ISSN 0003-2654
VOL. 120 NO. 5 MAY 1995

The Analyst

An international analytical science journal

GEOANALYSIS 94

An International Symposium on the Analysis of Geological and Environmental Materials

Special Issue: Geoanalysis

The Analyst

The Analytical Journal of The Royal Society of Chemistry

Analytical Editorial Board

Chairman: J. N. Miller (*Loughborough, UK*)

M. Cooke (*Sheffield, UK*)
C. S. Creaser (*Nottingham, UK*)
A. G. Davies (*London, UK*)
A. G. Fogg (*Loughborough, UK*)
J. M. Gordon (*Cambridge, UK*)
G. M. Greenway (*Hull, UK*)
S. J. Hill (*Plymouth, UK*)
D. L. Miles (*Keyworth, UK*)
R. M. Miller (*Gouda, The Netherlands*)
B. L. Sharp (*Loughborough, UK*)
M. R. Smyth (*Dublin, Ireland*)
Y. Thomassen (*Oslo, Norway*)
P. Vadgama (*Manchester, UK*)

Advisory Board

J. F. Alder (*Manchester, UK*)
A. M. Bond (*Victoria, Australia*)
J. G. Dorsey (*Cincinnati, OH, USA*)
L. Ebdon (*Plymouth, UK*)
A. F. Fell (*Bradford, UK*)
J. P. Foley (*Villanova, PA, USA*)
M. F. Giné (*Sao Paulo, Brazil*)
T. P. Hadjiioannou (*Athens, Greece*)
W. R. Heineman (*Cincinnati, OH, USA*)
A. Hulanicki (*Warsaw, Poland*)
I. Karube (*Yokohama, Japan*)
E. J. Newman (*Poole, UK*)
J. Pawliszyn (*Waterloo, Canada*)
T. B. Pierce (*Harwell, UK*)
E. Pungor (*Budapest, Hungary*)
J. Růžička (*Seattle, WA, USA*)
R. M. Smith (*Loughborough, UK*)
K. Štulík (*Prague, Czechoslovakia*)
J. D. R. Thomas (*Cardiff, UK*)
J. M. Thompson (*Birmingham, UK*)
K. C. Thompson (*Sheffield, UK*)
P. C. Uden (*Amherst, MA, USA*)
A. M. Ure (*Aberdeen, UK*)
C. M. G. van den Berg (*Liverpool, UK*)
A. Walsh, KB (*Melbourne, Australia*)
J. Wang (*Las Cruces, NM, USA*)
T. S. West (*Aberdeen, UK*)

Regional Advisory Editors

For advice and help to authors outside the UK

Professor Dr. U. A. Th. Brinkman, Free University of Amsterdam, 1083 de Boelelaan, **1081 HV Amsterdam,** THE NETHERLANDS.
Professor P. R. Coulet, Laboratoire de Génie Enzymatique, EP 19 CNRS-Université Claude Bernard Lyon 1, 43 Boulevard du 11 Novembre 1918, **69622 Villeurbanne Cedex,** FRANCE.
Professor O. Osibanjo, Department of Chemistry, University of Ibadan, **Ibadan,** NIGERIA.
Professor F. Palmisano, Universitá Degli Studi-Bari, Departimento di Chimica Campus Universitario, 4 Trav. 200 Re David—**70126 Bari,** ITALY.
Professor K. Saito, Coordination Chemistry Laboratories, Institute for Molecular Science, Myodaiji, **Okazaki 444,** JAPAN.
Professor M. Thompson, Department of Chemistry, University of Toronto, 80 St. George Street, **Toronto,** Ontario, CANADA M5S 1A1.
Professor Dr. M. Valcárcel, Departamento de Química Analítica, Facultad de Ciencias, Universidad de Córdoba, **14005 Córdoba,** SPAIN.
Professor J. F. van Staden, Department of Chemistry, University of Pretoria, **Pretoria 0002,** SOUTH AFRICA.
Professor Yu Ru-Qin, Department of Chemistry and Chemical Engineering, Hunan University, **Changsha,** PEOPLES REPUBLIC OF CHINA.
Professor Yu. A. Zolotov, Kurnakov Institute of General and Inorganic Chemistry, 31 Lenin Avenue, 117907, **Moscow V-71,** RUSSIA.

Editorial Manager, Analytical Journals: Janice M. Gordon

Editor, *The Analyst*
Harpal S. Minhas
The Royal Society of Chemistry,
Thomas Graham House, Science Park,
Milton Road, Cambridge, UK CB4 4WF
Telephone +44(0)1223 420066.
Fax +44(0)1223 420247.
E-Mail:Analyst@RSC.ORG(Internet)

US Associate Editor, *The Analyst*
Dr Julian F. Tyson
Department of Chemistry,
University of Massachusetts,
Box 34510 Amherst MA
01003-4510, USA
Telephone +1 413 545 0195
Fax +1 413 545 4846

Assistant Editors

Sarah Williams Caroline Seeley Yasmin Khan

Editorial Secretary: Claire Harris

Advertisements: Advertisement Department, The Royal Society of Chemistry, Burlington House, Piccadilly, London, UK W1V 0BN. Telephone +44(0)171-287 3091. Fax +44(0)171-494 1134.

Information for Authors

Full details of how to submit material for publication in *The Analyst* are given in the Instructions to Authors in the January issue. Separate copies are available on request.

The Analyst publishes original research papers, critical reviews, tutorial reviews, perspectives, news articles, book reviews and a conference diary.

Original research papers. The Analyst publishes full papers on all aspects of the theory and practice of analytical chemistry, fundamental and applied, inorganic and organic, including chemical, physical, biochemical, clinical, pharmaceutical, biological, environmental, automatic and computer-based methods. Papers on new approaches to existing methods, new techniques and instrumentation, detectors and sensors, and new areas of application with due attention to overcoming limitations and to underlying principles are all equally welcome.

Full critical reviews. These must be a critical evaluation of the existing state of knowledge on a particular facet of analytical chemistry.

Tutorial reviews. These should be informally written although they should still be a critical evaluation of a *specific* topic area. Some history and possible future developments should be given. Potential authors should contact the Editor before writing reviews.

Perspectives. These articles should provide either a personal view or a philosophical look at a topic relevant to analytical science. Alternatively, they may be relevant historical articles. Perspectives are included at the discretion of the Editor.

Particular attention should be paid to the use of standard methods of literature citation, including the journal abbreviations defined in Chemical Abstracts Service Source Index. Wherever possible, the nomenclature employed should follow IUPAC recommendations, and units and symbols should be those associated with SI.

Every paper will be submitted to at least two referees, by whose advice the Editorial Board of *The Analyst* will be guided as to its acceptance or rejection. Papers that are accepted must not be published elsewhere except by permission. Submission of a manuscript will be regarded as an undertaking that the same material is not being considered for publication by another journal.

Regional Advisory Editors. For the benefit of potential contributors outside the UK and N. America, a Group of Regional Advisory Editors exists. Requests for help or advice on matters related to the preparation of papers and their submission for publication in *The Analyst* can be sent to the nearest member of the Group. Currently serving Regional Advisory Editors are listed in each issue of *The Analyst.*

Manuscripts (four copies typed in double spacing) should be addressed to:

H. S. Minhas, Editor, *or*
J. F. Tyson, US Associate Editor

All queries relating to the presentation and submission of papers, and any correspondence regarding accepted papers and proofs, should be directed either to the Editor, or Associate Editor, *The Analyst.* Members of the Analytical Editorial Board (who may be contacted directly or *via* the Editorial Office) would welcome comments, suggestions and advice on general policy matters concerning *The Analyst.*

There is no page charge.

Fifty reprints are supplied free of charge.

The Analyst (ISSN 0003–2654) is published monthly by The Royal Society of Chemistry, Thomas Graham House, Science Park, Milton Road, Cambridge, UK CB4 4WF. All orders, accompanied with payment by cheque in sterling, payable on a UK clearing bank or in US dollars payable on a US clearing bank, should be sent directly to The Royal Society of Chemistry, Turpin Distribution Services Ltd., Blackhorse Road, Letchworth, Herts, UK SG6 1HN. Turpin Distribution Services Ltd., is wholly owned by the Royal Society of Chemistry. 1995 Annual subscription rate EC £408.00, USA $749.00, Canada £428.00 (excl. GST), Rest of World £428.00. Purchased with *Analytical Abstracts* EC £807.00, USA $1472.00, Canada £841.00 (excl. GST), Rest of World £841.00. Purchased with *Analytical Abstracts* plus *Analytical Proceedings* EC £925.00, USA $1699.00, Canada £971.00 (excl. GST), Rest of World £971.00. Purchased with *Analytical Proceedings* EC £492.00, USA $905.00, Canada £517.00 (excl. GST), Rest of World £517.00. Air freight and mailing in the USA by Publications Expediting Inc., 200 Meacham Avenue, Elmont, NY 11003.

USA Postmaster: Send address changes to: *The Analyst,* Publications Expediting Inc., 200 Meacham Avenue, Elmont, NY 11003. Second class postage paid at Jamaica, NY 11431. All other despatches outside the UK by Bulk Airmail within Europe, Accelerated Surface Post outside Europe. PRINTED IN THE UK.

© The Royal Society of Chemistry, 1995. All rights reserved. No part of this publication may be reproduced, stored in a retrieval system, or transmitted in any form, or by any means, electronic, mechanical, photographic, recording, or otherwise, without the prior permission of the publishers.

Guest Editor—Dr. Michael H. Ramsey

Geoanalysis 94: An International Symposium on the Analysis of Geological and Environmental Materials

Dr. Michael H. Ramsey MSc, DIC, PhD, C. Chem., FRSC

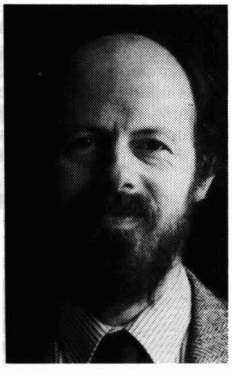

Born and educated in North Yorkshire, Michael Ramsey graduated with joint honours in Chemistry and Geology from Hull University in 1974. He then moved south to Birmingham to study for an MSc in Mineral Chemistry in 1975, and then further south to Imperial College, London, where he gained his PhD in Analytical Geochemistry in 1986.

In 1975 he went to work for a mining company on the Zambian Copperbelt for three years. This initially involved the development of new analytical methods, based mainly on emission spectrometry, but rapidly progressed into supervision and finally to the management of an analytical laboratory with a staff of 30.

Returning to the UK, he joined the Applied Geochemistry Research Group in the Geology Department at Imperial College in 1979. This necessitated keeping a stimulating balance between research into new analytical methods while managing a suite of laboratories analysing some 20 000 samples per annum. The research was directed mainly towards devising geochemical applications of the newly developed ICP-AES, initially under the supervision of Dr. Michael Thompson, who pioneered this application at Imperial.

The main focus of his research interests has been measurement uncertainty; its estimation, its reduction and finding objective methods to set targets for acceptable levels of this uncertainty. Initially this work concentrated on analytical error, particularly from ICP-AES, and looked at correlated variance between multielement determinations. This resulted in the development of the parameter-related internal standard method (PRISM) of reducing both random and systematic errors, and the award of the Ronal Belcher Memorial Lectureship in 1986.

While assessing the effect of measurement uncertainty on particular geochemical interpretations, it became evident that the sampling error, rather than the analytical error, was often the limiting factor. This led to the development of the idea of integrated sampling and analytical quality control schemes (SAQCS = SAX), that has been applied to both environmental and exploration geochemistry. His current research includes developing methods for the estimation of sampling errors, both random and systematic.

With his team of research students at Imperial College, Dr. Ramsey is now looking at the implications of measurement uncertainty on a range of geochemical investigations. These include quantifying the geochemical processes that control the downward migration of heavy metals beneath ancient smelting sites. A related topic is aimed at separating 'natural' from 'anthropogenic' sources of metal contamination using geographical information systems (GIS). This system should be particularly useful for assessing the ramifications of the sampling and analytical uncertainties.

On the domestic front, Michael Ramsey is happily married with two daughters, the family gained a rare insight into the fraternity of geoanalysts by visiting GEOANALYSIS 94, and by joining in the glorious weather and convivial atmosphere of the boat trip on lake Windermere. The musical sessions at both of the geoanalytical conferences have become a regular feature, with Dr. Ramsey on the piano, often Dr. Thompson on the flute, and a hearty chorus of geoanalysts. This has led to the development of the most crucial document of the conference, 'The Geoanalytical Song Book'.

ห้องสมุดกลาง จุฬาลงกรณ์มหาวิทยาลัย
15 ธ.ค. 2538

Foreword

Geonalysis 94: An International Symposium on the Analysis of Geological and Environmental Materials

Geoanalysis 94 held in Ambleside, in the English Lake District, on September 18–22, 1994 brought together an enthusiastic community of some 120 geoanalysts from 25 countries. It has built on the firm foundations laid at the first Geoanalysis conference held in Canada at Grandview in the Ontario Muskoka Lakes, and seems to suggest that geoanalysts have a natural affinity for the serenity of such idyllic settings.

This special issue of *The Analyst* brings together 44 of the papers that were presented at Geoanalysis 94. The diversity of the content of the papers illustrates the extraordinary range of analytes and types of sample with which the geoanalyst has to contend. The challenges of this analytical task may be one of the reasons for the appreciation of serene settings for our conferences! More seriously, the meeting provided a rare opportunity for workers in many relatively isolated areas of geoanalysis to compare notes and to recognize a large number of common problems and many common solutions.

The scope of the conference encompassed all the main geoanalytical techniques in common use (ion and electron probe microscopy, NAA, ICP-MS, ICP-AES, XRF, TIMS and SIMS), and the more exotic synchrotron-based techniques XANES, EXAFS (see Smith, p. 1231) and accelerator-based MS (see Rucklidge, p. 1283). The main applications were geochemical research, either pure (*e.g.*, petrogenesis), environmental or for mineral exploration. The papers in this issue are of three types that reflect the styles of lectures that were given. The majority are papers describing primary research, others are reviews of particular subject areas, and the third category are papers describing broad perspectives of subject areas, often deriving from plenary or invited lectures.

As Guest Editor, I perceived several main themes that arose from the conference. I have tried to be objective in their selection, but they probably reflect some of my personal interests to some extent. These themes can be exemplified by many of the papers in this issue. Spatially resolved analysis was barely discussed at the 1990 meeting, yet by 1994 it has become obvious that this is an approach with a large potential for answering geochemical questions. Not only were there reports on the characterization of separate mineral grains (see Watling *et al.*, p. 1357) but also spatial-resolved elemental mapping within grains (see Smith, p. 1231), typified by the keynote lecture given by Professor K. O'Nions.

Isotope geochemistry was one of the main themes of this conference, although there had been little involvement of this topic in the 1990 meeting. The precision achieved on isotope ratio determinations for bulk samples are often amazing to other geoanalysts, but it was remarkable that precisions of around 0.1% are now achievable for $^{18}O/^{16}O$ even for microprobe systems (see Lyon *et al.*, p. 1321). The increasing use of ICP-MS for isotopic measurements made an interesting comparison with the determinations by more traditional MS techniques. This was particularly clear in the investigations of boron isotopes by ICP-MS (see Porteous *et al.*, p. 1397) and TIMS (see Aggarwal *et al.*, p. 1301).

Developments in the assessment of analytical data quality was a common theme of the conference. An invited lecture by Dr. M. Thompson described the forays made by analytical chemists, and geoanalysts, onto the 'Data Quality Isles' (see Appendix). This lecture clarified the meaning of an increasing array of technical terms, many of which are liable to baffle the average geoanalyst, (*e.g.*, trueness, traceability and uncertainty). Unfortunately, this lecture was not written up as a paper but a list of definitions of data quality terminology distributed at the lecture, is given in the Appendix. One of the new areas of endeavour in data quality is the estimation of the errors generated in field sampling, rather than in the laboratory. Initial work has shown that random errors in sampling can be estimated and compared with those arising from analysis. Systematic errors in sampling can also be estimated, at least between different sampling protocols (see Ramsey *et al.*, p. 1353). The characterization of reference materials for the estimation of systematic analytical error has itself been improved by the use of new analytical techniques such as ICP-MS (see Kane, p. 1505).

Geoanalysis using field portable instruments is also making geoanalysts more aware of the possibilities of investigating problems at first hand rather than being presented with an anonymous sample of unknown provenance and quality. The performance of a new field portable XRF with relatively low detection limits, was shown to have high potential in such a role (see Potts *et al.*, p. 1273). Multi-element detectors have also been evaluated for *in situ* determinations down bore holes (see Sams *et al.*, p. 1407).

A lively session on applications of geoanalysis to environmental problems illustrated the diversity of the challenges facing this community. These ranged from the determination of sub-parts per billion concentrations of Se in natural waters (see Adkins *et al.*, p. 1433) to the strategies required for mapping the geochemistry of the whole planet within a reasonable budget (see Xie, p. 1497).

The final session concentrated on innovations in geoanalysis. The possibilities of spatial analysis were extended even further to include speciation analysis, with an example of Se speciation across a plant root/soil interface. Excitation from synchrotron-generated high-energy X-rays enables spatial mapping of phases containing Se^{VI}, Se^{IV} and finally Se^{0} across this interface (see Smith, p. 1231). This form of geoanalysis, although currently very specialized, opens the way for a much clearer understanding of geochemical processes in such environments. Accelerator mass spectrometry is another specialized technique that is usually applied to radionuclides with long half-lives. One example, demonstrated the power of the technique by mapping atmospheric dispersion of ^{129}I from Sellafield over the Lake District, through the analysis of mosses (see Rucklidge, p. 1283).

Aside from the science, the conference was also notable for its very friendly and positive atmosphere. This was doubtless facilitated by the social events, such as the cruise on Lake Windermere one glorious sunny afternoon, and the conference dinner in a splendid hotel overlooking the lake. More fundamentally, the atmosphere derived from the feeling amongst the delegates that they were among like minds, and that they often faced similar analytical challenges. The general consensus was that the sharing of experience and the personal contacts made at Geoanalysis 94 were of enormous benefit in advancing the science of geoanalysis amongst an international fraternity of geoanalysts.

Michael H. Ramsey
Guest Editor
Imperial College, London

Appendix

The Data Quality Isles*

The island group has seen colonization by various tribes of analytical chemists moving into the area from the West. Most of the tribes were represented in the small islands of the Sea of Basic Concepts by the early 20th Century and are now firmly established, although the outlying island of Traceability has apparently been little explored until recently. The twin islands Statistics and Experimental Design are well known but not permanently inhabited. On the Big Island some of the more enterprising tribes, such as the Geochemists and the Clinical Biochemists are thoroughly established at the western end in the Quality Assurance and Quality Control regions, and most of the tribes are now represented to a degree. At the eastern end the territories of Uncertainty and Fitness-for-Purpose are well known only around the easily accessible coastline. The rugged hinterland has not been settled and known only from the accounts of the few expeditions that have penetrated the area. (See next page for definitions.)

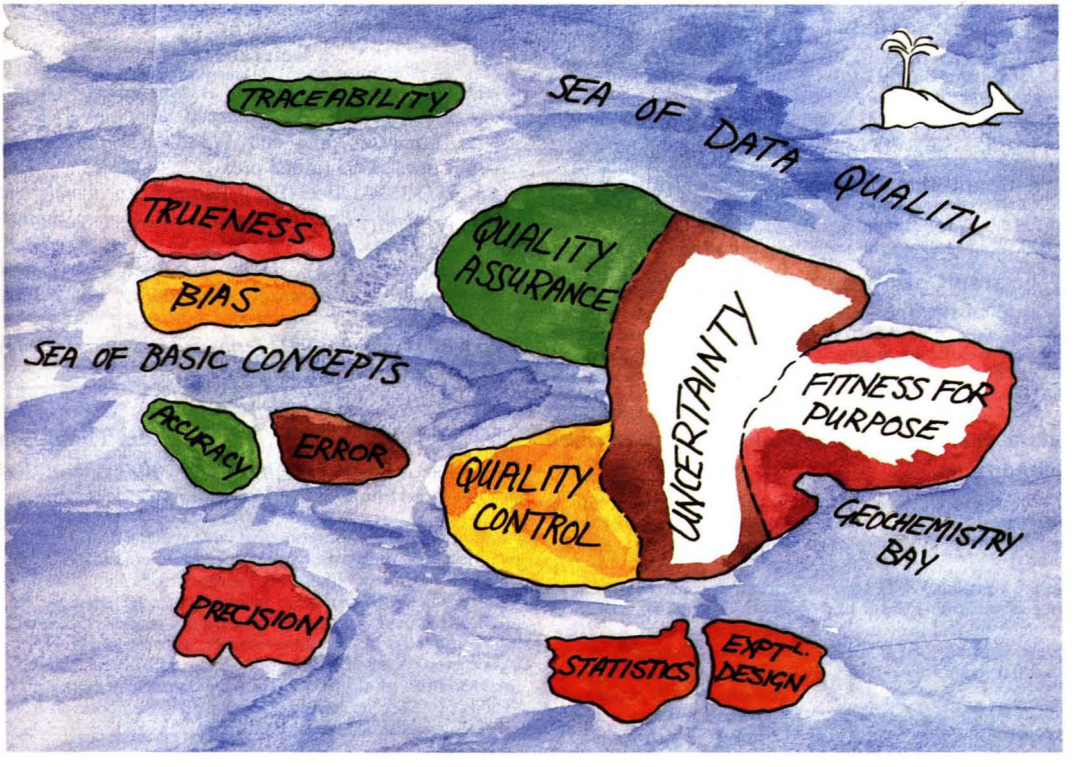

* Presented at Geoanalysis 94: An International Symposium on the Analysis of Geological and Environmental Materials, Ambleside, England, September 18–22, 1994.

Definitions

Quality Assurance

All those planned and systematic actions necessary to provide adequate confidence that a product or service will satisfy given requirements for quality.[1]

Internal Quality Control

The set of procedures undertaken by laboratory staff for the continuous monitoring of operation and the results of measurements in order to decide whether results are reliable enough to be released.[2]

Trueness

The closeness of the agreement between the average value obtained from a large series of test results and an accepted reference value.[3]

Bias

The difference between the expectation of the test results and an accepted reference value.[3]

Accuracy

The closeness of the agreement between a test result and the accepted reference value.[4]

Error

The result of a measurement minus the true value of the measurand.[4]

Precision

The closeness of agreement between independent test results obtained under prescribed conditions.[5]

Uncertainty

A parameter, associated with the result of a measurement, that characterizes the dispersion of the values that could reasonably be attributed to the measurand.[4]

Traceability

A property of the result of a measurement or the value of a standard whereby it can be related, with a stated uncertainty, to stated references, usually national or international standards, through an unbroken chain of comparisons.[4]

Fitness-for-purpose

The degree to which data produced by a measurement process enables a user to make technically correct decisions for a stated purpose.[2]

References

1 ISO 8402:1994. *Quality Assurance and Quality Management—Vocabulary.*
2 Thompson, M., and Wood, R., *Pure Appl. Chem.*, 1995 (in the press).
3 ISO 3534-1:1993 (E/F). *Statistics, Vocabulary and Symbols—Part 1 Probability and General Statistical Terms.*
4 *International Vocabulary for Basic and General Terms in Metrology*, 2nd edn., 1993, ISO, Geneva.
5 ISO Guide 30:1992. *Terms and Definitions Used in Connection with Reference Materials.*

Michael Thompson
Birkbeck College, London

Tutorial Review

Synchrotron X-Ray Sources: Instrumental Characteristics. New Applications in Microanalysis, Tomography, Absorption Spectroscopy and Diffraction*

Joseph V. Smith†

Department of Geophysical Sciences and Center for Advanced Radiation Sources, University of Chicago, Chicago, IL, USA 60637

Summary of Contents

Introduction
Synchrotron X-Ray Sources
  Beamlines and Experimental Stations
    Experimental station for X-ray fluorescence analysis
    Experimental stations for X-ray diffraction
    Experimental station for X-ray absorption spectroscopy
    Detectors
    Design of an experimental facility at the APS
Use of a Synchrotron Source
Analytical Procedures and Interpretation
  Comparison With Other Microanalytical Techniques
  Illustrative Applications and Future Advances
    Coal
    Cosmic dust
    Element partitioning and diffusion couples
    Environmental
    Inclusions in minerals
    Earth's mantle
    Meteorites and the moon
    Ore mineralogy
    Soil mineralogy and agriculture
    Miscellaneous
References

Keywords: *Synchrotron X-ray source; X-ray diffraction; X-ray fluorescence; X-ray spectroscopy; X-ray tomography; review*

Introduction

The current state of microanalysis using synchrotron X-ray techniques is reviewed. Only the broadest concepts are presented here. For technical details, see ref. 1 which contains a detailed bibliography up to April 1994, which is updated here to December 1994. Synchrotron-related science spans many interdisciplinary topics covered in various books, review articles and workshop reports.[2-26]

Particularly important is the concept of combining fluorescence, diffraction and absorption spectroscopy to determine the bulk chemical composition, the atomic positions in the unit cell, and the type of chemical bonding in a single crystal. Chemical reactions can be followed on a millisecond scale.

This review describes the current technical capabilities and analytical applications, and concludes with speculations about future analytical capabilities made possible by further technical developments. Emphasis is placed on societal applications involving agriculture, toxic waste, organic–inorganic systems, geochemical processes involving coal and ore deposits, and atmospheric aerosols.

Synchrotron X-ray Sources

Synchrotron X-ray sources utilize narrow bunches of electrons circulating at near the velocity of light in a horizontal vacuum ring (Fig. 1). The near-circular flight path of the string of bunches is constrained by an electromagnetic system.

Kinetic energy is imparted to the electrons by synchronous pulsing from an electromagnetic oscillator. Inward acceleration by a bending magnet causes tangential emission of a very narrow beam of white X-rays (Fig. 2): white is the term used for a continuous energy band analogous to the optical spectrum.

The narrow beam is so brilliant that a sub-millimetre sample can be examined. Brilliance is a technical term that specifies the number of photons hitting a tiny analytical sample, typically a few micrometres in diameter.

Instantaneously, the tangential jet is circular in cross-section, and its angular divergence is only a 1 mrad across. The horizontal arc at the bending magnet is typically about 20 mrad. Generally a mask absorbs the inner region of the beam to yield two X-ray beams, each a few mrad wide, which can be used simultaneously (Fig. 3).

Each white beam can be used either directly or after focusing by a mirror. The small angular divergence of a synchrotron X-ray beam is very favourable for sophisticated design of mirror optics. The brilliance at a micro-sample can be increased 10- to 100-fold with a focusing mirror which demagnifies the source (*i.e.* electron bunch). However, the angular divergence increases at the analytical sample, and the mirror will have an upper-energy cut-off. A monochromator can be inserted.

The much wider angular dispersion from a laboratory source makes it more difficult to design focusing mirrors. Most X-rays from a laboratory source are wasted in analysis of a tiny sample, and the specimen size is commonly in the millimeter range.

Multiple reflection inside a tapered glass capillary[27-28] can concentrate a synchrotron beam into an even more intense jet, and a sub-micrometre final jet with sufficient flux for analysis can be obtained. However, the emerging jet is perforce more divergent than the incoming one, and the working distance to the sample is sub-millimetre.

Many experiments with micrometre samples will probably continue to use brute force. A very intense synchrotron beam confined by crossed slits is much more tolerant of alignment problems and irregular sample morphology than an expensive system using complex optics.

Monochromator design involves very subtle factors, includ-

* Presented at Geoanalysis 94: An International Symposium on the Analysis of Geological and Environmental Materials, Ambleside, England, September 18–22, 1994.

† Also at Department of Applied Science, Brookhaven National Laboratory, Upton, NY, USA 11973.

ing compensation for mechanical distortion caused by heating, and the possible addition of multiple surface layers to increase the reflectivity for a particular energy range. In general, it is easy to obtain reliable monochromators up to 15 keV, but increasingly difficult towards 40 keV.

Synchrotron sources are designed either for high energy (2–200 keV photon energy) or low energy (< 2 keV). The low-energy ones are mainly used for experiments in the soft X-ray, UV and IR regions. This review will not cover these experiments, except to state that (*i*) soft-X-ray microscopy[29-31] can give sub-micrometre images of light elements including C and N that are particularly useful in biology, while (*ii*) IR spectroscopy has the potential to image atomic vibrations on 1000-fold smaller samples than for conventional instruments. Surface phenomena involving adsorbed ionic species and molecular complexes will undoubtedly be studied by pioneering analysts using standing waves generated by glancing incidence.[32-34]

High-energy sources[35] are more suitable than the low-energy ones for studying diffraction, absorption spectroscopy and fluorescence of the materials examined at most analytical laboratories. A white synchrotron beam from a bending magnet has a continuous (white) energy profile (Fig. 4), similar to that from a laboratory tungsten source, but with a different shape.

The critical energy (defined as the median energy of the photons) ranges from 2–5 keV for beamlines at existing synchrotron radiation facilities to about 20 keV for the new ones coming into operation. A substantial flux is still available at six times the critical energy. Thus for a bending magnet atthe X-ray ring of the National Synchrotron Light Source (NSLS) at Brookhaven National Laboratory, the critical energy is 5 keV, with only a 10-fold reduction in brightness at

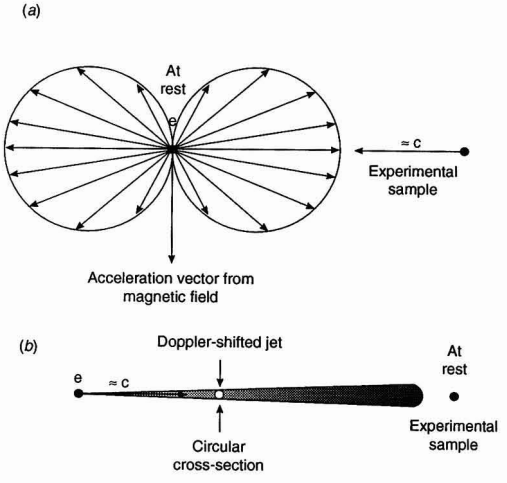

Fig. 2 Angular emission of X-rays from an accelerated electron. (*a*) The amplitude of the instantaneous emission in the reference plane of the electron, e, is governed by a torus-shaped pattern. The torus is symmetrical about the acceleration vector. In a symmetrical synchrotron ring, the acceleration vector is the inwards radial vector. The experimental sample is moving towards the electron at nearly the velocity of light, *c*. (*b*) Switching to the reference plane of the sample requires that the dipole pattern undergoes a Doppler shift. Essentially the electron 'pulls' the dipole pattern into a narrow jet with a circular cross-section. The higher the energy of the electron, the narrower the jet.

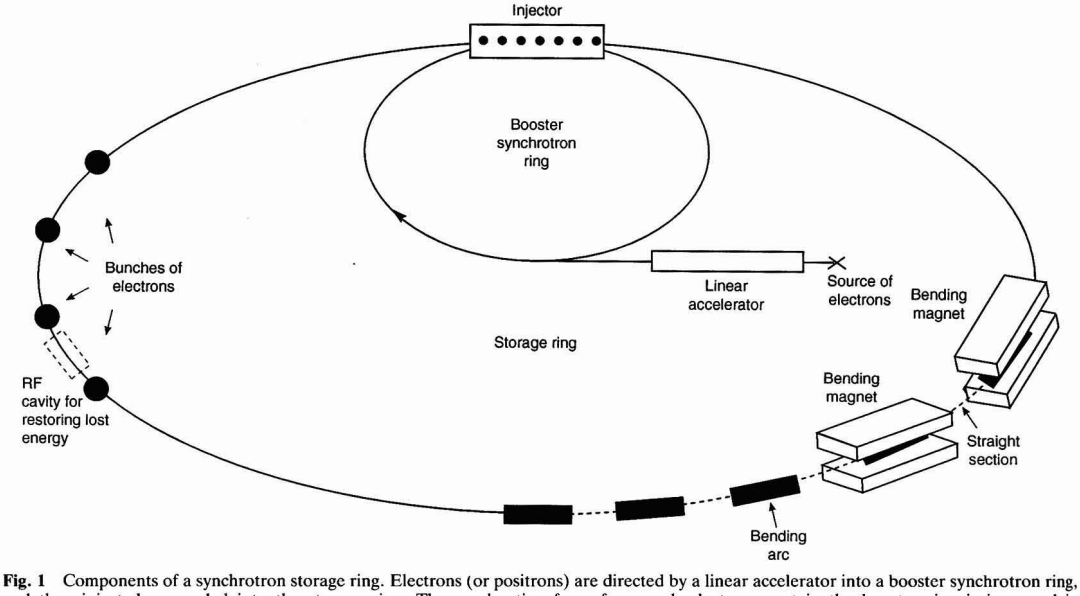

Fig. 1 Components of a synchrotron storage ring. Electrons (or positrons) are directed by a linear accelerator into a booster synchrotron ring, and then injected as needed into the storage ring. The accelerating force from each electromagnet in the booster ring is increased in synchronisation with the circulation time as the kinetic energy of the electrons is increased. The bending magnets of the storage ring have constant magnetic field, and the kinetic energy of the electrons remains constant. Each ring consists of bending arcs joined by straight sections. The electrons are injected as bunches. To maintain control of the electrons, which tend to repel each other, the bunches are continuously 'tightened' by special electromagnetic systems. The 'tighter' the electron bunch, the more brilliant the X-ray beams, and the better for microanalysis. Wandering from the desired orbit is inhibited by positional sensors and feedback electromagnetic deflectors. Electrons are lost by collisions with residual gases in the ring vacuum. Generally, the electrons are discarded when the electron current becomes halved, and new bunches are injected from the booster ring.

30 keV (Fig. 4). For the bending magnets at the Advanced Photon Source (APS) in the Argonne National Laboratory, and the European Synchrotron Research Facility (ESRF), the critical energy is about 20 keV, with substantial flux at and above 100 keV.

First-generation bending magnets were shoe-horned into fortuitous empty sections of existing nuclear accelerators. Although service was erratic, excellent pioneering experiments were performed. Second-generation synchrotrons are fully dedicated, and were tailored for bending magnets. Adjacent bending magnets are connected by a short straight section, where there is no inward acceleration, to complete a near-polygonal ring. The electron bunches in the old nuclear accelerators were broad, while the ones in the new synchrotron sources were deliberately made as small as possible to increase the brilliance of the beams for microanalysis. Typically there are several dozen beamlines at each ring, and several thousand users over a year. Examples are the Synchrotron Radiation Source (SRS), and the NSLS. Although the cost per individual analysis is comparable with that for advanced laboratory instruments (*e.g.*, ion microprobe), the over-all cost of operations at a synchrotron source is high.

There are two rings at the NSLS, a low-energy ring (0.7 GeV kinetic energy of the electrons) for experiments with IR to soft X-ray photons, and a medium-energy ring (2.5 GeV) for hard X-rays (1–40 keV). The former ring is shown in Fig. 5. The concrete safety wall around the storage ring can be seen in the middle distance nearly under the supply duct. One of the tangential beamlines projects to the middle front, and another projects to the left. Almost every square inch is used for auxiliary equipment, and vertical stacking is typical.

The next technical advance was installation of a multiple array of magnets (known as an insertion device, ID) into a long straight section between two bending magnets. Pioneering IDs were developed on existing synchrotron sources, often in non-optimal configurations. Third-generation sources, now coming into operation, are deliberately optimized for such multiple arrays of magnets. Fig. 6 shows an experimental ID

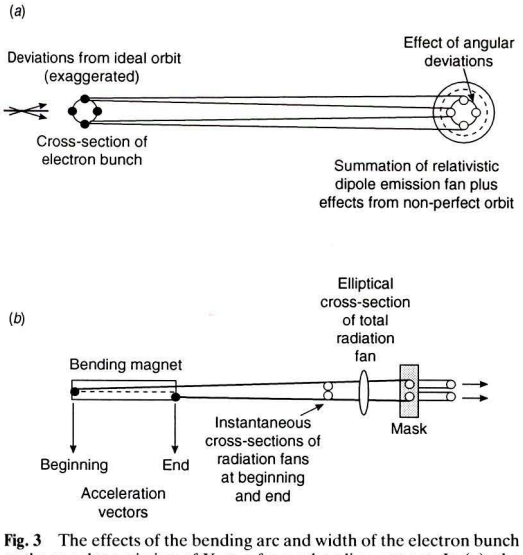

Fig. 3 The effects of the bending arc and width of the electron bunch on the angular emission of X-rays from a bending magnet. In (*a*), the circular radiation fans for four points on the circumference of the circular cross-section of the electron bunch are shown. The combined fan for all points in the bunch is circular. In (*b*), the summation of instantaneous circular fans for a curved arc generates an elliptical fan. A mask absorbs the central region to generate two outer beams that can be used simultaneously.

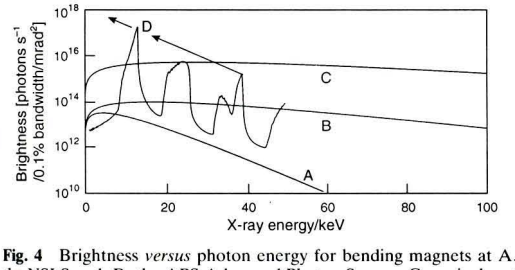

Fig. 4 Brightness *versus* photon energy for bending magnets at A, the NSLS and, B, the APS Advanced Photon Source, C, a wiggler at the APS, and, D, an undulator operating at its highest photon energy (~13 keV in the first harmonic). The second harmonic is broader than the first harmonic, and the third harmonic is split, simply because the magnets are not point scatterers and produce 'ghosts'. The arrows show the increase of brightness as the undulator is tuned to lower photon energy. The spectral profile retains its shape. Note that details will vary as designs are fine tuned.

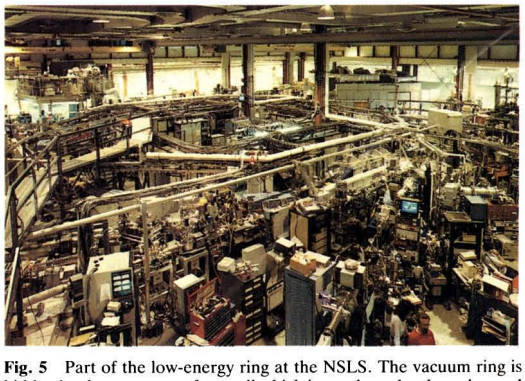

Fig. 5 Part of the low-energy ring at the NSLS. The vacuum ring is hidden by the concrete safety wall which is nearly under the polygonal supply duct. Two metal tubes carrying X-ray beams are shown at middle front and left. Photograph CN7-378-97 from the NSLS Archive.

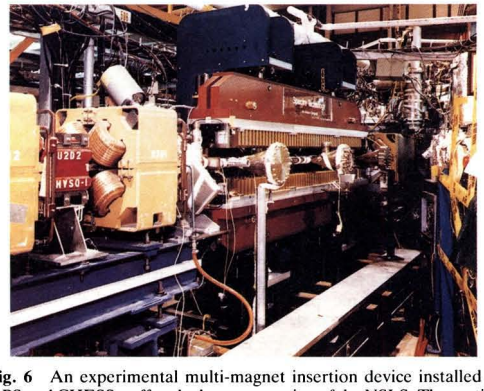

Fig. 6 An experimental multi-magnet insertion device installed by APS and CHESS staff at the low-energy ring of the NSLS. The vertical pairs of magnets of alternating polarity straddle the vacuum tube of the storage ring. Also visible are the electromagnetic components at the flanking bending magnets and a front end of a beamline. Argonne National Laboratory Photograph 9851K.

inserted into the low-energy ring at NSLS to gain experience for design of the APS.

There are two types of ID, wiggler and undulator, both of which cause each electron bunch to oscillate symmetrically about the straight path between the curved arcs from the adjacent bending magnets. Just as for a single bending magnet, a tangential jet of X-rays is emitted at each magnet of an ID. For N magnets of alternating polarity, there will be $N/2$ jets to the outside and $N/2$ to the inside.

If the magnets deflect the electrons strongly, the two circular $N/2$ jets merely add up to give a single elliptical jet of N-fold higher flux (wiggler). Fig. 4 shows the same spectral profile for a bending magnet and a wiggler at the APS, with a vertical displacement of brightness corresponding to the 20 poles of wiggler together with a geometrical factor related to the cross-sections of the beams. In some older synchrotron sources, the magnets of the wiggler are superconducting. The six-fold higher field over that for a simple magnet increases the critical energy. Thus the five-pole superconducting wiggler on beamline X-17 at the 2.5 GeV NSLS has a spectral profile with critical energy similar to that of the bending magnet of the 7 GeV APS.

If the deflections are smaller, the jets remain in the same phase space and undergo constructive interference as for visible light scattered from a diffraction grating (undulator). The combined jet is essentially circular and even narrower than for a single bending magnet (10-fold for a typical undulator in a third-generation source). The white beam of a bending magnet and a wiggler is replaced by harmonic peaks for an undulator (Fig. 4). For $N = 100$, the energy peaks are effectively about 2% wide in $\Delta E/E$ (some broadening and fine structure occurs because the magnets are not point scatterers).

By varying the magnetic field, the energy can be varied: this is equivalent to rotating a crystal monochromator in a conventional X-ray spectrometer. In Fig. 4, the spectral profile of an APS undulator is shown at its highest energy with the first harmonic at 13 keV, the second at 26, and the third at 39 keV (note the broadening and splitting of the higher harmonics). At the lowest energy, the harmonics are at 4, 9 and 13 keV, thus providing continuous tuning from 4 to 39 keV. The brightness increases 10-fold for lower energy (Fig. 4, arrows). Brightness is a technical term used for experiments using a simple collimator rather than a focusing mirror for which brilliance is appropriate.

In theory, the first harmonic is on axis, the second is a symmetrical off-axis dipole, and the third has a central jet with side bands: the polarization is correspondingly complex. In practice, the finite size and orbital irregularity of the electron bunches and the imperfection of the magnets will cause blurring of each harmonic to give near-circular, concentric jets for each harmonic. Complex development studies will be needed to optimize the brightness and polarization for each particular experiment.

For a diffraction experiment, one of the harmonic peaks from an undulator can be selected, and used directly for very fast experiments (μs to ns). Alternatively, ΔE can be reduced by a crystal monochromator at the expense of reducing the flux at least 100-fold. There are fascinating details on the best use of undulators for Bragg and Laue diffraction.

For fluorescence analysis, the magnetic field can be varied so that a harmonic peak sweeps successively through an absorption edge of each element of interest. Symmetrical tilting of a rack of magnets causes broadening of the harmonics, and a ΔE of about 1 keV is used for absorption spectroscopy. (This is also useful for Laue diffraction.) A crystal monochromator is used to sweep through an absorption edge which sits in the broadened harmonic of the tilted undulator.

Increase of the magnetic field turns an undulator into a wiggler. The number of harmonics increases, and they ultimately merge into a continuum. There are many technical advantages of a hybrid undulator–wiggler that cannot be detailed here.

As the magnetic energy of an undulator must be weak with respect to the kinetic energy of the circulating electrons, it is necessary to have a high electron energy in order to be able to tune the harmonics of an undulator into the hard X-ray region. Thus the ESRF, the APS, and the Spring-8 source(Japan) operate with a kinetic energy of 6, 7 and 8 GeV, respectively, to obtain combined tunability of the first three harmonics from about 5 to about 30 keV. This higher energy brings the critical energy of the bending magnets (and wigglers) up to about 20 keV, with useable flux to above 100 keV. Hence, measurements with the wigglers and bending magnets can be made in the K spectrum for all elements.

Early non-dedicated synchrotrons were frustrating to use because of breakdowns, closures for upgrading, and competition with particle physicists. Dedicated synchrotrons are now achieving an operating reliability of better than 95% for over 200 days per year scheduled for users, plus another 100 days for planned maintenance and upgrades. Electrons are lost by collision with the residual gases in the vacuum system, but the lifetime for each fill of electrons into the very hard vacuum is now at least one day, instead of the few hours of a decade ago. (The APS uses positrons which interact with residual ions even less than electrons.) In early experiments, broad electron bunches wandered by up to a millimetre from the desired orbit, but in the latest operations tight bunches are rigorously controlled to 1–10 μm at most.

The circuit time of each electron bunch is a few microseconds for a third-generation source (3.5 μs for the APS), and each bunch generates X-rays for only a small fraction of a nanosecond. In principle for a millimetre sample, a simple analysis can be performed using a single bunch, and the analysis can be repeated every few microseconds. Generally, a synchrotron operates with 10 to 100 bunches, which may or may not be equally spaced, but a single bunch or a cluster can be used. Obviously there is the possibility of analytical chemistry on the micro- to nanosecond scale. However, most chemical analysts will simply use the time-averaged beam.

Beamlines and Experimental Stations

Each beamline consists of a complex front end which protects the ring vacuum from the beamline, a beam transport system which consists of a shielded tube enclosing optical components, *etc.*, and a safety hutch which holds the experimental equipment and sample (Fig. 7). The design of mirrors and monochromators is optimized by computer programs whose output is reviewed by several experts and iterated to match the perceived needs for the various analytical instruments before installation is permitted. The optical components in a flexible beamline can be switched in or out to permit analysis with white or monochromatic beam, either focused or straight through.

The safety protocol is extremely complex because of the need to protect human operators from radiation hazards. For high-energy sources with photon energies of >100 keV, at least 1 in of lead and steel is needed with labyrinth protection at joints. All the equipment in the hutch must be controlled from a computer terminal outside the hutch once the safety door is locked and the synchrotron beam is released. It is not practical to enter the hutch frequently to adjust the specimen position. A telemicroscope with a video output is essential.

A key consideration in the design of equipment at a synchrotron source is that the electric vector of the X-rays is polarized in the plane of the electron ring. Compton and Rayleigh scattering can be essentially eliminated by collecting

data at 90° to the incoming beam in the plane of the electron ring. Hence, the spatial orientation of spectrometers and diffractometers must be optimized. At beamline X26A of the NSLS, the solid-state detector, which is very sensitive to background, is placed exactly at 90° (Figs. 8 and 9), while the less-sensitive crystal spectrometer is tilted away (13° downwards, Fig. 9). Owing to the insignificant background at 90°, very weak peaks can be detected in diffraction experiments (for powder diffraction, the peak : background ratio is typically around 4000 compared with about 200 with laboratory instruments). A solid-state detector at 90° can be used in fluorescence analysis of trace elements (but only if the intensity from major elements is reduced with an absorption filter so that the limited count capability is not monopolized). Polarized X-ray absorption spectroscopy[36] can map the electronic structure and chemical bonding in three dimensions for an atomic site in a crystal.

Experimental station for X-ray fluorescence analysis

The X-ray fluorescence analysis station is the main facility for most chemical analyses at a synchrotron source.

The X26A beamline at the NSLS during the pioneering days of micro-XRF studies in 1986 is shown in Fig. 7. The X-ray beam travels down the metal pipe (left), and enters the safety hutch, whose interlocked door is open.

Fig. 8 shows the components for a micro-XRF experiment. Primary and secondary apertures define the incident beam from one side of a bending magnet. A double-crystal monochromator and a focusing mirror can be inserted. The beam on the specimen is defined by crossed slits driven by computer-controlled digital motors. The X-ray detector is placed at 90°, and the specimen is mounted on an *x-y-z* digital stage. The operator views the specimen with a microscope of long working distance.

Fig. 9 shows the micro-XRF apparatus at the X26A beamline in the 1990s.[4,24,37-42] The essential features remain the same. An additional feature is a wavelength spectrometer whose upper surface is visible under the solid state detector. Not visible are many improvements in hardware and software that have increased the sensitivity and accuracy of the analyses.

Experimental stations for X-ray diffraction

Apparatus for X-ray diffraction at a synchrotron source is essentially the same in principle as that for a standard laboratory.[13,14,20] Obvious key differences are that the incident X-ray beam is almost parallel and is much more brilliant. Equally important is the fact that X-rays of higher energy are available from a synchrotron source; a narrow energy band of high intensity can be obtained for chemical speciation using anomalous scattering; the electron bunches allow time-resolved experiments; and the polarization can be controlled accurately. The details of the various types of experimental stations cannot be explored here. Let it suffice that surface diffraction[8] must become one of the major analytical tools of the future as third-generation sources become established.

X-ray powder diffraction[14] is technically straightforward for sample identification, though there are many useful variants and experimental tricks. More sophisticated is the use of Rietveld profile analysis and phase-seeking methods to solve the crystal structure. When a large amount of sample is available, powder is loosely enclosed in a 1 mm capillary. The diffraction peaks for a well crystallized sample will be less than 0.02° wide on a good beam line, at least seven times sharper

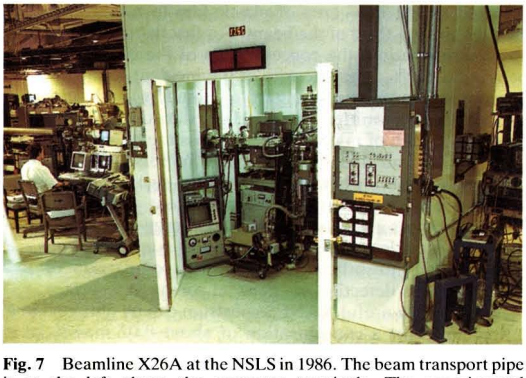

Fig. 7 Beamline X26A at the NSLS in 1986. The beam transport pipe is at the left above the computer terminals. The experimental apparatus is inside a safety hutch, whose interlocked door is open. Photograph CN9.649.86 from the BNL Archive.

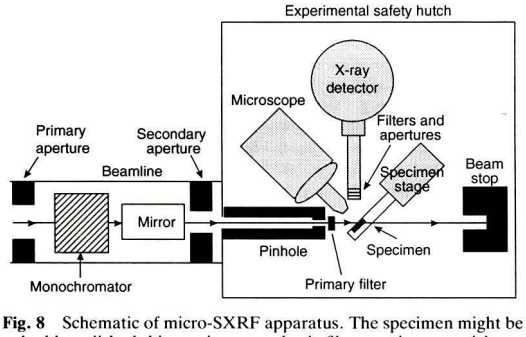

Fig. 8 Schematic of micro-SXRF apparatus. The specimen might be a doubly polished thin section or a plastic film carrying a particle.

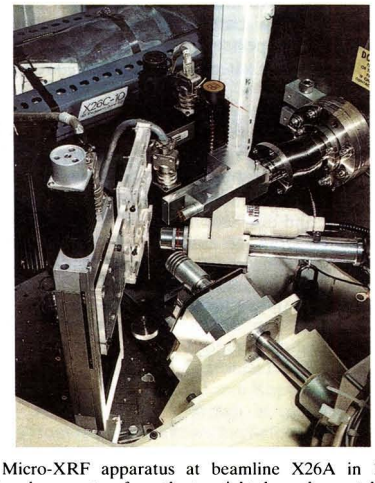

Fig. 9 Micro-XRF apparatus at beamline X26A in 1993. The synchrotron beam enters from the top right through a metal bellows to allow positional adjustment. The specimen is mounted in the assembly of plastic plates driven by digital motors. The microscope is at centre right. At bottom right is the entrance pipe of a solid-state detector, which is at 90° in the horizontal plane to essentially eliminate background scattering. A filter projects from the entrance tube. Just visible at bottom right is the upper surface of a crystal spectrometer which is perforce at 13° below the horizontal plane.

than for most in-house instruments. The wavelength can be chosen to match sample properties, and indeed anomalous scattering can be used to search for the structural location of particular elements. Precision can be sacrificed, and a line detector used, to allow observation of fast phase transitions and chemical changes. In particular, peak width can be used to discriminate between different phases in a mechanical mixture. Thus for a mud rock, the clays give their usual broad low peaks while well-crystalline phases, including feldspars, give sharp spikes that can be characterized even for a concentration of less than 1%. The X-ray beam can be 'skidded off' a sample to pick off a surface film, while missing the bulk phase. Industrial chemists can follow catalytic reactions with powder diffraction.[43]

Single-crystal X-ray diffraction is potentially an important analytical tool. There are enough photons for diffraction analysis of a single crystal only a few micrometres across. Currently, it is easier to work with crystals of greater than 20 μm, but progress will be made towards 1 μm ones. Mounting of such tiny crystals is a severe challenge to be resolved, but embedding them in a thin stretched sheet of polymer appears promising. Commercial diffractometers must be improved at least ten-fold in geometrical alignment of component parts. It is very important to reduce the background from scattered radiation.

If the crystal has a well-ordered structure, Laue diffraction can be used.[13,44] Overlap of orders at the same angular position can be reduced by using a restricted band of wavelengths instead of a completely white beam. The diffraction data for a 'good' crystal of about 0.1 mm across can be collected in less than 1 min using the white-light Laue technique and an area detector. Software is just becoming adequate to turn the diffraction data rapidly and almost automatically into a list of atomic coordinates.

Monochromatic radiation and Bragg diffraction is necessary for poorly crystallized samples, and gives somewhat higher precision than Laue diffraction for well-ordered samples. Choice of wavelength allows the use of anomalous scattering for determination of structural location of chosen elements. Even more sophisticated is the determination of valence state for an element in a particular crystallographic site by combined diffraction/spectroscopy.[13,45]

Experimental station for X-ray absorption spectroscopy

Since X-ray absorption spectroscopy (XAS) is not fully familiar to all analysts, it is important to describe the technique[11,46] and equipment in somewhat more detail than for fluorescence and diffraction.

For an isolated atom, an absorption edge rises abruptly at the photon energy required for ejection of a specific bound electron, and then falls monotonically as the photon energy increases [Fig. 10(*a*)]. For an isolated diatomic molecule, the outgoing photoelectron carries a wave function which interacts with those of the electrons in the adjacent atom. The resulting interference function perturbs the absorption edge to give a fine structure [Fig. 10(*b*)]. This interference function becomes more complex for atoms in the crystalline, amorphous and liquid states. As the energy of the incident photon increases, the outgoing photoelectron gains kinetic energy and interacts less strongly with the bound electrons of the parent atom and more strongly with the electrons of the neighbouring atoms. The low-energy region, denoted XANES (X-ray absorption near-edge structure), typically defined as within 40 eV of the classical edge, gives information mainly on the electronic (valence) state and how it depends on the local bonding (*e.g.*, tetrahedral *versus* octahedral coordination). The high-energy region, denoted EXAFS (extended X-ray absorption fine structure), contains ripples whose Fourier inversion gives a radial distribution function of the electrons in neighbouring atoms. In a solid, the wave functions of the bound electrons are spatially anisotropic, and the chemical bonding can be mapped out in three dimensions by rotating a single crystal in the polarized synchrotron beam (*e.g.*, for Cu coordinated to four O atoms in a square). Most experiments use a fine powder which produces an isotropic mechanical average.

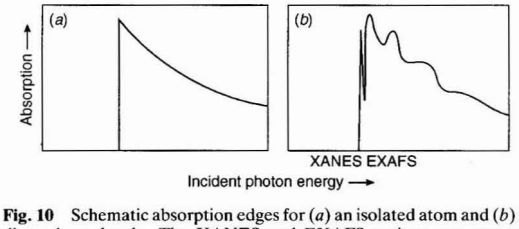

Fig. 10 Schematic absorption edges for (*a*) an isolated atom and (*b*) a diatomic molecule. The XANES and EXAFS regions are, respectively, at the low-energy and high-energy sides of the formal absorption edge.

It is essential to measure with high precision and accuracy the change of absorption as a near-monochromatic beam sweeps through the absorption edge of the element of interest. Because the energy changes in the XANES region from one type of solid to another are only a few electron volts, the monochromator must give a narrow energy band.

If there is a large amount of powdered sample, it is usually smeared on a 1 mm^2 area of plastic film to a thickness that absorbs about a third of the beam. For fast data collection and easy interpretation, the concentration of the element should be around 1–2%. The intensity of the incident X-ray beam is monitored (*e.g.*, by scattering from a thin film) and ratioed to that of the transmitted beam. High statistical precision is needed for each of many energies across the edge.

For minor and trace elements, it is impossible to achieve sufficient precision when the transmission signal is dominated by other elements. Hence, the fluorescent photons or the Auger electrons are detected with an energy-sensitive detector which excludes unwanted photons. As Auger electrons are more strongly absorbed than photons, comparison of the signals permits detection of chemical zoning at a surface.

In practice, a useful XANES spectrum can be obtained in a few minutes for a concentration of about 0.02 mass% of a transition element like Fe at a bending-magnet source. An EXAFS spectrum is much more difficult to acquire because a greater energy range is needed, and a higher statistical precision plus excellent accuracy of background subtraction is needed for Fourier inversion.

Another method is to pass a divergent beam through the sample and record the signal on a linear detector. The resultant spectrum is not as precise as the point-by-point scanning of the usual technique, but is good enough to follow chemical changes on a ms time scale. Such a time scale is very useful for following valence and coordination changes in gels and dynamic biological systems.

For further details of synchrotron analytical techniques, see the review articles[10,11,23,36,40,45–47] and study guides.[4,24]

Detectors

Detectors are a key to success in synchrotron experiments and major development programs are underway. The standard detectors used in electron microprobes and X-ray diffractometers retain their value for synchrotron experiments yielding a low signal. For intense signals, a solid-state detector

is severely limited by pulse overlap[47] and associated energy distortion caused by its long dead-time (about 50 μs). Thirteen-element Si(Li)/Ge detectors are coming into use, and monolithic 100-element detectors are being developed. A consequent gain of three in statistically-limited sensitivity should increase to 10. For diffraction experiments, photographic film and proportional counters are being replaced by image plates (fast exposure, but 5 min read-out in a separate apparatus) while charge coupled device (CCD) detectors [48] (fast exposure and read-out) are being seen as the detectors of the future. Area detectors with about 1024 × 1024 pixels are becoming available, and a 4 × 4 grid array should allow imaging with about 4096 × 4096 resolution. On-line computer processing is advancing rapidly, and pixels for a diffraction peak can be isolated, summed and outputted very rapidly. Although the cost of these new detectors is very high ($100 000–$1 000 000), they are financially advantageous with respect to the total cost per effective photon.

Design of an experimental facility at the APS

Fig. 11 shows the current design of the GeoSoilEnviroCARS sector at the APS, which will be adjacent to the BioCARS sector for structural biology. This design is undergoing final adjustments before submission to the Preliminary Design Review Committee in February 1995. (See the figure legend next for an overview.) Microanalysis will be carried out on both the insertion device and bending magnet beamlines. Only experience will tell what will be the optimum mix of experiments. Digital tracking of experimental stations and sample positions in holders will permit rapid movement of experimental stations into the X-ray beams, and movement of a sample from one station to another. Obviously, there are a myriad of details for the construction phase, but the actual operation should be made readily accessible to the users by advanced computer graphics both on and off site.

Use of a Synchrotron Source

When using the complex equipment at a synchrotron facility a number of factors need to be borne in mind.

Firstly, even at the best facility the staff cannot spend much time teaching you how to run an experiment. Secondly, a considerable amount of time may need to be spent on administration and safety precautions.

It may be best to work with a synchrotron operator on a project to be published jointly. Even when you know all the physics and mineralogy, etc., there are details best known to the day-to-day operators. It is best to give the synchrotron operator a test sample that can be slotted in one day when an unexpected vacancy comes up to establish whether it is worth starting a big project.

It is best to characterize the sample as much as possible prior to analysis with the synchrotron source. For example, for trace-element analyses of minerals in a rock, a doubly polished thin section should be characterized with an electron microprobe. The major and minor elements can be used as internal standards for the synchrotron analysis. There may be erratic zoning patterns that require very careful selection of spots for analysis. The section should have uniform thickness, or the thickness profile should be known accurately. Samples should be kept scrupulously clean. The time needed for each analysis should be calculated and a plan developed in which sufficient data can be obtained in about half the allotted synchrotron time. This should allow tolerance for mistakes and unexpected lucky discoveries. Allowance should be made for exhaustion. Most successful synchrotron work is carried out by a small team sharing the load over a 24 h working day. A check-list should be prepared to guard against mistakes.

With use of electronic mail, synchrotron data of immense density can be transmitted almost instantly to a user's home laboratory. This brings the possibility of remote working from the user's laboratory.

Analytical Procedures and Interpretation

X-ray fluorescence (XRF) analysis is a standard technique for analysis of rocks and minerals.[2,19] When an X-ray photon drives out an electron from a bound state, the excited atom regains equilibrium by emission of either an X-ray photon or an Auger electron. Measurement of the energy of the emitted X-ray photon or electron identifies the type of atom (except for accidental overlap within the experimental resolution). Determination of the flux of a particular type of photon with respect to the total flux from all X-ray photons from all atoms in a sample provides a measure of the atomic concentration in the bulk sample. There are many details but the technique is fundamentally straightforward and potentially accurate to better than 1% of the amount present when suitable standards are used. Classical XRF analysis is technically easiest for those elements whose fluorescent photons have energies from 1 to 20 keV. Complexity increases from the K to the L and M series.

Trace element analysis involves a balance between sample size, atomic concentration, and duration of data collection. Trace elements cannot be measured on a micrometre-sized sample with a conventional hot-cathode source, and a higher brilliance of synchrotron source is needed.[1,37-42,49-54] Present bending magnet sources permit simple XRF analysis with a solid-state detector for a 10 μm beam at a 1 ppm detection level for most elements in many samples from, *e.g.*, Mn to Ba in 5 min, and below 10 ppm for 'difficult' elements and samples. Thus As and Se in a sulfide,[55] Rb in a feldspar,[56] and Br in a volcanic dust particle[57] are easily accessible to a synchrotron source, but very rarely to an electron microprobe.

An undulator source tuned just above the edge of a particular element will permit analysis of most of the above elements down to 0.01–0.1 ppm.[50] The spot size can be reduced to 2 μm for minor elements using second-generation synchrotron sources, but will decrease to this spatial resolution for trace elements using the third-generation sources.

For this range of elements in the middle of the Periodic Table, the technical problems are generally trivial for concentrations of >10 ppm. Light elements are difficult to analyse because of uncertainty in the absorption of the outgoing photons and in the excitation functions. Heavy elements are becoming easier to analyse as the higher kinetic energy of synchrotron sources allows data collection in the K spectrum. Surface analysis has great potential. Reflection at a few milliradians from a flat surface allows analysis of surface species. The experiments require a high level of photons, and will become more feasible with the third-generation sources.

Some illustrative spectra are now given in order of increasing sophistication. Fig. 12, one of the earliest test spectra, is for NBS glass, 1 ppm nominal, Si(Li) energy-dispersive detector, white light from a NSLS bending magnet, 0.4 mm Al first absorber and 0.1 mm Kapton second absorber. The very low background, which is partly due to elastic scattering from the glass, allows the detection of Cu and Pb at the ppm level. Fig. 13 is a spectrum for a marcasite (FeS_2) impurity in coal from the Littlewood Quarry Borehole, Nottinghamshire.[55] The heavier matrix in comparison with the NBS glass increases the background scattering, and reduces the sensitivity. Nevertheless, Se at 55 ppm and Mo at 11 ppm are easily detectable. Fig. 14 shows how REEs can be detected in the K spectrum for perovskite ($CaTiO_3$) when the signals from the light elements are reduced by absorption with a brass foil. Fig. 15 illustrates how a wavelength-dispersive system

ห้องสมุดกลาง เพื่อบริการ

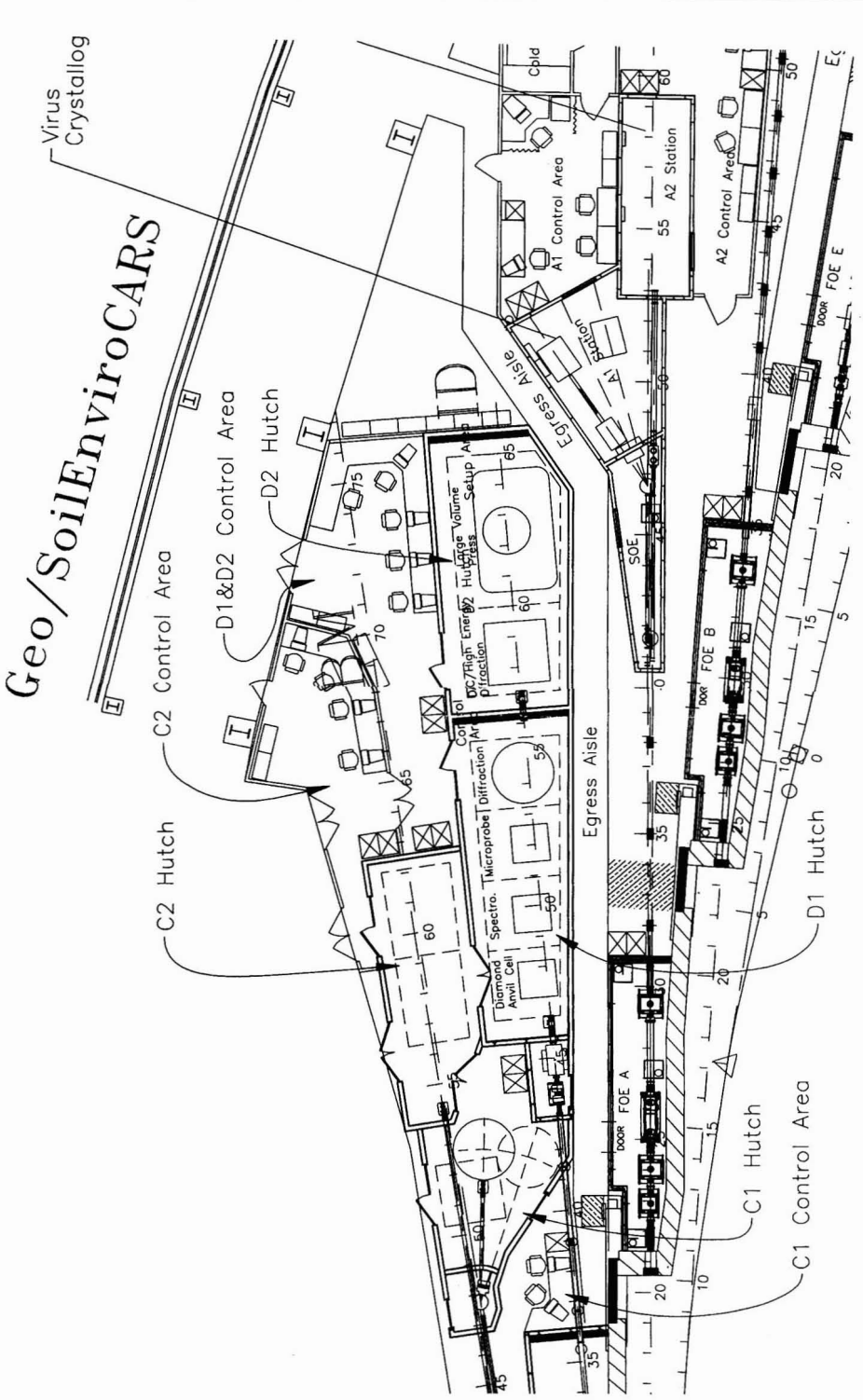

Fig. 11 Schematic for the GeoSoilEnviroCARS Sector at the Advanced Radiation Source plus part of the BioCARS Sector. Numbers and tick marks are in metres from the positron ring. The coarse diagonal shading shows the notched safety wall around the ring. Each sector contains a bending magnet and a straight section. The straight section is 5 m long and can contain two insertion devices. In the GSE Sector, the ID beamline supplies X-rays to two hutches D1 and D2. Each of these safety enclosures contains more than one experimental apparatus which can be inserted into the beam or withdrawn. For microanalysis, the D1 hutch contains apparatus for XAS, XRF (denoted microprobe), and diffraction. The bending-magnet beamline also contains two safety hutches. Two X-ray beams enter the C2 hutch, one from the left and one from the right of the fan, as in Fig. 3. The C1 hutch uses a deflected beam, which might be obtained from a Laue–Bragg monochromator. This optical device deflects part of the beam and transmits the rest. The front ends of the Jessie sector are essentially the same as those shown for the Bio-sector. Details of this design have changed since the first draft of this paper was prepared in October 1994.

allows detection of Co and Cu in the Fe,Ni phases of iron meteorites, in contrast to an EDS system.[58] The much better energy resolution permits sufficient discrimination from the dominant beta peaks of Fe and Ni. Peaks for gallium and germanium are detected by both systems, but the peak : background ratio is more favourable for the WDS system. The additional resolution comes at the cost of a hundred-fold signal reduction per incident photon. Since the EDS system is photon limited by the long dead-time, the loss of intensity in a WDS system is not important for a strong synchrotron source.

X-ray diffraction (XRD) is not currently regarded as a tool for chemical analysts. Of course, X-ray powder diffraction is a routine tool for phase identification, and a measurement of a cell dimension may imply a chemical composition in certain simple systems. But what are the implications of a rapid crystal structure determination using synchrotron diffraction? Bragg diffraction can be carried out on a 10 μm crystal using data collected over a few minutes with an area detector. For the emerging technique of synchrotron Laue diffraction, less than 30 s of data collection was required for a test solution of an unknown inorganic crystal structure by standard phase-seeking methods (J. J. Pluth *et al.*, to be published). One could consider sprinkling a powder or a heavy-mineral separate on a film, and running from grain to grain as fast as the computers could process the data.

X-ray absorption spectroscopy (XAS) is rapidly becoming a prime tool for microanalysis. Fig. 16 shows the pre-edge peak in the XANES region for hexavalent Cr.[59] This particular spectrum was collected on beamline NSLS-X26A in 3 hours with a 20 μm monochromatic beam for a chromate sample doped with 2% Cr^{6+}. A multi-element detector will allow reduction of the counting time by the number of detector elements (currently 13). Increase of the spot size to 0.2 mm allows detection of Cr^{6+} in a Cr^{3+}-rich sample down to 5 ppm.

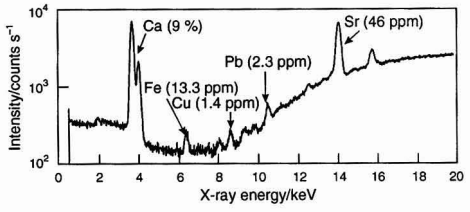

Fig. 12 XRF spectrum for NBS glass, 1 ppm nominal. See text for conditions.

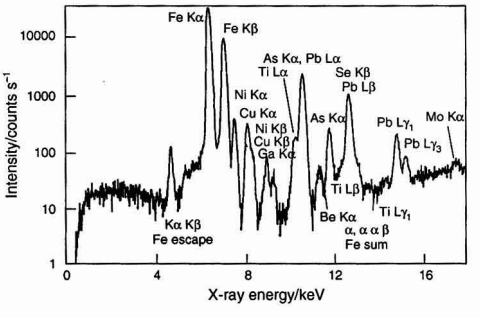

Fig. 13 XRF spectrum for marcasite from Littlewood Quarry Borehole, Nottinghamshire. This spectrum clearly shows the escape peak for the Fe Kα dominant peak. The Fe sum peaks are just visible in the background. Concentration levels are: Ni, 2600 ppm; Cu 1300; Se 55; As 1640; Tl 375; Pb 1600; Mo 11. Note the well-known overlap of As and Pb spectra.

With a third-generation source, this trade-off between beam diameter, counting time and detection level will be much improved.

Fig. 17 shows how spectra for synthetic olivines doped with Cr^{2+} and Cr^{3+} were used as references for determination of the valence state of Cr in minerals for lunar basalt 15555. Lunar olivine (not shown) contains divalent Cr, while lunar pyroxene has a mixture of di- and trivalent Cr.[60]

Fig. 18 shows XANES spectra of $MnSO_4$ and birnessite ($Na_4Mn_{14}O_{27}{\cdot}9\ H_2O$) used as references for study of Mn in soils.[61] The quadrivalent Mn in birnessite is easily distinguishable from the divalent Mn in the sulfate.

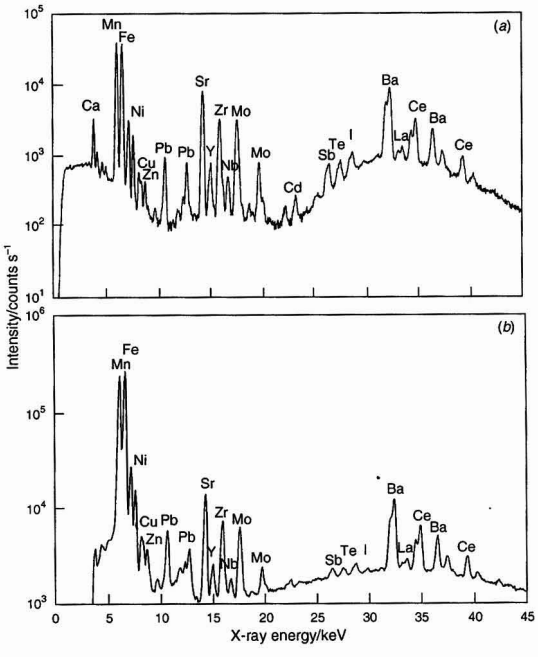

Fig. 14 XRF spectrum for perovskite sample MO-3. To reduce the signal from the dominant light elements Ca and Ti, a 0.25 mm brass foil was used. This allowed detection of REEs in the K spectrum using a Si(Li) detector and bending magnet radiation at the NSLS-X26A beamline. Aperture 10 × 40 μm; data collected for 600 s. (*a*) Perovskite sample MO-3 and (*b*) USGS standard manganese crust.

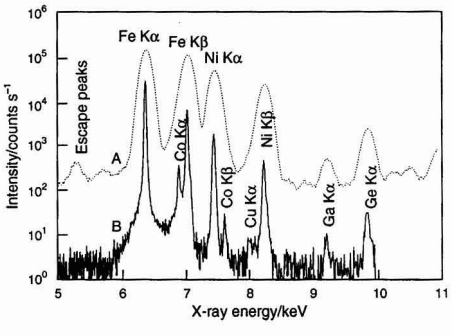

Fig. 15 Comparison of energy- and wavelength-dispersive detectors for iron meteorites. A, Si(Li) detector, Odessa and; B, WDS detector, Canyon Diablo.

Fig. 19 shows XAS data for staurolite.[62] The Ti spectra for staurolite and three reference standards demonstrate that the Ti is tetravalent and is octahedrally coordinated to oxygen. The Fe, Mn and Zn spectra have similar profiles indicating that all three elements are divalent and in tetrahedral coordination with oxygen. Small differences in peak positions correspond to changes in bond length. Subtle perturbations for Zn may indicate that some Zn is in octahedral coordination.

Comparison With Other Microanalytical Techniques

Synchrotron X-ray microanalysis allows combination of fluorescence with diffraction and absorption spectroscopy to obtain not only the concentration of an element but also its electronic state and topochemistry. The physics of X-ray interaction with matter is reasonably straightforward. X-rays deposit little energy in a sample, and most samples can be studied in air. The inherent polarization of a synchrotron beam plus tuning through an absorption edge allows better detection than for conventional XRF. The higher the atomic number, and the more refractory an element, the greater is the advantage of synchrotron-based techniques over competitors. Multi-component particles can be 'flooded' with the X-ray beam to get a bulk analysis. Tomography[63–68] can give a three-dimensional image. A synchrotron study can be followed by destructive techniques. Good specimen preparation is mandatory, and doubly polished thin sections with near-parallel surfaces are desirable. If a beam of hard X-rays penetrates right through a sample, the depth resolution is governed by the sample itself.

Electron microprobe analysis (EMPA) retains its advantage for analysis of major and minor elements in thin sections of stable minerals to the 2–10 μm level of spatial resolution, but the Bremsstrahlung limits the detection of trace elements. Moreover, the sensitivity of EMPA is reduced seriously for $Z > 30$. Glasses, liquids, and minerals containing volatile elements and molecules are difficult or impossible to analyse by EMPA, though cooling the sample is reducing the thermal and electronic damage (Steele, to be published).

Secondary ion mass spectroscopy (SIMS) is valuable for determination of isotopic ratios for certain elements; depth profiling with nanometer resolution downwards and about 10 μm sideways; and very high sensitivity for easily ionized elements. Disadvantages are problems in modelling the sputtering process; sensitivity to variation of electrical conductivity across grain boundaries; and migration of impurities, especially ones containing H, into the sputtered area. For certain light elements, including Li and Na, the sensitivity is very high. The technique is insensitive to refractory elements with high work function: here, SXRF has a considerable technical advantage.

Particle-based techniques, commonly using a proton or a deuteron, have unique advantages. Nuclear reaction analysis (NRA) is excellent for certain light elements. Particle-induced gamma-ray emission (PIGE) is very good for F above the 10 ppm level: SIMS is more sensitive, but more difficult to quantify. Particle-excited X-ray emission (PIXE) is easy to quantify in refractory samples thick enough to stop the beam (> 20 μm), but the sensitivity is reduced severely for $Z > 30$. The heating from the heavy particles severely limits the combination of small spot and trace concentration. The billiard-ball technique of Rutherford back scattering (RBA) is useful for depth profiling at the sub-micrometre level, but has severe limitations on minimum element concentration.

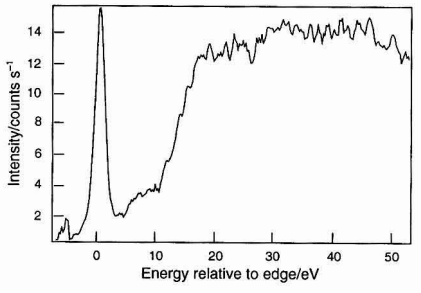

Fig. 16 XANES spectrum for Cr^{6+}. The chromate sample was doped with 2% Cr^{6+}. Conditions: 3 h scan with 13-element detector and 20 μm beam at NSLS-X26A beamline.

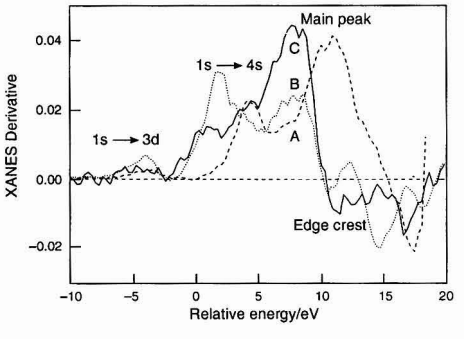

Fig. 17 XANES spectra for divalent and trivalent Cr in synthetic olivines bracket the XANES spectrum for pyroxene from lunar basalt 15555. A, Cr^{3+} (Ito); B, Cr^{2+} (GRR-1690); and C, lunar pyroxene.

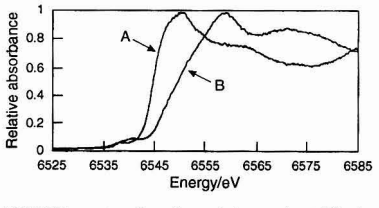

Fig. 18 XANES spectra for di- and tetravalent Mn in synthetic sulfate and the mineral birnessite. A, $MnSO_4$ (Mn^{2+} standard); and B, birnessite (Mn^{4+} standard).

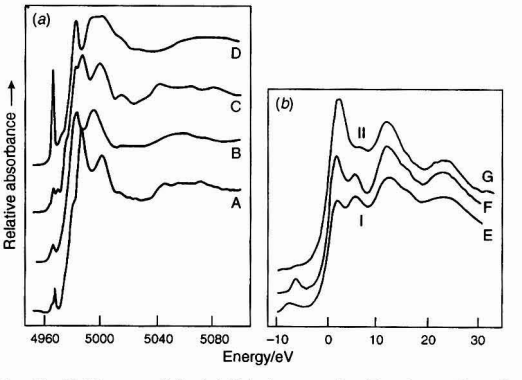

Fig. 19 XAS spectra[62] for (*a*) Ti in A, staurolite, B, sphene, C, rutile and D, Ba_2TiO_4 reference standards, and (*b*) E, Fe; F, Mn; and G, Zn in staurolite. Note the difference in peaks I and II in (*b*).

Synchrotron techniques have a huge advantage for unstable samples, and this increases for the heavier elements.

Electron microscopy has special features, including diffraction and imaging towards the atomic level. Analytical electron microscopy has excellent spatial resolution, but is limited to major element ratios: however, progress is being made towards identification of small atomic clusters. Scanning electron microscopy is used extensively for determination of shape, but quantitation of the X-ray signal from a rough surface is difficult. Heating and electrical damage is a problem, and synchrotron soft X-ray microscopy should carve a niche to the sub-micrometre level.[69]

Illustrative Applications and Future Advances

It is impossible to give detailed literature citations and credits to all the hundred or more scientists who have pioneered new applications. This section should be taken as an impressionistic overview. Furthermore, there is a strong tendency to refer to studies at NSLS about which I have personal knowledge, and for which I know enough about the provenance to select the important aspects in a concise manner. XRF studies at the SRS, Daresbury,[70,71] and the Photon Factory[72] complement those at the NSLS.

Coal

Bulk analyses of trace elements have demonstrated geographic trends across coal basins, but detailed microanalysis of the individual components has not been carried out. Systematic study of petrographically identified plant remains might prove useful to paleobotanists. The mineral components of coal are a useful indicator of the chemical deposition from fluids that have entered the coal bed and its adjacent sedimentary rocks, including shales. Nickel, Cu, Zn, Ga, Ge, As , Se, Rb, Sr, Mo, Tl and Pb in pyrite and marcasite[55] have environmental significance. Systematic sampling across coal seams (especially of U-shaped spatial profiles indicative of incomplete diffusion-driven chemical exchange) and basins, when coupled with isotopic analyses, should provide useful characterization of the chemical nature and timing of migrating fluids. Analyses of pyrite, marcasite, clays, calcite[73] and other minerals are much easier than for the organic components, simply because of higher elemental concentrations.

Cosmic dust

The Earth is bombarded by small particles of bulk compositions similar to, but more rich in volatile compounds than, those of carbonaceous chondrites. The divergent concentrations of certain 'volatile' elements in the chondritic particles may indicate the existence of more primitive classes of chondritic material closer to the supposed primary compositions of the various types of stars. Particles are collected on special 'shock-absorbing' panels carried by high-flying planes and satellites, and fragments surviving after atmospheric heating are collected most efficiently from lake beds fed by melting Greenland ice and moving Antarctic glaciers. Interpretation is complicated by the atmospheric heating and perhaps by scavenging of stratospheric aerosols carrying residues from volcanic eruptions. Pioneering studies of bulk particles[57,74–78] will be extended to tomographic analysis of individual minerals.[68]

Element partitioning and diffusion couples

Element partitioning among co-existing phases is important for establishing crystal–liquid differentiation,[79] metamorphic re-equilibration, ore deposition, *etc*. The SXRF microprobe is particularly useful for trace elements that are inaccessible to the other microanalytical methods. Furthermore, micro-XAS yields information on the electronic state and stereochemical bonding. Pioneering experiments on basalt–rhyolite diffusion couples[80,81] and several zoned minerals,[82–84] including sector-zoned ones, have demonstrated the importance of synchrotron techniques for measuring trace elements (including Kr in feldspar and glasses[85]), and these will be pushed down to the sub-micrometre level.

Environmental

The migration of an element in nuclear waste depends strongly on how it is chemically bonded. Coupled XRF and XAS analyses are pin-pointing the particular host minerals in a complex matrix, and identification of the 'hot-spots' should help in thinking about remediation. The electronic state of uranium and other high-Z elements in lake sediments may change during the year in response to chemical events triggered by overturning of the water layers. The bonding of an element in a glass, and the resistance to leaching, depend on the electronic state. These, and other, phenomena are being quantified by synchrotron microprobe studies of carefully chosen samples.

Chromium and technetium are important in low-level waste disposal. The oxidized species diffuse faster than the reduced ones. XANES measures the ratio of hexavalent to total chromium with an accuracy of 5% at a minimum detection level of 10 ppm Cr^{6+} for a 150 μm X-ray beam on the NSLS-X26A microprobe.[59] Sediments around uranium processing facilities generally contain hexavalent U, but some tetravalent U is present.[86,87] The hexavalent U is associated mainly with Fe and Mn, perhaps on the surface of oxyhydroxide minerals. The tetravalent U, and some of the hexavalent U, is correlated with Cu, perhaps indicating the presence of a discrete Cu, U-containing phase.

A second area of study involves aerosols and fly ash in the atmosphere. Fly ash from power stations is easy to analyse.[88] The chemical composition of atmospheric aerosols is important for human health and the vigour of plants and trees. The days of thick fogs in the UK and the USA, but not in all countries, have gone as the burning of soft coal in open fires has been replaced by natural gas, and as some coal power stations have been retro-fitted with scrubbers. Smog from photochemical oxidation of hydrocarbons from automobiles and other sources remains a major problem in the industrialized world. The residue from volcanic eruptions descends from the stratosphere into the troposphere to increase the haze from industrial and other sources. As frontal systems move around the world the chemistry of the aerosols changes. Atmospheric chemists need to monitor the changes in the aerosols, and synchrotron-XRF provides a useful tool. At the simplest level, a filter loaded with captured aerosol can be chemically analysed with a broad beam to the ppm level.[89] At a more advanced level, individual droplets could be characterized. In addition to XRF analysis, one can envisage the XAS study of the electronic state and chemical bonding.

A third area involves the leaching from waste heaps from coal and metal mines, and the seepage of fluids from municipal waste heaps. Widely apparent are the yellow–brown–black deposits in certain streams and ponds. Synchrotron-XAS, -XRF and possible -XRD should yield fascinating scientific data, as they have for the results on geothermal brine sludge.[90]

Inclusions in minerals

Analysis of trapped melts and vapours in minerals provides major analytical challenges. Ingenious methods include mechanical release into a mass spectrometer, and electron

microprobe analysis of a frozen sample. Synchrotron-XRF[91] and XAS[92] provide interesting possibilities that are particularly useful for medium- to high-Z elements accessible to hard X-rays. Ideally the host mineral has a simple composition (*e.g.*, quartz) with a uniform content of light elements. A polished thin section or cleavage fragment should be prepared with some inclusions intact and just under the surface.

Pioneering experiments have been made on Ca-, Mn- and Zn-chlorides enclosed by quartz;[91] melt inclusions with Cu-rich spots in late-stage quartz phenocrysts from Pantelleria rhyolite;[93] hypersaline fluids containing Fe, S, Pb, P, Li, Sn, Cu, Be, Sr and Be in topaz of a Sn–W–Cu–Pb–Zn-mineralized granite;[94] and brine inclusions from rocks dredged at mid-oceanic ridges;[95] and metals in porphyry copper deposits.[96]

Concentration of Rb, but not Sr, in the twin boundaries of albite was demonstrated by anomalous X-ray scattering of X-ray streaks using a hot-cathode source.[97] There is an unlimited field of analytical applications to the internal surfaces of minerals. With the intense third-generation synchrotron sources, it should be possible to analyse arrays of dislocations for minor and perhaps trace elements.

Earth's mantle

Some rock and mineral fragments in kimberlites and alkali-basalts contain inclusions that have been preserved from alteration during transport. Particularly interesting are inclusions in diamonds: differences in the $Cr^{2+}:Cr^{3+}$ ratio, measured by XANES, of several olivine inclusions indicate variations of the redox state.[98,99] The next step is to couple the SXAS measurements with isotopic age determinations to test whether there are temporal and spatial variations of redox state in the Earth's mantle. SXRF data for many sulfide inclusions carefully selected from peridotite and other xenoliths indicate fascinating variations in ore-forming trace elements. However, the presence of numerous micrometre-sized spots containing Rb and other elements indicative of infiltration by kimberlitic fluid indicates the need for high-resolution tomography with third-generation sources.

Meteorites and the moon

SXRF and SXAS are very useful for analysis of meteorites and lunar rocks and minerals because of the complex microtextures and rarity of samples. Exemplary studies are: (*i*) nickel and copper correlation with associated kamacite and taenite lamellae in iron meteorites which indicate migration of Cu to exsolving metal during sub-solidus equilibration;[58] (*ii*) evidence of complex source regions in the Moon from trace elements in coloured spheres of over-all Mg-rich basaltic composition at the lunar surface.[100] These have been ascribed to volcanic fire fountains driven by deep-seated eruptions. Perhaps the currently fashionable hypothesis that the Moon is essentially the product of a single glancing impact that tore off part of the Earth may need extension to cover multiple reservoirs related to events that include capture of planetesimals and proto-moons; and (*iii*) evidence for a wide range of redox conditions in meteorites and the Moon, because each transition metal of the first series has its own characteristic redox property, an oxygen fugacity grid for nebular and planetary geochemistry can be explored using synchrotron-XANES, *e.g.*, Cr in olivine from an Apollo 15 basalt is entirely divalent;[60] trace elements in plagioclase from Apollo 16 breccias;[101] abundances of Ni, Cu, Zn and Ga in magmatically-zoned pyroxene from the Zagami shergottite basalt, believed to have crystallized on Mars; analysis of Ni, Cu, Zn, Ga, Ge and Se in the rims of chondrules in an unequilibrated CO_3 carbonaceous chondrite.[102] The rims are compositionally homogeneous, and their richness in volatile elements implies a source distinct from that of the chondrule cores.

Ore mineralogy

The SXRF microprobe is particularly valuable for the study of sulfide ore minerals because of its good sensitivity for medium- to high-Z elements, including Fe–Se, Mo–Te and Re–Bi. Most sulfide minerals in igneous and metamorphic rocks occur as tiny grains in the interstices of the coarser silicate grains, and are often aggregated or intergrown. Thus the high-temperature M-type Fe–Ni–Cu solid solution is typically represented at low temperature by a one micrometre intergrowth of pyrrhotite and pentlandite rimmed by atolls of chalcopyrite. The mineralogical literature contains many reports of tiny grains rich in noble metals. Synchrotron-XRF, -XRD and -XAS should open up a new world of micromineralogy.

Metasomatic ore deposits commonly have very complex textures and intergrowths ranging down to the submicrometre level. SXRF analysis of minor and trace elements in associated gangue minerals such as calcite is generally easier than for the sulfide minerals because of the lightness of the major elements. Some examples are: analysis of pyrite and marcasite in coal; analysis of fluid inclusions related to porphyry copper deposits; location of gold in Carlin-type ore deposits;[103] zoned carbonate gangue in Mississippi Valley-type deposits;[84] ore metals in titanate minerals from the Tuolomne Intrusive Suite, California;[104] rare earth elements in the Bayan Obo deposits, China; and fluid inclusions in Questa molybdenum deposit.[105] Also relevant are analyses of hydrothermal flume particles.[106]

Soil mineralogy and agriculture

A soil is a complex assemblage of inorganic and organic constituents whose properties depend on the source rocks, climate and meteorology, and the time of year. Soils used for agriculture undergo modification depending on the type of crop and intensity of cultivation. Trace elements in soils are affected by microbial activity, and by external factors, including the chemistry of rain and aerosols. Some pioneering applications[21] are: take-all disease of wheat (rotting of root and foot) is caused by the fungus *Gaeumannomyces graminis* var. *triti.*, synchrotron-XANES[107] has shown that fungal activity is related to oxidation of divalent Mn to tetravalent Mn. Combined synchrotron-XRF and -XAS techniques should yield interesting chemical information on the Mn-rich nodules that occur in certain soils. Comparison with data for nodules in oceans and lakes should also be fascinating. Manganese is also involved in bacterial infection of rice; the Se content in soils has become of environmental concern. Prolonged flow of water into an evaporation basin without an outflow can cause build-up of elements like Se to toxic levels, as at the Kesterson Reservoir, California: synchrotron-XRF and XAS is providing fascinating data, including implications for bacterial reduction of Se in rotting plant roots.[108]

Mineralogical studies relevant to soil chemistry include: XAS of Se oxyanions on α-FeOOH;[109] polarized EXAFS of hematite clusters on Fe-diaspore;[110] distribution of Fe in micas by polarized EXAFS;[111] and EXAFS of coprecipitated and adsorbed arsenate on ferrihydrite.[112]

Speculations on mobilization of trace elements in soil minerals and adjacent trees and plants are testable by synchrotron techniques. The trace element chemistry of galls and other pernicious growths also appears to be another profitable target. Many bacteria and lichens have a specific affinity for trace elements, and determination of the microchemistry cannot fail to yield important scientific results with implications for human welfare.

Miscellaneous

Further useful studies are: XANES of Fe in pumpellyite minerals;[113] EXAFS of Fe-bearing tetrahedrites;[114,115] XRF

of REEs;[116] X-ray reflectivity of adsorbed water on the surface of calcite;[117] EXAFS of gold(III) in aqueous chloride solution;[118] EXAFS of sulfur in bitumen and asphaltene;[119] XAS of S in sphalerite, chalcopyrite and stannite;[120] XAS of Ti in amphiboles;[120] XAS of Cu in tetrahedrite minerals;[122] XANES of S in heavy petroleum.[123]

It has been my privilege to collaborate with physicists at the Department of Applied Science of Brookhaven National Laboratory (particularly K. Jones), geoscientists of GeoSync, soil and environmental scientists (particularly D. Schulze and P. Bertsch) belonging to SoilEnviroCARS, and biologists (particularly K. Moffat). Special thanks are given to A. Gaines and D. Weill (NSF-EAR-Instrumentation), W. Luth (DOE-Basic Energy Sciences-Geochemistry) and D. Bogard (NASA- Planetary Science) for their keen insight into the scientific basis for funding the instrumental development and accompanying pioneering research. S. Sutton, M. Rivers and S. Bajt are thanked for their assistance in operating the NSLS-X26A beamline, and for providing detailed information for this manuscript. S. Rice (Dean of Physical Sciences) and F. Stafford (Director, Special Projects) at the University of Chicago are thanked for their support. Personal thanks, are also due to N. Weber, J. Viccaro, W. Schildkamp and J. Talsma. Finally, the author thanks the hundreds of scientists, engineers and administrators at the synchrotron sources.

The GeoSoilEnviro organizing groups that make synchrotron facilities available around the world can be contacted through the author.

References

1 Smith, J. V., and Rivers, M. L., in *Microprobe Techniques in the Earth Sciences*, eds. Potts, P., Bowles, J. F. W., Reed, S. J. B., and Cave, M. R., Chapman and Hall, London, 1995, ch. 5.
2 *X-ray Fluorescence Analysis in the Geological Sciences: Advances in Methodology*, ed. Ahmedali, S. T., 1989, Geological Association Canada Short Course 7, Toronto, Canada, 297 pp.
3 Attwood, D., *Physics Today*, 1992, **8**, 24.
4 Bajt, S., *Workshop on X-ray Microfocusing Techniques and Applications*, NSLS, Upton, May 19, 1993.
5 Baruchel, J., Hodeau, J-L., Lehmann, M. S., Regnard, J-R. and Schlenker, C., *Neutron and Synchrotron Radiation for Condensed Matter Studies. Vol. 1 Theory, Instruments and Methods*, Springer, Berlin, 1993.
6 Bassett, W. A. and Brown, G. E., Jr., *Ann. Rev. Earth Planet. Sci.*, 1990, **18**, 387.
7 *Chemical Applications of Synchrotron Radiation: Workshop Report.*, eds. Beno, M., and Rice, S., Argonne National Laboratory/Advanced Photon Source/TM-4, 1990.
8 Brennan, S., Tompkins, W., Takaura, N., Pianetta, P., Laderman, S. S., Fischer-Colbrie, A., Kortright, J. B., Madden, M. C., and Wheery, D. C., *Nucl. Instrum. Methods Phys. Res., Sect. A*, 1994, **347**, 417.
9 *Handbook of Synchrotron Radiation*, eds. Brown, G., and Moncton, D. E., North Holland, Amsterdam, 1991, vol. 3.
10 Brown, G. E., Jr., *Rev. Mineral.*, 1990, **23**, 309.
11 Brown, G. E., Jr., and Parks, G. A., *Rev. Geophys.*, 1989, **27**, 519.
12 Cooke, P. M., *Anal. Chem.*, 1990, **62**, R423.
13 Coppens, P., *Synchrotron Radiation Crystallography*, Academic Press, London, 1992.
14 Finger, L. W., *Rev. Mineral.*, 1989, **20**, 309.
15 *Handbook of Synchrotron Radiation*, ed. Koch, E. E., North Holland, Amsterdam, 1983, vol. 1.
16 Kunz, C., *Synchrotron Radiation: Techniques and Applications*, Springer, Berlin, 1979.
17 Margaritondo, G., *Introduction to Synchrotron Radiation*, Oxford University Press, New York, 1988.
18 Markowicz, A. A., and Van Grieken, R. E., *Anal. Chem.*, 1988, **60**, R28.
19 Potts, P.J., *A Handbook of Silicate Rock Analysis*, Blackie, London, 1987.
20 Prewitt, C. T., Coppens, P., Phillips. J. C., and Finger, L. W., *Science (Washington, D. C., 1883–)*, 1987, **238**, 312.
21 *Synchrotron X-ray Sources and New Opportunities in the Soil and Environmental Sciences: Workshop Report.*, eds. Schulze, D. G., and Smith, J. V., 1990, Argonne National Laboratory/Advanced Photon Source/TM-7.
22 *Synchrotron X-ray Sources and New Opportunities in the Earth Sciences: Workshop Report.*, eds. Smith, J. V., and Manghnani, M. H., 1990, Argonne National Laboratory/Advanced Photon Source/TM-3.
23 Stöhr, J., *NEXAFS Spectroscopy*, Springer, Heidelberg, 1992.
24 Sutton, S. R., *Workshop on Applications of Synchrotron Radiation to Earth Materials*, SRS, Chicago, 1992.
25 Williams, K. L., *Introduction to X-ray Spectrometry: X-ray and Electron Microprobe Analysis*, Allen and Unwin, London, 1987.
26 *Synchrotron Radiation Research*, eds. Winick, H., and Doniach, S., Plenum Press, New York, 1980.
27 Thiel, D. J., Bilderback, D. H., and Lewis, A., *Rev. Sci. Instrum.*, 1993, **64**, 2872.
28 Hoffman, S. A., Thiel, D. J., and Bilderback, D. H., *Nucl. Instrum. Methods Phys. Res., Sect. A*, 1994, **347**, 384.
29 Rarback, H., Shu, D., Feng, S. C., Ade, H., Kirz, J., McNulty, I., Kern, D. P., Chang, T. H. P., Vladimirsky, Y., Iskander, N., Attwood, D., McQuaid, K., and Rothman, S., *Rev. Sci. Instrum.*, 1988, **59**, 52.
30 Kirz, J., Ade, H., Anderson, E., Buckley, C., Chapman, H., Howells, M., Jacobsen, C., Ko, C.-H., Lindaas, S., Sayre, D., Williams, S., Wirick, S., and Zhang, X., *Nucl. Instrum. Methods Phys. Res., Sect. B*, 1994, **87**, 92.
31 Howells, M. R., Kirz, J., and Sayre, D., *Sci. Am.*, 1991, **2**, 88.
32 Jach, T., and Bedzyk, M. J., *Acta Crystallogr., Sect. A Found. Crystallogr.*, 1993 **49**, 346.
33 Qian, Y., Sturchio, N. C., Chiarello, R. P., Lyman, P. F., Lee, T.-L., and Bedzyk, M. J., *Science (Washington, D.C., 1883–)*, 1994, **265**, 1555.
34 Streli, C., Wobrauschek, P., Ladisich, W., Rieder, R., Aiginger, H., Ryon, R. W., and Pianetta, R., *Nucl. Instrum. Methods Phys. Res., Sect. A*, 1994, **345,** 399.
35 Winick, H., *Nucl. Instrum. Methods Phys. Res., Sect. B*, 1994, **87,** 112.
36 Waychunas, G. A., and Brown, G. E., Jr., *Phys. Chem. Minerals*, 1990, **17**, 420.
37 Jones, K.W., *Handbook of X-Ray Spectrometry*, eds. Van Grieken, R. E., and Markowitz, A. A., Marcel Dekker, New York, 1992, pp. 411–452.
38 Rivers, M. L., Sutton, S. R., and Jones, K. W., *Synchrotron Radiation News*, 1991, **4(2)**, 23.
39 Rivers, M. L., Thorn, K. S., Sutton, S. R., and Jones, K. W., *Lunar Planet. Sci.*, 1992, **XXIV**, 1203.
40 Smith, J. V., *Inst. Phys. Conf. Ser.*, 1992, **130**, 605.
41 Sutton, S. R., Rivers, M. L., Bajt, S., and Jones, K. W., *Nucl. Instrum. Methods Phys. Res., Sect. B*, 1993, **75**, 553.
42 Sutton, S. R., Rivers, M. L., Bajt, S., Jones, K., and Smith, J. V., *Nucl. Instrum. Methods Phys. Res., Sect. A*, 1994, **347**, 412.
43 Puxley, D. C., Squire, G. D., and Bates, D. R., *J. Appl. Crystallogr.*, 1994, **27**, 585.
44 Moon, K. J., Allinson, N. M., and Helliwell, J. R., *Nucl. Instrum. Methods Phys. Res., Sect. A*, 1994, **348**, 631.
45 Stragier, H., Cross, J. O., Rehr, J. J., and Sorensen, L. B., *Phys. Rev. Lett.*, 1992, **69**, 3064.
46 Brown, G. E., Jr., Calas, G., Waychunas, G. A., and Petiau, J., *Rev. Mineral.*, 1988, **18**, 431.
47 Cousins, C. S. G., Gerward, L., Laundy, D., Meads, R. E., Staun Olsen, J., and Sheldon, B. J., *Nucl. Instrum. Methods Phys. Res., Sect. A*, 1993, **324**, 598.
48 Clarke, R., *Nucl. Instrum. Methods Phys. Res., Sect. A*, 1994, **347**, 529.
49 Giauque, R. D., Thompson, A.C., Underwood, J. H., Wu, Y., Jones, K. W., and Rivers, M. L., *Anal. Chem.*, 1988, **60**, 855.
50 Gordon, B. M., and Jones, K. W., *Nucl. Instrum. Methods Phys. Res., Sect. B.*, 1985, **10/11**, 293.
51 Jones, K. W., and Gordon, B. M., *Anal Chem.*, 1989, **61**, A341.

52 Sparks, C. J., Jr., in *Synchrotron Radiation Research*, eds. Winich, H., and Doniach, S., Plenum, New York, 1980, p. 459.
53 Sutton, S. R., Rivers, M. L., Smith, J. V., Brown, G. E., Jr., and Jones, K. W., *Eos*, 1988, **69**, 1666.
54 Chen, J. R., Chao, E. C. T., Minkin, J. A., Back, J. M., Jones, K. W., and Rivers, M. L., *Nucl. Instrum. Methods, Sect. B*, 1990, **49**, 533.
55 White, R. N., Smith, J. V., Spears, D. A., Rivers, M. L., and Sutton, S. R., *Fuel*, 1989, **68**, 1480.
56 Lu, F.-Q., Smith, J. V., Sutton, S. R., Rivers, M. L., and Davis, A. M., *Chem. Geol.*, 1989, **75**, 123.
57 Sutton, S. R., and Flynn, G. J., *Proceedings of the 20th Lunar and Planetary Science Conference*, Lunar and Planetary Institute, Houston, 1990, 357.
58 Sutton, S. R., Delaney, J., Smith, J. V., and Prinz, M., *Geochim. Cosmochim. Acta*, 1987, **51**, 2653.
59 Bajt, S., Clark, S. B., Sutton, S. R., Rivers, M. L., and Smith, J. V., *Anal. Chem.*, 1993, **65**, 1800.
60 Sutton, S. R., Jones, K. W., Gordon, B., Rivers, M. L., and Smith, J. V., *Geochim. Cosmochim. Acta* , 1993, **57**, 461.
61 Schulze, D. G., Sutton, S. R., and Bajt, S., *Soil Sci. Soc. Am. J.*, 1995, submitted for publication.
62 Henderson, C. M. B., Charnock, J. M., Smith, J. V., and Greaves, G. N., *Am. Mineral.*, 1993, **78**, 477.
63 Dilmanian, F. A., Garrett, R. F., Thomlinson, W. C., Berman, L. E., Chapman, L. D., Hastings, J. B., Luke, P. N., Overshizen, T., Siddons, D. P., Slatkin, D. N., Stojanoff, V., Thompson, A. C., Volkow, N. D., and Zeman, H. D., *Nucl. Instrum. Methods, Sect. B*, 1991, **56–57**, 1208.
64 Kinney, J. H., Hampt, D. L., Nichols, M. C., Breunig, T. M., Marshall, G. W., Jr., and Marshall, S. J., *Nucl. Instrum. Methods, Sect A.*, 1994, **347**, 480.
65 Lindquist, W. B., Kaufmann, A. E., Spanne, P., Jones, K. W., Smith, J. V., Rivers, M. L., and Sutton, S. R., *Eos*, 1992, **73**, 208.
66 Spanne, P., and Rivers, M. L., *Nucl. Instrum. Methods Phys. Res., Sect. B*, 1987, **24–25**, 1063.
67 Spanne, P., Jones, K. W., Lindquist, W. B., Coker, D. A., and Lee, S.-M., *Eos* , 1993, **74**, 626.
68 Sutton, S. R., Spanne, P., Rivers, M. L., and Jones, K. W., *Lunar Planet. Sci.*, 1992, **XXIII**, 1393.
69 Janssens, K. H., van Langevelde, F., Adams, F. C., Vis, R. D., Sutton, S. R., Rivers, M. L., Jones, K. W., and Bowen, D. K., *Adv. X-ray Anal.*, 1992, **35**, 1265.
70 van Langevelde, F., Tros, G. H. J., Bowen, D. K., and Vis, R. D., *Nucl. Instrum. Methods Phys. Res., Sect. B*, 1990, **49**, 544.
71 van Langevelde, F., and Vis, R. D., *Anal. Chem.*, 1991, **63**, 2253.
72 Saito, J., Nakamura, T., Yamaguchi, A., Saiki, K., and Takeda, H., *Mineralogical J.*, 1993, **16**, 258.
73 Kolker, A., and Chou, C.-L., *J. Geol.*, 1994, **102**, 111.
74 Chevallier, P., Jehanno, C., Maurette, M., Sutton, S. R., and Wang, J., *J. Geophys. Res.*, 1987, **92**, E649.
75 Flynn, G. J., and Sutton, S. R., *Proceedings of the 20th Lunar and Planetary Science Conference*, Lunar and Planetary Institute, Houston, 1990, 335.
76 Flynn, G. J., and Sutton, S. R., *Proceedings of the 21st Lunar and Planetary Science Conference*, Lunar and Planetary Institute, Houston, 1991, 549.
77 Flynn, G. J., and Sutton, S. R., *Proceedings of the 22nd Lunar and Planetary Science Conf.*, Lunar and Planetary Institute, Houston, 1992, 171.
78 Flynn, G. J., Sutton, S. R., and Bajt, S., *Lunar Planet. Sci.*, 1993, **XXIV**, 495.
79 Dalpe, C., Baker, D. R., and Sutton, S. R., *Eos*, 1992, **73**, 607.
80 Baker, D., *Geochim. Cosmochim. Acta*, 1989, **53**, 3015.
81 Baker, D. R., *Contrib. Mineral. Petrol.*, 1990, **104**, 407.
82 Northrup, P., and Reeder, R., *Am. Mineral.*, 1995, submitted for publication.
83 Staudt, W. J., Reeder, R. J., and Schoonen, M. A. A., *Geochim. Cosmochim. Acta*, 1994, **54**, 2087.
84 Kopp, O. C., Reeves, D. K., Rivers, M. L., and Smith, J. V., *Chem. Geol.*, 1990, **81**, 337.
85 Carroll, M. R., Sutton, S. R., Rivers, M. L., and Woolum, D. S., *Chem. Geol.*, 1993, **109**, 9.
86 Bertsch, P. M., Hunter, D. B., Sutton, S. R., Bajt, S., and Rivers, M. L., *Environ. Sci. Technol.*, 1995, in the press.
87 Chisholm-Brause, C., Conradsen, S. D., Buscher, C. T., Eller, P. G., and Morris, D. E., *Geochim. Cosmochim. Acta*, 1994, **58**, 3625.
88 Tuniz, C., Jones, K. W., Rivers, M. L., Sutton, S. R., and Török, Sz., *Environ. Sci. Technol.*, 1994, submitted for publication.
89 Grant, R. H., Schulze, D. G., and Sutton, S. R., *Atmos. Environ.*, 1995, submitted for publication.
90 Premuzic, E. T., Kwiatek, W. M., Lin, M., and Jones, K. W., *Geothermal. Sci. Techn.*, 1989, **2**, 125.
91 Frantz, J. D., Mao, H. K., Zhang, Y.-G., Wu, Y., Thompson, A. C., Underwood, J. H., Giauque, R. D., Jones, K. W., and Rivers, M. L., *Chem. Geol.*, 1988, **69**, 235.
92 Anderson, A. J., Mayanovic, R. A., Bodnar, R. J., Mavrogenes, J. A., Bajt, S., Rivers, M. L., and Sutton, S. R., *Geol. Soc. Am. Abstr. Progr.*, 1993, **25**, A316.
93 Lowenstern, J. B., Mahood, G. A., Rivers, M. L., and Sutton, S. R., *Science (Washington, D.C., 1883–)*, 1991, **252**, 1405.
94 Rankin, A. H., Ramsey, M. H., Coles, B., van Langevelde, F., and Thomas, C. R., *Geochim. Cosmochim. Acta*, 1992, **56**, 67.
95 Vanko, D. A., Sutton, S. R., Rivers, M. L., and Bodnar, R. J., *Chem. Geol.*, 1990, **109**, 125.
96 Bodnar, R., Mavrogenes, A., Anderson, A., Bajt, S., and Sutton, S., *Eos* , 1993, **74**, 669.
97 Berthold, T., and Jagodzinski, H., *Z. Kristallogr.*, 1990, **193**, 85.
98 Sutton, S. R., Bajt, S., Rivers, M. L., Smith, J. V., Meyer, H. O. A., and Jones, K. W., *Eos*, 1992, **73**, 651.
99 Sutton, S. R., Bajt, S., Rivers, M. L., and Smith, J. V., *Lunar Planet. Sci.*, 1993, **XXIV**, 1383.
100 Delano, J. W., Sutton, S. R., and Smith, J. V., *Lunar Planet. Sci.*, 1991, **XXII**, 311.
101 Delaney, J. S., Sutton, S. R., and Smith, J. V., *Lunar Planet. Sci.*, 1989, **XX**, 238.
102 Brearley, A. J., Bajt, S., and Sutton, S. R., *Lunar Planet. Sci.*, 1995, **XXVI**, 169.
103 Chen, J. R., Chao, E. C. T., Minkin, J. A., Back, J. M., Bagby, W. C., Rivers, M. L., Sutton, S. R., Gordon, B. M., Hanson, A. L., and Jones, K. W., *Nucl. Instrum. Methods, Sect. B*, 1987, **22**, 369
104 Candela, P. A., Piccoli, P. M., and Rivers, M. L., *Geol. Soc. Am. Abstr. Progr.*, 1991, **23**, A465.
105 Vanko, D. A., Sutton, S. R., Ghazi, A. M., and Cline, J. S., *Eur. J. Mineral.*, 1995, **ECROFI XII** (Special Issue), in the press.
106 Campbell, A. C., Cramer, S., Rivers, M. L., and Sutton, S. R., *Eos*, 1990, **71**, 1621.
107 Schulze, D. G., McCay-Buis, T., Sutton, S. R., and Huber, D. M., *Agron. Abstr.*, 1993, **S9–18**.
108 Tokunaga, T. K., Sutton, S. R., and Bajt, S., *Soil Sci.*, 1994, **158**, 421.
109 Hayes, K. F., Roe, A. L., Brown, G. E., Jr., Hodgson, K. O., Leckie, J. O., and Parks, G. A., *Science, (Washington, D.C., 1883–)*, 1987, **238**, 783.
110 Hazemann, J. L., Manceau, A., Sainctavit, Ph., and Malgrange, C., *Phys. Chem. Miner.*, 1992, **19**, 25.
111 Manceau, A., Bonnin, D., Stone, W. E. E., and Sanz, J., *Phys. Chem. Miner.*, 1990, **17**, 363.
112 Waychunas, G. A., Rea, C. C., Fuller, J. A., and Davis, J. A., *Geochim. Cosmochim. Acta*, 1993, **57**, 2251.
113 Artioli, G., Sacchi, M., Balerna, A., Burattini, E., and Simeoni, S., *N. Jb. Miner. Mh.*, 1991, 413.
114 Charnock, J. M., Garner, C. D., Pattrick, R. A. D., and Vaughan, D. J., *Mineral. Mag.*, 1989, **53**, 193.
115 Charnock, J. M., Garner, C. D., Pattrick, R. A. D., and Vaughan, D. J., *J. Solid State Chem.*, 1989, **82**, 279.
116 Chen, J. R., Chao, E. C. T., Back, J. M., Minkin, J. A., Rivers, M. L., Sutton, S. R., Cygan, G. L., Grossman, J. N., and Reed, M. J., *Nucl. Instrum. Methods Phys. Res., Sect. B*, 1993, **75**, 576.
117 Chiarello, R. O., Wogelius, R. A., and Sturchio, N. C., *Geochim. Cosmochim. Acta*, 1993, **57**, 4103.

118 Farges, F., Sharps, J. A., and Brown, G. E., Jr., *Geochim. Cosmochim. Acta*, 1993, **57**, 1243.
119 Kasrai, M., Bancroft, G. M., Brunner, R. W., Jonasson, R. G., Brown, J. R., Tan, K. H., and Feng, X., *Geochim. Cosmochim. Acta*, 1994, **58**, 2865.
120 Li, D., Bancroft, G. M., Kasrai, M., Fleet, M. E., Yang, B. X., Feng, X. H., Tan, K., and Peng, M., *Phys. Chem. Miner.*, 1994, **20**, 489.
121 Paris, E., Mottana, A., Della Ventura, G., and Robert, J.-L., *Eur. J. Miner.*, 1993, **5**, 455.
122 Pattrick, R. A. D., van der Laan, G., Vaughan, D. J., and Henderson, C. M. B., *Phys. Chem. Miner.*, 1993, **20**, 395.
123 Waldo, G. S., Carlson, R. M. K., Moldowan, J. M., Peters, K. E., and Penner-Hahn, J. E., *Geochim. Cosmochim. Acta*, 1991, **55**, 801.

Paper 4/06409G
Received October 19, 1994
Accepted January 17, 1995

Trace Element Standards for the Electron Microanalyser Using Layered and Ion-implanted Materials*

G. Remond
BRGM, DR/GGP, BP6009, 45060 Orleans Cedex 2, France

R. H. Packwood
CANMET-EMR, Metals Technology Laboratories, 568 Booth Street, Ottawa, Ontario, Canada

C. Gilles
BRGM, DR/GGP, BP6009, 45060 Orleans Cedex 2, France

The merits and limitations of thin surface film deposition and ion implantation for preparing reference materials for quantitative analysis of trace elements using wavelength-dispersive X-ray spectrometry with the electron probe microanalyser are illustrated and discussed. The objective is to generate X-ray intensities typical of elements present at trace levels and to relate the measured intensities to the mass concentration of these elements when assumed to be homogeneously distributed within bulk materials. For this purpose, X-ray intensity calculations based on the use of analytical expressions for both the depth–ionization and the depth–concentration distributions, respectively, are presented. It will be demonstrated that gold-layered and materials ion implanted with gold can be advantageously used to validate the experimental approaches used for X-ray intensity measurements in the presence of distortions in the shape of an X-ray peak and the underlying continuous emission distribution, and also to test the algorithms and the physical parameters used in the analytical descriptions of the ionization and concentration profiles as a function of depth. The contribution of layered and ion-implanted compounds to a better understanding of surface and bulk charging phenomena in strongly insulating specimens is also presented.

Keywords: *X-ray spectrometry; wavelength-dispersive spectrometry; surface coating; ion implantation; X-ray intensity measurement; insulating material; surface charging; bulk charging; trace element standard*

Introduction

The modern computer-controlled electron probe microanalyser (EPMA) for spatially resolved chemical analysis by X-ray spectrometry (XRS) offers a tremendous capability for repetitive analyses, on a routine basis, of a variety of materials. Quantitative analysis requires the use of standards. According to the so-called 'standardless-based approach' the reference X-ray intensities are calculated using a physical parameter database, including the ionization cross-sections, the energy loss function, the relative intensity of the X-ray lines belonging to the K, L, or M series, the absorption coefficients, *etc.* Some of these parameters are not known accurately and the method must be used carefully. The use of external standards is still preferred to derive accurate quantitative data from X-ray spectrometry. A variety of metallic and non-metallic compounds are available with certified chemical compositions determined according to a rigourous testing procedure as discussed by Marinenko.[1] These certified materials are primary standards suitable for the development of a large collection of secondary standards needed for the analysis of minerals the composition and crystallography properties of which may vary to a large extent. Using wavelength-dispersive spectrometry (WDS), it is usually acceptable to measure the intensity of an X-ray emission as the peak height of the emission line. The approach based on X-ray peak height measurement in WDS has been proved experimentally to be quite sufficient for quantitative analysis of major constituents in a variety of materials. However, this approach only remains valid as long as the peak height remains proportional to the integrated peak area and as long as no chemical peak shift exists between the X-ray emission line measured at the surface of the specimen and the reference material. Consequently, the reference and the unknown specimens must have similar chemical properties in order to minimize peak shifts resulting from this effect, which will affect the reliability of the X-ray intensities when the peak height measurement procedure is used. In addition, Fialin[2] showed that a discrepancy occurred between measured and calculated concentrations of Zn bearing minerals analysed with the soft Zn Lα emission line and a pure Zn specimen for standard. When using soft X-ray emission bands (K lines of low atomic number elements or L and M emission bands of intermediate and high atomic number elements), Remond *et al.*[3] reached the conclusion that when analysing insulating materials, the electrical conductivity as well as the chemical composition must be considered for optimizing the choice of the reference materials.

The choice of the reference material is particularly crucial in the analysis of elements present at trace levels, *i.e.*, when the intensity of the analysed characteristic X-ray peak is of the same order of magnitude as that of the underlying continuous emission distribution.

Recalibration procedures during quantitative analysis may be used for correcting peak shifts resulting from instrumental factors or from chemical effects. Marion and Vannier[4] have suggested that two successive measurements on each side of the expected peak position should be made and the actual peak maximum be derived from a theoretical description of the peak around its maximum. These authors showed that this procedure accounted for a small non-reproducibility in the

* Presented at Geoanalysis 94: An International Symposium on the Analysis of Geological and Environmental Materials, Ambleside, England, September 18–22, 1994.

monochromator positioning or for small chemical shifts. Direct peak integral measurements or multiple least squares fitting techniques to process digitally recorded wavelength-dispersive spectra are to be preferred to peak height measurements. Using modern computer-controlled EPMAs, peak areas can be easily obtained by integrating the number of counts in each successive channel analysed by displacing the monochromator step-by-step. Peak integration obviates the need for recalibration when peaks are shifted in wavelength by chemical bonding (Fialin *et al.*[5]) or by instrumental factors that may alter the reproducibility of the monochromator positioning over a long period of time for repetitive quantitative analyses. However, whilst peak integration permits cancellation of the effect of asymmetry of X-ray peaks on the intensity measurements it neglects the origins of the phenomena leading to the asymmetry, which in turn may vary with the specimen composition and the experimental conditions as illustrated by Remond and co-workers.[6–8] In some instances, peak area measurement based on the least-square fitting of the experimental data to an analytical description of the emission band is to be preferred to the on-line measurement of peak integrals. The spectral decomposition of digitally recorded WDS X-ray spectra has been illustrated by Remond and co-workers,[6–8] and its importance will be illustrated in the analysis of gold-bearing compounds using the Au Lα and Au Mα emission peaks, both of which exhibit asymmetrical shapes resulting from instrumental effects and spectroscopic phenomena leading to the presence of non-diagram bands accompanying the characteristic diagram emission bands. (The term 'diagram' refers to X-rays produced by simple shell-to-shell electron transitions.)

Optimizing the X-ray intensity measurement procedure together with the statistical precision is necessary; however, non-sufficient conditions for accurate quantitative analysis and the source of errors that arise from the sample itself must also be examined. EPMA is a technique that is very sensitive to surface composition changes and false data can arise from non-uniform distribution of the element of interest, either in a lateral or a vertical direction, with respect to the specimen surface. Changes in surface composition may be introduced during the polishing procedure, resulting in a contamination of the surface by species carrying the elements in question. Surface composition that changes with respect to the bulk material leads to a calculated composition that varies with the incident energy values, *i.e.*, with the sampling depth below the specimen surface, as reported by Remond and co-workers.[9,10] These authors added to the analytical scheme an additional correction accounting for the contribution of surface layer to the X-ray signal originating from the bulk material. The approach used consisted of combining analytical models describing both the ionization and the concentration distributions as a function of depth. This study led the authors to the idea that the artifacts resulting from the presence of surface films could be used advantageously to generate controlled concentration/distribution reference materials and the use of layered and ion-implanted materials as possible reference specimens for XRS with the EPMA have been briefly mentioned by Remond *et al.*[11]

Besides the need for an accurate micro-characterization of thin films on substrates and ion-implanted profiles for the improvement of the manufacture of materials used in modern technology there is also a need to account for the presence of surface coating films in the data reduction procedures used in X-ray quantitative analysis with EPMA. Correction of the measured X-ray intensities for absorption through the coating films is particularly necessary when using soft X-ray emission bands for analytical purposes with the EPMA as reported by Remond *et al.*[8] These correction procedures are based on the use of analytical description of both the ionization and concentration distributions as a function of depth, and several algorithms have been developed for this purpose (see, for example, Packwood,[12] Pouchou and Pichoir[13]).

The general aspects of ion implantation have been intensively reviewed, the topics covered include instrumentation, physical parameters controlling the depth depositions and applications have been summarized by Donnelly[14] amongst abundant literature on the subject. The use of ion implantation was first introduced by McIntyre *et al.*[15] for the calibration of the ion microprobe (SIMS) in order to quantify trace element analyses in sulfides. The merits of ion-implanted materials for the quantiative analysis of precious metals in minerals with SIMS has been illustrated in detail by Cabri and co-workers.[16,17] and by Chryssoulis.[18,19] It is the purpose of this paper to give a detailed investigation of the merits and limitations of materials with a controlled concentration–depth distribution to the procedures involved in quantitative X-ray analysis with EPMA. The fundamental relationships used in this study for the prediction of X-ray intensities observed at the surface of targets exhibiting changes in composition as a function of depth will be presented first. The use of layered and implanted specimens will be discussed with a view to providing a test for: (*i*) the experimental procedure used for X-ray intensity measurement accounting for non-symmetrical shape of the analysed lines resulting from spectroscopic or instrumental effects, (*ii*) the evaluation of matrix correction procedures and the choice of the physical parameters to be used (mass absorption coefficients amongst others); and (*iii*) the investigation on electrical charging effects in insulating materials by varying the depth deposition of trapped charges with respect to the surface conductive layer or the depth distribution of the implanted metallic ions.

Materials and Methods

Specimens

A silicon wafer and a gold-free natural arsenopyrite (AsFeS) were gold-implanted using the Pelletron heavy-ion mass separator installed at the Atomic Energy of Canada Ltd. Research, in Chalk River, Ontario, Canada. The experimental procedure has been discussed by Chryssoulis[18] who developed quantitative gold ion implantation to determine the gold concentration in common sulfide and sulfo-arsenide minerals from refractory ores. For the specimens used in the present study, the implanted area was about 1 cm^2. The lateral homogeneity of the implant was evaluated to be 5% by Chryssoulis[18] studying the gold-implanted Si wafer by Rutherford backscattering spectroscopy (RBS). The depth distribution of the implant was studied by SIMS profiling which has a reproducibility of about 10% for the depth of the maximum of the implant profile.

The mass per cent. of gold at the maximum of the depth distribution, C_M was derived from the SIMS profile according to:

$$C_M = 0.197 F I_M n_c / N \rho I_b D \quad (1)$$

where F, is the implant fluence (or dose in atoms cm^{-2}), I_M the measured number of counts at the profile maximum, n_c the number of cycle measurements in the the depth profile, N the Avogadro number, ρ the density (in g cm^{-3}), I_b the integrated background counts and, D the depth (in nm).

For the implanted silicon wafer, the implant dose was 2.5×10^{15} atoms cm^{-2}. The gold concentration at the maximum of the profile was 1.9 mass-%. The maximum of the distribution was located 320 nm below the specimen surface with a 160 nm width. An implanted arsenopyrite specimen previously analysed with SIMS by Chryssoulis *et al.*[20] was also studied. The Au implantation was 10^{15} atoms cm^{-2}, the maximum of the

implant corresponding to 0.45 mass-% of Au was located 236 nm below the specimen surface.

Two synthetic ZnS crystals were Ga implanted. The two synthetic crystals were manufactured by Morton International (Woburn, MA, USA). One specimen is colourless and transparent and referred as Cleartran, the second specimen is yellow coloured.The polycrystalline synthetic ZnS specimens were grown by chemical vapour deposition (CVD) using Zn vapour and H_2S in an argon carrier gas at around 700 °C. X-ray diffraction showed that the ZnS crystals have a cubic structure. The specimens are polycrystalline with grain sizes in the range 5–10 μm. According to the manufacturer, the resistivities are $\approx 10^{12}$ Ω cm for the yellow coloured crystal and $>10^{13}$ Ω cm for the Cleartran specimen. The relative permittivity is $\varepsilon_r \approx 8.3$. The two synthetic ZnS crystals were Ga implanted with a Wickham ion implanter at the University of Sussex. The implantation was carried out with a 175 keV energy and at 5×10^{16} ions cm^{-2}.

Instrumentation

For X-ray spectrometry, the automated computer-controlled EPMA installed in the joint BRGM–CNRS laboratory was used. The EPMA is equipped with five WDSs. In the present study, the Au Mα peaks were analysed with a pentacrytritol, $C_5H_{12}O_4$, monochromator (PET, $2d = 0.874$ nm). An LiF ($2d = 0.4026$ nm) monochromator was used for the analysis of Au Lα emission line. The ZnS crystals were also analysed using an energy-dispersive spectrometer (EDS) attached to a scanning electron microscope (SEM).

Experimentation

Varying the Apparent Concentrations as a Function of the Analysed Depth Below the Specimen Surface

For a layered target (thin layer deposited on top of a substrate) or for a graded composition as a function of depth below the specimen surface (implant), the number of atoms of the element in the surface layer or in the implant contributing to the measured X-ray intensity will vary as a function of the sampling depth, *i.e.*, as a function of the incident energy.

In the present study, two intensity measurement procedures were used to vary the apparent concentration of the analysed element:

(*i*) Using a stationary electron beam at the surface of a coated surface or ion-implanted specimen but, varying the incident energy, *i.e.*, varying the depth distribution of the X-ray excitation with respect to the depth distribution of the ion implant [Fig. 1(*a*)].

(*ii*) Using a fixed incident energy, but varying the beam location along a direction travelling down a SIMS crater wall. For an ion-implanted target, the depth concentration profile can be revealed by making a groove in the surface and analysing the implant by moving the incident electron beam across the groove. Such a procedure, surface analysis by X-ray emission (SAXE) has been previously illustrated by Packwood and Remond[21] for a thick Si–Ge layer buried in a Si matrix. Similar to the SAXE procedure, a step-by-step quantitative analysis along a line scan crossing the crater wall resulting from ion depth profiling with the SIMS allows different regions of the implanted element to be analysed as a function of the beam location [Fig. 1(*b*)].

A three-dimensional view of the SIMS craters and a two dimentional contour map of the same depth are shown in Fig. 2. Although the SIMS crater is only around 300 nm in depth, the resulting topography when crossing the crater wall may lead to errors in the X-ray intensity measurement and processing. The SIMS crater changes slope near the upper rim, and even through the slope measured from the profilometer trace was only 1 : 100, it was still sufficient to create a shadowing effect, so that the specimen orientation cannot be ignored when measuring the X-ray intensity along a line scan crossing the crater wall.

Data Acquisition and Processing

Intensity measurement procedures

Two X-ray intensity measurement procedures were used.

Peak height measurement. The net intensity is obtained by measuring the total number of counts for the monochromator set at the Bragg angle corresponding to the analysed emission, followed by repositioning the monochromator to measure the continuum intensity on each side of the peak. The usual peak height intensity measurement may fail to apply when the X-ray emission bands exhibit an asymmetrical shape resulting from the presence of non-diagram lines (satellites) or from instrumental distortions as reviewed by Remond and co-workers[6,8] for X-ray peaks measured with wavelength dispersive spectrometers of the EPMA. In the presence of asymmetrical X-ray emission peaks, peak area measurements may be preferred to the usual peak height intensity measurement procedure.

Peak area measurement. Digital recording of the analysed X-ray emission peak was used for the case of peak integral measurement or spectral decomposition of X-ray peaks, the shape of which was strongly asymmetrical due to either the presence of satellite lines or to instrumental distortions. The monochromator was moved in a step-count fashion and the

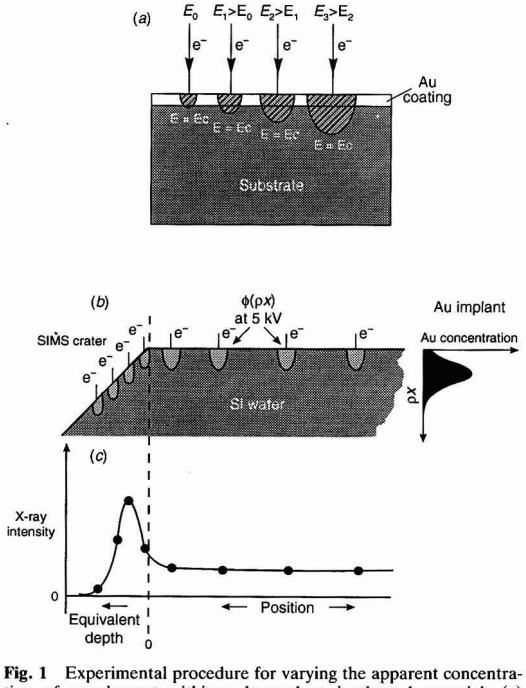

Fig. 1 Experimental procedure for varying the apparent concentration of an element within a layered or implanted material: (*a*) variations in the sampling depth by changing the incident energy and, (*b*) variations in the concentrations along the vertical direction of the implant profile revealed when crossing the crater wall produced by SIMS analysis and, expected line scan (*c*).

measurements stored for spectral decomposition by a least-square fitting technique using an analytical description specific to the experimental spectra in question.

The observed peak profile, $P(\lambda)$, was described by an empirical pseudo-Voigt-function, *i.e.*, a linear combination of a Gaussian and a Lorentzian distribution according to :

$$P(\lambda) = C_g\, G(\lambda) + C_l\, L(\lambda) \qquad (2)$$

where $0<C_g<1$ and $C_l = 1 - C_g$ are the contributions of the Gaussian, $G(\lambda)$ and Lorentzian, $L(\lambda)$ of same half-width and centred at the same position.

To describe asymmetrical peak shapes, Remond and co-workers.[6–8] showed that adding Gaussian or pseudo-Voigt offsets to the major pseudo-Voigt diagram line profile was a good enough approximation to describe a complex peak containing several discrete spectroscopic features, *e.g.*, diagram and non-diagram contributions and possible instrumental effects.

Calculation of X-ray intensities from layered and ion-implanted specimens

The prediction of the characteristic X-ray intensity of an element assumed to be homogeneously diluted within the bulk specimen and that which would be measured at the surface of a layered specimen or of an ion-implanted material (concentration varying as a function of depth below the specimen surface) can be performed when analytical descriptions are known for both the ionization and the concentration distributions as a function of depth.

For elements homogeneously distributed in a bulk solid, quantitative data with the EPMA are obtained by applying correction factors to the experimentally measured concentrations, *i.e.*, the intensity measured at the surface of the unknown normalized to that of a reference compound. The correction factor accounts for the difference between the number of generated photons and the number of emitted photons; the difference resulting from: (*i*) interactions between the incident electrons and the target (atomic number correction involving the energy loss function and the loss of ionization due to the backscattered electrons leaving the specimen surface) and (*ii*) interactions between the generated photons and the matrix (absorption correction, A and fluorescence correction, F).

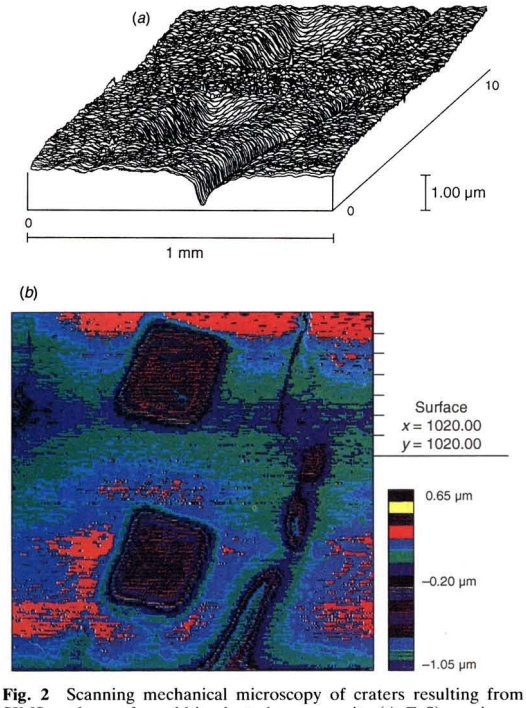

Fig. 2 Scanning mechanical microscopy of craters resulting from SIMS analyses of a gold-implanted arsenopyrite (AsFeS) specimen: (*a*) three-dimensional view of the craters and, (*b*) contour map of iso-depth levels.

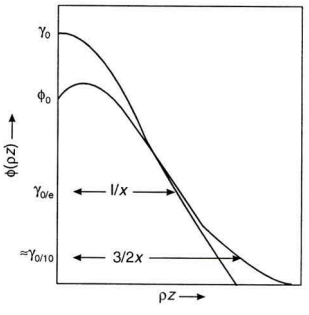

Fig. 3 Description of the ionization depth distribution, $\phi(\rho z)$ based on the modified surface gaussian (MSG) model according to Packwood and Brown,[23] where:

$$\gamma_0 = 10\pi \frac{U_0}{U_0 - 1}\left[1 + \frac{10}{\ln U_0}\left(U_0^{-0.1} - 1\right)\right]$$

$$\phi_0 = 1 + 2.7\,\eta\left[1 - \exp\left(\frac{1 - U_0}{Z}\right)\right]$$

$$\alpha = \frac{5.5\,10^5}{E_0^{0.75}}\left(\frac{Z - 1.3}{Z}\right)\left(\frac{Z}{A}\right)^{0.5}\left(\frac{\frac{Z}{A}\ln\frac{166\left(\frac{E_0 + E_c}{2}\right)}{J}}{E_0^2 - E_c^2}\right)^{0.5}$$

$$\beta = 0.4\,\alpha\, Z^{0.6} \qquad U_0 = \frac{E_0}{E_c} \qquad J = 1.15\,10^{-3}\,Z$$

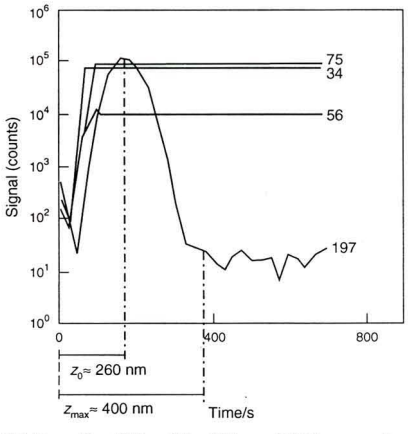

Fig. 4 SIMS profiles ^{197}Au, ^{75}As, ^{56}Fe, and ^{16}S ion mass for the case of a gold-implanted arsenopyrite (analysis by Chryssoulis).[19] For EPMA calculations the gold implant profile was approximated by eqn. (5).

These two interactions can be treated separately using analytical description of the Z, A, and F correction factors. It has been shown that the integration of the ionization distribution, $\phi(\rho z)$ as a function of the mass depth ρz, below the specimen surface rather than the analytical functions Z and A, leads to an improvement in the accuracy of quantitative data. For analytical expressions of the ionization distribution function see, for example, Scott and Love,[22] Packwood[12] and Pouchou and Pichoir.[13]

The model we used in the present study, called the modified surface-centred gaussian (MSG) is derived from the observations reported by Packwood and Brown[23] on several hundreds of $\phi(\rho z)$ curves showing that the plot of $\ln[\phi\rho(z)]$ as a function of $(\rho z)^2$ exhibited a linear relationship so that:

$$\phi(\rho z) = \gamma_0 \exp[-(\alpha\rho z)^2]\left[1 - \frac{\gamma_0 - \phi(0)}{\gamma_0}\exp - (\beta\rho z)\right] \quad (3)$$

The above equation expresses $\phi(\rho z)$ in terms of two Gaussian distributions: a Gaussian of amplitude γ_0 centred at the surface with a standard deviation $(2\alpha)^{-1/2}$ and a transient term $1 - [\gamma_0 - \phi(0)/\gamma_0]\exp(-\beta\rho z)$ where $\phi(0)$ is the value of the ionization distribution at the surface. The values of the parameters in eqn. (3) are given in Fig. 3, and their meaning has been discussed by Packwood.[12]

The emerging intensity is obtained directly by algebraic or numerical integration of the parametric description of $\phi(\rho z)$ without the separate calculations of the absorption effect and the atomic number effect, *i.e.*, the effects of stopping power and backscattering, which are treated implicitly rather than separately as it is done using the ZAF model. For the conventional specimen of uniform elemental concentration with ρz, we have for the observed intensity, I_{obs}:

$$I_{obs} = C_A\left(\frac{\sqrt{\pi}}{2\alpha}\right)\left\{\gamma_0 \exp\left(\frac{\chi}{2\alpha}\right)^2 \cdot \mathrm{erfc}\left(\frac{\chi}{2\alpha}\right) - (\gamma_0 - \phi_0)\exp\left[\frac{\chi+\beta}{2\alpha}\right]^2 \cdot \mathrm{erfc}\left[\frac{\chi+\beta}{2\alpha}\right]\right\} \quad (4)$$

where the error function of the variable x [erf(x)] and the complementary error function [erfc(x)] are approximated by numerical calculation (see Appendix)

The above depth distribution function [eqn. (3)] can also be used for the microanalysis of thin layers deposited on substrates. X-ray intensities from stratified samples were derived by Packwood and Milliken[24] and applications were illustrated by Packwood[12] and by Packwood and Remond.[21]

It is also possible to extend the calculations for the case of continuously varying concentrations as a function of depth below the specimen surface. Of particular interest in the present study is the case of a concentration gradient following a Gaussian depth distribution centred below the specimen surface, consistent with the SIMS depth profiles shown in Fig. 4. For the ion-implanted specimens used in the present study, the Au implant was accurately approximated by the following Gaussian distribution

$$C_A = C_0 \exp[-\kappa^2(\rho z - \rho z_0)^2] \quad (5)$$

i.e., a Gaussian of height C_0, centred at mass depth ρz_0 and having a full width at 1/e given by $2/\kappa$.

For a Gaussian concentration distribution centred at mass depth ρz_0 of height C_0 and of half-width at half-maximum determined by κ, we have:

$$I_A^{imp} = C_A \exp(-K^2\rho^2 z_0^2)\frac{\sqrt{\pi}}{2\alpha'}\left[\gamma_0 \exp\left(\frac{\chi'}{2\alpha'}\right)\mathrm{erfc}\left(\frac{\chi'}{2\alpha'}\right) - (\gamma_0 - \Phi_0)\exp\left(\frac{\beta+\chi'}{2\alpha'}\right)\mathrm{erfc}\left(\frac{\beta+\chi'}{2\alpha'}\right)\right] \quad (6)$$

with

$$\alpha'^2 = \alpha^2 + \kappa^2$$

$$\chi' = \chi - 2\kappa^2\rho z_0$$

This equation is similar to that established for a conventional specimen [eqn. (4)] when replacing the α, χ and β variables by new values as shown in Fig. 5, so that the predicted intensities for models of concentrations following an exponential distribution, or a Gaussian distribution, as a function of depth, can be easily derived by parameter substitution in the expression giving the predicted intensity for the same matrix in which the element of interest is homogeneously distributed.

Electron Probe Microanalysis of Gold-implanted Materials

Preliminary Observation

When analysing elements present at trace levels, using the peak height intensity and a linear interpolation of two measurements on each side of the peak to determine the intensity of the continuous emission associated with the analysed line, it is a frequent occurrence to obtain negative intensities, *i.e.*, a background intensity higher than that of the characteristic peak. This can arise from counting statistics, both quantities being in the same order of magnitude, or because of the curvature of the continuum intensity with wavelength.

This situation has been encountered for the Au Lα intensities measured on gold-implanted and gold-free areas and of a silicon wafer. The beam energy was 20 keV, with a 20 nA beam current and 30 s counting time. For the gold-free area, the continuum intensity N_B was greater than the total number of counts N_P measured at the Au Lα peak position. The absolute difference $|N_P - N_B|$ was equivalent to a concentration of 0.06% compared with the intensity of a pure gold specimen. For the case of the gold-implanted area, the net Au Lα peak $N_P(Au)$ was greater than the corresponding continuous intensity $N_B(Au)$ and the difference $N_P(Au) - N_B(Au)$ was statistically significant, *i.e.*, $N_P(Au) \geqslant 3\sqrt{N_B(Au)}$. The measured k-ratio, *i.e.*, the measured x-ray intensity relative to that of the pure element was 0.06 mass-%. Based on the analysis of the gold-free area, the continuous emission intensity is over-estimated by an amount equivalent to 0.06%. Correcting the intensities measured at the surface of the implanted area by an equivalent amount leads to a measured Au concentration of 0.12 mass-% within the implanted area. This concentration, corrected for the over-estimate of the continuous intensity, is in a fairly good agreement with the calculated value equal to 0.14 mass-%. For these calculations eqn. (6) was used with eqn. (5) describing the gold depth profile measured with SIMS.

In order to explain the over-estimation of the continuous emission intensity and the subsequent deviation between the measured and calculated Au Lα k-ratios for the gold-implanted silicon wafer, we investigated the shape of the analysed X-ray peak and the corresponding continuous emission.

Gold-implanted Arsenopyrite Specimens (AsFeS)

The Au Lα emission peak for a pure gold target and a 20 keV incident energy is shown in Fig. 6. A LiF monochromator (200 planes, $2d = 0.4026$ nm) was used. For that crystal the first-order reflection of the Au Lα emission occurs at Bragg angle, $\theta = 18.48°$. At such a low Bragg angle instrumental distortions and high-energy satellites resulting from multiple ionization may combine to give rise to the asymmetric Au Lα emission band.

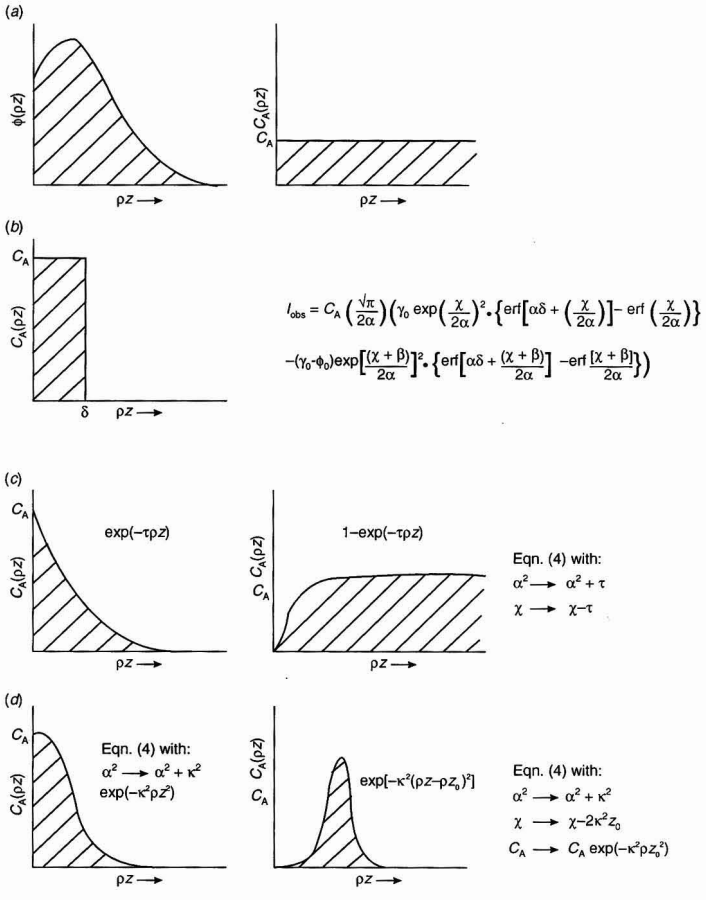

Fig. 5 Some concentration distributions with algebraic solutions for the observed intensity ratios. (*a*) conventional [see eqn. (4) in text]; (*b*) surface layer; (*c*) exponential and (*d*) Gaussian. Note that for surface layer and gradient concentrations, the observed intensities are obtained by parameter substitution in the general eqn. (4).

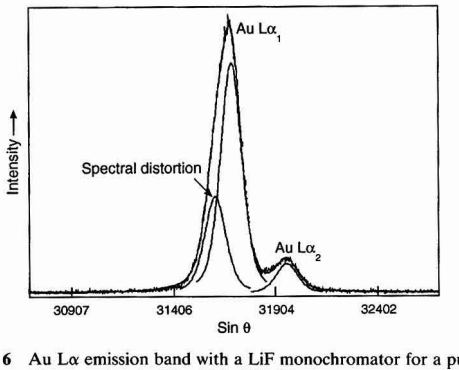

Fig. 6 Au Lα emission band with a LiF monochromator for a pure gold specimen analysed with a 20 keV incident energy.

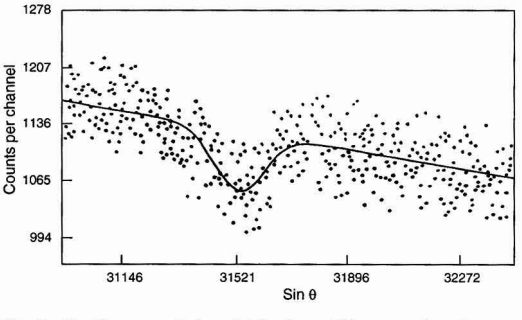

Fig. 7 Continuous emission distribution within a wavelength range centred on the Au Lα emission band observed at the surface of a gold-free arsenopyrite specimen analysed with a LiF monochromator and a 20 keV incident energy.

As discussed by Remond *et al.*,[6] instrumental distortions contribute more to the Au Lα peak asymmetry than the existence of satellite lines such as those associated with Coster–Kronig transitions for the case of the Au Lα X-ray emission spectrum. The Au Lα emission peak analysed with the LiF monochromator was therefore described by a pseudo-Voigt profile [eqn. (2)] associated with the diagram line, with a Gaussian offset accounting for the instrumental distortion on the high-energy side (short-wavelength side) of the peak, as illustrated in Fig. 6.

For the analyses of gold present at low concentration levels, the shape of the continuous emission associated with the Au Lα peak was then carefully examined. As shown in Fig. 7 for the case of a gold-free arsenopyrite specimen, a sharp decrease in the continuous intensity was observed at $\sin\theta = 0.31650$, *i.e.*, $\theta = 18.42°$. The position of the 'hole' in the continuum remained independent either of the incident energy or of the nature of the specimen analysed with the LiF monochromator, and this feature must be regarded as resulting from some intrinsic property of the LiF crystal. Recently, Self *et al.*[25] calculated the positions of 'holes' occurring at specific wavelengths in the continuous spectrum by considering diffraction from all crystallographic planes of the LiF monochromator.

Since the position of the anomalous continuum intensity decrease depends only on the monochromator crystal, we derived an analytical expression for the continuum distribution within a narrow wavelength range centred at the Au Lα peak position. For this purpose gold-free pyrite (FeS_2) and arsenopyrite (AsFeS) specimens, oxides and pure elements were analysed and their continuum distributions $B(\lambda)$ measured within the $\sin\theta$ interval $0.32944 < \sin\theta < 0.32444$. The readings were digitally recorded and processed using eqn. (7) as a fitting function:

$$B(\lambda) = a\lambda + b - H_H \exp[-\ln 2\,(\lambda - \lambda')/\Gamma_H]^2 \qquad (7)$$

where a is the slope of the average linear variation of the continuum intensity, b its ordinate at the origin of the scan, H_H is the amplitude of a Gaussian distribution centred at the 'hole' wavelength λ', having a half-width at half-maximum of Γ_H.

The hole at $\theta = 18.42°$, in the continuous emission of any specimens analysed with the LiF (200) monochromator occurs in a wavelength range containing the Au Lα emission band. The Au Lα emission peak observed on a gold-implanted arsenopyrite analysed at 20 keV incident energy is shown in Fig. 8. It is obvious from Fig. 8 that the shape of the observed emission band is the result of combining the high energy tail with the Au Lα peak and the 'hole' in the continuous emission distribution (the position of the 'hole' corresponds to that of the Gaussian off-set used in the fitting function to correct the asymmetry of the peak). At low Au concentrations, *i.e.*, at low Au Lα peak-to-background ratios, a change in the Au Lα peak shape (*i.e.*, area), height and position may thus occur with respect to the Au Lα emission band of a pure gold specimen.

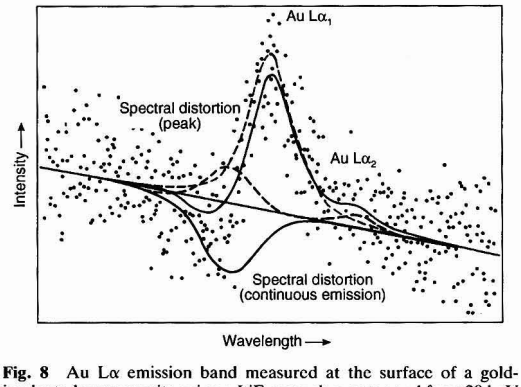

Fig. 8 Au Lα emission band measured at the surface of a gold-implanted arsenopyrite using a LiF monochromator and for a 20 keV incident energy.

We first investigated the change in the peak area values derived from channel-by-channel integration, N_{sum} and from spectral decomposition to derive the area of the diagram peak, N_{diag} accounting for both the asymmetry of the Au Lα peak and the 'hole' in the background, respectively. In order to avoid the effect of heterogeneities when comparing the X-ray intensities all values of N_{sum} and N_{diag} for the implanted specimen and the pure gold specimen were derived from a single spectrum digitally recorded on the unknown and reference materials, successively. Each spectrum measured at 15, 20 and 25 keV, successively, contained 500 channels with a 1 s counting time per channel. As shown in Table 1, the values derived from integrated peak areas, *i.e*, neglecting the 'hole' in the background, differ from those based on the area of the diagram peak derived from the spectral decomposition procedure, because the 'hole' in the background and the asymmetry of the Au Lα peak, occurring within the same wavelength domain, and so cannot be distinguished experimentally by analysing the Au Lα peak step-by-step. As previously reported, the amplitude of the Gaussian offset (asymmetry of the Au Lα band) relative to that of the pseudo-Voigt profile (diagram line) remained independent of the specimen composition. Thus, the peak amplitude of the symmetrical pseudo-Voigt profile describing the Au Lα diagram emission peak led to the same results as those obtained by using the peak areas derived from the fitting procedure. However, the digital recording of the Au Lα emission band aims to increase the statistical precision of the total number of counts within the analysed wavelength range but, the statistical precision in each channel is poor because of the short acquisition time per channel. The Au Lα k-ratios derived from peak area measurement from a single point analysis were compared with the data obtained by using the conventional peak height measurement procedure used for repetitive quantitative analyses.

The Au Lα peak height measurement was combined with a linear interpolation of two measurements on each side of the peak to determine the continuum intensity. For each incident energy used, *i.e.*, 15, 20 and 25 keV, successively, 20 point measurements were made on the surface of the gold-implanted arsenopyrite specimen and on the pure gold specimen, successively. The presence of the 'hole' in the continuum distribution leads to a peak shift of the Au Lα emission

Table 1 Measured Au Lα k-ratios for a gold-implanted AsFeS specimen as a function of the Au Lα intensity measurement procedure

	Au Lα k-ratio		
E_p/keV	Peak integral*	Peak decomposition*	Peak height†
15	ND‡	0.32	0.28 ± 0.02
20	0.08	0.18	0.17 ± 0.02
25	0.01	0.10	0.10 ± 0.01

* Au Lα intensities derived from the same digital Au Lα emission band recorded at the surface of the implanted specimen and the pure gold as reference.

† Average Au k-ratios from 20 Au Lα intensity measurements using the peak height intensity procedure.

‡ ND, Not detected.

observed at the surface of the implanted specimen with respect to that of the pure metal. A difference equal to 25×10^{-5} of the sin θ value was observed between the Au Lα maximum position measured at the surface of the pure gold and the gold-implanted specimen. The difference in peak position corresponds to a variation $\Delta I/I = 5\%$ for the peak height of the Au Lα peak measured at the surface of the Au-implanted arsenopyrite specimen. However, the error in the measured concentration resulting from the shift between the peak maxima for the unknown and reference compounds was found to be smaller than the error resulting from statistics and heterogeneity of the Au implanted distribution.

As shown in Table 1, the average Au Lα *k*-ratios derived from the usual peak height intensity procedure are consistent with the data derived from the spectral decomposition procedure applied to a single spectrum measured for each incident energy value.

The experimental Au Lα *k*-ratios were compared with the calculated data, using eqn. (6) with eqn. (5) for the implant profile. The area below the Gaussian curve describing the implant depth profile represents the number of implanted ions within the matrix. Thus, solving eqn. (6) has no unique solution because for a given $\phi(\rho z)$ ionization function, the same calculated *k*-ratios will be obtained by varying the maximum concentration or the width of the implant in such a way that the area of the implant will remain constant.

For calculations reported in Table 2, we first used the description of the gold implant derived from SIMS analysis of the implanted arsenopyrite (Chryssoulis[19]), *i.e.*, the maximum of the implant ($C_0 = 0.45\%$) located 265 nm below the specimen surface. The calculated *k*-ratio corresponding to a given implant shape is proportional to the C_0 concentration at the profile maximum. Independent of the incident energy the change in the calculated *k*-ratios will remain proportional to the change in the C_0 value. However, varying the width of the implant distribution will lead to a change in the calculated *k*-ratios depending on the incident energy, *i.e.*, a change in the depth ionization distribution. This effect is shown in Table 2 by comparing the *k*-ratios calculated with $\kappa = 6250$ and $\kappa = 8000$ successively, the z_0 and C_0 parameters remaining constant. The depth maximum of the gold implant derived from SIMS data differs from the theoretical depth profile for the implantation conditions used indicating that the maximum of the implant should be located 135 nm below the specimen surface, a value which is approximately half that derived from the SIMS analysis. The best fit between the measured and the calculated *k*-ratios was obtained for a gold concentration at the implant maximum of 0.6 mass-% located 130 nm below the specimen surface. It is possible to adjust the calculated data to the measured concentrations by varying the C_0 value. Obviously, such a procedure can only be applied if a change in the width and position of the implant has a smaller effect on the final result than that of a change of the maximum concentration. This condition will depend on the ion implant profile relative to the ionization distribution, *i.e.*, for a given implant profile will depend on the energy of the analysed X-ray photons, the incident electron energy, and the matrix .

From data in Table 2 it appears that the best agreement between the observed and calculated *k*-ratios is obtained when the position of the maximum of the implant profile is moved towards the specimen surface and subsequently the width of the implant is narrowed ($\kappa = 1/\rho z_0$) with respect to those values predicted from the SIMS measurements. The C_0 concentration at the maximum of the implant profile is then higher than the expected 0.45 mass% value.

In order to estimate the uncertainty in the calculated *k*-ratios resulting from an error in the description of the implant profile, the gold-implanted arsenopyrite specimen was analysed using the Au Mα (2123 eV) emission band.

The Au Mα *k*-ratios for a 10 keV incident energy were first measured along a line scan crossing the crater wall of an area previously analysed with SIMS. The line scan was performed using 2 μm steps starting in the ion-etched area at a depth below the Au implant, crossing the implanted layer and finally analysing on the top surface. The peak height procedure was used to measure the Au Mα intensities. The Au Mα *k*-ratios (Au Calc 5000 and Au Calc 6250) were calculated using the implant maximum and implant position of the implant profile derived from the SIMS data and by setting the κ parameter [eqn. (5)] equation to 5000 and 6250 successively. As shown in Fig. 9, the shape of the experimental line scan was consistent with the calculated profiles but all measured Au Mα *k*-ratios were found to be systematically greater than the calculated data. Adjusting the calculated profiles to the experimental line scan (Au Adj 5000, Au Adj 6250) led to a constant factor of 1.33 between the measured and predicted profiles.

The Au Mα peak analysed with a PET monochromator was asymmetrical because of a broad tail on its short wavelength side. While the asymmetry of the distorted Au Lα peak was associated with instrumental distortion, Remond *et al.*[6] showed that the Au Mα peak resulted mainly from high energy satellite bands leading to a peak shape dependent on

Table 2 Measured and calculated Au Lα *k*-ratios for a gold-implanted AsFeS specimen as a function of the description of the gold-implant profile.

			E_p/keV		
			15	20	25
			k(Au Lα)*		
			0.28 ± 0.02	0.17 ± 0.02	0.11 ± 0.02
κ	z_0/nm	C_0(%)	Calculated Au Lα *k*-ratios		
6250	265	0.45	0.25	0.21	0.15
8000	205	0.43	0.24	0.17	0.11
10000	164	0.50	0.26	0.16	0.10
12500	131	0.60	0.29	0.16	0.11

* Average *k*-ratios derived from 20 point measurements using the peak height intensity measurement procedure.

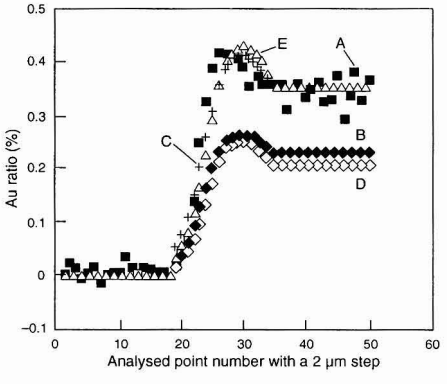

Fig. 9 Observed and calculated Au Mα *k*-ratios for a 10 keV incident energy along a line scan crossing a SIMS crater wall on a gold-implanted arsenopyrite specimen. For purpose of calculation the Au concentration at the maximum of the implant was set equal to $C_0 = 0.45\%$ (SIMS data) and the width of the Gaussian implant profile was $\kappa = 6250$ and $\kappa = 5000$, successively. A, Measured Au ratio (%); B, Au Calc 5000; C, Au Adj 5000; D, Au Calc 6220; and E, Au Adj 6220.

the composition and the experimental conditions (absorption). However, for a given incident energy the shape of the Au Mα emission band remained approximately independent of the gold concentration (Remond *et al.*[6]). A modification of the Au Mα peak shape as a function of the matrix composition and experimental conditions is not a sufficient self explanation for the observed deviation between the measured and the calculated data shown in Fig. 9.

As a second possible explanation of the 1.33 factor between the observed and the calculated Au Mα *k*-ratios, we investigated possible errors in the data reduction procedure used to express the measured data in terms of concentrations. The S Kα emission (2308 eV) is close to that of the M_4 absorption edge of gold and is strongly absorbed by that element leading to a fluorescence enhancement of the Au Mα emission line. However, the observed increase in the measured Au Mα *k*-ratios relative to the calculated data neglecting such phenomena is too high to result from fluorescence alone. Furthermore, when approaching an absorption discontinuity, the mass absorption coefficient (MAC) values are often uncertain as is the case for the S Kα absorption in gold the values for which are reported to be $\mu/\rho = 3880$ in Heinrich's Table and were calculated as $\mu/\rho = 2200$ by Pouchou and Pichoir.[26] Even so, difference in the MAC values was not sufficient to explain the increase in the measured *k*-ratios with respect to the calculated data. Similar discrepencies may also occur for the high MAC value for the Au Mα line in As ($\mu/\rho = 2999$ according to the Heinrich's tables). Assuming a 10% error in the MAC value led to a 3% variation of the Au Mα *k*-ratio for 0.2 mass-% Au homogeneously diluted within an arsenopyrite specimen.

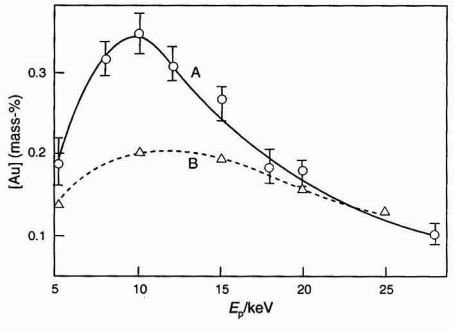

Fig. 10 Observed and calculated Au Mα *k*-ratios as a function of the incident energy for the gold-implanted arsenopyrite specimen. In these calculations, the implant profile derived from SIMS analysis was used. A, Observed and B, calculated using an Au implant from SIMS profile.

A more likely explanation for the observed discrepencies between the measured and calculated data may result from the parameters used for describing the gold-implant depth profile. The calculated data remained consistent with each other when the width of the implant, κ, was set equal to κ = 6250 (SIMS profile data) or decreased to κ = 5000. For both widths of the gold implant the best fit of the measured concentrations to the calculated values was obtained when the C_0 concentration at the implant maximum was set equal to $C_0 = 0.6$ instead of the $C_0 = 0.45$ derived from the SIMS analysis. This ratio is significant because the value of 1.33 is equal to the ratio 0.6:0.45 where 0.60 was the Au concentration at the maximum of the implant leading to the best fit of the experimental data to the measured Au Lα *k*-ratios, and 0.45 was the value of the maximum concentration derived from the SIMS profile.

In order to confirm such a difference between the concentration at the maximum of the implant derived from the SIMS analysis and that from the fitting procedure used on the measured Au Mα *k*-ratios together with a theoretical description of the gold implant, the analyses were repeated on the gold-implanted AsFeS specimen this time varying the incident energy.

The Au Mα *k*-ratios were measured with a stationary electron beam at various incident energies so changing the sampling depth through the gold implant. As for the case of the line scan crossing the wall of the SIMS crater (see Fig. 9) the peak height of the Au Mα emission band was used for intensity measurements, and a pure gold specimen was used for reference. As shown in Fig. 10, the variations of the measured *k*-ratios as a function of the incident energy had a maximum for a 10 keV energy.

The measured data were compared with those predicted from various assumed depth profiles for the gold implant. Results of calculations are shown in Table 3. These results show that for descriptions of the implant profile, a concentration of $C_0 \geqslant 0.60$ led to a better fit of the experimental data to the calculated *k*-ratios than the value $C_0 = 0.45$ derived from the SIMS data.

Gold-implanted Silicon Wafer

The uncertainty of the *k*-ratios for an ion-implanted specimen analysed either by varying the incident energy or by crossing a SIMS crater wall, mainly results from the uncertainty of the implant depth profile used for calculations. In order to validate the approaches used for comparing measured and calculated *k*-ratios, a gold-implanted silicon wafer was chosen for these comparisons because the implant peak profile derived from SIMS analysis was very consistent with the calculated peak profile assuming a Gaussian distribution for the implant depth profile. Based on these observations, the error resulting from the parameters used to describe the

Table 3 Measured and calculated Au Mα *k*-ratios at the surface of the gold-implanted arsenopyrite specimen as a function of the incident energy

			E_p/keV							
			5	8	10	12	15	18	20	28
			Measured *k*-ratio							
			0.19	0.31	0.32	0.31	0.24	0.19	0.19	0.11
κ	z_0/nm	C_0(%)	Calculated *k*-ratio							
6250	265	0.45	0.14	0.18	0.20	0.21	0.19	0.17	0.15	0.11
6250	265	0.60	0.19	0.24	0.27	0.28	0.25	0.23	0.20	0.15
6600	210	0.66	0.27	0.32	0.33	0.32	0.28	0.24	0.22	0.15
8500	210	0.66	0.20	0.28	0.29	0.28	0.24	0.22	0.19	0.13
12500	130	0.60	0.24	0.28	0.26	0.22	0.17	0.14	0.12	0.05

implant profile is then expected to be low, making possible the comparisons between measured and calculated *k*-ratios at the surface of ion-implanted targets.

The Au Mα *k*-ratios across a SIMS crater wall were measured with a 5 and a 10 keV incident energy, successively. A graph of the Au-implant profile and predicted Au Mα *k*-ratios in Si at 5 keV are shown in Fig. 11. The calculated data using the SIMS profile of the gold implant were scaled to the experimental data and the position of the maximum was adjusted to a value 20 nm lower than the initial estimate of 320 nm. The value of 20 nm is in the order of reproducibility of the maximum position of the implant derived from several SIMS depth profiles. From calculations, it has been shown that a 5 keV incident energy is very sensitive to the maximum position of the implant below the specimen surface. By varying the maximum position by only 20 nm led to large change in the predicted Au Mα signals, but this effect rapidly decreased with energy and predictions were quite insensitive for incident energies above 10 keV. While the gold implant was clearly shown on the line scan through the crater wall at 5 keV, it rapidly became lost at higher energies. Observed and calculated Au Mα *k*-ratios along a line scan crossing a SIMS crater wall are in a good agreement using the expected depth profile of the implant resulting from theoretical calculations and SIMS data.

The Au Mα *k*-ratios were measured at the surface of the gold-implanted area with beam energy increasing from 5 to 10, 15 and 20 keV, successively. The measured data for the 5 keV incident energy were scattered indicating the presence of local enrichment of the Au concentration at the surface of the specimen. The measured concentrations were compared with the calculated data. For these calculations, the maximum depth of the implant was set equal to 300 nm, consistent with the results obtained for the case of the line scan across the crater wall at 5 keV energy. Experimental and calculated data are given in Table 4 and show a satisfactory agreement between both sets of data.

Discussion

The change in the calculated *k*-ratios as a function of the shape of the implant (assuming a Gaussian distribution) will be more or less pronounced depending on the maximum position of the implant with respect to that of the ionization depth distribution. The depth ionization functions for several incident energies were calculated for the Au Lα and the Au Mα emission lines for the analysed silicon and arsenopyrite specimens, and compared with the gold-implant Gaussian distributions derived from SIMS analysis. As shown in Fig. 12(*a*), for the Au Lα emission line, the maximum of the gold implant is very close to that of the ionization depth distribution for both matrices and incident energy values. This result contrasts with the situation encountered in the analysis of the Au Mα emission line. As shown in Fig. 12(*b*), the gold implant maximum is located deeper than the maximum depth of the ionization distribution for the silicon and arsenopyrite specimens; and a smaller dependence of the implant shape on *k*-ratio calculations is expected for the Au Mα than for the Au Lα X-ray photons. The closer the maximum of the ion implant is to the maximum of the ionization depth distribution, the more sensitive the calculated *k*-ratios will be to a small change

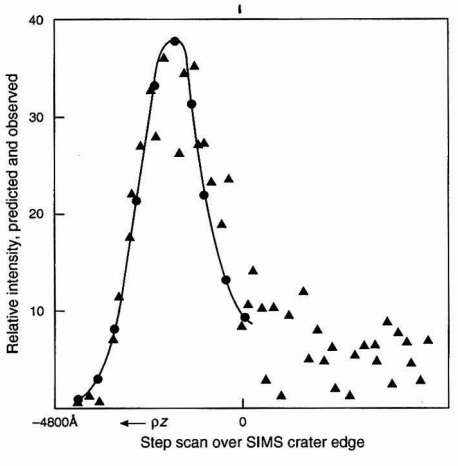

Fig. 11 Observed and calculated Au Mα *k*-ratios for a 5 keV incident energy taken along a line scan crossing a SIMS crater in a Au implanted Si wafer. ●, Calculated, and, ▲, experimental.

Table 4 Measured and calculated Au Mα *k*-ratios at the surface of the gold-implanted Si wafer as a function of the incident energy

E_p/keV	Observed* *k*-ratios	Calculated† *k*-ratios
5	0.18	0.19
10	0.30	0.30
15	0.16	0.16
20	0.11	0.10

* Peak height and † Gaussian peak centred at 300 nm (*i.e.*, 20 nm lower than SIMS position) (C_0 = 1.9 mass-%; implant width equal to 160 nm).

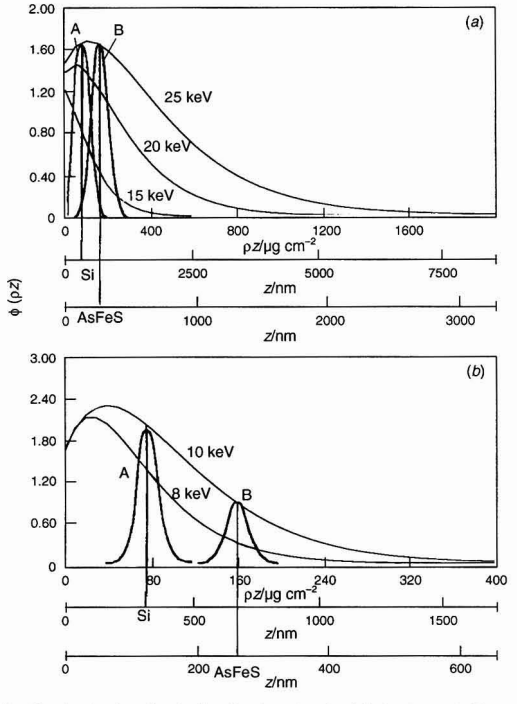

Fig. 12 Ionization depth distributions for the (*a*) Au Lα and (*b*) Au Mα and Au implant profile within an arsenopyrite specimen and an Si wafer, respectively. A, Gold-implant profile in Si and B, gold-implant profile in AsFeS.

in the shape of the implant. For a deep implant with respect to the ionization distribution, the calculated k-ratios will mainly vary with the C_0 concentration at the maximum of the implant. Such an effect was encountered for the case of the Au Mα k-ratios measured along the crater wall at the surface of the gold-implanted arsenopyrite. As shown in Fig. 9, the calculated Au Mα k-ratios remained unchanged when the width of the gold implant was set equal to $\kappa = 5000$ and $\kappa = 6220$, successively. However the calculated k-ratios were found to rapidly vary with the C_0 value (see Table 3). Such a situation is the more favourable case to validate an experimental procedure by the use of ion-implanted materials. The uncertainty in the shape of the ion implant depends on the analytical method used for studying the ion-implanted depth and also depends on the ion-implantation procedure and the intrinsic properties of the implanted substrates. Ion implantation is known to cause considerable damage to the crystalline lattice of the implanted substrate. The degree of damage depends upon the energy of the incident projectile, the atomic number and mass of the incident ion and target atoms successively (Donnelly[14]). Less damage occurs for low implantation fluences and with light atoms. When high fluences are used or when heavy atoms are implanted into crystalline substrates, an amorphous layer is created at the surface. The existence of the amorphous layer has been revealed by SEM observations of As-implanted Si wafer (Takahashi *et al.*[27]) and by optical reflectance property changes of silicon damaged by ion implantation (Hummel and Hagmann[28]). Above a critical incident dose, the amorphous layer becomes wider and buried below the specimen surface. In addition, the depth profile of the implant has been shown to depend on the electrical properties of the substrates as discussed by Oyoshi *et al.*[29] Positive surface charging at the surface of semiconductors and insulating crystals occurs during the ion implantation procedure. The effect of charging on ion implantation of glasses has been discussed by Oyoshi *et al.*[29] by comparing depth profiles obtained with and without surface charge neutralization, using an external electron flood gun, metal film coatings and electron generation from ion-irradiated metals. These authors showed that because of charging phenomena, the implanted-ion depth profile was shifted towards the surface and that the actual dose decreased with respect to the implanted profile obtained with surface charge compensation. In addition, lateral heterogeneities resulted from charging effect during the implantation procedure. The observed discrepancies between the theoretical and the measured gold implant profile within the arsenopyrite specimen may be a result of the damages induced during the implantation and the sputtering yield during SIMS analyses and it is difficult to separate both effects.

Surface Layer Deposition *Versus* Ion Implantation: Application to the Study of Surface and Bulk Charging in Insulators

Thin Surface Film Deposition as a Function of the Electric Properties of the Substrates

In this section, we investigated the reliability of calculated and measured data for metallic (gold) surface films as a function of the electrical properties of the substrates. For this purpose, a gold film was sputter-deposited on top of a pure nickel specimen, at the surface of the silicon wafer (1.1 eV band gap), and, on a natural and two synthetic ZnS specimens (3.7 eV band gap), respectively. Each specimen was separately prepared as a polished section. The full surface of each specimen was first coated. Using masks, half of the coated area at the surface of each specimen was again coated with a second gold layer deposited under the same conditions as those used for the first deposition layer. The thickness of the layer depends on the residual gas pressure in the coater chamber, the ion beam current and the time of gold sputtering. During the deposition time, the pressure and beam current may vary slightly, and the experimental conditions are maintained constant by manually adjusting these experimental factors. At the surface of the same specimen that is coated by several independent coating procedures, the reproducibility of the gold layer thicknesses was found to be better than ±5%.

The Au Lα k-ratios using a pure gold specimen as reference were measured at a 20 keV electron beam energy. Results in Table 5 show that: (*i*) the observed k-ratios, *i.e.*, the thickness of the gold layer(s), measured on surfaces that having received two gold layers are twice the k-ratios derived from measurements on surfaces coated with a single layer, supporting the reproducibility of the gold deposition procedure; and (*ii*) an increase in the gold layer thicknesses, much greater than the expected 10% reproducibility, is obtained for the insulating ZnS specimen compared with the thickness of the layers deposited on top of the conductive pure Ni and the semiconductor Si wafer.

The differences in the Au Lα k-ratios as a function of the substrates may reflect an actual thickness difference or may be an apparent variation resulting from the model and the parameters used for calculations, or from the mechanisms for dissipating the incident energy leading to discrepancies between the $\phi(\rho z)$ expressions for a conducting and an insulating material, respectively.

A possible source of error may arise from the calculations as in eqn. (6) (used for the layered specimens), it is assumed that the $\phi(\rho z)$ equation is not disrupted by the change in physical parameters at the interface of the two compounds having different atomic numbers. One approach consists of treating the electron distribution in the layer as the sum of two distributions, the first one being associated with the forward scattered electrons and the second resulting from the fraction, η_s, of electrons backscattered at the layer/substrate interface. A second approach consists of using a single expression for $\phi(\rho z)$ while taking account of the backscattering contribution by adjusting some of the parameters. Both approaches and the different means for weighting the parameters have been discussed by Hunger and Rogaschewski,[30] Packwood[12] and by Pouchou and Pichoir.[13]

In the MSG model [eqn. (3)] used for describing the ionization depth distribution, both $\phi(0)$ and β parameters are strongly dependent on the atomic number, Z, *i.e.*, strongly dependent on the backscatter coefficients at the outer surface of the layer and at the interface between the layer and the substrate. According to Packwood,[12] an effective backscatter coefficient η_{eff} can be used in the $\phi(\rho z)$ equation for the layer/substrate assembly according to

$$\eta_{eff} = \eta_{sub} + \mathrm{erf}(2\alpha\ \rho z)(\eta_{layer} - \eta_{sub}) \qquad (8)$$

Calculations based on the use of a weighted backscatter coefficient has been proved to be a satisfactory approximation by Packwood and Remond[21] who compared measured and calculated data for a variety of metal layers deposited on top of metallic substrates. In the present study, because the pure Ni

Table 5 Au Lα-ratios and calculated thickness of gold layer(s) on top of several substrates (20 keV incident energy)

	Single Au surface layer		Two superimposed Au surface layers	
Specimen	Au k-ratio (%)	d/nm	Au k-ratio (%)	d/nm
Si	5.7	19	—	
Ni	6.7	21	13.8	40
ZnS*	8.9	27.5	17.4	50

* Natural ZnS specimen from the Santander deposit (Spain).

substrate and the ZnS crystals have close atomic numbers, the deviation between the calculated gold layer thicknesses cannot only result from the use of an effective backscatter coefficient for calculations, and the observed deviation must be regarded as a consequence of the strong insulating nature of the ZnS substrates compared with the Ni metal and Si semiconductor.

We examined the role of the near sub-surface ion-implanted area on the analysis of gold layers deposited on top of an insulating substrate. For this purpose, the Ga-implanted synthetic ZnS specimens were analysed.

Thin Surface Film Deposition on Top of Implanted and Non-implanted Insulating Substrates

The two Ga-implanted synthetic ZnS specimens were used. The Cleartran ZnS specimen has an electrical resistivity greater than 10^{13} Ω cm and the yellow-coloured ZnS substrate has a 10^{12} Ω cm resistivity.

The two independently prepared polished sections containing the clear and yellow ZnS crystals that were partly Ga implanted, were gold sputter-coated. Using masks, non-implanted and implanted areas were gold coated, some areas of these surfaces remaining uncoated. The Au Mα *k*-ratios using a pure gold specimen as reference were measured on both the Ga-implanted and non-implanted ZnS substrates, sucessively. The *k*-ratios were measured with a 8 keV incident energy. As shown in Table 6, for both the yellow and the clear synthetic ZnS specimens, the Au Mα *k*-ratios were found to be higher when measured on the non-implanted area than those measured for the gold layer deposited on top of the Ga-implanted ZnS area.The average relative *k*-ratios for the Au Mα emission peak, $k'(\text{Au M}\alpha) = k$ (Ga-implanted area)/ k (non-implanted area) varied from 1.06 ± 0.06 for the case of the yellow crystal to 1.03 ± 0.03 for the case of the clear crystal.

Because of the presence of Ga ($Z = 31$), the mean atomic number of the first hundreds of nanometres in thickness of the implanted area is higher than that of the same thickness of the non-implanted material. This effect should lead to an increase in the number of backscattered electrons at the gold/implanted area interface than that occurring at the gold layer/non-implanted interface. Consequently, the contribution of the number of backscattered electrons to the production of X-ray photons within the gold surface layer should lead to a higher Au Mα *k*-ratios at the surface of the Ga-implanted areas than those measured at the surface of the non-implanted specimens, while the opposite situation is observed in Table 6. In addition, the differences in the Au Mα *k*-ratios measured at the surface of the clear and yellow ZnS specimens are greater than the expected experimental error resulting from the layer deposition reproducibility. These observations lead to the conclusion that the differences in the measured thicknesses are apparent variations to be related with the differences in the electrical properties of the analysed specimens as previously discussed by Remond *et al.*[31] studying the X-ray and cathodoluminescence emissions of similar specimens.

In order to illustrate the role of electrostatic charging phenomena on the apparent increase in the gold layer thicknesses as a function of the substrates, energy dispersive X-ray spectra were performed on an uncoated ZnS area and on an uncoated Ga-implanted area. The incident beam energy was 5 keV. As shown in Fig. 13(*a*) the Duane–Hunt limit for the continuous emission for the analysed uncoated area was 2.5 keV indicating that a 2.5 kV retarding potential had developed at the surface. The Duane–Hunt limit is the maximum energy of the emitted X-ray photons, thus indicating the maximum kinetic energy for the electrons scattered into the volume of the insulating specimen exposed to the electron beam. Thus, the Duane–Hunt limit shows the presence of surface charging sufficient to reduce the energy of the incident electrons. As shown in Fig. 13(*b*) the Duane–Hunt limit observed when analysing the ion-implanted area was equal to the incident energy value showing that no retarding field existed, *i.e.*, the excess of electrical charges was evacuated to the ground potential through the ion-implanted zone.

During the electron bombardment, the electric potential is not equal to zero outside an insulating material bounded with vacuum. As discussed by Cazaux,[32,33] inside the insulator, the field is not constant, the normal component of the built-up electrical field is expected to change direction from the surface into the bulk for a vacuum/dielectric interface, this component is first directed towards the surface, then becomes zero at an inversion point, and is then directed towards the bulk with an increasing amplitude exhibiting a maximum close to the end of the real charge distribution (maximum penetration depth of the incident electrons). The existence of a surface retarding potential has been illustrated by studying the change in the Duane–Hunt limit of the continuous X-ray emission distribution at the surface of uncoated Ga-implanted and non-implanted ZnS surfaces. When the specimen surface is coated with a thin conductive layer at earth potential, the surface potential is equal to zero and no beam displacement can occur, because the electric potential in the vacuum is also equal to zero. However, while the surface coating prevents against surface charging (*i.e.*, making it possible to observe insulating materials with the SEM), charge trapping within the bulk compound still occurs, and the internal electric field may be very strong. The presence of the internal retarding electric fields resulting from a bulk negative trapped charge tends to reduce the depth of complete penetration of the incident electrons and simultaneously to push the point of complete diffusion towards the specimen surface. Consequently, these phenomena will reduce the absorption pathlength for the

Table 6 Au Mα *k*-ratios for a 8 keV incident energy measured at the surface of gold-coated synthetic ZnS specimens

Specimen	k(Au Mα) (%) Non-implanted area	k'(Au Mα) (%) Ga-implanted area	k/k'
Clear ZnS	28.4 ± 0.4	27.5 ± 0.3	1.03
Yellow ZnS	35.6 ± 0.7	33.7 ± 0.6	1.06

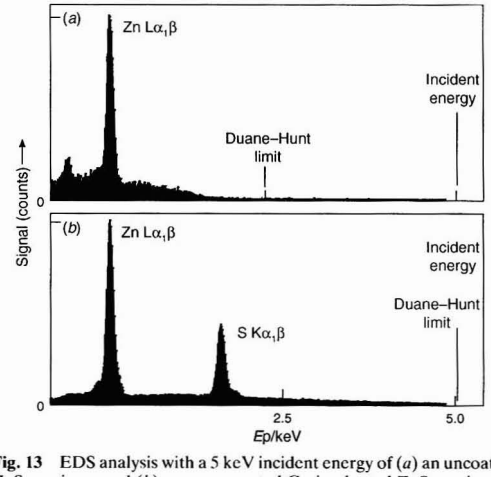

Fig. 13 EDS analysis with a 5 keV incident energy of (*a*) an uncoated ZnS specimen and (*b*) on an uncoated Ga-implanted ZnS specimen.

generated photons before they escape the insulating specimen with respect to the absorption found for a metallic target, the latter not being affected by the development of internal electrical fields. Simultaneously, the internal field in the insulating materials tends to increase the electron backscatter coefficient leading to an increase in the loss of ionization and an increase in the ionization function, $\phi(0)$, at the specimen surface. These effects are supported by the electrostatic theory, discussed by Cazaux[32,33] and by Monte-Carlo simulation for the trajectories of electrons in presence of internal electric fields induced by a pre-irradiation dose as calculated by Kotera and Suga[34] and computer simulation of the transport equation as calculated by von Fitting *et al.*[35]

The development of bulk charging leading to a change in the electron distributions within the ZnS crystals may lead to an increase of the number of backscattered electrons contributing to the production of Au photons in addition to those created by the electrons moving in the forward direction and consequently, leading to the appearance of an increase in the thickness of the gold surface films on top of the insulating substrates compared with the thickness of the layers on top of conductive substrates. This effect was illustrated by comparing the Au Mα k-ratios for a gold surface film deposited on top of an ion-implanted and a non-implanted area of the same ZnS specimen. In addition, the apparent increase in the surface film was found to depend on the electrical conductivity of the ZnS substrates. The continuous change in the conductivity as a function of depth resulting from ion implantation avoids the sharp electrical discontinuity resulting from a surface film deposition onto a substrate and may offer an approach for studying the depth distribution of the internal electrical fields by modifying the ionization depth distribution within insulating materials.

Conclusion

By using thin film deposition and ion implantation we aimed to create a controlled heterogeneity as a function of depth within the EPMA analysed volume. For this purpose the apparent concentrations were varied by varying the incident energy, *i.e.*, changing the sampling depth below the specimen surface and, by traversing the ion-implanted region revealed by making a groove or a SIMS crater in the surface of the specimen. The use of such methods and materials is justified because the technology is available to produce known deposit and implantation profiles and because theoretical models are available to predict the number of generated and emitted X-ray photons as a function of depth.

Coated and ion-implanted materials offer an original approach for creating reference compounds for the analysis of elements present at low levels with the EPMA. However, rather than just being used for routine analytical purposes, a major use for these materials is to validate the limits of detection for the EPMA, which are often derived solely on statistical grounds and which neglect the accuracy of the measurements. Statistical limits of detection can only be calculated after the experimental approach for obtaining accurate data has been validated. The particular example of analysis of Au at trace levels using the Au Lα emission peak shows that the attempt to improve the statistical precision by the use of peak integration may, in some circumstances, be accompanied by a decrease in the accuracy of quantitative data and a careful examination of the peak shape must be performed before deciding on the appropriate X-ray intensity measurement procedure.

The use of ion-implanted materials for quantitative analysis may not be suitable for a general application because of uncertainties in our knowledge of the ion implantation profile although to some extent they can be theoretically predicted or, alternatively, measured by an independent analytical technique such as SIMS. In some instances, a satisfactory agreement between observed and calculated profiles is obtained and the implanted materials can easily be used for reference materials.

The insulating behaviour of the substrate may affect both the depth distribution of the implanted ions and the electron loss mechanisms, *i.e.*, the ionization depth distribution, during the EPMA analysis with respect to these distributions for a conductive material. Ion implantation may be an original approach to continuously modify the electrical conductivity as a function of depth in order to better understand charging phenomena of insulating materials during EPMA analyses.

The authors are grateful to S. L. Chryssoulis for providing the gold-implanted arsenopyrite and silicon specimen analysed by SIMS. The authors thank Professor P. D. Townsend for the implantation of the synthetic ZnS. This work was financially supported by a BRGM research project (BRGM contribution number 95015).

Appendix

The error function erf(x) and the complementary error function erfc(x) are defined by

$$\mathrm{erf}(x) = \frac{2}{\sqrt{\pi}} \int_0^x \exp(-t^2)\,\mathrm{d}t$$

and

$$\mathrm{erfc}(x) = \frac{2}{\sqrt{\pi}} \int_x^\infty \exp(-t^2)\,\mathrm{d}t$$

with

$$\mathrm{erf}(x) + \mathrm{erfc}(x) = 1$$

For most EPMA applications the numerical computation of erf (x) is based on the polynomial approximation

$\mathrm{erf}(x) = 1 - (a_1 t + a_2 t^2 + a_3 t^3) \exp(-x^2) + \varepsilon(x)$
$t = 1/(1 + px)$ and $\varepsilon(x) \leq 2.5 \times 10^{-5}$
$p = 0.47047$, $a_1 = 0.3480242$, $a_2 = -0.0958798$, $a_3 = 0.7478556$

References

1 Marinenko, R. B., in *Electron Probe Quantitation*, ed. Heinrich, K. F. J., and Newbury, D. E., Plenum Press, New York, 1991, pp. 251–260.
2 Fialin, M., *X-Ray Spectrom.*, 1990, **16**, 169.
3 Remond, G., Cazaux, J., Fialin, M., and Packwood, R. H., *Microbeam Anal.*, submitted for publication.
4 Marion, C., and Vannier, M., *J. Microsc. Spectrosc. Electron.*, 1983, **8**, 31.
5 Fialin, M., Henoc, J., and Remond, G., *Scanning Microsc.*, 1993, Suppl. 7, 153–166.
6 Remond, G., Campbell, J. L., Packwood, R. H., and Fialin, M., *Scanning Microsc.*, 1993, Suppl. 7, 89–132.
7 Remond, G., and Campbell, J. L., in *Microbeam Analysis*, ed. Michael, J. R., and Ingram. P., San Francisco Press, San Francisco, 1990, pp. 59–66.
8 Remond, G., Fialin, M., Packwood, R. H., Gilles, C., and Rouer, O., *Microbeam Anal.*, submitted for publication.
9 Remond, G., Giraud, R., and Packwood, R. H., *Scanning Electron Microsc.*, 1984, **I**, 151.
10 Remond, G., Holloway, P. H., Kosakewitch, A., Ruzakowski, P., Packwood, R. H., and Taylor, J. A., 1985, *Scanning Electron Microsc.*, 1985, **IV**, 1305.

11 Remond, G., Packwood, R. H., Gilles, C., and Chryssoulis, S., *Proceedings of the 50th Annual Meeting of the Electron Microscopy Society of America*, ed. Bailey, G. W., Bentley, J., and Small, J., San Francisco Press, San Francisco, 1992, pp. 1652–1653.
12 Packwood, R. H., in *Electron Probe Quantitation*, ed. Heinrich, K. F. J., and Newbury, D. E., Plenum Press, New York, 1991, pp. 83–104.
13 Pouchou, J. L., and Pichoir, F., in *Electron Probe Quantitation*, ed. Heinrich, K. F. J., and Newbury, D. E., Plenum Press, New York, pp. 31–76.
14 Donnelly, J. P., in *III-V Semiconductor Materials and Devices*, ed. Malik, R. J., Elsevier, Amsterdam, 1989, pp. 331–428.
15 McIntyre, N. S., Cabri, L. J., Chauvin, W. J., and Laflamme, J. H. G., *Scanning Electron Microsc.*, 1984, **III**, 1139.
16 Cabri, L. J., Chryssoulis, S. L., De Villiers, J. P. R., Laflamme, J. H. G., and Buseck, P. R., *Can. Mineral.*, 1989, **27**, 353.
17 Cabri, L. J., Chryssoulis, S. L., Campbell, J. L., and Teesdale, W. J., *Appl. Geochem.*, 1991, **6**, 225–230.
18 Chryssoulis, S. L., *Ion Probe Microanalysis of Gold in Common Sulphide Minerals and Applications of Enhanced Recovery From Refractory Gold Ores*, CANMET contract Report 79037–01-SS, p. 380.
19 Chryssoulis, S. L., Cabri, L. J., Salter, R. S. in *Proceedings of the International Symposium on Gold Metallurgy, Refractory Gold*, ed. Salter, R. S., Wyslouzil, M. C. and Donald, G. W., Pergamon Press, Toronto, 1987, pp. 235–244.
20 Chryssoulis, S. L., Cabri, L. J., and Lennard, W., *Econ. Geol.*, 1989, **84**, 1684.
21 Packwood, R. H., and Remond, G., *Scanning Microsc.*, 1993, **6**, 367.
22 Scott, V. D., and Love, G. in *Electron Probe Quantitation*, ed. Heinrich, K. F. J., and Newbury, D. E., Plenum Press, New York, 1991, pp. 19–30.
23 Packwood, R. H., and Brown, J. D., *X-Ray Spectrom.*, 1981, **10**, 138.
24 Packwood, R. H., and Milliken, K. S., *A General Equation for Predicting X-ray Intensities From Stratified Samples in the Electron Microprobe*, CANMET report, PMRL/85–25 (TR), 1985.
25 Self, P. G., Norrish, K., Milnes, A. R., Graham, J., and Robinson, B., *X-ray Spectrom.*, 1990, **19**, 59.
26 Pouchou, J. F., and Pichoir, F., in *Microbeam Analysis*, ed. Newbury, D. E., Plenum Press, New York, 1988, pp. 319–324.
27 Takahashi, Y., Yabuuchi, Y., Inazato, S., Ogura, K., and Ono, A., *Jpn. J. Appl. Phys.*, 1993, **32**, 1477.
28 Hummel, R. E., Xi, W., and Hagmann, D. R., *J. Electrochem. Soc.*, 1990, **137**, 3583.
29 Oyoshi, K., Tagami, T., and Tanaka, S., *Jpn. J. Appl. Phys.*, 1993, **32**, 5170.
30 Hunger, H. J., and Rogaschewski, S., *Scanning*, 1986, **8**, 257.
31 Remond, G., Cazaux, J., Chapoulie, R., Ermakoff, P., Fialin, M., and Packwood, R. H., *Microbeam Anal.*, submitted for publication.
32 Cazaux, J., *J. Microsc. Spectrosc. Electron.*, 1986, **11**, 293.
33 Cazaux, J., in *Ionization of Solids by Heavy Particles, NATO, Advanced Research Workshop*, ed. Baragiola, R. A., *NATO ASI Series*, Plenum Press, New York, 1993, Series B: Physics **306**, 325–350.
34 Kotera, M., and Suga, H., *J. Appl. Phys.*, 1988, **63**, 261.
35 von Fitting, H. J., Glaefeke, H., Wild, W., Frank, M., and Muller, X., *Phys. Status Solidi A*, 1979, **27**, 13.

Paper 5/00184F
Received January 11, 1995
Accepted March 10, 1995

Method of X-ray Fluorescence Analysis For Environmental Lead, Especially in Household Dust, Using Thin-film Principles*

Jacques Renault and Chris McKee
New Mexico Bureau of Mines and Mineral Resources Division, New Mexico Institute of Mining and Technology, Campus Station, Socorro, NM 87801, USA

Environmental lead in a variety of matrices can be determined by wavelength-dispersive X-ray fluorescence (XRF) spectrometry using thin-film principles. Transfer tape or double-coated adhesive tape is attached to a disc that fits the spectrometer's sample changer and a powdered sample is applied to the tape. Except for direct interferences, matrix effects are absent and the graph of net counts per second per unit mass against concentration is linear and passes through the origin. Using a single reference standard, lead concentration is calculated using the equation $[Pb]_x = (C_x m_s / C_s m_x)[Pb_s]$, where [Pb] is lead concentration, C is net count rate, m is mass and subscripts x and s designate unknown and standard, respectively. A test of the method using Canadian CCRMP reference materials FeR-1 and SY-2, American USGS standard GXR-2 and French ANRT standard VS-N, which cover the range from 85 to 5200 μg g^{-1} Pb, shows that lead can be determined by this method with an analytical error of 10% relative. Details of the procedure are given and the device for mounting and attaching the adhesive tape and for mounting the sample is shown. A practical application of the method to the determination of lead in household dust at the 540 μg g^{-1} level with 5% precision for samples weighing about 10 mg is described and it is shown that the method compares favourably with flame atomic absorption spectrometry for 0.5 g samples.

Keywords: Lead determination; dust; X-ray fluorescence spectrometry; thin film; sample preparation

Introduction and Theory

At a National Institute of Standards and Technology (NIST) workshop held at Boulder, CO, in 1993 to review the use of X-ray fluorescence (XRF) spectroscopic analysis of environmental lead, entitled 'Accuracy of Lead Measurements of Paint, Soil, and Dust Samples by Laboratory-based X-ray Fluorescence,' the principal consideration was the poor correlation of XRF results compared with flame atomic absorption spectrometry (FAAS) and inductively coupled plasma (ICP) results reported in Williams *et al.*.[1] Although the XRF analyses reported by the EPA study were internally consistent, they were unacceptably lower than the FAAS and ICP analyses.

The low XRF results for lead were attributed to a general lack of suitable reference materials available for environmental XRF analysis. In addition, there is a considerable variation in XRF protocols for lead determination. Important variations in XRF protocols are found in the methods of matrix correction.

In 1993, Austin *et al.*[2] reported on the use of the thin-film method for the determination of Pb in heavy mineral fractions of contaminated soil at the 1% m/m level. Renault and McKee[3] presented preliminary results of a more refined thin-film XRF method of Pb determination at the Boulder, CO, meeting. This method presents to the X-ray spectrometer a sample of very fine powder dusted onto an adhesive substrate. Since then, our methodology has been further tested, simplified and refined. We present here a review of our method and give further results.

The XRF analysis of powders in the form of thin films has been known for many years. Salmon[4] applied the thin-film method to the analysis of mineral samples. His approach was to encapsulate the powdered sample between sheets of Mylar and present it upside down to the X-ray beam in a spectrometer using inverted geometry. He experienced difficulties in the preparation of uniform samples and in attenuation of the X-ray beam by the Mylar film.

During the last 30 years, the application of the thin-film method to mineral powders has been reported on very little, but we have found it attractive for environmental lead determination at environmental agency action levels greater than 100 μg g^{-1}. Modern XRF spectrometers with closely coupled X-ray tube–sample geometries and upright sample positioning favour the elimination of the Mylar film covering the sample and make the thin-film method for mineral powders more feasible than it was.

It is important that the film is thin enough for absorption effects to be insignificant. Tertian and Claisse[5] presented the theory of thin-film analysis and gave the following rule of thumb for the film thickness required to ensure linearity of count rate *versus* concentration:

$$\rho x \ll \frac{100}{\mu'}$$

where ρ is density, x is film thickness and

$$\mu' = \frac{\mu_1}{\sin \psi_1} + \frac{\mu_2}{\sin \psi_2}$$

μ_1 and μ_2 being the mass absorption coefficients for the film at the incident and secondary wavelengths, respectively, and ψ_1 and ψ_2 the incident and take-off angles of the spectrometer, respectively.

Consider a thin film of household dust composed of 10 μm grains of 50% m/m calcite and 50% m/m quartz. Ignoring the void space, its average density is 2.68. Its mass absorption coefficients for Rh Kα and Pb Lβ are 3.8 and 14.4, respectively. The incident and take-off angles for our spectrometer are 90° and 37.2°, so μ' is calculated to be 27.5. If the film of the dust is composed of non-overlapping grains, is 10 μm thick and has $\rho x = 0.00268$ g cm^{-2}, which is much less than $100/\mu' = 3.62$, under these circumstances the mass of sample on a 2.54 cm diameter disc is 0.0136 g, which is consistent with the sample masses we measured in our tests.

* Presented at Geoanalysis 94: An International Symposium on the Analysis of Geological and Environmental Materials, Ambleside, England, September 18–22, 1994.

The advantages of the method over conventional XRF geochemical methods are that only 10–20 mg of sample material are required and that matrix effects are essentially eliminated. A small sample size is of considerable advantage in collecting dust from surfaces in an occupied dwelling. The disadvantages are that the count rates require long counting times for good precision and that several weighing steps are required. Inhomogeneity can be a problem with small samples and the analyst must minimize this by using samples that have a very fine grain size of the order of 5–10 μm and by spinning the sample in the spectrometer. If large amounts of sample are available, say several grams, another method should be used in order to avoid the sampling errors inherent with samples of only a few milligrams.

The absence of matrix effects allows a simplified calculation of results that is based on linear proportionality between an unknown and a single standard. The count rate per concentration per unit mass is the same for both unknown and standard when there are no interferences. Using the determination of Pb as an example:

$$\frac{C_x}{[Pb_x]m_x} = \frac{C_s}{[Pb]_s m_s} \quad (1)$$

where C is net count rate, m is mass and subscripts s and x represent the standard and an unknown, respectively. Rearranging eqn. (1) for the determination of the unknown, $[Pb]_x$,

$$[Pb]_x = \frac{C_x m_s}{C_s m_x}[Pb_s] \quad (2)$$

An additional benefit of the thin-film method is that it allows X-ray diffraction (XRD) analysis on the mount used for XRF analysis.

Procedure

The sample, as a fine powder, is mounted on the sticky surface provided by double-coated adhesive film or transfer tape previously attached to a mount substrate appropriate to the spectrometer. The mount substrate can be conveniently made by compressing microcrystalline cellulose in a die designed for making pressed powder briquettes. The prepared mount is first tared, the sample powder is applied, then the mounted sample is re-weighed and the net mass of the sample is determined.

We investigated the XRF and XRD properties of various transfer tapes and double-coated tapes with paper and polyester carriers. All the test adhesives were manufactured by 3M (St. Paul, MN, USA) and are sold under the Scotch brand name.* A summary of our tape tests is given in Table 1.

Microcrystalline cellulose was used for mounting the tapes because it has no characteristic XRF lines of any consequence. In addition, discs compressed in a briquetting die fit naturally in the spectrometer's sample carrier and are easy to make. The major disadvantages of cellulose as a substrate for adhesive are that it gives a high XRF background and has a diffraction pattern. For XRD studies, glasses make better mount substrates. Quisefit *et al.*[6] discussed methods of reducing the background in thin-film analysis.

We found no interferences for Pb in any of the tapes, but the tapes with a paper carrier have a strong Zn signal and complex XRD patterns. The XRD patterns of the double-coated polyester tapes and the transfer tapes (tapes without a carrier) have the simplest XRD patterns.

Double-coated adhesive films of almost any type work well provided that they contain no interfering elements. The tapes with a protective liner are easiest to manipulate. If an X-ray diffraction pattern is to be obtained from the same mount, tapes with paper carrier should be avoided. We found that 3M transfer tape No. 927 has the lowest XRD background signal of any of the tapes we tested. It is thin and has no carrier.

For the occasional use, the film cutter shown in Fig. 1 can be used to cut a 1 in circle from film attached to a 37 mm disc that rides in the spectrometer's sample changer. For more frequent use, it is convenient to purchase 'dots' of transfer tape that have been cut to the appropriate diameter. The dots can be centred on the carrier by means of the film cutter. At present, 1000 × 1 in dots of No. 927 cost $178 from R. S. Hughes (Albuquerque, NM, USA).

Whether the tape is cut as needed or applied as pre-cut dots, it is important that the adhesive disc is precisely centred on the carrier. This is because the X-ray flux is not uniform across the

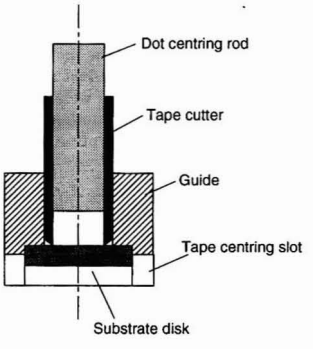

Fig. 1 Cutter for making discs of double-coated and transfer tapes.

Table 1 Summary of adhesive tapes tested

3M No.	Family	Type*	Carrier	Adhesive	Thickness/ mm	XRF lines	XRD pattern max./counts s^{-1}
400	R50	DC	Paper	Rubber	0.13	Zn	Very complex, >1500
410	R50	DC	Paper	Rubber	0.13	Zn	Complex, >2500
415	A40	DC	Polyester	Acrylic	0.10	None	Simple, >10000
443PC	R40	DC	Polyester	Rubber	0.13	None	Simple, >7500
444	A60	DC	Polyester	Acrylic	0.10	None	Simple, >6000
927	A60	ATT	None	Acrylic	0.05	None	Simple, ≈500
9460PC	A10	VHB	None	Acrylic	0.05	None	Simple, >500
9473PC	A10	VHB	None	Acrylic	0.25	None	Moderate, >5000
9500PC	A25	DC	Polyester	Acrylic	0.14	None	Simple, >6500

* DC = Double-coated; ATT = adhesive transfer tape; VHB = very high bond strength.

* The listing of trade names and company names is for information only and does not imply endorsement by the New Mexico Bureau of Mines and Mineral Resources.

sample and the unknown must occupy the same position as the standard. This matter was discussed by Quisefit *et al.*[6] Sample spinning is always important in X-ray spectrometry.

Procedure for Mounting Uncut Tape

1. Apply tape.
   a. Invert guide with slots up, and place it on a table.
   b. Insert labelled substrate disc, label towards the table.
   c. Apply tape to disc through centring slot.
   d. Remove disc and tape, and trim tape to edge of disc.
2. Cut disc.
   a. Place disc on table with tape up.
   b. Place guide over disc with slot towards the table.
   c. Lower cutter with dot centring rod into guide until they rest on tape, and press the tape down with rod.
   d. Grip disc through tape centring slot.
   e. Rotate cutter on tape several times back and forth to cut through to the substrate.
3. Remove guide leaving cutter on disc.
4. Hold disc plus cutter together and remove waste tape.
5. Store disc with its protective liner in a dust-free place prior to weighing if the sample is not to be applied immediately.

Procedure for Mounting Pre-cut Dots

1. Insert Teflon rod into the cutter and place the liner surface of a dot on the rod's end.
2. Insert substrate disc into guide.
3. Insert cutter, rod and dot into the guide, with exposed adhesive facing the substrate.
4. Push the rod with its dot onto the substrate and press them firmly together.
5. Dismantle and store the completed mount with its protective liner until ready for weighing.

The sample should be a powder with a grain size as fine as possible, as it is important that the grains fill the available space without overlap and consequent shadowing.

Procedure for Applying Sample to Tape

1. Tare the prepared briquette and tape after removing the protective liner.
2. For large amounts of sample, use the disc cutter as a guide.
   a. Align the disc cutter cylinder edge with the edge of the adhesive.
   b. Pour the sample into the cylinder and onto the adhesive.
   c. Completely cover adhesive with sample powder by shaking it in the cylinder.
   d. Brush off any sample adhering to the perimeter of the mount.
   e. Use a soft artist's brush to distribute the sample evenly if necessary.
   f. Pour off excess of sample powder and tap the mount upside down to remove what remains.
   g. Carefully wipe out inside of disc cutter.
3. For microsamples.
   a. Transfer sample onto adhesive surface with a soft artist's brush or press adhesive surface lightly on dust surface.
   b. Tap mount upside down to remove excess of sample.
   c. Brush off any sample adhering to the perimeter of the mount.
4. Re-weigh and subtract tare.

Tests of the Method

The method was tested by using several geochemical reference materials having a comprehensive range of lead concentrations. In addition, a sample of household dust collected from the attic of an occupied dwelling near an EPA 'Emergency Response Site' of a Pb contamination site was analysed by FAAS and the results were compared with XRF thin-film results from the same sample. The reference materials used are listed in Table 2.

Data were collected using a Rigaku 3064 Geigerflex wavelength-dispersive X-ray spectrometer operating at 60 kV and 45 mA. An LiF(200) analyser crystal was used with a 'coarse' collimator. Except for reference materials, 200 s fixed counts were collected on the Pb Lβ line at 28.14° 2θ, and 100 s fixed counts collected on background positions at 25.60° 2θ and 28.64° 2θ. The sample spinner was always used. The background intensity was initially determined on blanks for the measurements on standards. Later, for work with unknowns, the background was interpolated to the peak position where the signal-to-noise ratio (S/N) is 1.117 for the standard VS-N, which has a lead concentration of 1000 μg g^{-1}. The peak count rate for the standard is about 2860 counts s^{-1}. Three standard deviations of the interpolated background 200 s count is 11 counts s^{-1} (or 15 counts s^{-1} at 100 s). The limit of detection is about 37 μg g^{-1} Pb under these conditions.* Our experience shows that with low signal-to-noise ratios, interpolated backgrounds are more reliable than blank backgrounds.

Tests With Reference Materials

Samples were prepared in triplicate following the procedures given above. The 3M No. 400 tape was mounted and cut on 37 mm diameter microcrystalline cellulose briquettes weighing about 5 g and briquetted at 20 tons total load. The background was corrected after measuring the peak intensity on a blank. The data were reduced using eqn. (2) and the reference materials were treated as unknowns. The results were calculated once using VS-N and again using FeR-1. The results are summarized in Table 3.

Inspection of the last column of Table 3 shows that the precision of the analysis is of the order of 10%. The average errors for FeR-1, VS-N, GXR-2, and SY-2 are 11%, 5% 10% and 8%, respectively. Excluding FeR-1b, the accuracy is good for the two higher concentrations, moderate at 690 μg g^{-1} and poor at 85 μg g^{-1}. The dispersion shown by sample FeR-1b is attributed to inhomogeneity of the reference material at the sample sizes used. Reference material VS-N is an artificial glass reported Pb concentration of which carries a 10% relative error.[7] It shows the best reproducibility.

Table 2 Reference materials

Sample No.	Agency*	Material	Certified Pb content/μg g^{-1}
FeR-1	CCRMP	Iron formation	5200
GXR-2	USGS	Soil	690
SY-2	CCRMP	Syenite	85
VS-1	ANRT	Glass	1000

* CCRMP = Canadian Certified Reference Materials Project; USGS = United States Geological Survey; ANRT = Association National de la Recherche Technique.

* *i.e.* $\frac{11 \text{ counts s}^{-1}}{0.30 \text{ counts s}^{-1}/\mu\text{g g}^{-1}}$, where the denominator is net peak intensity per unit Pb concentration.

Columns 3 and 4 of Table 3 show that results calculated by using FeR-1b (5200 μg g^{-1}) are systematically lower than those calculated by using VS-Na (1000 μg g^{-1}). However, this bias is substantially less than the analytical variation among replications.

Fig. 2 shows a least-squares linear fit of thin-film intensity as a function of reported Pb concentration in the various reference materials. It shows that the variation in net count rate per milligram of sample *versus* reported Pb concentration is substantially linear over a range of three-orders of magnitude. This allows samples as diverse as soils, paint and household dust to be analysed with a single well-characterized standard.

Fig. 3 shows a least-squares linear fit of measured *versus* reported Pb concentrations in reference materials using the thin-film XRF method described here. It shows that calculated and reported Pb concentrations in the reference materials used for this study correspond closely.

Application to the Determination of Lead in Household Dust

Substrate discs were prepared by briquetting microcrystalline cellulose in a standard briquetting die as described for the reference materials. Dots 25.4 mm in diameter of 3M transfer tape No. 927 were applied to the substrates as described in the procedure above. It was determined that the mean mass of seven dots less their liners was 29.26 mg with an estimated standard deviation (s_{est}) of 0.55 mg. The mean mass of the adhesive dots 15 h later was 23.21 mg with an s_{est} of 1.25 mg. The 3M Industrial Specialties Division informed us that the mass loss is due to evaporation of water and a volatile resin that controls the adhesive's tackiness. It is apparent that if samples are collected in the field directly on the adhesive surface, they should remain covered until collection and weighed as soon as possible after collection.

Dust was collected from an occupied residence located about 100 m north of an EPA 'Emergency Response Site' in central New Mexico. The site was the location of a lead smelter during World War I. Within the site is an agricultural field of less than 10 acres containing soil with lead levels varying from 1000 to 3000 μg g^{-1}. During the windy season, the prevailing wind is from the south.

The residence is an occupied adobe dwelling of unknown age. Dust was collected from the upper horizontal surfaces of a 0.5 × 0.5 × 0.25 m cardboard box in the dwelling's attic. The box had lain undisturbed since 1981 when the roof of the dwelling was replaced. The box contained miscellaneous wire.

The sample mounts were transported to the site with their protective liner tape in place, and the liners were removed immediately prior to charging the adhesive. Ten samples of several milligrams each for thin-film XRF analysis were collected by sweeping dust from various places on the cardboard onto the tared mounts. A 13 mm artist's brush was used to sweep more than enough sample onto the adhesive, where it was lightly brushed to give an even distribution of dust. The disc was then inverted and tapped to remove non-adhering dust. After mounting, the discs were stored in closed plastic boxes until they could be weighed about 1 h later.

A several-gram sample of the dust was collected from one portion of the cardboard box and prepared for FAAS analysis in the New Mexico Bureau of Mines and Mineral Resources chemistry laboratories. The sample was homogenized by cone and quartering and then divided into two parts. One part was further divided into 1 g aliquots, which were analysed blind. The second part was analysed in three aliquots by the thin-film XRF method. Four FAAS analyses yielded 540, 550, 520 and 510 μg g^{-1} with a mean of 530 μg g^{-1} Pb. The three XRF analyses yielded 577, 571 and 574 μg g^{-1} with a mean of 574 μg g^{-1} Pb.

The ten samples for thin-film XRF analysis had a mean dust mass of 10.7 mg with an s_{est} of 2.1 mg. Each sample was counted twice for a total of 400 s (*i.e.*, 100 s on each of two backgrounds and 200 s on the peak) with each of three preparations of VS-N as a standard. The instrumental conditions were as given above 2 except that the background was measured on either side of the analytical peak and interpolated at the peak position.

The mean relative standard deviation (s_r) of the ten six-fold determinations was 0.0549% with an s_{est} of 0.0261 μg g^{-1}. The range of relative error using s_r as a measure was from 2.5 to

Table 3 Results of tests with reference materials using VS-N and FeR-1. Concentrations are in μg g^{-1}. Column 2 gives the reported concentrations of Pb in the reference materials. Columns 3 and 4 show the analysed results treating the reference materials as unknowns and using VS-Na and FeR-1a as the single reference materials. Column 5 shows the masses of material in each thin film and column 6 the XRF intensity per milligram

Sample No.	Reported	Anal./ VS	Anal./ FcR	Unk./ mg	Intensity/ counts s^{-1} mg^{-1}
FeR-1a	5200	5352	5200	18.4	8.46
FeR-1b	5200	4216	4096	15.3	6.67
FeR-1c	5200	5669	5508	16.4	8.96
VS-Na	1000	1000	971	10.5	1.58
VS-Nb	1000	929	902	9.6	1.47
VS-Nc	1000	1077	1046	11.1	1.70
GXR-2a	690	524	509	7.6	0.83
GXR-2b	690	474	460	4.4	0.75
GXR-2c	690	608	591	8.0	0.96
SY-2a	85	159	155	9.1	0.25
SY-2b	85	181	176	10.1	0.29
SY-2c	85	196	191	10.6	0.31

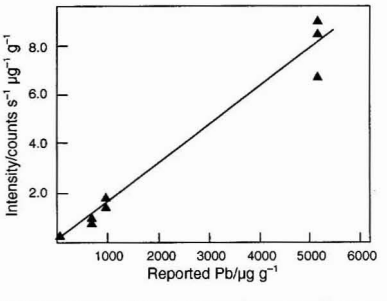

Fig. 2 Linearity of XRF thin-film intensity *versus* Pb concentration.

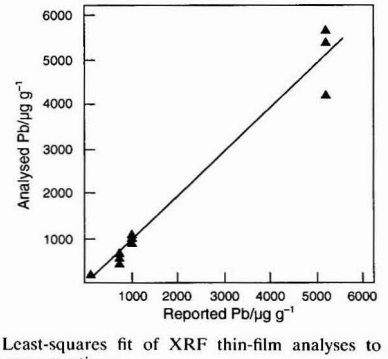

Fig. 3 Least-squares fit of XRF thin-film analyses to reference material concentrations.

11.3%. There was no correlation of s_r with sample mass. The mean of all 60 determinations on the ten samples was 544.92 μg g^{-1} with an s_r = 0.22%.

The mean Pb concentration determined on the split of the several-gram composite dust sample is 574 μg g^{-1} as compared with the mean of 530 μg g^{-1} obtained by FAAS on the composite sample and 544 μg g^{-1} found for the ten thin-film samples. The range of values is about 12% of their average.

The wide spread in the results for the ten thin-film samples is probably due to the method of their collection. No attempt was made to clean the samples of insect debris, and the surface on which the dust had collected over the years may have been inhomogeneous for a number of reasons. The composite samples, on the other hand, were cleaned of debris, which included lint and spider web and finally homogenized.

Conclusion

A method of XRF analysis to determine environmental Pb has been presented with a practical example of the analysis of household dust. Samples of the order of 10 mg are applied to an acrylic transfer tape for presentation to the spectrometer. The concentration of lead is determined with reference to the geochemical standard VS-N, which is an artificial glass containing 1000 μg g^{-1} Pb. The reproducibility of a single preparation of dust using three preparations of the standard is about 5% and the reproducibility of three preparations of a homogenized dust sample using one standard is effectively the same. The variability in lead determined in ten spot samples collected over 0.25 m^2 is about 22%.

The mean of 574 μg g^{-1} Pb determined by the thin-film XRF method on triplicates of a composite dust sample compares favourably with 530 μg g^{-1} determined by FAAS on the same composite. The mean lead concentration in the ten spot samples as determined by the thin-film XRF method is 544 μg g^{-1}, which compares well with the composite samples, and its large s_r of over 20% reflects real compositional variations at the sampling site.

The principal disadvantage of the method as compared with conventional XRF analysis of powders is that more than one weighing step is required. A second disadvantage of the method, as we have presented it, is the low S/N (1.11), requiring high count times on the peak and two background positions (400 s total). The small S/N can generate large errors in the net peak if the background is not carefully determined. It is advisable to use a substrate that is strongly absorbing in order to improve the S/N. We recommend counting the background on both sides of the peak and interpolating the background to the peak position.

The advantages of the method are its freedom from matrix correction and its applicability to measure lead in very small amounts of sample. These characteristics are significant to sampling in occupied dwellings found in diverse geological settings. The method is applicable to environmental 'action level' evaluation of total lead in finely divided materials in general. The method is exceptionally direct and free from the assumptions ordinarily found in XRF analyses. It does require careful weighing of small amounts of sample and attention to the analytical procedure. We think that its most practical use will be in the analysis of dust collected from selected locations in dwellings.

The authors thank B. Popp of the New Mexico Bureau of Mines and Mineral Resources FAAS laboratory for comparison dust analyses and P. Dalheim for directing us to the work of M. L. Salmon. The publication of this paper is authorized by the director of the New Mexico Bureau of Mines and Mineral Resources, C. Chapin.

References

1 Williams, E. E., Binstock, D. A., and Gutkecht, W. F., *USEPA Report, No. 600/R-93/235*, Atmospheric Research and Exposure Laboratory, Research Triangle Park, NC, December, 1993.
2 Austin, G. S., Brandvold, L. A., and Renault, J., *Min. Eng.*, 1993, **45**, 396.
3 Renault, J., and McKee, C., *New Mexico Bureau of Mines and Mineral Resources Open File Report*, No. 395, New Mexico Bureau of Mines and Mineral Resources, Socorro, NM, 1993.
4 Salmon, M. L., *Adv. X-Ray Anal.*, 1962, **5**, 389.
5 Tertian, R., and Claisse, F., *Principles of Quantitative X-Ray Fluorescence Analysis*, Heyden, London, 1982, pp. 278–304.
6 Quisefit, J. P., de Chateaubourg, P., Garivait, S. and Steiner, E., *X-Ray Spectrom.*, 1964, **23**, 59.
7 Govindaraju, K., *Geostand. Newsl.*, Special Issue, July 1989, 94.

Paper 4/05851H
Received September 26, 1994
Accepted November 11, 1994

Analysis and Characterization of Water Treatment Plant Sludges by X-ray Fluorescence Spectrometry*

H. Margaret West and Jess Cawley
Materials Research Institute, Sheffield Hallam University, Sheffield, UK S1 1WB

Robert Wills†
School of Science, Sheffield Hallam University, Sheffield, UK S1 1WB

Samples of sludge from various processes in an electroplating works were analysed for elemental content by X-ray fluorescence (XRF) spectrometry prior to disposal by landfill. The samples were first examined in compressed powder pellet form using a semiquantitative package in order to establish the analytes present before being fused into glass beads and analysed on a wide range oxide calibration prepared specifically for these sludges. The quantitative analytical programme used a previously developed novel calibration method which was tested using a suite of certified reference materials. Sample preparation reproducibility and instrumental precision trials were also performed. The carbon and sulfur contents of the sludges were determined using an induction furnace combustion technique and an attempt was made to characterize the sludges by X-ray diffraction. The project shows that the XRF approach using a combination of semiquantitative and quantitative analysis provides a rapid, comprehensive and cost effective means of ensuring that the waste products are thoroughly characterized prior to disposal.

Keywords: Electroplating process sludge; X-ray fluorescence spectrometry; wide range oxide calibration

Introduction

Legislation introduced to control the environmental consequences of industrial processes has resulted in challenges for both the analyst and the industrialist. Waste is subject to close scrutiny in order to ensure that the producer complies with the law with regards to its disposal. In the metal finishing industry, sludges generated during the process often contain concentrations of heavy metals and phosphates that are known to be particularly damaging to the ecosystem. Collaboration between the Forschungsinstitute fur Edelmetalle und Metallchemie (FEM), Schwabisch Gmund, Germany and Sheffield Hallam University has resulted in a project to analyse these sludges by XRF.

* Presented at Geoanalysis 94: An International Symposium on the Analysis of Geological and Environmental Materials, Ambleside, England, September 18–22, 1994.

† Present address: Oxford Instruments, Industrial Analysis Group, 19/20 Nuffield Way, Abingdon, Oxon, UK OX14 1TX.

Phosphating Process

The sludges examined were residues from a phosphating process used in the preparation of under layers for paint finishes and the production of sealed corrosion protection.

The process is dependent upon the fact that divalent zinc forms primary, secondary and tertiary phosphates, the first being soluble, the second sparingly soluble and the last insoluble. The primary phosphates form in hot, dilute phosphoric acid solution and the object of the operation is to precipitate tertiary phosphate onto the metal surface in a three-stage mechanism. Coatings therefore consist of mixed phosphates, but once the initial layers have been formed the subsequent layers consist mainly of zinc phosphate with the over-all composition corresponding to $Zn_3(PO_4)_2{\cdot}Zn(OH)_2$ or $Zn_3(PO_4)_2{\cdot}H_2O$. The coated object is then rinsed to remove all soluble phosphates.

After oxidation of the cyanides, present from a number of sources, such as alkaline cleaners used to prepare the substrate and the reduction of chromates, the soluble metallic contents of the effluents are precipitated out as insoluble compounds and removed as a semi-solid sludge. Following a de-watering process to increase the solid content to approximately 50% by mass the sludge is ready for disposal by landfill.

As sludges from this type of process must be treated as unknowns, an initial semiquantitative analysis was used to identify the elements present in order to ensure that the analyst adopted the appropriate analytical method(s) to provide the producer with the necessary data for compliance with the disposal legislation.

The semi-quantitative method used for this project was the Philips Uniquant 2 program which provides data on elements from fluorine to uranium in the periodic table. The package allows the user to input prior knowledge of the sample such as the dilution, sample area, mass/viewed area, the sample's chemical nature and can correct for binders and backings used in the sample preparation.

The 19 elements identified in the five sludges examined were then quantified using the method described by Giles *et al.*,[1] which is based on the use of theoretical correction coefficients (Alphas) introduced by de Jongh[2,3] in 1973 and further explored in 1979. The technique uses only two 'standards' to define each calibration line, a blank or zero concentration, and a top standard made from a pure source of each element of interest. A set of Alpha coefficients is used to correct for matrix effects.

As the calibration standards and unknowns were prepared as glass beads fused with lithium tetraborate at 1250 °C, there

would be significant loss of volatiles such as carbon and sulfur, these analytes were determined by an induction furnace combustion technique.

Experimental

Five samples of sludge were made available by FEM.

(*i*) G1A: a fine, dry powder, beige–yellow in colour with no odour. This sample was received in a dried and homogenized state with a quoted moisture content but no detail as to the preparation methods used.

(*ii*) G1B: the raw form of G1A consisting of solid, brittle particles with some smaller coarse grains. Again beige–yellow with no odour.

(*iii*) G2: a particulate, dark brown sludge, very moist with a pungent, unpleasant odour.

(*iv*) G3: a very moist, grey sludge which was coarse grained and contained some small brown particulates and was odourless.

(*v*) G4: a moist, green sludge with mainly coarse grains and some large, brittle particles and odourless.

Moisture Content and Loss on Ignition

The moisture content of samples G1B to G4 was determined by drying at 105 °C for 24 h and compared with the moisture value quoted for G1A. All five samples were then ground in agate to pass through a 75 × 10 nm sieve. Agate was selected as the grinding medium to minimize contamination.

A loss on ignition (LOI) was determined at 1000 °C for 2 h on all five samples. Whilst the loss corresponds to the oxidation of volatiles such as sulfur and carbon, and to the loss of residual water molecules, it is also possible for samples to show a mass gain on ignition if there are elements present that may be oxidized to a higher state.

Each sample was prepared for the semiquantitative XRF analysis by compressing 20 g of the dried, ground material into a 40 mm diameter aluminium cup at 30 kN for 10 s. The resultant pellets were robust and able to withstand the vacuum medium in the spectrometer.

The Uniquant 2 XRF package was used to calibrate the spectrometer and provide semiquantitative analyses. The spectrometer measures intensities at 2θ angles corresponding to the major K or L emissions of the analytes. A suite of 60 calibration samples, covering each element to be quantified, and a Teflon sample (used for fluorine and background intensities) were measured to produce a calibration line for each element.

When an unknown sample is measured, the program uses a series of 'kappa' algorithms to relate the intensities from the unknown to the calibrations. The kappas are sensitivity values for each element and are used with a fundamental parameters approach to calculate the matrix effects. The analysis time is approximately 12 min.

Quantitative XRF Analysis

When powdered materials are analysed by XRF, particle size effects and macro-scale inhomogeneities may be minimized by grinding and pelletizing but not completely removed as the harder compounds are not broken down and segregation by particle size may occur during pressing. In some materials softer compounds may coat harder particles (smearing) and hence the analytical surface becomes unrepresentative of the whole.

The sample preparation method adopted for the quantitative analysis of the sludges overcame these mineralogical effects by fusing the material with a flux, $Li_2B_4O_7$ and thereby forming a glass bead. However, the dilution used, 1 part of sample to 10 parts of flux, leads to a higher limit of determinability (five times the limit of detection) then that achieved with a pressed powder pellet.

The spectrometer was calibrated for 19 elements detected in the five sludges by the Uniquant 2 program. Correlation between the net count rate and the chemical concentration may only be linear for a limited concentration range and in most instances the calibration line deviates from linearity owing to absorption effects. Corrections for these commonly termed matrix effects are applied to 'pull' the calibration back to linearity and thereby provide a wide range calibration.

In the past, laboratories have calibrated spectrometers using large numbers of certified reference materials to establish the primary calibration line and calculate empirical inter-element correction coefficients (Alphas). This generation of the Alpha factors by regression analysis on each line using an iterative fitting procedure to refine the calibration was time consuming.

The method described by Giles *et al.*,[1] in which the use of theoretically based correction coefficients and the concept of 'apparent concentration' which is related linearly to the measured intensity, was adopted for this work. The procedure was actually one of recalibration using the measurement parameters for the analytical program, GERMAN as shown in Table 1. The algorithm used is in the form

$$C_i = D_i - \sum_l L_{i,l}Z_l + E_i \frac{R_j}{R_{\text{int rat}}} \times \left[1 + \sum_j a_{i,j}\frac{Z_j}{100} + \sum_k b_{i,k}\frac{Z_k}{100 + C_i} + \sum_{m,n} g_{i,m,n}\frac{Z_m Z_n}{10\,000}\right]$$

Where C_i is the calculated concentration of the element i; D_i is the correction for fixed background of element i; $L_{i,l}$ is the line overlap correction factor for line overlap of element i by element l; E_i is the calibration constant representing the inverse slope of the calibration line for element i; R_i is the net count rate for element i; $R_{\text{int rat}}$ is the net count rate of internal ratio channel (if no internal channel is used $R_{\text{int rat}}$ is set to 1); $a_{i,j}$ is the constant representing the matrix correction for element j on element i; $b_{i,k}$ is the constant representing matrix correction for the element k on element i; $g_{i,m,n}$ is the constant representing matrix correction for the combination of element m and element n on element i; and Z_q is the count rate in kcounts s^{-1} or concentration, expressed as a percentage by mass of element q, where q represents j, k, l, m and n.

The measured X-ray intensity of an analyte may be subject to errors from spectral line overlaps from adjacent emission lines. These effects may be corrected by measuring the single element standards as unknowns on the 'new' calibration. The reported concentrations of the elements, j, other than the calibrant, i, should be zero (±0.02%). Where the reported concentration for an element, j, was found to be significantly higher, this was owing to a line overlap. The correction factor for such an effect is given by

$$L = C_j/C_i$$

where L is the line overlap correction factor for element j on element i expressed as %j per %i; C_j is the reported concentration of oxide j; and C_i is the known concentration of calibrant oxide i.

The complete calibration was then tested for accuracy and precision prior to the analysis of the sludges.

Carbon and Sulfur Determination

It is known that volatile components such as sulfur are lost during the preparation of fused beads and that whilst the latest generation of X-ray spectrometers are able to analyse carbon in metals, the analysis of carbon in powders is still an

'adventure'. An alternative to the XRF method was needed for the accurate determination of these components. Therefore the samples were analysed using a Leco CS444 induction furnace combustion analyser and the results checked against BCS 489-1 and BCS 484-1 certified reference materials.

X-ray Diffraction

The dried samples were also examined by X-ray diffraction to give information on any crystalline structures present in the samples.

Results and Discussion

Moisture Content and Loss on Ignition

The moisture content of the sludges is given in Table 2, sample G2 was found to be hygroscopic. The moisture determination on sample G1A was performed by FEM and quoted with the dried sample.

The 24 h drying time at 105 °C ensured removal of the free moisture from the sludges whilst the loss on ignition at 1000 °C removed any chemically bound water present as ligands in the metal ion complexes and those volatiles such as carbon and sulfur, either in their free elemental state or as constituents in compounds. The loss on ignition data, expressed on a dry mass basis, are given in Table 3.

Semiquantitative XRF Analysis

Care must be exercised when selecting and performing any sample preparation procedure to avoid contamination of the samples from equipment such as grinding mills. For this reason the sludges were pulverized in agate. Laboratory staff must also take appropriate action to avoid inhalation of dusts whilst handling powders.

The compressed powder pellets used for the semiquantitative analysis can be prepared in 2 min. After pressing, the pellets were immediately introduced into the spectrometer to avoid any moisture take up: a problem sometimes associated with compacted powders, which tends to distort the analytical surface. Following analysis the samples were stored in a desiccator. The sample preparation, analysis and data evaluation by Uniquant 2 package took 20 min. The results of the semiquantitative analysis are given in Table 4. This analytical approach is particularly useful in the analysis of 'unknowns' as it provides data for almost all the elements in the periodic table without the need for previously analysed reference materials. Where more comprehensive quantitative data is required, the appropriate calibration may be selected or prepared if not already available. For many applications the information obtained from Uniquant 2 is sufficient to characterize the sample and meet the customer's requirements.

X-ray Diffraction

The X-ray diffraction examination of sample G1A identified the compound $Zn_3(PO_4)_2{\cdot}4H_2O$ as being present. Scans from

Table 2 Moisture content

	Moisture content (%)		
Sample	1	2	Average (%)
G1A			50.7
G1B	55.78	54.83	55.31
G2	66.49	64.27	65.38
G3	64.17	64.16	64.16
G4	71.86	71.85	71.86

Table 3 Loss on ignition

	Loss on ignition (%)		
Sample	1	2	Average (%)
G1A	15.84	16.97	16.41
G1B	18.25	17.65	17.95
G2	14.44	14.31	14.38
G3	19.03	18.60	18.82
G4	25.92	24.95	25.45

Table 1 Measurement parameters for the analytical program

Element	Line	Potential/ kV	Current/ mA	Collimator space/mm	Crystal	2θ (degrees)	Offset	Detector*	LL†	UL‡
Mo§	Kα	60	50	0.15	LiF220	28.8174	See Sr	SC	25	75
Sr	Kα	60	50	0.15	LiF220	35.7756	−4.86	SC	20	75
Zn§	Kα	30	30	0.30	LiF220	60.5468	See Fe	SC	20	80
Cu§	Kα	50	60	0.15	LiF220	65.5033	See Fe	DU	21	75
Ni§	Kα	50	60	0.15	LiF220	71.2163	See Fe	DU	14	70
Co§	Kα	50	60	0.15	LiF220	77.8451	See Fe	DU	11	75
Fe	Kα	50	60	0.15	LiF220	85.6784	+5.00	DU	16	75
Mn§	Kα	50	60	0.15	LiF220	95.1288	See Cr	DU	17	75
Cr	Kα	50	60	0.15	LiF220	107.0364	−4.08	DU	12	75
Ti	Kα	50	60	0.15	LiF200	86.1365	−1.46	FL	8	75
Ca	Kα	50	60	0.15	LiF200	113.0925	−8.99	FL	19	75
K	Kα	50	60	0.15	LiF200	136.6398	−8.75	FL	25	75
Zr§	Lα	50	60	0.70	PE	87.7276	See Si	FL	25	75
S§	Kα	50	60	0.70	PE	75.5954	See Si	FL	25	75
P§	Kα	50	60	0.70	PE	89.3854	See Si	FL	25	75
Si	Kα	50	60	0.70	PE	109.0170	+11.48	FL	25	75
Al	Kα	50	60	0.70	PE	144.8346	See Si	FL	25	75
Mg	Kα	50	60	0.70	PXI	22.4698	See Na	FL	25	62
Na	Kα	50	60	0.70	PXI	27.1351	+10.4	FL	25	68

* SC, scintillation counter; DU, gas flow + sealed xenon; FL, gas flow proportional.

† LL, lower level discriminator.

‡ UL, upper level discriminator.

§ Shared background offsets: Sr offset used for Mo background; Fe offset used for Zn, Cu, Ni and Co backgrounds; Cr offset used for Mn background; Si offset used for Zr, S and P backgrounds; Na offset used for Mg background.

the other samples produced broad, poorly resolved 'peaks' on high backgrounds which it was not possible to identify. Such traces are obtained from weakly crystalline phases that are possibly found in sludges.

Quantitative XRF Analysis

An assessment of a method of analysis would be incomplete without reference to precision and accuracy to give the technique credibility. The accuracy of the calibration used for the analysis of the sludges was assessed by analysing certified reference materials (CRMs). In the absence of appropriate CRMs covering all the elements found in the samples under investigation, a range of reference materials was examined to prove the calibration. For a result to be acceptable, the analysis of a CRM should be within $0.07\sqrt{(\text{concentration})}$ as discussed by Hughes and Hurley.[4] In Table 5 the results are given for one of the reference materials examined, ECRM 776-1 showing that the method is as good as internationally accepted standard methods of analysis.

Repeatability of the preparation of the fused bead samples was demonstrated by preparing 11 beads of ECRM 776-1. The statistics package in the Philips software was used to assess the data (see Table 6). This trial includes errors such as weighing, the possibility of incomplete dissolution and the state of the analysed surface of the beads. The manganese is quoted as Mn_3O_4 and not MnO because Mn_3O_4 is the stable oxide at the fusion temperature.

Similarly the instrument repeatability is shown in Table 7 where a single bead was measured 11 times. This trial includes errors such as photon counting statistics and short-term instrument drift including the re-setting of instrument parameters and sample presentation. The stability of the spectrometer and the technique used to prepare the beads is clearly demonstrated. The intensity measurements obtained using this analytical programme used the absolute mode, there was no ratio to a drift monitor sample. The stability of the spectrometer was monitored by measuring ECRM 776-1 at regular intervals. The quality of these results was used as a measure of the need for recalibration using the appropriate

Table 4 Semiquantitative analysis

	Concentration (mass%)				
Analyte	G1A	G1B	G2*	G3	G4
ZnO	47.1	46.2	0.076	0.019	49.8
P_2O_5	22.7	21.8	22.5	10.8	14.7
Fe_2O_3	5.9	6.2	26.8	3.16	5.1
MnO	1.98	1.91	0.124	0.037	0.052
CaO	4.5	4.23	37.4	57.0	15.2
SiO_2	0.29	0.45	5.4	1.36	2.67
Al_2O_3	6.3	6.6	0.51	9.4	2.62
S	6.7	7.0	1.31	12.7	0.59
Na_2O	1.7	2.5	0.10	0.23	—
MgO	0.086	0.030	0.84	0.57	4.09
K_2O	0.85	0.91	0.030	0.015	0.054
Cr_2O_3	0.13	0.13	0.014	3.69	4.11
TiO_2	0.013	0.011	0.029	0.62	0.013
Co_3O_4	0.006	—	0.019	—	0.21
NiO	0.15	0.16	0.012	0.18	0.043
CuO	—	—	0.088	0.005	0.064
SrO	—	—	0.037	0.018	0.056
MoO_3	0.014	0.013	0.011	0.031	—
ZrO_2	—	—	—	0.025	—
Cl	1.39	1.78	0.18	0.059	0.58

* Sample was also found to contain 4.1% F.

Table 5 Accuracy of calibration for ECRM 776-1

	Concentration (mass%)	
Analyte	XRF	Certificate
ZnO	—	—
P_2O_5	0.05	0.06
Fe_2O_3	1.40	1.43
Mn_3O_4	0.02	—
CaO	0.33	0.31
SiO_2	63.13	62.76
Al_2O_3	29.28	29.28
SO_3	0.11	—
Na_2O	0.51	0.49
MgO	0.52	0.48
K_2O	2.95	2.92
Cr_2O_3	0.02	0.02
TiO_2	1.60	1.62
Co_3O_4	0.02	—
NiO	0.03	—
CuO	0.02	—
SrO	0.02	—
MoO_3	0.00	—
ZrO_2	0.05	—

Table 6 Fused bead sample repeatability using ECRM 776-1

Analyte	RMS sample	Analyte	RMS sample
P_2O_5	0.002	Na_2O	0.008
Fe_2O_3	0.008	MgO	0.006
CaO	0.004	K_2O	0.014
SiO_2	0.160	Cr_2O_3	0.003
Al_2O_3	0.039	TiO_2	0.006

Table 7 Instrument repeatability using ECRM 776-1

Analyte	RMS instrument	Analyte	RMS instrument
P_2O_5	0.002	Na_2O	0.007
Fe_2O_3	0.006	MgO	0.005
CaO	0.004	K_2O	0.009
SiO_2	0.061	Cr_2O_3	0.002
Al_2O_3	0.021	TiO_2	0.007

Table 8 XRF analysis of waste sludges from German electroplating works analysis performed using Philips PW2400 sequential XRF spectrometer

	Concentration (mass%)				
Channel	G1A	G1B	G2	G3	G4
ZnO	33.40	32.67	0.04	0.01	30.18
P_2O_5	25.43	24.91	20.13	8.57	12.79
Fe_2O_3	5.64	5.72	22.14	2.17	4.21
Mn_3O_4	1.91	1.84	0.14	0.04	0.08
CaO	4.75	4.15	33.35	41.12	14.01
SiO_2	0.10	0.13	4.19	1.04	1.91
Al_2O_3	4.27	4.39	0.32	7.41	1.87
SO_3	1.17	0.74	0.17	1.38	0.02
Na_2O	3.80	4.00	0.00	0.01	0.91
MgO	0.00	0.00	0.54	0.32	2.83
K_2O	0.77	0.78	0.02	0.00	0.03
Cr_2O_3	0.13	0.14	0.02	2.70	3.68
TiO_2	0.01	0.00	0.02	0.40	0.01
Co_3O_4	0.01	0.01	0.02	0.00	0.11
NiO	0.14	0.14	0.00	0.13	0.04
CuO	0.03	0.04	0.04	0.04	0.06
SrO	0.00	0.00	0.03	0.01	0.05
MoO_3	0.02	0.02	0.01	0.03	0.07
ZrO_2	0.00	0.00	0.00	0.02	−0.00

Table 9 Carbon and sulfur determinations

Sample		Carbon (%)	Sulfur (%)
BCS489-1		2.884	0.1550
		2.825	0.1586
		2.879	0.1581
		2.865	0.1595
		2.887	0.1560
	Average	2.868	0.1574
	Certificate	2.86	0.155
BCS484-1		3.217	0.2423
		3.215	0.2418
		3.206	0.2353
		3.340	0.2363
		3.221	0.2367
	Average	3.240	0.2385
	Certificate	3.20	0.230
G1A		1.033	3.858
		1.001	3.746
	Average	1.017	3.802
G1B		1.076	3.915
		1.045	3.944
	Average	1.061	3.930
G2		1.588	0.7463
		1.559	0.7384
	Average	1.574	0.7424
G3		1.192	6.048
		1.202	5.944
	Average	1.197	5.996
G4		4.983	0.3518
		5.428	0.3280
	Average	5.206	0.3399

single element calibration bead and the blank. The results of the analysis on the five sludges are shown in Table 8.

Carbon and Sulfur Determinations

The calibration of the Leco CS444 analyser was assessed by measuring two CRMs five times, the results are shown in Table 9 along with the sludges measured in duplicate.

Conclusion

Semi-quantitative analysis using the Uniquant 2 software is a very useful first method of analysing unknown materials. The combination of semi-quantitative and quantitative methods makes XRF an ideal technique for the analysis and characterization of sludges and by implication, many other waste products.

The preparation methodologies of pressed powder pellets and fused beads are well established and accepted techniques which proved eminently suitable for this type of investigation. It is recognized that comparative analysis by conventional techniques must be conducted and it is the intention of this laboratory to complete this investigation and report further results in the scientific literature.

References

1 Giles, H. L., Hurley, P. W., and Webster, H. W. M., unpublished work.
2 de Jongh, W. K., *X-Ray Spectrom.*, 1972, **2**, 151.
3 de Jongh, W. K., *X-Ray Spectrom.*, 1979, **8**, 52.
4 Hughes, H., and Hurley, P. W., *Analyst*, 1987, **112**, 1445.

Paper 4/06024E
Received October 3, 1994
Accepted January 17, 1995

Analysis of Silicate Rocks Using Field-portable X-ray Fluorescence Instrumentation Incorporating a Mercury(II) Iodide Detector: A Preliminary Assessment of Analytical Performance*

Philip J. Potts, Peter C. Webb and Olwen Williams-Thorpe

Department of Earth Sciences, The Open University, Walton Hall, Milton Keynes, UK MK7 6AA

Richard Kilworth

Thermo Electron Ltd., Analytical Instruments Division, 910 Birchwood Boulevard, Birchwood, Warrington, Cheshire, UK WA3 7QN

An assessment is reported of the performance of a field-portable energy dispersive X-ray fluorescence analysis system using ^{55}Fe, ^{109}Cd and ^{241}Am excitation sources and a high resolution mercury(II) iodide detector. Seventy international reference materials, mainly of silicate composition, were analysed as compressed powder pellets. Results from spectra recorded for live times of 200 s (per source) showed that the major elements K, Ca, Ti, Mn and Fe and the trace elements Ba, Nb, Rb, Sr, Y and Zr could be determined routinely in 'normal' silicate rocks and in addition Co, Cr, Cu, Ga, La, Nd, Ni, V and Zn at higher concentrations or in mineralized samples. Detection limits for the most sensitively measured trace elements (Rb, Sr, Y, Zr, Nb) were found to be in the range 6–14 μg g^{-1} and for Ba (K-line), 21 μg g^{-1}. Precision in the determination of the major elements was generally in the range 0.45–2% (relative standard deviation) and a high degree of accuracy was achieved when judged from a self-consistent comparison of analysed values with the expected compositions of the 70 reference materials. Having characterized performance in the laboratory with 'ideal' control over sample presentation, work is now in progress to evaluate additional discrepancies that will be encountered in the analysis of geological and archaeological samples in the field.

Keywords: *Portable energy dispersive X-ray fluorescence analysis system; mercury(II) iodide detector; radioisotope excitation; accuracy; precision; detection limit*

Introduction

X-ray fluorescence (XRF) analysis is a well established laboratory technique for the elemental analysis of many sample types, including rocks, ores, minerals, refractories, and ferrous and non-ferrous metals (see, for example, refs. 1–4). In quality control and research laboratories operating in these areas, wavelength dispersive XRF spectrometry is often regarded as the technique of choice in view of the ease of sample preparation, analytical accuracy and high precision. Energy dispersive (ED) XRF spectrometry also has an important role to play in low-cost instruments dedicated to specific applications (*e.g.*, sulfur in oil) and in fingerprinting applications such as the characterization of forensic samples. However, EDXRF spectrometry can also achieve high accuracy and precision, as demonstrated in an earlier series of publications which showed that tube-excited EDXRF spectrometry is capable of the quantitative analysis of the major and trace elements in silicate rocks, with detection limits of 2–5 μg g^{-1} for some geochemically important trace elements.[4–9]

Although XRF spectrometry is best known as a laboratory-based technique, it is also one of the few atomic spectrometric techniques that can be adapted for true field-portable use. In this form, it offers several important advantages over conventional laboratory-based analysis, including: (i) immediate analytical results, so that measurement programmes can be undertaken interactively, which is important, for example, in assessing sites contaminated with heavy metals[10,11] or in identifying the extent of mineralization in geological exploration applications;[12] (ii) the non-destructive analysis of objects that can neither be sampled nor removed to the laboratory for analysis, for example, in the analysis of museum samples, including works of art[13] and in provenancing studies of archaeological artefacts.[14–17]

Field-portable XRF instrumentation based on gas proportional counters and Si(Li) detectors has been available for a number of years and has already found extensive use in environmental applications, particularly in the assessment of heavy metal contamination.[18] In such applications, the degree of accuracy is often limited by poor sampling precision caused by localized variations in the distribution of the elements of interest. If, indeed, the objective is to locate 'hot-spots' of contamination, high absolute accuracy may not be critical to the interpretation of results. However, our interest is in the analysis of geological and archaeological samples, where the accuracy and precision are much more important than in many environmental applications. In order to provenance archaeological lithic artefacts (*e.g.*, Roman columns or stone axes) to their source areas (*i.e.*, quarrying sites), it is essential that accuracy and precision are sufficiently high so that analytical results taken from the artefact can be compared with literature data representative of potential source regions, measurements on which would normally have been undertaken by standard laboratory-based techniques.[19,20]

In this paper, the performance of a recently introduced portable XRF instrument is assessed with the above applications in mind. The instrument incorporates three radioisotope excitation sources (^{55}Fe, ^{109}Cd and ^{241}Am) and a mercury(II) iodide ED detector capable of high resolution operation

* Presented at Geoanalysis 94: An International Symposium on the Analysis of Geological and Environmental Materials, Ambleside, England, September 18–22, 1994.

without requiring liquid nitrogen cooling. The objective here is to measure realistic levels of accuracy, precision and detection limits under ideal laboratory conditions where silicate rock samples were analysed as compressed powder pellets, which could be positioned accurately and reproducibly on the analyser. On the basis of these results, work is now in hand to apply this instrumentation to the analysis of real geological and archaeological samples in the field, where reproducible sample presentation conditions cannot as easily be satisfied.

Experimental

Measurements were made using a Spectrace 9000 field-portable XRF instrument (TN Technologies, Round Rock, TX, USA), which was originally supplied by Tracor Europa (now by Thermo Electron, Warrington, Cheshire, UK). This instrument consists of a portable analyser, incorporating ^{55}Fe (1.8 GBq), ^{109}Cd (180 MBq) and ^{241}Am (180 MBq) excitation sources and a solid-state mercury(II) iodide X-ray detector (resolution 260 eV full width at half maximum at 5.9 keV) connected to a separate portable data acquisition and data analysis unit. All measurements were undertaken using the laboratory stand configuration in which compressed powder pellet samples were reproducibly placed in the analysis position on an adaptor ring under a removable, hinged, safety shield.

Spectra were obtained by exciting samples with each source in turn, the acquisition of these data being controlled by the instrument automation software. A live time of 200 s per source was used, except for some repeatability measurements which were made with a reduced, 100 s count time. Spectra from each source were recorded by a 2000-channel multichannel analyser and peak intensities determined using the TN spectrum analysis software, based on multiple window integrations. A typical spectrum from each source is shown in Fig. 1. The Sn and Cd lines in the ^{241}Am excited spectrum appear to be artefacts produced by the instrument.

Spectral intensities were corrected and quantified using the TN Fundamental Parameter program (see, for example, ref. 21) which operated in the portable analyser using coefficients that had been calculated off-line using an applications package. These coefficients were calculated using an off-line personal computer (PC) for a silicate rock matrix and were then down-loaded into the portable analyser. The facility to store complete sets of spectra in the portable analyser (up to 40 sets can be stored) was not used routinely. Instead, data files of results (derived from the analysis of individual samples) were accumulated in the portable analyser (a maximum of up to 300 individual results files can be stored). After each operating session, these results were transferred to a PC for further manipulation using a spreadsheet program.

A wide range of international reference materials was analysed to investigate instrument performance. These reference materials consisted of silicate rocks, silicate minerals, sediments, a few carbonate rocks and silicate ore samples. The identifiers of these reference materials are as follows (further details about their origin and composition can be found in ref. 22): AC-E, BHVO-1, BIR-1, CZN-1, DH-1, DNC-1, DR-N, DT-N, FK-N, G-2, GA, GH, GXR-4, HV-1, IGS-21, IGS-22, IGS-23, JA-1, JA-2, JA-3, JB-1a, JB-2, JCh-1, JF-1, JF-2, JG-1, JG-1a, JG-2, JG-3, JGb-1, JLK-1, JP-1, JR-1, JR-2, JSD-1, JSD-2, JSL-1, JSL-2, GFS-400, GFS-401, GFS-402, MA-1, MAG-1, MICA-Fe, MICA-Mg, MP-1, NIST SRM 679, NIST SRM 97b, NIST SRM 98B, NIM-D, NIM-L, NIM-N, NIM-P, NIM-S, PM-S, SARM-7, QLO-1, RGM-1, SCo-1, SDC-1, STM-1, SU-1a, SY-2, SY-3, UM-1, UM-1A, UM-2, UM-4, W-2, WS-E. Samples were prepared as compressed powder pellets using conventional techniques.[4]

The groups of elements chosen for determination were influenced in part by the excitation capabilities of the individual sources (commented on further below) and in part by the concentration range in the above suite of rocks. The final selection, by source (with justifications), was as follows:

^{55}Fe. This source decays by electron capture, emitting Mn K-lines, and so is capable, in geological applications, of exciting a similar range of elements to a Cr anode X-ray tube. The elements K, Ca, Ti, V and Cr (K-lines) were measured from ^{55}Fe-excited spectra [see Fig. 1(*a*)]. X-rays of lower atomic number elements suffered excessive attenuation in air and so could not be detected. Determinations of Cr were severely affected by a spectral overlap interference from the Mn Kα lines scattered from the source.

^{109}Cd. This source decays by electron capture and emits Ag K-lines. Its excitation capabilities are similar to those of an Ag anode X-ray tube. However, some spectral differences arise because, unlike an X-ray tube, the ^{109}Cd source does not emit continuum radiation, only characteristic Ag K-lines. Thus, the ^{109}Cd source is able to excite most efficiently the fluorescence lines of elements with absorption edge energies below but close to the Ag K-line energy. The excitation efficiency for elements with more remote absorption edges falls off more rapidly than with tube excitation, which benefits from a continuum contribution to excitation. However, the absence of continuum radiation from the radioactive source reduces the background under the analytical lines of interest, compared with a tube-excited spectrum in which a significant contribution to background intensity arises from scatter of the continuum component. The ^{109}Cd source-excited spectra benefit, therefore, from more favourable peak-to-background

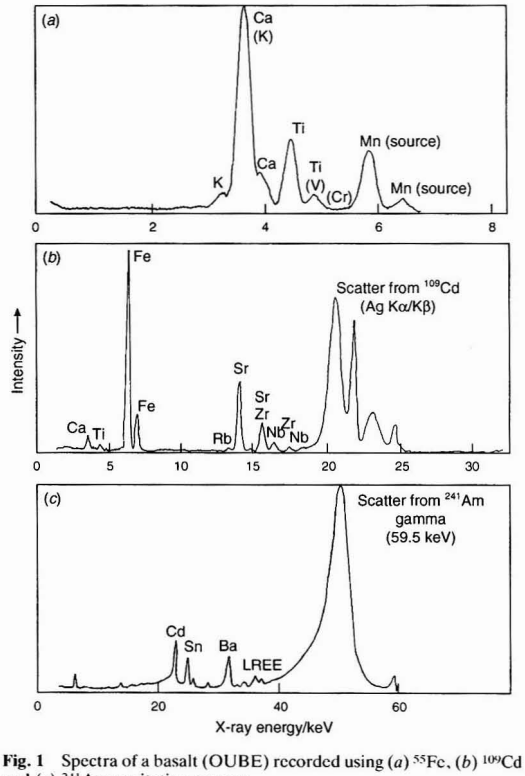

Fig. 1 Spectra of a basalt (OUBE) recorded using (*a*) ^{55}Fe, (*b*) ^{109}Cd and (*c*) ^{241}Am excitation sources.

ratios which compensate to some extent for the over-all lower excitation intensities from a source compared with an X-ray tube. The elements Nb, Zr, Y, Sr, Rb, Ga, Zn, Cu, Ni, Co, Fe and Mn (all K-lines) and Pb (L-lines) were measured from ^{109}Cd-excited spectra [see Fig. 1(*b*)].

^{241}Am. This source emits 59.5 keV gamma rays and the closest equivalent in tube-excited XRF spectrometry is a W anode X-ray tube operated at a sufficiently high voltage to excite the W K-lines. In fact, such conditions are not frequently encountered using laboratory XRF instrumentation, in part because modern instruments fitted with end window tubes are normally limited to a maximum operating potential of 60–75 kV (although some side-window tubes can be powered up to 100 kV). In consequence, the ^{241}Am source is capable of exciting the K-lines of higher atomic number elements which would normally be analysed using the lower energy L-lines with conventional tube-excited instrumentation. The lines measured in this work were the K-lines of Ba, La and Ce [see Fig. 1(*c*)].

Table 1 Comparison of detection limits obtained by field-portable XRF spectrometry. All values in μg g^{-1}

Source	Element	'Instrumental'* (siliceous matrix) (manufacturer's data)	'Working'† (silicate rock) (this work)	Laboratory EDXRF spectrometry‡ (tube-excited) (silicate rock)
^{55}Fe	K	150	360	
	Ca	70	225	
	Ti	55	120	
	V	50	49	
	Cr	90	1080	
^{109}Cd	Mn	200	354	
	Fe	110	424	
	Co	100	354	
	Ni	65	116	12
	Cu	50	80	8
	Zn	40	63	7
	Ga	35	58	6
	Rb	5	13	3
	Sr	4	14	3
	Y	4	9	3
	Zr	3	9	3
	Nb	4	6	3
	Pb-L	15	39	7
^{241}Am	Ba-K	9	21	—
	La-K	8	—	—
	Ce-K	8	14	—

* 'Instrumental': 200 s count time per source on a siliceous matrix (Spectrace TN9000, manufacturer's data).

† 'Working': 200 s count time per source on a silicate rock matrix (this work).

‡ Laboratory EDXRF spectrometry: 800 s count time, Si(Li) detector, Ag tube-excited, silicate rock.[4]

Results and Discussion

Detection Limit Performance

Detection limits were estimated from the results obtained from the analysis of a wide range of reference materials using a live time of 200 s per source. Each set of results listed the analysed concentration and associated standard deviation derived from a combination of counting statistics and the spectrum fitting error. This fitting error took into account the uncertainty attributable to background subtraction as well as the effect (if any) of spectrum overlap interferences. The results file for each sample was examined to identify circumstances where an elemental analysis had a value equivalent to or less than that of the corresponding fitting error. The value of this fitting error was then recorded as the standard deviation representing the uncertainty in fitting a background to the spectrum of the fluorescence line of interest. After examining results files for all 70 samples, a small range of standard deviation values was recorded for each element, ranging from 3 to 12 values (the number varied according to the number of samples in which the element abundance was at or below the detection limit level). The detection limit of the technique in silicate rock analysis was calculated as three times the average value of this standard deviation.

Detection limit values obtained in this way are compared in Table 1 with the manufacturer's data, based on the analysis of a 'siliceous matrix' (using a comparable live time of 200 s per source). Other detection limit values, representative of tube-excited EDXRF spectrometry using an 800 s live count time, are also listed in Table 1. As can be seen, detection limit data obtained in this work are typically between two and three times higher than the data from the 'siliceous' matrix. Nevertheless, it is noteworthy that detection limits for Nb, Zr, Y, Sr and Rb obtained from silicate rocks fall in the range 6–14 μg g^{-1} for a 200 s count time for the ^{109}Cd source, compared with values of about 3 μg g^{-1} obtained by tube-excited EDXRF spectrometry using an Ag anode X-ray tube and an 800 s count time. This favourable response of the radioisotope-excited instrument appears to result from an increased

Table 2 Precision (repeatability) in the analysis of Whin Sill dolerite (powder pellet)

		100 s count time (n = 10)			200 s count time (n = 8)		
Element	Expected/ μg g^{-1}	Analysed/ μg g^{-1}	s*/ μg g^{-1}	s_r† (%)	Analysed/ μg g^{-1}	s*/ μg g^{-1}	s_r† (%)
K	8302	13046	512.2	3.9	13093	210.2	1.6
Ca	64540	70152	794.9	1.1	70240	313.0	0.45
Ti	14560	17799	382.0	2.1	17445	311.2	1.8
V	349	470.5	60.6	12.9	484.3	19.3	4.0
Mn	1320	1531.0	375.2	24.5	1523.2	206.3	13.5
Fe	93380	104020	1396	1.3	104079	1585	1.5
Rb	27	38.8	8.3	21.4	42.0	4.0	9.5
Sr	422	513.9	22.2	4.3	508.4	11.1	2.2
Y	34	37.5	6.3	16.8	31.4	4.4	14.0
Zr	206	240.4	8.1	3.4	234.5	7.5	3.2
Nb	18	14.2	3.8	26.8	13.6	4.0	29.4
Ba	350	385.3	27.7	7.2	392.9	7.7	2.0

* s = Standard deviation.

† s_r = Relative standard deviation.

signal-to-background ratio owing to the absence of a significant continuum component from the excitation source, as mentioned above.

The detection limits of 21 μg g^{-1} for the Ba K-line and 14 μg g^{-1} for the Ce K-line obtained by ^{241}Am excitation are also noteworthy, these data approaching the routine performance expected of a wavelength dispersive instrument measuring the corresponding L-lines. Conversely, detection limits for the trace elements Co, Cr, Cu, Ga, Ni, V and Zn are not adequate for the routine determination of these elements in silicate rocks, except at higher levels and in mineralized samples. The detection limit for Cr, in particular, appears to be degraded by an overlap interference caused by scatter of the Mn K-lines from the ^{55}Fe excitation source.

Precision

The short-term precision (repeatability) of the instrumentation was assessed by the repeated analysis of a powder pellet of Whin Sill dolerite, this sample being chosen because it has analysable concentrations of a wide range of elements. The averages of a sequence of ten analyses using a count time of 100 s per source are compared with data for eight analyses using a count time of 200 s per source in Table 2. Data for elements approaching detection limit levels are not listed in Table 2 because, for these elements, limitations in performance are better assessed by detection limit data in Table 1. Results in Table 2 show that for the 200 s count spectra, the best precision is 0.45% relative standard deviation (s_r) for the major element, Ca, excited with the ^{55}Fe source; 2.2% s_r for the trace element, Sr, at the 500 μg g^{-1} level; 1.5% s_r for Fe at the 9.3 mass% level excited with ^{109}Cd and 2.0% s_r for Ba (K-line) at the 390 μg g^{-1} level excited by ^{241}Am. Corresponding s_r results from the 100 s count time spectra are 1.1% (Ca), 4.3% (Sr), 1.3% (Fe) and 7.2% (Ba). The low values of these data suggest that, as with other XRF techniques, the dominant contribution to precision is associated with Poisson counting statistics, the instrument component being relatively small when repetitive counts are undertaken without moving the sample.

Accuracy

An assessment of accuracy was based on analyses of the 70 international reference materials, listed above, comparing analysed results with expected values listed by Potts *et al.*[22] On plotting expected *versus* analysed values, most elements showed strong linear trends. Selected data are plotted in Fig. 2 for the following elements: (*a*) K, the lowest atomic number major element that could be determined routinely; (*b*) Cu, representing an element for which the technique is not sufficiently sensitive for routine determination in 'normal' silicate rocks, except for samples with unusually high contents (Cu > about 200 μg g^{-1}); (*c*) Sr, representing a geochemically important element for which sensitivity is high; and (*d*) Ba, demonstrating the performance in the determination of Ba from its K-line (^{241}Am excited), rather than the L-line which would normally be measured in routine wavelength dispersive XRF spectrometry.

These data are considered to demonstrate excellent linearity (with the exception of Cu, where many of the data are at or below detection limit level). The occasional discrepancy could be caused by uncertainties in the expected composition, or errors in the matrix correction for samples that are not strictly 'silicate' in composition (a small number of carbonates and oxide ores were included in the sample set analysed).

Further examination of these lines (Fig. 2) showed that, although the linearity of the data was excellent, small deviations could be seen in the slope of the line from an ideal one-to-one line of equivalence. These deviations varied from element to element from a slope factor of about 1.0 (*i.e.*, equivalence between analysed and expected values) to about 0.8 (analysed values about 20% low). It is thought that these discrepancies could have arisen from minor inaccuracies in the assumptions programmed into the fundamental parameter matrix correction procedure, which required an estimate to be made of the composition of non-analysable matrix elements, for which a single 'average' composition was taken to

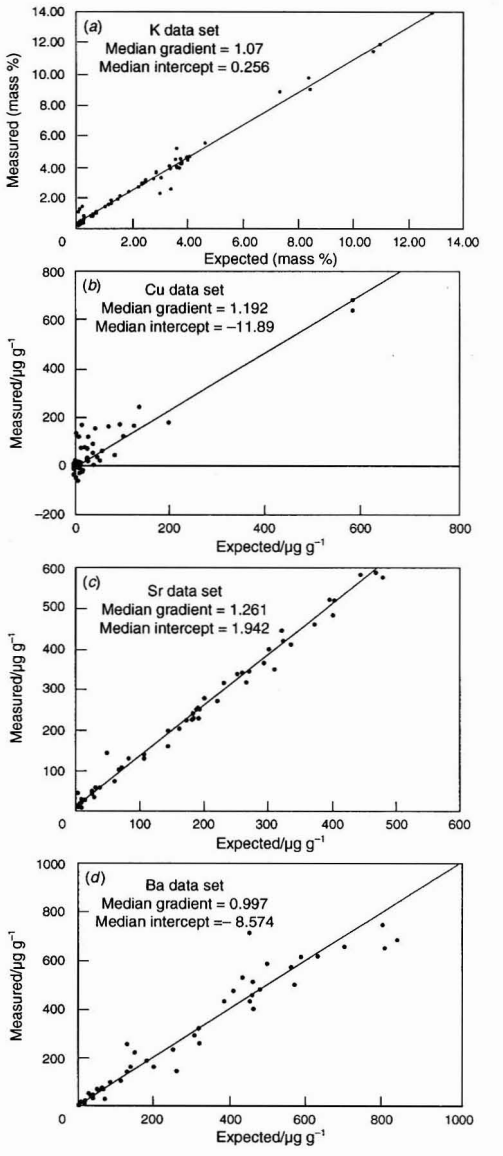

Fig. 2 Results for (*a*) K, (*b*) Cu, (*c*) Sr and (*d*) Ba (K-line) derived from the analysis of 70 international reference materials. Portable EDXRF analysed data are plotted against expected compositions (taken from Potts *et al.*[22]). The best fit lines shown were calculated by Thiel's incomplete method.[23]

represent all samples. In order to correct small discrepancies of this nature, the software allows the user to specify and apply a slope correction factor.

The normal way of estimating a correction factor from these data sets would be to perform a least-squares fit of analysed to expected concentrations. However, previous experience has shown that serious bias can arise in the least-squares fitting procedure if individual data points that deviate significantly from the general trend of the remaining data are included. In these circumstances, the fitted line can be distorted from the general trend of the data to accommodate a 'rogue' point and it is then necessary to make arbitrary decisions about discarding such outliers if the over-all fit to the data is to be acceptable. In order to avoid this problem, an alternative procedure, based on Thiel's incomplete method,[23] was used to calculate slope correction factors. This procedure, which has been used previously in the successful assessment of XRF calibration data,[24] is based on the median value of the slope calculated from a set of slope values obtained from pairs of data points. The first value of the slope is calculated from the first and $(n/2 + 1)$th data point, the second from the second and $(n/2 + 2)$th value, and so on, until all pairs of points have contributed a slope value (n is the total number of points in the data set and must have an even value). The median of these slope values is taken as representative of the full data set. The effect of outliers on this value is effectively suppressed. A median intercept may be derived from a set of intercepts calculated by applying the median slope (calculated as above) to each data point in turn and extrapolating the resulting notional line until it intercepts the x-axis. The median intercept is then derived from the array of values calculated in this way. As a result, realistic estimates of the slope and intercept coefficients of a best fit line can be derived and used to adjust data to correct for systematic discrepancies in the fundamental parameters calibration.

After applying this subsidiary correction to the analytical results, corrected results for selected samples are listed in Table 3 to indicate the potential accuracy of the technique. Data listed in Table 3 are a sub-set of the complete data, chosen to represent some of the more reliably characterized rock reference materials. Data are listed for the elements Rb, Sr, Y, Zr, Nb and Ba, and show the excellent over-all agreement between expected and analysed values. As the data in Table 3 are the best fit results based on an analysis of all 70 reference materials, they represent a measure of the relative, rather than the absolute, accuracy of the technique. However, this method represents the only practical way in which the performance of the portable XRF technique can be demonstrated. These results show that, provided that sample positioning is reproducible, a high degree of accuracy can be achieved with this technique, even down to concentration levels of 10 μg g^{-1}.

Conclusions

In assessing the performance of the radioisotope-excited portable EDXRF instrument incorporating a mercury(II) iodide detector in the analysis of silicate rocks, it was found that the most sensitive elements (Rb, Sr, Y, Zr, Nb) could be determined down to the 6–14 μg g^{-1} level using a 200 s count with the ^{109}Cd source and that Ba (detection limit 21 μg g^{-1}), V (49 μg g^{-1}) and the major elements K, Ca, Ti, Mn and Fe could be determined routinely in 'normal' silicate rocks. These elements benefit from favourable signal-to-background ratios caused by the proximity of their absorption edges to the excitation source lines and a lower contribution to scattered backgrounds in comparison with tube-excited EDXRF spectrometry. Conversely, detection limits for Cr, Co, Cu, Ga, Ni and Zn were in the range 58–1080 μg g^{-1}, adequate only for measurements at the higher end of the concentration range in silicate rocks or in mineralized samples. These elements have absorption edges more remote from the radioisotope excitation lines and do not benefit from supplementary excitation from a continuum emission (as would be the case in tube-excited EDXRF spectrometry).

Short-term precision (*i.e.*, repeatability) using a 200 s count time per source was found to be in the range 0.45–1.8% s_r for the major elements (> 1 mass%) and 2–5% s_r for trace elements in the range 100–500 μg g^{-1}. Based on the analysis of 70 international reference materials prepared as compressed powder pellets, a high degree of linearity was observed between analysed and expected values. Excellent agreement was observed when analysed values were compared with expected compositions, after applying a small correction for calibration bias. These impressive performance characteristics were obtained using samples prepared as compressed powder pellets, which were reproducibly positioned on the instrument for analysis. Although fully representative of what can be achieved in the laboratory, additional discrepancies will be encountered in field analysis, caused by non-ideal sample geometry, mineral inhomogeneity effects and weathered surfaces. Work is currently in progress to evaluate the magnitude of these effects.

The authors are very grateful to Tracor Europa Ltd. (now Noran Instruments, UK) for loan of the TN 9000 instrument and to J. Watson for technical assistance. An earlier version of this paper was presented at the joint Atomic Spectrometry

Table 3 Assessment of accuracy based on a comparison of analysed composition (with Thiel's calibration refinement method) *versus* the expected value for selected international silicate reference materials. All values in μg g^{-1}

Reference material	Rb		Sr		Y		Zr		Nb		Ba	
	XRF*	RM†	XRF*	RM†	XRF*	RM†	XRF*	RM†	XRF*	RM†	XRF*	RM†
AC-E	146	152	3.2	3	176	184	731	780	105	110	61	55
BHVO-1	11	11	406	403	23	28	178	179	16	19	159	139
BIR-1	−2.4	0.3	105	108	13	16	30	22	−0.6	2	15	8
DNC-1	4.1	4.5	151	145	21	18	43	41	4	3	103	114
G-2	166	170	451	478	18	11	298	300	11	13	1618	1880
QLO-1	67	74	321	336	18	24	182	185	11	10	1251	1370
RGM-1	137	149	97	108	35	25	219	219	10	9	650	807
SDC-1	130	127	173	183	38	40	269	290	18	18	616	630
STM-1	118	118	694	700	51	46	1197	1210	233	268	569	560
W-2	21	20	194	194	18	24	94	94	10	8	185	182

* XRF = Analysed value (this work).

† RM = Expected composition from Potts *et al.*[22]

Updates/Atomic Spectrometry Groups meeting in Ambleside, UK, March, 1994. One of the authors (O. W. T.) acknowledges support for her contribution to this work from the Leverhulme Trust (Grant No. F.269P; S903248).

References

1 Bacon, J. R., Ellis, A. T., McMahon, A. W., Potts, P. J., and Williams, J. G., *J. Anal. At. Spectrom.*, 1994, **9**, 267R.
2 Bennett, H., and Oliver, G. J., *XRF Analysis of Ceramics, Minerals and Allied Materials*, Wiley, Chichester, 1992.
3 *Handbook of X-ray Spectrometry, Methods and Techniques*, eds. van Grieken, R. E., and Markowicz, A. A., Marcel Dekker, New York, 1993.
4 Potts, P. J., and Webb, P. C., *J. Geochem. Explor.*, 1992, **44**, 251.
5 Potts, P. J., Webb, P. C., and Watson, J. S., *X-ray Spectrom.*, 1984, **13**, 2.
6 Potts, P. J., Webb, P. C., and Watson, J. S., *Analyst*, 1985, **110**, 507.
7 Potts, P. J., Webb, P. C., and Watson, J. S., *Geostand. Newsl.*, 1990, **14**, 127.
8 Webb, P. C., Potts, P. J., and Watson, J. S., *Geostand. Newsl.*, 1990, **14**, 361.
9 Webb, P. C., Potts, P. J., and Watson, J. S., *J. Anal. At. Spectrom.*, 1993, **8**, 293.
10 Harding, A. R., and Walsh, J. P., *Adv. X-ray Anal.*, 1990, **33**, 647.
11 Bernick, M., Berry, P. F., Voots, G. F., Prince, G., Ash, J. B., Patel, J., and Gupta, P., *Adv. X-ray Anal.*, 1992, **35B**, 1047.
12 Zhou, S.-h., Xie, T.-z., and Ge, L.-q., *Nucl. Sci. Tech.*, 1992, **3**, 191.
13 Cesareo, R., Gigante, G. E., Iwanczyk, J. S., and Dabrowski, A., *Nucl. Instrum. Methods Phys. Res., Sect. A*, 1992, **322**, 583.
14 LaBrecque, J. J., Rosales, P. A., and Carias, O., *Adv. X-ray Anal.*, 1991, **34**, 307.
15 Giauque, R. D., Asaro, F., Stross, F. H., and Hester, T. R., *X-ray Spectrom.*, 1993, **22**, 44.
16 Yap, C. T., *Appl. Spectrosc.*, 1993, **47**, 330.
17 Yamada, T., Yamada, E., Sukigara, T., Tabuchi, H., and Sato, M., *X-sen Bunseki no Shinpo*, 1991, **22**, 81.
18 Raab, G. A., Enwall, R. E., Cole, W. H., Kuharic, C. A., and Duggan, J. S., *Environ. Sci. Res.*, 1991, **42**, 155.
19 Peacock, D. P. S., Williams-Thorpe, O., Thorpe, R. S., and Tindle, A. G., *Antiquity*, 1994, **68**, 209.
20 Kelley, S., Williams-Thorpe, O., and Thorpe, R. S., *Archaeometry*, 1994, **36**, 209.
21 Sparks, C. J., *Adv. X-ray Anal.*, 1976, **19**, 19.
22 Potts, P. J., Tindle, A. G., and Webb, P. C., *Geochemical Reference Material Compositions: Rocks, Minerals, Sediments, Soils, Carbonates, Refractories and Ores Used in Research and Industry*, Whittles Publishing, Caithness, and CRC Press, Boca Raton, FL, 1992.
23 Miller, J. C., and Miller, J. N., *Statistics for Analytical Chemistry*, Ellis Horwood, Chichester, 1984, pp. 132–134.
24 Potts, P. J., Wright, D. W., Watson, J. S., and Webb, P. C., *Chem. Geol.*, 1987, **63**, 345.

Paper 4/06360K
Received October 18, 1994
Accepted January 3, 1995

Merits of Using Barium as a Heavy Absorber in Major Element Analysis of Rock Samples by X-ray Fluorescence: New Data on ASK-1 and ASK-2 Reference Samples*

T. Gnaneshwara Rao and Pradip K. Govil

National Geophysical Research Institute, Uppal Road, Hyderabad 500 007, India

It has been demonstrated that XRF analysis of fused discs doped with Ba instead of La can give acceptable results for major element analysis of silicate rock samples, which are comparable to those obtained from La-doped fused discs. Replicate analysis of reference samples using Ba-doped fused discs indicated an analytical precision of approximately 1% and an accuracy of better than 3% for most of the elements. Another advantage of using Ba as a heavy absorber was that it allows simultaneous determination of Na along with other major elements on the same disc. Sodium levels determined by this method are in good agreement with the results of XRF analysis using pressed powder pellets. However, with Ba-doped discs there could be some difficulty in the determination of Ti and Mn as Ba Lα1 and Lτ2 lines are in close proximity to Ti and Mn Kα lines, respectively, causing enhancement of the background signals of Ti and Mn. This can be avoided by carefully selecting suitable background angles. New major elemental analytical data are provided for the Norwegian reference samples ASK-1 (larvikite) and ASK-2 (schist) as the recommended values for these are not available in the literature.

Keywords: *Heavy absorber; lanthanum; barium doping; fused discs; reference sample*

Introduction

Problems that arise in the major element analysis of silicate rocks by X-ray fluorescence (XRF) spectrometry include particle size effects, sample inhomogeneity and inter-element (matrix) effects. A variety of sample preparation and data reduction techniques have been proposed to overcome these problems. Fused discs are generally preferred for the major element analysis of rock samples to minimize the particle size effect and sample inhomogeneity. It was shown that when the sample is diluted sufficiently with flux (1:100), the matrix effect becomes constant and there is a simple linear relationship between concentration and intensity.[1] A major problem with such extreme dilution, however, is that the estimation of low concentration elements like Ti, Mn and P becomes difficult, as the concentration of these elements falls to below the detection limits. Norish and Hutton,[2] and Rose *et al.*[3] used low dilution techniques but introduced La as a heavy absorber to minimize matrix effects. However, La is not only expensive but also hinders the simultaneous analysis of Na in La-doped samples due to interference of La lines with Na Kα lines (Haukka and Thomas[4]). Thus Na had to be analysed separately in pressed powder pellets. On the other hand, Spangenberg *et al.*[5] used a fusion method of high dilution ratio (sample-to-lithium tetraborate ratio, 1:10), but to reduce matrix effects an intensity-based correction was applied for the determination of major and minor elements. The recent advances in X-ray instrumentation permits accurate analysis of major elements by applying corrections of inter-elemental effects by computer methods (Kodama *et al.*[6]).

Aim of Study

The aims of the present study are (1) to develop a simple and cost effective analytical method for the acurate determination of sodium and other major elements in rock samples by using a single fused disc and (2) to provide new major element analytical data for Analytisk Sporelement Komite ASK-1 and ASK-2, as recommended values for these reference samples are not available in the literature.

Experimental

Sample Preparation

Lanthanum and barium were used as heavy absorbers to reduce inter-elemental effects, accordingly two sets of fusion mixtures were prepared. The first consisted of lithium tetraborate, lithium metaborate and lanthanum oxide in the ratio 2:1:0.45, respectively. In the second set, barium oxide replaced lanthanum oxide. The salts were dried at 300 °C separately for about 4 h in an oven and cooled in a desiccator before mixing with the fluxes. Sample powders were also dried and cooled under similar conditions.

A 0.5 g amount of each sample powder was mixed thoroughly with 2.5 g of the flux and placed in a platinum gold crucible (Pt:Au, 95:5), and heated for 20 min in a Herzog (Germany) (HAG 12/1500) automatic fusion machine at 1200 °C. A built-in rocking device was used for 10 min during fusion to achieve homogeneity and to eliminate air bubbles from the melt. The crucible containing the melt was cooled gradually by exposing it to filtered compressed air and vacuum suction, simultaneously. This yielded clear discs of 31 mm diameter. It was observed that the method produces stable glass discs for rocks of different compositions varying from ultramafic to felsic.

Instrumentation

A Philips (Eindhoven, The Netherlands) PW-1400 microprocesser-controlled wavelength-dispersive, sequential X-ray fluorescence spectrometer with a 100 kV X-ray generator was used for the analysis. A Philips P851 online dedicated minicomputer was used for preparing calibration graphs of concentration *versus* intensity.

* Presented at Geonalysis 94: An International Symposium on the Analysis of Geological and Environmental Materials, Ambleside, England, September 18–22, 1994.

The Philips X-14 software available for the computer enabled dead time, background and line overlap corrections to be made and provided an output as concentration in mass-% in ppm (after converting the counts into concentration with the help of calibration graphs). For further details of Philips X-14 software, the reader is referred to Govil.[7] A spinner was used during measurement for uniform counts. A pulse height discriminator was used for all the elements while a fine collimator was used for some elements to achieve better resolution. All elements were analysed by using a Sc–Mo dual target X-ray tube in a vacuum medium. P-10 gas was used in the gas flow proportional counter. A poly(propylene) counter window of 2 μm thickness was used. The operating conditions are shown in Table 1.

Procedure

Calibration graphs of concentration *versus* intensity were prepared by using the geological reference samples of the United States Geological Survey (USGS), the Canadian Certified Reference Material Project (CCRMP) and the Geological Survey of Japan (GSJ). The concentration of the reference samples were taken from Govindaraju.[8] The internal ratio (I/I_0) technique (Rose *et al.*[9]) was adopted to reduce the instrumental drift error: the background corrected counts of each element for the standards and unknown were divided by the background corrected counts of monitor sample. The method yielded satisfactory linear regression curves over a wide compositional range (*i.e.*, from dunite to granite) for most of the elements. No empirically calculated multi-element correction coefficients are necessary for the samples if there is not much variation in the composition of the samples from the standards used.

The above method also works for extreme compositions, *e.g.*, banded iron formations, provided that the compositions of the standards used for preparation of calibration graphs are similar to those of the samples (*e.g.*, FeR-1, FeR-2, FeR-3 and FeR-4 of CCRMP.

Results and Discussion

Advantage of Ba *Doping*

Major element calibration graphs obtained for a wide compositional range of international reference materials using La- and Ba-doped fused discs are shown in Figs. 1–5. Both La- and Ba-doped discs have given similar linear regression lines for most of the elements. The distinct advantage of Ba doping is particularly evident in the case of Na, where Ba-doped discs give a reliable linear fit, in contrast to the La-doped samples (Fig. 6). The scatter in the La-doped discs is due to the interference of La lines with Na Kα lines. The study also reveals that the presence of La is also a hinderence in the determination of Mg, Ti and Mn (see Haukka and Thomas[4]).

It is observed that even with a Ba-doped set of samples, there is a minor hinderence in the estimation of Ti and Mn, as Ba Lα1 (87.70) and Ba Lτ2 (64.80) lines are in close proximity to Ti Kα (86.70) and Mn Kα (63.60) lines, respectively. Hence, the background of Ti and Mn increases owing to the presence of Ba. This problem was avoided by carefully selecting suitable background angles, *i.e.*, Ti background angle at 86.10° and Mn background angle at 62.90°.

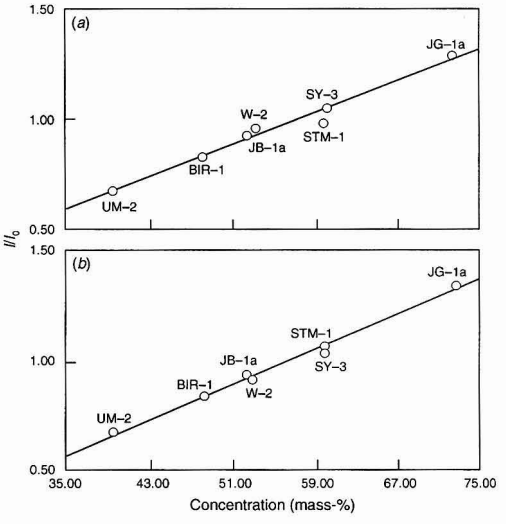

Fig. 1 Major element calibration graphs for (*a*) SiO_2 (La doped), r = 0.986 and (*b*) SiO_2 (Ba doped), r = 0.998. Intensity (I/I_0) *versus* concentration where I and I_0 are the net count rates of the sample and monitor sample, respectively. Standards used for calibration: JG-1a, granodiorite (GSJ); JB-1a, basalt (GSJ); BIR-1, basalt (USGS); W-2, diabase (USGS); STM-1, syenite (USGS); SY-3, syenite (CCRMP); and UM-2, ultramafic (CCRMP).

Table 1 Instrumental parameters of CRF analysis*

	Parameters†									Time/s	
ELE	COL	XTL	UPL	LWL	*E*/kV	*I*/mA	Angle	+OFFS	−OFFS	Peak	Background
Si	C	PET	80	20	40	30	109.80	1.20	—	20	10
Al	C	TlAP	80	20	40	30	38.40	1.20	—	20	10
Ti	F	LiF200	82	10	45	30	86.70	—	0.60	20	10
Fe	F	LiF220	75	15	50	30	86.30	2.40	—	20	10
Ca	F	LiF200	80	20	40	30	113.70	1.60	—	20	10
Mg	C	TlAP	75	20	40	30	45.70	0.70	—	40	20
Na	C	TlAP	70	20	40	30	55.70	1.10	—	40	20
K	C	LiF200	75	18	40	30	137.30	1.00	—	20	10
Mn	F	LiF200	70	30	45	30	63.60	—	0.70	40	20
P	F	PET	80	20	40	30	90.20	1.20	—	40	20

* An Sc–Mo dual target tube was used in the determination of all elements.

† ELE, element; COL, collimator [F, fine (300 μm); C, coarse (150 μm)]; XTL, crystal; *E*, potential; *I*, current; UPL, upper level; LWL, lower level (thresholds of pulse height discriminator); Angle, 2θ angle of goniometer; +OFF, background angle (positive side of peak); and −OFF, background angle (negative side of peak).

The reference samples of Institut Geokhimii, Irkutsk (IGI) USSR, CR-1A (granite) and USGS, DNC-1 (basalt) were used as unknowns in the determination of major elements using Ba-doped discs and corresponding calibration graphs in order to check the validity of the Ba doping technique. The results are tabulated along with the published literature values of Govindaraju[8] in Table 2. It may be noted that the results are in good agreement with values published in the literature and vary within ±3% in most of the cases.

Table 2 also shows the Na concentrations in two geological reference samples of the IGI and USGS obtained by this method. It is evident that the results of Na obtained from the Ba-doped set of samples are in good agreement with the previously reported values of Govindaraju[8] and those obtained using pressed powder pellets. These results encourage the usage of Ba as a heavy absorber in fused discs in place of La, thus avoiding the time consuming preparation of a separate pressed pellet for the determination of Na.

Major element composition (averages) based on replicate analyses of the Norwegian reference samples ASK-1 and ASK-2 are given in Table 3. The discs for these analyses were prepared in triplicate by using Ba-doped flux mixture and each

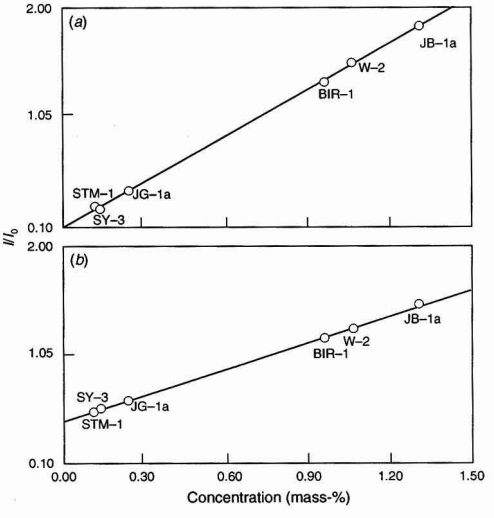

Fig. 2 Major element calibration graph for (*a*) TiO_2 (La doped), r = 1.00 and (*b*) TiO_2 (Ba doped), r = 1.00. For further explanation see Fig. 1.

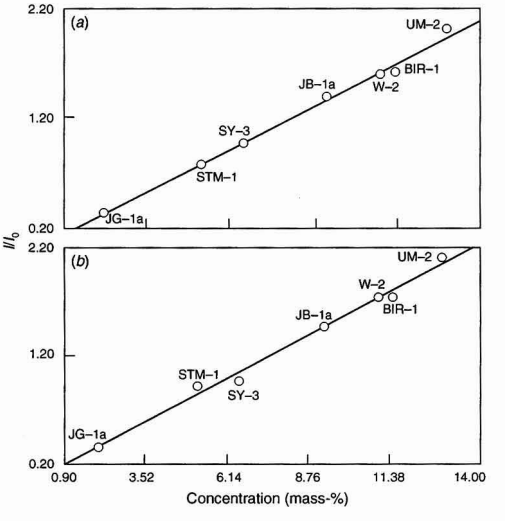

Fig. 4 Major element calibration graph for (*a*) Fe_2O_3 (La doped), r = 0.997 and (*b*) Fe_2O_3 (Ba doped) r = 0.995. For further explanation see Fig. 1.

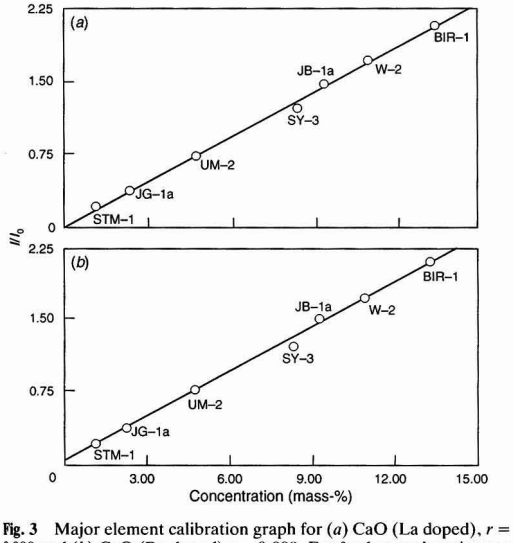

Fig. 3 Major element calibration graph for (*a*) CaO (La doped), r = 0.999 and (*b*) CaO (Ba doped) r = 0.999. For further explanation see Fig. 1.

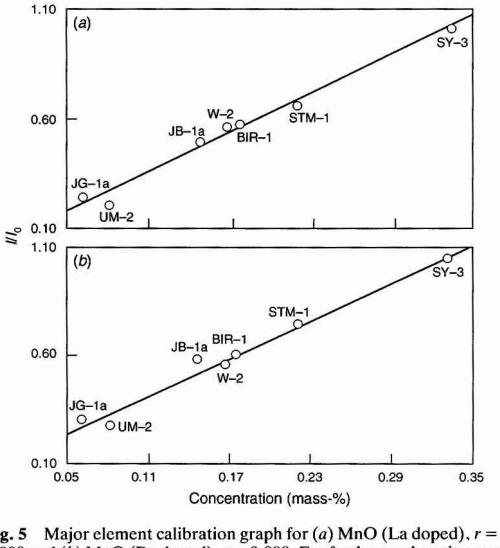

Fig. 5 Major element calibration graph for (*a*) MnO (La doped), r = 0.990 and (*b*) MnO (Ba doped), r = 0.990. For further explanation see Fig. 1.

Table 2 Analytical data for DNC-1 and CR-1A obtained by XRF in the present study and reported values from Govindaraju[8] in mass-%

	DNC1				CR-1A			
Element	A*	B†	Present study‡	*s*	A*	B†	Present study‡	*s*
SiO_2	47.04		47.85	0.35	73.36		73.88	0.37
Al_2O_3	18.30		18.19	0.20	13.84		14.15	0.21
TiO_2	0.48		0.47	0.01	0.07		0.06	0.01
Fe_2O_3§	9.93		10.05	0.02	2.19		2.15	0.04
CaO	11.27		11.54	0.01	0.14		0.15	0.02
MgO	10.05		9.83	0.02	0.054		0.035	0.01
Na_2O	1.87	1.96	1.74	0.08	5.46	5.50	5.35	0.07
K_2O	0.23		0.24	0.05	4.14		4.10	0.06
MnO	0.15		0.165	0.04	0.195		0.185	0.03
P_2O_5	0.085		0.09	0.01	0.013		0.01	0.01

* Values from Govindaraju.[8]
† Sodium values obtained from pressed pellet.
‡ Average of six values.
§ Total iron.

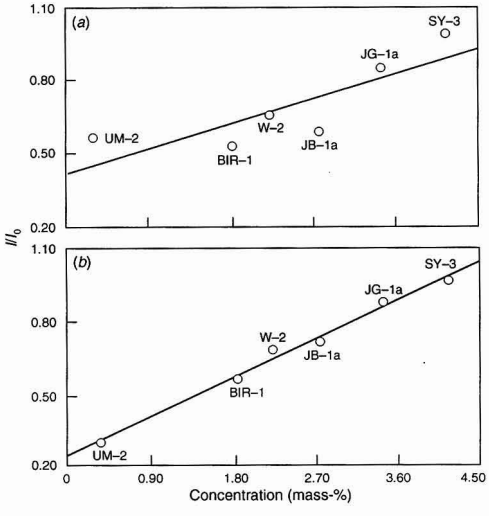

Fig. 6 Graph of intensity *versus* concentration for (*a*) Na_2O (La doped), $r = 0.814$ and (*b*) Na_2O (Ba doped), $r = 0.992$. For further explanation see Fig. 1.

disc analysed three times. For comparison, published literature values are also given in Table 3. The P_2O_5 values for ASK-1 and ASK-2 are not available in literature: the P_2O_5 values obtained by this method could, therefore, be useful.

The authors thank Dr. S. M. Naqvi for constant encouragement, Dr. Y. J. Bhaskar Rao for help during review of the paper and Dr. H. K. Gupta, Director of the National Geophysical Research Institute, Hyderabad, for granting permission to publish this work.

Table 3 Analytical data for ASK-1 and ASK-2 obtained by XRF in the present study and reported values from Govindaraju[8] in mass-%

	ASK-1			ASK-2		
Element	A*	Present study†	*s*	A*	Present study†	*s*
SiO_2	59.50	59.10	0.370	54.20	54.70	0.380
Al_2O_3	18.60	18.10	0.216	18.80	19.20	0.214
TiO_2	1.16	1.06	0.019	0.92	1.00	0.008
Fe_2O_3‡	4.60	4.02	0.040	6.90	6.04	0.042
CaO	3.20	2.75	0.011	0.75	0.81	0.070
MgO	1.10	1.60	0.041	2.00	2.40	0.050
Na_2O	6.50	6.05	0.090	0.80	0.73	0.060
K_2O	4.20	4.10	0.017	5.30	5.06	0.043
MnO	0.14	0.15	0.037	0.04	0.05	0.047
P_2O_5	—	0.40	0.011	—	0.15	0.010

* Values from Govindaraju.[8]
† Average of nine values.
‡ Total iron.

References

1 Claisse, F., *Que. (Prov.) Dept. Mines*, 1956, 327.
2 Norish, K., and Hutton, J. T., *Geochim. Cosmochim. Acta*, 1969, **33**, 431.
3 Rose, H. J., Adler, I., and Flanagan, F. J., *U.S. Geol. Surv., Prof. Pap.*, 1962, **450B**, 80.
4 Haukka, M. T., and Thomas, I. L., *X-Ray Spectrom.*, 1977, **6**, 204.
5 Spangenberg, J., Fontbote, L., and Pernicka, K., *X-Ray Spectrom.*, 1994, **23**, 83.
6 Kodama, H., Brydon, J. E., and Stone, B. C., *Geochim. Cosmochim. Acta*, 1967, **31**, 649.
7 Govil, P. K., *J. Geol. Soc. India*, 1985, **26**, 38.
8 Govindaraju, K., *Geostand. Newsl.*, 1989, **13**, 3.
9 Rose, W. I., Bornhorst, T. J., and Sivonen, S. J., *X-Ray Spectrom.*, 1986, **15**, 55.

Paper 4/05860G
Received September 26, 1994
Accepted January 26, 1995

Accelerator Mass Spectrometry in Environmental Geoscience*

A Review

John Rucklidge

IsoTrace Laboratory, Department of Geology, University of Toronto, Toronto, Ontario, Canada M5S 3B1

Using accelerator mass spectrometry (AMS), ratios as low as 10^{-14} can be measured for rare compared with abundant isotopes of an element. Attaining such an extreme ratio can be achieved through the elimination of interfering molecular ions by high energy dissociation, avoidance of isobaric interference through negative ion discrimination, and reduction of detector background by high-energy ion counting. Carbon-14 is the best known nuclide routinely determined by AMS, because samples with as little as 10^6 atoms of ^{14}C (less than 1 mg of modern carbon) can be measured more rapidly and precisely than is possible by the beta-counting method. AMS can be applied to rare stable nuclides, but most of the applications have been with rare radionuclides the half-lives of which are so long as to preclude decay counting: ^{10}Be, ^{14}C, ^{26}Al, ^{36}Cl and ^{129}I belong to this group, whose half-lives range from 5000 to 16 000 000 years, and which are all produced naturally as well as anthropogenically. Chlorine-36 and iodine-129 have both been used in groundwater tracing studies, and ^{129}I is becoming a more widely applied radionuclide in this respect; one reason being its association with nuclear fuel reprocessing facilities. A radioactively benign nuclide, because of its long half-life, ^{129}I has been released in relatively large amounts into the atmospheric and oceanic environments, where backgrounds have risen several orders of magnitude over pre-bomb levels. The point sources (*e.g.*, Sellafield, Cap la Hague) produce plumes in the North Sea, Barents Sea and Western Atlantic from which transport models can be built. Atmospheric dispersion of ^{129}I from Sellafield over the Lake District has been documented through analysing mosses down-wind from the plant. The immobilization of iodine over the limestone bedrock in the northeast of the region can be seen dramatically in the ^{129}I moss data. Beryllium-10 and aluminium-26, produced continuously by cosmic-ray spallation in the atmosphere, are delivered to the surface by precipitation. Their accumulation in ice cores yields paleo-cosmic-ray flux data, and their presence in soils may allow estimates of creep rates to be made. Additionally, ^{10}Be and ^{26}Al are produced in surface rocks by *in situ* cosmic-ray bombardment, and this leads to a method of estimating exposure or erosion ages of landforms. There are more radionuclides in the environment, about which little is known because of their rarity. One by one, AMS is uncovering their secrets and opening up new frontiers in environmental geoscience.

Keywords: Accelerator mass spectrometry; iodine-129; chlorine-36; beryllium-10; aluminium-26

* Presented at Geoanalysis 94: An International Symposium on the Analysis of Geological and Environmental Materials, Ambleside, England, September 18–22, 1994.

Introduction

Several modern analytical methods have attained the capability of measuring most elements at the ppb (ng g^{-1}) level or even lower. The study of trace elements in the environment has therefore advanced accordingly. But in attempting to extend these methods to substantially lower levels of detection such as 10^{-12} (pg g^{-1}), or even 10^{-15} (fg g^{-1}), problems inevitably arise. In the case of mass spectrometry, for instance, detector backgrounds, and molecular and isobaric interferences impose a practical limit which, except in certain special cases, has only been passed in the technique of accelerator mass spectrometry (AMS). The atomic species of interest at these low levels are mostly long-lived radionuclides since by their very nature they rarely attain higher concentration levels by natural processes. Stable nuclides, on the other hand, often become less interesting in this background region.

Radionuclides are usually determined by counting the gamma or beta rays emitted when they decay. Providing the activity is reasonably high, this works well, but where the radionuclide has a long half-life, and additionally may be present at very low levels, counting is realistically impossible. In these situations the solution would be to count the atoms by mass spectrometry, but this runs into severe problems because there are invariably stable nuclides with the same nominal mass (isobars) that are present in much greater abundance. A mass spectrometer with high resolution might be able to separate them, but with such a loss in efficiency that it could not be tolerated when dealing with such low concentrations. For example, ^{14}C is present at a level of 1 part in 10^{12} of modern carbon while nitrogen is ubiquitous. Even in carefully purified samples of carbon the presence of ^{14}N impurities would prevent the ^{14}C being measured, and with the additional mass overlap of molecules such as $^{12}CH_2$ and ^{13}CH there is no possibility of detecting ^{14}C unambiguously. Isotope ratios less than 10^{-6} cannot in practice be measured with conventional, low energy, mass spectrometers because of molecular and isobaric interferences, and detector background noise. The method of AMS which employs high (MeV) energies largely solves these problems.

In Fig. 1 the relative efficiency of measuring various radionuclides by decay counting and by AMS in samples of elementally pure material where the radionuclide has a concentration of 10^{-12} are compared. For radionuclides with a half-life greater than one year, decay counting produces count rates greater than 1 cps in sample sizes of 1 mg. For longer half-lives in such small samples the rates become unacceptably low. Neutron activation may succeed in transforming the weakly active radionuclide into a more active species (*e.g.*, ^{129}I to ^{130}I) and this reduces the time needed for any one measurement, but the sample mass threshold for detection of ^{129}I is still in the region of 1 g total iodine. AMS, on the other hand, gives count rates that are independent of half-life and sample size and are typically in the range 1–100 cps.

Radionuclides that are currently of interest in environmental geoscience are at present rather few. This may be largely because the environmental behaviours of the various radionuclides have not been established, the number of facilities where measurements can be made are relatively few, and the range of radionuclides studied rather limited. However, several radionuclides occur both naturally and anthropogenically with such long half-lives (5000 to 16 000 000 years), such low concentrations and, therefore, such low radioactivities, that from a radio-toxicity perspective they are completely benign biologically and environmentally: yet, they present the opportunity of being applied as tracers and indicators in a wide variety of systems. A major advantage of using AMS on these radionuclides is that extremely small samples are needed and measurements can be rapid. Instead of tens or even hundreds of litres of water being needed to make an ^{129}I measurement in sea-water, less than a litre may now suffice. This obviously alters the experimental strategy in studies where sample collection time and storage is critical, as on ocean cruises.

The AMS Method

AMS, which uses a tandem electrostatic accelerator, is not to be confused with tandem mass spectrometry. While both have two mass spectrometers in sequence and ions suffer charge modification in passing from one to the other, the former uses multi-megavolt acceleration potentials to eliminate molecular ions from the ion beam. AMS thus employs the methods and equipment of nuclear and particle physics, and most AMS laboratories have developed from this root. A complete description of AMS can be found in many review articles (*e.g.*, Litherland *et al.*,[1] Elmore and Phillips[2]) therefore only a brief outline of the essential features will be given here.

As ^{14}C was the first radionuclide to be studied by AMS, this will be used to illustrate the method. Samples are prepared in a pure, solid form, which, in the case of carbon, frequently takes the form of graphite. Carbon dioxide is derived from the raw sample by combustion, hydrolysis, *etc.*, and after conversion through lithium carbide, acetylene is cracked to deposit a layer of graphite (ideally 1 to 10 mg) on an aluminium substrate. This becomes the 'target' for sputtering by a Cs^+ ion beam in an ion source, and negative ions of C^- are extracted to form the beam for analysis. Fig. 2 illustrates schematically the essential features of an AMS system.

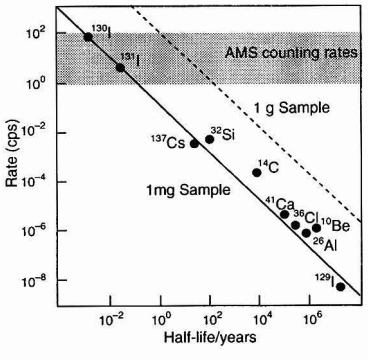

Fig. 1 Counting rate for a number of radionuclides *versus* half-life (λ) for a 1 mg sample and a concentration of 10^{-12} for the radionuclide in an elementally pure material. Solid line serves as a guide. Expected counting rate for a 1 g sample is also shown. On the same plot, the range of typical counting rates for an AMS system is delineated by the shaded area. Actual counting rates will depend upon a number of physical and instrumental parameters such as negative-ion formation efficiency, ion-source intensities and transmission factors.

The beam passes through the electric and magnetic sectors of a mass spectrometer to select negative ions of mass 14, which are then injected into the tandem accelerator and raised to at least 2 MeV energy in the 'terminal' of the accelerator. Here the ions pass through a gas 'stripper' which removes one or more electrons from the ions in the beam. The voltage on the terminal is chosen such that most ions in the beam lose at least 4 electrons bringing the positive ionic charge to 3+. Selection of the charge state 3+ ensures that only monoatomic ions continue in the beam, as molecules cannot form stable bonds against the large coulomb repulsive forces encountered within multiply charged molecules. The destruction of the molecules removes molecular ions from the beam. Hence the resolving power required of the magnets is reduced, and the system can be optimized for maximum transmission efficiency.

Subsequent acceleration by -2 MV in the second part of the tandem brings the ions back to ground potential with an energy of 8 MeV at charge 3+. Further electric and magnetic sector analysis at the high energy end of the machine results in the removal of molecular fragments from the beam and the passage of monoatomic atoms of mass 14 to the detector.

The atomic isobar discrimination against ^{14}N takes place in the ion source, because nitrogen, having a negative electron affinity, cannot form a negative ion and therefore never enters the beam. This serendipitous situation works perfectly in the instance of ^{14}C and also ^{129}I, the isobar of which is the noble gas Xe; other isobars are less obliging. Chlorine-36 has the stable isobar ^{36}S, and both these species form negative ions readily and therefore separation has to be accomplished by range discrimination in the detector after acceleration. Unfortunately this requires acceleration to considerably higher energies ($\approx$32 MeV) than can be attained in a 'small' accelerator, so ^{36}Cl and radionuclides with similar isobar problems can only be measured on 'big' machines. Beryllium-10 presents another problem in that Be does not form a negative ion in the ion source. The solution in this instance is to optimize the production of BeO^- in the ion source and then select Be^{3+} from the break-up of molecules in the terminal of the accelerator. Each radionuclide which is to be analysed presents a separate set of difficulties that must be worked out with patience and ingenuity. In no way can AMS be considered to be a 'turn-key' system! Table 1 lists the various AMS laboratories currently active, along with radionuclides in which they specialize.

Iodine-129 in the Environment

Iodine-129 is a radioactive isotope of iodine with a half-life of 1.57×10^7 years. It has the potential for use as a geochronometer on time scales of the order of 10^8 years and attempts

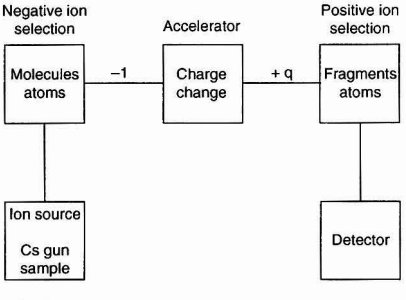

Fig. 2 Principles of a basic tandem-accelerator mass spectrometer shown schematically. Both the negative ion and positive ion blocks represent combinations of electric and magnetic analysers which select energy and ion momentum.

to use it in the characterization of oil formations and associated salt brines have been described.[3] It has also found applications in hydrological studies, particularly when used in conjunction with other long-lived radionuclides such as ^{36}Cl.[4] The natural provenance of ^{129}I has been ascribed to:

(*i*) cosmic ray spallation of Xe isotopes,[5]
(*ii*) spontaneous fission of ^{238}U,[6]
(*iii*) neutron induced fission of ^{235}U,[6] and
(*iv*) meteoritic debris,[7]

but none of these processes has been established with any degree of precision. It is not improbable that the major source of natural ^{129}I is fission related and emerges through volcanism or de-gassing of the lithosphere.[8] However, by far the greatest source of ^{129}I in recent years has been through nuclear activity in the form of atmospheric weapons testing and nuclear fuel reprocessing.

An indication of the magnitude of the weapons testing programme input to the ^{129}I inventory has been documented by Kilius *et al.*,[8] who studied contemporary and archived seaweed collected around the coast of North America. Samples dating from the pre-bomb era had $^{129}I/^{127}I$ ratios two orders of magnitude less than samples that had grown since the testing began. The pre-bomb ratios lie in the range 10^{-12}–10^{-11}, while post-bomb values exceed 10^{-10}. These samples of seaweed, taken more or less randomly from coastal locations, document clearly the global dispersion of ^{129}I owing to nuclear activity. Because of the long half-life of ^{129}I, it has become a permanent contaminant on a human time scale, but by the same token it is a harmless one, being biologically indistinguishable from the stable ^{127}I.

The value of ^{129}I as a tracer cannot be overestimated. For example, ^{129}I can serve as a monitor for the release of other biologically harmful highly radioactive iodine isotopes such as the shorter-lived ^{131}I (half-life 8 d). Within a few weeks (about 10 half-lives) the ^{131}I has decayed below detection limits, but the ^{129}I record remains and integrates the total exposure.

Hence today there exists a unique opportunity to study the distribution and transport of iodine within the biosphere, and this arises through the fortunate coincidence of three developments. Firstly, regions exist where there are high concentrations of ^{129}I due to human activity. Nuclear facilities such as Hanford and Savannah River in North America, Sellafield and Cap la Hague in Europe, act as point sources from which the ^{129}I can be followed. At such point sources ^{129}I will enter the global circulation slowly and will not become uniformly distributed. The residence time of iodine in the atmosphere is about 15 d[9] compared with 10 years for ^{14}C. Unless the pulse extends well into the stratosphere, a release of ^{129}I will redeposit locally, whether it be in the ocean or on land.

The second relevant development is the ability to measure ^{129}I at background levels on small samples using AMS. Before the advent of AMS, only ^{129}I significantly above the natural background could be measured, and only then using large samples, neutron activation and long counting times.

The third aspect of this situation concerns the rather poor understanding of the iodine cycle in the atmosphere, hydrosphere, lithosphere and biosphere. With ^{129}I to act as a tracer, this problem can be tackled, but there is an urgency to proceed before the background levels rise even higher and the tracer becomes homogenized.

Columbia River

In responding to the challenge issued above, a study of dispersion of ^{129}I from the mouth of the Columbia River was undertaken.[10] The estuary of the Columbia is a convenient

Table 1 Accelerator mass spectrometry laboratories

Institution	Species analysed	Date or status
New laboratories with specialized instruments—		
Research Lab for Archaeology, Oxford, UK	^{14}C	1981
Dept. of Physics, University of Arizona, USA	^{14}C	1981
IsoTrace laboratory, University of Toronto, Canada	^{14}C, ^{129}I, trace precious metals	1981
University of Nagoya, Japan	^{14}C	1981
CNRS, Gif sur Yvette, France	^{10}Be, ^{14}C, ^{26}Al	1982
NOSAMS, Woods Hole Oceanographic Inst., USA	^{14}C	1990
University of Gröningen, Netherlands	^{14}C	1993
Leibnitz Laboratory, University of Kiel, Germany	^{14}C	1995
Existing laboratories with upgraded instruments—		
Far East		
University of Kyoto, Japan	^{10}Be, ^{14}C, ^{26}Al	5%
University of Osaka, Japan	^{41}Ca	5%
University of Tokyo, Japan	^{10}Be, ^{14}C, ^{26}Al	25%
Peking University, China	^{10}Be, ^{14}C, ^{26}Al, ^{36}Cl	100%
Shanghai Institute for Nuclear Research, China	^{10}Be, ^{14}C, ^{26}Al	Shared
Australian National University	^{10}Be, ^{14}C, ^{26}Al, ^{36}Cl	Shared
Australian Nuclear Scientific & Technology Organization	^{10}Be, ^{14}C	Shared
New Zealand Institute of Geological & Nuclear Sciences	^{14}C	100%
Europe		
University of Uppsala, Sweden	^{10}Be, ^{14}C	Shared
University of Utrecht, Netherlands	^{10}Be, ^{14}C	Shared
Paul Sherrer Institute, Zürich, Switzerland	^{10}Be, ^{14}C, ^{26}Al, ^{36}Cl	Shared
Weizmann Institute, Rehovoth, Israel	^{14}C, ^{26}Al, ^{129}I	Shared
Technische Universität, Munich, Germany	^{36}Cl, ^{41}Ca	Shared
North America		
Chalk River Laboratories, Canada	^{14}C, ^{36}Cl, ^{129}I	Shared
Lawrence Livermore National Laboratory, USA	^{3}H, ^{10}Be, ^{14}C, ^{26}Al, ^{36}Cl, ^{129}I	Shared
University of North Texas, USA	Semiconductor impurities	Shared
University of Pennsylvania, USA	^{3}H, ^{10}Be, ^{14}C, ^{26}Al, ^{36}Cl, ^{129}I	Shared
PRIME Laboratory, Purdue University, USA	^{10}Be, ^{36}Cl	100%
University of Rochester, USA	^{36}Cl, ^{129}I	Shared
University of Washington, USA	^{14}C	Shared

source from which to trace the transport of ^{129}I by coastal currents along the west coast of North America because large quantities of ^{129}I are known to exist at the Hanford nuclear fuel reprocessing facility[11] approximately 300 km up-stream in the state of Washington, and the estuary of the Columbia is at the apex of the northerly flowing Alaskan current and the southerly flowing Californian current.

It has been estimated that there are approximately 8×10^8 l of high level nuclear waste in storage at Hanford. Wells in the area have been found to contain ^{129}I concentrations in the range 10^{10}–10^{17} atoms l^{-1},[11] though in the nearby Columbia River the levels reported were lower (up to 10^9 atoms l^{-1}). However, thyroids taken from goldfish in the Gable Mountain Pond on the Hanford Reservation Area had concentrations of 2.2×10^{15} atoms g^{-1}; the equivalent $^{129}I/^{127}I$ isotopic ratio would be 1.2×10^{-2}!

The high level on-site ^{129}I distributions are well known, but the transport of ^{129}I away from the Columbia River estuary has been fragmentary because of the much lower concentrations that are difficult to measure by non-AMS methods. Samples of algae were collected along the coast both south and north of the estuary, and iodine was extracted from these to form targets for AMS analysis in the form of AgI.[10] The results of this study are reproduced in Fig. 3 where empirical exponential functions have been fitted to the data. Symmetrical dispersion curves exist on both sides of the estuary, and the baseline is consistent with the level of fallout-contaminated ocean water in the northern hemisphere.[8] The average initial $^{129}I/^{127}I$ input level determined from these curves is 1.8×10^{-9}, which is about 10 times higher than the 2×10^{-10} value measured in seaweed in 1975.[12]

Atmospheric Transport of ^{129}I Over Land

Fuge[13] has shown that iodine in the secondary environment is derived from the oceans by way of the atmosphere, and as a result near-coastal soils and surface waters are greatly enriched relative to inland areas. It appears that appreciable quantities of iodine are recycled from soils, lakes and rivers by volatilization. In acid soils and waters, iodine is present as the I^- ion which can be oxidized to I_2 and volatilized. In alkaline conditions the iodine is more likely to be present as IO_3^-, which is not converted to I_2. Soils and waters in limestone regions may therefore be equally enriched in iodine compared with those in other geological terrains, but the iodine is not volatilized and hence is unavailable to plants and animals by atmospheric transfer. To test this hypothesis a study was undertaken to utilize the effective point source of isotope specific iodine in the form of ^{129}I released at the Sellafield Nuclear facility on the coast of Cumbria, England, and to sample the downwind plume to the northeast of the plant by analysing moss.[14] The south-westerly prevailing wind from Sellafield crosses the heart of the English Lake District, which consists of mountains rising to almost 1000 m, composed mainly of Ordovician slate and meta-volcanic rocks. Beyond the mountains lies a band of Carboniferous limestone and beyond that Triassic sandstone. This combined geological and industrial situation provides an ideal setting for testing the theory of iodine transport and fixation.

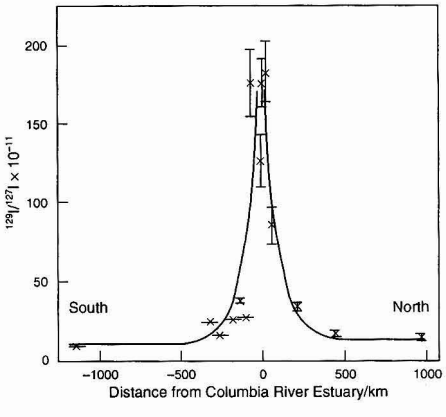

Fig. 3 Iodine-129 ratios ($\times 10^{-11}$) plotted as a function of distance from the mouth of the Columbia River. Solid curves are derived from a least squares fit to the southern and northern portions of the measured iodine distribution.[10]

In Fig. 4 sample locations and important geological boundaries are shown. Approximately 1 g dry mass of sphagnum moss sufficed to provide a AgI target sufficient for ^{129}I analysis. Even with this amount, large dilutions (up to 10 000 times) were necessary because of the high ratios.

The results of the $^{129}I/^{127}I$ ratio measurements and total iodine analyses are shown Table 2. The ratios vary over a wide range from 6.7×10^{-5} to 1.5×10^{-7}. For comparison Kilius *et al.*[8] report an average value close to 10^{-10} for 'post-bomb' seaweed from the Atlantic and Pacific shores of North America while 'pre-bomb' is less than 10^{-11}. The Lake District mosses are 4 to 6 orders of magnitude greater than this 'baseline' figure.

In attempting to understand the data the following premises were assumed. Iodine in moss is obtained directly from the atmosphere. The ^{129}I in the samples is assumed to be mostly derived from the plume from the Sellafield plant. The stable ^{127}I also comes with the wind from the coast but mostly from the soil, except where it lies over limestone. Hence the highest

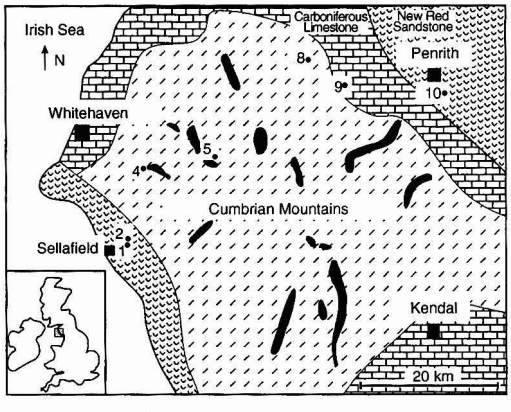

Fig. 4 Map of the English Lake District showing important geological boundaries and locations of moss samples collected for ^{129}I analysis.[14]

Table 2 Iodine ratios and total iodine measured in moss samples

Sample	$^{129}I/^{127}I$ ($\times 10^{-8}$)	Total I (ppm)
1	6693.0 ± 1188	5.1
2	14.72 ± 8.9	8.9
3	214.2 ± 15.5	24.5
4	78.65 ± 4.94	2.0
5	142.7 ± 80.5	6.8
9	653.0 ± 830	2.8
10	25.85 ± 1.96	2.3

ratios of $^{129}I/^{127}I$ are found in dry moss close to the plant, and in moss over limestone at the extreme end of the traverse. In between there is a general falling off of ^{129}I with distance from Sellafield. One anomalous sample, number 2, was taken from the banks of a stream in a heavily wooded valley quite near the plant. This sample must have been periodically washed with running water which would tend to remove the ^{129}I and possibly exchange it with stable ^{127}I being brought down from the hills where it originally derived from the wind from the sea.

The high values of $^{129}I/^{127}I$ ratios measured in the Lake District, the remarkable variation of the ratio over relatively small distances, and the amazing influence of limestone bedrock on the ratio calls for further work to establish the details of this process. To put these data in a different perspective, it should be noted that the ^{129}I concentrations measured in the mosses exceed the values found in soils collected near Chernobyl after the 1986 accident.

Iodine-129 in the North Atlantic and Arctic Oceans

In the pre-nuclear era the concentration of ^{129}I in the oceans of the world has been estimated[8,15] to be 3×10^5 atoms l^{-1} corresponding to a $^{129}I/^{127}I$ ratio of 10^{-12} assuming an oceanic ^{127}I concentration of 60 mg l^{-1}.[16] The input of ^{129}I from nuclear weapons testing, $\approx 2 \times 10^{26}$ atoms,[17] increased the concentration in ocean surface water to $\approx 3 \times 10^7$ atoms l^{-1}. It is now estimated that during the last 25 years the nuclear fuel reprocessing facilities at Sellafield (UK) and Cap la Hague (France) have added $\approx 5 \times 10^{27}$ atoms, or about 1200 kg of ^{129}I, most of which is transported up the West European coast into the North Atlantic and Arctic Oceans.[18]

Studies of the distribution of ^{129}I in this region have been initiated by Zhou *et al.*[18] who have used the AMS technique, which is capable of detecting as little of 10^6 atoms of ^{129}I. Based on the concentrations now known to be present in the oceans, it is clear that water sample volumes much less than a litre are adequate, and in the Eastern Atlantic in the vicinity of the sources, as little as 1 ml suffices. Their data, measured on water and seaweed samples, show $^{129}I/^{127}I$ ratios ranging from a high of 3.7×10^{-6} at Herquemoulin close to Cap la Hague to a low of 2.4×10^{-10} in the Vestmarnaeyjar off the coast of Iceland. A few of their data are reproduced in Table 3. The values in the Irish Sea, close to Sellafield, are considerably lower than the French values. It is possible to correlate the changes in $^{129}I/^{127}I$ in seaweeds from archived collections from Goury, near Cap la Hague, with the quantities of fuel reprocessed year by year.[18]

It is clear from these data that currents carry the ^{129}I emissions north along the coast of Europe into the Arctic from whence they may go west into the south flowing East Greenland current, or east into the Barents and Kara Seas. Further work by Raisbeck *et al.*[20] shows that even in the Kara Sea, where there is reputed to be extensive dumping of nuclear debris by the former USSR, the $^{129}I/^{127}I$ ratios are slightly lower than in the Barents Sea to the west. Contrary to earlier measurements of ^{137}Cs,[19] there is no indication of significant increase in ^{129}I with depth, thus arguing against any important contribution from sources on the sea bed. However, Raisbeck *et al*[20] report that there are enhanced $^{129}I/^{127}I$ ratios along with lower ^{129}I concentrations at stations influenced by water flowing in from the Ob river. This is owing to the fact that stable iodine in fresh water is typically an order of magnitude less than in sea-water, and hence there may be sources of ^{129}I inland being carried down the river.

Although it is not at present possible to measure ^{137}Cs by AMS (the measurement of ^{134}Cs, ^{135}Cs and ^{137}Cs is currently under development at the IsoTrace Laboratory, University of Toronto) existing data show that the $^{129}I/^{137}Cs$ ratio in emissions from nuclear fuel reprocessing is substantially larger than in unreprocessed nuclear releases. For example,[18] the $^{129}I/^{137}Cs$ ratio from recent releases from Sellafield and Cap la Hague are >3000, while the production ratio from ^{235}U fission is ≈ 0.1. Thus by measuring such a ratio it is possible to impose constraints on the origin of the radioactivity observed in the oceans, and a powerful fingerprinting tool becomes available.

Beryllium-10, Aluminium-26 and Chlorine-36

These three radionuclides have half lives of 1.6×10^6, 7.2×10^5 and 3.01×10^5 years, respectively. Beryllium-10 and aluminium-26 are relatively easily measured using a 'small' accelerator, and Raisbeck *et al.*[19] give an account of a laboratory specializing in these radionuclides at Gif-sur-Yvette. The stable isobar of ^{10}Be, ^{10}B, is of higher atomic number than Be, and being a light element can be discriminated against by dE/dx rejection in the detector. The stable isobar of ^{26}Al, ^{26}Mg, does not form negative ions, and so is

Table 3 Iodine ratios in seaweed and water from the coasts of western Europe[19]

Location	Sample type	Sample/mg or ml	$^{129}I/^{127}I$ measured ($\times 10^{-11}$)	^{127}I/mg l^{-1}	$^{129}I/^{127}I$ in sample ($\times 10^{-10}$)
Doélan, France	Seaweed	17.53	95.0 ± 20	—	9.5 ± 2.0
Doélan, France	Water	100.0	0.29 ± 0.04	120.0 ± 6.0	12.3 ± 1.8
Roscoff, France	Seaweed	11.76	50.3 ± 1.1	990.0 ± 50	500.0 ± 30
Cancale, France	Seaweed	11.30	343.0 ± 23	300.0 ± 15	3 400.0 ± 300
Carteret, France	Seaweed	18.42	124.0 ± 2	650.0 ± 65	7 600.0 ± 800
Herquemoulin, France	Seaweed	11.03	213.0 ± 6	690.0 ± 70	37 000.0 ± 3800
Fermanville, France	Seaweed	12.07	185.0 ± 5	754.0 ± 75	15 000.0 ± 1500
Gatteville, France	Seaweed	7.40	796.0 ± 63	310.0 ± 15	8 000.0 ± 700
Luc sur Mer, France	Seaweed	11.18	310.0 ± 19	340.0 ± 17	3 100.0 ± 250
Lowestoft, England	Water	100.0	3.9 ± 0.9	46.5 ± 2.3	430.0 ± 60
Heysham, England	Water	100.0	32.0 ± 4	36.5 ± 1.8	8 900.0 ± 1200
Maryport, England	Water	100.0	18.0 ± 2	36.2 ± 1.8	5 100.0 ± 600
Lossiemouth, Scotland	Water	100.0	1.8 ± 0.2	57.8 ± 2.9	160.0 ± 20
Thorshavn, Faroe Islands	Seaweed	7.31	29.0 ± 4	—	2.9 ± 0.4
Sørvagur, Faroe Islands	Seaweed	10.01	39.0 ± 5	—	3.9 ± 0.5
Vestmarnaeyjar, Iceland	Seaweed	18.01	24.0 ± 5	—	2.4 ± 0.5
Grimsy, Iceland	Seaweed	17.60	39.0 ± 6	—	3.9 ± 0.6
Raudfjorden, Svalbard	Seaweed	1.94	26.0 ± 0.5	194.0 ± 8	37.2 ± 1.2
Adventfjorden, Svalbard	Seaweed	1.92	0.23 ± 0.004	1.90 ± 0.06	32.2 ± 1.1

rejected in the same way that ^{14}N is prevented from interfering with ^{14}C. Chlorine-36, as mentioned above, has the isobaric interference ^{36}S, which has never been rejected by a small machine, being both lower in atomic number than Cl, and also being in the medium atomic mass range where the dE/dx discrimination requires higher energies. Chlorine-36 at the present time can only be measured using a large, at least 8 MV, accelerator, and it can be seen from Table 1 that there are relatively few laboratories that handle this radionuclide.

Beryllium-10, aluminium-26 and chlorine-36 are all produced by cosmic ray spallation in the atmosphere, and they arrive on Earth's surface by precipitation. These are the so-called 'garden variety' of these radionuclides,[21] and are so named to distinguish them from the same radionuclides produced by spallation of solid material at Earth's surface. Chlorine-36 inevitably ends up in solution in groundwater, rivers, lakes and oceans, and in the groundwater environment can be a valuable tracer. Vogt *et al.*[22] report on ^{36}Cl studies on water in some shallow wells on perched aquifers from the American Mid-West; they concluded that the recharge water dated from before the nuclear weapons testing era, and showed that the ^{36}Cl in the wells was not significantly different from that of present-day precipitation, at a level of $^{36}Cl/Cl$ of 10^{-12}.

Another recent study utilizing ^{36}Cl concerns the origin of waters in a granite batholith in south-eastern Manitoba, and is part of the Underground Research Laboratory of the Canadian Nuclear Fuel Waste Management Study.[23] In this instance ^{36}Cl in the shallower levels of the batholith appears to be mainly cosmogenic, *i.e.*, from atmospheric spallation, with a possible bomb component suggested by the occasional presence of ^{3}H. In fracture zones the $^{36}Cl/Cl$ ratios are significantly higher (by 1.5 to 2.5 times) than the ratios in undisturbed rock, and this may be explained by the fact that U and Th are typically enriched in these areas, thereby producing a greater neutron flux, and hence local generation of ^{36}Cl by neutron capture on ^{35}Cl.

The use of ^{36}Cl in groundwater studies is still in its infancy, but because of the small samples required when using AMS it has a great potential, though the need to use large expensive machines for the measurements has doubtless discouraged rapid application of this radionuclide. The complex behaviour pattern in the environment still needs to be worked out in detail. In basinal aquifers, ^{36}Cl may provide the information for determining palaeorecharge conditions, and in unsaturated zones, the presence of the 'bomb pulse' offers a significant advance compared with other methods in the determination of the recharge rate.[24]

In contrast to ^{36}Cl, which is soluble, ^{10}Be and ^{26}Al attach to particulates and accumulate in the sedimentary environment, such as the ice caps of Greenland and Antarctica,[25] or in ocean floor sediments. In the former ^{36}Cl, ^{10}Be and ^{26}Al provide a detailed record of recent cosmic ray flux and hence are important in interpreting climatic history; ^{10}Be data from the Vostok ice core has established a precise age calibration back to 2.20×10^5 years BP.[25] In the sedimentological area these isotopes also have potential geochronological use,[26] and a novel application of using ^{10}Be to measure bedrock-to-soil conversion rates has recently been described by Monaghan and Elmore.[21] Precipitation from atmospheric spallation is the dominant source of this radionuclide in soils, and the amount found in the soil depends upon the length of time the soil has been exposed, the chemical and physical removal rates, and the decay constant of ^{10}Be. Working on soil on hill slopes in the Coast range of California it has been shown that measurement of ^{10}Be allows a distinction to be made between increasing and decreasing bedrock-to-soil conversion rates as on moving downslope, and also provides quantitative estimates of bedrock-to-soil conversion rates as a function of position on a hill slope. Slopes seem to change shape with a characteristic time of about 75 000 years, while the transit time of soil on the slope is about 12 500 years. Knowledge of these rates is important for developing soil conservation strategies and understanding landscape evolution.[21]

Surface Exposure Age Dating

Although the dominant source of cosmogenic nuclides at the Earth's surface is from cosmic ray spallation in the atmosphere, they may also be generated in exposed rocks, albeit at a much lower rate. It has only become feasible to measure this *in situ* production of radionuclides by cosmic rays since the advent of AMS. Typical reactions involve ^{10}Be and ^{14}C from the nuclear spallation of O, ^{26}Al from spallation of ^{28}Si and negative mu-meson capture in ^{28}Si,[27] and ^{36}Cl from spallation on Ca. Production rates are low, and depend not only on depth below the exposed surface, but also on altitude and latitude. In 1 g of quartz at mountain altitudes, only 10 to 100 atoms of ^{26}Al and ^{10}Be are produced per year,[27] but nevertheless the build-up over time produces enough atoms in a 10–20 g sample that it can be measured by AMS. Fig. 5 shows how the radionuclide builds up to within 1% of saturation after a period of 7 half-lives. At saturation the production rate matches the decay rate, and corresponds to about 2×10^7 atoms g^{-1} of ^{10}Be and ^{26}Al in quartz at sea level. This value would rise to about 5×10^8 atoms g^{-1} at an altitude of 5 km where the atmospheric shielding is much less.[27] Production rates are reported normalized to sea level and 'high latitude'. Details of these rates and other related data are shown in Table 4.

A requirement for the mineral phase is that it should have a low content of the elements of interest in order to produce a measurable ratio. Quartz is ideal in this respect, although occasionally the Al content is high enough to give trouble. Based on the models outlined below it is possible to measure the length of time a surface has been exposed, say after the removal of ice cover, or alternatively by the processes of erosion.

The typical depth of penetration (L) of cosmic rays in surface rocks is short ($L \approx 50$ cm for reduction in intensity by 1/e) so nuclides do not begin building up appreciably until the rocks in question are close to the surface.[30] If T_{ero}, the average time for L cm to be removed by erosion, is long compared with T_m, the mean life of the nuclide, the nuclide in the rock would be in secular equilibrium with the radioactive decay, while if $T_{ero} \ll T_m$ the nuclide concentration is in erosion equilibrium. Only an upper limit can be determined for the erosion rate in

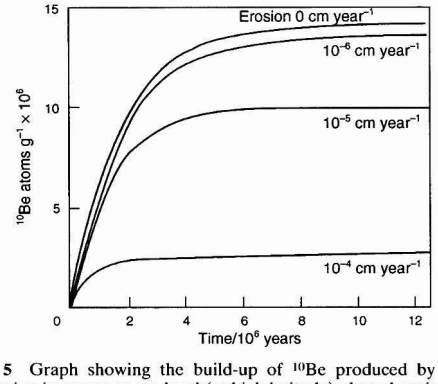

Fig. 5 Graph showing the build-up of ^{10}Be produced by *in situ* spallation in quartz at sea level (at high latitude) plotted against time for various erosion rates.

Table 4 *In situ* production data for ^{10}Be, ^{14}C, ^{26}Al and ^{36}Cl

	^{10}Be	^{14}C	^{26}Al	^{36}Cl
Material	Quartz	Basalt	Quartz	Calcite
Altitude/m	3340	1445	3340	3005
Latitude (°N)	44	38.9	44	37.9
Half-life/years	1.6×10^6	5.73×10^3	7.2×10^5	3.01×10^5
Production rate/atoms g^{-1} $year^{-1}$	61.9 ± 3.0	55 ± 10	373.6 ± 27	250
Sea level, high latitude/atoms g^{-1} $year^{-1}$	6.03 ± 0.29	21 ± 4	36.8 ± 2.7	29.3
Reference	27	28	27	29

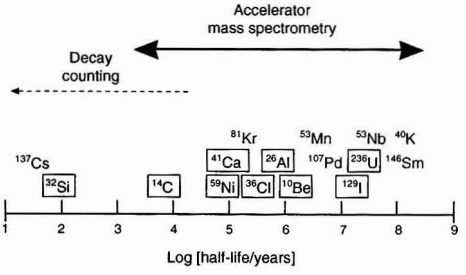

Fig. 6 Some cosmogenic nuclides with various half-lives. Nuclides shown in boxes have been measured by AMS.

the former instance, but when $T_{cro} \leq T_m$ the erosion rates can be determined easily. The estimates are very sensitive to production rates when $T_{cro} \approx T_m$, and in practice several nuclides have to be used to determine geomorphological changes on different time scales.[30] Hence it is important to know the *in situ* production rates accurately and this has now been done for the nuclides under discussion here. By measurement of granitic rocks in the Sierra Nevada of California, which were polished by glacial action in the Tioga period 10 000 to 11 000 years ago, and in which the erosion has been less than 1 mm, it has been possible to acquire the necessary data.[28]

Brown *et al.*[31] have used ^{10}Be and ^{26}Al to determine the surface exposure ages of Antarctic moraines. Ages ranging from 5×10^4 to 2.5×10^6 years were found to be in accordance with other geological evidence. Further development of the method by using the ratio of production rates of nuclides with different half-lives[32] has shown that more precise measurements can be obtained; the results are less dependent on the absolute production rates, which may vary due to changes in the primary cosmic ray flux. This, of course, requires more complex measurement strategy because the different radionuclides must be measured independently, using different samples and experimental conditions, perhaps even different accelerators.

An interesting consequence of the build up of ^{10}Be in surface rocks, whether by *in situ* production or by precipitation, is the purity of commercial aluminium. Bauxite (Al ore) from Haiti has been found to contain $\approx 6 \times 10^9$ atoms of ^{10}Be per gram, which leads to 5.7×10^{10} atoms of ^{10}Be per gram in the refined Al.[33] As aluminium is frequently used in the samples used for analysis by AMS this may lead to significant levels of contamination.

Chlorine-36 is a relative newcomer to the *in situ* production field. It is produced by a variety of cosmic reactions on Ca and is ideally suited for the measurement of limestone erosion rates. The concentration of muon-produced ^{36}Cl from Ca, as opposed to spallation, persists to greater depths and therefore responds more slowly to erosion than ^{36}Cl at the surface. Deep samples therefore integrate erosion over longer periods than surface samples, and combined measurements can be used to detect past changes in erosion rates. Samples from Australia and New Guinea yielded limestone erosion rates ranging from 5 μm $year^{-1}$ in arid regions to 200 μm $year^{-1}$ in the equatorial highlands.[29]

Carbon-14 is also a candidate for *in situ* measurements from the spallation on O in surface rocks. A problem is that it must be carefully distinguished from the ^{14}C of the 'garden variety' that greatly dominates the environment. This radionuclide has been studied extensively in meteorites where methods distinguishing spallogenic from non-spallogenic carbon have been developed.[34] Applying these methods to basalts from Utah, Jull *et al.*[28] have succeeded in showing that this radionuclide, too, can be used for exposure dating on shorter time scales than the other radionuclides discussed here.

Conclusions

AMS has provided access to a field of low-level long-lived radionuclides that could formerly only be detected at unnaturally high levels. The ability to determine these at the natural background levels provides a host of possibilities for applications in a range of studies of natural and anthropogenic processes. Many more similar radionuclides exist, for which the analytical problems have still to be solved. Fig. 6 shows a list of cosmogenic radionuclides found in meteorites; many of these also occur on earth, and the only method by which they may be accessed is AMS. Attempts are being made to bring the more difficult, heavy radionuclides into the range of the small machines.[35] One such radionuclide is ^{129}I, which until recently was thought to be only accessible on a large accelerator, but careful design of the low energy options has shown this not to be the situation.[36] But the problem of isobar separation in AMS still remains formidable and, while ingenuity may succeed occasionally,[37] no universal solution seems likely. Development of powerful new ion sources, coupled with new methods of sample preparation, and perhaps laser ionization methods, lead to the expectation that these frontiers will be pushed back and problems unimagined at present will be tackled.

The author thanks colleagues at the IsoTrace AMS Laboratory for many hours of stimulating discussion. In particular T. Litherland, L. Kilius, G. Wilson and R. Cresswell are thanked. Part of the work described in this paper has been supported by a grant from the Natural Sciences and Engineering Research Council of Canada.

References

1 Litherland, A. E., Allen, K. W., and Hall, E. T., *Philos. Trans. R. Soc. London, Ser. A*, 1987, **323**, 1.
2 Elmore, D., and Phillips, F. M., *Science*, 1987, **236**, 543.
3 Fehn, U., Tullai-Fitzpatrick, S., Teng, R. T. D., Gove, H. E., Kubik, P. W., Sharma, P., and Elmore, D., *Nucl. Instrum. Methods Phys. Res. Sect. B*, 1990, **52**, 446.
4 Fabryka-Martin, J., Davis, S. N., and Elmore, D., *Nucl. Instrum. Methods Phys. Res., Sect. B*, 1987, **29**, 361.

5 Edwards, R. R., *Science*, 1962, **236**, 543.
6 Sabu, D. D., *J. Inorg. Nucl. Chem.*, 1971, **33**, 1509.
7 Kohman, T. P., and Edwards, R. R., *US AEC Report*, NYO-3624-1, 1966, p. 41.
8 Kilius, L. R., Litherland, A. E., Rucklidge, J. C., and Baba, N., *Appl. Radiat. Isot.*, 1992, **43**, 279.
9 Kocher, D. C., *Environ. Int.*, 1981, **5**, 15.
10 Kilius, L. R., Rucklidge, J. C., and Soto, C., *Nucl. Instrum. Methods Phys. Res., Sect. B*, 1994, **92**, 389.
11 Brauer, F. P., and Rieck, Jr., H. G., *Battelle Pacific Northwest Laboratory Report*, BNWL-SA-4478, 1973.
12 Brauer, F. P., and Tenny, H., *Battelle Pacific Northwest Laboratory Report*, BNWL-SA-5287, 1975.
13 Fuge, R., *Appl. Geochem.*, 1990, **5**, 357.
14 Rucklidge, J. C., Kilius, L. R., and Fuge, R., *Nucl. Instrum. Methods Phys. Res., Sect. B*, 1994, **92**, 417.
15 Fabryka-Martin, J., Bentley, H., Elmore, D., and Airey, P. L., *Geochim.Cosmochim. Acta*, 1985, **49**, 337.
16 Wong, G. T. F., *Aquat. Sci.*, 1991, **4**, 45.
17 Chamberlain, A. C., *Radioactive Aerosols*, Cambridge University Press, 1991 p. 254.
18 Raisbeck, G. M., Yiou, F., Zhou, Z. Q., and Kilius, L. R., *J. Marine Systems*, 1995, in the press.
19 Raisbeck, G. M., Yiou, F., Bourlès, D., Brown, E., Deboffle, D., Jouhanneau, P., Lestringuez, J., and Zhou, Z. Q., *Nucl. Instrum. Methods Phys. Res. Sect. B*, 1994, **92**, 43.
20 Raisbeck, G. M., Yiou, F., Zhou, Z. Q., Kilius, L. R., and Dahlgaard, H., *Proceedings of an International Conference on Environmental Radioactivity in the Arctic and Antarctic, Kirkenes, Norway*, 1993, 125.
21 Monaghan, M. C., and Elmore, D., *Nucl. Instrum. Methods Phys. Res. Sect. B*, 1994, **92**, 357.
22 Vogt, S., Elmore, D., and Fritz, S. J., *Nucl. Instrum Methods Phys. Res. Sect. B*, 1994, **92**, 398.
23 Gascoyne, M., Sharma, P., and Kubik, P. W., *Nucl. Instrum. Methods Phys. Res., Sect. B*, 1994, **92**, 389.
24 Fontes, J.-C., and Andrews, J. N., *Nucl. Instrum. Methods Phys. Res., Sect. B*, 1994, **92**, 367.
25 Jouzel, J., Barkov, N. I., Barnola, J. M., Bender, M., Chappellaz, J., Genthon, C., Kotlyakov, V. M., Lipenkov, V., Lorius, C., Petit, J. R., Raynaud, D., Raisbeck, G., Ritz, C., Sowers, T., Stievenard, M., Yiou, F., and Yiou, P., *Nature*, 1993, **364**, 407.
26 Wilson, G. C., Litherland, A. E., and Rucklidge, J. C., *Chem. Geol.*, 1984, **44**, 1.
27 Nishiizumi, K., Lal, D., Klein, J., Middleton, R., and Arnold, J. R., *Nature*, 1986, **319**, 134.
28 Jull, A. J. T., Lifton, N., Phillips, W. M., and Quade, J., *Nucl. Instrum. Methods Phys. Res., Sect. B*, 1994, **92**, 308.
29 Stone, J., Allan, G. L., Fifield, L. K., Evans, J. M., and Chivas, A. R., *Nucl. Instrum. Methods Phys. Res., Sect. B*, 1994, **92**, 311.
30 Nishiizumi, K., Winterer, E. L., Kohl, C. P., Klein, J., Middleton, R., Lal, D., and Arnold, J., *J. Geophys. Res.*, 1989, **94B**, 17907.
31 Brown, E. T., Edmond, J. M., Raisbeck, G. M., Yiou, F., Kurz, M. D., and Brook, E. J., *Geochim. Cosmochim. Acta*, 1991, **55**, 2269.
32 Brown, E. T., Brook, E., Raisbeck, G. M., Yiou, F., and Kurz, M. D., *Geophys. Res. Lett.*, 1992, **19**, 369.
33 Middleton, R., Klein, J., Dezfouly-Arjomandy, B., Albrecht, A., Xue, S., Herzog, G. F., and Gregory, J., *Nucl. Instrum. Methods Phys. Res., Sect. B*, 1994, **92**, 362.
34 Cresswell, R. G., Beukens, R. P., Rucklidge, J., and Miura, Y., *Nucl. Instrum. Methods Phys. Res., Sect. B*, 1994, **92**, 505.
35 Litherland, A. E., *Nucl. Instrum. Methods Phys. Res., Sect. B*, 1994, **92**, 207.
36 Kilius, L. R., Rucklidge, J. C., and Litherland, A. E., *Nucl. Instrum. Methods Phys. Res., Sect. B*, 1987, **29**, 72.
37 Kilius, L. R., Nadeau, M.-J., Rucklidge, J. C., and Litherland, A. E., *Nucl. Instrum. Methods Phys. Res., Sect. B*, 1987, **29**, 57.

Paper 4/05863A
Received September 26, 1994
Accepted November 9, 1994

Recent Developments in Thermal Ionization Mass Spectrometric Techniques for Isotope Analysis*

A Review

K. G. Heumann, S. Eisenhut, S. Gallus, E. H. Hebeda, R. Nusko, A. Vengosh and T. Walczyk

Institut für Anorganische Chemie der Universität Regensburg, Universitätsstraße 31, D-93040 Regensburg, Germany

Thermal ionization mass spectrometry in the positive or negative ionization mode can be used for precise isotope ratio determinations of most elements. The preferably formed ions are M^+, M^- and MO_x^- (x = 1–4). Recent interesting developments in this field, which are relevant in geology, are the U/Th and Re/Os dating methods, re-determinations of the relative atomic masses of elements by more precise and more accurate isotope ratio measurements, the determination of isotope variations in geological and cosmic samples and the analysis of trace and ultra-trace amounts of elements and elemental species in the environment. In order to measure accurately a low abundant isotope in addition to a high abundant isotope (up to ratios of 10^9), thermal ionization mass spectrometers with deceleration lens systems have been constructed which fulfil the required abundance sensitivities. Chromium (III)/chromium(VI) speciation below the μg l^{-1} level in different river water samples is reported as an example of the application of positive thermal ionization mass spectrometry in connection with the isotope dilution technique. Rhenium/osmium determinations in iron meteorites of group IIA and IAB are performed by using a corresponding separation procedure with an OsO_4 distillation step and rhenium isolation by anion-exchange chromatography. The isochron for the IIA iron meteorites results in an age of (4.54 ± 0.08) × 10^9 years. These precise measurements also indicate small deviations of the IAB silicate-rich iron meteorite data from the IIA isochron. Precise boron isotope ratio measurements by negative thermal ionization mass spectrometry are applied to determine anthropogenic influences in groundwater samples.

Keywords: *Isotope ratio measurement; positive and negative thermal ionization; abundance sensitivity; chromium(III)/chromium(VI) speciation; isotope dilution mass spectrometry; rhenium/osmium dating; boron isotope variation; review*

Introduction

To date, ionization at the surface of a hot metal filament (thermal ionization) is the most precise and accurate method in mass spectrometry to determine isotope ratios of solid samples. Single-, double- and triple-filament ion sources are used in thermal ionization mass spectrometry (TIMS). The evaporation and ionization process takes place on the same filament with a single-filament arrangement, whereas double- and triple-filament ion sources are used if the evaporation process is better separated from the ionization process.

Positive and negative thermal ions can be formed at a hot metal surface. The ion yield β (ratio of emitted ions to the sum of ions and neutrals) in positive ion thermal ionization mass spectrometry (PITIMS) is theoretically described by the Langmuir–Saha equation[1]

$$\beta^+ = \left[1 + \frac{g_0}{g^+} \times \exp \frac{(I - W)}{k \times T}\right]^{-1} \quad (1)$$

and in negative ion thermal ionization mass spectrometry (NITIMS) by a modified equation[2]

$$\beta^- = \left[1 + \frac{g_0}{g_-} \times \exp \frac{(W - EA)}{k \times T}\right]^{-1} \quad (2)$$

where g is a statistical factor, I the first ionization potential or EA the electron affinity of the atom or molecule to be analysed, W the electron work function of the filament material used, T the temperature and k the Boltzmann constant. From these theoretical considerations it follows that high positive thermal ion currents can be expected for compounds with a low first ionization potential and by using filament materials of high W values. High negative ion beams can be obtained for substances with high electron affinities and filaments with low values of W. More detailed descriptions of thermal ion sources, their filament materials and the ionization process are given elsewhere.[3]

The most important characteristics of PITIMS and NITIMS are summarized in Table 1. With respect to eqns. (1) and (2), elements with a first ionization potential of less than 7 eV are preferably analysed by PITIMS. On the other hand, an electron affinity of at least 2 eV is necessary for elements or molecules to be analysed by NITIMS.[3–5] Normally, singly charged positive atomic ions M^+ are formed in the PITI mode; negative atomic ions M^- or oxide ions MO_x^- (x = 1–4) are formed in the NITI mode. The special features of TIMS are a

Table 1 Comparison of PITIMS with NITIMS

	PITIMS	NITIMS
Preferably analysed compounds	Elements with I <7 eV	Elements or molecules with EA >2 eV
Normally detected ions	M^+	M^-, MO_x^- (x = 1–4)
Sensitivity	High	Very high
Ion current characteristics	Increase with temperature	Maximum at definite temperature
Interferences	Seldom	Very seldom
Filament preparation	Silica gel	Lanthanum or barium salts

* Presented at Geoanalysis 94: An International Symposium on the Analysis of Geological and Environmental Materials, Ambleside, England, September 18–22, 1994.

high sensitivity in connection with an excellent selectivity, which means that isobaric interferences are very rare. In some instances, ion formation must be promoted using different filament preparation techniques. The silica gel technique with addition of phosphoric acid[6] or boric acid[7] is one of the possibilities for an ion current enhancement in PITIMS; the addition of lanthanum or barium salts for reduction of the electron work function of filament materials[3–5] with the corresponding promotion of the negative thermal ion current are preparation techniques in NITIMS. Even if elements with low *I* or high *EA* values are analysed, the thermal ionization process is usually endothermic. This means that high filament temperatures should increase the ionization yield with respect to eqns. (1) and (2). This is found in PITIMS where filament temperatures between 800 and 2000 °C are applied depending on the element to be analysed. Contrary to the correlation given by eqn. (2), a maximum ion current is observed in NITIMS at definite temperatures, which is due to secondary effects such as electron emission from the filament material.[3]

In the Periodic Table of the elements, represented in Fig. 1, all elements are marked with horizontal and vertical lines, respectively, where the positive and negative thermal ionization mode is preferably used for isotope ratio determination. Elements, where at least one radioactive isotope (with a sufficiently long half-life for mass spectrometric investigations) must be used for isotope ratio determinations, are indicated by a black bar on top of the element box. Isotope ratio determinations of non-marked elements must either be carried out by electron impact gas mass spectrometry, *e.g.*, for mercury and the noble gases, or they have only one stable or long-lived radioactive isotope, *e.g.*, phosphorus or actinium. As can be seen from Fig. 1, two different groups of elements are preferably analysed by NITIMS. One is the transition metals Mo, Tc, W, Re, Os, Ir and Pt where MO_x^- ions are measured for isotope ratio determination.[3,8–11] Here, oxygen isotopic corrections must be carried out for the measured MO_x^- ions to determine the corresponding isotope ratio of the transition metal. Secondly, the isotopic composition of many of the non-metals and semi-metals can be determined by measuring MO_2^- ions (B, N and Si), CN^- ions (C and N), and M^- atomic ions (S, Se, Te, Cl, Br and I).[3–5,12–15]

Modern Trends in the Application of PITIMS

Investigations Relevant to Geoanalysis

During the last few years, isotope ratio determinations by PITIMS have been applied to the following topics:

(a) Precise thorium isotope ratios have been measured to determine the age of corals by the U/Th disequilibrium method.[16]

(b) Precise and accurate determinations of natural isotope abundances[7–19] have resulted in a re-determination of the relative atomic masses of the elements titanium, iron and antimony with much higher precision compared with former data.[20]

(c) In meteorites, isotope anomalies have been investigated, for example, of titanium, chromium and iron,[21–23]

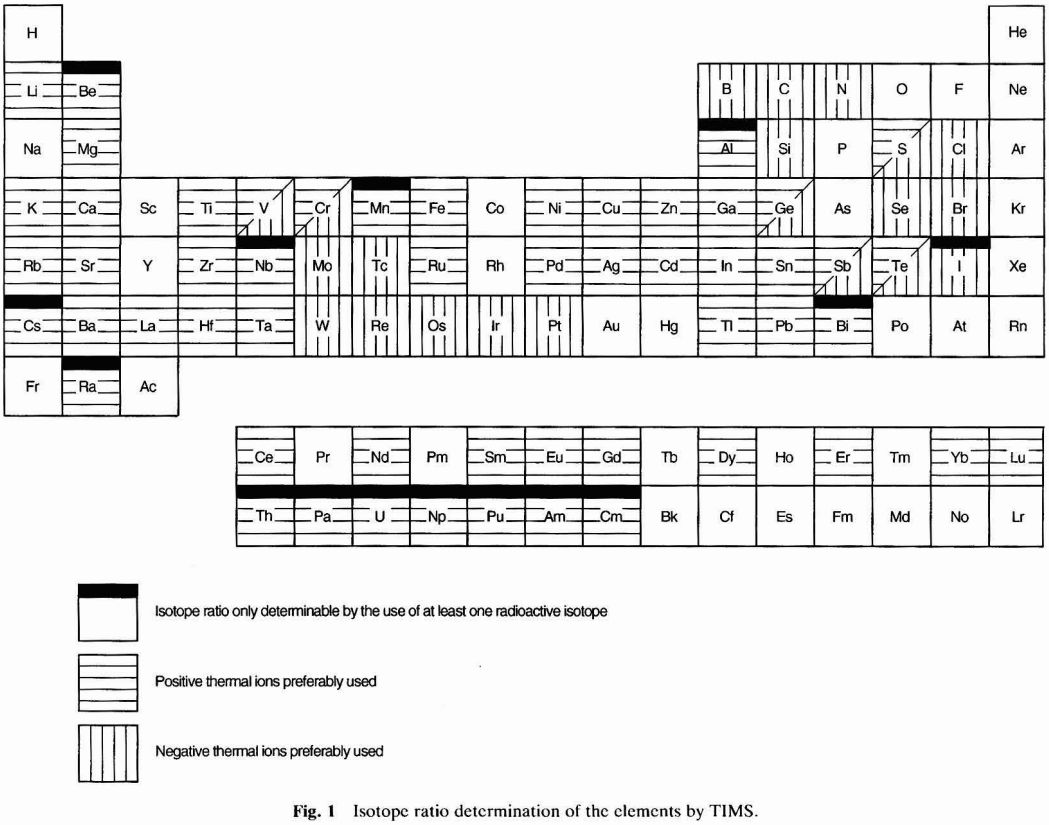

Fig. 1 Isotope ratio determination of the elements by TIMS.

which resulted in more detailed information regarding specific nucleosynthetic processes and their possible astrophysical provenance.

(d) Accurate determinations of femtogram amounts of radioisotopes in geological samples have been carried out by isotope dilution mass spectrometry (IDMS). The analysis of trace amounts of ^{226}Ra and ^{231}Pa in rock samples is an excellent example of this type of ultra-trace analysis.[24–26]

(e) The determination of trace element species in the environment by IDMS has become of great importance. For example, the geochemical mobility of elements strongly depends on the chemical form in which the corresponding element exists. Under certain preconditions, heavy metal speciation can be studied using PITIMS.[27,28]

Two topics of special interest are discussed in the following sections in more detail.

TIMS Instrument for Enhanced Abundance Sensitivity

For some geological applications, the abundance sensitivity (contribution of a high abundant isotope peak to the intensity of a low abundant isotope peak) cannot be sufficiently determined using common magnetic sector field TIMS instruments. For example, a number of geological investigations of thorium require the determination of $^{230}Th/^{232}Th$ isotope ratios in the range of 10^{-6} to 10^{-8}.[29] For such high precision determinations of ratios of 10^{-6} or less, new types of mass analyser systems have been developed with enhanced abundance sensitivity.

One instrument of this type, which has been described by Schwieters and Bach,[30] is represented in Fig. 2. An extended geometry 90° magnetic sector field instrument was coupled with a retarding potential quadrupole (RPQ) filter lens system. A conventional multi-collector Faraday cup array is used for detection of the higher abundant isotopes, an ion counting system for detection of the low abundant isotopes.

Scattered ions, which are lower in energy and/or have false flight directions, reduce the abundance sensitivity. The RPQ system acts as a sensitive energy and direction filter lens, which rejects ions of false direction and energy. Such equipment has an abundance sensitivity of at least 10^{-9}. Fig. 3 demonstrates the significant enhancement of the abundance sensitivity by measuring a thorium sample with an isotope ratio $^{230}Th/^{232}Th$ of about 6×10^{-6} by an instrument with the RPQ filter lens system compared with a 'normal' TIMS configuration.[31]

Chromium Speciation in the Environment by IDMS

Isotope dilution mass spectrometry is a method of proven high accuracy, which means that it is a technique for which the sources of systematic error are understood and controlled. More detailed information on the fundamental principles, advantages, restrictions and possibilities of IDMS can be found in several reviews.[3,32–35] Because it provides reliable analytical results, IDMS is now also used for elemental speciation. Chromium speciation in the environment is of particular importance because Cr^{III} is essential for plants and animals whereas Cr^{VI} is toxic and carcinogenic. Furthermore, the geochemical mobility strongly depends on the oxidation state of this element.

The treatment of water samples for chromium speciation is represented in Fig. 4 as an example of elemental speciation in the environment by IDMS. More details of the experimental conditions are described in a recent paper.[28] Some examples of Cr^{III} and Cr^{VI} determinations in different river water samples by IDMS are listed in Table 2. As can be seen, chromium species can be determined down to 60 ng l^{-1}. The reliability of the applied IDMS method had been demonstrated in an interlaboratory comparison where a standard solution containing 24 μg l^{-1} of Cr^{III} and 16 μg l^{-1} of Cr^{VI} by mass was analysed with different analytical methods. Whereas IDMS resulted in the given concentrations within the limits of error, other methods used by various laboratories showed a significant spread of the analytical results (last line of Table 2).

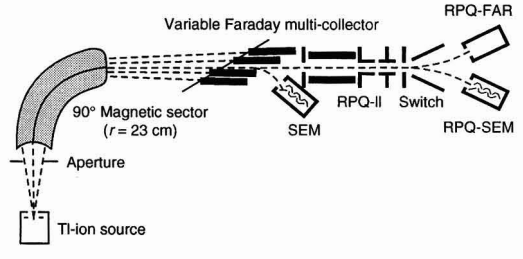

Fig. 2 Schematic diagram of a TIMS instrument with enhanced abundance sensitivity.[30]

Modern Trends in the Application of NITIMS

Investigations Relevant to Geoanalysis

NTI-MS has particularly improved results in the following areas:

(a) Determinations of the Re/Os systematics.

(b) Precise and accurate determinations of natural isotope abundances of W,[36] Os[8] and Ir[10] were used to re-determine the relative atomic masses of these elements.[20,37]

(c) Accurate determinations of ultra-trace amounts of technetium are a precondition to detect ^{99}Tc contaminants from the nuclear industry in the environment or to measure the flux of high-energy solar neutrinos over the past several million years in technetium isolated from molybdenite ores.[38] PITIMS measurements of technetium are not sufficient for

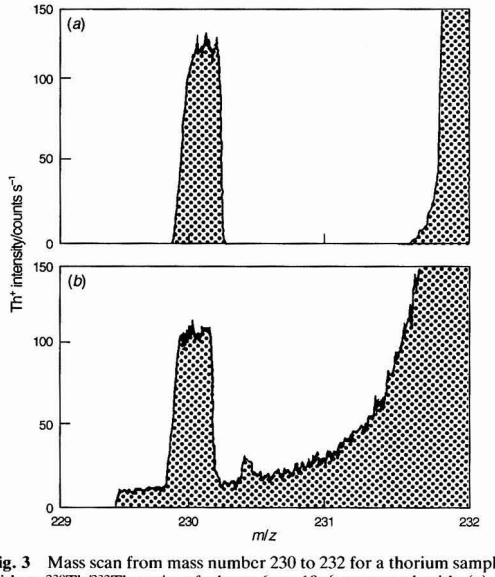

Fig. 3 Mass scan from mass number 230 to 232 for a thorium sample with a $^{230}Th/^{232}Th$ ratio of about 6×10^{-6} measured with (*a*) a retarding potential quadrupole (RPQ) system and (*b*) a 'normal' TIMS instrument.[31]

that purpose because of interferences by molybdenum isotopes from all the filament materials tested and the low sensitivity due to the high first ionization potential of technetium. NITIMS is more sensitive for technetium and, in addition, produces TcO_4^- and MoO_3^- ions, respectively, which prevents isobaric interferences.[3,39] Based on NITIMS, an IDMS method for the determination of sub-picogram amounts of technetium in geological samples has recently been developed.[40]

(d) Elemental speciation by IDMS is also an important feature in NITIMS. The determination of inorganic and organic selenium and iodine species in the environment was possible by this technique, *e.g.*, at the ng l^{-1} level for trimethylselenonium $[(CH_3)_3Se^+]$ in aquatic systems[41] and at the ng m^{-3} level of hypoidous acid (HOI) in the atmosphere.[42]

(e) Many of the light elements show significant natural isotope variations. Precise isotope ratio determinations can therefore be used to identify possible sources of an element by its isotopic composition. For example, the direct measurement of the nitrogen isotopic composition in nitrate samples by NITIMS[14] may be a potential tool to identify nitrate sources in the environment. Isotope variations of boron in geological samples can be used to obtain information on geochemical processes,[43,44] and can also be applied to the identification of anthropogenic sources, which may, in some instances, have different isotopic compositions.[45]

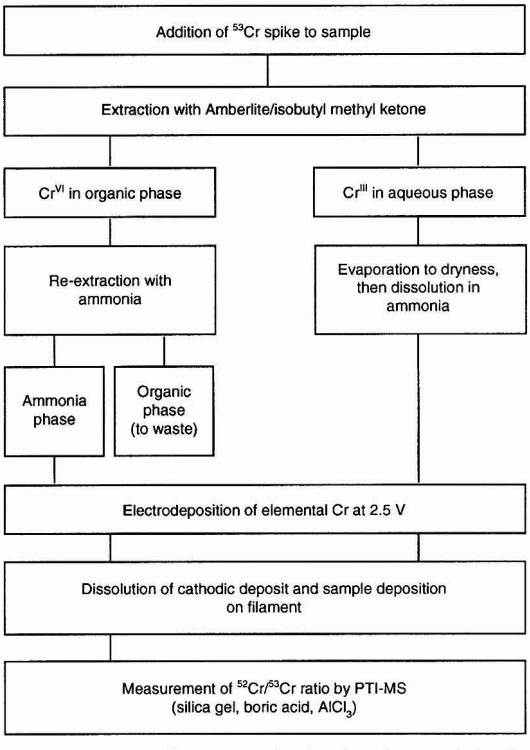

Fig. 4 Treatment of water samples for chromium speciation by IDMS.[28]

Table 2 Chromium speciation by IDMS in river water samples and analysis of a standard solution within an interlaboratory comparison

	Concentration/μg l^{-1}	
Sample	Cr^{III}	Cr^{VI}
River Danube	2.85	0.12
River Regen	3.45	0.18
Creek (forest)	2.03	0.06
Standard solution:		
By mass	24.0	16.0
IDMS	23.4 ± 1.5	16.3 ± 1.6
Other methods	14.8–34.9	12.3–21.9

Use of NITIMS for Re/Os Systematics

The introduction of NITIMS for determination of the Re/Os systematics of geological and cosmic samples is one of the highlights in this analytical field. Geological age determinations by the Re/Os method are possible owing to the β^- decay of the naturally occurring ^{187}Re into the stable osmium isotope ^{187}Os with a half-life of 4.23×10^9 years. A former problem in the application of Re/Os datings was the lack of sensitive and precise methods to measure osmium isotope ratios. In the 1980s, rhenium isotope ratio measurements were performed by NITIMS.[12,29] However, significant contributions from the filament materials limited the analysis of trace amounts of rhenium. Recent developments have overcome these problems.

Osmium isotope ratios were first sensitively and precisely measured by NITIMS in 1989.[33,34] At the beginning of 1991 two papers were published almost simultaneously, one by Völkening *et al.*[18] and the other by Creaser *et al.*,[46] where improved NITIMS techniques for osmium isotope ratio determinations were described. The most precise and most sensitive technique has subsequently been developed by Walczyk *et al.*[9] by introducing oxygen gas into the ion source during the heating up and measuring procedure. Since then many laboratories have adapted the NITIMS technique,[47–50] which may become a standard method in the future for Re/Os datings and other investigations into the Re/Os systematics.

The present 'state-of-the-art' in rhenium and osmium isotope ratio measurements by NITIMS is summarized in Table 3. The use of nickel filaments, coated with a homogeneous layer of V_2O_5, results in almost blank-free rhenium isotope ratio measurements.[11] Independent of the chemical form of the sample, ReO_4^- and OsO_3^- are the most abundant ions in NITIMS. These oxide ions are therefore used for isotope ratio determinations. The high sensitivity of the NITIMS technique is demonstrated by ionization efficiencies

Table 3 Experimental conditions and parameters in rhenium and osmium isotope ratio measurements by NITIMS[8,9,11,51]

Parameter	Rhenium	Osmium
Ion source	Single-filament	Double-filament
Filament material	Nickel, coated with V_2O_5 and vacuum-heated	Platinum
Ion current promoter	$Ba(OH)_2$	$Ba(OH)_2$
Detected ions	ReO_4^- (most abundant)	OsO_3^- (most abundant)
	ReO_3^-	OsO_4^-, OsO_2^-
Temperature (evaporation filament)	Not heated	800–850 °C
Temperature (ionization filament)	840–860 °C	760–820 °C
Ionization efficiency	up to 20%	up to 30%
Oxygen bleeding	No effect	Ion current enhancement

of up to 20 and 30%, respectively, which permits the detection of sub-nanogram amounts of rhenium and osmium.

The $^{185}Re/^{187}Re$ ratio can be determined with relative standard deviations of 0.04% (1*s* values) in nanogram samples of rhenium, preferably loaded as perrhenate. The progress in the osmium isotope ratio determination by the application of NITIMS compared with former measurements with resonance ionization mass spectrometry (RIMS) and secondary-ion mass spectrometry (SIMS) can be seen from the results listed in Table 4.

Re/Os Determinations in Iron Meteorites

Because iron meteorites contain relatively high osmium and rhenium concentrations, this type of sample is an ideal subject for Re/Os investigations. A possible treatment for iron meteorite samples successfully used for the isolation of osmium and rhenium is represented in Fig. 5.[51,54] By using this sample treatment procedure, Re/Os age determinations can be performed by analysing the present $^{187}Os/^{186}Os$ isotope ratio of the sample and the osmium and rhenium concentrations by IDMS. One critical point in the analysis of osmium is the isotope equilibration between sample and spike osmium when applying the isotope dilution technique. Digestion in a closed glass ampoule by H_2SO_4 and CrO_3 at 150 °C was found to be the best method to prevent non-equilibration, which can lead to incorrect results. In addition to other procedures described in the literature,[55] distillation of OsO_4 from the solution after digestion of the sample and absorption of osmium in a H_2O_2 solution improves the osmium isolation step. Afterwards, purification of the osmium sample by a second distillation of OsO_4 and absorption in a mixture of HCl and ethanol is essential to guarantee high precison and sensitivity of the isotope ratio measurement.

The Re/Os systematics of some IIA (Boguslavska, Lombard, Coahuila) and IAB (Four Corners, Landes, Zagora, Campo de Cielo/El Taco) iron meteorites are represented in Fig. 6.[51] The isochron calculated from the data for the IIA iron meteorites is plotted in the figure. This isochron plot results in an age of $(4.54 \pm 0.08) \times 10^9$ years with an initial $^{187}Os/^{186}Os$ ratio of 0.8014 ± 0.0087. The initial osmium isotope ratio agrees very well with other NITIMS determinations of this group of iron meteorites, where $^{187}Os/^{186}Os$ values of 0.800747 and 0.803348 were obtained. Also, the age of the IIA iron meteorites of 4.54×10^9 years, calculated from the slope of the isochron in Fig. 6, agrees well with the data of recently published investigations (4.60×10^9 and 4.61×10^9 years, respectively)[47,48] but deviates considerably from the result of 4.17×10^9 years from SIMS measurements by Luck and Allègre.[52] Errors in the $^{187}Re/^{186}Os$ ratio influence the

Table 4 Progress in osmium isotope ratio determination by NITIMS [for NITIMS, 1 ng of osmium in the form of hexachloroosmate(VI) was used]

Technique	Isotope ratio	s_r (%)*	Reference
SIMS	$^{184}Os/^{188}Os$	11	Luck and Allègre[52]
	$^{187}Os/^{188}Os$	0.06	
RIMS	$^{187}Os/^{186}Os$	3.2	Walker and Fassett[53]
	$^{190}Os/^{192}Os$	1.3	
NITIMS	$^{184}Os/^{189}Os$	0.3	Walczyk and co-workers[9,51]
	$^{187}Os/^{186}Os$	0.04	
	$^{189}Os/^{192}Os$	0.004	

* s_r = Relative standard deviation (1*s* values).

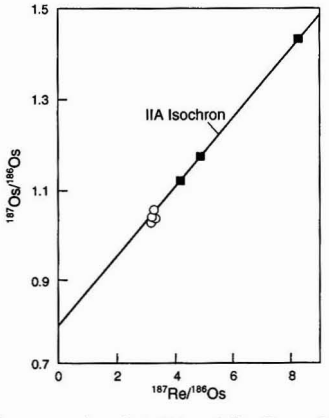

Fig. 6 Re/Os systematics of ■, IIA and ○, silicate-rich IAB iron meteorites and IIA isochron.[51] Age from slope of IIA isochron: (4.54 ± 0.08) × 10^9 years.

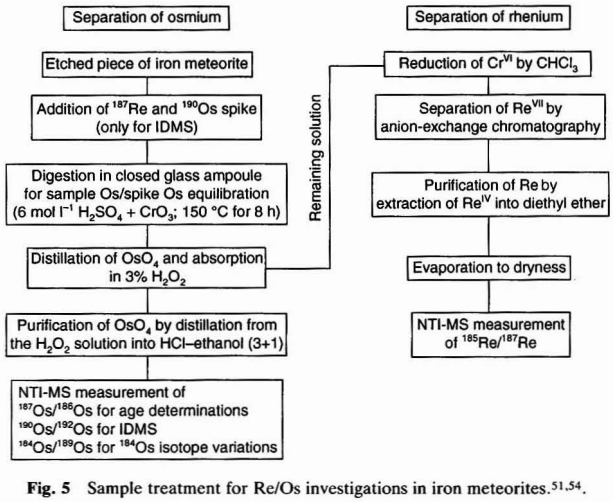

Fig. 5 Sample treatment for Re/Os investigations in iron meteorites.[51,54]

accuracy of the determined age. Accurately characterized osmium standard solutions have to be prepared, which has, so far, proved to be a problem.[56]

The four IAB iron meteorites investigated, which are all silicate-rich samples, differ only slightly in their Re/Os ratio so that an isochron could not be obtained from these samples. The results for these meteorites do not exactly fit the isochron plot of the IIA iron meteorites. The precise isotope ratio determinations by NITIMS indicate that the IAB values lie slightly below the IIA isochron. This becomes obvious from a plot of δ(‰) values *versus* the $^{187}Re/^{186}Os$ ratio (Fig. 7), where the deviation δ is defined as

$$\delta(‰) = \left[\frac{(^{187}Os/^{186}Os)_{IAB}}{(^{187}Os/^{186}Os)_{IIA\ isochron}} - 1\right] \times 10^3 \qquad (3)$$

Possible interpretations for this deviation are the different ages of the IAB and IIA iron meteorites, differences in the initial $^{187}Os/^{186}Os$ ratio or Re/Os mobilization in IAB meteorites after their formation. Further investigations are necessary to clarify this interesting effect.

Search for Possible ^{184}Os Isotope Variations in Iron Meteorites

Osmium-184 isotope variations may occur in meteorites owing to the very high neutron cross-section of 3000 barn for this osmium isotope. High neutron fluxes in space can therefore reduce the ^{184}Os abundance compared with the terrestrial isotopic composition. Neutrons in space are produced by nuclear reactions with cosmic rays or they can appear from a supernova.

Osmium-184 is the least abundant osmium isotope by only 0.02%. Therefore, extreme osmium isotope ratios (the $^{184}Os/^{189}Os$ ratio is about 10^{-3}) must be precisely determined to be able to identify ^{184}Os variations in meteorites. For isolation, the osmium line of the sample treatment scheme in Fig. 5 without the isotope dilution step was applied.

Two iron meteorites (Campo de Cielo/El Taco and Henbury) have been analysed for their $^{184}Os/^{189}Os$ isotope ratios and were compared with the results for 14 different samples of platinum group mineral nuggets (osmiridium) from Tasmania/Australia (Fig. 8). As can be seen from Fig. 8 the isotope ratios of the analysed iron meteorites agree within an error of 1*s* (standard deviation) with the terrestrial $^{184}Os/^{189}Os$ ratio measured in different platinum group mineral nuggets.

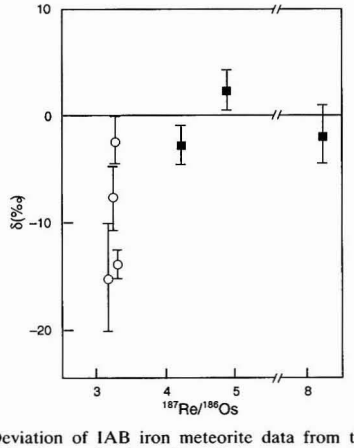

Fig. 7 Deviation of IAB iron meteorite data from the isochron calculated by the results from the IIA iron meteorites.[51] ○, IAB silicate-rich iron meteorites and ■, IIA iron meteorites.

Although no significant ^{184}Os variation could be detected in these two iron meteorites, the represented NITIMS measurements are the most precise $^{184}Os/^{189}Os$ results at present with relative standard deviations (1*s*) of less than 0.3%.

Boron Isotope Variations as Indicators of Anthropogenic Influences

Natural boron isotope variations are well known.[43–45] The variation of $\delta^{11}B(‰)$ values of different minerals and seawater samples is presented in Fig. 9. The $\delta^{11}B$ values range from about −30 to about +60‰, where $\delta^{11}B$ is related to the National Institute of Standards and Technology (NIST) Standard Reference Material (SRM) 951 (boric acid):

$$\delta^{11}B = \left[\frac{(^{11}B/^{10}B)_{Sample}}{(^{11}B/^{10}B)_{Standard}} - 1\right] \times 10^3\,(‰) \qquad (4)$$

Washing powder and detergents, which are one of the major contaminants of natural water systems, contain considerable amounts of boron as perborate. Our investigations have shown that many of the washing powders used, at least in Europe, contain boron isotopic compositions similar to those of the NIST SRM 951 (see Fig. 9). This may be because perborate for washing powders is produced only from a few natural borate mineral sources, *e.g.*, in Turkey and California. If boron from a natural source is mixed with sewage containing boron from washing powder, the $\delta^{11}B$ value may be shifted. Such an isotopic shift may be used as an indicator

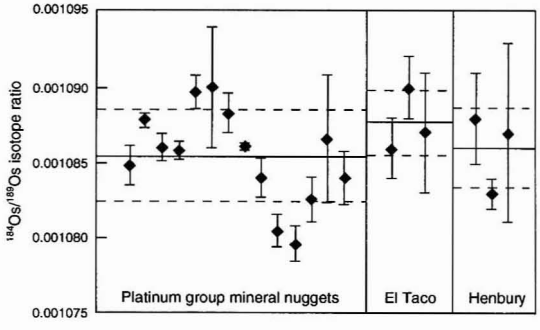

Fig. 8 $^{184}Os/^{189}Os$ isotope ratio of different platinum group mineral nuggets compared with two iron meteorites.[51] (Each point with standard deviation represents ten isotope ratios for the mineral nuggets measured by direct loading of one nugget on the filament.[10] For the iron meteorites three different pieces of each meteorite were analysed after isolation of osmium according to Fig. 5).

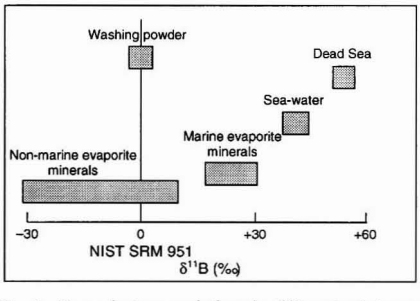

Fig. 9 Boron isotope variations in different substances.

of anthropogenic influences, for example, in groundwater samples.

Precise boron isotope ratio measurements are the most important precondition for the determination of isotope variations in the per mil range. Different ionization techniques in mass spectrometry have been used for boron isotope ratio measurements. Inductively coupled plasma mass spectrometry (ICP-MS), PITI- and NITIMS are the most precise mass spectrometric techniques. Characteristic data, including the advantages and disadvantages of these techniques, are summarized in Table 5. ICP-MS has the advantage that all boron compounds soluble in water can be directly investigated, but the sensitivity is low and the precision is not sufficient to determine most of the isotope variations that may occur. In the PITIMS mode, sodium borate or caesium borate must be prepared from the samples because $Na_2BO_2^+$ and $Cs_2BO_2^+$ ions, respectively, are detected. Measurement of caesium borate ion intensities has the advantage of no interferences. Even if the sensitivity is not high in PITIMS, microgram amounts of a sample can yield relative standard deviations as low as 0.03%.

In NITIMS, BO_2^- thermal ions can be formed from any boron compound. The applied NITIMS technique is based on the investigations of Zeininger and Heumann,[13] and on some other recent developments.[60] Extremely high BO_2^- ion currents of more than 10^{-11} A at the detector side of the mass spectrometer can be obtained from nanogram amounts of boron in a single-filament ion source by using $La(NO_3)_3$ as an ionization promoter.[13] However, in this instance the measured boron isotope ratio depends on the sample size (see Fig. 10).[61] When applying $Ba(OH)_2$ instead of $La(NO_3)_3$ no effect on the sample amount could be observed as can be seen by the results plotted in Fig. 10.[60] In addition, more stable ion currents and, hence, more precise isotope ratio measurements with relative standard deviations of 0.08% can be obtained by adding about 2 μg of $MgCl_2$ as an aqueous solution onto the rhenium filament before deposition of the boron sample. Possible interferences at mass numbers 42 and 43 by CNO^- ($^{12}C^{14}N^{16}O^-$ and $^{13}C^{14}N^{16}O^-$ or $^{12}C^{15}N^{16}O^-$, respectively), formed by organic impurities during the heating-up procedure, are prevented by separating organics from the boron sample to be measured by NITIMS.[62]

Table 5 Different techniques for boron isotope ratio determinations

Technique	Measured ion	s_r (%)*	Advantages/ disadvantages	Reference
ICP-MS	B^+	0.5–1	Any boron compound Low sensitivity	57
PTI-MS	$Na_2BO_2^+$	0.08–0.25	Only sodium borates Low sensitivity Interference by $^{88}Sr^+$ and $^{89}Y^+$	58
	$Cs_2BO_2^+$	0.03	Only caesium borates Low sensitivity No interference	59
NTI-MS	BO_2^-	0.08–0.2	Any boron compound High sensitivity No interference	60

* s_r = Relative standard deviation.

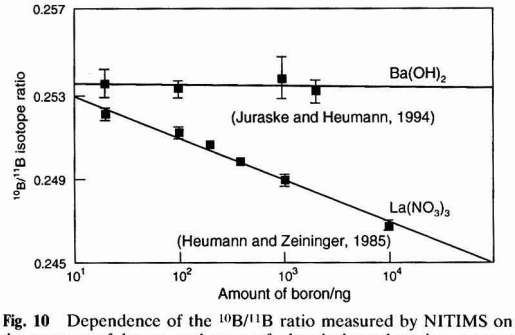

Fig. 10 Dependence of the $^{10}B/^{11}B$ ratio measured by NITIMS on the amount of boron and type of chemical used as ion current promoter.[60,61]

The applicability of boron isotope variations for indication of anthropogenic influences in groundwater samples is demonstrated by the results represented in Fig. 11.[45] Whereas the chloride and boron concentrations continuously increase in the order uncontaminated, less contaminated, contaminated groundwater and sewage, the $\delta^{11}B$ value continuously decreases in this direction. As mentioned above, the boron isotope variation is due to perborate in washing powder used in households.

In many instances it would be easier to analyse the chloride or boron concentration in groundwater samples as anthropogenic parameters instead of the boron isotopic composition. Results from groundwater of the Yavne Region, Israel (Fig. 12) demonstrate that the chloride or boron concentration may lead to incorrect interpretations whereas the boron isotope ratio measurement results in the correct answer.[45] The high chloride concentration in groundwater samples of the Yavne Region suggests anthropogenic influences. Also, the boron concentration cannot give a definite answer to the question because it lies between uncontaminated and contaminated

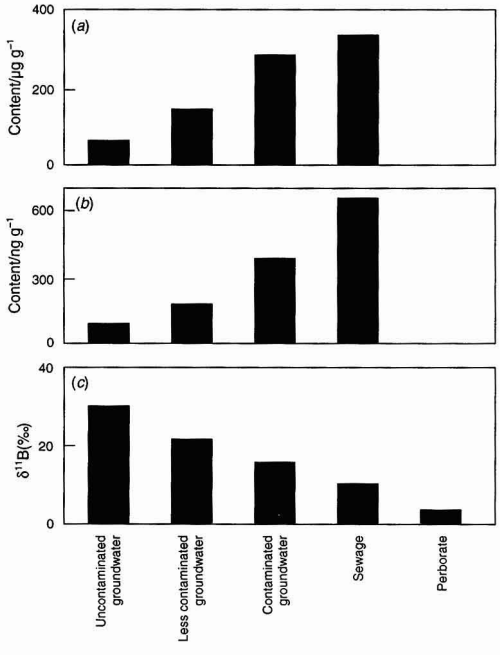

Fig. 11 Boron isotope variation in different groundwater samples and sewage of the Dan Region, Israel, compared with the corresponding chloride and boron concentrations.[45] (All columns represent the mean value of at least three independent analyses of each sample). (*a*) Chloride concentration; (*b*) boron concentration; and (*c*) boron isotope variation.

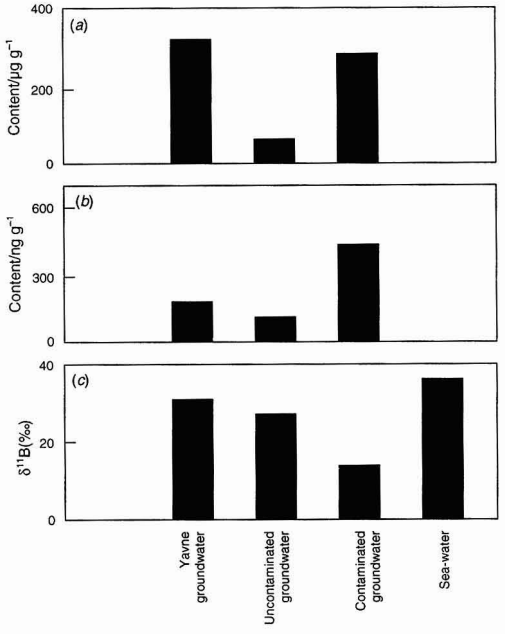

Fig. 12 Identification of saline influences on groundwater by measuring the boron isotopic composition (Yavne, Israel).[45] (Representation of columns as in Fig. 11.) (*a*) Chloride concentration; (*b*) boron concentration; and (*c*) boron isotope variation.

groundwater samples. However, by measuring the boron isotopic composition it was possible to identify natural saline influences for this groundwater, because the $\delta^{11}B$ value of boron in the Yavne water was found to be between the corresponding values of uncontaminated groundwater and sea-water (Fig. 12).

Conclusion

Although other mass spectrometric techniques such as ICP-MS have expanded rapidly during recent years, TIMS is still an important method in geoanalysis. This is especially valid for precise isotope ratio analyses in connection with geological age determinations, determinations of isotope variations in geological and cosmic materials, and also in the trace and ultra-trace analysis of elements and elemental species in geological and other environmental samples by IDMS.

References

1 Langmuir, I., and Kingdon, K. H., *Proc. R. Soc. (London)*, 1925, **107**, 61.
2 Kawano, H., and Page, F. M., *Int. J. Mass Spectrom. Ion Phys.*, 1983, **50**, 1.
3 Heumann, K. G., in *Inorganic Mass Spectrometry*, eds. Adams, F., Gijbels, R., and van Grieken, R., Wiley, New York, 1988, pp. 301–376.
4 Wachsmann, M., and Heumann, K. G., *Int. J. Mass Spectrom. Ion Processes*, 1991, **108**, 75.
5 Wachsmann, M., and Heumann, K. G., *Int. J. Mass Spectrom. Ion Processes*, 1992, **114**, 209.
6 Barnes, I. L., Murphy, T. J., Gramlich, J. W., and Shields, W. R., *Anal. Chem.*, 1973, **45**, 1881.
7 Völkening, J., and Heumann, K. G., in *Advances in Mass Spectrometry 1985*, ed. Todd, J. G. J., Wiley, New York, 1986, part B, pp. 1059–1060.
8 Völkening, J., Walczyk, T., and Heumann, K. G., *Int. J. Mass Spectrom. Ion Processes*, 1991, **105**, 147.
9 Walczyk, T., Hebeda, E. H., and Heumann, K. G., *Fresenius' J. Anal. Chem.*, 1991, **341**, 537.
10 Walczyk, T., and Heumann, K. G., *Int. J. Mass Spectrom. Ion Processes*, 1993, **123**, 139.
11 Walczyk, T., Hebeda, E. H., and Heumann, K. G., *Int. J. Mass Spectrom. Ion Processes*, 1994, **130**, 237.
12 Heumann, K. G., Schindlmeier, W., Zeininger, H., and Schmidt, M., *Fresenius' Z. Anal. Chem.*, 1985, **320**, 457.
13 Zeininger, H., and Heumann, K. G., *Int. J. Mass Spectrom. Ion Phys.*, 1983, **48**, 377.
14 Unger, M., and Heumann, K. G., *Int. J. Mass Spectrom. Ion Phys.*, 1983, **48**, 373.
15 Renner, M., Lamberty, A., and De Bièvre, P., *Analusis*, 1992, **20**, 229.
16 Edwards, R. L., Chen, J. H., Ku, T.-L., and Wasserburg, G. J., *Science*, 1987, **236**, 1547.
17 Shima, M., and Torigoye, N., *Int. J. Mass Spectrom. Ion Processes*, 1993, **123**, 29.
18 Taylor, P. D. P., Maeck, R., and De Bièvre, P., *Int. J. Mass Spectrom. Ion Processes*, 1992, **121**, 111.
19 Chang, T.-L., Qian, Q.-Y., Zhao, M.-T., and Wang, J., *Int. J. Mass Spectrom. Ion Processes*, 1993, **123**, 77.
20 IUPAC Commission on Atomic Weights and Isotopic Abundances, *Pure Appl. Chem.*, 1994, 66, 2423.
21 Jungck, M. H. A., Shimamura, T., and Lugmair, G. W., *Geochim. Cosmochim. Acta*, 1984, **48**, 2651.
22 Birck, J.-L., and Allègre, D. J., *Geophys. Res. Lett.*, 1985, **12**, 745.
23 Völkening, J., and Papanastassiou, D. A., *Astrophys. J.*, 1989, **347**, L43.
24 Volpe, A. M., Olivares, J. A., and Murrell, M. T., *Anal. Chem.*, 1991, **63**, 913.
25 Cohen, A. S., and O'Nions, R. K., *Anal. Chem.*, 1991, **63**, 2705.
26 Pickett, D. A., Murrell, M. T., and Williams, R. W., *Anal. Chem.*, 1994, **66**, 1044.
27 Heumann, K. G., in *Metal Speciation in the Environment*, eds. Broekaert, J. A. C., Gücer, S., and Adams, F., NATO ASI Series, vol. G23, Springer, Heidelberg, 1990, pp. 153–168.
28 Nusko, R., and Heumann, K. G., *Anal. Chim. Acta*, 1994, **286**, 283.
29 Goldstein, S. J., Murrell, M. T., and Janecky, D. R., *Earth Planet. Sci. Lett.*, 1989, **96**, 134.
30 Schwieters, J. B., and Bach, P., *Proceedings of the 2nd A.O. Nier Symposium on Inorganic Mass Spectrometry, Durango, CO, 1994*, ed. Rokop, D. J., Delmore, J. E., and Green, L. W., Chalk River Laboratory, in the press.
31 Tuttas, D., and Habfast, K., *Application New No. 4*, Finnagan-MAT, Bremen, 1993.
32 Fassett, J. D., and Paulsen, P. J., *Anal. Chem.*, 1989, **61**, 643A.
33 Heumann, K. G., *Mass Spectrom. Rev.*, 1992, **11**, 41.
34 Heumann, K. G., *Int. J. Mass Spectrom. Ion Processes*, 1992, **118/119**, 575.
35 De Bièvre, P., *Fresenius' J. Anal. Chem.*, 1994, **350**, 277.
36 Völkening, J., Köppe, M., and Heumann, K. G., *Int. J. Mass Spectrom. Ion Processes*, 1991, **107**, 361.
37 IUPAC Commission on Atomic Weights and Isotopic Abundances, *Pure Appl. Chem.*, 1992, **64**, 1519.
38 Cowan, G. A., and Haxton, W. C., *Science*, 1982, **216**, 51.
39 Heumann, K. G., Kastenmayer, P., Schindlmeier, W., Unger, M., and Zeininger, H., *Proceedings of the 31st ASMS Conference on Mass Spectrometry and Allied Topics, Boston, MA, 1983*, pp. 581–582.
40 Dixon, R. P., Rokop, D. J., Curtis, D. B., and Fabryka-Martin, J. T., *Proceedings of the 2nd A.O. Nier Symposium on Inorganic Mass Spectrometry, Durango, CO, 1994*, ed. Rokop, D. J., Delmore, J. E., and Green, L. W., Chalk River Laboratory, in the press.
41 Tanzer, D., and Heumann, K. G., *Anal. Chem.*, 1991, **63**, 1984.
42 Gäbler, H.-E., and Heumann, K. G., *Fresenius J. Anal. Chem.*, 1993, **345**, 53.
43 Barth, S., *Geol. Rundschau*, 1993, **82**, 640.
44 Vengosh, A., Chivas, A. R., McCulloch, M. T., Starinsky, A., and Kolodny, Y., *Geochim. Cosmochim. Acta*, 1991, **55**, 2591.

45 Vengosh, A., Heumann, K. G., and Juraske, S., *J. Environ. Sci. Technol.*, 1994, **28**, 1968.
46 Creaser, R. A., Papanastassiou, D. A., and Wasserburg, G. J., *Geochim. Cosmochim. Acta.*, 1991, **55**, 397.
47 Horan, M. F., Morgan, J. W., Walker, R. J., and Grossman, J. N., *Science*, 1992, **225**, 1918.
48 Creaser, R. A., Papanastassiou, D. A., and Wasserburg, G. J., *Lunar Planet. Sci.*, 1993, **24**, 339.
49 Hauri, E. H., and Hart, S. R., *Earth Planet. Sci. Lett.*, 1993, **114**, 353.
50 Reisberg, L., Zindler, A., Marcantonio, F., White, W., Wyman, D., and Weaver, B., *Earth Planet. Sci. Lett.*, 1993, **120**, 149.
51 Walczyk, T., *PhD Thesis*, University of Regensburg, 1994.
52 Luck, J.-M., and Allègre, C. J., *Nature (London)*, 1983, **302**, 130.
53 Walker, R. J., and Fassett, J. D., *Anal. Chem.*, 1986, **58**, 2923.
54 Gallus, S., *Diploma Thesis*, University of Regensburg, 1994.
55 Walker, R. J., *Anal. Chem.*, 1988, **60**, 1231.
56 Papanastassiou, D. A., Ngo, H. H., and Wasserburg, G. J., *Lunar Planet. Sci.*, 1994, **25**, 1041.
57 Gregoire, D. C., *J. Anal. At. Spectrom.*, 1987, **59**, 2749.
58 Swihardt, G. H., Moore, P. B., and Callis, E. L., *Geochim. Cosmochim. Acta*, 1986, **50**, 1297.
59 Nakamura, E., Ishikawa, T., Birck, J. L., and Allègre, C. L., *Chem. Geol.*, 1992, **94**, 193.
60 Eisenhut, S., *Diploma Thesis*, University of Regensburg, 1994.
61 Heumann, K. G., and Zeininger, H., *Int. J. Mass Spectrom. Ion Phys.*, 1985, **67**, 237.
62 Henning, N. G., and Hanson, G. N., *Chem. Geol.*, 1994, **114**, 147.

Paper 4/06998F
Received November 16, 1994
Accepted January 3, 1995

Boron Isotope Analysis*
A Review

Jugdeep K. Aggarwal† and Martin R. Palmer
Department of Geology, University of Bristol, Wills Memorial Building, Queen's Road, Bristol, UK BS8 1RJ

Over the last ten years there has been a rapid increase in the number of studies of the boron isotope composition of natural samples. These studies have employed a variety of methods, with varying degrees of accuracy and precision. The relevant techniques are discussed in this paper and the problems associated with the measurement of boron isotope are divided into those dealing with (*i*) the extraction of boron from different types of samples (*ii*) purification of the extracted boron and (*iii*) mass spectrometric analysis of boron isotopes. The advantages and disadvantages of the different techniques are discussed. In addition, some refinements of these published methods and a new purification stage are presented. No one single method is appropriate for all studies; instead the choice of analytical method depends on the type of sample under consideration, the level of precision required to solve the problem, and the analytical equipment that is available. There is, however, a general requirement for more consideration to be given to assessing the reproducibility of some techniques and there is also a need for the development of working standards appropriate to the different types of natural samples, and the natural range of boron isotope ratios in these different types of samples.

Keywords: *Boron isotope analysis; extraction; purification; ion exchange; pyrohydrolysis; digestion; distillation; mass spectrometry*

Introduction

Boron has two stable isotopes, ^{10}B and ^{11}B, which have average relative abundances of approximately 20 and 80%, respectively. Boron isotope compositions are generally as $\delta^{11}B$ values, where

$$\delta^{11}B = \left[\left\{ \frac{^{11}B/^{10}B_{sample}}{^{11}B/^{10}B_{standard}} \right\} - 1 \right] \times 10^3$$

The standard is NBS boric acid SRM 951, prepared from a Searles Lake borax[1] and as with any other isotope standard the measured value varies slightly between laboratories; at our laboratory $\approx$ 100 analyses of this standard over three years have yielded an average $^{11}B/^{10}B$ ratio of 4.0529 $\pm$ 0.1‰ (2σ), or 4.0529 $\pm$ 0.0004.

Over the last ten years there has been growing interest in the analysis of boron isotope ratios in the natural environment. This work has included analyses of a wide range of materials including, alumino-silicate rocks and sediments,[2,3] boron-rich minerals,[4,5] carbonates,[6] and high- and low-temperature saline and non-saline waters.[7–10] Overall, $\delta^{11}B$ values range from +60‰ in salt lakes[9] to −30‰ in non-marine evaporite minerals[4] (Fig. 1). These studies have yielded much valuable information concerning geological and environmental processes, but analysis of boron isotope ratios in natural samples is not a routine procedure. The volatility of boron in some acid media makes extraction and purification procedures difficult. In addition, the fact that boron only has two stable isotopes means that instrumental isotope fractionation during mass spectrometry cannot easily be corrected for, if only analysing for the boron stable isotopes.

In this paper we review the difficulties inherent to the three stages of boron isotope analysis (extraction, purification and mass spectrometry), and examine some of the ways in which these problems have been overcome. A new purification stage using ion-exchange resins is detailed. The confines of this review mean that a detailed exposition of all of the techniques is not possible, however, various aspects of boron isotope analysis in some papers will be discussed in some detail. Those interested in applying the methods outlined here should consult the original papers.

Extraction

Problems of extraction of boron from solutions are dealt with under the heading of purification. This section is concerned with the extraction of boron from solid samples.

Tourmalines and Borates

Boron generally has a low average abundance in the earth, but where present, it is frequently concentrated in boron-rich minerals. The most common of these are tourmaline and a variety of evaporite borate minerals.

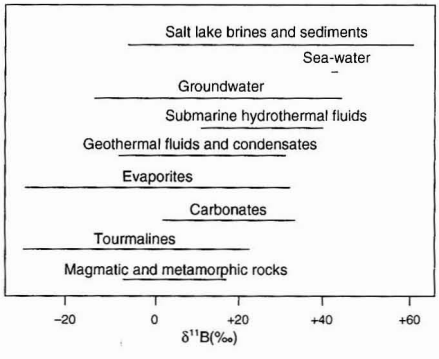

Fig. 1 Range of $\delta^{11}B$ values in natural samples, after Barth.[11]

* Presented at Geoanalysis 94: An International Symposium on the Analysis of Geological and Environmental Materials, Ambleside, England, September 18–22, 1994.

† Present address: Institute of Geological and Nuclear Sciences, P.O. Box 31312, Lower Hutt, New Zealand.

Tourmaline is a complex borosilicate mineral with the basic formula $NaR_3Al_6B_3Si_6O_{27}(OH,F)_4$, where R can be Fe^{2+}, Mg or (Al + Li).[12] Tourmaline is extremely resistant to acid digestion, but can be decomposed by fusion with sodium carbonate.[4] This method has been successfully applied,[13] but it requires extensive purification of the fusion cake before the sample is suitable for mass spectrometric analysis. In addition, it can be difficult obtaining fluxing agents that have low boron blanks. An alternative approach to extraction of the boron is by pyrohydrolysis.[5,14] In this method 4–5 mg of tourmaline are placed in a Pt boat and heated to 1400 °C in an alumina tube. Steam is passed over the sample at a rate of ≈ 20 ml h^{-1} of H_2O and the condensate collected with a quartz condensor. For tourmaline grains < 1 mm diameter, >99% of the boron is extracted within 4 h.

Non-marine evaporates are the major economic source of boron and borate minerals frequently form a major component of these deposits.[15] Most evaporite minerals are very soluble in water so it is possible to extract boron from them by dissolving the sample in water. However, post-depositional metamorphism or diagenesis of the minerals can produce less soluble forms. In addition, incomplete or incongruent dissolution of the sample could result in significant boron isotope fractionation. For these reasons pyrohydrolysis for extraction of the boron is favoured. For borate minerals complete boron extraction from the sample takes 2.5 h using the conditions described above.

One of the major advantages of pyrohydrolysis of borates and tourmalines is that few other species are transported with the steam phase so a relatively pure solution of boron is collected. Problems are encountered where samples contain high levels of other volatile elements, such as sulfur. In these instances purification of the condensate is required. Repeated runs of the splits of the same samples of tourmaline and borates show that the method is reproducible for these phases (Fig. 2).

Alumino-silicates

Pyrohydrolysis

Most alumino-silicate rocks contain < 50 ppm of boron. As 1–10 μg of boron can be required by mass spectrometric methods to obtain a reliable result, this can require processing of several grams of material. In these instances pyrohydrolysis is less suitable for extraction of boron. For example, up to 12 h are required to extract all the boron from 7 g of fresh mid-ocean ridge basalt.[7] This requires large volumes of water, lengthening the time required to process the condensate and increasing the chance of sample contamination. The low viscosity of basaltic melts also means that the melted rock can creep up the sides of the Pt boat and spread through the alumina tube. This makes cleaning of the apparatus difficult. In addition, it is possible that some boron remains in a refractory phase and is not completely extracted from the rock.[16] As the sample melts completely it is unlikely that there would be significant isotope fractionation between any residual boron and the steam phase at temperatures of 1400 °C, but retention of boron in the sample would result in an underestimation of the boron concentration.[17] The pyrohydrolysis of alumino-silicates also yields appreciable amounts of Na, Cl and significant amounts of Si as well as B. The Si must be especially removed as it interferes with the ionization of B.

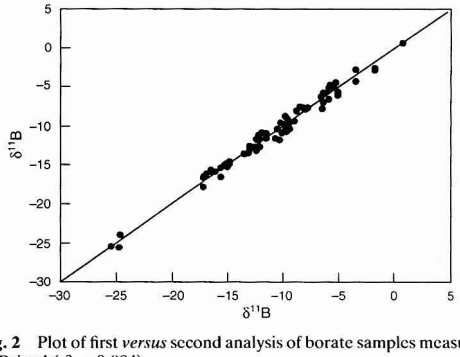

Fig. 2 Plot of first *versus* second analysis of borate samples measured at Bristol (r^2 = 0.984).

Fusion

The alternatives to pyrohydrolysis extraction of boron from alumino-silicates are fusion or acid dissolution of the sample.

Aspects of the fusion technique have been explored by Musashi *et al.*[18] A 0.5–1.0 g amount of powdered sample is fused with Na_2CO_3 or NaOH in a Pt or Ni crucible at 900–1500 °C. The ratio of flux-to-rock varies from 8 : 1 for Na_2CO_3 to 5 : 1 for NaOH. After cooling, the fusion cake is dissolved in 5% HCl and heated at 90–100 °C until the cake is dry. Boron is extracted from the dried fusion cake by methyl borate distillation (see below). The advantage of this method is that it is rapid and relatively large amounts of samples can be processed, enabling rocks with low boron concentrations to be analysed. The major disadvantage of the technique is that <90% of the total boron in the sample is extracted. Although isotope dilution studies suggest there is no isotope fractionation of the boron during processing of the fusion cake, it is possible that there is isotope fractionation between the extracted and residual boron. This is more likely to be a problem when using a NaOH flux as it has a low melting point (500 °C). The other problem is that the flux requires extensive cleaning (particularly for NaOH) with a boron-selective resin to remove impurities.

Acid dissolution

Acid dissolution (using combinations of HF, HNO_3, $HClO_4$) is the most common technique used for extracting elements such as Sr, Nd and Pb for isotopic analysis. Application of this method to preparation of samples for boron isotope analysis is complicated by the fact that BF_3 is highly volatile and easily lost from the dissolved sample with the potential for isotope fractionation. Boron volatilization can be suppressed by the use of mannitol during acid dissolution.[19] In this technique up to 0.5 g of powdered sample is soaked in a 1% mannitol solution in 0.1 mol l^{-1} HF before dissolution using 30 mol l^{-1} HF in a sealed Teflon beaker at 80 °C. The sample is then evaporated to dryness at 70 °C before conversion to the chloride by addition of 6 mol l^{-1} HCl and further evaporation. This technique has the advantage that the reagents can be easily cleansed of boron impurities, and boron extraction from the sample is complete, obviating any problems of isotope fractionation.

Purification

Before introduction of the sample into the mass spectrometer it is necessary to separate boron from impurities in the sample to eliminate isobaric interferences, avoid suppression of the ionization of the boron species analysed and maintain a good vacuum in the mass spectrometer. Some impurities in the sample can result in the fractionation of the ion beams during analysis yielding imprecise isotope ratios. Separation of boron

from impurities can be carried out by methyl borate distillation and/or ion exchange separation.

Distillation

Methyl borate distillation uses the volatility of trimethyl borate to separate boron from more refractory species and is particularly useful in removing silica from the sample, which cannot be readily separated from boron using non-specific ion-exchange resins.[14] In this technique 12 ml of anhydrous H_2SO_4 are slowly added to 150 ml of anhydrous methanol in an open quartz round-bottomed flask. The mixture is boiled for 30 min at a distillation rate of < 0.75 ml min^{-1} to remove boron impurities in the reagents. Up to 3 ml of aqueous sample are then added and a distillation head attached. The method is also suitable for extracting the boron from fusion cakes. In this instance the dried cake is added to the distillation vessel after the initial portion of methanol has been distilled off. A 35 ml volume of distillate is then collected in 50 ml of H_2O to hydrolyse the methyl borate. This solution is evaporated down to 1 ml at <50 °C. The method is simple and applicable to a wide variety of aqueous samples and the products of fusion and pyrohydrolysis extractions. The disadvantages are that only 3 ml of sample can be added to the distillation apparatus to ensure complete recovery of the boron (if more sample is used the boron remains partially hydrolysed and is not distilled, resulting in isotope fractionation of boron). Hence, low-boron concentration aqueous samples (< 500 μm kg^{-1}), such as meteoric waters must be preconcentrated (by ion exchange or evaporation) before they can be distilled. The distillation procedure is rapid (≈90 min), but subsequent evaporation takes approximately 1 d (faster evaporation leads to loss of boron from the distillate).

The ion-exchange techniques can be divided into those using boron-specific resin and those using non-specific anion and cation resins. The boron-specific resin techniques will be discussed later.

The products of the methyl borate distillation may contain small amounts of more volatile elements, such as Cl, and some elements that are carried over with the distillate such as Na, which can interfere later with mass spectrometric analyses. These can be removed from the sample by passing it through a mixed anion–cation exchange column (previously treated with HCl and NaOH to convert the resins to their H^+ and OH^- forms).[14] The resin is washed with H_2O to remove any contaminant boron from the column. Approximately 1 ml of sample is added to the column and the boron eluted off using H_2O; the anions and cations being left on the column. Many ion-exchange resins contain loosely bound organic material, some of which is collected with the boron. These organics can inhibit ionization of the boron species in the mass spectrometer and must, therefore, be removed. This can be accomplished by exposing the sample to a UV source for several hours. The major advantage of this method is that no acids are used in the column elution procedure so the problems of boron volatilization are reduced; however, the fact that a mixture of anion and cation resins is used means that the resin must be discarded after each use. This necessitates the UV stage to destroy the labile organics that may otherwise be removed during repeated use of the resin and adds an additional 24 h to the time required to process each sample.

For low boron concentration aqueous samples, the sample may be preconcentrated prior to distillation by a simple evaporation stage. However, if the sample contains significant amounts of total dissolved solids or a high alkalinity, then during the evaporation stage a precipitate may form. For high alkalinity samples, this precipitate has been found to co-precipitate boron into the carbonate structure. It is, therefore, inadvisable to use the evaporation stage prior to distillation for samples that contain low boron concentrations.

Ion Exchange

An alternative ion-exchange procedure has been developed for the products of the acid-dissolution technique.[19] In this instance the sample is loaded onto a cation-exchange column as a boron–mannitol complex in 0.1 mol l^{-1} HCl and eluted off the column using 0.02 mol l^{-1} HF. The boron–mannitol complex behaves as an anion and is not adsorbed onto the column, whereas the major cations in the solution are retained on the resin. A further purification step involves the use of an anion-exchange column, (AG1-X4). In this instance BF_4^- is adsorbed onto the column more strongly than the major anions and cations in the solution (despite the presence of mannitol). After purification of the sample through the cation resin, 3 mol l^{-1} HF is added to the sample in a sealed container, and warmed. This sample is then loaded onto the anion resin. The boron is eluted off the column following the major elements using a mixed acid composed of 2 mol l^{-1} HCl and 0.5 mol l^{-1} HF. This technique has the advantage of using small volumes of reagents and is, therefore, relatively rapid. The only disadvantage is that boron is highly volatile in the acid media used, so great care needs to be taken to avoid loss of boron at each stage.

Boron specific ion-exchange resin

An alternative method for analysing boron isotope ratios in low boron concentration fluids has involved the use of boron-specific ion-exchange resins. There are a number of methods in the literature that have used Amberlite 743 for the separation of boron from the other elements.[20–23] This Amberlite resin contains a hydrophobic styrene backbone and a tertiary amine group that will only absorb boron in the alkaline form $[B(OH)_4^-]$.

A new method has been developed for the determination of boron isotope ratios in low boron concentration aqueous samples using a combination of a boron-specific ion-exchange resin and a cation-exchange resin. The boron-specific resin (Amberlite 743), is used to concentrate the boron and provide an initial stage of purification, and the cation-exchange resin eliminates all of the other cations that the Amberlite resin does not remove.

The high ion-exchange capacity of the Amberlite 743 resin, means that only a small quantity (1.5 ml) of ground resin (80–100 mesh) is needed for the preparation of 15 μg of purified boron. Flow rates through the ion-exchange resin are adjusted to less than 0.5 ml min^{-1}. The resin is conditioned by the addition of 10 ml sub-boiling distilled water, 10 ml of 2 mol l^{-1} HCl, 10 ml of sub-boiling distilled water, 10 ml of 3 mol l^{-1} ammonia solution and finally 10 ml of sub-boiling distilled water.

The sample is adjusted to a pH of at least 10 and loaded onto the conditioned resin. The column is rinsed with 10 ml of a pH 10 ammonia solution, followed by two washes of 1 ml of sub-boiling distilled water with boron being eluted off the resin by the addition of 30 ml of 2 mol l^{-1} HCl, into a Teflon beaker containing 15 μl of (1.82 mass%) mannitol. Fig. 3 shows the elution of B during all of the wash and elution stages. The contents of the beaker are then evaporated down to about 1 ml under an IR lamp in a filtered air chamber. About 15 ml of sub-boiling distilled water are added to the sample prior to cation exchange to reduce the concentration of the acid from 6 to less than 1 mol l^{-1}.

A 5 ml volume of Dowex 50X W8 cation-exchange resin is placed in an ion exchange resin holder and is conditioned by the addition of 20 ml of 6 mol l^{-1} HCl, followed by 40 ml of

sub-boiling distilled water. The diluted sample is then loaded onto the resin followed by 30 ml of sub-boiling distilled water, and the eluate collected. To the eluate is added 33 μl of a caesium carbonate solution (7.62 μg ml^{-1}) and 15 μl of the mannitol solution. The sample is then exposed to UV light overnight to destroy any labile organics.[14] A 5 μl volume of the mannitol solution is then added to the sample before being evaporated down to a few microlitres.

The literature shows a number of methods that use the Amberlite boron-specific resin. The pH of the solutions used in this technique is critical to their success. In aqueous samples, boron occurs as both the $B(OH)_3$ and the $B(OH)_4^-$ species. In acidic solutions the $B(OH)_3$ species predominates, and in the more alkaline solutions the $B(OH)_4^-$ species dominates, (Fig. 4). At a pH of about 9, both species occur in equal proportions. Of these two borate species it is the $B(OH)_3$ that tends to contain the lighter isotope.[24] As the Amberlite resin only absorbs the boron in the anionic form, it is crucial that all of the boron is converted into the $B(OH)_4^-$ species by the addition of alkali. It is, therefore, interesting to note that Leeman *et al.*,[23] adjust the sample pH to 8; Davidson and Bassett[20] suggest that the sample should be adjusted to a pH of at least 5; and Hemming and Hanson[21] adjust to a pH of 8.2. In all of these methods there is likely to be unabsorbed

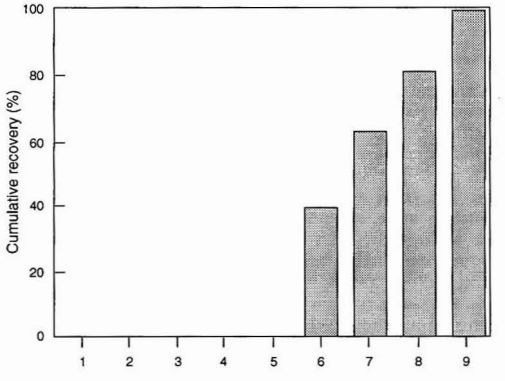

Fig. 3 Recovery of B during washes of the boron-specific resin: 1, sample loaded onto the resin; 2, addition of 5 ml of pH 10 ammonia wash; 3, addition of second 5 ml aliquot of pH 10 ammonia wash; 4, addition of third 5 ml aliquot of pH 10 ammonia wash; 5, addition of 5 ml of sub-boiling distilled water; 6, addition of 5 ml aliquot of 2 mol l^{-1} hydrochloric acid; 7, addition of second 5 ml aliquot of 2 mol l^{-1} hydrochloric acid; 8, addition of third 5 ml aliquot of 2 mol l^{-1} hydrochloric acid; and 9, addition of forth 5 ml aliquot of 2 mol l^{-1} hydrochloric acid.

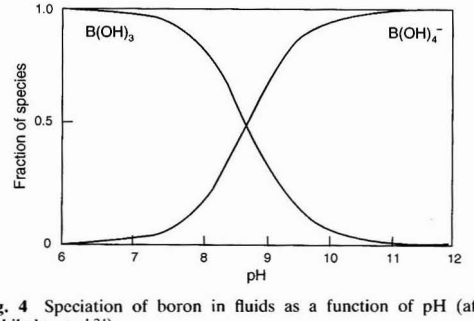

Fig. 4 Speciation of boron in fluids as a function of pH (after Kakihaha *et al.*[24])

$B(OH)_3$ in solution, resulting in fractionation of the boron isotope ratios. Adjusting the pH of the sample to a pH of at least 10 ensures that all of the boron is converted into the tetrahedral form, which can then be quantatively absorbed onto the ion-exchange resin.

In the proposed method, the pH of the sample is adjusted to a pH of at least 10. At this high pH precipitates of notably iron, calcium and magnesium hydroxides form and can be retained on the Amberlite resin as precipitates. These precipitates are dissolved by the acid used to elute the boron off the Amberlite resin, and are subsequently removed by the cation resin. Further improvements have been made by careful selection of solutions to wash the boron-specific ion-exchange resin. Washing the resin with a solution of ammonia at a pH of 10, rather than water, ensures that all of the boron remains adsorbed onto the resin. A wash at lower pH may release some boron and result in isotope fractionation. A wash of just 2 ml of sub-boiling distilled water ensures that no ammonia solution remains on the resin, which would otherwise fractionate the ion beams.

Davidson and Bassett,[20] have eliminated the need for a second ion-exchange resin by carrying out further purification of the sample using the methyl borate distillation. In order to use the distillation stage, boron is eluted off 10 ml of the Amberlite resin, using 100 ml of 0.1 mol l^{-1} nitric acid. This sample is then evaporated down sufficiently prior to the distillation stage. Elution of boron using nitric acid eliminates any problems of boron volatility encountered during the use of hydrochloric acid (without the mannitol), however, it does use large qualities of acid during the elution stage. We have modified this method in order to reduce the volume of acid used in the elution stage, by increasing the concentration of the nitric acid to 1 mol l^{-1}.

Mass Spectrometry

There have been attempts to determine boron isotope ratios using methods other than mass spectrometry, but the lack of precision and/or large sample sizes required do not make them suitable for natural samples. Some early measurements of boron isotope ratios were made using a gas source mass spectrometer by analysis of the isotope ratio of BF_4^-, but the reactive nature of this species introduced large memory effects and led to degradation of the equipment.

Apart from thermal ionization mass spectrometry (TIMS), the two other mass spectrometric techniques used to determine boron isotope ratios are inductively coupled plasma-mass spectrometry (ICP-MS) and secondary ion mass spectrometry (SIMS).

ICP-MS

In the ICP-MS method,[25] an aqueous solution of boron is aspirated into the plasma *via* a Meinhard nebulizer and the isotope ratio determined from the ratio of the peak intensities at masses 11 and 10. One advantage of this technique is that the throughput of samples is very high (up to 100 samples per day). In addition, careful purification of the boron is not required as there are no isobaric interferences with the two boron masses and there is little or no suppression of boron ionization unless the solution contains high levels of dissolved salts. There are, however, a number of major disadvantages that do not make the technique suitable for the majority of geological applications. Firstly, the precision of the technique is only ±14‰ (2σ), compared with ±0.4‰ for the most precise TIMS methods (see below). The isotope ratios determined by ICP-MS are strongly dependent on the matrix of the solution, to the extent that there is approximately a 10% difference in the boron isotope ratio determined for a boron standard

containing 3000 ppm Na and one containing 6000 ppm (Fig. 5).

SIMS

As noted above, one of the major problems in analysing boron isotope ratios in alumino-silicate materials is extracting and purifying the boron without loss of boron from the sample (with the problems of inducing isotope fractionation effects). SIMS offers the possibility of avoiding these problems by direct analysis of solid samples.[26] A polished thin section of the sample is placed in an ion microprobe and sputtered with a primary beams of Ga^-, or Cs^+ or more usually O^-, and the secondary positive boron beams are measured at masses 10 and 11. Standardization is carried out by analysis of a sample of known boron isotope composition and similar chemical composition to reduce matrix effects. The advantage of this technique is that no chemical sample processing is required and small amounts of material (>150 μm sized grains) can be analysed for boron concentrations as low as 1 ppm.[27] The resolution of the O^- primary beam allows measurement of 25 μm spot sizes, the Cs^+ allows spot analyses of about 1–2 μm, and the Ga^- primary ion beam allows spot analyses of sub-micrometer size, should analyses at these fine spacial resolutions be required. Different matrices provide different ion yields of the boron, so absolute concentration determinations are difficult; however, isotope ratio measurements are more straightforward. The major disadvantage is that the precision of the analyses is only ±4‰ (2σ), which is considerably poorer than TIMS analyses. In addition, difficulties are encountered in the analysis of the more volatile phases such as carbonate and borates.

TIMS

TIMS methods can be divided into those using positive ions (PITIMS) and those using negative ions (NITIMS).

PITIMS

PITIMS techniques involve measurement of the isotopic composition of an alkali-borate complex. After purification of the boron an appropriate amount of an alkali salt (usually the carbonate or hydroxide) is added and the solution evaporated to dryness on an out-gassed Ta filament. The amount of boron required varies according to the sensitivity of the mass spectrometer but typical sample sizes are 10–50 μg of boron. Initial studies used the $Na_2B_4O_7$ salt, and analysed the $Na_2BO_2^+$ species at masses of 88 and 89. Although a number of interesting studies have been performed using this method[4,13] there are several problems with the technique. Significant isotope fractionation is frequently observed during the course of an individual analysis, with the $^{11}B/^{10}B$ ratio becoming progressively heavier during the course of the run[28] (Fig. 6). As there are only two stable isotopes of boron it is not possible to carry out an on-line correction for this isotope fractionation so this problem limits the precision of the Na-borate method to ±2–3‰ (2σ). A further, though less significant, problem is that isobaric interference is possible from $^{88}Sr^+$ if the sample is not sufficiently pure or if the mass spectrometer is also used for analysis of Sr isotopes.

The problem of in-run isotope fractionation can be reduced by increasing the molecular mass of the alkali-borate species analysed. Potassium borate complexes are not suitable because the presence of three K isotopes (^{39}K, ^{40}K and ^{41}K) leads to overlapping $K_2BO_2^+$ peaks in the mass spectrum that are not easily deconvoluted. The two isotopes of Rb (^{85}Rb and ^{87}Rb) are separated by two u so that overlapping $Rb_2BO_2^+$ peaks are not such a problem and the masses are sufficiently high (212–217, not including the minor oxygen isotope peaks) that instrumental mass fractionation is greatly reduced. However, as with all alkali-borates the size of the alkali ion beam is frequently two orders of magnitude greater than the alkali-borate ion beam. This results in a significant build of alkali in the source of the mass spectrometer that is difficult and time-consuming to remove. For Rb this creates major problems if Sr isotopes are run on the same mass spectrometer as there is frequently a significant memory effect of $^{87}Rb^+$ that causes isobaric interference on ^{87}Sr.

These problems are largely avoided by analysis of the $Cs_2BO_2^+$ species[13,28] at masses of 308 and 309 (Fig. 6). The method has been modified by the use of a graphite slurry and mannitol during the loading procedure[29] so that the sample size can be reduced to 1 μg of boron with an analytical precision of <±0.4‰ on most mass spectrometers. The graphite slurry has been employed in most techniques for boron isotope analysis, as it has been found to significantly improve the ionization efficiency of the sample off the filaments. Using a reduced sample size there is still a significant build up of Cs in the mass spectrometer source. This has a number of deleterious effects on the mass spectrometer performance. Cs has a very low ionization energy so deposition of Cs on the lens stack results in charging of the lenses and drift in the focus position during the course of the run. This can be reduced by lowering the Cs:B ratio loaded onto the filament from 1:2 down to 1:7, and thorough

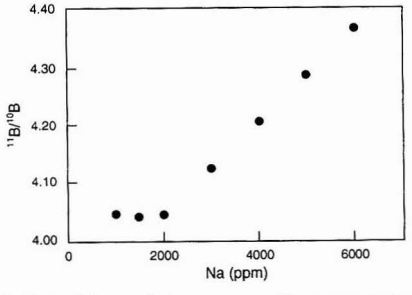

Fig. 5 Plot of boron isotopes *versus* Na concentrations from Gregoire.[25]

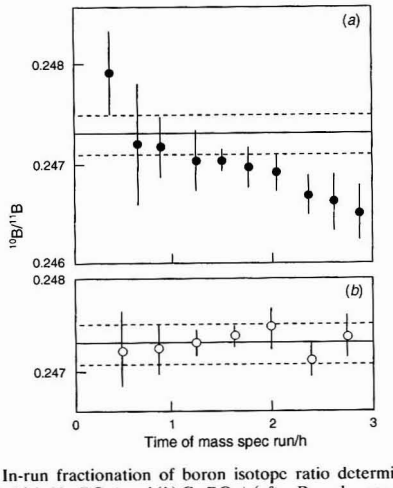

Fig. 6 In-run fractionation of boron isotope ratio determined by PITIMS of (*a*), $Na_2BO_2^+$ and (*b*) $Cs_2BO_2^+$ (after Ramakumar *et al.*[28])

cleaning of the lens stack, but it is difficult to eliminate the problem entirely. A more serious problem is encountered if the same mass spectrometer is used for isotope analyses requiring a high filament current (*e.g.*, Nd or Hf). This causes heating of the source and volatilization of Cs deposited on surfaces. The low ionization energy of Cs can cause suppression of the Nd^+ signal and lens charging compromises attempts to obtain high precision ($\pm 10^{-5}$) data. These problems have meant that relatively few laboratories have developed a major boron isotope analytical programme.

NITIMS

Some of the problems associated with analysis of alkali-borate salts can be avoided by analysis of negative ions. In this instance the ion of interest is BO_2^-, measured at masses of 42 and 43. After purification the boron is loaded onto a single Re filament together with $La(NO_3)_3$ to lower the electron work function of the filament.[30] The major advantage of this technique is that the ion yield is of the order of 1000 times higher than that for PITIMS, which allows samples containing <1 ng of boron to be run.[30] In addition, the degree of purification of boron required to perform the analyses is not so high as for analysis of the alkali-borates so that the boron isotope composition of some aqueous samples can be analysed by loading the solution directly onto the filament without any purification.[31] The major disadvantage of the technique is that the low mass numbers of the species analysed means that there is severe isotope fractionation during the course of the run[30] leading to precisions of $\pm 0.8‰$ (2σ). Improved precision can be attained by integrating the ion beam yields from the entire run for an individual beam.[32]

One disadvantage that the NITIMS suffers from over the PITIMS is that of isobaric interference at the low masses. CNO^- of mass 43 ($^{12}C^{15}N^{16}O^-$, $^{13}C^{14}N^{16}O$, can interfere with the $^{11}B^{16}O^{16}O^-$, yielding higher $^{11}B/^{10}B$ ratios, and $^{12}C^{14}N^{16}O^-$ can interfere with $^{11}B^{16}O^{16}O^-$ at a mass of 42. Monitoring of the CN^- peak at mass 26 often indicates whether this isobaric interference on the borate peak is significant.[6]

Discussion

There are a variety of extraction, purification and mass spectrometric methods available for the study of boron isotope ratios in natural samples. The choice of approach depends on a number of factors including: the sample type analysed, the level of precision required and the equipment available for the preparation and analysis of samples (Table 1).

If the problem under consideration requires data with good precision then the mass spectrometric technique with the highest precision is the Cs-borate method. Both aqueous and alumino-silicate samples require extraction and purification of the boron for this method. For aqueous samples the ion-specific resin technique is the most flexible in terms of the size of sample that can be processed and the speed with which the sample can be prepared. For boron-rich minerals the pyrohydrolysis extraction method is the simplest and there is less problem with loss of boron during processing of the sample. For solid samples with lower boron concentrations the acid dissolution technique appears to be the most reliable.

If precision of the data is not critical then for aqueous samples the negative ion thermal ionization technique is more suitable and requires far less sample processing than other methods. For solid samples, the SIMS method is by far the most straightforward in that minimum sample processing is required; however, ion microprobes are not common pieces of equipment in geological laboratories and there is a shortage of appropriate boron isotope standards. In the absence of access to SIMS the extraction and sample processing are similar for

Table 1 Summary of the advantages/disadvantages of the techniques available for isotope analysis

		Advantages	Disadvantages
Extraction	Pyrohydrolysis	No fractionation of B.	Only suitable for solid samples with high B concentrations
Fusion		High yields	Difficult to prepare reagents at pure enough grade
	Acid digestion	Samples with low B concentrations can be analysed	Volatilization of B may be a problem. Extraction method is arduous and involves many stages where contamination may arise
Purification	Distillation	Well proven technique	Purification stage is time consuming and only a few samples may be prerpared at a time. Method is only suitable to aqueous samples with relatively high B concentrations
	Ion exchange	Able to tolerate samples with low B concentrations	Volatilization of B needs to be suppressed. Purification stage involves much sample handling
Mass spectrometry	ICP-MS	Requires little or no sample preparation. High sample throughput	Precision is relatively poor ($\approx \pm 14‰$)
	PITIMS	High levels of precision may be attained ($\approx \pm 0.3‰$)	Requires that sample analysed is as pure as possible
	NITIMS	Relatively high levels of precision with minimal amounts of preparation	Precision of $\approx \pm 1‰$
	SIMS	No sample preparation required	Significant instrumental mass fractionation needs to be corrected for. Poor precision of $\approx \pm 4‰$ is typical

both negative and positive ion thermal ionization mass spectrometry.

All the mass spectrometric techniques have to deal with the fact that boron only has two stable isotopes so that on-line correction for instrumental isotope fractionation is not possible. Experience at Bristol has shown that careful attention has to be made in focusing the ion beam to ensure optimum peak shape if reliable data are to be obtained. Where possible our practice is to run duplicates of every sample to check this problem. Operation of this quality control procedure reveals that approximately 5% of all runs yield erroneous isotope ratios (defined as repeat runs differing by more than 1‰). The effect appears to be random in the sense that a poorly focused beam does not systematically produce lighter or heavier isotope ratios. In these instances two further analyses are made of the same sample to confirm the true boron isotope ratio.

As with other stable isotope techniques it is important that isotope ratios are reported for standard materials. For boron the standard used in virtually all studies is NBS SRM 951 boric acid. Generally this involves loading a solution (in the appropriate form) of this standard directly onto the filament. It would also be useful to have international standard samples that can be processed through the extraction and purification techniques to ensure their reliability. For aqueous samples the obvious choice is sea-water as its boron isotope ratio is constant throughout the World's oceans[14] and it is in plentiful supply. Because of the greater analytical problems involved there have been fewer studies of solid samples and there is no obvious isotope standard at present. It is hoped that intercalibration of the boron isotope composition of a suitable international rock standard may be possible in the future.

The level of precision of the various methods employed are variable so that it is important that these are quoted for each sample, with a specification as to whether the errors are at the 1 or 2σ level. In addition, replicate analyses of at least some samples should be performed and reported as a check on the reproducibility of the technique employed as this is the true measure of the accuracy and precision of an analytical method.

Conclusions

Over the last decade there has been a considerable increase in the interest in boron isotope geochemistry. A range of analytical methods have been developed to cope with a variety of sample types, analytical equipment available and the level of precision required. Analytical methods have developed to the point where there are now reliable and precise techniques for most of the problems of interest to geochemists.

It is hoped that common practices will be developed whereby laboratories measuring boron isotope ratios can agree on the use of appropriate working standards for different types of samples. There is also a need for checks on the reproducibility of the analytical methods employed in a particular study.

This work has been supported by a NERC grant GR3/7681 and The Royal Society. We are also grateful to our colleagues at Bristol (A. Lewis and S.-Y. Jiang) and in the wider boron isotope community for their advice and encouragement.

References

1 Cantanzaro, E. J., Champion, C. E., Garner, E. L., Marinenko, G., Sappenfield, K. M., and Shields, W. R., *NBS Spec. Pub. (U.S.)*, 1970, **260–17**.
2 Spivack, A. J., Palmer, M. R., and Edmond, J. M., *Geochim. Cosmochim. Acta*, 1987, **51**, 1939.
3 Palmer, M. R., *Geology*, 1991, **19**, 215.
4 Swihart, G. H., Moore, P. B., and Callis, E. L., *Geochim. Cosmochim. Acta*, 1986, **50**, 1297.
5 Palmer, M. R., and Slack, J. F., *Contrib. Mineral. Petrol.*, 1989, **103**, 434.
6 Hemming, N. G., and Hanson, G. N., *Geochim. Cosmochim. Acta*, 1992, **56**, 537.
7 Spivack, A. J., and Edmond, J. M., *Geochim. Cosmochim. Acta*, 1987, **51**, 1033.
8 Palmer, M. R., and Sturchio, N. C., *Geochim. Cosmochim. Acta*, 1990, **54**, 2811.
9 Vengosh, A., Starinsky, A., Kolodny, Y., and Chivas, A. R., *Geochim. Cosmochim. Acta*, 1991, **55**, 1689.
10 Aggarwal, J. K., Palmer, M. R., Ragnarsdottir., K. V., *Proceedings of the 7th International Symposium on Water-Rock Interactions*, Park City, July 13–18, 1992, ed. Kharaka, Y. K., and Maest, A. S., Balkema, Rotterdam, 1992, pp. 893–897.
11 Barth, S., *Geol. Rundsch.*, 1993, **82**, 640.
12 Dietrich, R. V., *The Tourmaline Group*, Van Nostrand Reinhold, New York, 1985, p. 300.
13 Swihart, G. H., and Moore, P. B., *Geochim. Cosmochim. Acta*, 1989, **53**, 911.
14 Spivack, A. J., and Edmond, J. M., *Anal. Chem.*, 1986, **58**, 31.
15 Hardie, L. A., *Amer. J. Sci.*, 1984, **284**, 193.
16 Leeman, W. P., personal communication.
17 Palmer, M. R., London, D., Morgan, G. B., and Babb, H. A., *Chem. Geol.*, 1992, **101**, 123.
18 Musashi, M., Oi, T., Ossaka, T., and Kakihana, H., *Anal. Chim. Acta*, 1990, **231**, 147.
19 Nakamura, E., Ishikawa, T., Birck, J. L., and Allègre, C. J., *Chem. Geol.*, 1992, **94**, 193.
20 Davidson, G. R., Bassett, R. L., *Environ. Sci. Technol.*, 1993, **27**, 172.
21 Hemming, N. G., Hanson, G. N., *Chem. Geol.*, 1994, **114**, 147.
22 Kiss, E., *Anal. Chim. Acta*, 1988, **211**, 243.
23 Leeman, W. P., Vocke, R. D., Beary, E. S., and Paulsen, P. J., *Geochim. Cosmochim. Acta*, 1992, **55**, 3901.
24 Kakihana, H., Kotaka, M., Satoh, S., Nomura, M., and Okamoto, M., *Bull. Chem. Soc. Jpn.*, 1977, **50**, 158.
25 Gregoire, D. C., *Anal. Chem.*, 1987, **59**, 2479.
26 Chaussidon, M., and Albarède, F., *Earth Planet. Sci. Lett.*, 1992, **108**, 229.
27 Chaussidon, M., and Jambon, A., *Earth Planet. Sci. Lett.*, 1994, **121**, 277.
28 Ramakumar, K. L., Parab, A. R., Khodade, P. S., Almaula, A. I., Chitambar, S. A., and Jain, H. C., *J. Radioanalo. Nucl. Chem.*, 1985, **94**, 53.
29 Xiao, Y. K., Beary, E. S., and Fassett, J. D., *Int. J. Mass Spectrom. Ion Processes*, 1988, **85**, 203.
30 Zeininger, H., and Heumann, K. G., *Int. J. Mass. Spectrom. Ion Phys.*, 1983, **48**, 377.
31 Vengosh, A., Chivas, A. R., and McCulloch, M. T., *Chem. Geol.*, 1989, **79**, 333.
32 You, C. F., Spivack, A. J., Smith, J. H., and Gieskes, J. M., *Geology*, 1993, **21**, 207.

Paper 4/05862C
Received September 26, 1994
Accepted November 4, 1994

Determination of Hydrogen in Silicates by Secondary Ion Mass Spectrometry*

Luisa Ottolini, Piero Bottazzi and Alberto Zanetti

C.N.R.—Centro di Studio per la Cristallochimica e la Cristallografia, I-27100 Pavia, Italy

Riccardo Vannucci

Dipartimento di Scienze della Terra, Università degli Studi di Pavia, I-27100 Pavia, Italy

A quantitative procedure for the determination of hydrogen in silicates was developed for incorporation in the general procedure used with the Cameca IMS 4f ion microprobe for light and trace elements. The procedure employs a static $^{16}O^-$ primary beam and the 'energy filtering' technique. Moreover, it allows the analysis of samples placed on separate mounts with respect to standards and, in particular, of mineral grains directly in thin sections of rock. Factors influencing the hydrogen background were studied in order to ascertain the appropriate analytical conditions and to develop a specific procedure for the determination of low hydrogen contents. A low and reproducible background was obtained with simple heating and de-gassing of the sample. The background value was equivalent to 0.007–0.015% H_2O and its fluctuation over a 1 week working session indicated that the detection limit was ≈0.015% H_2O. The results obtained confirm that the use of high-energy ions reduces the influence of the matrix composition on the ionization of hydrogen (relative to that of Si); effects related to the structure of the sample appear to be negligible. Residual matrix composition effects are related, to a first approximation, to the Si content of the sample. As such effects could not be completely removed, two separate ion yields were used for samples with SiO_2 contents in the range 27–51% and for rhyolites (≈72% SiO_2). The reproducibility of the measurements was typically ≈3% and the accuracy for the former group of samples was 15% for H_2O contents >0.1% and 30% for H_2O contents of ≈0.05%.

Keywords: *Hydrogen determination; silicate; secondary ion mass spectrometry; ion microprobe*

Introduction

In the study of hydrogen in melt inclusions (between 50 and 300 μm width) or whenever measurements are required on very small crystals or on micro-areas of thin sections of rock, a microanalytical tool reveals information of fundamental importance. Secondary ion mass spectrometry (SIMS) is, in principle, ideal for hydrogen determination because it requires only a small analytical volume and limited (solid) sample preparation, with a minimum consumption of material during analysis; its sensitivity for hydrogen is high, and the mass spectrum in the region of the ^1H peak is free from interferences. Furthermore, hydrogen can be measured in conjunction with several other elements of interest. A specific feature of SIMS is that it measures all the hydrogen present in the sample, as it is not able to discriminate between the various hydrogen species. Two analytical problems have hampered its development as a routine technique in earth sciences: (i) the background level of hydrogen present and detected by the instrument, which can be equivalent to several per cent. of H_2O; (ii) the presence of matrix effects, *i.e.*, the influence that the chemical composition and the structure of the matrix can exert on the ionization of hydrogen.

Hydrogen is a constituent of the residual vacuum gases within the instrument, and hence will adsorb onto the surface of the sample. This adsorbed hydrogen will be ionized during sputtering and will contribute to the hydrogen detected during analysis. SIMS analyses for elements that are also constituents of the residual vacuum gases are often limited by the background signal introduced when these gases strike and adhere to the sample surface and are subsequently ionized during sputtering. Also, the implantation of hydride species present as impurities in the primary ion beam is a source of this background; however, the use of a mass-filtered primary beam reduces the hydride impurities. Hydrogen atoms, sputtered from the extraction plate in the sample chamber, can be re-deposited onto the analysed area, contributing to the secondary ions (memory effect). Another source of contamination is due to adsorbed hydrogen, present on the sample surface, related to contamination of the environment and sample preparation. If the sensitivity of the analysis is sufficient, it is this background that defines the operational detection limit.

The determination of hydrogen by SIMS carried out using low-energy ions[1–3] suffers from two major problems: (i) a high intercept of the calibration graph; and (ii) severe matrix effects (factor >3), which make it compulsory to calibrate hydrogen signals on standard samples of similar chemical composition to the unknown. Matrix effects constitute a major drawback, as homogeneous reference materials for hydrogen are scarce, and the use of standards of composition appropriate to all samples is not generally practicable for complex matrices, such as staurolites or micas. Hervig and Williams[4] found that a marked reduction of both problems occurs when the secondary beam is 'energy filtered', *i.e.*, when high-energy ions are used. According to Hervig and Williams,[4] the application of a voltage offset to the sample eliminates the effects related to hydrogen ions formed by electron stimulated desorption (ESD). The abundant secondary electrons produced by the primary ion beam ionize surface hydrogen very efficiently; moreover, the secondary electron yield depends on the chemistry of the sample, which will cause the ESD ion yield of hydrogen to vary with the nature of the matrix. As ESD ions have a narrow energy distribution,[5,6] however, even a small offset voltage effectively eliminates them.

A very low intercept (corresponding to 0.3 ppm by mass) was also found for quartz by Yurimoto *et al.*[7] using the energy filtering technique and an intense primary beam (≈100 nA).

* Presented at Geoanalysis 94: An International Symposium on the Analysis of Geological and Environmental Materials, Ambleside, England, September 18–22, 1994.

In preliminary work,[8] using a rastered 50 nA primary beam of O^- ions and no thermal treatment of the samples, we obtained a working curve for hydrogen in silicates accurate to ≈20%. The starting point for the development of updated methodology for the Cameca IMS 4f ion microprobe was to find an analytical procedure by which hydrogen could be measured routinely on micro-areas in all the silicates of interest. For this purpose, we adopted the instrumental conditions generally used for the analysis of various trace and light elements in silicates,[9,10] *i.e.*, microspot analysis of energy-filtered secondary ions, combined with procedures to reduce the hydrogen background, *i.e.*, cold-trap and sample de-gassing treatments.

Experimental

A description of the general features of the Cameca IMS 3f/4f ion microprobe/ion microscope is given in ref. 11. For this work, a static 10 nA, mass-filtered $^{16}O^-$ primary beam accelerated to 17 kV was focused on the sample surface to obtain a 15–20 μm beam diameter. The second aperture on the primary-beam mass selector (400 μm) was used to prevent $^{16}O^1H^-$ ions, which form a weak second spot on the sample (clearly visible in anhydrous samples), from reaching the sample chamber (SC). Positive secondary ions from the sample were extracted by a 4.5 kV accelerating voltage and transferred into the mass spectrometer by the 25 μm secondary ion optics. Secondary ions were then 'energy-filtered' in the electrostatic sector of the IMS 4f instrument by offsetting the sample accelerating voltage by −100 V and closing the energy slit to a width corresponding to 50 eV; this instrumental set-up allows ions with an emission energy in the range ≈75–125 eV to be collected. Entrance and exit slits were left wide open.

Standards used for the investigation of hydrogen ion yields and reference samples used to test the validity of the procedure are listed in Tables 1 and 2, respectively, with their reference silica and total H_2O content, and with methods used for the determination of hydrogen.[12–18] For most of the standards and reference samples, the accuracy of their H_2O reference value is unknown. Portions of each sample, with grain sizes from about 50 μm to several millimetres, were mounted in epoxy resin, polished and gold-coated to a thickness of ≈50 nm. A maximum of five samples were placed on each mount as close to the centre as possible. This mounting procedure is that normally used for ion probe analysis of separate mineral grains; most mounts were in fact already available because they had been employed previously for calibration of other elements. Hydrogen and silicon ion intensities, H^+ and Si^+, respectively, were collected at the electron multiplier as ^1H and ^{30}Si, together with other signals (not reported here), by peak-jumping through the mass spectrum and repeating the mass loop for 14 min (24 cycles). Signal loss owing to the deadtime of the counting chain and the background of the electron multiplier were negligible. Counting times per cycle were 4 s for ^1H and 2 s for ^{30}Si. These counting times allow counting statistics better than 1% relative to be achieved, even in less favourable situations. Before measuring ^{30}Si, the magnet was allowed to settle for 2 s; a longer delay (6 s) was used for ^1H to account for the slower settling of the magnet after the jump from 30 to 1 u. The first 7 min of each run were rejected owing to non-steady-state sputtering conditions; the following 12 cycles, corresponding to ≈7 min, were accepted. The H^+ and Si^+ intensities were corrected for isotopic abundance, and the H-to-Si intensity ratios were averaged. The normalization to an internal standard allows compensation for small fluctuations in the instrumental conditions over a long period of time.

The measurements for the construction and testing of the working curve spanned 3 months, and were divided into three separate sessions of 7–10 d each. Over this time, the SC vacuum was always $<7 \times 10^{-7}$ Pa (typically 3×10^{-7} Pa) with primary ion source and primary beam on. Prior to insertion in the sample chamber, sample mounts were de-gassed under a rotary-pump vacuum (<1 Pa) with mild heating (≈50 °C). Literature data[1,19–21] indicate the usefulness of different heating (60–120 °C) and de-gassing treatments of samples. A systematic investigation of the influence of thermal treatments on hydrogen background reduction could not be carried out because the epoxy mount of the samples did not allow the latter to be heated at temperatures higher than 50 °C. A few results obtained for samples with low hydrogen contents, however, showed a significant reduction of the background for treated samples; in sample MH1 (0.05% reference H_2O), for instance, a reduction of ≈0.15% in the H_2O-equivalent signal was observed (after a 2 h residence time in the SC) on

Table 1 Standard samples with reference H and Si concentrations and relative-to-Si H ion yield

Sample	Description	SiO_2 (%)	H_2O (%)	Method	H ion yield
71-60E	Staurolite	27.79	2.27	Vacuum extraction + manometry[12]	0.136 ± 0.005
ER-70	Staurolite	26.97	1.48	Vacuum extraction + manometry[12]	0.122 ± 0.002
DL-5	Amphibole	39.60	0.67	Karl Fischer titration[13]	0.131 ± 0.010
MH17	Amphibole	40.91	0.74	Karl Fischer titration[13]	0.113 ± 0.004
Great Bear Lake	Cordierite	48.11	1.24	Infrared spectroscopy[14]	0.133 ± 0.003
Manitouwadge	Cordierite	48.00	1.45	Infrared spectroscopy[14]	0.138 ± 0.004
CY82-29-1V	Basaltic glass	49.52	0.09	Vacuum extraction + manometry[15]	0.136 ± 0.010
CLDR01-5V	Basaltic glass	50.43	0.16	Vacuum extraction + manometry[15]	0.141 ± 0.004
MacBr	Rhyolite	72	0.17	Vacuum extraction + manometry[15]	0.205 ± 0.004
ME 35D	Rhyolite	72	5.11	Wet chemistry[16]	0.188 ± 0.023
Macusani	Rhyolite	72.30	0.43*	Wet chemistry[17]	0.209 ± 0.003

* Average of two values:[17] 0.40, 0.46.

Table 2 Control samples with reference H and Si concentrations and H values obtained by SIMS

Sample	Description	SiO_2 (%)	H_2O (%)	Method	H_2O by SIMS (%)
Kaersut	Amphibole	39.99	0.69	Karl Fischer titration[13]	0.69 ± 0.02
DH	Amphibole	38.40	0.24	Karl Fischer titration[13]	0.21 ± 0.02
MH1	Amphibole	38.40	0.05	Karl Fischer titration[13]	0.035 ± 0.006
Topaz Mt.	Topaz	32.74	0.04	Element analyser in V_2O_5 flux[18]	0.045 ± 0.004

applying the preliminary treatment. Subsequently, mounts were allowed to de-gas in the sample chamber. A liquid nitrogen cold-trap (commercially available for the Cameca IMS 4f instrument) was used to reduce H_2O vapour and volatiles in the vicinity of the sample. The cold-trap was filled with liquid nitrogen at least 120 min before starting the analysis, and it was regularly checked during the day.

It was assumed that the signal, measured at relative atomic mass 1, was the sum of the H^+ signal from the sample plus the H^+ signal from the background. Only one reference sample (quartz) was available to determine the background signal through measurement of its H^+/Si^+ intensity ratio. Its hydrogen content is 45 atoms per 10^6 Si atoms,[16] and it can be considered to be anhydrous for our purposes. It is not known whether background H^+ experiences the same matrix effects as H^+ sputtered from the sample; here it was assumed that the error in the background determination, related to possible matrix effects, was, to a first approximation, negligible compared with its over-all uncertainty. In order to take into account the different silica contents of the samples (which range from about 27 to 72%), an empirical manipulation was made: the H^+ signal from quartz was normalized to that of silicon ratioed to the silica content in the quartz (*i.e.*, $b = H^+/Si^+ \times SiO_2\%$); H^+/Si^+ intensity ratios, measured in standards and test samples, were then corrected for background, calculated using the b value obtained in each analytical session, corrected for the silica content of the sample, *i.e.*, $b/(\%\ SiO_2$ in the sample). The H-ion yield was then calculated according to:

$$\text{Relative-to-Si ion yield of H} = \frac{\text{H ion intensity normalized to Si ion intensity}}{\text{H atomic concentration normalized to Si atomic concentration}}$$

where ion intensities were corrected for background and for isotopic abundance. A total of 4–5 analyses were carried out on each sample, except for the kaersut sample, for which two measurements were made.

Results and Discussion

Hydrogen Background

Quartz was mounted on a separate specimen holder; for this reason, and owing to the duration of various de-gassing treatments, a daily check of the background level was not possible. The background estimation refers to 2–3 d within each analytical session. The value of b for quartz was obtained with an analysis performed after preliminary heating for 1 d and de-gassing for 12 h in the SC; such de-gassing conditions will be referred to hereafter as 'normal'. These treatments allow a low and stable background to be achieved: the b values determined were 0.011 in the first analytical session, 0.009 in the second and 0.019 in the third; the standard deviation of b was ± 0.002–0.003. The within-day reproducibility of b, corresponding to 10–20% relative (1σ), was higher than expected from counting statistics (<1% for quartz). This might be due to small variations in the stability of the instrument both during analysis (for instance, primary beam wander, which contributes to the background from the edge of the crater) and between analyses (a slight variation in the focusing conditions of the primary beam can result in variations in primary beam density on the sample surface).

In the absence of well characterized anhydrous silicates, three samples were used to define upper limits for the background in silicate matrices. Two garnets (andradite and pyrope) and a synthetic rhyolite, with an unknown hydrogen content, but expected to be anhydrous, were analysed and their over-all H^+ signal was assumed, pessimistically, to be due to the background. The values of b obtained under normal de-gassing conditions were similar (within $\pm 20\%$) to those for quartz and showed that the background level for anhydrous silicate samples is of the same order or lower than for quartz. The value for the background for quartz was equivalent to ≈ 0.007–0.014% H_2O (depending on the analytical session), as calculated using the H-ion yield for rhyolites (see below). As the sensitivity (4×10^4–10×10^4 ions counted per second per 1% of H_2O under the present conditions) is sufficiently high, detection limits (defined as 6σ of the background) can be estimated from the within-session reproducibility to be $\approx 0.015\%$ H_2O.

The dependence of the hydrogen background, under normal de-gassing conditions, on several analytical parameters was also tested in order to control the sources of the background itself more effectively under the operational conditions used and to design a specific procedure for the determination of low hydrogen contents.

In samples with a low hydrogen content, an intense hydrogen peak (up to 10^5 counts s^{-1} compared with 1×10^3–2×10^3 counts s^{-1} for quartz under steady-state conditions) is observed at the start of sputtering. As reported above, this part of the analytical run is rejected for quantification purposes. However, as the primary beam density is higher in the centre of the beam and decreases at the edges, the outermost part of the crater is eroded at a slower rate than the centre under micro-beam conditions. Ions sputtered from this part of the sample surface are collected during analysis, as the secondary-ion imaged field is larger than the primary beam spot. The contribution of the edge of the crater was therefore considered. Analysis was carried out on quartz using the second field-aperture (750 μm diameter), resulting in a nominal imaged field of ≈10 μm. In fact, a reduction of the H^+/Si^+ ratio in the range 30–60% relative was observed. The use of such a method can be considered for the analysis of samples with very low H_2O contents if the samples are mounted very closely on the same specimen holder. However, accurate day-to-day re-positioning of the field aperture relative to the primary ion beam is cumbersome and the background reproducibility is not improved.

Sisson and Layne[19] rastered (70×70 μm^2) the primary ion beam on the area to be analysed in order to remove surface contamination. In the present work, the effectiveness of this procedure in reducing the hydrogen background was tested by analysis after a preliminary 2 min raster (50×50 μm^2) of several samples (quartz, pyrope, synthetic rhyolite and MH1 amphibole). The H^+/Si^+ ratios were compared with those obtained immediately afterwards, but without the raster cleaning procedure. In most instances the two values coincided; furthermore, increasing the duration of the raster cleaning procedure to 10 min did not result in any reduction of the hydrogen signal. In the third analytical session a lower background value was obtained for quartz and for synthetic rhyolite (≈0.013% as H_2O), but not for pyrope (≈0.021% as H_2O). Thus, the effect of the preliminary raster is not systematic and it is significant only in the session with the higher background; therefore, it was not considered worthwhile to use it in the proposed procedure.

Coating the sample surface with gold before and after heat treatment did not result in any significant variation in the H^+/Si^+ intensity ratio under steady-state sputtering conditions.

The importance of the proposed procedure is that it allows the background to be routinely determined from reference samples that are placed on separate mounts; it is then possible to analyse, in particular, minerals on thin section of rock, thus preserving the petrological context and the mutual spatial relationships among phases. However, for accurate determination of low hydrogen concentrations it is recommended that reference samples for background evaluation and unknown

samples are mounted together and that the analysis is performed within a short period of time. This would allow a higher measurement reproducibility to be achieved. Heat treatments at temperatures >50 °C could be potentially useful in reducing the duration of de-gassing in the SC, and, therefore, in increasing the sample throughput.

Hydrogen Ion Yield and Matrix Effects

The average values and standard deviations of the relative-to-Si ion yield of hydrogen determined in standard samples are given in Table 1. Only measurements obtained under normal de-gassing conditions were used. The background correction, roughly equivalent to 0.01–0.02% H_2O, was almost negligible for most samples, as the standard with the lowest concentration of H_2O (CY82-29-1V) contains 0.09% H_2O, and the correction is, therefore, about 10–20% relative (depending on the analytical session). For ME 35D (with 5.11% H_2O), analyses carried out over a period of 1 d showed a slightly lower scatter than that reported in Table 1. For most samples, analyses were carried out within a particular session; hence, the standard deviations reported in Table 1 give the within-session reproducibility, which was 3% (1σ) relative on average. Repeated analyses over a 3 month period gave consistent results, but a statistical evaluation was not possible owing to the small number of analyses carried out.

The most obvious result is that rhyolites show an ion yield systematically greater than that of any other matrix. Rhyolite ion-yield values lie in the range 0.188–0.209 and do not overlap with those for the remaining samples, *viz.*, 0.113–0.141. The most discriminating features between rhyolites and the other matrices are their high silica and low Fe contents. Matrix effects related to structure can be excluded as glassy basalts did not show any enhanced hydrogen ionization; in fact, Yurimoto *et al.*[7] did not find any difference in the yield of high-energy H ions from crystalline and glassy quartz. Previous investigations of matrix effects on the ionization of hydrogen, carried out using low-energy ions,[1–3] showed that the H^+ yield, either absolute or normalized to Si^+ (or to O^+), is higher in low-silica samples, with a 3-fold variation between basalt and rhyolite.[1] In contrast, we observed the opposite behaviour when looking at high-energy secondary ions: the relative-to-Si ion yield in basalt is ≈30% lower than in rhyolite (and ≈40% for the absolute yield; not reported). This finding is in agreement with the results of Hervig and Williams,[4] who found that the high-energy absolute H ion yield in basalt was ≈30% lower than in rhyolites. It is interesting that a similar behaviour was found for Li,[9] the ion yield of which at low energies correlates inversely both with that at high energies and with the Si content in the matrix. Hence, the use of high-energy ions not only effectively removes most of the hydrogen background,[4] but also significantly reduces matrix-related discrimination of the relative ion yield.

As the Si and Fe contents in the samples studied here show an approximate inverse correlation, their effect on the ionization of hydrogen could not be separated; to a first approximation, it was assumed that matrix effects are related to Si. The set of samples was sub-grouped for quantitative purposes into 'low-silica' samples (27–51% SiO_2) and rhyolites (≈72% SiO_2), the latter being the only samples representative of 'high-silica' samples. Relative-to-Si ion yields were averaged over the two groups and were 0.131 ± 0.009 (1σ) for low-silica samples and 0.201 ± 0.011 for rhyolites. As regards the first group, the results for MH17 amphibole deviate by 14% from the mean value, whereas the results for the other samples lie within ±8% of the mean value.

In previous work,[8] where a 50 nA, 100 × 100 μm² rastered primary beam and no heat treatment of the sample was adopted, it was impossible to discriminate between the two groups because of the poor reproducibility of the measurements: *viz.*, ± 15 and ±20% relative for within- and between-day data, respectively. Therefore, a unique working curve was constructed for all the samples. If a unique ion yield, intermediate between the low silica and the 'rhyolite' ion yields, is also assumed for the results obtained here, the error related to matrix effects for the two groups would be ±21%. The improved short- and long-term reproducibility is probably due to better control of the vacuum conditions and to the sample treatment procedures adopted.

The working curve for low-silica samples was applied to some control samples; the results are reported in Table 2.

The kaersut sample is similar to other amphiboles investigated as far as silica and H_2O contents are concerned, but it was mounted differently. For this analysis it was necessary to use a different specimen holder for which the sample surface was a little closer (some 0.3 mm) to the extraction electrode; it is therefore suitable for testing discrimination due to the positioning of the sample relative to the extraction electrode. The H_2O value determined by SIMS coincides with the reference value within the uncertainty of measurement, *viz.*, 0.02% (1σ) H_2O.

DH amphibole is characterized by a low H_2O content (0.24%). This sample was chosen in order to test the validity of the proposed procedure at low H_2O contents within the range of the working curve; the ion probe result agrees with the reference value to within 2 standard deviations.

MH1 and topaz have H_2O contents beyond the range covered by the working curve. Runs carried out under normal de-gassing conditions gave, after background correction, values of 0.035 ± 0.006 (1σ)% for MH1 and 0.045 ± 0.004 (1σ)% for topaz.

The accuracy of the working curve for low-silica (and Fe-bearing) matrices, with the background determined on anhydrous samples, can therefore be estimated to be 15% for >≈0.1% H_2O and 30% at ≈0.05% H_2O.

The authors are indebted to R. L. Hervig, M. Chaussidon and F. C. H. Hawthorne for their generosity in providing standards, without which this work would not have been possible. In particular we thank R. L. Hervig for providing suggestions about hydrogen analysis, and F. C. H. Hawthorne for his constructive criticism of the manuscript. The paper benefited from the advice and encouragement given to us by N. Shimizu to follow up our studies. Finally, M. Palenzona is thanked for technical support and for maintaining the microprobe in good working order.

References

1 Delaney, J. R., and Karsten, J. L., *Earth Planet. Sci. Lett.*, 1981, **52**, 191.
2 Jones, A. P., and Smith, J. V., *Neues Jahrb. Mineral., Monatsh.*, 1984, **1984**, 228.
3 Steele, I. M., *Neues Jahrb. Mineral., Monatsh.*, 1986, **1986**, 193.
4 Hervig, R. L., and Williams, P., in *Secondary Ion Mass Spectrometry, SIMS VI*, ed. Benninghoven, A., Huber, A., and Werner, H. W., Wiley, Chichester, 1988, pp. 961–964.
5 Wittmaack, K., *Phys. Rev. Lett.*, 1979, **43**, 872.
6 Williams, P., *Phys. Rev. B*, 1981, **23**, 6187.
7 Yurimoto, H., Kurosawa, M., and Sueno, S., *Geochim. Cosmochim. Acta*, 1989, **53**, 751.
8 Ottolini, L., Bottazzi, P., and Zanetti, A., in *Secondary Ion Mass Spectrometry*, ed. Benninghoven, A., Nihei, Y., Shimizu, R., and Werner, H. W., *SIMS IX*, Wiley, Chichester, 1994, pp. 191–194.
9 Ottolini, L., Bottazzi, P., and Vannucci, R., *Anal. Chem.*, 1993, **65**, 1960.

10 Bottazzi, P., Ottolini, L., Vannucci, R., and Zanetti, A., in *Secondary Ion Mass Spectrometry*, ed. Benninghoven, A., Nihei, Y., Shimizu, R., Werner, H. W., *SIMS IX*, Wiley, Chichester, 1994, pp. 927–930.
11 Lepareur, M., *Rev. Tech. Thomson-CSF*, 1980, **12**, 225.
12 Holdaway, M. J., Dutrow, B. L., Borthwick, J., Shore, P., and Harmon, R. S., *Am. Miner.*, 1986, **71**, 1135.
13 Hawthorne, F. C. H., personal communication.
14 Vry, J. K., Brown, P. E., and Valley, J. W., *Am. Miner.*, 1990, **75**, 71.
15 Chaussidon, M., personal communication.
16 Hervig, R. L., personal communication.
17 Pichavant, M., Herrera, J. V., Boulmier, S., Briqueu, L., Joron, J.-L., Juteau, M., Marin, L., Michard, A., Sheppard, S. M. F., Treuil, M., and Vernet, M., in *Magmatic Processes: Physicochemical Principles*, ed. Mysen, B. O., The Geochemical Society, Special Publication, 1987, vol. 1, pp. 359–373.
18 Barton, M. D., Haselton, H. T., Jr., Hemingway, B. S., Kleppa, O. J., and Robie, R. A., *Am. Miner.*, 1982, **67**, 350.
19 Sisson, T. W., and Layne, G. D., *Earth Planet. Sci. Lett.*, 1993, **117**, 619.
20 Deloule, E., Albarède, F., and Allé, P., in *Secondary Ion Mass Spectrometry, SIMS VIII*, ed. Benninghoven, A. Janssen, K. T. F., Tümpner, J., and Werner, H. W., Wiley, Chichester, 1992, pp. 69–72.
21 Deloule, E., Chaussidon, M., and Allé, P., *Chem. Geol.*, 1992, **101**, 187.

Paper 4/05896H
Received September 27, 1994
Accepted January 3, 1995

Ion Probe Measurements of National Institute of Standards and Technology Standard Reference Material SRM 610 Glass, Trace Elements*

R. W. Hinton and B. Harte

Department of Geology and Geophysics, University of Edinburgh, West Mains Road, Edinburgh, UK EH9 3JW

G. Witt-Eickschen

Mineralogisch-Petrographisches Institüt der Universität Köln, Köln, Germany

Ion microprobe measurements have been made of 22 trace elements in the National Institute of Standards and Technology (NIST) glass standard, standard reference material SRM 610; this silicate glass standard nominally contains 500 ppm of 61 trace elements. Computer-controlled point-by-point analyses across 1 mm of a single glass fragment indicates that SRM 610 is homogeneous on a very small scale and that it can be used to check microanalytical precisions to at least 0.2%. Although it is not possible to exclude a single small volume differing from the average composition by a few per cent., there is no evidence for heterogeneity (except for F). It is likely that all variations observed in the analyses presented in this work are owing to instrument tuning effects. Variations observed between fragments of the SRM 610 glass obtained from a number of laboratories were essentially identical to those observed on a single fragment. Interlaboratory comparisons using different aliquots of the SRM 610 glasses do not introduce errors greater than 1%. SRM 610 can be considered homogeneous on the 10 μm–1 cm scale.

Keywords: Ion probe; standard reference material; NIST SRM 610 glass; homogeneity

Introduction

Unlike X-ray probe techniques secondary-ion mass spectrometry (SIMS) has no well-defined physical model to permit a direct conversion of measured secondary-ion signal to absolute concentration. Quantification is only possible by the direct comparison of secondary-ion intensities measured on a standard with those measured on the 'unknown' material. However, the major element composition of the substrate can influence not only the absolute number of ions formed but also the differences in ionization between elements. Thus, quantification ideally requires standards of known trace element chemistry with a major element composition similar to that of the unknown under investigation. However, apart from the very large number of standards required, natural mineral standards analysed by bulk techniques often have only partial element coverage and may be flawed because of zoning, alteration or inclusions. Although it has been shown that where glass standards and minerals have closely matched major element chemistry the ion yields are similar,[1,2] glass standards may also be inhomogeneous or poorly characterized. It has been shown that ion yields do follow predictable trends[1] and therefore the combination of a single glass standard, with full element coverage coupled with a mineral standard with only partial element coverage, might be one method for improving the accuracy of trace element data.

The Standard Reference Material SRM 600 series of glasses were manufactured by the National Bureau of Standards (now National Institute of Standards and Technology, NIST) with considerable care to have a constant concentration of 61 trace elements (at levels of 500, 50 and 1 ppm). These standards were designed for bulk analysis and no claims were made for the homogeneity over a small scale for all elements. However, initial analyses[1] indicated tht this standard was reasonably uniform. Although the concentrations have not been certified for many elements, analyses of the 50 ppm SRM 612/3 standard indicates that trace elements were doped at a constant level. The average for certified values for both SRM 610 and 612 glasses are close to the certified concentrations of the two elements that have been studied in the greatest detail, U and Th. The U and Th contents are therefore probably the best guide to the concentration of the trace elements that have not been determined (with the exception of the particularly volatile elements). The SRM 610 500 ppm standard has been used routinely in the ion microprobe laboratory at the University of Edinburgh as an internal standard and comparisons have been made between this glass and natural standards. This standard is now being used for a number of microanalytical techniques; improved knowledge of the homogeneity of these glasses on a small scale is therefore becoming increasingly more important. After a few unpublished reports of inhomogeneities for this material it was decided to make further checks on the homogeneity of the SRM 610 glass standard over the 10 μm to 2–3 mm scale and also to investigate if there were any differences between fragments of wafers acquired from 5 ion microprobe laboratories.

Analytical Technique

Ion microprobe measurements were made, using a Cameca ims-4f (Courbevoie Cedex, France), on fragments broken off 5 different SRM 610 glass wafers. The glass fragments were mounted in Araldite, polished optically flat and finally gold-coated. A 15 keV ^{16}O-primary beam was used to sputter a pit of approximately 10–15 μm diameter, ^{16}O-primary beam currents range 4.5–5.5 nA. All measurements described here were made at low mass resolution using the energy filtering technique to reduce molecular interferences (as described by Zinner and Crozaz[3] and Hinton[1]). Positive secondary ions in the energy range 55–95 eV were measured, the absolute

* Presented at Geoanalysis 94: An International Symposium on the Analysis of Geological and Environmental Materials, Ambleside, England, September 18–22, 1994.

positioning of the energy window was checked at frequent intervals, usually at the end of the analysis. Measured secondary ion count-rates were dead-time corrected but as only trace elements and minor isotopes of the major elements were recorded, corrections were less than 0.3%. The individual peaks measured (in order of increasing mass) were: ^{7}Li, ^{11}B, ^{16}O, ^{19}F, ^{30}Si, ^{26}Mg, ^{42}Ca, ^{47}Ti, ^{85}Rb, ^{88}Sr, ^{89}Y, ^{90}Zr, ^{93}Nb, ^{98}Mo, background 130.5, ^{133}Cs, ^{138}Ba, ^{139}La, ^{140}Ce, ^{143}Nd, ^{149}Sm, ^{165}Ho, ^{208}Pb, ^{232}Th and ^{238}U. Corrections were made for the overlap of SmO on Ho. Where the point analysed was changed by moving the sample stage under computer control all the masses noted above were measured only once at each point. Where the points analysed were chosen by manually moving the sample, all 26 masses were measured 5 times (cycles) at each point. The secondary-ion count rate for the isotope of each element was normalized to that of ^{30}Si (the Si concentration is assumed to be constant at all points analysed). The normalization to Si reduces the effects of changes in secondary-ion count rate; these are principally owing to changes in the primary beam current. Clearly the degree to which homogeneity can be assessed is dependent on the precision of the individual point analyses. It will be shown that observed variations in Si-normalized secondary-ion count rates are probably related to small changes in analytical conditions rather than any changes in trace element concentrations between points analysed. Absolute variations from standard to standard were therefore portrayed as changes in apparent ion yields, relative to Si, rather than changes in trace element concentrations. Ion yields relative to Si were calculated from the Si-normalized count rates using certified abundance's or the nominal 500 ppm values (see Table 1 and Hinton[1] for concentrations used).

Variations of Single Glass Fragment

Measurements were made of 22 trace elements and 2 major elements (Ca and O) on a single chip of SRM 610 glass (origin: Lancaster University). The sample was moved under computer control beneath the primary beam in 50 μm steps. Twenty-one points were analysed sequentially, the first analysis was discarded as the conditions for this analysis differed slightly from the others (longer pre-sputter time). This created a line of analysis points 1 mm long. For each point of analysis, the primary beam sputtered the sample for 1 min prior to a single measurement of the secondary-ion intensities of 26 masses in order of increasing mass. Each peak was measured for 5 s. Standard deviations of the 20 points were calculated as percentages of the mean ion yield (*i.e.*, as a percentage relative standard derivatives) and are given in Table 1 and Fig. 1. All standard deviations quoted in this paper are 1 σ (unless otherwise stated) and are those observed for each single point measurement. Also given in Table 1 is the expected standard deviation based on Poisson counting statistics (again expressed as a percentage of the mean value) and the extremes of the measured ion yields. The primary beam current was very stable over the period of this analysis (approximately 90 min for 21 analysis points) and there was virtually no difference between the standard deviation of the absolute count rates measured for each isotope at all 20 points and that of the calculated ion yields normalized to Si (on average Si normalization only improved the standard deviation by 0.05%).

It is clear from Table 1 and Fig. 1 that the variations observed across 1 mm of a single fragment of SRM 610 glass are very close to those expected from Poisson counting statistics. On average, the standard deviation was only 0.1% higher than that expected from Poisson counting statistics (F and Pb were excluded from this comparison due to their large counting errors). As such, no heterogeneity can be demonstrated. The standard deviation for Pb appears somewhat smaller than that calculated, but this is not unexpected given that there will be a variation in the standard deviation itself. Even if the extreme range of the individual measurements are considered, for all 22 trace elements measured, no measured value exceeds 2σ (calculated) by more than 1%. The close correspondence between measured and calculated standard deviations suggests that the concentrations of the elements measured are sufficiently homogeneous that multiple analyses

Table 1 Relative standard deviation and mean ion yield of 20 point analyses of SRM 610 glass

Element	s_r* Measured (%)	s_r* Expected (%)	Ion yield relative to Si	Minimum	Maximum	Concentration (ppm)
Li	0.41	0.26	1.216	1.205	1.231	500
B	0.75	0.57	0.560	0.551	0.565	351
O	0.32	0.25	0.0029	0.0029	0.0030	49.4%
F	4.77	5.00	0.0070	0.0062	0.0075	500
Mg	1.36	1.03	1.887	1.838	1.928	500
Ca	0.31	0.34	3.214	3.197	3.234	8.36%
Ti	2.02	1.59	2.652	2.559	2.760	437
Rb	1.26	1.15	0.945	0.925	0.966	426
Sr	0.81	0.60	2.654	2.626	2.703	516
Y	0.64	0.56	3.185	3.154	3.220	411
Zr	1.13	0.89	2.010	1.974	2.058	500
Nb	0.55	0.83	1.221	1.209	1.239	500
Mo	2.23	2.17	0.758	0.730	0.784	500
Cs	1.69	1.45	0.565	0.542	0.580	500
Ba	1.09	1.00	1.737	1.699	1.786	500
La	0.95	0.80	1.903	1.871	1.939	514
Ce	0.82	0.86	1.837	1.811	1.864	524
Pr	0.79	0.79	2.069	2.029	2.099	500
Nd	2.14	2.24	2.093	2.033	2.181	505
Sm	2.36	2.03	2.357	2.278	2.462	500
Ho	0.91	0.84	2.080	2.053	2.115	500
Pb	7.6	10.0	0.041	0.035	0.048	426
Th	1.77	1.48	1.045	0.999	1.079	457
U	1.18	1.51	1.021	0.988	1.044	461

* Relative standard deviation, s_r (%) = 100 × (s/mean ion yield).

of a single fragment of SRM 610 can be used to check the performance of any microsampling trace element technique on a scale of 10 μm to 1 mm. Given a reasonable number of repeat measurements, the inhomogeneity in the standard should introduce an error of less than 0.2% in point-to-point standard deviation calculated. This is probably an overestimate of the variability given that small changes in the primary ion current will increase variability in the ratio of individual elements relative to the ^{30}Si reference mass. While the minima and maxima in the ion yields shown in Table 1 could reflect the extreme variations in trace element concentrations this could only occur in a few instances before a significant increase in the standard deviation of the population was observed.

Variations Between Different Glass Samples

Where point analyses are made of minerals and glasses widely distributed about a 2.54 cm (1 inch diameter) thin/thick section changes in surface topography necessitate that some manual tuning of the instrument is required. Therefore, a number of point analyses were made on a single glass fragment to establish first the precision with which element ratios can be made when the sample is moved manually and the instrumental conditions manually 'optimized' for each point of analysis. Similar point analyses were then made on fragments of the glass standard obtained from 5 different laboratories in order to establish the homogeneity between different wafers of the same standard. In all, over 50 repeat point analyses of SRM 610 glasses were made in 8 sessions over 3 d. For each session (of between 3 and 10 point analysed) changes to instrument tuning and primary beam focus were kept to a minimum. For each point analysed the surface was sputtered for 3 min prior to the start of the measurement cycle in order to remove the gold coat and permit the secondary-ion signal to stabilize. During this time the magnetic field setting was determined for each isotope measured. As with the computer-controlled point-by-point analyses, the secondary ion intensities of 22 trace and 2 major elements were measured in order of increasing mass. However, in this case 5 cycles of the 26 individual masses were made for each point analysed; for each measurement cycle the secondary-ion intensities were normalized to ^{30}Si. In a single point analysis the internal/within run (cycle to cycle) standard deviation is assumed to be close to that expected from Poisson counting statistics. This is routinely observed in ion microprobe measurements when the primary beam current is stable and is more readily demonstrated when the count rates are high.[4]

Single Fragment/Analytical Reproducibility

Point analyses were made on a single glass fragment in five analytical sessions (3, 10, 6, 7 and 3 points analysed). The

Table 2 Measured variations in SRM 610 glass

	s_r* (Single analyses)			Extremes (as percentage of mean for each session) 51 analyses	
	Single source (%)	Different source (%)	Poisson statistics (%)	Maximum (%)	Minimum (%)
	1	2	3	4	5
Li	1.11	1.16	0.11	2.8	−2.9
B	0.82	1.14	0.25	1.8	−2.9
O	0.82	1.05	0.10	2.5	−2.2
F	5.97	7.36	2.80	11	−16
Mg	0.70	0.55	0.46	1.5	−1.4
Ca	0.61	0.34	0.14	1.0	−1.9
Ti	0.76	0.79	0.71	1.7	−2.0
Rb	1.29	0.85	0.53	2.1	−2.9
Sr	1.09	0.78	0.26	1.4	−2.2
Y	1.05	0.95	0.25	2.8	−1.9
Zr	0.96	1.01	0.40	3.0	−1.7
Nb	0.96	1.06	0.37	2.2	−2.1
Mo	1.56	1.52	0.95	3.7	−3.4
Cs	1.22	1.56	0.66	2.6	−3.8
Ba	1.12	1.15	0.45	2.1	−2.4
La	1.10	1.01	0.36	1.6	−2.8
Ce	1.15	1.39	0.38	2.3	−3.1
Pr	1.12	1.06	0.35	1.5	−2.5
Nd	1.36	1.52	1.01	2.8	−3.0
Sm	1.41	1.56	0.90	3.0	−4.4
Ho	1.14	1.18	0.38	2.0	−2.3
Pb	3.67	4.80	3.80	8.5	−8.7
Th	1.92	1.73	0.67	3.7	−4.3
U	2.05	1.64	0.68	3.1	−5.5

* Relative standard deviation s_r (%) = 100 × (s/mean ion yield).

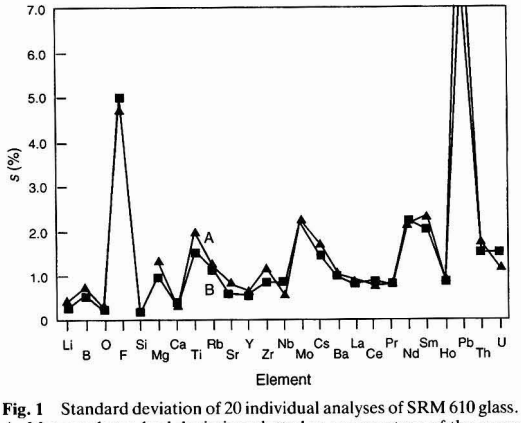

Fig. 1 Standard deviation of 20 individual analyses of SRM 610 glass. A, Measured standard deviation plotted as a percentage of the mean (Si normalized) ion yield and B, standard deviation calculated from Poisson counting statistics, including the error on both the element and Si.

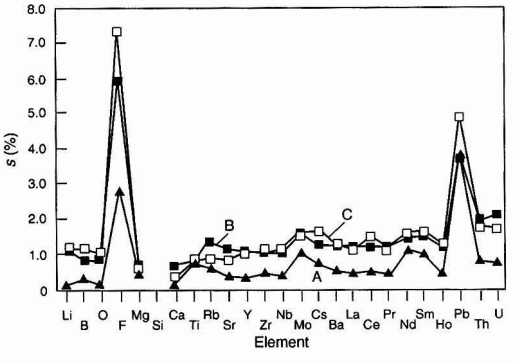

Fig. 2 Average standard deviation for each individual analysis of SRM 610 glass plotted as a percentage of the mean (Si normalized) ion yield. A, Poisson Counting Statistics B, standard deviations calculated from 5 analyses of the Chicago SRM 610 fragment, comprising 3, 10, 6, 7 and 3 repeat measurements; and C, average standard deviation for individual analyses calculated from 3 sessions of 6, 7 and 9 analyses of glass fragments from 5 different laboratories (plus one unknown).

distance between one analysis and the next varied between 50 μm and 2 mm. Primary beam position and focus, and secondary-ion tuning were checked at each point analysed. The standard deviation of each element was determined for each session (3 or more points analysed). As the standard deviation is itself subject to variation, the standard deviations calculated for the 5 individual sessions were averaged to give a more precise measure of the analytical errors ('Single source' standard deviation Table 2, column 1). The over-all homogeneity was assessed by determining, for every point analysed, the difference in the ion yield of each element from the average ion yield for the whole session. This permitted any extreme values (minima and maxima, Table 2, columns 4 and 5) to reflect potential variability in the standard rather than instrument tuning effects.

While the standard deviations predicted from Poisson counting statistics are considerably improved by recording each isotope 5 times at each point analysed, on average the observed standard deviation of the populations were 0.7% higher than that predicted (Table 2, columns 1 and 3 and Fig. 2). Indeed, the observed variations were only similar to, and in some instances larger than, those observed for the computer-controlled point-by-point analyses on a single sample (Table 1) despite the fact that 5 times more counts were recorded for each element. One possible explanation is that manual changes to instrument tuning causes small differences in the energy and the angular distribution of the secondary ions measured. Small changes in the primary beam focus (and hence the beam density) may also change the amount of oxygen implanted into the volume of the matrix analysed. As the oxygen concentration has a strong influence on the degree of ionization,[5] and any change in ionization may not be the same for all elements, variations in the beam density could potentially change the element ratios measured. In these analyses the heaviest masses appear to have the largest standard deviations, reinforcing the possibility that the variability is related to instrument effects rather than sample heterogeneity. As the computer-controlled point-by-point analyses have demonstrated that heterogeneity in a single glass fragment will decrease the precision of the analysis by less than 0.2%, it appears that manual changes to instrument tuning decreases the accuracy of element ratio measurements such that the measured precision is 0.6–1.0% (increasing with mass) in excess of that expected by counting statistics.

SRM 610 From Different Laboratories

Five fragments of SRM 610 from different sources were mounted together in a single sample mount. The samples were from the Universities of Lancaster, Cambridge, Chicago, Manchester and Karlsruhe. Also included was an unidentified fragment from one of these 5 samples. Analyses were made, in three sessions (6, 7 and 9 point analyses), in an identical manner to those given for the single fragment (above). The only difference between the two sets of analyses was that the analysis sites could be up to 2 cm apart on the polished mount rather than all within 2 mm. Again instrumental conditions were kept as constant as possible to permit the absolute ion yields to be used to detect any potential variation between individual glasses from different origins. At least one measurement was made of each different sample of SRM 610 in each session. The standard deviations were calculated assuming that the glasses from each session are all from the sample population.

The standard deviations calculated for the repeat analyses of the different glasses (given as 'Different source', Table 2, Column 2 and Fig. 2) were virtually identical to those observed for measurements on a single fragment (*i.e.*, 0.7% greater than counting statistics would predict). If the absolute differences in the average ion yields for the 5 glasses are considered (Table 3, Fig. 3) virtually all trace elements fall within the ±1% band. The ion yields for the Lancaster University fragment would appear to be significantly different from the mean of all fragments. The mean ion yields for elements heavier than Rb in the Lancaster University fragment was about 0.5–1.0% higher than the mean of all the

Table 3 NBS/NIST SRM 610 on yields relative to Si (average of 3 sessions)

	Ion yield relative to Si						
	Chicago 1	Lancaster 2	Manchester 3	Cambridge 4	Karlsruhe 5	Unknown 6	Average 1–6
Li	1.272	1.272	1.277	1.279	1.296	1.279	1.279
B	0.564	0.559	0.558	0.567	0.570	0.559	0.563
O	0.0031	0.0030	0.0031	0.0031	0.0031	0.0031	0.0031
F	0.0041	0.0040	0.0033	0.0040	0.0040	0.0038	0.0039
Mg	1.908	1.907	1.914	1.913	1.918	1.920	1.913
Si	1.000	1.000	1.000	1.000	1.000	1.000	1.000
Ca	3.424	3.421	3.424	3.419	3.419	3.419	3.421
Ti	2.763	2.775	2.779	2.725	2.755	2.756	2.759
Rb	0.970	0.980	0.960	0.974	0.969	0.970	0.970
Sr	2.864	2.876	2.864	2.858	2.852	2.855	2.862
Y	3.418	3.445	3.427	3.419	3.448	3.422	3.430
Zr	2.141	2.156	2.150	2.146	2.168	2.148	2.152
Nb	1.317	1.336	1.317	1.322	1.323	1.322	1.323
Mo	0.835	0.852	0.835	0.846	0.842	0.838	0.841
Cs	0.609	0.615	0.597	0.609	0.609	0.608	0.608
Ba	1.884	1.905	1.888	1.888	1.872	1.893	1.888
La	2.079	2.092	2.074	2.079	2.074	2.087	2.081
Ce	2.024	2.043	2.022	2.012	2.005	2.020	2.021
Pr	2.273	2.286	2.267	2.268	2.260	2.270	2.271
Nd	2.263	2.326	2.266	2.248	2.280	2.276	2.277
Sm	2.599	2.642	2.612	2.603	2.607	2.618	2.614
Ho	2.291	2.327	2.306	2.292	2.299	2.313	2.305
Pb	0.048	0.050	0.047	0.050	0.050	0.051	0.049
Th	1.174	1.193	1.176	1.180	1.175	1.183	1.180
U	1.168	1.185	1.174	1.172	1.172	1.176	1.175

glasses. In contrast, the elements lighter than Si are 0.5–1.0% lower. Similar, mass-related changes can be generated by changing the beam density (beam focus) and are almost certainly due to instrumental/matrix effects (see above) and probably are not an indication of sample heterogeneity. Only F varies significantly from sample to sample and this element does not appear to be homogeneous. Provided a reasonable number of repeats of the SRM 610 glass are made (≥ 3) and the sampled area is greater than 10 μm, less than 1% of any measured variation can be attributed to variability of the SRM 610 standard glass.

If all the individual point analyses are compared to the mean of each session (51 repeats in 8 sessions normalized to the mean of each session, including sessions with the 5 different glass samples) then the total spread of element ion yields is less than ±3% (Fig. 4), *i.e.*, no single analysis point is more than 3% different than the mean of 3 or more points measured at the same time. The extreme values tend to increase with increasing mass; again this is likely to be an analytical effect related to changes in the primary beam density or secondary-ion energy recorded. As such extremes in the individual point analyses are to be expected if the analytical precision of the population is limited to 0.7–0.8% (1σ), there is no evidence that any inhomogeneity exists on scales of 10 μm to >2 cm for any element (other than F).

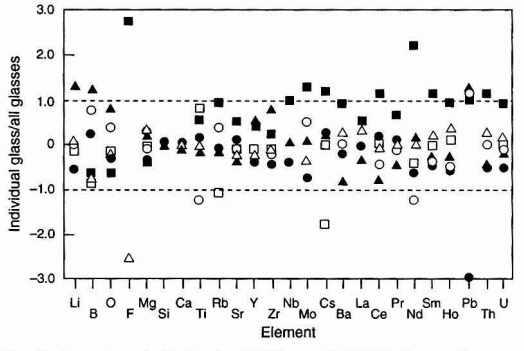

Fig. 3 Mean ion yields for the 5 different SRM 610 glasses plus one unknown (from 3 sessions) calculated as a percentage of the over-all mean ion yield for all glasses (see Table 3, column 7): ●, Chicago; □, Manchester; ■, Lancaster; ○, Cambridge; ▲, Karlsrue; and △, unknown.

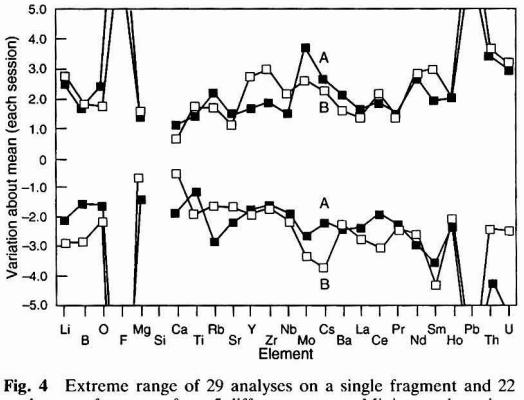

Fig. 4 Extreme range of 29 analyses on a single fragment and 22 analyses on fragments from 5 different sources. Minima and maxima for SRM 610 are calculated relative to the mean ion yield for each element for each session. A, Single and B, different source.

Sample Change

Three repeat measurements of SRM 610 were made after a sample change to gauge whether potentially more extreme changes in tuning and sample height had any major effect on the measured element ratios. The mean of three analyses made after the sample change agreed with the previous measurements to within 1.3%. The largest differences were for the heaviest and lightest elements, U and Li, and can therefore be attributed to instrument effects rather than sample variability. Fluorine was the only element that was different at the 2σ level. This is similar to observed differences between all unknowns and the Lancaster University SRM 610 fragment (see above). The major elements O and Ca were within 0.2% of the previous measurements. The over-all effect of removing the sample from the instrument, inserting an 'unknown', subsequent retuning of the primary beam focus and secondary-ion extraction optics, is less than 1% for all but the heaviest elements.

Conclusions

With the exception of F, no significant variations are observed in the microsampling of the SRM 610 glass standard. For the 22 elements analysed variations in the trace element content of the glass on the 50 μm–1 mm scale are unlikely to exceed 1%. A single 10–20 μm analysis of SRM 610 is unlikely to differ by more than 3% from a bulk analysis of any fragment of SRM 610. Repeat analyses suggest that different wafers of SRM 610 differ in trace element content by less than 1%. SRM 610 glass can be considered homogeneous both on a small, as well as a large scale, and can therefore be used to check the reproducibility of microprobe measurements. The measured standard deviation of repeat sampling of micro-volumes of the standard glass over a 1 mm^2 area will be increased by, at most, 0.2% owing to standard inhomogeneity. Although the uncertainty for any variations introduced by sampling volumes over a larger area, or even different wafers, is 0.8%, this higher value probably reflects poorer analytical precision rather than any large scale variability. Analyses of the trace element concentrations of SRM 610 glass are now being made in a number of laboratories. More certified abundance's would permit a more accurate assessment of ion yields of SRM 610 relative to those of mineral standards.

The authors acknowledge Dr. R. Macdonald (Lancaster) Drs. M. Seitz and A. Rochall (Karlsruhe), Dr. I. Lyon (Manchester) and Dr. J. V. P. Long (Cambridge) for providing fragments of SRM 610. The authors also acknowledge NERC Scientific Services and NERC research grants for funding the ion microprobe facility at Edinburgh.

References

1 Hinton, R. W., *Chem. Geol.*, 1990, **83**, 11.
2 Macrae, N., Botazzi, P., Ottolini, L., and Vannucci, R., *Chem. Geol.*, 1993, **103**, 45.
3 Zinner, E., and Crozaz, G., *Int. J. Mass Spectrom. Ion Phys.*, 1986, **69**, 17.
4 Valley, J. W., and Graham, C. M., *Contrib. Mineral. Petrol.*, 1991, **109**, 38.
5 Anderson, C. A., *Int. J. Mass Spectrom. Ion Phys.*, 1970, **3**, 413.

Paper 4/06190J
Received October 11, 1994
Accepted December 16, 1994

High-precision, *In Situ* Oxygen Isotope Ratio Measurements Obtained From Geological and Extra-terrestrial Materials Using an Isolab 54 Ion Microprobe*

John M. Saxton, Ian C. Lyon and Grenville Turner

Department of Earth Sciences, The University of Manchester, Manchester, UK M13 9PL

We have developed an ion probe technique for the *in situ* measurement of oxygen isotope ratios, $^{18}O/^{16}O$ and $^{17}O/^{16}O$, with high spatial resolution in polished thin sections of silicate minerals. This technique allows the isotopic analysis of samples as small as picomoles of material which represents only 10^{-7} of the sample size required by conventional fluorination oxygen isotope measurement methods and thus has wide application to the study of many terrestrial and extra-terrestrial samples that have heterogeneous oxygen isotope compositions on a scale of tens of micrometres. To illustrate the breadth of studies that are made possible by the ion probe, we report here oxygen isotope measurements from an authigenic quartz overgrowth obtained from the Penrith sandstone, UK, and measurements of magnetite grains from the Orgueil and Yamato 82162 carbonaceous chondrites which may be used to constrain possible formation mechanisms of the magnetite.

Keywords: Ion probe; oxygen isotope; high spatial resolution; geological and extra-terrestrial samples.

Introduction

Oxygen isotopes are widely used to address problems in geo- and cosmo-chemistry.[1] They may be used, for example, as tracers to constrain the sources of minerals,[2,3] and fluids[4,5] and for isotope thermometry.[6,7] Conventional oxygen isotope measurement techniques are mainly refinements of a fluorination technique first developed by Clayton and Mayeda[8] and are widely and routinely applied to geological and cosmochemical problems. The technique yields high-precision measurements (±0.1‰) of $^{18}O/^{16}O$ but typically a few milligrams of material are required (corresponding to a cube of material of the order of 1 mm^3) and this limits the spatial resolution at which samples may be studied. Some *in situ* measurements have been made using laser probes, in which silicate minerals are heated by a focused IR laser beam in a bromine pentafluoride atmosphere but a large alteration aureole is formed around the analysed spot (itself typically 100 μm or more in both diameter and depth) and spatial resolution can be as poor as several hundred micrometres.[9,10] Very recent reports[11,12] indicate that the formation of an alteration aureole may be avoided by the use of UV lasers which release oxygen through a photochemical reaction rather than by heating, but large sample sizes are still required.

The major alternative to the laser probe is SIMS in which the sample is bombarded by a focused beam of heavy ions. Atoms and molecules are sputtered from the surface, a small fraction emerging as ions. These ions may be accelerated and focused into a mass spectrometer where the isotopes may be separated and detected by suitable ion detectors.

We have used an Isolab 54 ion microprobe, (VG Isotech, Manchester, UK) to develop techniques for making high spatial resolution *in situ* measurements of $^{18}O/^{16}O$ with an accuracy of 1‰ and $^{17}O/^{16}O$ to 2‰. Although less precise than bulk fluorination techniques, this disadvantage is offset by the advantage of high spatial resolution afforded by the ion probe. We have acquired oxygen isotope analyses from a volume with a diameter of 10 μm and depth of 2–3 μm which represents approximately 3 pmol of material, only 10^{-7} of the material required by conventional fluorination techniques. Oxygen isotope analyses have previously been acquired using ion probes, but typically only on conducting samples[13,14] although progress has also recently been reported in making *in situ* measurements on insulating materials.[15–17] The ion probe offers us an entirely new window onto the isotope systematics of microscopically heterogeneous samples.

The Isolab 54 Ion Microprobe

Fig. 1 shows a schematic representation of the Isolab 54 ion microprobe illustrating relevant components. Primary ions are produced from a caesium ion gun held at 10 kV, and focused and steered onto the sample by sets of deflector plates and lenses. The sample is held at −8 kV so that negative secondary ions from the surface are accelerated into a second system of ion optics that focuses the secondary ions onto the source slit of a mass spectrometer. Ions transmitted through the source slit are dispersed, first by energy in an electrostatic analyser (ESA) and then by momentum in a magnetic field where they are mass analysed and focused into ion detectors. A slit between the ESA and magnet limits the range of ion energies passed through to the magnet to 22 eV. The trajectory of an ion through the magnet depends on its energy as well as its mass, so an ion beam having a finite energy spread cannot normally be brought to a sharp focus at the detectors. In the Isolab, however, the energy dispersion of the ESA is arranged to be equal and opposite to that of the magnet, an arrangement known as double focusing.[18] A well focused ion beam is essential if high mass resolution is to be achieved. Mass resolution is a measure of the ability of the instrument to separate two nearly isobaric ion beams; it depends on both the ion beam width and the detector slit width and may be defined as $(m/\Delta m)$ where two ion beams of average mass m are just resolved when their mass difference is Δm.

We employ multicollection to measure all three oxygen isotopes simultaneously in different detectors: $^{16}O^-$ ions are measured by a Faraday cup and the $^{17}O^-$ and $^{18}O^-$ beams by a new type of detector, a small channeltron with a conversion

* Presented at Geoanalysis 94: An International Symposium on the Analysis of Geological and Environmental Materials, Ambleside, England, September 18–22, 1994.

dynode (CDS detector)[17] developed by Fison's Instruments. The magnet poles are shaped so that the isotopes are all focused along a plane orthogonal to the beam axis, simplifying the design of the multicollector. Multicollection makes efficient use of the measurement time (desirable in view of the low abundance ^{17}O and ^{18}O), makes the ratio insensitive to slight changes in the primary and secondary ion beam intensities, and overcomes dynamic range problems incurred when trying to measure oxygen isotopes on a single detector (since $^{16}O/^{18}O \approx 500$, $^{16}O/^{17}O \approx 2650$). The CDS detectors are only exposed to low count rates, and have exhibited a high and stable ion-to-pulse conversion efficiency (Lyon *et al.*,[17] see also Fig. 2). Use of these detectors has been essential in obtaining accurate and reproducible results with this instrument. We determined the efficiency of the CDS used for ^{18}O measurement as part of an experiment to measure the dead time of the counting equipment, in which ^{16}O beams of differing intensities were switched between the CDS and a Faraday detector. The efficiency was found to be 100.9 ± 0.6%; the fact this is greater than 100% probably results from uncertainty in the precise absolute resistance of the resistor used to measure the Faraday current for ^{16}O. The efficiency of the CDS used for ^{17}O measurement has not been directly determined. It is therefore not possible to calculate precise absolute isotope ratios. Precise absolute ratios are unnecessary, however, since the observed ratios are calibrated by making measurements of a well characterized standard in addition to the unknown mineral.

Many of the samples we wish to study are silicates, which are electrical insulators. The samples are gold or carbon coated, but we must still use a focused electron beam to charge neutralize the analysed spot, which would otherwise rapidly charge positive (once the coating is sputtered away), through gaining Cs^+ ions and losing secondary electrons and negative ions. Our gun delivers a 7 keV, approximately 1 μA, electron beam into an area a few hundred micrometres in diameter, and with it we obtain stable secondary ion beams. The stability of the secondary ion energy spectrum indicates that the potential of the sputtered spot does not change by more than 1 V with respect to the rest of the sample.

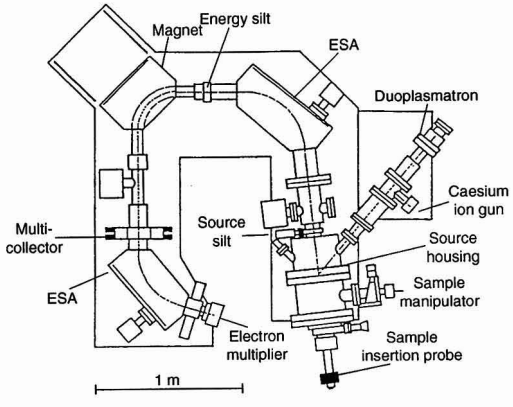

Fig. 1 A schematic view of the Isolab 54 ion microprobe. Primary caesium ions are produced by the caesium ion gun and accelerated into the primary ion column where the ions are focused and steered by a series of lenses and deflector plates. The Cs^+ ions sputter the sample and secondary ions leave the surface to be focused and steered by the secondary ions optics to the source slit of the mass spectrometer. The ions are energy dispersed by an ESA and a fraction of the ions selected by the intermediate energy slit. After passing through the slit the ions are dispersed by momentum in the magnet and focused at the multicollector. The multicollector consists of five Faraday detectors and two miniature CDS electron multipliers. The positions of these detectors in the focal plane (normal to the ion beams) may be adjusted, allowing up to five ion beams to be measured simultaneously.

Experimental Procedures

The measurement of accurate isotope ratios by SIMS is hindered by variable isotopic fractionation which appears as a natural consequence of the secondary ionization process. This fractionation must be carefully controlled, so that the standard and unknown minerals are measured under the same conditions in order to obtain meaningful and accurate results. There are two main causes of this fractionation: the dependence of the ionization probability for each isotope on the matrix chemistry and the large energy spread of the secondary ions. We discuss these effects below.

The variation of the ionization probability for different isotopes with matrix chemistry is commonly referred to as the 'matrix effect'.[19–21] It is observed as a difference between the measured isotopic ratios and the known isotopic composition of the sample. The ionization process may be considered as the breaking of the chemical bonds between the sputtered atom/ion and the target,[22] so that it is expected to be matrix dependent. It is therefore necessary to choose a standard mineral of the same composition as the unknown mineral, or at least to calibrate the matrix effect between the two materials. One mineral we wish to study is olivine, which forms an isomorphous series between forsterite (Mg_2SiO_4) and fayalite (Fe_2SiO_4), and we have observed that the matrix effect depends upon the Mg/Fe ratio. To calibrate the matrix effects for this mineral, we selected several olivine samples whose oxygen isotopic compositions were known from conventional measurements performed by Clayton and coworkers.[23] Initially three olivines were studied: pure forsterite designated 'Allied' and 5 mol% fayalite (Fa_5) designated 'Crestmore' and olivine (Fa_{12}) from the Brenham pallasite meteorite. The Allied and Crestmore samples were provided by Dr. I. Steele and are described by Hervig *et al.*,[19] and, on the basis of their work, and our own repeated measurements on different grains, we believe these olivine standards to be homogeneous. Fig. 3 shows the measured matrix effects for these materials relative to Brenham. We are currently

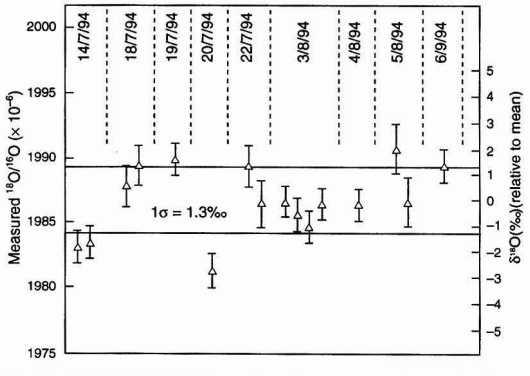

Fig. 2 Measured $\delta^{18}O$ values of spot measurements acquired on a quartz standard (seed quartz, $\delta^{18}O = -4.79‰$) over a period of 8 weeks. The values reported are derived directly from the ion currents measured by the Faraday and CDS detectors [although no correction has been applied for the efficiency (≈99%) of the CDS detector], and the values from each day have not been normalized to values obtained from other days.

studying more olivines to calibrate the matrix effect over a greater range of fayalite compositions.

The large energy spread of the secondary ions causes isotopic fractionation in various ways. First, the ions of different isotopes have slightly different energy spectra (this is both expected theoretically and known from previous experiments; *e.g.*, see, Gnaser and Hutcheon[24]), so that selecting a different portion of the ion energy spectrum will change the isotopic fractionation. We are, therefore, always careful to use the same part of the energy spectrum when comparing the unknown and standard minerals.[17]

Second, the electrostatic ion optical elements of the ion probe are inherently energy dispersive so that each isotope is focused differently onto the mass spectrometer source slit. We term this effect 'chromatic aberration', by analogy with the effect that occurs when white light is focused by a simple lens. When transmission through the source slit is less than 100% (such as occurs when the slit is narrowed to obtain high mass resolution), the isotopes are transmitted unequally, and even slight variations in the shape or position of the focused spot on the source slit (as inevitably occurs whilst retuning the instrument) may change the isotopic fractionation by up to several per mil. We have found an elegant solution to this problem in sweeping the whole beam linearly back and forth across the slit, so that the spatial distribution of each isotope is integrated. The problem and its solution are discussed more fully elsewhere.[17] We have found that a small amount of chromatic aberration remains, apparently related to the vertical distribution of the ion beam, but this is only a problem (a few ‰) if the sample tilt is allowed to vary by large angles (several degrees) and we have developed techniques for ensuring that the sample surface is always kept to within a fraction of a degree of vertical.

The typical reproducibility of measurements of a single standard obtained with our technique has been reported previously[17] and we can here extend this data set to include all $^{18}O/^{16}O$ measurements obtained on a quartz standard over a period of 8 weeks. This standard was known as seed quartz and has $\delta^{18}O_{SMOW} = -4.79‰$, *i.e.*, $1000[(^{18}O/^{16}O_{quartz})/(^{18}O/^{16}O_{SMOW}) - 1] = -4.79$, where SMOW refers to a recognized standard isotopic composition (standard mean ocean water). These data are illustrated in Fig. 2 which shows the $^{18}O/^{16}O$ measurements for different spots obtained from the seed quartz standard over this period of time. The spread in values obtained from the standard has generally been found to be less than 1‰ for measurements obtained during a day whilst conditions remained constant and the value obtained for a particular day was used as the calibration for that day. However, the day-to-day stability of the ratios (1σ = 1.3‰ over 8 weeks) is also quite remarkable when it is considered that the ratios are derived directly from the ion currents measured by the Faraday and CDS detectors and ratios from each day have not been normalized with the values from other days. The scatter arises from counting statistics, any fluctuation in the relative gains of the CDS and the Faraday detector over the 8 week interval, any sample charging, resulting in different parts of the energy spectrum being sampled, any residual chromatic aberration incurred due to the sample tilt changing slightly between loadings (the measurements shown were interspersed with measurements on other samples), and any inhomogeneity in the standard.

The virtual elimination of variable instrumental fractionation effects and the gain in stability of our detectors gave us confidence in applying these techniques to measuring oxygen isotope compositions in geological and extra-terrestrial samples.

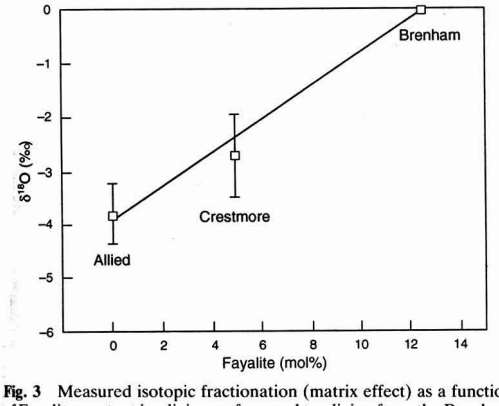

Fig. 3 Measured isotopic fractionation (matrix effect) as a function of Fayalite content in olivines referenced to olivine from the Brenham pallasite (Fa_{12}).

Applications

Authigenic Quartz Overgrowths

Quartz overgrowths are volumetrically the most important diagenetic mineral cement in many sandstone basins worldwide. Authigenic quartz precipitates at temperatures <150 °C from fluids of variable salinity and composition and can commonly amount to more than 20% of bulk sandstone volume, occluding virtually all the available intergranular

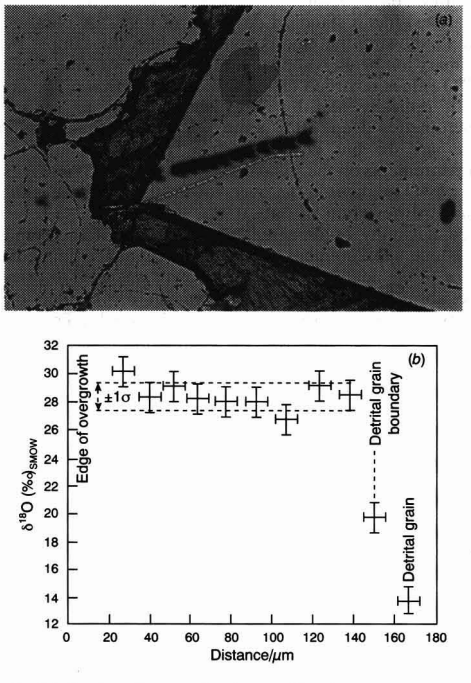

Fig. 4 (*a*) A microphotograph of an authigenic quartz overgrowth from a sandstone, Penrith, UK, showing ion beam induced craters from which quartz was sampled to obtain $\delta^{18}O$ measurements. (*b*) Measured $\delta^{18}O$ values obtained from this sample showing clearly the capability of resolving isotopically distinct sections of a sample with very high spatial resolution. Mean $\delta^{18}O$ on overgrowth = +28.5‰, 1σ = 0.9‰.

porosity.[25,26] Despite the scientific and economic interest in establishing the geological conditions and history necessary to form authigenic quartz overgrowths, the source of the silica and the origin of source fluids which carry the silica remain in most cases essentially unproven.[27–29] Analytical difficulties arise because of the chemical purity of both the authigenic quartz and the detrital grains, and the small scale of the overgrowths (typically 50 μm diameter) which precludes isotopic analysis by conventional methods on individual overgrowths. Some conventional oxygen isotope measurements have been obtained by abrading overgrowths from detrital grains and measuring essentially a bulk composition of many overgrowths. By estimating the percentage of contamination from detrital material, end-member compositions of the authigenic quartz and detrital grains may be estimated,[30] but the process is exceedingly time consuming and cannot resolve any evolution of the $\delta^{18}O$ composition across the overgrowth.

We report here the results of very high spatial resolution $\delta^{18}O$ measurements acquired from an authigenic quartz overgrowth obtained from the Penrith Sandstone (Lower Permian) in the Vale of Eden, Cumbria, UK. A $\delta^{18}O$ profile was obtained by focusing the primary ion beam to a well resolved spot (approximately an 11 × 18 μm ellipse in this case) and moving the sample in steps of 10–15 μm to acquire a series of measurements. The profile was completed when the detrital grain was reached. The profile was normalized to an absolute SMOW value by measuring the $^{18}O/^{16}O$ value of a standard of known isotopic composition (in this case 'seed' quartz: see Fig. 2). Seven analyses of this standard made over the three days (before, after, and the day of, the overgrowth analyses) had a standard deviation of 0.9‰. A photomicrograph showing the craters sputtered into the sample by the primary ion beam is shown in Fig. 4 along with the measured $\delta^{18}O$ values recorded for each spot. Inspection of the craters both optically and by SEM shows them to be several micrometres deep, after about 1 h analysis time. The error bars are 1σ but do not include the uncertainty in the measurements on the standard. Although there is a suggestion of a $\delta^{18}O$ gradient in the overgrowth, the nine values show a standard deviation of only 0.9‰, which is the same as the reproducibility of repeated measurements of the standard. The one measurement of the standard made immediately prior to the analyses of the overgrowth was used to calculate the absolute $\delta^{18}O$ values. The mean $\delta^{18}O$ value of the overgrowth is then found to be +28.5 ± 1.0‰. The error in this value was obtained by combining 0.9‰ (from the reproducibility of the standard measurements) and 0.3‰ (from the combined analyses of the overgrowth) in the quadrature. This value contrasts strongly with the measured value on the detrital grain of +13.5‰ which is characteristic of quartz produced by igneous processes.

Meteoritic Magnetite

Magnetite occurs in many meteorites, in particular in the more oxidized carbonaceous chondrites. The magnetite grains display a variety of distinctive morphologies, for example stacks of platelets (plaquettes), and spherical clusters of tiny grains (framboids).[31,32] Some of these are illustrated in Fig. 5. These meteorites show extensive evidence for aqueous alteration, but the mode of formation of the magnetite is unclear. Kerridge *et al.*[33] suggested that the magnetites formed from an aqueous solution on the meteorite parent body. On the other hand, the extremely old I–Xe age for some magnetite[31] suggests that at least some of the grains may be of nebular origin.

We studied magnetite separates from two CI chondrites, Orgueil and Y-82162, to see if the oxygen isotope systematics could constrain the formation mechanism. The magnetite grains were pressed onto gold foil for analysis. We originally wished to analyse individual grains of different morphologies, but unfortunately, being magnetic, the grains tended to clump together. For Orgueil we therefore analysed several clumps, each consisting of many grains of different morphologies. The Y-82162 grains were rather more dispersed and our analyses are of groups of several grains, although each group still generally contained a mixture of different morphologies. The results are shown in Fig. 6. The large size of the error bars for the Y-82162 sample are a result of the small sample size. Within the error, the averages of both Orgueil and Y-82162 magnetite samples lie on the same fractionation line.

Our average composition for Orgueil magnetite ($\delta^{17}O = 3.6 \pm 1.7‰$, $\delta^{18}O = -0.2 \pm 0.6‰$) is in good agreement with the results of Hyman *et al.*[34] The average for Y-82162 magnetite ($\delta^{17}O = 7.4 \pm 1.5‰$, $\delta^{18}O = 8.8 \pm 1.1‰$) is significantly heavier than for Orgueil. The quoted errors were derived by dividing the standard deviation of the n measures by $n^{\frac{1}{2}}$; they do not include the additional possible error of ≈1‰ due to uncertainties in the calibration. The Y-82162 data also show some evidence for inter-grain variation. During the course of six successive measurements of one particular clump, which consisted chiefly of two large plaquettes, the observed $^{18}O/^{16}O$ ratio decreased by 10‰, which was outside the possible variation expected from counting statistics. If the small grains were sputtered away first, so that the final, isotopically light, signal came from the plaquettes, these data would suggest that the plaquettes are isotopically light. Note that this was the

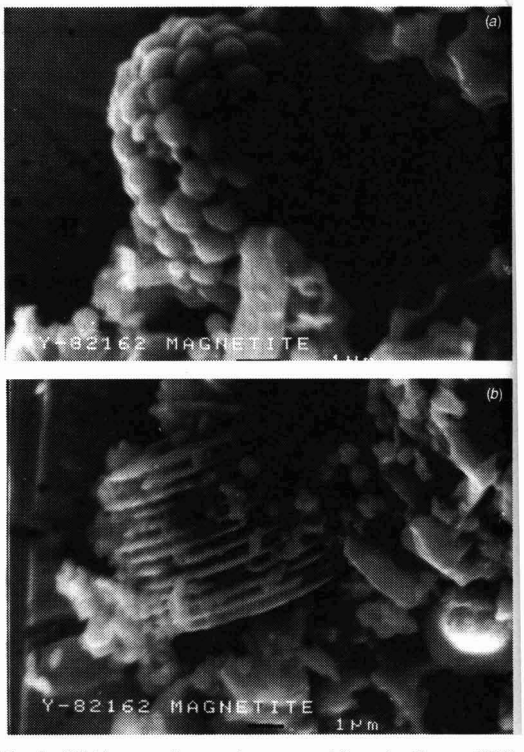

Fig. 5 SEM images of magnetite separated from the Yamato 82162 carbonaceous chondrite showing two morphologies: (*a*) a framboid, consisting of a cluster of small grains, and (*b*) a plaquette, consisting of a stack of thin plates. The scale bar is 1 μm.

only Y-82162 clump known to consist chiefly of plaquettes (the other analysed clumps were known to be mixtures of different sorts of grains, except for two where no high-resolution SEM images were obtained prior to analysis).

Löhn[31] made an extensive study of magnetites in Y-82162, Orgueil and other carbonaceous chondrites, and found that the magnetites sometimes occur in clusters; some clusters contain grains of a single morphology, whilst others contain grains of different morphologies. Since one would expect different morphologies to reflect different formation conditions, he concluded that *in situ* formation for all the magnetite was not plausible. Our limited evidence for inter-grain variability in Y-82162 is consistent with a variety of different formation mechanisms for the grains, and argues against a single formation event for all the magnetite in this meteorite.

We are not sure why Y-82162 magnetite should have a higher average $^{18}O/^{16}O$ value than Orgueil magnetite. Bulk Y-82162 ($\delta^{17}O = 12‰$, $\delta^{18}O = 22‰$) is isotopically heavier than bulk Orgueil ($\delta^{17}O = 9‰$, $\delta^{18}O = 17‰$, values read from Fig. 1 of the work of Mayeda and Clayton[35]). If the magnetite were formed by parent body processes, one would expect its composition to be related to that of the bulk meteorite. However, both bulk analyses lie practically on the terrestrial fractionation line (slope 0.52 in a plot of $\delta^{17}O$ *versus* $\delta^{18}O$), whilst the magnetite compositions appear to lie above it (an observation which agrees with the data of Hyman *et al.*[34]), which suggests that at least some of the magnetite was never in isotopic equilibrium with the bulk meteorite.

It would be very desirable to make *in situ* oxygen isotope analyses of the magnetite clusters found by Löhn,[31] especially those that consist of a single morphology. This would be the best way of determining whether isotopic composition is correlated with morphological type. Our ability to acquire *in situ* oxygen isotope analyses should allow us to do this with greater precision than for the isolated grains.

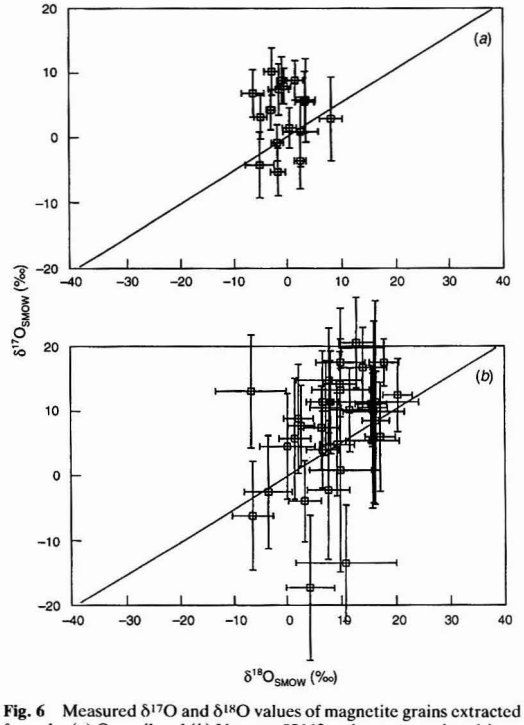

Fig. 6 Measured $\delta^{17}O$ and $\delta^{18}O$ values of magnetite grains extracted from the (*a*) Orgueil and (*b*) Yamato-82162 carbonaceous chondrites.

Conclusions

We have developed techniques to measure $^{17}O/^{16}O$ and $^{18}O/^{16}O$ *in situ* with the ion microprobe, with an accuracy of between 1 and 2‰, for both ratios. The reduced accuracy compared with conventional (bulk) oxygen isotope measurement techniques is offset by the ability to measure isotopic ratios *in situ* and with a spatial resolution of 10–20 μm. This offers us a new window onto the isotope systematics of microscopically heterogeneous samples. We are initially pursuing three avenues of inquiry:

(*i*) Authigenic quartz overgrowths in sandstones. A $\delta^{18}O$ profile on an authigenic quartz overgrowth which formed in a sandstone from the Vale of Eden shows a high $\delta^{18}O$ value indicative of an isotopically heavy source fluid. This study demonstrates the capability of measuring $\delta^{18}O$ values to a precision of at least 1‰ and with a spatial resolution down to 10 μm.

(*ii*) Magnetite in primitive carbonaceous meteorites. Although some carbonaceous chondrites show much evidence for aqueous alteration, the mode of formation of the magnetite is unclear. Initial oxygen isotopic results indicate a variety of origins for the magnetite grains, and do not appear consistent with formation of all the magnetites in a single event. This suggests that at least some of the magnetites may be of solar nebular origin.

(*iii*) Olivine in primitive meteorites. The different meteorite groups have different and characteristic oxygen isotopic compositions. Some of the olivine in these meteorites consists of grains that appear to predate the accretion of the meteorite and may be expected to preserve a history of events in the solar nebula. We have begun a program of study of these grains, in order to learn about solar nebula processes, in particular those through which the isotopic signatures of the different meteorite groups were established.

This work was supported by the Science and Engineering Research Council (now PPARC) who also provided a research followship for one of us (J. M. S.). The authors thank Dr. S. Burley, Dr. P. McKeever and Dr. S. Guscott who provided the authigenic quartz sample and for many helpful discussions. Dr. McKeever also undertook conventional fluorination $\delta^{18}O$ measurements of our quartz standards. We would also recognize the early contributions made to the development of these techniques by P. van Lierde and E. Chatzitheodoridis. We also wish to thank Dr. B. Löhn and Professor A. El-Goresy (Max Planck Institut für Kernphysik, Heidelberg) who separated the magnetite grains from Orgueil and Y-82162, Professor R. N. Clayton and Dr. I. Steele for providing samples of their olivine standards and Dr. J. Valley for providing samples of his magnetite standard (LP204). We also gratefully acknowledge the skilful technical support of D. Blagburn and B. Clementson.

References

1 Faure, G., *Principles of Isotope Geology*, Wiley, New York, 2nd edn., 1986, ch. 24 and 25.
2 Hoefs, J., *Stable Isotope Geochemistry*, Springer-Verlag, Berlin, 2nd edn., 1980.
3 Epstein, S., and Taylor, H. P., in *Researches in Geochemistry, Volume 2*, ed. Abelson, P. H., J. Wiley, New York, 1967, pp. 29–62.
4 Friedman, I., and O'Neill, J. R., in *Data Geochemistry*, ed. Fleischer, M., *U.S. Geol. Surv. Prof. Paper*, 440-KK, 1977.
5 Craig, H., *Science (Washington, D.C., 1883–)*, 1961, **133**, 1702.

6 Deines, P., *Geochim. Cosmochim. Acta*, 1977, **41**, 1709.
7 Anderson, A. T., Clayton, R. N., and Mayeda, T. K., *J. Geol.*, 1971, **79**, 715.
8 Clayton, R. N., and Mayeda, T. K. *Geochim. Cosmochim. Acta*, 1963, **27**, 43.
9 Sharp, Z. D., *Chem. Geol.*, 1992, **101**, (*Isotope Geoscience Special Issue*, **15**), 3.
10 Elsenheimer, D., and Valley, J. W., *Chem. Geol.*, 1992, **101**, (*Isotope Geoscience Special Issue*, **15**), 21.
11 Valley, J. W., Eiler, J. M., Kohn, M. J., Spicuzza, M. J., Baumgartner, L. P., Elsenheimer, D., and Graham, C. M., *Mineral. Mag.*, 1994, **58A**, 924.
12 Weichart, U., and Hoefs, J., *Mineral. Mag.*, 1994, **58A**, 973.
13 Valley, J. W., and Graham, C. M., *Contrib. Mineral. Petrol.*, 1991, **109**, 38.
14 Valley, J. W., and Graham, C. M., *Science (Washington, D.C., 1883–)*, 1993, **259**, 1729.
15 Jamtveit, B., and Hervig, R. L., *Science (Washington, D.C., 1883–)*, 1994, **263**, 505.
16 Ricciputi, L. R., and Paterson, B. A., *Mineral., Mag.*, 1994, **58A**, 770.
17 Lyon, I. C., Saxton, J. M., and Turner, G., *Rapid Commun. Mass Spectrom.*, 1994, **8**, 837.
18 Benninghoven, A., Rudenauer, F. G., and Werner, H. W., in *Secondary Ion Mass Spectrometry: Basic Concepts, Instrumental Aspects, Applications and Trends, Chemical Analysis Volume 86*, ed. Elving, P. J., and Winefordner, J. D., Wiley, New York, 411.
19 Hervig, R. L., Williams, P., Thomas, R. M., Schauer, S. N., and Steele, I. M., *Int. J. Mass Spectrom. Ion Processes.*, 1992, **120**, 45.
20 Deline, V. R., Katz, W., and Evans, C. A., *Appl. Phys. Lett.*, 1978, **33**(9), 832.
21 Havette, A., and Slodzian, G., *J. Phys. Lett.*, 1980, **41**, L247.
22 Lu, M. L., and Mann, K., *Phys. Rev. Lett.*, 1986, **57**, 1476.
23 Steele, I., and Clayton, R. N., 1994, personal communication.
24 Gnaser, H., and Hutcheon, I. D., *Phys. Rev. B*, 1987, **35**, 877.
25 Ehrenburg, S. N., *Am. Assoc. Petrol. Geol. Bull.*, 1990, **74**, 1538.
26 Guscott, S. C., and Burley, S. D., *Geofluids '93 Contributions to an International Conference on Fluid Evolution, Migration and Interaction in Rocks, Torquay, 1993*, ed. Parnell, J., Ruffell, A. H., and Moles, N. R., pp. 323–328.
27 Ramm, M., *Mar. Petrol. Geol.*, 1992, **9**, 553.
28 Bloch, S., *Am. Assoc. Petrol. Geol. Bull.*, 1991, **70**, 1145.
29 McBride, E. F., *Earth Sci. Rev.*, 1989, **26**, 69.
30 Fallick, A., 1994, personal communication.
31 Löhn, B., PhD Thesis, Ruprecht-Karls-Universität, Heidelberg, 1994.
32 Lewis, R. S., and Anders, E., *Proc. Natl. Acad. Sci. U.S.A.*, 1975, **72**, 268.
33 Kerridge, J. F., MacKay, A. L., and Boynton, W. V., *Science (Washington, D.C., 1883–)*, 1979, **205**, 395.
34 Hyman, M., Zinner, E. K., and Rowe, M. W., *Meteoritics*, 1994, **26**, 350.
35 Clayton, R. N., and Mayeda, T. K., *Proceedings of the Twentieth Lunar and Planetary Science Conference*, Lunar and Planetary Institute, Houston, TX, 1989, pp. 169–170.

Paper 4/05959J
Received 29 September, 1994
Accepted 8 March, 1995

A New Type of Synthetic Geochemical Reference Material—SynTERM*

David Cohen

Department of Applied Geology, University of New South Wales, Sydney, Australia NSW 2052

Rolf Beck

Water Research Laboratory, University of New South Wales, Manly Vale, Australia NSW 2093

Analytical data reported for natural geological reference materials (GRMs) indicates uncertainty in the recommended element concentrations, varying levels of both inhomogeneity in the distribution of trace elements and chemical/physical instability. Two types of silica gel-based synthetic trace element reference materials (SynTERM) have been developed as alternatives to natural GRMs: (*i*) high-purity reference materials and (*ii*) standard additions to existing natural geological materials. Wide variations in the concentration and combination of trace elements have been successfully formulated. The gel is formed by the rapid alkaline hydrolysis of tetraethyl orthosilicate (TEOS). Depth profiling by X-ray photoelectron spectrometry indicates that the trace metals are homogeneously distributed throughout gel particles of mean size 25 μm. Relative variation in results for trace elements in the high-purity reference materials (inhomogeneity) was less than ± 1.5% for a 1 g sample and less than ± 12% for 0.05 g samples. Compared with many natural GRMs SynTERM reference materials are more homogeneous, cheaper to produce and of potentially infinite supply.

Keywords: Synthetic reference material; homogeneity; calibration; silica gel

Need for Reference Materials or Standards

In environmental and exploration geochemical programs, the majority of trace metal analyses of geological materials are performed using comparative spectral methods such as atomic absorption spectrophotometry (AAS), inductively coupled plasma mass spectrometry (ICP-MS), instrumental neutron activation analysis (INAA) and X-ray fluorescence (XRF). Although these methods provide rapid acquisition of multi-element data they are subject to a variety of matrix interferences. Suitable reference materials are essential in calibrating the selected analytical technique. Subsequent determination of analytical accuracy, including the monitoring of transitory variation in analytical quality, is largely dependent on the analysis of reference materials.

Analytical accuracy within ±2% is critical for soil, dust or sediment samples collected as part of environmental audits of industrial and extractive industry sites.[1,2] Detailed site assessments, or even a requirement for site remediation, may be triggered in instances where a small proportion of samples collected exceed regulatory environmental standards. In geochemical exploration the demand for high-accuracy analyses may be relaxed; however, interlaboratory or inter-batch variations in analytical accuracy and precision may inhibit differentiation between background and subtly anomalous geochemical signatures (and increase the risk of failing to detect mineralization). In both situations, analytical accuracy needs to be monitored by use of geological reference materials (GRMs).

GRMs may be divided into two types: (*i*) natural reference materials derived from geological material and physically modified by comminution, and (*ii*) synthetic reference materials derived from either 'pure' laboratory reagents or from the chemical treatment of natural materials. GRMs should exhibit the following characteristics:

(*i*) well defined trace element concentrations close to those of the samples being analysed,
(*ii*) a matrix that matches the samples being analysed,[3]
(*iii*) homogeneity to a level specified by the end use; the finer the grain size, the easier a reference material is to homogenize but the greater the risk of physical separation of different minerals especially particulate gold and platinum group elements (PGEs),
(*iv*) sufficient supply, which could be of the order of tens of kg per year for a single laboratory (a number of international reference materials are now exhausted), and
(*v*) long-term physical and chemical stability.

For a range of geological, geochemical and environmental applications and sample types, the existing collection of natural 'international' and in-house reference materials do not meet these requirements.

Problems Inherent in Natural GRMs

The principle method for producing GRMs has been to collect, crush, sieve and homogenize a large amount of raw natural materials such as rock, ore, sediment or vegetation. Some attempts have been made to produce a range of component concentrations by mixing natural reference materials. Natural GRMs may display a range of deficiencies.

Uncertainty in 'True' Values

The element contents recommended for natural reference materials (central values) are effectively determined on the basis of consensus between laboratories using a range of analytical methods and statistical manipulation of the ensuing data.[4–6] The recommended values must take into account the substantial variability that usually exists between the different laboratories. Although these values may closely estimate the

* Presented at Geoanalysis 94: An International Symposium on the Analysis of Geological and Environmental Materials, Ambleside, England, September 18–22, 1994.

true values, the true value is an ideal that cannot be perfectly known.[7]

Reported data in collaborative programs can be incoherent and often display severely skewed distributions.[8] The use of a few selected laboratories and 'ideal' analytical methods to establish 'true' values for new reference materials should assist with improvement of the characterization of natural reference materials, but there remains the problem of how these laboratories are to be chosen and the cost of such exercises. Although certified values are subject to occasional review as new data or analytical methods become available, updates of recommended values for most reference materials have not significantly reduced the level of uncertainty regarding the mean or true value from the original testing.[9] Instances of significant between-bottle variation for exploration GRMs of the GXR series has also been noted in addition to significant variations between analytical methods and laboratories.[10,11]

Inhomogeneity

It is difficult to produce a completely homogeneous reference material by crushing, grinding, sieving and mixing a large volume of natural material. An extreme case of this is gold, where the entire gold content of a bulk sample may be bound up in a few grains and in which the number of gold grains cannot be readily increased by grinding owing to ductility.[12] High relative standard deviations (s_r values) on replicate gold analyses of reference materials have been reported.[13] It is possible to partition the components of analytical variance into analytical error and inhomogeneity within the reference materials themselves. In the same way that analytical precision is a function of concentration,[14] the degree of homogeneity may be a function of sample mass. In other instances quoted in the literature, the relationship between analytical sample mass and variation in mean contents is difficult to explain. A comparison of variation in the fire assay-INAA-determined gold contents of three to six 1, 5 and 10 g sub-samples of some United States Geological Survey (USGS) reference rocks[15] indicated a much higher relative standard deviation for the 1 g sub-samples than the 5 or 10 g sub-samples (Table 1) for two of the three reference materials analysed, but the reverse for the third. There was no explanation given for the puzzling trend in mean gold contents such that $Au_{1g} \gg Au_{10g} > Au_{5g}$.

Table 1 Variations in mean gold contents and s_r values for selected USGS reference materials

	Mean gold contents (ppb)			s_r (%)		
Size/g	BHVO-1	BIR-1	DNC-1	BHVO-1	BIR-1	DNC-1
1	3.52	2.62	2.99	45	122	35
5	0.74	0.84	0.92	39	82	66
10	1.15	1.08	1.96	33	16	68

Instability and Restricted Compositions

Reference materials may be chemically or physically unstable. Oxidation, adsorption of moisture or chemical reaction between components may be difficult to control once reference materials are exposed to the atmosphere. Stratification or settling of particles due to variations in particle size and density also occurs[16] with the effects of such particle segregation on mean metal contents demonstrated for base metal ore GRM MP-1a.[17] Although a large number of GRMs are available, there is actually a paucity of reference materials in terms of the types of matrices, combinations and concentrations of trace metals. This is particularly true for Au, PGEs and some REEs.

A Synthetic Alternative

A variety of synthetic reference material types have been developed including mixed high-purity powders, glasses, solution dosing of powders and various types of co-precipitation gels. Glasses are homogeneous to the mg level but require complete digestion for quantitative extraction of trace elements[18] and some trace elements may be volatilized during fusion.[19] Silica gels have been used previously as a co-precipitation medium,[19,20] however, many aspects of their use for trace metal reference materials and as viable alternatives to natural GRMs have not been investigated.

Two forms of synthetic reference material have been developed. The first is a pure, silica gel-based material and the second involves dosing of selected rock powders, soils or sediments. The dosed materials are designed to be analysed in parallel with the parent raw material (akin to the process of analysis by standard addition).

Experiment

Stock Solutions

Accurately weighed quantities of (at least) analytical-reagent grade metals or metal compounds of greater than 99.9% purity were dissolved in either nitric acid or dilute sodium hydroxide. In rare instances HF was used to assist digestion. For multi-element reference materials, the solutions were combined and evaporated by gentle heating to minimize the total quantity of aqueous phase. The reagents and solvents are listed in Table 2 and were purchased from Johnson and Matthey (Sydney), and Selby Scientific (Sydney). Fluka Chemika (Sydney) tetraethyl orthosilicate (TEOS) [$(C_2H_5O)_4Si$; density, 0.931 kg l^{-1}; bp, 163 °C] was obtained from Bioscientific (Sydney) ammonia solution from Selby Scientific (Sydney) and ammonia gas from CIG (Sydney). Quartz sandstone crushed to >97% (300 mesh) was obtained from Commercial Minerals (Sydney): the trace element contents are listed in Table 3. The bulk chemistry of the sandstone was determined by XRF and the results have been used to calculate the mineral composition (Table 3) using a sedimentary norm program.[21]

Table 2 Form of (at least) analytical-reagent grade metals and solvents used in SynTERM reference materials

Form	Solvent	Metals
Pure metals	*Aqua regia* or HF–HNO_3	Ag, Au, In, Ni, Ta, Zr
Oxides	HNO_3	Bi, Cd, Cu, Mn, Nb, Pb, REEs, Tl, Zn
Oxides	Dilute NaOH	As, Mo, Sc, Te, V, W
Nitrates	HNO_3 or water	Co, Rb, Sr, Th
Chloro-ammonium salts	HNO_3	PGEs
Other	HNO_3	$Cr[K_2Cr_2O_7]$, $Sb[KSbO]$, $U[UO_2(NO_3)_2 \cdot 6H_2O]$

Pure SynTERM Reference Materials

In a typical formulation, 460 g of tetraethyl orthosilicate (TEOS) and the aqueous metals solutions were combined in a borosilicate glass beaker, forming immiscible liquid phases. Ethanol was added until a single homogeneous phase developed. If required, the alkaline aqueous phase was added at this stage with sufficient nitric acid added to neutralize the alkaline solution and prevent premature gelling of the TEOS. While stirring vigorously concentrated ammonia solution was added, causing rapid gelling of the TEOS (the reaction was complete within 2–10 s).

After setting, the material was dried at 80 °C for 12 h to evaporate excess of adsorbed or incorporated ethanol and to remove ammonia, then heated at 120 °C for 12 h to remove excess of water. The material was ignited at 200–300 °C overnight, resulting in collapse of the silica gel into a non-hygroscopic amorphous silica and conversion of metal nitrates to oxides or to element form. The material was sieved through 80-mesh nylon cloth to reduce the size of gel clusters and ensure homogeneity of the final reference material.

The ultimate metal concentrations were calculated on the basis of the mass of ignited material and mass of element added. Loss-on-ignition (1050 °C) values for the pure and quartz sand matrix reference materials did not exceed 0.2%, even after 14 d exposure to the atmosphere, indicating the reference materials to be non-hygroscopic.

Dosed SynTERM Reference Materials

The TEOS–ethanol–metal solutions were combined with 1870 g of rock pulp or soil, which had been sieved to <0.075 mm, to form a very thick slurry. The ammonia solution (or gas) was added to gel the TEOS and the same drying procedure described above followed. In initial tests on the efficiency of ammonia gas in initiating gelling analytical-reagent grade ammonia gas was bubbled from the base of the reaction vessel through the end of a 2 mm diameter PTFE tube at a flow rate of around 1 l s^{-1}. This resulted in rapid gelling.

Solid Mixtures

To test the rate and efficiency of mixing of SynTERM with other powders, five smooth-sided 2 l polythene bottles were filled to 40% capacity with 980 g of crushed quartz sand and 40 g of one formulation (designated as SynTERM-12) placed on top of the sand without mixing. The bottles were gently rested on a roller with opposing cams, which provided a ± 10° oscillation from the horizontal and rotated at a rate of 30 rev min^{-1}. Individual bottles were removed after 1, 4, 16, 64 and 256 min and six 10 g sub-samples removed from parts of the bottle using polythene tubing. The results are described below.

The compositions of SynTERM reference materials discussed in this paper are listed in Table 4.

General Analytical Programme

Analysis of selected reference materials has been performed using a range of digestion and analytical techniques. The majority of the analytical work was performed by commercial laboratories within Australia and Canada, with a focus on gold. The analytical programme is summarized in Table 5. In most instances 3–16 sub-samples of a given references material were analysed with 2–5 readings. Analysis of variance was used to partition total analytical variance into contributions by analytical error and by the combination of sample inhomogeneity and sample-processing errors.

Particle Sizing

To examine the effect of matrix type and trace element composition on the size of the gel particles formed, particle size distributions of SynTERM-12, 13 and 14 were determined using Malvern Instruments laser particle sizers SB.0B and M3.1. Samples were analysed following 5 and 15 min of ultrasound disaggregation. The data was analysed using interactive probability plots[22] to identify and characterize particle size populations.

Depth Profiling and SEM

The distribution of metals within the silica gel was examined using and X-ray photoelectron spectrometry (XPS) at the UNSW Surface Analysis Facility. Grains of a pure high concentration Ni and Co reference material (SynTERM-14) were mounted on In foil, coated with carbon and a 100 μm hole etched to a depth of 1 mm at the rate of 2.2 Å s^{-1}. At

Table 3 Chemical composition and normative mineralogy of crushed sandstone matrix used in formulation of reference materials

Oxide	Percentage by mass	Trace element	Concentration (ppm)	Trace element	Concentration (ppm)
SiO_2	98.64	Ag	<1	Ni	<0.1
TiO_2	0.07	As	0.2	Os	<0.001
Fe_2O_3	0.14	Au	<0.001	Pb	<0.1
Al_2O_3	0.67	Cd	<0.1	Pd	<0.001
K_2O	0.03	Ce	8.8	Pt	<0.001
Na_2O	0.14	Co	0.12	Rb	<5
CaO	0.02	Cr	3.3	Sm	0.88
SO_3	0.04	Cu	<0.1	Sr	<1
MnO	<0.01	Eu	0.12	Th	1.8
MgO	<0.01	Ir	<0.005	U	0.5
P_2O_5	<0.01	La	4.7	V	<1
Loss-on-ignition	0.20	Mn	<20	Zn	<50
		Mo	<2		

Mineral	Percentage by mass
Quartz	97.64
Rutile	0.07
Hematite	0.14
Illite	0.30
Kaolinite	1.44
Na-clays	0.14
Gypsum	0.06

various depths, the Ni and Co contents were determined using a CMS spectrometer. Photomicrographs of SynTERM-13/1 (sand matrix) and SynTERM-13/4 (matrix-free) were obtained by SEM.

Results

Physical Characteristics of SynTERM

Laser particle sizing and SEM

Based on population decomposition using probability plots, the gel particles sizes typically range from around 2 to 50 μm with mean sizes of about 25 μm (Table 6). For pure SynTERM there is a second size distribution (gel B) with population mean sizes that suggest fused double grains. The size appears to be relatively unaffected by the nature of the supporting matrix, although the mean particle sizes were smaller for the pure reference materials (around 15 μm). Ultrasounding beyond 15 min had little effect on the mean gel particle sizes. In the dosed materials, the gels were weakly bound to matrix surface (Fig. 1). The spongy nature of the gel has presented problems in producing polished sections for electron microprobe analysis.

Table 4 Composition of SynTERM reference materials (concentrations are in ppm)

	SynTERM reference material													
Element	1	2	12	16	7	8	9	13/1	13/5	14	15B	15G	15S	15L
Ag	26.3	2.6	113	—	0.26	0.52	4.16	—	—	—	—	—	—	—
As	100	10	46.8	197	—	—	—	—	—	—	50.1	54.9	67.3	57.2
Au	2.01	0.5	19.7	0.005	0.2	0.6	8.01	—	—	—	5.1	5.1	6.0	5.2
Cd	—	—	46.9	—	—	—	—	—	—	—	—	—	—	—
Co	21	2.1	48.9	—	—	—	—	≈20	≈40	—	95.7	57.1	83.3	76.5
Cr	498	200	468	—	—	—	—	—	—	—	—	—	—	—
Cu	104	10.2	93.6	50.6	—	—	—	—	—	—	—	—	—	—
Mn	847	340	—	980	—	—	—	—	—	—	—	—	—	—
Mo	40	4	46.9	—	—	—	—	—	—	—	—	—	—	—
Ni	103	10.3	93.8	—	—	—	—	≈100	≈200	≈25 000	—	—	—	—
Pb	50	5	93.4	115	—	—	—	—	—	—	—	—	—	—
Rb	217	87	—	—	—	—	—	—	—	—	—	—	—	—
Sr	249	100	480	—	—	—	—	—	—	—	—	—	—	—
Th	27	4.2	—	—	—	—	—	—	—	—	—	—	—	—
U	46	4.6	46.9	—	—	—	—	—	—	—	—	—	—	—
V	200	20	187	—	—	—	—	—	—	—	—	—	—	—
Zn	498	200	467	97.6	—	—	—	—	—	—	—	—	—	—
56	10.6	—	—	—	—	—	—	—	—	—	—	—	—	—
Dy	20	4	—	—	—	—	—	—	—	—	—	—	—	—
Eu	11.3	2.3	—	—	—	—	—	—	—	—	—	—	—	—
La	54	14	—	—	—	—	—	≈100	≈200	—	—	—	—	—
Nd	50	10	—	—	—	—	—	—	—	—	—	—	—	—
Sm	26	6	—	—	—	—	—	—	—	—	—	—	—	—
Tb	10.4	2.1	—	—	—	—	—	—	—	—	—	—	—	—
Tm	17	3.4	—	—	—	—	—	—	—	—	—	—	—	—
Ir	—	—	—	—	0.05	0.16	2.06	—	—	—	—	—	—	—
Os	—	—	—	—	0.04	0.12	0.81	—	—	—	—	—	—	—
Pd	—	—	—	—	0.98	2.01	4.02	—	—	—	—	—	—	—
Pt	—	—	—	—	2.45	5.0	10.0	—	—	—	—	—	—	—
Re	—	—	—	—	0.41	1.26	4.21		—	—	—	—	—	—
Matrix*	Sand	Sand	Sand	Lat	Sand	Sand	Sand	Sand	None	None	Basalt	Granite	Bl	Lat

* Sand, quartz sand; Lat, lateritic soil; and Bl, smectitic black soil.

Table 5 Interlaboratory analytical programme

Laboratory	SynTERM	INAA	ICP–MS	ICP–MS solvent	AAS*	AAS solvent	FA†	BLEG‡	XRF	XPS§
A	12	•	•	*Aqua regia*						
B	12		•	*Aqua regia*–HF	•	*Aqua regia*–HF	•	•		
C	1, 2, 7–9	•								
	12–15	•								
D	12		•	*Aqua regia*–HF			•			
	13		•	*Aqua regia*–HF						
	1, 2		•	Hot nitric			•			
E	1, 2		•	*Aqua regia*–HF	•	*Aqua regia*–HF	•			
	7–9		•	*Aqua regia*–HF		*Aqua regia*–HF	•			
	12		•	*Aqua regia*–HF	•	*Aqua regia*–HF	•	•		
F	1,2						•			
G	12				•	*Aqua regia*			•	•
H	15, 16				•	*Aqua regia*			•	•
I	12	•	•	Hot nitric						

* AAS, atomic absorption spectrometry, air–acetylene flame.
† FA, fire assay with Pb collection and AAS finish.
‡ BLEG, bulk (cyanide) leach extractable gold, active 24 h leach with AAS finish.
§ XPS, X-ray photoelectron spectrometry.

Sizing of gold particles

Estimation of effective gold particle size using the GOLDCALC program indicates the effective gold particle size in the reference materials to be relatively uniform and in the order of 1 μm (Table 7). These size estimates are somewhat larger than indicated by the SEM work and suggest that the measured variability in gold contents of the reference materials (inhomogeneity) are over-estimates.

Table 6 Particle size distributions for selected SynTERM reference materials (pure and matrix supported)

SynTERM	Time in ultrasound/ min	Population	Mean/ μm	*s*/μm	Range* μm
12	15	Gel	27.0	10.3	6.4—47.6
		Matrix	64.8	17.5	29.7—99.8
13/1	2	Gel	25.1	11.4	2.4—47.8
		Matrix	52.5	10.6	31.3—73.7
13/1	15	Gel	22.2	10.0	2.2—42.2
		Matrix	62.2	15.6	31.0—93.4
13/4	2	Gel A	15.8	7.2	1.5—30.2
		Gel B	35.8	5.7	24.4—47.2
13/4	15	Gel A	15.1	6.8	1.5—28.7
		Gel B	34.7	6.1	22.5—46.9
14	2	Gel A	14.4	7.2	0.0—29.0
		Gel B	45.8	17.3	11.2—80.5
14	15	Gel A	11.1	5.2	0.8—21.4
		Gel B	30.2	11.4	7.5—52.9

* 95% Confidence interval.

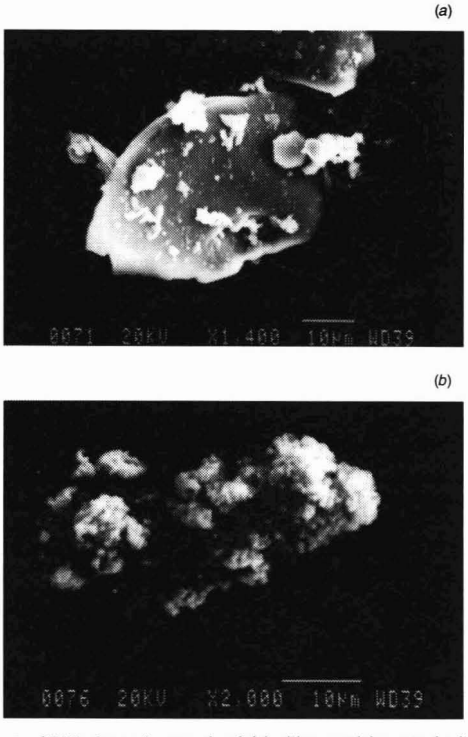

Fig. 1 SEM photomicrograph of (*a*) silica particles attached to a quartz grain in sandstone matrix-based SynTERM-13/1 and (*b*) spongy agglomerations of silica particles in pure reference material SynTERM-13/4.

Chemical Characteristics

Surface analysis and depth profiling

The binding energy peaks derived from the XPS analysis confirms that both Ni and Co are present as the oxide and homogeneously distributed within the gel grains (Fig. 2). The low relative surface concentration is due to adsorption of water and C coating. This implies a high level of internal homogeneity is achievable for the reference materials at the mg level and is of particular relevance to analytical methods such as laser ablation, where small quantities of material are analysed.

Comparison between analytical methods

The behaviour of the reference materials varied between digestion/analytical methods and between elements (Fig. 3). In the instance of gold, the combination of fire assay or *aqua regia*–HF digestion with AAS generally attained the expected metal concentrations (slightly low in some instances). INAA under-estimated the amount of gold present in SynTERM-12 and 1-9, although laboratory C was generally within 2% of the expected value for other reference materials tested. In the instance of cobalt and chromium, INAA provided close to the true values. The results from ICP-MS were highly variable, but appeared to be dependent on the type of acid digestion. *Aqua regia*–HF provided near total extraction of the metals whereas hot nitric acid provided an incomplete and variable extraction. Iridium concentrations determined by INAA was consistently within 1% of the expected value for SynTERM-7, 8 and 9.

Two active leach BLEG methods tested succeeded in extracting only around 50% of the gold, less than 60% of the copper, and around 90% of the silver.

Homogeneity

Using analysis of variance methods on multiple analyses of some of the reference materials, the total analytical variance has been partitioned between sub-sample and analytical error to establish the level of homogeneity within the reference materials. The relative standard deviation of the analyses (s_r) attributable to inhomogeneity within the reference material (which includes all errors beyond counting or measurement) is less than 1.5% for all elements, and for all analytical methods (Table 8). These s_r values are significantly less than values normally quoted in the literature regarding natural GRMs. There is no apparent effect on the metal homogeneity within the reference materials of gel size, support matrix or metal concentration. The theoretical limit to homogeneity of the reference materials formulated with a matrix may be predicted using the expected variability of metal distribution in multimineralic mixture.[23] If gel grains of mean diameter 20 μm comprised 1% of the total material present and the metals are homogeneously distributed though the gel, then the expected relative standard deviations would be 0.012% for 10 g sub-samples, rising to 3.8% for 0.1 mg sub-samples.

Element concentration correlations

In the instance of SynTERM-12, both INAA and ICP-MS results indicate some correlation between metal values. The strength of these correlations vary, with most being statistically insignificant. The implications are that there is some intrinsic inhomogeneity in metal distributions and this suggests the component of total variance attributed to inhomogeneity may be statistically significant. There were some problems with excess of liquid phase in this reference material after gelling and formation of what appeared to be a silver salt

prior to setting, which may contribute to this apparent minor inhomogeneity. The problem of excess of liquid phase has been addressed by using ammonia gas rather than ammonia solution to gel the reference material.

Relationship between homogeneity and sample mass

For sample mass in the range 0.06–10 g, the mean INAA and flame-AAS values for elements analysed were unaffected by sample mass (Fig. 4). The total variability increased as sample mass decreased; however, this is a function of inherent reduction in precision as concentrations approach the analytical detection limits.

Mixing and effects of support matrix

In the instance of Au, the expected bulk Au value was obtained within 16 min of mixing and the s_r values reduced below 5% (which includes sample preparation and analytical error as well as sample inhomogeneity) within 256 min. This suggests that a range of reference materials may be produced by mixing powders rather than dosing matrix materials. Variations in matrix type do not appear to affect the size of gel particles or the homogeneity of metal distributions within the reference materials (Table 9).

Discussion

The technique developed in this study differs from previous gelling techniques using TEOS[20] in the rate at which gelling proceeds and in the number of elements that have been incorporated into single stage formulations. Batches as large as 12 kg have been gelled in less than 5 s, depending on the rate at which the ammonia was introduced and the concentration of trace metals (which appears to promote rapid gelling). The formulation produces only negligible quantities of residual liquids after setting and minimizes the risk of metals partitioning into the liquid phase or adsorbing onto reaction vessel walls, thereby ensuring homogeneity and accuracy in the reference materials.

The size of the silica gel particles (15–25 μm) and their adhesion to matrix grains should limit the physical segregation or settling of the gel particles during transport and eliminate the need to rehomogenize the reference materials before use. Based on the XPS work and a comparison of the proportion of metals released by different digestion techniques, the metals appear to be homogeneously incorporated within the gel particles. This makes the reference materials ideal for analytical methods where no digestions are required (INAA, XRF and the various micro-ablation methods) or where digestion is complete (fire assay). Providing there is no transient inhomogeneity in the solutions during the gelling process, the size of gel particles formed from the TEOS does not appear to affect the size of trace element colloids or aggregations, or the homogeneity of their distribution throughout the gel.

The use of replicate analyses has permitted the partitioning of total analytical variance into analytical error and the composite sub-sample inhomogeneity plus sample preparation errors. In most instances the apparent inhomogeneity in the reference materials is less than ±1.5%, and usually less than ± 1.0%. This is probably an over-estimation of intrinsic inhomogeneity in the reference materials. The existence of some inhomogeneity in the sand-based SynTERM-12 in

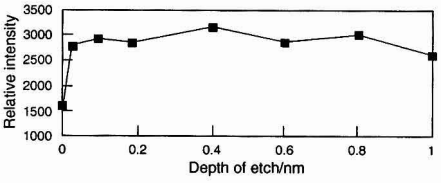

Fig. 2 Variation in Ni concentrations within SynTERM-14 determined using XPS and expressed as relative intensities.

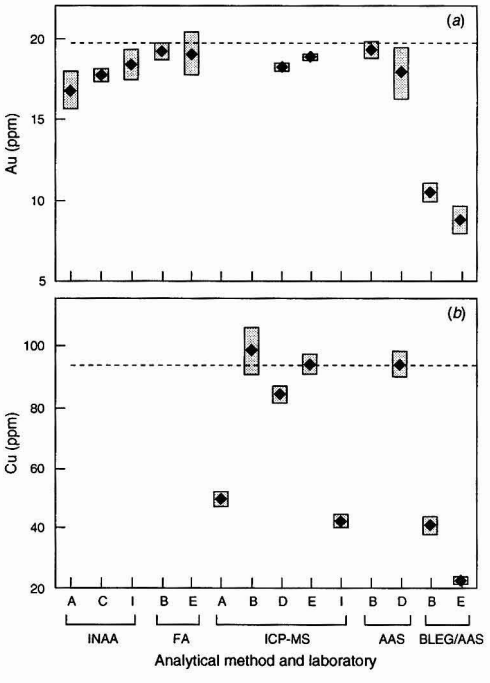

Fig. 3 Mean and 2s spread for (*a*) Au and (*b*) Cu on SynTERM-12 for a range of analytical methods and laboratories. Expected metal values are shown (dashed line).

Table 7 Gold particle sizing of selected SynTERM-12 based on analytical data and application of the GOLDCALC statistical sizing method

SynTERM	1	12	12	12	13/1	13/5	13/5
Analytical method	INAA	INAA	INAA	ICP-MS	INAA	INAA	INAA
Sample mass/g	30	30	10	1	10	6.5	10
Mean concentration (ppm)	2.10	18.70	18.45	17.3	4.62	8.20	8.20
s (ppm)*	0.02	0.05	0.16	0.3	0.07	0.18	0.15
Number of gold particles†	110 26	139 877	15 130	3818	4357	2328	3432
Gold sphere diameter/μm	0.8	0.7	1.2	0.8	1.0	1.3	1.1

* Related to calculated sample inhomogeneity.
† Expected at the 95% confidence limit.

indicated by moderate correlations between some elements (r^2 of 0.5 to 0.7). For matrix-free SynTERM reference materials it should be possible to routinely produce GRMs where the level of inhomogeneity in the trace metal contents is restricted to ±0.5% for 0.05 g sub-samples. Providing that this level of homogeneity can be established and no loss of elements occurs during formulation, confidence can be placed in the accuracy of the expected values.

The pure reference materials do not replicate natural materials as well as the dosed-matrix formulations. Major elements, such as Fe can be added, but problems arise in maintaining solubilities of elements prior to gelling and limiting the ratio of aqueous phase to TEOS. For dosed matrix SynTERM formulations, it is essential that the trace elements of interest are homogeneously distributed. As with any natural GRM, there will be uncertainty as to the true trace element content in the matrix material; however, if the trace elements of interest are homogeneously distributed in the raw material then the difference between the two materials (dosed and raw) will be well defined. It is the differential value which would be used in analytical calibration or the monitoring of analytical quality. Where the trace element contents of the raw material are significant, a sequence of two or more incremental dosed standards would be produced.

For analytical techniques requiring digestions and where the digestions tend to produce incomplete sample dissolution (*e.g.*, various combinations of strong acids or bulk cyanide leaching) the recovery of metals from SynTERM as well as for natural materials is generally incomplete. As a means of monitoring analytical accuracy, SynTERM may therefore be more applicable to solid powder sample methods such as INAA and XRF. SynTERM would, however, be useful in techniques involving sample dissolution as a means of verifying sample preparation procedures or monitoring variations in sample digestion conditions, even if total extraction of metals is not required for the SynTERM material.

High-quality gold-bearing natural GRMs are notoriously difficult to develop, especially if gold concentrations exceed ppb levels. The ability to incorporate gold into SynTERM reference materials in the ppm range, yet maintain gold particle sizes below 1 μm and ensure the absence of 'nuggets' cannot be matched by the existing set of natural GRMs.

Table 8 Average analytical variability in SynTERM reference materials

	s_r (%) due to inhomogeneity	s_t (%) total
Method—		
AAS	—	2.2 ± 0.9
BLEG	—	3.8 ± 0.7
FA	—	1.7 ± 1.2
ICP–MS	1.0 ± 0.7	2.9 ± 1.2
INAA	0.9 ± 0.6	1.7 ± 0.8
Overall	1.0 ± 0.7	2.4 ± 1.2
Element—		
As	0.6 ± 0.1	2.4 ± 1.6
Au	1.5 ± 1.2	2.3 ± 1.4
Cd	0.5 ± 0.2	2.4 ± 1.0
Co	1.5 ± 0.7	2.1 ± 0.8
Cr	0.7 ± 0.3	2.3 ± 1.1
Cu		2.9 ± 0.9

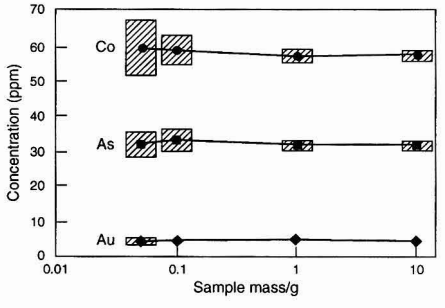

Fig. 4 Variation in means and standard deviations for Au, As and Co contents of SynTERM-13/5 (determined by INAA) *versus* analytical sample mass.

For high-quality natural GRMs, the ability to produce a sufficient quantity of material with a homogeneous trace element content is difficult. Natural GRMs are usually produced from a single source and are therefore limited in quantity. Natural GRMs are usually produced from a single source and are therefore limited in quantity. Natural GRMs are usually produced from a single source and are therefore limited in quantity.

Conclusion

The SynTERM synthetic GRMs display a more homogeneous metal distribution at the sub-μm scale than natural GRMs. This is particularly relevant to methods of analysis such as laser ablation-ICP, where very small quantities of sample are analysed. Unlike natural GRMs, where the true content of trace elements is difficult to establish, the true concentration of SynTERM is well defined providing homogeneity of the reference materials can be established. Any variation of analytical results from the established concentrations must be a function of sample processing and analytical errors.

The synthetic reference materials are more flexible than natural GRMs in terms of the combination and concentration of metals which may be incorporated and the choice of supporting matrix. The results of the project to date and feedback from analytical laboratories and potential end-users

Table 9 Comparison between AAS results for 15 replicates of SynTERM-16 and its support matrix (Fe-rich lags from Cobar area, New South Wales, Australia)

	Cr (ppm)	Cu (ppm)	Fe (%)	Pb (ppm)	Zn (ppm)
Support matrix—					
Mean	310.6	30.5	32.6	98.2	83.0
s_r (%)	4.9	2.6	2.5	8.4	2.2
SynTERM-16—					
Expected mean	289.8	78.5	30.5	206.6	175.1
Mean	293.3	77.6	30.5	206.1	161.3
s_r (%)	5.9	3.3	2.5	3.3	2.8
Comparison—					
Difference between mean and expected mean (%)	1.2	−1.9	0.0	−0.3	−7.8
t-test on difference between means	0.80	2.18	0.0	0.34	12.27
Result*	NS	NS	NS	NS	SIG

* NS/SIG, difference between mean and expected mean (not significant/significant) at 95% confidence limit.

indicate that SynTERM reference materials are a suitable low cost alternative to natural GRMs.

This study was supported by funds from the Australian Research Council. The authors thank E. Fellenberg and S. Alipour for assistance with the analytical work and are grateful to D. Rice and I. Wainwright for their constructive comments on this paper.

References

1 National Health and Medical Research Council, *Draft Australian Guidelines for the Assessment and Management of Contaminated Sites*, 1990, Government Printer, Melbourne.
2 United States Environmental Protection Authority (US EPA), *Methods for the Evaluation of the Attainment of Clean-up Standards*, US EPA publication 230/02, 1989.
3 Ingamells, C. O., *Geostand. Newsl.*, 1983, **7**, 1.
4 Ellis, P. J., and Steele, T. W., *Geostand. Newsl.*, 1982, **6**, 207.
5 Levinson, A. A., *Introduction to Exploration Geochemistry*, 1980, Applied Publishers, Illinois, pp. 51–80.
6 Fleischer, M., *Geochim. Cosmochim. Acta*, 1969, **33**, 65.
7 Youden, W. J., *Anal. Chem.*, 1960, **32**, 23A.
8 Abbey, S., *Geostand. Newsl.*, 1991, **15**, 3.
9 Kane, J. S., *Geostand. Newsl.*, 1991, **15**, 13.
10 Kane, J. S., Siems, D. F., and Arbogast, B. F., *Geostand. Newsl.*, 1992, **16**, 45.
11 Allcott, G. H., and Lakin, H. W., *USGS Open file report*, 1974.
12 Cohen, D. R., Booth, G. W., Govett, G. J. S., and Beck, R. W., *J. Geochem. Explor.*, 1991, **43**, 1.
13 Gladney, E. S., and Burns, C. E., *Geostand. Newsl.*, 1983, **7**, 3.
14 Thompson, M., and Howarth, R. J., *Analyst*, 1976, **101**, 690.
15 St Louis, R. M., *Geostand. Newsl.*, 1987, **11**, 151.
16 Flanagan, F. J., *U.S. Geol. Surv. Bull.*, 1986, 1582, p. 70.
17 Steger, H. G., and Sutarno, R., *Geostand. Newsl.*, 1983, **10**, 93.
18 Myers, A. T., Havens, R. G., Connor, J. J., Conlin, N. M., and Rose, H. J., *U.S. Geol. Surv. Prof. Paper*, 1976, **1013**, 29.
19 Date, A. R., *Analyst*, 1978, **103**, 84.
20 Hamilton, D. L., and Henderson, C. M. B., *Mineral. Mag.*, 1968, **36**, 832.
21 Cohen, D. R., and Ward, C. R., *Comput. Geosci.*, 1991, **17**, 1235.
22 Stanley, C. R., *PROBPLOT* program, *Association of Exploration Geochemists, Spec. vol. 14, 1987.*
23 Rickwood, P. C., in *Handbook of Exploration Geochemistry*, ed. Govett, G. J. S., 1982, Elsevier, Amsterdam, vol. 3, p. 24.

Paper 4/05885B
Received September 26, 1994
Accepted January 13, 1995

Application of Analytical Transmission Electron Microscopy to Identifying Intercrystal Variations in the Composition of Clay Minerals*

Balwant Singh

Department of Soil Science, The University of Reading, Whiteknights, Reading, UK RG6 2DW

R. J. Gilkes

Soil Science and Plant Nutrition, The University of Western Australia, Nedlands, WA 6009, Australia

Two examples of the use of analytical transmission electron microscopy (AEM) in solving mineralogical problems are reported. In the first instance, a beidellite-type smectite was identified using X-ray diffraction (XRD) in the clay fraction of a lateritic pallid zone from south-western Australia. The beidellite mineral constitutes <5% of the kaolin-dominated clay fraction of the sample and, thus, it is not possible to derive the chemical formula using bulk chemical analysis. The AEM analysis of beidellite indicates that this mineral is similar in chemical composition to an ideal beidellite, but is anomalous in that it contains large amounts of non-exchangeable K (K_2O = 2.2%). The second example is the determination of Fe in soil kaolinites using AEM. Analyses of the bulk clay fractions of soil kaolinites indicate the presence of ≈2.4% Fe_2O_3. It is uncertain to what extent this Fe is present as discrete impurities (such as iron oxides) and whether it is a constituent of kaolinite. Furthermore, the bulk analyses gave no indication of whether there was a range in values of Fe content between individual kaolinite crystals. AEM analysis of twenty single crystals for each of seven soil-kaolinite samples confirmed the presence of 1.96–2.83% Fe_2O_3 in kaolinite and that there was a considerable variation (*s* values of 0.66–1.21% Fe_2O_3) in iron content between kaolinite crystals in each sample.

Keywords: *Analytical transmission electron microscopy; beidellite; kaolinite; clay mineral; iron*

Introduction

The reactivity of clay minerals in soil may be explained on the basis of their chemistry and their variation between crystals. Clay minerals in soils are chemically analysed using X-ray fluorescence spectrometry (XRF) or wet-chemical analysis, where bulk samples of the clay-size (<2 μm) fraction, which often contain several mineral species, provide an average analysis. It is usually possible to identify the various crystalline minerals in a clay fraction using X-ray diffraction (XRD), thermal methods or other spectrometric methods, but these techniques are insensitive and often cannot detect poorly crystalline phases. As for the chemical composition, the mineralogical analyses represents the bulk material so that it is not possible to derive accurate structural formulae of the individual minerals in a mixture. The problem is accentuated by the variable chemical compositions of individual clay mineral species in soils, which is likely to be of a greater extent than is reported for reference minerals of geological origin.

The modern-day analytical transmission electron microscope is a powerful tool for detailed morphological, structural and chemical analysis of single crystals of clay minerals. Thus, the above mentioned problems, associated with the analysis of bulk samples, are eleminated due to its high spatial resolution. The use of analytical transmission electron microscopy (AEM) in solving two mineralogical problems is reported in this paper.

Experimental

Case Study 1: Boddington Beidellite

This material was obtained from a depth of 300 cm from the pallid zone of a deeply-weathered lateritic profile at the Hedges Gold Mine, Boddington, Western Australia. A reference mineral, Black Jack Mine (BJM) beidellite (#NMNH 24679) was supplied by the Smithsonian Institution, Washington, DC. The samples were dispersed in 0.01 mol dm^{-3} NaOH. The clay fraction (<2 μm) of BJM was used for the study, whereas for the Boddington sample, a coarse clay fraction (2–0.2 μm) was used, as the beidellite-like mineral was the most abundant in this fraction.

Case Study 2: Iron in Soil Kaolinites

Clay fractions of seven soils containing only kaolinite as the clay mineral, and representing major soil types of south-western Australia, were examined. The soils of the region are mostly derived from deeply weathered Precambrian igneous rocks (mainly granite and gneiss with the occasional intrusion of doleritic dykes). Complete descriptions and other details of the samples have been published by Singh and Gilkes.[1] The <2 μm fraction of the soil samples used for this study was made free of iron oxides by dithionite–citrate–hydrogencarbonate treatment.

Procedures

XRD patterns of the clay fraction coated onto a ceramic plate were made using monochromated CuKα radiation with a computer-controlled goniometer. The diffraction patterns were obtained after various pre-treatments to enable the identification of clay mineral species (Brown and Brindley[2]). The Greene-Kelly[3] test was employed to distinguish montmorillonite from beidellite.

* Presented at Geoanalysis 94: An International Symposium on the Analysis of Geological and Environmental Materials, Ambleside, England, September 18–22, 1994.

For AEM, a drop of well-dispersed Ba-saturated suspension was placed onto a carbon film supported on a Cu grid. Barium saturation was performed by washing the clays five times with 1 mol dm^{-3} $BaCl_2$ and the excess of salts were removed by repeatedly washing with de-ionized water. A Philips EM 430 analytical transmission electron microscope operated at 200 kV fitted with an EDAX PV9900 X-ray energy dispersive system was used for the study (at the Electron Microscopy Centre of the University of Western Australia, Nedlands, Western Australia). Energy dispersive X-ray spectra (EDS) for single crystals were collected at 1000–2000 counts per second (cps) for 100 live-time seconds, using a spot size of ≈10 nm. The spectra were collected from the edges of well-separated single crystals (overlapping crystals were avoided for such analyses). The analyses were performed with a liquid nitrogen cold stage and the detector was fitted with a thin (<10 μm) Be window. A tilt angle of 25° towards the detector was used for all the analyses. After background stripping, intensities were converted to analyses using *k*-factors derived from the spectra of standard minerals. All the iron was assumed to be in the Fe^{3+} form for formula calculations. The structural formulae were calculated on the basis of 44 and 28 equivalent negative charges for beidellite and kaolin, respectively.

Results and Discussion

Case Study 1: Boddington Beidellite

The XRD patterns of oriented specimens of Boddington- and BJM-beidellite samples are shown in Fig. 1. The very strong reflections observed at ≈7.2 Å indicating the presence of kaolin in the Boddington sample are not shown in this figure. For both of the samples, smectite produced a peak of ≈14 Å for Mg-saturated air-dried samples expanding to ≈18 Å on glycerol solvation and collapsing to ≈10 Å for the K-saturated and heated (to 550 °C) samples. The Greene-Kelly test for the determination of the source of negative charge indicated that BJM beidellite swelled extensively after glycerol solvation of Li-saturated and heated (to 300 °C) samples. These results indicate that the net negative charge was in the tetrahedral layer, due to the substitution of Al^{3+} for Si^{4+}.

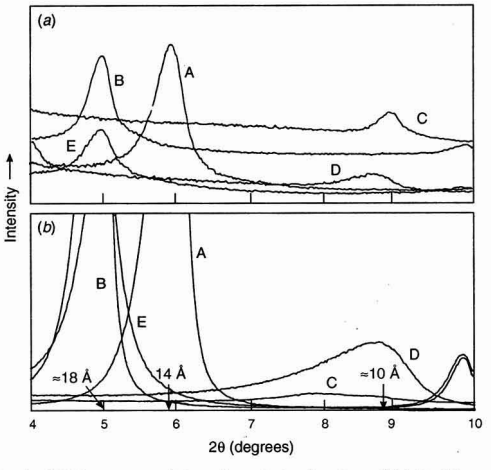

Fig. 1 XRD patterns of the oriented clay fraction of (*a*) Boddington beidellite and (*b*) BJM beidellite after A, Mg-saturation; B, Mg-saturation and glycerol-solvation; C, K-saturation and heating to 550 °C; D, Li-saturation and heating to 300 °C; and E, Li-saturation and glycerol-solvation.

As the Boddington clay contained abundant kaolin it was not possible to derive a structural formula for the beidellite from chemical analyses of the whole samples. AEM is perhaps the only available technique for quantitative chemical analysis of phases in such mixtures, as morphologically distinct single crystals may be analysed and contributions from other phases avoided (Curtis *et al.*[4]). Electron micrographs of Boddington- and BJM-beidellite samples with corresponding selected area diffraction (SAD) patterns and EDS are shown in Fig. 2. BJM beidellite consists of thin, predominantly ribbon-shaped flakes, which are several micrometres in length. A typical multiply-folded ribbon of BJM beidellite is shown in Fig. 2(*a*)(*i*) and is identical in morphology to a sample from this locality described by Güven and Pease.[5] The SAD of this mineral gave a characteristic spacing d(060) ≈1.50 Å. The EDS spectrum indicates abundant Si and Al, with lesser Ba, small amounts of Fe and Mg, and little or no K, which is consistent with the chemical analysis of the bulk sample. Electron micrographs of the Boddington clay fraction show that kaolinite, halloysite and beidellite each have a characteristic crystal morphology. These distinct morphologies, *i.e.*, euhedral to sub-hedral hexagonal plates of kaolinite, tubular halloysite and large (1–10 μm) thin sheets of beidellite resembling mica, enabled the unambiguous identification of crystals of these minerals prior to their chemical analysis by AEM. The EDS of kaolinite and halloysite are identical and show that they have a much higher Al:Si ratio than for beidellite, and also contain little Fe and no K. The Boddington beidellite contains K, which is an abnormal constituent of this mineral, as indicated by the EDS spectrum for BJM beidellite. The electron diffraction pattern of the Boddington beidellite is identical to that of the BJM beidellite, being the usual pseudo-hexagonal pattern of dioctahedral clay minerals with d(060)

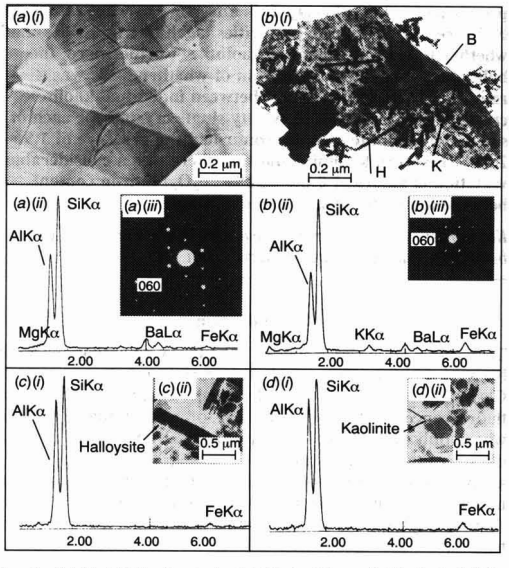

Fig. 2 (*a*)(*i*) AEM of a typical folded ribbon of Black Jack Mine beidellite with (*ii*) EDS spectrum and (*iii*) and SAD pattern. (*b*)(*i*) AEM of the 2–0.2 μm fraction of the Boddington clay. (B = beidellite, H = halloysite and K = kaolinite), (*ii*) EDS spectrum of a Ba-saturated crystal of Boddington beidellite and (*iii*) SAD of the beidellite crystal. (*c*)(*i*) EDS spectrum of the tubular halloysite crystal shown in (*ii*). (*d*)(*i*) EDS spectrum of the euhedral kaolinite crystal shown in (*ii*).

≈1.50 Å with the characteristic of two very strong (11, 02) reflections (Güven and Pease[5]).

AEM analyses for Ba-saturated BJM-beidellite and minerals in the Boddington sample are given in Table 1. The data for the BJM beidellite, halloysite and kaolinite are consistent with published analyses of bulk samples of these minerals. The cation-exchange capacity (CEC) of BJM beidellite based on the Ba content determined by AEM was 83 $cmol_c kg^{-1}$ [centimole charge (+) per kilogram of material]. For Boddington beidellite, the CEC value was 45 $cmol_c kg^{-1}$ but the inter-layer cation charge, including the contribution from the non-exchangeable K (47 $cmol_c kg^{-1}$), was 92 $cmol_c kg^{-1}$ which is similar to the inter-layer charge value for BJM and to other published values for reference beidellites.[6] Thus, the Boddington beidellite differs considerably from reference beidellites, in that almost exactly half of the layer charge was balanced by non-exchangeable K (structural formulae for the minerals derived from AEM analyses are shown in Table 2). The values of the tetrahedral charge, indicated by the structural formulae, are consistent with the XRD results of the Greene-Kelly test. Table 1 indicates that there is some variation in composition between beidellite crystals. Variations in the chemical composition of different size-fractions of the same beidellite sub-sample have been reported by Nadaeu *et al.*[7] Accurate and precise values of basal spacings for Mg-saturated and glycerol-solvated Boddington beidellite were obtained using octacosane as an internal standard and a scanning speed of 0.25° 2θ min^{-1}. The almost perfect integral series of basal spacings for a glycerol-solvated sample [d(001) = 17.87 ± 0.15 Å] indicates that the beidellite is not an interstratified smectite-mica, but a true smectite. This, an apparently freely swelling beidellite, contains about one sixth of the fixed K content of a mica. The existence of such a mineral has been postulated by various workers[8] on the basis of bulk chemical and XRD analyses of soil clays, but AEM analysis of single crystals has provided unambiguous evidence for the chemical composition of this mineral. Another important result obtained from this study was the greater variation in chemical composition of the Boddington beidellite compared with associated kaolinite and halloysite (and also BJM beidellite).

Case Study 2: Iron in Soil Kaolinites

The clay fraction of many of the major soils in south-western Australia is dominated by kaolinite.[1] The soil kaolinites give

Table 1 AEM analyses of single crystals in Ba-saturated Boddington clay and BJM beidellite

	BJM beidellite		Boddington beidellite		Boddington halloysite		Boddington kaolinite	
Element oxide (%)	Mean ($n = 18$)	s	Mean ($n = 19$)	s	Mean ($n = 12$)	s	Mean ($n = 6$)	s
SiO_2	57.38	0.50	61.34	2.81	53.76	0.85	54.38	0.68
Al_2O_3	33.81	0.48	27.25	2.43	43.15	1.48	42.25	0.16
Fe_2O_3	0.46	0.18	3.69	0.47	1.05	0.33	1.80	0.46
MgO	1.26	0.29	2.40	0.56	1.11	0.23	1.03	0.53
BaO	6.38	0.53	3.48	0.61	nd†	—	0.22	0.04
K_2O	0.08	0.04	2.20	0.34	nd	—	nd	—
Total	99.43	—	100.36	—	99.07	—	99.68	—
CEC* ($cmol_c kg^{-1}$)	83.4	—	45.4	—		—	2.87	—
			$K = 46.9$					

* Calculated from BaO content.
† nd = Not detectable.

Table 2 Structural formulae of beidellite, halloysite and kaolinite in the Boddington clay derived from analytical transmission electron microscopy (AEM) analyses of Ba-saturated single crystals together with a published formula for beidellite

Sample	Structural Formula	Total interlayer charge (M^+)	Tetrahedral substitution (M^+)
BJM beidellite	$[Si_{7.03}Al_{0.97}][Al_{3.92}Mg_{0.23}Fe^{3+}_{0.04}]O_{20}(OH)_4Ba_{0.31}K_{0.01}$	0.63	0.97
BJM beidellite (Weir and Greene-Kelly[6])	$[Si_{6.96}Al_{1.04}][Al_{3.96}Mg_{0.02}Fe^{3+}_{0.04}]O_{19.96}(OH)_4Na_{0.90}K_{0.02}$	1.00	1.04
Boddington beidellite	$[Si_{7.44}Al_{0.56}][Al_{3.34}Mg_{0.43}Fe^{3+}_{0.34}]O_{20}(OH)_4Ba_{0.17}K_{0.34}$	0.66	0.56
Kaolinite	$[Si_{4.07}][Al_{3.72}Mg_{0.11}Fe^{3+}_{0.10}]O_{10}(OH)_8Ba_{0.01}$	0.04	—
Halloysite	$[Si_{4.02}][Al_{3.80}Mg_{0.23}Fe^{3+}_{0.02}]O_{10}(OH)_8$	0.05	—

Table 3 Contents (Mean ± s) of major elements derived from AEM analyses of 20 single crystals of seven soil kaolinite samples and Georgia kaolinite

	SiO_2 (%)		Al_2O_3 (%)		Fe_2O_3 (%)		K_2O (%)		BaO (%)	
Sample	Mean	s	Mean	s	Mean	s	Mean	s	Mean	s
#124	52.24	0.79	44.35	1.16	2.75	0.87	0.24	0.39	0.42	0.73
#150	52.02	0.65	44.93	1.11	2.55	1.21	0.14	0.15	0.37	0.31
#167	55.73	3.18	41.66	2.88	1.96	0.66	0.32	0.20	0.34	0.35
#169	54.43	2.02	42.48	2.02	2.57	0.98	0.18	0.08	0.34	0.40
#175	55.77	2.09	41.09	2.34	2.66	0.75	0.21	0.32	0.27	0.30
#235	58.31	3.74	38.79	3.54	2.65	0.78	0.19	0.16	0.06	0.04
#239	57.78	2.52	38.92	2.71	2.83	0.93	0.30	0.22	0.31	0.27
Georgia kaolinite	53.96	1.57	45.28	1.50	0.31	0.17	0.28	0.20	0.16	0.17

broad basal XRD reflections and have a poorly ordered structure. Compared with reference geological kaolinites, soil kaolinites have higher surface area, cation-exchange capacity and P-sorption capacity, and lower dehydroxylation temperature. They also contain much more Fe (median value 2.4% Fe_2O_3 for 16 samples) than geological kaolinite (typically 0.4% Fe_2O_3). Seven soil kaolinites and one reference kaolinite (Georgia kaolinite) containing no detectable accessory minerals (on the basis of XRD, DTG, Mössbauer and electron microscopy results) were investigated by AEM to measure the iron in kaolinite crystals.

Electron micrographs and the EDS spectra of single crystals of Ba-saturated Georgia kaolinite and a typical soil kaolinite (#235) are given in Fig. 3. The crystal size of soil kaolinites (median value, 0.06 μm to 0.12 μm) is considerably smaller than for Georgia kaolinite (0.28 μm). The EDS show the presence of Fe in soil-kaolinite crystals. The chemical

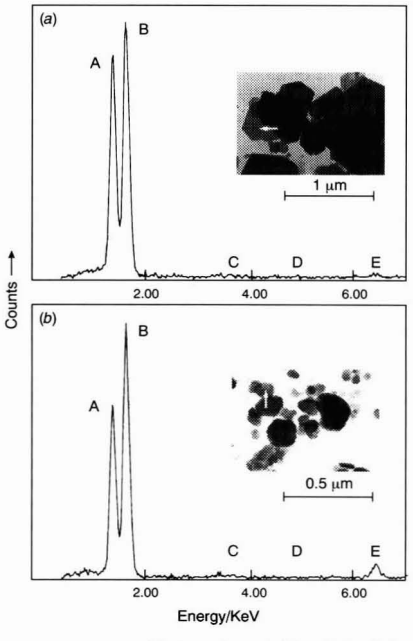

Fig. 3 EDS spectra for (*a*) Georgia and (*b*) soil kaolinite (#235) single crystals similar to those indicated by the arrows in the micrographs. A, AlKα; B, SiKα; C, KKα; D, BaLα; and E, FeKα.

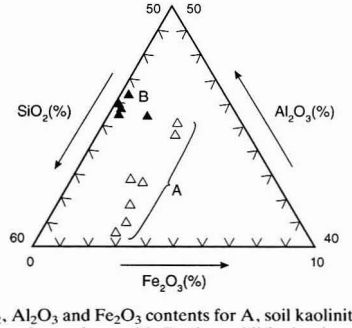

Fig. 4 SiO_2, Al_2O_3 and Fe_2O_3 contents for A, soil kaolinites derived from AEM analyses along with B, the published values for some reference kaolinites.

composition of Georgia and soil kaolinites derived from EDS analyses of 20 crystals is given in Table 3. The samples had been Ba-saturated, but only very small amounts of Ba were present (due to the small CEC of the kaolinite). Within each sample, crystals of both Georgia kaolinite and soil kaolinite varied considerably in their contents of SiO_2, Al_2O_3, Fe_2O_3, K_2O and BaO. The variations in composition between crystals are not solely due to the instrumental variability, as much lower values of *s* for these elements were observed for a pallid-zone kaolinite (Table 1) using the same procedure. It appears that there is an appreciable variation in the composition of individual crystals in both soil- and Georgia-kaolinites.

The high iron content for soil kaolinites determined by XRF analysis of bulk clay samples is consistent with the AEM results, which gave mean Fe_2O_3 values for soil kaolinites of between 1.96 and 2.83% in comparison with 0.31% for Georgia kaolinite. These data are compared with published values for some reference geological kaolinites as shown in Fig. 4. Soil kaolinites generally have higher Fe_2O_3 and SiO_2 contents and a lower Al_2O_3 content than reference kaolinites. As no evidence for associated Fe minerals was observed, it is concluded that Fe is present in the structure of kaolinite. The conclusion is consistent with the Mössbauer spectra of these specimens which showed that most of the iron is Fe^{3+} and is present in the octahedral layer of kaolinite.[9] The CEC of soil kaolinite, as indicated by the BaO analyses, are low and owing to the very low X-ray count rates are not precise. However, in general, single crystals of soil kaolinite have higher CEC values than the crystals of Georgia kaolinite (in accordance to CEC values for bulk-clay samples). The K_2O content of soil kaolinites ranged from 0.14 to 0.32%. If we assume that all K is present as the inter-layer cation of muscovite (≈10% K_2O), the soil kaolinites contain 1.4 to 3.2% muscovite layers which could not be identified by XRD but are consistent with the broad basal reflections of the kaolinite. For Georgia kaolinite which contains 0.28% K_2O, some discrete mica was identified by XRD, so that little or no inter-stratification with muscovite occurred. An important result of this study is that there is a large degree of variation in the chemical composition of kaolinite crystals within a single sample of soil kaolinite.

We have demonstrated that AEM provides information on the composition and variability of micro-minerals that could not be obtained by other techniques. It is, however, a time-consuming technique. The detection limit for most elements is of the order of 0.5 mass% in micrometre-sized crystals [this limit is much larger for lower atomic number ($Z < 10$) elements.[10,11]] Atom displacement, ionization and heating in the electron beam may cause considerable damage to samples and errors in analyses. For the close-placed peaks, overlapping can cause considerable analytical errors. A strong diffracting orientation should be avoided during AEM analysis. The analysis system requires regular calibration and monitoring and, thus, it is difficult to study a large number of samples.

The authors acknowledge the assistance of T. M. Armitage.

References

1 Singh, B., and Gilkes, R. J., *J. Soil Sci.*, 1992, **43**, 645.
2 Brown, G., and Brindley, G. W., in *Crystal Structures of Clay Minerals and Their X-ray Identification*, ed. Brindley, G. W., and Brown, G., Mineralogical Society, London, 1980, pp. 305–359.
3 Greene-Kelly, R., *J. Soil Sci.*, 1953, **4**, 233.
4 Curtis, C. D., Hughes, C. R., Whiteman, J. A., and Whittle, C. K., *Mineral. Mag.*, 1985, **49**, 375.
5 Güven, N., and Pease, R. W., *Clay Miner.*, 1975, **10**, 427.
6 Weir, A. H., and Greene-Kelly, R., *Am. Mineral.*, 1962, **47**, 137.

7 Nadeau, P. H., Farmer, V. C., McHardy, W. J., and Bain, D. C., *Am. Mineral.*, 1985, **70**, 1004.
8 Ross, G. J., and Mortland, M. M., *Soil Sci. Soc. Am. Proc.*, 1966, **30**, 337.
9 St. Pierre, T. G., Singh, B., Webb, J., and Gilkes, B., *Clays Clay Miner.*, 1992, **40**, 341.
10 Peacor, D. R., in *Minerals and Reactions at the Atomic Scale: Transmission Electron Microscopy*, ed. Buseck, P. R., Mineralogical Society of America, Washington, DC, 1992, pp. 113–140.
11 Hughes, C. R., Curtis, C. D., Whiteman, J. A., Heping, S., Whittle, C. K., and Ireland, B. J., in *Electron–Optical Methods in Clay Science*, ed. Mackinnon, I. D. R., and Mumpton, F. A., The Clay Minerals Society, Colorado, USA, 1990, pp. 70–88.

Paper 4/05884D
Received September 26, 1994
Accepted December 1, 1994

Reconstruction of *In Situ* Pore-water Compositions Obtained by Aqueous Leaching of Drill Core: An Evaluation Using Multivariate Statistical Deconvolution*

Mark Cave and Shaun Reeder

Analytical Geochemistry Group, British Geological Survey, Keyworth, Nottingham, UK NG12 5GG

A method for reconstructing pore-water compositions from aqueous leachate data obtained from milled and dried drill core is described. The method uses principal component analysis (PCA) to construct an abstract model of the aqueous leachate data which separates out the contaminating components, arising from rock dissolution and drilling fluid contamination, from the pore-water residual solutes component. Iterative target factor analysis (TFA) is used to quantify this pore-water component based on the assumptions that halides in the aqueous leachate are mainly attributable to the pore-water and that the lithium tracer in the drilling fluid is not present in the pore-water. The method is tested on a simulated data set and on data obtained from a deep borehole in Sellafield, Cumbria. The results demonstrate that the proposed method, although requiring further development, has potential use as a powerful investigative tool in a wide range of environmental applications.

Keywords: Pore-water; aqueous leaching; principal component analysis; target factor analysis

Introduction

A site near Sellafield, north-west England, is currently being assessed by UK Nirex for its suitability to host a radioactive waste repository. At this site, a sequence of relatively permeable sedimentary cover rocks, consisting mainly of Permo-Triassic red beds, overlies a sequence of low permeability Ordovician volcanic basement rocks, the Borrowdale Volcanic Group (BVG).

A major part of the investigation has been the chemical characterization of the groundwaters in these varied lithologies, in order to aid the interpretation of groundwater flow paths and water–rock interaction. This has involved sampling groundwaters from deep (up to approximately 2 km) boreholes. However, the coverage of such sampling is restricted by the relatively low frequency of features from which groundwater flow can be induced and from which waters can be collected. This means that often only relatively large-scale hydrochemical variations down a borehole may be resolved using samples obtained from these zones. It is therefore desirable to construct continuous geochemical profiles down the boreholes using alternative sources of data as an additional interpretation tool.

One such alternative source of data is the pore-water within the core rock samples removed from the test boreholes. For consolidated rocks with high porosity, pore-water can be removed from the core material by centrifugation.[1–3] However, the majority of the core material removed from the Sellafield boreholes has moisture contents less than 2%. In such rocks, characterization of pore-water compositions by aqueous leaching of residual solutes from drill core is the only appropriate method.[4–7] The use of aqueous leachates is complicated, however, in that their composition is not only derived from residual solutes from the pore-water but also are affected by two sources of contamination: (*i*) the pore-water in the core samples, particularly those from the more permeable Permo-Trias, is contaminated and diluted to varying extents with fluid used for collection of the core material during drilling; and (*ii*) residual solute data obtained by aqueous leaching is modified principally by dissolution of the rock during the experimental procedure.

Correction for these contamination effects is not a trivial problem as the number of source components in the raw aqueous leachate data is unknown: there is likely to be more than one groundwater component, the drilling fluid composition is known but it is likely that its composition is altered by filtration effects within the core, and the number of minerals contributing to the rock dissolution effects is unknown. All of these effects will be variable at different depths and lithologies within the borehole.

Principal component analysis (PCA) and derivative methods have been used widely in geochemical applications to identify source components within naturally occuring materials.[8] The multivariate statistical approach would seem to be the most suitable method for removing the interfering effects described above leading to the identification and quantification of the true pore-water component.

A number of workers[9–12] have applied PCA specifically to the chemical compositions of naturally occurring waters to identify source components, although this approach does not appear to have been applied to the interpretation of data from aqueous leaching of rocks. In these studies the number of components were identified, but only qualitative data on the component compositions was obtained. More recently, a number of more specialized multivariate statistical methods have been developed to allow the number of components in a mixture to be deduced and the composition of the components and the amount of each component present in the mixture to be quantified. Evolving factor analysis, originally described by Gamp *et al.*,[13] has been shown to be very successful for evolutionary processes where components appear and disappear in an ordered fashion (*e.g.*, in chromatographic applications) but is unlikely to be successful in resolving and quantifying rock dissolution effects from residual solutes from pore-waters where the concentration profiles are less well behaved. Rank annihilation factor analysis[14,15] allows the quantification of one component of interest in a complex

* Presented at Geoanalysis 94. An International Symposium on the Analysis of Geological and Environmental Materials, Ambleside, England, September 18–22, 1994.

mixture without concern for other components. However, this method requires that either the composition of the component or the concentration profile of the component be known for the algorithm to be successful, which again makes this method unsuitable for quantifying the groundwater component from the raw aqueous leachate data.

A promising methodology for using PCA to arrive at pore-water chemistries has been described by Alpert and Hopke[16] in which PCA is used to determine the number of components in a chemical data set derived from a number of different chemical sources and to set up an abstract model of the components which can be used to test whether given components fit the data using a procedure known as target factor analysis (TFA). If the test components were found to fit the model then they could be positively identified as being true components of the data. In this study the composition of the target vectors was known, but in the application described here the composition of the components are unknown. Because, however, there is some geochemical knowledge of the system under study and some individual constituents of the test factors can be estimated, it should be possible to use TFA in combination with the PCA model, as described by Malinowski,[17] to predict the missing data. The purpose of this paper is to test the proposed method for arriving at the true composition of pore-waters from raw aqueous leachate data on a simulated data set to verify the methodology and then to use the method on a real data set derived from aqueous leaching of core material from a Sellafield borehole.

Theory

Chemical analysis of aqueous leachates obtained from core material produces data arising from a combination of sources, including residual solutes from pore-water, residual solutes from contaminating drilling fluid, residual solutes from fluid inclusions, dissolution of rock minerals, and non-linear water–rock interaction processes (*e.g.*, ion exchange). If the leachate is derived predominantly from a linear combination of components and the non-linear interactions are minimal, the data can be modelled by PCA. Fig. 1 shows how PCA reduces a data matrix of samples with different combinations of different components into a series of 'score' column vectors, which are abstract representations of the chemical compositions of each component, and a series of 'weight' row vectors, which are abstract representations of the proportion of each component in each sample. The first few components represent true constituents in the data and the final components represent error in the measurements.

Once the number of significant underlying factors in the data has been determined, a matrix containing the abstract factors (concentrations of each analyte) can be calculated. The abstract factors are not recognizable as meaningful chemical compositions as the reference axes are generated to yield a purely mathematical solution. Reconstruction must be accomplished by transforming the reference axes so that they become aligned with the fundamental properties of the chemical system. Malinowski[17] shows that the following eqn. (1), derived from a least squares fitting approach, can be used

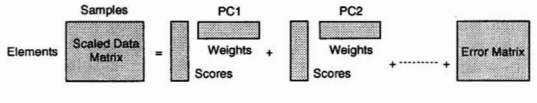

Fig. 1 Illustration of how PCA reduces a data matrix into scores and weights vectors.

to test if a given combination of element concentrations is a true factor by a process known as TFA:

$$\boldsymbol{T}_t = [\lambda]^{-1}\,[\boldsymbol{R}]^T\boldsymbol{R}_t \qquad (1)$$

where $\boldsymbol{T}_t$ is the transformation vector; $[\lambda]$ is a diagonal matrix composed solely of primary eigenvalues (the superscript –1 indicates the inverse of the matrix); $[\boldsymbol{R}]$ is the abstract factor matrix (the superscript T indicates the transpose of the matrix) and $\boldsymbol{R}_t$ is the test vector.

Both $[\lambda]$ and $[\boldsymbol{R}]$ are obtained by the PCA analysis of the raw data and subsequent selection of the number of factors. Values for $\boldsymbol{R}_t$ must be chosen with some prior knowledge of the system under test. Once $\boldsymbol{T}_t$ has been calculated, the following calculation is performed:

$$\boldsymbol{R}_p = [\boldsymbol{R}]\boldsymbol{T}_t \qquad (2)$$

where $\boldsymbol{R}_p$ is the predicted vector from the transformation. If $\boldsymbol{R}_t$ and $\boldsymbol{R}_p$ are equal to within an acceptable error then the test vector, $\boldsymbol{R}_t$, is a true factor of the model.

Hopke[18] has shown that the target testing procedure can be carried out iteratively. If a value for $\boldsymbol{R}_t$ is chosen that is not a true factor, then the calculated $\boldsymbol{R}_p$ value is used as the new $\boldsymbol{R}_t$. The process is repeated until the test vector converges on a true factor. Certain constraints can be built into the iterative TFA step to eliminate inappropriate factors, *e.g.*, a lower boundary of zero can be set for all analytes to prevent potential factors converging on meaningless negative values. As there are an infinite number of 'true factors', however, the key requirement of a successful TFA is to identify factors that are meaningful to the chemical system under study. TFA, therefore, has two very important properties that can be utilized to give quantitative information from the abstract PCA model. Firstly, if there are candidate geochemical components arising from independently derived sources of data, these can be tried to see if they fit the model. Secondly, if there is a component for which some of the determinand values are quantified then, by holding these values constant and taking the component through iterative TFA, quantified values for the unknown determinands are predicted which fit the PCA model. This second property is the basis of the proposed method used in this study.

In the specific case of aqueous leachates obtained from drill core as part of this study, two assumptions can be made which help the formulation of the trial test factor.

(*i*) It is known from the chemistry of the different lithologies within the borehole that the chloride and bromide concentrations in the rock matrix are low (< 5 μg g^{-1}) and that the chloride and bromide concentrations in the groundwaters sampled from the borehole are about 50 000–100 000 mg l^{-1} and 50–100 mg l^{-1}, respectively. It can, therefore, be assumed that the chloride and bromide found in the aqueous leachates is derived solely from the pore-water component.

(*ii*) Lithium is added to the drilling fluid at 1000 mg l^{-1} as a tracer, the rock matrix contains less than approximately 10 μg g^{-1} lithium and the groundwater extracted from an adjacent borehole of similar salinity contained < 10 mg l^{-1} lithium. Therefore, it can be assumed that the lithium found in the aqueous leachates of core material is derived solely from the drilling fluid contamination.

By using target factors in which chloride and bromide are held constant at their concentration in the pore-water and lithium is held constant at zero concentration, iterative TFA, with all other determinands initially set to zero, should produce values for these determinands which converge on concentrations representative only of the pore-water.

To validate this hypothesis, the proposed method was tested on a simulated data set and on a real data set derived from aqueous leachate analysis of core material from a single borehole.

Experimental

Computing

PCA was performed using the NIPALS algorithm, as described by Wold *et al.*,[19] and the iterative TFA using an algorithm based on the equations from Malinowski[17] discussed under Theory. The algorithms were programmed in Microsoft Visual Basic on a Dell 486D/50 PC. The cluster analysis was performed using Statsoft Statistica on the same computer.

Simulated Data Set

The synthetic data set is made up of a score matrix (Table 1) consisting of five separate chemical components, each with 15 chemical determinands, which represent a gypsum dissolution component (Gypsum), an alumino-silicate dissolution component (WRI), a drilling fluid component (Mud) and two groundwater components (Water 1 and Water 2). These components are broadly based on actual components that are thought to be present in the real data set studied in the second part of the study. The concentrations of each determinand are scaled between 0 and 1 and approximate the proportions of the different elements typically found in the aqueous leachates of these types of material. The weights matrix (Table 2) represents a simulated depth profile in which the proportion of each component in each test sample is varied.

The proportions of each component have been varied to reflect trends typically found in borehole profiles. The simulated gypsum component is generally a minor constituent except for a sequence of test samples which represents a gypsum rich lithology. For the drilling fluid component, the contribution decreases down the borehole, simulating the effect of lower porosity in the deeper rocks and, therefore, less drilling fluid intrusion. The alumino-silicate component is higher in the deeper, crystalline rocks and is quite variable down the borehole. Mixing of two source groundwater components is represented by a shallow, meteoric groundwater with a higher proportion at shallow depths and a deeper, more saline water with an increasingly higher proportion as depth increases.

By multiplying the weights matrix by the scores matrix, a simulated aqueous leachate data set was obtained (Table 3). This matrix was subjected to PCA to produce an abstract PCA model. Before TFA can be carried out on the PCA model it is necessary to identify the number of true components in the data so that those components that describe error are not included in the reconstruction. This can be achieved by many different methods (*e.g.*, Malinowski[18]) although in this study a fairly simple approach has been used. By plotting eigenvalues, which are proportional to the amount of variance explained by a particular principal component (PC) against component numbers, breaks in the continuity of the curve can be used to indicate the transition between real factors and those factors due to error. This can be accentuated by plotting ratios of successive eigenvalues and identifying maxima in the resulting plot. Fig. 2 shows the eigenvalue and eigenvalue ratio values plotted against component number for the simulated data set. In this case, as the simulated data set contains five pure components and no error the plot clearly shows that there are five components in the data as indicated by the discontinuity of the eigenvalue and the maximum in eigenvalue ratio at five components. The other components are made up of rounding off errors in the computation of the principal components, with the second peak in the eigenvalue ratio effectively being a 'noise' peak caused by differences in the error eigenvalues.

Pore-water data was reconstructed using the proposed iterative TFA, *i.e.*, chloride and bromide held constant and lithium held low, allowing the other determinands to be predicted by the model.

Real Aqueous Leachate Data Set

Sample preparation

Core samples were preserved at approximately 25 m intervals by wrapping in plastic film and aluminium foil then coating with a thick layer of wax immediately on removal of the core from the borehole. On return to the laboratory, the samples were unwrapped and the outer 1–2 cm annulus trimmed from the core and discarded. The remaining material was broken into fragments of <1 cm diameter and the moisture content determined by heating at approximately 110 °C, in excess of 12 h.

Aqueous leaching was performed on a sample milled to <350 μm diameter and dried at approximately 110 °C for a minimum of 12 h before weighing accurately approximately 5 g into a centrifuge tube. De-ionized water (30 ml) was added to the centrifuge tube and the sample shaken at room temperature for about 24 h. The mixture was then centrifuged and the supernatant leachate filtered to 0.45 μm. The sample for cation analysis was acidified to 1% with 16 mol l^{-1} nitric acid. The remainder of the unacidified sample was used for anion and pH determination.

Table 1 Simulated chemical components (scores matrix) in arbitrary units

	Gypsum	WRI	Water 1	Water 2	Mud
Cl	0.01	0.01	1	0.5	0.2
Br	0.01	0.01	1	0.7	0.1
Li	0.01	0.01	0.01	0.01	1
Ca	1	0.2	0.2	0.1	0.1
Mg	0.5	0.6	0.2	0.1	0.2
Na	0.01	0.5	1	0.5	0.2
K	0.1	1	0.2	0.3	0.1
Sr	1	0.2	0.1	0.1	0.05
Ba	0.1	0.01	0.1	0.1	0.05
TIC	0.1	1	0.3	0.1	0.8
SO_4	1	0.01	0.4	0.1	0.1
NO_3	0.01	0.01	0.01	0.1	1
Si	0.1	1	0.01	0.01	0.2
Al	0.1	1	0.01	0.01	0.3
Fe	0.01	1	0.1	0.1	0.3

Table 2 Simulated depth profiles for each simulated component (weights matrix) in arbitrary units

Depth	Gypsum	WRI	Water 1	Water 2	Mud
1	0.01	0.1	0.01	1	0.5
2	0.01	0.1	0.01	1	0.5
3	0.01	0.1	0.01	0.8	0.3
4	0.2	0.1	0.01	0.8	0.2
5	0.5	0.2	0.1	0.7	0.2
6	0.7	0.2	0.2	0.5	0.2
7	1	0.3	0.2	0.4	0.3
8	1	0.2	0.2	0.3	0.2
9	0.5	0.1	0.4	0.1	0.1
10	0.4	0.5	0.4	0.1	0.1
11	0.1	0.6	0.7	0.05	0.05
12	0.01	0.6	0.8	0.02	0.05
13	0.01	0.1	0.6	0.01	0.02
14	0.01	0.4	0.5	0.01	0.02
15	0.01	0.5	0.5	0.01	0.01
16	0.01	0.5	0.5	0.01	0.01
17	0.01	0.4	0.6	0.01	0.01
18	0.01	0.6	0.7	0.01	0.01
19	0.01	0.3	0.8	0.01	0.01
20	0.01	0.2	0.9	0.01	0.01

During the sample preparation the sample is dried to ensure that the milling procedure can be performed without the sample sticking to the milling apparatus causing malfunction and greater potential for cross contamination between samples. The drying process will obviously alter the chemistry of the water sample. Thus, when the residual salts from the pore-water are rehydrated, the more reactive species such as bicarbonate, nitrate, and the pH will not be truly representative of the original pore-water. However, the ions that make up the bulk chemistry of the pore-water (Na^+, K^+, Ca^{2+}, Mg^{2+}, Cl^- and SO_4^{2-}) may have their actual chemical speciation changed but the absolute amount present will still be an accurate reflection of the original values in the pore-water.

The abstraction of residual solutes by dispersive aqueous leaching was carried out on 35 samples. Seven of the samples were tested in duplicate (*i.e.*, separate aliquots of sample were prepared by crushing and milling and treated as individual samples for purposes of leaching and subsequent chemical analysis). Each of these duplicate samples was tested twice to provide replicate leachates for chemical characterization thus enabling statistical analysis to assess the repeatability of the leaching process.

Chemical analysis

Alkalinity and pH were determined by automated titration using a Radiometer VIT90 Video Titrator Controller module with an ABU93 autoburette and a SAM 90 sample station. The sample (1 ml) was pipetted into a small cup mounted on a titration stand with an integral magnetic stirrer and pH sensing glass electrode. The electrode was calibrated at pH 4, 7 and 10 (Whatman high resolution pH buffers, Whatman, Maidstone, Kent, UK) prior to analysis. The initial pH of the sample was noted and then titrated to pH 2.5 with 0.01 mol l^{-1} sulfuric acid (BDH Convol, now Merck, Poole, Dorset, UK). The titration curve is stored in the titrator controller and the bicarbonate content of the sample is equivalent to the number of moles of sulfuric acid added to the inflection point at pH 4.5.

Metal concentrations (Na, K, Ca, Mg, Ba, Sr, Mn, Fe, Al and Li) and silicon concentration were determined by ICP-AES using a Perkin-Elmer Plasma II sequential scanning system with twin 1 m vacuum monochromators. Monochromator A has a 3600 line/mm grating and wavelength range of 160–400 nm and the second, B, has a 1800 line/mm grating and wavelength range of 160–800 nm. The monochromator gratings, plasma power, plasma gas flows, plasma viewing height, 50-position autosampler, and nebulizer peristaltic pump were all under computer control. The emission wavelengths used for the analysis are summarized in Table 4. The instrument was operated under its standard operating conditions with argon flow rates of 15 l min^{-1} coolant, 1 l min^{-1} auxiliary flow and 1 l min^{-1} nebulizer flow to the torch, viewing height of 15 mm above the load coil and 1000 W forward power. The system was calibrated with three solutions: a major element standard containing 1000 mg l^{-1} Na and 100 mg l^{-1} Ca, Mg and K made from AnalaR grade salts in

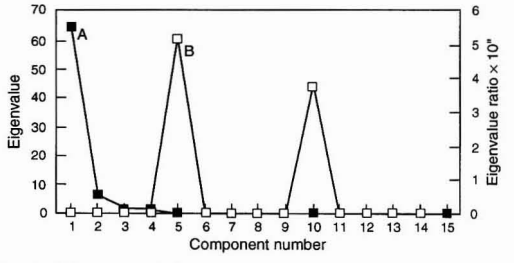

Fig. 2 Eigenvalue (A) and eigenvalue ratio (B) plots for the simulated data set.

Table 4 Emission wavelengths used for ICP-AES analysis

Element	Wavelength/nm
Al	396.152
Ba	455.403
Ca	315.887
Fe	259.940
K	766.490
Li	670.781
Mg	279.079
Mn	257.610
Na	589.592
Na	330.237
Si	251.611
Sr	407.771

Table 3 Simulated aqueous leachate data (arbitrary units)

Depth	Cl	Br	Li	Ca	Mg	Na	K	Sr	Ba	TIC	SO_4	NO_3	Si	Al	Fe
1	0.6111	0.7611	0.5112	0.182	0.267	0.6601	0.453	0.156	0.128	0.604	0.165	0.6012	0.2111	0.2611	0.3511
2	0.6111	0.7611	0.5112	0.182	0.267	0.6601	0.453	0.156	0.128	0.604	0.165	0.6012	0.2111	0.2611	0.3511
3	0.4711	0.6011	0.3092	0.142	0.207	0.5201	0.373	0.126	0.098	0.424	0.125	0.3812	0.1691	0.1991	0.2711
4	0.453	0.593	0.2111	0.322	0.282	0.502	0.382	0.311	0.112	0.363	0.305	0.2831	0.1681	0.1881	0.243
5	0.497	0.617	0.215	0.65	0.5	0.595	0.5	0.63	0.142	0.51	0.632	0.278	0.298	0.318	0.345
6	0.499	0.579	0.216	0.85	0.6	0.597	0.48	0.82	0.152	0.54	0.852	0.261	0.317	0.337	0.337
7	0.473	0.523	0.319	1.17	0.82	0.62	0.59	1.135	0.178	0.74	1.153	0.355	0.466	0.496	0.46
8	0.402	0.442	0.217	1.13	0.73	0.5	0.45	1.1	0.162	0.55	1.132	0.244	0.345	0.365	0.32
9	0.476	0.486	0.111	0.62	0.42	0.525	0.27	0.575	0.106	0.36	0.681	0.12	0.175	0.185	0.185
10	0.479	0.489	0.114	0.6	0.61	0.724	0.66	0.555	0.1	0.75	0.585	0.123	0.565	0.575	0.584
11	0.742	0.747	0.0645	0.37	0.565	1.036	0.77	0.2975	0.0935	0.865	0.396	0.069	0.6275	0.6325	0.691
12	0.8261	0.8251	0.0643	0.297	0.537	1.1201	0.772	0.2145	0.0915	0.883	0.343	0.0661	0.6192	0.6242	0.6971
13	0.6101	0.6101	0.0272	0.153	0.19	0.6591	0.226	0.092	0.064	0.298	0.254	0.0281	0.1111	0.1131	0.1671
14	0.5131	0.5131	0.0292	0.193	0.35	0.7091	0.506	0.142	0.057	0.568	0.217	0.0301	0.4101	0.4121	0.4571
15	0.5121	0.5131	0.0202	0.212	0.408	0.7571	0.605	0.1615	0.0575	0.66	0.217	0.0211	0.5081	0.5091	0.5541
16	0.5121	0.5131	0.0202	0.212	0.408	0.7571	0.605	0.1615	0.0575	0.66	0.217	0.0211	0.5081	0.5091	0.5541
17	0.6111	0.6121	0.0202	0.212	0.368	0.8071	0.525	0.1515	0.0665	0.59	0.256	0.0211	0.4091	0.4101	0.4641
18	0.7131	0.7141	0.0232	0.272	0.508	1.0071	0.745	0.2015	0.0785	0.82	0.298	0.0241	0.6101	0.6111	0.6741
19	0.8101	0.8111	0.0212	0.232	0.348	0.9571	0.465	0.1515	0.0855	0.55	0.335	0.0221	0.3111	0.3121	0.3841
20	0.9091	0.9101	0.0212	0.232	0.308	1.0071	0.385	0.1415	0.0945	0.48	0.374	0.0221	0.2121	0.2131	0.2941

a 1% HNO_3 matrix; a trace element standard containing 10 mg l^{-1} Na and 1 mg l^{-1} Al, Ba, Fe, Li, Mn and Sr made from 1000 mg l^{-1} single element stock solutions (BDH SpectrosoL) in 1% HNO_3 solution; a 10 mg^{-1} silicon standard made from 1000 mg l^{-1} stock solution (BDH SpectrosoL). Two emission lines were used for Na; the more sensitive higher wavelength line for concentrations <100 mg l^{-1} and less sensitive lower wavelength line for concentrations >100 mg l^{-1}. The instrument was standardized every 10 samples and independent quality control checks analysed after every 20 samples.

The ions Cl^-, SO_4^{2-}, NO_3^- and Br^- were determined by ion chromatography using a Dionex 2000i instrument with an AutoIon 100 control unit and autosampler. The data was processed using a Spectra Physics 4270 computing integrator and WINNER data capture and manipulation software. The sample (50 µl) was injected onto an AG4A guard column and an AS4A separator column with a $NaHCO_3$–Na_3CO_3 eluent (0.1425 and 0.191 g l^{-1}, respectively) pumped at 1.8 ml min^{-1}. After separation on the column, the background conductivity signal was chemically suppressed using an anion micromembrane suppressor. The ions Cl^-, SO_4^{2-} and NO_3^- were detected with a conductivity detector and Br^- was detected with a Phillips PU4110 UV/VIS detector set at 210 nm run in series with the conductivity detector. The system was calibrated with three solutions made from AnalaR grade salts in a de-ionized water matrix: standard 1 containing 100 mg l^{-1} Cl^- and SO_4^{2-} and 5 mg l^{-1} Br^-; standard 2 containing 50 mg l^{-1} Cl^- and SO_4^{2-} and 2.5 mg l^{-1} Br^-; standard 3 containing 10 mg l^{-1} Cl^- and SO_4^{2-} and 2.5 mg l^{-1} Br^-. The instrument was standardized every 11 samples and a quality control standard was run at the same frequency. The data was collected by the integrator which was pre-programmed to identify the peaks by their retention times and calculate peak areas for quantification.

In general, the leaching procedure is repeatable and the experimental errors were found to be sufficiently small for true geochemical trends to be observed for all determinands.

Multivariate Statistical Analysis of Aqueous Leachate Chemistry Data

Before PCA reduction of the aqueous leachate chemistry data was carried out, the raw concentration values have to be converted to a form suitable for the PCA data reduction. Values in the aqueous data matrix which were below detection limit were replaced by half the value of that limit. As pH is a logarithmic measurement and is not additive, these values were converted into their equivalent hydrogen ion concentrations, assuming that $pH = -\log [H^+]$. The aqueous leachate data were converted to the mass of analyte leached per unit mass of rock (µg g^{-1}) and is summarized in Table 5. Finally, to avoid the major elements dominating the PCA and masking the trends in the trace analytes, the data were 'scaled', using the standard procedure descibed by Wold *et al.*,[19] by subtracting the mean value for each analyte and dividing by the standard deviation of that particular analyte over the whole data set.

Following PCA reduction of the scaled data set, an evaluation of the true number of components in the data was carried out, as descibed for the simulated data set. The eigenvalue and eigenvalue ratio data are shown in Fig. 3 and identify major breaks in continuity at component numbers 4, 7, 11 and 14. In order to provide further evidence for the number of true factors, a second method was used. As the moisture content of the core material shows strong evidence for being a true factor of the data (see Results and Discussion) the closeness with which moisture content fits the PCA model for increasing number of factors should give an indication of how many factors are optimal. Fig. 4 shows how the root mean square difference between the actual moisture content and the moisture content predicted after TFA falls rapidly after the first three components, stays relatively constant from 4 to 9 components, decreases again from 9 to 11 components and then remains relatively constant from 11 to 16 components. Although somewhat subjective, the two methods used to estimate the number of true factors suggest 11 factors were optimal. It was therefore decided to use 11 components as a suitable compromise between selecting real structure in the data and not selecting additional factors which only contribute error. Reconstruction of the pore-water compositions was carried out using the same TFA procedure as applied to the simulated data set.

Results and Discussion

Simulated Data

Reconstructed pore-water data are shown in Table 6. The actual contribution from the pore-water (Table 7) is obtained by multiplying the weights and scores from the pore-water components in Tables 1 and 2. In all cases multivariate statistical deconvolution has substantially eliminated those components that are not associated with the pore-water contribution. The agreement between reconstructed values and the actual pore-water contribution is, however, somewhat variable.

Comparisons between the reconstructed data and the original data are shown in Figs. 5–8. The data labelled 'A' represents the contribution from the actual pore-water, 'B' represents the raw leachate data with the contributions from the pore-water, the drilling fluid and the rock dissolution components, and 'C' represents the TFA predicted value for the pore-water alone. The reconstruction works very well for iron (Fig. 5) and, to a slightly lesser extent, sulfate. For sodium (Fig. 6) and total inorganic carbon (TIC), the agreement is particularly good for samples in which the drilling fluid component is a minor constituent. With increasing drilling fluid contribution, however, these determinands, which are most significantly associated with the drilling fluid, are not sufficiently eliminated from the reconstructed data. This probably arises from an inconsistency in the boundary conditions applied during the iterative TFA in that chloride is held constant, in the assumption that it is solely derived from pore-water, when there is actually a small contribution from the drilling fluid (Table 1). The attempted removal of the drilling fluid component by holding lithium low, therefore, is restricted because of the constraint imposed on the chloride which results in some determinands associated with the drilling fluid not being sufficiently removed.

Some determinands, including potassium (Fig. 7), calcium, magnesium and barium, reconstruct to levels which follow the pore-water profile but are marginally over corrected with respect to the actual compositions. Despite these deviations from accuracy, the TFA predicted values closely follow the trends in the actual pore-water data which are totally obscured in the uncorrected data. Silicon (Fig. 8), aluminium and, to a lesser extent, nitrate are reduced to levels substantially lower than the actual pore-water compositions. This is related to the very low levels of these determinands in the pore-water relative to concentrations in the other components.

Further work is required to optimize the constraints applied during the iterative TFA procedure and to determine the factors governing the accuracy and precision of reconstruction. Nevertheless, the results of this preliminary investigation, on simulated data, have validated the principle of the proposed technique.

Pore-water Aqueous Leachate Data

The scaled aqueous leachate data is summarized in Table 5 and the scaled reconstructed pore-water component arrived at by the TFA method are shown in Table 8.

For the data obtained from analysis of aqueous leachate samples, there are more uncertainties than for the simulated data set. Firstly, for the proposed procedure to work it is necessary to know that the aqueous leachate data conforms to the conceptual model, *i.e.*, that the data are derived from a number of discrete components mixing in different proportions in each of the different samples. Qualitative indications of this can be obtained by examining the abstract scores and weight vectors obtained by the PCA data reduction.

A cluster algorithm was applied to the PCA scores and plotted as a dendrogram (Fig. 9) to show qualitative relationships between the determinands in the PCA model. The distance axis represents the degree of association between groups of determinands such that the lower the level at which determinands are joined on the distance axis, the more significant is their association. Three clear groupings are evident: one strongly associated with calcium, sulfate, magnesium and strontium, which is possibly related to dissolution of

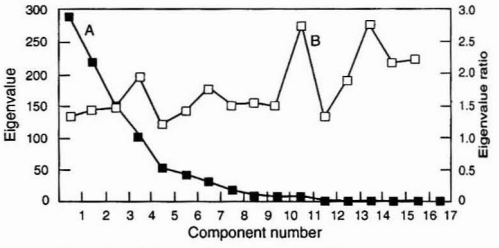

Fig. 3 Eigenvalue (A) and eigenvalue ratio (B) plots for the aqueous leachate data set.

Table 5 Scaled aqueous leachate data (arbitrary units)

Depth/m	Cl	Br	Li	H^+	Ca	Mg	Na	K	HCO_3	SO_4	NO_3	TIC	Si	Ba	Sr	Mn	Al
725.46	0.56	0.97	1.84	−0.18	−0.45	−0.22	0.43	−0.39	−0.01	−0.49	−0.07	0.03	−0.21	−0.96	−0.46	−0.42	−0.45
749.80	2.06	1.98	3.36	−0.18	−0.41	0.64	1.81	−0.34	−0.31	−0.46	−0.25	−0.26	−0.30	−0.48	−0.34	−0.42	−0.49
802.67	1.09	1.30	3.86	−0.17	−0.42	0.00	0.83	−0.88	−0.53	−0.48	−0.88	−0.55	−0.24	−0.66	−0.39	−0.37	−0.49
852.50	1.69	1.64	1.04	−0.18	−0.41	0.68	1.29	−0.60	−0.20	−0.48	−0.34	−0.08	−0.18	−0.50	−0.38	−0.37	−0.49
908.46	1.27	1.26	0.36	−0.16	−0.42	0.90	1.09	−0.39	−0.34	−0.48	−0.07	−0.07	−0.21	−0.65	−0.41	−0.33	−0.50
981.25	2.49	2.26	1.82	−0.15	−0.40	1.13	2.28	−0.27	−0.43	−0.47	−0.88	−0.22	−0.02	0.19	−0.32	−0.42	−0.51
981.25	2.29	1.93	1.66	−0.17	−0.40	1.17	2.34	−0.27	−0.06	−0.47	0.56	−0.08	0.58	0.12	−0.33	−0.42	−0.51
981.25	2.71	2.21	1.74	−0.16	−0.40	1.16	2.17	−0.25	−0.42	−0.47	−0.34	−0.16	0.09	0.43	−0.32	−0.42	−0.50
981.25	2.25	1.78	1.74	−0.18	−0.40	1.16	2.11	−0.18	−0.07	−0.47	0.55	0.02	0.47	0.42	−0.33	−0.42	−0.51
1028.05	1.84	2.02	−0.10	−0.17	−0.41	1.25	1.61	−0.60	−0.37	−0.48	0.20	−0.12	0.14	0.97	−0.35	−0.37	−0.51
1134.45	0.45	0.55	−0.54	−0.18	−0.47	−0.73	0.67	−0.70	0.97	−0.49	0.20	1.57	0.31	−1.24	−0.51	−0.37	−0.25
1180.08	−0.41	−0.81	−0.38	0.01	2.74	2.06	−0.21	0.37	−0.82	2.61	2.44	−0.95	−0.24	−0.48	2.75	−0.24	−0.44
1180.08	−0.53	−0.81	−0.34	7.32	2.81	2.05	−0.22	0.22	−0.82	2.61	1.72	−0.96	−0.22	−0.45	3.00	−0.21	−0.41
1180.08	−0.51	−0.81	−0.37	−0.10	2.64	2.23	−0.25	0.46	−0.82	2.77	3.07	−0.94	−0.21	−0.40	2.68	−0.22	−0.41
1180.08	−0.52	−0.82	−0.48	0.00	2.37	1.68	−0.44	0.12	−0.82	2.63	3.82	−0.96	−0.35	−0.52	2.65	−0.29	−0.45
1237.16	−0.40	−0.81	−0.14	0.09	1.95	2.67	0.21	0.59	−0.82	2.12	0.02	−0.68	−0.16	−0.35	2.25	−0.35	−0.46
1324.93	−0.44	−0.81	−0.52	0.41	0.51	0.51	−0.61	0.74	−0.82	0.55	−0.88	−0.86	−0.75	0.38	0.23	1.20	−0.47
1370.41	−0.53	−0.81	−0.78	−0.09	−0.38	−0.45	−0.61	0.48	−0.82	−0.33	−0.88	−0.60	−0.60	1.71	−0.39	−0.34	−0.46
1370.41	−0.56	−0.81	−0.80	−0.08	−0.36	−0.38	−0.62	0.45	−0.82	−0.30	−0.88	−0.63	−0.68	1.45	−0.37	−0.28	−0.47
1370.41	−0.55	−0.81	−0.78	−0.16	−0.39	−0.45	−0.56	0.69	−0.51	−0.33	−0.88	−0.60	−0.61	1.89	−0.39	−0.42	−0.46
1370.41	−0.57	−0.81	−0.79	−0.16	−0.36	−0.38	−0.61	0.48	−0.56	−0.31	−0.34	−0.63	−0.68	1.50	−0.38	−0.30	−0.47
1390.20	−0.40	−0.81	−0.08	0.02	0.29	0.19	−0.52	1.33	−0.82	0.36	−0.88	−0.85	−0.48	0.31	0.09	0.60	−0.49
1414.75	−0.36	−0.81	−0.44	−0.04	2.44	1.66	−0.48	1.83	−0.82	2.26	−0.88	−0.71	−0.56	1.10	2.12	5.15	−0.43
1446.31	−0.58	−0.81	−0.34	−0.14	2.90	2.21	−0.69	1.25	−0.82	2.71	−0.88	−0.71	−0.52	0.30	2.39	4.19	−0.39
1477.29	−1.04	−0.81	−0.31	−0.16	−0.43	−0.65	−1.43	−1.67	−0.82	−0.52	−0.88	−0.69	−1.25	−0.15	−0.44	−0.37	−0.28
1500.06	−1.04	−0.81	0.12	−0.16	−0.44	−0.63	−1.37	−1.44	−0.54	−0.50	−0.34	−0.63	−1.11	−1.09	−0.45	−0.37	−0.32
1500.06	−1.03	0.21	0.01	−0.15	−0.44	−0.61	−1.37	−1.36	−0.53	−0.50	−0.16	−0.59	−1.09	−1.17	−0.44	−0.37	−0.32
1500.06	−1.04	−0.81	0.11	−0.16	−0.44	−0.65	−1.37	−1.44	−0.56	−0.50	−0.25	−0.65	−1.20	−1.09	−0.46	−0.42	−0.35
1500.06	−1.03	0.02	0.02	−0.16	−0.44	−0.62	−1.37	−1.37	−0.51	−0.50	−0.16	−0.62	−1.10	−1.13	−0.45	−0.42	−0.33
1522.86	−1.06	−0.81	−0.39	−0.16	−0.45	−0.57	−1.38	−1.37	−0.28	−0.51	−0.07	−0.56	−0.97	−1.13	−0.40	−0.42	−0.27
1556.13	−0.70	0.55	−0.17	−0.15	−0.42	−0.56	−1.11	−1.78	−0.82	−0.52	−0.43	−0.83	−1.45	−0.26	−0.19	−0.42	−0.45
1577.56	−1.04	−0.81	−0.53	−0.17	−0.45	−0.59	−1.34	−1.35	−0.33	−0.51	0.29	−0.45	−0.90	−1.20	−0.43	−0.42	−0.28
1605.25	−1.02	−0.81	−0.78	−0.18	−0.46	−0.70	−1.20	−1.26	−0.01	−0.49	−0.34	−0.11	−0.54	−1.24	−0.46	−0.42	−0.22
1628.12	0.72	0.93	−0.14	−0.16	−0.43	−0.71	0.90	1.55	−0.27	−0.29	−0.88	−0.36	−0.02	0.63	−0.43	−0.42	−0.34
1628.12	0.71	0.78	−0.13	−0.17	−0.43	−0.72	1.04	1.34	−0.33	−0.28	−0.88	−0.41	−0.30	0.44	−0.43	−0.42	−0.42
1628.12	0.65	0.83	−0.16	−0.15	−0.41	−0.68	0.89	1.85	−0.48	−0.26	0.55	−0.56	−0.09	0.48	−0.40	−0.42	−0.43
1628.12	0.70	0.74	−0.16	−0.16	−0.41	−0.68	1.03	1.56	−0.51	−0.24	−0.34	−0.59	−0.32	0.44	−0.40	−0.42	−0.46
1650.06	−0.57	−0.81	−0.46	−0.17	−0.47	−0.75	−0.58	−0.41	0.21	−0.43	1.37	0.18	0.77	−0.92	−0.51	−0.20	0.34
1676.52	−0.26	−0.81	−0.52	−0.18	−0.48	−0.74	−0.36	−0.60	0.48	−0.51	0.02	0.47	1.39	−0.64	−0.51	−0.09	1.00
1700.96	0.02	0.02	0.95	−0.17	−0.46	−0.75	0.23	0.44	−0.05	−0.37	−0.16	−0.08	0.25	−0.64	−0.50	−0.42	0.03
1728.51	−0.01	0.16	0.17	−0.17	−0.47	−0.56	0.25	−0.27	1.40	−0.50	−0.88	1.63	2.59	0.78	−0.51	1.22	3.15
1753.23	−0.03	0.07	−0.09	−0.12	0.22	−0.39	0.27	1.55	−0.82	0.43	−0.88	−0.89	−0.34	1.42	0.46	−0.42	−0.48
1753.23	−0.01	−0.40	−0.08	−0.12	0.28	−0.38	0.34	1.60	−0.82	0.38	−0.25	−0.83	−0.33	1.36	0.48	−0.42	−0.48
1753.23	−0.27	−0.17	−0.35	−0.12	−0.20	−0.55	0.03	1.81	−0.82	0.02	−0.88	−0.83	−0.26	0.36	−0.19	−0.42	−0.49
1753.23	−0.28	0.12	−0.40	−0.12	−0.18	−0.57	0.03	1.61	−0.82	−0.02	−0.43	−0.90	−0.20	0.27	−0.19	−0.42	−0.49
1772.91	−0.72	−0.81	−0.82	−0.18	−0.47	−0.68	−0.50	−0.35	2.30	−0.51	−0.88	2.32	3.30	3.24	−0.51	0.75	3.10
1802.55	−0.69	−0.81	−0.63	−0.18	−0.47	−0.76	−0.41	−0.74	2.27	−0.51	−0.88	1.60	1.01	−0.88	−0.52	−0.03	0.36
1827.34	−0.71	−0.81	−0.85	−0.18	−0.47	−0.75	−0.64	−0.18	1.44	−0.51	−0.34	1.26	0.66	−0.30	−0.51	0.67	0.55
1851.15	−0.46	−0.81	−0.78	−0.18	−0.47	−0.75	−0.38	0.01	1.35	−0.51	−0.07	1.18	0.15	−0.46	−0.51	0.34	0.46
1877.82	−0.39	−0.81	−0.51	−0.18	−0.47	−0.61	−0.22	−0.43	2.40	−0.51	0.47	2.10	3.58	1.92	−0.51	0.59	4.47
1877.82	−0.37	−0.81	−0.42	−0.18	−0.47	−0.69	0.20	−0.74	2.29	−0.51	0.91	2.50	1.85	1.01	−0.51	0.29	2.12
1877.82	−0.06	0.35	−0.65	−0.18	−0.47	−0.74	0.03	0.02	1.46	−0.51	1.19	1.34	0.45	−0.75	−0.51	0.11	0.48
1877.82	−0.39	−0.81	−0.43	−0.18	−0.47	−0.75	−0.22	−0.87	2.21	−0.51	−0.16	2.41	0.91	−0.69	−0.52	−0.22	0.79
1900.86	−0.07	0.40	−0.67	−0.18	−0.47	−0.74	0.04	0.11	1.55	−0.51	0.74	1.58	0.58	−0.56	−0.51	0.40	0.73
1925.80	−0.28	0.31	−0.52	−0.18	−0.45	−0.51	−0.07	0.41	0.47	−0.37	0.92	0.73	−0.37	−1.06	−0.49	−0.42	−0.39
1949.77	−0.60	−0.81	−0.95	−0.18	−0.47	−0.74	−0.57	−0.36	1.36	−0.51	0.82	1.26	0.05	−1.04	−0.51	−0.09	0.26

gypsum from the core material; a second showing a strong association between sodium, chloride, bromide and lithium, which is probably related to the interstitial pore-water component; and a final group consisting of TIC, hydrogen carbonate, silicon and aluminium, which is possibly a water–rock interaction component.

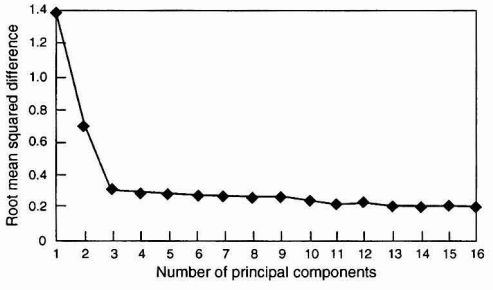

Fig. 4 Roof mean square difference between the measured moisture content and the predicted sample moisture content after target factor analysis plotted against the number of principal components used in the PCA model.

Further evidence for the origin of the different components is obtained by looking at the correlation between the original data, the PCA weights for the first seven factors and the moisture contents for each sample. Principal component 1 (PC1) weights are highly correlated (r^2 >0.9) with calcium, sulfate and strontium but are not correlated to moisture

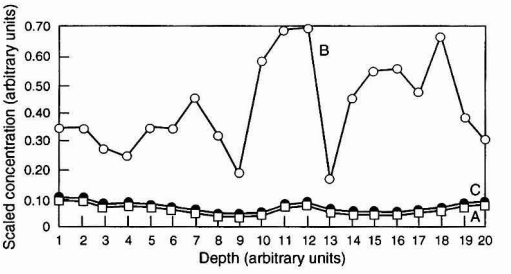

Fig. 5 Graph of actual pore-water data (A), uncorrected pore-water data (B) and TFA predicted pore-water values (C) for iron in the simulated data set.

Table 6 TFA predicted pore-water values for simulated data set (arbitrary units)

Depth	Cl	Br	Li	Ca	Mg	Na	K	Sr	Ba	TIC	SO_4	NO_3	Si	Al	Fe
1	0.61459	0.724727	0.0001	0.033662	0.078469	0.615535	0.225111	0.0001	0.079801	0.14535	0.101968	0.050602	0.00054	0.0001	0.088053
2	0.61459	0.724727	0.0001	0.033662	0.078469	0.615535	0.225111	0.0001	0.079801	0.14535	0.101968	0.050602	0.00054	0.0001	0.088053
3	0.473892	0.571607	0.0001	0.022802	0.058979	0.474699	0.186173	0.0001	0.064405	0.108557	0.069079	0.044805	0.000528	0.0001	0.071147
4	0.455726	0.563008	0.0001	0.018627	0.055227	0.456691	0.192355	0.0001	0.06492	0.10093	0.056437	0.049088	0.000831	0.000284	0.072014
5	0.499818	0.587626	0.0001	0.027832	0.064045	0.500582	0.181356	0.0001	0.064506	0.11872	0.084258	0.040378	0.000442	0.0001	0.071181
6	0.501559	0.553611	0.0001	0.036883	0.6862	0.502115	0.146509	0.0001	0.056642	0.129122	0.111517	0.024271	0.000166	0.0001	0.062301
7	0.475247	0.501553	0.0001	0.040668	0.067811	0.475648	0.116201	0.0001	0.048508	0.128746	0.122877	0.012631	2.06E-06	0.0001	0.053229
8	0.403883	0.424037	0.0001	0.035124	0.057908	0.404216	0.096598	0.0001	0.040732	0.110043	0.106085	0.009759	0.0001	0.0001	0.044691
9	0.477543	0.469457	0.0001	0.049677	0.072452	0.477606	0.08275	0.0001	0.041089	0.139592	0.149461	0.0001	0.0001	0.0001	0.044864
10	0.480545	0.472374	0.0001	0.049999	0.072912	0.480607	0.083235	0.0001	0.04134	0.140482	0.150427	0.0001	0.0001	0.0001	0.045136
11	0.743239	0.725015	0.0001	0.07893	0.113491	0.743089	0.123024	0.0001	0.062772	0.219284	0.237021	0.0001	0.0001	0.0001	0.068335
12	0.826554	0.803443	0.0001	0.088572	0.12658	0.826271	0.133921	5.5E-05	0.069212	0.244911	0.265788	0.0001	0.0001	0.0001	0.075265
13	0.610561	0.593764	0.0001	0.065327	0.09347	0.610374	0.099228	1.02E-05	0.051182	0.180847	0.196092	0.0001	0.0001	0.0001	0.055697
14	0.513483	0.499359	0.0001	0.054961	0.078626	0.51333	0.083468	3E-05	0.043048	0.152114	0.164929	0.0001	0.0001	0.0001	0.046857
15	0.512627	0.498947	0.0001	0.054757	0.078442	0.512491	0.083754	2.36E-05	0.043064	0.151704	0.164336	0.0001	0.0001	0.0001	0.046884
16	0.512627	0.498947	0.0001	0.054757	0.078442	0.512491	0.083754	2.36E-05	0.043064	0.151704	0.164336	0.0001	0.0001	0.0001	0.046884
17	0.6117	0.595296	0.0001	0.06534	0.093593	0.611529	0.099843	8.24E-06	0.051367	0.19614	0.164336	0.0001	0.0001	0.0001	0.055907
18	0.713766	0.694577	0.0001	0.076282	0.10918	0.713556	0.116438	3.64E-05	0.05993	0.211224	0.228934	0.0001	0.0001	0.0001	0.065202
19	0.810837	0.78898	0.0001	0.086656	0.124065	0.810593	0.132202	2.72E-05	0.068066	0.239952	0.260101	0.0001	0.0001	0.0001	0.074042
20	0.909909	0.885331	0.0001	0.097248	0.13922	0.909628	0.148293	2.15E-05	0.076371	0.269272	0.291912	0.0001	0.0001	0.0001	0.083064

Table 7 Actual pore-water component for the simulated data set (arbitrary units)

Depth	Cl	Br	Li	Ca	Mg	Na	K	Sr	Ba	TIC	SO_4	NO_3	Si	Al	Fe
1	0.51	0.71	0.0101	0.102	0.51	0.302	0.101	0.101	0.103	0.104	0.1001	0.0101	0.0101	0.0101	0.101
2	0.51	0.71	0.0101	0.102	0.51	0.302	0.101	0.101	0.103	0.104	0.1001	0.0101	0.0101	0.0101	0.101
3	0.41	0.57	0.0081	0.082	0.082	0.41	0.242	0.081	0.081	0.083	0.084	0.0801	0.0081	0.0081	0.081
4	0.41	0.57	0.0081	0.082	0.082	0.41	0.242	0.081	0.081	0.083	0.084	0.0801	0.0081	0.0081	0.081
5	0.45	0.59	0.008	0.09	0.09	0.45	0.23	0.08	0.08	0.1	0.11	0.071	0.008	0.008	0.08
6	0.45	0.55	0.007	0.09	0.09	0.45	0.19	0.07	0.07	0.11	0.13	0.052	0.007	0.007	0.07
7	0.4	0.48	0.006	0.08	0.08	0.4	0.16	0.06	0.06	0.1	0.12	0.042	0.006	0.006	0.06
8	0.35	0.41	0.005	0.07	0.07	0.35	0.13	0.05	0.05	0.09	0.11	0.032	0.005	0.005	0.05
9	0.45	0.47	0.005	0.09	0.09	0.45	0.11	0.05	0.05	0.13	0.17	0.014	0.005	0.005	0.05
10	0.45	0.47	0.005	0.09	0.09	0.45	0.11	0.05	0.05	0.13	0.17	0.014	0.005	0.005	0.05
11	0.725	0.735	0.0075	0.145	0.145	0.725	0.155	0.075	0.075	0.215	0.285	0.012	0.0075	0.0075	0.075
12	0.81	0.814	0.0082	0.162	0.162	0.81	0.166	0.082	0.082	0.242	0.322	0.0	0.0082	0.0082	0.082
13	0.605	0.607	0.0061	0.121	0.121	0.605	0.123	0.061	0.061	0.181	0.241	0.007	0.0061	0.0061	0.061
14	0.505	0.507	0.0051	0.101	0.101	0.505	0.103	0.051	0.051	0.151	0.201	0.006	0.0051	0.0051	0.051
15	0.505	0.507	0.0051	0.101	0.101	0.505	0.103	0.051	0.051	0.151	0.201	0.006	0.0051	0.0051	0.051
16	0.505	0.507	0.0051	0.101	0.101	0.505	0.103	0.051	0.051	0.151	0.201	0.006	0.0051	0.0051	0.051
17	0.605	0.607	0.0061	0.121	0.121	0.605	0.123	0.061	0.061	0.181	0.241	0.007	0.0061	0.0061	0.061
18	0.705	0.707	0.0071	0.141	0.141	0.705	0.143	0.071	0.071	0.211	0.281	0.008	0.0071	0.0071	0.071
19	0.805	0.807	0.0081	0.161	0.805	0.163	0.081	0.081	0.081	0.241	0.321	0.009	0.0081	0.0081	0.081
20	0.905	0.907	0.0091	0.181	0.181	0.905	0.183	0.091	0.091	0.271	0.361	0.01	0.0091	0.0091	0.091

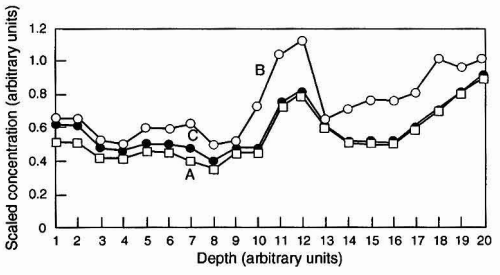

Fig. 6 Graph of actual pore-water data (A), uncorrected pore-water data (B) and TFA predicted pore-water values (C) for sodium in the simulated data set.

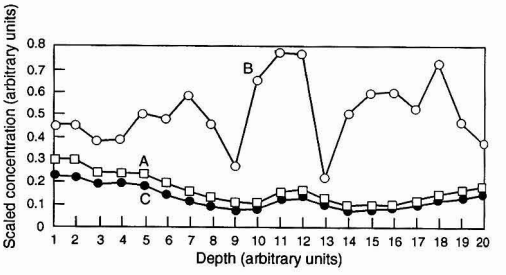

Fig. 7 Graph of actual pore-water data (A), uncorrected pore-water data (B) and TFA predicted pore-water values (C) for potassium in the simulated data set.

Table 8 Scaled pore-water composition as predicted by the TFA method (arbitrary units)

Depth/m	Cl	Br	H^+	Ca	Mg	Na	K	HCO_3	SO_4	NO_3	TIC	Si	Ba	Sr	Mn	Al
725.46	0.56	0.97	−0.08	−0.39	0.78	0.11	−1.43	−0.99	−0.52	−0.82	−0.79	−0.75	−1.06	−0.41	0.04	−0.53
749.80	2.06	1.98	0.01	−0.33	1.92	1.53	−1.28	−0.97	−0.52	−0.45	−0.61	−0.13	0.92	−0.40	0.40	−0.53
802.67	1.09	1.30	−0.05	−0.37	1.19	0.61	−1.38	0.98	−0.52	−0.69	−0.73	−0.53	−1.01	−0.41	0.17	−0.53
852.50	1.69	1.64	−0.01	−0.35	1.68	1.18	−1.32	−0.98	−0.52	−0.53	−0.66	−0.25	−0.95	−0.41	0.32	−0.53
908.46	1.27	1.26	−0.03	−0.37	1.41	0.78	−1.35	−0.98	−0.52	−0.62	−0.71	−0.38	−0.97	−0.42	0.22	−0.53
981.25	2.49	2.26	0.04	−0.32	2.25	1.94	−1.23	−0.97	−0.52	−0.34	−0.56	0.05	−0.88	−0.40	0.50	−0.53
981.25	2.29	1.93	0.03	−0.33	2.19	1.74	−1.25	−0.97	−0.52	−0.37	−0.59	0.04	−0.88	−0.42	0.46	−0.53
981.25	2.71	2.21	0.06	−0.31	2.50	2.13	−1.20	0.96	−0.52	−0.27	−0.54	0.21	−0.84	−0.41	0.56	−0.53
981.25	2.25	1.78	0.04	−0.33	2.21	1.69	−1.26	−0.96	−0.52	−0.37	−0.60	0.06	−0.87	−0.43	0.45	−0.53
1028.05	1.84	2.02	−0.01	−0.34	1.66	1.33	−1.31	−0.98	−0.52	−0.52	−0.63	−0.29	−0.97	−0.38	0.34	−0.53
1134.45	0.45	0.55	−0.07	−0.40	0.85	−0.01	−1.41	−0.99	−0.52	−0.82	−0.81	−0.66	−1.03	−0.44	0.03	−0.53
1180.08	−0.41	−0.81	−0.08	−0.43	0.54	−0.85	−1.43	−0.98	−0.52	−0.96	−0.94	−0.72	−1.02	−0.52	−0.18	−0.53
1180.08	−0.53	−0.81	−0.09	−0.44	0.40	−0.96	−1.43	−0.98	−0.52	−1.00	−0.95	−0.80	−1.05	−0.52	−0.20	−0.53
1180.08	−0.51	−0.81	−0.09	−0.44	0.43	−0.94	−1.43	−0.98	−0.52	−0.99	−0.95	−0.78	−1.04	−0.52	−0.20	−0.53
1180.08	−0.52	−0.82	−0.09	−0.44	0.42	−0.94	−1.43	−0.98	−0.52	−0.99	−0.95	−0.79	−1.04	−0.52	−0.20	−0.53
1237.16	−0.40	−0.81	−0.08	−0.43	0.55	−0.84	−1.43	−0.98	−0.52	−0.95	−0.94	−0.71	−1.02	−0.52	−0.17	−0.53
1324.93	−0.44	−0.81	−0.08	−0.44	0.51	−0.87	−1.43	−0.98	−0.52	−0.97	−0.94	−0.74	−1.03	−0.52	−0.18	−0.53
1370.41	−0.53	−0.81	−0.09	−0.44	0.41	−0.96	−1.43	−0.98	−0.52	−1.00	−0.95	−0.80	−1.05	−0.52	−0.20	−0.53
1370.41	−0.56	−0.81	−0.10	−0.44	0.37	−0.98	−1.44	−0.98	−0.52	−1.01	−0.95	−0.81	−1.05	−0.52	−0.21	−0.53
1370.41	−0.55	−0.81	−0.10	−0.44	0.39	−0.97	−1.43	−0.98	−0.52	−1.00	−0.95	−0.81	−1.05	−0.52	−0.21	−0.53
1370.41	−0.57	−0.81	−0.10	−0.45	0.36	−0.99	−1.44	−0.98	−0.52	−1.01	−0.95	−0.82	−1.05	−0.52	−0.21	−0.53
1390.20	−0.40	−0.81	−0.08	−0.43	0.55	−0.83	−1.43	−0.98	−0.52	−0.95	−0.94	−0.71	−1.02	−0.52	−0.17	−0.53
1414.75	−0.36	−0.81	−0.07	−0.43	0.60	−0.80	−1.42	−0.97	−0.52	−0.94	−0.93	−0.68	−1.01	−0.52	−0.16	−0.53
1446.31	−0.58	−0.81	−0.10	−0.45	0.35	−1.00	−1.44	−0.98	−0.52	−1.01	−0.96	−0.83	−1.06	−0.52	−0.22	−0.53
1477.29	−1.04	−0.81	−0.14	−0.47	−0.16	−1.41	−1.46	−1.00	−0.52	−1.18	−1.01	−1.13	−1.14	−0.49	−0.35	−0.53
1500.06	−1.04	−0.81	−0.14	−0.47	−0.16	−1.41	−1.46	−1.00	−0.52	−1.18	−1.01	−1.13	−1.14	−0.49	−0.35	−0.53
1500.06	−1.03	0.21	−0.18	−0.45	−0.56	−1.37	−1.62	−1.00	−0.52	−1.25	−0.95	−1.47	−1.21	−0.38	−0.37	−0.47
1500.06	−1.04	−0.81	−0.14	−0.47	−0.16	−1.41	−1.46	−1.00	−0.52	−1.18	−1.01	−1.12	−1.14	−0.49	−0.35	−0.53
1500.06	−1.03	0.02	−0.17	−0.45	−0.48	−1.38	−1.59	−1.00	−0.52	−1.23	−0.96	−1.43	−1.20	−0.40	−0.36	−0.51
1522.86	−1.06	−0.81	−0.15	−0.47	−0.17	−1.42	−1.46	−1.00	−0.52	−1.18	−1.01	−1.13	−1.14	−0.49	−0.36	−0.53
1556.13	0.70	−0.55	−0.17	−0.44	−0.36	−1.06	−1.60	−1.00	−0.52	−1.18	−0.91	−1.40	−1.20	−0.37	−0.30	−0.51
1577.56	−1.04	−0.81	−0.14	−0.47	−0.15	−1.41	−1.46	−1.00	−0.52	−1.18	−1.00	−1.12	−1.14	−0.49	−0.35	−0.53
1605.25	−1.02	−0.81	−0.14	−0.46	−0.13	−1.39	−1.46	−1.00	−0.52	−1.17	−1.00	−1.11	−1.14	−0.49	−0.35	−0.53
1628.12	0.72	0.93	−0.06	−0.39	0.97	0.26	−1.40	−0.99	−0.52	−0.77	−0.77	−0.63	−1.03	−0.42	0.09	−0.53
1628.12	0.71	0.78	−0.06	−0.39	1.02	0.24	−1.39	−0.98	−0.52	−0.75	−0.78	−0.58	−1.01	−0.44	0.09	−0.53
1628.12	0.65	0.83	−0.07	−0.39	0.93	0.18	−1.41	−0.99	−0.52	−0.78	−0.79	−0.64	−1.03	−0.43	0.07	−0.53
1628.12	0.70	0.74	−0.06	−0.39	1.03	0.23	−1.39	−0.98	−0.52	−0.76	−0.78	−0.57	−1.01	−0.44	0.08	−0.53
1650.06	−0.57	−0.81	−0.10	−0.45	0.36	−0.99	−1.44	−0.98	−0.52	−1.01	−0.96	−0.82	−1.05	−0.52	−0.21	−0.53
1676.52	−0.26	−0.81	−0.06	−0.42	0.71	−0.70	−1.41	−0.97	−0.51	−0.91	−0.92	−0.61	−0.99	−0.52	−0.14	−0.53
1700.96	0.02	0.02	−0.09	−0.42	0.62	−0.42	−1.42	−0.99	−0.52	−0.90	−0.87	−0.75	−1.05	−0.47	−0.07	−0.53
1728.51	−0.01	0.16	−0.10	−0.42	0.53	−0.45	−1.44	−0.99	−0.52	−0.92	−0.87	−0.83	−1.07	−0.45	−0.08	−0.53
1753.23	−0.03	−0.07	−0.09	−0.42	0.55	−0.46	−1.44	−0.99	−0.52	−0.92	−0.88	−0.80	−1.06	−0.46	−0.09	−0.53
1753.23	−0.01	0.40	−0.11	−0.42	0.42	−0.43	−1.47	−0.99	−0.52	−0.95	−0.86	−0.92	−1.09	−0.43	−0.09	−0.53
1753.23	−0.27	−0.17	−0.10	−0.43	0.40	−0.69	−1.45	−0.99	−0.52	−0.97	−0.91	−0.87	−1.07	−0.47	−0.14	−0.53
1753.23	−0.28	0.12	−0.12	−0.43	0.27	−0.69	−1.48	−1.00	−0.52	−1.00	−0.90	−0.98	−1.10	−0.44	−0.15	−0.53
1772.91	−0.72	−0.81	−0.11	−0.45	0.20	−1.12	−1.45	−0.99	−0.52	−1.06	−0.97	−0.92	−1.08	−0.51	−0.26	−0.53
1802.55	−0.69	−0.81	−0.11	−0.45	0.23	−1.10	−1.44	−0.99	−0.52	−1.05	−0.97	−0.90	−1.08	−0.51	−0.25	−0.53
1827.34	−0.71	−0.81	−0.11	−0.45	0.21	−1.11	−1.45	−0.99	−0.52	−1.05	−0.97	−0.91	−1.08	−0.51	−0.25	−0.53
1851.15	−0.46	−0.81	−0.08	−0.44	0.48	−0.89	−1.43	−0.98	−0.52	−0.97	−0.94	−0.75	−1.03	−0.52	−0.19	−0.53
1877.82	−0.39	−0.81	−0.07	−0.43	0.56	−0.83	−1.43	−0.98	−0.52	−0.95	−0.93	−0.70	−1.02	−0.52	−0.17	−0.53
1877.82	−0.37	−0.81	−0.07	−0.43	0.58	−0.81	−1.42	−0.97	−0.52	−0.95	−0.93	−0.69	−1.01	−0.52	−0.17	−0.53
1877.82	−0.06	0.35	−0.11	−0.42	0.40	−0.48	−1.47	−0.99	−0.52	−0.96	−0.87	−0.93	−1.09	−0.43	−0.10	−0.53
1877.82	−0.39	−0.81	−0.07	−0.43	0.56	−0.83	−1.43	−0.98	−0.52	−0.95	−0.93	−0.70	−1.02	−0.52	−0.17	−0.53
1900.86	0.07	0.40	−0.11	−0.42	0.36	−0.49	−1.48	−1.00	−0.52	−0.96	−0.87	−0.95	−1.10	−0.43	−0.11	−0.53
1925.80	−0.28	0.31	−0.12	−0.42	0.19	−0.68	−1.50	−1.00	−0.52	−1.02	−0.89	−1.05	−1.12	−0.42	−0.16	−0.53
1949.77	−0.60	−0.81	−0.10	−0.45	0.33	−1.02	−1.44	−0.98	−0.52	−1.02	−0.96	−0.84	−1.06	−0.52	−0.22	−0.53

content (r^2 <0.2), confirming that this component is not related to an interstitial pore-water content but is more likely due to gypsum dissolution. Principal component 2 (PC2) weights are highly correlated (r^2 >0.79) with moisture content, sodium, chloride, bromide and lithium, which suggests that this component arises from residual salts obtained from a true interstitial pore-water contaminated with drilling fluid. The majority of the remaining variance of chloride is assocated with PC3, which is also significantly correlated with moisture content ($r^2 = -0.46$), and suggests that this PC is also a pore-water component. That there are two such components suggests that the pore-water within the core material tested is derived from two sources, although it is unclear at this stage whether this is a leaching effect or a reflection of the true geochemistry.

The high correlation of moisture content with PC2 weights ($r^2 = 0.85$) suggests that moisture content is a true factor of the data. This is confirmed by using moisture content (scaled by mean centring) as a target factor which produces a predicted vector very close to the original values (Fig. 10). It is interesting to note that chemical analysis of aqueous leachates obtained from dry crushed core material could be used to independently predict values for *in situ* moisture content.

These qualitative data show strong evidence that the PCA has identified components that have true geochemical meaning. Those that are most clearly defined are: a component due to gypsum dissolution; a component due to carbonate dissolution; and two components derived from pore-water residual solutes. This is very close to the conceptual model with the exception that a component due to drilling fluid contamination is not clearly identified.

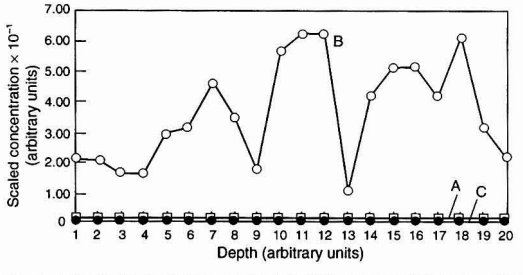

Fig. 8 Graph of actual pore-water data (A), uncorrected pore-water data (B) and TFA predicted pore-water values (C) for silicon in the simulated data set.

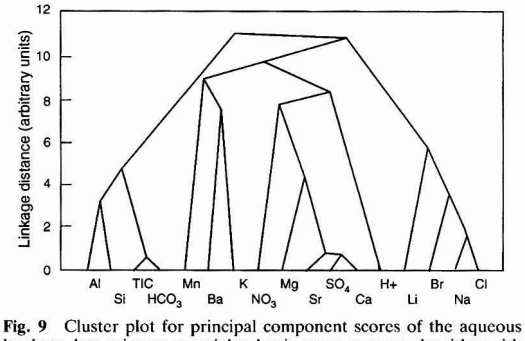

Fig. 9 Cluster plot for principal component scores of the aqueous leachate data using an unweighted pair group average algorithm with euclidean distances.

For the results of the TFA data reconstruction to be meaningful it is also necessary that the halides (chloride and bromide) are substantially derived from the pore-water. Although the actual pore-water compositions are unknown for this borehole, there are data available from 6 zones down the borehole where groundwater flow could be induced by discrete extraction tests (DETs). The composition of these groundwaters may not be the same as the pore-water compositions but are, at present, the only source of independently derived data that can be compared with the pore-water data obtained from aqueous leaching. By taking the moisture content of the nearest rock sample to each DET sampling zone, the flowing groundwater data were converted to micrograms of determinand per gram of rock, scaled and directly compared to the aqueous leachate data. Fig. 11 shows the chloride data for the aqueous leachates and the DET values and shows reasonable agreement at shallower depths and excellent agreement for the deepest DETs. This provides strong evidence that the assumption regarding the halides is correct. The graphs show how the higher density of data obtained by aqueous leaching compared to DETs gives rise to fine structure in the salinity profiles that would otherwise not be apparent.

In a similar manner to that shown in the simulated data set, the degree of success for the reconstruction of each determinand is variable. In all cases, however, the often significant enhancements caused by localized gypsum dissolution and dissolution of the bulk core material have been substantially eliminated.

Comparisons between the reconstructed data and the original data are shown in Figs. 12–15 with the same designation of data as for the simulated data set. Hydrogen carbonate data (Fig. 12), give reconstructed values that not only eliminate non-pore-water components but also agree very closely with the groundwater data. Reconstructed calcium (Fig. 13), barium, strontium and TIC data also

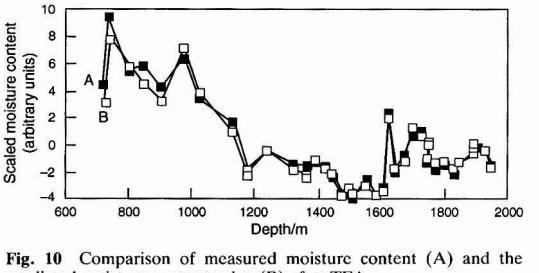

Fig. 10 Comparison of measured moisture content (A) and the predicted moisture content value (B) after TFA.

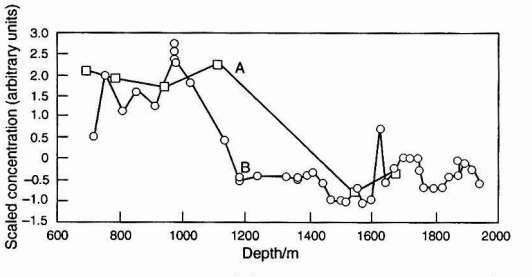

Fig. 11 Graph of DET data (A) and uncorrected pore-water data (B) for chloride in the aqueous leachate data set.

eliminate enhanced components arsing from dissolution of the core material and give compositions that are of the same order as the DET data. Reconstructed magnesium and sodium values are not substantially changed from the aqueous leachate data and are similar to DET values which suggests

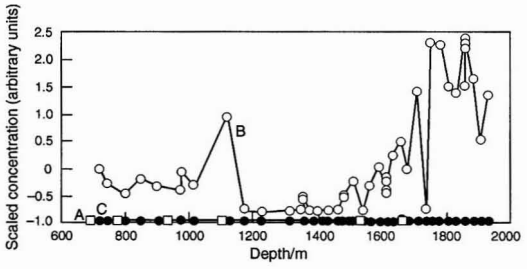

Fig. 12 Graph of DET data (A), uncorrected pore-water data (B) and TFA predicted data (C) for hydrogen carbonate in the aquoues leachate data set.

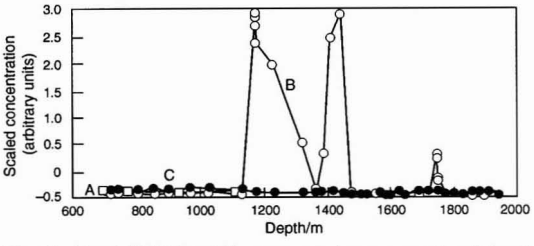

Fig. 13 Graph DET data (A), uncorrected pore-water data (B) and TFA predicted data (C) for calcium in the aqueous leachate data set.

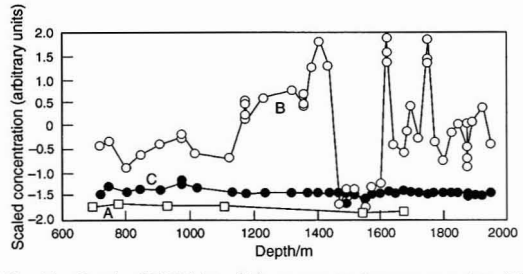

Fig. 14 Graph of DET data (A), uncorrected pore-water data (B) and TFA predicted data (C) for potassium in the aqueous leachate data set.

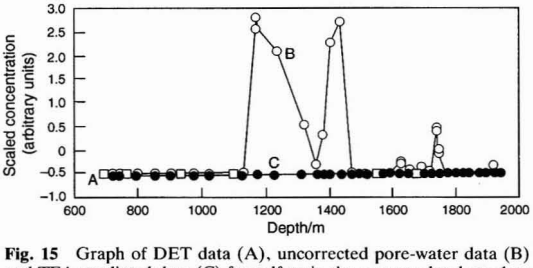

Fig. 15 Graph of DET data (A), uncorrected pore-water data (B) and TFA predicted data (C) for sulfate in the aqueous leachate data set.

that most of these leached salts are derived from pore-water sources.

For potassium (Fig. 14), silicon, sulfate (Fig. 15) and aluminium the corrected data are very much less than the raw aqueous leachate data suggesting that a large proportion of these determinands is derived from rock dissolution. Despite the substantial correction by the TFA method, the DET values for these determinands are significantly different from the corrected values; potassium and silicon still giving data significantly enhanced with respect to DET compositions, whilst aluminium and sulfate are reduced to scaled values almost equivalent to zero concentration. At this stage, it is not known if this is caused by a bias in the reconstruction procedure or whether the data represent true differences between flowing groundwater and pore-water compositions.

Conclusions

A multivariate statistical method for reconstructing pore-water compositions from aqueous leachate data has been proposed. The method has been successfully tested on a simulated data set. The assumptions used in the procedure have been tested on aqueous leachate data from a Sellafield borehole and there is strong evidence that these assumptions hold true in real samples. The method has been applied to the real data set producing data that are consistent with independently derived groundwater data from the borehole for most determinands.

The method requires further work to understand fully the limitations of the procedure and further studies, possibly using core material spiked with synthetic pore-waters, to help fully validate this statistical approach. The procedure does have the potential to be of use as an extremely powerful investigation tool in a wide range of environmental applications.

The authors are grateful to J. K. Trick, P. A. Blackwell and K. A. Green for carrying out the experimental and analytical work and to Dr. C. J. B. Gowing for helpful comments on the text. The authors also acknowledge UK Nirex for funding this investigation. This paper is published with the approval of Director, British Geological Survey (NERC).

References

1 Sholkovitz, E., *Geochim. Cosmochim. Acta*, 1973, **37**, 2043.
2 Edmunds, W., and Bath, A. H., *Environ. Sci. Technol.*, 1976, **10**, 476.
3 Swalan, J. J., and Murray, J. W., *Earth Planet Sci. Lett.*, 1983, **64**, 213.
4 Manger, G. E., and Wertman, W. T., *U.S. Geol. Surv. Prof. Pap.* 1967, 575C, 192.
5 Murthy, A. S. P., and Ferrell, R. E., *Clays Clay Miner.*, 1972, **20**, 317.
6 Schmidt, G. W., *Bull. Am. Assoc. Petrol. Geol.*, 1973, **57**, 321.
7 Acquilina, L., Boulegue, J., Sureau, J. F., and Bariac, T., *Appl. Geochim.*, 1994, **9**, 657.
8 Reyment R. A., Jöreskog, K. G., and Marcus, L. F., *Applied Factor Anlaysis in the Natural Sciences*, Cambridge University Press, Cambridge, 2nd edn., 1993.
9 Dawdy, D. R., and Feth, J. H., *Water Resour. Res.*, 1967, **3**, 505.
10 Hitchon, B., Billings, K. G., and Klovan, J. E., *Geochim. Cosmochim. Acta*, 1971, **35**, 567.
11 Knudson, E. J., Duewer, D. L., Christian, G. D., and Larson, T. V., in *Chemometrics: Theory and Application*, ed. Kowalski, B. R., *ACS Symposium Series 52*, ACS, Washington, D.C., 1977, pp. 80–116.
12 Zhang, P., Dudley, N., Ure, A. M., and Littlejohn, D., *Anal. Chim. Acta*, 1992, **258**, 1.
13 Gamp, H., Maeder, M., Meyer, C. J., and Zuberbuhler, A. D., *Talanta*, 1985, **39**, 315.

14 Ho, C. N., Christian, G. D., and Davidson, E. R., *Anal. Chem.*, 1978, **52**, 1108.
15 Burns, D. H., Callis, J. B., and Christian, G. D., *Anal. Chem.*, 1986, **58**, 2805.
16 Alpert, D. J., and Hopke, P.K., *Proceedings of the Conference on Quality Assurance Environmental Measures*, Denver, CO, 1978, 204.
17 Malinowski, E. R., *Factor Analysis in Chemistry*, Wiley, New York, 2nd edn., 1991.
18 Hopke, P. K., *Chemom. Intell. Lab. Syst.*, 1989, **6**, 7.
19 Wold, S., Esbenson, K., and Geladi, P., *Chemom. Intell. Lab. Syst.*, 1987, **2**, 37.

Paper 4/06233G
Received October 12, 1994
Accepted March 6, 1995

Estimation of Sampling Bias Between Different Sampling Protocols on Contaminated Land*

Michael H. Ramsey and Ariadni Argyraki
Department of Geology, Imperial College, London, UK SW7 2BP
Michael Thompson
Department of Chemistry, Birkbeck College, London, UK WC1H 0PP

A method has been devised for the estimation of sampling bias between different sampling protocols on contaminated land. A pilot study was conducted at one site of contaminated land near Wirksworth in Derbyshire. Four sampling schemes (simple regular grid taking single auger samples, regular grid taking five-fold composite samples, herringbone and stratified random) were applied to sample topsoil. The samples were decomposed with nitric and perchloric acids and analysed using ICP-AES for 24 elements. The interpretation of the results was focused on the study of two elements with contrasting properties: lead, which shows high geochemical variability across the field and copper, with very low geochemical variation. Although the mean lead concentrations vary markedly between the different sampling protocols (*e.g.*, 5680–6868 μg g^{-1}) the differences are not statistically significant owing to the high geochemical variability of lead, quantified as geochemical variance. For copper with much lower geochemical variance a significant sampling bias of 2.45 μg g^{-1} was detected between two of the sampling designs (*i.e.*, the simple regular grid and the stratified random design). The methodology could be applied for more demanding studies such as interlaboratory trials for estimating sampling bias between different sampling organizations at this site.

Keywords: *Sampling; bias; sampling protocol; quality control; heavy metal contamination*

Introduction

Sampling is an integral part of the measurement process that is often neglected in terms of the errors that it generates. Systematic error in sampling, expressed as sampling bias affects the results of every environmental survey to some extent. Specifically, undetected sampling bias within measurements for the classification of contaminated land has implications that are both financial and medical owing to the potential toxicity of the soils to human health. The presence of sampling bias can invalidate the interpretation of chemical analyses no matter how high the quality. The full importance of sampling bias cannot be judged at present because of the lack of any method for its determination.

There are four main types of measurement error in environmental geochemistry. Analytical and sampling precision describe the random measurement errors and are often expressed as variances, s^2 (the square of the standard deviation, s) whereas the analytical and sampling bias describe the systematic errors. Methods have now been developed for the estimation of the first three types of error. Such methods utilize the collection of duplicate samples with duplicated analyses for the estimation of sampling and analytical precision[1] and use certified reference materials for the estimation of analytical bias.[2] No method has yet been described for the estimation of sampling bias in general or for this particular application of environmental sampling.

There are many texts that give information on general sampling practice in different environmental media[3] but the emphasis has been on how to improve sampling technique rather than on estimating the errors introduced. Gy has suggested that sampling bias can be avoided by ensuring correctness in the sampling procedure and, in effect, he denies the possibility of estimating systematic error in sampling.[4] However the idea of devising methods for the estimation of sampling bias that are analogous to the methods already in use for the estimation of analytical bias has recently been suggested.[5]

This paper discusses the feasibility of measuring sampling bias, by considering the simplest case; bias between different sampling protocols on a single area of contaminated land. These findings are then used to assess the experimental design that would be required for the estimation of sampling bias between different organizations. The ultimate estimation of absolute sampling bias using such an area as a reference sampling target (RST), analogous to the use of a reference material (RM) for the estimation of analytical bias, is also considered.

Experimental

A pilot study was conducted at one site of contaminated land near Wirksworth, Derbyshire in the English Midlands, originally described by Maskall.[6] This site was considered appropriate when judged by several criteria: *i.e.*, (*i*) substantial concentrations of heavy metals at the site (owing, in this case, to use of the site for lead smelting in medieval times (1300–1550 AD); (*ii*) the absence of factors that might cause short term variation of the metal concentration (*e.g.*, flooding); (*iii*) no recent or current cultivation or remediation (this field was last ploughed in 1948); (*iv*) dimensions that are typical of contaminated land investigations (in this instance 1.76 ha); and finally (*v*) the cooperation of the owner.

Four different sampling protocols were applied to sample the topsoil (0–15 cm) (Fig. 1). They were selected on the basis of representativeness and common usage. These protocols were: (*a*) a simple regular grid design taking a single auger sample every 20 m described by Webster;[7] (*b*) a composite regular grid being the same as (*a*) but taking five-fold composite auger samples in a shape of X over a 1 m^2 area; (*c*) a herringbone design with an alternate 5 m offset the regular square grid,[8] and (*d*) a stratified random design.[7] In the

* Presented at Geoanalysis 94: An International Symposium on the Analysis of Geological and Environmental Materials, Ambleside, England, September 18–22, 1994.

random design (*d*), the coordinates of sampling within each 20 m square were taken from a uniform random number distribution generated within a statistical spread sheet (MINITAB). Designs (*a*), (*c*) and (*d*) all used single auger samples at each sampling point (diameter 2.5 cm). In all the designs the sampling precision was estimated by taking sampling duplicates at 2 m distance away from the initial sampling point in random direction. This distance was selected to represent the possible error in the location of the sampling point in the field and therefore to make a realistic estimate of the sampling repeatability variance.

All soil samples were dried at 65 °C, disaggregated in a pestle and mortar and the <2 mm fraction was ground (<100 μm). Analytical test portions of these samples were decomposed in a mixture of nitric and perchloric acids and analysed by ICP-AES for a suite of 24 elements.[9] Analytical duplicates were prepared for each sampling duplicate, for the estimation of sampling and analytical precision.[1] Reagent blanks and six certified soil reference materials were analysed at random positions between the sample test portions for the estimation of analytical bias.[2]

Results

The statistical interpretation of analytical measurements focused on the study of two elements with contrasting properties, lead and copper. Lead shows a high geochemical variability (*i.e.*, high variance of the true metal concentration between the sampling points) across the site whilst copper shows very little geochemical variation. This would apply to lateral variability but also to the vertical variance of metal concentration in this soil profile discussed by Maskall and Thornton.[6]

The measurement errors can be considered to have two aspects. Firstly, sampling and analytical quality control as previously described, was applied to estimate only the random measurement errors of lead and copper;[1] and secondly, for the estimation of sampling and analytical precisions, a nested design of sample and analytical duplicates was used. Robust analysis of variance (ANOVA) was applied to the concentrations measured for the sampling and analytical duplicates so as to estimate separately the geochemical, sampling and analytical variances.[1] Pie charts for the lead variance in soil using the data from all four protocols (Fig. 2) show that the analytical precision is acceptable as it contributes less than 4% to the over-all variance.[10] Similarly the combined sampling and analytical precision is also acceptable contributing less than 20% to the over-all variance. The pie charts also give a clear indication of the effect of composite sampling, showing a significant improvement of sampling variance (from 5.2% for single auger samples to 2.7% for composite samples) in the instance of lead. This change in variance was shown to be statistically significant using the *F*-test at the 95% confidence level. For copper data from all the sampling designs the analytical variance (1.7% over total variance) is well within the 4% limit but the large sampling variance of 29.7% of total, makes the measurement precision to be over the 20% acceptable for spatial interpretation of the concentration estimates. However, the mean concentration results can be interpreted within their stated uncertainties. The high proportion of sampling error, in this instance, is due primarily to the relatively low geochemical variance of copper.

The frequency distribution for the mean Pb concentration at each sampling point show a positive skew and approaches a lognormal distribution (Fig. 3). The concentration of lead is

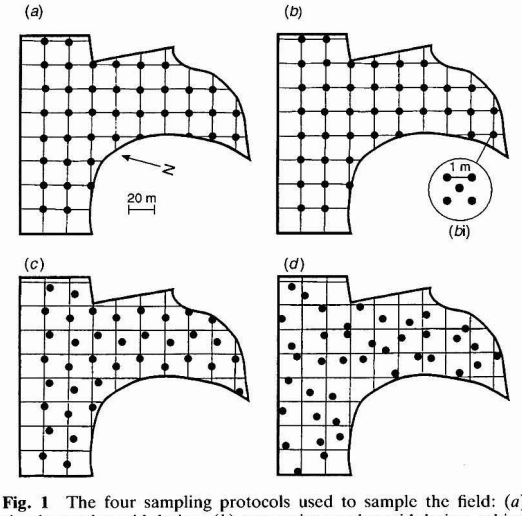

Fig. 1 The four sampling protocols used to sample the field: (*a*) simple regular grid design; (*b*) composite regular grid design, taking five-fold composite auger samples at each sampling point (*bi*); (*c*) herringbone design with alteration 5 m offset the regular square grid; and (*d*) stratified random design.

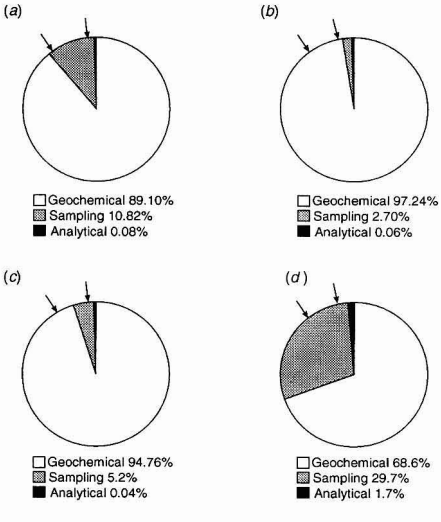

Fig. 2 Relative importance of measurement errors (from sampling and analysis) and geochemical variability, both expressed as proportions of total variance. Estimates of variance were made using Robust ANOVA and were compared with the accepted levels of 4% of the total for analytical variance and 20% of the total for measurement variance (from Ramsey *et al.*,[10]), indicated by arrows on the charts. (*a*) Proportions of sampling, analytical and geochemical variances for Pb data from the four sampling protocols combined, showing acceptable levels of measurement variance (<20% of total variance). Significant improvement of sampling variance was obtained by taking (*b*) five-fold composite samples at each sampling point instead of (*c*) single auger samples on the regular grid. (*d*) Proportions of measurement and geochemical variances for Cu data from all the sampling designs, showing high sampling variance of 29.7% due to the relatively low geochemical variance of 68.6%.

generally high with a geometric mean of 6000 μg g^{-1} and a maximum of 30000 μg g^{-1} in the soil. The distribution of copper is closer to the normal distribution with a mean of around 27 μg g^{-1}, about double the natural background concentration expected in a soil of 15 μg g^{-1}.[11]

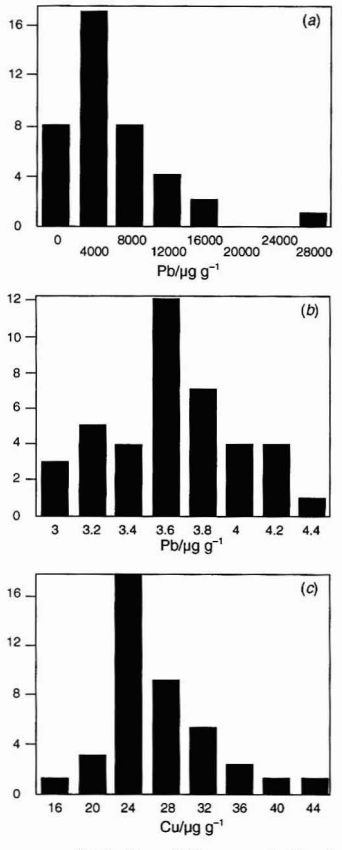

Fig. 3 Frequency distribution of Pb concentration in soil for the simple regular grid design, showing (*a*) positively skewed population, that approximates (*b*) the log-normal distribution. (*c*) Frequency distribution of Cu concentration in soil for the simple regular grid design, showing a slight positive skew.

For the systematic measurement errors the estimates of analytical bias made from the six certified reference materials were generally small (<5%) for both lead and copper (Table 1). Most of the estimates of bias were not statistically different from zero, using the *t*-test with 95% confidence interval. The analytical bias was also estimated over a range of concentrations by fitting a maximum likelihood functional relationship (MLFR) between the measured and certified elemental concentrations.[12] The MLFR technique resolves the bias into its translational component (*i.e.*, fixed μg g^{-1} bias) and its rotational component (*i.e.*, the bias as a fixed proportion of the concentration). It also takes into account the uncertainties on both the measured and the certified values, unlike least squares regression. No translational bias was detected, but significant rotational bias of −3.3% was found for both lead and copper, suggesting that the cause might be volumetric.

The mean concentrations of lead measured by the four different sampling protocols vary widely between 5680 μg g^{-1} and 6868 μg g^{-1} (Table 2). When sampling bias is calculated between each of these values and the best estimate of the 'true value' (the grand mean of 6233 μg g^{-1}) the bias values range from −8.9 to +10.2%. However, when the sampling bias between the geometric mean Pb concentrations is estimated by selected pairs of the four sampling protocols, using the two-sample *t*-test on the log-transformed data, these differences are not statistically significant. This is primarily the result of the high natural variability in the lead concentration (*i.e.*, high geochemical variance). When the medians are compared using the Mann–Whitney test they are similarly indistinguishable statistically.

For any subsequent survey the sampling bias that could be detected, by comparison with the grand mean lead concentration, was estimated as 726.5 μg g^{-1} (11.7%), again using the *t*-distribution.

For copper the geochemical variance was much lower (equivalent to 4.1 μg g^{-1} or 68.6%) and therefore smaller levels of sampling bias could be detected (0.8 μg g^{-1} or 2.7%). A significant sampling bias of 2.45 μg g^{-1} (8.7%) was detected between two protocols (the simple regular grid and the stratified random protocol) but not between the other protocols.

A methodology has been demonstrated that is capable of detecting sampling bias in the measurement of metals in contaminated land. Although no bias was detected in this instance (except for two protocols for Cu) the methodology is potentially applicable to more demanding studies.

Table 1 Analytical bias for lead and copper concentration estimated from six CRMs (*x*, mean concentration; *s*, standard deviation; and *c*, certified value)

CRM ($n = 4$)	x/μg g^{-1}	s/μg g^{-1}	s/x (%)	c/μg g^{-1}	Bias/μg g^{-1}	Bias (%)
Lead—						
NBS2709	19.7	3.2	16	18.9	+0.8	+4
NBS2710	5352	138	3	5532	−180	−3
NBS2711	1121.4	14.7	1	1162	−40.6*	−3*
BCR141	34.4	3.9	11	29.4	+5	+17
BCR142	36.2	4.6	13	37.8	−1.6	−4
BCR143	1297.5	33	3	1333	−35.5	−3
Copper—						
NBS2809	32.7	1	3	34.6	−1.9*	−6*
NBS2710	2878.8	82.1	3	2950	−71.2	−2
NBS2711	108.5	0.6	0.6	114	−5.5	−5
BCR141	31.3	1.2	4	32.6	−1.3	−4
BCR142	25.4	0.5	2	27.5	−2.1*	−8*
BCR143	235.4	6.8	3	236.5	−1.1	−1

* Bias statistically significant with 95% confidence interval.

It is possible to use the present finding to select the optimum sampling protocol among those tested, for the estimation of the mean concentration. As no significant difference was detected between the different sampling designs for lead in this case, logistics implies that the optimal sampling scheme should be the easiest to set up and that is the regular grid. Although the five-fold composite improved the sampling precision, the simple single auger protocol gave an acceptable sampling precision contributing 5.2% to the total variance.

Conclusions

It is possible to estimate sampling bias between different sampling protocols implemented on an area of contaminated land. The natural heterogeneity of the elemental concentration over the site is a factor limiting the size of bias that can be detected. The size of the sampling bias that can be detected at any site therefore varies according to the geochemical variance of the element. This has been demonstrated for Pb and Cu at a particular site for which the minimum sampling bias that is demonstrable is 726.5 μg g^{-1} for Pb and 0.8 μg g^{-1} for Cu.

No significant difference was found between the mean concentrations estimated by the different sampling designs for lead. The optimal sampling scheme for this objective therefore appears to be the regular grid because it is the fastest to set up and least prone to locational errors.

Duplicate sampling is a useful method for the estimation of sampling precision for various sampling protocols. The improvements in sampling precision obtained by using a five-fold composite sample at each regular grid point is significant (5.2–2.7% of variance) but judged not to be worthwhile when well below the limit of 20% for sampling variance.

The particular site studied is judged to be suitable for inter-organizational sampling trials such as a sampling proficiency test and a collaborative sampling trial. These trials would be analogous to the methodologies applied in the comparison of analytical bias between different laboratories. The selection of a site to become a reference sampling target should use the criteria of having relatively low geochemical variance, which should minimize the sampling bias that can be detected between the results given by different samplers.

The site studied might also be suitable for establishment as a reference sampling target for the absolute estimation of sampling bias. This is analogous to the use of a reference material for the estimation of analytical bias. Further work and experimentation is required to evaluate the feasibility of such a proposal. This work illustrates that sampling error is an integral part of measurement uncertainty and needs to become measured and considered in the interpretation of environmental measurements.

Table 2 Lead and copper concentrations estimated from the four different sampling protocols and bias (%) from the grand mean of 6229 μg g^{-1} for lead and 27.9 μg g^{-1} for copper (n, number of samples for each design)

Sampling design	n	Mean/ μg g^{-1}	Median/ μg g^{-1}	s/ μg g^{-1}	Bias (%) (from grand mean)
Lead—					
Regular grid (composite samples)	40	6322	4320	5633	+1.4
Regular grid (single samples)	40	6046	3915	5321	−3.0
Herringbone Stratified	39	5680	4470	4420	−8.9
Stratified random	40	6868	4860	6837	+10.2
Copper—					
Regular grid (composite samples)	40	27.4	26.1	4.9	−1.8
Regular grid (single samples)	40	26.9	25.7	5.3	−3.6
Herringbone	39	28.2	27.3	5.6	+1.1
Stratified random	40	29.4	28.3	7.3	+5.4

References

1 Ramsey, M. H., *Appl. Geochem.*, 1993, **2**, 149.
2 Ramsey, M. H., Thompson, M., and Banerjee, E. K., *Anal. Proc.*, 1987, **24**, 260.
3 *Principles of Environmental Sampling*, ed. Keith, L. H., American Chemical Society, Washington, D. C., 1988.
4 Gy, P. M., *Sampling of Particulate Materials: Theory and Practice*, Elsevier, Amsterdam, 1979, p. 568.
5 Thompson, M., and Ramsey, M. H., *Analyst*, 1995, **120**, 261.
6 Maskall, J., and Thornton, I., *Land Contam. Reclamation*, 1993, **1**, 92.
7 Webster, R., *Quantitative and Numerical Methods in Soil Classification and Survey*, Clarendon Press, Oxford, 1979, pp. 55–60.
8 Ferguson, C. C., *Ground Eng.*, 1992, **25**, 34.
9 Thompson, M., and Walsh, J. N., *A Handbook of Inductively Coupled Plasma Spectrometry*, Blackie, Glasgow, 1989, pp. 143–144.
10 Ramsey, M. H., Thompson, M. and Hale, M., *J. Geochem. Explor.*, 1992, **44**, 23.
11 Rose, A. W., Hawkes, H. E., and Webb, J. S., *Geochemistry in Mineral Exploration*, Academic Press, London, 1979.
12 Ripley, B. D., and Thompson, M., *Analyst*, 1987, **112**, 377.

Paper 4/06135G
Received October 10, 1994
Accepted December 13, 1994

Analysis of Diamonds and Indicator Minerals for Diamond Exploration by Laser Ablation–Inductively Coupled Plasma Mass Spectrometry*

R. John Watling, Hugh K. Herbert, Ian S. Barrow and Allen G. Thomas
Chemistry Centre (WA), 125 Hay Street, East Perth, Western Australia 6004

A method has been developed, using laser ablation–inductively coupled plasma mass spectrometry (LA–ICP-MS), for the semiquantitative determination of 43 elements in diamonds, chromites and garnets. Samples of diamonds from five countries have been analysed and the interrelationship between the trace elements gives distinctive patterns for each source. The data indicate that this technique could form the basis of a provenance identification protocol for diamonds. This would produce an analytical technique to assist police forces in tracing the origin of stolen material. LA–ICP-MS can also be used to establish the trace element distribution in indicator minerals for diamond exploration, such as garnets and chromites. Of particular significance in this data set in the comparison of the relative distributions of the rare earth elements, tantalum and hafnium, which indicates a consistent inter-element relationship for garnets associated with diamondiferous kimberlites. This relationship is considerably different from that found in garnets obtained from non-diamondiferous and other sources. Application of the principle of trace element partitioning pattern recognition to chromites has indicated the potential of the technique to identify also a kimberlitic or non-kimberlitic provenance for this mineral. The data presented here are the result of preliminary investigations. A more detailed study is currently being undertaken and will be the subject of future papers.

Keywords: Laser ablation–inductively coupled plasma mass spectrometry; diamond; indicator mineral

Introduction

The illegal appropriation of diamonds at all points in their production from source mine to final product nets a significant income for all those involved. Once on the 'open market' diamonds are notoriously difficult to source and their small size, easy transportability and large value make them a superb international Black Market currency. Attempts to 'fingerprint' diamonds have, thus far, met with limited success. However, the use of laser ablation–inductively coupled plasma mass spectrometry (LA–ICP-MS) to obtain element compositional data for diamonds heralds a new age in the search for an analytical technique that can establish the provenance of recovered stones.

Although LA–ICP-MS has the potential to provide quantitative data, this necessitates the use of accurately calibrated standards, a situation that is difficult to achieve in this instance as certified standards for diamonds would be extremely difficult to produce and of course none exist at this stage. However, the analytical method employed in this study requires only that instrument response functions and lasing conditions are as near identical as possible from sample to sample and from day to day because trace element associations, rather than element concentrations, are the basis of the interpretative protcol applied to the data.

The classification of garnets, into groups indicative of the provenance of the mineral, has been used successfully to identify the diamondiferous potential of the host rock.[1,2] Analyses, associated with this exercise, have centred on quantification of the partitioning of nickel between chrome-pyrope and olivine, the so-called 'nickel thermometer' effect. This methodology, based on proton microprobe analysis,[3] accurately identifies whether the garnet under investigation is formed in the so-called 'diamond window'[4,5] of the Earth's mantle and hence whether the kimberlite or lamproite that is being assessed has a significant potential for diamond production.

Initial research, using LA–ICP-MS, was undertaken to assess the potential of the technique to produce quantitative data for comparison with proton microprobe results for garnets. However, while the data obtained for selected elements using both techniques compared favourably, and will be the subject of a future paper, it was also possible to obtain data for a wide selection of other analyte elements and thereby identify trace element distribution patterns that appeared to correlate with the diamondiferous potential of the host rock. It is these data that have the potential of being used to establish a novel method of geochemical exploration for diamondiferous rocks. The same approach was applied to chromites from a known kimberlitic and non-kimberlitic environment. Here again, trace element distribution patterns, especially for the rare earth elements (REEs), indicated the potential of the 'fingerprint' concept to identify the provenance of the material.

In additional to its obvious potential for use in diamond exploration, LA–ICP-MS has considerable additional potential as a means of identifying the primary or secondary nature and metamorphic history of garnets and chromites and their host rocks. As the use of LA–ICP-MS becomes more widespread, and the analysis of discrete mineral grains becomes more practical,[6–13] it is possible that the elemental associations and the recognition of inter-element association patterns, such as those described in this paper, will feature more significantly in geochemical exploration initiatives.

Experimental

Sample Preparation

Sample preparation for this type of analysis can be as simple or as complex as the analyst requires. In general, provided that the sample fits directly inside the laser cell and is no more than 5 mm above the sample stage, analysis can be performed

* Presented at Geoanalysis 94: An International Symposium on the Analysis of Geological and Environmental Materials, Ambleside, England, September 18–22, 1994.

directly on the original material with very little preparation. It must be remembered, however, that laser ablation of original material can result in the incorporation of surface debris, derived from the host material or a variety of other anthropogenic sources. Analytical data will be compromised if this occurs. Accordingly, unpolished garnets and chromites are pre-cleaned by heating in concentrated hydrochloric acid for 10 min, washing in de-ionized water and acetone and drying at 60 °C prior to ablation. Diamonds are cleaned by heating in a mixture of concentrated hydrochloric and hydrofluoric acids (1 + 1) for 1 h at 120 °C, washing in water and acetone and also drying at 60 °C prior to lasing. Obviously, if the sample is pre-cut or is in the form of a polished mount this type of cleaning is both impractical and unnecessary. Unpolished material is mounted directly on plastic blocks using cyanoacrylate glue, with up to 25 samples being mounted in an appropriate array on the same block. These samples can also be mounted in small holes in the plastic block which are then backfilled with quick-setting plastic. The mount is then polished to expose the surfaces of the samples. Samples prepared in this way are suitable for additional investigation using scanning electron microscopic energy dispersive X-ray analysis and/or electron microprobe analysis. In most instances, it is difficult to prepare polished mounts of diamonds and consequently they are usually analysed after surface-mounting on the plastic blocks.

Instrumentation

A VG Turbo Plus inductively coupled plasma mass spectrometer fitted with an 'S'-Option sensitivity upgrade and fine focus LaserProbe accessory were used for the experimental work. The LaserProbe is built around a 500 mJ pulsed Nd:YAG laser operating at a wavelength of 1064 nm. The fine focus optics facilitate the production of laser craters of less than 30 μm in the free running mode and less than 100 μm in the Q-switched mode for the sample matrices analysed.

Laser Optimization

The use of LA–ICP-MS could imply a degradation in precision of results, when compared with equivalent solution ICP-MS data, simply because of variations in volatilized sample mass between samples. This would be of serious concern if the use of the trace element partitioning pattern protocol required the production of quantitative data. The concepts associated with interpretation of data produced under this experimental protocol have already been described in detail[14] and rely on the presence, association or lack of association, of specific suites of analyte elements. Consequently, quantitative data are not as important as they are in more conventional analytical methodologies.

Establishment of the optimum laser ablation conditions, for all mineral types analysed, is undertaken using the same general experimental matrix. Significant variation in the characteristics of the physical matrix exists between samples of the same mineral. Variations in colour, surface texture and sample orientation with respect to crystal planes all facilitate variability in laser coupling.[15] Hence, the amount of material ablated will vary from sample to sample and, therefore, the apparent analyte concentration will also vary. Consequently, it is again stressed that quantitative analysis, using the present laser configuration, is not practical at this time but is also not required for data interpretation because the association of elements, and not their actual concentrations, is used to establish the element distribution pattern.

It has already been established that there can be selective volatilization of elements from given matrices.[13,16] Therefore, at this preliminary stage of analytical method development, the use of an internal standard is neither advocated nor, in our opinion, necessary. Nevertheless, it is necessary to establish an optimum compromise series of parameters for laser ablation for each sample type to ensure that a robust comparison mechanism is achieved for different samples of the same mineral.

The two variables of major significance, which were chosen for this investigation, were laser power and repetition rate of laser shots. Preliminary studies indicated that analysis of garnets and chromites would be undertaken using a free running lasing mode, whereas analysis of diamonds would be undertaken using Q-switched lasing conditions. Whenever possible the free running lasing mode was used as it facilitated the development of the smallest craters. This was possible for both garnets and chromites; however, while it was possible to couple a free running laser pulse to dark, inclusion-rich diamonds, it was impossible to couple to clear diamonds. Consequently, in order to ensure uniformity of analytical conditions, all diamonds were analysed using a Q-switched laser.

Diamonds

For the analysis of diamonds, three sites on the surface of the in-house reference samples were pre-ablated, in Q-switched mode, for 15 s at 750 V laser power and a frequency of 6 Hz. The coordinates of each ablated area were recorded by computer in order that the sites could be re-located and ablated when establishing the final lasing conditions. Although the period of pre-ablation is not as long as traditionally accepted to ensure a steady-state signal, the concept of pre-ablation in this experimental protocol was not simply to establish uniform analyte release conditions, but more importantly to clean the surface of any attached or incorporated extraneous material. In this way it was possible to ensure that element association patterns resulted from the ablation of matrix rather than from incorporated material. Laser power was varied between 500 and 750 V and shot frequency between 1 and 10 Hz.

Garnets and Chromites

In order to determine the optimum lasing conditions for the analysis of garnets and chromites, laser power was varied between 600 and 1000 V and repetition rate between one and five shots s^{-1} for 1 s ablation at each specific site. A total of 10 sites, across the surface of each sample, was used for each experiment. The samples were not pre-ablated prior to analysis.

The study was repeated on six separate occasions and results were averaged to produce response intensities for each analyte. The response characteristics of 45 analytes were investigated. The experimental matrix, designed to establish the optimum set of analytical conditions, was essentially similar to that established for previous investigations into gold fingerprinting.[15] Results indicate a trend in the analyte response under the different conditions that is essentially related to the melting and boiling characteristics of the compounds of the individual analyte elements and the selective partitioning of these elements between vapour, melt and solid phases present during the ablation event.[13] When establishing the optimum compromise set of ablation parameters, it is necessary to ensure that variations in response between two sets of experimental conditions are as small as possible. This increases the robustness of the method and ensures that variations in the trace element partitioning patterns are minimal when the analysis is undertaken on different instruments or on different days.

Spot size should be as small as possible, while still providing sufficient material for analysis. In this way small samples can

be ablated under the same conditions as large samples, thereby maintaining the relevance of intercomparison of the fingerprint. Lower laser power and reduced shot numbers are to be preferred as this significantly reduces cross-contamination and memory effects.

Ablation conditions were established for the three sample types as follows:

Diamonds: Q-switched mode; 625 V and 6 Hz

Garnets: free-running mode; 750 V with a double pulse at each site

Chromites: free-running mode; 700 V with a single pulse at each site

Where possible, samples should be ablated at a number of sites per sample. However, it may only be possible to use one site when dealing with very small samples. Acquisition time for each mass spectrum is usually set at a minimum of 100 s. In this way it is possible to use the multichannel analyser to watch the fingerprint accumulate and reject data that have resulted from ablation of inclusions. This is evidenced by sudden increases in analyte response. A long potential acquisition time also allows the analyst to move the sample and ablate different spots, thereby ensuring better precision and providing a more intense spectrum for comparison.

Optimization of Long-term Data Intercomparability

The instrument operating parameters were optimized using National Institute of Standards and Technology (NIST) Standard Reference Materials (SRMs) NIST SRM 610, 612 and 614 glass standards. The choice of this material (and not one of the actual experimental matrices) is based on the premise that experimental optimization for this type of analysis requires only the production of a reproducible set of analytical and instrumental conditions which can be re-established on a daily basis. To this end, the use of a reference material, rather than an inhomogeneous sample matrix, was preferred. The fact that glass and the minerals under study are 'similar' matrices is an advantage. The use of NIST SRM glasses has proved to be robust and convenient and facilitates reproducible instrument optimization.

Once optimization had been achieved, in-house reference samples (three diamonds, four garnets and three chromites) were used where appropriate to ensure data intercomparability on a daily basis and to provide a cross-reference comparison with previously obtained data. The data thus produced facilitated maintenance of long-term quality control and ensured intercomparability of fingerprint data. Because the technique was not designed to provide quantitative data, it was only necessary to confirm comparability of the element associations within the sample with data from previous analyses of the same sample prior to undertaking the analysis of a new series of samples. This cross-calibration procedure usually required about 1 h to complete.

Results and Discussion

Diamonds

Obviously, only a limited number of samples (six from each deposit) have been analysed at this point in the research

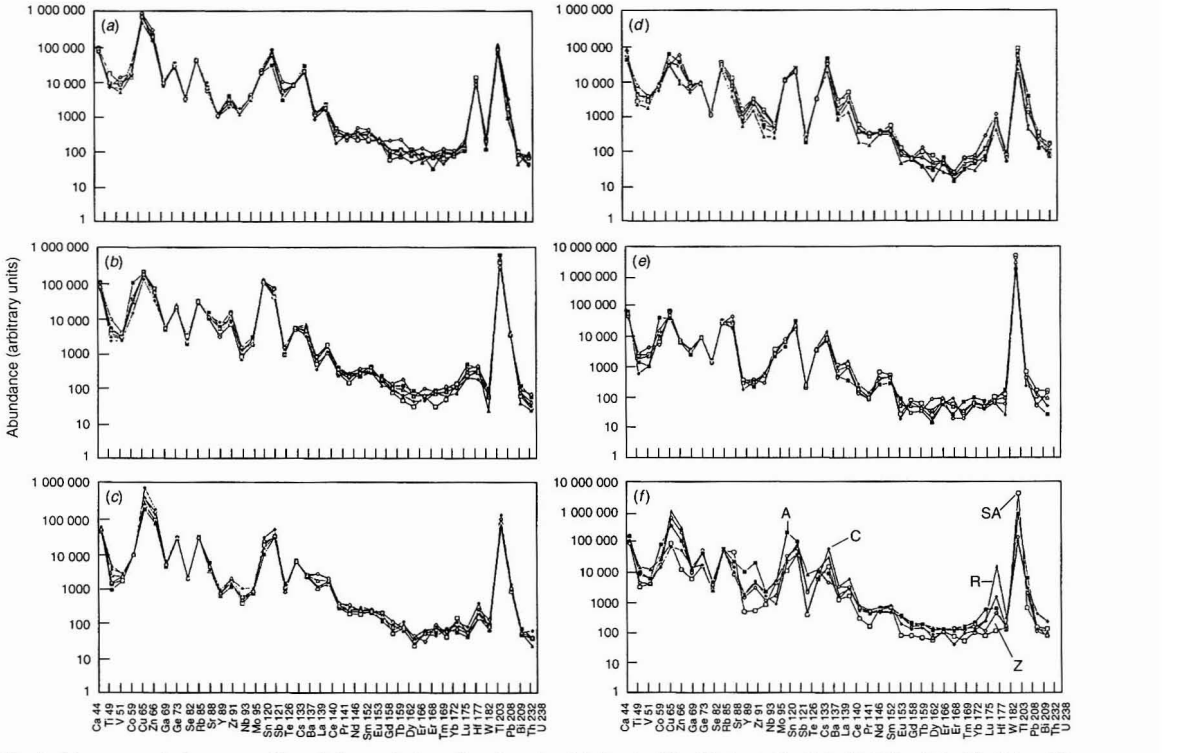

Fig. 1 Mass spectral element profiles of diamonds from five deposits. (*a*) Russia (R); (*b*) Australia (A); (*c*) Zaire (Z); (*d*) China (C); (*e*) South Africa (SA), and (*f*) composite average for each deposit.

programme as uncut diamonds are extremely expensive and difficult to obtain from international producers. However, it is anticipated that, once the potential of the technique is fully recognized, international producers will be more co-operative in supplying diamonds and the problems associated with obtaining a significant number of stones from each deposit, with which to establish a robust methodology, will be overcome.

The mass spectral elemental profiles of diamonds from the five deposits so far investigated are shown in Fig. 1(*a*)–(*e*). The ordinate scale is an indication of the abundance of the analyte isotope being measured. No attempt has been made to relate isotopic abundance to elemental abundance as the concept of inter-element association patterns relies on relative abundances of analytes and not on their concentrations. Consequently, provided that the same isotope of an element is compared between profiles, and as there are no interfering isobaric overlaps, spectral comparisons are readily facilitated. The reproducibility of the spectral pattern within a deposit is evident in all profiles. This suggests a common origin for the analysed diamonds from each deposit. This is obviously of fundamental importance as, if significant variations in element profile did occur, the potential of the technique to establish a definitive provenance of diamonds would be severely degraded.

Although the over-all elemental distribution pattern for each of these deposits appears, at first sight, to be similar, significant differences do occur between them. The significance of these variations is illustrated in Fig. 1(*f*) where average data are compared directly. Of particular note are differences in the relative abundances of copper, zinc, yttrium, zirconium, tungsten, lead and thorium as well as within the REE assemblage. In order to demonstrate these differences more effectively, conventional ternary diagrams were constructed. Because ternary variation diagrams use ratio percentages, the plots do not require data to be quantitative, only reproducible. They provide a means of comparing the relationship between individual sets of data. Consequently, they are ideally suited to interpreting the type of data produced using LA–ICP-MS under the experimental protocol described in this paper.

Selected ternary plots are presented in Fig. 2(*a*)–(*f*). Although there is some spread in the data points within a deposit, each deposit forms a relatively coherent cluster of points that are essentially isolated from those of a different deposit. It must be remembered that these data are of a preliminary nature and further refining of the technique will

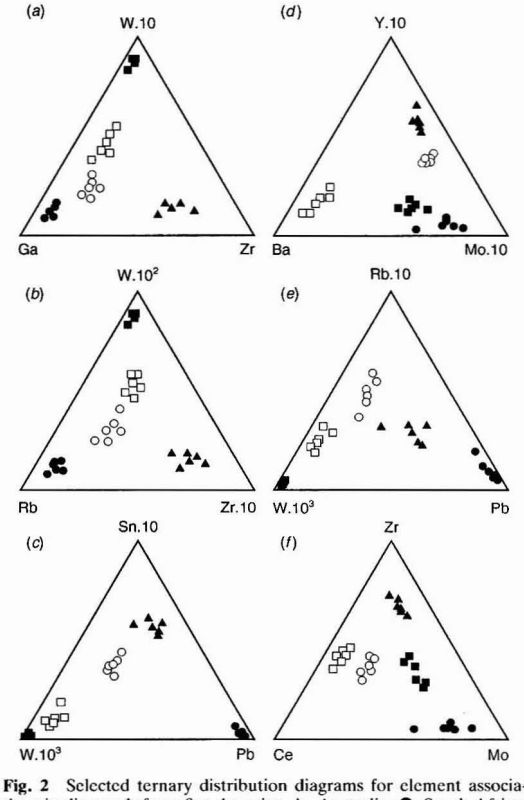

Fig. 2 Selected ternary distribution diagrams for element associations in diamonds from five deposits: ▲, Australia; ●, South Africa; □, China; ○, Zaire; and ■, Russia.

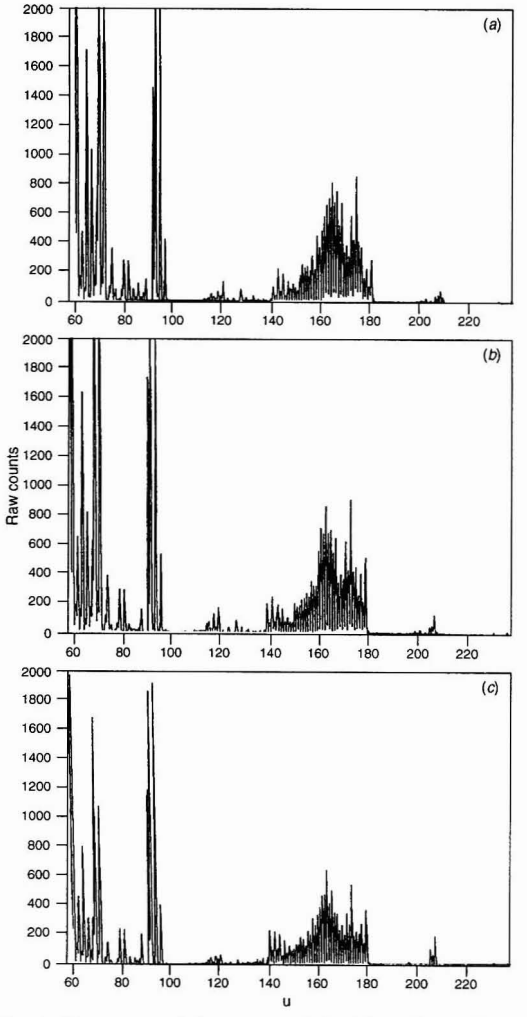

Fig. 3 Mass spectra of three garnets derived from diamondiferous host rocks.

undoubtedly lead to closer associations of points. To date, it has not been possible to find a suitable element with which to normalize data internally. Consequently, only uncorrected raw data are plotted. This means that differences in element release, caused by variation in ablation conditions between samples, remain uncorrected.

From the data shown in Fig. 2(*a*)–(*f*), it is clear that tungsten is a major discriminatory element for the Russian deposit, whereas lead, molybdenum and rubidium are the predominant discriminatory elements for the South African deposit investigated. The occurrence of high concentrations of lead in diamonds from the South African deposit is surprising in that this element is extremely volatile and usually not associated with ultramafic magmas. One possibility is that the lead has been incorporated during transport and emplacement of the deposit during the geological evolution of host eclogite and/or garnet peridotite, or that it results from sub-cratonic metasomatic processes. Significant lasing of these diamonds only marginally reduces the lead content and confirms that the lead is pervasive throughout the diamonds.

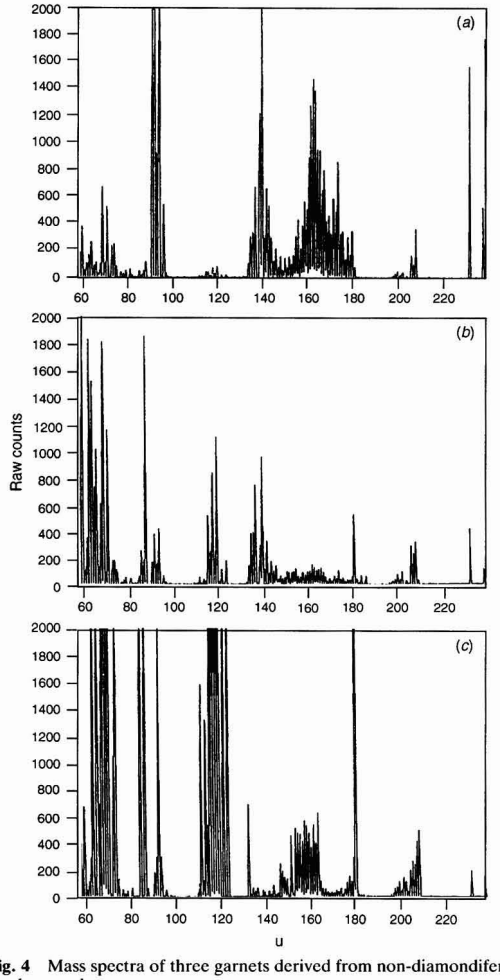

Fig. 4 Mass spectra of three garnets derived from non-diamondiferous host rocks.

Garnets

A series of 11 garnets from two diamondiferous deposits and 86 garnets from known igneous and metamorphic environments were prepared for analysis. The mass spectra of three representative garnets typical of diamondiferous deposits are presented in Fig. 3(*a*)–(*c*), while those from the non-diamondiferous host rocks are shown in Fig. 4(*a*)–(*c*).

The mass spectra of garnets from the diamondiferous deposits all indicate a similar trace element pattern. Zinc (64, 66, 67, 68 and 70 u), gallium (69 and 71 u) and zirconium (90, 91, 92, 94 and 96 u) are relatively enhanced, whereas yttrium (89 u) has been removed from the spectral scan as its concentration is often so high that it trips the ion multiplier, resulting in the loss of data. The element distribution pattern for garnets from non-diamondiferous host rocks contrasts sharply with that for garnets associated with diamondiferous deposits, while the elemental assemblage also appears much more variable. Elements such as uranium (235 and 238 u) thorium (232 u), lead (204, 206, 207 and 208 u), mercury (196, 198, 199, 200, 201, 202 and 204 u), tin (112, 114, 115, 116, 117, 118, 119, 120, 122 and 124 u), strontium (84, 86, 87 and 88 u) and rubidium (85 and 87 u), which are traditionally associated with crustal rocks, are significantly more abundant. As with lead from the South African diamonds investigated in this study, these elements may reflect metasomatic events or they may be inherited from host rock evolutionary processes.

Of particular interest in all the spectra is the REE (139–176 u) distribution pattern. The distribution of these elements, in garnets from the diamondiferous deposits, when chondrite-normalized,[17] indicates a significant depletion in the lighter REE and enhancement in the heavier REE. The characteristic pattern exhibited by the indicator garnets from the two diamondiferous deposits is shown in Fig. 5(*a*) and (*b*). The two profiles, while different in detail, are remarkably similar, both within and between deposits. Conversely, the chondrite-normalized REE profile of garnets from a high temperature and pressure eclogitic environment [Fig. 5(*c*)] exhibits much more variable characteristics with a far less pronounced depletion in the lighter REEs compared with the heavier REEs. In most samples there is also a suggestion of minor europium depletion, while one sample illustrates europium enrichment. The REE profiles of garnets from a low temperature metamorphic environment indicate no enhancement of heavy REEs or depletion in light REEs [Fig. 5(*d*)]. In fact, some of the garnets indicate that there has been a significant enhancement in the lighter REEs. Hafnium and tantalum also do not show the characteristic downward slope pattern that characterizes their association in garnets from diamondiferous deposits and in garnets from eclogites. In order to discriminate better between the types of garnets, ternary diagrams were again prepared [Fig. 6(*a*)–(*f*)]. From these diagrams the identification of garnets derived from two diamondiferous and two non-diamondiferous host rocks is readily apparent. Plots of elemental associations in garnets from the two diamondiferous deposits are essentially overlapping whereas the data from the non-diamondiferous host rocks are scattered almost over the entire plotting area. However, it is interesting that while there is considerable scatter of the non-diamondiferous data, very few data points overlap into the diamondiferous field.

Chromites

Six chromites each from kimberlitic and non-kimberlitic host rocks were analysed and the elemental association patterns are presented in Fig. 7(*a*)–(*d*). The reproducibility of the elemental signature for both types of chromite was essentially excellent [Fig. 7(*a*) and (*c*)]. However, there appeared to be an anomalous sample in the kimberlitic chromite suite [Fig.

7(*a*)]. The ablation characteristics for this sample were also different from the other chromites in this suite. When the element profile for this sample was removed and the data were replotted [Fig. 7(*b*)], a much more reproducible elemental pattern resulted.

A comparison of the average element profile for the two suites of samples is shown in Fig. 7(*d*). Here, the differences between the two sample suites are clear. Kimberlitic chromites contain significantly more rubidium, strontium, yttrium, zirconium, niobium, barium, hafnium, tantalum, thorium and uranium and the entire REE suite than do chromites from the non-kimberlitic rocks. Ternary plots of these data (Fig. 8) elegantly confirm the definitive identification of the two suites of chromites. Furthermore, the one 'suspect' chromite from the kimberlite is, in all instances, intimately associated with data from the non-kimberlitic chromites. It is felt that this chromite represents material entrained from higher crustal levels during ascent of the kimberlitic magma.

Conclusions

In Australia, as in other diamond-producing countries, stolen diamonds represent major losses of revenue to producing companies through direct loss and reduced sales, of dividends to investors, of tax to Government and of loss of foreign revenue. More dramatically, diamond theft is illegal and can result in death or injury to innocent bystanders and should be discouraged. However, until now, identification of the provenance of diamonds, as a means of assisting the authorities in criminal investigations, has not been possible.

Studies so far have shown that it is possible to identify the provenance of different diamonds on the basis of their unique trace element association patterns. The method is rapid and relatively simple, although interpretation of spectra requires considerable experience. Ultimately, it is hoped that the identification of a particular diamond will be achieved using a computerized database of mass spectra.

Application of the technique to the analysis of garnets and chromites has produced data for a wide range of analyte elements which, until now, have been at concentrations below

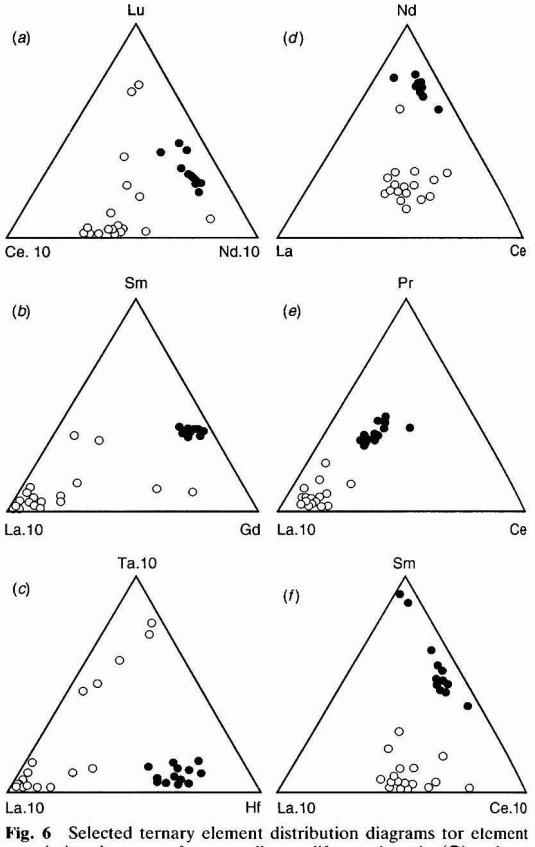

Fig. 6 Selected ternary element distribution diagrams for element associations in garnets from two diamondiferous deposits (●) and two non-diamondiferous host rocks (○).

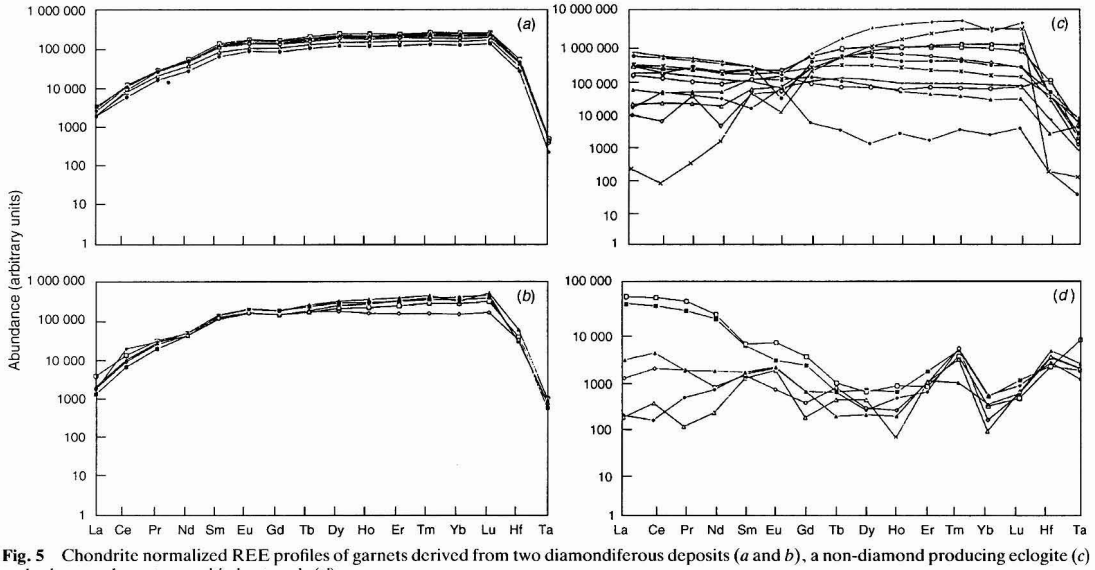

Fig. 5 Chondrite normalized REE profiles of garnets derived from two diamondiferous deposits (*a* and *b*), a non-diamond producing eclogite (*c*) and a low-grade metamorphic host rock (*d*).

the analytical sensitivity for most conventional techniques. The data for this increased range of analytes have facilitated the identification of trace element association patterns that have not previously been available to geologists and geochemists and which can be used for provenance identification of the minerals concerned. Such data have the potential of being applied in association with conventional geochemical data for improving the use of indicator minerals in the exploration for diamond deposits.

The methodology described in this paper further demonstrates the application of LA–ICP-MS to the area of forensic mineralogy and provides the experimental design to transfer this technology to other aspects of the analysis of solid samples. It is not designed to provide quantification of analyte concentrations in a sample, but rather to provide a distribution pattern of elements present within a particular sample, under conditions that are robust and reproducible between the same type of sample on a day-to-day basis. Interpretation of results is based on the association of elements within a sample and comparison of these associations with reference samples or samples in a database.

Although it is possible to discriminate between diamonds from the deposits studied, between garnets from diamondiferous and non-diamondiferous host rocks and between chromites from kimberlitic and non-kimberlitic host rocks using simple ternary diagrams, the potential of improved discrimination, using tetrahedral plots and more complicated multivariate statistical software, is being investigated. Again, it must be stressed that all data presented in this paper are preliminary and represent the analysis of a limited sample base. Significant further research and development must be undertaken before the true potential of the technique can be demonstrated. However, the initial data for all sample types are extremely encouraging.

The authors thank the Director of the Research Centre for Advance Mineral and Materials Processing, University of Western Australia, for financial support in running the LA–ICP-MS facility and the Director of the Chemistry Centre (WA) for permission to publish this work.

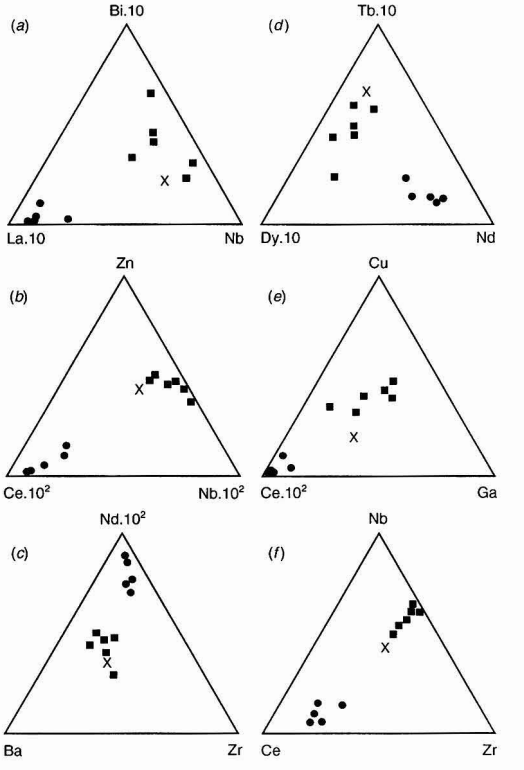

Fig. 8 Selected ternary distribution diagrams for element associations in chromites from kimberlitic and non-kimberlitic host rocks. ●, Kimberlitic and ■, non-kimberlitic. ×, Garnet from a kimberlitic host rock showing non-kimberlitic characteristics.

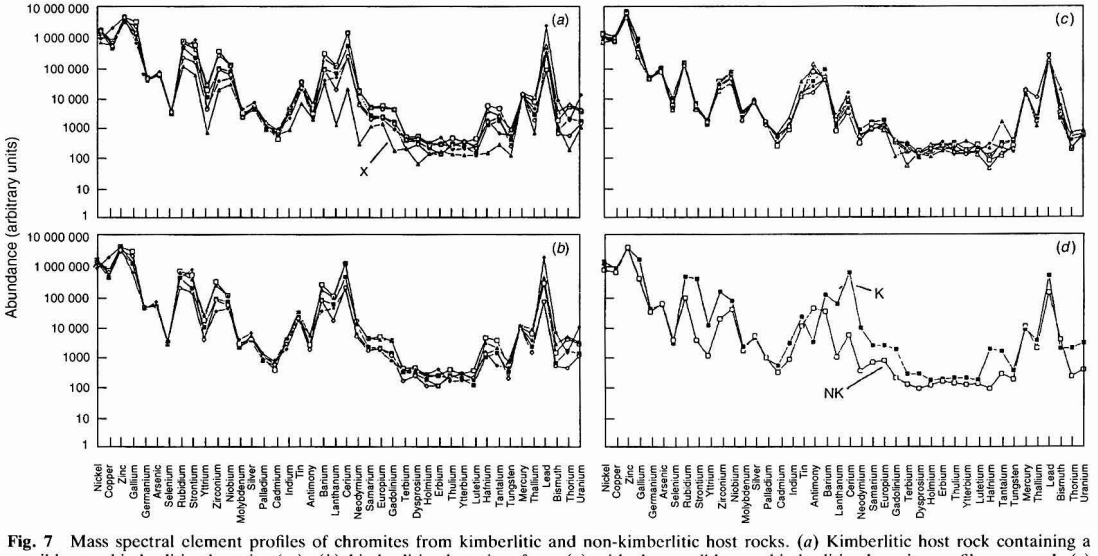

Fig. 7 Mass spectral element profiles of chromites from kimberlitic and non-kimberlitic host rocks. (*a*) Kimberlitic host rock containing a possible non-kimberlitic chromite (×), (*b*) kimberlitic chromites from (*a*) with the possible non-kimberlitic chromite profile removed, (*c*) non-kimberlitic and (*d*) average comparison. K, Kimberlitic and NK, non-kimberlitic.

References

1 Griffin, W. L., Cousens, D. R., Ryan, C. G., Sie, S. H., and Suter, G. F., *Contrib. Mineral. Petrol.*, 1989, **103**, 199.
2 Griffin, W. L., Gurney, J. J., and Ryan, C. G., *Contrib. Mineral. Petrol.*, 1992, **110**, 1.
3 Griffin, W. L., Jaques, A. L., Sie, S. H., Ryan, C. G., Cousens, D. R., and Suter, G. F., *Contrib. Mineral. Petrol.*, 1988, **99**, 143.
4 Kennedy, C. S., and Kennedy, G. C., *J. Geophys. Res.*, 1976, **81**, 2467.
5 Griffin, W. L., and Ryan, G. C., in *Mineralogy in the Service of Mankind*, Program and Abstracts International Congress on Applied Mineralogy, ICAM '93, Perth, Western Australia, ed. Griffin, B., Graham, J., and Linge, H., pp. 280–284.
6 Broadhead, M., Broadhead, R., and Hager, J. W., *At. Spectrosc.*, 1990, **11**, 205.
7 Broadhead, M., *At. Spectrosc.*, 1991, **12**, 45.
8 Crain, J. S., and Gallimore, D. L., *J. Anal. At. Spectrom.*, 1992, **7**, 605.
9 Imai, N., *Anal. Chim. Acta*, 1990, **235**, 381.
10 Pearce, N. J. G., Perkins, W. T., Abell, I., Duller, G. A. T., and Fuge, R., *J. Anal. At. Spectrom.*, 1992, **7**, 53.
11 Perkins, W. T., Pearce, N. J. G., and Jeffries, T. E., *Geochim. Cosmochim. Acta*, 1993, **57**, 475.
12 Reed, S. J. B., *Chem. Geol.*, 1990, **83**, 1.
13 Watling, R. J., Herbert, H. K. and, Abell, I. D., *Chem. Geol.*, in the press.
14 Watling, R. J., Herbert, H. K., Delev, D., and Abell, I. A., *Spectrochim. Acta, Part B*, 1994, **49**, 205.
15 Jeffries, T., Perkins, W. T., and Pearce, N. J. G., *Analyst*, 1995, **120**, 1365.
16 Chenery, S., Hunt, A., and Thompson, M., *J. Anal. At. Spectrom.*, 1992, **7**, 647.
17 Nakamura, N., *Geochim. Cosmochim. Acta*, 1974, **38**, 757.

Paper 4/06997H
Received November 16, 1944
Accepted January 3, 1995

Comparisons of Infrared and Ultraviolet Laser Probe Microanalysis Inductively Coupled Plasma Mass Spectrometry in Mineral Analysis*

Teresa E. Jeffries, William T. Perkins and Nicholas J. G. Pearce
Institute of Earth Studies, University of Wales, Aberystwyth, Dyfed, UK SY23 3DB

The application of an infrared and an ultraviolet laser probe microanalysis ablation system, coupled to an inductively coupled plasma mass spectrometer is described for the analysis of olivine, garnet, phlogopite, magnetite, apatite, calcite, quartz and feldspar. These minerals represent a range of composition, absorption characteristics and physical properties (for example cleavage) and were prepared both as cut blocks and thin sections. The analytical performance of the two laser probe systems is compared for each mineral type in terms of lateral and vertical resolution, duration of ablation, and the importance of mineral orientation. Lower limits of detection are presented for the two laser systems. Lateral resolution in the ultraviolet system is a function of laser power and can be varied from less than 5 to >70 μm. For the infrared system, laser power is essentially fixed and lateral resolution is a function of mineral type and sample preparation. Mineral orientation is an important factor in analysis using the infrared system but for the ultraviolet system this is of no significance. For the ultraviolet laser system, lower limits of detection are dependent on the amount of material ablated which is a function of laser power density and range from hundreds to thousands of ppm at low power to sub-ppm levels at high power. The removal of material by the ultraviolet laser probe system is facilitated by the strong absorption in the ultraviolet region of the electromagnetic spectrum that all the minerals in this study possess. The ultraviolet laserprobe system provides a superior analytical performance for mineral microanalysis when compared with the infrared system.

Keywords: Laser ablation; inductively coupled plasma mass spectrometry; mineral microanalysis; infrared; ultraviolet

Introduction

During the last 10 years interest in laser ablation as a means of solid sample introduction to plasmas has steadily increased. Laser ablation (LA) was first coupled to an inductively coupled plasma mass spectrometer (LA–ICP-MS) by Gray[1] who demonstrated the application of a ruby laser to the analysis of geological materials. Subsequently, Arrowsmith[2] described the use of a neodymium yttrium aluminium garnet (Nd:YAG) laser ablation system to the analysis of metals. The Nd:YAG laser ablation system provides a lateral resolution of approximately 150 μm when operated at its fundamental wavelength in the infrared region at 1064 nm in focused Q-switched mode and has found application in the bulk analysis of a variety of materials (see for example Perkins *et al.*[3]).

However, a major advantage of laser ablation is the potential to perform *in situ* spatial analyses of solids and much of the development of laser ablation techniques in recent years has been towards improvement in lateral resolution. To this end, a recent development employing a Nd:YAG laser ablation system, operating at its fundamental wavelength in the infrared region (1064 nm), has been the modification of the laser optics to give a lateral resolution of 20–40 μm in geological materials (Pearce *et al.*,[4] Jackson *et al.*[5]). This technique is referred to here as infrared laser probe microanalysis (IR-LPMA).

Whilst it is possible to analyse most minerals of 100 μm diameter or larger, prepared as blocks by IR-LPMA, material prepared in this way is of limited value for geological applications where many minerals of interest are less than 100 μm diameter and where the material is typically prepared as thin section. An example of the use of thin sections is electron probe microanalysis (EPMA) which may provide data for use as internal standardization in LA–ICP-MS techniques. Many abundant pale coloured minerals such as calcite, quartz and feldspar, and indeed the glass slide of thin sections, are transparent to infrared light and this means that the analysis of all minerals prepared as thin section, and in particular these pale-coloured minerals, is difficult by IR-LPMA. However, most minerals and glass absorb strongly in the ultraviolet region of the electromagnetic spectrum[6] and thus most recent developments in LA–ICP-MS have concentrated on wavelength modification to produce ultraviolet laser light. Such a system employing the use of a Nd:YAG laser has been described recently by Chenery and Cook[7] who demonstrate the analysis of rare earth elements (REEs) in monazite, (a REE phosphate) as well as the formation of craters of less than 5 μm diameter in a variety of minerals. This technique is referred to here as ultraviolet LPMA (UV-LPMA).

In this paper the ablation characteristics of IR- and UV-LPMA in the analysis of a variety of mineral types prepared both as cut blocks and thin section are investigated and compared. Data are presented to describe the following ablation characteristics: lateral and vertical resolution, duration of ablation, importance of mineral orientation and limits of detection.

Instrumentation

Two configurations of a VG Laser Lab laser ablation system have been used in the present work and are described below. These were coupled to a VG Instruments (Fisons Instruments Elemental, Winford, Cheshire, UK) Plasma Quad PQII+ ICP-MS. The VG Laser Lab is based on a Spectron Laser Systems 500 mJ pulsed Nd:YAG laser operating at its fundamental wavelength in the infrared region at 1064 nm. In the unmodified VG Laser Lab (operating in focused Q-

* Presented at Geoanalysis 94: An International Symposium on the Analysis of Geological and Environmental Materials, Ambleside, England, September 18–22, 1994.

switched mode) crater diameters of approximately 150 μm result in most geological materials. In this configuration power density is approximately 3.8×10^{11} W cm^{-2}.

For a full description of the laser and ICP-MS instrumentation and analysis methodology the reader is referred to Perkins and Pearce.[8]

Laser Probe Microanalysis: Laser Modifications

Infrared

In IR-LPMA the laser beam is attenuated by placing a 1 mm ceramic aperture (producing TEM_{00}) in the beam path at the exit of the laser cavity. The attenuated beam is then focused through a (20×) Nikon super long working distance (25 mm) microscope objective lens. Laser power is reduced to 4 mJ but as the beam diameter is reduced to approximately 10 μm, the power density at 3.4×10^{11} W cm^{-2} is similar to the unmodified laser. Because of the damage that high power laser light can cause to the compound objective used in this configuration, it is necessary to carefully control the laser power and hence power density. For most applications therefore, laser power is set at its minimum to achieve coupling to the sample and is usually approximately 4 mJ per shot.

Green

In Green-LPMA the Laser Lab optics are modified as above and the attenuated infrared beam is passed through a frequency doubling potassium di-deuterium phoshate (KD*P) crystal to produce a second harmonic. Harmonic separation and beam steering is achieved using 3 mirrors with a dielectric coating for 532 nm. The advantage of this technique, apart from the safety a visible laser affords, is that the laser may be used in conjunction with an ordinary refracting objective.

Ultraviolet

In UV-LPMA the Laser Lab optics are modified as above and the attenuated beam is passed through two frequency doubling KD*P crystals to produce a fourth harmonic. Harmonic separation and beam steering is achieved using 3 mirrors with a dielectric coating for 266 nm. The beam is focused through a (15×) long working distance (23 mm) microscope reflecting objective with a dielectric coating for 266 nm. In UV-LPMA laser power can be varied by changing the voltage to the flashlamp from a minimum coupling power (power required to produce a visible crater in the sample) of 0.05 mJ to a maximum output of 3.2 mJ (power density ranges from approximately 1.7×10^{10} to 1.1×10^{12} W cm^{-2}) without apparent damage to the objective.

In IR-LPMA it is possible to operate the laser in both fixed-Q and Q-switched mode. Q-switched mode has only been used in this study, however, as for some minerals analysis may only be performed in Q-switched mode and because Q-switched mode must be used in UV-LPMA to produce the short duration high intensity pulse required by the crystals.

Green-LPMA has been demonstrated by a number of workers (see for example, Chenery *et al.*;[9] Huang *et al.*[10]) but as this technique appears to offer no advantage in mineral microanalysis above IR- or UV-LPMA described below, it will not be considered further here.

Experimental

Sample Preparation

LPMA–ICP-MS techniques require only minimal sample preparation. In this study material was prepared both as cut blocks and unpolished thin sections. Blocks were sawn to approximately 30 × 20 × 5 mm to fit the sample analysis chamber (53 mm id, height 10 mm). Whilst it is possible to use both blocks and thin sections either in polished and unpolished form, in this work unpolished material was used to minimize surface reflectance of the laser light. The sample is positioned in the laser beam path and moved by a motorized *X*–*Y* stage.

Materials Analysed

The following minerals have been analysed in this study:

Olivine, $(Mg,Fe)_2SiO_4$, Fo_{90} *(Mg rich olivine).* In a tholeiitic basalt from Stapafell Quarry, Reykjanes Peninsula, South West Iceland. Fresh, euhedral, optically unzoned, up to 3 mm length.

Garnet, $(Mg,Fe,Mn,Ca)_3Al_2Si_3O_{12}$. In an anorthosite from South Harris igneous complex, Northwest Highlands, Scotland, up to 5 mm length.

Phlogopite, $KMg_3(AlSi_3O_{10})(OH,F)_2$. In a coarse, phlogopite facies, ultrabasic pegmatoid from Palabora carbonatite suite, South Africa. Fresh, up to 2 cm length, randomly oriented.

Magnetite, Fe_3O_4. In a layered gabbro from The Cuillins, Isle of Skye, Northwest Highlands, Scotland. Massive grains up to 1 cm length.

Apatite, $Ca_5(PO_4)_3(F,Cl,OH)$. Single crystal from the mineralogy collection at University of Wales, Aberystwyth. Large, clear, euhedral, 8 mm diameter, locality unknown.

Calcite, $CaCO_3$. In a carbonatite from Igaliko dyke swarm, South West Greenland. Fresh, strongly cleaved, up to 3 mm length.

Quartz, SiO_2. In a granite from Bodmin, Cornwall, South West England. Grey, up to 5 mm diameter.

Alkali feldspar, $(Na,K)AlSi_3O_8$. In a granite from Bodmin, Cornwall, South West England. Slightly altered, up to 5 mm length.

With the exception of the apatite, which was analysed as a single mineral separate, the above minerals were analysed *in situ* in whole rock samples. To determine the ablation characteristics of the two laser systems in the analysis of minerals a series of experiments were conducted and are described below.

Lateral and Vertical Resolution

To determine the lateral resolution and assess the vertical resolution of the two laser probe techniques each sample, prepared both as cut block and thin section was ablated and the resultant craters were viewed, measured and photographed using a scanning electron microscope (SEM) (Stereoscan 120, Cambridge Instruments). For the cut block samples and thin sections laser power for IR-LPMA was determined by the mineral sample and set at the lowest level to achieve coupling, (*i.e.*, the lowest power necessary to produce a visible crater). For all samples this was approximately 3–4 mJ. For UV-LPMA laser power was set at 0.2 mJ for all minerals. In cut blocks for both IR- and UV-LPMA ablation was continued at 5 Hz (pulses of laser) for 1 min, or until ablation stopped, whichever was sooner. (Ablation may cease when the laser becomes grossly out of focus because of the removal of sufficient material from the sample surface.) The laser was focused on the sample surface at the start of the ablation and remained unchanged throughout. This provided a maximum crater size. A minimum crater size was determined in cut blocks by firing the laser 20 times at the sample surface. Laser power was as outlined above.

For thin sections a single crater size was determined for both IR- and UV-LPMA, and was based on firing the laser 20 times at the sample surface. Laser conditions were otherwise as stated above.

To determine the range of lateral resolution available in UV-LPMA a glass slide was ablated at various laser power settings between 0.05 and 3.2 mJ for 1 min at 4 Hz and 1 min at 8 Hz.

Duration of Ablation

Duration of ablation for each mineral prepared as a cut block was determined by continuously ablating the sample at 4 Hz. The laser was focused at the sample surface at the start of each determination and the focus was unchanged throughout. For IR-LPMA laser power was approximately 4 mJ corresponding to a power density of approximately 3.4×10^{11} W cm^{-2}. For UV-LPMA laser power was set at approximately 0.8 mJ to provide a similar power density to the infrared system. Data was acquired by scanning the mass spectrometer across the range *m/z* 6–239 and integrated every 30 s until the signal fell to an 'unacceptable' level or ablation ceased, whichever occurred first.

For the analysis of material prepared as thin section (but not including the quartz and feldspar samples), data was acquired using the time resolved analysis application of the VG PlasmaQuad software. This allows for rapid continuous peak jumping or scanning across the range *m/z* 6–239 and by limiting the number of sweeps per scan, data can be integrated in 1–2 s time slices. In this study the 'peak jumping' time resolved analysis method was used. In all of the analyses ^{29}Si was monitored to determine the point at which the glass slide was sampled. (A background signal for ^{29}Si was present for most minerals but is increased in the glass slide.) In addition to ^{29}Si one or two other isotopes were monitored from the mineral itself (*e.g.*, ^{57}Fe, ^{43}Ca) and these were selected on the basis of mineral type. The samples were ablated continuously at 4 Hz until the signal from the glass slide dominated the total ion signal or ablation ceased. For IR-LPMA laser power was determined by the mineral type and set at the lowest level to achieve coupling. For all minerals this was approximately 3–4 mJ. For UV-LPMA laser power was set at 0.2 mJ as this was the lowest power required to provide a usable signal.

Importance of Mineral Orientation

The effect of mineral orientation on ablation characteristics was assessed using samples containing variously oriented minerals prepared as thin section only. These were calcite in the carbonatite, olivine in the tholeiite, feldspar in the granite and phlogopite in the ultrabasic pegmatoid. For each of the samples mineral orientation was determined using a petrological microscope. The laser was fired 20 times at the surface of each mineral and the resultant craters were viewed and photographed using an SEM. To determine if there was any significant difference in signal from the variously oriented minerals, spectra were acquired from appropriate regions of the mass range. Data reduction and manipulation was performed off-line.

Detection Limits

For the determination of detection limits data was acquired by scanning 65 isotopes in the range *m/z* 6–239 whilst ablating the reference material NIST SRM 610 for 1 min at 5 Hz. For IR-LPMA laser power was 4 mJ corresponding to a power density of approximately 3.4×10^{11} W cm^{-2}. For UV-LPMA data was acquired for each of the following laser powers: 0.05, 0.2, 0.35, 0.6, 1.1, 1.8, 2.5 and 3.2 mJ corresponding to power densities in the range 1.7×10^{10} (0.05 mJ)–1.1×10^{12} W cm^{-2} (3.2 mJ). Data reduction and manipulation was performed off-line. Concentrations for the trace elements in the NIST SRM 610 reference material used in the calculation of detection limits are taken from the NIST certification and Pearce *et al.*[11]

Results and Discussion

For the purposes of discussion it is convenient to divide the minerals analysed in this study into two major groups. Firstly, minerals that have a strong absorption in the near-infrared region of the electromagnetic spectrum as well as in the ultraviolet. This behaviour is typical of the ferro-magnesian minerals.[6] This group includes olivine, garnet, phlogopite and magnetite. Secondly, minerals that have a poor absorption in the near-infrared region of the electromagnetic spectrum but a strong absorption in the ultraviolet. This behaviour is characteristic of light coloured minerals and here includes apatite, calcite, quartz and feldspar.

Lateral and Vertical Resolution

In the first set of experiments the lateral and vertical resolution of both IR- and UV-LPMA in the analysis of minerals in cut block and thin section was investigated using SEM imaging. For IR-LPMA lateral resolution appears to be related to mineral type. In the analysis of the ferro-magnesian minerals, circular, 20–40 μm diameter craters were formed in cut block whilst larger, 50 μm diameter craters were formed in the light minerals prepared in this way. Geertsen *et al.*[12] have recently described the formation of complex plasmas above the sample surface during infrared laser ablation and it is considered that removal of material from the sample is in part a result of plasma erosion rather than ablation caused by absorption of the laser energy. The increased crater diameters observed in our poorly IR-absorbing light minerals compared with the smaller crater diameters produced in our strongly IR-absorbing ferro-magnesian minerals are in accordance with this conclusion. The smaller craters in the ferro-magnesian minerals may reflect a greater degree of direct ablation than would occur in the light minerals.

In the analysis of thin sections by IR-LPMA circular craters 20–40 μm in diameter were again formed in ferro-magnesian minerals, but craters of up to 200 μm diameter formed in light minerals. This large crater formation in thin section is the result of a catastrophic ablation which usually occurs after 2 or 3 laser shots (see Fig. 1). As neither the mineral nor the glass

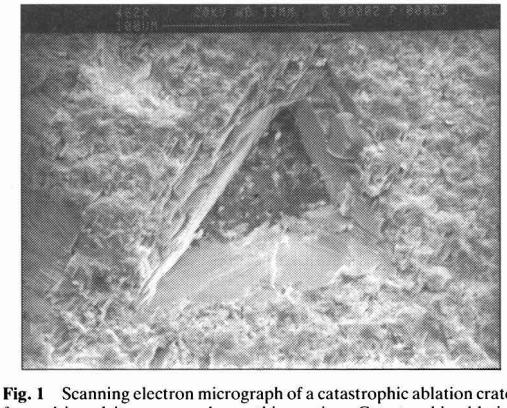

Fig. 1 Scanning electron micrograph of a catastrophic ablation crater formed in calcite, prepared as a thin section. Catastrophic ablation occurred after 1 laser shot in an analysis by IR-LPMA. Flat area at the base of the crater represents the sample slide interface. See text for laser settings. Scale bar, 100 μm.

slide absorb the incoming laser light, some of the energy may be absorbed in the intervening bonding material (epoxy resin). This rapidly volatilizes causing a large area, often a cleavage fragment, of the sample to flake off.

Lateral resolution in UV-LPMA is controlled by laser power and does not appear to be a function of mineral type. Craters in the region of 5 μm diameter were produced in both light and ferro-magnesian minerals under the experimental conditions outlined above when prepared both as cut block and thin section. Geertsen *et al.*[12] suggest that plasmas formed above the sample surface in ultraviolet laser ablation are simple in comparison to those formed in infrared laser ablation. They conclude that a greater proportion of the material removed from the sample is from direct ablation caused by absorption of the laser energy in the ultraviolet than by plasma erosion. Again our observations are in agreement with this finding.

Craters produced in a glass slide ranged from less than 5 to >70 μm diameter with increasing laser power, from 0.05 to 3.2 mJ (Fig. 2). Interestingly, increasing laser power above 1.5 mJ to its maximum at 3.2 mJ made little difference in the crater diameter produced, although the surrounding damage in the form of conchoidal fracturing in the glass slide increased. The size of the fragments produced in this conchoidal fracturing may be too large to be transported to the plasma.

Crater depth, or vertical resolution has received little attention in the literature, although it is an important consideration in the analysis of minerals in a cut block. When material is prepared in this way it is very often difficult to determine the boundaries of the mineral of interest, and thus it may be difficult to avoid sampling adjacent material as well as the mineral during an analysis. Vertical resolution is difficult to assess by SEM imaging as this technique provides no direct means of measuring depth. However, qualitatively, crater depth appears to be related not only to mineral type but also laser wavelength. For IR-LPMA it appears that in ferro-magnesian minerals relatively deep craters are produced both in cut blocks and thin sections [Fig. 3(*a*)]. For light minerals, ablation is often in the form of cleavage fragments, the loss of which may be catastrophic in thin section. Conversely, for UV-LPMA it appears that shallow craters are formed in some ferro-magnesian minerals prepared both as cut blocks and thin sections [Fig. 3(*b*] whilst deep craters are formed in light minerals. An exception to this is the magnetite sample in our study in which deep, narrow craters were rapidly formed by both IR- and UV-LPMA and the appearance of which resembled craters formed in metals.[13]

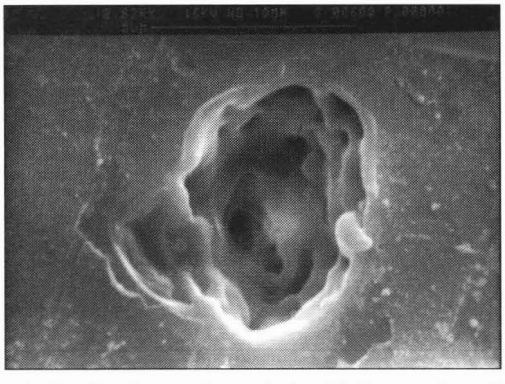

Fig. 2 Scanning electron micrograph of an ablation crater formed in glass by UV-LPMA after 1 min of ablation at 8 Hz. Laser power, 0.05 mJ. Slightly oval shape of this crater is caused by instrument vibration. Scale bar, 5 μm.

Duration of Ablation

An important consideration in the analysis of any material, but particularly material prepared as thin section is duration of ablation and this is partly associated with crater depth. Duration of ablation was investigated in the second set of experiments by repeatedly scanning during ablation of the cut block material and by rapid, continuous scanning in time resolved analysis during ablation of the thin sections.

In IR-LPMA a usable signal can be maintained for 5–10 min in ferro-magnesian minerals prepared as cut blocks without the need to change focus. For light minerals prepared in this way ablation continues for only approximately 20 s and this is indicative of the poor absorption characteristics of these minerals in the infrared region of the electromagnetic spectrum. Similarly, for thin sections, ablation continues for approximately 1 min in ferro-magnesian minerals but lasts just a few shots in light minerals before a catastrophic failure occurs.

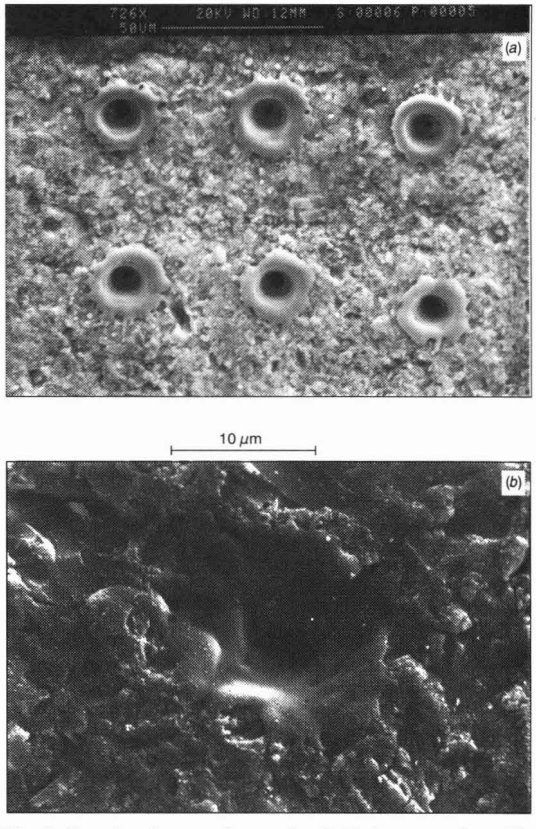

Fig. 3 Scanning electron micrographs of ablation craters formed in garnet prepared as a thin section. See text for laser settings. (*a*) Six craters resulting from analysis by IR-LPMA. Craters are neat cylindrical pits that appear as deep as they are wide. A rim of molten ejected material is deposited around each crater. Scale bar, 50 μm. (*b*) Crater resulting from analysis by UV-LPMA. This crater is a roughly circular shallow pit. Scale bar, 5 μm.

For both ferro-magnesian and light minerals prepared as cut block in ablation by UV-LPMA a usable signal can be maintained for up to 10 min without the need to change focus. In the analysis of thin sections by UV-LPMA the ability of the laser to couple to and ablate the glass slide can be exploited to lengthen the duration of ablation. For most minerals a strong signal from the thin section continues after the glass slide is met so that provided there is no analyte of interest in the glass slide or binder, ablation may be continued through the sample slide interface. By using this method usable signals can be maintained for up to 2 min in both ferro-magnesian and light minerals. Such a determination of an apatite is represented in Fig. 4(*a*). In this sample the ^{43}Ca signal from the apatite at the start of the analysis lasts for approximately 40 s before the ^{29}Si signal from the glass slide starts to rise and continues strongly for some 20 s after this. The ^{43}Ca signal does not return to background for a further 30 s or so, making a total analysis time of 90 s. Similar patterns are also seen in the ferro-magnesian minerals with the exception of the magnetite sample. Fig. 4(*b*) shows the analysis of the magnetite in thin section. In this sample the usable ^{57}Fe signal lasts for approximately 30 s and is finished before the ^{29}Si signal from the glass slide is full. This is perhaps indicative of the rapid formation of deep narrow craters observed in the magnetite sample, reminiscent of the analysis of metals (*op. cit*).

Importance of Mineral Orientation

In the third set of experiments the significance of mineral orientation was investigated by monitoring the signal from each sample during ablation, and by viewing, measuring and photographing the resultant craters with the aid of an SEM. For IR-LPMA mineral orientation has a significant effect on the size and shape of resultant craters in strongly cleaved minerals. An extreme example of this was the analysis of the mica phlogopite. When ablating the {001} face of the crystal, *i.e.*, perpendicular to the cleavage plane, fairly neat, circular craters are observed [Fig. 5(*a*)]. However, when ablating parallel to the cleavage plane, elongate, cleavage fragments are removed and catastrophic ablation occurs [Fig. 5(*b*)]. This results in a 100× signal loss when ablating parallel to the cleavage, and indicates that the cleavage fragments ablated in this orientation are too large to be transported to the plasma. For poorly-cleaved minerals such as olivine, orientation had no significant effect on either crater formation or signal intensity. Catastrophic ablation of the light minerals occurred regardless of orientation.

Mineral orientation does not appear to be important in UV-LPMA for either the ferro-magnesian or light minerals. Although cleavage fragments are ablated from the strongly cleaved light minerals in some orientations, there was no loss of signal. This indicates that the fragments were sufficiently small to be transported to the plasma.

Lower Limits of Detection

The final set of experiments concern detection limits. With the move towards ever smaller lateral resolution in laser ablation techniques comes a degradation in detection limit.

In UV-LPMA laser power and thus crater diameter and volume of material ablated can be controlled and this offers the analyst a range of lateral resolutions and detection limits. Fig. 6 and Table 1 show that at very low power, crater diameters of less than 5 μm result in geological materials, but lower limits of detection based on 1 min ablation time [calculated as $(3 \times \sqrt{\text{background counts}})$/slope of the calibration curve (counts/ppm), Potts[14]] range from hundreds to thousands of ppm and this sensitivity is insufficient for most

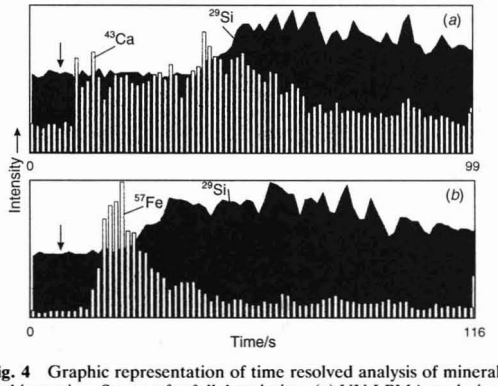

Fig. 4 Graphic representation of time resolved analysis of minerals in thin section. See text for full description. (*a*) UV-LPMA analysis of apatite and (*b*) UV-LPMA analysis of magnetite. Arrows indicate laser on.

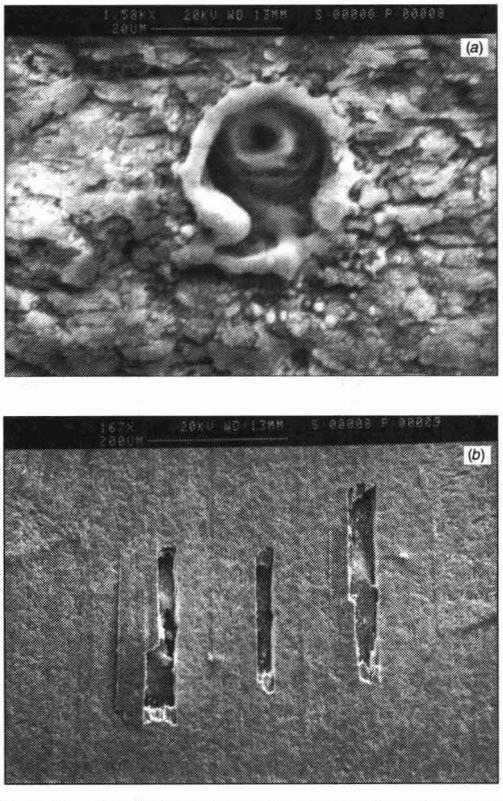

Fig. 5 Scanning electron micrographs of craters formed in phlogopite by IR-LPMA. See text for full description. (*a*) Ablation on to the {001} face, *i.e.*, perpendicular to the cleavage plane. Scale bar, 20 μm. (*b*) Ablation on to the {010} face, *i.e.*, parallel to the cleavage plane. Scale bar, 200 μm.

geological applications. Increasing the laser power to give a lateral resolution of 10–20 μm reduces this lower limit of detection to ppm–tens of ppm and this would find reasonable application to geological materials. Sub-ppm lower limits of detection are achieved by increasing the laser power to produce crater diameters in the 20–40 μm range. Interestingly, increasing the laser power still further provides little reduction in lower limits of detection and this corresponds to the maximum crater diameter of 70 μm observed at less than maximum laser power above.

IR-LPMA provides no such control over lateral resolution and lower limits of detection. Interestingly, for the same power density and crater diameter produced in IR-LPMA the corresponding lower limit of detection in the ultraviolet system is 10 times smaller (see Fig. 6). This would indicate that the production of transportable particulate during ablation is greater in the ultraviolet than in the infrared and is a result of greater absorption of the ultraviolet in the sample.

All of the lower limits of detection presented in this study may be improved by either increasing the duration of ablation and therefore increasing the amount of ablated material or reducing the number of isotopes scanned.

Conclusion

Differences in the ablation characteristics of an infrared and ultraviolet laser used in LPMA–ICP-MS are demonstrated in this paper.

The lateral resolution achieved by laser sampling of material prepared as cut block and thin section for the UV laser is determined by the power density of the laser and at low power is approximately 4 μm in most minerals. For the IR laser lateral resolution is determined by the absorption characteristics of the mineral and the extent to which plasma erosion is responsible for the removal of material from the sample. In the instance of light minerals prepared as thin section a catastrophic ablation will result and this technique is unsuitable for the analysis of such material. Vertical resolution in both IR- and UV-LPMA appears to be related to the absorption characteristics of the mineral.

Table 1 LPMA–ICP-MS lower limits of detection

	UV-LPMA–ICP-MS								IR-LPMA
Power/mJ	0.05	0.2	0.35	0.6	1.1	1.8	2.5	3.2	4
Crater diameter/μm	4	6	8	21	42	60	70	70	40
Power density /W cm^{-2}	1.7×10^{10}	6.79×10^{10}	1.19×10^{11}	2.04×10^{11}	3.73×10^{11}	6.11×10^{11}	8.48×10^{11}	1.09×10^{12}	3.39×10^{11}
Isotope/element	Lower limits of detection (ppm)								
^{7}Li	6331	39.6	5.59	2.16	0.967	0.627	0.572	0.519	5.26
^{11}B	304	78.5	15	7.71	3.18	2.15	1.87	1.79	ND*
^{45}Sc	4118	48.2	6.37	2.33	0.948	0.545	0.514	0.459	35.4
^{47}Ti	219	19.3	3.4	1.29	0.511	0.311	0.295	0.269	210
^{51}V	405	44.4	5.92	2.43	1.01	0.667	0.618	0.563	10.2
^{52}Cr	176	59.4	8.82	3.47	1.45	0.926	0.866	0.814	26.9
^{59}Co	696	66.8	7.64	3.47	1.58	0.988	0.929	0.873	8.11
^{60}Ni	283	107	25.4	11.3	4.51	2.96	2.91	2.6	ND
^{65}Cu	259	195	139	57.9	30.4	21.9	22.3	19.9	187
^{66}Zn	ND	180	27.3	10.8	4.44	2.97	2.84	2.62	36.4
^{69}Ga	304	18.4	3.17	1.28	0.564	0.347	0.341	0.297	8.63
^{85}Rb	623	128	16.2	6.05	2.65	1.68	1.63	1.38	25.8
^{88}Sr	181	34.4	4.3	1.6	0.659	0.379	0.357	0.329	9.61
^{89}Y	ND	80	11.4	3.64	1.54	0.863	0.831	0.757	9.95
^{90}Zr	639	65.6	15.5	5.99	2.06	1.39	1.27	1.18	23.2
^{93}Nb	657	41.9	6.69	2.5	1.09	0.618	0.59	0.521	10.1
^{115}In	273	12.7	2.39	0.85	0.396	0.239	0.238	0.206	7.1
^{133}Cs	512	21.5	3.51	1.3	0.591	0.351	0.337	0.305	23.9
^{135}Ba	ND	88.9	16.9	5.78	2.16	1.34	1.26	1.15	84.4
^{139}La	212	14.7	2.3	0.77	0.307	0.174	0.166	0.153	7.1
^{140}Ce	120	11.3	1.92	0.69	0.294	0.172	0.167	0.154	5.38
^{141}Pr	149	11.5	1.65	0.59	0.234	0.134	0.133	0.118	6.2
^{143}Nd	439	44.8	6.74	2.27	0.945	0.517	0.503	0.458	62.3
^{147}Sm	ND	39.3	5.7	1.87	0.763	0.437	0.418	0.38	49.6
^{153}Eu	394	15.8	2.04	0.73	0.296	0.170	0.164	0.147	14.6
^{157}Gd	797	36.2	4.7	1.74	0.673	0.392	0.373	0.349	30.6
^{159}Tb	250	11.6	1.81	0.65	0.254	0.143	0.137	0.126	6.98
^{163}Dy	168	17.6	2.6	1.03	0.422	0.233	0.221	0.199	46.1
^{165}Ho	153	9.1	1.25	0.44	0.178	0.099	0.094	0.087	8.79
^{166}Er	505	15.8	3.23	1.04	0.437	0.238	0.229	0.207	24.2
^{169}Tm	241	10.6	1.56	0.54	0.218	0.122	0.114	0.102	8.47
^{172}Yb	3640	38.3	5.52	1.78	0.729	0.394	0.383	0.354	32.9
^{175}Lu	173	7.92	1.3	0.42	0.166	0.094	0.086	0.081	11.4
^{178}Hf	232	1.2	1.73	0.61	0.247	0.131	0.127	0.114	31.2
^{181}Ta	103	5.11	0.78	0.26	0.106	0.061	0.058	0.052	9.49
^{208}Pb	208	17.8	2.74	0.91	0.401	0.258	0.229	0.209	27.8
^{232}Th	235	8.03	1.2	0.41	0.166	0.091	0.088	0.078	17.4
^{238}U	83.5	3.76	0.51	0.15	0.071	0.042	0.038	0.036	9.62

* ND, Not detected.

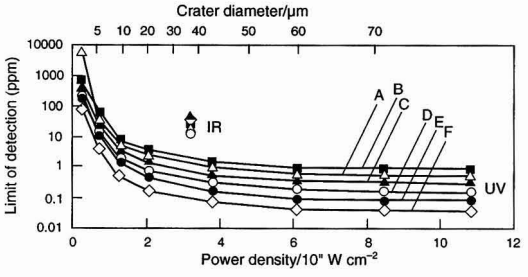

Fig. 6 LPMA–ICP-MS lower limits of detection *versus* power density and crater diameter for A, Li; B, Co; C, Cs; D, Ce; E, Lu; and F, U. See text for full description. Conditions: 1 min of ablation, 5 Hz; NIST SRM 610; scanning *m/z* 6–239.

The duration of ablation in IR-LPMA is similarly related to the absorption characteristics of the mineral and for light minerals is as little as 20 s in cut block and a single laser shot for thin sections. In ferro-magnesian minerals duration of ablation ranges from 5–10 min in cut blocks and is approximately 1 min in thin sections. For UV-LPMA a usable signal can be maintained for any mineral in cut blocks for approximately 10 min. For thin sections the duration of a usable signal may be lengthened to approximately 2 min by continuing the ablation through the sample slide interface.

Mineral orientation is an important consideration for IR-LPMA and in the analysis of an inappropriately oriented mineral a 100× signal reduction or catastrophic ablation may occur. For UV-LPMA mineral orientation is not significant.

In UV-LPMA lower limits of detection are a function of power density and range from thousands of ppm to sub-ppm levels. For the same power density produced in IR-LPMA the corresponding lower limit of detection for the ultraviolet system is 10 times smaller and this results from the greater production of transportable particulate in the UV system.

In all of the ablation characteristics investigated here, UV-LPMA offers significant advantages over IR-LPMA. In particular, the reduction in lateral resolution, decrease in lower limits of detection and the ability to analyse all minerals in thin section in UV-LPMA makes this the most appropriate technique for mineral microanalysis.

T. E. J. thanks Fisons Instruments Elemental and The Institute of Earth Studies, University of Wales, Aberystwyth for financial support. W. T. P. gratefully acknowledges financial support from The Royal Society (Research grant 13188) for modifications to the laser system. (Institute of Earth Studies publication number 377).

References

1 Gray, A. L., *Analyst*, 1985, **110**, 551.
2 Arrowsmith, P., *Anal. Chem.*, 1987, **59**, 1437.
3 Perkins, W. T., Pearce, N. J. G., and Jeffries, T. E., *Geochim. Cosmochim. Acta*, 1993, **57**, 475.
4 Pearce, N. J. G., Perkins, W. T., Abell, I., Duller, G. A. T., and Fuge, R., *J. Anal. At. Spectrom.*, 1992, **7**, 53.
5 Jackson, S. E., Longerich, H. P., Dunning, G. R., and Fryer, B. J., *Can. Mineral.*, 1992, **30**, 1049.
6 Burns, R. G., *Mineralogical Applications of Crystal Field Theory*, Cambridge University Press, Cambridge, 1970, p. 224.
7 Chenery, S., and Cook, J. M., *J. Anal. At. Spectrom.*, 1993, **8**, 299.
8 Perkins, W. T., and Pearce, N. J. G., in *Microanalytical Techniques in the Geosciences*, ed. Potts, P. J., Bowles, J. F. W., Reed, S. J. B., and Cave, M. R. Chapman and Hall, London, 1995, pp. 291–325.
9 Chenery, S., Hunt, A., and Thompson, M., *J. Anal. At. Spectrom.*, 1992, **7**, 647.
10 Huang, Y., Shibata, Y., and Morita, M., *Anal. Chem.*, 1993, **65**, 2999.
11 Pearce, N. J. G., Perkins, W. T., Westgate, J. A., Gorton, M. P., Jackson, S. E., and Neal, C. R., *Geostand. Newsl.*, submitted for publication.
12 Geertsen, C., Briand, A., Chartier, F., Lacour, J.-L., Mauchien, P., Sjöström, S., and Mermet, J.-M., *J. Anal. At. Spectrom.*, 1994, **9**, 17.
13 Watling, R. J., Herbert, H. K., Delev, D., and Abell, I. D., *Spectrochim. Acta, Part B*, 1994, **49**, 205.
14 Potts, P. J., *A Handbook of Silicate Rock Analysis*, Blackie and Sons, Glasgow, 1987, p. 622.

Paper 4/05894A
Received September 27, 1994
Accepted November 16, 1994

Preparation of Glasses for use as Chemical Standards Involving the Coprecipitated Gel Technique*

David L. Hamilton and Timothy C. Hopkins
Department of Geology, University of Manchester, Manchester, UK M13 9PL

Homogeneous glasses of known compositions have been prepared using the coprecipitated gel technique for use as chemical standards. Three of the glasses produced have been tested in a collaborative study to assess their suitability as chemical standards for laser ablation inductively coupled plasma mass spectrometry.

Keywords: Glass chemical standards; coprecipitated gel technique; laser ablation inductively coupled plasma mass spectrometry

Introduction

The object of this investigation was to produce homogeneous glasses of known compositions for use as chemical standards in electron probe microanalysis (EPMA), X-ray fluorescence (XRF), laser ablation inductively coupled plasma mass spectrometry (LA–ICP-MS) and other associated techniques.

Silicate compositions for use in phase-equilibria experiments made by the coprecipitation gel technique were first investigated in 1960 by Hamilton and MacKenzie;[1] the method being based on an idea published by Roy.[2] The phase-study required the synthesis of a number of compositions, each of sufficient mass so that many aliquots could be taken from them for individual experiments. Usually 5 g batches were made, from which about 0.1 g aliquots were removed for study. To be of any use the 5 g batch must be of the desired composition and it must be homogeneous so that each aliquot is of the same composition. These two properties are exactly those required for a standard glass composition from which smaller samples are taken for distribution and analysis. It therefore seemed reasonable in 1992 to use this expertise at preparing gel compositions in the preparation of standard glasses. Chemical analyses of three glasses produced by the gel technique are reported from four laboratories to test their suitability as chemical standards for LA–ICP-MS.

Experimental

Gelling Technique

The technique depends on the fact that certain SiO_2-rich (also TiO_2 and ZrO_2) liquids may be made to set very rapidly producing a stiff 'gel'. The structure of a pure SiO_2-gel consists of a 3D-framework of Si–O linkages with a large porosity; the pores (diameters measured in Å), will be filled with the liquid used in the gel preparation, normally water and alcohol. Upon drying, the gel-structure is destroyed by the surface tension forces operating at the liquid/vapour interface in each pore and the end-result is a fine-grained, soft, crypto-crystalline powder of SiO_2-composition. If other components are added to the silica liquids as solutions, *e.g.*, nitrates, and immiscibility avoided by adding alcohol then, upon gelling the silica, the pores of the gel will contain this solution. During drying, the solution in each pore will deposit its originally dissolved load into its pore space. Surface tension within each pore will collapse the gel structure and the end-product should be a fine-grained, soft powder the chemical components of which are mixed on a very fine scale (*i.e.*, Å scale). At this stage the nitrates are still present so it is necessary to 'fire' the gel, usually to about 700 °C, to decompose these. After firing to about 700 °C or below, the 'gel' will have contracted 30 to 50% but will remain soft and may easily be ground and mixed by hand in agate.

The method of gel making used for all the glass compositions described here is described in Hamilton and Henderson[3] and briefly is as follows. All components except SiO_2 are contained in a single solution as nitrates. About an equal volume of ethanol is stirred into this solution followed by the required mass of tetraethyl orthosilicate (TEOS). The liquid is vigorously stirred until a single homogeneous liquid results. Additional ethanol might be needed to accomplish this because TEOS is immiscible with water. Concentrated ammonia solution is now added while vigorous stirring continues. This causes the SiO_2 and aluminium hydroxide to gel and the whole contents of the beaker should become semi-solid in a few minutes, thus producing a homogeneous mixture as a gel.

This description excludes two complicating issues met in many chemical systems, (*i*) not all elements will dissolve in nitric acid at the required concentrations, *e.g.*, Cr, Ti and Ce. In these instances we accept a nitrate solution with fine-grained suspension of the insoluble components, (*ii*) in Al-bearing compositions, on adding the ammonia to gel the system, the Al will form a gel before the Si does which will cause an uneven distribution of Al and Si. The inhomogeneity caused by (*i*) and (*ii*) is minimized by hand mixing the 'gel' at two stages during drying and firing followed by a mechanical mixing just prior to melting. Melting also will tend to remove any compositional gradients.

Glass Making

Each 'gel' composition was melted in a platinum crucible at 1450 ± 50 °C for about 16 h before quenching by pouring onto a mild steel plate. In some cases the melt was rolled flat using a small roller made from mild steel.

Tests for Homogeneity

It is essential that any material used as a standard for an analytical technique with high spatial resolution, such as EPMA or LA–ICP-MS, is homogeneous. Three separate tests were performed to check for homogeneity in glasses produced by the gel method. (1) Hamilton and Henderson[3] sampled a

* Presented at Geoanalysis 94: An International Symposium on the Analysis of Geological and Environmental Materials, Ambleside, England, September 18–22, 1994.

Na–K–Al–Si raw gel (*i.e.*, a gel before drying or decomposition of the nitrates) from several places within its structure and found no significant variation in Na or K levels. (2) A REE glass (based on Si–Al–Ca) produced as a standard for EPMA containing Y, Pr, Dy and Er each at 4.0 mass% has been subjected to line scan analysis using an EMPA. The result is shown in Fig. 1, over a 2 mm scan length there is no significant variation in REE or Ca concentration. (3) DLH6, DLH7 and DLH8 are three glasses made for use as standards for LA–ICP-MS instruments. DLH6 has no minor elements added and is intended as a blank; its composition is: SiO_2, 72.0; CaO, 12.0; Na_2O, 14.0; and Al_2O_3, 2.0 mass%. DLH7 is similar to DLH6 plus 43 elements added at levels of 75 ppm and Y at 225 ppm. DLH8 is again similar to DLH6 plus 44 elements added at the 150 ppm concentration level.

Three of our co-operating laboratories have analysed glasses DLH6, 7 and 8 using LA–ICP-MS analysis, they all ablated material from a minimum of five positions on the 10 mm^2 glasses. It is not possible to show all these data, Table 1 shows the data for the elements V, Sr, Pr, and U only. The calibration was obtained by the standard solution method (described later under Glass Compositions), the five analyses for V are within ±12 ppm of the mean value of 151.4 ppm and the results for Pr are the best being within ±4 ppm of the mean value. Proportioning the error between inhomogeneity and analytical problems cannot be made at this stage. To test for coarser inhomogeneity several pieces of the glass specimen were dissolved and the separate solutions analysed. The results are shown in Table 2. The standard deviations (*s* values) for this method are smaller than those obtained for the laser analysis method.

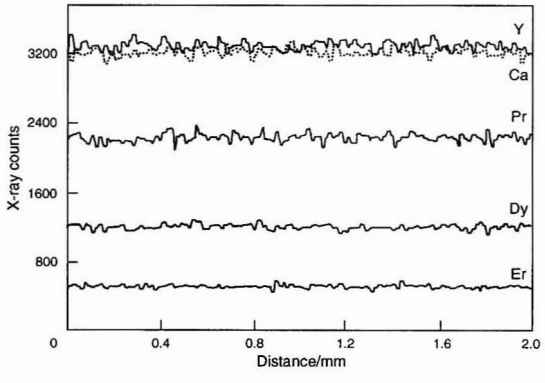

Fig. 1 Microprobe analysis of glass DLH1, which has 4 mass% each of Pr, Dy, Er, and Y in a base glass of SiO_2, 62; CaO, 23.5; and Al_2O_3, 14.5 mass%. The figure represents a 128 point line scan over a 2 mm distance, the counting time was 20 s per point (analyst: T. C. Hopkins).

Table 1 Chemical test for homogeneity, DLH8, 150 ppm. Five spots on the same glass fragment were laser ablated and analysed by ICP-MS using the solution method to calibrate (analyst: Aberystwyth University)

	Concentration (ppm)						
Element	1	2	3	4	5	Mean (ppm)	*s* (ppm)
V	140.0	148.0	148.9	159.0	161.2	151.4	8.7
Sr	138.8	144.7	152.3	149.3	158.3	148.7	7.3
Pr	144.0	149.5	142.8	152.2	151.2	148.0	4.3
U	155.6	161.1	152.4	163.2	168.2	160.1	6.3

Glass Compositions

Four glass compositions have been determined by four different laboratories. All results were obtained from ICP-MS instruments but 3 different analytical methods were used *viz.* the following:

(1) Calibration by standard solutions (either produced in the laboratory or obtained commercially) and the glass specimens dissolved, the solution is then compared with the standard solution; this method will be referred to as the solution–solution method.

(2) Calibration by standard solution as in (1) but the glass specimens are laser ablated; referred to as the solution–laser method.

(3) Calibration by ablating NIST (National Institute of Standards and Technology, formerly the NBS) standard glasses 610 and 612 then laser ablating the glass specimens; referred to as the laser–laser method.

Glass DLH10

This glass, intended for use as an XRF analysis standard, contains 23 elements, each at 1000 ppm concentration. Manchester University used the solution–solution method to

Table 2 Mean analyses of three glass fragments taken from a single batch of glass each individually dissolved and analysed by the solution–solution method. The small standard deviations reflect the good homogeneity of the glass (analyst: Aberystwyth University)

Element	Mean (ppm)	*s* (ppm)
V	134.0	1.9
Sr	140.0	1.4
Pr	138.9	1.2
U	152.7	2.0

Table 3 ICP-MS analyses of two glass chips from melt DLH10a and melt DLH10b. Chips were dissolved and the solution analysed using standard solutions, *i.e.*, the solution–solution method (analyst: Manchester University)

Element	Atomic No.	Expected analysis (ppm)	DLH10a analysis (ppm)	DLH10b analysis (ppm)
Sc	21	1000	968.9	986.0
Ti	22	1000	987.2	1018.9
V	23	1000	1125.4	1294.5
Cr	24	1000	332.1	374.3
Mn	25	1000	1005.9	1027.0
Co	27	1000	1003.5	1016.7
Ni	28	1000	949.7	963.4
Cu	29	1000	881.6	869.0
Zn	30	1000	947.5	932.1
Ga	31	1000	1045.3	1058.1
Rb	37	1000	943.1	944.5
Sr	38	1000	1085.7	1073.4
Y	39	1000	1012.5	1005.7
Zr	40	1000	820.0	884.0
Nb	41	1000	nd*	nd*
Mo	42	1000	280.3	312.4
Sn	50	1000	nd*	nd*
Ba	56	1000	963.0	970.2
La	57	1000	892.3	929.1
Ce	58	1000	1029.4	1028.5
Nd	60	1000	932.0	935.0
W	74	1000	267.3	252.3
Pb	82	1000	070.3	085.3

* nd, Not determined.

analyse two pieces of the glass from two different melt castings to produce the results shown in Table 3, and one set of results is shown in Fig. 2. The two sets of analyses are quite similar in that 17 elements are reasonably close to the expected 1000 ppm level but Cr, Mo, W and Pb are all very much lower. Lythgoe (Manchester University) has suggested that Mo and W levels are probably low owing to the difficulty in getting the glass into solution. Lead is probably lost during the 1500 °C melting process and Pearce (Aberystwyth University) has suggested that $CrCl_2$ might be lost in the vapour during the digestion of the glass.

Glasses DLH6, DLH7 and DLH8

Four laboratories have analysed these glasses, the results are given in Tables 4, 5 and 6 which also shows the type of analytical method used, *i.e.*, solution–solution, solution–laser or laser–laser. No laboratory submitted a determination for Fe although this element was added to DLH7 at a concentration 75 ppm and to DLH8 at a concentration of 150 ppm. The average (s_{av}) and standard deviation (s) are calculated for each element both (*i*) for all results and (*ii*) for selected results. The latter excludes analyses that 'appear to be discordant' with the main data set. For DLH7 (75 ppm) the selective average and selective standard deviation have excluded values below 50 and above 100 ppm, and for DLH8 (150 ppm) values below 100 and above 200 ppm have been excluded. The 'selected' data probably gives a better indication of the compositions of the glasses.

Results and Discussion

DLH6, Blank

Most of the data in Table 4 show that the glass is indeed 'blank' which is encouraging for the reagents used in the synthesis. A few elements gave a high value, *e.g.*, Mn (2.8 ppm) but this result is based on only two laboratories having provided data of 0.9 and 4.8 ppm. Zinc (4.7 ppm), again, if the high value of 11 ppm is excluded from the mean calculation, then the mean becomes 1.6 ppm which is a more acceptable result. Yttrium (2.5 ppm), and Mo (3.9 ppm) are difficult to explain, whether these amounts are due to impurities, contamination or analytical errors cannot be determined.

DLH7, 75 ppm

It is premature in the 'round-robin' type characterization of these glass standards to discuss in detail every one of the trace elements, so a few general points will be made followed by some specific points. Identifying a concentration within ±5 ppm of the intended value as 'good' within ±15 ppm as 'intermediate' and outside these ranges as 'bad', on referring to the selective average in Table 5 there are 23 good, 16 intermediate and 3 bad results (however the results for K might well be left out for reasons of sparsity of data). Most of the results are lower than the theoretical values and this could be due to shortcomings of the synthesis method. For instance, probably the Tl has been completely lost by volatilization during heating (most likely at the melting stage) and both K and Pb are known to be lost from melts. The possibility that all elements are lost to some small extent during melting cannot be excluded at this stage. A more likely explanation soon to be reported by Pearce *et al.*[4] is that when samples are dissolved in various acids prior to a solution analysis some loss by volatilization of compounds of chloride and fluoride takes place. The analysis of such a depleted solution might account for the lower than expected analyses in Table 5.

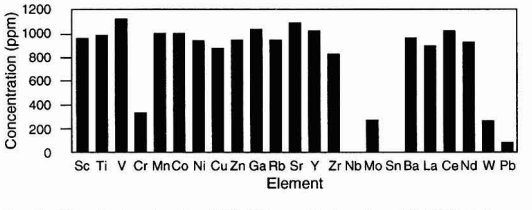

Fig. 2 Graph showing the ICP-MS results for glass DLH10a (shown in Table 2). The glass was made up to contain 1000 ppm of all the minor elements shown. Nb and Sn are present but not determined.

Table 4 DLH6, no added minor elements. Base glass composition is SiO_2, 72; Al_2O_3, 2; CaO, 12; and Na_2O, 14 mass%

Laboratory*	Aber	Aber	BGS	
Calibration method†	S	L	S	
Analysis method†	S	L	L	Av‡
Li	0.3			0.3
B	0.0	6.1		3.1
Mg	nd	nd	14.2	14.2
K	nd	nd		
Sc	0.1	0.8		0.4
V	0.3	0.3	−1.7	−0.4
Cr	3.7	3.3	−7.2	−0.1
Mn	nd	0.9	4.8	2.8
Co	0.3	0.3	0.3	0.3
Ni	2.8	1.6	−13.1	−2.9
Cu	6.7	8.7	11.9	9.1
Zn	0.8	2.4	11.0	4.7
Ga	0.0	0.2		0.1
Rb	0.0	0.4		0.2
Sr	1.4	1.8		1.6
Y	2.4	2.7		2.5
Zr	1.5	1.7		1.6
Nb	0.2	0.5		0.3
Mo	3.6	4.2		3.9
Ag	0.1			0.1
Cd	<0			
In	0.1		0.1	0.1
Ba	0.3	0.6		0.4
Ta	0.0	0.0		0.0
W	nd			
Tl	<0.01			
Pb	0.1	0.3	1.0	0.5
Bi	0.7			0.7
La	0.2	0.3	0.4	0.3
Ce	0.1	0.2	0.7	0.3
Pr	0.0	0.1	0.1	0.1
Nd	0.9	1.0	1.0	1.0
Sm	0.1	0.1	0.0	0.1
Eu	0.1	0.1	−0.1	0.0
Gd	0.1	0.2	0.1	0.1
Tb	0.9	1.0	0.7	0.9
Dy	0.1	0.1	0.0	0.0
Ho	0.1	0.1	0.1	0.1
Er	0.0	0.1	−0.1	0.0
Tm	0.1	0.1	0.0	0.0
Yb	0.1	0.2	0.1	0.1
Lu	1.0	1.1	0.8	1.0
U	0.0	0.0	−0.1	0.0

* Aber, Aberystwyth University; BGS, British Geological Survey.
† S, solution and L, laser methods.
‡ Av, average value.

The large spread in the results from the various laboratories leading to large *s* values shown in Table 5 may be explained by the following:

(*i*) The glass samples are inhomogeneous. However, the whole synthesis process was directed towards producing a homogeneous glass and the repetitive results shown in Table 1 show only minor variations in compositions supporting the proposition of good homogeneity.

(*ii*) The various analytical procedures *e.g.*, solution–laser and laser–laser methods used by the various participating groups and the variety of standards used have contributed errors leading to the rather large *s* values seen in Table 5.

DLH8, 150 ppm

A similar survey of the results for DLH8 in Table 6 leads to the following breakdown: good, 19(23); intermediate, 16(16); and bad, 7(3). These figures are quite close to those for DLH7 (shown in parentheses).

Conclusions

Before making any firm pronouncements about the genuine compositions of the glasses described in this paper we feel that more analyses by different laboratories and in some instances using different analytical techniques, *i.e.*, neutron activation analysis (NAA) are essential. From the data presented we conclude that: (*i*) the glasses are essentially homogeneous; (*ii*) Tl is completely lost probably by vapour loss during melting; (*iii*) Pb and K are similarly lost but not so completely; (*iv*) there are some problems with B, Cr and Ag, which might be due to LA–ICP-MS analysis errors rather than to errors in the method of synthesis; and (*v*) the remaining minor elements

Table 5 DLH7, minor elements added to 75 ppm except for Y at 225 ppm. Selective average column and selective *s* column ignore analyses outside the range 50–100 ppm (except Y)

Laboratory*	Aber	Aber	Fis	Man	BGS			Selective	Selective
Calibration method†	S	L	L	S	S			av	*s*
Analysis method†	S	L	L	S	L	Av‡	*s*		
	(ppm)	(ppm)	(ppm)	(ppm)	(ppm)	(ppm)	(ppm)	(ppm)	(ppm)
Li	73.7		58.6			66.2	07.5	66.2	7.5
B	<0.01	31.7	75.0	18.9		41.9	24.0	75.0	0.0
K			56.4			56.4	00.0	56.4	0.0
Sc	65.7	69.9	61.1	69.1		66.5	03.5	66.5	3.5
V	66.5	72.9	71.8	140.0	77.0	85.6	27.4	72.1	3.7
Cr	50.7	51.7	63.1	72.8	45.0	56.7	10.0	59.6	9.1
Mn	nd	64.2	70.7	65.5	68.0	67.1	02.5	67.1	2.5
Co	63.3	71.0	68.4	128.3	68.0	79.8	24.4	67.7	2.8
Ni	60.7	53.7	70.7	70.9	52.0	61.6	08.1	61.6	8.1
Cu	41.6	58.9	64.7	373.6	84.0	124.6	125.2	69.2	10.7
Zn	100.2	63.0	47.1	61.8	60.0	66.4	17.8	61.6	1.2
Ga	72.0	61.1	72.1	132.0		84.3	27.9	66.6	5.2
Rb	67.5	59.3	71.2	70.1		67.0	04.7	67.0	4.7
Sr	68.7	75.2	73.8	70.5		72.0	02.6	72.0	2.6
Y	227.4	262.8	228.4	224.5		235.8	15.7	235.8	15.7
Zr	72.5	73.9	74.1	66.1		71.6	03.3	71.6	3.3
Nb	21.8	81.4	72.8			58.7	26.3	77.1	4.3
Mo	59.2	51.4	78.4	57.4		61.6	10.1	61.6	10.1
Ag	21.1		76.0			48.6	27.5	76.0	0.0
Cd	30.4		66.1	76.2		57.6	19.6	71.1	5.0
In	75.5		74.1		65.0	71.5	04.7	71.5	4.7
Ba	68.6	61.4	75.5	78.6		71.0	06.6	71.0	6.6
Ta	9.7	84.0	76.2	6.6		44.1	36.1	80.1	3.9
W			78.7	21.1		49.9	28.8	78.7	0.0
Tl	1.3		0.0	0.0					
Pb	51.6	48.3	69.3	85.7	50.0	61.0	14.5	64.1	8.7
Bi	55.6		76.1	68.4		66.7	08.5	66.7	8.5
La	67.2	73.1		75.6	67.0	70.7	03.7	70.7	3.7
Ce	62.3	65.4	77.6	76.7	69.0	70.2	06.1	70.2	6.1
Pr	71.1	76.9	76.7	80.5	72.0	75.4	03.5	75.4	3.5
Nd	60.8	75.3	74.6	71.4	62.0	68.8	06.2	68.8	6.2
Sm	57.4	64.3	71.0	71.4	60.0	64.8	05.7	64.8	5.7
Eu	67.6	77.0	78.4	79.1	68.0	74.0	05.1	74.0	5.1
Gd	69.9	82.3	80.0	77.5	69.0	75.7	05.4	75.7	5.4
Tb	73.1	82.4	77.5	76.1	65.0	74.8	05.7	74.8	5.7
Dy	71.0	85.0	78.4	71.1	67.0	74.5	06.4	74.5	6.4
Ho	74.8	83.6	80.1	73.9	66.0	75.7	06.0	75.7	6.0
Er	68.0	83.0	80.1	79.6	66.0	75.3	06.9	75.3	6.9
Tm	73.4	83.5	77.9	75.4	65.0	75.0	06.1	75.0	6.1
Yb	73.3	93.9	79.1	72.4	66.0	76.9	09.4	76.9	9.4
Lu	78.5	93.0	81.5	79.3	65.0	79.5	08.9	79.5	8.9
U	75.0	75.2	79.8	68.7	78.0	75.3	03.8	75.3	3.8

* Aber, Aberystwyth University; Fis, Fisons Instruments; Man, Manchester University; BGS, British Geological Survey.
† S, solution; L, laser methods.
‡ Av, average value.

Table 6 DLH8, minor elements added to 150 ppm. Selective numbers ignore value outside the range 100–200 ppm

Laboratory*	Aber	Aber	Fis	Man	BGS				
Calibration method†	S	L	L	S	S			Selective	Selective
Analysis method†	S	L	L	S	L	Av‡	*s*	av	*s*
	(ppm)	(ppm)	(ppm)	(ppm)	(ppm)	(ppm)	(ppm)	(ppm)	(ppm)
Li	154.1		136.0	nd		145.1	9.0	145.1	9.0
B	0.0	36.3	115.4	21.8		43.4	43.5	115.4	0.0
Mg	nd§		133.0	nd	138.0	135.5	2.5	135.5	2.5
K	nd		231.8	nd		231.8	0.0	231.8	0.0
Sc	135.4	143.3	158.4	146.8		146.0	8.3	146.0	8.3
V	134.0	151.4	144.6	170.0	157.0	151.4	12.1	151.4	12.1
Cr	61.3	100.0	140.6	126.8	112.0	108.1	27.1	119.9	15.3
Mn	nd	135.9	166.4	138.2	137.0	144.4	12.7	144.4	12.7
Co	124.9	148.2	151.8	204.3	140.0	153.8	26.9	141.2	10.4
Ni	119.2	122.8	172.2	145.6	129.0	137.8	19.5	137.8	19.5
Cu	81.1	112.1	154.0	323.1	186.0	171.3	83.9	150.7	30.3
Zn	195.9	118.9	176.6	146.4	134.0	154.4	28.1	154.4	28.1
Ga	142.8	130.4	153.4	218.4		161.2	34.0	142.2	9.4
Rb	133.1	134.1	158.6	140.3		141.5	10.2	141.5	10.2
Sr	140.0	148.7	156.2	144.9		147.4	5.9	147.4	5.9
Y	154.1	167.0	166.6	160.3		162.0	5.3	162.0	5.3
Zr	146.2	143.8	145.4	112.8		137.0	14.0	137.0	14.0
Nb	28.9	154.1	158.4	nd		113.8	60.1	156.3	2.1
Mo	109.9	90.2	146.4	102.3		112.2	21.0	119.5	19.2
Ag	34.9		100.4	nd		67.7	32.8	100.4	0.0
Cd	56.7		152.0	88.3		99.0	39.6	152.0	0.0
In	152.4		156.4		139.0	149.3	7.4	149.3	7.4
Ba	135.8	127.5	156.0	160.0		144.8	13.6	144.8	13.6
Ta	10.1	177.2	151.6	20.7		89.9	75.1	164.4	12.8
W	nd		156.8	46.8		101.8	55.0	156.8	0.0
Tl	0.5		0.0	0.0		0.2	0.2	0.2	0.2
Pb	105.9	102.1	nd	144.2	112.0	116.0	16.6	116.0	16.6
Bi	119.1		173.8	114.5		135.8	26.9	135.8	26.9
La	132.3	147.5		152.0	127.0	139.7	10.4	139.7	10.4
Ce	125.4	131.5	151.4	154.4	136.0	139.8	11.3	139.8	11.3
Pr	138.9	148.0	150.4	156.5	135.0	145.8	7.8	145.8	7.8
Nd	121.2	151.6	156.2	157.8	121.0	141.6	16.8	141.6	16.8
Sm	115.2	142.2	142.6	149.5	114.0	132.7	15.0	132.7	15.0
Eu	133.7	159.0	150.8	157.7	129.0	146.0	12.4	146.0	12.4
Gd	139.1	162.4	152.6	153.2	131.0	147.7	11.2	147.7	11.2
Tb	151.6	168.2	156.6	161.2	131.0	153.7	12.6	153.7	12.6
Dy	141.0	173.3	150.6	149.4	130.0	148.9	14.3	148.9	14.3
Ho	151.4	179.3	153.0	151.7	131.0	153.3	15.4	153.3	15.4
Er	136.5	175.0	150.0	157.5	132.0	150.2	15.4	150.2	15.4
Tm	150.0	178.7	150.4	153.3	128.0	152.1	16.1	152.1	16.1
Yb	147.6	187.5	146.2	151.0	130.0	152.5	19.0	152.5	19.0
Lu	158.7	188.2	153.4	158.6	130.0	157.8	18.5	157.8	18.5
U	152.7	160.1	132.4	135.9	165.0	149.2	13.0	149.2	13.0

* Aber, Aberystwyth University; Fis, Fisons Instruments; Man, Manchester University; BGS, British Geological Survey.
† S, solution; L, laser methods.
‡ Av, average value.
§ nd, not determined.

are probably present at a concentration close to, or a few ppm below, their theoretical value.

The authors are grateful to the following four groups for their excellent co-operation and encouragement: Aberystwyth University, N. Pearce; BGS Keyworth, S. Chenery; Fisons Instruments, A. Raith and J. Godfrey; and Manchester University, P. Lythgoe.

References

1 Hamilton, D. L., and MacKenzie, W. S., *J. Petrol.*, 1960, **1**, 56.
2 Roy, R., *J. Am. Ceram. Soc.*, 1956, **39**, 145.
3 Hamilton, D. L., and Henderson, C. M. B., *Mineral. Mag.*, 1968, **36**, 832.
4 Pearce, N. J. G., Perkins, W. T., Westgate, J. A., Gorton, M. P., Jackson, S. E., and Neal, C. R., *Geostand. Newsl.*, submitted for publication.

Paper 4/06094F
Received October 6, 1994
Accepted January 18, 1994

Determination of Trace Elements in Petroleum Exploration Samples by Inductively Coupled Plasma Mass Spectrometry and Instrumental Neutron Activation Analysis*

Samuel D. Olsen

RF-Rogaland Research, P.O. Box 2503, Ullandhaug, 4004 Stavanger, Norway

Roy H. Filby

Department of Chemistry, Washington State University, Pullman, Washington, USA

Trond Brekke

Brekke CHEMO, Leirstad 26, 6800 Førde, Norway

Gary H. Isaksen

Exxon Production Research Co., P.O. Box 2189, Houston, Texas, USA

A suite of geochemical oil samples from a wide geographic area and a variety of depositional environments was analysed by INAA and ICP-MS. Good correlation between the two techniques was obtained for V, Ni and Co ($r = 0.95$–0.90). The correlation decreased in the order: Zn ($r = 0.87$), Fe, Sb, Se, U, Ti, La, As, Ba, Mn and W ($r = 0.18$). The contribution of trace elements to oils from produced waters, drilling fluids, biodegradation and migration has been suggested by some of the samples for which there was disagreement. Laboratory experiments confirmed that barite contributes Mn, Fe, Ga and Pb to oil samples that have not been filtered. On the ICP-MS $^{130}Ba^{2+}$ interferes with $^{65}Cu^{+}$ whereas $^{63}Cu^{+}$ suffers from interference by $^{51}V^{12}C^{+}$. If formation water and produced water is not removed from the oil, the water contribution of elements *e.g.*, As and Br is superimposed onto the organically bound contents in the oils. In such instances, it appears that these elements are not useful in fingerprinting and classifying oils. However, when the formation water contribution is removed, elements *e.g.*, As are shown to be geochemically significant. It has thus been demonstrated that it is important to water wash and filter oil samples before analysing for geochemical exploration purposes. This work has also shown that metals such as Zn, Cd and Pb are picked up by oils migrating through ore bodies of these metals. Prior to examining the contributions of water, barite and migration, oils could only be classified using their V, Ni and Co contents. The new understanding acquired from this work, has made it possible to identify and eliminate samples with severe contamination. Application of multivariate statistics to the V, Ni, Co, Mo, As, Sb, Fe, Mn, Zn and Bi data for the Exxon oils enabled appropriate oils to be correlated with each other.

Keywords: Oil; metal; trace element; oil–oil correlation; petroleum geochemistry; inductively coupled plasma mass spectrometry; instrumental neutron activation analysis; Exxon oil set

* Presented at Geoanalysis 94: An International Symposium on the Analysis of Geological and Environmental Materials, Ambleside, England, September 18–22, 1994.

Aim of Investigation

Crude oils contain organic complexes of metal ions. The current low oil price, and the tariff ($3 per barrel for some North Sea oils) charged by refineries for processing oils with high metal content and acid number, has made oil companies realize the importance of knowledge about metals at the exploration and engineering stages. It is necessary to build up geochemical knowledge of how metals enter oils and knowledge of the secondary factors[1] that control their contents. Understanding of the molecular association of metals in heavy oils will provide insight into rapid[2] and cost-effective methods for their removal.

Refineries[3] and legislating[4] authorities are carrying out work to ensure low levels of toxic metals like Cd, Hg and Pb in petroleum products.

A recent concise overview of trace elements in petroleum is given by Filby.[1] Representing practising petroleum geochemists in the oil industry, Curiale[2] states that the application of metal information to petroleum geochemistry is still in its infancy. He predicts that the information from metal organic complexes in crude oils will be routinely used to complement that provided from analysis of hydrocarbon fractions.

Further to the intercomparison of instrumental neutron activation analysis (INAA) and inductively coupled plasma mass spectrometry (ICP-MS) by Filby and Olsen,[5] the 25 oils which are part of the Exxon oil set,[6] were analysed in the work reported here. The aim of the investigation was to increase confidence in the measured metal content of oils by identifying the sources of contamination from formation water, drilling fluids, production equipment and chemicals as well as from the containers used to store the oils. Work has also been carried out to determine how migration alters the metal content. Samples from wells that produced a mixture of oil and water were examined to see the influence of water cut on the metal contents of oils. Branthaver and Filby[7] indicate that trace elements of a source rock leave an imprint on its derived crude oils. If this imprint is not too greatly altered during secondary processes such as migration and production, then it might be possible to establish correlations among crude oils and source rocks based on the relative amounts of metals. If, however, the distribution of metals or porphyrin suites of a crude oil are significantly altered during migration or after implacement in

reservoirs in an unpredictable fashion, then they will not be useful in correlation studies. Several successful correlation studies,[8–10] using metal distributions, have been reported. Hirner,[10] for example only used Ni, V and Co of the 12 metals analysed to classify the oils studied. The secondary factors that obscure the usefulness of the other trace elements analysed are investigated in this work. By the intercomparison with INAA, an attempt was made to determine the sources of error due to problems such as isobaric interferences on the ICP-MS.

With the background knowledge regarding factors such as migration and drilling fluid contamination, the trace element data was applied to classify the oils of the Exxon set into families.[11] Three of the 25 samples, the metal contents of which were significantly altered, could be identified as outliers, thus providing a more accurate and clearer oil correlation. The principal component analysis plot was therefore not dominated and skewed by samples, the trace element fingerprints of which were altered significantly by migration through mineralized regions or contaminated during production and storage.

Experimental

Instrumental Neutron Activation Analysis

The INAA method used is described in Filby and Olsen[5] and in Jacobs and Filby.[12]

Inductively Coupled Plasma Mass Spectrometry

The conditions used on the VG PlasmaQuad PQ2+ ICP-MS system were the same as previously described[5] except that 1.5 kW of power was used. The Pt sampling cone orifice is 1.0 mm and that of the skimmer is 0.75 mm. The sample preparation for ICP-MS has been modified and is therefore described here.

Sample preparation for ICP-MS oil analysis

Samples (1.5 g) were diluted 1 + 9 in xylene. A Sartorius MC 1 balance was used for weighing the oil and xylene. Indium internal standard (in xylene) was added so that the diluted samples (15 g) and standards contained 100 ng g^{-1} In. Condensates were diluted 1 + 3 as the concentration of metals is generally very low in these samples.

Polyethylene scintillation tubes (22 ml, from Zinsser Analytic GmbH, Frankfurt, Germany) were used for the dilutions. Samples were vigorously shaken to dissolve the oil in xylene in the proportions mentioned above. A 2 cm^3 volume of de-ionized water (Milli-RO Plus 6/Milli-Q plus, Millipore, Milford, MA, USA) was then added to the solution of oil in xylene and again shaken vigorously to extract water soluble salts from the oil. Samples were centrifuged at 5000 rpm for 5 min (Hermle Z 380). The organic phase was then pipetted (Finntip 10 ml) and a 0.2 μm Teflon filter (Millex-FG50, Millipore) attached to the poly(propylene) pipette tip before it was dispensed to a new polyethylene scintillation tube. The sample was passed through the filter. The filtered xylene solution was then stored in this new polyethylene scintillation tube and closed tightly. PFA Teflon spray bottles were used to dispense the xylene and de-ionized water.

The time between making up of samples and standards and their use in analysis was limited as much as possible. Samples were stored in a refrigerator if it was unavoidable to wait a few days before analysis.

Solvents and Standards

Xylene and dekalin (*pro analysi*, Merck, Darmstadt, Germany) were tested for their suitability as solvents of oil analysed by ICP-MS. Dekalin had higher blanks and thus 30 times higher detection limits for Zn, Ni and Pb than xylene. We thus chose xylene as solvent for the standards and crude oils reported in this paper. Calibration standard solutions of metals were prepared from Conostan elemental standards (Conoco, Ponca City, OK, USA), *i.e.*, Ag, As, B, Ba, Cd, Co, Cr, Cu, Fe, Hg, La, Li, Mg, Mn, Ni, Pb, Sb, Se, Sn, Sr, Ti, V, W, Y, Zn. These were diluted to give standards with concentrations between 10 and 5000 ng g^{-1}. Iodine (*pro analysi*, Fluka, Buchs, Switzerland) was dissolved directly in xylene. Bromine standards from Micrographics (Tahoe Sierra Corporation, NV, USA) were diluted to the required concentrations. Metals for which organic-solvent based standards were not available (*e.g.*, U) were analysed using the semiquant mode.

Analytical Procedure

The xylene blank and standards were analysed using 6 repeat runs. The nebulization system was then rinsed with xylene and thereafter with 5% suprapure HNO_3 for an extended period (15 min). Condensates and light oils were analysed first. The dark heavier oils were analysed later in order to minimize contamination from carry-over. Between samples a xylene rinse was given for about 3 min.

Each sample dilution was analysed using 3 runs. Blanks were analysed after every third sample. In addition, the multichannel scaler (MCS) video display of the spectrum being collected was monitored to ensure that the Sn, Hg, and Pb levels in the samples were low. Where high levels of metal showing memory effect such as Sn, Hg and Pb were observed in the blank, a 3 min rinse using 5% suprapure HNO_3 followed the 3 min xylene rinse. Following this rinse, the blank levels were checked with a fresh xylene rinse before proceeding with the next analysis.

Accuracy and Precision

The NIST SRM 1634b fuel oil is used as a test of the accuracy of the ICP-MS method. Table 1 shows values obtained for SRM 1634b. These are within the standard deviation of the certified values for Co, Mn, Ni and Zn. Barium is systematically higher than the recommended value. It is possible that the Ba in SRM 1634b is contributed by particulate barite as will be discussed later. The bottle supplied for this work probably had a higher content of barite particles than that in samples

Table 1 Analysis of NIST SRM 1634b by ICP-MS

	Certified value/ng g^{-1}		Found/ng g^{-1}		
Element	Average	s^*	Average	s^*	Error (%)†
As	120	20	142	17	+18
Ba	1300‡		2804	187	190
Co	320	40	324	3	+1
Cr	700‡		1275	124	+82
Fe§	31.6	2	27.2	2	−14
Mn	230	30	206	2	−10
Ni§	28	2	26.8	1	−4
Pb	2800‡		3054	92	+9
Se	180	40	240	30	+33
V§	55.4	1.1	49.6	1	−10
Zn	3000	200	3062	147	+2

* Standard deviation (s) was calculated from 6 replicates.

† Error (%) is the difference between the average value found and the average certified value expressed as a percentage.

‡ Value recommended only, not certified.

§ Concentration listed in μg g^{-1}.

analysed during certification of this oil. Chromium-53 determined by ICP-MS in organics suffers from interference by $^{40}Ar^{12}C^{1}H$ and the extent of this interference varies with the nature of the sample.

Relative standard deviation values, when analysing metal-organic standards for 6 repeat runs of the same sample, were generally 15% at 20 ng g^{-1} and between 2 and 10% in the region 200–5000 ng g^{-1}. Detection limits are given in Filby and Olsen.[5]

Formation Water and Produced Water Analysis

Samples were analysed to determine their Na content. They were generally diluted 1 : 10 with de-ionized water. Synthetic standards were matrix-matched for Na using NASS-3 (NRC, Canada) open ocean sea-water.

SRM 1634b Oil and Asphaltene Extraction Experiments Using Disodium EDTA and Formation Water From Field B (New Well)

Duplicate 2 g samples of oil were added to 13 g of 0.23 mol dm^{-3} Na_2EDTA solution in polyethylene vials. This experiment was conducted to test if metal complexing agents in water would extract metals from oil. The mixtures were heated at 100 °C for 0.5 h and shaken thoroughly while hot. They were then left in an oven at 100 °C for the night. Samples were then left standing at room temperature for 8 months (to ensure a long time of contact between oil and water).

Two 3 g portions of SRM 1634b oil were weighed out and 10 cm^3 of formation water (pH 6.4) from field B were added. The same heating and agitation described above was used.

Asphaltenes of SRM 1634b oil were obtained by mixing 40 volumes of pentane with a xylene solution of the oil. The 0.07 g of asphaltene collected was added to 10 g of formation water. The above heating and agitation procedure was again repeated for this sample.

After these extractions portions (2 g) of the Na_2EDTA and formation water samples were carefully pipetted, filtered through a 0.45 μm Whatman filter (Clifton, NJ, USA) and diluted 8 times with de-ionized water before analysis.

Experiments to Test Contamination During Storage and Production of Oil

Container materials

NIST SRM 1083 base oil (10 g) was stored in polyethylene, aluminium and tin containers at room temperature for 1 week.

Production tubing

A piece of steel tubing (14 g) cut from drill pipe, which had been used on the RF-Drilling Rigg, was left in contact with 10 g of SRM 1083 oil in a polyethylene vial for 1 week.

Barite

A mixture of 1.5 g of barite, 2 cm^3 of de-ionized water and 10 g of SRM 1083 oil was shaken together thoroughly and left overnight. A portion of this SRM 1083 oil was diluted with xylene, internal standard added and the homogenized solution filtered through a 0.2 μm Teflon filter. A 1 g amount of barite was dissolved in HNO_3 (1 + 1 v/v) under pressure (according to the Norwegian Standard Method NS 4770) and the metals in the acid extract analysed by ICP-MS.

Reservoir rock samples

About 25 g of the rock were ground in an agate mortar and pestle. A 4 g amount of xylene containing 100 ng g^{-1} In was added and the grinding continued for 1 min. The sample was then transferred into a poly(propylene) centrifuge vial. A 25 cm^3 volume of de-ionized water was added, the vial stopper closed and the mixture shaken thoroughly. This sample was then placed in the Hermle centrifuge and centrifuged for 10 min at 5000 rpm. The xylene oil layer was siphoned off and filtered through 0.2 μm Teflon filter and the sample analysed on the ICP-MS. The water sample was collected after filtering the sample.

Experiment to Test Whether Metals are Picked up by Oils in Contact With Ore Minerals

Galena (3 g), sphalerite (2 g), barite (2.5 g) and fluorite (2.5 g) grains from samples taken at Windy Knoll and Odin Mine (West Derbyshire District, UK) were used. A 10 g amount of SRM 1083 base oil was added to these grains in a polyethylene vial. The mixture was heated for 0.5 h at 100 °C, shaken vigourously for 5 min and then left overnight at 100 °C. The sample was left at room temperature for a week before a portion of the oil was removed, internal standard added, diluted with xylene, filtered and analysed.

Results and Discussion

Intercomparison of INAA and ICP-MS

In the previous intercomparison,[5] 6 crude oils and an asphaltene-rich bitumen were analysed by both INAA and ICP-MS. The agreement between INAA and ICP-MS data for this set was generally good and no systematic bias between the methods could be recognized. In the work reported here, the intercomparison has been expanded to include 25 oils from the Exxon oil set.[6] Linear regression by least squares method has been applied to all the INAA *versus* ICP-MS pairs. An example of a pair with correlation better than 0.9 is shown in Fig. 1 where the results for Co are plotted against each other. For Co the correlation between INAA and ICP-MS is r = 0.92. However, the INAA readings are approximately 30% lower than the ICP-MS values. Interference on ^{59}Co is not significant when using ICP-MS for these samples. The reason for the offset must be sought in the Co calibration standards used for ICP-MS.

INAA and ICP-MS show good agreement for V; the offset is low (INAA values are 10% higher than ICP-MS) and the correlation between INAA and ICP-MS data is r = 0.95. For

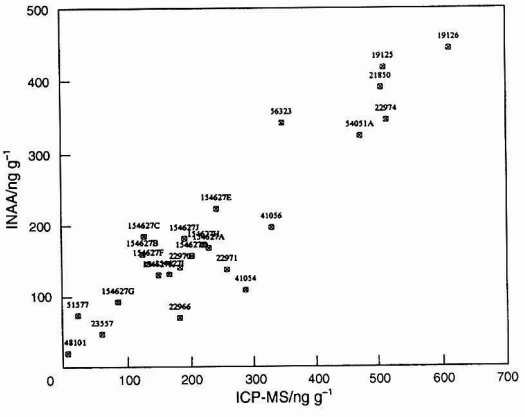

Fig. 1 Linear regression by least squares method to show the match between INAA and ICP-MS analysis for Co in the 25 Exxon oils (r = 0.92).

Ni, the offset is insignificant and the correlation between INAA and ICP-MS is $r = 0.87$ for ^{58}Ni and $r = 0.9$ for ^{60}Ni, respectively.

The correlation coefficients obtained for the elements analysed on both techniques are plotted in the bar diagram in Fig. 2. These results have provided a basis for learning regarding the interferences on ICP-MS and the contamination due to formation water, drilling fluid and production chemicals.

Interference due to Carbonaceous Species

The lack of correlation between ICP-MS values for ^{47}Ti, ^{53}Cr, ^{77}Se and ^{81}Br seen in Fig. 2, is partly or wholly due to isobaric overlap of Ar and C species. The probable species interfering on m/z 53 and 81 are $^{40}Ar^{12}C^{1}H$ and $^{40}Ar_2{}^{1}H$ respectively. We are unable to propose a suggestion for a species interfering at m/z 77. Fig. 3 shows the strong correlation between ^{47}Ti and ^{53}Cr. Sample 23557 has the highest values for ^{53}Cr and ^{47}Ti by ICP-MS. The sample is in fact a wax with very low metal content and illustrates the fact that light oils and waxes appear to have the highest interferences from carbonaceous species. Species that potentially could overlap with ^{47}Ti are $^{31}P^{16}O$, $^{32}S^{14}N^{1}H$, $^{12}C^{17}O_2{}^{1}H$ and $^{14}C^{16}O_2{}^{1}H$. The observation of highest interference in light oils referred to above, where polar compounds containing S, N, P and metals are low, favours an allocation of a species such as $^{14}C^{16}O_2{}^{1}H$ as the cause of this interference with ^{47}Ti. Because of the variation of $^{40}Ar^{12}C^{1}H$ interference with oil type, it appears that ICP-MS cannot be used for the analysis of Cr in oils using ^{53}Cr.

Titanium-48 can be used in ICP-MS analyses of low sulfur oils. More work is needed to determine a method of correcting for sulfur interference on ^{48}Ti. The INAA results for Ti were an order of magnitude higher than those obtained using ICP-MS. This suggests that perhaps the INAA results were not corrected for the interfering reaction known to affect Ti in high V oils. Further experience is needed with the analysis of Br in real samples before we can use ^{81}Br with confidence. Br was contributed by formation water to the samples analysed by INAA, whereas samples analysed by ICP-MS had the formation water removed. The intercomparison does not, therefore, give an indication of the extent of the influence of Ar_2H interference on the accuracy of determining ^{81}Br using ICP-MS in real samples.

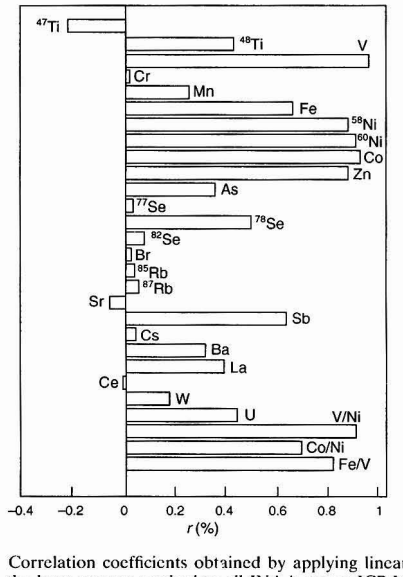

Fig. 2 Correlation coefficients obtained by applying linear regression by the least squares method to all INAA *versus* ICP-MS pairs. INAA is the dependent variable (y) and ICP-MS the independent variable (x).

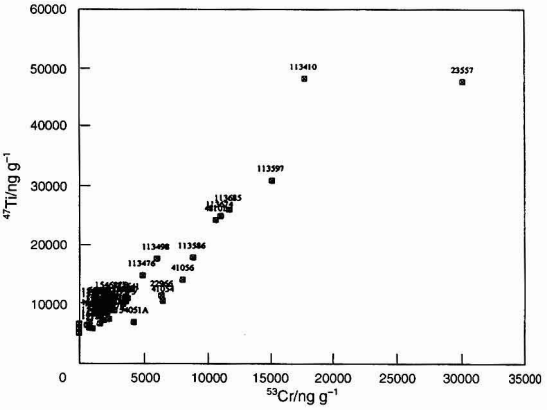

Fig. 3 ^{47}Ti *versus* ^{53}Cr illustrating the linear relationship that exists for masses that suffer interference from Ar and C species.

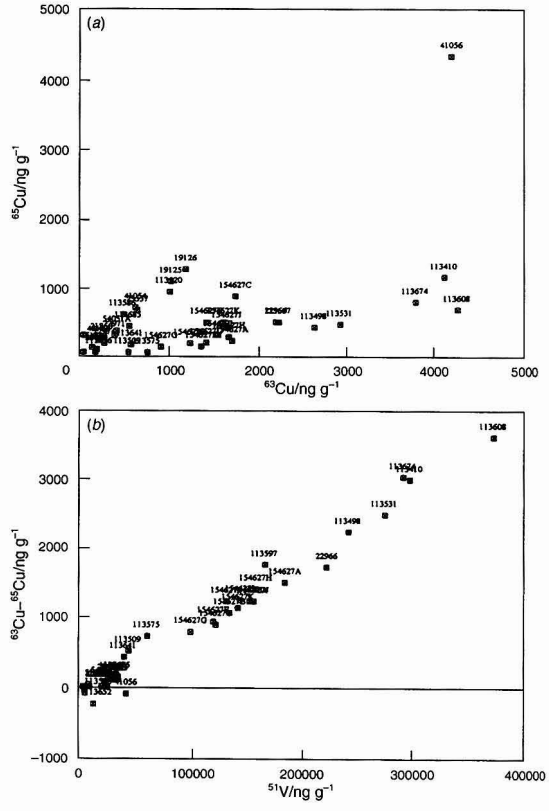

Fig. 4 Interference on ^{63}Cu: (*a*) showing the poor agreement between the results for Cu using ^{63}Cu and ^{65}Cu for oils; and (*b*) evidence substantiating the interference of $^{51}V^{12}C^{+}$ on ^{63}Cu.

Fig. 4(*a*) shows plots of the ^{65}Cu *versus* ^{63}Cu values obtained by ICP-MS. For samples with high V such as 113410 (297 μg g^{-1} V), the correlation between ^{65}Cu and ^{63}Cu is poor and the interference of $^{51}V^{12}C$ on ^{63}Cu is more evident than for samples with low levels of V. The strong interference on ^{63}Cu due to $^{51}V^{12}C$ is shown in Fig. 4(*b*). The cross plot of (^{63}Cu–^{65}Cu) *versus* ^{51}V shows that the interference of $^{51}V^{12}C$ occurs for all these samples. [Note that the correlation coefficient is $r = 0.99$ for this relationship in Fig. 4(*b*).] The $^{51}V^{12}C$ species gives an error in the ^{63}Cu readings of 0.97 ± 0.02% of the V concentration found at *m/z* 51.

Observations Regarding the Influence of Produced and Formation Water

Metals contained in both oils and formation water

The oils analysed by ICP-MS were water-washed and filtered prior to analysis. The oils analysed by INAA were analysed without prior treatment. Eleven oils from the Hondo field in California were part of the Exxon set. These oils were produced with differing amounts of water as shown by the water cut (%) in Table 2.

The INAA *versus* ICP-MS plot for As is shown in Fig. 5. The Hondo oils are the oils labelled 154627A to 154627K in Fig. 5(*a*). When the Hondo oils are included, as in Fig. 5(*a*), there is not a good correlation between the As data from the two techniques ($r = 0.35$). The concentrations of As determined in 154627A to C in Fig. 5(*a*) are substantially higher by INAA than that determined by ICP-MS. The water wash for 154627G and 154627D did not, apparently, break the emulsion effectively. There appears to have been Cl left in the emulsion of 154627G, which resulted in an enhanced signal at *m/z* 75 from $^{40}Ar^{35}Cl$.

When the linear regression by least squares method is applied to the As data in which the Hondo oils are excluded, Fig. 5(*b*) is obtained. The correlation increases to $r = 0.87$.

The example of As illustrates that some trace elements are inherent components of oil, the concentration of which can be masked by additional supply from formation or produced water.

The relative amount of water that was mixed with the Hondo oils during production is given as the water cut (%). This term is defined by Exxon as the water removed when oil and water are separated in a separator at well-site. Some elements were contributed almost entirely to the oil by the water. This is illustrated for Na *versus* water cut (%) in Fig. 6. As a check of the well-site determination of water cut, the water content was measured in the laboratory using the Karl Fischer titration technique (Metrohm 702 SM Titrino, Herisau, Switzerland). The results are shown in Table 1. The Karl Fischer determination yielded water contents of 48.1 ± 0.2% and 4.59 ± 0.32% for samples 154627G and 154627A respectively (three repeat titrations). Although the water was removed at well-site, stable emulsions had formed in the Hondo oils; the amount of emulsion being proportional to the water cut (%). Future water washing procedures need to be modified in order to break the stable emulsions more effectively.[13,14] This could involve repeating the mixing and centrifuging steps. The addition of methanol to the de-ionized water will be considered; however, the organically complexed metals may be affected by methanol.

The correlation coefficients for the water cut (%) *versus* all the concentration data of the elements determined by both

Table 2 Water content of the Hondo oils measured using the Karl Fischer technique compared with that given from well-site measurements of water cut

Sample number	Karl Fischer (%)	Water cut (%)
154627G	48.1	46.9
154627C	35.9	38.8
154627F	36.9	36
154627B	30.6	34.7
154627K	26	27
154627I	20.5	18
154627E	22.1	16.7
154627D	11.8	6.8
154627J	20.6	6.5
154627H	8.4	5.6
154627A	4.6	4

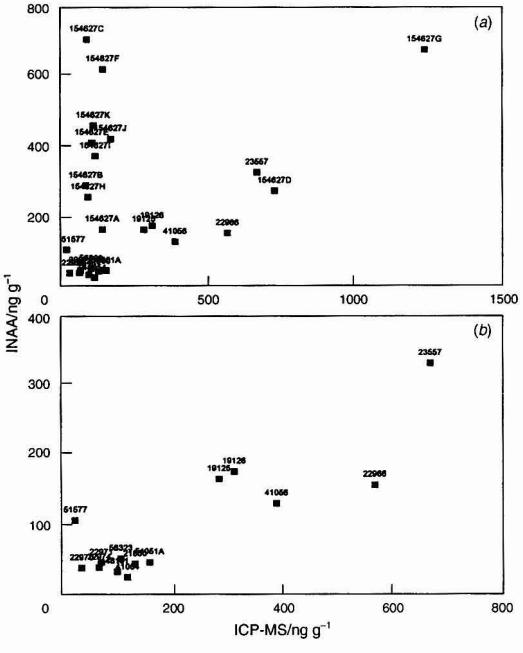

Fig. 5 Arsenic levels obtained by INAA in the Exxon Oil Set *versus* As levels by ICP-MS: (*a*) with the Hondo oils included, water contributes additional As to the INAA values ($r = 0.35$); and (*b*) when the Hondo oils are excluded ($r = 0.87$).

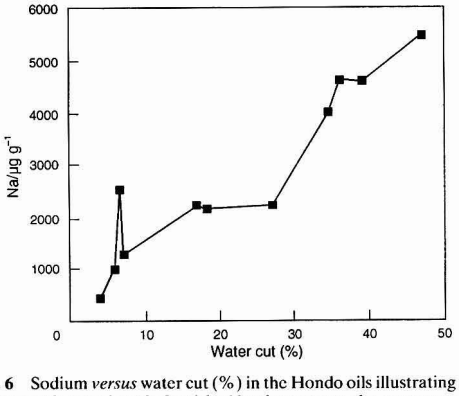

Fig. 6 Sodium *versus* water cut (%) in the Hondo oils illustrating that some metals were largely furnished by the water to the measurements made by INAA.

ICP-MS and INAA in the Hondo oils are depicted in the bar diagrams in Fig. 7. The elements such as Na and Mg, which are largely contributed to these oils by the produced water, show a correlation coefficient close to +1 in Fig. 7. In this figure, the ICP-MS element isotope measured, *e.g.*, ^{58}Ni, is used to distinguish it from the INAA measured element *e.g.*, Ni.

It can be seen that, similarly to the case of Na in Fig. 6, water contributes most of the Mg, Cl, K, Ca, Ga, As, Br, Cs, La and W to these Hondo oil samples. In his classification of the types of metal species found in crude oils and source rock bitumens, Filby[1] included I and SO_4^{2-} in the 'entrained formation waters' group of elements.

Decrease in Absolute Concentrations of Metals in High Water Cut Hondo Oils

The negative correlation coefficient between water cut and certain metals such as ^{51}V, V, ^{60}Ni, Ni, ^{59}Co, Co, Cr, ^{98}Mo *etc.*, in Fig. 7 is better illustrated in Fig. 8 where V is plotted against water cut. It is observed (similar plots to Fig. 8 were obtained for metals such as Ni and Co) that there is a decrease in the absolute concentration of organically bound metals as the percentage of water increases. The percentage of saturates, aromatics, polars or resins and asphaltenes (SARA fractions) were determined in the 11 Hondo oils by means of Iatroscan (Iatron, TH 10). The values obtained are shown in Table 3. There is no systematic decrease in either the resin or asphaltene contents of the Hondo oils with increasing water cut. The decrease in metal content is thus not due to precipitation of the asphaltenes from oils in vigorous contact with water. The decrease appears to be due to dilution of the co-produced oil with water which forms an emulsion with the oil. In the ICP-MS analyses, the emulsion with the produced water is broken during the vigorous washing with de-ionized water and centrifuging. However, it appears that the oil in contact with de-ionized water results in an emulsion forming again on being left to stand.

Fig. 9 shows a plot of V/(V + Ni) against Co for the 25 Exxon oils. In this figure, it can be seen that the V/(V + Ni) ratio for the Hondo oils (154627 A to K) remains very similar

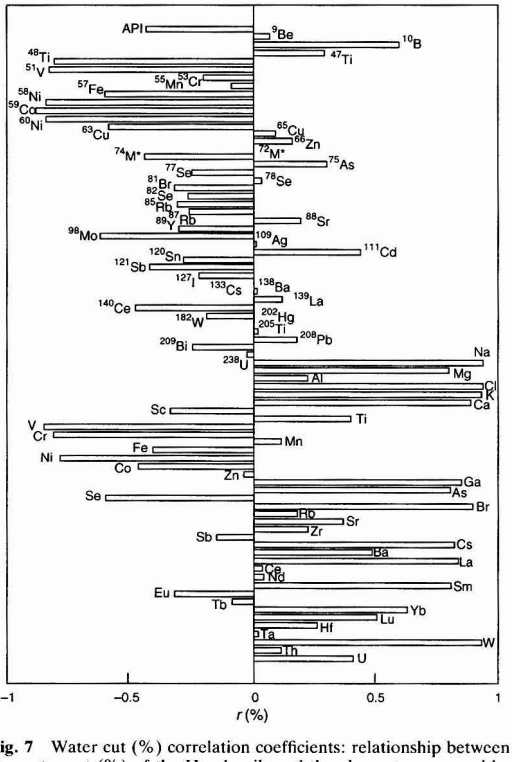

Fig. 7 Water cut (%) correlation coefficients: relationship between the water cut (%) of the Hondo oils and the elements measured by INAA (element symbols *e.g.*, As) and by ICP-MS (isotope of element used *e.g.*, ^{75}As).

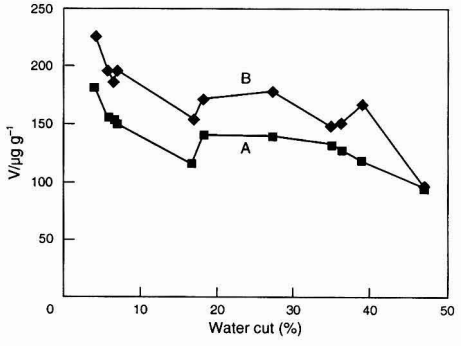

Fig. 8 Vanadium *versus* water cut (%) for the Hondo oils: A, ICP-MS and B, INAA.

Table 3 Molecular fractions determined by Iatroscan in the Hondo oils. Oils listed in order of decreasing water cut

Sample	Saturates (%)	Aromatics (%)	Resins (%)	Asphaltenes (%)
154627G	10	19	60	11
154627C	12	23	48	17
154627F	11	27	48	14
154627B	13	26	46	15
154627K	11	28	47	14
154627I	13	28	45	14
154627E	10	24	51	15
154627D	11	26	48	15
154627J	9	26	44	20
154627H	12	31	46	12
154627A	11	28	49	12

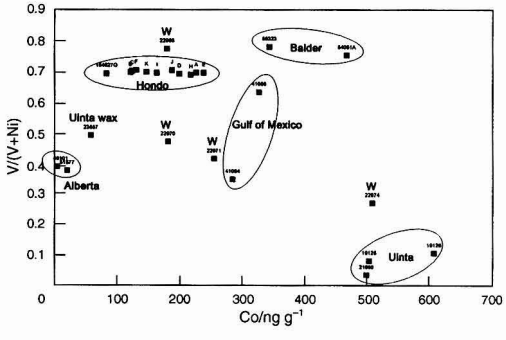

Fig. 9 Classification of the oils in the Exxon oil set using V/(V + Ni) *versus* Co.

despite the fact that the absolute concentrations of V and Ni have decreased drastically.

Metals Contained in Oils Compared With Metals in Waters From the Same Wells

In the course of work to determine the toxic metal content of formation and produced waters, we have been able to analyse some North Sea oils and waters from the same wells. Table 4 shows results for 3 such pairs.

The results for oil and formation water from a New Well Field B (Oil S7, Formation Water S7) represents the closest to 'uncontaminated composition' of oil and water in a reservoir. The results in Table 4 show that there is no relation between the metal contents of the oils to that of the waters. Metals are inherent components of the oil and are not supplied by formation and produced water. The metals such as Na and As, which in the case of the Hondo oils were contributed by entrained water, can be removed by washing the oil with de-ionized water prior to analysis of the oil.

Generally, V and Ni are the elements in highest abundance in oils. Where oils have been known to be biodegraded, Fe has been observed to be in highest abundance (see the metal composition of biodegraded oil M12 in Table 4 and that of biodegraded oil 6507/7-2 DST 2 in Table 7. Elevated Fe is also seen in Table 5 for the Pennine seep which is heavily degraded. One possible source for these elevated Fe levels in oils is microbially induced corrosion of steel in the production tubing and production tank. Lee *et al.*[15] discuss how biofilms influence the corrosion process of steel.

Laboratory experiments with formation water and SRM 1634b were performed to test if metals such as V and Ni were

Table 4 Comparison of metals in oils and waters from the same wells (*c*, concentration; *s*, standard deviation)

		Older established well field A				New well field B				Production well H7F			
		Oil M12		Produced water M12		Oil S7		Formation water S7		Oil H7F		Produced water	
Metal	Mass (*m/z*)	*c*/ng g^{-1}	*s*/(±) ng g^{-1}	*c*/ng g^{-1}	*s*/(±) ng g^{-1}	*c*/ng g^{-1}	*s*/(±) ng g^{-1}	*c*/ng g^{-1}	*s*/(±) ng g^{-1}	*c*/ng g^{-1}	*s*/(±) ng g^{-1}	*c*/ng g^{-1}	*s*/(±) ng g^{-1}
V	51	3150	200	<20		5014	260	<20		8450	238	<20	
Cr	52			<0.6		<100		6	1			16	2
Mn	55	582	150	840	26	<1		34	1	<1		1065	22
Fe	57	7300	2600	6480	150	65	60	840	80	<60		2700	70
Co	59	12	9	<1		127	2	<1		27	6	3163	40
Ni	58/60	425	84	<0.3		3795	237	<0.3		1530	108	23800	390
Cu	63/65	1100	63	<0.1		3800	8	<7		180	3	1810	7
Zn	66	1300	440	<2		118	3	<2		1114	64	665	5
As	75	280	120	<1		45	26	<8		<60		<180	
Sr	88	10	7			<1				28	1		
Mo	98	35	10	<10		<2		<10		<2		90	15
Ag	109	24	5	<0.2		<1		<0.2		<1		<0.2	
Cd	111	80	50	<0.3		<3		<0.3		<3		6	2
Sn	120	17	3	<1		12	6	<1		<1		<1	
Ba	138	<90		51000	710			2000	200	1200	61		
W	182	<1		204	20	<1		<1		<1		874	40
Hg	202	101		9.5	1	215	73	<1		780	17	171	5
Pb	208	<10		48	5	73	9	<0.5		<1		4	0.3
U	238	<2		<2		<2		<2		<2		<2	

Table 5 Evidence for metals added during migration (*c*, concentration; *s*, standard deviation)

		Base oil: NIST SRM 1083		Pennine Seep, UK associated Pb, Zn, Ba minerals	
Metal	Mass (*m/z*)	Base in polyethylene/ng g^{-1}	Galena (Pb) sphalerite (Zn)/ng g^{-1}	*c*/μg g^{-1}	*s*/(±)μg g^{-1}
V	51	<11	<11	9	1
Mn	55	<8	<8	97	9
Fe	57	<120	<120	8500	206
Co	59	<0.3	<0.3	17	0.8
Ni	58/60	<3	<3	150	5
Cu	63/65	11	22	12	1
Zn	66	<4	312	7130	44
As	75	<15	<15	115	6
Se	82	<140	<140	96	7
Sr	88	1	<0.3	26	1
Mo	98	<8	<8	27	2
Ag	109	2	<1	0.7	0.1
Cd	111	4	<3	7.5	0.2
Sn	120	<1	<1	61	5
Sb	121	<1	<1	3	0.2
Ba	138	2	2	33	2
Hg	202	<2	<2	4	0.3
Pb	208	12	1260	315	26

extracted from oils or asphaltenes after extensive contact with the water. See Table 6.

Where wells are prepared for production, as is the case of well H7F in Table 4, the results for the water sample analysed suggest that chemicals were used that supplied Co, Cu, Ni and Zn to the water. The oil supplied to us from this well has a similar content of V, Ni, Co, Cu and Zn to that of the DST (drill stem test) oils from this oil field, *e.g.*, 6507/7-2 DST 2 in Table 7. When cores were examined, this same contamination with Co, Cu, Ni and Zn was evident (see the discussion of Table 7 in text).

Removal of Metals From Oil by Formation Water and a Disodium EDTA Solution

Table 6 summarizes the results obtained from an experiment where NIST SRM 1634b oil was shaken together with disodium EDTA solution and formation water, respectively.

The concentration of elements contained in SRM 1634b are shown in Table 1. The elements analysed in the disodium EDTA solution are shown and compared with the concentrations measured in this same solution after it had been shaken with the oil. (See Experimental for details.) Pb was found to increase in concentration from <0.5 to 81 ng g^{-1}. The increase of from <1 to 3 ng g^{-1} for Co is noted with interest, but the value is too close to the blank level in EDTA to attach strong significance.

The results for formation water extraction in Table 6 do not show any evidence that metals other than Mn are transferred from the oil or asphaltenes into the water.

Work to Determine the Influence of Reservoir Rock Minerals on Metals in Oil

Five core samples from oil bearing zones in the Ekofisk, Statfjord, Snorre and Heidrun oil fields have been examined.

Table 6 Data from experiments to examine the removal of metals from oils by Na_2 EDTA and formation water (*c*, concentration; *s*, standard deviation)

		0.23 mol dm^{-3} Na_2EDTA				Formation water–oil/asphaltene 1634b mixture					
		Na_2EDTA solution		Na_2EDTA–1634b oil mix		Formation water S7		Formation water–oil mix		Formation water–asphaltene	
Metal	Mass (*m/z*)	*c*/ng g^{-1}	*s*/(±) ng g^{-1}	*c*/ng g^{-1}	*s*/(±) ng g^{-1}	*c*/ng g^{-1}	*s*/(±) ng g^{-1}	*c*/ng g^{-1}	*s*/(±) ng g^{-1}	*c*/ng g^{-1}	*s*/(±) ng g^{-1}
V	51	<11		<11		<11		<11		<11	
Cr	52	237	20	215	5	6	1	<1		<1	
Mn	55	<2		<2		34	1	250	10	316	11
Fe	57	<800		<800		840	80	<800		<800	
Co	59	<1		3	1	<1		<1		<1	
Ni	58/60	<7		<7		<7		<7		<7	
Zn	66	<6		<6		<6		<6		<6	
As	75	<8		<8		<8		<8		<8	
Se	82	<140		<140		<140		<140		<140	
Pb	208	<0.5		81	2	<0.5		<0.5		<0.5	

Table 7 Well 6507/7-2. Metals in oil, reservoir rock oil, rock minerals and water (*c*, concentration; *s*, standard deviation)

		6507/7-2 DST 2 oil		Reservoir rock oil		Wash water		Metals in reservoir rock by XRF	
Metal	Mass (*m/z*)	*c*/ng g^{-1}	*s*/(±)ng g^{-1}	*c*/ng g^{-1}	*s*/(±)ng g^{-1}	*c*/μg g^{-1}	*s*/(±)ng g^{-1}	*c*/μg g^{-1}	*s*/(±)μg g^{-1}
V	51	11 940	1135	2 505		<30		<15	
Mn	55	3 584	30	17 120		5356	327	1182	60
Fe	57	124 800	8800	398 000		117	50	16	5
Co	59	67	14	4 820		670	67	100	20
Ni	58/60	3 062	249	9 980		1300	140	21	4
Cu	63/65	471	6	3 600		46	2	52	11
Zn	66	1 789	306	5 590		157	4	27	5
As	75	171	43	576		<33			
Sr	88	28	3	300		1087	71		
Mo	98	<2		<2		59	16		
Ag	109	<1		<1		<1			
Cd	111	<3		173		5	1		
Sn	120	<1		<1		<1			
Sb	121	<1		140		5	2		
Ba	138	57		6 550		93	24	1373	70
La	139	<1		104		<1			
Ce	140	<1		176		<1			
W	182	<1		<1		2.7	0.5		
Hg	202	14	10	493		<2			
Pb	208	2 400	280	35 500		36			
Bi	209	12	5	1 400		<1			
Th	232	<1		13		<1			
U	238	<2		15		<2			
V/(V + Ni)		0.796		0.201					

The oils extracted with xylene from these cores were analysed and the results compared with that of the respective DST oils. The remaining sediment was then washed with de-ionized water and the water analysed for its metal content. All fluid samples were filtered through 0.2 μm Teflon filters prior to analysis. The extracted and water washed reservoir rock was then analysed by XRF (Siemens SRS 300) and XRD (Siemens D 500).

In the oils extracted from the 5 core samples, contamination of Ni and Co was evident which resulted in completely different V/(V + Ni) ratios for these oils from those of the DST oils. The example of 6507/7-2 is chosen because this was the most extreme case of contamination. The oil in this reservoir is heavily biodegraded.[16]

The composition of the 6507/7-2 DST 2 oil resembles that of the Spekk[16] source rock bitumen. The oil extracted (reservoir rock oil) from the core of 6507/7-2 has a metal composition which is totally different from that of the 6507/7-2 DST 2 oil. It would appear that chemicals added during the taking of reservoir cores or during production (see produced water data for H7F in Table 4) are taken up into the oil and overshadow the source inherited metal fingerprint of the 6507/7-2 reservoir rock oil in Table 7. The metal content of the water used to wash this core is also shown here. The type of contamination discussed here is alarming to those who wish to use metals for geochemical purposes.

Work by Norheim and Barth[17] showed that the oil remaining on water-wet quartz grains in cores had an asphaltene content of 65% compared with the 5% asphaltene content in the original crude oil. Any drilling fluid components, corrosion and scale inhibitors used that contained metals could furnish these metals to the asphaltene. Our work on another core showed that slightly more metals (Ni, Co, Zn, Cu, Fe) were contained in water soluble than in xylene soluble components (comparison of xylene extract and acetic acid extract).

The Ba content of 1373 μg g^{-1} found by XRF in the reservoir rock is evidence of contamination by drilling fluid containing barite. Work is in progress to identify the chemical that provides the high Co and Ni contents and other metals introduced as contaminants shown in Tables 4 and 7.

Table 8 presents the minerals identified in the reservoir rock of 6507/7-2. It can be seen that there are not any minerals that would naturally contain such high levels of Co. The high Co in the whole rock analysis in Table 7 is likely to be contained in the barite and asphaltene particles interspersing the mineral grains.

Table 8 Phase analysis by XRD of reservoir rock 6507/7-2, depth 2418 m

Identified mineral	Chemical formula	Estimated amounts*
Quartz	SiO_2	46
Na-feldspar	$NAlSi_3O_8$	1
K-feldspar	$KAlSi_3O_8$	37
Calcite	$CaCO_3$	Trace
Dolomite	$CaMg(CO_3)_2$	Trace
Siderite	$FeCO_3$	—
Goethite	FeOOH	—
Gypsym	$CaSO_4{\cdot}2H_2O$	—
Barite	$BaSO_4$	—
Pyrite	FeS_2	—
Fluor-apatite	$Ca(PO_4)_3F$	—
Amphibole		—
Kaolinite/chlorite	$Al_2Si_2O_5(OH)_4$ (kaolinite)	5
Illite/mica	$KAl_2Si_3AlO_{10}(OH)_2$	9
Mixed-layer Clay		—
Smectite(montmorillonite)		—
Talc		—

* Semiquantitative estimates with a relative uncertainty of 20–30%. Trace, only traces (<0.5% of the mineral is detected); —, not present, or below the limit of detection.

Metal Contamination due to Barite

Laboratory experiments were conducted in which finely powdered barite, with the composition shown in Table 9 (extreme right), was mixed with de-ionized water and SRM 1083 base oil. The xylene-diluted and filtered oil sample was then analysed. The metal content of this barite-contaminated oil was then compared with that of the uncontaminated (polyethylene) SRM 1083 oil. After contact with barite, the base oil in Table 9 was found to contain higher Mn, Fe, Cu, Zn, Sr, Ba and Pb. (The increase in ^{65}Cu is possibly due to Ba^{2+} interference. Copper-63 should be monitored in oils with very high levels of barite.) It appears that particles finer than 0.2 μm remain suspended in the oil and pass through the nebulizer to the plasma for analysis.

While working with DST oils from the North Sea, oil samples were at first not filtered and water washed. Contamination of a number of oils was evident by the extremely high

Table 9 Evidence for metals added during production and storage

		Base oil: NIST SRM 1083/ng g^{-1}				
Metal	Mass (*m/z*)	Polyethylene	Aluminium (Sn)	Steel tube	Barite particulate	Metals in barite μg g^{-1}
V	51	<11	<11	<11	<11	3
Mn	55	<8	<8	<8	80	150
Fe	57	<120	<120	<120	250	5400
Co	59	<0.3	<0.3	<0.3	<0.3	1
Ni	58/60	<3	<3	<3	<3	2
Cu	63/65	11	<11	13	70	195
Zn	66	<4	<4	46	16	390
As	75	<15	<15	<15	<15	18
Sc	82	<140	<140	<140	<140	0.2
Sr	88	1	<0.3	<0.3	39	320
Mo	98	<8	<8	<8	<8	6
Ag	109	2	<1	<1	<1	2
Cd	111	4	<3	<3	<3	5
Sn	120	<1	<1 (25 ppm)	<1	<1	5
Sb	121	<1	<1	<1	<1	22
Ba	138	2	<1	2	1100	
Hg	202	<2	<2	<2	<2	0.7
Pb	208	12	6	11	84	5800

Ba contents (29400 ng g^{-1}) as shown in Table 10 for oil 2/12-1 DST 1 when not filtered. When the sample was filtered through a 0.2 μm Teflon filter and then analysed, the concentrations of Ba, Sr, Fe, Ga and Mn were drastically reduced. Other elements that were reduced were elements such as La, Nd, Pb, U, Y and Zn. The geochemically important elements V, Ni, Cu and Br were not affected by filtering. The particulates obtained from this contaminated 2/12-1 DST 1 oil were investigated by means of electron microscopy and X-ray diffraction. An EDAX XRF (Philips SEM 515 with EDX) spectrum and photo micrograph are shown in Fig. 10 and clearly identified most of the particles as barite ($BaSO_4$).

Table 10 Illustration of contamination by drilling fluid with 2/12-1 DST 1 (*c*, concentration; *s*, standard deviation)

	Oil not filtered		Filtered oil	
Element	*c*/ng g^{-1}	*s*/ng g^{-1}	*c*/ng g^{-1}	*s*/ng g^{-1}
Ag	<0.07		<0.07	
As	1.3	0.6	<0.3	
B	3891	832	6713	1278
Ba	29400	2850	16	6
Be	1.3	1	2	1
Bi	0.6	0.3	0.01	
Br	19	3.5	14	3
Cd	<0.3		<0.3	
Co	0.8	0.1	0.1	
Cr	<300		<300	
Cu	49	7	36	4
Fe	2200	94	37	5
Ga	1860	150	4	1
Hg	16	5	26	7
I	<4		<4	
La	2.4	0.1	<0.02	
Li	5	2	2	
Mn	388	20	7.6	1
Mo	0.7	0.3	<0.1	
Nd	6	2	<1	
Ni	36	5	30	4
Pb	22	4	6	1
Sc	<1		<1	
Sn	<1		<1	
Sr	1093	4	0.8	0.5
Ti	72	14	15	2
U	0.2	0.05	<0.03	
V	10.3	0.4	11	0.4
W	0.5	0.3	<0.05	
Y	0.9	0.3	<0.02	
Zn	48	2	16	1

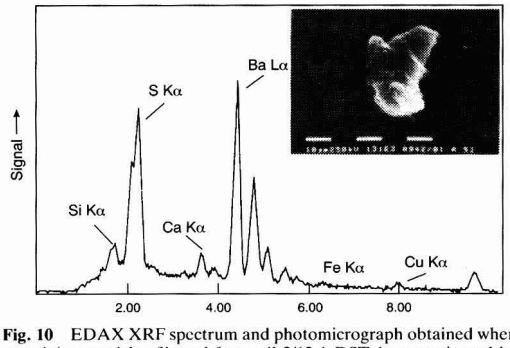

Fig. 10 EDAX XRF spectrum and photomicrograph obtained when examining particles filtered from oil 2/12-1 DST 1 contaminated by drilling fluid.

Experiments With Different Containers and Lightly Corroded Steel

Experiments were conducted in which base oil SRM 1083 was stored in polyethylene, aluminium and tin containers. In another experiment, a piece of production tubing was left in contact with SRM 1083. These oils were then filtered and analysed for their metal contents. The results are shown in Table 9. The results for the analysis of SRM 1083 contained in new clean aluminium and tin containers were identical. However, extremely high values of Sn were observed in oils contained in a corroded tin container. It appears that fine particles of SnO_2 pass through the 0.2 μm filter and contribute a large Sn signal. The most detrimental effect of Sn contamination is the isobaric interference that occurs from ^{115}Sn on ^{115}In. When In is used as internal standard, serious errors are introduced in the measured concentrations of all the trace elements ratioed against In.

Table 9 also illustrates that where oil contacts steel tubing, contamination due to Fe and alloying elements does not occur. Strongly acidic conditions and a high asphaltene content in the oils such as those suggested for biodegraded oils in steel containers are required to result in Fe contamination (see the discussion of Tables 4 and 7).

Evidence for Metals Added During Migration

The Exxon oil set included two Uinta oils, 19125 and 19126, with unusually high levels of Zn, Cd, Sn and Pb. Filby[1] reported that oils from the Cymric field, Kern County, California contained up to 23 μg g^{-1} of Hg. Geological evidence was given that the oil acquired the Hg as it passed through cinnabar deposits. It is highly likely that the 250 μg g^{-1} of Pb found in 19125 oil are owing to this oil migrating over a region mineralized with galena and minerals that would furnish lesser amounts of Zn (14 μg g^{-1}), Cd (7 μg g^{-1}) and Sn (3 μg g^{-1}).

Laboratory experiments with galena, sphalerite, barite and fluorite were conducted to test whether an oil like SRM 1083 would indeed acquire Pb, Zn and Ba from the minerals. The results from analysing the 0.2 μm filtered oil treated in this way are given in the galena/sphalerite column of Table 5. The results shown in Table 5 were obtained using the ICP-MS. The Zn content increases from <4 to 312 ng g^{-1} and that of Pb from 12 to 1260 ng g^{-1}. These metals are possibly complexed more readily. Drilling fluids use finely ground barite. As noted in the discussion of Table 9, the Ba signal is high (1100 ng g^{-1}) due to particles <0.2 μm passing into the oil. In the above laboratory migration experiment, large crystals of barite were used; hence the Ba concentration given in Table 5 is only 2 ng g^{-1}. We have thus demonstrated that Zn and Pb are indeed picked up when oils migrate over mineralized regions.

For purposes of comparison, the Pennine seep sample was also analysed. This seep at Windy Knoll (West Derbyshire District, UK) is associated with galena, sphalerite, barite and fluorite which was used in the experiment reported above. The very high Zn and Pb values for this seep can be seen in Table 5. (Because the seep was so viscous, it was not possible to filter it.) The seep occurs near to a sphalerite deposit, whereas galena and barite occur further away. This could explain the higher Zn than Pb found in the seep.

Classification of Oils Using Trace Elements

Fig. 9 shows a plot of V/(V + Ni) against Co for the 25 Exxon oils analysed by ICP-MS. Most of the oils were clearly distinguished from oils of other fields using these three metals. Error in correctly determining the very low levels of Ni and V

in the solid wax sample 23557 from Uinta is the reason why it does not group with the other Uinta oils.

Rinaldi[18] reported that the source rock depositional environments of oils in the Williston region range from coastal swamp to marine. These varying depositional environments are confirmed by the V/(V + Ni) and Co results in Fig. 9. The coastal swamp section of the source rock produced Williston oil W 22974. The section of rock from the coastal depositional environment produced Williston oils W 22970 and 22971 and that from the marine environment produced Williston oil W 22966. (Note the systematic increase in Co as the depositional environment becomes more oxic.) The use of Ni/Co for indicating the paleo-redox conditions has been discussed by Jones and Manning[19] during their work on Draupne, Heather and Kimmeridge Clay Formations. Gendron *et al.*[20] carried out work on the Laurentian Trough sediments and found that in an estuary, Co will be concentrated in the oxidized layer of the sediments and tends to migrate landward. It thus appears that the Co content of the Williston oils may be an indication of the proximity of the respective Williston source rocks to land during diagenesis.

The very similar V/(V + Ni) for the different Hondo and Balder oils, respectively, are noted. Alteration of the absolute concentrations of the V and Ni discussed earlier did not affect the V/(V + Ni) for the Hondo oils.

The widely different V/(V + Ni) for the Gulf of Mexico oils suggest that oil 41054 is from the siliciclastic shale (terrigenous) of the Tuscaloosa Formation whereas oil 41056 is from the calcareous Smackover Formation.

Although Hirner[10] analysed V, Cr, Fe, Co, Ni, Zn, Sc, Br, Ag and I in petroleum samples from the Molasse basin, he found that differention of the two oil families in the data set could only be achieved from the Ni, V and Co data. For the Exxon oil sample set, we have applied principal component (PC) analysis on a selection of elements measured by both ICP-MS and INAA (*i.e.*, Co, Zn, Mo, Ni, V, Sb, Bi, As, Fe and Mn). Principal components are linear combinations of the variables in the data that represent axes of maximum spread among the samples. The contributions from the variables (*e.g.*, metal type and concentration) to the PCs is given by their loadings. Variables are standardized prior to PC analysis. Sample scores on the PCs thus provide multivariate classification of the samples according to the main statistical factors in the data. The variable loadings show how the variables relate to each other. Massart *et al.*[21] deals with the use of PC analysis in chemistry.

Principal component score and loading plots for the whole Exxon oil sample set are given in Fig. 11. After eliminating three samples which are contaminated, the plots shown in Fig. 12 were obtained.

The score plot in Fig. 11 is dominated by Uinta oils 19125 and 19126 which are suspected of migration through mineralized zones. These samples had unusually high contents of Bi, Cd, Mn, Zn, Pb, U and Fe. Balder sample 54051A was apparently left out during the ICP-MS sample pre-treatment. It showed evidence of contamination by its unusually elevated levels of Sr, Zn and Fe. When these three samples are removed, we obtain the PCs shown in Fig. 12. Here the variables are the concentrations of Co, Zn, Mo, Ni, V, Sb, Bi, As, Fe and Mn. The Hondo oils together with the single Williston sample 22966 remain in one relatively dense class of oils. A reasonable correspondence between oils from the same regions emerges in Fig. 12(*a*). The exceptions are samples 23557 and 22966.

The Uinta sample 23557 is a wax and has very low levels of all metals (low content of polar components) except Fe and Mn. This Fe is possibly due to contamination of the wax during handling of the solid wax with corroded metal tools. We thus

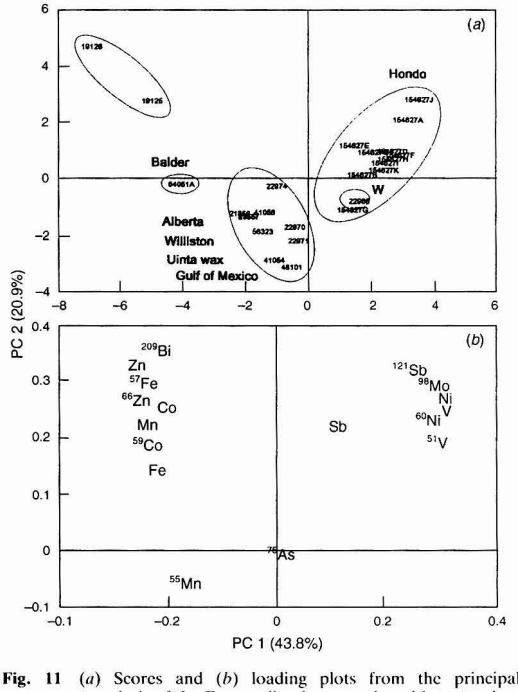

Fig. 11 (*a*) Scores and (*b*) loading plots from the principal component analysis of the Exxon oils when samples with contamination were included.

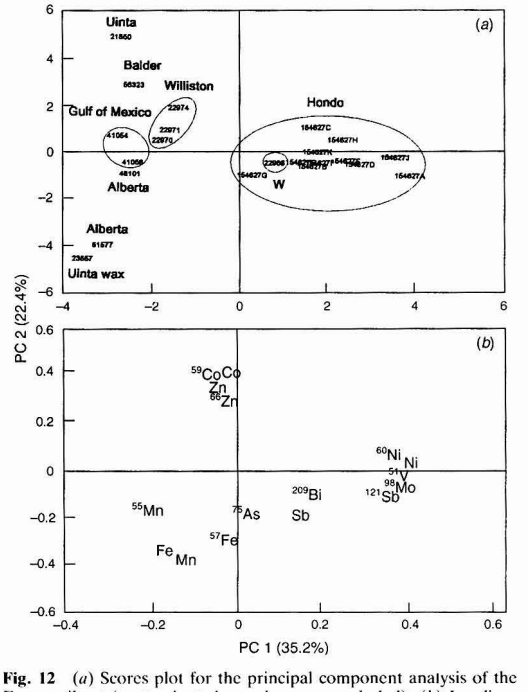

Fig. 12 (*a*) Scores plot for the principal component analysis of the Exxon oil set (contaminated samples were excluded). (*b*) Loadings plot for the principal component analysis of the Exxon oil set.

have a fourth sample, the trace element signature of which is obscured because of contamination and because the metals inherited from the source rock are below the detection limits of ICP-MS and INAA. The assemblage of metals and their concentration levels in the marine Williston sample 22966 are very similar to that found in the Hondo oils. This oil and the Hondo oils appear to have derived from similar calcareous source rocks which were deposited under similar E_h/pH conditions, but at different geographical locations.

Along PC1 of Fig. 12(*a*), Ni, V, Mo and ^{121}Sb are largely responsible for the difference in the classification of, *e.g.*, the Hondo oils from the Gulf of Mexico oils. Both these groups have middle of the range levels of Co, Zn, Fe and Mn.

Along PC2 of Fig. 12(*a*), the Uinta sample 21850 has a high content of Co and Zn and low levels of Fe and Mn. In contrast, the Alberta sample 51577 is relatively high in Mn and Fe and low in Co and Zn.

The very tight clustering of Co and Zn in Fig. 12(*b*) strongly suggests an association of these two metals in natural petroleum. As discussed earlier, Co seems characteristic for an oxic depositional environment or an environment with terrigeneous input. It would appear that the clusters of three groups of metals in the loading plot in Fig. 12(*b*) represent three different geochemical factors. The clusters are (1) Co and Zn, (2) Ni, V, Mo, Sb and Bi, and (3) Mn and Fe. Note that both INAA and ICP-MS data show the three associations of trace elements. Curiale[2] reported evidence that the behaviour and molecular association of Ni, V and Mo was similar. The behaviour he found for these three metals was different from that of Co, Cu, Fe, Mn and Zn. The data from the Exxon oils [Fig. 12(*b*)] confirms this and suggests yet further differentiation in the molecular association of Curiale's latter group into the Co, Zn group and the Mn, Fe group.

Conclusion

Intercomparison between INAA and ICP-MS showed agreement between the Co, Ni and V in oils. This is because they are least affected by the contamination sources discussed here.

Difference in sample preparation prior to analysis by INAA and ICP-MS resulted in marked differences for elements like Mn, As and W. Barite in the oil samples contributes Ba, Sr, Mn, Fe, Ga, Pb and possibly Cu and Zn, thus complicating the analysis for these metals in oil. Formation and produced water contributes Na, Mg, K, Ca, Ce, Br, As, Ga, Cs and W. When oils are filtered and washed with de-ionized water, the contamination due to barite and formation water is removed. Oil in contact with steel production tubing does not appear to pick up metals. No contamination was observed when polyethylene and aluminium containers were used for oil. Biodegraded oils appear to be contaminated with Fe and W. Oils that migrate through ore bodies acquire metals such as Zn, Cd and Pb. The Exxon oils oils were classified into families using Co, Zn, Mo, Ni, V, Sb, Bi, As, Fe and Mn. Where oils were severely contaminated, the classification was still possible using V/(V + Ni) *versus* Co.

This work was made possible by Esso Norge A.S. who have funded a Geoscience Research Program at RF-Rogaland Research. E. Clarke and T. Whitfield of the University of Newcastle performed the Karl Fischer and Iatroscan determinations on the Hondo oils, respectively. L. Dybvik (RF) performed the electron microscopy and J. O. Thorsplass (Westlab) the XRF and XRD work. The reservoir rock and DST oil samples were obtained from the Norwegian Petroleum Directorate (NPD). The formation water, produced water and corresponding oils were obtained from Statoil. Permission by Exxon EPR, the NPD and Statoil to publish the results is acknowledged.

References

1 Filby, R. H., in *Geofluids: Origin, Migration and Evolution of Fluids in Sedimentary Basins*, ed. Parnell, J., Geological Society Special Publication No. 78, London, 1994, pp. 203–218.
2 Curiale, J. A., in *Exploration for Heavy Oil and Bitumen*, American Association of Petroleum Geology Research Conference, Santa Maria, California, October 28–November 2, 1984, AAPG, 1, pp. 1–39.
3 Wolf, N. O., personal communication.
4 Gjerald, E., personal communication.
5 Filby, R. H., and Olsen, S. D., *J. Radioanal. Nucl. Chem.*, 1994, **180**, 285.
6 Isaksen, G. H., *Org. Geochem. J.*, 1992, **18**, i.
7 Branthaver, J. F., and Filby, R. H., in *Metal Complexes in Fossil Fuels*, ed. Filby, R. H., and Brandhaver, J. F., *ACS Symp. Ser. No. 344*, American Chemical Society, Washington, DC, 1987, pp. 84–99.
8 Hitchon, B., and Filby, R. H., *AAPG Bull.*, 1984, **68**, 838.
9 Curiale, J. A., in *Metal Complexes in Fossil Fuels*, ed. Filby, R. H., and Brandhaver, J. F., *ACS Symp. Ser. No 344*, American Chemical Society, Washington DC, 1987, pp. 135–145.
10 Hirner, A. V., in *Metal Complexes in Fossil Fuels*, ed. Filby, R. H., and Brandhaver, J. F., *ACS Symp. Ser. No 344*, American Chemical Society, Washington, DC, 1987, pp. 146–153.
11 Isaksen, G. H., *Exxon Oil-Set Program*, Exxon Production Research Company, Houston, 1992.
12 Jacobs, F. S., and Filby, R. H., *Anal. Chem.*, 1983, **55**, 74.
13 Acevedo, S., Layrisse, I., and Rivas, H., *J. Dispersion Sci. Technol.*, 1984, **5**, 1.
14 Clarke, E. L., personal communication.
15 Lee, W.-C., Levandowski, Z., Characklis, W. G., and Nielsen, P. H., in *Biofouling and Biocorrosion in Industrial Water Systems*, ed. Geesy, G. G., Levandowski, Z., and Flemming, H.-C., Lewis Publishers, London, 1994, pp. 205–212.
16 Olsen, S. D., Report RF-4/93, Rogalandsforskning, 1993, pp. 1–50.
17 Norheim, E., and Barth, T., unpublished work.
18 Rinaldi, G. G. L., *Org. Geochem. J.*, 1988, **13**, 373.
19 Jones, B., and Manning, D. A. C., *Chem. Geol.*, 1994, **111**, 111.
20 Gendron, A., Silverberg, N., Sunby, B., and Lebel, J., *Geochim. Cosmochim. Acta*, 1986, **50**, 741.
21 Massart, D. L., Vandeginste, B. G. M., Deming, S. N., and Kaufman, L., *Chemometrics: a textbook*, Elsevier Science Publishers, Amsterdam, 1988.

Paper 4/05852F
Received September 26, 1994
Accepted January 13, 1995

Determination of Platinum, Palladium, Ruthenium and Iridium in Geological Samples by Isotope Dilution Inductively Coupled Plasma Mass Spectrometry Using a Sodium Peroxide Fusion and Tellurium Coprecipitation*

Jacinta Enzweiler† and Philip J. Potts‡

Department of Earth Sciences, The Open University, Walton Hall, Milton Keynes, UK MK7 6AA

Kym E. Jarvis

NERC ICP-MS Facility, Centre for Analytical Research in the Environment, Imperial College at Silwood Park, Buckhurst Road, Ascot, Berkshire, UK SL5 7TE

A method was developed for the determination of Ru, Pd, Ir and Pt in geological samples by isotope dilution inductively coupled plasma mass spectrometry. After fusion of the sample with sodium peroxide, the platinum group elements were preconcentrated by Te coprecipitation. Results obtained for the reference materials WGB-1, TDB-1, UMT-1, WPR-1, WMG-1 and SARM-7 are in excellent agreement with the recommended values for elements above the detection limit level of 0.3–2.0 ng g^{-1} (whole rock). Although the method used only 0.5 g of sample, no errors were found that could be associated with sample inhomogeneity effects in the analysis of the above reference materials. Further measurements indicated that the technique could be extended to the determination of Rh and Au by external calibration.

Keywords: Platinum group element determination; geological sample; sodium peroxide fusion; isotope dilution; inductively coupled plasma mass spectrometry

Introduction

The development of methods for the determination of the platinum group elements (PGEs; Ru, Rh, Pd, Os, Ir and Pt) in geological samples has attracted considerable interest in recent years for several reasons. The economic importance of these elements has stimulated the development of analytical techniques appropriate for geochemical exploration and ore processing.[1] However, there is also increasing academic interest in the geochemistry of these elements in studies of, for example, mantle and metallogenetic processes[2,3] and the Cretaceous–Tertiary boundary layer with its associated Ir anomaly.[4] This resurgence of interest has been further stimulated by the recent development of isotopic techniques for Os/Re geochronometry studies.[5,6]

The low concentration of PGEs in geological samples (with typical background levels of a few ng g^{-1}) makes the determination of PGEs a challenge. Appropriate analytical procedures generally have three steps: chemical decomposition of the sample, separation of the PGEs from the matrix (*i.e.*, preconcentration) and finally elemental determination. One of the most successful methods for both decomposing the sample and concentrating the PGEs is the nickel sulfide fire assay procedure coupled to the high sensitivity of inductively coupled plasma mass spectrometry (ICP-MS) instrumentation for the determination stage,[7,8] later improved by an intermediate Te coprecipitation step.[9–12] The nickel sulfide fire assay method offers the advantage of accepting large sample aliquots (routinely 20–50 g), which is essential in the analysis of any sample that might contain discrete PGE minerals. In such circumstances, serious sampling errors are likely to occur (caused by the 'nugget effect') if techniques that employ smaller sample masses (*e.g.*, <1 g) are used. However, the nickel sulfide procedure has some disadvantages. One is the relatively large amounts of reagents used and the contribution they may make to the analytical blank unless very high purity reagents are used. Another potential difficulty is that judgement is required to optimize flux composition in the analysis of some sample types (*e.g.*, chromite and sulfide-bearing samples or kimberlites).[13–15] A third potential difficulty is that some investigations have indicated that PGE recoveries by nickel sulfide fire assay may not always be quantitative, with losses occurring during the fusion procedure itself[16] and during subsequent crushing[17] and dissolution of the nickel sulfide button.[9] Alternative procedures are often used for the analysis of mantle rocks, in Os/Re isotope studies for example, where geochemical and thermodynamic constraints would indicate that discrete PGE grains are unlikely to be present. In these circumstances, a low blank decomposition procedure is more important than the capability to analyse 50 g sample aliquots and indeed, many studies have been undertaken successfully using techniques requiring less than 1 g of sample.[18–20]

In the analysis of mantle rocks, several approaches have been used to dissolve the sample. Some of the most common are those based on acid attack (total or partial)[21,22] and fusion procedures.[23,24] The digestion with *aqua regia* in sealed tubes[25,26] is also being used because of its effectiveness in dissolving PGE-bearing phases and the low blank levels, the latter being crucial in Re/Os geochemistry. The fusion of powdered samples with oxidizing fluxes such as sodium

* Presented at Geoanalysis 94: An International Symposium on the Analysis of Geological and Environmental Materials, Ambleside, England, September 18–22, 1994.

† Present address: Universidade Estadual de Campinas, Instituto de Geociências, Campinas, SP, P.O. Box 6152, CEP 13081, Brazil.

‡ To whom correspondence should be addressed.

peroxide has been widely used both to decompose resistant minerals after a preliminary acid attack[27] and to decompose the entire sample in radiochemical neutron activation analysis methods.[20] Indeed, fusions with oxidizing fluxes have the advantage that they are very effective in dissolving both resistant and sulfide mineral phases.[28] However, such procedures must normally be restricted to small samples, usually 1 g or less, in applications such as those referred to above where sampling errors are not likely to occur.

In this work, a method has been developed for the determination of Ru, Pd, Ir and Pt using a fusion with sodium peroxide to decompose the sample in glassy carbon crucibles. After dissolution of the fused cake, the sample solution was spiked and the PGEs were separated by Te coprecipitation prior to determination of the PGEs by isotope dilution ICP-MS. The method was applied to five Canada Centre for Mineral and Energy Technology (CANMET) PGE reference materials: WGB-1 (gabbro rock), TDB-1 (diabase rock), UMT-1 (ultramafic ore tailings), WPR-1 (altered peridotite) and WMG-1 (mineralized gabbro), and to the mineralized ore of the South African Bureau of Standards (SARM)-7. Additional studies were carried out to evaluate the determination of the mono-isotopic elements Rh and Au by conventional external calibration. The fusion and Te coprecipitation procedure described here is similar to that used in the radiochemical neutron activation method of Stone and Crocket.[20] The over-all method is similar to the isotope dilution ICP-MS procedure described by Sen Gupta and Gregoire.[29] However, instead of using a two-stage sample dissolution procedure based on an initial acid attack, followed by fusion of any residue with sodium peroxide, we have adopted a single-stage digestion based on a sodium peroxide fusion and have included Pt in the list of analysed elements.

Experimental

Reagents

Quartz-distilled HCl and sub-boiling distilled HNO_3 were used in the analytical procedure. De-ionized water was used and all other reagents were of analytical-reagent grade. Poly(tetrafluoroethylene) (PTFE), glassware and glassy carbon crucibles were cleaned by soaking in freshly prepared *aqua regia* and then repeatedly soaking and rinsing with de-ionized water.

A standard solution of the PGE (100 μg g^{-1}, Spex Industries Edison, NJ, USA) was used to check natural isotope ratios and to prepare a mixed solution (monitor) with the spike solutions to correct the measured ratios of the samples for instrumental mass bias.[30] Isotope dilution was undertaken using enriched stable spike solutions of ^{101}Ru, ^{105}Pd, ^{193}Ir and ^{194}Pt (US Services, Summit, NJ, USA, courtesy of Dr. D. C. Gregoire, Geological Survey of Canada, Ottawa, Canada). Spike solution concentrations were determined against the standard by isotope dilution ICP-MS.

Spike solutions were always weighed instead of only measuring the required volume. The same procedure was carried out with the standard solution used to prepare the monitor solution.

Tellurium solution (1 mg ml^{-1}). Tellurium (0.1 g) was dissolved in 5 ml of *aqua regia* and the solution evaporated to dryness. The residue was converted into $TeCl_4$ by evaporating to dryness three times with 2 ml portions of HCl (6 mol l^{-1}). The residue was dissolved in 2 mol l^{-1} HCl, diluted to 100 ml with the same acid and stored in a PTFE bottle.

Tin(II) chloride solution (1 mol l^{-1}). Small amounts of this solution were prepared before use to ensure that it was fresh. The required amount (4.5 g) of tin(II) chloride was dissolved by heating gently in 6 ml of 6 mol l^{-1} HCl. De-ionized water was added to dilute the solution to a final volume of 20 ml.

Sample Decomposition

Samples were dried at 105 °C overnight and cooled in a desiccator before weighing. Conical crucibles made of glassy carbon with a capacity of 60 ml (Sigri, Meitingen, Germany) were used in the sample fusion procedure. In order to protect the crucible from attack by the sodium peroxide flux, a layer of sodium carbonate (3.5 g) was used to line the bottom and walls of the crucible before each fusion. Sodium peroxide (0.5 g), sample (0.5000 g) and then more sodium peroxide (1.5 g) were weighed into the crucible onto the sodium carbonate lining. The sample and sodium peroxide were carefully mixed using a nickel spatula. The crucible was covered with a lid and transferred into a cold furnace. The temperature of the furnace was raised to 200 °C and left for 15 min and then raised to 490 °C and left for 1 h. The crucible was then removed from the furnace and allowed to cool. With the crucible transferred into a 400 ml beaker (covered with a watch-glass) the cake was dissolved in 50 ml of warm de-ionized water, swirling the contents periodically. After dissolution, the spike solution containing Pt, Pd, Ir and Ru was added to the alkaline sample solution. The crucible was removed from the beaker using a PTFE tweezer and rinsed repeatedly with small volumes of de-ionized water and 6 mol l^{-1} HCl to ensure quantitative transfer of the contents into the beaker. More acid was added (total 45 ml) to dissolve completely the hydroxides and to acidify the solution. The solution was then gently boiled for a few minutes to destroy peroxides. Any precipitated silica was removed by filtration using a Millipore filtration apparatus (with Whatman No. 4 filter-paper) and the filtrate collected in a 250 ml Pyrex filter-flask. The original beaker and the precipitate were washed with hot 1 mol l^{-1} HCl (20 ml), which was added to the filtrate.

The filter-flask containing the solution was then heated to boiling and 2 ml of Te solution were added. The solution was brought back to boiling and tin(II) chloride solution (10 ml) was slowly added. The solution was boiled for a few minutes until the black precipitate was thoroughly coagulated. At this point, more Te solution (1 ml) was added. The solution was boiled again for 5–10 min to coagulate the precipitate. The flask was removed from the hot-plate and allowed to cool for a while to settle the precipitate. The mixture was filtered using a Millipore membrane filter (Type HA, 0.45 μm) using suction provided by a water-pump. The precipitate was rinsed with hot 1 mol l^{-1} HCl (approximately 100 ml). The filter membrane was transferred into a 30 ml PTFE flask (Savillex) using small plastic tweezers and while holding it bent inside the flask, the precipitate was dissolved by dropping concentrated HNO_3 onto the membrane. In this way, the precipitate could be dissolved, avoiding the necessity to dissolve the membrane. In order to ensure quantitative dissolution, the membrane, and any precipitate adhering to the filtering apparatus, was rinsed with a few more drops of HNO_3. The resulting solution was evaporated to dryness by placing the beaker in a PTFE vessel, through which filtered air was passed, and heating with an infrared lamp. The residue was dissolved in 1 ml of dilute *aqua regia* (6 mol l^{-1} HCl–concentrated HNO_3, 6 + 1) by re-heating the PTFE flask with its screw cap lid in place. This reagent was used in a slightly diluted form because 6 mol l^{-1} HCl was the highest concentration that could be purified by sub-boiling distillation. The resulting solution was stored awaiting analysis and diluted with de-ionized water just before the ICP-MS measurements. Blank samples were prepared using the same procedure but omitting the addition of the spike solution.

During the development of this procedure, some difficulties were encountered in achieving quantitative recoveries of the Te precipitate. Attempts to use centrifugation to separate the precipitate as suggested by Sun *et al.*[11] were not successful because when the supernatant was decanted, a small amount of the loosely settled precipitate was lost because it was found to float on the surface of the supernatant solution. The procedure described above was found to give reliable quantitative recoveries, which although not necessary for a method based on isotope dilution, was important in extending the technique to elements (such as Au and Rh) that must be determined by external calibration.

ICP-MS Measurements

The sample solutions were analysed by ICP-MS using the upgraded prototype instrument at the NERC ICP-MS Facility, Centre for Analytical Research in the Environment (CARE), Imperial College at Silwood Park. A summary of the operating parameters used is given in Table 1. Ten runs were obtained for each isotope.

Several potential isobaric interferences with the isotopes measured here have been mentioned in the literature, mainly from Y, rare earth elements and hafnium oxides formed during ionization. It has been suggested that the addition of HF to the solution before the Te precipitation inhibits the coprecipitation of Hf.[20] However, this precaution was not found to be necessary in this work because no significant interferences were found.

Isotope Dilution Calculations

As the reference materials analysed in this work have a wide range of PGE concentrations, care had to be taken to optimize isotope dilution measurements. According to Heumann,[31] the highest precision in an isotope ratio measurement can usually be achieved when the ratio A/B is approximately unity (where A and B are the abundances of the heavier and lighter isotope selected for analysis). However, in isotope dilution applications, to minimize the uncertainty introduced by the propagation of errors through the isotope dilution equation (see below), this isotope ratio (A/B) should be close to the geometric mean of its value in the spike and sample. The amount of spike added to each sample in this work was chosen so that the spiked sample had an isotopic ratio of between 1 and the geometric mean value (Heumann[31]). The target ratios were approximately as follows: $^{108}Pd/^{105}Pd = 0.5$, $^{195}Pt/^{194}Pt = 0.6$, $^{101}Ru/^{99}Ru = 12$ and $^{193}Ir/^{191}Ir = 8$. The high values for the Ru and Ir ratios arose from the unusual isotope concentration of the spike available in this work, that is, for these two elements, the more abundant naturally occurring isotope was the isotope that was enriched in the spike.

The concentration (ng g^{-1}) of the element in the sample [$El_{(sample)}$] was calculated from the standard isotope dilution equation listed by Heumann[31] [eqn. (3), p. 304], rearranged to make calculations simpler, as follows:

$$[El_{(sample)}] = \frac{\text{spike mass (ng)}}{\text{sample mass (g)}} \times \frac{AW_{(natural)}}{AW_{(spike)}} \times \frac{A_{(spike)} - [R \times B_{(spike)}]}{[R \times B_{(natural)}] - A_{(natural)}}$$

where $AW_{(natural)}$ and $AW_{(spike)}$ are the relative atomic masses of the natural element and spike, A and B are the abundances (%) of the heavier and lighter isotopes, respectively, and R is the measured ratio A/B. Data in Table 2 show the isotopes selected for analysis and their natural and spike compositions. These isotopes were selected to avoid mass interferences in ICP-MS. Thus, although $^{102}Ru/^{101}Ru$ might be a better choice for Ru than $^{101}Ru/^{99}Ru$, the former was avoided because of ^{102}Pd interference. The measured ratios of the samples were corrected for instrumental mass bias using a spiked standard solution with isotopic ratios similar to those of the spiked samples.[30] Non-spiked procedural blanks were analysed and the blank count rate was subtracted from those of the samples before isotope ratios were calculated.

Table 1 ICP-MS operating conditions

Instrument	Surrey research instrument
Plasma gas	Ar
Plasma power	1300 W
Reflected power	<5 W
Nebulizer	Cross flow
Outer gas flow rate	14 l min^{-1}
Intermediate gas flow rate	0.5 l min^{-1}
Nebulizer gas flow rate	0.75 l min^{-1}
Sample uptake rate	0.5 ml min^{-1}
Spray chamber coolant temperature	5 °C
Scan regions	93.6–200.4 u, skip region 114.4–186.6
Run time per sample	30 s
Run mode	Scanning

Results and Discussion

Detection Limits

In order to evaluate the detection limits, count rates of ^{99}Ru, ^{108}Pd, ^{191}Ir and ^{195}Pt were measured on the procedural blank sample. These isotopes were chosen because they are the less abundant in the spiked samples and therefore define a more realistic detection limit signal. The signal corresponding to three standard deviations ($+3s$) on the average of ten count rate measurements of these isotopes was taken and compared with the average count rate from a standard solution of known composition. The resulting detection limit values are listed in Table 3. These data are representative of the entire sample preconcentration procedure and include an allowance for small day-to-day variations in instrument response. Detection limit values for the elements Ru, Pd, Ir and Pt all lie in the range 0.3–2 ng g^{-1} (whole rock), based on the analysis of a 0.5 g sample.

Results for Certified Reference Materials

Concentrations for Ru, Pd, Ir and Pt obtained from an analysis of selected reference materials are listed in Table 4. In general, two sample aliquots were analysed, but for some samples none, one or three results are shown for some of the

Table 2 Abundances of isotopes (%) and relative atomic masses (A_r) of the natural and spike elements used in isotope ratio measurements

	Ru			Pd			Ir			Pt		
	99	101	A_r	105	108	A_r	191	193	A_r	194	195	A_r
Natural	12.7	17.1	101.07	22.34	26.46	106.42	37.3	62.7	192.22	32.9	33.8	195.08
Spike	0.24	96.3	101.15	96.58	0.46	105.06	0.67	99.33	192.99	95.06	3.78	194.10

elements and the reasons for this are as follows: (i) in samples WGB-1 and TBB-1, Ir could not be determined because the count rates were below the detection limit; (ii) for the same samples, there is only one result for Ru because in only one set of measurements on duplicate test portions were the count rates sufficiently above the procedural blank to obtain meaningful data; (iii) in sample UMT-1 three values are shown for Ru, Pd and Ir and only two for Pt because the procedure was repeated an additional time for this sample, to provide more data for the low Pt results (see below) and (iv) only one set of results for SARM-7 is presented in Table 4 because this sample was only used for the first trials in developing the procedure. In any event, this reference sample is not fully representative of the type of rock for which the procedure was developed, because of its high concentration of PGEs.

The results for Ru, Pd and Ir shown in Table 4 are in excellent agreement with the recommended values and the excellent precision between the duplicate determinations shows that the method is very effective for determining these elements, provided that concentrations are above the detection limit level. The results for Pt for samples WGB-1, TDB-1 and SARM-7 are in excellent agreement with the certified values but for samples UMT-1, WPR-1 and WMG-1, lower results than the expected values were found. It is suggested that the reason for this discrepancy in Pt is related to difficulties in ensuring equilibration between spike and sample solution. In fact, the way in which the spike solution was added to the sample mixture was found to be the critical step. When the spike solution was weighed directly into a clean glassy carbon crucible and evaporated to dryness before the addition of sample and flux, good results were found for Ru and Pt, but not for Ir and Pd, indicating that some physical or chemical reaction may occur between these elements and the crucible material. When the spike solutions were added to an acidified solution of the sample obtained after dissolution of the fused cake, good agreement was found for Ru, Pd and Ir, while Pt gave very low values. Only when the spike was added to the strongly alkaline sample solution obtained after dissolution of the cake were good results obtained for all elements. For Pt, these findings appear to be related to the aqueous chemistry of this element. Previous work in our laboratory (Enzweiler and Potts[32]) showed that when alkaline solutions containing Pt salts are acidified with HCl, the Pt appears to be only partially converted into soluble chloro-complexes. We surmise, therefore, that the addition of a chloroplatinate spike solution to the sample solution after acidification with HCl prevents complete equilibration between the spike solution and the (apparently) unreactive Pt species present, so causing low recoveries. By comparison, better equilibration occurs when the spike is added to the strongly alkaline solution. Thus, it was observed that in three trial analyses of sample UMT-1, the results for Pt obtained when the acidified sample solution was spiked were in good agreement among themselves, but still had an average value of only 64% of the recommended value. These discrepancies did not affect simultaneous determinations of Ru, Pd and Ir, nor determinations of Pt at lower abundance in other reference samples (Table 4). It is possible that these low Pt values in UTM-1 may have arisen because insufficient time was allowed for equilibration in view of the higher concentrations of Pt in UTM-1, although a full explanation is still not possible.

Precision of the technique cannot be adequately judged from the small number of replicate results listed in Table 4. However, estimates of precision were made from the standard deviation data derived from the ten runs made for each isotope ratio measurement by ICP-MS (see under Experimental). Assuming no other contribution to the precision of the final analysis, typical values for the relative standard deviation (%) were calculated as follows: Pt in WMG-1: 2.7% (for Pt at the 631 ng g^{-1} level); Pd in WGB-1: 5.1% (for Pd at the 14 ng g^{-1} level); Ir in UMT-1: 3.4% (for Ir at the 8 ng g^{-1} level); Ru in WPR-1: 7.7% (for Ru at the 21 ng g^{-1} level).

Table 3 Detection limits (3*s*) for ^{99}Ru, ^{105}Pd, ^{191}Ir and ^{194}Pt based on measurements from procedural blanks. Values (ng g^{-1}) were recalculated to whole rock assuming that 0.5 g of sample was taken for analysis

Ru	Pd	Ir	Pt
0.4	1.0	0.3	2.0

Table 4 Determination of Ru, Pd, Ir and Pt in reference materials by sodium peroxide fusion, isotope dilution, Te coprecipitation and measurement by ICP-MS. All values are in ng g^{-1}. Values marked with an asterisk are provisional or information values. All others are certified values. ± means 95% confidence limits

Reference material		Ru	Pd	Ir	Pt
WGB-1	This work	0.28	14.1; 14.0	—	5.9; 5.4
	Average		14.1		5.7
	Recommended	0.3*	13.9 ± 2.1	0.33*	6.1 ± 1.6
TDB-1	This work	0.37	23.0; 21.9	—	5.9; 5.5
	Average		22.4		5.7
	Recommended	0.3*	22.4 ± 1.4	0.15*	5.8 ± 1.1
UMT-1	This work	9.5; 9.7; 10.4	108; 107; 105	8.2; 8.5; 8.6	109; 91
	Average	9.9	107	8.4	100
	Recommended	10.9 ± 1.5	106 ± 3	8.8 ± 0.6	129 ± 5
WPR-1	This work	20.4; 21.8	233; 240	14.4; 14.7	263; 261
	Average	21.1	236	14.6	262
	Recommended	22 ± 4	235 ± 9	13.5 ± 1.8	285 ± 12
WMG-1	This work	31; 32	370; 390	45; 39	662; 600
	Average	32	380	42	631
	Recommended	35 ± 5	382 ± 13	46 ± 4	731 ± 35
SARM-7	This work	412	1506	70	3792
	Recommended	430 ± 57	1530 ± 32	74 ± 12	3740 ± 45

One limitation of the procedure described here is the relatively small amount of sample (0.5 g) taken for analysis, in comparison with fire assay procedures, for example. The only precaution taken in selecting this test portion was to mix the sample in the bottle before weighing, as recommended by the certified reference material suppliers. However, examination of duplicate or triplicate determinations on independent test portions listed in Table 4 shows excellent agreement between the measurements, indicating the absence of sample inhomogeneity effects in the samples studied here. The main disadvantage of the small amount of sample taken for analysis was the impossibility of determining routinely Ru and Ir in low-level samples. This problem might be overcome if the final volume (8–10 ml) prepared for ICP-MS analysis in the scheme described above were further reduced to obtain a higher preconcentration factor.

From the results obtained, it is possible to conclude that the fusion procedure was very efficient in attacking the PGEs and relatively rapid if compared with other procedures in which an initial acid attack is followed by fusion of any remaining insoluble residue.[27] The temperature selected for fusion (490 °C) was a compromise between the minimum temperature required to fuse the sodium peroxide flux and the maximum temperature to ensure the thermal stability of the glassy carbon crucibles.

The modified procedure used in this work to dissolve the Te precipitate from the filtration membrane (without having to dissolve the entire membrane) was much easier and more rapid than the alternative in which the membrane and contents are decomposed by acid attack,[27] and was shown to be quantitative.

In order to investigate the extension of the procedure to the determination of Au and Rh (elements that are monoisotopic and cannot, therefore, be determined by isotope dilution), previously prepared sample solutions of WPR-1 and WMG-1 were re-analysed using the appropriate external calibration. The results for these measurements are shown in Table 5. Good agreement was obtained for Rh in the two analysed samples and this indicates that the procedure can probably be extended to the determination of all PGE (except for Os, which is lost as the tetroxide when the acidified sample solution is boiled). For Au, good agreement was obtained for sample WPR-1, but low results in comparison with the expected value were obtained for sample WMG-1. It was not possible to identify the reasons for these poor results and further studies may be necessary to evaluate whether Au can be included in the list of analysed elements.

Conclusions

A method has been developed for the determination of Ru, Pd, Ir and Pt at ng g^{-1} levels in geochemical samples by isotope dilution ICP-MS after fusion of the sample with sodium peroxide and a Te coprecipitation procedure. Results from the analysis of selected reference materials show that good to excellent agreement can be obtained when the spike solution is added to the strongly alkaline solution obtained by dissolution of the fusion cake. Low values for Ir and Pd were observed if the spike solution was evaporated directly into the glassy carbon crucible and of Pt if the spike was added after acidifying the solution obtained from the fusion cake. Detection limits were of the order of 0.3–2 ng g^{-1} (recalculated to whole rock). Further studies showed that the technique could be extended to the determination of Rh and possibly Au by external calibration. Sample inhomogeneity effects were not observed with the samples studied here, although as only 0.5 g was taken for analysis, this factor is likely to restrict application of the technique to mineralized samples that contain discrete PGE mineral grains.

Table 5 Determination of Rh and Au by ICP-MS after sodium peroxide fusion and Te coprecipitation, using an external calibration. All values are in ng g^{-1}

Reference material		Rh	Au
WPR-1	This work	14.3; 16.2	45; 39
	Average	15.3	42
	Certified	13.4 ± 0.9*	42 ± 3*
WMG-1	This work	28; 27	53; 72
	Average	28	63
	Certified	26 ± 2*	110 ± 11*

* ± Means 95% confidence limits.

The authors thank C. Gregoire (Geological Survey of Canada) for donation of the spikes used in this work. J. E. acknowledges financial support from the Brazilian agency FAPESP.

References

1 Sutcliffe, R. H., in *Analysis of Geological Materials*, ed. Riddle, C., Marcel Dekker, New York, 1993, pp. 1–35.
2 Brügmann, G. E., Arndt, N. T., Hoffmann, A. W., and Tobschall, H. J., *Geochim. Cosmochim. Acta*, 1987, **51**, 2159.
3 Sun, S. S., Wallace, D. A., Hoaston, D. M., Glikson, A. Y., and Keays, R. R., *Precamb. Res.*, 1991, **50**, 1.
4 Alvarez, L. W., Alvarez, W., Asaro, F., and Michel, H. V., *Science*, 1980, **208**, 1095.
5 Luck, J. M., Birck, J. L., and Allegre, C. J., *Nature (London)*, 1980, **283**, 256.
6 Morgan, J. W., *J. Geophys. Res.*, 1986, **91**, 12375.
7 Robért, R. V. D., van Wyk, E., and Palmer, R., *Natl. Inst. Metall. Repub. S. Afr. Rep.*, 1971, No. 1371.
8 Date, A. R., Davis, A. E., and Cheung, Y. Y., *Analyst*, 1987, **112**, 1217.
9 Jackson, S. E., Fryer, B. J., Gosse, W., Healey, D. C., Longerich, H. P., and Strong, D. F., *Chem. Geol.*, 1990, **83**, 119.
10 Denoyer, E., Ediger, R., and Hager, J., *At. Spectrosc.*, 1989, **10**, 97.
11 Sun, M., Jain, J., Zhou, M., and Kerrich, R., *Can. J. Appl. Spectrosc.*, 1993, **38**, 103.
12 Reddi, G. S., Rao, C. R. M., Rao, T. A., Lakshmi, S. V., Prabhu, R. K., and Mahalngam, T. R., *Fresenius' J. Anal. Chem.*, 1994, **348**, 350.
13 Robért, R. V. D., and van Wyck, E., *Natl. Inst. Metall. Repub. S. Afr. Rep.*, 1975, No. 1705.
14 Asif, M., and Parry, S. J., *Analyst*, 1991, **116**, 1071.
15 McDonald, I., Hart, R. J., and Tredoux, M., *Anal. Chim. Acta*, 1994, **289**, 237.
16 Palmer, R., and Watterson, J. I. W., *Natl. Inst. Metall. Repub. S. Afr. Rep.*, 1971, No. 1185.
17 Boisvert, M., Bergeron, M., and Turcotte, J., *Anal. Chim. Acta*, 1991, **246**, 365.
18 Brügmann, G. E., Gorton, M. P., and Hancock, R. G. V., *J. Geochem. Explor.*, 1990, **37**, 25.
19 Evans, N. J., and Crocket, J. H., *Geostand. Newsl.*, 1990, **16**, 71.
20 Stone, W. E., and Crocket, J. H., *Chem. Geol.*, 1993, **106**, 219.
21 Walker, R. J., *Anal. Chem.*, 1988, **60**, 1231.
22 Gowing, C. J. B., and Potts, P. J., *Analyst*, 1991, **116**, 773.
23 Morgan, J. W., *Anal. Chim. Acta*, 1965, **32**, 8.
24 Crocket, J. H., Keays, R. R., and Hsiegh, S., *J. Radioanal. Chem.*, 1968, **1**, 487.

25 Shirey, S. B., and Walker, R. J., *Eos Trans.*, 1994, **75**, 355.
26 Pearson, D. G., personal communication.
27 Sen Gupta, J. G., *Talanta*, 1989, **36**, 651.
28 Sulcek, Z., Povondra, P., and Dolezal, J., *CRC Crit. Rev. Anal. Chem.*, 1977, **6**, 255.
29 Sen Gupta, J. G., and Gregoire, D. C., *Geostand. Newsl.*, 1989, **13**, 197.
30 Colodner, D. C., Boyle, E. A., and Edmond, J. M., *Anal. Chem.*, 1993, **65**, 1419.
31 Heumann, K. G., in *Inorganic Mass Spectrometry*, eds. Adams, F., Gijbels, R., and van Grieken, R., Wiley, New York, 1988, pp. 301–376.
32 Enzweiler, J., and Potts, P. J., *Talanta*, in the press.

Paper 4/06271J
Received October 13, 1994
Accepted January 3, 1995

Measurement of Boron Isotope Ratios in Groundwater Studies*

Nikki C. Porteous and J. Nick Walsh

Geology Department, Royal Holloway College, University of London, Egham, Surrey, UK TW20 OEX

Kym E. Jarvis

NERC ICP-MS Facility, CARE, Imperial College, Silwood Park, Ascot, Berkshire, UK SL5 7TE

Boron is present at low levels in groundwater and rainfall in the UK, ranging between 2 and 200 ng ml^{-1}. A sensitive technique has been developed using inductively coupled plasma mass spectrometry (ICP-MS) to measure boron isotope ratios at low concentrations with a precision (s_r) of between 0.1 and 0.2%. Samples were evaporated to increase elemental boron concentrations to 200 ng ml^{-1} and interfering matrix elements were removed by an adapted cation-exchange separation procedure. The validity of measuring boron isotopic ratios by ICP-MS at this concentration level is discussed in relation the theoretical instrument precision attainable based on counting statistics. Using the developed procedure it is possible to use ICP-MS to establish a reliable database documenting the natural variation in boron isotope compositions in aquifers and rain water in the UK. Preliminary results demonstrate a trend in boron isotopic compositions with increasing boron concentration. The method may be used to evaluate possible levels of boron pollution from anthropogenic inputs into natural aqueous systems.

Keywords: Boron isotopes; inductively coupled plasma mass spectrometry; ion exchange

Introduction

Boron has two stable isotopes of atomic masses 10 and 11, which have natural abundances of 18.98 and 81.02%, respectively. This large difference in atomic mass has led to significant isotopic fractionation of boron and suggests that differences in isotopic ratio may be used to identify distinctive sources for boron in geological and environmental situations.

Boron isotopic compositions are difficult to measure accurately and with an acceptable level of precision. There are two methods of interest for the measurement of boron isotopes; thermal ionization mass spectrometry (TIMS) and inductively coupled plasma mass spectrometry (ICP-MS). The majority of the literature is concerned with determination by TIMS which has an established methodology.[1] The measurement of boron isotopes in a number of environments has been summarized by Bassett;[2] although at that time the measurement of boron isotopes by ICP-MS was in its infancy and was therefore not discussed. A limited number of papers describing the potential of ICP-MS for boron isotopic measurement have been published.[3–5] In each case ICP-MS was chosen for both its sensitivity and simplicity when measuring boron isotopes in simple matrices like groundwater. Little or no sample preparation is normally required, as the sample is already in solution, and can therefore by introduced directly into the instrument using conventional nebulization. By contrast, TIMS whilst having good precision and an established methodology,[2,4,6] requires extensive sample preparation even for simple matrices like water. Sample preparation for ICP-MS by comparison is relatively straightforward, and samples can be analysed in less than 10 min with a precision (s_r) typically better than 0.15%, which is acceptable for this application. In previous work by Gregoire boron isotopic ratios were determined using ICP-MS at concentrations of 0.5 μg ml^{-1} with a precision of 0.7% (s_r). The precision was further improved in later work on freshwater and brine samples; where precision was lowered to 0.5% (s_r) for the former samples.[5]

In the present work, a methodology has been developed for the measurement of boron isotopic ratios in groundwater by ICP-MS achieving a precision of 0.15% (s_r) or less. This level of precision is required to record differences in the natural variation of boron isotopes.

Variation in boron isotope ratios is described by the $\delta^{11}B$ notation where

$$\delta^{11}B = \left[\frac{^{11}B/^{10}B_{Sample}}{^{11}B/^{10}B_{Standard}} - 1 \right] \times 1000$$

The standard used is usually NIST SRM 951 which has a $^{11}B/^{10}B$ ratio of 4.04367. The large mass difference between ^{10}B and ^{11}B provides the potential for extensive fractionation and reported isotopic values for $\delta^{11}B$ range from −31‰ for terrestrial rocks to +40‰ for sea-water.[2]

Boron is present at low concentrations (between 2 and 200 ng ml^{-1}) in UK rainfall and groundwaters and is of great interest as a tracer element, particularly because it is contained in many waste substances that are deposited in landfill sites, effluent ponds, *etc.* There are a number of problems encountered when analysing boron isotope compositions (reliably) at low boron concentrations because of the relationship between precision and count rate. The method described below has been developed to achieve the necessary precision for a wide range of boron concentrations. The technique described here permits precise isotope ratio determination for low boron concentrations to be obtained, and has a quick and simple sample preparation procedure. The analysis of the samples by ICP-MS produces results with a precision of around 0.15% (s_r).

Experimental

Procedure

Sample collection

Volumes of 500–1000 ml of the aqueous sample were collected from boreholes and filtered using 0.45 μm Whatman (Maidstone, Kent, UK) membrane filters. Samples were acidified on

* Presented at Geoanalysis 94: An International Symposium on the Analysis of Geological and Environmental Samples, Ambleside, England, September 18–22, 1994.

collection using 1% v/v high-purity 16 mol l^{-1} nitric acid and stored in acid-washed poly(propylene) bottles. The acidification was necessary to retain trace and major cations in solution, which were subsequently determined by ICP-atomic emission spectrometry (AES).

Preconcentration

Analysis of the groundwater samples by ICP-AES revealed boron concentrations ranging from 2 to 200 ng ml^{-1}. With levels at the lower end of the concentration range it was not possible to obtain the optimum precision when the isotopic ratios were measured by ICP-MS (see discussion below). Thus, a simple evaporative preconcentration method was used so that the signal obtained was sufficient to produce $^{11}B/^{10}B$ precision of 0.15% (s_r) or better. Fig. 1 shows the signal for ^{11}B required to obtain a theoretical isotopic ratio precision of 0.15% (s_r) or better. It also illustrates the point that for counts in excess of 9×10^6 there is no great improvement in the theoretical precision, as count rate and precision are related by a square-root function. The instrument used for this work incorporates an enhanced sensitivity interface (FI elemental) and for ^{11}B, 10×10^6 counts s^{-1} ppm^{-1} can be obtained. Therefore 200 ng ml^{-1} total boron gives a count rate of 2.5×10^6 counts s^{-1} which would correspond to a theoretical precision of 0.13% (s_r).

Matrix effects

Simple evaporation of natural water samples will enhance boron levels but also enhances matrix element concentrations (Ca, Mg and Na). This is especially severe where preconcentration factors of 20 or 30 are used. The enhanced sensitivity interface on the ICP-MS instrument is intolerant to concentrations of Ca (for example) that exceed $\approx$ 100 μg ml^{-1}, and matrix effects are more severe than those experienced using lower sensitivity instruments. The major element data for two preconcentrated borehole samples, one from the Lower Greensand aquifer of South-east England and the other from the Lincolnshire Limestone aquifer are shown in Table 1. Attempts to measure boron isotope ratios on samples with these Na, Ca and Mg levels after preconcentration resulted in poor precision for the isotope ratio measurements. To reduce the level of matrix elements present in the preconcentrated solution a simple cation-exchange technique was adapted.

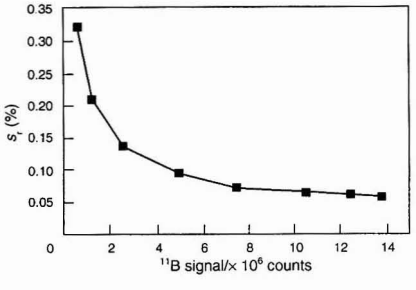

Fig. 1 Variation of theoretical $^{11}B/^{10}B$ precision with ^{11}B signal.

Table 1 Typical levels of major elements after preconcentration by simple evaporation

Sample number	B ng ml^{-1}	Ca μg ml^{-1}	Mg μg ml^{-1}	Na μg ml^{-1}	K μg ml^{-1}	Fe μg ml^{-1}
LGS17	18	386	45.9	107	15.3	2.87
LINCS3	35	798	41	88	13.8	0.69

Ion-exchange procedure

For this work, glass columns of 200 mm length and 10 mm diameter were used. A 5 ml volume of Dowex AG50W-X8 (200–400 mesh) (Bio-rad Laboratories, Richmond, CA, USA) cation-exchange resin was placed in each column (see column resin preparation procedures below), 20 ml of preconcentrated sample solution were loaded onto the column and allowed to drain through. This solution contained the boron for analysis while the major cations were retained on the resin. A small amount of boron was also retained on the resin; however, boron recoveries were better than 90%. The removal of cations and the cleaning of the resin was performed using a 3 stage wash-out procedure. The wash-out procedure involved 250 ml of 4 mol l^{-1} HCl to be washed through the columns, followed by 150 ml of 1 mol l^{-1} HCl and a further 100 ml of 0.25 mol l^{-1} HCl. All wash-out solutions were discarded and the columns were then ready for the loading of new samples.

Boron isotopic determination

Table 2 shows the ICP-MS operating conditions. The operating conditions incorporate some adaptations from the standard instrument operating procedure. The spray chamber (usually made of borosilicate glass), was replaced with a quartz chamber to reduce the likelihood of boron being retained within the system. A free running Meinhard nebulizer was chosen because it does not contribute to background noise and should produce the best precision.[8] Data was collected using the peak hopping mode of acquisition. There are no spectroscopic interferences at *m/z* 10 and 11 and the dwell-time spent at each mass position was the same.

Isotope ratio measurements obtained by ICP-MS are subject to some degree of mass bias owing to differences in the degree of ion transmission for each mass through the interface and ion lenses. This feature is not a mass fractionation effect and, depending on the *m/z* of the isotopes concerned can be a negative or positive bias. This is particularly true for boron isotopes. Using a conventional ICP-MS instrument, which has a steep mass response at the light end, the bias nearly always results in an 'apparent' loss of the light isotope. The use of an enhanced sensitivity interface, however, gives a much flatter mass response and similar sensitivities can be achieved for boron and cobalt (for example). Optimization of the ICP-MS instrument on one of the boron isotopes may result in an 'apparent' loss of the heavy isotope and hence a negative bias.

Table 2 ICP-MS instrument operating conditions

Instrument	FI elemental analysis plasmaquad STE
Interface	enhanced sensitivity
Forward power/W	1350
Reflected power/W	<5
Coolant gas flow/l min^{-1}	14
Auxillary gas flow/l min^{-1}	0.5
Nebulizer gas flow/l min^{-1}	0.9
Nebulizer	Meinhard
Spray chamber	quartz
Mode of data collection	peak hopping
No. of data points per peak	3
Dwell time/ms	10.24
Total analysis time/s	60
Ion lenses	optimized at ^{11}B
Rest mass	8

A mass bias correction factor was applied to all measurements using NIST SRM 951 (boric acid), which has a boron isotopic composition of 4.04367 for $^{11}B/^{10}B$. The measured mass bias recorded during this work was around +5%, although a range of values ranging from 1 to 12% were recorded on some occasions. The measured mass bias over a typical 5 h period is shown in Fig. 2. To correct for mass bias each sample was bracketed between NIST SRM 951 standards and a correction factor calculated from the mean measured ratio was applied to the sample.

Instrument optimization and analytical protocol

The instrument was opimized at ^{11}B whilst aspirating a 200 ng ml^{-1} solution of NIST SRM 951. Torch alignment, ion lenses and nebulizer gas flow were initially adjusted to give maximum sensitivity. The mass spectrometer was then set to transmit only ^{10}B ions and was re-optimized. This routine was carried out to minimize the degree of mass bias. Peak integral counts were collected for ^{10}B and ^{11}B only using the peak hopping mode of data acquisition. The time spent on each isotope was the same. Background count rates were at least 2 orders of magnitude lower than that of the calibration standard. For each sample and standard analysis, ten 60 s replicate measurements were made and the mean and relative standard deviation were calculated in each case. If the precision (1s) was worse than 0.25% (s_r), the analysis was rejected and then repeated. Each sample was bracketed by the NIST SRM 951 standard to monitor signal change and mass bias. The mean of the two NIST SRM 951 standard runs were taken and used to correct for bias in the ratio measurement for the unknown sample. The degree of correction was typically <5% on the $^{11}B/^{10}B$ ratio. Accuracy was assessed by analysing NIST 951 as an 'unknown' sample between two further solutions of the same material. Table 3 (column A) records the repeat determinations of NIST SRM 951 measured as an unknown sample (incorporating the correction noted above). The recorded NIST SRM 951 value is 4.04346 ± 0.00414, this has a precision of 0.10% (s_r).

Repeatability was assessed by analysing the same sample on three separate occasions (seven replicates of each run) during a 5 h period. Results from Table 3 show that the precision was 0.13% (s_r) over this period of time. Reproducibility was assessed by analysing the same sample on two repeat days. Results show this sample was within 1s.

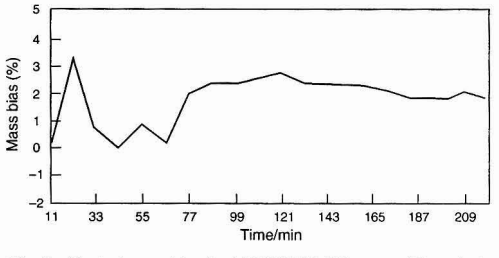

Fig. 2 Typical mass bias for NIST SRM 951 over a 5 h period.

Results and Discussion

An important aspect of the validation of the method was to demonstrate that the preconcentration procedure did not produce any fractionation of the boron isotopes. Table 3 shows the results of the three stages of the sample preparation: procedure A, untreated standard solution; B, after evaporation to preconcentrate to 200 ng ml^{-1} and C, after cation exchange to remove matrix elements. It can be seen that within the error of the measurements there is no disernable differences between the original sample, the evaporated sample and the evaporated samples passed through the columns. The results also confirm that there has been no significant change in the boron isotope composition by using glass columns for the ion-exchange procedure.

Groundwater samples were collected from Lower Greensand boreholes in Woburn and Slough in South-east England, (Fig. 3). These samples form the basis of a wider study covering aquifers in the UK and were selected for method evaluation. The relationship between boron concentration and $\delta^{11}B$ is shown in Fig. 4. For each data point (n = 10) the

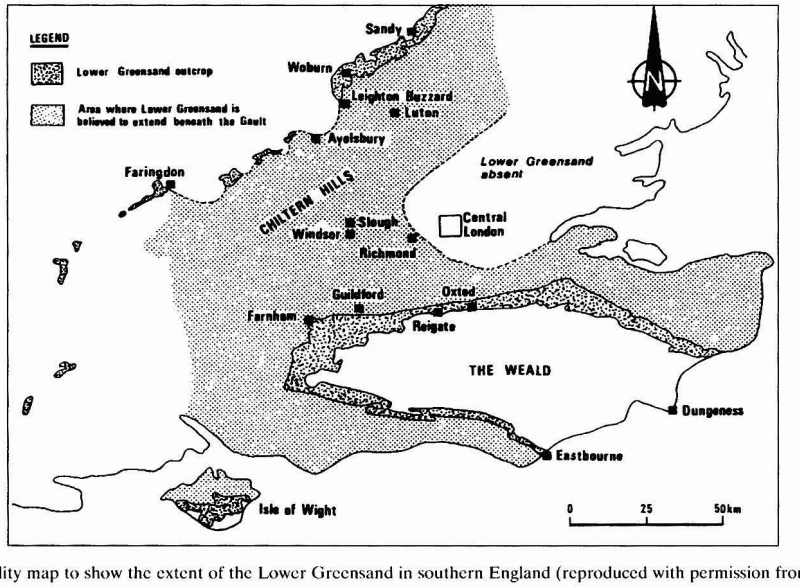

Fig. 3 Locality map to show the extent of the Lower Greensand in southern England (reproduced with permission from ref. 4).

error (1σ) is shown. With a precision of 0.13% (s_r), the data broadly show an increase in isotopic ratio with increasing boron content although this trend is not clear below levels of 40 ng ml^{-1}.

Conclusions

A method has been developed for the accurate determination of boron isotopes in groundwater and rainfall at levels of 200 ng ml^{-1}. Reliable results have been obtained on natural water samples with less than 20 ng ml^{-1} boron concentration using the preconcentration and separation procedures described. Results presented demonstrate that these procedures do not cause any fractionation of the boron isotopes.

Further work is needed to verify this relationship between boron concentration and $\delta^{11}B$ seen in Fig. 4 and to determine whether it is due to water–rock interaction in the Lower Greensand aquifer. The data illustrate the wide range of $\delta^{11}B$ values found in some aquifers in the UK. The precision attained (± 0.13%) is very low in comparison with the range of $\delta^{11}B$ values. The data does clearly demonstrate that the methodology is appropriate for precise boron isotope ratio determination in groundwater samples. Further work would be required to evaluate the applicability of the method for other sample types such as sea-water.

Table 3 Assessment of isotopic fractionation during sample preparation for $^{11}B/^{10}B^*$ for NIST SRM 951

A†	B†	C†
4.03665	4.02123	4.01792
4.04386	4.05861	4.04875
4.04940	4.04285	4.03031
4.04073	4.06042	4.02755
4.04711	4.03991	4.02366
4.04302		4.04957
4.04347		
Average‡ =	Average‡ =	Average‡ =
4.04346 ± 0.00414	4.04460 ± 0.01595	4.03269 ± 0.01322

* NIST SRM 951 reference value for $^{11}B/^{10}B$ = 4.04367.

† A, untreated standard solution; B, standard solution after evaporation; and C, standard solution after evaporation and preconcentration.

‡ Errors quoted are ± 1*s*.

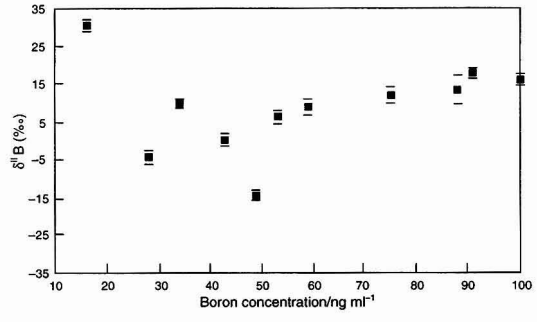

Fig. 4 Preliminary results for the northern boreholes of the Lower Greensand in South-east England.

The NERC ICP-MS Facility is partly supported by the Natural Environment Research Council and this support is gratefully acknowledged. This work was carried out whilst one of us (N. P.) was in receipt of a NERC studentship. The authors also thank B. C. H. Gibson and J. D. Wills for technical assistance and advice.

References

1 Spivack, A. J., and Edmond, J. M., *Geochim. Cosmochim. Acta*, 1987, **51**, 1033.
2 Bassett, R. L., *Appl. Geochem.*, 1990, **5**, 551.
3 Russ, G. P., and Bazan, J. M., *Spectrochim. Acta, Part B*, 1987, **42**, 49.
4 Gregoire, D. C., *Am. Chem. Soc.*, 1987, **59** (20), 2479.
5 Gregoire, D. C., *J. Anal. At. Spectrom.*, 1990, **5**, 623.
6 Zeininger, H., and Heumann, K. G., *Int. J. Mass Spectrom. Ion Phys.*, 1983, **48**, 377.
7 Egerton, R. H. L., *Q. J. Eng. Geol.*, 1994, **27**, S57.
8 Jarvis, K. E., Gray, A. L., and Houk, R. S., *Handbook of Inductively Coupled Plasma Mass Spectrometry*, Blackie, London, 1992.

Paper 4/06272H
Received October 13, 1994
Accepted February 1, 1995

Comparative Study on the Trace and Rare Earth Element Analysis of an Indian Polymetallic Nodule Reference Sample by Inductively Coupled Plasma Atomic Emission Spectrometry and Inductively Coupled Plasma Mass Spectrometry*

V. Balaram and K. V. Anjaiah
National Geophysical Research Institute, Hyderabad-500 007, India
M. R. P. Reddy
Centre for Materials for Electronic Technology, Hyderabad-500 762, India

The results of the semi-quantitative and quantitative characterization of an Indian polymetallic nodule reference sample (No. 2388) using ICP-AES and ICP-MS methods are presented. Acid dissolution using HF, HNO_3, $HClO_4$ and H_2O_2 in a PTFE beaker was adopted for sample dissolution. The calibration was performed with synthetic reference solutions that contained the reagents used for sample dissolution. The data thus obtained were corrected using the data obtained on United States Geological Survey (USGS) polymetallic nodule reference samples (NOD-A-1 and NOD-P-1) to minimize matrix and other effects. Over 30 trace elements were determined using both techniques. The accuracy of the determination was assessed by comparing the values obtained with the certified values for three RIAP reference samples. Indicative values were obtained on sample No. 2388 for about 60 elements by semi-quantitative analysis using ICP-MS.

Keywords: Inductively coupled plasma mass spectrometry; inductively coupled plasma atomic emission spectrometry; polymetallic nodule reference sample; trace element; rare earth element

Introduction

Data on rare earth elements (REEs) and trace elements in manganese nodules contribute to the understanding of the chemical and mineralogical compositions and the processes that control their genesis.[1] REE concentrations, in particular in manganese nodules and the associated phases, have helped in constraining models for REE cycling in the ocean environment.[2] These studies require sensitive, precise, accurate and rapid determinations of several trace elements in a large number of samples. The analytical procedures adopted in most instrumental methods require the use of appropriate reference samples which help to minimize the analytical uncertainties such as matrix effects and inter-element interferences. Two well certified manganese nodule reference samples (NOD-A-1 and NOD-P-1) have been available from the United States Geological Survey (USGS) since 1980.[3] Three more manganese nodule reference samples (OOPE 601, OOPE 602 and OOPE 603) have been made available more recently by the Research Institute of Applied Physics (RIAP) jointly with the Institute of Oceanology of the USSR Academy of Sciences.[4] These three samples also have reasonably good major, minor, trace and REE data.[5] Recently Roelandts[6] supplemented the trace element data by providing some new REE data on all these five reference samples.

In India, an ocean bed polymetallic nodule reference sample (No. 2388) from the Indian Ocean was prepared by the National Metallurgical Laboratory, Jamshedpur, jointly with the National Institute of Oceanography, Goa, in 1981. Subsequently, a collaborative investigation of the sample was carried out by ten National Research Laboratories including NGRI, details of which were given by Pandey.[7] 'Certified values' are assigned for only six of the major and minor elements, namely Si, Fe, Mn, Ni, Co and Cu (Table 1), most crucial from the exploration point of view, and data are not available on several other geochemically significant trace elements such as REEs, U and Th.

In this work, we attempted to provide working values on several geochemically significant trace elements in this reference sample by using two of the most popular multi-element analytical techniques, inductively coupled plasma atomic emission spectrometry (ICP-AES) and inductively coupled plasma mass spectrometry (ICP-MS). Indicative values were obtained for several other trace elements using semi-quantitative analysis by ICP-MS.

Experimental

Reagents, Calibration Standards and Internal Standard for ICP-MS

Electronic and analytical-reagent grade acids and high-purity doubly distilled water were used throughout. Three sets of

Table 1 Certified data on sample No. 2388 for some major and minor elements[7]

Component	Concentration (% m/m)*	s_r (%)
SiO_2	16.07	2.80
Fe	14.94	3.28
Mn	21.28	3.05
Ni	0.71	5.63
Co	0.14	7.14
Cu	0.49	4.08

* Average of 8 or 9 determinations.

* Presented at Geoanalysis 94: An International Symposium on the Analysis of Geological and Environmental Materials, Ambleside, England, September 18–22 1994.

multi-element stock standard solutions (10 μg ml^{-1}) were prepared from certified 1000 μg ml^{-1} single-element solutions obtained from Spex Industries (Edison, NJ, USA) and Merck (Darmstadt, Germany): (i) Y, Sc and REEs, 10 μg ml^{-1}, 5% HNO_3; (ii) U, Th, V, Cr, Co, Ni, Cu, Ba, Rb, Sr and Cs, 10 μg ml^{-1}, 5% HNO_3; and (iii) Nb, Zr, Hf and Ta, 10 μg ml^{-1}, 2% HCl and 1% HF. From these three solutions, a working standard solution containing Y, Sc, REEs, U, Th, V, Cr, Co, Ni, Cu, Ba, Rb, Sr, Cs, Nb, Zr, Hf, Ta and the internal standard Rh at 100 ng ml^{-1} in 5% HNO_3 was prepared. Another standard solution containing Be, Mg, Co, In, Rh, Pb and U at 100 ng ml^{-1} in 2% HNO_3 was also prepared independently from the stock standard solutions for use in instrument optimization and semi-quantitative work. These calibration standards were found to be stable for 1 month without any problem.

Calibration Standards for ICP-AES

Four sets of calibration solutions of 1 and 10 μg ml^{-1} of the combinations (i) Sc, Y and REs in 5% HNO_3, (ii) V, Cr, Co, Ni, Cu, Zn, Pb, U and Th in 5% HNO_3, (iii) Rb, Sr, Cs and Ba in 5% HNO_3 and (iv) Zr, Nb, Hf and Ta in 2% HCl and 0.5% HF were prepared for use in ICP-AES measurements. These combinations did not cause any significant problems in the stability of these calibration solutions over a period of 2 months. No internal standards were used in the ICP-AES measurements.

Sample Preparation

Sample preparation for both ICP-MS and ICP-AES was done separately. In both instances the samples were dried at 105 °C for 12 h before weighing. Amounts of 100 mg each of the samples and standards were weighed into PTFE beakers and each sample was moistened with a few drops of water. To each beaker 5 ml of HCl, 3 ml of HNO_3, 1 ml of $HClO_4$ and 7 ml of HF were added. The beakers were kept overnight for digestion after adding 1 ml each of 10 μg ml^{-1} rhodium solution to act as an internal standard. The next day the beakers were heated on a hot-plate at 200 °C for about 1 h, after which the lids were removed and the contents were evaporated nearly to dryness. This process was repeated again with further addition of 2 ml of HNO_3, 1 ml of $HClO_4$ and 3 ml of HF. Then the contents were dissolved using a mixture of 5 ml of 1 + 1 HNO_3 and 5 ml of 1 + 1 HCl. The dark residue that remained was dissolved by the addition of 5 ml of 30% hydrogen peroxide. Excess of peroxide was removed by gentle boiling.[8] The resultant solution was cooled and made up to 100 ml using doubly distilled water. These solutions were used for ICP-MS measurements.

Sample preparation for ICP-AES measurements was carried out by taking 1 g of the samples and standards and by adding appropriate amounts of different acids using a method similar to that described by Fries and Lamothe.[8] Solutions of 1% concentration were prepared for this purpose and clear solutions were obtained. Five replicate solutions of the Indian polymetallic reference sample were prepared in both instances. Solution of NOD-A-1 and NOD-P-1 manganese nodule reference samples from the USGS were also prepared using both methods. Solutions of 0.1% of the three RIAP manganese nodule reference samples (OOPE 601, OOPE 602 and OOPE 603) were prepared for ICP-MS analysis. The solutions prepared by the fusion method using lithium metaborate flux in graphite crucibles (samples-to-flux ratio 1 : 5) did not yield clear solutions in dilute nitric acid medium, so all measurements were made using solutions prepared by acid decomposition procedures only.

ICP-MS Instrumentation, Operation and Data Acquisition

The instrument used was a VG PlasmaQuad PQ1 (Fisons Instruments) equipped with a Tracor Northern multichannel analyser. The instrument configuration and other details are given elsewhere.[9] The operating parameters given in Table 2 were kept constant throughout this study. The following isotopes were used in analytical determinations: ^{45}Sc, ^{51}V, ^{52}Cr, ^{59}Co, ^{62}Ni, ^{63}Cu, ^{64}Zn, ^{71}Ga, ^{85}Rb, ^{88}Sr, ^{89}Y, ^{90}Zr, ^{93}Nb, ^{103}Rh, ^{133}Cs, ^{137}Ba, ^{139}La, ^{140}Ce, ^{141}Pr, ^{146}Nd, ^{147}Sm, ^{151}Eu, ^{157}Gd, ^{162}Dy, ^{166}Er, ^{174}Yb, ^{175}Lu, ^{178}Hf, ^{181}Ta, ^{208}Pb, ^{209}Bi, ^{232}Th and ^{238}U. These isotopes were selected taking into consideration their abundance levels and freedom from interference effects from other elements present in the sample.[10] Some isotopes such as ^{232}Th are monoisotopic and therefore no choice was available.

The results presented here were acquired in the mass scanning mode covering all the elements including the internal standard in a single scan. Sample solutions were introduced into the ICP-MS instrument by conventional pneumatic nebulization with a peristaltic pump at a solution uptake rate of 0.8 ml min^{-1}. The system was operated in the mass scanning mode after tuning the ion lenses using a 100 ng ml^{-1} solution of ^{9}Be, ^{23}Mg, ^{59}Co, ^{115}In, ^{208}Pb and ^{238}U to yield a response that is relatively uniform across the mass range. Each standard or sample or blank was aspirated for about 2 min to enable the nebulizer–spray chamber system to equilibrate before acquisition of data. The blank, standards and samples were run (three runs) in that order with a wash time of 2 min between each sample.

Table 2 Instrument configuration and operating conditions of ICP-MS instrument (PlasmaQuad PQ1)

Plasma—	
Incident power at 27 MHz	1.35 kW
Reflected power	<5 W
Coolant gas flow rate	12 l min^{-1}
Auxiliary gas flow rate	0.7 l min^{-1}
Nebulizer gas flow rate	0.70 l min^{-1}
Nebulizer type	Standard Meinhard (TR-30-C3)
Sample uptake (pumped)	0.8 ml min^{-1}
Spray-chamber cooled to	9 °C
Washout time	120 s
Interface—	
Sampling depth	10 mm
Sampling cone	Nickel sampler (1.0 mm orifice)
Skimmer cone	Nickel skimmer (0.75 mm orifice)
Vacuum—	
Expansion stage	2.3 mbar
Intermediate stage	<10^{-4} mbar
Analyser stage	2×10^{-6}
Mass analyser—	
Quadrupole type	12–12 S (VG Isotopes)
Mass resolution at 10% of peak height	0.8 u
Data acquisition—	
Detector type (Channeltron)	Galileo Model No. 4870V
Detector mode	Pulse counting
Quantitative mass scanning range	44–240 u
Skipped mass regions	46–50, 53–58, 65–70, 72–84, 94–102, 104–132, 182–207, 210–231, 233–237 u
Sweeps	120
Dwell time	500 ms
Channels	2048
Total analysis time per run	≈90 s

ICP-AES Instrumentation and Data Acquisition

A Jobin-Yvon 24R ICP atomic emission spectrometer system was used. The system consists of a high-frequency rf generator, a plasma torch, a sample nebulizer and a monochromator. The experimental facilities and the operating conditions are summarized in Table 3. The REEs and other trace elements were determined directly on 1% solutions without any separation or preconcentration from the rock matrix as the concentrations of these elements in manganese nodule samples are relatively high.

Results and Discussion

The ICP mass spectrum of the reference sample No. 2388 in the mass range 134–240 is illustrated in Fig. 1. This spectrum gives a good overview of the concentrations of various trace elements such as Ba, REEs, Pb, Bi, Th and U. The spectrum indicates very high concentrations of these elements in this particular sample. Such spectra are indispensable prior to quantitative analysis for the selection of proper analyte isotopes that are relatively free from interferences, in choosing the suitable internal standards, *etc.*

The matrix and the inter-elemental effects in ICP-MS determinations in geochemical samples are more pronounced, especially when elements such as Mn, Fe, Mg and Ti are present as major elements. The effect of Mn is found to be particularly severe on the signal of trace elements such as Th and U, depressing the signal[11] by more than 50%. To minimize these effects, the results for each element obtained using synthetic calibration graphs were corrected using the data obtained on the USGS polymetallic nodule reference samples, which were analysed along with samples under

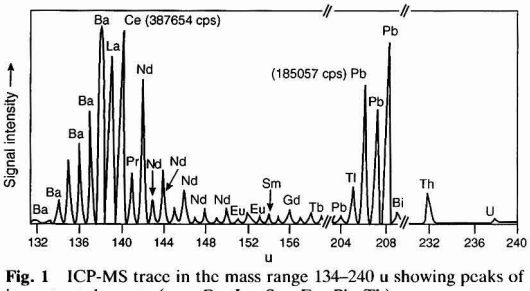

Fig. 1 ICP-MS trace in the mass range 134–240 u showing peaks of important elements (*e.g.*, Ba, La, Sm, Eu, Pb, Th).

Table 3 Instrument configuration and operating conditions of ICP-AES instrument (Jobin Yvon JY 24R)

Sequential spectrometer—	
Spectrometer	Jobin Yvon JY 24R 1 m Czerny–Turner
Gratings	Holographic, 3600 grooves mm^{-1} (120 × 140 mm)
Spectral range	150–500 nm
Slit width	20 nm for entrance and exits, adjustable
Linear dispersion	0.26 nm mm^{-1} (1st order)
Theoretical resolving power	504 000
Experimental resolution	0.006 nm (20 nm slit)
Aperture FWHM	*F* 7.5
Peak search	10 points, 0.0013 nm per step
Slew speed	800 nm min^{-1}
RF generator—	2.3 kV A, continuous; power stability better than 0.01%, 40.68 MHz; single phase 220 V; tuned oscillating circuit; automatic voltage and frequency regulator
Computer—	Adonics for instrument control and analytical processing of intensity data.
Plasma—	
Plasma torch assembly	Fused quartz with capillary injector
Nebulizer and spray chamber	Glass pneumatic nebulizer into dual-tube spray chamber
Forward power	1600 W
Reflected power	<10 W
Argon coolant gas flow rate	14 l min^{-1}
Argon plasma gas flow rate	1.5 l min^{-1}
Argon carrier gas flow rate	1 l min^{-1}
Observation height in plasma	15 mm above load coil

Wavelengths (nm) used—

Sc	361.384	La	408.672	Er	349.910
V	290.882	Ce	418.660	Tm	313.126
Cr	267.716	Pr	390.844	Yb	328.937
Co	238.892	Nd	430.358	Lu	261.542
Ni	231.604	Sm	446.734	Pb	220.353
Cu	324.754	Gd	335.047	Ti	334.941
Zn	213.856	Tb	350.917	Mo	379.825
Y	371.030	Dy	353.170		
Zr	343.823	Ho	345.600		

Table 4 Values obtained (μg g^{-1}) for different trace elements in the polymetallic nodule reference sample by ICP-AES and ICP-MS in comparison with recommended values

Element	ICP-AES*	ICP-MS*	Recommended value[7] (Table 1)	Average s_r (%)
Sc	9.80	11.10	NA†	6.37
V	776.00	750.00	NA	6.57
Cr	19.11	17.04	NA	5.08
Co	1309.00	1319.00	1400.00	3.47
Ni	7020.00	7196.00	7100.00	3.33
Cu	4910.00	4788.00	4900.00	2.30
Zn	879.30	763.30	NA	2.51
Ga	ND‡	12.29	NA	4.41
Rb	ND	12.06	NA	4.74
Sr	ND	1010.00	NA	5.01
Y	113.10	107.1	NA	4.83
Zr	535.12	510.33	NA	2.07
Nb	ND	27.60	NA	1.10
Cs	ND	0.56	NA	1.71
Ba	ND	1397.00	NA	1.36
La	223.27	187.70	NA	2.31
Ce	851.68	806.20	NA	3.35
Pr	ND	45.12	NA	4.50
Nd	243.60	182.40	NA	3.30
Sm	ND	43.80	NA	3.39
Eu	13.32	10.43	NA	4.10
Gd	43.65	44.52	NA	3.27
Tb	7.26	7.42	NA	4.71
Dy	ND	40.20	NA	2.31
Ho	ND	7.31	NA	3.81
Er	22.10	19.81	NA	4.77
Tm	ND	2.91	NA	5.09
Yb	18.70	17.85	NA	6.11
Lu	3.75	3.13	NA	3.10
Hf	ND	2.69	NA	2.23
Ta	ND	0.49	NA	4.47
Pb	ND	801.54	NA	6.69
Th	ND	58.82	NA	2.87
U	ND	5.04	NA	4.03

* Average of ten determinations.
† NA, not available.
‡ ND, not determined.

similar operating conditions. The major and minor element concentrations[3,7] of sample No. 2388 fit approximately between those of NOD-A-1 and NOD-P-1, particularly with respect to elements such as Mn, Ni and Cu. Hence this kind of correction should help to minimize the matrix effects to a large extent. Even in ICP-AES measurements the results obtained after comparison with the synthetic calibrations were corrected as above. To ensure adequate precision, each sample was prepared in five replicates and each replicate was analysed twice, and the means of ten determinations by both techniques are presented in Table 4.

The assessment of the accuracy of data is a problem particularly when dealing with several elements without any earlier data. An interlaboratory comparison cannot be made on several elements because of a lack of availability of data for many elements. Hence the accuracy of the determinations carried out on sample No. 2388 (Table 4) was assessed by comparing the results with those obtained on NOD-A-1 and NOD-P-1 (Table 5) and the three RIAP reference samples using ICP-MS (Table 6). There is good agreement for the values obtained by both ICP-AES and ICP-MS in most instances, with average precisions better than s_r = 6%. However, there is a pronounced difference in the data obtained by both techniques (Table 4) for elements such as Nd, La and V. The proposed values for Cr, Ga, Nb, Cs and Hf (Table 5) for NOD-A-1 and NOD-P-1 should be useful for indicative purposes. Some elements such as Rb, some of the REEs, U and Th were not determined using ICP-AES because of the poor detection. The ICP-MS data obtained for the RIAP reference samples (Table 6) show reasonable accuracy when compared with the reported data; in particular, the REE data are very close to those reported by Roelandts[6] recently.

A plot of REE contents normalized to chondrite abundances should yield a smooth graph[12] as shown in Fig. 2. REEs are mobile in aqueous systems and their solutions are sensitive to pH, which can lead to fractionation. In addition, the solubility is sensitive to oxidizing conditions of ocean waters. Under favourable conditions Ce can exist in the tri- or tetravalent state. Under oxidizing conditions, notably associated with the deposition of manganese nodules in oceans, cerium is oxidized to Ce^{4+}, with a consequent decrease in its radius. This results in the precipitation of cerium hydroxide and phosphates in managanese nodules and these compounds become enriched in Ce. Consequently, Ce enrichment should be seen in this kind of plot and a positive Ce anomaly is strikingly evident in this particular sample, which further supports the credibility of the reported data for REEs.

Semiquantitative analysis using ICP-MS provides a comprehensive survey of elements present in an unknown sample

Table 5 Trace element concentrations (μg g^{-1}) in NOD-A-1 and NOD-P-1 determined by ICP-AES and ICP-MS in comparison with reported values

	NOD-A-1			NOD-P-1			
Element	ICP-MS*	ICP-AES*	Reported value[14]	ICP-MS*	ICP-AES*	Reported value[14]	Average s_r(%)
Sc	10.86	9.21	10.80	9.46	8.41	9.30	5.36
V	752.85	ND†	770.00	568.70	ND	570.00	6.69
Cr	25.75	23.03	25.90	17.84	ND	NA‡	3.31
Co	3011.00	ND	3110.00	2296.00	ND	2240.00	2.01
Ni	6350.00	ND	6360.00	13 368.00	ND	13 400.00	4.77
Cu	1107.00	ND	1100.00	11 412.00	ND	11 500.00	2.22
Zn	584.27	ND	587.00	1613.00	ND	1595.00	5.17
Ga	11.73	ND	NA	32.33	ND	NA	1.07
Rb	10.22	ND	11.00	23.08	ND	22.00	4.49
Sr	1587.00	ND	1748.00	684.05	ND	680.00	2.84
Y	96.72	95.40	97.00	74.89	74.70	75.00	3.55
Zr	314.72	ND	317.00	276.40	ND	280.00	6.99
Nb	42.30	ND	NA	20.75	ND	NA	4.09
Cs	0.52	ND	NA	1.71	ND	NA	1.33
Ba	1637.00	ND	1670.00	3373.00	ND	3350.00	2.11
La	103.78	110.26	104.00	102.38	108.60	100.00	3.78
Ce	751.69	676.62	760.00	308.41	259.65	310.00	3.55
Pr	21.58	ND	21.70§	27.52	ND	27.50§	2.41
Nd	84.30	85.63	81.00	120.78	139.20	124.00	4.69
Sm	17.63	ND	18.00	21.42	ND	20.00	3.14
Eu	4.40	4.73	4.30	7.37	7.94	7.44§	2.88
Gd	25.99	ND	29.00	21.16	22.78	21.00	5.77
Tb	4.17	4.23	4.20§	4.81	5.06	4.53§	3.09
Dy	21.67	ND	20.00	27.28	ND	28.00	5.14
Ho	5.59	ND	5.80	6.27	ND	6.50	4.44
Er	13.89	13.90	14.60	13.38	14.30	13.60	3.23
Tm	2.16	ND	2.19§	1.75	ND	1.72§	5.49
Yb	12.68	13.10	13.20	11.73	12.20	11.80	4.16
Lu	2.66	2.848	2.80	2.02	1.68	1.70	5.04
Hf	6.48	ND	6.20	4.13	ND	4.30	5.87
Ta	1.01	ND	NA	0.36	ND	NA	7.76
Pb	ND	ND	346.00	554.04	ND	555.00	5.22
Th	25.93	ND	27.00	17.83	ND	17.50	4.89
U	6.79	ND	6.00	3.73	ND	4.00	3.09

* Average of six determinations.
† ND, not determined.
‡ NA, not available.
§ From ref. 2.

with a moderate degree of accuracy, *i.e.*, within about 30% of the correct result in most instances. Table 7 presents the semiquantitative data on manganese nodule sample No. 2388. Details of the procedure followed are presented elsewhere.[13] Over 60 elements were determined using this procedure and data on some of these elements are compared with those obtained in the quantitative mode. Although Rh and Bi are used as internal standards for the quantitative analysis of most rock samples in our laboratory, Bi was not used as an internal standard here because of the presence of about 20 μg g^{-1} of Bi in sample No. 2388 as indicated by semiquantitative analysis. This amount can cause significant problems if Bi is used as an internal standard. Hence a semi-quantitative analysis in the initial stages will be of great help in choosing a proper internal standard for a particular analytical programme. This feature is unique for ICP-MS and cannot be applied to ICP-AES.

Conclusions

If one compares the detection power of these two analytical techniques, undoubtedly ICP-MS is more sensitive than ICP-AES, allowing the direct determination of all the REE and other trace elements in 100 mg samples. The unique semi-quantitative analysis feature of ICP-MS offers the advantage of establishing the approximate concentrations of over 60 elements in an unknown sample within a few minutes. This helps immensely in proper planning for the quantitative analysis.

Further characterization of this sample is needed using other techniques such as XRF, INAA and TIMS, and a great deal of work needs to be carried out on many other elements not considered in this study before assigning certified data for all the trace elements for this valuable standard.

The authors are grateful to Dr. H. K. Gupta, Director, National Geophysical Research Institute, Hyderabad and Dr. S. G. Patil, Executive Director, Centre for Materials for

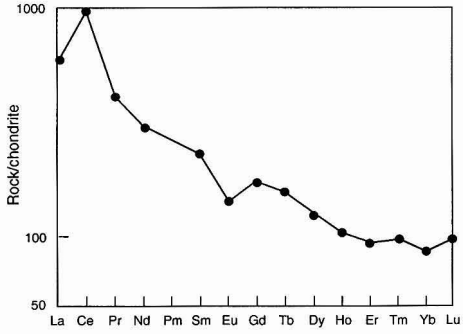

Fig. 2 Chondrite-normalized REE patterns for manganese nodule sample No. 2388.

Table 6 Trace element concentrations (μg g^{-1}) in OOPE 601, OOPE 602 and OOPE 603 by ICP-MS in comparison with the reported values

	OOEP 601			OOPE 602			OOPE 603			
Element	This study*	Roelandts[6]	Govindaraju[14]	This study*	Roelandts[6]	Govindaraju[14]	This study*	Roelandts[6]	Govindaraju[14]	Average s_r (%)
Sc	13.53	NA†	12.00	12.43	NA	11.00	12.74	NA	13.00	6.01
V	639.72	NA	400.00	570.37	NA	430.00	721.00	NA	480.00	5.49
Cr	21.39	NA	17.00	21.88	NA	18.00	21.80	NA	19.00	5.37
Co	3032.55	NA	3100.09	2225.00	NA	2200.00	4450.40	NA	4700.00	2.41
Ni	8329.35	NA	8400.87	12853.00	NA	13700.00	4398.52	NA	4200.00	2.18
Cu	5286.57	NA	5100.00	9917.40	NA	10100.00	2395.11	NA	2200.00	5.30
Zn	785.73	NA	770.00	1188.71	NA	1200.00	601.53	NA	580.00	4.41
Ga	17.51	NA	20.00	26.82	NA	10.00	13.44	NA	7.00	6.29
Rb	18.06	NA	16.00	21.93	NA	21.00	10.78	NA	10.00	5.80
Sr	1034.40	NA	900.00	719.72	NA	640.00	1260.93	NA	1100.00	4.18
Y	160.85	NA	160.00	123.16	NA	110.00	165.77	NA	140.00	3.42
Zr	452.92	NA	600.00	328.75	NA	320.00	634.33	NA	600.00	2.09
Nb	42.80	NA	48.00	25.98	NA	20.00	88.54	NA	90.00	2.69
Cs	0.78	NA	30.00	1.15	NA	30.00	0.38	NA	30.00	1.28
Ba	1976.32	NA	1900.00	2327.10	NA	1800.00	1608.00	NA	1700.00	5.58
La	186.07	184.00	150.00	106.94	110.00	90.00	185.79	182.00	140.00	5.41
Ce	663.82	735.00	500.00	270.13	300.00	200.00	833.03	1210.00	900.00	6.38
Pr	45.27	NA	NA	27.74	NA	NA	38.46	NA	NA	3.37
Nd	191.60	209.00	150.00	118.68	133.00	80.00	158.98	168.00	140.00	6.45
Sm	45.55	49.90	40.00	28.92	32.70	22.00	34.72	37.60	30.00	5.37
Eu	10.67	12.04	10.00	7.42	8.10	8.00	8.28	8.99	10.00	2.70
Gd	45.90	47.30	50.00	28.62	31.40	40.00	42.21	37.90	40.00	4.85
Tb	7.71	NA	8.00	5.09	NA	5.00	6.40	NA	5.00	6.00
Dy	43.24	42.00	30.00	29.50	28.60	20.00	37.19	36.00	30.00	4.65
Ho	8.51	NA	3.00	6.01	NA	1.00	8.14	NA	3.00	5.38
Er	21.11	NA	20.00	14.27	NA	3.00	19.51	NA	10.00	3.58
Tm	2.99	NA	2.00	2.11	NA	0.60	3.00	NA	0.90	4.31
Yb	20.81	21.40	21.00	14.58	15.00	13.00	21.13	20.80	14.00	3.36
Lu	3.18	3.14	2.00	2.18	2.15	2.00	3.16	3.09	2.00	1.24
Hf	1.15	NA	10.00	5.06	NA	8.00	12.42	NA	10.00	1.03
Ta	0.11	NA	5.00	0.44	NA	5.00	2.02	NA	2.00	5.05
Pb	742.52	NA	710.00	474.17	NA	400.00	1064.97	NA	980.00	3.29
Th	33.61	NA	31.00	18.45	NA	17.00	40.45	NA	38.00	5.95
U	6.28	NA	5.00	4.19	NA	4.00	8.19	NA	8.00	3.11

* Average of six determinations.
† NA, not available.

Table 7 Semi-quantitative values (μg g^{-1}) of elements in polymetallic reference sample No. 2388 by ICP-MS

Element	Semiquantitative ICP-MS*	Quantitative ICP-MS values	Element	Semiquantitative ICP-MS*	Quantitative ICP-MS values
^{7}Li	37.36	NA†	^{127}I	6.42	NA
^{9}Be	2.93	NA	^{128}Te	2.68	NA
^{11}B	19.82	NA	^{133}Cs	0.68	0.56
^{31}P	1472	NA	^{138}Ba	1175	1397
^{45}Sc	12.68	11.10	^{130}La	169.70	187.70
^{46}Ti	3935	4175‡	^{140}Ce	728.82	806.20
^{51}V	776	750	^{141}Pr	50.28	45.12
^{52}Cr	30.70	17.04	^{146}Nd	204.05	182.40
^{59}Co	1556	1319	^{152}Sm	46.58	43.80
^{60}Ni	7587	7196	^{153}Eu	12.65	10.43
^{63}Cu	5429	4788	^{158}Gd	50.76	44.52
^{65}Cu	5277	4788	^{159}Tb	7.59	7.42
^{66}Zn	803	763.3	^{163}Dy	38.59	40.20
^{68}Zn	795	763.3	^{165}Ho	6.97	7.31
^{69}Ga	23.24	12.29	^{166}Er	17.90	19.81
^{72}Ge	3.91	NA	^{169}Tm	3.08	2.91
^{75}As	138.65	NA	^{172}Yb	16.08	17.85
^{77}Se	66.72	NA	^{175}Lu	3.09	3.13
^{81}Br	42.30	NA	^{178}Hf	3.78	2.69
^{85}Rb	13.59	12.06	^{181}Ta	0.44	0.49
^{88}Sr	1192	1010	^{182}W	1.41	NA
^{89}Y	145.22	107.10	^{187}Re	0.04	NA
^{90}Zr	485.35	510.33	^{192}Os	0.01	NA
^{93}Nb	25.23	27.60	^{193}Ir	0.05	NA
^{98}Mo	483	494‡	^{195}Pt	0.10	NA
^{102}Ru	0.04	NA	^{197}Au	0.54	NA
^{103}Rh	0.01	NA	^{202}Hg	6.47	NA
^{106}Pd	0.68	NA	^{205}Tl	78.10	NA
^{108}Pd	0.20	NA	^{208}Pb	884	801.54
^{111}Cd	8.73	NA	^{209}Bi	22	NA
^{115}In	1.92	NA	^{232}Th	59.11	58.82
^{120}Sn	387	NA	^{238}U	7.50	5.04

* Average of six determinations.
† NA, not available.
‡ ICP-AES value.

Electronics Technology, Hyderabad. Grateful thanks are due to Dr. L. P. Pandey (NML, Jamshedpur) and our colleague Dr. Nirmal Charan at NGRI for critical reading of the manuscript and helpful suggestions for its improvement.

The reference material nodule reference sample No. 2388 together with a certificate of analysis can be obtained from Dr. L. P. Pandey, Head, Analytical Chemistry and Standard Samples Division, National Metallurgical Laboratory, Jamshedpur-7, India.

References

1 Baturin, G. N., *The Geochemistry of Manganese Nodules in the Ocean*, Riedel, Dordrecht, 1988.
2 Nagender Nath, B., Balaram, V., Sudhakar, M., and Pluger, W. L., *Mar. Chem.*, 1992, **38**, 185.
3 Flanagan, L. J., and Gottfried, D., *U.S. Geol. Surv. Prof. Pap.*, 1980, No. 1155.
4 Berkovits, L. A., Obolyaninova, V. G., and Baturin, G. N., *Oceanology*, 1990, **33**, 445.
5 Berkovits, L. A., Obolyaninova, V. G., Parshin, A. K., and Romanovskaya, A. R., *Geostand. Newsl.*, 1991, **15**, 85.
6 Rolandts, I., *Spectrochim. Acta, Part B*, 1992, **47**, 947.
7 Pandey, L. P., *Certificate of Analysis of Sample No. 2388*, National Metallurgical Laboratory, Jamshedpur, 1992.
8 Fries, T., and Lamothe, P. J., *Anal. Chim. Acta*, 1984, **159**, 329.
9 Balaram, V., *J. Indian Chem. Soc.*, 1991, **68**, 600.
10 Balaram, V., Manikyamba, C., Ramesh, S. L., and Anjaiah, K. V., *At. Spectrosc.*, 1992, **13**, 19.
11 Balaram, V., in *Proceedings of National Seminar on Modern Trends in Analytical Techniques—Applications in Chemistry*, ed. Bhattacharyya, K. G., Department of Chemistry, Gauhati University, Assam, 1992, pp. 162–175.
12 Jarvis, I., and Jarvis, K. E., *Chem. Geol.*, 1985, **53**, 335.
13 Balaram, V., *At. Spectrosc.*, 1993, **14**, 174.
14 Govindaraju, K., *Geostand. Newsl.*, 1994, **18**, Special Issue, Appendix I, p43.

Paper 4/05897F
Received September 27, 1994
Accepted December 15, 1994

Validation of a Geochemical Logging Tool for *In Situ* Major Element Analysis in Boreholes Using Inductively Coupled Plasma Atomic Emission Spectrometry*

Mark S. Sams, Peter J. Watkins† and Michael H. Ramsey

Department of Geology, Imperial College of Science, Technology and Medicine, London, UK SW7 2BP

The geochemical logging tool (GLT) provides *in situ* measurement of the concentrations of 10 elements commonly found in sedimentary rocks: Si, Al, Fe, Ca, K, Ti, S, Th, U, and Gd. The element abundances thus determined can be used to derive lithology, sand class, mineralogy, porosity, permeability and cation-exchange capacity. The usefulness of this tool will depend upon the precision and bias of measurements. This paper describes the results of deploying a GLT at the Imperial College borehole test site in a sequence of finely layered siliciclastic and carbonate rocks. The bias of the GLT was quantified for six elements (Si, Al, Fe, Ca, K and Ti) by comparison with measurements on corresponding core samples made by inductively coupled plasma atomic emission spectrometry (ICP-AES). The high density of core measurements (approximately every 25 cm) allowed them to be averaged over a depth interval equivalent to the vertical resolution of the GLT thus reducing errors due to differences in sample size. A statistically significant bias for the GLT for all elements was calculated from a simple linear regression; values were between −55 and +5%. The detection limits and dependence of precision on concentration for Si, Al, Fe, Ca, K and S were determined using duplicate analyses from two logging runs in the same borehole. Values for the detection limits ranged from 0.26 for Fe to 2.70 mass-% for Si. When the precision varied with concentration, the high level precision was found to be less than 6.5% in most cases. It was found that the processing applied to the raw counts data obtained from the GLT played a major role in the determination of detection limits, precision and also the accuracy of measurements obtained using the GLT.

Keywords: *Inductively coupled plasma atomic emission spectrometry; neutron activation; gamma-ray spectrometry; borehole logging; bias*

Introduction

Geochemical logging has opened up a new dimension for wireline logging.[1] The ability to measure element concentrations of the rock matrix in a continuous fashion permits an estimate of mineralogy,[2] porosity and, consequently, cation-exchange capacity, permeability and other properties[3–5] of the rock mass on a scale which, in the past, has only been achievable by extensive coring. Previous comparisons of log data with core data have shown the technique to be very effective.[1] However, an objective, independent analysis of the precision and bias of the geochemical logging tool (GLT) has not been carried out. Some statistical analysis of the bias of the GLT has been attempted previously by comparing means and standard deviations of log data and core data (analysed by X-ray fluorescence) and by cross correlation.[6] However, this comparison was limited by the small variation in element concentrations and by the problem of different sample size.

Laboratory techniques make measurements on core samples which are typically about 30 g in mass (12 cm^3) whereas the GLT responds to a volume of rock with a radius of approximately 30 cm (11 000 cm^3). Thus the GLT effectively smoothes variations in depth (assuming lateral homogeneity) and potentially introduces bias in a comparison with core analyses. Owing to this difference in sample volume, estimation of bias between GLT measurements and analyses of core samples by inductively coupled plasma atomic emission spectrometry (ICP-AES) will therefore contain inevitable components of both sampling and analytical bias. It is an assessment of the over-all bias of the GLT in practical use that is the main objective of this study, together with the determination of realistic precision and detection limits of analyses made using the GLT.

Core measurements were made using a sampling interval of approximately 25 cm. The element concentrations of these core samples were determined by ICP-AES after fusion with $LiBO_2$,[7] and the depth interval over which these analyses are smoothed was optimized in order to maximize the correlation between the two techniques. This is a different approach which does not seem to have been used in previous studies.[1,6]

Experimental

Imperial College Borehole Test Site

The data used for this study were obtained from the Imperial College borehole test site at Whitchester farm in Northumberland.[8] This site comprises a suite of four boreholes that penetrate at least five cyclothems of the Upper Namurian limestone sequence to a depth of 250 m. Borehole 1 was fully cored with an excellent recovery in excess of 95%. The borehole was logged with an extensive suite of tools including the GLT.

Core measurements were concentrated on a single cyclothem, the Corbridge cyclothem (140–180 m), which was chosen as it displayed the greatest range of rock types. Three sub-environmentally associated facies groupings were resolved: (*i*) a carbonate interval denoted full open marine conditions with a minimum of terrestrial influence; (*ii*) a delta front sequence represented the progradation of terrigenous siliciclastics into a marine domain; and (*iii*) a delta plain sequence recorded the progressive establishment and re-establishment of predominantly subaerial conditions. A sequence of different rock types was analysed therefore,

* Presented at Geoanalysis 94: An International Symposium on the Analysis of Geological and Environmental Materials, Ambleside, England, September 18–22, 1994.

† To whom correspondence should be addressed.

including sandstones, mudstones, limestones and three bands of coal (Fig. 1). Each lithology type presented a wide range of different compositions over which to compare the performance of the two measurement techniques.

GLT Analysis

The GLT has been described in detail by Hertzog *et al.*[9] and uses three different measurement techniques.

(*i*) The natural radioactivity of K, Th and U is used for their determination with a natural gamma-ray spectrometer (NGS). The count rates obtained are directly proportional to the mass per cent. of the element, providing that a borehole correction factor is applied.

(*ii*) A neutron source of ^{252}Cf, emitting neutrons at about 2.3 MeV is used to activate Al. The ^{28}Al isotope produced decays as follows

$$^{27}Al(n,\gamma)\,^{28}Al \xrightarrow[2.24\ min]{\beta} {}^{28}Si^{*} \longrightarrow {}^{28}Si + \gamma\,(1779\ keV)$$

The 1779 keV gamma-ray produced is measured using an aluminium activation clay tool (AACT). Results obtained are proportional to the mass per cent. of Al after an environmental correction is applied.

(*iii*) After neutron capture from a burst of 14 MeV neutrons, Si, Fe, Ca, Ti, S and Gd are determined using a tau-gated thermal neutron capture spectrometer with a gamma spectrometer (GST). This procedure only provides relative concentrations of these elements, and they have to be converted to absolute values by imposing a closure relationship on the results obtained.

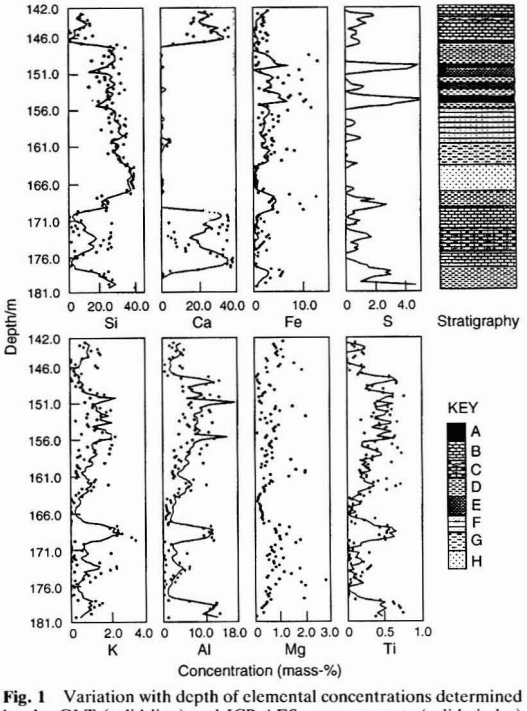

Fig. 1 Variation with depth of elemental concentrations determined by the GLT (solid line) and ICP-AES measurements (solid circles) across the Corbridge cyclothem. (Note that Mg was not detected by the GLT and S was not determined by ICP-AES.) Geological log of the borehole is included to show correlations between lithologies (*e.g.*, coal) and bias between the GLT and ICP-AES (*e.g.*, Si, Al, K): A, coal; B, limestone; C, clayey-limestone; D, mudstone; E, gannister (sandstone seat earth); F, layered mudstone-sandstone; G, clayey sandstone; and H, clean sandstone.

Oxide closure

In order to derive element concentrations from the raw GLT data a closure relationship is imposed on the results. It is assumed that each element occurs as a single oxide or carbonate in the formation and that the sum of the oxide and carbonate fractions is unity. This assumption is known to be in error, but it is considered that the errors involved will be small (<5%) for most lithologies.[9] The equation to be solved is

$$F(\Sigma X_i Y_i/S_i) + X_K W_K + X_{Al} W_{Al} = 1.0 \qquad (1)$$

where F is a calibration factor to be determined at each depth point; Y_i is the fraction of the measured prompt gamma rays attributed to element i; S_i is the tool sensitivity for element i; and X_i is the ratio of the mass of the associated oxide or carbonate to the mass of element i.

The mass fractions of potassium and aluminium (W_K and W_{Al}) must first be corrected for porosity to give a dry mass per cent. This is normally determined from the density log by assuming a quartz matrix.

If the presence of Mg or Na is suspected, the above equation should be modified, and solved by incorporating an additional factor that compares the predicted photo-electric factor to the measured photo-electric factor obtained from the lithodensity logging tool.[9]

Core Analysis

Sampling strategy

Core sampling was aimed at investigating the vertical variations in bulk rock geochemistry and mineralogy over a single sedimentary cycle using the same depth interval as the GLT (140–180 m). Exact correspondence of the volume of rock analysed by both GLT and ICP-AES is clearly impossible. The rationale behind the sub-sampling of the core used for analysis is that it should characterize the geochemistry of the core at small intervals (*e.g.*, 25 cm), so that subsequent mathematical smoothing of results can be employed to approximate the sampling volume analysed by the GLT (11 000 cm^3). The inevitable sampling bias introduced by lithologies of widths less than 25 cm (*e.g.*, iron-rich sideritic nodules) can then be estimated and recognized as a systematic difference between the two techniques.

Discrete samples of about 30 g were selected with an average vertical spacing of 25 ± 5 cm between samples, the rock chips being taken to represent the full lateral hetereogeneity of the sequence. A total of 147 analytical specimens were collected over the entire depth interval. These chips were powdered in an agate Tema mill to less than 75 μm.

Analytical procedure

After drying at 110 °C, 0.25 g of powder was mixed with 0.75 g of Johnson Matthey Spectroflux 100B (Royston, Cambridge, UK), transferred into a graphite crucible and fused in an electric muffle furnace for 30 min. The fused bead was dissolved in dilute nitric acid and diluted to 250 ml in a calibrated flask. This solution was filtered to remove particles of graphite and stored in a sealed plastic bottle.[7]

ICP-AES measurements were obtained using an ARL 34000 simultaneous spectrometer. Short-term fluctuations were reduced by ratioing all elements to Li, used as an internal standard. Longer term drift was corrected by linear interpolation of a drift correction solution. Calibration graphs were

obtained by linear regression of corrected intensities obtained from the measurements of 10 international reference materials.[7] Each group of 30 samples analysed also included a blank, four in-house reference materials to monitor data quality, and five duplicate preparations.

A loss on ignition determination on each sample was made by igniting 4 g of sample at 1000 °C for 16 h, starting from room temperature.

Results and Discussion

Bias

The bias of the GLT was determined by comparing the logging results with values obtained from core samples using ICP-AES. The method employed used simple linear regression to determine the rotational and translational components of bias. This method requires that data used as the independent variable be free from random error. However, it has been shown that simple linear regression gives accurate estimates of bias if the results from the method with the smaller variance are used as the independent variable.[10] In this instance the ICP-AES data were used as the independent variable as it has been shown that the precision of such data is <0.7%.[7] An additional requirement is that samples cover the concentration range from zero up to the maximum concentration measured in a uniform manner. Translational bias occurs when the intercept of the regression line is statistically significantly different from zero. Rotational bias occurs when the slope of the regression line is statistically different from unity. The test for significance used in this study was the Student's *t*-test with a probability of 0.05.

Before comparing results obtained using the two techniques the question of sample size must be addressed. Samples collected for laboratory analysis represent a depth of approximately 1 cm. The GLT responds to an approximately spherical volume of rock with a radius of about 30 cm. Assuming that there is lateral homogeneity, the GLT response is a weighted depth average of vertical variations. In addition, it is usual to apply a vertical smoothing process to the raw data before the oxide closure is performed. A running average of 5 data points, or just over 60 cm in depth, was used for the current data. Therefore, raw measurements obtained from the GLT and ICP-AES represent significantly different depth intervals of rock. In order to make a comparison that is not biased by this difference, the ICP-AES data must be depth averaged in a comparable manner to the GLT data, although this assumes that each laboratory measurement is representative of a 25 cm depth interval, *i.e.*, the sampling interval. Smoothing was applied to the ICP-AES data using windows of varying lengths. The window chosen was one that gave maximum correlation between the GLT and ICP-AES data, and a square window 1.4 m wide (equivalent to six analyses) was found to be the best. Thus the smoothed ICP-AES results, at any particular depth, are based on six separate determinations around that depth. The unsmoothed and smoothed ICP-AES data are plotted alongside the GLT data against depth in Fig. 1 and 2, respectively.

In order to compensate for the difference in sample interval the GLT determinations were interpolated using a cubic spline and depths equivalent to the ICP-AES sampling were taken. It was also necessary to apply a static depth shift of 0.5 m to the GLT data to account for a difference between drilling depth and logging depth. A comparison of element concentrations obtained from GLT and ICP-AES measurements against depth given in Fig. 2 highlights the effect of two coal layers on the GLT results. These coals occur at depths of 150 m and 154.3 m. Both Al and K show a higher value when measured using the GLT than when measurements are made using ICP-AES, whereas Si shows a lower result using the GLT. The dry mass per cent. of Al and K were found by correcting the mass per cent. obtained from the GLT by the porosity, which was determined from the density log by assuming a matrix density of 2.65 gm cm^{-3}. As the density of coal is much less than this value the porosity will be incorrectly determined causing errors in the calculation, and these errors will propagate through to the other elements through the oxide closure. The results at these depths were therefore ignored in the following discussion although they are included in the graphs.

A statistical comparison of element concentrations determined by the GLT and ICP-AES is given in Table 1. Significant bias was found for the six elements common to GLT and ICP-AES determinations: Si, Al, Fe, Ca, K and Ti. The GLT data are plotted against smoothed ICP-AES data in Fig. 3. Magnesium has been ignored as the GLT predicts zero (or negative) Mg, presumably due to the relatively low concentrations present (<2 mass-%).

Bias for Each Element

Silicon shows a statistically significant intercept (*i.e.*, translational bias) of −1.53 mass-%, but the slope is not significantly different from unity (Table 1). However, it can be seen from Fig. 3 that the relationship is not strictly linear and that there is a bias that varies with concentration. Indeed, when the

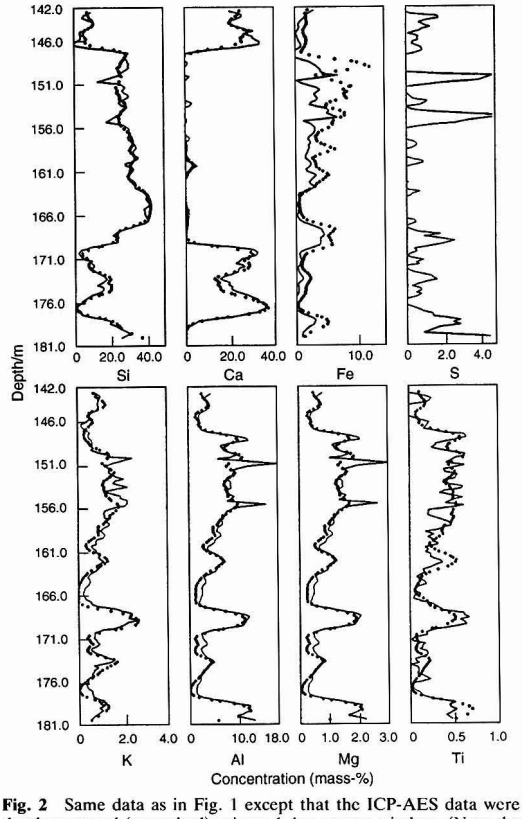

Fig. 2 Same data as in Fig. 1 except that the ICP-AES data were depth averaged (smoothed) using a 1.4 m square window. (Note the effect of the two coal bands on the GLT data at depths of 150 and 154.3 m.)

Si concentration is below 25 mass-% the majority of data points fall below the regression line.

This contrasts with the bias for Ca where the majority of data points lie above the regression line when the Ca concentration is greater than 10 mass-%. This trend produces a small but statistically significant difference from unity for the slope for Ca (4.3%). This over-estimation of Ca (and consequent under-estimation of Si) in the carbonates by the GLT suggests that the sensitivity factor for calcium, S_{Ca} in eqn. (1), is too low. This will have the largest effect in absolute terms at intermediate concentrations because of the oxide closure. For example, in pure calcite 40 mass-% Ca will be determined whatever the sensitivity associated with Ca as all other elements will sum to zero.

Iron shows significant bias in both slope and intercept with the GLT consistently under-estimating the Fe content. There are two possible causes for this. Firstly, it is possible that the sensitivity factor for iron, S_{Fe}, is too high. Secondly, it is possible that occasionally the sampling procedure used for ICP-AES determinations dramatically over-estimates the Fe content of samples. As mentioned earlier, the ICP-AES data is assumed to be representative of a 25 cm depth interval. However, in the case of Fe this may not be true. Iron occurs mainly as sideritic nodules in the mudstones. If present in a core sample these nodules could produce an analysis of up to 30 mass-% Fe, which is probably a gross over-estimate of the average value for the 25 cm depth interval. If a nodule is not sampled then the average value for the Fe concentration of the 25 cm interval will not be as severely over-estimated.

Aluminium, potassium and titanium display similar plots which show that the regression lines for all three elements have a slope that is statistically significantly different from unity, due to bias at low concentrations. This bias can be eliminated by progressively removing lower values from the regression line until the slope shows no statistically significant deviation from unity. These results are also tabulated in Table 1. The concentration values above which no bias in the GLT results is evident are 1.9, 0.50 and 0.08 mass-% for Al, K and Ti, respectively. The bias at low concentrations of Ti is difficult to observe from the data plot (Fig. 3), and there is some suggestion from this graph that the bias varies with concentration. This may be a result of the bias in Si and Ca concentrations obtained from the GLT, which has been propagated through to Ti through the oxide closure.

Aluminium and potassium concentrations are not affected by the oxide closure as they represent absolute estimates; nor are biases due to layering finer than the sampling interval of the laboratory samples as they occur systematically over large depth intervals as shown in Fig. 2, *e.g.*, from 160–166 m. Aluminium shows a slightly non-linear relationship with a tendency for the GLT to over-estimate Al at all concentrations, as indicated by the significant intercept of around 0.9 mass-%, both before and after the 1.9 mass-% lower cut-off value (Table 1). The GLT Al values are derived after a complicated environmental correction, which depends on the neutron moderation and absorption properties of the formation and borehole, and on changes in gamma-ray transport properties.[9] A correction is also applied to account for the continuous movement of the tool during logging. These values are converted to dry mass per cent. using a porosity value calculated from the density log assuming a quartz matrix. It is possible that bias is introduced through one or all of these

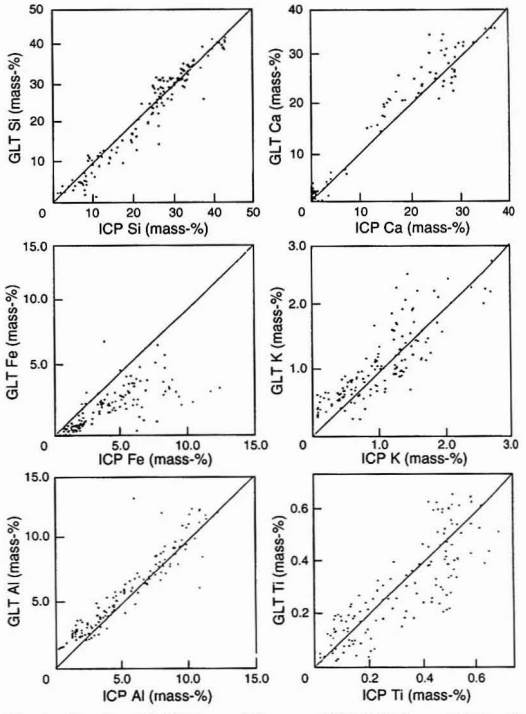

Fig. 3 Graphs of GLT (mass-%) *versus* ICP-AES (mass-%) for Si, Fe, Al, Ca, K and Ti showing analytical bias between the two techniques. Solid lines represent zero bias, having zero intercepts and gradients of unity.

Table 1 Comparison of GLT and ICP-AES derived concentrations for six elements. Correlation coefficients are shown for raw and depth averaged (smoothed) ICP-AES data

Element	Range (mass-%)	Correlation coefficient		Linear regression coefficients		Bias (%)
		ICP raw	ICP smooth	Intercept (mass-%)	Slope	
Si	0–44	0.977	0.994	−1.53 ± 0.57*	1.035 ± 0.022	3.5
Al	0–12.5	0.940	0.987	1.12 ± 0.15*	0.899 ± 0.026*	−10.1*
Fe	0–13	0.793	0.938	0.34 ± 0.16*	0.454 ± 0.033*	−54.6*
Ca	0–38	0.949	0.989	0.38 ± 0.25	1.043 ± 0.017*	4.3*
K	0–2.8	0.894	0.961	0.31 ± 0.05*	0.791 ± 0.042*	−20.9*
Ti	0–0.7	0.921	0.949	0.023 ± 0.017	0.845 ± 0.046*	−15.5*
Al†	1.9–12.5	0.967	0.991	0.86 ± 0.22*	0.933 ± 0.034	−6.7
K†	0.5–2.8	0.943	0.969	0.20 ± 0.09*	0.864 ± 0.071	−13.6
Ti†	0.08–0.7	0.934	0.952	0.003 ± 0.021	0.889 ± 0.056	−11.1

* Regression parameters and per cent. bias show statistically significant differences from zero intercept or slope of unity ($p = 0.05$).
† Additional statistics are shown where a bias in the regression slope can be reduced by applying a low concentration cut-off value.

corrections. The increased bias at low concentrations occurs below the effective detection limit of the GLT for Al (see next section), a condition that also holds true for K.

To summarize, the largest bias occurs with Fe, which is most probably due to an incorrect sensitivity factor applied in the oxide closure. An incorrect sensitivity factor has probably also been used for Ca, resulting in a slight bias at intermediate Ca concentrations resulting in an opposite bias for Si in the limestone sequences. The corrections applied to the Al counts have caused an over-estimation by the GLT. Some bias will be caused by layering finer than the sampling interval of the core measurements. Bias in any one element will be propagated through to the other elements by the oxide closure.

Precision

The precision of GLT measurements was studied using the method of Thompson and Howarth.[11] This approach enabled the high-level precision and detection limit to be estimated for 6 elements (Si, Al, Fe, Ca, K and S) by using a dataset consisting of 600 duplicate borehole measurements taken over a section between 110 and 230 m in depth.

The duplicate determinations obtained for each element were ordered into a set of increasing concentration means. This set was then divided into groups of 11 results, starting with the lowest 11 values. For each group of 11, the median value (Y_m) of the absolute differences was plotted against the mean value (X_m) of the mean values of the group. In this instance 54 groups were used for the regression. From the regression line obtaned it was possible to calculate values for the precision and detection limits of the GLT technique using the following equation

$$s = s_0 + kc$$

where s is the standard deviation at a particular concentration; s_0 the standard deviation at zero concentration; c the concentration (mass-%); and k the slope of the regression line of Y_m against X_m.

The detection limit is related to s_0, provided that s_0 is statistically different from zero, and the high-level precision is related to k, provided that k is statistically different from zero. If the regression line does not produce a significant intercept the maximum method detection limit (MMDL) can be calculated and if the slope does not differ significantly from zero an average precision value can be estimated.[7]

The duplicate dataset consisted solely of raw counts that had not been processed through the oxide closure. The original dataset consisted of absolute values of elements that had been processed through the oxide closure, with corresponding raw count data also being available. In order to achieve comparability, the original dataset was divided by the corresponding raw counts for each element at a particular depth. This procedure gave a value for the factor FX_i/S_i, and both F and S_i should be constant at a constant depth. If the raw counts for an element taken from the duplicate dataset are now multiplied by the corresponding value of FX_i/S_i, an estimate of the absolute value for that element at a particular depth can be made. This procedure is not quite the same as comparing data obtained from two runs processed independently.

Precision data for Si, Al, Fe, Ca, K and S are plotted as standard deviation (s) against concentration (c) in Fig. 4 and tabulated in Table 2. The same results are transformed into the more usual form of relative precision ($100s/c$) in Fig. 5. Where possible the effects of bias were minimized: *i.e.*, for Al and K only values above the cut-off value quoted in the previous section on bias were used. The high-level precision is an estimate of the precision the method approaches at high concentrations. It should be noted that in many cases this value is much higher than the theoretical limit for the concentration of the element. Results obtained for each element will be discussed and compared, wherever possible, with results presented by Hertzog *et al.*[9] for a similar sedimentary sequence and similar borehole environment.

Silicon

The detection limit (DL) for Si was found to be 2.70 mass-% Si with a precision of under 4% at 47 mass-% Si. Hertzog

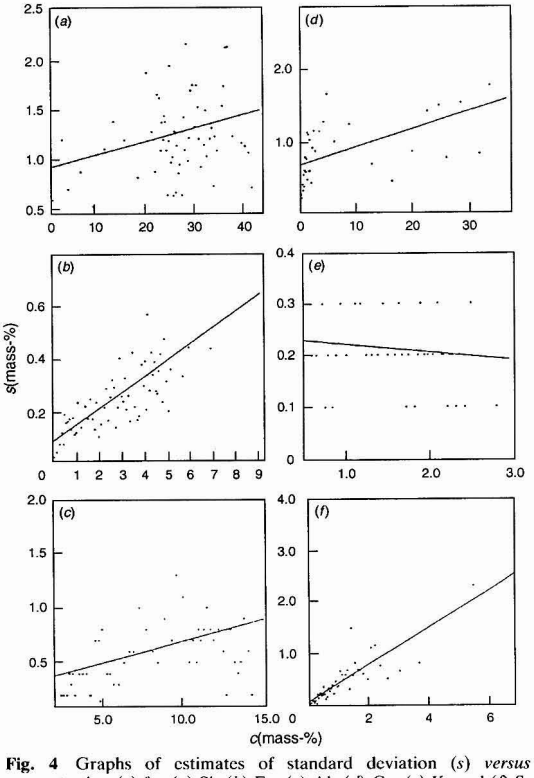

Fig. 4 Graphs of estimates of standard deviation (s) *versus* concentration (c) for (*a*) Si, (*b*) Fe, (*c*) Al, (*d*) Ca, (*e*) K, and (*f*) S. Dots represent median absolute differences of groups of 11 analyses and solid lines represent simple linear regressions through the data points.

Table 2 Estimation of precision of GLT determinations from the analysis of 600 duplicate measurements

Element	Intercept (mass-%)	DL (mass-%)	Slope	High-level precision (%)
Si	0.86 ± 0.17*	2.70	1.29 ± 0.59*	1.35
Al	0.29 ± 0.10*	0.92	3.65 ± 1.13	3.83
Fe	0.08 ± 0.02*	0.26	5.77 ± 0.67*	6.05
Ca	0.61 ± 0.09*	1.92	2.39 ± 0.78*	2.51
K	0.23 ± 0.04*	0.71	-1.52 ± 2.27	nd†
S	0.08 ± 0.05	0.56	33.82 ± 3.23*	35.45

* Statistically significant differences from zero intercept or slope ($p = 0.05$). The detection limit (DL) indicated for sulfur is the maximum method detection limit since the intercept is not significantly different from zero (see text).

† nd, Not determined due to over-rounding of results.

et al.[9] do not give a standard deviation at zero mass-% but give precisions of 25.6 and 4.9% at 25 and 47 mass-% Si, respectively.

Aluminium

The DL for Al was found to be 0.93 mass-% Al with a precision of just over 6% at 15 mass-% Al. These values are slightly higher than those presented by Hertzog *et al.*[9] (DL of 0.3 mass-% Al and 5% precision) for a similar concentration range (assuming the DL of Hertzog *et al.* was 3 times the standard deviation at zero concentration).

Iron

It is difficult to calculate values for the DL and precision of Fe determinations owing to the bias in results mentioned in the previous section. If it is assumed that this bias is mainly due to an incorrect sensitivity factor, S_{Fe}, a correction factor of 2.2 applied to the GLT data will produce a line of best fit for the GLT *versus* ICP-AES data. This procedure will not affect the value of high-level precision obtained, but the intercept used to calculate the DL will need to be multiplied by 2.2. After making these adjustments a DL of 0.57 mass-% Fe and a precision of 8% at 5 mass-% Fe were calculated. Hertzog *et al.* quote a precision of 30% at 1 mass-% Fe and one of 16% at 5 mass-% Fe, but there is no indication as to whether their values for Fe were biased in any way.

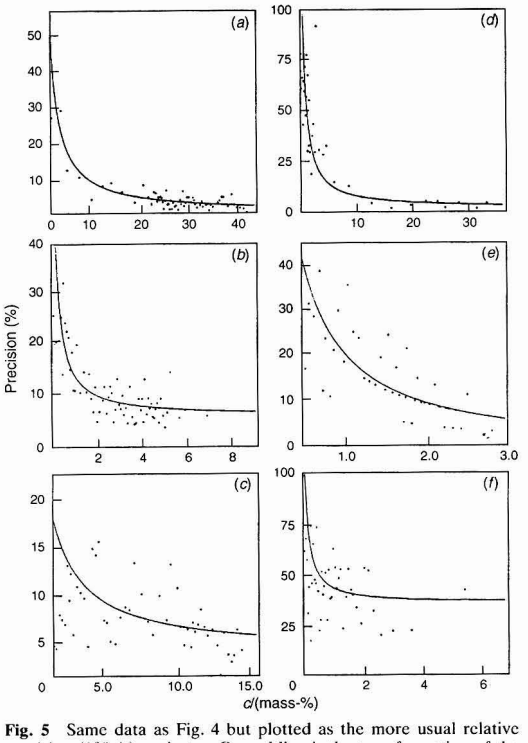

Fig. 5 Same data as Fig. 4 but plotted as the more usual relative precision ($100s/c$) against c. Curved line is the transformation of the regression line of Fig. 4 and shows the improved precision at higher concentrations: (*a*) Si, (*b*) Fe, (*c*) Al, (*d*) Ca, (*e*) K and (*f*) S.

Calcium

The DL for Ca was found to be 1.92 mass-% Ca with a precision of about 5% at 40 mass-% Ca. However, the distribution of calcium concentrations is non-Gaussian which casts some doubt over these values. The detection limit given by Hertzog *et al.* is 12.6 mass-% Ca with a precision of 4% at 40 mass-% Ca.

Potassium

It is possible to see from Fig. 4 that differences in duplicate measurements take discrete values, with a value of 0.1 mass-% K representing the digital resolution of the instrument. The distribution of values is therefore non-Gaussian and the method of Thompson and Howarth[11] is not valid. However, it is possible to see that the median absolute differences are not changing with concentration and a precision of 5% at 4 mass-% K is a good estimate. No information was given by Hertzog *et al.*

Sulfur

No significant intercept was found for S so only a maximum method detection limit could be calculated.[7] This was found to be 0.54 mass-% S. The precision was found to be over 30% at all concentrations. No information was given by Hertzog *et al.*, and as S was not determined by ICP-AES there is no indication to show whether the GLT results are biased.

It has been found during this work that, for elements affected by the oxide closure calculation (Si, Fe, Ca and S), analysis of the duplicate raw counts obtained from the GLT gave DLs and precisions that were much smaller in value than those obtained from duplicate determinations independently processed through the oxide closure. This fact seems to suggest that using such a closure operation imposes some constraints and limitations on the DLs and precision of the GLT analysis. It will be interesting to investigate the effect of such analytical errors on the subsequent estimation of mineralogy and other derivatives, but this will be the subject of a future paper.

Conclusions

The results of running a GLT in a borehole through a finely layered sedimentary sequence have been assessed. The bias of the results have been determined by simple linear regression against ICP-AES measurements on corresponding core samples. Values ranged from −55% for Fe to +4.3% for Ca. The core measurements were depth-averaged before comparison in order to account for differences in sample size. Some bias was found, which could be explained by the use of incorrect sensitivity factors when converting the raw counts data from the GLT to absolute abundances. Additional bias was observed when the ICP results indicated concentrations below the detection limit of the GLT. However, part of the measured bias may be due to bias in the sampling procedures used for the core in regions where elements are concentrated in fine layers or nodules, *e.g.*, Fe. Although bias originating in the sampling procedure is not strictly a quality of the analytical method used, the sampling procedures employed are typical of routine procedures and would therefore currently reflect typical measurement errors in the analysis produced by these techniques. The use of the oxide closure in processing the raw GLT data causes bias in one element to be matched by opposite bias in other elements.

The detection limits and precision of analysis of the GLT for some elements were investigated by a method using duplicate analysis. The DL values obtained ranged from 0.26 mass-% for Fe to 2.70 mass-% for Si and, apart from S, the high-level

precision values calculated were 6.5% or less. Unfortunately, owing to limitations of the data available, it was not possible to compare data that had been independently processed through the oxide closure. However, this allowed the impact of the oxide closure to be investigated by comparing our results with those derived from replicates that had been independently processed through the oxide closure. It was found that the detection limits and precisions were much higher for the independently processed data. This suggested that the oxide closure plays a major role in determining the detection limits and precision of elements affected by it (Si, Fe, Ca, Ti, S and Gd).

The oxide closure, therefore, also plays a major role in determining the accuracy of the GLT. This closure propagates bias from one element to another, and raises the detection limit whilst degrading precision. It is possible that some bias could be reduced by the application of improved sensitivity factors. However, despite the analytical errors involved, the GLT provides an efficient method of determining the abundances of the major elements found in sedimentary rocks.

The authors thank D. Filmer for performing the ICP-AES analyses. The authors also thank Agip, Amoco, BP, Elf, Mobil, NERC, Schlumberger and Statoil for funding the Imperial College borehole test site. M. S. S. also acknowledges assistance given by Petronas Research and Scientific Services to enable this work to be completed.

References

1 Herron, M. M., and Herron, S. L., in *Geological Applications of Wireline Logging*, ed. Hurst, A., Lovell, M. A., and Morton, A. C., Geological Society Special Publication No. 48, Geological Society, London, 1990, pp. 165–175.
2 Herron, M. M., *Clays Clay Miner.*, 1990, **34**, 204.
3 Herron, M. M., *Nucl. Geophys.*, 1987, **1**, 197.
4 Herron, M. M., *Transactions of The Society of Professional Well Log Analysts 28th Annual Logging Symposium*, The Society of Professional Well Log Analysts, Houston, 1987, paper HH.
5 Herron, M. M., and Grau, J. A., unpublished work.
6 Herron, M. M., *J. Sediment. Petrol.*, 1988, **58**, 820.
7 Ramsey, M. H., Potts, P. J., Webb, P. C., Watkins, P. J., Watson, J. S., and Coles, B. J., *Chem. Geol.*, in the press.
8 Sams, M. S., Worthington, M. H., King, M. S., and Shams-Khanshir, M., *Geophys. Prospect.*, 1993, **41**, 189.
9 Hertzog, R., Colson, L., Seeman, B., O'Brien, M., Scott, H., McKeon, D., Grau, J., Ellis, D., Schweitzer, J., and Herron, M., in *Proceedings of the Society of Petroleum Engineers Annual Technical Conference*, The Society of Petroleum Engineers, Richardson, 1987, paper SPE 16792, pp. 447–460.
10 Thompson, M., *Analyst*, 1982, **107**, 1169.
11 Thompson, M., and Howarth, R. J., *Analyst*, 1976, **101**, 690.

Paper 4/05889E
Received September 26, 1994
Accepted January 13, 1995

Chemical Partitioning of the New National Institute of Standards and Technology Standard Reference Materials (SRM 2709–2711) by Sequential Extraction Using Inductively Coupled Plasma Atomic Emission Spectrometry*

Xiangdong Li

Centre for Environmental Technology, Royal School of Mines, Imperial College, London, UK SW7 2BP

Barry J. Coles and Michael H. Ramsey

Department of Geology, Royal School of Mines, Imperial College, London, UK SW7 2BP

Iain Thornton

Centre for Environmental Technology, Department of Geology, Royal School of Mines, Imperial College, London, UK SW7 2BP

Three new NIST standard reference materials (2709–2711) have been analysed by a widely-used sequential chemical extraction method to provide analyte levels that are particularly useful for the characterization of contaminated soils. Each chemical fraction is operationally defined as follows: (*i*) exchangeable; (*ii*) bound to carbonates or specifically adsorbed; (*iii*) bound to Fe–Mn oxides; (*iv*) bound to organic matter and sulfides; and (*v*) residual. The extraction solutions resulting from the five steps have been analysed for 15 elements (Al, Ca, Cd, Co, Cu, Fe, K, Mn, Ni, P, Pb, Sr, Ti, V, and Zn) using ICP-AES. The over-all recovery rates (the sum concentrations from the five steps/ the certified total concentrations) were observed to lie between 90 and 105% for most of the elements. The precision was estimated to be approximately 5% (2*s*) for most extraction steps. The high concentrations and proportions of trace elements in the exchangeable fraction (step 1) in NIST 2710 suggest that this reference material can be especially appropriate for studies of mobility and bioavailability of heavy metals in contaminated soils. Using sequential extraction methods, the elemental concentrations in these reference materials determined by ICP-AES for some major elements (Al, Ca, Fe, K, Mn, P and Ti) help to indicate the mineralogical compositions actually dissolved in each step.

Keywords: *Sequential extraction; reference material; inductively coupled plasma atomic emission spectrometry; soil contamination*

Introduction

Concern over the possible health and ecological effect of the ever increasing accumulation of heavy metal contaminants in the environment has prompted numerous investigations. It is now well recognized that the development of effective strategies to solve the problems of contaminated land will depend greatly on our knowledge of the mobility and bioavailability of heavy metals in soils and sediments (Förstner[1] and Kramer and Allen[2]).

In characterizing heavy metals in soils and sediments, sequential chemical extraction is one of the most commonly used methods. Many schemes of extraction have been developed using different reagents and under various conditions (Lake *et al.*;[3] Tessier and Campbell[4]). However, the limitations of sequential extraction have been addressed by several researchers (Jouanneau *et al.*;[5] Khebonian and Bauer;[6] Rauret *et al.*[7]). These include technical difficulties associated with achieving selective dissolution of specific chemical forms and re-adsorption of metals to other geochemical phases during extraction. Despite its inherent limitations, the sequential extraction scheme is still a very useful method for characterizing solid-phase associated trace metals in soils and sediments (Belzile *et al.*;[8] Xian;[9] Kim and Fergusson[10]).

The lack of uniformity of sequential extraction methods makes the comparison between different researchers very difficult. Moreover, the absence of suitable international reference materials for this type of analysis prevents an effective quality control programme being implemented. There is a recognized need for adequately characterized geostandards in environmental research and monitoring programmes (Flegal[11] and Ure *et al.*[12]). This paper aims to present the sequential extraction results for the new NIST (National Institute of Science and Technology) standard reference materials (SRMs 2709–2711) using a widely adopted extraction scheme (Tessier *et al.*[13]) coupled to ICP-AES analysis (Li *et al.*[14]). The discussion will be focused on the suitability of these reference materials on metal speciation and bioavailability studies of contaminated soils.

Materials and Methods

The three new SRMs from NIST are all soil materials with different total metal concentrations, that are intended primarily for use in the analysis of soil, sediments, or other similar materials. SRM 2709 is an agricultural soil from a ploughed field in San Joaquin Valley in central California, which has baseline trace element concentrations. SRM 2710 is

* Presented at Geoanalysis 94: An International Symposium on the Analysis of Geological and Environmental Samples, Ambleside, England, September 18–22, 1994.

a highly contaminated soil from pasture land along Silver Bow Creek in the Butte, Montana area. The sampling site periodically floods depositing sediment with high concentrations of Cu, Mn, Pb, and Zn from the settling ponds of a local industrial plant. SRM 2711 is a moderately contaminated agricultural soil collected in the till layer of a wheat field. All the three soils were oven-dried, sieved and ground to pass through a 74 μm screen (NIST[15]).

The sequential extraction scheme developed by Tessier *et al.*[13] was chosen in this study because of its wide application in soil and sediment researches. The details of the sequential chemical extraction procedure using ICP-AES have been described by Li *et al.*[14] The extraction was carried out progressively on an initial mass of 1.0 g of test material. The extractants and operationally defined chemical fractions are as follows:

(1) Fraction 1: exchangeable. Soil was extracted with 8 ml of 0.5 mol l^{-1} $MgCl_2$ at pH 7.0 for 20 min, with continuous agitation at room temperature.

(2) Fraction 2: bound to carbonate and specifically adsorbed. Residue from step 1 was leached for 5 h with 8 ml of 1 mol l^{-1} CH_3CO_2Na (adjusted to pH 5.0 with CH_3CO_2H) at room temperature. Continuous agitation was maintained during the extraction.

(3) Fraction 3: bound to Fe–Mn oxides. Residue from step 2 was extracted with 20 ml of 0.04 mol l^{-1} $NH_2{\cdot}OH{\cdot}HCl$ in 25% (v/v) CH_3CO_2H for 6 h. The extraction was performed at 96 °C with occasional agitation. After extraction, the extract solutions were diluted to 20 ml with de-ionized water and subjected to continuous agitation for 10 min.

(4) Fraction 4: bound to organic matter and sulfide. A 3 ml volume of 0.02 mol l^{-1} HNO_3 and 5 ml of 30% H_2O_2 (adjusted to pH 2.0 with HNO_3) were added to the residue from step 3. The sample was heated progressively to 85 °C, and maintained at this temperature for 2 h with occasional agitation. A second 3 ml aliquot of 30% H_2O_2 (adjusted to pH 2.0 with HNO_3) was then added, and the mixture was heated again at 85 °C for 3 h with intermittent agitation. After cooling, 5 ml of 3.2 mol l^{-1} $CH_3CO_2NH_4$ in 20% (v/v) HNO_3 were added, followed by dilution to a final volume of 20 ml with de-ionized water. The tubes were then continuously agitated for 30 min.

(5) Fraction 5: residual phase. The residue from step 4 was digested with 4 ml of concentrated HNO_3 (70%), 2 ml of $HClO_4$ (60%) and 15 ml of HF (40%) to dryness using the following heating regime: 90 °C for 6 h; 120 °C for 10 h; 190 °C for 6 h. The remaining material was then taken up in 5 ml of 4 mol l^{-1} HCl at 70 °C for 1 h, and diluted to 25 ml with 0.3 mol l^{-1} HCl.

The extractions (except the last HF–$HClO_4$–HNO_3 step) were conducted in 50 ml of polysulfone centrifuge tubes (Nalgene, Rochester, NY, USA, Catalog No. 3115-0050). Following each extraction, the mixtures were centrifuged at 2000 rpm for 20 min at room temperature. An aliquot of the supernatant was decanted into clean glass test-tubes using a pipette. Prior to the start of the next extraction step, samples were shaken with 8 ml of de-ionized water for 5 min, and the wash solution discarded after 20 min of centrifuging. The final extraction step (HF–$HClO_4$–HNO_3 digestion) was carried out in PTFE tubes after the residue had been transferred from the polysulfone tubes by repeated suspension in de-ionized water using a vortex mixer, and subsequent decanting of the suspension.

In order to ensure one uniform matrix for ICP-AES analysis, the different extraction matrices from steps 1–4 were digested with concentrated HNO_3. A 1 ml volume of HNO_3 (concentrated, 70%) was added to the solutions, and heated to dryness on an aluminium heating block at 140 °C. The residue in the tubes was then leached with 2 ml of 5 mol l^{-1} HCl, and made-up to final volume of 10 ml with de-ionized water.

Multi-element analysis was performanced by ICP-AES using an ARL3580B Model (see Table 1). The calibration scheme was based on that described by Thompson and Walsh[16] with a matrix of 1 mol l^{-1} HCl and approximate matrix-matching with 2000 μg g^{-1} Na in the trace element calibration solutions. Calibration solutions were also run at regular intervals throughout each batch and at the end of the analysis, to compensate for drift.

Results and Discussion

The sequential chemical extraction results for NIST SRMs 2709, 2710 and 2711 are given in Tables 2–4. The results are reported for mean value and 2 × standard deviation (2*s*) for five or six replicate determinations in different batches.

The precision for each extraction step was estimated from analyses of soil samples in duplicate using the method modified from that described by Thompson and Howarth.[17] Most of the elements determined using ICP-AES have a precision (2*s*) of around 5% at each extraction step (Li *et al.*[14]). The precision for many of the elements analysed for these three SRMs at each step are normally better than 10%, with the majority being 5% in the last three steps (Tables 2–4). The poor precision of some major elements (*e.g.*, Al, Fe and P) at the first two steps is probably due to the effects of the low concentrations of these elements and the high contents of Mg and Na in the extraction solutions.

In order to assess the over-all accuracy of the sequential extraction using ICP-AES, the sum of the concentrations from the five steps were compared with the certified total values for the total concentrations (see Tables 2–4). The over-all recovery rates from the five steps for the three SRMs are in the range 80–120% for all of the 15 elements determined, with an average of 93%. The over-all recovery for SRM 2710 is illustrated in Fig. 1. These results were based on six observations for SRM 2710 in different batches compared with the certified total concentrations. The error bars show 95% confidence intervals for the results summed over all of the extraction steps. The high over-all recovery rates (> 80%) indicate accepted accuracy by this method for most applications of the multi-element determination in sequential chemical extraction.

The chemical partitioning patterns of the 15 elements can be calculated from the sequential extraction results. However, the following discussion is mainly based on Pb, Zn, Fe and Ca as examples in use of these data. The operationally defined speciation patterns of these four elements are shown in Figs. 2 and 3.

The most important fraction for Pb in SRM 2709 is the residual fraction (last step) as has been shown in many other studies of uncontaminated soils and sediments (Tessier *et al.*[13] and Förstner[1]). For SRM 2711, the carbonate/specifically adsorbed and Fe–Mn oxide fractions (steps 2 and 3) are the

Table 1 Instrumental operating conditions

ICP-AES	Applied Research Laboratories, ARL 3580B, 1 m vacuum spectrometer
Forward power	650 W at 27 MHz
Viewing height	9 mm above the load coil
Torch	Fassel type
Gas flow rate:	
Coolant	7.5 l min^{-1}
Plasma	0.8 l min^{-1}
Carrier	0.8 l min^{-1}
Spray chamber	conical
Nebulizer	concentric glass (Meinhard TR-30-K3)
Solution uptake rate	1.0 ml min^{-1} (pumped)
Pre-flush, integration time	45 s and 3 × 5 s

Table 2 Sequential extraction results for NIST SRM 2709 (μg g^{-1}) with ± 2*s* (*n* = 5)

	Extraction steps*						
Element	1	2	3	4	5	Σ†	CTV‡
Al	14 ± 6	172 ± 88	946 ± 260	1440 ± 70	62 200 ± 7 200	64 800 ± 7 200	75 000 ± 600
Ca	3670 ± 160	7370 ± 1120	1330 ± 100	503 ± 60	5 320 ± 300	18 200 ± 1 200	18 900 ± 500
Cd	<0.1	<0.4	<0.1	<0.1	<0.3	—	0.38 ± 0.01
Co	<0.1	1.1 ± 0.6	3.7 ± 0.6	0.9 ± 0.2	7.2 ± 0.4	13.0 ± 1.0	13.4 ± 0.7
Cu	<0.2	0.7 ± 0.2	1.2 ± 0.2	1.3 ± 0.2	31.0 ± 0.4	34.4 ± 0.6	34.6 ± 0.7
Fe	2.9 ± 1.6	60 ± 36	1930 ± 720	133 ± 36	32 000 ± 3 200	34 100 ± 3 400	35 000 ± 1 100
K	378 ± 10	247 ± 136	242 ± 18	156 ± 80	17 700 ± 1 000	18 700 ± 1 000	20 300 ± 600
Mn	16.7 ± 1.0	93 ± 16	182 ± 20	41.8 ± 7.4	244 ± 16	578 ± 32	538 ± 17
Ni	<0.4	2.5 ± 1.0	16.4 ± 4.6	9.0 ± 1.0	50.0 ± 1.2	80.0 ± 5.0	88 ± 5
P	3.3 ± 0.2	15.0 ± 8.0	70.0 ± 8.0	31.4 ± 4.8	417 ± 24	537 ± 28	620 ± 50
Pb	<1.0	<4.0	<0.7	<0.7	24.2 ± 0.6	24.2 ± 0.6	18.9 ± 0.5
Sr	30.7 ± 1.4	26.7 ± 3.6	11.1 ± 1.0	4.9 ± 1.2	129 ± 10	203 ± 11	231 ± 2
Ti	<0.1	<0.4	<0.1	21.1 ± 5.6	3 180 ± 60	3 200 ± 60	3 420 ± 240
V	<0.1	<0.4	9.1 ± 1.0	7.0 ± 0.8	91.7 ± 3.0	108 ± 3	112 ± 5
Zn	<0.2	1.9 ± 0.4	11.8 ± 2.6	2.3 ± 0.4	83.5 ± 4.0	99.5 ± 4.8	106 ± 3

* Following the sequential extraction steps described in the text: step 1, exchangeable fraction; step 2, fraction bound to carbonate and specifically adsorbed *etc*.

† Σ represents the sum of the five fractions.

‡ CTV is the certified total concentration.

Table 3 Sequential extraction results for NIST SRM 2710 (μg g^{-1}) with ± 2*s* (*n* = 6)*

	Extraction steps						
Element	1	2	3	4	5	Σ	CTV
Al	44 ± 14	64 ± 40	489 ± 70	910 ± 74	62 600 ± 5 100	64 100 ± 5 100	64 400 ± 800
Ca	1620 ± 60	323 ± 86	218 ± 26	152 ± 14	10 400 ± 1 000	12 700 ± 1 000	12 500 ± 300
Cd	9.7 ± 0.3	3.0 ± 0.5	3.3 ± 0.3	0.7 ± 0.1	3.9 ± 0.8	20.6 ± 1.0	21.8 ± 0.2
Co	0.5 ± 0.2	0.7 ± 0.4	1.9 ± 0.2	0.4 ± 0.1	5.7 ± 0.6	9.3 ± 1.1	(10)
Cu	147 ± 12	753 ± 48	704 ± 110	657 ± 72	385 ± 30	2 650 ± 140	2 950 ± 130
Fe	37 ± 16	168 ± 76	5150 ± 1820	468 ± 200	28 100 ± 2 600	33 900 ± 3 200	33 800 ± 1 000
K	586 ± 42	407 ± 160	251 ± 14	145 ± 18	18 400 ± 1 600	19 800 ± 1 600	21 100 ± 1 100
Mn	912 ± 68	395 ± 76	4660 ± 870	629 ± 40	3 830 ± 240	10 400 ± 900	10 100 ± 400
Ni	<0.2	<0.8	0.4 ± 0.3	0.3 ± 0.2	9.6 ± 0.8	11.4 ± 1.2	14.3 ± 1.0
P	3 ± 2	14 ± 7	108 ± 8	50 ± 25	702 ± 90	877 ± 102	1 060 ± 150
Pb	553 ± 20	1300 ± 100	1250 ± 220	900 ± 110	1 080 ± 90	5 080 ± 280	5 532 ± 80
Sr	33.0 ± 1.8	8.4 ± 1.4	9.5 ± 1.1	7.6 ± 0.6	259 ± 32	318 ± 32	(240)
Ti	1.6 ± 1.0	0.8 ± 0.4	0.5 ± 0.3	0.9 ± 0.6	2 670 ± 50	2 670 ± 60	2 830 ± 100
V	<0.1	1.0 ± 0.7	8.8 ± 1.2	2.2 ± 1.0	60.1 ± 5.4	72.3 ± 6.0	76.6 ± 2.3
Zn	743 ± 22	450 ± 40	2010 ± 260	387 ± 26	2 860 ± 350	6 450 ± 440	6 952 ± 91

* For further explanation see Table 2.

Table 4 Sequential extraction results for NIST SRM 2711 (μg g^{-1}) with ± 2*s* (*n* = 5)*

	Extraction steps						
Element	1	2	3	4	5	Σ	CTV
Al	13 ± 10	80 ± 50	623 ± 11	972 ± 56	61 200 ± 5 300	62 900 ± 5 300	65 300 ± 900
Ca	3040 ± 130	12 300 ± 1 300	2320 ± 220	462 ± 18	8 390 ± 2 140	26 500 ± 2 500	28 800 ± 800
Cd	8.7 ± 0.2	18.7 ± 1.7	8.5 ± 1.2	0.9 ± 0.1	2.1 ± 1.0	38.9 ± 2.4	41.7 ± 0.25
Co	<0.1	1.4 ± 0.6	2.3 ± 0.3	0.5 ± 0.1	5.1 ± 0.4	9.3 ± 0.8	(10)
Cu	0.9 ± 0.1	7.0 ± 1.0	14.2 ± 1.5	17.7 ± 2.2	66.0 ± 4.0	106 ± 5	114 ± 2
Fe	6.4 ± 3.0	32.2 ± 10	1440 ± 190	104 ± 26	26 900 ± 1 200	28 500 ± 1 200	28 900 ± 600
K	486 ± 20	160 ± 40	260 ± 24	167 ± 79	20 800 ± 1 100	21 900 ± 1 100	24 500 ± 800
Mn	16.7 ± 1.0	167 ± 44	170 ± 80	26.2 ± 4.0	265 ± 8	645 ± 92	638 ± 28
Ni	<0.2	1.7 ± 0.6	3.3 ± 1.0	1.5 ± 0.1	12.7 ± 0.8	19.4 ± 1.5	20.6 ± 1.1
P	9.8 ± 7.0	24.0 ± 2.6	71.5 ± 8.2	54.5 ± 14.0	522 ± 10	682 ± 20	860 ± 70
Pb	2.3 ± 0.4	506 ± 78	372 ± 54	116 ± 12	90.0 ± 13.8	1 090 ± 100	1 162 ± 31
Sr	8.6 ± 0.2	15.8 ± 1.4	4.4 ± 0.5	2.1 ± 0.1	184 ± 38	215 ± 38	245.3 ± 0.7
Ti	0.4 ± 0.2	1.1 ± 0.6	0.3 ± 0.1	23.2 ± 5.1	2 800 ± 40	2 820 ± 40	3 060 ± 230
V	<0.1	0.7 ± 0.3	4.2 ± 0.4	3.5 ± 0.2	68.7 ± 3.4	77.1 ± 3.6	81.6 ± 2.9
Zn	0.5 ± 0.2	29.5 ± 3.4	89.6 ± 16.8	24.9 ± 1.0	171 ± 11	316 ± 20	350.4 ± 4.8

* For further explanation see Table 2.

dominant phases for Pb. In case of SRM 2710, however, the five operationally defined fractions all have a role in differentiating the high Pb, especially the much higher concentration and proportion in the exchangeable phase (step 1).

The majority of the Zn in all the three SRMs is in the residual fraction, particularly in SRM 2709. The reducible fraction (Fe–Mn oxides) is the next important phase for Zn. As for Pb, SRM 2710 has much higher Zn concentration in the exchangeable fraction.

Most of the Fe in these soils is in the residual fraction, which indicates the presence of crystallized Fe oxides and the Fe in silicate minerals as in the study by Tessier *et al.*[13] The Fe–Mn oxide form is the second most important phase for Fe, which probably represents the amorphous Fe oxides in soils and sediments (Förstner[1]).

Most of the Ca is in the residual fraction in SRM 2710, with very little carbonate phase (step 2). This may indicate that most of the Ca is in silicate form in this soil. However, the carbonate and residual fractions are the dominant for Ca in SRM 2709 and SRM 2711, which suggest that the carbonate form (calcite) is possibly one of the major minerals for Ca in these two soils. Therefore, the sequential extraction results of the major elements, such as Fe and Ca, will provide additional information on the possible mineralogical forms actually dissolved in each step.

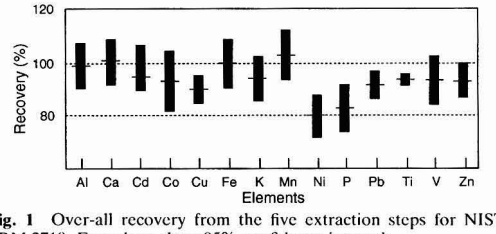

Fig. 1 Over-all recovery from the five extraction steps for NIST SRM 2710. Error bars show 95% confidence intervals.

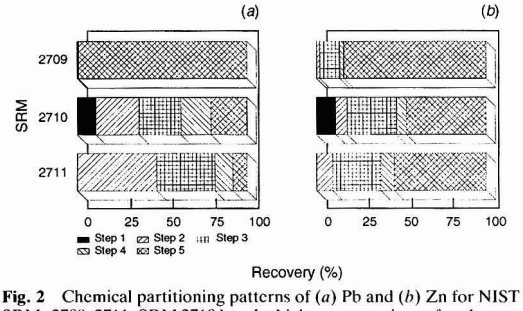

Fig. 2 Chemical partitioning patterns of (*a*) Pb and (*b*) Zn for NIST SRMs 2709–2711. SRM 2710 has the highest proportions of exchangeable Pb and Zn (extracted in step 1) and would therefore be useful for environmental studies of metal bioavailability.

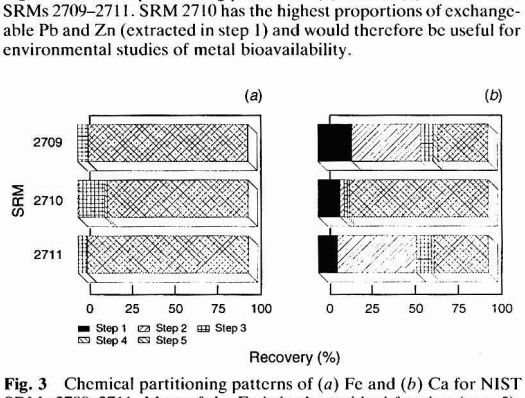

Fig. 3 Chemical partitioning patterns of (*a*) Fe and (*b*) Ca for NIST SRMs 2709–2711. Most of the Fe is in the residual fraction (step 5). The carbonate phase (step 2) of SRM 2709 and 2711 contains the largest proportion of Ca, confirming the dissolution of $CaCO_3$ in step 2.

The mobility and bioavailability of metals in soils is thought to decrease approximately in the order of the extraction sequence, from readily available to unavailable, because the strength of extraction reagents used increases in this sequence (Harrison *et al.*[18] and Förstner[1]). Hence, the exchangeable fraction may indicate the form of the metals that is most available for plant uptake. The second step extracts metals bound to carbonate and specifically adsorbed phases, which can easily become mobile and available under the condition of lower soil pH. In a recent study (Li *et al.*;[14] Li[19]), different patterns of metal chemical partitioning between the old mining and smelting areas in Derbyshire, England were recognized using the sequential extraction method, and the plant uptake of Pb and Zn was significantly correlated with the exchangeable Pb and Zn (extracted in step 1) in the contaminated soils.

Most of the other CRMs and SRMs that have been used in sequential extraction methods (*e.g.*, USGS MAG-1, NBS SRM 1645 and BCR 141–143) have very low concentrations of heavy metals in the exchangeable fraction, usually below the detection limits (Tessier *et al.*;[20] Mahan *et al.*;[21] Li *et al.*[14]). This has limited the use and reliability of these reference materials in environmental monitoring and research programmes. The high concentrations and proportions of Pb, Zn and other common heavy metals in the exchangeable fraction in SRM 2710 suggest its suitability for studies on the mobility and bioavailability of metals in contaminated soils.

Conclusions

Multi-element concentrations and measurement uncertainties have been determined from the five-step sequential extraction for the three new NIST soil SRMs using a single calibration by ICP-AES with acceptable precision and accuracy. These results will be very useful in comparisons between different laboratories and various extraction methods.

The high concentrations and proportions of heavy metals in the exchangeable phase of SRM 2710 suggest that this reference material will be particularly useful in the study of the mobility and availability of heavy metals in contaminated soils.

Using sequential extraction methods, the elemental concentrations for some major elements (Fe, Ca *etc.*) in these reference materials determined by ICP-AES may help to indicate the mineralogical compositions actually dissolved in each step. This should clearly be a more reliable indication of the possible mineralogy dissolved than the nominal designation given in the operational definition.

References

1 Förstner, U., in *Chemical Methods for Assessing Bio-Available Metals in Sludges and Soils*, ed. Leschber, R., Davis, R. D., and L'Hermite, P., Elsevier, Amsterdam, 1985, pp. 1–31.
2 Kramer, J. R., and Allen, H. E., *Metal Speciation: Theory, Analysis and Application*, Lewis Publishers, Michigan, USA, 1988.
3 Lake, D. L., Kirk, P. W. W., and Lester, J. N., *J. Environ. Qual.*, 1984, **13**, 175.
4 Tessier, A., and Campbell, P. G. C., in *Metal Speciation: Theory, Analysis and Application*, ed. Kramer, J. R., and Allen, H. E., Lewis Publisher, Michigan, USA, 1988, pp. 183–199.
5 Jouanneau, J. M., Latouche, C., and Pautrizel, F., *Environ. Technol. Lett.*, 1983, **4**, 509.

6 Khebonian, C., and Bauer, C., *Anal. Chem.*, 1987, **59**, 1417.
7 Rauret, G., Rubio, R., and Lopez-Sachez, J. F., *Int. J. Environ. Anal. Chem.*, 1989, **36**, 69.
8 Belzile, N., Lecomte, P., and Tessier, A., *Environ. Sci. Technol.*, 1989, **23**, 1015.
9 Xian, X., *Plant Soil*, 1989, **113**, 257.
10 Kim, N. D., and Fergusson, J. E., *Sci. Total Environ.*, 1991, **105**, 191.
11 Flegal, A. R., *Geostand. News..*, 1980, **4**, 17.
12 Ure, A. M., Quevauviller, Ph., Muntau, H., and Griepink, B., *Int. J. Environ. Anal. Chem.*, 1993, **51**, 135.
13 Tessier, A., Campbell, P. G. C., and Bisson, M., *Anal. Chem.*, 1979, **51**, 844.
14 Li, X., Coles, B. J., Ramsey, M. H., and Thornton, I., *Chem. Geol.*, 1995, in the press.
15 NIST, National Institute of Standard and Technology, Gaitherburg, Maryland, USA, Certificate of Analysis, 1993.
16 Thompson, M., and Walsh, J. N., *A Handbook of Inductively Coupled Plasma Spectrometry*, Blackie, London, 2nd edn., 1989.
17 Thompson, M., and Howarth, R. J., *Analyst*, 1976, **101**, 690.
18 Harrison, R. M., Laxen, D. P. H., and Wilson, S. J., *Environ. Sci. Technol.*, 1981, **15**, 1378.
19 Li, X., PhD Thesis, University of London, UK, 1993.
20 Tessier, A., Campbell, P. G. C., and Bisson, M., *Geostand. Newsl.*, 1980, **4**, 145.
21 Mahan, K. I., Foderaro, T. A., Garza, T. L., Martinez, R. M., Maroney, G. A., Trivisonne, M. R., and Willging, E. M., *Anal. Chem.*, 1987, **59**, 938.

Paper 4/06142J
Received October 10, 1994
Accepted January 23, 1995

Improved Detection Limits for Transient Signal Analysis of Fluid Inclusions by Inductively Coupled Plasma Atomic Emission Spectrometry Using Correlated Background Correction*

Barry J. Coles, Sarah A. Gleeson, Jamie J. Wilkinson and Michael H. Ramsey
Department of Geology, Royal School of Mines, Imperial College of Science, Technology and Medicine, London, UK SW7 2BP

The detection limits for ICP-AES bulk analysis of fluid inclusions by thermal decrepitation are limited by fluctuations in background emissions from the plasma. The transient nature of the analyte signal prevents sequential off-peak estimation of background levels. The established technique of time-interpolation of background signals measured between the analyses of samples gives somewhat unrealistic estimates because the background is not measured during the decrepitation event. A new procedure, correlated background correction (CBC), uses the high degree of correlation between the relative fluctuations in the spectral background at different wavelengths to effectively predict the background emission under transient analyte peaks. An estimate of the spectral background is made at a wavelength with no analyte signal or spectral interference, in this case 371.030 nm which is otherwise used to measure yttrium. The relative fluctuation in this intensity is used to predict the background emission intensity at all analyte wavelengths during the decrepitation event. The detection limits achieved using CBC are improved typically by a factor of five over those estimated without any correction of background fluctuation, thus increasing the range of sample material amenable to analysis.

Keywords: *Inductively coupled plasma atomic emission spectrometry; transient signal; fluid inclusion; background correction*

Introduction

Transient signals, such as those produced during the analysis of fluid inclusions by thermal decrepitation,[1] provide a challenge to traditional techniques of background correction in ICP-AES.[2,3] Off-peak correction is not possible because of the rapid variation in emission signal that occurs during the decrepitation event which prevents a representative background wavelength being scanned and measured. The method of background correction that has been traditionally employed for inclusion analysis by decrepitation[4] is on-peak time interpolation of interspersed 'blank' measurements. These 'blank' measurements are performed using the same procedure that is used for samples, but in the absence of sample material. The background emission intensity of the plasma is known, however, to fluctuate during decrepitation of inclusions and this places a limitation on the efficiency of the time interpolation method.

A strong correlation has been observed between the variation in the inherent background emission intensities over a broad range of wavelengths (250–800 nm) *e.g.*, Fig. 1. This correlated behaviour can be used to make a prediction of the background emission intensity at an analyte wavelength during the decrepitation process. The predicted background emission facilitates an improved background correction which results in lower detection limits. This is analogous to, but distinct from, the use of internal standards for the correction of variations in the sensitivity of analyte emission intensity.

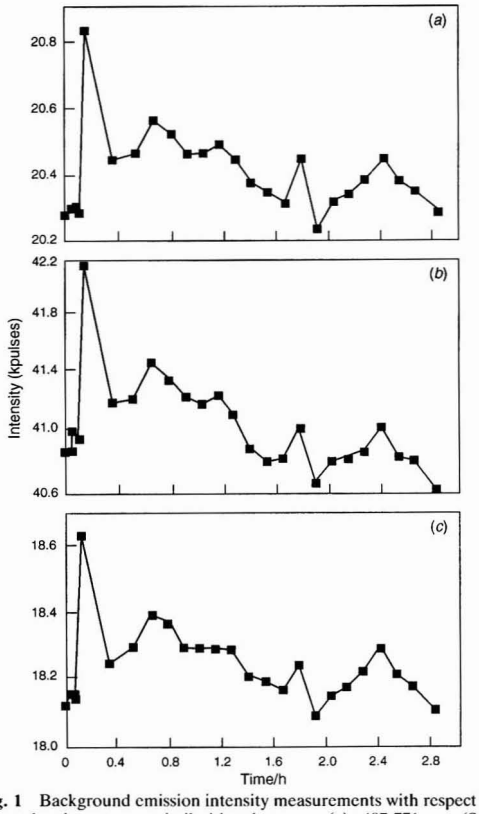

Fig. 1 Background emission intensity measurements with respect to time showing strong similarities between (*a*) 407.771 nm (Sr), (*b*) 588.990 nm (Na) and (*c*) 371.030 nm (Y) during a typical batch of analyses.

* Presented at Geoanalysis 94: An International Symposium on the Analysis of Geological and Environmental Materials, Ambleside, England, September 18–22, 1994.

Experimental

Instrumental Operating Conditions

All measurements were performed using a Fisons Instruments ARL 3580B simultaneous/sequential ICP-AES (Luton, Bedfordshire, UK) operating under the conditions described in Table 1. Because of the transient nature of the signal produced from the decrepitation event only the simultaneous spectrometer (polychromator) was used in this study. All measurements, therefore, are performed concurrently on-peak. The polychromator wavelengths used for the analyte determinations are listed in Table 2.

Decrepitation Analysis of Fluid Inclusions

Fluid inclusions are microscopic droplets of fluid trapped in minerals during their growth. They are of great interest to geochemists because they provide the only direct evidence of the composition of palaeofluids that once flowed through the Earth's lithosphere and can be used to constrain a wide range of geological processes.[5]

Table 1 Instrumental operating conditions

ICP-AES instrument	Fisons Instruments, ARL 3580B, 1m vacuum spectrometer
RF forward power	650 W at 27 MHz
RF reflected power	<10 W
Observation height	9 mm above the load coil
Argon flow-rate	
Coolant/l min^{-1}	7.5
Plasma/l min^{-1}	0.8
Carrier/l min^{-1}	0.8
Nebulizer	Concentric glass (Meinhard TR-30-K3)
Spray chamber	Conical
Solution uptake rate (pumped)/ml min^{-1}	1.0
Pre-flush time/s	10
Integration time/s	45

Table 2 Spectral emission lines measured

Element	Ion/Atom	Wavelength/nm	Order	Element	Ion/Atom	Wavelength/nm	Order
Ag	I	328.070	2	Mg	II	279.080	2
Al	I	308.215	2	Mn	II	257.610	2
As	I	189.040	3	Mo	II	202.030	3
B	I	249.680	3	Na	I	588.990	1
Ba	II	455.403	1	Nd	II	430.360	1
Be	II	313.040	2	Ni	II	231.603	3
Bi	I	222.820	2	P	I	178.287	3
Ca	II	317.930	2	Pb	II	220.350	3
Cd	II	226.502	2	Pr	II	422.290	1
Ce	II	413.770	1	S	I	180.730	3
Co	II	228.620	3	Sb	I	217.589	3
Cr	II	267.716	3	Sc	II	361.380	2
Cu	I	324.754	2	Se	I	196.090	2
Dy	II	353.170	2	Si	I	288.157	2
Er	II	390.630	2	Sm	II	359.260	2
Eu	II	381.960	2	Sr	II	407.771	1
Fe	II	259.940	2	Ti	II	337.280	2
Gd	II	310.050	2	V	II	290.880	2
Ho	II	345.600	2	Y	II	371.030	2
K	I	766.490	1	Yb	II	369.420	2
La	II	398.850	2	Zn	I	213.860	3
Li	I	670.784	1	Zr	II	339.190	2
Lu	II	261.540	2				

Decrepitation ICP-AES is one method developed for the bulk determination of cations in fluid inclusions. The apparatus used for decrepitation analysis (Fig. 2) was originally described in detail by Thompson *et al.*[1] and subsequently revised by Rankin *et al.*[4] with the introduction of a ten-port valve which allowed a more rapid and convenient means of sample interchange. The heating of grains of quartz (0.3 g of 1–2 mm diameter) to about 750 °C causes the fluid inclusions within the grains to rupture and the contents of the inclusions are carried in a stream of argon into the plasma for analysis. A single estimate of intensity is obtained for each analyte wavelength by integrating the emission over the time period of the decrepitation event (45 s). The sensitivity of the system is calibrated by the nebulization of aqueous standards subsequent to each batch of decrepitation samples. The background emission intensity at each analyte wavelength is usually measured at regular intervals, generally after three or four sample measurements, during a batch; such 'blanks' are measured by heating an empty tube through the decrepitation cycle.

In this study, 20 samples comprising pure quartz grains were analysed using the decrepitation method. During the course of the batch run of almost 3 h duration, three replicate splits of each sample were analysed in succession, with a blank measurement after each group. The resulting blank data were used for the evaluation of a new method for background correction of transient signals.

Correlated Background Correction (CBC)

A strong correlation was observed between simultaneous background emission intensity measurements for a range of analyte wavelengths in each of the 24 blank integrations. The covariance of the background emission intensities with respect to time for three wavelengths of interest (*a*) 407.771 nm (Sr), (*b*) 588.990 nm (Na) and (*c*) 371.030 nm (Y) is shown in Fig. 1. When these fluctuations are compared on a scatter graph [Fig. 3(*a*) and (*b*)] a strong linear relationship is apparent and confirmed by significant correlation coefficients of 0.985 for (Sr)/(Y) and 0.906 for (Na)/(Y); however, the slope is different for each pair of elements. If the relative background intensities for each analyte wavelength, defined by the ratio of the measured emission intensity (I_x) to the average emission intensity for the entire run (I_{x^0}), are compared, the slope is statistically indistinguishable from unity [Fig. 3(*c*) and (*d*)], *i.e.*,

$$\frac{I_x}{I_{x^0}} = \frac{I_y}{I_{y^0}} \quad (1)$$

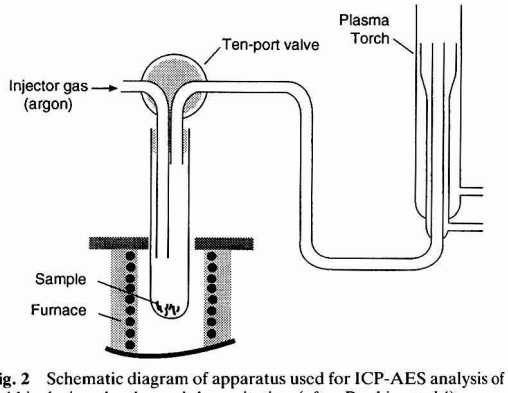

Fig. 2 Schematic diagram of apparatus used for ICP-AES analysis of fluid inclusions by thermal decrepitation (after Rankin *et al.*[4]).

where x and y are the two analyte wavelengths. It is therefore possible to predict the background emission at any analyte wavelength ($I_{x_{pred}}$) during analysis of a transient signal using the background emission measured at a different (reference) wavelength (I_{ref}), *i.e.*,

$$\frac{I_{x_{pred}}}{I_{x^0}} = \frac{I_{ref}}{I_{ref^0}} \quad (2)$$

The predicted background for each analyte is obtained using the transposed equation:

$$I_{x_{pred}} = \frac{I_{ref}}{I_{ref^0}} I_{x^0} \quad (3)$$

The predicted background level can then be subtracted from the analyte peak intensity ($I_{x_{meas}}$) to obtain the background corrected intensity.

Conversion of the intensity measurement to 'pseudo' concentration c_x (in equivalent μg ml^{-1}) is achieved by a sensitivity factor S_x (μg ml^{-1}/kpulses), obtained from the nebulization of calibration solutions:

$$c_x = (I_{x_{meas}} - I_{x_{pred}})S_x \quad (4)$$

The final 'pseudo' concentration is produced after conventional correction for inter-element translational interferences by the on-peak method. The calculated concentration is termed 'pseudo' because it is not the actual μg ml^{-1} in the inclusion, as the analysed volume is unknown. For geochemical interpretation of the data, however, a ratio of elements in the inclusions is determined and this limitation disappears.

Choice of Reference Wavelength

On a polychromator system, the reference wavelength chosen should represent an element that is known to be effectively absent in the sample of interest. The choice of element wavelength for monitoring the background is critical. The background emission at 371.030 nm (Y) seems to fulfil many necessary criteria for this application. Firstly, it has a high correlation ($r > 0.9$) with a large number of element wavelengths (see Fig. 4). Secondly, yttrium, with a relatively low crustal abundance (35 μg g^{-1}),[6] is not present in significant concentrations in many geological samples and has not been reported in fluid inclusions; and thirdly, yttrium exhibits no significant spectral interferences, such as line overlaps. The background emission at other wavelengths, such as

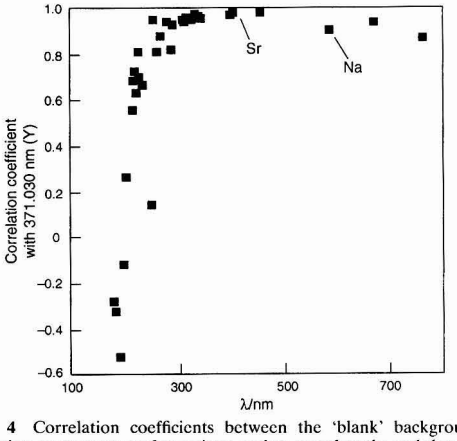

Fig. 4 Correlation coefficients between the 'blank' background emission measurements for various analyte wavelengths and that for 371.030 nm (Y) plotted against wavelength, showing the spectra range over which the CBC method may be applicable.

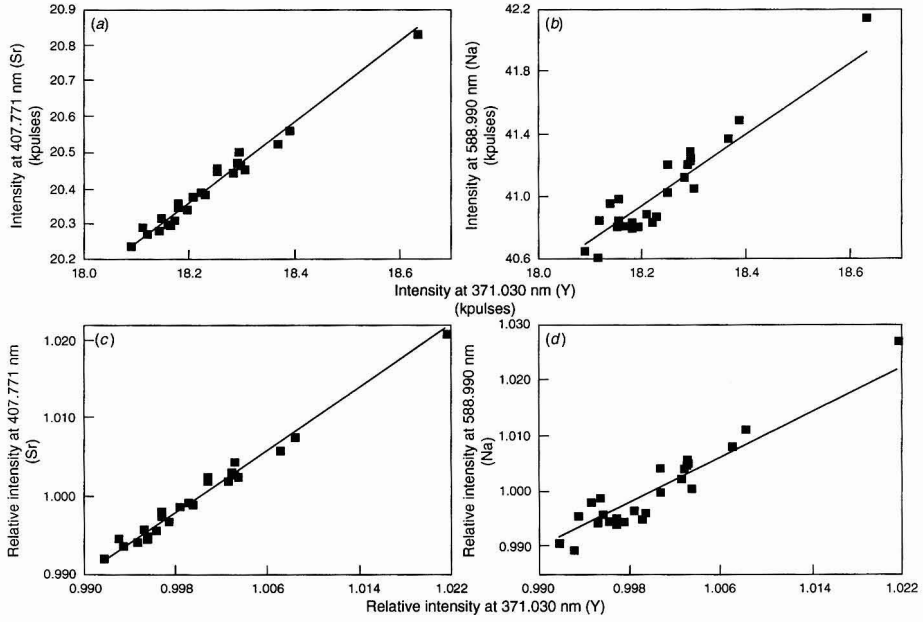

Fig. 3 Scatter graphs of background emission intensity data showing correlation between 371.030 nm (Y) and [(*a*) and (*c*)] 407.771 nm (Sr) and [(*b*) and (*d*)] 588.990 nm (Na). Graphs (*a*) and (*b*) show raw intensity whereas (*c*) and (*d*) are relative intensity. The line plotted indicates a relative slope of unity in all cases.

345.600 nm (Ho) and 381.960 nm (Eu), show similar background fluctuations to yttrium, and could be used to cross-check these assumptions.

Wavelength Limitation of CBC

If the correlation coefficient with background at 371.030 nm (Y) is plotted as a function of wavelength (Fig. 4), strong correlations, greater than 0.9, between background emissions are in evidence for a range of wavelengths measured above 250 nm. The background emissions at lower wavelengths (*i.e.*, below 250 nm) do not vary systematically with respect to that at the yttrium wavelength. Further examination of the correlation matrix failed to produce any significant correlation coefficients between the background variation of any of these low wavelength emission lines. Background emissions at these low wavelengths cannot therefore be effectively predicted by any method relying on such correlations.

Effect of CBC on Detection Limits

Previously, a simple estimate of the detection limit for decrepitation analysis was made using 3 standard deviations of the background emissions for each element.[4] If, using this method, a typical background at the Sr wavelength (407.771 nm) over an entire batch of samples is considered (Fig. 5), a detection limit of 0.006 (equivalent μg ml^{-1}) is obtained. The effect of applying CBC to the strontium background emission (Fig. 5) is to reduce substantially both the systematic and short term, apparently random, fluctuations in the background data. This approach yields a new estimate of the detection limit of 0.0008 (equivalent μg ml^{-1}), improving the detection limit by a factor of eight.

Detection limits were calculated for both the uncorrected and CBC-corrected background intensities of a range of elements and the improved detection limit ratios (uncorrected/corrected) are shown in Fig. 6. The detection limit ratio varies from element to element and typically shows an improvement of 400–500%. The greatest improvements are for elements measured around the yttrium wavelength [between 339.190 nm (Zr) and 398.850 nm (La)]. This is probably owing to improved correlation between the background in this spectral region as illustrated in Fig. 4.

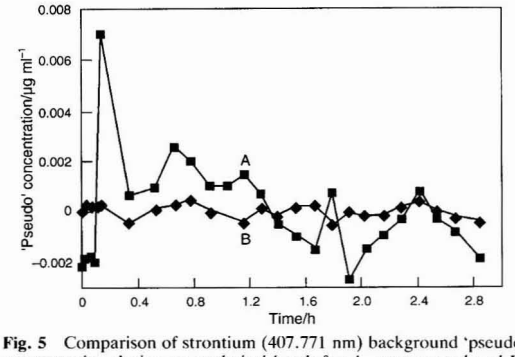

Fig. 5 Comparison of strontium (407.771 nm) background 'pseudo' concentration during an analytical batch for A, uncorrected and B, CBC-corrected measurements.

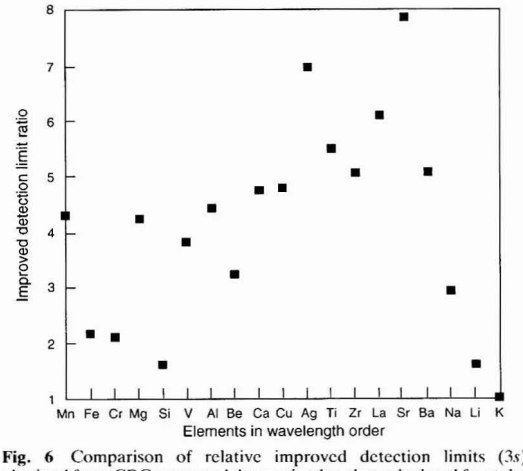

Fig. 6 Comparison of relative improved detection limits (3*s*) obtained from CBC-corrected data ratioed to that calculated from the uncorrected blank emission measurements for elements in the wavelength range 250–800 nm. The average improvement, by a factor of four, shows a peak around the yttrium wavelength [between 339.190 nm (Zr) and 398.850 nm (La)].

Additional Effects Resolved by CBC

Using CBC processing, unexpected background emission behaviour was observed. When the estimated blank emissions under the analyte signals ($I_{x_{pred}}$) were compared with the machine blanks measured between samples, a slight negative bias became apparent (Fig. 7). This suppression of background emission during sample decrepitation may be caused by the introduction of inclusion fluid into the plasma reducing the plasma excitation temperature. The degree of suppression is dependent, therefore, on the amount and composition of the inclusion fluids in each sample. The ability of CBC to resolve such analytical phenomena is of major significance to ICP-AES analysis in general and it is conceivable that the method may be used to compensate for such previously unrecognized effects.

Conclusions

Correlated background correction successfully improves the detection limit for decrepitation analysis of fluid inclusions by

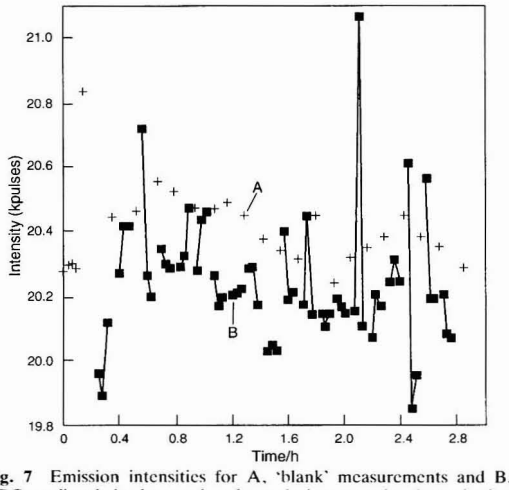

Fig. 7 Emission intensities for A, 'blank' measurements and B, CBC-predicted background values during sample decrepitation measurements at 407.771 nm (Sr). The lines join CBC-predicted background measurements for the three replicate splits of each sample analysed.

reducing the effect of both systematic and random fluctuations in background plasma emissions. This is achieved by a more accurate estimation of the background emission at the point of transient signal analysis. An improvement of at least 400% is achieved for 11 elements (Ag, Al, Ba, Ca, Cu, La, Mg, Mn, Sr, Ti and Zr) and of greater than 200% for a further 4 elements (Be, Cr, Fe and Na). Measurements at low wavelength (<250 nm), often used to determine elements such as As, B, Mo, P, S and Se, fail to show statistically significant correlations and are not improved by the CBC method. It is possible that CBC may also be used to correct for the apparent suppression of background emissions occurring during decrepitation ICP-AES analysis. Similarly, laser ablation ICP-AES produces transient signals that require realistic background correction.[7,8] Therefore, the CBC approach should be of great benefit to the further development of this technique.

S. G. was supported in the course of this work by a Research Studentship funded by Shell International Oil Company Ltd. and J. J. W. by a Lectureship funded by Minorco UK Ltd.

References

1 Thompson, M., Rankin, A. H., Walton, S. J., Halls, C., and Foo, B. N., *Chem. Geol.*, 1980, **30**, 121.
2 Thompson, M., and Walsh, J. N., *A Handbook of Inductively Coupled Plasma Spectrometry*, Blackie and Son, Glasgow, 1983.
3 Dawson, J. B., Snook, R. D., and Price, W. J., *J. Anal. At. Spectrom.*, 1993, **8**, 517.
4 Rankin, A. H., Herrington, R. J., Ramsey, M. R., Coles, B., Christoula, M., and Jones, E., *Proceedings of the 8th Quadrennial International Association of Geologists in Ore Deposits Symposium*, Schweizerbart, Stuttgart, 1993, 183.
5 Roedder, E., *Rev. Mineral.*, 1984, **12**, 644.
6 Krauskopf, K. B., *Introduction to Geochemistry*, McGraw-Hill, New York, 2nd edn., 1979.
7 Ramsey, M. H., Coles, B. J., Wilkinson, J. J., and Rankin, A. H., *J. Anal. At. Spectrom.*, 1992, **7**, 587.
8 Wilkinson, J., Rankin, A. H., Mulshaw, S. C., Nolan, J., and Ramsey, M. H., *Geochim. Cosmochim. Acta*, 1994, **58**, 1133.

Paper 4/06268J
Received October 13, 1994
Accepted February 2, 1995

Inductively Coupled Plasma Atomic Emission Spectrometric Determination of Rare Earth Elements in Granites and Greisens Using Thin-layer Chromatographic Preconcentration*

Natalia S. Safronova and Svetlana S. Matveeva

Geochemistry Division, Geological Department, Lomonosov State University, Moscow, 119899, Russia

Yury I. Fabelinsky and Valentin A. Ryabukhin

Vernadsky Institute of Geochemistry and Analytical Chemistry, Russian Academy of Sciences, ul. Kosygina 19, Moscow, 117975, Russia

A method for the determination of individual rare earth elements and yttrium in granites and greisens was developed on the basis of a combination of thin-layer chromatographic separation and clean-up of the rare earth element group on a Dowex 50-X8 cation exchanger in combination with inductively coupled plasma atomic emission spectrometry (ICP-AES). The detection limit of the latter varies from 0.25 to 5.0 ppm and the relative standard deviation is 0.04–0.08. A water-cooled burner was used in a Plasma-701 apparatus for ICP-AES. Spectra were observed along the discharge axis from the top of the burner. The separation of rare earth elements and yttrium using thin-layer chromatography is universal with regard to the materials analysed. It can be used in combination with other methods of element determination. It has the advantages over column chromatographic methods that a small initial mass and small aliquots of solutions can be used.

Keywords: *Rare earth element; yttrium; granite; thin-layer chromatography; inductively coupled plasma atomic emission spectrometry*

Introduction

More and more papers are appearing in which data on rare earth elements (REEs) are used to solve numerous problems in petrology and ore formation. Revealing fluid sources and their evolution in ore formation processes is one of the most important aspects of using REE and Y indicator properties for hydrothermal deposits. REEs possess all the main properties of geochemical indicators of hydrothermal solution genesis: REE composition for waters of different origin is specific, and this specificity of the solutions is preserved in exchange reactions between rock and solutions in fluid flow processes to metal formation zones. Variations in lanthanide concentrations in hydrothermal minerals and rocks reflect the chemical specificity of solution and physico-chemical conditions of mineral formation (*i.e.*, temperature, pressure, Eh, pH).

The determination of the REE composition in minerals and rocks within individual deposits provides relevant information on fluid sources and on temporal and spatial changes in ore formation conditions. However, large-scale application of REE indicator properties requires the availability of information and observation data on REE contents in rocks and minerals. The episodic character of such information can be explained primarily by analytical difficulties. The diversity and complexity of the composition of environmental materials requires serious methodological studies for each type of mineral or rock.

Granites and greisens of the Akchatau deposits (Kazakhstan) were studied in this investigation. The total REE concentrations in these deposits are 160 and 40 ppm (mg kg^{21}), respectively. The contents of the main components in granites and greisens are SiO_2 76 and 94%, Al_2O_3 12.4 and 2.1%, TiO_2 0.14 and 0.11%, ΣFe_2O_3 1.5 and 1.9%, MnO 0.02 and 0.02%, MgO 0.2 and 0.2%, CaO 0.4 and 0.16%, Na_2O 3.6 and 0.12% and K_2O 4.6 and 0.5%, respectively.

Choice of Analytical Methods

Rare earth elements with similar chemical properties are usually found together in natural materials, and it is very difficult to separate one element from another. Methods widely used to determine individual REEs in natural materials are highly sensitive neutron activation analysis (NAA),[1,2] inductively coupled plasma mass spectrometry (ICP-MS)[3,4] and atomic emission spectrometry (AES).[5–11] NAA is difficult to use, expensive and time consuming, and does not provide information on the whole series of REEs. ICP-MS is useful for REE determination, but expensive. AES is widely used to determine REEs in rocks and minerals. The complexity of the electron shell structure ($4f^k\ 6s^2$ and $4f^k\ 6s$ are the normal configurations of atoms and ions; $k = 2, 3, \ldots, 14$) and the low ionization potential (5.4–6.5 eV) typical of REE lead to the complexity and multilinearity of both atomic and ionic spectra.[12] Sample excitation in the arc discharge and also in the ICP method give rich ionic spectra of REEs and yttrium. Dense wide molecular CN bands, located in the most informative (for REEs) optical range of the spectrum (350–450 nm) are the main obstacles to the application of arc sources in studying REE spectra. Thus arc sources can be used efficiently only in special chambers, with a nitrogen-free environment.

In ICP-AES, the presence of OH bands (mainly in the 306–320 nm region) and a relatively poor argon spectrum do not create any serious obstacles for REE determination. However, the use of ICP-AES for the determination of REEs in granites at their background concentrations requires preconcentration. The following criteria were taken into account while selecting the preconcentration techniques: high sensitivity, possibility of quantitative separation of REE from the rocks and availability and simplicity of the analytical procedure.

* Presented at Geoanalysis 94: An International Symposium on the Analysis of Geological and Environmental Materials, Ambleside, England, September 18–22, 1994.

At present, the most promising and widely used methods of REE preconcentration involve sorption. We chose thin-layer cation-exchange chromatography.[13] A variant of its combination with NAA was developed for the determination of REEs in different types of rocks.[2] This method is being used in combination with ICP-AES on an ICAP-61 50-channel spectrometer (Thermo Jarrell Ash) for determining REEs and Y in rocks with a high content of REEs.[5]

The main aims of this work were to investigate the possibilities of a Russian device for the ICP-AES determination of REEs in granites and greisens at the level of their background concentrations,[14] and to find optimum conditions for the application of thin-layer chromatography (TLC) for the preliminary separation of REEs from the rocks with low REE contents.

Experimental

Apparatus

The instrumentation (Fig. 1) was based on a Plasma-701 source of spectrum excitation (developed in St. Petersburg, Russia) and a DFS-13 high-resolution spectrograph (LOMO, St. Petersburg, Russia). The analytical possibilites of the Plasma-701 have not been studied. The design of the plasmochemical block of the Plasma-701 device envisages the possibility of using of two types of burner: a Fassel burner with gas cooling of the walls (15 l min^{-1}) and a flame blowing out from the burner (the analytical zone is located within this flame),[15] and a Britske–Sukach burner with water cooling of the walls.[16]

A modified water-cooled burner was chosen because earlier we had obtained some positive results in investigating the analytical possibilities of such a burner. This burner was used in combination with a VCG2-4/27 generator.[17,18]

In the Plasma-701 the burner is installed vertically. Observation is implemented along the discharge axis. Irradiation of the analytical zone from the top of the burner is projected with the help of a flat mirror and a quartz lens ($F = 250$ mm) on the inlet slit of the spectrograph (Fig. 1). The source of high-frequency energy is a free-running generator connected with the impedance-matching device of the inductor by a cable.

There are indicators of both forward and reflected waves. The generation frequency is 27.12 MHz and the output power is 0.5–4.5 kW (with a standard setting of 1.7 kW). The inductor coil has two turns, its height is 36 mm and the diameter of the winding tube is 12 mm. The burner and the inductor are cooled by water at a flow rate of 1.5 l min^{-1}. The quartz welded burner has an inner diameter of 32 mm. The injector is made of quartz tubing without tapering off; its inner diameter is 6 mm. The argon flow rate for the nebulizer is 2 l min^{-1} and the flow rate of the plasma-forming argon is 1.5 l min^{-1}. Hence the total flow rate of argon is several times less than that in a gas-cooled burner. The nebulizer is concentric and the sample flow rate is 1.5 ml min^{-1}.

Parameters of DFS-13 spectrograph are as follows: grating, 600 groves mm^{-1}; reciprocal linear dispersion, 0.4 nm mm^{-1}; spectral resolving power, 72000; resolution, 0.008 nm; focal length, 4000 mm; and spectral range, 200–800 nm. Photographic registration allows for the simultaneous registration of a spectral range of 100 nm.

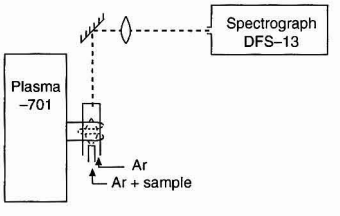

Fig. 1 Scheme of the spectroanalytical set-up.

Reagents and Materials

Concentrated mineral acids and ammonia of analytical-reagent or ultrapure grade, aqueous solutions of acids at concentrations varying from 0.1 to 5.0 mol l^{-1} and 0.1 mol l^{-1} oxalic acid solution were used. A 2 mol l^{-1} solution of NH_4Cl was prepared by neutralization of HCl with concentrated ammonia solution.

Fixion 50-X8 sheet material with a layer of Dowex 50-X8 cation exchanger on the polymer base was used for the chromatographic separation of REEs on discs with diameters of 21 and 50 mm.

Individual REE oxides with purity exceeding 99.9% were used to prepare a stock standard solution with a concentration of 1 g l^{-1}. The stock standard solution served for the preparation of standard mixtures for ICP-AES.

Spectral Type II and UFSh-3 photographic plates (Khimfotoproekt, Moscow, Russia) were used for spectrum registration.

Sample Preparation

Sample decomposition

A rock sample with mass varying from 0.6 to 1.0 g was wetted in a platinum cup with several drops of water, then 2–3 ml of $HClO_4$ and 20–40 ml of HF were added and the mixture was evaporated to dryness. High contents of SiO_2 in granites require the procedure to be repeated twice. Complete removal of fluoride ions was achieved after additional treatment of the samples with perchloric acid. Non-decomposed residue of the rock was melted with a 5–10-fold excess of NaOH or Na_2O_2 in a corundum crucible. The salt obtained was then dissolved in 5 mol l^{-1} HCl.[5]

Hydroxide precipitation

The aqueous phase from rock decomposition was diluted to 600 cm^3 with acid of concentration varying from 1 to 2 mol l^{-1}. Metal hydroxides were precipitated with ammonia solution, obtained from the purified liquified gas by dissolution in boiled (for CO_2 removal), doubly distilled water. Hydroxides were filtered off and transferred into 0.1 mol l^{-1} HCl to be used later in the work with a sorption disc of diameter 50 mm.

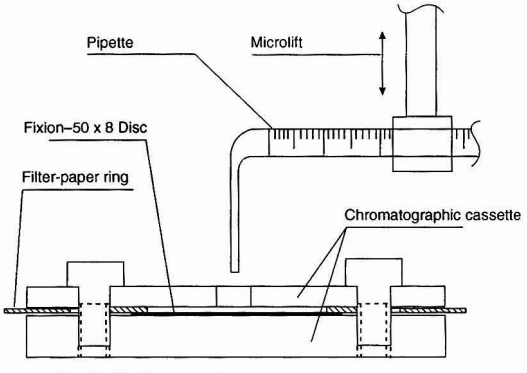

Fig. 2 Device for implementing chromatographic stages of REE and Y separation.

Chromatographic separation of REEs and Y

Chromatographic stages of the preparation of REE concentrate were carried out in a casette (Fig. 2), consisting of two round Plexiglas plates, between which a disc of the thin-layer material Fixion 50-X8 and a ring strip of filter-paper were sandwiched, so that the edge of the inner cut of the paper was superimposed on the disc edge by 1.5–2.0 mm. All the solutions required for chromatography were supplied to the centre of the thin-layer disc *via* a slot in the casette lid using a 0.1 ml graduated pipette, fixed horizontally in the microlift. Thus, the chromatographic device is a plane, semi-sealed, knock-down column with radial movement of the solution, filled sequentially with the cation exchanger and paper.

The chromatographic procedure of REE separation from the rock consisted of the following stages:

(*i*) passing an aliquot of the analyte solution corresponding to 60–300 mg of rock through the chromatographic device with a thin-layer cation-exchange disc (stage of cation sorption);

(*ii*) passing eluting solutions, *i.e.*, 0.1 mol l^{-1} oxalic acid–2 mol l^{-1} NH_4Cl at pH levels varying from 7.5 to 8.5 (stage of purification), for removal of outside elements from the disc due to complex compound formation or displacement with ammonia ions; and

(*iii*) desorption of the REE group with 5 mol l^{-1} HCl solution onto a new paper strip, its ashing in the platinum crucible at 500 °C, followed by dilution of the residue with 5 ml of 1 mol l^{-1} HCl and the use of the solution obtained for the determination of REEs by ICP-AES.

ICP-AES

A 5 ml volume of 1 mol l^{-1} HCl containing the REEs separated from 60–300 mg of the rock was used for the analysis.

The exposure time was 100 s. Spectra of a standard solution and the analyte samples were recorded on the photographic plate. Calibration graphs were plotted as $\log I_l/I_b$ *versus* $\log C$, where I_l and I_b are the intensities of the analytical lines of the REEs and the background, respectively. Two groups of stock standard solutions were used: a cerium group (from La to Gd) and an yttrium group (from Tb to Lu and Y). The ratio of concentrations in the stock standard solutions corresponded to the ratio of the average concentrations of individual REEs in granites and greisens: La 40, Ce 100, Pr 12.8, Nd 60, Sm 20, Eu 4, Gd 40, Tb 8.8, Dy 39.6, Ho 11, Er 30, Tm 4, Yb 28, Lu 4 and Y 100 mg l^{-1}. Working standard solutions were prepared by diluting the two stock standard solutions with 1 mol l^{-1} HCl. Standard solutions were prepared by dilution of the stock standard solution in the proportions 1 + 4, 1 + 9, 1 + 39, 1 + 79, 1 + 159, 1 + 499 and 1 + 999. The number of standard solutions depended on two factors: the lowest level of measurement for each element and the photographic plate which was used as a detector. With photographic recording the calibration graph has a non-linear section and requires many measurements for its confident construction.

In order to have a wavelength standard, which is necessary for the identification of spectra on the photographic plate, a solution of a mixture of REEs and Y was used. The concentrations in the solution were five times less than those of the individual elements in the stock standard mixtures, and Fe solution (1 g l^{-1}) was also used. The reliability of the results obtained was verified using international geological reference materials (granites G-2, GB and SG-1A).

Table 1 Conditions for thin-layer separation of a REE group

Condition	Scheme 1	Scheme 2
Rock sample mass/mg	20–50	50–300
Disc diameter/cm	2.1	5.0
Flow rate of solution/ml h^{-1}	0.6	0.6
Sorption of initial probe solution, 0.1 mol l^{-1} HCl/ml	0.5	1.0
Desorption of impurities with 0.1 mol l^{-1} oxalic acid/ml	0.3	1.5
Desorption of impurities with 2 mol l^{-1} NH_4Cl/ml	0.3	none
Desorption of REE group with 5 mol l^{-1} HCl/ml	0.5	1.5

Results and Discussion

Separation of REE and Y

In order to determine REEs in granites and greisens at the level of their background concentrations, the previously used TLC technique[13] was modified. This variant of the TLC technique in combination with ICP-AES is effective for rocks with high contents of REEs (over 1000 ppm) if an initial sample of mass 20 mg is used. In rocks with a low content of REEs, with the help of this technique we only managed to determine four or five elements (La, Ce, Y, Pr, Nd).

The need to increase the initial sample mass required modification of the sample preparation scheme. As the chromatographic stages are the basis of the separation technique and affect the output and quality of the REE concentrate obtained, the main problems in the investigation were to determine the optimum concentration and volume of loading and eluting solutions, and also the mass of samples analysed, depending on the rock macrocomposition.

Table 1 presents a comparison of stages of the chromatographic process at various initial sample masses from 20 to 50 mg (21 mm disc) and from 50 to 300 mg (50 mm disc). Work with large masses (50–300 mg) required preliminary precipitation of hydroxides to increase the dynamic capacity of the sorbent. In this instance, it is possible to exclude the stage of elution with ammonium chloride solution.

The analysis of the output chromatograms of individual components obtained using Dowex 50-X8 and 5.0 mol l^{-1} HCl showed that the affinity of the cations in the cation-exchange resin increases in the series Fe, Al, Mg, Ca. This means that calcium has the greatest displacement effect on REE ions and greatly diminishes the maximum size of the aliquot to be analysed. This effect of cations depends on the rock composition with regard to the main rock-forming cations and limits the maximum load of the sorption layer on the chromatographic disc (Table 2). It is clear from Table 2 that the maximum mass of the rock sample varies within the range 10–50 mg for sorption discs 21 mm in diameter and for a complete mixture of cations in the initial solution (Scheme 1 in Table 1). However, the preliminary separation of alkaline and alkaline earth elements allows one to increase appreciably the load of

Table 2 Maximum mass of rock sample analysed with Scheme 1 (21 mm disc)[2]

	Rock composition (%)				
Rock sample	Fe_2O_3 + FeO	Al_2O_3	MgO	CaO	Maximum mass/mg
Basalt BM	9.7	16.2	7.5	6.5	30
Basalt BE-N	12.1	10.2	13.3	13.3	10
Granite GM	2.0	13.6	0.4	1.1	50
Anorthosite AN-G	13.1	29.8	1.8	15.8	100
Slate TB	6.9	20.6	1.9	0.3	30
Limestone KH	0.9	2.4	0.7	47.8	20–50
Limestone KH*	0.9	2.4	0.7	47.8	50–300

* With preliminary hydroxide precipitation.

the sorption layer and to increase the mass of sample (*e.g.*, several-fold for limestone). After this operation the analysed solution contains mainly iron, as a macrocomponent, and partially aluminium and magnesium, which are separated from the REEs later in the chromatographic stage. These elements together with the disc diameter control the chemical yield of REEs in the last separation stage. This is why, when analysing rocks poor in REEs, preliminary hydroxide precipitation is obligatory. The use of a larger diameter disc allows one also to increase the sample mass to values that ensure the determination of elements with low detection limits (Scheme 2). In this instance, the degree of load of the sorption layer was investigated for granite samples with initial mass varying from 60 to 300 mg.

The optimum sample mass for the conditions mentioned above is 200 mg. Such a mass ensures an 80–85% REE output in the final solution. When the mass is 300 mg, REE losses at the chromatography stage could be observed. As the content of the main rock-forming components is several orders of magnitude (>2) higher than the REE content, these components control the stage of cation sorption on the ion-exchange layer on the disc. Therefore, the REE recovery after chromatographic purification depends only on the initial mass of rock sample analysed and the sorption disc diameter. Using discs larger than 50 mm in diameter demands a much longer time for chromatographic treatment of the disc. Decreasing the initial sample mass diminishes the sensitivity of analysis. The chemical yield of REEs of 85% corresponds to the selected compromise (disc diameter 50 mm, sample mass 200 mg).

ICP-AES Determination of REE and Y

The choice of the optimum conditions for ICP-AES for the determination of REE separated from granites and greisens is important. Analysis of the individual REE and Y spectra allowed us to choose the most sensitive lines for each element. Mutual REE spectral interferences were determined. Possible spectral interferences of other elements (Fe, Ti) that could enter the analyte solution during sample preparation (mainly at the stage of the chromatographic separation of the REE group) were revealed. Detection limits were calculated

Table 3 Analytical characteristics of ICP-AES

Element	Analytical line/nm	Interference/ nm	Detection limit (ppm)	Akchtau deposit, NAA (ppm)		Average content in granites ($SiO_2 > 70\%$)[14] (ppm)
				Granites	Greisens	
La	II 408.672	Ce II 408.642	0.35			
	II 412.320	Nd II 412.300	0.35	50	17	50
		Sm II 412.300				
Ce	II 413.765		5.0			
	II 413.380	Pr II 413.360	5.2	96	20	100
	II 418.659		5.2			
Pr	II 390.844*	Ce II 390.841	1.25			
	II 414.311*	Eu II 414.297	1.25			11.4
		Dy II 414.311				
	II 417.939		1.38			
Nd	II 401.225	Ce II 401.238	2.5			
	II 430.358*	Pr II 430.359	3.7			46
	II 406.109*	Sm II 406.104	4.8			
Sm	II 359.262*	Nd II 359.259	5.0			
	II 442.430	Gd II 442.410	6.3	7.0	0.56	8.3
	II 360.948		6.6			
Eu	II 381.967*	Nd II 381.970	0.25			
		Fe I 382.043		1.05	0.019	1.1
	II 412.970	Sm 412.990	0.39			
Gd	II 342.247*	Sm II 342.247	5.0			
	II 336.223	Tm II 336.261	7.14			7.6
	II 335.047	Er II 335.025	7.5			
Tb	II 350.917	Ho II 350.937	2.0	1.11	0.086	1.12
	II 384.873		7.78			
Dy	II 353.170*	Ho II 353.174	0.75			
	II 364.54		1.72			
Ho	II 345.600	Dy II 345.601	1.25			1.62
	II 339.898	Dy II 339.834	2.8			
		Er II 339.894				
Er	II 337.271	Ti II 337.280	1.0			4.7
	II 349.910*	Ho II 349.908	1.7			
Tm	II 346.220	Ho II 346.196	2.0			
	II 384.802	Tb II 384.788	2.39			0.74
	II 342.508	Ho II 342.535	2.46			
Yb	II 328.937		0.5	4.85	0.99	4.8
	II 369.419	Sm II 369.399	0.83			
		Fe I 369.401				
Lu	II 261.542	Fe II 261.500	0.25	0.81	0.24	0.78
	II 339.707		2.5			
Y	II 371.030*	Eu II 371.029	1.25	51		42
	II 360.073	Sm II 360.125	1.70			

* See text.

according to the 3σ criterion[19] on the basis of standard samples (Table 3).

The spectral interferences shown in Table 3 were revealed at high concentrations of individual REEs (12–16 mg l^{-1}). To decrease the effect of spectral interferences as much as possible, a high-resolution apparatus (0.008 nm) with an aperture ratio of 1:40 was used. In several instances the resolution of the spectrograph is insufficient to avoid interferences. These line pairs are marked with asterisks. However, these interferences do not constitute a problem because the real ratios of REE components in granites and the corresponding intensities of analytical and interfering lines permit these interferences not to be taken into consideration.

The analysis of the individual REE spectra showed that the distribution of lines according to their intensity with the burner utilized is close to the distribution obtained by Wing *et al.*,[19] who used a Fassel burner of smaller diameter with gas cooling of the walls and registration of spectra from one side, which is normal to the burner axis. Fig. 3 presents a comparison of these two types of burner from the viewpoint of spectrum observation. Analytical zones whose irradiation passes into the spectral device are shaded. With the Fassel burner, the analytical zone is situated above the body of the burner; in the water-cooled burner, this zone is situated inside the burner, and is wider.

The spectral excitation conditions change along this zone. For the elements with low excitation potential, the analytical zone seems to be larger than that for hardly excitable elements. This is why for easily excitable elements (in particular for REEs) lower detection limits can be obtained than for elements with higher excitation potential. It was shown earlier that the signal-to-background ratio for REEs in such a water-cooled burner is better than in the Fassel burner, if the observation is made from one side.[18] It should be noted that the diameter of the zone in which the optimum signal-to-background ratio is achieved for this burner is 6 mm.

Important parameters of the spectral excitation source are the excitation temperature, T_{exc}, and the electron concentration N_e. Results obtained with a water-cooled burner[17] showed that T_{exc} measured in the analytical zone using the Ornstein method was (5.5–6.5) × 10^3 K. The density of electrons, N_e, measured according to the Shtark expansion of the H_β line, was 10^{19}–10^{20} m^{-3}. It should be noted that the configuration of the contour of the H_β line does not agree with the Gaussian or Lorentzian distribution, because it has high wings. If we calculate the value of the electron density at which such wings could appear due to the Shtark expansion of the H_β line, we find that this value of N_e is 10^{21} m^{-3}.

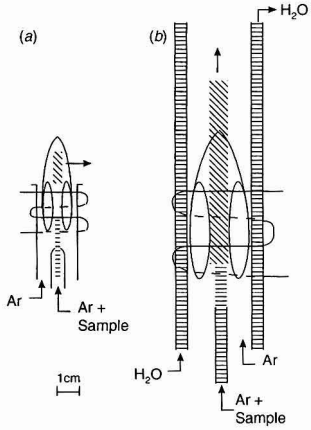

Fig. 3 Comparison of analytical zones of (*a*) the Fassel burner and (*b*) the water-cooled burner.

Thus, favourable conditions for the excitation of a large number of elements are created in the source. In projecting the analytical zone from the end face of the burner along its axis, the spectra of all the elements excited in the plasma, fall on the slit of the spectrograph. This is why when determining REE with complex multilinear spectra, it is necessary to have a high-resolution optical device for recording spectra, allowing the use of not one line, but a set of analytical lines for each element. In addition, it is very important to use a method of preliminary relative concentration with a high selectivity with regard to REEs, allowing one to avoid disturbances from macro- and microcomponents of rocks. In operation of the Plasma-701, changes in the output power of the generator due to the temporal drift or introduction of easy-to-ionize elements were found to increase the reflected power. This is why the power given to the plasma is much more stable than the output power of the generator. This affects the reproducibility of the results. Relative standard deviations, s_r (n = 11), based on the mid-point of the analysed concentration intervals (0.04–0.6 mg l^{-1}), varied in the range 0.03–0.05 depending on the elements. Calculation of s_r was performed both with standard solutions and with rock samples passed through all stages of the procedure. In the latter instance the s_r (n = 5) values were in range 0.04–0.08.

Conclusions

While analysing rocks with a high content of REEs, it is possible to implement the chromatographic separation of the REE and Y group on cation-exchange discs with a diameter of 21 mm for sample masses of 20 mg. The duration of the chromatographic stage is 2 h. For low concentrations of REEs in granites and greisens, this variant of the ICP-AES method can ensure the determination of the following five elements (La, Ce, Y, Pr, Nd).

The use of sorption discs with a diameter of 50 mm in the preliminary precipitation of hydroxides for granites makes it possible to use samples of initial mass 60–250 mg. The duration of the chromatographic stage is up to 5 h. The number of elements determined by ICP-AES can be increased up to ten (in addition to Tm, Tb, Ho, Cd, Sm).

As a result of these investigations, a method for determining ten individual elements of the REE group in granites was developed with the following detection limits: La 0.35, Ce 5.0, Pr 1.25, Nd 2.5, Sm 5.0, Eu 0.25, Gd 5.0, Tb 2.0, Dy 0.75, Ho 1.25, Er 1.0, Tm 2.0, Yb 0.5, Lu 0.25 and Y 1.25 ppm. The relative standard deviation varies from 0.04 to 0.08, depending on the element and concentration.

This work was supported by grant 93-05-08190 from the RFFI. The authors thank Professor V. A. Zharikov for helpful suggestions and interesting discussions.

References

1 Terakado, Y., Fujitani, T., and Takada, J., *J. Radioanal. Nucl. Chem., Articles*, 1989, **129**, 23.
2 Ryabukhin, V. A., Volynets, M. P., and Myasoedov, B. F., *Zh. Anal. Khim.*, 1990, **45**, 279.
3 Moraes, N. M. P., and Iyer, S. S., *Anal. Chim. Acta*, 1990, **236**, 487.
4 Casetta, B., Giaretta, A., and Mezzacasa, G., *At. Spectrosc.*, 1993, **11**, 222.
5 Kuz'min, N. M., Pukhovskaya, V. M., Varshal, G. M., Spirakov, B. Ya., Maryutina, Y. A., Volynets, M. P., Ryabukhin, V. A., Chkhetiya, D. N., Grebneva, O. N., and Pavlutskaya, V. I., *Zh. Anal. Khim.*, 1993, **48**, 898.
6 Zuieger, E., and Erzinger, J., *Fresenius' Z. Anal. Chem.*, 1988, **332**, 140.

7 Bauer-Wolf, E., Wegscheider, W., Posch, S., and Knapp, G., *Talanta*, 1993, **40**, 9.
8 Serdobova, L. I., Kataeva, Z. T., and Andreeva, I. P., *Zh. Anal. Khim.*, 1988, **43**, 2206.
9 You, X., Jiang, Z., and Zhe, Y., *J. Chin. Rare Earth Soc.*, 1990, **8**, 133.
10 Smirnova, E. V., Kuznetsova, A. I., and Chumacova, N. L., *Atomic Emission Analysis in Geochemistry*, Nauka, Novosibirsk, 1993, pp. 131–151 (in Russian).
11 Thompson, M., and Walsh, J. N., *A Handbook of Inductively Coupled Plasma Spectrometry*, Blackie, Glasgow, 1983, pp. 116–126.
12 Yel'ashevich, M. A., *Spectra of Rare Earths*, GITTL, Moscow, 1953 (in Russian).
13 Volynets, M. P., and Ryabukhin, V. A., *Avt. Svid. USSR*, No. 1442860, 1988; *Bull. Izobret.*, 1988, **45**, 162.
14 Balashov, Yu. A., *Geochemistry of REE*, Nauka, Moscow (in Russian).
15 Wendt, R. H., and Fassel, V. A., *Anal. Chem.*, 1965, **37**, 920.
16 Britske, M. A., and Sukach, Y. S., *Zh. Prikl. Spektrosk.*, 1976, **25**, 5.
17 Safronova, N. S., Fabelinsky, Yu. I., Savinova, E. N., and Vul'fson, E. K., *Zh. Anal. Khim.*, 1990, **45**, 737.
18 Pliesovska, N., Solltes, P., and Fabelinsky, Yu. I., *XXVI Colloquim Spectroscopicum Internationale, Selected Papers*, ed. Tsalev, D. L., Sofia, 1989, p. 232.
19 Wing, R. K., Peterson, V. J., and Fassel, V. A., *Appl. Spectrosc.*, 1979, **33**, 210.

Paper 4/05867D
Received September 26, 1994
Accepted December 9, 1994

Inductively Coupled Plasma Atomic Emission Spectrometric Analysis of Low Levels of Selenium in Natural Waters*

Rob L. Adkins and Nick Walsh

Department of Geology, Royal Holloway, University of London, Egham Hill, Egham, Surrey, UK TW20 0EX

Mike Edmunds and Janice M. Trafford

BGS Hydrogeology Research Group, Maclean Building, Crowmarsh Gifford, Wallingford, Oxon, UK OX10 8BB

Selenium is an environmentally important element that is difficult to determine in natural waters owing to its low concentrations. Research has shown that selenium levels are typically <0.5 μg l^{-1} in most waters sampled. The increased environmental interest in selenium has promoted the modification of analytical methods with the aim to improve analysis at the sub-μg l^{-1} level. The determination of selenium by hydride generation has been widely documented by a number of authors. Selenium may be reduced to a gaseous hydride by reaction with sodium tetrahydroborate and introduced directly into the base of the ICP torch. This allows almost 100% efficiency of sample injection compared with only 2–5% by standard nebulization, hence improving sensitivity. Hydride generation represents a greatly improved method of selenium analysis and detection limits of 1 μg l^{-1} or lower may be obtained. However, when measuring selenium in most natural waters, samples must be preconcentrated to further lower detection limits into the usual range of occurrence. Coprecipitation with lanthanum hydroxide is a rapid and efficient method of concentrating selenium. In natural groundwaters and similar environments, selenium occurs mostly as Se^{VI} (selenate) although small amounts of Se^{IV} (selenite) may also be present. This research has shown that the dominant form of selenium (selenate) is not effectively precipitated with lanthanum hydroxide. Previously documented methods have therefore been modified here by reducing all Se to selenite prior to preconcentration and analysis. A method is described that allows selenium levels as low as 0.06 μg l^{-1} to be analysed rapidly and accurately. The selenium in each sample is reduced to selenite by heating with HCl and KBr. Selenite is then coprecipitated with lanthanum hydroxide and separated by centrifugation. The resulting precipitate is dissolved in an acid solution and introduced into the ICP in the form of gaseous hydride. Standard solutions show very good linear calibration across the range 0–10 μg l^{-1}.

Keywords: *Selenium; groundwater; preconcentration; reduction; hydride generation*

Introduction

There is currently very little data available on background Se levels in natural waters, mainly as a result of analytical difficulties. A low detection limit is vital in view of the need to investigate potential deficiencies of this biologically important element. Conventional inductively coupled plasma atomic emission spectrometry (ICP-AES) with pneumatic nebulization is not sensitive enough to measure the low levels of Se in most groundwaters. A 3σ detection limit of 0.14 mg l^{-1} was obtained using standard ICP methods and this is clearly not sensitive enough to study background selenium concentrations. Hydride generation is now widely used as a very effective means of increasing sensitivity for those elements capable of forming water-insoluble gaseous hydrides (As, Sb, Se, Te, Ge, Sn and Pb). This method is equally valuable in both inductively coupled plasma and atomic absorption techniques and has been thoroughly reviewed by Nakahara.[1]

Hydride generation ICP-AES allows reliable and rapid analyses of selenium, permitting potential detection limits of <1 μg l^{-1} to be obtained.[2–4] Pretorius *et al.*[5] obtained a detection limit for Se of 3 μg l^{-1} whilst 1.3 μg l^{-1} was obtained by Pyen and Browner[6] and 0.3 μg l^{-1} by Pruszkowska *et al.*[7] Although these detection limits are significantly lower than those obtained using standard nebulization, preconcentration of samples prior to analysis is required to further lower the detection limits into the range of natural waters. Thompson *et al.*[2–4] describe the improvement of the hydride generation technique by introducing a lanthanum preconcentration step. This method involves the addition of lanthanum nitrate to an acidified water sample followed by the addition of ammonia solution, which causes coprecipitation of lanthanum and selenium. Similarly, Skogerboe *et al.*[8] developed a method based on the reaction of sodium tetrahydroborate coupled with a carrier (indium in the case of selenium) which permits the separation of several ions by co-precipitation. Recoveries reported using this technique are good (typically 92%) and large concentration factors up to 1000-fold can potentially be achieved. An evaporation technique was employed by Wang *et al.*[9] to preconcentrate selenium in a study of waters from Finland. Although a detection limit of 6.5 ng l^{-1} was claimed, evaporation techniques are considered inferior methods of selenium concentration as samples are exposed to the atmosphere in open vessels for long periods of time, the loss of volatile species is possible and the over-all procedure is very time consuming. This research has aimed to develop a rapid and accurate method for the routine analysis of background levels of selenium. Although the techniques summarized above may be suitable for the analysis of Se-polluted waters, none was considered to be directly applicable to the study of natural groundwater. For this work, a lanthanum preconcentration technique was chosen. The method described by Thompson *et al.*[3] was originally followed, although modifications were necessary to enable reliable analysis of selenium in groundwater.

* Presented at Geoanalysis 94: An International Symposium on the Analysis of Geological and Environmental Materials, Ambleside, England, September 18–22, 1994.

Experimental

Apparatus

Data were collected using a Philips PV8050 ICP system (Cambridge, UK). The instrument was used in combination with a commercially available PS Analytical hydride generator (Kemsing, Sevenoaks, Kent, UK). The hydride generator pumps three liquid streams (sample, acid blank and $NaBH_4$ reducing agent) continuously at a rate of 12 ml min^{-1} for sample and acid blank and 4 ml min^{-1} for $NaBH_4$. Two liquid streams (the reducing agent and either the sample or acid blank) meet at a capillary T-junction where a vigorous reaction occurs, forming gaseous SeH_2. The third stream passes directly to the drain.

The mixture of liquid and gaseous products is continually pumped from the T-junction into a glass phase separator. The phase separator possesses two inlet tubes: one for the test solution and $NaBH_4$, and one connected to an external argon supply. The argon is released into the phase separator from where it carries the gaseous selenium hydride *via* an outlet tube to the base of the ICP torch. The remaining unused test solution collects in a U-tube at the base of the phase separator. This causes sufficient back pressure to drive the gases through to the ICP torch as well as acting as a drain for waste liquid.

The PS Analytical hydride generator incorporates a Teflon switch-over valve, which allows an instantaneous switch from blank to sample after a programmed time interval synchronized with the ICP. This keeps hydrogen production rates constant and maintains stable plasma conditions. This instantaneous switch-over is essential when high molarity acid is being used as any instability tends to extinguish the plasma. However, if 1 mol l^{-1} acid is used, instabilities caused by air entering the system are less dramatic and it is possible to perform the switch-over manually.

The Philips ICP system used as a detector for selenium had the following argon flow rates to the torch: plasma 1.2 l min^{-1}, auxiliary 0.2 l min^{-1}. A 20 s integration time was used and the selenium analytical wavelength at 196.026 nm (measured in the first order) was used.

Reagents

Distilled water was used in the preparation of all reagents. Hydrochloric acid (1 mol l^{-1}) was used as an acid blank and also to dissolve preconcentrated samples. A stock solution of sodium tetrahydroborate was prepared daily by dissolving 5 g of $NaBH_4$ in 500 ml of 0.1% sodium hydroxide. A 5% m/v lanthanum oxide solution was prepared for use in the preconcentration step. Three sets of calibration standards were prepared using SpectrosoL standard selenium solution, sodium selenite pentahydrate and sodium selenate.

Results and Discussion

Optimization of Hydride Generation

The main controls on the sensitivity and signal intensity were found to be sample and $NaBH_4$ flow rates, ICP anode current and argon flow rate. Signal intensity increased greatly as the sample and $NaBH_4$ flow rates were increased. Narrow bore tubing, pumping at a rate of 12 ml min^{-1} for samples and 4 ml min^{-1} for $NaBH_4$, gave optimum sensitivity. An increase in argon flow rate to the base of the torch produced an increase in sensitivity of up to 1 l min^{-1} above which sensitivity was seen to decrease.

Signal intensities for 1 mg l^{-1} and 10 mg l^{-1} standards were seen to show a slight linear increase as the HCl concentration was increased (Fig. 1). However, the plasma was not stable when high molarity acid was used; therefore, it was decided to use 1 mol l^{-1} HCl which allowed excellent plasma stability and only slightly lower output intensities.

Moisture carryover originating during the gas–liquid separation process was seen to cause loss of sensitivity and over-all plasma instability. A simple physical moisture trap (as described by Corns *et al.*[10]) was essential to overcome this problem.

Optimization of Reduction and Preconcentration Techniques

The preconcentration method was based on that described by Thompson and Walsh.[11] For this work, 1 ml of 5% m/v lanthanum oxide (dissolved in 1 mol l^{-1} HCl) was added to a 200 ml water sample. This was subsequently precipitated by the addition of a few drops of ammonia solution and centrifuged at 4000 rpm for 150 s. The resulting precipitate was reduced by heating with KBr and HCl, then dissolved in 7.5 ml 1 mol l^{-1} HCl ready for introduction to the ICP *via* the hydride generator.

This method works well when using SpectrosoL standard solutions and the 3σ detection limits obtained in two separate laboratories were 0.06 μg l^{-1}* and 0.09 μg l^{-1}.† Output intensities of preconcentrated SpectrosoL standards were linear over the range 0.1–100 μg l^{-1} Se. However, experiments using natural water samples show that this method cannot be applied directly to the analysis of environmental samples.

Selenium in groundwater occurs mostly as Se^{VI} (selenate) as any Se^{IV} (selenite) present in the system tends to be adsorbed by iron oxides or clay minerals.[12–14] For efficient hydride generation, the selenate must be reduced to selenite prior to analysis by ICP-AES. The method described by Thompson[11] uses a KBr and HCl solution combined with moderate heating after the lanthanum preconcentration step to reduce the selenium. However, groundwater samples preconcentrated using the above method gave consistently low intensities, often at levels comparable to that of the blank. This suggested that selenate was not being reduced and that the failure of the pre-reduction process was not noticeable from the SpectrosoL standards as these solutions evidently contain selenium in its reduced selenite state.

Stock solutions were prepared from SpectrosoL, sodium selenate and sodium selenite pentahydrate using the procedure described earlier. Output intensities obtained after preconcentration are given in Table 1.

These results confirm that reduction was very inefficient with even 100 μg l^{-1} selenate failing to give an easily measured intensity. The low selenate intensities may be explained either by a failure in the reduction step after preconcentration, or simply by the fact that selenate does not precipitate out with lanthanum oxide. Stock solutions were prepared containing

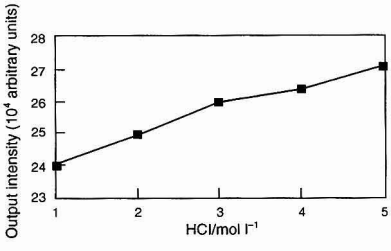

Fig. 1 Effect of changing acid molarity on the output intensity of a 1 mg l^{-1} standard solution.

* Royal Holloway, University of London.
† British Geological Survey, Wallingford.

selenite and selenate at levels above the detection limit for direct analysis by ICP. The coprecipitation procedure was followed on both forms of selenium and after centrifuging the standards at 4000 rpm for 150 s, the clear centrifugate was analysed. Analysis showed that most of the selenite was precipitated out of solution whilst much of the selenate remained. This contradicts the findings of Saisho and Fujimara.[15] The field treatment of samples could potentially account for the observations seen. Hence fresh groundwater was spiked with selenate just after filtration and acidification (0.5% v/v HCl), as documented by Thompson.[4] After 24 h, the lanthanum coprecipitation step still failed to recover the selenate, suggesting that field treatment has little effect on the outcome of the concentration technique. Therefore, lanthanum oxide does not effectively co-precipitate selenate. Previously published methods involve the reduction of selenium after the lanthanum preconcentration step; however, the results from this research suggest that such methods do not allow for the determination of selenate, and hence reduction of the water sample prior to preconcentration is preferable.

Various pre-reduction methods are available, including the addition of KBr, HCl or KI to a sample. Potassium iodide was not chosen as it is reported to reduce selenium to its zero oxidation state from which no hydride is formed.[16] Concentrated HCl is widely used as a reductant although large amounts combined with strong heating was necessary.

Stock solutions of 100 μg l^{-1} selenite and selenate were prepared and 11.7 mol l^{-1} HCl was added to 15 ml batches of selenate to give strengths of 1, 3 and 4 mol l^{-1} HCl. Standards were heated at 65 °C for 1 h, cooled, and analysed by hydride generation ICP-AES. Intensities were compared with those of the 100 μg l^{-1} selenite standard to evaluate the efficiency of selenate reduction. Allowances were made for the varying dilution factors of the samples and it was noted that recoveries improved as the acid concentration increased. Fig. 2(*a*) shows the 4 mol l^{-1} acid solution gave an average of 76% reduction of selenate to selenite although this quantity acid is not practical for the treatment of 200 ml water samples.

KBr was also found to be an efficient reductant and a 15% m/v solution reduced an average 88% of the selenate to selenite after heating [Fig. 2(*b*)]. Maximum selenate reduction was obtained by combining KBr and HCl to give stock selenate solutions containing 10% m/v KBr and 1 mol l^{-1} HCl. Duration of heating time was found to have little effect on reduction although samples heated for 30 min had a slightly lower recovery than those heated for 60 and 90 min (Fig. 2(*c*)]. Combining HCl and KBr allowed almost 100% reduction of selenate to selenite. When working with 200 ml water samples, maximum reduction is achieved by adding 25 ml concentrated HCl and 20 g of KBr to each sample. The samples are then heated at 65 °C for 50 min and standard solutions containing 0, 0.5, 1, 5, and 10 μg l^{-1} selenate are prepared with each set of samples.

After reduction to selenite, samples may be effectively concentrated by using an adaptation of Thompson's method. A 1 ml volume of 5% m/v La_2O_3 (dissolved in 1 mol l^{-1} HCl) is added to each 200 ml sample and sufficient ammonia solution is added to raise the pH to slightly above neutral (approximately 25 ml). A white precipitate forms which is separated by centrifugation at 4000 rpm for 150 s. The clear centrifugate is discarded and the precipitate is dissolved in 7.5 ml of 1 mol l^{-1} HCl. Thus, the selenium contained in a 200 ml water sample is reduced and concentrated into 7.5 ml: a concentration factor of 26.7.

Table 1 Output intensities after preconcentration and reduction of various selenium standards (arbitrary units)

	Output intensity (arbitrary units)		
Concentration/μg l^{-1}	SpectrosoL	Selenate	Selenite
100	302.52	1.68	306.79
50	146.20	0.42	157.38
10	26.59	0.39	29.94
1	2.79	0.01	2.08

Conclusions

The inability of the lanthanum oxide solution to coprecipitate selenate illustrates the need to reduce the selenium in each sample prior to preconcentration. Failure to pre-reduce samples will give recoveries for total selenite and this in effect

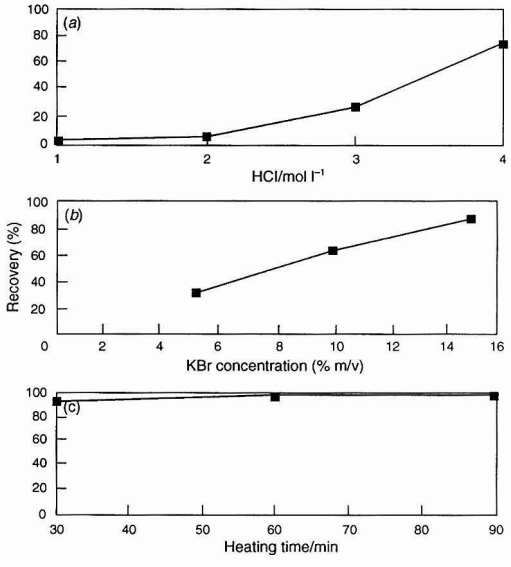

Fig. 2(*a*) Effect of acid molarity on selenate reduction, (*b*) effect of KBr concentration on selenate reduction and (*c*) effect of heating time on selenate reduction (5% m/v KBr and 1 mol l^{-1} HCl).

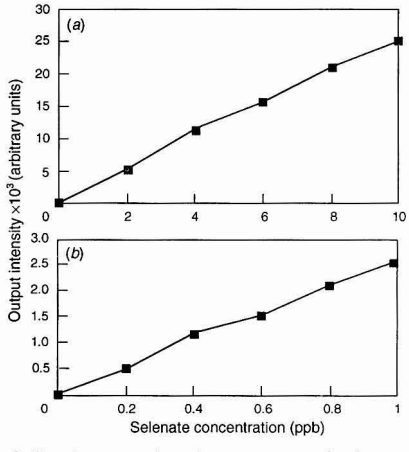

Fig. 3 Calibration curves for selenate concentration between (*a*) 0–10 and (*b*) 0–1 ppb.

allows speciation studies to be made. The ability to study Se speciation is a valuable feature of this method although selenite levels are rarely above detection limit in the British groundwaters analysed to date.

The pre-reduction and preconcentration techniques described above have allowed selenium in groundwaters to be measured satisfactorily at concentrations as low as 0.06 μg l^{-1}. Prepared selenate standards show good linear correlation both at the low concentrations found in groundwaters and also at higher levels up to 10 μg l^{-1}. Fig. 3(*a*) shows the good linearity between output intensities of blank corrected selenate standards between 0 and 1 μg l^{-1} (the range into which most groundwaters fall). The linearity continues up to 10 μg l^{-1} [Fig. 3(*b*)]. Results obtained were checked by dual analysis of several samples at Royal Holloway, University of London and the British Geological Survey in Keyworth. Comparable concentrations were obtained in each laboratory (Table 2), and analysis of SRM NIST 1643c also produced an acceptable result. The s_r values obtained from 12 repeat sample runs show the good precision and repeatability of the method (Table 2) which has allowed for the routine determination of selenium concentrations in many British groundwaters. Selenium has been found to be strongly dependent on redox conditions with most concentrations below 1 μg l^{-1} and usually below 0.5 μg l^{-1}.

The described method is simple to implement and the results obtained are accurate and repeatable. The procedure is fairly rapid with production of around 30 samples per day including blanks.

Table 2 Accuracy and precision data illustrated by 1, interlaboratory data; 2, s_r values; and 3, analysis of NIST SRM 1643c

	Se concentration determined/μg l^{-1}	
	RHUL	BGS
Interlaboratory—		
Amen Corner	0.11	0.15
Everton	0.70	0.77
Chequer House	0.21	0.21
s_r *Values (%)—*		
Acid blank	0.77	
Standard (5 μg l^{-1})	0.73	
NIST SRM 1643c—		
Specified concentration	12.7 ± 0.7 μg l^{-1}	
Determined	12.2 μg l^{-1}	

This research was financed as part of the NERC/AFRC Joint Initiative on Pollutant Transport in Soils and Rocks. The ICP-AES facility at Royal Holloway, University of London is funded by NERC Scientific Services. The analytical assistance of S. James is gratefully acknowledged.

References

1 Nakahara, T., *Prog. Anal. At. Spectrosc.*, 1983, **6**, 163.
2 Thompson, M., Pahlavanpour, B., Walton, S. J., and Kirkbright, G. F., *Analyst*, 1978, **103**, 568.
3 Thompson, M., Pahlavanpour, B., Walton, S. J., and Kirkbright, G. F., *Analyst*, 1978, **103**, 705.
4 Thompson, M., Pahlavanpour, B., and Thorne, L. T., *Water Res.*, 1981, **15**, 407.
5 Pretorius, I., Kempster, P. L., Van Vliet, H. R., and Van Staden, J. F., *Fresenius J. Anal. Chem.*, 1992, **342**, 391.
6 Pyen, G. S., and Browner, R. F., *Appl. Spectrosc.*, 1988, **42**, 262.
7 Pruszkowska, E., Barrett, P., Ediger, R., and Wallace, G., *At. Spectrosc.*, 1983, **4**, 94.
8 Skogerboe, R. K., Hanagan, W. A., and Taylor, H. E., *Anal. Chem.*, 1985, **57**, 2815.
9 Wang, D., Alfthan, G., Aro, A., Kauppi, L., and Soveri, J., in *Trace Elements in Health and Disease*, Proceedings Jt. Nordic Trace Element. Society, Helsinki, ed Aitio, A., 1991, pp. 49–56.
10 Corns, W. T., Ebdon, L., Hill, S. J., and Stockwell, P. B., *Analyst*, 1992, **117**, 717.
11 Thompson, M., and Walsh, J. N., *Handbook of Inductively Coupled Plasma Spectrometry*, Blackie, London, 2nd edn., 1989.
12 Balistrieri, L. S., and Chao, T. T., *Geochim. Cosmochim. Acta*, 1990, **54**, 739.
13 Bar-Yosef, B., and Meek, D., *Soil Sci.*, 1987, **144**, 11.
14 Hamdy, A. A., and Gissel-Nielsen, G., *Z. Pflanzenernaehr. Bodenkd.*, 1977, **140**, 63.
15 Saisho, H., and Fujimura, Y., *Anal. Sci.*, 1990, **6**, 619.
16 De Oliveira, E., McLaren, J. W., and Berman, S. S., *Anal. Chem.*, 1983, **55**, 2047.

Paper 4/05857G
Received September 26, 1994
Accepted December 2, 1994

Epithermal Neutron Activation Analysis of Mosses Used to Monitor Heavy Metal Deposition Around an Iron Smelter Complex*

M. V. Frontasyeva

Frank Laboratory of Neutron Physics, Joint Institute for Nuclear Research, 141980 Dubna, Moscow Region, Russia

E. Steinnes

Department of Chemistry, University of Trondheim, AVH N-7055 Dragvoll, Norway

The moss *Hylocomium splendens* was used as a biomonitor to study changes in the atmospheric deposition of metals around an iron smelter complex in Northern Norway between 1989 and 1993. Samples representing the last three years' growth of moss, collected on the ground at 25 sites located 1–25 km from the source area, were analysed by instrumental neutron activation analysis using epithermal neutrons. A total of 38 elements were determined, including most of the heavy metals known to be released into the air from this kind of industry. A re-orientation of the industrial production occurred around 1990; the most important developments being the closing of an iron smelter and the starting-up of a new ferrochrome smelter. Accordingly, the Cr deposition in the vicinity of the smelter increased by about a factor of 100, while the Fe deposition decreased by almost a factor of 10. Other elements showing a decrease over this period were Mo, Sr, Se, Zr, Re, Hf, Ta, Th, and U, while there was an appreciable increase for Ni, W, and Au. Most other elements, including V, Mn, Co, Cu, Zn, As and Sb, had similar levels as before. A new method for the graphical representation of deposition levels is introduced. Instead of constructing isopleths based on the observed concentration values, each value is divided by a number representing the background level found in moss in the area. The resulting ratios are then used as a basis for the construction of isopleths. Examples are shown for Cr, Fe and V levels in 1989 and 1993 respectively.

Keywords: *Instrumental neutron activation analysis; epithermal neutron; biomonitor;* Hylocomium splendens; *metal smelter; trace element; air pollution*

Introduction

Mosses can be favourably used as biomonitors of the atmospheric deposition of trace elements because they lack a root system and therefore depend on supply of chemical substances derived from above. Analysis of naturally growing mosses to monitor heavy metal deposition is a well established technique[1,2] and has been shown to be useful in studies on a local[3–5] as well on a large[6–8] scale. Studies of a limited number of elements using atomic absorption spectrometry have been reported most frequently, but also multi-element techniques, such as instrumental neutron activation analysis (INAA)[8–11] and inductively coupled plasma mass spectrometry (ICP-MS)[12] have been employed. INAA using epithermal neutrons was shown to be feasible for the determination of more than 40 elements,[11] including some elements not yet reported in moss studies.

Among the local pollution problems studied using moss analysis is metal deposition in the vicinity of iron and steel manufacturing industries.[3,13] In 1989, the moss technique was

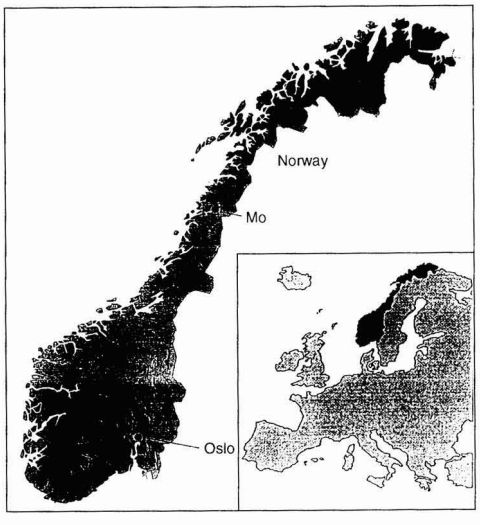

Fig. 1 Location of study area and individual sampling points (originally 39 points were sampled as shown, but only the 25 marked with filled circles were included in this work).

* Presented at Geoanalysis 94: An International Symposium on the Analysis of Geological and Environmental Materials, Ambleside, England, September 18–22, 1994.

used to investigate the deposition of selected heavy metals near an iron smelter complex at Mo, a small industrial town in northern Norway.[14] For certain elements, very high deposition rates were observed. In 1993, after a re-orientation of the industrial production, the most important parts of which were to close a large iron smelter, and replacing it with the production of ferro-alloys, the study was repeated. As the application of INAA in moss monitoring studies related to iron industries had not been previously reported, it was decided to submit the moss samples collected from the two different years to INAA in the IBR-2 reactor at Dubna, using a very high ratio of epithermal to thermal neutrons, in order to study simultaneously how the deposition patterns had developed for a large number of elements.

Table 1 Characteristics of the irradiation channels

Irradiation site	Neutron flux density/ 10^{12} n cm^{-2} s^{-1}			T/°C
	Thermal	Resonance	Fast	
Ch1	Cd coat	0.23 ± 0.03	1.4 ± 0.16	70
Ch2	0.54 ± 0.06	0.12 ± 0.014	0.64 ± 0.04	60

Experimental

Sampling

Samples of the feather moss *Hylocomium splendens*, which grows on organic topsoils in forests and other natural environments, were collected at 25 sites situated 1–25 km from the smelter complex. The network of sampling sites is shown in Fig. 1. The sampling was carried out according to a procedure described in detail elsewhere.[7] For each site 5–10 subsamples were taken within a 50 × 50 m area and these were combined in the field. The unwashed samples were air-dried at 30 °C and extraneous plant material was removed. The three youngest fully developed segments of each *Hylocomium* plant were taken for analysis. No further homogenization of the samples was performed.[10] Disposable polyethylene gloves were used during all handling of samples.

Analysis

Moss samples of about 0.5 g were packed in aluminum cups for long-term irradiation and heat-sealed in polyethylene foil bags for short-term irradiation. Neutron flux density characteristics and the temperature in the channels equipped with a pneumatic system are given in Table 1.

Table 2 Summary of results obtained for 38 elements in 25 moss samples from the vicinity of an iron smelter complex

Element	Radio-nuclide used	E_γ measured/ keV	1993			1989		
			Mean (ppm)	Range (ppm)	No. of samples <DL*	Mean (ppm)	Range (ppm)	No. of samples <DL*
Na	^{24}Na	2753.6	310	127–732		294	93–635	
Mg	^{27}Mg	1014.4	2015	781–6520		1861	556–4230	
Al	^{27}Al	1778.9	1186	293–4460		1244	243–3100	
Cl	^{38}Cl	2168.0	201	88–375		294	50–1110	
K	^{42}K	1524.7	3470	1640–4770		3845	1930–7160	
Ca	^{49}Ca	3084.4	1903	995–4830		2871	1450–6740	
Sc	^{46}Sc	889.2	0.20	0.03–0.70		0.41	0.06–1.41	
V	^{52}V	1434.1	4.10	0.79–19.0		5.72	1.05–31.0	
Cr	^{51}Cr	310.1	390	4.3–3900		11.7	0.5–50	
Mn	^{56}Mn	1810.7	325	61–917		384	89–1460	
Fe	^{59}Fe	1291.6	2440	300–8700		12 280	700–72 100	
Co	^{60}Co	1332.4	0.68	0.07–3.0		0.61	0.06–2.2	
Ni	^{58}Co	810.8	2.84	<0.5–15.6	4	1.69	<0.5–6.96	5
Cu	^{64}Cu	511.0	8.23	3.5–20.3		12.3	2.9–29.0	
Zn	^{65}Zn	1116.0	88	16–542		99	31–397	
As	^{76}As	559.1	0.37	0.06–1.56		0.62	0.06–2.20	
Sc	^{75}Sc	264.7	0.31	0.16–0.75		0.47	0.21–1.17	
Br	^{82}Br	776.5	6.36	3.5–11.4		6.94	3.6–12.2	
Rb	^{86}Rb	1976.6	12.5	3.3–26.4		17.2	6.7–46.2	
Sr	^{85}Sr	514.0	8.9	<4–52	1	19.9	<4–50	1
Zr	^{95}Zr	756.7	3.0	<2–24	17	11.0	<2–46	7
Mo	^{99}Tc^{m}	140.5	0.16	<0.08–0.76	6	0.87	<0.08–3.85	4
Ag	^{110}Ag^{m}	657.7	0.057	<0.03–0.18	6	0.059	<0.03–0.16	3
Sb	^{124}Sb	1691.0	0.166	<0.03–0.69	1	0.250	<0.05–0.76	
I	^{128}I	442.9	1.82	<1.0–3.3	4	2.26	<1.0–4.3	4
Cs	^{134}Cs	795.8	0.28	0.05–0.89		0.37	<0.05–1.03	1
Ba	^{131}Ba	496.8	26.7	15–57		33.1	12–83	
La	^{140}La	1596.5	0.45	<0.10–1.38	1	0.69	<0.10–2.87	4
Sm	^{153}Sm	103.2	0.139	0.04–0.45		0.33	0.05–1.34	
Eu	^{152}Eu	1407.5	0.016	<0.01–0.13	10	0.031	<0.01–0.12	6
Tb	^{160}Tb	879.4	0.020	<0.005–0.096	7	0.019	<0.005–0.067	5
Yb	^{169}Yb	198.0	0.032	<0.010–0.120	6	0.069	<0.010–0.230	2
Hf	^{181}Hf	482.0	0.097	<0.04–0.36	7	0.179	<0.04–0.71	4
Ta	^{182}Ta	1221.4	0.011	<0.003–0.038	6	0.043	<0.003–0.180	1
W	^{187}W	685.8	1.68	<0.6–9.4	2	1.71	<0.6–6.4	12
Au	^{198}Au	411.8	0.0042	0.0006–0.037		0.0002	<0.0001–0.010	4
Th	^{233}Pa	312.0	0.114	0.02–0.47		0.267	0.04–1.10	
U	^{239}Np	228.2	0.035	0.03–0.22	11	0.143	<0.03–0.51	1

Long-lived isotopes were determined using channel 1 (Ch1). Samples were irradiated for 5 d, re-packed and then measured twice after 4–6 and 20 d of decay, respectively. Measuring time varied from 1 to 5 h. To determine the short-lived isotopes of Cl, V, I, Mg, Cu, Al and Mn, channel 2 (Ch2) was used. Samples were irradiated for 5 min and measured twice after 3–5 and 20 min of decay for 5–8 and 20 min, respectively. To determine Cu, K, Na the same samples were irradiated for an additional 30 min, and after 12–15 h of decay measured for 30 min.

Table 3 Interference by fast neutron reactions*

Intended reaction	Interfering reaction	Level of interference/ng†
$^{23}Na(n,\gamma)^{24}Na$	$^{24}Mg(n,p)^{24}Na$	3×10^5
	$^{27}Al(n,\alpha)^{24}Na$	1.5×10^6
$^{26}Mg(n,\gamma)Mg^{27}$	$^{27}Al(n,p)^{27}Mg$	9×10^8
$^{27}Al(n,\gamma)^{28}Al$	$^{28}Si(n,p)^{28}Al$	3×10^7
	$^{31}P(n,\alpha)^{28}Al$	9×10^6
$^{41}K(n,\gamma)^{42}K$	$^{42}Ca(n,p)^{42}K$	—‡
	$^{45}Sc(n,\alpha)^{42}K$	1.5×10^6
$^{51}V(n,\gamma)^{52}V$	$^{52}Cr(n,p)^{52}V$	1×10^4
$^{50}Cr(n,\gamma)^{51}Cr$	$^{54}Fe(n,\alpha)^{51}Cr$	4×10^5
$^{55}Mn(n,\gamma)^{56}Mn$	$^{56}Fe(n,p)^{56}Mn$	7×10^4
$^{58}Fe(n,\alpha)^{59}Fe$	$^{59}Co(n,p)^{59}Fe$	2.3×10^8
$^{63}Cu(n,\gamma)^{64}Cu$	$^{64}Zn(n,p)^{64}Cu$	5×10^6

* Cr and Fe were determined in Ch1, all other elements mentioned here in Ch2 (see Table 1).

† As compared with 1 gram of the interfering element.

‡ Cross section not available.

Gamma spectra were measured using Ge(Li) detectors with a resolution of 2.5 keV for the ^{60}Co 1332.4 keV line, with an efficiency of about 6% relative to a 3 × 3″ NaI detector for the same line. Radionuclides and γ-energies used are given in Table 2. Data processing and element concentration determination was performed on the basis of certified reference materials and flux comparators, using software developed in FLNP JINR.[15]

For long-term irradiations in Ch1 single comparators of Au (1 μg) and Zr (10 mg) were used. For short-term irradiations in Ch2 a comparator of Au (10 μg) was used. Concentrations of elements yielding long-lived isotopes were also determined using certified reference materials: SDM (International Atomic Energy Agency, Vienna) and moss DK-1.[11]

Results and Discussion

Mean values and ranges for 38 elements in moss samples collected at the same 25 sites in 1989 and 1993, respectively, are given in Table 2. The number of samples showing values below the detection limit are also listed. The detection limits were generally somewhat inferior to those observed in the previous study[11] of mosses from areas with low air pollution exposure using the same technique. The main reason for this was the very high levels of ^{59}Fe and ^{51}Cr (particularly in the 1993 samples) which complicated the measurement of other long-lived radionuclides. Data for elements such as Sn and the rare earth elements Nd, Gd, Tm and Lu, which were determined in the previous paper,[11] are therefore not reported here. Also Ce proved to be very difficult to determine using the 145.4 keV peak owing to the very

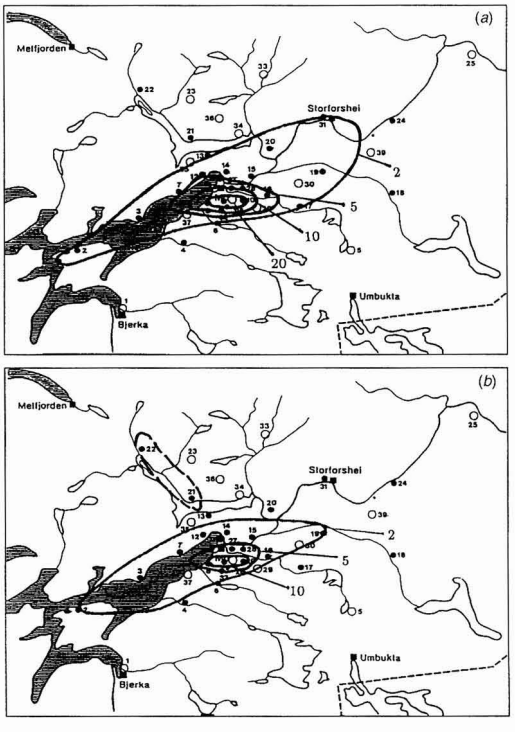

Fig. 2 Isopleths showing deposition pattern of V around the Mo iron smelter complex relative to background level, constructed for the (*a*) 1989 and (*b*) 1993 sampling data. See text for details.

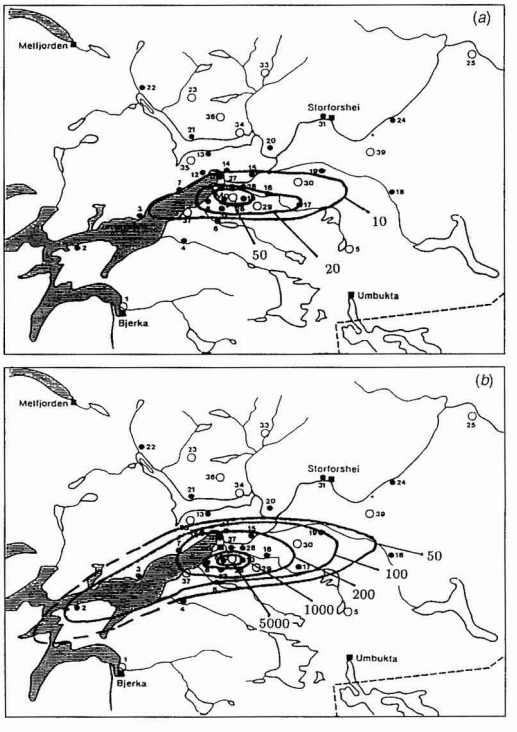

Fig. 3 Isopleths showing deposition pattern of Cr around the Mo iron smelter complex relative to background level constructed for the (*a*) 1989 and (*b*) 1993 sampling data.

intensive 142.8 keV peak of ^{59}Fe. However, the determination of Cu and Mo was shown to be feasible in the present study.

Also reported are data for the main constituents (Na, Mg, Al, K and Ca) which were not given in the previous paper[11] due to interferences from nuclear reactions associated with the high fast-neutron component in the IBR-2 reactor.

The high density of fast neutrons in the irradiation channels used provided favourable conditions for the determination of Ni by the ^{58}Ni(n,p)^{58} Co reaction. However, problems with interfering nuclear reactions are evident in a number of instances, as shown in Table 3. The character of the problems depends on the concentration ratios of the elements concerned in the samples, which in some instances varied over quite wide ranges. In most instances the concentrations of the potentially interfering elements were known. An exceptional case is Al, where data for the interfering elements Si and P were not available for the actual samples. Considering the fact that the Si:Al ratios in most crustal materials vary within relative narrow ranges (crustal mean, 3.5), and the P concentration of mosses is normally of the order of 800 ppm (Kemp and Steinnes[16]), it appears that the corrections are relatively small in most instances. The interference of Ca in K determination is not known because of the lack of cross section data, but is probably not very serious considering the high and constant level of K in mosses.

The spatial distribution of multi-site pollution data is often expressed in the form of isopleths based on observed single values. In the present work an alternative approach is presented: Background levels of the individual elements in *Hylocomium splendens* in the actual region of Norway are established on the basis of data from nationwide deposition surveys in 1985[10] and 1990.[16] The observed values from the present work are divided by the corresponding background values and the resulting ratios, expressing the enrichment factors over the background levels, are used as a basis for isopleth construction instead of the primary concentration values. Examples of such isopleths are shown for 3 elements that are strongly enriched in the area around the smelter complex in Fig. 2 (V), Fig. 3 (Cr) and Fig. 4 (Fe).

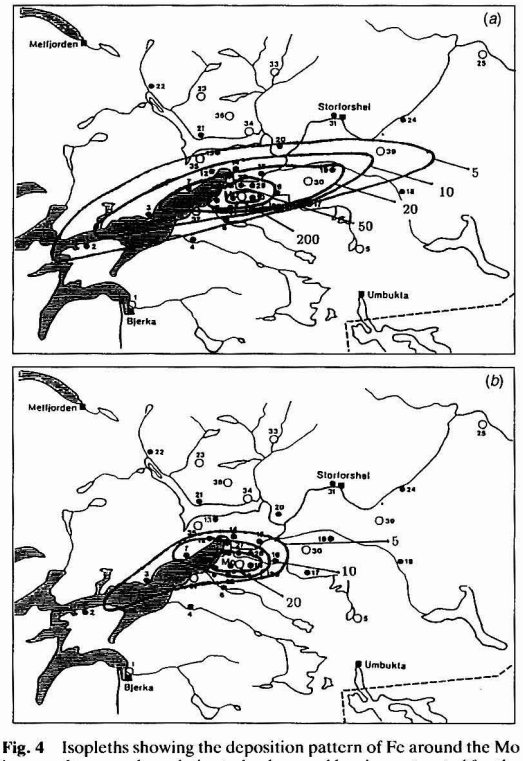

Fig. 4 Isopleths showing the deposition pattern of Fe around the Mo iron smelter complex relative to background level, constructed for the (*a*) 1989 and (*b*) 1993 sampling data.

Chromium shows the most dramatic difference between the samples collected in 1989 and the samples collected in 1993, with an increased deposition by a factor of 100, which is clearly associated with the new ferrochrome plant started after 1989. Also for Ni, W and Au (not shown) there has been a fairly clear increase in the moss metal-levels in the vicinity of the industrial complex. The deposition of Fe, however, has decreased substantially after the closing of the iron smelter. A similar decrease is observed for Mo, to a lesser extent Sr, and some of the refractory lithophilic elements (Sc, Zr, Re, Hf, Ta, Th, U). Most of these elements are enriched in moss samples near the industry, which indicates that there must be a mineral dust problem, possibly associated with the handling of iron ore, and, perhaps also disposal of slag from the smelting processes.

For V the changes in industrial activity have not had any strong influence on the deposition levels. A separate discussion of the temporal and spatial pattern of each element and their relations to details in the local industrial development is beyond the scope of this paper.

In conclusion, ENAA appears to be a very useful technique in studying air pollution problems associated with iron and steel industries, employing moss as a biomonitor. The most significant metal pollutants associated with such industries can thus be determined. Furthermore, the present investigation is an example showing that recent changes in industrial practice can sometimes lead to worse heavy metal contamination problems than before.

References

1 Rühling, A., and Tyler, G., *Water, Air, Soil Pollut.*, 1973, **2**, 445.
2 Rasmussen, L., and Johnsen, I., *Oikos*, 1976, **27**, 483.
3 Ellison, G., Newham, J., Pimchin, M. J., and Thompson, I., *Environ. Pollut.*, 1975, **11**, 167.
4 Andersen, A., Hovmand, M. F., and Johnsen, I., *Environ. Pollut.*, 1978, **17**, 133.
5 Folkeson, L., *Ann. Bot. Fenn.*, 1981, **18**, 245.
6 Gydesen, H., Pilegaard, K., Rasmussen, L., and Ruhling, A., *Bulletin SNV PM 1670*, Swedish Board of Environmental Protection, Stockholm, 1980, p. 44.
7 Ruhling, A., Rasmussen, L., Pilegaard, K., Makinen, A., and Steinnes, E., *Report NORD 1987: 21*, Nordic Council of Ministers, Copenhagen, 1987, p. 44.
8 Steinnes, E., Ramback, J. P., and Hanssen, J. E., *Chemosphere*, 1992, **25**, 735.
9 Steinnes, E., *J. Radioanal. Chem.*, 1980, **58**, 357.
10 Steinnes, E., Hanssen, J. E., Ramback, J. P., and Vogt, N. B., *Water, Air, Soil Pollkut.*, 1994, **74**, 121.
11 Frontasyeva, M. V., Nazarov, V. M., and Steinnes, E., *J. Radioanal. Nucl. Chem.*, 1994, **181**, 363.
12 Steinnes, E., Johansen, O., Royset, O., and Odegard, M., *Environ. Monit. Assess.*, 1993, **25**, 87.
13 Pilegaard, K., *Water, Air, Soil Pollut.*, 1979, **11**, 77.
14 Steinnes, E., Andersson, E. M. and Sjobakk, T. E., *Report 495/92*, Norwegian State Pollution Control Authority, Oslo, 1992, p. 18.
15 Ostrovnaya, T. M., Nefedyeva, L. S., Nazarov, V. M., Borzakov, S. B., and Strelkova, L. P., in *Activation Analysis in Environment Protection*, JINR, D14-93-325, Dubna, 1993, p. 319.
16 Kemp, K., and Steinnes, E., unpublished work.

Paper 4/06441K
Received October 21, 1994
Accepted December 20, 1994

Determination of Platinum, Palladium, Iridium and Gold in Selected Geological Reference Materials by Radiochemical Neutron Activation Analysis: Comparison of Procedures Based on *Aqua Regia* Leaching and Sodium Peroxide Sintering*

Claudio A. Nogueira and Ana M. G. Figueiredo

Supervisão de Radioquímica, Instituto de Pesquisas Energéticas e Nucleares, CNEN/SP, Caixa Postal 11049, São Paulo, SP, Brazil

A rapid and sensitive neutron activation method for the determination of platinum, palladium, iridium and gold in rocks is described. The procedure consists of thermal neutron irradiation of about 250 mg of sample, followed by chemical treatment of the rock, precipitation of gold and the platinum group elements with tellurium and high-resolution gamma-ray spectrometry with a hyper-pure Ge detector. Two different methods were used for the chemical treatment of the rock: *aqua regia* leaching and sintering with sodium peroxide. The procedures were evaluated by analysis of the certified reference material SARM-7 and the reference material CHR-Pt+. Sintering with sodium peroxide and precipitation with tellurium were more appropriate for the determination of Pd, Pt and Ir, giving results in good agreement (within ±10%) with literature values. For gold, *aqua regia* leaching gave more accurate results (relative errors from 0 to 6%). The detection limits for the analytical conditions employed were 0.1 μg kg^{-1} Au, 10 μg kg^{-1} Pd, 20 μg kg^{-1} Pt and 0.2 μg kg^{-1} Ir. The procedure employing fusion with sodium peroxide was applied to the analysis of the reference material CHR-Bkg and the concentrations of Au, Pt, Pd and Ir obtained are presented.

Keywords: *Platinum, palladium, iridium and gold determination; geological sample; neutron activation analysis;* aqua regia *leaching; sintering with sodium peroxide*

Introduction

In recent years, the development of sensitive and reliable techniques for the determination of the platinum group elements (PGEs) and gold in terrestrial materials has attracted great interest. This is due not only to the growing economic interest in PGEs and gold as mineral resources, but also to the information that these elements can provide on metal geochemistry. The determination of very low amounts of iridium is particularly important on account of some anomalies in iridium distribution in sedimentary rock samples, related to catastrophic events.[1]

The concentration of PGEs in many geological samples is in the ng g^{-1} or even sub-ng g^{-1} range, so sensitive and accurate techniques must be used to achieve reliable results. Neutron activation analysis (NAA) and inductively coupled plasma mass spectrometry (ICP-MS) are the most widely used techniques for PGE determination in rocks.[2,3] NAA is one of the preferred methods of analysis because of its sensitivity, accuracy and freedom from contamination. Nevertheless, even when sensitive techniques are employed, it is necessary to separate the PGEs from matrix elements and concentrate them before analysis. Classical fire assay with lead collection and cupellation remains the most widely used technique for the preconcentration of PGEs, making possible the quantitative recovery of Au, Pt, Pd and Rh.[4] When analysing samples containing elements approaching detection limit concentrations, Ag must be added to the charge if Au, Pt and Pd are to be determined and Au if Rh is to be determined. For Ru, Os and Ir, the composition of the flux and the fusion conditions must be carefully controlled to avoid losses of these elements.[5] Nickel fire assay with radiochemical NAA has been used in recent years,[6,7] offering sensitivities at the ng g^{-1} level. However, this procedure requires reagents of high purity and the processing time may make difficult the determination of short-lived isotopes such as ^{109}Pd ($t_{1/2}$ = 13.5 h). Alternative procedures using alkali fusion and acid dissolution with PGE concentration by Te precipitation and NAA gave good results for Au, Pt, Pd, Ir, As, Sc.[8] *Aqua regia* sample decomposition followed by tellurium precipitation with electrothermal atomic absorption spectrometry has also been used,[9] giving accurate results for Au, Pt, Pd and Rh, but not for Ir.

This paper describes a simple and rapid radiochemical NAA method for the determination of Pt, Pd, Ir and Au in small geological samples (<500 mg). The procedure represents a modification of the procedure described by Stockman,[10] and consists of sample irradiation in a nuclear reactor, chemical treatment of the sample, precipitation with tellurium and high-resolution gamma-ray spectrometry. Two different methods were used for chemical treatment of the rock: *aqua regia* leaching and sintering with sodium peroxide at 480 °C. The accuracy of the procedures and detection limits were verified by analysis of the reference material SARM-7 (platinum ore) distributed by the South Africa Bureau of Standards, representative of silicate materials, which has certified values for all the PGEs. The new reference materials of chromitite CHR-Pt+, which is enriched in the PGEs, and CHR-Bkg, which has much lower PGE concentrations, were also analysed. These were prepared and distributed by CRPG (Centre de Recherches Petrographiques et Geochimiques), and represent important reference materials to chromitite matrices, with which PGEs are frequently associated. The results obtained by the two procedures employed are compared and discussed. Since the first compilation data about the proposed chromitite reference materials CHR-Pt+ and CHR-

* Presented at Geoanalysis 94: An International Symposium on the Analysis of Geological and Environmental Materials, Ambleside, England, September 18–22, 1994.

Bkg were reported recently,[11] this paper is also a contribution to Pt, Pd, Ir and Au values.

Experimental

Chemical Standards

Standard solutions were prepared by dissolving accurately weighed amounts of the salts $PdCl_2$, $H_2PtCl_6 \cdot 6H_2O$ (Merck) and $IrCl_4$ (Aldrich Chemical) in dilute nitric acid (1 + 9) and Au metal in *aqua regia* [HCl–HNO_3 (3 + 1)]. A convenient aliquot of each standard solution was pipetted onto a 1 cm^2 piece of Whatman No. 40 filter-paper, evaporated to dryness under an infrared lamp and packed in a polyethylene vial. Each individual standard contained 14.6 μg of Pd, 1.0 μg of Pt, 419 ng of Ir and 106 ng of Au. The chemical standards were irradiated together with the samples.

Carriers

Carrier solutions containing 0.5 mg ml^{-1} of Pt, Ir and Au and 1.0 mg ml^{-1} of Pd were prepared as described for the standard solutions. Aliquots of 0.100 ml for Au, Pd and Ir and of 0.250 ml for Pt were used as carriers in the radiochemical procedure.

Tellurium and Tin(II) Chloride Solutions

A solution containing 1 mg ml^{-1} of Te was prepared by dissolving Te metal in *aqua regia*. The nitrates were removed by repeated evaporations to dryness with concentrated hydrochloric acid, to ensure a non-oxidant medium. The tellurium chloride formed was taken up in dilute hydrochloric acid (1 + 9). A tin(II) chloride solution was prepared fresh just before use by dissolving 5.5 g of $Sn_2Cl_2 \cdot H_2O$ in 5 ml of concentrated HCl and diluting the resulting solution to 25 ml with distilled water.

Irradiation

Irradiation was carried out at the IEA-R1 nuclear reactors of the Instituto de Pesquisas Energéticas e Nucleares, Comissão Nacional de Energia Nuclear, SP. Aliquots of about 250 mg of the powdered samples were weighed in pre-cleaned Al foils and placed, with the chemical standards, inside aluminium irradiation vessels, specially developed for use in the IEA-R1 reactor. Samples and standards were irradiated for 8 h at a thermal flux of about 10^{16} nm^{-2} s^{-1}. The cooling period before the radiochemical procedure was about 48 h.

Table 1 Radioisotopes used and their nuclear data

Radioisotope	Production	Half-life	Energy/keV
^{198}Au	$^{197}Au(n,\gamma)$	2.7 d	411.8
^{109}Pd	$^{108}Pd(n,\gamma)$	13.5 h	88.0
^{199}Au	$^{198}Pt(n,\gamma,\beta^-)$	3.15 d	158.3
^{192}Ir	$^{191}Ir(n,\gamma)$	74.4 d	316.5

Radiochemistry

Aqua regia *leaching*

The irradiated sample was transferred into a beaker with 6 ml of freshly prepared *aqua regia* and carriers. The resulting solution was heated to boiling, evaporated to dryness and a further 6 ml of *aqua regia* were added. This procedure was repeated three times. The resulting solution was filtered through Whatman No. 42 filter-paper (4 cm diameter). The filtrate was evaporated to dryness and the residue was dissolved in concentrated HCl, to eliminate nitrates, and finally was dissolved in 10 ml of dilute HCl (1 + 2).

Sintering with sodium peroxide

The procedure employed was described by Enzweiler[12] for the determination of Ti, Cr, Al, Fe and Mg in chromitites. The irradiated sample was transferred into a nickel crucible and was throughly mixed with 1.5 g of sodium peroxide. After this, 0.75 g of sodium peroxide was added to the mixture. The crucible was covered with a nickel lid and introduced into a cold furnace. The temperature was raised to 200 °C for 30 min and then to 480 °C for 90 min. After sintering had finished, the crucible was transferred into a 400 ml beaker, with the addition of about 60 ml of warm water (60 °C), 10 ml of dilute HCl (1 + 2) and carriers. The crucible was removed from the beaker and was rinsed with distilled water.

Tellurium coprecipitation

The resulting solutions from the two procedures described for the chemical attack of the rock were boiled and 2 ml of Te solution were added to the beaker. Then, 10 ml of tin(II) chloride solution were added to precipitate a black cloud of metallic Te. The solution was boiled to coagulate the precipitate and then 1 ml of tin(II) chloride solution was added and the solution was boiled for 5 min. The precipitate was filtered onto a 4 cm Millipore filter (RA) and was rinsed with dilute HCl (1 + 9). The precipitate was dried under an infrared lamp and sealed in a plastic envelope.

Counting and gamma spectrometry

The measurements of the induced gamma-ray activity were carried out in a GMX, hyper-pure Ge detector, connected to an ADCAM 100 Multichannel Buffer (EG & G Ortec) and to a personal computer. The resolution (FWHM) of the system was 1.90 keV for the 1332 keV gamma ray of ^{60}Co. The gamma-ray spectra were processed by using the program VISPECT, developed at IPEN by Piccot,[13] from Saclay, France. This program locates peak positions and calculates gamma-ray energies and net areas. The counting times were about 10 h for the samples and 1 h for the chemical standards. The radioisotopes measured and their nuclear data are presented in Table 1. The determination of Pt was performed with the radioisotope ^{199}Au, produced by the nuclear reaction ^{198}Pt (n,γ,β^-) ^{199}Pt. The interference of Au, by the reaction

Table 2 Concentrations (mg kg^{-1}) of gold, palladium, platinum and iridium in the reference materials SARM-7 and CHR-Pt+. Number of measurements (n) = 5; results presented correspond to the mean ± standard deviation

	CHR-Pt+			SARM-7		
Element	*Aqua regia* leaching	Sintering (Na_2O_2)	Proposed values[11]	*Aqua regia* leaching	Sintering (Na_2O_2)	Certified values[14]
Au	4.3 ± 0.3	3.8 ± 0.3	4.3	0.29 ± 0.02	0.26 ± 0.02	0.31 ± 0.015
Pd	63 ± 4	84 ± 4	80.8	1.40 ± 0.09	1.4 ± 0.1	1.53 ± 0.032
Pt	34 ± 3	55 ± 4	58	3.21 ± 0.09	3.41 ± 0.03	3.74 ± 0.045
Ir	0.13 ± 0.07	5.6 ± 0.5	6.2	0.032 ± 0.003	0.076 ± 0.009	0.074 ± 0.012

$^{197}Au(2n,\gamma)$ ^{199}Au, was corrected for by the irradiation of a pure gold source, from which the production of ^{199}Au from Au could be evaluated. According to Crocket and Cabri,[5] only ultramafic rocks are matrices in which the $(2n,\gamma)$ interference is negligible.

Results and Discussion

The results obtained for the reference materials SARM-7 and CHR-Pt+, and also certified and proposed values,[11,14] are presented in Table 2. The reproducibility of the method was tested by five replicate analyses of the sample, and the errors associated with the data represent one standard deviation.

It can be observed that for Au, *aqua regia* leaching gave more accurate results for the two reference materials analysed, showing relative errors between 0 and 6% and good precision (average relative standard deviation s_r = 7%), confirming the efficiency of *aqua regia* to extract Au from geological samples.[2,9]

For Pd, both chemical treatments gave similar results for SARM-7 (relative errors less than 10% and $s_r \approx 7\%$), but for CHR-Pt+ much better results were obtained when sintering was used, the relative errors for recommended values falling from 22% to 4%.

For Ir and Pt, the improvement in the results was remarkable when sintering was applied, for both SARM-7 and CHR-Pt+. In the latter, almost no Ir was extracted from the rock by partial attack with *aqua regia*, whereas an almost quantitative yield (more than 90%) was achieved by using the sintering procedure. These data agree with results reported by Gowing and Potts[2] and may be explained by the fact that dominant minerals containing Pt and Ir in CHR-Pt+ are insoluble in *aqua regia*. These observations indicate that the solubility of some PGE minerals may be a limiting factor for the use of *aqua regia* for PGE determination. It must be noted that, in the analysis of CHR-Pt+ using *aqua regia* leaching and flame atomic absorption spectrometry, Potts *et al.*[11] reported a higher concentration for Pt (45.17 μg g^{-1}), indicating an improved leaching efficiency.

The experimental quantitative detection limits for the analytical conditions described, in the analysis of SARM-7 when sintering with sodium peroxide and Te precipitation were used, calculated considering the Currie criterion,[15] were 0.1 μg kg^{-1} of Au, 10 μg kg^{-1} of Pd, 20 μg kg^{-1} of Pt and 0.2 μg kg^{-1} of Ir. The detection limits (L_d) were calculated according to the equation

$$L_d = 2.71 + 4.65\sqrt{B}$$

where B is the measured background area of a specific energy range in the gamma-ray spectra.

It is concluded that sintering with sodium peroxide followed by coprecipitation with tellurium seems to be more appropriate for the determination of Pd, Pt and Ir. Gold was successfully determined by using *aqua regia* leaching.

The sintering procedure was applied to the analysis of chromitite CHR-Bkg, and the results obtained for four determinations are given in Table 3, together with proposed values. For Pt and Pd, substantial discrepancies are observed between replicate analyses, with outliers in relation to proposed values, mainly for Au and Pt. Potts *et al.*[11] also reported 'gross' outliers for Au and Pd in CHR-Bkg, probably owing to minerological effects, and recommended the analysis of 10 g sub-samples, in duplicate, for the determination of Au and PGEs. For Ir, however, the results obtained showed good agreement with proposed values and relative standard deviations between replicate analyses of about 3%, which may indicate smaller differences in mineralogical behaviour for this element.

Table 3 Concentrations (μg kg^{-1}) of gold, palladium, platinum and iridium in the reference material CHR-Bkg. Number of measurements (n) = 4; results presented correspond to the mean ± standard deviation

Element	Sintering (Na_2O_2)	Proposed values[11]
Au	6.6 ± 0.9	28
Pd	43 ± 16	70
Pt	77 ± 12	50
Ir	31.0 ± 0.9	28

Compared with fire assay-based techniques, the procedure has the advantage of avoiding contamination, with strict control of reagent purity, being a relatively simple and rapid analytical procedure. The time consumed from the beginning of the rock attack until the recording of the gamma-ray spectra is about 20 h and several samples may be treated at the same time if gamma-ray spectrometers are available. Nevertheless, the milligram-sized samples (250 mg) may cause errors, mainly in the determination of gold, owing to the heterogeneous distribution in PGE minerals. The proposed method may be used in the determination of iridium anomalies in studies to associate the impact of an extra-terrestrial object with extinctions at the Cretaceous–Tertiary boundary, as typical iridium anomalies lie in the range 1–100 μg kg^{-1}.[16] For the particular case of Ir, owing to its relatively long half-life, detection limits may be improved by taking a larger amount of sample for analysis and applying the radiochemical procedure some days after irradiation, to avoid activity from short-lived radioisotopes.

The whole procedure is simple and rapid, giving accurate and precise results, and can be applied to different matrices in which minerals of PGEs are associated. Results obtained for Au, Pt, Pd and Ir in the proposed geostandards CHR-Pt+ and CHR-Bkg are a contribution to concentration values.

FAPESP is acknowledged for financial support.

References

1 Alvarez, I. W., Alvarez, W., Asaro, F., and Michel, H. V., *Science*, 1980, **208**, 1905.
2 Gowing, C. J. B., and Potts, P. J., *Analyst*, 1991, **116**, 773.
3 Cocherie, A., Volfinger, M., and Meyer, G., *J. Radioanal. Chem., Articles*, 1987, **113**, 133.
4 Haffty, J., Riley, L. B., and Goss, W. D., *U.S. Geol. Surv. Bull.*, 1977, No. 1445.
5 Crocket, J. H., and Cabri, L. J., in *Platinum-Group Elements: Mineralogy, Geology and Recovery*, ed. Cabri, L. J., The Canadian Institute of Mining and Metallurgy, Ontario, 1981, Special Volume 23, pp. 71–79.
6 Asif, M., and Parry, S., *Analyst*, 1989, **114**, 1057.
7 Shazali, I., Van't Dack, L., and Gijbels, R., *Anal. Chim. Acta*, 1987, **196**, 49.
8 Stone, W. E., and Crocket, J. H., *Chem. Geol.*, 1993, **106**, 219.
9 Sighinolfi, G. P., Gorgoni, C., and Mohamed, A. H., *Geostand. Newsl.*, 1984, **8**, 25.
10 Stockman, H. W., *J. Radioanal. Chem.*, 1983, **78**, 307.
11 Potts, P. J., Gowing, C. J. B., and Govindaraju, K., *Geostand. Newsl.*, 1992, **16**, 81.
12 Enzweiler, J., *Geochim. Brasil.*, 1990, **4**, 119.
13 Piccot, D., personal communication.
14 Steel, T. W., Levin, J., and Copelowitz, I., *Nat. Inst. Metall. Repub. S. Afr. Rep.*, 1975, No. 1696.
15 Currie, L. A., *Anal. Chem.*, 1968, **40**, 586.
16 Millard, H. T., Jr., *J. Radioanal. Chem., Articles*, 1987, **113**, 125.

Paper 4/05892E
Received September 26, 1994
Accepted December 8, 1994

Neutron Activation Analysis Investigation of the Composition and Geochemical Peculiarities of Lake Baikal Bottom Sediments*

A. I. Bulnayev

Irkutsk State Technical University, Lermontov St. 83, 664074 Irkutsk, Russia

Concentrations of 18 trace elements were determined in 40 samples of bottom sediments of Lake Baikal by instrumental neutron activation analysis. The absence of anthropogenic pollution of sediments by minor elements was found. The main geochemical peculiarities of Lake Baikal bottom sediments are enrichment by light rare earth elements (REEs) and a deficit of caesium and tantalum. The distribution of REEs in Lake Baikal bottom sediments is of a specific type that is intermediate between riverine and sea types.

Keywords: Lake Baikal; bottom sediment; neutron activation analysis; trace element; anthropogenic pollution

Introduction

Lake Baikal is a unique phenomenon in nature. The constant interest of investigators in Lake Baikal is conditioned by its numerous peculiarities: exceptional cleanliness of the water, diversity of its flora and fauna, great depth, morphology of the depression, character of its seismic activity and others.

Different research centres and scientific institutes in Irkutsk, Novosibirsk and Ulan-Ude deal with the study of Baikal but more successful in this direction is the work of the Limnological Institute of the Siberian Branch of the Russian Academy of Sciences (Irkutsk). At the instigation of this Institute, the Baikal International Centre for Ecological Research (BICER) was created in 1991, its founding members being Russia, USA and Japan.

Complete and accurate information about the history and development of the lake and its depression can be obtained by the analysis of sediments. Recently this problem has been studied in depth.[1] Detailed maps of sediments were compiled on the basis of special surveys performed on the lake bottom. Lifted from the bottom, cores of the silt were studied in detail in order to obtain information about the substance of the sediments, sources, conditions of formation, *etc.*

The modern stratum of the bottom sediments of Lake Baikal and the chemical composition of its macrocomponents have been studied more or less completely. However, the microcomponents composition has been very poorly studied.

In connection with the problem of anthropogenic pollution of the Lake Baikal ecosystem, it is important to study the composition and distribution of trace elements in bottom sediments of the lake. The solution of this task will help to establish the presence or absence of anthropogenic pollution of sediments by minor elements. If the answer is positive, it may be possible to evaluate the pollution intensity and the area of its distribution. If there is no pollution, investigation of trace elements in Lake Baikal bottom sediments should make it possible to establish its geochemical peculiarities reflecting the character of the processes of sediment accumulation in the lake.

Publications on trace element concentrations in water and sediments of Lake Baikal are inadequate, owing to the complexity of the solution of this problem.

The concentrations of minor elements in the surface stratum of bottom sediments of Southern Baikal were determined for the first time in 1954.[2] There were 12 elements: Be, Pb, Cu, Co, Ni, Zr, Ga, Cr, V, Ba, Sr and Ti. These elements were found in different concentrations in all types of sediments. Three elements (As, Se and Mo) were found only in some samples.

Later, investigations of Baikal sediments by the same spectral analysis made it possible to determine concentrations of minor elements, decreasing in the order Ti, Sr, Zr, V, Cr, Ga, Pb, Co, Ni, La, Y, Sc.[3] Copper, Be, As and Se, mentioned previously,[2] were not found at all.

In 1982, Goldyrev[1] published results of the spectral determination of 46 elements in Baikal sediments. In all analysed samples collected at 21 stations, the following elements were determined: Ti, Mn, Ba, Sr, Zr, Zn, V, Cu, Ni, Co, Cr, Ga, Y, Be, Pb, Sc. In several samples P, Li, Nb, Ag, Sn were found. Bismuth was determined in one sample only and Ta, In, W, As, Sb, Ge, Hf, Ce, La, Gd, Ir, Pt, Th and U were not found in any sample.

From the results, Goldyrev concluded that trace elements are present in the surface layer of Baikal sediments. However, he did not give any explanation for the huge fluctuations of element concentrations. It should be noted that for the majority of trace elements originally determined,[1] their concentrations were at the level of the sensitivity of the spectral analysis applied; the accuracy of determinations became extremely low and wide dispersion of the results occurred.

Hence, to solve the task of the investigation of Baikal bottom sediment composition it is necessary to use a more sensitive analytical method than emission spectral analysis. Such a method is neutron activation analysis. Its main advantage is the combination of high sensitivity of element determination and the accuracy of results.[4] At present in Russia neutron activation analysis is not widely used in geochemical investigations. However, this method has great possibilities for the solution of geochemical problems because it can determine many trace elements simultaneously at the level of or below the average crustal abundances of the elements (Clark concentrations).[5]

The Laboratory of Activation Analysis of Irkutsk State Technical University is the only one to have developed this method in the region of Eastern Siberia. The difficulty with the technique of instrumental neutron activation analysis (INAA) is the great distance between the nuclear reactor (in

* Presented at Geoanalysis 94: An International Symposium on the Analysis of Geological and Environmental Materials, Ambleside, England, September 18–22, 1994.

St. Petersburg) and the spectrometric laboratory (in Irkutsk). Therefore, we use an intensive flux of reactor neutrons to irradiate samples and long-lived radionuclides of elements to determine concentrations. Metrological characteristics of the INAA technique were obtained as the result of a detailed study of Russian and international geochemical reference samples.[6,7]

In 1991 at the Institute of Geochemistry, Siberian Branch of the Russian Academy of Sciences, a standard sample of deep-water bottom silt from lake Baikal BIL-1, was created. It is used as a reference sample for the evaluation of the pollution of the lake ecosystem.[8]

The INAA of standard sample BIL-1 carried out in a process of attestation allowed the determination of 19 trace elements and iron.[9] The results of INAA for reference sample BIL-1 show that this method allows one to determine the concentrations of elements in the bottom silt of Baikal that cannot be determined by spectral analysis, namely Ce, Cs, Eu, Gd, Hf, Ho, Lu, Nd, Sb, Sm, Ta, Tb, Th, Tm, U and Yb.

Table 1 Characteristics of samples of Baikal bottom sediments obtained for INAA

No. of station	Depth of bottom/m	Sampling layer/cm	Sample code	Characteristic
Samples from region of BPPP (collection of Limnology Institute)—				
3	180	0–3	3-1	Silt
		3–8	3-2	Silt
15	520	0–5	15-1	Silt
		5–10	15-2	Silt
21	800	0–5	21-1	Silt
		5–10	21-2	Silt
25	973	0–5	25-1	Silt
		5–10	25-2	Silt
		20–25	25-3	Clay
26	1025	0–5	26-1	Silt
		5–10	26-2	Silt
28	1210	0–5	28-1	Sand
		5–10	28-2	Find sand with mica
29	1130	0–5	29-1	Sand
		5–10	29-2	Fine sand with mica
		15–20	29-3	Silt
30	43	0–5	30-1	Silt
		5–10	30-2	Fine sand with mica
31	30	0–5	31-1	Sand
		5–10	31-2	Fine sand with mica
Samples from regions remote from BPPP (collection of Institute of Geochemistry)—				
278	1370	14–18	278-1	Silt
		60–61	278-2	Silt
		162–175	278-3	Silt
		255–260	278-4	Silt
38	250	100	38-1	Silt
		101	38-2	Silt
32	1230	76	32-1	Silt
		78	32-2	Silt
28/1	50	68	28/1-1	Silt
		69	28/1-2	Silt
27	640	64	27-1	Silt
		67	27-2	Silt
22	890	51	22-1	Silt
		52	22-2	Silt
2	18	2	2-1	Silt
		3	2-2	Silt
9	190	17	9-1	Silt
		18	9-2	Silt
18	260	29	18-1	Silt
		30	18-2	Silt

Thus, the results of multi-element INAA of standard sample BIL-1 allowed us to formulate a study for the investigation of bottom sediments of Lake Baikal by INAA in order to evaluate the anthropogenic pollution by trace elements and to establish its geochemical peculiarities reflecting the character of the sediment accumulation in the lake.

The basis of the investigation was a detailed sampling of Baikal sediments during a number of special expeditions in 1991–92. In 1991 a Russian–American expedition took samples from the southern depression of the lake, the shore of which is subjected to maximum industrial effect. The aim of this work was to study the influence of a pulp and paper plant (PPP) in the town of Baikalsk on the ecosystem of the southern part of the lake.

Experimental

Characteristics of Samples

A series of samples of Baikal bottom sediments from the collection of the Limnological Institute and Institute of Geochemistry, Siberian Branch of the Russian Academy of Sciences, was used for INAA (Table 1). Sites of sampling (stations) are shown in Fig. 1.

Samples of bottom sediments from the region of the Baikalsk PPP (BPPP) were obtained by the members of the Russian–American expedition in summer 1991 with the help of an underwater submersible. At each station samples were collected from several layers of sediments from the surface of the bottom in order to estimate anthropogenic pollution of sediments. Samples of sediments from regions remote from BPPP were collected by the expedition of the Institute of Geochemistry in 1991–92 from onboard a research vessel using special immersion tubes.

Two international geochemical standards, andesite AGV-1 (USA) and granite GM (Germany),[10] and a Russian standard

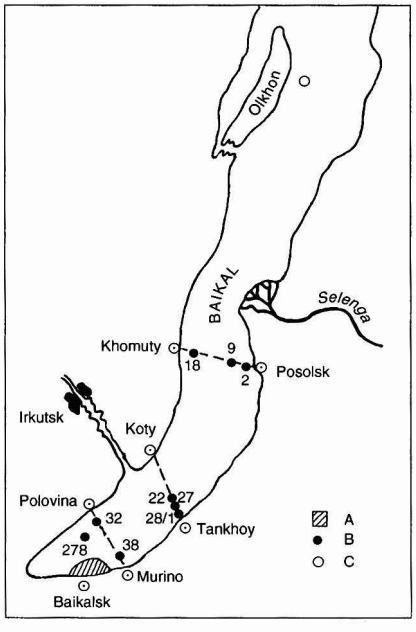

Fig. 1 Scheme of bottom sediment sampling regions. A, Region of Baikalsk pulp and paper plant (BPPP); B, stations remote from the BPPP; and C, point of sampling for reference material BIL-1.

sample, akaline granite SG-3,[11] were used as multi-element monitors.

Samples and Irradiation

Samples of sediments collected for INAA were dried at about 100 °C. Precisely weighed aliquots of each sediment sample and the three monitor samples, AGV-1, GM and SG-3, were placed in vials of spectrally pure quartz and sealed. The purity of the quartz was established by irradiation of an empty vial simultaneously with the samples. Each sediment portion was about 50 mg and monitor portions 100 mg. The sealed vials were placed in a nuclear reactor for irradiation. About 60 vials containing the samples of sediments and monitors were irradiated in the reactor core simultaneously. To ensure determination of the maximum number of elements, the irradiation period was 100 h at a flux of thermal neutrons of about 5×10^{13} n cm^{-2} s^{-1}. Samples and monitors were in nearly identical radial and vertical positions with respect to the reactor core and the sample container was rotated to ensure a uniform neutron flux.

Equipment and Measurements

Two semiconductor detectors were used to measure the spectra of irradiated samples, a BDER-2K type made of highly pure germanium (HPGe) with an analytical sensitive area of 20 mm^2, and a DGDK-40B type, coaxial Ge(Li) detector with a 35 cm^3 volume sensitivity sphere. The HPGe detector with an energetic resolution of 0.530 keV for the 121.8 keV ^{152}Eu gamma-line covers the energy range from 20 to 150 keV. The efficiency of registration of gamma-ray by the HPGe detector in this energy range varies from 100 to 1%. The Ge(Li) detector has a resolving power of 2.7 keV for the 1332.5 keV ^{60}Co line and covers the energy range from 150 keV to 2 MeV with an efficiency of detection from 100 to 3%.

Spectra of the gamma-radiation from the activated samples were observed with a 4096-channel pulse analyser (NTA-1024, Hungary) equipped with a magnetic tape drive. A detailed amplitude analysis allowed us to measure the energy of peaks with an error of ±0.1 keV in spectra registered by the HPGe detector, and with an error of less than ±0.5 keV in spectra registered by the Ge(Li) detector. The results obtained allowed complete data decoding. The measuring time of the gamma-radiation spectra varied from 500 to 2000 s, depending on sample activity. The statistical error associated with the number of counts in the peaks of analytical lines was within a few per cent.

Data from the analyser memory were processed by the EMG-666B computer (Hungary) included in the measuring equipment system. The amount of element in the sample was calculated from the ratio of the peak area in the sample spectrum to the area of corresponding peak in the monitor spectrum. The full area method for the determination of analytical peak area was used.

The irradiated container with the Baikal bottom sediments was delivered to the laboratory on the 12th day after the irradiation was stopped. The samples were etched in acidic solution to remove any surface pollution, then washed with distilled water. This was followed by the first series of gamma-spectra measurements to determine concentrations of elements with a half-life period within a few days. Later, each sample was measured repeatedly following different cooling times to promote the best conditions for the calculation of a particular group of element concentrations.

Results and Discussion

Check Analysis

The use of three geostandards, AGV-1, GM and SG-3, studied in detail makes it possible to evaluate the errors of the INAA technique. Results of the check analysis are presented

Table 2 Results of INAA of control samples

					Element concentration (ppm)				
						GM		SG-3	
Nuclide	Half-life	Time after irradiation/d	Energy/keV	Detector*	AGV-1 Att.†[10]	Att.†[10]	INAA	Att.†[11]	INAA
^{141}Ce	32.51 d	75	145.41	1	67	65 ± 7.2	66	90 ± 10	91
^{60}Co	5.26 yr	120	1332.5	2	15.3	3.7 ± 0.73	4.4	1.3 ± 0.3	1.1
^{51}Cr	27.8 d	50	320.1	2	10.1	11 ± 1.6	10.4	31 ± 3	26.1
^{134}Cs	2.05 yr	120	795.8	2	1.28	8.1 ± 0.54	8.1	4.5 ± 0.5	4.6
^{152}Eu	12.7 yr	120	121.78	1	1.64	0.6 ± 0.04	0.6	0.4 ± 0.1	0.4
^{153}Gd	242 d	75	97.52	1	5.0	(5.2)	—	—	4.0
^{181}Hf	42.45 d	75	133.2	1	5.1	5.1 ± 0.35	5.1	12 ± 2	12.0
^{166}Ho	26.9 h	12–13	80.60	1	0.67	(1.0)	1.33	—	1.18
^{177}Lu	6.74 d	12–13	208.34	1	0.27	0.4 ± 0.01	0.45	0.9 ± 0.2	0.91
^{147}Nd	11.06 d	12–13	91.10	1	33	30 ± 4.7	30.0	50 ± 10	50.4
^{124}Sb	60.4 d	75	1691.0	2	4.3	(0.51)	0.61	(0.5)	0.56
^{46}Sc	83.9 d	120	889.3	2	12.2	4.8 ± 0.73	5.13	4.6 ± 0.8	3.94
^{153}Sm	47.1 h	12–13	103.18	1	5.9	4.9 ± 0.50	—	10 ± 1	10.4
^{182}Ta	115.1 d	120	1221.4	2	0.90	1.7 ± 0.46	1.60	1.1 ± 0.2	1.17
^{160}Tb	72.1 d	75	86.79	1	0.70	0.7 ± 0.28	—	1.7 ± 0.3	1.46
^{170}Tm	134.2 d	75	84.26	1	0.34	—	—	—	0.71
Th (^{233}Pa)	27.4 d	50	311.9	2	6.5	36 ± 3.1	39.8	8 ± 1	7.23
U (^{239}Np)	2.35 d	12–13	106.30	1	1.92	6.4 ± 0.97	—	1.8 ± 0.3	1.65
^{169}Yb	31.83 d	75	63.11	1	1.72	3.1 ± 0.33	3.25	7 ± 1	6.96
^{59}Fe	45.64 d	75	152.33	1	4.73‡	2.01 ± 0.2‡	1.94‡	—	4.41‡

* Detector: 1 = HPGe; 2 = Ge(Li).
† Att. = attested value.
‡ Fe concentrations in %.

in Table 2. The check was carried out by determining of 19 trace elements and iron in GM and SG-3 standard samples, the monitor being AGV-1. In addition to the INAA data we have listed in Table 2 certified concentrations of elements and energies of analytical lines, half-lives of nuclides, time delay after irradiation and recommended detectors.

The results in Table 2 show that there is good agreement between the INAA results and certified values for most elements indicating a high accuracy of our INAA technique.

It should be noted that in the irradiation spectra of AGV-1, GM and SG-3, which were measured with the Ge(Li) detector, weak peaks of ^{85}Sr, ^{86}Rb, ^{95}Zr and ^{140}La nuclides were observed. However, owing to a large statistical error in measuring these peak areas and to the low precision of determinations, lanthanum, rubidium, strontium and zirconium abundances were not determined in Baikal bottom sediments.

In the gamma-ray spectra of the monitors and standard sample BIL-1 that were registered by the HPGe detector in the first series of measurements (cooling time 12–13 d), clean peaks of analytical lines of short-lived nuclides were observed (^{166}Ho, ^{239}Np, ^{153}Sm).

Analysis of Sediments

Results of INAA of Lake Baikal bottom sediments are given in Tables 3–5 and Fig. 2.

Table 3 shows that bottom sediments of Lake Baikal, on the whole, have more or less similar concentrations of trace elements. This allowed us to use mean values of element concentrations for certain groups of samples for the interpretation of INAA data.

Mean arithmetic values of element concentrations in bottom sediments from the region of BPPP and their standard deviations are given in Table 4. The data show that trace element concentrations in the near-surface layer of sediments almost coincide with their concentrations in samples from deeper layers of sediments for both silts and sands. This allows us to conclude that there is no anthropogenic pollution by trace elements of bottom sediments of Lake Baikal in the

Table 3 Results of INAA of Lake Baikal bottom sediments

	Concentration of element (ppm)																	
Samples	Ce	Nd	Sm	Eu	Gd	Tb	Ho	Tm	Yb	Lu	U	Th	Cr	Co	Cs	Ta	Hf	Ba
3-1	85	42	8.52	1.69	5.53	1.04	1.73	0.40	3.44	0.44	5.80	5.98	107	22.9	3.49	0.51	5.92	572
3-2	87	45	8.83	1.76	5.66	1.15	1.29	0.44	3.07	0.48	6.39	5.78	105	36.7	3.90	1.15	5.75	575
15-1	67	35	6.17	1.61	5.16	1.03	0.93	0.47	2.78	0.46	2.93	6.12	63.9	28.9	3.51	1.35	5.06	
15-2	81	42	6.69	1.67	4.87	1.00	0.89	0.51	3.73	0.32	2.35	2.88	37.0	25.3	3.15	1.09	5.42	343
21-1	81	39	7.66	1.60	6.79	1.08	1.21	0.39	3.52	0.52	6.62	5.97	103	31.7	4.17	0.50	5.54	403
21-2	97	51	8.36	1.75	5.34	1.28	1.64	0.40	3.53	0.51	4.17	6.81	89.6	29.5	3.32	1.03	6.04	587
25-1	137	70	12.4	1.70	5.46	1.48	1.31	0.41	3.22	0.37	5.94	10.0	84.0	30.7	4.07	1.12	5.55	487
25-2	86	40	7.60	1.76	6.26	1.22	1.09	0.42	2.84	0.47	5.26	8.95	85.7	30.0	5.18	0.82	4.92	
25-3	86	41	7.54	1.79	6.51	1.09	1.09	0.42	2.81	0.40	6.07	11.1	79.1	31.9	4.18	1.07	5.64	
26-1	37	19	3.31	1.22	4.06	0.51	0.44	0.26	2.23	0.29	1.08	3.78	111	18.0	1.49	0.82	3.85	1629
26-2	62	46	6.05	1.48	5.97	0.80	0.77	0.30	2.98	0.33	4.86	4.05	81.8	26.1	2.96	0.83	4.57	360
28-1	53	25	4.88	1.29	5.72	0.65	0.77	0.35	2.46	0.45	2.79	5.68	311	23.3	2.78	1.01	3.97	
28-2	48	26	3.81	1.17	5.55	0.60	0.51	0.31	2.20	0.29	1.81	3.73	262	24.8	2.67	0.68	3.90	974
29-1	49	27	5.02	1.28	4.76	0.75	0.70	0.40	2.60	0.34	2.05	6.37	267	28.5	2.74	0.89	5.17	
29-2	48	24	4.17	1.13	4.19	0.67	0.47	0.27	1.86	0.23	1.67	2.92	83.1	18.8	1.85	0.72	4.25	510
29-3	58	30	5.81	1.43	3.78	0.94	0.88	0.33	3.09	0.37	2.50	1.64	82.4	26.8	2.85	0.68	5.06	273
30-1	66	35	6.04	1.54	4.64	1.01	1.09	0.31	2.85	0.38	1.75	2.75	94.1	20.9	1.50	0.80	5.40	271
30-2	62	31	5.92	1.48	7.13	0.90	1.21	0.51	2.91	0.40	2.80	2.26	145	26.9	3.24	1.13	6.11	476
31-1	60	35	6.33	1.47	6.74	0.88	0.75	0.46	2.83	0.45	3.58	2.44	64.7	24.5	3.08	1.02	5.21	570
31-2	70	35	7.48	1.56	6.18	0.91	0.88	0.39	3.22	0.45	4.57	4.68	128	27.6	3.16	0.81	5.85	
278-1	85	40	7.35	1.57	8.10	1.10	0.99	0.58	3.22	0.30	4.67	4.77	87.4	24.2	4.59	1.41	5.29	563
278-2	96	49	9.53	1.87	7.32	1.05	0.95	0.54	3.65	0.53	11.7	8.15	83.5	29.6	6.25	0.94	5.86	561
278-3	101	54	9.80	1.76	6.71	1.25	1.09	0.45	3.80	0.47	5.88	6.79	64.1	31.0	5.47	1.11	5.85	460
278-4	83	35	6.22	1.61	5.42	0.99	0.86	0.45	3.31	0.36	2.52	4.87	62.9	27.0	5.33	1.11	5.06	
38-1	88	41	7.58	1.56	7.04	1.07	1.17	0.40	3.33	0.43	5.78	7.41	63.3	25.9	4.95	0.80	5.89	505
38-2	84	46	7.69	1.60	7.23	1.06	1.34	0.45	3.37	0.41	5.51	9.83	60.8	22.8	5.93	1.28	5.33	296
32-1	272	109	21.0	1.99	8.64	2.88	1.54	0.86	7.64	0.70	6.49	51.0	95.0	21.4	2.85	1.53	20.5	1714
32-2	175	91	14.9	1.93	9.05	2.27	1.63	0.79	5.56	0.59	5.06	32.6	119	18.0	3.56	1.27	15.4	991
28/1-1	98	45	9.18	1.62	5.17	1.18	1.03	0.47	4.13	0.54	3.29	11.6	83.8	20.2	3.75	1.15	7.51	
28/1-2	85	41	7.21	1.56	5.93	1.00	1.12	0.46	3.02	0.43	2.51	7.79	41.7	18.9	3.97	0.94	7.23	304
27-1	83	44	8.79	1.60	4.43	1.13	1.09	0.34	3.67	0.47	3.45	11.5	45.5	16.9	3.69	0.81	6.29	1855
27-2	22	10.5	2.00	0.89	2.68	0.29	0.42	0.15	1.26	0.19	1.20	2.76	37.0	4.02	1.03	0.37	2.87	671
22-1	89	36	7.01	1.52	5.88	0.99	0.73	0.48	2.74	0.37	3.75	4.69	37.5	24.0	5.24	1.30	5.34	701
22-2	85	39	7.03	1.53	5.19	1.00	0.93	0.47	2.77	0.32	3.57	4.32	28.6	25.3	5.06	1.16	4.91	290
2-1	77	39	6.85	1.52	4.88	0.92	0.92	0.41	2.98	0.35	4.90	5.68	47.7	24.4	4.35	0.86	4.78	
2-2	76	33	6.24	1.42	4.79	0.95	0.85	0.42	2.91	0.48	2.39	5.82	33.3	16.3	3.56	1.02	5.67	401
9-1	86	38	7.01	1.41	6.43	0.99	1.07	0.51	2.77	0.40	7.10	14.1	52.9	21.8	5.66	0.93	4.56	1666
9-2	81	36	6.97	1.40	5.14	0.98	0.75	0.38	3.48	0.46	5.21	9.32	52.7	19.5	5.86	1.09	4.46	271
18-1	96	38	8.40	1.89	7.02	1.05	0.89	0.44	2.95	0.54	2.59	10.6	27.6	11.8	2.38	1.09	9.23	649
18-2	96	46	7.68	1.69	5.27	1.05	0.83	0.43	2.84	0.56	3.36	20.8	43.4	7.65	2.46	0.86	16.1	1340

region of BPPP. The BPPP has been operating for about 30 years and contamination of lake sediments by its effluent probably occurred during that period. The rate of sediment accumulation in Lake Baikal according to data from different workers varies from 0.04[12] to 1.00 mm year^{-1}.[13] With this range of accumulation rate samples collected from depths below 5 cm of the sediment surface cannot contain anthropogenic contamination.

Comparative analysis of element concentrations in different facies of sediments shows that silts, on the whole, have considerably greater concentrations of light lanthanides (Ce and Nd) than sands. Concentrations of intermediate rare earth elements (REE) (Sm, Eu, Tb, Ho) are slightly higher in silts than in sands, and heavy REE (Tm and Lu) concentrations in both facies of sediments are almost identical. The mean concentrations of Ta, Hf, Cs, Co, Th and Ba are similar. However, there is a difference in the concentrations of U and especially of Cr for silts and for sands. It should be noted that for coarse-grained sands from the near-surface layer of sediments a higher mean concentration of chromium (214 ppm) with a larger relative standard deviation (61.2%) was determined. For the fine sands with mica from deeper layers of sediments these parameters were lower (155 ppm and 49.0%, respectively). Therefore, the origin of the chromium anomaly in Lake Baikal bottom sediments is obvious. Fragments of chromium-containing minerals in the river-wash that enters the lake with the flow give such an anomaly.

Anomalous Samples

Comparison of the data in Tables 3 and 4 shows some anomalous samples, *e.g.*, samples collected at station No. 32,

Table 4 Concentrations of trace elements (ppm) in bottom sediments from the region of BPPP

Element	Silts from surface layer ($n = 6$)*	Silts from deeper layers ($n = 6$)†	Silts from region of BPPP, average ($n = 12$)	Sands from surface layer ($n = 3$)‡	Sands from deeper layers ($n = 4$)§	Sands from region of BPPP, average ($n = 7$)
Ce	79 ± 33	79 ± 15	79 ± 25	54 ± 6	57 ± 11	56 ± 8
Nd	40 ± 17	42 ± 7	41 ± 12	29 ± 5	29 ± 5	29 ± 5
Sm	7.4 ± 3.1	7.2 ± 1.2	7.3 ± 2.2	5.4 ± 0.8	5.4 ± 1.7	5.4 ± 1.3
Eu	1.6 ± 0.2	1.6 ± 0.2	1.6 ± 0.2	1.4 ± 0.1	1.3 ± 0.2	1.3 ± 0.2
Gd	5.3 ± 0.9	5.3 ± 0.9	5.3 ± 0.9	5.7 ± 1.0	5.8 ± 1.2	5.8 ± 1.0
Tb	1.0 ± 0.3	1.1 ± 0.2	1.1 ± 0.2	0.8 ± 0.1	0.8 ± 0.2	0.8 ± 0.1
Ho	1.1 ± 0.4	1.1 ± 0.3	1.1 ± 0.4	0.7 ± 0.1	0.8 ± 0.4	0.8 ± 0.3
Tm	0.4 ± 0.1	0.4 ± 0.1	0.4 ± 0.1	0.4 ± 0.1	0.4 ± 0.1	0.4 ± 0.1
Yb	3.0 ± 0.5	3.2 ± 0.4	3.1 ± 0.4	2.6 ± 0.2	2.6 ± 0.6	2.6 ± 0.5
Lu	0.4 ± 0.1	0.4 ± 0.1	0.4 ± 0.1	0.4 ± 0.1	0.3 ± 0.1	0.4 ± 0.1
U	4.0 ± 2.4	4.3 ± 1.6	4.1 ± 1.9	2.8 ± 0.8	2.7 ± 1.3	2.8 ± 1.0
Th	5.8 ± 2.5	5.0 ± 2.7	5.4 ± 2.5	4.8 ± 2.1	3.4 ± 1.1	4.0 ± 1.6
Cr	94 ± 18	80 ± 23	87 ± 21	214 ± 131	155 ± 76	180 ± 98
Co	25.5 ± 5.7	29.1 ± 4.2	27.3 ± 5.1	25.4 ± 2.7	24.5 ± 4.0	24.9 ± 3.3
Cs	3.0 ± 1.2	3.6 ± 0.9	3.3 ± 1.1	2.9 ± 0.2	2.7 ± 0.6	2.8 ± 0.5
Ta	0.9 ± 0.3	0.9 ± 0.2	0.9 ± 0.3	1.0 ± 0.1	0.8 ± 0.2	0.9 ± 0.2
Hf	5.2 ± 0.7	5.3 ± 0.6	5.3 ± 0.6	4.8 ± 0.7	5.0 ± 1.1	4.9 ± 0.9
Ba	672 ± 546	428 ± 144	550 ± 398	570	653 ± 278	633 ± 231

* Samples 3-1, 15-1, 21-1, 25-1, 26-1, 30-1.
† Samples 3-2, 15-2, 21-2, 25-2, 26-2, 29-3.
‡ Samples 28-1, 29-1, 31-1.
§ Samples 30-2, 28-2, 29-2, 31-2.

Table 5 Concentrations of trace elements (ppm) in Lake Baikal bottom sediments in comparison with reference samples

Element	Sediments from region of BPPP ($n = 20$)*	Sediments from regions remote from BPPP ($n = 20$)†	Sediments from southern depression, average ($n = 40$)	Reference sample BIL-1[9]	Platform clays[14]	Clark concentration for sediment, rocks[15]
Ce	71 ± 22	98 ± 49	85 ± 40	82.5 ± 3.7	70	50
Nd	37 ± 11	46 ± 21	41 ± 17	41 ± 2.1	33.2	23
Sm	6.6 ± 2.1	8.4 ± 3.8	7.5 ± 3.1	7.57 ± 0.72	6.9	6.5
Eu	1.5 ± 0.2	1.6 ± 0.2	1.6 ± 0.2	1.30 ± 0.10	1.34	1.0
Gd	5.5 ± 0.9	6.1 ± 1.6	5.8 ± 1.3	5.50 ± 0.37	6.0	6.5
Tb	1.0 ± 0.2	1.2 ± 0.5	1.1 ± 0.4	1.09 ± 0.07	1.0	0.9
Ho	1.0 ± 0.4	1.0 ± 0.3	1.0 ± 0.3	1.43 ± 0.17	1.2	1.0
Tm	0.4 ± 0.1	0.5 ± 0.2	0.4 ± 0.1	0.46 ± 0.05	0.5	0.25
Yb	2.9 ± 0.5	3.5 ± 1.3	3.2 ± 1.0	2.76 ± 0.10	3.2	3.0
Lu	0.4 ± 0.1	0.5 ± 0.1	0.4 ± 0.1	0.38 ± 0.05	0.5	0.7
U	3.8 ± 1.8	4.6 ± 2.3	4.2 ± 2.1	8.79 ± 0.24		3.2
Th	5.2 ± 2.6	11.7 ± 11.5	8.5 ± 8.9	10.5 ± 1.3		11
Cr	119 ± 74	53 ± 25	89 ± 62	59.5 ± 7.6		100
Co	26.7 ± 4.6	20.5 ± 6.8	23.6 ± 6.5	21.5 ± 1.6		20
Cs	3.1 ± 0.9	4.3 ± 1.4	3.7 ± 1.3	5.60 ± 0.44		12
Ta	0.9 ± 0.2	1.1 ± 0.3	1.0 ± 0.3	0.91 ± 0.05		3.5
Hf	5.2 ± 0.7	7.4 ± 4.6	6.3 ± 3.4	4.41 ± 0.51		6.0
Ba	574 ± 351	779 ± 535	686 ± 466	710 ± 70		800

* Samples 3-1, 3-2, 15-1, 15-2, 21-1, 21-2, 25-1, 25-2, 25-3, 26-1, 26-2, 28-1, 28-2, 29-1, 29-2, 29-3, 30-1, 30-2, 31-1, 31-2.
† Samples 278-1, 278-2, 278-3, 278-4, 38-1, 38-2, 32-1, 32-2, 28/1-1, 28/1-2, 27-1, 27-2, 22-1, 22-2, 2-1, 2-2, 9-1, 9-2, 18-1, 18-2.

which was represented by yellow silts. As anomalous concentrations of trace elements were found both in surface (32-1) and deeper (32-2) layers of sediments, one cannot consider anthropogenic pollution of sediments in the region of this station. As samples from station No. 32 show maximum enrichment by thorium combinations having low solubility in water and adsorption on the surface of sediment particles, it may be assumed that bottom silt in the region of station No. 32 contains small fragments of Th minerals with high concentrations of other trace elements that were brought by riverine sedimented particles. As samples 32-1 and 32-2 show, in addition to Th, enrichment by REEs and Hf, it may be also assumed that this mineral is zircon, having concentrations of thorium and REEs of a few per cent. and hafnium of 20%.

Sample 25-1 has higher concentration of light lanthanides (Ce, Nd, Sm) and Th, but the reason of this enrichment is obviously different. In comparison with samples from station No. 32, sample 25-1 shows no Hf enrichment. As will be shown below, enrichment by light REEs is a specific peculiarity of clean silt facies.

Anomalously low concentrations of all determined trace elements were shown by sample 27-2, which was collected from the layer of clean diatomite white silt.

Low concentrations of trace elements were also present in sample 26-1, which was collected from the surface layer of the bottom sediments. However, it differs from sample 27-2 in having a high concentration of chromium (111 ppm). As was shown before, this is a specific peculiarity of sediments having sandy facies.

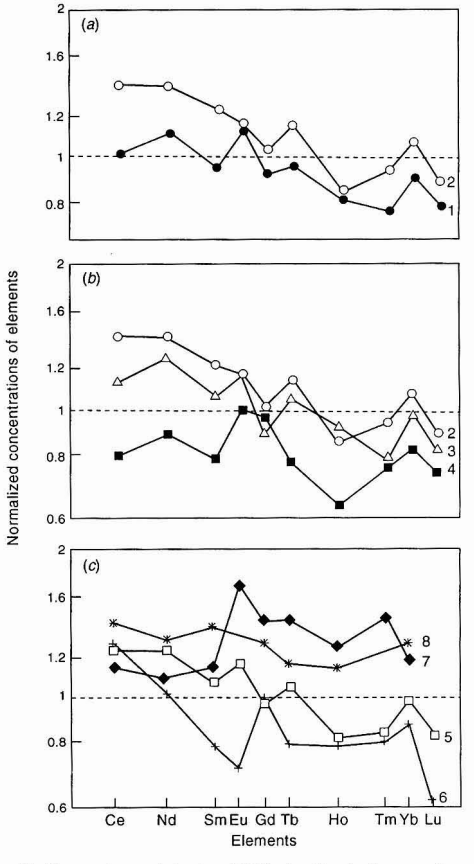

Fig. 2 Comparison plots for REEs in the bottom sediments, normalized to REE abundances in platform clays. (*a*) Distribution of REEs in bottom sediments from different regions of the southern depression of Lake Baikal: 1, sediments from the BPPP region (silts and sands); and 2, sediments from regions remote from the BPPP (silts). (*b*) Distribution of REEs in different facies of Baikal bottom sediments: 2, silts from regions remote from the BPPP; 3, silts from the region close to the BPPP; and 4, sands from the region close to the BPPP. (*c*) Distibution of REEs in different types of bottom sediments: 5, sediments from the southern depression of Lake Baikal, on the whole; 6, riverine sediments;[14] 7, sea pelitic sediments;[14] and 8, ocean pelitic sediments.[18]

Geochemical Peculiarities of Sediments

Let us use the data in Table 5 for the determination of the origin of the enrichment of Lake Baikal sediments by light lanthanides and uranium. The mean concentrations of trace elements in bottom sediments are given in Table 5 together with data for reference sample BIL-1, clays of platforms and Clark concentrations of elements for sedimentary rocks.

As was mentioned above, a reference sample of deep-water bottom silt of Lake Baikal, BIL-1, is used as a standard of clean sediment without any anthropogenic contamination in the evaluation of the pollution of the lake ecosystem. The material was sampled in the middle of the lake in the central depression as deep as 1620 m (Fig. 1). The median composition of platform clays is used as a reference sample in the study of geochemical peculiarities of sedimentary processes.[14] Clark concentrations of trace elements for the sedimentary rocks were given by Voytkevich *et al.*[15]

Table 5 shows that sediments from regions remote from BPPP with the exception of Cr have similar concentrations of trace elements to those from the region of BPPP. The difference in chromium concentration is connected with the fact that the first group of sediments consist only of silt samples whereas the second group includes some sand samples.

Comparison of the mean concentrations of trace elements in the bottom sediments from the southern depression of Baikal with the data for the reference sample BIL-1 shows that they almost coincide. This is additional confirmation of the absence of anthropogenic pollution in bottom sediments of Lake Baikal. However, it should be noted that concentrations of U and Cs in sediments of the southern depression and in the reference sample BIL-1 are significantly different. Our data for the concentrations of uranium and caesium in BIL-1 are well correlated with those of Gavshin *et al.*[16] for their concentrations in peltic silts of the central depression of Lake Baikal, 7.5 ± 1.6 and 7.8 ± 0.6 ppm, respectively. This indicates lower concentrations of U and Cs in bottom sediments of the southern depression than in sediments of the central depression of Baikal.

At the International Conference on Baikal as a Natural Laboratory for Global Change held in Irkutsk (1994), a hypothesis was made on the possibility of the use of the U concentration change in sediments as a geochronometer.[12] In another report,[13] a hypothesis on the reason for uranium enrichment of diatom silts of Lake Baikal was presented.

Comparison of the concentrations of trace elements in the bottom sediments from the southern depression with the Clark concentrations for sedimentary rocks shows their enrichment by light lanthanides and an obvious deficit of caesium and tantalum on the background of almost identical concentrations of intermediate and heavy REEs, U, Th, Cr, Co, Hf and Ba. The similarity of the concentrations of Cs and Ta in sediments from southern and central (BIL-1) depressions of the lake suggests the possibility of the caesium and

tantalum deficit as a geochemical peculiarity of Baikal bottom sediments.

REE Anomaly

Let us consider the main interesting geochemical peculiarity of Lake Baikal bottom sediments, namely an enrichment of deep water silts by light REEs. REEs are widely used in geochemistry as indicators of natural processes,[14,17,18] but data on their behaviour in the lytogenesis are inadequate.

Comparison of the lanthanide concentrations in Lake Baikal bottom sediments with their concentrations in the clays of platforms are given in Fig. 2. The ordinator gives the REEs in order of increase in atomic number and the abscissa gives the concentrations of elements in bottom sediments normalized to their concentrations in platform clays.

Fig. 2(*a*) shows that Lake Baikal bottom sediments are enriched by light REEs as compared with platform clays. Sediments from regions remote from BPPP which are represented only by silts (curve 2) show higher concentrations of REEs than sediments from the region of BPPP (curve 1).

Plots of REE distribution in different facies of bottom sediments are presented in Fig. 2(*b*). The group of samples from the region of BPPP was divided into two parts: silts and sands. Fig. 2(*b*) shows that the characters of two curves of REE distribution for silts from different parts of the lake are very similar (curves 2 and 3), but the type of curve for sands (curve 4) is different. The identical type of distribution of REEs for silts from different parts of the bottom of the lake allows us to assume the action of the same process, which results in the enrichment of silts by light lanthanides and that does not influence other facies of Baikal sediments.

To understand the mechanism of the enrichment of Lake Baikal sediments by light REEs, it is necessary to know that these elements can enter the bottom sediments by three routes: (1) in the composition of solid terrigenous component of riverine suspended matter; (2) in the form of colloidal high molecular mass organic combinations with REEs that are adsorbed on the surface of suspended particles; and (3) in the form of combinations of REEs dissolved in the water.

It may be assumed that the reason for enrichment of Lake Baikal deep water silts by REEs is the deposition of combinations of these elements that were adsorbed on the surface of suspended particles. Sand facies of Baikal sediments representing a solid component of the suspended matter is not enriched by REEs, and the contribution of the deposition of lanthanides from solution is very small and almost identical for all types of sediments.

According to data of Balashov,[14] adsorbed REEs make up 30–60% of the balance of all lanthanides of the solid component of river flow. Moreover, in their composition there is predominance of light and intermediate REEs. In this work, the concentrations of Ce and Nd in silts from BPPP are 29.1% and 29.3%, respectively, higher than in sands. For silts from regions remote from BPPP the concentrations of Ce and Nd are 42.8% and 37% higher. This is in good correlation with the data of Balashov and confirms the correctness of the supposition made.

In Fig. 2(*c*), the results of a comparison of the REE distribution in Lake Baikal bottom sediments with that in riverine, sea[14] and ocean[18] sediments is presented. The results show that the type of REE distribution in riverine sediments (curve 6) is similar to that for Lake Baikal sediments (curve 5). There is a noticeable enrichment by Ce, a smaller one by Nd and small deficit of other lanthanides with respect to platform clays.

It is obvious that the lower absolute concentration of REEs in riverine sediments is connected with a shorter period of sedimentation of adsorbed elements under riverine conditions. In this respect, the character of curves 7 and 8 is interesting. They show enrichment of sea (curve 7) and ocean (curve 8) sediments by light, intermediate and heavy lanthanides. Evidently, the reason of this enrichment is connected with the increase in the middle parts of sea and ocean basins of pelitic facies of sediments enriched in adsorbed REEs and with long period of sedimentation.

We shall make one more supposition. We determined that the main reason for the enrichment of deep-water bottom sediments of the lake by light lanthanides is the sedimentation of REE combinations that are adsorbed on the surface of suspended particles. The adsorption ability of suspended matter depends on the temperature of the water in the basin. Therefore, the concentration of light REEs in sediments is a function of temperature. This gives us the possibility of using the change in light REE concentrations in bottom sediments as a geothermometer for reconstruction of the climate in the past by studying sediment composition at different depths from the bottom surface.

Conclusions

Multi-element INAA of bottom sediments of Lake Baikal has shown the absence of anthropogenic pollution by trace elements. The concentrations of trace elements in bottom sediments of Lake Baikal correspond, on the whole, to the Clark values for sedimentary rocks. Enrichment by light REEs and a deficit of caesium and tantalum are the main geochemical peculiarities of Lake Baikal bottom sediments. The reason for the enrichment of deep-water bottom sediments of Lake Baikal by light REEs is the sedimentation of lanthanide combinations that were adsorbed at the surface of suspended particles. The distribution of REEs in Lake Baikal bottom sediments is of a specific type, intermediate between riverine and sea (ocean) types.

The author is grateful to Dr. I. S. Lomonosov and Dr. M. S. Shimaraeva, research scientists at the Limnological Institute and Institute of Geochemistry of the Russian Academy of Sciences, for the supply of samples of Lake Baikal bottom sediments.

This study was carried out with the support by Russian State Committee on High Education (Grant No. 93-7-12).

References

1 Goldyrev, G. S., *Sedimentation and Quaternary Period of History of Lake Baikal Depression*, Nauka, Novosibirsk, 1982 (in Russian).
2 Knyazeva, L. M., in *Sedimentation in the Modern Basins*, Publishing House of USSR Academy of Sciences, Moscow, 1954, pp. 180–236 (in Russian).
3 Goldyrev, G. S., in *Limnology of Near Baikal Delta Areas, Selenginsky Region*, Nauka, Leningrad, 1971, pp. 13–64 (in Russian).
4 Winchester, J. W., *Activation analysis in mineral prospecting* in *Nuclear Techniques in Mineral Exploration and Exploitation*, Vienna, 1971, pp. 1–5.
5 *Activation Analysis in Geochemistry and Cosmochemistry., Proceedings of the NATO Advanced Study Institute*, ed. Brunfelt, A. O., and Steinnes, E., Univ.-Forl., Oslo, 1971 (in Norwegian).
6 Bulnayev, A. I., Vaganov, P. A., Kuznetsov, R. A., and Pankratov, V. B., in *Applied Nuclear Spectroscopy*, Atomizdat, Moscow, 1978, vol. 8, pp. 232–42 (in Russian).
7 Bulnayev, A. I., and Vakhromeyev, G. S., *Instrumental Neutron Activation Analysis of Russian State Reference Samples*, VINITI (Russian State Institute of Scientific and Technical Publication), Irkutsk, 1994 (in Russian).
8 Petrov, L. L., Kornakov, Yu. N., Persikova, L. A., Vlasov, A. V., Malykh, V. V., and Prokopjeva, A. Z., *Geostand. Newsl.*, 1991, **15**, 135.

9 Bulnayev, A. T., and Vakhromeyev, G. S., *Geostand. Newsl.*, 1993, **17**, 205.
10 Govindaraju, K., *Geostand. Newsl.*, 1989, Special Issue.
11 Petrov, L. L., Kornakov, Yu. N., and Persikova, L. A., *Reference Samples of Mineral Substances*, Prepared at the Institute of Geochemistry Siberian Branch of USSR Academy of Sciences (Catalogue), Irkutsk, 1988.
12 Edgington, D. N., Gustin, M. P., Orlandini, K. A., Robbins, J. A., Granina, L. Z., and Grachev, M. A., in *Proceedings of International Conference on 'Baikal as a Natural Laboratory for Global Change'*, LISNA, Irkutsk, 1994, vol. 2, pp. 9–10.
13 Bobrov, V. A., Gavshin, V. M., Bogdanov, Yu. N., and Prokopenko, A., in *Proceedings of International Conference on 'Baikal as a Natural Laboratory for Global Change'*, LISNA, Irkutsk, 1994, vol. 3, p. 19.
14 Balashov, Yu. A., *Geochemistry of Rare Earth Elements*, Nauka, Moscow (in Russian).
15 Voytkevitch, G. V., Kokin, A. V., Miroshnikov, A. W., and Prokhorov, V. G., *Reference Book on Geochemistry*, Nedra, Moscow, 1990 (in Russian).
16 Gavshin, V. M., Bobrov, V. A., and Bogdanov, Yu. A., *Uranium Anomalies in Deep Water Sediments of Lake Baikal*, Reports of the Russian Academy of Sciences, 1994, **334**(3), 356 (in Russian).
17 Haskin, L. A., Frey, F. A., Schmitt, R. A., and Smith, R. H., *Meteoritic, Solar and Terrestiral Rare Earth Distribution*, ed. Mineyev, D. A., MIR, Moscow, 1968 (in Russian).
18 Aleksiev, E., *Geochemistry of Rare Earth Elements*, Publishing House of Bulgarian Academy of Sciences, Sofia, 1974 (in Russian).

Paper 4/06186A
Received October 11, 1994
Accepted December 2, 1994

Evolution, Using Instrumental Neutron Activation Analysis, of the Element Composition of Coal and Oil Shale Fuel at Consecutive Stages of Its Combustion*

Peter A. Vaganov
Faculty of Geology, University of St. Petersburg, 199034, Russia
Zhou Rongsheng
Chengdu College of Geology, 610059, China
Liidia I. Pets
Technical University of Tallinn, EE0001, Estonia

Instrumental neutron activation analysis (INAA) was used to measure the concentrations of 40 elements in coal and oil shale and in products of their combustion at power plants: slag, ash from different aggregates and fly ash. Particular attention was paid to the fine size fractions of fly ash because micrometre and sub-micrometre particles are responsible for the long-range transport of air contaminants. The determination limits of all the elements considered were lower than their mean abundances in the Earth's crust. Concentrations of heavy metals, including radioactive U and Th, and also Cr, Co, Ni, Zn, Mo, Cd, Hg, *etc.*, and toxic non-metals (As, Se, Br, Sb) were determined in the initial fuel and in its combustion products at two power plants. The first, in the city of Chengdu (China), was coal-fired; the second, in Estonia, was oil shale-fired. There were many similar features in the changes in the trace element composition of the combustion products at the two types of power station. Most of the elements enriched in fly ash were volatile. The behaviour of these elements, as revealed by INAA, corresponds to the model of volatilization and condensation processes occurring during combustion of solid fuel.

Keywords: Instrumental neutron activation analysis; coal; oil shale; ash; fly ash; aerosol; trace element

Introduction

Solid fossil fuels, coal and oil shale, will remain for the foreseeable future the most economic, generally acceptable and readily available fuels for power production within vast regions of the world. Coal resources are abundant compared with other fossil fuels. Internationally, the availability of oil and gas can be measured in terms of a few decades, whereas identified coal reserves indicate that there will be coal for many hundreds of years, thus ensuring the long-term availability of coal at an increasingly competitive cost.

The total annual coal output worldwide is currently about 3.5 billion tons; the leading countries in coal production are China, the USA and Russia. China produces 1 billion tons of coal annually, which makes up 75% of China's total energy supply. Seventy per cent. of dust emissions and 90% of discharged sulfur dioxide originate from coal burning.

In Russia also coal remains an important source of energy and there is a serious problem concerning the deterioration of its quality. During recent years the mean ash content of coal has increased by about 30%. Hence there are related changes in the chemical composition of its combustion products. The mean ash content of industrial shale has also increased.

Medlin and Simon,[1] in considering the role of the characterization of solid fuel as a multivariant system, indicated that analysis of coal samples (and it may be added of its combustion products also) should not be restricted to those determinations that are of purely economic interest but should also include as many minor and trace elements as posible. In fact, these elements are being remobilized by the mining and combustion processes and are consequently released into the environment. Although many elements are present in coal in trace amounts, the large amounts of coal being burned mean that the potential for contamination from toxic trace elements is high. As an example, 50000 tons of the toxic trace element As are released into the environment annually as a result of coal combustion.[1]

Virtually every improvement in the technology of fossil fuel combusition is accompanied by some change in the chemical composition of the combustion products: slag, ash from different aggregates of a power plant, and fly ash. Modernization of the equipment for removal of suspended particulates (cyclone collectors, different types of filters, *etc.*) also changes the chemical composition of ash and particularly fly ash, where some type of re-distribution of elements between different phases occurs. In order to observe these changes, a sensitive multi-element analytical technique has to be used.

In the study of the combustion products of solid fuel, particular attention must be paid to the fine fractions of fly ash. The settling velocity of small particles is very low and they are, therefore, liable to remain in suspension for periods of several days. Hence, micrometre and sub-micrometre particles are responsible for the long-range transport of air contaminants. Fine sized particles penetrate into the lungs and may stay there ('respirable' particles). It was observed[2] that small particles usually contain the highest amounts of some toxic elements; evidently they are more harmful to man than larger particles.

The aim of this work was to investigate the evolution of the element composition of solid fuel at consecutive stages of the processes of its combustion using instrumental neutron activation analysis (INAA).

Experimental

The element composition of different combustion products generated at two large power plants using solid fossil fuel was studied. The first plant was a 330 MV power station fired by

* Presented at Geoanalysis 94: An International Symposium on the Analysis of Geological and Environmental Materials, Ambleside, England, September 18–22, 1994.

coal and located in the city of Chengdu (China, Sichuan province). The second plant was a 1000 MW power station fired by oil shale and located in Estonia, near the town of Narva. In both instances the chemical composition of the fuel and of the different types of bottom ash and fly ash was determined. Moreover, the study in China included analysis of aerosols (urban dust) collected at different distances from the power plant. The sites of the aerosol sampling were chosen with due regard for the prevailing wind direction.

For INAA, a reactor with a high neutron flux was used; the ratio of the epithermal flux to the thermal flux was about 0.1. The samples of solid fuel, ash, fly ash and aerosols were packed in quartz vials or in aluminium foil. The mean sample mass was about 40 mg. The samples, together with a set of multi-element geochemical standards, were irradiated for 10 or 24 h with epithermal neutrons with a total flux density of 5×10^{17} m^{-2} s^{-1}. With the aid of certified reference materials and the internal standard method, the concentrations of 40 elements were measured: Na, K, Ca, Sc, Ti, Cr, Fe, Co, Ni, Zn, As, Se, Br, Rb, Sr, Zr, Mo, Ag, Cd, Sb, Cs, Ba, La, Ce, Nd, Sm, Eu, Tb, Ho, Tm, Yb, Lu, Hf, Ta, W, Ir, Au, Hg, Th and U. The gamma spectral lines of the radionuclides selected for the determination of these elements were free from interferences; hence INAA provided the required selectivity. The determination limits of all these elements were lower than their mean abundances in the Earth's crust (K). The precision and accuracy of the determination for most of the elements considered did not exceed 20%.

Results and Discussion

Fig. 1 shows the results of the study carried out at the coal-fired power station. The changes in the concentrations of some elements on going from coal (I) to slag in the power plant fire-chamber (II), then to ash immediately after this fire-chamber (III), then to ash from the cyclone collectors (IV) and finally to fly ash (V) can be seen. In addition, the mean concentrations of the same elements in aerosols collected at a distance of 1.5 km (VI) and 2 km (VII) from the power plant are shown. The values of the mean abundances of the elements in the Earth's crust are marked by horizontal lines with the indexes K_U, K_{Th}, *etc.* The K values were taken from Ovtchinnikov's review published in 1990.[3]

The behaviour of the radioactive elements, U and Th, in the technological process of coal combustion is virtually identical. Slag contains much more U and Th compared with coal. The concentrations of these elements in ash are also fairly high, but in the aerosol samples taken at distances of 1.5 and 2 km from the power plant they are lower. Hence, U and Th remain preferentially at the power station and in its immediate vicinity.

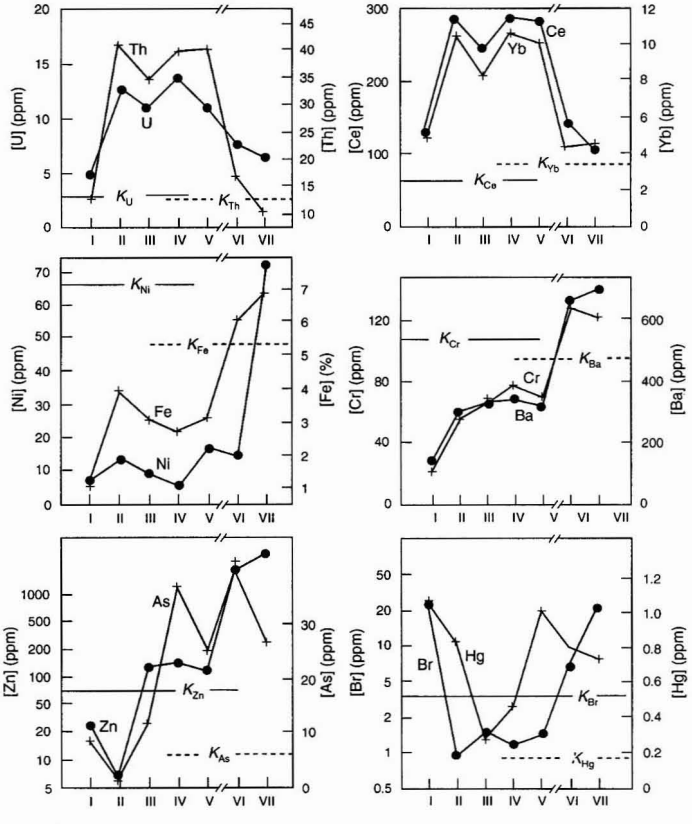

Fig. 1 Concentrations of U, Th, Ce, Yb, Fe, Ni, Cr, Ba, Zn, As, Br and Hg determined by INAA in coal, its combustion products and aerosols (I, coal; II, slag from a fire-chamber; III, ash after a fire-chamber; IV, ash from cyclone collectors; V, fly ash; VI, aerosols taken at a distance of 1.5 km from the power station; and VII, aerosols taken at a distance of 2 km from the power station). K = mean crustal abundance.

The patterns for the rare earth elements (REEs) are similar. Fig. 1 shows the changes in the concentrations of one of the light REEs (Ce) and one of the heavy REEs (Yb). As with U and Th, the concentrations of the REEs in coal are higher than their mean abundances in the Earth's crust. In slag and in ash of different aggregates the REEs are strongly enriched, but in distant aerosols their contents are close to the mean crustal concentrations. Evidently, there is no long-range air transport of the radioactive elements and REEs from the power station.

Fig. 1 also shows the changes in the iron group element concentrations (Fe, Ni, Cr) together with the behaviour of Ba. Relative to coal, Fe, Cr and Ba are enriched both in slag and in ash. However, in contrast to the elements mentioned above, the amounts of Fe, Ni, Cr and Ba in aerosols are high

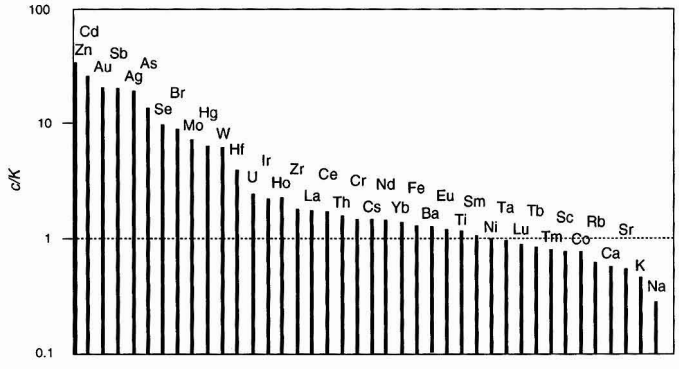

Fig. 2 Results of INAA of the aerosol samples taken at a distance of 2 km from the coal-fired power station expressed as c/K ratios (c = concentration in aerosol; K = mean crustal abundance).

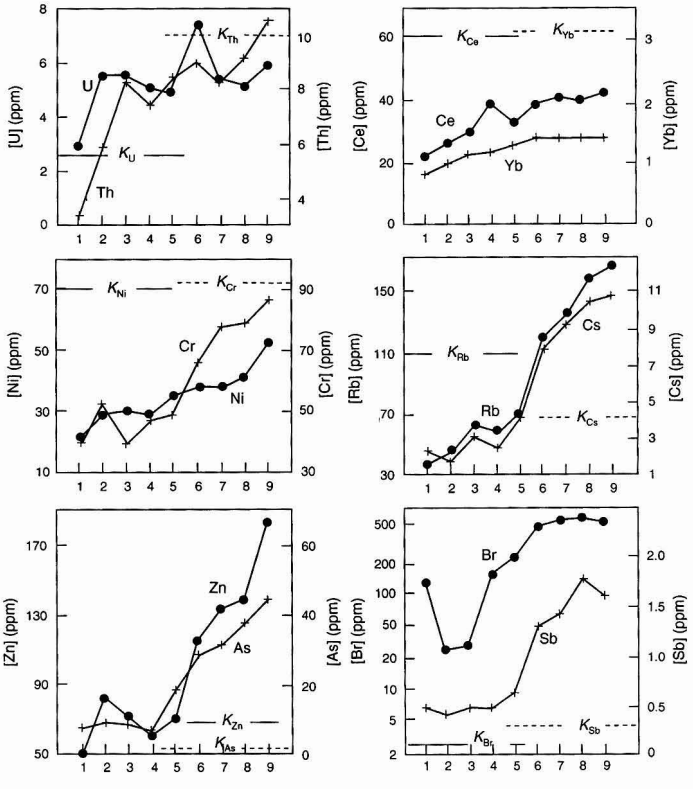

Fig. 3 Concentrations of U, Th, Ce, Yb, Ni, Cr, Rb, Cs, Zn, As, Sb and Br determined by INAA in oil shale and its combustion products (1, oil shale; 2, slag from a fire-chamber; 3, ash from steam overheating aggregates; 4, ash from cyclone collectors; 5–8, ash from different zones of electrofilters; and 9, fly ash from the stack). K = mean crustal abundance.

compared with those in the ash remaining at the power station.

Fig. 1 further shows the evolution of the concentrations of some volatile elements: Zn, As, Br and Hg. The content of Zn in coal is less than the K_{Zn} value, whereas the contents of As, Br and particularly Hg in this fuel are higher than their mean crustal abundances. Compared with coal, slag contains reduced amounts of these volatile elements, whereas their concentrations in ash are higher than in the initial fuel. As regards urban dust (aerosols), the concentrations of these elements are even higher, particularly of Zn.

The behaviour of volatile elements corresponds to the model of volatilization and condensation processes.[4,5] According to this model, volatile components would be vaporized during combustion and later condense on the surface of the ash particles during cooling. Because a unit mass of fly ash would have a much larger surface area among the finer size fractions, these volatile compounds would be enriched in the finer size fractions of the ash as condensation products.

In Fig. 2 the results of INAA of aerosols taken at a distance of 2 km from the Chengdu coal-fired power station are shown. It can be seen that there is a group of trace elements enriched in aerosols: Zn, Cd, Au, Sb, Ag, As, Se, Br, Mo, Hg, *etc.* Most of these elements are volatile. The capacity of fine aerosol particles to carry elements with high volatility has been observed previously.[2] The high value of the ratio of the concentration to the mean crustal abundance (c/K ratio) confirms the technogenic origin of the elements considered. Indeed, trace elements such as As, Se and Hg can be used as indicators of air pollution caused by coal burning. According to recent studies, about 65% of the anthropogenic emission of Hg into the atmosphere is due to coal burning.[6] Moreover, after observing the regional variations in Hg content it was suggested that these variations are due to deposition of anthropogenic Hg not in the gaseous state but in particulate form.[7] Selenium may be the most enriched element in coal relative to its mean crustal abundance.[8] High As enrichment in coal fly ash was established; this fact is evident from the recent determinations of As in some fine fly ash reference materials.[9,10]

In Fig. 3, data from the INAA study of the composition of oil shale and its combustion products at the power plant in Estonia are presented. In this instance, the analysis of ash was more detailed. In addition to the samples of oil shale (1) and slag from a fire-chamber (2), the following samples of ash were studied: ash from steam overheating aggregates (3), ash from cyclone collectors (4), ash from different zones of electrofilters (5–8) and fly ash from the stack (9).

It can be seen that the main features of the element composition evolution are similar to those that were observed for coal. Conversion from oil shale to slag is accompanied by an increase in the contents of U, Th and the REEs. The concentrations of U, Ce and Yb in the different types of ash are virtually identical; only the concentrations of Th exhibit a slight increase in fly ash. The absolute amounts of the REEs in ash are small; they are less than their mean abundances in the Earth's crust.

Nickel and Cr show an increase in their slag concentrations compared with the initial fuel. Their concentrations in ash increase gradually, reaching maxima in fly ash from the stack. However, the contents of Ni and Cr never reach the values of their mean crustal abundances.

Fig. 3 also shows results obtained for the volatile elements. The concentrations of the rare alkali metals, Rb and Cs, in slag are virtually unchanged compared with those in oil shale, but the ash samples taken along the line of collection at the power station show a gradual increase in the amounts of Rb and Cs. In the last zones of the electrofilters and in fly ash from the stack, the concentrations of these metals exceed their mean abundances in the Earth's crust.

Similar behaviour is demonstrated by Zn and As. The ash samples from the last electrofilters and from the stack are characterized by Zn and As concentrations that are many times higher than the K_{Zn} and K_{As} values. As regards the changes in the contents of Sb and Br (Fig. 3), it can be seen that again the amounts of both elements increase gradually in the direction of the line of ash collection. There is only one difference in the behaviour of Br: the process of oil shale combustion leads to a sharp decrease in the content of this element in slag. The concentrations of Sb and particularly Br in all the samples studied significantly exceed the mean concentrations of these elements in the Earth's crust. Hence, the results of the INAA study of variations in the element composition of oil shale products confirm the model of volatilization and condensation processes.

Conclusions

Application of INAA to the study of the trace element composition of solid fossil fuels and their combustion products showed many similar features for coal and oil shale. In both instances, volatile compounds tend to accumulate on the surface of the fine particle fraction of ash. INAA is a very effective technique for evaluating different quality parameters of fuel. It has been proposed that coal beds be characterized by a set of 128 parameters including many minor and trace elements.[1] By using INAA, most of these elements can be determined not only in the initial fuel, but also in all its combustion products.

Of course, INAA is fairly expensive for use in routine measurements. However, it is convenient for a detailed study of any changes in the element composition of the combustion products caused by some essential alteration in the technology of solid fuel combustion aimed at improving its efficiency, in particular to reduce the pollution of the atmosphere by heavy metals and toxic elements. In this instance, the use of INAA prevents inter-technique biases which would hamper interpretation of the results. INAA is useful also in different control studies, for example, for intercalibration measurements or in interlaboratory and intertechnique comparisons.

References

1 Medlin, J. H., and Simon, F. O., in *Proceedings of U.S. Geological Survey Workshop on Environmental Geochemistry*, ed. Doe, B. R., U.S. Geological Survey Circular 1033, Denver, CO, 1990, pp. 105–118.
2 Kulmatov, R. A., Abdullaev, B., and Kist, A. A., *Geokhimiya*, 1983, No. 10, 1477 (in Russian).
3 Ovtchinnikov, L. N., *Applied Geochemistry*, Nauka Publishers, Moscow, 1990 (in Russian).
4 Natusch, F. S., Wallace, J. R., and Evans, C. A., Jr., *Science*, 1974, **183**, 202.
5 Davison, R. L., Natusch, F. S., Wallace, J. R., and Evans, C. A., Jr., *Environ. Sci. Technol.*, 1974, **8**, 1107.
6 Slem, F., and Langer, E., *Nature (London)*, 1992, **355**, 434.
7 Nater, E. A., and Grigal, D. F., *Nature (London)*, 1992, **358**, 139.
8 Naftz, D. L., and Rice, J. A., *Appl. Geochem.*, 1989, **4**, 565.
9 Masumoto, K., and Yagi, M., *J. Radioanal. Nucl. Chem., Articles*, 1991, **152**, 55.
10 Dybczynski, R., *Geostand. Newsl.*, 1991, **15**, 163.

Paper 4/05886K
Received September 26, 1994
Accepted January 3, 1995

Neutron Activation Analysis of Environmental Materials

Gennady M. Kolesov

Vernadsky Institute of Geochemistry and Analytical Chemistry, Russian Academy of Sciences, Kosygin St. 19, 117975, Moscow, V-334, Russia

Several possible methods for the analysis of important environmental materials have been examined. The role of nuclear-physical methods, including activation methods using reactor neutrons is highlighted. The main steps of analysis (sample preparation, irradiation conditions, information processing and interpretation of results) is discussed. Attention is also paid to the necessity of using other methods of analysis, and the coordination and widening of International collaborative programme in the field of ecological investigations.

Keywords: Neutron activation analysis; environmental objects; nuclear-physical methods.

Introduction

The rapid technological progress in the world has led to increased destruction and damage to the natural world, resulting in serious environmental changes. Such effects are reflected in the deforestation causing oxygen disequilibrium between the Earth and atmosphere; depletion in the ozone layer that forms an essential barrier to ultraviolet radiation; and damage to pastures, fields, reservoirs, and food materials. Therefore, many countries, including Russia, are realizing the need for environmental protection; in particular the Russian Academy of Sciences holds yearly meetings and as a result has devised the 'Programme of biosphere and environmental investigations'.[1]

General Aim of Investigation

The over-all problem of environmental protection is intrinsically linked to Man's understanding and interaction with natural biospheric processes. This involves gaining information on the anthropogenic factors that affect the stability of biological systems and the various ways in which anthropogenic loads interact within these systems. This is an important environmental problem, the solution to which is linked with land area (*i.e.*, the continent on the whole), water levels (*i.e.*, rivers, lakes, oceans), air (*i.e.*, the atmosphere) and, in general, all of the natural systems[2] represented in Fig. 1.

The system (presented in Fig. 1) is mainly affected by technogenic processes, transportation and population growth, and to a lesser extent by natural processes like volcanic activity, earthquakes *etc.* This situation requires an understanding of the ecological processes and the monitoring of communal domestic activities which creates analytical problems.

The main environmental materials that can be analysed are: plants, cereals, soil, rocks, natural water, sediments, atmospheric fall-outs, aerosols, sewage water, agrochemicals, dust and gases. The most damaging compounds are pesticides, Freons, phenols, amines, certain oxides (*e.g.*, carbon and nitrogen), derivatives of phosphorous, antimony, chlorine, fluorine *etc.*

The main elements that influence the environment are grouped as follows (Table 1). (1) Elements that characterize the over-all ecological situation: As, Be, Cl, Mn, Pb, Sb, Se, Tl, V. (2) Indicator elements that often introduce matter into ecologically important materials: Al, Ba, Fe, Zr, REEs. (3) Toxic elements: As, Cd, Cr, Hg, Ni, Pb and others. Of these, As, Hg, Pb and V are distinguished by their universal characteristics and fall into all three separate elemental groups.

Categorizing the above-mentioned elements into the three groups can be used as a guide in selecting an appropriate method of analysis. Generally, the following factors are considered to be most important in chemical analyses in general and in the analysis of environmental materials:[3] a low detection limit of the order of <0.1 ppm ($1\ \mu g\ g^{-1}$); a small analytical error; a high selectivity (particularly, in the analysis of biological products); a low minimum sample mass requirement (of <10 mg), the possibility of performing an analysis in the presence of a high flux is particularly important for water and air sample analysis, and the possibility of instrumentation automatization *etc.*

At present, spectrophotometry (in particular using new reagents), gas chromatography, mass spectrometry, atomic absorption and atomic emission spectrometry coupled with inductively coupled plasma and nuclear-physical methods are routinely used as the fulfil the requisites and requirements of environmental analysis. Of the nuclear-physical methods neutron activation analysis (NAA) is the most important.[4]

The interest in nuclear-physical methods started at the end of 1970 and its popularity continued until 1986 (particularly in

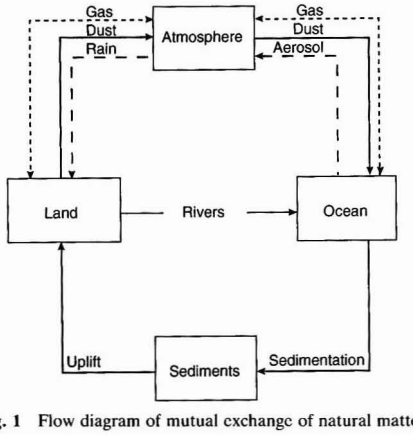

Fig. 1 Flow diagram of mutual exchange of natural matter.

* Presented Geoanalysis 94: An International Symposium on the Analysis of Geological and Environmental Materials, Ambleside, England, September 18–22, 1994.

the former USSR) until the Chernobyl Atomic Power Station accident. In the USA, for example,[4] NAA methods are mostly used at universities (46%), at laboratories under government control (27%), at industrial laboratories (16%), and at medical schools and hospitals (11%) (*i.e.*, 24% of the total NAA work is carried out in methodological processing and 76% in applied investigations). Out of the applied studies, 30% are industrial studies and 22% are for environmental studies, 21% are for medicine, 22% are for geochemistry (cosmochemistry and oceanology) and 5% are for archaeology. For example, during the periods 1950–71 and 1976–86 90% of total activation analyses were carried out by the NAA method, 5.5% by charged particle analysis and 4.5% by the gamma activation method.

In most investigations, neutron reactors (76%), accelerators (1.7%), isotopic sources (6%) and neutron generation (16.3%) are used. In most investigations thermal neutrons (90%) are used. However, recently analysis using epithermal neutrons has decreased (6%). In many analyses preference has been given to isotopic sources with fluxes of 10^{13} n cm^{-2} s^{-1}.

Over the years that neutron activation methods of analysis have been used: instrumental NAA (53%); radiochemical NAA (18.3%); preconcentration of elements; (8.4%) 'prompt' gamma-radiation (9.9%) and slow and fast impulse neutrons (10.4%) types of reactor were used. In recent years the use of INAA has increased. A similar trend is also observable in the former Soviet Union evidenced by the conferences held concerning NAA and other nuclear-physical methods.[5] NAA methods, in particular using reactor neutrons, has many advantages. Among the advantages are the availability of high neutron fluxes; the simplicity of sample irradiation and sample analysis; the high selectivity with low detection limits and the non-destructivity of samples with small masses (in most cases).

A variety of methods of analysis in NAA can be implemented and are given below:

(*i*) Analysis using very short-lived isotopes.[6] Good metrological determination characteristics (Table 2) are obtained for F, V, Se and Rh. This method is completely automated.

(*ii*) Analysis using average-life ($t_{1/2}$ > 1–2 d) and long-lived ($t_{1/2}$ > 20–100 d) radionuclides (this is the most commonly used type of analysis used in many experiments). It is seen

Table 2 Neutron activation analysis of elements using short-lived isotopes ($t_{1/2}$ < 5 min) ($t_{irradiation}$ = 5 min or 1000 disintegrations s^{-1}; flux, 10^{13} n_t cm^{-2} s^{-1} and 10^{12} n_{ep} cm^{-2} s^{-1})*

Element	Radionuclide	$t_{1/2}$/s	Detection limits/g
Li	^{8}Li	0.84	5×10^{-8}
B	^{12}B	0.022	2.13×10^{-1}
N	^{16}N	7.13	1.7
O	^{19}O	26.9	3.6×10^{-3}
	$(n,p)^{16}N$	7.13	3.3
F	^{20}F	11.0	2.2×10^{-6}
	$(n,p)^{19}O$	20.9	1.2×10^{-5}
Ne	^{23}Ne	37.6	1.4×10^{-6}
Al	^{28}Al	2.24	2.0×10^{-8}
V	^{52}V	3.76	9.0×10^{-10}
Se	$^{77}Se^{m}$	17.4	1.0×10^{-8}
Rb	$^{86}Rb^{m}$	61.0	1.2×10^{-7}
Rh	$^{104}Rh^{m}$	4.34	2.5×10^{-9}
	^{104}Rh	42.3	3.5×10^{-9}
Pb	$^{207}Pb^{m}$	0.81	1.7

* n_t and n_{ep} are thermal and epithermal neutrons, respectively.

Table 1 Elements of ecological importance and their determination by activation methods

	Information about			Method of analysis*		
Element	Total pollution	Pollution of matter	Toxic materials	INAA	IGAA	CPAA
Al		●		+	—	
Ag		●		+	+	
As	●	●	●	+	+	
B	●			—	—	
Ba		●		+	+	
Be	●		●	—	—	
Br		●		+	—	+
C		●		—	—	+
Ca		●		+	+	+
Cd	●		●	+	+	+
Cl	●		●	+	+	
Co		●		+	+	
Cr	●		●	+	+	+
F	●	●		+	—	
Fe		●		+	+	+
Hg	●	●	●	+	+	
I		●		+	—	+
K		●		+	+	
Mn	●	●		+	+	
Na		●		+	+	
Ni	●	●	●	+	+	+
Pb	●	●	●	—	+	+
Rb		●		+	+	+
S	●			+	—	+
Sb	●	●		+	+	
Se	●		●	+	+	+
Sn		●		+	+	
Te	●		●	—	+	
V	●	●	●	+	+	
Zn		●	●	+	+	

* INAA, instrumental neutron activation analysis; IGAA instrumental gamma activation analysis; CPAA, charged particle activation analysis.

from the obtained data (Table 3) that around 50 elements can be determined at the order of <0.01 ppm. The applications of this method can be widened further by using Cd- and B-filters, *i.e.*, by changing the energy spectrum of the neutrons (given in Fig. 2). The success of the method (particularly, RNAA) depends on the preconcentration and separation of the elements. For this purpose, sorption, ion-exchange and extraction methods are used.

(*iii*) Analysis using neutron sources ^{252}Cf, ^{124}Sb–Be and others are important and very useful, particularly in field investigations such as in the construction of mobile laboratories. In this way up to 55 elements can be determined with elemental concentrations of the order of 10–100 ppm (Table 4).

(*iv*) Analysis using the fast neutrons (energy 14 MeV) of generators. This method is more suitable for the determination of O, Si and Al.

As a general example the role of INAA in obtaining analytical data on rock samples (also soil and other materials)[7] is shown in Fig. 3. Of the analysis methods considered, NAA was capable of determining the largest number of elements at concentrations of the order of <1 ppm (40). These include Hf, Ta, Th, Y, U, REEs, noble metals, As, Sb, V and others.

Table 3 Elemental detection limits (DLs) obtained by neutron activation analysis (flux, 1.2×10^{-13} n cm^{-2} s^{-1}; $t_{irradiation}$, 20 h; $t_{cooling}$, <1, 1–2, 7–14 and >30 d for columns 1, 3, 5 and 7, respectively

1 Element	2 DL/g	3 Element	4 DL/g	5 Element	6 DL/g	7 Element	8 DL/g
Cl	10^{-8}	Na	10^{-11}	Ca	10^{-6}	Sc	10^{-13}
Mn	10^{-11}	K	10^{-10}	Sn	10^{-8}	Cr	10^{-9}
Ni	10^{-7}	Cu	10^{-8}	Ba	10^{-6}	Fe	10^{-7}
Eu	10^{-11}	Zn	10^{-8}	Ce	10^{-9}	Co	10^{-10}
Dy	10^{-11}	Ga	10^{-10}	Nd	10^{-8}	Rb	10^{-9}
Er	10^{-10}	As	10^{-9}	Yb	10^{-10}	Zr	10^{-8}
		Br	10^{-9}	Lu	10^{-11}	Ag	10^{-8}
		La	10^{-10}	Au	10^{-10}	Sb	10^{-8}
		Pr	10^{-8}	U(Np)	10^{-10}	Cs	10^{-9}
		Sm	10^{-10}			Tb	10^{-9}
		Gd	10^{-9}			Tm	10^{-9}
		Ho	10^{-9}			Hf	10^{-10}
		W	10^{-10}			Ta	10^{-10}
		Os	10^{-10}			Hg	10^{-10}
		Ir	10^{-11}			Th(Pa)	10^{-10}

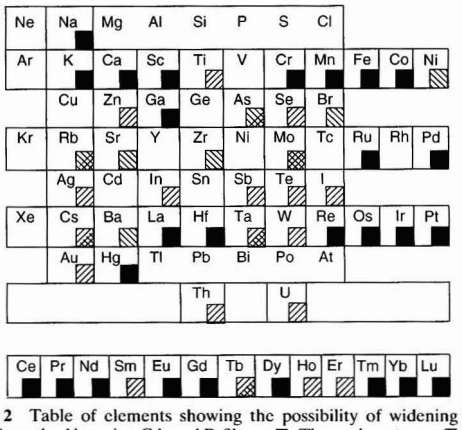

Fig. 2 Table of elements showing the possibility of widening the NAA method by using Cd- and B-filters. ■, Thermal neutrons; ▨ and ▧, epithermal neutrons using Cd- and B-filters, respectively.

The use of instrumental neutron activation analysis and also analysis using gamma quantum radiations and charged particles in the determination of ecologically important elements[8] was mentioned earlier. It is important to emphasize the use of other techniques currently used in the analysis of environmental samples and industrial materials in addition to NAA. The advantage of combining NAA with other methods, for example, atomic absorption, is discussed.

In recent years, X-ray fluorescence methods, using mainly X-rays produced by the interaction of gamma quanta from radioisotope sources (for example ^{55}Fe, ^{57}Co, ^{109}Cd and ^{241}Am) and synchronized radiation have given way to X-ray fluorescence analysis.[9]

Neutron activation analysis, like other nuclear-physical methods, are developed at nuclear centres, as such laboratories have access to linear accelerators, betatrons, microtrons, cyclotron, generators, reactors *etc.* Every investigation centre of the former USSR has developed and applied the above methods, particularly in the analysis of manganese nodules, sediments, ores, soil, water, petroleum products, biological samples, agricultural products and other environmental objects.[5,10]

Various examples are given (principally methodological) of the application of NAA at the Vernadsky Institute of Geochemistry and Analytical Chemistry which partially reflects the popularity of their use in the country as a whole at the present time. The applications are assessed by considering the main parts of the analysis.

Experimental

Sample Preparation

Different types of materials are chosen for NAA, preferably in solid form. Plant and plankton samples are usually dried and

Table 4 Neutron activation determination of elements using a radioactive source (^{252}Cf)

Element	Detection limit (ppm)
Eu, Dy	10^{-3}
Mn, In, Ir, Au, Lu, Ho, Sm, Re	10^{-3}–10^{-2}
Na, Sc, Co, Ga, Br, Ag, Sb, Cs, La, Tm, Yb, Ta, W, As, Se	10^{-2}–10^{-1}
K, Cr, Y, Cu, Cd, Ce, Nd, Gd, Tb, Er, Hg, Hf, Ge, Sr	10^{-1}–1
Cl, Zn, Mo, Ru, Rh, Pd, Ba, Os, F, Mg, Al	1–10
Mg, Al, Ti, Ni, Sn, Rb, Y	10–10^2
Ca, Fe, Zr	10^2–10^3

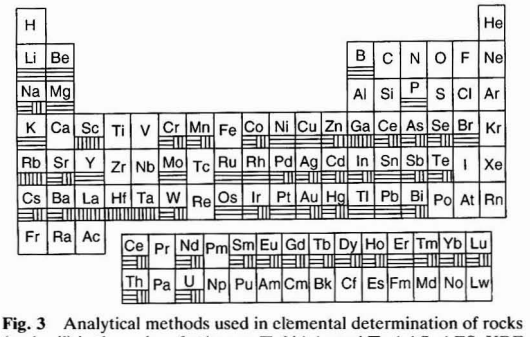

Fig. 3 Analytical methods used in elemental determination of rocks (and soil) in the order of <1 ppm: ▥, NAA; and ▤, AAS, AES, XRF and other methods.

ashed; aerosol samples are analysed along with the filters; natural water samples are evaporated or subjected to a chemical preconcentration method prior to analysis. The sample masses used range from 1 mg to 1 g. Samples are prepared by ashing and acid digestion using a microwave ashing system which is particularly suitable for the analysis of food materials, concretes, chromites and ores.[11]

For the preconcentration of elements or for radiochemical methods of analysis tertiary amine sorbents Polyorgs-IV and Polyarsenazo-N, in addition to microfire assay and coupling simultaneous dissolution and separation of groups of elements are used. For example, the sorbents Polyarsenazo-N and Polyorgs-IV consist of complexing groups (Fig. 4) with a polymeric matrix of copolymer of poly[styrene-*co*(divinyl benzene)] (10%) and polymeric matrix of polystyrene, respectively.

Irradiation

Various irradiation and cooling regimes, and activity measurements of samples are choosen according to the automatization of the method and the energy spectrum of the neutrons (while using a Cd- or B-filter[12,13]). This gives an idea of how to plan the experiment and how to achieve better metrological characteristics, for example, a detection limit.

Information Processing

De-coding multicomponent gamma spectra of radionuclides, calculation elemental concentrations, correction of interfering reactions and isotopes *etc.* are carried out with the help of automation of the method using programmes such as KROKO, OBRAZ and ASPRO.[12–14]

Results and Discussion

Interpretation and Verification of Results

Internal standards are widely used to verify results: the standards and samples are analysed simultaneously and the results obtained are compared. Analytical precision and background comparisons are used in methods such as X-ray fluorescence and inductively coupled plasma atomic emission spectrometry. Normalization, where the obtained values are divided by the elemental concentrations (used in chondrites, clays or soils) is used to explain the anomalous distribution of elements, and to account for sources of their entrance and transfer into matter. On the whole, this complex approach allows for the determination of 25–45 elements in a single sample with a detection limit of 1–100 ppm.[12]

Many different ecological problems have been solved by using NAA.[15,16] Finding a suitable method for the determination of: the chemical composition of a sample; the potential pollution level of material objects; of the quantity (in large amounts) of introducing matter and then possibilities of improving the ecosystem with the help of specialists are all essential requirements that an analyst has to fulfil.

Polyarsenazo

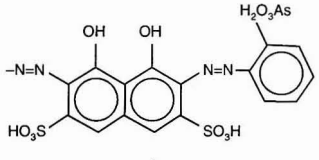

1

Polyorgs IV

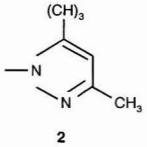

2

Fig. 4 Complexing group of sorbents used in the preconcentration of REEs (**1**) and noble metals (**2**).

Conclusions

It is apparent that NAA has developed significantly and is now a fairly universal technique. NAA has the potential to be used for increasing the number of material standards available, and to elaborate on the simple and universal schemes for routine analyses of samples and group isolation of elements, and in the construction of mobile measuring complexes (including ^{124}Sb-Be, ^{109}Cd and ^{57}Co).

Realizing these new applications and, in particular, combining NAA with other methods of analysis the role of NAA in the study of natural and environmental sample composition can be widened further. Furthermore, the solution of the problem of ecological protection depends largely upon the coordination of the research programme and the widening of international co-operation and support.

References

1 Marchuk, G. I., *Vestn. Acad. Nauk SSSR*, 1989, **5**, 4.
2 Valkovic, V., *Nucl. Instrum. Methods Phys. Res.*, 1989, **280**, 459.
3 *Analytical Chemistry Articles*, ed. Zolotov, Yu. A., Khimya, Moscow, 1977, p. 112.
4 Erdman, I., *Neutron Activation Analysis With Research Reactor: Applications and Techniques, Proceedings of an International Symposium*, Grenoble, 1987, IAEA-SM-300/18, pp. 447–474.
5 *Activation Analysis. Methodology and Application*, ed. Shtan, A. C., FAN, Tashkent, 1990, p. 224.
6 Grass, F., *J. Radioanal. Nucl. Chem.*, 1987, **112**, 347.
7 *Methods for Geochemical analysis*, ed. Baedecker, F. A., *U.S. Geol. Surv. Bull.*, 1987, **1**, 1770.
8 Vandecasteele, C., *Activation Analysis With Charged Particles*, New York, Wiley, 1988, p. 171.
9 Barishev, V. B., Kolmagorov, Yu. P., Kulipanov, G. N., and Skrinski, A. N., *Zh. Anal. Khim.*, 1986, **41**, 389.
10 *5th All Soviet Union Conference on Activation Analysis and other Radioanalytical Methods, Tashkent, May 26–28*, 1987, Abstracts, **2**, pp. 384–426.
11 Sedykh, E. M., Bannykh, L. N., Ostronova, M. M., Istimiyanova, G. R., Tatsii, Yu. G., Orlova, V. A., Myasoedova, G. V., and Kuz'min, N. M., *Zh. Anal. Khim.*, 1993, **48**, 526.
12 Kolesov, G. M., *Zh. Anal. Khim.*, 1994, **49**, 56.
13 Shubina, N. A., and Kolesov, G. M., *Zh. Anal. Khim.*, 1993, **48**, 889.
14 Shubina, N. A., and Kolesov, G. M., in *Mathematic Methods and Electronic Computers in Analytical Chemistry*, Nauka, Moscow, 1989, pp. 77–81.
15 Anikiev, V. V., Dudarev, O. V., Kolesov, G. M., and Shumilin, E. N., *Geokhimiya*, 1993, **5**, 709.
16 Kolesov,G. M., Prasad, S. K., Anikiev, V. V., and Sedykh, E. M., *Anal. Chem.*, 1993, **38**, 625.

Paper 4/05854B
Received September 26, 1994
Accepted December 19, 1994

Neutron Activation Determination of Noble Metals in Samples of Terrestrial and Cosmic Origin Using Microfire Assay Concentration*

Gennady M. Kolesov and Dmitry Yu. Sapozhnikov

V.I. Vernadsky Institute of Geochemistry and Analytical Chemistry, Russian Academy of Sciences, Kosygin St. 19, 117975 Moscow, Russia

The effects of various factors (composition of mixture, relationship between the mass of mixture and sample, value of the Ni:S ratio, fusion time, and temperature) on the conditions of the fire assay concentration of the noble metals with nickel sulfide were investigated, and a method proposed for their quantitative separation from different geological matrices with a neutron activation determination for up to 10^{-1}–10^{-3} ppb. The proposed method is used to analyse geological samples, *i.e.*, ores, stones, iron meteorites, chromites, soil and lunar rocks.

Keywords: Fire assay preconcentration; platinum group elements; silver; gold; neutron activation analysis; geological materials

Introduction

Determination of the platinum group elements (PGEs), silver and gold in geological samples is difficult because their concentration in the samples varies (to less than 10^{-3} ppb) and their distribution is not similar. Therefore, a universal method is necessary. Neutron activation analysis (NAA) can be used for this task as it has high sensitivity, low detection limits, and allows the analysis of a sample containing a wide range of elements. NAA can be used both in radiochemical (RNAA) and instrumental variants (INAA).[1]

We modified and developed earlier methods for the determination of noble metals (NMs)[2–6] by using them in conjunction with microfire assay preconcentration. This offers the advantages of simultaneous sample decomposition and concentration of the elements.

Various collectors are used for fire assay preconcentration, *e.g.*, Pb, Bi, Sn, Ag, Ni and NiS.[7–13] We used NiS as it was the most appropriate for all the PGEs, silver and gold.

The main objective of the present work was to ascertain the most effective RNAA method for the determination of noble metals in geological matrices of different masses and compositions using fire assay concentration of elements by nickel sulfide.

Experimental

Reagents and Apparatus

The reagents used were as follows: for fusion nickel carbonyl, elemental sulfur, a mixture of potassium tetraborate (or lithium borate), sodium carbonate and silicon dioxide; for formed fusion dissolution concentrated hydrochloric acid; for noble metal extraction control polyvinylbenzylmethylpyrazol sorbent (PVB-MP-10T).[14] All reagents were of analytical-reagent grade and were from Khimreactiv, Russia. The degree of extraction and the detection limits for elements were determined by the activities of the radionuclides ^{103}Ru, ^{109}Pd, ^{110}Ag, ^{191}Os, ^{192}Ir, ^{197}Pt and ^{198}Au. Fusion of samples was carried out in china crucibles of 10–25 ml volume in a muffle furnace; sorption of elements was carried out in a 100 ml conical flask by heating and mechanical stirring.

The radioactivity was counted on a gamma spectrometer equipped with a 4096 channel analyser LP-4900 (Nokia, Finland) or ICA-70 (FMG, Hungary) and high resolution Ge(Li) and Ge detectors. Spectrometric sources were used for instrumental calibration (^{152}Eu, ^{137}Cs, ^{90}Y, *etc.*) Spectral interpretation and elemental composition calculations were carried out according to a particular computer program.[1]

Standards were prepared from stock solutions of single elements with concentrations ranging from 0.10 to 10.0 μg ml^{-1}. Reference materials PCC-1, BCR-1, SARM-7, Cu–Ni sulfide ores VT-1, G-3, stony meteorite Allende, *etc.*, were also used.

Fire Assay Procedure

The powdered sample (0.1–10 g) was placed in a crucible, 1–2 ml of solution were added (containing ^{192}Ir and radionuclides of determinable elements) and the flux mixture, the mixture was then stirred, fused and cooled. Determination of the nickel button containing the NMs was carried out by crushing the crucible and counting the radioactivity. When necessary (for reducing background activity level) the button was dissolved in concentrated HCl with heating and the NM radionuclides were filtered onto a Synpor or Millipore membrane filter for subsequent activity counting.

Results and Discussion

The influence of various factors on the sample decomposition and the NM yield was investigated in detail.

These factors were: the composition of the mixture; the ratio of mixture components; the Ni yield; the value of Ni:S ratio; the duration of fusion; the fusion temperature; the influence of non-noble metals (for example Co, Sc, Cr, Fe, As and Sb); the effect of added non-isotopic carrier, particularly tellurium, on the NM extraction; NM separation from the collector; NM collection using sorbents.

Some of experimental data are given in Figs. 1–5 and Tables 1–3.

Thus the dependence of the chemical yield of nickel in matte (*i.e.*, molten nickel) with respect to the components of mixture is given in Table 1. One can see that when changing the ratio of mixture components from 1 to 10 the nickel yield is, on average, 93 ± 3% reaching the maximum value at approximately 99% at a ratio of 5.

From the data given in Fig. 1 it can be seen that the maximum nickel yield of 95–99% can be achieved when the ratio of mass of Ni:S is 1–1.7.

* Presented at Geoanalysis 94: An International Symposium on the Analysis of Geological and Environmental Materials, Ambleside, England, September 18–22, 1994

Fig. 2 shows that the high iridium yield occurs when the ratio of mixture components is between 1 and 5; when the ratio is outside this range the iridium yield decreases. Iridium duplicates the nickel yield dependence.

Table 2 shows that the dependence of the NM yield on the fusion time for 5–60 min. During the first few minutes of fusion, the nickel yield is very high and then it falls. The highest iridium, osmium and ruthenium yield is observed when a 10 min fusion time is used.

The yield of these elements for 5 g samples (see Table 2) fused for 10–30 min are lower by 5–10% than for 1 g samples; also, the yield is higher by 15–20% when the fusion time is increased to 60 min.

The dependence of Ir chemical yield on temperature, can be seen in Fig. 3. Maximum (100%) yield occurs at 1050 ± 50 °C.

The dependence of the NM (*e.g.*, Ir) microfire assay concentration on the ratio of the masses of mixture and sample are given in Fig. 4. The dependence is different for sedimentary rocks (curve 1) and ultrabasic rocks (curve 2) and has a maximum ratio value in the range 4–20. This is why, regardless of the mineral and petrochemical composition of the samples, we used usually 2–3 fold excess for reliability.

Similar experimental investigations allowed us to ascertain the optimum conditions for fire assay concentration, to evaluate the NM yield and finally to propose an analytical procedure. This procedure is summarized in Fig. 5 as a scheme.

So the mixture content for a sample of 1 g mass is: nickel, 0.66 g; sulfur, 0.4 g, sodium tetraborate (or lithium borate), 4 g; sodium carbonate, 2 g; and silica-gel, 0.3–0.4 g. The irradiation time is close to 20 h with a neutron flux of 1.3 ×

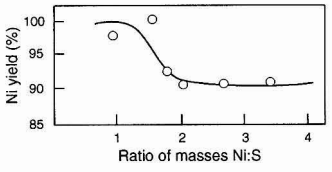

Fig. 1 Dependence of nickel yield on the ratio of the masses of Ni and S.

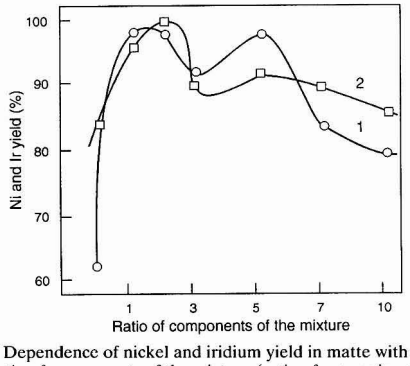

Fig. 2 Dependence of nickel and iridium yield in matte with respect to the ratio of components of the mixture (ratio of masses in ref. 9). 1, Nickel and 2, iridium.

Table 2 Chemical yield dependence of nickel, iridium, ruthenium and osmium in matte on fusion time for samples of different mass with a mixture composition as in ref. 9 (n = 2)

Sample number	Mass of sample/g	Fusion time/min	Chemical yield (%) Ni	Ir	Ru	Os
1	1.0	5	98	60	51	53
2	1.0	10	99	97	98	89
3	1.0	20	76	98	99	96
4	1.0	30	77	88	97	76
5	1.0	60	64	47	51	50
6	5.0	5	95	55	56	59
7	5.0	10	88	92	90	81
8	5.0	20	75	92	88	81
9	5.0	30	70	79	74	70
10	5.0	60	74	71	66	59

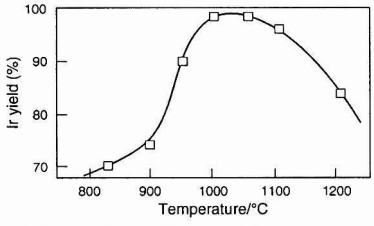

Fig. 3 Dependence of iridium yield on temperature.

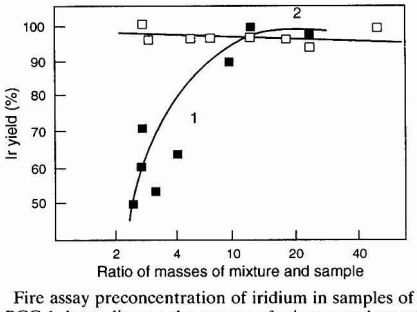

Fig. 4 Fire assay preconcentration of iridium in samples of 1, SM-4 and 2, PCC-1 depending on the masses of mixture and sample.

Table 1 Chemical yield dependence of nickel in matte with respect to the ratio of components of the mixture (n = 3)

Sample number	Mass/g Ni	S	Sample	Na_2CO_3	$Na_2B_4O_7$	SiO_2	Ratio of components	Chemical yield of Ni (%)
1*	0.33	0.2	1.0	1.0	2.0	0.2	1	95
2	0.33	0.2	3.0	3.0	6.0	0.6	3	97
3	0.33	0.2	5.0	5.0	10.0	1.0	5	99
4	0.33	0.2	7.0	7.0	14.0	1.4	7	94
5	0.33	0.2	10.0	10.0	20.0	2.0	10	90

* 'General' ratio of components in the mixture.[9]

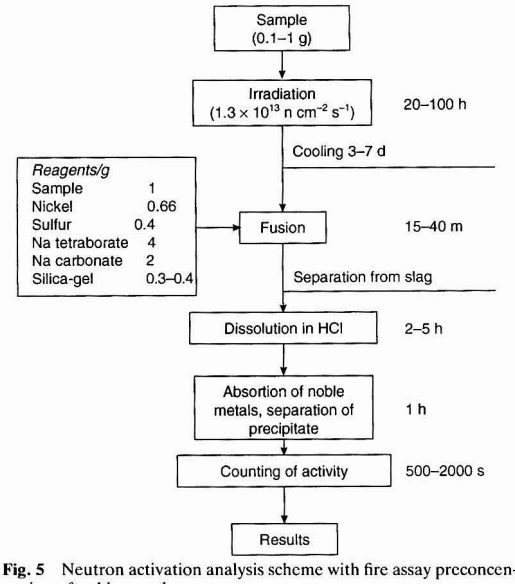

Fig. 5 Neutron activation analysis scheme with fire assay preconcentration of noble metals.

10^{13} n cm^{-2} s^{-1}, the sample is then cooled, melted, separated from the slag and its activity measured. When necesssary, the nickel matte can be dissolved in 9 mol l^{-1} HCl, the NM sorption carried out on sorbent PVB-MP-10T, and the radioactivity measured to calculate the NM content (see Fig. 5).

When the uranium content is high a correction had to be made for the determination of ruthenium.

The detection limits for the elements were also calculated. They were low and similar to the values obtained for minimum detectable concentrations of the individual elements. These data are given in Fig. 6, curve 2, and the signal is a result of the following concentrations: Ir and Au, 0.005 ppb; Os, Ru and Ag, 0.5 ppb; Pd and Pt, 1.0–5.0 ppb (mass of sample, 1.0 g; s_r = 0.05–0.20).

The proposed method can also be used when NMs are preconcentrated (before sample irradiation); but the detection limits in this instance increase by a factor of 1–2 as possible interferences from As or Sb are likely to occur (see Fig. 6, curve 1).

Overall, the proposed method is relatively simple, and it can be used to process 10 samples over 12 h.

When the NM content is high (more than 1.0 ppm) INAA can be used directly.

Control samples were determined using ICP-AES and an agreement of between 5–10% was obtained.

The proposed method was tested by analysis of reference materials and the samples of stoney meteorites; ultrabasic,

Table 3 Results of the microfire assay neutron activation analysis determination of noble metals in some geological materials (ppb*)

Samples	Au	Ag	Ru	Os	Ir	Pt	Ref.
Meteorites—							
Sikhote-Alin	1100 ± 100 1100–1400	— 180–200	4900 ± 200 5400–6000	37 ± 6 27–30	26 ± 5 21–30	4030 ± 200 4100–4400	1
Canyon Diablo	1200 ± 100 1060–2000	— 46.5	5900 5300–7300	2400 ± 200 2000–2900	2200 1800–2400	4900 ± 300 5700–9900	18
Allende	130 145	— 107	760 1150	530 690–850	730 785	1200 1200–1500	19
Standards—							
Peridotite PCC-1	0.91 ± 0.03 0.76–3.2	— —	8.1 ± 0.6 7.4–11.2	8.6 ± 0.5 8.8–12.3	4.2 ± 0.2 3.0–6.6	10.0 ± 0.8 3.5–11.0	20
Basalt BCR	0.9 0.8	— 30–35	0.84 1.0	0.0004 —	0.006 0.004	2.6 2.0	20
Pyroxenite SARM-7	250 ± 25 310 ± 100		520 ± 70 430 ± 60	66 ± 9 63 ± 7	76 ± 8 74 ± 12	3500 ± 500 3740 ± 300	21
Chromites—							
KM-20-5	2.8 —	— —	75 —	140 —	58 —	10 11†	17
KM-II	55 50†	— —	24 —	3 —	16 —	18 18.7†	17
Sediment rocks—							
SM-4	7.0 ± 0.2 5–6	74 ± 10 1000	9 ± 1 9	10 ± 1 1.2	12 ± 1 9–14	58 ± 4 63	3
SDO-1	3.9 4.0	— —	0.8 —	1.2 —	0.75 —	13 —	22
Sulfur–copper–nickel ores—							
VT-1	210 ± 10 260 ± 40	530 —	120 ± 50 105 ± 55	52 ± 5 —	42 ± 3 41 ± 12	2700 ± 200 2550 ± 340	23
G-3	100 ± 10 120 ± 20	— —	190 ± 10 190 ± 15	80 ± 5 —	64 ± 5 54 ± 26	1100 ± 100 1160 ± 110	23

* Numerator = results of present work and denominator from literature values.
† Results from atomic absorption method.

basic, sedimentary rocks, chromites and other samples mentioned earlier. Some of the data obtained are given in Table 3. From these results we can conclude that there is good agreement between the results obtained and the literature data.

The proposed method can be used for almost any geological material. It found most use in our laboratory for the analysis of: sedimentary earth rocks with different stratigraphic boundaries;[3] ultra-refractory inclusions in chondrites,[5] stoney and iron meteorites,[6] soil and lunar rocks.[1]

Conclusion

Neutron activation analysis with microfire assay concentration with nickel sulfide as collector may be used for the determination of very low levels of noble metals in the various geological samples with small masses from 0.1 to 1 g or more.

The use of the microfire assay concentration method for the preliminary enrichment of noble metals is appropriate when they are present at >1 ppb and after irradiation of samples, if they are present at <1 ppb.

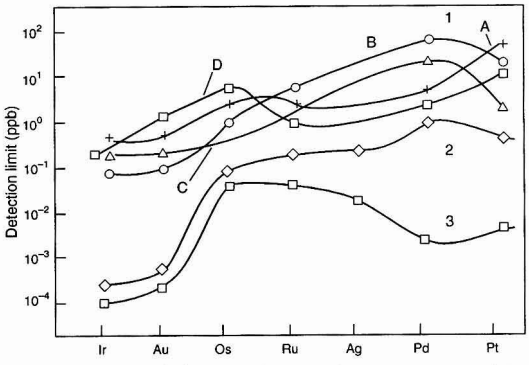

Fig. 6 Detection limits of noble metals in different types of fire assay–neutron activation analysis of rocks. 1, Preconcentration: A, results of present work; B, Hoffman *et al.*[9]; C, Kvasov[15]; D, Shazali *et al.*[16] 2, Concentration of NMs after irradiation. 3, Analysis of the artificial mixture of individual elements.

References

1 Kolesov, G. M., *Z. Anal. Chem.*, 1994, **49**, 65.
2 Kolesov, G. M., Sapozhnikov, D. Yu., and Miklishansky, A. Z., unpublished work.
3 Alekseev, A. S., Nazarov, M. A., Barsukova, L. D., Kolesov, G. M., Nizhegorodova, J. V., and Maniyazov, K. N., *Bull. Moscow Soc. Nat. Exam.*, 1988, **63**, 55.
4 Kapustkina, I. G., Kolesov, G. M., and Feldman, V. I., *Rep. AN USSR.*, 1985, **280**, 755.
5 Lyul, A. Yu., Kolesov, G. M., and Lavrukhina, A. K., *Activation Analysis: Methodology and Application*, Tashkent, 1990, p. 166.
6 Zaslavskaia, N. I., Kolesov, G. M., Barsukova, L. D., and Migdisova, L. F., *Meteoritika*, 1984, **43**, 30.
7 Beamish, F. E., *Analytical Chemistry of Noble Metals*, Mir, Moscow, 1969, pp. 202–254.
8 Brugman, G. E., Gorton, M. P., and Hancock, R. G. V., *J. Geochem. Explor.*, 1990, **37**, 25.
9 Hoffman, E. L., Naldrett, A. J., Van Loon, J. C., Hancock, R. G. V., and Mason, A., *Anal. Chim. Acta*, 1978, **102**, 157.
10 Parry, S. J., *J. Radioanal. Chem.*, 1982, **74**, 605.
11 Parry, S. J., *Z. Anal. Chem.*, 1994, **49**, 65.
12 Artemiev, O. I., Stepanov, V. M., and Madianov, T. N., *Z. Anal. Chem.*, 1987, **42**, 499.
13 Artmemiev, O. I., Stepanov, V. M., Adasbaeva, R. A., and Haldeeva, N. V., *Zavod. Lab.*, 1985, **51**, 11.
14 Myasoedova, G. V., *Fresenius J. Anal. Chem.*, 1991, **341**, 586.
15 Kvasov, A. I., *Geochemistry*, 1987, **7**, 1045.
16 Shazali, I., Van't Dack L., and Gijbels, R., *Anal. Chim. Acta*, 1987, **196**, 49.
17 Kuzmin, N. M., Puhovskaia, V. M., Varshal, G. M., Spivakov, B. Ya., Marytina, T., Volgnets, M. P., Ryebukhin, V. A., Chkbiya, N. N., Grebneva, O. N., and Pavlutskaya, V. M., *Z. Anal. Chem.*, 1993, **48**, 898.
18 Permicko, E., Wasson, J. T., *Geochim. Cosmochim. Acta*, 1987, **51**, 1717.
19 Anders, E., and Ebihara, M., *Geochim. Cosmochim. Acta*, 1982, **46**, 2363.
20 Abbey, S., *Geostand. Newsl.*, 1980, **44**, 163.
21 Rice, T. D., *Certificate of Analysis Platinum Ore SARM-7*, Department of Mineral Resources, Australia, 1988.
22 Standard Sample SDO-1, *GSO 1757-80*, Irkutsk, 1980, p. 11.
23 Standard Sample VT-1 and G-1, *Minzvetmet USSR*, Krasnojarsk, 1977, p. 3 and 10.

Paper 4/05853D
Received September 26, 1994
Accepted January 17, 1995

Analysis of Weathering Products Formed on Saxonean Cretaceous Sandstones*

K. Russ, S. Machill and W. E. Steger

Institute for Analytical Chemistry, University of Technology, 01062 Dresden, Germany

The most obvious appearance of weathering on Saxonean Cretaceous sandstones is the formation of black layers on the surface. The origin of these layers may be increased atmospheric pollution, different climatic conditions, the sandstone itself and the activity of micro-organisms. Various techniques, particularly infrared spectroscopy, X-ray diffraction and Mössbauer spectroscopy, were used to identify accessory minerals in the bulk of different sandstones and to investigate the nature of the weathering products on the surfaces. Salt-like components present are predominantly gypsum. Different iron oxides such as hematite, maghemite and magnetite are involved in the formation of the black layers and explain their dark colour to some extent. The exposure to rain and sunshine has an important influence on the selection or formation of various iron minerals. The main source of the iron is the interior of the sandstone.

Keywords: *Sandstone; black weathering layer; Fourier transform infrared spectroscopy; X-ray diffraction; Mössbauer spectroscopy*

Introduction

Famous buildings all over the world are endangered by increasing atmospheric pollution leading to different kinds of damage. Less compact rocks such as sandstones with a great porosity are highly susceptible to atmospheric attack. Sulfur dioxide is the main factor as it forms the acid rain which causes material damage to natural and artificial stones.[1–3] The acid rain leads to the dissolution of salts, oxides and clay minerals within the stone and the transport of their components to the surface. Hence the black layer and salt efflorescences are formed by mobilized material from within the stone and also by dry or wet deposition of pollutants.[4,5]

Most of the black layers are very thin and hard. These layers contain, in addition to quartz, gypsum and clay minerals and also various iron minerals. Secondary ferrimagnetic oxides resulting from the chemical transformation of iron compounds in soils and parent rocks produce either magnetite or maghemite.[6] The magnetic susceptibility of these compounds is often much greater than that of the parent rocks.[7]

From the documented changes in the appearance of buildings in Dresden it follows that this phenomenon of weathering develops nowadays 10 times faster than 100 years ago. This results from an increased amount of aggressive components in the atmosphere.

Together with physical and chemical processes the presence of micro-organisms on the stone surface has to be taken into account.[8] Inorganic and organic acids, slimes and several other organic compounds from biological activities contribute to the mobilization of stone material and to the destruction of natural stones.[9] The organic matter must be considered also in order to understand the redox processes concerning the iron species.

The salt efflorescences consist mainly of sulfates with their respective hydrates (especially gypsum). The accumulation of sulfates in the porous system of sandstones results in mechanical stress[10,11] and leads to stone destruction by exfoliation of the stone surface. Much is known about the salt efflorescences.[12,13] We have identified, in addition to different sulfate salts, various nitrates, carbonates and occasionally silicate minerals such as kaolinite. Various types of salt efflorescences were also observed on building stones in Sweden and different causes for the creation of the damaging salt layers such as, for instance, anthropogenic sources, groundwater penetration, weather, and so on, were described.[14,15]

The aim of this study was the identification of the non-salt-like components of the black layers in Saxonean Cretaceous sandstones. A comparison of the compounds present before and after weathering was carried out in order to show the participation of material from within the stones themselves in the formation of the weathering crust. The transport and deposition of neogenic minerals of iron is one component of the dark colour of sandstone surfaces.

Experimental

Samples

Fresh sandstone samples provided from different quarries in Saxon Switzerland were analysed to define their state before weathering. The selected types represented the sandstones used for construction of historic monuments in Dresden. They were either quartz-cemented sandstones of type Posta or sandstone of type Cotta with a high content of accessory minerals (up to 10%[16]). The sandstone from Reinhardtsdorf had an intermediate content of accessory minerals.

Corresponding weathered samples from Zwinger, Dreikönigskirche, Kreuzkirche and Kunstakademie in Dresden were available for this study.

Sampling Procedures and Analytical Methods

The quarry-fresh samples were crushed and ground to the size of quartz particles and the accessory minerals were picked out from the quartz matrix under a microscope. The weathered samples also required some preconcentration. Two crusts were rubbed against each other under water. The water was decanted from the settled material. Both fractions were air-dried and investigated.

Infrared spectra were obtained by means of a Bruker Model IFS 88 Fourier transform infrared (FTIR) spectrometer equipped with a deuteriated triglycine sulfate detector. A 'Praying Mantis' attachment (DRA) from Harrick Scientific Corporation was used for diffuse reflection spectroscopy.

* Presented at Geoanalysis 94: An International Symposium on the Analysis of Geological and Environmental Materials, Ambleside, England, September 18–22, 1994.

FTIR spectra were recorded in the range 4800–200 cm^{-1}. The spectral resolution was 2 cm^{-1}. The samples were mixed with KBr in a ratio of 1:200. The discs used for transmittance spectroscopy in the range 500–200 cm^{-1} were prepared by mixing 1 mg of sample with 100 mg of polyethylene.

X-ray powder diffraction measurements were performed at room temperature using a URD 6 counter diffractometer (Freiberger Präzisionsmechanik) with monochromatized Co Kα radiation.

Iron-57 transmittance Mössbauer spectra were obtained at room temperature from powdered samples. The absorber sample contained 10 mg cm^{-2} of Fe. Signals were recorded in a constant acceleration mode on a multichannel analyser with 512 channels. Isomer shifts were calculated with respect to α-Fe.

Results

Investigation of the Bulk Material

The samples selected under the microscope were mainly investigated by IR spectroscopy in the range 4000–400 cm^{-1}. The content of accessory minerals in the varieties of sandstones from Saxon Switzerland is very different[17,18] (Table 1).

Sandstone from type Posta

The quartz-cemented sandstone from type Posta is the hardest sandstone because it contains a very small amount of accessory minerals. Infrared spectra of the bulk material without preconcentration show only the absorption bands of pure quartz. A small amount of kaolinite [$Al_2Si_2O_5(OH)_4$] exists in a few samples. Other clay minerals and also salts such as carbonates or nitrates were not found. Therefore, salt efflorescences on sandstones from type Posta are rare.

All samples contain iron compounds, as disclosed by the reddish-brown colour and from analysis by atomic emission spectrometry (AES). When using IR spectroscopy, the amount of iron compounds in a quartz sample must be higher than 10% m/m for identification of iron oxides and iron oxyhydroxides. The concentration of iron in sandstone from type Posta is not sufficient for identification.

The analysis of the X-ray data using the International Centre for Diffraction Data (ICDD) data files helped to identify the iron phases. The discussion of X-ray data was restricted to the most probable iron minerals. The diffraction peaks were assigned to hematite (α-Fe_2O_3) (Table 1).

Sandstone from type Cotta

The mostly yellow sandstone from type Cotta is a very fine-grained sandstone composed of argillaceous matter. Fig. 1 shows the IR spectrum of the bulk material. The high content of kaolinite is particularly striking and accounts for almost all of the clay mineral content. Its identification by IR spectroscopy is very reliable because of the high intensity and characteristic location of the four OH stretching vibrations (ν_{OH}) in the range 3700–3600 cm^{-1}. Additional positions of kaolinite are at 1033, 1010, 938 and 914 cm^{-1}. The absorption bands at 1167, 1095, 797, 778 and 693 cm^{-1} show that quartz is also present. The absorption bands at 537 and 470 cm^{-1} are due to kaolinite and quartz.[19,20]

A small amount of illite {$(K, H_3O)(Al, Mg, Fe)_2(Si, Al)_4O_{10}[(OH)_2, H_2O]$} exists in a few samples. Of the iron minerals, only goethite (α-FeOOH) was identified by IR spectroscopy. Additional silicate minerals such as nacrite [$Al_2Si_2O_5(OH)_4$], microcline ($KAlSi_3O_8$) and illite/montmorillonite [$KAl_4(Si, Al)_8O_{20}(OH)_4 \cdot xH_2O$] could be identified by X-ray diffraction (Table 1).

Sandstone from Reinhardtsdorf

The sandstone from Reinhardtsdorf has an intermediate content of accessory minerals. Its physical and chemical behaviour is similar to that of the stone from Cotta, but the composition of the accessory minerals is partially different. Kaolinite is present again. Also, a small amount of microcline was clearly identified by X-ray diffraction.

From the brown veins in the sandstone from Reinhardtsdorf, a concentrate of well crystallized iron minerals was prepared. Goethite (α-FeOOH) and lepidocrocite (γ-FeOOH) were analysed together, *e.g.*, in the IR spectra in Fig. 2. The clearly observed absorption band in the OH stretching region at 3143 cm^{-1} and the corresponding bending vibrations δFe–OH at 896 and 797 cm^{-1} are those of goethite.

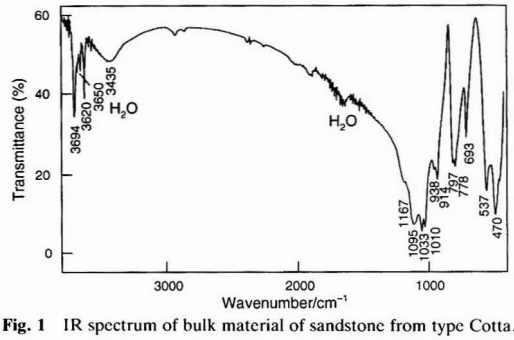

Fig. 1 IR spectrum of bulk material of sandstone from type Cotta.

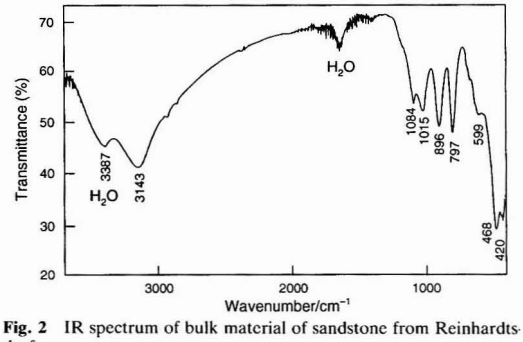

Fig. 2 IR spectrum of bulk material of sandstone from Reinhardtsdorf.

Table 1 Results of measurements of the bulk materials

Variety of sandstone	Accessory minerals*	IR spectroscopy	X-ray diffraction
Type Posta	<1%	Quartz, kaolinite	Quartz, hematite
Type Cotta	Up to 10%	Quartz, kaolinite, illite, goethite	Quartz, kaolinite, nacrite, microcline, illite/montmorillonite
From Reinhardtsdorf	4–7%	Quartz, kaolinite, goethite, lepidocrocite	Quartz, kaolinite, microcline, goethite

* Ref. 18.

Hydroxy group deformation bands occur at 1154, 1022 and 742 cm^{-1} for lepidocrocite.[19] In Fig. 2 only the deformation band at 1015 cm^{-1} is visible. Comparisons show that the less intense second band at 742 cm^{-1} may disappear with increasing amounts of goethite into the flank of the band at 797 cm^{-1} of the latter. The absorption bands at 468 and 420 cm^{-1} are primarily due to goethite and lepidocrocite. A small amount of quartz in the sample indicated by the band at 1084 cm^{-1} also contributes to the 468 cm^{-1} frequency.

In the X-ray diffraction pattern, only goethite was identified. Lepidocrocite was not found. The absorption bands of the iron compounds appear broader than those of quartz, which may be connected with a less perfect crystallization. In such circumstances it may be that a minor component escapes detection by X-ray diffraction.

Infrared spectroscopy is a rapid and easily applied method for identifying different minerals even in mineral compositions provided that the amount of quartz present is not too high. Infrared and X-ray data of Saxonean sandstones show clearly that clay minerals, iron oxides and iron oxyhydroxides are present in all varieties. However, in the sandstone from Posta, clay minerals appear only in trace amounts and only occasionally.

Investigation of Weathering Layers

When collecting and treating samples from different buildings in Dresden, it was observed that the most noticeable differences were linked to the way in which the surfaces were exposed to rain (and snow). The group of K1–K4 (*cf.* also in Table 2) consists of samples with fairly thin weathering layers. G1 and G2 are much thicker crusts with the same appearance, but they were formed on the botton surface of a cornice or hand-rail. These crusts mainly consist of gypsum and also of quartz as the interior of the stone, but these components provide no explanation for the dark or black colour. The crusts are very hard and strongly attached to the surface. After removal from the stone they were prepared in the same way as the other samples.

Sample K1 contains, in addition to quartz, a small amount of kaolinite, according to the IR data but no further information could be obtained. X-ray diffraction shows the presence of microcline. The Mössbauer spectrum consists of a symmetrical sextet and a pronounced central doublet (Fig. 3) and appropriate curves were fitted to it. The parameters of the sextet (Table 3) correspond to hematite of probably small particle size, because the isomer shift is smaller. The presence of magnetite (Fe_3O_4) would give rise to two partially overlapping sextets.[21] The doublet may be attributed to

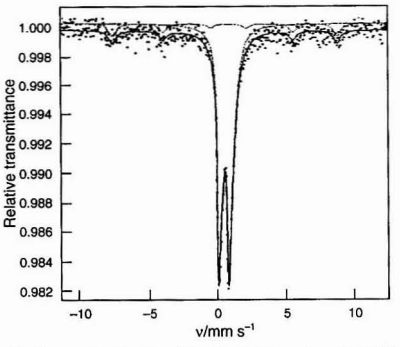

Fig. 3 Mössbauer spectrum of the top layer (sample K1) of the Dreikönigskirche.

Table 3 Values of Mössbauer parameters of the top layer (sample K1) and of the bottom surface (sample G1) of a cornice from the Dreikönigskirche

Sample	Isomer shift (δ/Fe)/ mm s^{-1}	Quadrupole splitting (ΔE_Q)/ mm s^{-1}	Peak width (Γ)/ mm s^{-1}	Area (%)
K1 sextet	0.33	−0.22	0.65	12.4
doublet	0.39	0.72	0.50	87.6
G1 sextet 1	0.36	−0.20	0.27	6.9
sextet 2	0.32	−0.14	0.69	13.8
sextet 3	0.41	0.06	2.26	27.8
doublet 1	0.39	0.74	0.55	43.1
doublet 2	0.90	2.46	1.56	8.5

Table 2 Results of measurements of the black layers

Sample	Description	IR spectroscopy	X-ray diffraction	Mössbauer spectroscopy
K1	Dreikönigskirche, southern facade of tower, rain exposed, cornice, top side, sampling approximately at a height of 60 m	Quartz, kaolinite	Quartz, kaolinite, microcline	Hematite
G1	As for sample K1, but from the bottom surface of the cornice	Quartz, kaolinite, magnetite, maghemite, hematite, (gypsum)	Quartz, albite, maghemite, hematite	Hematite, magnetite
K2	Zwinger, Wallpavillon, 1st story, balustrade of the balcony, top side	Quartz, kaolinite	Quartz, kaolinite, maghemite	NM*
G2	As for sample K2, but from the bottom surface	Quartz, kaolinite, (gypsum)	Quartz, albite, maghemite, hematite	Hematite, magnetite
K3	Kreuzkirche, southern facade at a height of 3–5 m	Quartz, kaolinite	Quartz, kaolinite, microcline	NM*
K4	Kunstakademie, casing of roof, facing west	Quartz, kaolinite	NM*	NM*

*NM = Not measured.

superparamagnetic iron oxides or oxyhydroxides or iron included in clay minerals. The conclusions from the combined results are summarized in Table 2.

Sample G1 shows a similar IR spectrum to sample K1. Quartz, kaolinite and also gypsum are present. Extraction of magnetic iron compounds with the help of magnets gives an enriched sample with a changed feature in the IR spectrum. The shoulder at 524 cm^{-1}, strongly overlapped by the band at 473 cm^{-1}, is split and shifted to 561 cm^{-1} (Fig. 4). The same behaviour, *viz.*, a shift in position with a change in the concentration of mixed iron oxides, has been observed in an investigation of corrosion products.[22] The IR band at 561 cm^{-1} is observed only if the amount of magnetic material is increased. The magnetic iron oxides are magnetite and maghemite. The major absorption band of magnetite is at 574 cm^{-1} (ref. 20) and that of maghemite near 562 cm^{-1}.[19,23] Because of the width of the band (the effect of very poor crystallinity) and the small difference between the major frequencies it is not possible to distinguish between the two iron oxides. This frequency also agrees with the major absorption band of hematite at 544 cm^{-1}. In all probability magnetite, maghemite and hematite are present and contribute to the intensity of this frequency.

X-ray diffraction shows that, in addition to the presence of quartz and albite [$(Na, Ca)Al(Si, Al)_3O_8$], maghemite and hematite are also present. Magnetite was not found, and this confirms the expectation that magnetite is fairly distant from a good crystallographic order.

The Mössbauer spectrum of sample G1 is more complex and shows that, in addition to the central doublet, the magnetic part is split into sub-spectra with different hyperfine field strengths (Fig. 5). The spectrum was fitted with three sextets and two doublets. The first sextet was assigned to hematite.[21] The parameters of the other two sextets suggest the presence of insufficiently crystallized magnetite. This assumption is supported by the asymmetry of the spectrum.

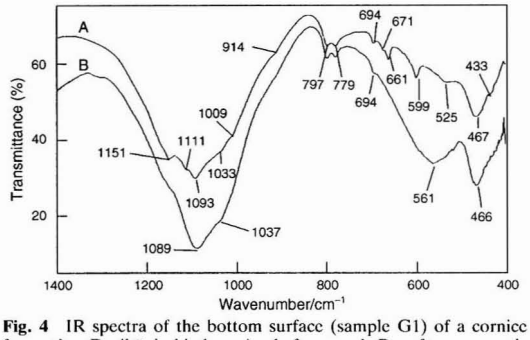

Fig. 4 IR spectra of the bottom surface (sample G1) of a cornice from the Dreikönigskirche: A, before and B, after magnetic extraction.

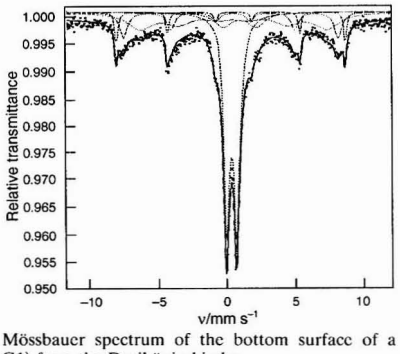

Fig. 5 Mössbauer spectrum of the bottom surface of a cornice (sample G1) from the Dreikönigskirche.

One of the sextets emerges from the fitting process with an isomeric shift of 0.41 mm s^{-1}. This is indicative of participation of Fe^{2+}. An almost surprising confirmation for magnetite is the ratio 28 : 14 = 2 : 1 of the intensities between the second and third sextets. The δ-value of the doublet provides further evidence for the participation of iron with mixed charge number. The doublet represents magnetite in its paramagnetic state and also some oxide–hydroxide, which explains the quadrupole splitting.

Samples K2 and G2 taken from the Zwinger were investigated in the same way. Quartz and kaolinite were detected by IR spectroscopy. Magnetite was not found. A magnetic concentration of iron compounds was not possible. In addition to quartz and kaolinite, maghemite was clearly identified by X-ray diffraction in sample K2. The results of X-ray diffraction and Mössbauer spectroscopy of sample G2 were similar to those for sample G1 (also shown in Table 2). The results for samples K3 and K4 were the same as for sample K1, although Mössbauer spectra were not available.

The spectra measured in the far-IR range do not contribute to further knowledge of the iron compounds contained in the black layer. Bands of quartz dominate and kaolinite is visible.

Essential differences were found in comparing the samples of the top layers (K1 or K2) with the samples of the bottom surfaces of a cornice (G1 or G2). Albite was found in the samples from the downward side whereas microcline exists on the top layer. Very small parts of feldspars enter the sandstone during sedimentation. Their weathering rates are high and the occasionally found orthoclase is one of the more resistant minerals. Kaolinite is the prevailing weathering product of feldspars. The feldspars found on the surfaces studied may be ascribed to deposition from the atmosphere in the form of dust transported from the open sand areas in the north of Dresden or from construction work within the city. The less resistant albite persists under protection from rain, the more durable microcline appears in the top layer.

The iron content in the samples from the bottom of the cornice is higher than in the thin black layers on the top according to results from AES. Hematite was mainly found on the surface, whereas in the bottom surface three different iron oxides were detected. Here the modes of exposure are perceptible again.

Dissolution and re-precipitation of iron oxides depend on pH and probably complexation. The Saxonean sandstones contain sufficient iron minerals which may be dissolved by acidic rain. Iron in solution forms $[Fe(H_2O)_6]^{3+}$. At suitable pH values, monomers react to form polymers by de-protonation. With increasing condensation goethite is formed.[21]

Iron may change its oxidation state and the salts of Fe^{2+} are much more soluble. Hence reducing agents would promote the dissolution. This could increase losses of iron with drainage, but the formation of magnetite requires the reduction of part of the iron from its Fe^{3+} state conserved in the bulk of the stone, for instance by abiotic reaction with organic material. Magnetite might be formed in the surface by biological processes, particularly by magnetotactic bacteria which occur in soils.[24]

In the absence of reducing agents, maghemite may be formed or transformed by oxidation of magnetite.[25] Maghemite is transformed into hematite at fairly high temperatures.

On a clear summer day the temperature of the stone surface can reach 50–60 °C.[26] Freshly formed iron products could be easily transformed into hematite. The availability of Al during the formation of iron compounds often leads to substitution of

Al for Fe, which also influences the transformation processes. On the bottom surface of the stone the end-product, hematite, is present together with maghemite and magnetite. Goethite was not identified on the surface, but a similar phase or an imperfectly ordered hydroxydic precursor is also present.

Depositions from the air caused by industry and traffic will also modify the surface but they are not the primary reason for the black layers. An enrichment of carbon on the surface of the sandstones is detectable in relation to the inside of the stone. The inorganic carbon is negligible; hence the carbon content is due to soot and organic compounds. Many of these organic compounds, resulting from depositions from air and mainly from micro-organisms, have been identified by gas chromatography and mass spectrometry in samples of weathered Saxonean sandstone.[27] Different iron oxides might serve as indicators of the type of environment in which they were formed. However, no firm conclusions can be drawn from the observations reported here.

Conclusions

The identification of all the substances involved in the weathering process requires complementary methods, as several phases are difficult to detect or to discern. The processes of dissolution, formation and transformation are influenced by many factors such as the concentrations or reactants, the presence of other ions and organic matter, and probably also the actions of micro-organisms.

Together with results from earlier quantitative work[17] on the distribution of iron and other metals in surface crusts, both near the surface and at greater depths, it can be concluded that iron on sandstone surfaces mainly originates from the interior of the stone. Goethite, lepidocrocite and hematite were identified inside the stone. Iron is also contained in clay minerals or rarer accessory minerals. The smaller part was not considered separately.

Other iron compounds were found on the surface and were different for varying states of exposure. Hence hematite was found mainly on the top of cornices and balustrades but magnetite, maghemite and hematite on the bottom. The α-phase is more stable than the γ-phase. Iron oxides formed on the top layer were transformed by exposure to light and higher temperature to α-Fe_2O_3. On the bottom surface this process was slower. A reducing agent is required for the formation of magnetite. This must be provided by organic compounds which are washed out by exposure to rain. The iron oxides, and particularly magnetite, are the main reason for the dark colour of the surface of sandstones.

Mössbauer spectroscopy was effective in disclosing the composition of the weathering layer. By using this method it was possible to estimate the part of this ill-defined iron compound, which has a structure between amorphous hydroxide and goethite. The identification of the iron oxides was not possible by IR spectroscopy because of the strong and broad absorption bands of quartz. They are also hard to detect by X-ray diffraction, as their small particles seem to be of an imperfect crystallographic order.

The authors are very grateful to Professor Dr. R. Salzer for granting the use of the facilities of the Institute for Analytical Chemistry, to Dr. P. Fricke and M. Cante, Institut Fresenius Gruppe, Angewandte Festkörperanalytik GmbH, for X-ray diffraction diagrams and to Dr. M. Krause and P. Wartewig, Universität Leipzig, Fakultät für Physik und Geowissenschaften, for the Mössbauer results. The authors acknowledge the help given by M. Hegner in recording the FIR spectra and also acknowledge the support of the DFG (Deutsche Forschungsgemeinschaft) and the Fond der Chemischen Industrie.

References

1 Fassina, V., Lazzarini, L., and Biscontin, G., *Int. Symp. Deterior. Build. Stones (Proc.)*, 1976, **2**, 201.
2 Nord, A. G., and Tronner, K., *Analysis Konservertingstekniska Studier—Rapport RIK 4*, The Central Board of National Antiquities, Stockholm, 1991.
3 Wolf, F., *Dissertation*, Fachbereich Chemie, TU Hamburg, 1991.
4 Nord, A. G., and Ericsson, T., *Studies Conservation*, 1993, **38**, 25.
5 Berryman, J. G., *J. Geophys. Res.*, 1992, **97**, 17409.
6 Mitra, S., *Applied Mössbauer Spectroscopy*, Pergamon Press, Oxford, 1992.
7 Le Borgne, E., *Ann. Geophys.*, 1955, **11**, 399.
8 Vieser, H., *Bild Wissenschaft*, 1987, **12**, 42.
9 Bock, E., and Krumbein, W. E., *Bautenschutz Bausanierung*, 1988, **Sonderheft**, 34.
10 Steiger, M., Wolf, F., and Danneckcr, W., *Conservation of Stone and Other Materials*, E & FN Spon, London, 1993.
11 Sperling, C. H. B., and Cooke, U., *Earth Surf. Processes Landforms*, 1985, **10**, 541.
12 Frost, B., Lunkwitz, R., and Steger, E., *Farbe Raum*, 1988, **2**, 43.
13 Goudie, A. S., *Earth Surf. Processes Landforms*, 1993, **18**, 369.
14 Nord, A. G., *GFF*, 1992, **114**, 423.
15 Schuh, J., *Münchner Geowissenschaftliche Abhandlungen*, 1989, **Reihe B.**
16 Steger, W. E., Lunkwitz, R., and Russ, K., *SPIE*, 1992, **1575**, 634.
17 Steger, W. E., and Russ, K., *DFG-Forschungsbericht*, Fakultät Mathematik und Naturwissenschaften, TU Dresden, 1993.
18 Grunert, S., *Freiberger Forschungshefte*, 1978, **A583**, 65.
19 Wilson, M. J., *Clay Mineralogy: Spectroscopic and Chemical Determinative Methods*, Chapman and Hall, London, 1994.
20 Salisbury, J. W., Walter, L. S., Vergo, N., and D'Aria, D. M., *Infrared Spectra of Minerals*, The John Hopkins University Press, Baltimore, MD, 1992.
21 Murad, E., and Johnston, J. H., *Mössbauer Spectroscopy—Applied to Inorganic Chemistry*, ed. Long, G. J., Plenum Press, New York, 1987, vol. 2.
22 Music, S., Gotic, M., and Popovic, S., *J. Mater. Sci.*, 1993, **28**, 5744.
23 Harder, U., *Praktikumsarbeit*, Analytisches Zentrum Berlin Aldershof, 1989.
24 *Biomineralization*, eds. Mann, S., Webb, J., and Williams, R. J. P., Verlagsgesellschaft, Weinheim, 1989.
25 Schwertmann, U., and Cornell, R. M., *Iron Oxides in the Laboratory*, VCH Verlagsgesellschaft, Weinheim, 1991.
26 Böhme, D., *Diplomarbeit*, TU Dresden, Fakultät Bau-, Wasser- und Forstwesen, 1991.
27 Machill, S., Russ, K., Steger, W. E., and Krumbein, W. E., unpublished work.

Paper 4/05895J
Received September 27, 1994
Accepted January 3, 1995

Trace Enrichment of Metals Using a Supported Liquid Membrane Technique*

Margareta Papantoni, Nii-Kotey Djane, Kuria Ndung'u, Jon Åke Jönsson and Lennart Mathiasson†

Department of Analytical Chemistry, University of Lund, P.O. Box 124, S-221 00, Lund, Sweden

The supported liquid membrane technique offers new possibilities for analytical enrichment, field sampling and speciation. The possibility of using the technique for the enrichment of metals in a flow system with off-line atomic absorption spectrometry in the final analysis step is outlined. Five metals (Cu, Cd, Co, Ni and Zn) have been used as model substances and different approaches to transport metals across the membrane are demonstrated. In one system 8-hydroxyquinoline was used as complexing agent in the sample (donor) solution. In a second system potassium thiocyanate was used in the donor solution and an extractant (Aliquat-336) in the membrane liquid. In a third system 8-hydroxyquinoline was used in the donor solution and Aliquat-336 in the membrane liquid. The parameters important for analytical enrichment are considered. These include factors for determining the extraction efficiency, the possibility of carry-over effects, matrix dependence and long-term membrane stability. The memory effects were below 2% and high concentrations of humic acids or salts did not interfere in the analysis. The long-term stability using di-*n*-hexyl ether in the membrane was 1–2 weeks and with the extractant Aliquat-336 incorporated in the membrane liquid it was 4 d. Determination of metals at levels <1 ppb was possible. The limiting factor for the determination at lower concentrations at present is the metal contamination in the reagents used.

Keywords: Trace enrichment; supported liquid membrane; flow system; metal; geological

Introduction

Liquid membrane technology for extraction in industrial processes is now, after about 25 years of development, well established. The methodology has reached the pilot plant stage in a number of applications. Emulsion liquid membranes (ELMs) have, for example, been used for the recovery of metals from waste waters.[1,2] Bulk liquid membrane (BLM) systems, with the donor and acceptor phases separated by an immiscible membrane phase and supported liquid membrane (SLM) systems, with the organic phase trapped in the pores of a porous polymer, are attractive to use because of their possible potential in the simultaneous enrichment and isolation of analytes from a complex matrix in a flow system. To enhance the mass transport rate, different types of hydrophobic organic compounds have been employed as extractants both for organic compounds[3] and metals.[4–6] Crown ethers, organophosphates and long chain amines are among the most frequently used extractants.

The use of SLM technology for analytical purposes is relatively new and was first demonstrated in 1986 by Audunsson for trace organic compounds.[7] Since then a large number of papers have appeared from the same research group[8–10] related to trace organic analysis, although in a recent paper[11] the possibility of using SLM for trace metal enrichment was briefly considered. Cox and Bhatnagar[12] and Parthasarathy and Buffle[4] have shown that SLM can be used for the analytical preconcentration of Cu and Zn. However, in neither of these two papers was a flow system used and the enrichment factor was linear for only about 30 and 20 min, respectively, giving enrichment factors of 11 and 4 for Zn and Cu, respectively. The use of SLM in flow systems for analytical purposes differs in some important respects from large scale procedures. In analytical SLM enrichment a stagnant acceptor is typically used. This permits the high concentration enrichment factors needed for preconcentration in trace analysis. For quantitative work the enrichment factors must be reproducible and independent of the analyte concentration, the time of enrichment and the sample matrix. However, it is not necessary that the extraction efficiency is close to 100%, as long as the value is constant. The extent of memory effects on the acceptor side must be low to minimize carry-over effects. This is especially important when the analyte concentration in different samples varies widely.

This paper presents the possibilities of using the SLM approach for the analytical preconcentration and clean-up of metals. Different approaches to achieve a transport of the analyte across the membrane are illustrated and important factors, which determine the usefulness of SLM as an analytical procedure for metals, are considered. These include factors determining the extraction efficiency, matrix dependence, long-term stability and the possibility of carry-over effects.

Theory

The liquid membrane enrichment methodology is based on diffusive transport of the analytes across a hydrophobic liquid membrane from a flowing aqueous solution (donor) to a stagnant aqueous solution (acceptor). The theory for mass transfer of analyte species from the sample donor solution to the acceptor solution as well as the conditions for trapping have recently been discussed from an analytical point of view.[13] The following conditions must be fulfilled for an efficient enrichment:

(*i*) The metal ions in the sample solution must form uncharged species before or in connection with the diffusive transport across the membrane.

(*ii*) An efficient trapping (conversion of the metal ion into an inactive form that prevents back-diffusion into the membrane) must take place on the acceptor side.

There are, in principle, two possible ways to form uncharged metal complexes. A combination can also be used. These two possibilities are illustrated in Fig. 1.

* Presented at Geoanalysis 94: An International Symposium on the Analysis of Geological and Environmental Materials, Ambleside, England, September 18–22, 1994.

† To whom correspondence should be addressed.

In extraction system 1, a complexing reagent is added to the sample solution before it passes through the membrane. Here it is important that both the complexing reagent and the formed complex are soluble in the aqueous donor solution. Conditions must be carefully selected so that the fraction of uncharged metal complex in the donor solution is as high as possible. The principle is illustrated in Fig. 1 using the complexing reaction between 8-hydroxyquinoline (8-HQ) and Cu as an example. Here it is possible to find conditions such that the uncharged species, $Cu(8\text{-}HQ)_2$ dominates. In the case of Co only a small fraction will be present as an uncharged species and this leads to low extraction efficiencies.

In extraction system 2 the metals are transported across the membrane using an extractant in the membrane, capable of forming an uncharged ion association complex with a metal ion or a metal complex on the donor side. As an example of extraction system 2, one can consider the enrichment of Co with thiocyanate ions in the sample solution and an ammonium ion (Aliquat-336) in the membrane. The trapping conditions must be such that as large a fraction (denoted α_A) as possible of the analyte is charged on the acceptor side to minimize back-transport to the donor side. When the concentration of uncharged analyte in the stagnant acceptor solution is equal to its concentration in the donor solution, no net transport of analyte occurs. Thus the maximum enrichment factor is $1/(1 - \alpha_A)$. For organic trace enrichment α_A values in the order of 0.001 are easily achieved by selecting a suitable pH in the acceptor solution.[13] Similar values are possible to achieve for the enrichment of metals in several ways. One way is to use a low pH resulting in a release of the metal ions when the complexing agent used for the transport of the metals across the membrane is protonated. A more efficient trapping can be obtained by adding a stronger complexing reagent to the acceptor solution. The complexes formed should be as water soluble as possible and charged. It should also be possible to use a masking metal ion to release the analyte metal ion from the complex used for its transport across the membrane.

Experimental

Membrane Equipment

The SLM device shown in Fig. 2 consists of two circular poly(vinylidene difluoride) (PVDF) blocks (diameter 120 mm, thickness 15 mm) with machined grooves like an Archimedes spiral (depth 0.25 mm, width 1.5 mm and length 250 cm giving a total volume of approximately 0.95 ml). A porous PTFE membrane with polyethylene backing (pore size 0.2 μm, porosity 0.70, total thickness 175 μm, of which 115 μm is polyethylene backing; Type FG, Millipore, Bedford, MA, USA) was impregnated by soaking for at least 15 min in di-*n*-hexyl ether containing 0–15% of Aliquat-336. The membrane was placed between the two PVDF blocks and clamped with eight screws. The screws were covered with a PTFE tube to prevent contact between the stainless-steel screws and the solution in the membrane channels. To avoid leakages a flat seal made of Viton rubber (width 3.0 mm and thickness 0.5 mm) was placed on the acceptor side between the membrane and the PVDF blocks. This construction is somewhat different to those previously used[14,15] where an O-ring of Viton and blocks made of PTFE (softer material) were used. PVDF is a harder polymer material and the purpose of using the flat seal is to cover the net-like structure of the polyethylene back-up of the membrane to ensure that no liquid transport between the two membrane compartments occurs.

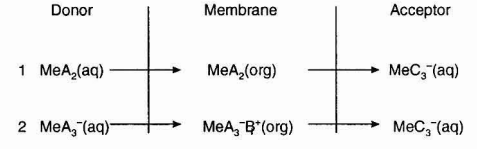

Fig. 1 Transport of a divalent metal ion, Me, using a soluble chelating reagent, HA (weak acid), in the sample solution and a positively charged monovalent ion-pairing reagent, B, in the membrane. The acceptor solution contains a trapping reagent, C, forming a stronger complex than A with the metal, Me. The metal can be transported across the membrane as uncharged MeA_2 (extraction system 1) as well as uncharged MeA_3B (extraction system 2).

Chemicals

8-Hydroxyquinoline *pro analysi*, diethylenetriaminepentaacetic acid (DTPA) *pro analysi*, boric acid, nitric acid 65% suprapur, barium nitrate, calcium chloride, cobalt nitrate *pro analysi*, lead nitrate, magnesium chloride, potassium bromide, potassium chloride, potassium thiocyanate *pro analysi*, silver nitrate *pro analysi*, sodium chloride *pro analysi*, sodium fluoride, sodium hydrogencarbonate, sodium hydroxide monohydrate suprapur, disodium tetraborate decahydrate (borax), sodium sulfate suprapur and zinc nitrate, all from Merck (Darmstadt, Germany); methyltrioctylammonium chloride (Aliquat-336) from Janssen Chimica (Beerse, Belgium); citric acid monohydrate, manganese nitrate, strontium chloride and copper nitrate *pro analysi* from Riedel-De Haen, (Hannover, Germany); di-*n*-hexyl ether from Sigma Chemicals (St. Louis, MO, USA); and humic acid from Fluka Chemika (Fluka Chemie AG CH-, 9470 Buchs, Switzerland) were used in the experiments. Reagent water was purified using Milli-Q-RO-4 (Millipore) equipment. Substitute ocean water was prepared in accordance with ASTM recommendations (ASTM D 1141-90).

Enrichment Procedure

Fig. 3 shows the set-up for the metal enrichment. Metal sample and ligand solutions were pumped from separate containers (A), and transported through the system using PTFE tubes (0.5 mm id) and acid resistant pump tubes (Elkay, Shrewsbury, MA, USA) with the help of a peristaltic pump B (Minipuls 2, Gilson, Villiers-le-Bel, France). After merging the two streams together in a T-connection (C) made of PTFE

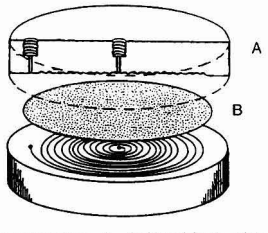

Fig. 2 Membrane separator: A, PVDF block with grooves and B, porous PTFE membrane with polyethylene backing.

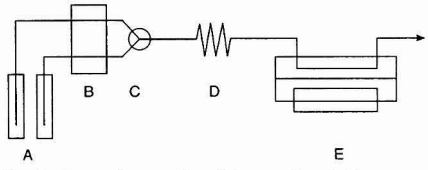

Fig. 3 Set-up for metal enrichment. For A–E see text.

and mixing in a coil (D) the solution enters the membrane separator unit (E). The flow rate of the sample and in the reagent channel was, in most cases, 0.5 ml min^{-1} giving a total flow rate of 1 ml min^{-1} through the membrane unit. After complete enrichment, the stagnant acceptor solution containing the enriched metal ions was transported into an autosampler vial using a peristaltic pump. For the analysis using electrothermal atomic absorption spectrometry (ET-AAS), 2 ml of acceptor solution were transferred directly into the carousel of the autosampler. For flame AAS (FAAS) measurements, 2–5 ml of acceptor solution were used. At a later stage in this investigation, the system was automated using four membrane devices that were processed simultaneously. Details concerning this set-up will be discussed elsewhere.[16] Two different ligands were used, 8-hydroxyquinoline (1×10^{-4} mol l^{-1}) and potassium thiocyanate (0.06 mol l^{-1}). The former was dissolved in a 5 mmol l^{-1} borate solution and the pH was adjusted to 9.8 with 0.1 mol l^{-1} NaOH solution to ensure that the 8-HQ in the donor solution was predominantly in the anionic form. The acceptor solution contained DTPA at different pH levels and at a concentration of between 2 and 100 mmol l^{-1}, with a 3 mmol l^{-1} solution being used in most experiments.

Instrumentation for Final Analysis

For the determination of sample concentrations at parts per billion levels, a Varian AA-1475 atomic absorption spectrometer fitted with a GTA-95 graphite tube atomizer was used. Sample solutions were delivered into the furnace using a Varian programmable GTA-95 sample dispenser. Background correction (deuterium lamp) was found to be important with the relatively high concentrations of organic complexing reagents in our samples. For samples at ppm-level, a Varian AA-6 atomic absorption spectrometer with an air–acetylene flame was used. The operating parameters used for the instruments, *e.g.*, wavelength, slit width, lamp-current and temperature programs were those recommended in the operation manuals.

Results

Extraction Efficiency Considerations

The results below are presented under two headings: extraction efficiency and quantitation. It is vital to know how the extraction efficiency is influenced by different parameters in the system, as this will have an impact on the detection limit as well as on the precision and accuracy of quantification.

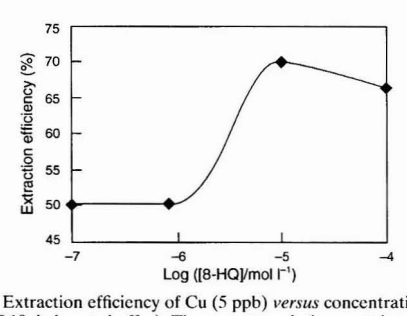

Fig. 4 Extraction efficiency of Cu (5 ppb) *versus* concentration of 8-HQ (pH 10, in borate buffer). The acceptor solution contained DTPA (2 mmol l^{-1}), with pH adjusted to 3 with a few drops of 0.1 mol l^{-1} NaOH solution.

Extraction efficiency versus *concentration of a soluble complexing reagent in the donor solution*

Fig. 4 shows the extraction efficiency of Cu (5 ppb) as a function of the 8-HQ concentration in the sample solution with di-*n*-hexyl ether as the membrane liquid (extraction system 1).

The increased concentration of 8-HQ first leads to the formation of a higher fraction of neutral $Cu(8\text{-}HQ)_2$, which increases the extraction efficiency. At too high concentrations of 8-HQ the increased fraction of negatively charged $Cu(8\text{-}HQ)_3^-$ leads, as expected, to somewhat lower extraction efficiency.

Extraction efficiency versus *concentration of an extractant in the membrane*

Fig. 5 shows how the extraction efficiency of Co (0.5 ppm) in an extractant mediated transport process is influenced by the concentration of the extractant Aliquat-336, dissolved in di-*n*-hexyl ether in the membrane (extraction system 2). The donor solution contained 0.06 mol l^{-1} KSCN.

As the concentration of Aliquat-336 increases, there is first a slight increase in extraction efficiency. The decrease in extraction efficiency at concentrations higher than 4% might be due to the formation of higher order ion association complexes that slow down the diffusive transport through the membrane. An extractant concentration of 4% was used in later experiments that permitted some loss of extractant without significantly changing the efficiency, thus prolonging the lifetime of the membrane.

Extraction efficiency versus *conditions in the acceptor solution*

To prevent changes in extraction efficiency with time, especially for prolonged process times, it is essential that conditions in the acceptor are chosen so that back-transport of analyte species towards the donor side can be neglected. This is the case when the concentration in the acceptor of the uncharged species immediately drops to virtually zero after passing through the membrane.

The trapping process involves breaking the uncharged metal complex and forming charged metal complexes with the trapping reagent DTPA. As both the reagents, 8-HQ and HSCN on the donor and the trapping reagent DTPA in the acceptor, are acids, the trapping efficiency might depend on both the concentrations of these reagents and on the pH of the acceptor solution. Accordingly, DTPA solutions with concentrations between 2 and 100 mmol l^{-1} were investigated and the pH in the acceptor was varied between 2 and 12.

Extraction system 1. Table 1 shows the results obtained for the lowest (2 mmol l^{-1}) DTPA concentration used in these experiments. The results for the other DTPA concentrations were similar.

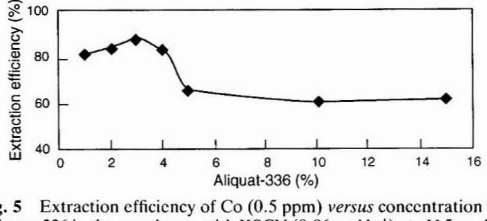

Fig. 5 Extraction efficiency of Co (0.5 ppm) *versus* concentration of Aliquat-336 in the membrane with KSCN (0.06 mol l^{-1}) at pH 5 on the donor side and DTPA (2 mmol l^{-1}) on the acceptor side with pH adjusted to 3 with a few drops of 0.1 mol l^{-1} NaOH solution.

The extraction efficiencies are satisfactory only for Cu. The efficiencies for all DTPA concentrations are generally highest around pH 3. One would expect values of about the same magnitude at higher pH, where the efficiency of the trapping reagent increases. However, the conditions at the interface between the organic liquid in the membrane and the aqueous acceptor solution seem to be important. Experiments with Cu have shown that the reason for the lower extraction efficiencies at higher pH can be explained by slow kinetics. This means that the membrane contains a substantial amount of the analyte, which slowly leaks out into the acceptor. Normally, 2–5 ml of buffer are pumped at flow rate of 1 ml min^{-1} during elution of the analyte in the acceptor. The corresponding time, 2–5 min is too short to remove the analyte from the membrane at pH 8. In fact, more than 2 h are needed. However, the kinetics at pH 3 are much faster, which is illustrated for Cu in Table 1. Obviously the protonation process of the complexing reagent is important and this is facilitated at low pH.

Extraction system 2. Table 2 shows the results obtained for the lowest and highest DTPA concentrations used in these experiments.

The extraction efficiency was independent of both pH and DTPA concentration in the intervals considered. However, there is a tendency for somewhat lower values when the DTPA concentration increases. These changes (of a few per cent.), are not statistically significant at the 95% confidence level. Thus compared to extraction system 1, system 2 is more robust.

Extraction efficiencies using different transport mechanisms

A comparison between the different approaches is given in Table 3.

Generally, the use of an ion-association complex (extraction system 2) seems to lead to higher extraction efficiencies than when only using a chelating reagent in the sample solution (extraction system 1). A combination of two extraction mechanisms can lead to higher extraction efficiencies for some metals. Of the metals considered, this is noted for Ni.

Extraction efficiency versus *flow rate*

The extraction efficiency dependence on flow rate is illustrated in Fig. 6.

Table 1 Extraction efficiency (%) of some metal ions at varying pH using extraction system 1.*

	Extraction efficiency (%)†		
pH	Cu	Cd	Zn
2.5	24(3)‡	8(3)	6(2)
3.0	64(2)	6(1)	7(1)
3.5	50(3)	10(1)	8(2)
4.0	19(2)	10(2)	6(1)
4.5	20(4)	8(2)	6(1)
5.0	20(3)	9(2)	5(1)
5.5	20(2)	9(2)	9(2)
6.0	21(3)	9(2)	8(2)
6.5	11(2)	11(3)	5(1)
7.0	13(3)	8(1)	5(1)
8.0	13(3)	8(1)	8(2)
10.0	6(1)	5(1)	8(2)

* Donor side: a 1 : 1 mixture of 0.1 mmol l^{-1} 8-HQ (pH 10, in borate buffer) and 0.5 mg l^{-1} metal ion solution (pH after mixing, 9.6); acceptor side: a 2 mmol l^{-1} DPTA solution, pH 2.5–10.0 adjusted with a few drops of 0.1 mol l^{-1} NaOH or 1 mol l^{-1} HNO_3.

† Each extraction efficiency is an average value of five experiments. Each analyte had a concentration of 0.5 mg l^{-1}.

‡ Values in parentheses are standard deviations.

At a flow rate of 0.2 ml min^{-1}, corresponding to a residence time of about 5 min of a sample plug passing the donor channel, the extraction efficiency is above 90% and can be further increased by decreasing the flow rate to about 0.1 ml min^{-1}, which is the lowest flow rate that gives good accuracy and precision with the peristaltic pumps used for the enrichment. However, with access to large sample volumes as, for example, in field sampling in natural waters, a high flow rate leads to a high rate of accumulation of metal in the acceptor. This gives lower extraction efficiency but higher concentration enrichment per unit time E_t (the quotient between the concentration in the acceptor phase and that in the donor phase divided with the enrichment time). The results illustrated in Fig. 6(*b*) are in good agreement with previous observations by Jönsson and Mathiasson.[11] For practical reasons a flow rate of 1 ml min^{-1} has typically been used for field measurements.[9]

Thus, even if it is possible to achieve extraction efficiencies close to 100%, the optimal working conditions are attained at far lower values. However, the recovery is still about 100%, as the unextracted part of the sample is found in the effluent from the donor channel and can be accounted for. This can be checked by measuring the concentration in the effluent. Such measurements have been made on numerous occasions by us with satisfactory results.

Influence of salt and humic substances

Two types of possible matrix interferents are especially interesting in natural waters. In freshwater systems, humic

Table 2 Mean extraction efficiency (%) of some metals over the pH range 2–12 using extraction system 2*

	Extraction efficiency (%)†	
Element	2 mmol l^{-1} DTPA	100 mmol l^{-1} DTPA
Cu	81(7)‡	77(6)
Cd	76(4)	80(6)
Co	83(6)	77(5)
Zn	76(4)	70(8)

* Donor side: a 1 : 1 mixture of 0.06 mol l^{-1} SCN^- at pH 5; acceptor side: as in Table 1.

† Each extraction efficiency is an average value of 88 experiments (8 repetitions at each whole pH in the interval). Each analyte had a concentration of 0.5 mg l^{-1}.

‡ Values in parentheses are standard deviations.

Table 3 Extraction efficiency (%) for some metals at concentrations of 0.5 mg l^{-1} using two different systems: A, 8-HQ as chelate in the donor solution (extraction system 1); B, thiocyanate as chelate in the donor solution and Aliquat-336 in the membrane liquid (extraction system 2); and C, 8-HQ in the donor solution and Aliquat-336 in the membrane liquid (extraction system 3)*

	Extraction efficiency (%)		
Element	A	B	C
Cu	70(5)†	85(7)	53(7)
Cd	6(1)	78(4)	37(5)
Co	7(1)	88(5)	49(7)
Ni	14(2)	14(4)	73(5)
Zn	7(1)	79(7)	60(6)

* Donor side: (A and C) a 1 : 1 mixture of 0.1 mmol l^{-1} 8-HQ (pH 10, borate buffer) and a solution of the metals, above pH 9.6 after mixing, (B) 1 : 1 mixture of 0.06 mol l^{-1} SCN^- and the metals at a pH of about 4; acceptor side (A, B and C): a 3 mmol l^{-1} DTPA solution at pH 3, adjusted with a few drops of 0.1 mol l^{-1} NaOH.

substances are often present in concentrations of several parts per million and in sea-water the high salt content might pose a problem. The extraction efficiencies of Cu (0.05 ppm) and Co (0.05 ppm) in reagent water spiked with different concentrations of humic acids is illustrated in Fig. 7. The enrichment times in these experiments were 30 min. For Cu, extraction system 1 was used and for Co extraction system 2.

Humic substances seem to have little influence on the extraction efficiency. This is probably due to a combination of the relative weakness of the complexes formed between humic acids and metals compared with the complexes formed with the added complexing reagents and by the relatively high excess of these complexing reagents compared with the concentration of humic acids in the sample solutions. The influence of high concentration of salt on the extraction efficiency was tested by extracting Co (0.1 ppm) in synthetic sea-water using extraction system 2. No significant effect was observed on the extraction efficiency compared with pure water solution and with 0.1 mol l^{-1} NaCl. From the results it seems likely that the methodology for metal enrichment can be applied to most types of natural waters.

Summary of results concerning extraction efficiency

In short, the conditions both in the membrane and in the acceptor, with respect to reagent concentration and the pH in the acceptor, need to be constant to ensure the same extraction efficiency from time to time. In this respect, ion association complexes seem to be less sensitive to minor changes. A constant extraction efficiency also demands a constant flow rate. The efficiency is not sensitive to high concentrations of salts and humic substances in the sample solution.

Quantitation in Trace Analysis

Memory effects in the membrane

After the enrichment step, there is a risk that a small fraction of the analyte, which remains in the membrane liquid, influences the results of the next sample enrichment (carry-over effect). This was investigated with Cu as a model metal solution and 8-HQ as a complexing reagent. An enrichment was carried out for 40 min, followed by a continuous pumping of liquid on the acceptor side at a flow rate of 1 ml min^{-1}. The volume of the liquid on the acceptor channel was 1 ml, which meant that the channel was swept with one acceptor volume each minute. Aliquots of 1 ml were consecutively collected from the acceptor side for analysis with FAAS. The results obtained are shown in Fig. 8 below.

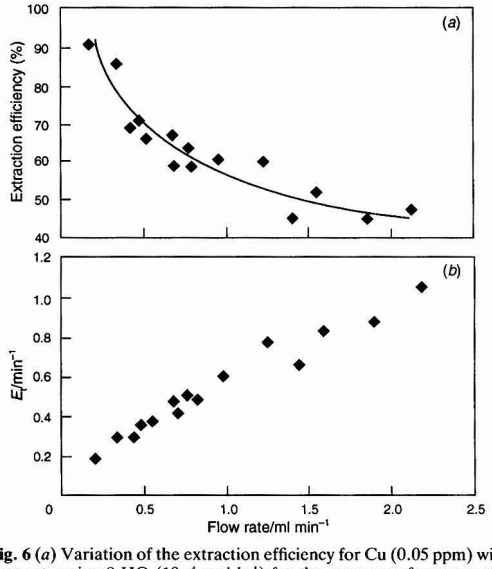

Fig. 6 (*a*) Variation of the extraction efficiency for Cu (0.05 ppm) with flow rate using 8-HQ (10^{-4} mol l^{-1}) for the mass transfer across the membrane and with DTPA (2 mmol l^{-1}) at pH 3 in the acceptor. (*b*) Influence of donor flow rate on the concentration enrichment per unit time (E_t), recalculated from the data used in (*a*).

The extraction efficiency is described satisfactorily by an exponential dilution process. This was confirmed as a linear relation between the logarithm of the detector signal and time. This behaviour can partly be explained by the fact that the net-like polyethylene back-up (115 μm) was directed towards the acceptor solution. However, the most important cause is probably a slow mass transport in the membrane/acceptor interface, as discussed under Extraction efficiency *versus* conditions in the acceptor solution.

Usually, 2–5 ml aliquots of acceptor solution are collected. According to Fig. 8, this means that more than 94% of the total enriched amount will be analysed. As the standards are processed in the same way, the error introduced by this procedure is small. This is especially true since, as shown below, the amount of analyte on the acceptor side increases linearly with analyte concentration on the donor side and with the enrichment time. Between each sample enrichment, the acceptor channel is swept for 5 min, which means that the carry-over effect is less than 1%.

Linearity in the extraction process when varying the analyte concentration

In these experiments, the concentrations in the donor solution of a number of metals, (Cu, Cd and Co) were varied between 1 and 500 ppb with a constant enrichment time of 30 min and the corresponding concentration in the acceptor solution was measured. Each concentration was run on four different membrane devices. In all cases linear relations were obtained. Using 8-HQ (system 1) the product–moment correlation coefficients for Cu, Cd and Co were 0.999, 0.994 and 0.983, respectively. The corresponding values for the thiocyanate system (system 2) for Cu, Cd and Co were 0.990, 0.996 and 0.992, respectively. In no case were the intercepts significantly different from zero at the 95% significance level. Thus the enrichment factor is independent of analyte concentration.

Linearity in the enrichment process when varying the enrichment time

In a typical experimental set-up the total flow rate was 1 ml min^{-1} with a 1 : 1 mixing of the sample and reagent streams, and a volume of 1 ml in both the donor and the acceptor channels. With an extraction efficiency of 70%, which can be obtained for all the metals investigated (see Table 3), a 24 h

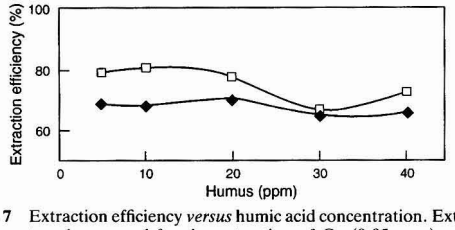

Fig. 7 Extraction efficiency *versus* humic acid concentration. Extraction system 1 was used for the extraction of Cu (0.05 ppm) whilst extraction system 2 was used for the extraction of Co (0.05 ppm).

enrichment then corresponds to a concentration increase in the acceptor of 500 times. To check the linearity in enrichment over long periods of time, Cu and Cd, each at a concentration of 2 ppb were enriched for periods varying from 30 min up to 24 h (six different time values). For each time period, enrichment values were obtained on four different membrane devices using the same two extraction systems as above. In all cases linear relationships were obtained between enrichment time and analyte concentration in the acceptor. With 8-HQ as the complexing reagent, the product–moment correlation coefficients for Cu and Cd were 0.984 and 0.990, respectively. In the thiocyanate system the figures for Cu and Cd were 0.998 and 0.982, respectively. In no case were the intercepts significantly different from zero at the 95% confidence level. Thus the enrichment factor is independent of enrichment time.

Long-term membrane stability

It is essential that the extraction efficiency does not change with time due to physical or chemical changes in the membrane. This has been investigated for membranes impregnated with pure di-*n*-hexyl ether or with 4% m/m of Aliquat-336 in di-*n*-hexyl ether. In the first case (extraction system 1), 8-HQ was used as complexing agent in the donor solution and in the second case (extraction system 2) KSCN was used as the complexing agent. Results indicate that a membrane impregnated with 100% di-*n*-hexyl ether is stable for at least 10 d of continuous use. The corresponding figure for a di-*n*-hexyl ether membrane containing 4% Aliquat-336 at a flow rate of 1 ml min^{-1} on the donor side is at least 4 d.

Limit of detection

The limit of detection using SLM enrichment is determined by several factors such as extraction efficiency, the trapping efficiency (which is related to the sample volume) and the purity of chemicals used in the enrichment. Presently, in sub-parts per billion measurements the background emanating from the metals in the chemicals is the limiting factor. Obviously, the most critical source of contamination is the chemicals on the donor side as impurities in these will be enriched. The concentration of metals in different reagents used in these investigations were determined by analysing concentrated aqueous solutions of the reagents by ETAAS or by ICP-MS. The results from such measurements are shown in Table 4.

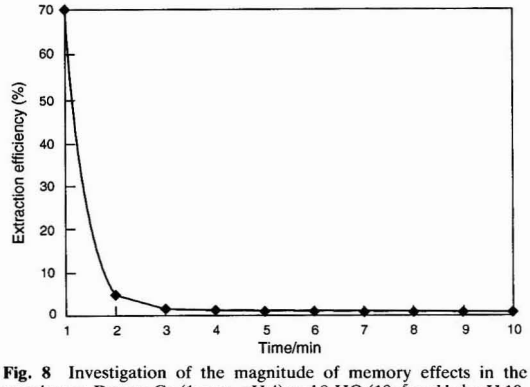

Fig. 8 Investigation of the magnitude of memory effects in the membrane. Donor: Cu (1 ppm, pH 4) and 8-HQ (10^{-5} mol l^{-1}, pH 10, borate buffer). Acceptor: DTPA (2 mmol l^{-1}), pH adjusted to 3 with a few drops of 0.1 mol l^{-1} NaOH solution.

Table 4 shows measured background concentrations. In some instances problems were encountered when attempting to obtain good precision due to the background from the reagents. From the values in Table 4, background contamination levels can be calculated. In extraction system 1 the concentrations of 8-HQ and sodium borate used for measurements at the parts per billion level were 0.0001 and 0.005 mol l^{-1}, respectively. This leads to background levels due to contamination on the donor side for Cu, Cd and Co of 0.06, 0.02 and 0.32 ppb, respectively. The contribution to the background from the small amounts of HNO_3 used on the donor side can be neglected. For sub-parts per billion measurements using 8-HQ and borate a further purification of the reagents is thus desirable. On the acceptor side, the largest contribution comes from DTPA. Using 3 mmol l^{-1} DTPA concentration gives contributions of less than 0.2 ppb of the metals considered. To obtain a sufficient signal in ETAAS measurement, the analyte is enriched up to at least 1 ppb, which means that the contribution from DTPA can usually be ignored. Using extraction system 2 the concentration of thiocyanate at ppb determinations was normally 0.03 mol l^{-1} resulting in background concentrations for Cu, Cd and Co of 0.4, 0.1 and 0.1 ppb, respectively. These values show that when using KSCN for sub-parts per billion determinations a purification is needed, especially for Cu.

A value corresponding to twice the background level can be considered as a reasonable detection limit, as the noise level in the determinations is low compared with the background level. In the final analysis step with ETAAS after the enrichment, the concentrations are so high (normally several parts per billion) that this determination will be more or less routine. Accordingly, one should achieve detection limits using 8-HQ as a chelating agent for Cu, Cd and Co of approximately 0.1, 0.05 and 0.6 ppb, respectively. Using thiocyanate and Aliquat-336, the values are higher for Cu and Cd but significantly lower for Co (about 0.2 ppb).

The detection limit can be further improved by decreasing the reagent concentrations, which in several cases can be achieved with an optimization of the enrichment procedure for each individual metal. This will, however, complicate the simultaneous enrichment of several metals in a mixture. A better way is to purify the reagents. Work in this direction using a supported liquid membrane technique is in progress and promising results have been obtained recently. However, when attempting to determine metals at concentrations of 1 ppt it will be necessary, even with ETAAS, to enrich the sample by three orders of magnitudes. This demands a very efficient trapping with an α_A value of less than 10^{-4} (see discussion in ref. 13). This might lead to the use of higher concentrations of the trapping reagents and hence to further increased demands on reagent purity.

Table 4 Concentrations (in ppb) of some metals in reagents used for membrane enrichment measured by AAS or ICP-MS

Element	NaOH 2.0 mol l^{-1}	HNO_3 1.0 mol l^{-1}	KSCN 0.5 mol l^{-1}	8-HQ 0.001 mol l^{-1}	Borax 0.1 mol l^{-1}	DTPA 0.05 mol l^{-1}
Cu	4.3	0.10	6.4	0.5	0.12	3.0
Cd	4.5	0.10	2.0	0.14	0.15	2.1
Co	4.4	0.30	2.0	2.2	2.1	1.8
Ni	0.10*	0.10	—†	—	—	—
Zn	1.2*	0.4*	—	2.6*	—	—

* Values obtained by ICP-MS.
† Not determined.

Discussion

The supported liquid membrane technique offers new possibilities for metal determinations at low concentrations in complex matrices. The most obvious application is to use the technique as a tool for metal determination in samples brought to the laboratory. Such samples can be water samples or urine and plasma samples, where previously the SLM technique has demonstrated its ability to offer very clean extracts. The possibility of enriching radioactive metal isotopes and analysing the sample using ICP-MS is also worthy of consideration. In this case, impurity of normal metal isotopes in the reagents will not be a problem. This also means that addition of a soluble complexation reagent to the donor could be useful. Otherwise, a system with an extractant in the membrane is to be preferred. Such a system would allow purification *in situ* before the enrichment of a real sample starts. Work is in progress concerning the use of organophosphorous compounds as extractants in the membrane and metal transport using only a pH gradient across the membrane as the driving force.

A second possibility is to use the technique for time-integrated field sampling in a manner similar to that previously described for phenoxy acids.[9,14] Here an enrichment time of 24 h is often advantageous. The experiments above concerning extraction efficiency as a function of enrichment time and long term stability experiments clearly show that 24 h sampling is possible. One advantage with time-integrated field sampling is that the enrichment step comes first in the analytical procedure, which decreases problems with contamination and analyte losses.

A third, and very important possibility, is the use of the technique for studies on metal speciation. Varying the strength of a soluble complexing reagent added to the sample gives an indirect way of studying the strength of naturally occurring metal complexing compounds as well as metal ion adsorption onto particulate matter. The only type of filtration needed in the SLM technique is the use of a 100 mesh net to prevent large particles and, especially in field sampling, small insects from clogging the sampling tube. Colloidal particles supposed to be responsible for transport of a considerable fraction of the total metal content in natural waters, can enter the sampling line and adsorbed metal ions can be stripped off with the aid of a complexing reagent in the donor solution. By incorporating delay coils between the sampling point and the membrane unit, the kinetics of adsorption and of different complexing reactions can also be studied. One great advantage using SLM technique is that natural systems can be studied with the metal concentrations typical for such systems.

A modern alternative to SLM is enrichment based on solid-phase immobilized ligands[17–19] or ion exchangers.[20–22] The procedure is normally performed in columns containing the material in a flow system, frequently with on-line connection to the final analysis equipment based on AAS[23,24] or ICP.[25,26] Compared with this column technique, SLM has both merits and disadvantages. With SLM there are less problems with dirty solutions containing particles or high concentration of organic substances[27] and virtually no breakthrough problems. The disadvantages, however, are that the enrichment per time unit is less than that achieved when using column techniques, the background is at present higher and memory effects due to slow mass transfer kinetics across the membrane may play a more important role. The SLM technique is easy to automate, which means that a slower enrichment can be compensated for by simultaneous enrichment on several parallel membrane devices.[16] Up until now the column approach has demonstrated better possibilities for simultaneous multisampling of metals. However, the organophosphorous extractants we are presently working on seem to be promising in this respect.

Conclusions

In this paper, we have shown the possibility of using supported liquid membranes for the enrichment of metals below the parts per billion level. With purification of reagents the possibility of reaching detection limits at the low parts per trillion level seems good. The stability of the membrane system makes 24 h time-integrated field sampling possible.

The authors are grateful to the Swedish Environmental Protection Agency and the Swedish Natural Science Research Council for providing financial support for this work. The authors also thank F. Malcus for assisting with the automation of the membrane enrichment system and I. Bergdahl for assisting with the ICP-MS measurements.

References

1 Raghuraman, B., Tirmizi, N., and Wiencek, J., *Environ. Sci. Technol.*, 1994, **28**, 1090.
2 Teresa, M., Reis, A., and Carvalho, J. M. R., *J. Membr. Sci.*, 1993, **84**, 201.
3 Shen, Y., Grönberg, L., and Jönsson, J. Å., *Anal. Chim. Acta*, 1994, **292**, 31.
4 Parthasarathy, N., and Buffle, J., *Anal. Chim. Acta*, 1994, **284**, 649.
5 Danesi, P. R., and Reichley-Yinger, L., *J. Membr. Sci.*, 1986, **27**, 339.
6 Danesi, P. R., Chiarizia, R., and Castagnola, A., *J. Membr. Sci.*, 1983, **14**, 161.
7 Audunsson, G., *Anal. Chem.*, 1986, **58**, 2714.
8 Jönsson, J. Å., Mathiasson, L., Trocewicz, J., Lindegård, B., and Olsson, A.-M., *J. Chromatogr.*, 1994, **665**, 259.
9 Knutsson, M., Nilve, G., Mathiasson, L., and Jönsson, J. Å., *J. Agric. Food Chem.*, 1992, **40**, 2413.
10 Nilve, G., Audunsson, G., and Jönsson, J. Å., *J. Chromatogr.*, 1989, **471**, 151.
11 Jönsson, J. Å., and Mathiasson, L., *Trends Anal. Chem.*, 1992, **11**, 106.
12 Cox, J. A., and Bhatnagar, A., *Talanta*, 1990, **37**, 1037.
13 Jönsson, J. Å., Lövkvist, P., Aundunsson, G., and Nilve, G., *Anal. Chim. Acta*, 1993, **277**, 9.
14 Mathiasson, L., Nilve, G., and Ulén, B., *Int. J. Environ. Anal. Chem.*, 1991, **45**, 117.
15 Nilve, G., and Stebbins, R., *Chromatographia*, 1991, **32**, 269.
16 Malcus, F., Djane, N.-K., Johansson, G., and Mathiasson, L., unpublished work.
17 Ljunggren, L., Altrell, I., Risinger, L., and Johansson, G., *Anal. Chim. Acta*, 1992, **256**, 75.
18 Elmahadi, H. A. M., and Greenway, G. M., *J. Anal. At. Spectrom.*, 1991, 6, **643.**
19 Malamas, F., Bengtsson, M., and Johansson, G., *Anal. Chim. Acta*, 1984, **160**, 1.
20 Hiraide, M., Hiramatsu, S., and Kawaguchi, H., *Fresenius' J. Anal. Chem.*, 1994, **348**, 758.
21 Ebdon, L., Fisher, A., Handley, H., and Jones, P., *J. Anal. At. Spectrom.*, 1993, **8**, 979.
22 Haraldsson, C., Lyven, B., Pollak, M., and Skoog, A., *Anal. Chim. Acta*, 1993, **284**, 327.
23 Rodriguez, D., Fernandez, P., Perez-Conde, C., and Camara, C., *Fresenius' J. Anal. Chem.*, 1994, **349**, 442.
24 Mohammad, B., Ure, A. M., and Littlejohn, D., *J. Anal. At. Spectrom.*, 1993, **8**, 325.
25 Porta, V., Sarzanini, C., and Mentasti, E., *Mikrochim. Acta*, 1989, **III**, 247.
26 Prakash, N., Csanady, G., Michaelis, M. R. A., and Knapp, G., *Mikrochim. Acta*, 1989, **III**, 257.
27 Mathiasson, L., Knutsson, M., Bremle, G., and Mårtensson, L., *Swed. J. Agric. Res.*, 1991, **21**, 147.

Paper 4/05058J
Received September 26, 1994
Accepted March 7, 1995

Enrichment of Metals in the Organic Surface Layer of Natural Soil: Identification of Contributions From Different Sources*

Eiliv Steinnes and Oddvar Njåstad
Department of Chemistry, University of Trondheim, N-7055 Dragvoll, Norway

The humus layer of natural soils is frequently used as a sampling medium in geochemical exploration surveys. This procedure has been questioned because the concentration level in the humus layer does not necessarily reflect the geochemistry in the underlying mineral material. Four sources of metals to the organic surface layer are identified: (1) bioturbation; (2) the 'vascular pump'; (3) atmospheric input of marine origin; and (4) airborne pollution. Two methods to define and discuss the contributions from these sources are presented for a survey of Norwegian soils. The first method is based on calculation of ratios of concentrations between humus and undisturbed subsoil within regions of similar topography, climate and air pollution. Concentration ratios consistently below 0.1 and low inter-region variation, such as for Al and Fe, characterize elements supplied to the humus by mixing-in of mineral soil, while concentration ratios appreciably higher than 0.1 identify some additional mechanism. The latter is evident for elements such as Pb, Zn and Cd (air pollution), Sr and Mg (atmospheric input of sea-salt), and Ca (the 'vascular pump'). The second method involves subtraction of the contributions from mineral matter, assuming that the ash content reflects the mass, and C-horizon soil the composition of the mineral matter in the humus layer. As mineral grains mixed into the humus layer are often fairly strongly weathered compared with the undisturbed mineral soil, this method will result in a certain over-compensation; nevertheless it leads to some interesting conclusions as is shown for Ba (the 'vascular pump'), and Zn and V (long-range transport and local air pollution).

Keywords: *Natural soil; metal; source identification; humus layer; mineral subsoil*

Introduction

In cool climates natural soils often have a several centimetre thick surface horizon mainly consisting of humic material, formed through the decay of dead plant material. This humus layer has been, and still is, a frequently used sampling medium in geochemical exploration surveys. Over the years it has become increasingly evident that an enhanced concentration level of a given metal in the humus layer is not necessarily connected to the geochemistry of the underlying mineral material,[1,2] but little seems to have been done to find ways of identifying the contribution from different mechanisms to the supply of metal to organic surface soil horizons.

In 1977, in connection with a large-scale survey in Norway using moss as a biomonitor of atmospheric deposition of heavy metals,[3,4] natural soil samples from the humus layer were also collected at 400 sites and analysed for their HNO_3-extractable contents of some metals.[3] An isopleth of the data obtained for Pb is shown in Fig. 1. The extremely regular geographic pattern with the greatest concentrations in the southern and south-western part of the country strongly suggests substantial influence from long-range transport of airborne Pb. Similar observations were made from investigations in other countries during the same period of time.[5,6]

However, the possibility could not be excluded that higher bedrock concentrations of Pb in the south could explain at least part of the observed pattern. In a subsequent nationwide sampling of soil samples in 1985[7] it was decided to collect samples from two different horizons in the mineral soil in addition to the humus layer. The main purpose of the present paper is to describe two approaches used in order to interpret data from the 1985 Norwegian soil survey with respect to contribution from different sources or mechanisms to the metal composition in the humus layer.

Experimental

Samples were collected from about 500 different sites with natural undisturbed soils regularly distributed over Norway (*cf.* Fig. 2). Most of the soils were podsols with a discrete eluvial horizon. Samples were taken at a depth of 2–5 cm in the

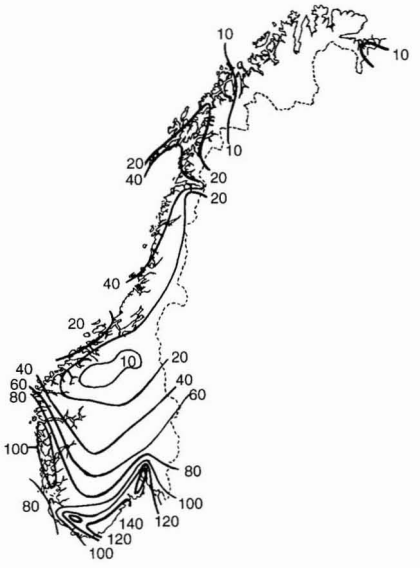

Fig. 1 Distribution of Pb (ppm) in Norwegian organic topsoil sampled in 1977.

* Presented at Geoanalysis 94: An International Symposium on the Analysis of Geological and Environmental Materials, Ambleside, England, September 18–22, 1994.

humus layer (A), in the illuvial horizon where the brown colour was most intense (B), in most instances at a depth of 10–15 cm in the mineral soil, and in the undisturbed subsoil (C) at a depth of about 60 cm.

In the laboratory the samples were dried, mechanically disintegrated and sieved (2 mm). Mineral samples were treated for about 15 h with hot 7 mol l^{-1} HNO_3. Humus samples were ashed at 450 °C and loss on ignition was determined. The residual material was treated with 7 mol l^{-1} HNO_3. After filtration and dilution to 2 mol l^{-1} HNO_3, the sample solutions were analysed with respect to 29 elements using inductively coupled plasma atomic emission spectrometry.[8] For the elements discussed in the following sections, duplicates analysed at different times generally showed an agreement within 15%. A detailed documentation of the data and further statistical analysis are reported elsewhere.[9]

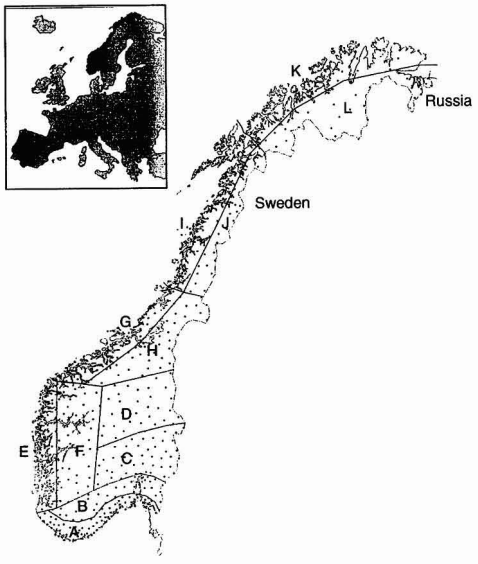

Fig. 2 Sampling sites for the present work. A–L denotes regions of comparably homogeneous topography, climate and air pollution.

Results and Discussion

The assumption originating from the 1977 survey that the large excess of Pb in the surface soils of Southern Norway is of pollution origin and mainly from areas in the other parts of Europe[10] was confirmed by the Pb data shown in Fig. 3 for all three horizons. While the B horizon still has a slightly enhanced level of Pb in the south, presumably from leaching of Pb–humus complexes from the humus layer, there is no such regularity in the C horizon. For Pb, therefore, it seemed easy to perform an analysis of contribution from different sources. For the remaining 28 elements, this process seemed much more difficult, and specific approaches would have to be developed.

Metals may be supplied to the organic surface layer by at least the following four mechanisms: (i) mixing with underlying soil, *e.g.*, by bioturbation; (ii) transfer from the mineral soil by root uptake in plants, and return to the humus layer by leaching or by decay of plant material ('vascular pump'); (iii) atmospheric transfer from the marine environment;[1,11] and (iv) atmospheric deposition of pollutants from local and distant sources.

Two different methods were developed to define and discuss contributions from different sources/mechanisms to the enrichment of metals in the humic surface horizon.

Method I

This method is based on the calculation of ratios of metal concentrations between the humus and undisturbed subsoil (*A*/*C*). For this purpose the country was divided into 12 regions (Fig. 2) according to topographical differences, climatic gradients and air pollution gradients.[4,10] The coastal regions, in particular G, I and K, are strongly affected by the oceanic environment. Regions A, E, B and C are affected by long-range transported air pollutants approximately in that order, while the remaining five regions are much less affected by atmospheric input in general, except for some air pollution influence in the far eastern part of region L due to industries in Russia. The number of sampling sites in each region was about 30–40.

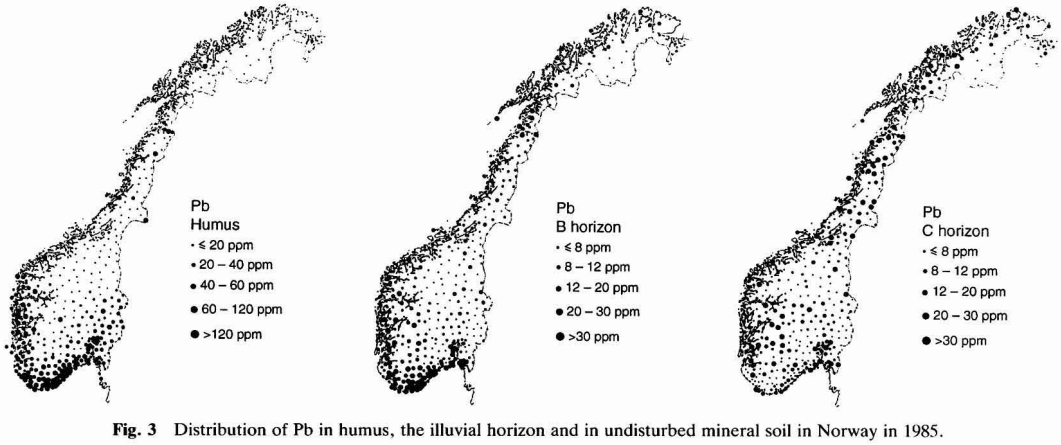

Fig. 3 Distribution of Pb in humus, the illuvial horizon and in undisturbed mineral soil in Norway in 1985.

In Table 1 concentration ratios (*A/C*) are given as median values for six of the above regions. Data for 13 selected elements with strongly different patterns in their geographical distribution are presented. As might be expected, these distributions differ substantially amongst the elements.

The data for the major crustal elements Al and Fe follow each other closely, and may be considered typical for elements supplied by mixing-in of mineral soil. The *A/C* ratios do not vary much between regions and are consistently low, ≤ 0.1. A higher ratio in region C may be interpreted as a generally higher influence from bioturbation in this region.

Any element showing an *A/C* ratio appreciably higher than 0.1 in a given region must be affected by some mechanisms other than mixing with underlying mineral soil. For Pb, as discussed above, the geographical trend indicates strong influence from air pollution. Even in the far north there is evidently a significant input from air pollution, as Pb is unlikely to be supplied either through plant uptake or by marine input. This is in agreement with previous findings based on analysis of peat cores from ombrotrophic bogs.[11] Other elements definitely supplied in significant amounts by long-range atmospheric transport are Zn and Cd. Also, for V, Cr, Ni and Cu the higher *A/C* values in the three southernmost regions may be ascribed to significant contributions from air pollution, as previously shown by analysis of aerosols[12] and mosses.[3,4]

Atmospheric input of sea-salt cations may influence the *A/C* ratio in two distinctly different ways. In some instances a net accumulation in the humus layer is observed, as indicated for Sr in Table 1 from high *A/C* values in marine districts and previously shown for Na and Mg,[1] halogens[13] and Se.[14,15] On the other hand, sea-salt cations such as Mg^{2+} may remove other cations from exchange positions in the humus layer. This effect seems to affect strongly the pattern of Mn (low *A/C* values in the marine regions E, G and H) and possibly also Ba and Ca.

For an element such as Ca, with very constant *A/C* ratios in all regions, the 'vascular pump' mechanism seems to be predominant. It is probably important also for Sr, Ba, Zn and possibly Cu.

Table 1 Median values of concentration ratios (*A/C*) of selected metals in corresponding soils from the A and C horizons for six regions in Norway

Region	A	C	E	G	H	L
Al	0.11	0.20	0.11	0.05	0.08	0.08
Ca	0.50	0.68	0.31	0.36	0.57	0.57
V	0.31	0.36	0.23	0.08	0.12	0.06
Cr	0.21	0.28	0.15	0.06	0.07	0.05
Mn	0.29	0.74	0.10	0.09	0.13	0.32
Fe	0.11	0.14	0.11	0.07	0.07	0.07
Ni	0.53	0.33	0.19	0.09	0.07	0.14
Cu	0.77	0.29	0.51	0.17	0.12	0.16
Zn	2.07	1.77	1.40	0.75	0.85	0.92
Sr	2.48	1.44	1.64	2.00	1.72	1.34
Cd	3.8	2.0	2.6	1.2	1.1	1.0
Ba	1.17	2.32	0.48	0.45	1.23	0.88
Pb	10.4	4.4	8.5	1.9	1.2	1.2

Method II

This method uses an entirely different approach, namely to try to calculate the contribution from mixing-in of mineral soil, subtract it, and use the residual values, which now represent contributions from the truly organic part of the soil, to construct isopleths.

If f is the fraction of an original humus sample remaining after ashing, and if we assume that this fraction consists of mineral material of the same composition as the C horizon, we may calculate the residual concentration R in the humic horizon as follows:

$$R = A - (C \times f) \quad (1)$$

As the mineral grains mixed into the humus layer are often fairly strongly weathered in comparison with C horizon material, the above calculation results in a certain over-compensation, sometimes yielding negative values for R for elements mainly introduced into the humus layer from mixing-

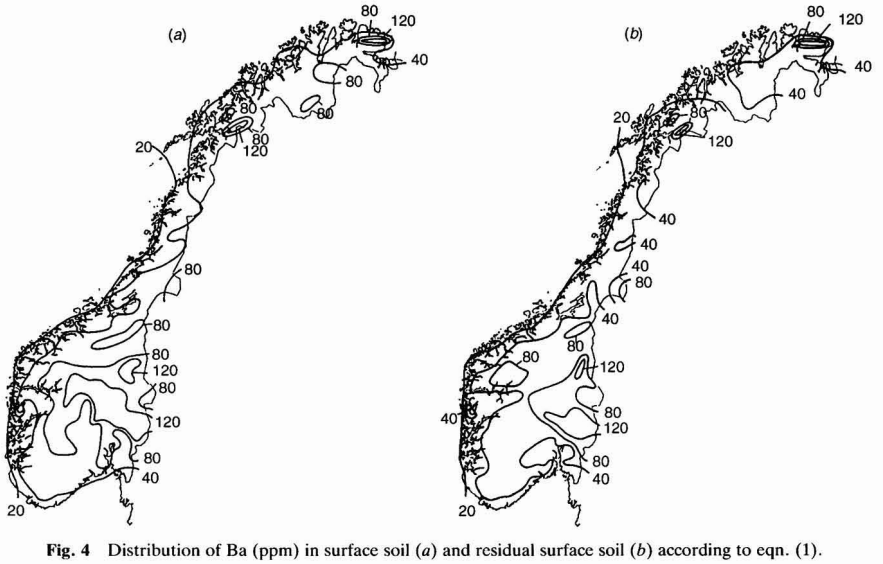

Fig. 4 Distribution of Ba (ppm) in surface soil (*a*) and residual surface soil (*b*) according to eqn. (1).

in of mineral subsoil. Samples of eluvial horizon material would have been preferred, if available. Nevertheless, the use of C horizon data still leads to some interesting conclusions.

In Figs. 4–6 isopleths are shown for three elements with appreciably different origin in topsoils, before and after applying the shown correction for mineral contribution.

For Ba (Fig. 4), which shows a fairly complicated geographical distribution, the correction hardly makes any difference. This may be interpreted as follows: the Ba concentration in the humus layer is mainly due to the 'vascular pump', and the Ba uptake in plants shows a geographical variation depending on the availability in the soil solution, which in turn bears clear connection with the geochemistry.

For Zn, the correction removes some features apparent in the original plot and presumably reflects the geochemistry. What remains is the contribution of Zn associated with air pollution from long-range transport and local sources, overlying a fairly constant level supplied by the 'vascular pump'. The low levels in coastal areas are probably due to the removal of Zn by ion exchange with sea-salt cations.

Considering the third example, the correction removes V almost totally. Small occurrences of residual V associated with

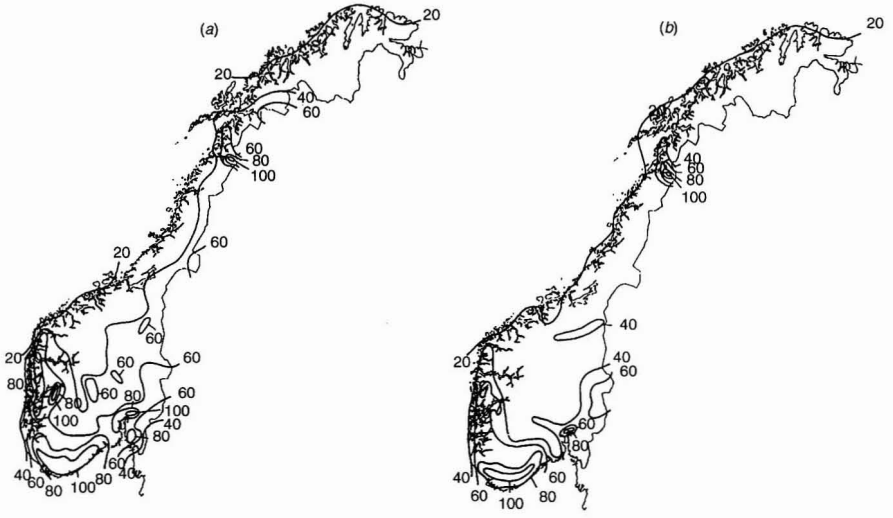

Fig. 5 Distribution of Zn (ppm) in surface soil (*a*) and residual surface soil (*b*) according to eqn. (1).

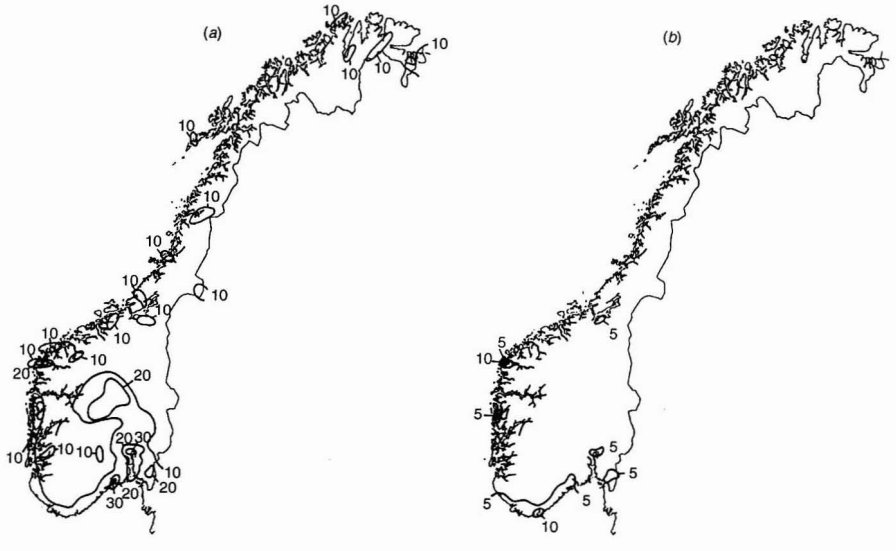

Fig. 6 Distribution of V (ppm) in surface soil (*a*) and residual surface soil (*b*) according to eqn. (1).

air pollution are found in the south (long-range transport) and around some major towns and smaller sites (local pollution).

References

1 Låg, J., *Acta Agric. Scand.*, 1968, **18**, 148.
2 Allen, R. O., and Steinnes, E., *Ecological Impact of Acid Precipitation*, eds. Drabløs, D., and Tollan, A., Sur nedbörs virkning på skog og fisk (SNSF) Project, Oslo-Ås, 1980, pp. 102–103.
3 Rambæk, J. P., and Steinnes, E., in *Nuclear Methods in Environmental and Energy Research*, ed. Vogt, J. R., US DOE CONF-800433, US Department of Energy, 1980, pp. 175–180.
4 Steinnes, E., Rambæk, J. P., and Hanssen, J. E., *Chemosphere*, 1992, **35**, 735.
5 Siccama, T. G., and Smith, W. H., *Environ. Sci. Technol.*, 1978, **12**, 593.
6 Heinrichs, H., and Mayer, R., *J. Environ. Qual.*, 1980, **9**, 111.
7 Bølviken, B., and Steinnes, E., in *Heavy Metals in the Environment*, eds. Lindberg, S. E., and Hutchinson, T. C., CEP Consultants, Edinburgh, 1987, vol. I, pp. 291–293.
8 Ødegård, M., *J. Geochem. Explor.*, 1981, **14**, 118.
9 Njåstad, O., Steinnes, E., Bølviken, B., and Ødegård, M., *NGU Rapport 94.027*, Geological Survey of Norway, Trondheim, Norway, 1994 (in Norwegian).
10 Steinnes, E., in *Lead, Mercury, Cadmium and Arsenic in the Environment*, eds. Hutchinson, T. C., and Meema, K. K., Wiley, New York, 1987, pp. 107–117.
11 Hvatum, O. Ø., Bølviken, B., and Steinnes, E., *Ecol. Bull. (Stockholm)*, 1983, **35**, 351.
12 Amundsen, C. E., Hanssen, J. E., Semb, A., and Steinnes, E., *Atmos. Environ.*, 1992, **26A**, 1309.
13 Låg, J., and Steinnes, E., *Geoderma*, 1976, **16**, 317.
14 Låg, J., and Steinnes, E., *Ambio*, 1974, **3**, 237.
15 Låg, J., and Steinnes, E., *Geoderma*, 1978, **20**, 3.

Paper 4/06270A
Received October 13, 1994
Accepted January 6, 1995

Distribution and Partitioning of Copper, Lead and Zinc in Stream Sediments Above and Below an Abandoned Mining and Milling Area Near Pecos, New Mexico, USA*

Lynn A. Brandvold, Virginia T. McLemore and Catherine O'Connor
New Mexico Bureau of Mines and Mineral Resources, Campus Station, Socorro, NM 87801, USA

Donald K. Brandvold
Chemistry Department, New Mexico Institute of Mining and Technology, Socorro, NM 87801, USA

A reconnaissance study of base metals and mercury in stream sediments from along the Pecos River from North-eastern to South-eastern New Mexico showed elevated levels of copper, lead and zinc at two areas: below an abandoned mine waste dump and below an inactive mill. Zinc was also present at elevated levels in the area of a fish hatchery. During subsequent sampling trips, stream-sediment samples were collected from tributaries as well as the main stem of the river from the Pecos Wilderness boundary south to Villanueva State Park, a distance of approximately 88 km. Sediments were sieved to obtain the 2 mm to 63 μm and <63 μm size fractions and analysed for copper, lead and zinc using *aqua regia* dissolution and flame atomic absorption spectrometry. The smallest size fraction, which typically constituted 10% or less of the mass of the sample, contained the highest concentrations of copper, lead and zinc with the exception of Willow Creek at the mine waste dumps and San Miguel, a site downstream. Partial dissolution techniques were employed on the size fractions from selected sites to estimate exchangeable, organic and oxide-bound metal forms. Copper was the only metal with a significant association with the organic fraction (about 26% with more than half the sites having 20% or greater). The largest amounts of copper and lead (about 56%) were in a form solubilized by *aqua regia* but not by the three extraction techniques. In contrast, the largest amount of zinc (about 52%) was associated with the iron and manganese oxide fraction. A significant amount of lead (about 38%) was associated with the oxide fraction with very little associated with either exchangeable or organic fractions. Zinc fractionation was low for the exchangeable and organic forms with the exception of significant amounts of exchangeable zinc at sites below the mine waste dump.

Keywords: *Stream sediment; metal partitioning; particle size fraction; copper, lead and zinc*

Introduction

A reconnaissance study of base metals and mercury in water and stream- and lake-sediment samples along the Pecos River in Eastern New Mexico (Fig. 1) was undertaken in 1992 in response to concerns about heavy metals from mineralized areas along the river travelling with the sediments and being deposited in reservoirs located on the river. A source area of particular concern was the upper Pecos River, a highly mineralized area where an old mine and waste tailings were located adjacent to the river (Fig. 2). The Lisboa Springs Fish Hatchery, located 18 km downstream of the mine site, lost 86 000 fish in March 1991 and the loss was blamed on heavy elements washed into the river from the abandoned mine area.[1] High levels of lead in the soil, some as high as 20 000 ppm, along the roads and campgrounds in the area were reported.[2] Residents and tourists were cautioned by the New Mexico Environment Department (NMED) against 'playing in the river during times of heavy runoff because that's when sediment containing heavy metals gets stirred up'.[3]

The reconnaissance study showed elevated levels of copper, lead and zinc in sediments at two areas in the upper Pecos River: below the abandoned mine waste dump (Pecos mine) and below an inactive mill.[4] Zinc was also found at elevated levels in the area of the Lisboa Springs Fish Hatchery.[4] An extensive sampling programme over a two year period was subsequently undertaken to include additional sample sites along the upper Pecos River and its tributaries in order to study the concentration, distribution and partitioning of

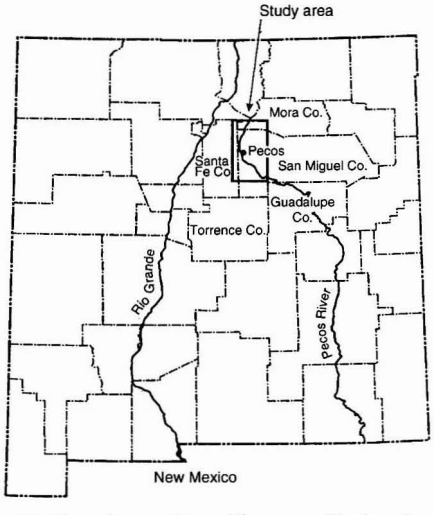

Fig. 1 Location of upper Pecos River area, North-eastern New Mexico, USA.

* Presented at Geoanalysis 94: An International Symposium on the Analysis of Geological and Environmental Materials, Ambleside, England, September 18–22, 1994.

copper, lead and zinc in the stream sediments. The Pecos River is the major river system of Eastern New Mexico and West Texas. The region is dependent on this river for irrigation water and recreation. Anything that shows potential for contaminating the river or its reservoirs is of major concern.

Metals that are released through weathering of mine waste dumps and mill tailings will eventually be partitioned into various chemical forms by complex chemical reactions such as adsorption, solubilization, precipitation and ion exchange.[5–7] Some knowledge of these forms is essential in estimating the transport and bioavailability of these metals. Partial dissolution techniques have been used by many researchers in an attempt to identify these various metal forms (for example, see refs. 8–14). These techniques differ from one another and each has various limitations.[15] The techniques are not generally selective in that a partial extractant designed to dissolve a certain chemical form may fall short of specificity in one way or another and may extract more or less of a component than intended. The extractants have also been applied singly or sequentially. Overlap can occur in both procedures because of the non-selective possibilities of the extractants and also in the sequential procedure because of the order in which they may be applied. Despite these limitations, extraction procedures are very useful for assessing the relative importance of the different metal forms that may be present in the sediments. For this study, the method of Levy *et al.*,[10] with some changes, was used because of similar geology, mineralogy and environmental concerns.

Study Area

The area of study covers the upper Pecos River with its many tributaries from the southern Pecos Wilderness southward to Pecos and Villanueva (Fig. 2). Elevations range from 1800 to nearly 4000 m. The climate varies from semi-arid in the lower elevations to alpine in the mountains. Vegetation and precipitation also vary according to changes in elevation, with greater amounts in the mountains.

The geology is diverse and structurally complex with rocks ranging in age from Proterozoic to Recent. Lithologies are likewise diverse, ranging from metamorphic and plutonic rocks to sandstones, shales and limestones. Mining has occurred sporadically in the area. The largest district is the Willow Creek district which includes the Pecos mine (Fig. 2). Total production from the Pecos mine amounts to over 2.1 million tonnes of ore grading 2.9% lead, 9.2% zinc, 0.4% copper, 82 g t^{-1} silver and 2.7 g t^{-1} gold worth over $40 million. Three additional districts: Glorieta, Tecolote and Santa Fe, also occur in the area, but production has been minor.

The Pecos mine was first operated in 1881, with production occurring in the early 1900s and again from 1927 to 1939. Production also occurred in 1943–44 from the dumps. The dumps, located at the mine site, consist of waste rock generated during mining activities and are now a source of acidic drainage causing elevated levels of metals and other elements to be released into the environment.[16] The acidic drainage is a result of meteoric water reacting with pyrite and other sulfide minerals. The dumps cover an area approximately 7.7 ha in size. Estimates of the volume of waste rock vary from 66 151 to 72 630 m^3 of material. The waste pile varies in thickness from 6 to 13 m. Mineralogically, the mine waste pile is very heterogeneous. The most common gangue minerals include quartz, clay minerals, altered feldspars, chlorite, iron and manganese oxides, and pyrite. Ore minerals include sphalerite, galena and chalcopyrite. Numerous discrete and diffuse seeps occur along the base of the mine waste pile. The number of seeps and amount of water varies according to daily storm events as well as year to year. Brown and while iron and aluminium oxide and hydroxide precipitates containing copper, lead and zinc are present along the course of the seeps, the drainage into Willow Creek and the adjacent wetlands area.

The ore mined at the Pecos mine was transported by aerial tramway approximately 19 km to the mill site in Alamitos Canyon (Fig. 2). The rejected material from the mill was conveyed to the tailings pond in the canyon and held in place by two earthen dams, 0.7 and 1.5 km downstream from the mill. Today the tailings pond occupies approximately 14 ha in the bottom of Alamitos Canyon.[17] During periods of high runoff, discharge from the tailings pile flows through Alamitos Canyon, and could reach the village of Pecos, and the Pecos River. Reclamation is currently underway with the construction of a stream channel through the tailings pile and stabilization of the tailings by covering with clay, gravel and soil.

The Lisboa Springs Fish Hatchery, located 18 km below the mine site, was constructed in 1921. In 1933, the Pecos Wilderness was established by the US Forest Service. In 1950 the New Mexico Game and Fish Department (NMGFD) purchased approximately 810 ha in the Pecos mine area, which includes the mine site, mine waste dumps and adjacent valley areas. The NMGFD and other government agencies utilized the mine waste dumps for road fill and base material in the campgrounds along the Pecos River from the 1930s to the late 1970s, resulting in wide dispersion of material containing copper, lead and zinc.

There are currently numerous multi-disciplinary studies ongoing in the upper Pecos River area. AMAX Resources

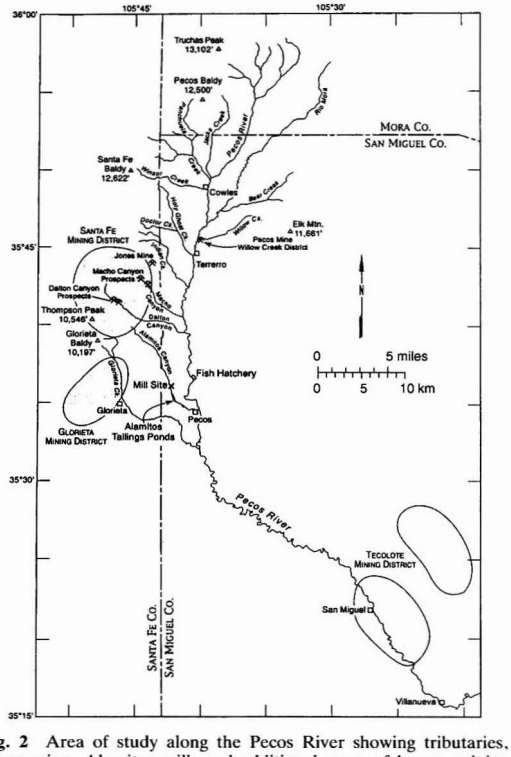

Fig. 2 Area of study along the Pecos River showing tributaries, Pecos mine, Alamitos mill, and additional areas of known mining districts.

Conservation Company and the NMED are conducting environmental evaluation and remedial studies in the immediate area of the Pecos mine. NMED is overseeing remediation at the mill site in Alamitos Canyon. The US Forest Service and the New Mexico State Highway and Transportation Department are removing the mine tailings from campgrounds and roads. The NMGFD and the US Fish and Wildlife Service are studying the fish kills at the Lisboa Springs hatchery.

Experimental

Sampling Sites

Sample sites are listed with a brief description in Table 1. Sites are also shown in Fig. 3. After the original reconnaissance trip in September 1992, six more sampling trips were undertaken, from November 1992 to May 1994, with additional sites added. A total of 31 different sites were sampled. Samples were collected at mid-stream where possible. High velocity stream flow and/or water depth made this impossible at many sites on the main stem of the river during spring run-off and at these sites, samples were collected close to the bank. Water depths varied from site to site as well as during high flow (May–June) and low flow (September–November) conditions. The maximum water depth was approximately 3 m. Natural sediment traps, such as bends in the river or large boulders, were sampled wherever possible. The main stem has many large rocks and pebbles so an effort was made to collect only the coarse-sand size and smaller grains. The samples are thus biased in this regard. The bias is towards forms of metal-containing compounds or particles that are transportable. This includes soluble substances and those particulates that may be mobilized by stream flow under any conditions.

Sample Treatment

Samples were stored in plastic zip-locked bags and transported in coolers. Samples were air-dried (2–14 d) and gently disaggregated, if necessary, by stirring in a mortar with a pestle. Chemical analyses on solids are typically performed on samples oven-dried at constant temperature, usually 80 or 105 °C.[18,19] The mercury content of samples in this study was also desired and concern for mercury losses on oven drying led to the air drying of samples. Oven drying may also alter the mineralogy of the sediment. Samples were not crushed for the work reported here because the intention was to determine the trace metals that were environmentally available without mechanical crushing, which could potentially release more metals. Samples were mixed by forming a cone and dividing the cone into four parts. Each opposite fraction was mixed and then the two halves were mixed. This method was repeated at least five times. The >2 mm size fraction was removed with a stainless-steel sieve. A portion of the <2 mm size fraction was split out and designated as 'whole' sample. The samples were then further sieved with stainless-steel sieves into 2 mm to 63 μm and <63 μm size fractions. All the fractions were weighed. The whole, the 2 mm to 63 μm and the <63 μm fractions were analysed for copper, lead and zinc by flame atomic absorption spectrometry (FAAS) following an *aqua regia* (15 ml HCl and 5 ml HNO_3) digestion of 1 g samples to dryness and reconstitution to 50 ml with 5% HNO_3. *Aqua regia* digestion more closely estimates the total amount of metals environmentally available and for this paper will be referred to as total metals with the realization that total metals obtained in this manner may not be the same as those obtained by a method such as X-ray fluorescence. Concentrations in whole samples (<2 mm fraction) are not reported in this paper.

Partitioning studies were carried out using essentially the method of Levy *et al.*[10] with the changes noted below. Even though overlap between extraction procedures with regard to the various forms undoubtedly exists, the terminology of Levy *et al.* will be used throughout this paper and each form is defined by the particular extraction procedure. Levy *et al.* used a single extraction scheme on air-dried sediments. However, because of sample size constraints, particularly in the <63 μm fraction, the exchangeable and oxide-bound extractions were performed on the same sample portion. The organic-bound extraction and the *aqua regia* digestion were carried out on separate portions of the sample. It was felt that combining the exchangeable and oxide-bound extractions would probably result in the least amount of overlap. For extraction of total metals, Levy *et al.* used 4 mol l^{-1} HNO_3 at 80 °C for 8 h as opposed to *aqua regia* digestion. Exchangeable metals (referred to as the exchangeable fraction) were extracted by weighing 2.000 g of sediment into a polyethylene centrifuge tube and treating with 25 ml of 1.0 mol l^{-1} $CH_3CO_2NH_4$ at pH 7.0. The suspension was shaken for 30 min, centrifuged at low speed to separate solids from liquid and the liquid portion decanted. Copper, lead and zinc were determined in the liquid portion by FAAS using matrix-matched standards. Metals adsorbed onto iron and manganese oxide surfaces (referred to as the oxide-bound fraction) were extracted by adding 25 ml of 0.25 mol l^{-1} NH_2OH–HCl in 25% CH_3COOH to the centrifuge tubes containing the sediments from which the exchangeable metals had previously been extracted. The tubes were heated to 90 °C for 8 h during which time the tubes were inverted several times to ensure mixing. The solutions were again analysed by FAAS for copper, lead and zinc using matrix-matched standards. Organic fraction-associated metals (referred to as the organic-bound fraction) were extracted by placing 1.000 g of sediment in a polyethylene centrifuge tube with 20 ml of a solution of 0.10 mol l^{-1} $Na_4P_2O_7$ and 0.10 mol l^{-1} NaOH at pH 13 and shaking for 16 h. Solutions were filtered through Whatman No. 42 filter-paper and the filtrates analysed for copper, lead and zinc by FAAS, again using matrix-matched standards. These procedures are shown diagrammatically in Fig. 4.

Results and Discussion

Particle size analyses were completed as part of this study but are not presented here. Several findings of the particle size analyses are of interest to this study. Particle size distribution varies from site to site. However, the <63 μm fraction represented the smallest mass per cent. of the sample collected, averaging approximately 8%. Six sites typically had amounts of the smallest size fraction exceeding 10%: (1) Willow Creek at the highway (WH), (2) Willow Creek below the seeps (BS), (3) Willow Creek at the confluence (WC), (4) Alamitos Creek below the mill (AM), (5) the Pecos at San Miguel (SM) and (6) the Pecos at Villanueva (V).

Mean, ranges and standard deviations for copper, lead and zinc for both size fractions are presented in Table 2. Duplicate samples were run with each batch of samples. Agreement between duplicates was within a relative 3% for copper, 8% for lead and 5% for zinc. Standard reference materials were included in runs ten times throughout the study. Canada Centre for Mineral and Energy Technology (CANMET) stream sediment reference materials STSD-1, STSD-2, STSD-3 and STSD-4 were chosen as reference materials because they were of similar matrix, and 'acid extraction' values as opposed to total values were available for these materials. The materials are newly available and confidence intervals have not yet been established. These quality control data are given in Table 3. Mean values of copper, lead and zinc in both size

fractions for each site are also shown graphically in Figs. 5, 6 and 7, respectively. The range of metal values at the same site on different trips was large in two regions: (1) from Willow Creek at the highway (WH) to the Pecos River confluence (WC) and downstream to Terrerro (T), and (2) from Alamitos Creek at the mill (AM) to the village (AV) and downstream to

Table 1 Description of sample sites along the Pecos River

Symbol	Name	Latitude	Longitude	Description
UP	Upper Pecos	35°49′30″	105°39′5″	* Near Pecos Wilderness boundary, along main stream of Pecos River
J	Jacks Creek	35°49′30″	105°39′7″	* Along Jacks Creek upstream of the confluence with the Pecos River approximately 1 m wide
P	Panchuela Creek	35°49′55″	105°39′55″	Along Panchuela Creek, upstream of the campground, approximately 1.2 km upstream of the confluence with Pecos River. Panchuela Creek is less than 1.5 m wide
BJ	Pecos below Jacks Creek	35°49′28″	105°39′14″	* West side of Pecos River approximately 50 m downstream of the confluence of Jacks Creek (upstream of bridge). Pecos River is approximately 4 m wide
Wi	Winsor Creek	35°48′56″	105°40′39″	Along Winsor Creek, upstream of the campground, approximately 1.8 km upstream of the confluence with Pecos River. Winsor Creek is less than 1.5 m wide
C	Pecos at Cowles	35°48′42″	103°39′30″	* Pecos River at Cowles, upstream of the bridge. Pecos River is approximately 4 m wide
RM	Rio Mora	35°46′44″	105°39′15″	Along Rio Mora, upstream from campground approximately 50 m, approximately 0.6 km upstream from confluence with Pecos River. Rio Mora is approximately 3 m wide
AW	Pecos above Willow Creek	35°45′43″	105°40′13″	* Along Pecos River on east side at Willow Creek campground, approximately 200 m upstream of Pecos mine. Pecos River is approximately 9 m wide
UW	Upper Willow Creek	35°45′42″	105°38′52″	* Along Willow Creek, approximately 2.2 km upstream of Pecos mine. Willow Creek is approximately 1.5 m wide
WH	Willow Creek at State Highway	35°45′34″	105°40′6″	From Willow Creek as it crosses the north-east edge of the Pecos mine waste pile, approximately 50 m upstream (east) of state highway
SE	Seep, below mine	35°45′33″	105°40′7″	From seep along drainage downstream of Pecos mine. Brown and white iron and aluminium oxide and hydroxide precipitates containing Cu, Pb and Zn occur along the course of the seep
BS	Below seep	35°45′33″	105°40′8″	From seep in wetlands, near Willow Creek, downstream of SE. Brown and white iron and aluminium oxide and hydroxide precipitates containing Cu, Pb and Zn occur along the course of the seep
WC	Willow Creek at Pecos	35°45′35″	105°40′89″	Approximately 15 m upstream of the confluence of Willow Creek with Pecos River, from Willow Creek
BW	Pecos below Willow Creek	35°45′27″	105°40′10″	* From Pecos River. Sample collected from sand bar or bank (depending on water flow) approximately 10 m downstream of the confluence with Willow Creek
T	Pecos at Terrerro campground	35°44′35″	105°40′30″	* From west side of Pecos River, 30 m upstream of Terrerro campground
HG	Holy Ghost Creek	35°44′30″	105°40′40″	* From Holy Ghost Creek, approximately 100 m upstream of confluence with Pecos River
D	Doctor Creek	35°46′3″	105°41′59″	* From Doctor Creek, approximately 10 m upstream of confluence with Holy Ghost Creek, approximately 3.5 km upstream of confluence of Holy Ghost Creek with Pecos River
I	Indian Creek	35°42′30″	105°41′5″	* From Indian Creek, approximately 500 m upstream of confluence with Pecos River. Indian Creek is approximately 1.5 m wide
WB	Pecos at Windy Bridge	35°41′50″	105°41′5″	* From Pecos River, east side at Windy Bridge campground, downstream of bridge
MA	Macho Canyon	35°40′35″	105°41′10″	* From Macho Canyon, approximately 0.6 km upstream of confluence with Pecos River
Da	Dalton Canyon	35°39′35″	105°41′7″	* From Dalton Canyon, approximately 0.4 km upstream of confluence with Pecos River
AH	Pecos above hatchery	35°37′00″	105°41′00″	* From Pecos River at small diversion dam approximately 1.0 km upstream of hatchery. Sample from west bank upstream of dam
BH	Pecos below hatchery	35°36′30″	105°41′00″	* From Pecos River approximately 10 m below discharge pipes from hatchery
AA	Pecos above Alamitos	35°35′15″	105°40′30″	* From Pecos River west of bridge on north edge of Pecos Village, north side of river
UA	Upper Alamitos Canyon	35°37′00″	105°42′35″	From Alamitos Canyon approximately 2.3 km upstream of tailings pile. Alamitos Canyon is less than 1 m wide
AM	Alamitos at mill site	35°35′45″	105°42′25″	From Alamitos Canyon downstream of mill site
AV	Alamitos in Pecos Village	35°34′45″	105°40′45″	From Alamitos Canyon, approximately 30 m west of state highway
BV	Pecos below village	35°34′32″	105°40′10″	* From Pecos River at bridge where Highway 223 crosses the river. Pecos River is approximately 12 m wide
SM	Pecos at San Miguel	35°22′00″	105°26′45″	From Pecos River at large dam south of San Miguel. Samples taken upstream of dam on west side of river
V	Pecos at Villanueva	35°15′30″	105°20′15″	From Pecos River south end of Villanueva State Park campground. Samples taken on north bank or middle of river (depending on water flow)

* Sample site consists of predominantly boulders. Sand-sized sediment collected from natural sand traps or bends in river.

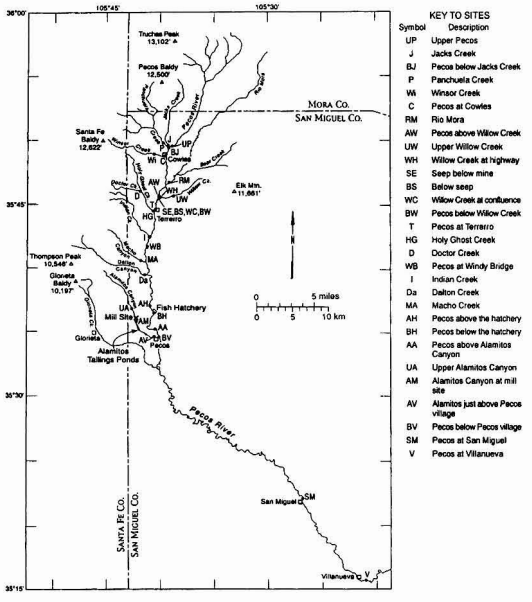

Fig. 3 Location of sample sites.

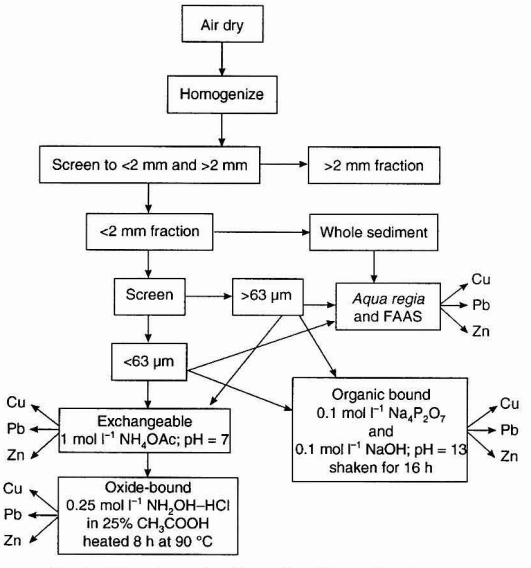

Fig. 4 Flow chart of sediment handling and analyses.

Table 2 Mean, range and standard deviation for copper, lead and zinc in <63 μm and 2 mm to 63 μm size fractions for *aqua regia* digestions. Values are in mg kg^{-1}. *s* = Standard deviation

Symbol	Sample site	No. of samples	Cu mean	<63 μm range	*s*	Cu mean	>63 μm range	*s*	Pb mean	<63 μm range	*s*
UP	Upper Pecos	6	21	17–32	6	13	6–18	4	37	19–60	20
J	Jacks Creek	5	20	13–40	10	12	6–15	5	44	24–76	21
P	Panchuela Creek	4	20	<15–35	10	7	5–10	2	26	18–29	5
BJ	Pecos below Jacks Creek	3	32	23–40	7	30	16–52	19	85	45–100	35
Wi	Winsor Creek	3	21	18–23	2	10	7–13	3	107	21–260	133
C	Pecos at Cowles	2	46	32–60	—	13	7–18	—	160	100–220	—
RM	Rio Mora	5	40	33–50	6	16	8–31	9	90	57–200	62
AW	Pecos above Willow Creek	5	42	18–57	15	29	12–52	19	86	60–111	21
UW	Upper Willow Creek	4	17	<15–22	6	17	15–21	3	38	20–63	22
WH	Willow Creek at State Highway	4	401	130–1100	406	673	160–1900	825	1281	400–3600	1551
SE	Seep, below mine	1	2100	—	—	1400	—	—	860	—	—
BS	Below seep	1	120	—	—	400	—	—	2900	—	—
WC	Willow Creek at Pecos	1	1200	—	—	510	—	—	1300	—	—
BW	Pecos below Willow Creek	4	288	110–310	113	192	23–280	115	289	130–470	141
T	Pecos at Terrerro Campground	5	83	46–107	27	27	12–65	22	104	73–122	23
HG	Holy Ghost Creek	1	36	—	—	13	—	—	59	—	—
D	Doctor Creek	2	35	31–38	—	8	6–8	—	39	38–39	—
I	Indian Creek	2	33	32–34	1	17	11–22	—	54	50–58	—
WB	Pecos at Windy Bridge	1	25	—	—	15	—	—	51	—	—
MA	Macho Canyon	2	20	16–24	—	9	8–9	—	41	34–48	10
Da	Dalton Canyon	1	25	—	—	14	—	—	26	—	—
AH	Pecos above hatchery	3	40	30–55	11	20	12–32	11	62	32–94	31
BH	Pecos below hatchery	4	46	35–53	7	22	12–32	10	80	43–153	50
AA	Pecos above Alamitos Canyon	3	26	21–30	4	11	8–15	4	43	35–51	8
UA	Upper Alamitos Canyon	2	25	23–27	—	11	10–12	—	36	27–44	—
AM	Alamitos at mill site	2	268	225–310	—	283	125–440	—	1198	895–1500	—
AV	Alamitos in Pecos Village	1	180	—	—	180	—	—	320	—	—
BV	Pecos below village	4	137	24–270	109	99	11–330	155	342	40–686	344
SM	Pecos at San Miguel	3	11	<15–19	8	23	14–35	11	33	27–46	11
V	Pecos at Villanueva	5	14	<15–45	17	6	5–6	1	32	17–44	16
Detection limit			5	(15 for trips 1 and 2)					12		

continued—

Table 2—*continued*

Symbol	Sample site	No. of samples	Pb mean	>63 μm range	*s*	Zn mean	<63 μm range	*s*	Zn mean	>63 μm range	*s*
UP	Upper Pecos	6	20	13–25	4	121	85–180	34	73	50–90	13
J	Jacks Creek	5	28	15–27	15	162	95–330	86	117	34–270	81
P	Panchuela Creek	4	12	<10	4	87	62–105	16	48	24–65	15
BJ	Pecos below Jacks Creek	3	38	20–65	20	210	130–330	86	160	110–210	41
Wi	Winsor Creek	3	18	14–23	4	84	64–108	18	49	40–58	7
C	Pecos at Cowles	2	27	18–36	—	210	170–250	—	85	77–93	—
RM	Rio Mora	5	18	15–26	4	180	120–226	48	72	35–157	44
AW	Pecos above Willow Creek	5	47	22–82	27	291	210–367	51	166	67–291	75
UW	Upper Willow Creek	4	19	14–24	4	80	75–87	5	84	65–129	26
WH	Willow Creek at State Highway	4	1263	350–3400	1248	2788	1000–7200	2558	5125	900–14400	5422
SE	Seep, below mine	1	610	—	—	20000	—	—	9800	—	—
BS	Below seep	1	1900	—	—	4300	—	—	4400	—	—
WC	Willow Creek at Pecos	1	660	—	—	12850	—	—	8150	—	—
BW	Pecos below Willow Creek	4	212	27–255	111	2511	1100–3100	828	2405	220–2900	1453
T	Pecos at Terrerro Campground	5	37	25–67	16	996	430–2000	543	493	260–1300	404
HG	Holy Ghost Creek	1	27	—	—	230	—	—	120	—	—
D	Doctor Creek	2	18	16–20	—	73	66–79	—	63	43–82	—
I	Indian Creek	2	20	15–25	—	94	77–110	—	53	47–59	—
WB	Pecos at Windy Bridge	1	28	—	—	145	—	—	97	—	—
MA	Macho Canyon	2	24	15–33	—	117	72–161	—	43	40–46	—
Da	Dalton Canyon	1	16	—	—	78	—	—	54	—	—
AH	Pecos above hatchery	3	38	18–60	17	798	450–1300	364	522	300–860	243
BH	Pecos below hatchery	4	46	20–80	22	743	650–831	88	367	270–500	89
AA	Pecos above Alamitos Canyon	3	23	16–29	5	366	288–470	77	239	187–310	52
UA	Upper Alamitos Canyon	2	23	12–34	—	105	100–110	—	56	35–76	—
AM	Alamitos at mill site	2	965	900–1030	—	2425	1550–3300	—	2270	1200–3340	—
AV	Alamitos in Pecos Village	1	260	—	—	860	—	—	670	—	—
BV	Pecos below village	4	182	20–342	159	654	285–990	254	458	240–900	265
SM	Pecos at San Miguel	3	45	25–65	16	90	51–110	28	115	110–120	4
V	Pecos at Villanueva	5	20	14–30	7	65	37–93	20	35	25–55	11
Detection limit						1					

Table 3 Quality control data using CANMET* stream sediment reference materials. Values are given in mg kg^{-1}

	Cu	Pb	Zn
STSD-1:			
Accepted acid extraction value†	36	34	165
Values obtained in this study	35, 33	40, 37	164, 161
Average of values	34	39	163
STSD-2:			
Accepted acid extraction value†	43	66	216
Values obtained in this study	42, 40, 41	67, 84, 77, 76	198, 213, 204, 205
Average of values	41	76	205
Standard deviation	0.94	6.98	6.16
STSD-3:			
Accepted acid extraction value†	38	39	192
Values obtained in this study	34, 37, 33	41, 50, 50	174, 180, 180
Average of values	35	47	178
Standard deviation	1.7	4.24	2.83
STSD-4:			
Accepted acid extraction value†	66	13	82
Values obtained in this study	57, 58	26, 21	75, 77
Average of values	58	24	76

* Canada Centre for Mineral and Energy Technology, Ottawa, Ontario, Canada.

† Extraction with concentrated HNO_3–concentrated HCl.

the Pecos below the village (BV). The wide range of values at these sites is probably real, as duplicate samples taken from the same site on the same sample trip (Table 4) produced large variations in metal concentrations (site BW) while duplicate samples from other areas (site WB) exhibited small variation. The variation cannot be attributed to experimental error as the per cent. difference, defined as the difference between duplicates divided by the average multiplied by 100, was greater for same-site duplicates than for within-batch duplicates. These sites with the widest range of values also had the highest values. Given the large concentration sources and the amount of precipitation (see Table 2, sites SE and BS) occurring at these sites these findings are not unexpected. Other sites, particularly sites on the tributaries, exhibited low metal values and little change from trip to trip. The <63 μm size fraction contained the highest metal concentrations with the exception of the sites at Willow Creek at the highway (WH) and at San Miguel (SM). Willow Creek, which flows through the mine waste dumps, would be expected to contain a significant amount of copper, lead and zinc in large sized particles. The site at San Miguel has very low metal concentrations and is not an environmental concern, but the higher metal values in the larger size fraction are interesting. The dam at San Miguel could be acting as a sediment trap for the larger particles.

The elevated levels of copper, lead and zinc in sediments noted on the first sampling trip at two areas, below the abandoned mine waste dump and below the mill site in

Alamitos Canyon, and the elevated level of zinc in the area of the fish hatchery were found to be elevated on all subsequent trips. Within relatively short distances downstream of each area the metal values dropped to background levels. Whether this is because of dilution or because the sediments do not move very far is not known. However, having witnessed the large amounts of sediments carried by the river during periods of heavy run-off, it is speculated that dilution is the likely cause.

Results of the partitioning study are presented in Tables 5 (<63 μm fraction) and 6 (2 mm to 63 μm fraction) and are displayed graphically in Fig. 8 (copper, <63 μm), Fig. 9 (lead, <63 μm), Fig. 10 (zinc, <63 μm), Fig. 11 (copper, 2 mm to 63 μm), Fig. 12 (lead, 2 mm to 63 μm) and Fig. 13 (zinc, 2 mm to 63 μm). Agreement between in-batch duplicates was within 7% for copper forms, 9% for lead forms and 5% for zinc forms. As mentioned previously some sites show wide variations in trace metal concentration from sample trip to sample trip. The extraction techniques applied to these samples also resulted in wide variations in extracted values. Converting the concentrations into percentage values allowed a more equivalent basis for comparison between samples. For instance, for one site the oxide-bound zinc ranged from 342–556 ppm but this range was only 76–78% of the totals. Therefore, these results are presented as percentages of the acid-extracted values (environmentally available total values).

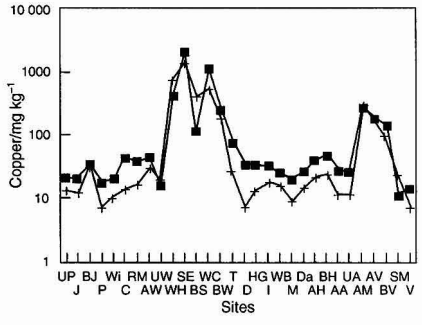

Fig. 5 Copper concentrations in +, 2 mm to 64 μm and ■, <63 μm stream-sediment size fractions.

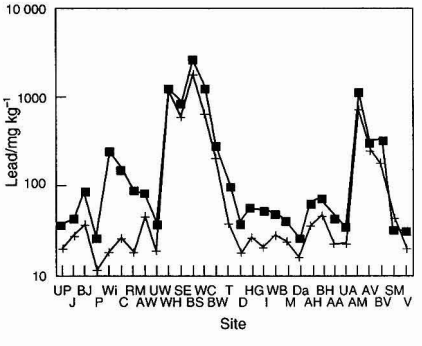

Fig. 6 Lead concentrations in +, 2 mm to 64 μm and ■, <63 μm stream-sediment size fractions.

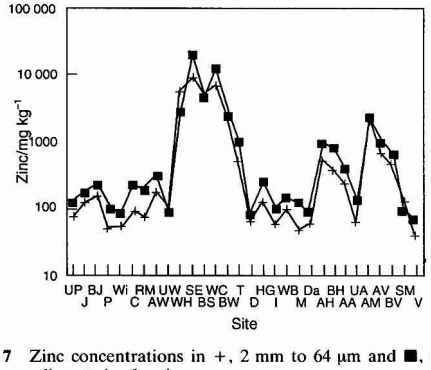

Fig. 7 Zinc concentrations in +, 2 mm to 64 μm and ■, <63 μm stream-sediment size fractions.

Because the organic-bound metal extraction was performed on a separate portion of sample, there is undoubtedly some overlap with the exchangeable metals. For copper, the exchangeable fraction is so low (below the detection limit in many instances) compared with the organic fraction that overlap is of little significance. For lead, both fractions are so low (again many were below the detection limit) that overlap has little significance. Zinc levels in the two extracted fractions were all above the detection limit, but are so low compared with the iron oxide bound fractions that overlap, again, has little significance.

Harrison *et al.*[20] have suggested that mobility and bioavailability of the metals decrease approximately in the order of the extraction sequence, hence the exchangeable fraction may indicate which metals are most available for plant uptake and other releases into the environment. As mentioned, the metal association with the exchangeable fraction was low (about 5%) for all three metals with the notable exceptions of copper (13.5%) and zinc (17.9%) at the seep (SE) and at Willow Creek below the seep (BS), *viz.*, copper (18.8%) and zinc (35.2%). The percentage of exchangeable copper and zinc at sites SE and BS translates into very high concentrations of available copper (180 and 320 mg kg^{-1}) and zinc (620 and 1600 mg kg^{-1}), respectively, in the sediments. This is of

Table 4 Comparison of concentrations in duplicate samples collected on the same trip and treated as separate samples. Concentrations given in mg kg^{-1} (ppm)

	Cu	Pb	Zn
Below Willow Creek:			
BW-A	610	700	10 800
BW-B	240	240	3 100
Average	425	470	6 950
Difference (%)*	87	98	111
Windy Bridge:			
WB-A	24	51	140
WB-B	25	51	150
Average	25	51	145
Difference (%)*	4	0	6.9
Above hatchery:			
AH-A	38	73	710
AH-B	33	46	580
Average	36	60	645
Difference (%)*	14	45	20
Below Village:			
BV-A	26	47	280
BV-B	23	34	290
Average	25	41	285
Difference (%)*	12	32	3.5
Average difference for in-batch duplicates (%)	3	8	5
Difference range (%)	0–7.5	0–28	1.4–9.7

* Difference between samples divided by average ×100.

definite environmental concern and the area is being addressed by NMED as mentioned previously. However, the NMED has not looked at the bioavailability of these metals and these data suggest that enlargement of the wetlands already in this area and introduction of the proper plants could prevent a large amount of copper and zinc from reaching the river.

Copper was the only metal with a significant association with the organic fraction (about 26%, with more than half the sites having 20% or greater). This is in agreement with previous studies.[9,10,21] The <63 μm fraction had the most significant association with organics (about 30.6%) with notable exceptions at two areas: the seep below the dump (SE) and the Alamitos (AM) and (AV). These are areas

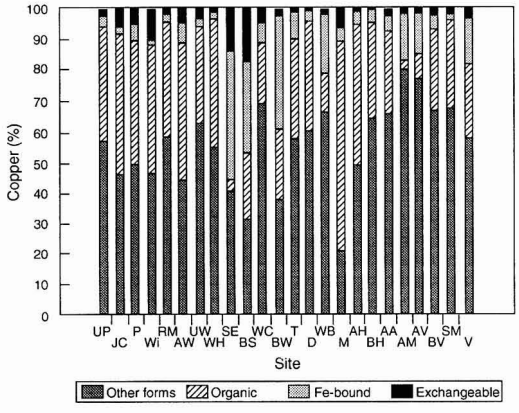

Fig. 8 Forms of copper in <63 μm size fraction.

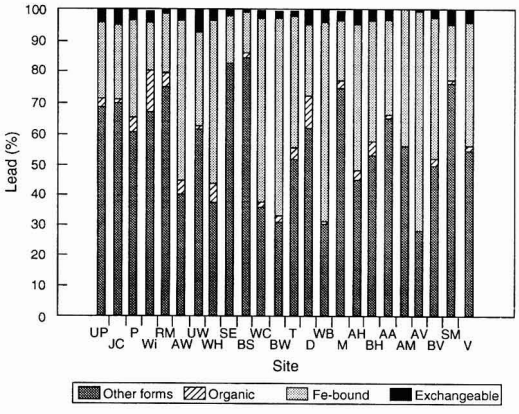

Fig. 9 Forms of lead in <63 μm size fraction.

Table 5 Chemical partitioning of copper, lead and zinc in <63 μm size fraction. Values are mean percentages except where only sample one was partitioned. Exchange = exchangeable; Fe-bound = bound to Fe–Mn oxides; Org = bound to organics; Other = other forms [100 − (Exchange + Fe-bound + Org)]

			Copper (%)*				Lead (%)*				Zinc (%)*			
Symbol	Site identification	No. of samples	Exchange	Fe-bound	Org	Other	Exchange	Fe-bound	Org	Other	Exchange	Fe-bound	Org	Other
UP	Upper Pecos	3	1.7†	3.5†	37.9	56.9	4.4†	24.8	3.1†	67.7	1.0	34.3	4	60.7
JC	Jacks Creek	2	5.3	2.8†	45.7	46.2	4.8†	24.8	0.9†	69.4	1.2	25.7	5.1	68.0
P	Panchuela	2	4.7	6.1	39.8	49.4	3.3†	32.8	5.3†	58.6	4.4	46.4	6.3	42.9
Wi	Winsor Creek	2	9.6	1.9†	42.5	45.9	4.0†	15.7	14.5	65.7	3.2	28.4	9.2	59.2
RM	Rio Mora	2	1.2†	2.5	37.9	58.3	1.5†	20.0	4.4†	74.2	4.1	39.3	4.3	52.4
AW	Pecos above Willow Creek	3	4.2	6.9	45.3	43.6	3.6†	52.9	5.0	38.5	2.0	54	4.2	39.8
UW	Upper Willow Creek	3 (2 Zn)	2.7†	2.5†	32.3	62.5	7.4	31.2	0.9†	60.5	1.7	32.5	2.9	62.9
WH	Willow Creek at highway	2	0.9	2.5	42.2	54.4	3.6	53.7	6.6	36.1	6.0	71.3	7.0	15.8
SE	Seep from dump	1	13.8	41.9	3.7	40.6	2.0	15.7	0.1	82.1	17.9	68.4	4.5	9.2
BS	Below seep	1	17.0	30.0	21.5	31.5	0.9	13.7	0.7	84.6	27.3	59.1	13.0	0.7
WC	Willow at Pecos Creek	1	4.2	6.8	20.0	69.0	2.8	60.8	1.0	35.5	4.4	78.6	5.7	11.4
BW	Pecos below Willow Creek	3	2.2	36.8	23.4	37.6	2.6	65.7	1.9	29.8	6.6	81.3	5.1	7.0
T	Pecos at Terrerro	2	1.1	8.3	32.9	57.7	1.7	44.1	3.5	50.7	3.1	52.3	3.7	41.0
D	Doctor Creek	1	0.6†	3.2	35.5	60.6	4.7†	23.9	10.3	61.1	5.0	36.3	8.3	50.5
WB	Pecos at Windy Bridge	1	1.0†	20.0	12.9	66.0	3.9	66.7	0.5†	28.9	2.4	51.4	1.4	44.8
M	Macho Canyon	1	5.6	4.4	68.8	21.3	3.5†	20	2.2†	74.3	1.6	42.2	7.5	48.7
AH	Pecos above fish hatchery	2	0.8†	4.8	45.0	49.3	4.6	48	3.5†	43.9	5.4	77.2	5.5	11.9
BH	Pecos below fish hatchery	3	0.7†	4.3	31.2	63.8	3.1†	40.6	4.0	52.3	3.8	74.9	7.4	14.0
AA	Pecos above Alamitos Canyon	3	1.9†	5.6	26.6	65.9	3.5†	31.5	0.8†	64.3	3.8	53.5	4.9	37.8
AM	Alamitos at mill	1	1.1	15.9	3.5	79.5	0.2†	45.2	0.1†	54.6	1.9	65.2	0.8	32.1
AV	Alamitos at Pecos Village	1	1.7	12.8	8.3	77.2	0.3†	72.5	0.1†	27.1	4.0	69.8	1.4	24.9
BV	Pecos below Pecos Village	3	1.9†	5.0	26.1	67	2.9†	46.6	1.9†	48.6	3.6	49.6	5.4	41.4
SM	Pecos at San Miguel	1	2.0†	2.0†	28.7	67.3	4.8†	18.5	1.1†	75.6	5.5	21.8	5.5	67.3
V	Pecos at Villanueva	3	2.7†	15.8	23.7	57.9	4.4†	40.6	1.1†	53.9	5.9	36.3	6.9	50.9
Detection limit (ppm in sediment)			0.5	0.5	1		3	3	5		0.2	0.2	0.5	

* Fractional percentages were calculated using the concentration extracted by each procedure divided by the concentration obtained by *aqua regia* treatment multiplied by 100.

† Extracted concentrations were below detection limit. Concentration of half the detection limit was used in calculations.

where available copper is high (Fig. 5) and there is probably a low amount of organic matter to be associated with in relation to other sites. Analysis of the organic content is currently underway and will be reported elsewhere. The 2 mm to 63 μm fraction at several other sites had copper association with organics of less than 20%: on the Pecos below Jack's Creek (BJ), at Cowles (C), at Windy Bridge (WB), and at Villanueva (V), and on Willow Creek (UW) and (WH). Lead associated

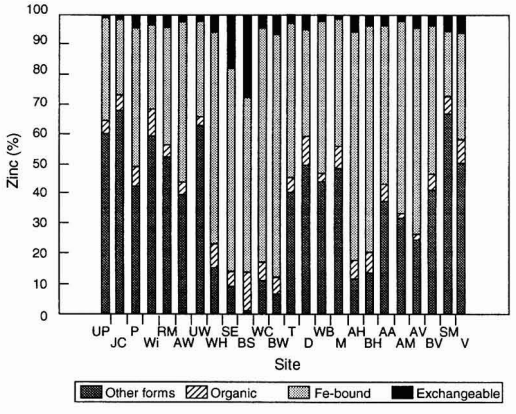

Fig. 10 Forms of zinc in <63 μm size fraction.

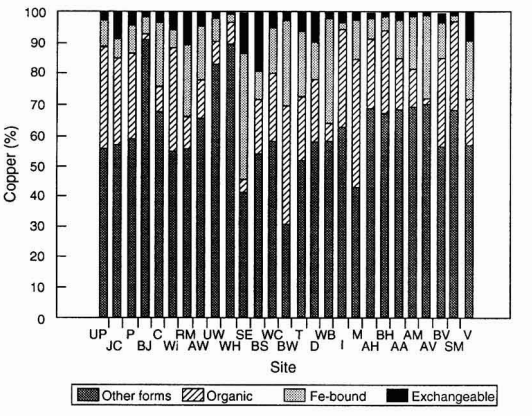

Fig. 11 Forms of copper in 2 mm to 63 μm size fraction.

Table 6 Chemcial partitioning of copper, lead and zinc in 2 mm to 63 μm size fraction. Values are mean percentages except where only one sample was partitioned. Exchange = exchangeable; Fe-bound = bound to Fe–Mn oxides; Org = bound to organics; Other = other forms [100 − (Exchange + Fe-bound + Org)]

			Copper (%)*				Lead (%)*				Zinc (%)*			
Symbol	Site identification	No. of samples	Exchange	Fe-bound	Org	Other	Exchange	Fe-bound	Org	Other	Exchange	Fe-bound	Org	Other
UP	Upper Pecos	3	3.5†	8.9†	32.4	55.8	4.7†	36.6	4.1	54.6	3.4	33.5	3.4	59.8
JC	Jack's Creek	2	8.1	7.9†	27.8	56.2	7.4	38.7	2.1†	51.8	3.0	45.8	4.5	46.6
P	Panchuela Creek	2	4.3†	9.8	27.1	58.8	2.2†	24.8	6.3	66.7	4.0	33.3	9.6	53.1
BJ	Pecos below Jacks Creek	1	1.3†	6.2	1.5	91	5.0†	65.0	1.3	28.8	0.9	26.9	2.4	69.8
C	Pecos at Cowles	1	3.6†	21.4	7.1	67.9	5.6†	72.2	1.4†	20.8	2.1	66.2	1.7	30.0
Wi	Winsor Creek	2	5.1†	7.0	33.4	54.4	5.0†	29.9	7.4†	57.7	5.1	35.2	3.8	55.9
RM	Rio Mora	3	10.3	24.2	9.8	55.7	4.1†	41.2	2.6†	52.2	6.2	43.5	4.7	45.7
AW	Pecos above Willow Creek	3	4.7	18	12.3	65	4.4†	55.4	2.5†	37.8	3.8	76.5	7.3	12.3
UW	Upper Willow Creek	3	2.0†	8.1	7.0	82.9	4.7†	31.5	1.3†	62.5	1.7	21.3	1.5	75.6
WH	Willow Creek at highway	2	0.4	3.1	7.0	89.5	2.1	44.7	2.9	50.3	1.5	32.1	2.1	64.2
SE	Seep from dump	1	13.5	41.7	3.7	41.1	2.0	15.7	0.1	82.1	17.9	68.4	4.5	9.2
BS	Below seep	1	18.8	11.3	16.5	53.5	0.9	26.3	0.2	72.6	35.2	52.3	11.4	1.1
WC	Willow at Pecos confluence	1	5.1	15.5	21.6	57.8	3.6	81.8	1.3	13.3	5.2	78.5	9.9	6.4
BW	Pecos below Willow Creek	3	2.5	28.7	38.3	30.5	2.7	60.3	1.7	35.3	7.0	72.4	9.2	11.5
T	Pecos at Terrerro	2	6.4	21.9	20.6	51.1	3.3†	55.6	2.6†	38.5	5.5	69.7	5.2	19.6
D	Doctor Creek	1	9.5	12.5	19	59	5.0†	31.5	3.0†	60.5	2.1	14.6	1.7	81.6
WB	Pecos at Windy Bridge	1	1.8†	35.0	5.7	57.5	3.4†	72.4	0.9†	23.3	4.9	71.1	4.1	20.0
I	Indian Creek	1	3.3	3.3	31.4	62	6.0†	36.4	5.6†	52.0	1.0	44.8	11.6	42.5
M	Macho Canyon	1	2.3†	14.4	41	42.3	3.3†	36.7	37.3	22.7	3.0	52.2	7.4	37.4
AH	Pecos above fish hatchery	2	1.9†	7.8	21.9	68.4	4.9†	40.6	2.3†	52.2	6.2	71.2	6.1	16.4
BH	Pecos below fish hatchery	3	1.2†	5.6	26.5	66.7	4.6†	56.8	4.9†	33.7	4.3	69.3	8.2	18.2
AA	Pecos above Alamitos Canyon	3	2.4†	13.6	16.2	67.8	3.4†	41.7	1.2†	53.8	4.0	68.6	4.6	22.8
AM	Alamitos at Mill	1	1.3	18.3	11.4	69	0.5†	71.8	0.3†	27.3	3.0	52.2	2.7	42.1
AV	Alamitos at Pecos Village	1	1.3	28.3	1.1	69.3	1.6	80.8	0.1†	17.6	3.4	62.7	3.3	30.6
BV	Pecos below Pecos Village	3	3.2	12.8	27.9	56.0	4.7	46.9	1.4†	47.0	4.4	72.9	3.5	19.3
SM	Pecos at San Miguel	1	1.8†	1.8†	28.6	67.9	6.4†	20.0	1.0†	72.6	5.5	21.8	8.2	64.5
V	Pecos at Villanueva	3	9.3	20.1	14.2	56.4	6.9	33.6	1.7†	57.9	14.4	36.1	9.9	39.6
Detection limit (ppm in sediment)			0.5	0.5	1		3	3	5		0.2	0.2	0.5	

* Fractional percentages were calculated using the concentration extracted by each procedure divided by the concentration obtained by *aqua regia* treatment multiplied by 100.

† Extracted concentrations were below detection limit. Concentration of half the detection limit was used in calculations.

with the organic fraction was low (about 3%) at all the sites except for Macho Canyon (37.3%). The association of zinc with the organic form was also low (about 5%).

There was a very strong association of zinc (about 52%) with the oxide fraction. Lead association with the oxide fraction was approximately 38%, while copper was only weakly associated (about 11%).

Copper (about 56%) and lead (about 55.6%) showed the strongest association with the fraction termed 'other' forms. This form represents forms solubilized by *aqua regia* minus the exchangeable, oxide-bound and organic forms. Hence, this form would not include silicates or minerals highly resistant to extraction. 'Other' forms most likely would include sulfides, such as PbS and CuS, other minerals containing copper, lead and zinc, as well as amorphous material containing copper, lead and zinc. Zinc was significantly less associated with 'other forms' (about 37.8%), and the sites at the seep (SE) (about 9%) and below the seep (BS) (about 1%) had very little zinc in 'other forms'. Here again given the many chemical reactions occurring at these sites this is not unexpected. Detailed mineralogical studies are underway to identify specifically the 'other forms' as well as any forms not solubilized by *aqua regia*.

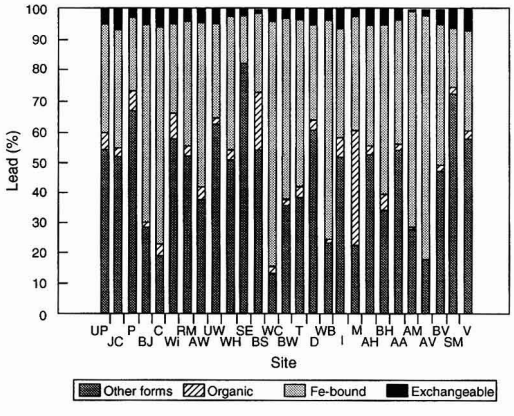

Fig. 12 Forms of lead in 2 mm to 63 μm size fraction.

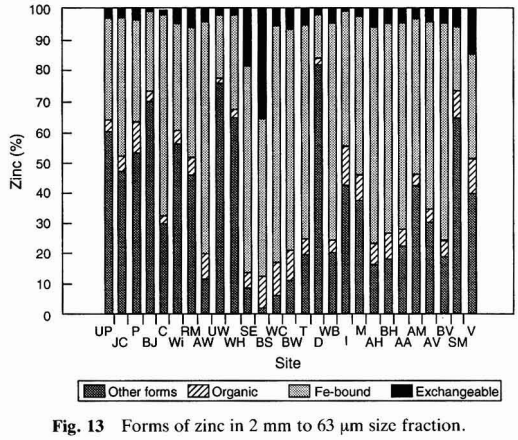

Fig. 13 Forms of zinc in 2 mm to 63 μm size fraction.

Conclusions

1. Copper, lead and zinc concentrations in sediments remain elevated at the two areas noted on the reconnaissance trip: below the abandoned mine and below the mill site. Zinc levels also remain elevated in the area of the fish hatchery. These concentrations rapidly drop to background levels downstream.

2. The smallest size fraction (<63 μm), typically represented the least amount of the sample by mass (<10%), but contained the highest concentrations of copper, lead and zinc, with the exception of Willow Creek at the highway (WH) and the Pecos River at San Miguel dam (SM).

3. Metal concentrations in two regions in particular varied greatly from sample trip to sample trip: from Willow Creek at the highway (WH) downstream to Terrerro (T) and Alamitos Creek at the mill site (AM) downstream to below Pecos village (BV). These areas contained the largest concentrated sources of metals and showed the highest concentrations of copper, lead and zinc in the stream sediments. Because of the available sources and variability of storm and run-off events, these findings are not surprising but are of environmental concern.

4. Typically, less than 5% (about 4.3%) of the metal values were found in the exchangeable fraction, the exceptions were for copper and zinc below seeps from the mine waste dump. Because this fraction is thought to be environmentally available and because the values are so high in this area, this finding is important.

5. Copper was significantly (about 26%) associated with the organic fraction of the sediments. The greatest percentage of copper (about 56%) was associated with the 'other' forms (speculated to be sulfide and other non-silicate minerals). Copper association with oxide forms averaged 11%.

6. Lead was significantly (about 38%) associated with the iron and manganese oxide fraction. It was similar to copper in that the greatest amount (about 55.6%) was associated with 'other' forms.

7. Zinc differed from both copper and lead in that the greatest amount was not associated with 'other' forms (about 37.8%) but rather with oxides (about 52%).

8. Elevated levels of copper, lead and zinc do not appear to be travelling with the sediments from the Upper Pecos area to downstream reservoirs.

The authors thank personnel from the New Mexico Game and Fish Department, Lisboa Springs Hatchery and the US Forest Service, Pecos District, for their assistance in collecting samples. The authors also acknowledge field assistance from C. Popp and T. Peace and laboratory assistance from D. Bright, D. Jones, R. Duncan, P. Martinez, T. Pease and D. Hack. Special thanks to J. Todd (AMAX) for providing data on remedial programmes at the Pecos mine. R. Titus drafted the figures and T. Telles typed the tables. Finally, the authors acknowledge financial support for this project from the US Bureau of Reclamation, NMBMMR (Charles Chapin, Director), and the Chemistry Department of NMIMT.

References

1 Neary, B., *Albuquerque J.*, 1991, May 9, pp. F-12.
2 Easthouse, K., *New Mexican*, 1991, October 4, pp. A-1.
3 Easthouse, K., *New Mexican*, 1991, October 6, pp. A-1.
4 McLemore, V. T., Brandvold, L. A., and Brandvold, D. K., *N.M. Geol. Soc. Guidebook, 44th Field Conference*, ed. Love, D. W., Hawley, J. W., Kues, B. S., Adams, J. B., Austin, G. S., and Barker, J. M., New Mexico Geological Society, Socorro, NM, 1993, pp. 339–351.
5 Jambor, J. L., in *Short Course Handbook on Environmental Geochemistry of Sulfide Mine Wastes*, ed. Jambor, J. L., and Blowes, D. W., Mineralogical Association of Canada, Short Course Handbook, Nepean, Ontario, Canada, 1994, vol. 22, pp. 59–102.

6 Ritchie, A. I. M., in *Short Course Handbook on Environmental Geochemistry of Sulfide Mine Wastes*, ed. Jambor, J. L., and Blowes, D. W., Mineralogical Association of Canada, Short Course Handbook, Nepean, Ontario, Canada, 1994, vol 22, pp. 133–161.
7 *Environmental Geochemistry of Sulfide Oxidation*, eds. Alpers, C. N., and Blowes, D. W., American Chemical Society, ACS Symposium Series 550, Washington, DC, 1994.
8 Tessier, A., Campbell, P. G. C., and Bisson, M., *Anal. Chem.*, 1979, **51**, 844.
9 Hickey, M. G., and Kittrick, J. A., *J. Environ. Qual.*, 1984, **13**, 372.
10 Levy, D. B., Barbarick, E. G., Siemer, E. G., and Sommers, L. E., *J. Environ. Qual.*, 1992, **21**, 185.
11 Arakel, A. V., and Hongjun, T., *Environ. Geol. Water Sci.*, 1992, **20**, 219.
12 Evans, D., and Davies, B. E., *Appl. Geochem.*, 1994, **9**, 45.
13 Fiedler, H. D., López-Sánchez, J. F., Rubio, R., Rauret, G., Quevauviller, Ph., Ure, A. M., and Muntau, H., *Analyst*, 1994, **119**, 1109.
14 Prusty, B. G., Sahu, K. C., and Godgul, G., *Chem. Geol.*, 1994, **112**, 275.
15 Chao, T. T., *J. Geochem. Explor.*, 1984, **20**, 101.
16 S. M. Stoller Corp., Tererro mine site, Pecos mine operable unit, San Miguel County, New Mexico: Background report prepared for AMAX Resource Conservation Co., 1993.
17 Sidle, R. C., Chambers, J. C., and Amacher, M. C., *J. Environ. Qual.*, 1991, **20**, 752.
18 Maxwell, J. A., *Rock and Mineral Analysis, Chemical Analysis Series Vol. 27*, Wiley-Interscience, New York, 1968.
19 Saheurs, J.-P., Wilson, W. P., and Sherwood, W. G., in *Analysis of Geological Materials*, ed. Riddle, C., Marcel Dekker, New York, 1993.
20 Harrison, R. M., Laxen, D. P. H., and Wilson, S. J., *Environ. Sci. Technol.*, 1981, **15**, 1378.
21 Tessier, A., Campbell, P. G. C., and Bisson, M., *Can. J. Earth Sci.*, 1980, **17**, 90.

Paper 4/05899B
Received September 27, 1994
Accepted January 3, 1995

The opinions expressed in the following article are entirely those of the author and do not necessarily represent the views of either The Royal Society of Chemistry or the Editor of *The Analyst*.

Perspective

Analytical Requirements in International Geochemical Mapping

Xie Xuejing

Institute of Geophysical and Geochemical Exploration, Langfang, Hebei, 102849, China

The history of the development of geochemical exploration has been closely connected with the progress of geoanalysis and instrumentation. International geochemical mapping is the inevitable outcome of the trends in the development of geochemical exploration. However, the analytical requirements in international geochemical mapping are markedly different from those in the earlier stages of its development owing to its international or global nature. Elements determined in existing regional or national geochemical mapping projects have been highly diversified. They should be unified in an international geochemical mapping programme in order to obtain a consistent global geochemical overview. Detection limits of trace and ultratrace elements should be lowered below their crustal abundances in order to make the geochemical maps of these elements much more informative. Unified data quality monitoring procedures and certified reference materials should be used to render the data produced by various mapping projects globally comparable, Multi-method, multi-element analytical schemes which could achieve these requirements should be developed. Geochemical maps produced in this way would be of immense value for monitoring the Earth's environment and for the appraisal of the world's mineral resources.

Keywords: *International geochemical mapping program; geochemical exploration; multi-element analysis; certified reference material*

Introduction

Geochemical exploration involves the systematic measurement of one or more chemical elements or compounds in rocks, soils, sediments, water, vegetation and air and the delineation and investigation of a variety of hierarchical geochemical patterns in these natural matrices. The hierarchical geochemical patterns may vary from local, regional, provincial, domainal, and continental to global scales.[1] The investigation of different types of geochemical patterns may provide different kinds of information for mineral exploration, metallogenesis, resource estimation, crustal growth, general geology, agriculture, human and animal health and the chemistry of the environment.

The historical development of geochemical exploration is from a very local scale to regional, national and then to international scale; from the prospecting of a single-element target to multi-element mineral exploration and multi-purpose, multi-element geochemical mapping. This development is closely connected with the progress of geoanalytical techniques and instrumentation. The application of emission spectrometry and colorimetry contributed much to the birth and initial growth of this new exploration technique. Extensive use of atomic absorption spectrometry in the 1960s highlighted local and semi-regional scale geochemical exploration worldwide.

The analytical requirements in geochemical prospecting in the 1960s have been well documented by Webb and Thompson.[2] According to these workers, the overriding requirements are low cost and high productivity. Analytical sensitivity at the ppm level and precision with a relative standard deviation (s_r) of 10–25% are acceptable for most exploration purposes. Absolute accuracy may not be essential because only the contrast between anomalous values and background values (not their absolute values) should be kept consistent for delineating targets meaningful for pinpointing new ores.

During the 1970s and 1980s great advances in analytical techniques and instrumentation were made, including the development of a wide range of decomposition and extraction procedures and analytical techniques and methods, and the commercialization and automation of a variety of sophisticated analytical instruments. All these advances have provided ample opportunities for geochemists to choose the techniques and instruments appropriate for different purposes in different geochemical exploration projects. The analytical requirements during this period have been summarized by Fletcher;[3] the importance of quality control of the analytical precision was emphasized in order to discriminate more subtle anomalies. The judicious choice of the element determined, and of the most suitable methods of sample processing, decomposition and determination, was considered the key to the success of any individual geochemical exploration project.[3]

These requirements are entirely suitable for local and semi-regional surveys, which have remained the main component of global geochemical exploration activities from the 1970s up to the present day. However, it is important to note that an entirely new type of geochemical survey (geochemical mapping), aimed not only at the discovery of local geochemical anomalies (dispersion halo or train) but also at the study of a hierarchy of more broad geochemical patterns, has emerged. From the 1970s up to the present day, about 40 regional and national geochemical surveys or geochemical mapping projects covering areas ranging from thousands to millions of square kilometres have been initiated.[4] The availability of automated techniques with multi-element analysis capability such as X-ray fluorescence (XRF) spectrometry, inductively

coupled plasma atomic emission spectrometry (ICP-AES) and instrumental neutron activation analysis (INAA) has been the main driving force in this development. Following this trend, international geochemical mapping is likely to be the inevitable outcome in the development of geochemical exploration both now and in the future. That the analytical requirements in regional, national and international geochemical mapping will be different from local and semi-regional geochemical exploration has been recognized only very slowly in the past 20 years during the development of such geochemical mapping practice. The most important difference is that geochemical exploration emphasizes the diversification of each project for its own special purposes while geochemical mapping emphasizes the standardization and unification of methods to meet its various goals, to render the data internationally comparable and to have short- and long-term and multi-purpose utilization. Geochemists and geoanalysts need to be fully aware of this difference before any geochemical maps produced could match the significance of geological maps.

International Geochemical Mapping Project

The International Geochemical Mapping Project was initiated in 1988, under the umbrella of the International Geological Correlation Program of UNESCO, UN, as the IGCP259 Project.[5] The aims of this project are: (1) standardization of the methodology of national and regional geochemical mapping projects to avoid the confusion caused by the lack of consistency in the methods used in different countries in the past 20 years; and (2) to investigate the possibility of wide-spaced sampling in order to obtain a geochemical overview of the Earth within a reasonably short time. This project terminated in 1993 and a final report on it will be published shortly.[6] Its successor project, 'Global Geochemical Baselines' (IGCP 360),[7] is concentrating its effort on the sophistication of wide-spaced sampling technology in order to collect 5000 representative samples covering the whole land surface of the Earth and to carry out multi-element analysis of 71 elements in the samples. The results will lead to the establishment of a global geochemical network for monitoring the delayed response of toxic materials on land surfaces of the Earth, and the delineation of a hierarchy of geochemical patterns for the appraisal of the world's mineral resources and the search for giant ore deposits.

For the purpose of consistency, the analytical requirements of newly initiated national and regional geochemical mapping projects should be the same as for the global wide-spaced sampling project.

A co-operative study could be carried out in which several competent laboratories would analyse these 5000 samples which would then serve as a geochemical reference sample set for assessing the quality of multi-element analyses in national and regional geochemical mapping.

Elements Determined

For many years, the elements determined in local and semi-regional geochemical exploration were highly diverse in both type and number and varied from project to project, the aim being specifically to locate mineral deposits with the greatest cost-effectiveness. However, for regional and national geochemical mapping, the number and type of elements determined should be unified to allow direct comparison and construction of geochemical maps from different regions and nations, in order to study broader patterns across regions or nations for a variety of purposes in exploration, and in environmental and basic studies. It is surprising to find that no single element has been determined in all of the 38 existing geochemical mapping projects (Table 1). The most commonly determined elements are Zn (determined in 35 out of 38 projects), Pb (33), Ni (31), Mn (31) and Co (30). Hence it is obvious that international agreement on a common range of elements is urgently needed.

This problem was discussed at several International symposia by members of the Analytical Method Committee (AMC) of the International Geochemical Mapping Program (IGCP 259) and by many other participants. After many discussions and modifications, the final recommendations advanced by the AMC concerning the unification of elements to be determined in both present and future geochemical mapping projects worldwide are shown in Fig. 1.

Although it is desirable that a common range of elements should be determined, some flexibility must be allowed owing to the diverse capabilities and facilities of different laboratories. The elements to be determined will be grouped into two categories: List One Elements for economic and environmental purposes include a group of rock-forming major elements and a group of minor, trace and ultratrace elements (totalling 51 in number) that should be determined in any new geochemical mapping project in order to render the maps more informative and valuable; List Two Elements that could be freely selected for determination depending on the aim and funding of the project and the capabilities and facilities of the laboratory.

Detection Limits

Another shortcoming which greatly reduces the scientific and practical value of most existing geochemical maps is the inconsistency of information for different element maps. This is because the detection limits used for many elements with very low crustal abundances are generally too high in most existing geochemical mapping projects in which these elements are determined; hence the contents of these elements in most of the samples collected from the mapped area are below their detection limits and cannot be reported and mapped (Table 2). The principle of lowering the detection limit below the crustal abundances of the elements to be determined is now universally accepted by geochemists engaged in geochemical mapping activity. However, the detection limits announced for some newly planned geochemical mapping projects are still not very satisfactory. This demonstrates the difficulty in striking a balance between cost-effectiveness and optimum methodology. Another difficulty in following this principle is that the crustal abundances of some elements may not have been correctly estimated. According to the data obtained from 1 million stream sediment samples covering 4×10^6 km^2, in China's National Geochemical Mapping Project,[7] the average Au content in stream sediment should be correctly estimated as 0.001 ppm, which is much lower than the published abundance of Au (0.004 ppm).[8] The published crustal abundances of other elements such as Hg, Ag and Bi may also be questionable according to information from this project.

Therefore, in establishing the guidelines for detection limits of those elements with very low crustal abundances, another

Table 1 Elements determined in 38 geochemical mapping projects

Elements determined in more than 30 geochemical mapping projects	Zn (35), Pb (33), Cu (32), Ni (31), Mn (31), Co (30)
Elements determined in 20–29 mapping projects	Mo (25), As (23), Fe (23), Cr (22)
Elements determined in 5–9 mapping projects	La (9), Cd (9), Sb (8), Th (8), Al (7), Au (7), B (6) Hg (6), Na (5), P (5), Rb (5), Si (5)
Elements determined in 1–4 mapping projects	Ga (4), Cs (2), Dy (2), Eu (2), F (2), Hf (2), Lu (2), S (2), Ta (2), Cl (1), Se (1), Tb (1), Yb (1)

complementary criterion is suggested, *viz.*, that the detection limit should be such that more than 80% of the samples in the mapped area should have reportable values in order to obtain informative geochemical maps. Table 2 shows the recommended detection limits which are based on a consideration of the existing crustal abundance data, the criterion of obtaining more than 80% reportable values, the vast amount of data obtained in China's Regional Geochemistry–National Reconnaissance Project and the current technical possibilities of multi-element analysis.

The detection limit is an important concept in trace analysis, but the literature is replete with various definitions. The detection limit has been commonly defined by the analytical community as that concentration of analyte producing a signal three times the standard deviation of the blank ($3s$). Does this blank represent only the acid used in the final dissolution step, for example (a typical instrument manufacturer's definition), or does it really represent the errors introduced during the entire sample preparation process (more realistic)? The Analytical Methods Committee of the Royal Society of Chemistry has published its recommendations on the term detection limit.[21] They proposed 'that the detection limit of an analytical system be defined as the concentration or amount corresponding to a measurement level $3s$ units above the value for zero analyte'. The quantity s is the standard deviation of the responses of field blanks. The only qualification to the detection limit should be the specification of the analytical system (*i.e.*, the complete analytical procedure).

Comparability

Comparability has long been a neglected concept in geochemical exploration analysis, because the geochemists were interested only in looking for the relative difference between anomalous values and background values. However, in international geochemical mapping, the analytical bias, whether interlaboratory or batch-to-batch within a laboratory, should be reduced to a minimum to make the data globally comparable. This could be effected by developing unified procedures for selecting optimum analytical methods and for routine monitoring of data quality. As drainage sediments are the most popularly used sampling medium in numerous geochemical mapping programmes, appropriate primary and secondary certified reference materials (CRMs) should be used in these procedures; the CRMs should be well documented with recommended values for many elements.

Primary CRMs could be used for selection of optimum analytical methods. Before the initiation of a geochemical mapping project, primary CRMs would be analysed for a variety of elements using different analytical methods. The method that yielded analytical data closest to the recommended values would be considered to be the optimum choice. If this procedure were to be followed by all newly initiated regional and national geochemical mapping projects, the analytical bias between different projects would be reduced to a minimum.

It is recommended that a set of primary CRMs should be inserted in each batch of 500 samples during routine multi-element analysis of the samples in a geochemical mapping project. The results obtained in different projects could be compared with the recommended values of the CRMs to study the analytical bias between different projects. The results could also be utilized for levelling the data so that they could be combined to construct geochemical maps covering the areas of several projects.

Secondary CRMs would be collected and prepared within the area covered by each individual mapping project. The sites for collecting the secondary CRMs should be representative of

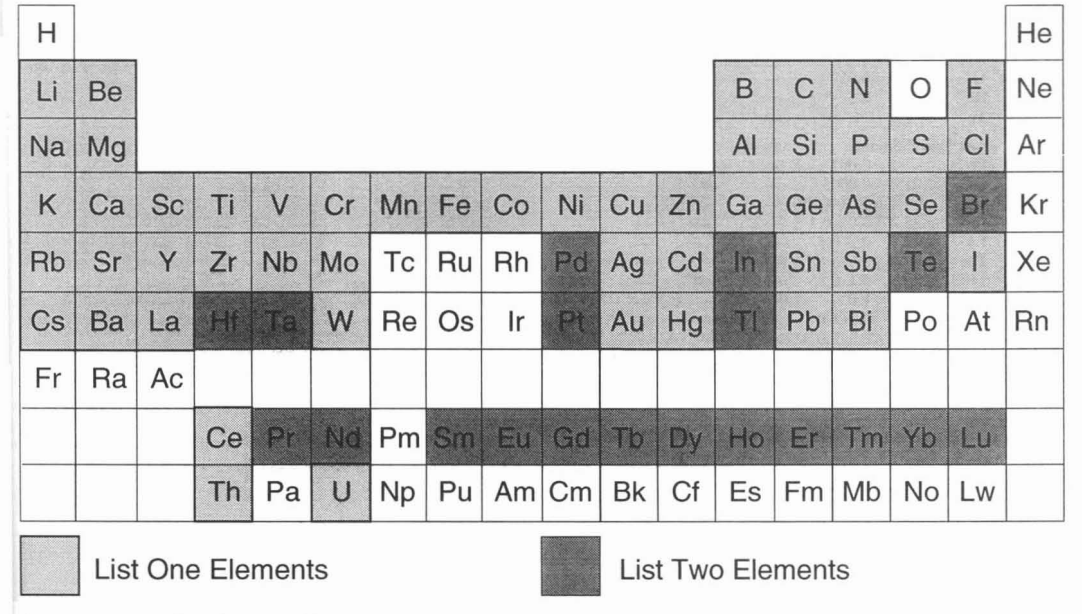

Fig. 1 List One Elements and List Two Elements for international geochemical mapping.

the main lithological units within the whole mapping area. It is recommended that four secondary CRMs should be inserted in each daily batch of 50 or 100 samples. These samples could be used for the monitoring of between-batch and between-map bias.

The logarithm of the deviation ($\Delta\log C$) of the determined values from the recommended values of primary or secondary CRMs can be used to monitor the between-batch, between-method and between-laboratory bias. The criteria established in China's national geochemical mapping project could be used for reference (Tables 3 and 4). If the data obtained for the CRMs during selection of optimum methods or during batch analysis of samples exceeded the allowed values, then either the method or the results obtained would not be accepted.

Precision

For many years in geochemical exploration practice, an acceptable precision has been an s_r of 10–25%.[2] Such a requirement is for a single element determination at a concentration above the ppm level. For multi-element analysis and for elements at concentrations below the ppm level, the challenge in achieving such precision will be greater. Statistics obtained in China's national geochemical mapping project show that major elements can be determined by XRF spectrometry with an s_r of 0.2–3% and minor and trace elements with an s_r of 0.4–25%. For elements (most of which are at very low concentrations) determined by methods other than XRF spectrometry, an s_r of 10–30% is common (Table 5).[26] These values are acceptable if factors such as current technical capabilities and cost-effectiveness are taken into account. However, it should be noted that any improvement in precision, particularly for those elements with very low crustal abundances, will increase proportionally the value of the geochemical mapping database.

Table 3 Allowance of bias in the determination of elements in primary CRMs

Concentration range	$\Delta\log C$
<3 DL*	$< \pm 0.3$
>3 DL	$< \pm 0.2$
1–5%	$< \pm 0.2$
>5%	$< \pm 0.1$

* DL = Detection limit.

Table 2 Detection limits (ppm) of elements with crustal abundances <3 of ppm for some past and on-going geochemical mapping projects

	1*	2†	3‡	4§	5¶	6‖	7**	8††	9‡‡	10§§	11¶¶	12‖‖
List One Elements:												
Au	0.001	0.0002	—	—	—	0.001	—	(0.05)***	—	—	0.0003	—
Bi	0.127	0.05–0.01	—	—	—	0.1	—	(5)	(0.3)	—	—	(4)
Se	0.05	0.02	—	—	—	—	—	(5)	—	—	—	—
Ag	0.075	0.02	(0.5)	—	—	0.02	(0.1)	(5)	—	(0.8)	(2.0)	(0.7)
Hg	0.085	0.01–0.05	—	—	—	0.05	(10)	—	—	(0.8)	—	—
Cd	0.15	0.05–0.1	—	(1.0)	—	—	—	—	—	—	—	(0.8)
Sb	0.2	0.04	—	—	—	0.2	—	(1)	—	—	0.1	—
Mo	1.2	0.5	0.4	0.5	1.0	0.5	1	—	—	1	1.0	—
W	1.25	0.2–0.5	1.0	—	—	1.0	2	(15)	(2)	—	2.0	—
As	1.8	0.5–1.0	1.0	(4.0)	—	1.0	—	(5)	—	—	0.3	—
Sn	2.3	1–2	(5.0)	(10)	—	1.0	—	(10)	—	—	(100)	—
U	2.7	0.05	—	—	—	1.0	—	0.01	—	0.1	0.3	—
Be	3.0	0.5	—	—	—	0.5	—	—	—	—	—	0.3
Ta	—	—	—	—	—	—	—	1	—	—	—	—
List Two Elements:												
Pt		0.001	—	—	—	—	—	—	—	—	—	—
Pd	0.015	0.0005	—	—	—	—	—	—	—	—	—	—
Te		0.01–0.02	—	—	—	—	—	—	—	—	—	—
In	0.25	0.05–0.1	—	—	—	—	—	—	—	—	—	—
I	0.45	0.2–0.5	—	—	—	—	—	—	—	—	—	—
Tm	0.52	0.5	—	—	—	—	—	—	—	—	—	—
Tl	0.85	0.1–0.5	—	—	—	—	—	—	—	—	—	—
Ho	1.3	1.0	—	—	—	—	—	—	—	—	—	—
Ge	1.5	0.5–1.0	—	—	—	—	—	—	—	—	—	—
Eu	2.0	0.5–1.0	—	—	—	—	—	—	—	—	—	—
Ta	2.0	1.0	—	—	—	—	—	1.0	—	—	—	—
Hf	3.0	1.2	—	—	—	—	—	—	—	—	—	—

* 1. Crustal abundance Au value according to our estimation; Bi value according to Taylor;[8,9] all other element values according to Ronov and Yaroshevsky.[10] All values in ppm.

† 2. Suggested detection limits in future geochemical mapping. These suggested detection limits (including those for the List Two Elements) are reasonable because they have been achieved in extensive studies carried out in China.

‡ 3. Sumatra (ref. 11).

§ 4. Wolfson Atlas (ref. 12).

¶ 5. Shetland (ref. 13).

‖ 6. RGNR Project, China (ref. 14).

** 7. NGR Project, Canada (ref. 15).

†† 8. Alaska Atlas (ref. 16).

‡‡ 9. W. Germany Atlas (ref. 17).

§§ 10. Nordkallot Project (ref. 18).

¶¶ 11. Finland Atlas (ref. 19).

‖‖ 12. Southern Scotland (ref. 20).

*** Figures in parentheses indicate that the detection limit is not satisfactory to meet international geochemical mapping requirements.

Multi-element Analytical Systems

When modern computerized analytical instruments with multi-element analysis capability such as the ICP atomic emission spectrometer and the XRF spectrometer began to become commercially available, many geochemists were optimistic that the simultaneous determination of 20–40 elements by a single instrument might be feasible in multi-element geochemical mapping.

Now, however, it is generally recognized that in order to fulfil the analytical requirements of international geochemical mapping, no single instrument, no matter how sophisticated, can cover all the elements to be determined. Multi-method approaches are now generally adopted in all geochemical mapping projects.

At present, funding, capabilities, facilities and the personal experience of individual laboratories lead to the use of a diverse combination of analytical methods in establishing multi-element analytical schemes, a diversity that can have an impact on the compatibility of the results. A period of extensive practice will be needed to identify the merits and drawbacks of the various combinations of methods. In general, ICP-AES provides good detection capabilities for the transition elements, and the alkali and alkaline-earth metals, whereas INAA is particularly effective in the determination of rare-earth and high field-strength elements (*e.g.*, Hf, Ta). XRF spectrometry has a justified reputation for high precision and for the ability to determine the suite of trace elements comprising Rb, Sr, Y, Zr, Nb, Pb and Th. Atomic fluorescence spectrometry (AFS) and atomic absorption spectrometry (AAS) are very sensitive for Au, Ag, As, Bi, Hg, Sb and Se. Polarography has an unmatchable advantage in the determination of W and Mo, as does laser-induced fluorescence (LIF) in the determination of U.

The relatively new technique of inductively coupled plasma mass spectrometry (ICP-MS) is generally viewed as the most sensitive technique currently available, and thus it shows great promise for the determination of elements of low crustal abundance such as the precious metals Tl, In, Se and Te.

The advantages and limitations of the principal analytical techniques currently used are discussed in detail in ref. 27, together with topics such as considerations in data quality and decomposition procedures employed to suit different objectives.

In order to achieve acceptable accuracy and precision in geoanalysis, judicious selection and care in sample preparation and processing are just as important as the technique (instrumentation) to be employed in the measurement stage. Unlike INAA and XRF spectrometry, the techniques of AAS, ICP-AES and ICP-MS are currently based on the nebulization of a solution containing the elements of interest. Such dissolution procedures increase the over-all analytical time and the likelihood of error, are subject to possible contamination and can yield low results owing to volatilization losses or incomplete digestion. Conversely, information can be obtained on the form(s) in which the element is bound in the sample by application of specific leachates designed to dissolve preferentially a certain phase of that sample (*e.g.*, elements bound to Fe/Me oxyhydroxides, or humic and fulvic compounds).

The determination of the total concentration of elements is the first priority, as these present the most reproducible values and could be compatible with a variety of purposes from mineral exploration, to environmental investigations to a

Table 4 Allowance of bias in the determination of elements in secondary CRMs

Concentration range	$\Delta \log C$
<3 DL*	$< \pm 0.2$
>3 DL	$< \pm 0.1$
1–5%	$< \pm 0.1$
>5%	$< \pm 0.05$

* DL = Detection limit.

Table 5 Precision of different analytical methods for the determination of different elements

Method*	Element or oxide	Content (%)	s_r (%)	Method*	Element	Content (ppm)	s_r (%)
XRF	SiO_2	57.32	0.43	ICP-AES	B	100	10.0
	Al_2O_3	12.74	0.77		Be	1.3	9.0
	Fe_2O_3	5.33	0.24				
	CaO	2.28	0.30	AES	Ag	0.064	10.1
	MgO	1.55	1.48		Sn	9.2	12.6
	K_2O	2.49	0.32				
	Na_2O	0.75	2.34	AAS	Li	19.8	7.1
		(ppm)					
	Ba	649	3.90		Cd	0.19	5.7
	Co	16	6.89	ETAAS			
	Cr	74	6.50		Mo	0.58	26.9
	Cu	29	4.87	POL	W	1.37	10.4
	Mn	888	1.21				
	La	34	23.80		F	360	13.9
	Nb	20	3.66	ISE			
	Ni	32	8.29		As	12.8	5.1
	P	1400	1.74	AFS	Sb	0.2	3.1
	Pb	39	7.14		Bi	0.24	13.7
	Sr	320	0.42		Hg	0.10	2.8
	Th	14	7.17				
	Ti	4650	1.08		U	4.6	12.9
	V	86	9.73	COL			
	Y	28	3.61		U	2.9	3.0
	Zn	100	2.15	LIF			
	Zr	270	0.99				

* XRF = X-ray fluorescence spectrometry; ICP-AES = inductively coupled plasma atomic emission spectrometry; AES = atomic emission spectrometry; AAS = atomic absorption spectrometry; ETAAS = electrothermal atomic absorption spectrometry; POL = polarography; ISE = ion-selective electrode; AFS = atomic fluorescence spectrometry; COL = colorimetry; and LIF = laser-induced fluoresence.

study of basic geology. Nitric acid digestion has been most commonly used in exploration geochemistry for many years, but it does not always provide a total extraction.[28] It is recommended that more rigorous acid decomposition methods should be used in geochemical mapping such as treatment with *aqua regia* (for Au, Pt metals and volatile metals) or with mixtures of HF–$HClO_4$–HNO_3 (for many trace metals), HF–$HClO_4$–HNO_3–*aqua regia* (for multi-element analysis using ICP-AES) or HF–H_2SO_4 (for some elements which will be tied up with residual fluoride). Some refractory elements not completely extracted by such rigorous acid decomposition can be released by physical means using XRF or INAA methods. Rigorous acid decomposition in closed vessels or in a microwave oven may also greatly improve the efficiency of extraction of refractory elements.

The selection of sample decomposition methods should be closely connected with the selection of analytical methods and with the development of a multi-element analytical scheme. The comprehensive review by Chao[28] on decomposition techniques could be used as a reference when planning such a selection. Decomposition by various methods of fusion should be avoided as far as possible, because of the introduction of large amounts of extraneous substances during analysis and the greater difficulty in streamlining the whole analytical procedure.

Major elements (Si, Al, Ca, Na, Mg, K, Fe) should be determined by XRF spectrometry following borate fusion into a glass disc. Chinese geoanalysts, however, have used powdered samples directly pressed into briquets without fusion.[29] This technique has been applied extensively to stream sediment samples with very good results. The key factors for success are a plentiful supply of reference materials with diverse matrix characteristics, and sophisticated computer software. The tendency to move from XRF spectrometry to ICP-AES for the 'whole rock' package should not be encouraged in international geochemical mapping because the accuracy of ICP-AES for major elements is far inferior to that of XRF spectrometry.

Examples of Analytical Schemes in Current Use in Mapping Projects

Multi-element analytical system based on extensive studies carried out in China

China's national geochemical mapping project, the Regional Geochemistry–National Reconnaissance (RGNR) Project, was initiated in 1978.[14] A joint project for developing analytical methods to be used in the RGNR Project was commenced in 1979 by many laboratories undertaking the analytical work of the RGNR Project. The general guidelines that all the researchers were to follow were: (1) a method and instrument with multi-element analysis capability should be used as the backbone of the analysis in order to scan a large number of elements simultaneously; (2) elements with low crustal abundances should be dealt with separately by whatever method could achieve the detection limits required.

A variety of methods and combinations of methods were developed by different laboratories. However, over a period of 6–8 years the scheme and also the analytical procedures were gradually unified and standardized.[26] This scheme has been designed to determine 39 elements (Table 6). They are all included in the list of 'List One Elements' which we now recommend for international geochemical mapping. The other 12 List One Elements not included in China's RGNR Project are S, Ga, Sc, Rb, Cs, Ce, Se, I, Cl, C, Ge and N; however, they could easily be incorporated in the existing scheme used in the RGNR Project. We now recommend this system for use in future geochemical mapping projects, because: (1) it was established by using the results from the analysis of 1 million samples over a period of about 12 years; (2) it is particularly suitable for developing countries, because only common analytical instruments are needed which are available in many laboratories. In the suggested multi-element analytical scheme based on the extensive studies carried out in China, the 51 List One Elements would be grouped into three packages to be determined with a variety of analytical methods successively (Fig. 2). Package 1 consists of ten rock-forming elements, *viz.*, Si, Al, Fe, Ca, Mg, K, Na, Mn, Ti and P, and 19 minor and trace elements, *viz.*, Cu, Pb, Zn, Cr, Ni, Co, Sr, Ba, Rb, Cs, Sc, Y, La, Zr, V, Nb, Th, Ce and S, which can be determined simultaneously in the same sample by XRF spectrometry. Package 2 consists of the remaining 20 List One Elements that must be determined on a more individual basis by a variety of methods: As, Sb, Bi, Hg and Se by AFS; W and Mo by polarography; Ag, Sn, B and Be by AES; (Ag), Cd, Li and Cs by AAS; U by LIF; Au by ICP-AES or electrothermal AAS; F by means of an ion-selective electrode; and I and Cl by ion chromatography. Package 3 consists of LOI and N, which must be considered in relation to each project. Packages 4, 5 and 6 contain the 20 List Two Elements that can be determined in a flexible way, either determined together with the List One Elements or determined at a later stage, or determined selectively. Package 4 consists of the 12 rare-earth elements which can be determined by ICP-AES. Package 5 consists of Pt and Pd, which can be determined by AES after preconcentration and Package 6 consists of Hf and Ta, which can be determined by AES with a special arc-concentration technique.[29] The other four List Two Elements can easily be incorporated with the Package 2 elements, if they are to be determined together (Fig. 2). Although List Two Elements are not included in the RGNR Project, a large amount of practical experience has already been accumulated in recent years using the methods described above to analyse tens of thousands of samples and obtain very good results. A detailed description of the scheme (in English) has been prepared by Qian Desun and can be supplied on request.

Detection limits achieved in this scheme meet all the requirements of international geochemical mapping (Table 7).

Conclusion

Some specific recommendations for analytical requirements in international geochemical mapping are set out below.

Table 6 Multi-element, multi-method analytical system used in the RGNR project with ICP-AES as the main component

System	Elements determined
X-ray fluorescence spectrometry	Al, Ba, Ca, Co, Cr, Cu, Fe, K, La, Mg, Mn, Na, Nb, Ni, P, Pb, Si, Sr, Th, Ti, V, Y, Zn, Zr
Atomic fluorescence spectrometry	As, Bi, Hg, Sb
Atomic absorption spectrometry	Ag, Cd, Li
Atomic emission spectrometry	(Ag), B, Be, Sn
Polarography	Mo, W
Ion-selective electrode	F
Colorimetry or laser-induced fluorescence	U
Atomic absorption spectrometry or electrothermal atomic absorption spectrometry with preconcentration procedure	Au

Elements Determined

A multi-element approach is recommended in international geochemical mapping in order to render the geochemical maps produced more valuable and informative. The list of elements determined should be unified. It is recommended that a group of 51 elements (List One Elements) should be determined in any on-going or newly initiated national geochemical mapping project so that the study is of practical and fundamental importance, and to facilitate the construction of internationally standardized geochemical maps or atlases. List Two Elements are not essential but are desirable in a major programme.

Total Extraction

The determination of the total amount of elements is the first priority, as these present the most fundamental and reproducible values. It is recognized that the $HF–HClO_4–HNO_3–HCl$ acid decomposition procedure is not total for elements bound in some refractory minerals but its universal acceptance and expediency lead us to recommend its usage for trace and minor elements. Although many types of weak partial extraction are informative for different purposes, results are generally operationally defined (with the probable exception of *aqua regia*) and hence the choice of extraction procedure will depend on the needs of each individual mapping project.

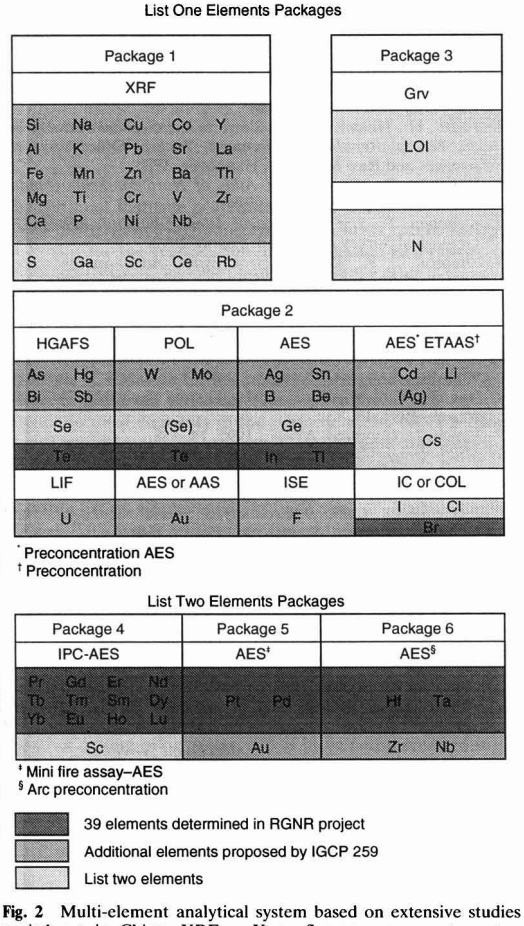

Fig. 2 Multi-element analytical system based on extensive studies carried out in China. XRF = X-ray fluorescence sspectrometry; HGAFS = hydride generation atomic fluorescence spectrometry; POL = polarography; AES = atomic emission spectrometry; ETAAS = electrothermal atomic absorption spectrometry; LIF = laser-induced fluorescence; AAS = atomic absorption spectrometry; ISE = ion-selective electrode; IC = ion chromatography; COL = colorimetry; and ICP-AES = inductively coupled plasma atomic emission spectrometry.

Detection Limits and Data Quality

The detection limits of all elements must be below their crustal abundances in principle. In each individual project the actual detection limits should be set such that more than 80% of the samples could yield reportable values of element concentrations above their respective detection limits. A list of suggested detection limits for elements with crustal abundances below 3 ppm is presented based on data for their crustal abundances, the experience from many geochemical mapping projects and the limitations of analytical technology. Various multi-element schemes based on XRF spectrometry, ICP-AES, INAA, *etc.*, incorporated with other techniques,

Table 7 Detection limits (ppm) of elements with crustal abundances of < 3 ppm. Multi-element analytical scheme based on extensive studies carried out in China

Element	1*	2†	3‡	4§
List One Elements:				
Au	0.001	0.0002	0.0001	Active C preconcentration ETAAS or AES
Bi	0.127	0.05–0.1	0.006	AFS
Se	0.05	0.02	0.005	AFS
Ag	0.075	0.02	0.03	AES or ETAAS
Hg	0.085	0.01–0.05	0.01	AFS
Cd	0.15	0.05–0.1	0.005	ETAAS
Sb	0.2	0.04	0.006	AFS
Mo	1.2	0.5	0.1	POL
W	1.25	0.2–0.5	0.1	POL
As	1.8	0.5–1.0	0.01	AFS
Sn	2.3	1–2	0.7	AES
U	2.7	0.05	0.05	LIF
Be	3	0.5	0.07	AES
Ta				
List Two Elements:				
Pt		0.001	0.0002	Mini fire assay–AES
Pd	0.015	0.0005	0.0001	Mini fire assay–AES
Te		0.01–0.02	0.001	AFS
In	0.25	0.05–0.1		AES
I	0.45	0.2–0.5	0.01	IC or COL
Tm	0.52	0.5	0.06	ICP–AES
Tl	0.85	0.1–0.5	0.05	AES
Ho	1.3	1		AES
Ge	1.5	0.5–1.0	0.02	ICP–AES
Eu	2	0.5–1.0		ICP–AES
Ta	2	1	1	Arc concentration–AES
Hf	3	1.2	0.3	Arc concentration–AES

* 1. Crustal abundance (ppm).
† 2. Suggested detection limits in future geochemical mapping.
‡ 3. Detection limits, multi-element analytical scheme based on extensive studies carried out in China.
§ 4. Methods used, multi-element analytical scheme based on extensive studies carried out in China. ETAAS = electrothermal atomic absorption spectrometry; AES = atomic emission spectrometry; AFS = atomic fluorescence spectrometry; POL = polarography; LIF = laser-induced fluorescence; IC = ion chromatography; COL = colorimetry; and ICP-AES = inductively coupled plasma atomic emission spectrometry.

can be employed provided that the criteria for the detection limit, precision and accuracy are met. Analytical accuracy or bias should be carefully monitored in order to produced high quality and internationally comparable data of major and diverse scientific value.

Primary and secondary CRMs should be used to monitor the analytical accuracy: primary CRMs to monitor the international or interlaboratory bias, and secondary CRMs to monitor the routine between-batch bias within a laboratory.

The Chinese GSD, GSS and the Canadian STSD standard samples are recommended for use as primary CRMs in geochemical mapping.

The logarithm of the deviation ($\Delta\log C$) of the determined value from the recommended value of a CRM or the average logarithm of the deviation ($\Delta\log C$) of the determined values from the recommended values of a set of CRMs can be used to estimate the interlaboratory or between-batch analytical bias. In order to achieve global comparability of data, it is recommended that before the commencement of a large-scale analytical operation in each newly established regional or national geochemical mapping project, a set of primary CRMs should be analysed several times for the elements to be determined in the samples. If the logarithm of the differences between the recommended values and the average values of replicate determinations are less than a certain limit, then the methods are acceptable.

Secondary CRMs should be collected and prepared within the area covered by each individual mapping project. The sites for collecting the secondary CRMs should be distributed more or less evenly within the whole mapping area. It is recommended that the analytical results for the secondary CRMs be utilized for the construction of global geochemical maps by wide-space global sampling.

Approximately one set of primary CRMs should be inserted in each batch of 500 samples. Four secondary CRMs and one duplicate sample should be inserted in each daily batch of 50 or 100 samples. The analytical precision will depend on the method used and the element determined. In general, the s_r for the major elements should be less than 3%, for minor and trace elements it should be less than 10% and for certain trace and ultratrace elements it should be less than 30%.

The author is very grateful to G. M. Hall for her many valuable comments and suggestions. Thanks are also given to my colleagues in the steering committee of IGCP 259/360 and to many geochemists and geoanalysts from different countries for their support and valuable exchange of opinions.

References

1 Xie, X., and Yin, *J. Geochem. Explor.*, 1993, **47**, 109.
2 Webb, J. S., and Thompson, M., in *Analytical Chemistry in Exploration, Mining and Processing of Materials*, ed. Strashein, A., Pergamon Press, Oxford, 1978, pp. 1507–1518.
3 Fletcher, W. K., *Analytical Methods in Geochemical Prospecting*, Elsevier, Amsterdam, 1981.
4 Plant, J. A., Hall, G. M., and Ridgway, J., *Trans. Inst. Mining Metal., Sect. B*, 1988, **97**, B116.
5 Darnley, A. G., *J. Geochem. Explor.*, 1990, **39**, 1.
6 Darnley, A. G., Bjorklund, A., Bolviken, B., Gustarsson, N., Koval, P., Plant, J. A., Stienfelt, A., Tauchid, M., and Xie, X., *A Global Geochemical Database*, Final report of IGCP 259, 1994, in the press.
7 Darnley, A. G., *J. Geochem. Explor.*, 1993, **48**, 97.
8 Taylor, S. R., *Geochim. Cosmochim. Acta*, 1964, **28**, 1273.
9 Taylor, S. R., and McLennan, S. M., *The Continental Crust, its Composition and Evolution*, Blackwell, Oxford, 1985, p. 312.
10 Ronov, A. B., and Yaroshevsky, A. A., *'Chemical Composition of the Earth's Crust'*, *Am. Geophys.* 13-D, Special Issue, 1969.
11 Stephenson, B., Ghazali, S. A., and Widjaja, H., *Regional Geochemical Atlas Series of Indonesia: I. Northern Sumatra*, Institute of Geological Sciences, Nottingham, 1982.
12 Webb, J. S., *The Wolfson Geochemical Atlas of England and Wales*, Oxford University Press, Oxford, 1978.
13 Bowie, S. H. U., and Plant, J., *Regional Geochemical Atlas, Shetland*, Institute of Geological Sciences, London, 1978.
14 Xie, X., and Ren, T., *Trans. Inst. Mining Metal.*, 1991, **100**, B57.
15 Coker, W. B., and Ellwood, D. J., *Open Files 730–749 Inclusive*, Geological Survey of Canada, Ottawa, 1981.
16 Weaver, T. A., Freeman, S. H., Broxton, D. E., and Bolivar, S. L., *Geochemical Atlas of Alaska*, Los Alamos National Laboratory, New Mexico, 1983.
17 Fauth, H., Hindel, R., and Siewers, U., *Geochemical Atlas of the Federal Republic of Germany*, Federal Office for Geosciences and Raw Materials, Hannover, 1985.
18 Bolviken, B., *Geochemical Atlas of Northern Fennoscandia*, Nordic Council of Ministers, 1986.
19 Koljonen, T., *The Geochemical Atlas of Finland, Part 2: Till*, Geological Survey of Finland, Espoo, 1992.
20 Simpson, P. R., *Regional Geochemical Atlas, Southern Scotland*, Institute of Geological Sciences, Nottingham, 1993.
21 Analytical Methods Committee, *Analyst*, 1987, **112**, 199.
22 Govindaraju, K., *Geostand. Newsl.*, 1994, **18**, Special Issue, 158.
23 Xie, X., Yan, M., Li, L., and Shen, H., *Geostand. Newsl.*, 1985, **9**, 83.
24 Xie, X., Yan, M., Wang, C. Li, L., and Shen, H., *Geostand. Newsl.*, 1989, **13**, 83.
25 Lynch, J., *Geostand. Newsl.*, 1990, **14**, 153.
26 *Multi-element Analytical Methods and Data Quality Monitoring System in Regional Geochemical Surveys*, ed. Xu, D., *Geol. Lab.*, Special Issue, 1987 (in Chinese).
27 *J. Geochem. Explor., Geoanalysis* Special Issue, ed. Hall, G. E. M., Elsevier, Amsterdam, 1992, p. 349.
28 Chao, T. T., and Sanzolone, R. F., in *J. Geochem. Explor., Geoanalysis* Special Issue, ed. Hall, G. E. M., Elsevier, Amsterdam, 1992, pp. 65–106.
29 Li, G., Zhang, Y., Xu, L., and Zhong, P., *Rock Mineral Anal.*, 1987, **6**, 15 (in Chinese).
30 Shen, R., *Proceedings of the Symposium on National Measuring and Testing Base of Rare Elements, Part 1*, National Commission of Science and Technology, Beijing, 1964, p. 198 (in Chinese).

Paper 4/06669C
Received November 1, 1994
Accepted January 10, 1995

The opinions expressed in the following article are entirely those of the author and do not necessarily represent the views of either The Royal Society of Chemistry or the Editor of *The Analyst*.

Perspective

Impact of Inductively Coupled Plasma Mass Spectrometry on Certification Programmes for Geochemical Reference Materials

Jean S. Kane

Standard Reference Materials Program, National Institute of Standards and Technology, Gaithersburg, Maryland 20899, USA

Ellyn S. Beary, Karen E. Murphy, and Paul J. Paulsen

CSTL, National Institute of Standards and Technology, Gaithersburg, Maryland 20899, USA

The National Institute of Standards and Technology (NIST) began using inductively coupled plasma mass spectrometry (ICP-MS) for the certification of its Standard Reference Materials (SRMs)* in 1986, only a few years after instruments first became commercially available. The United States, Canadian and Ontario Geological Surveys (USGS, CGS, and OGS, respectively) also made early use of the method to provide new data for existing certified reference materials (CRMs) and other non-certified geochemical reference materials (GRMs). The application of ICP-MS extends to most elements in the periodic table. NIST's efforts have focused largely on environmentally important trace elements. However, the impact of ICP-MS analysis in geochemistry is greatest in providing certified values for the platinum group elements (PGEs) and the rare earth elements (REEs). This paper will review the growing impact of ICP-MS analyses on the certification of CRMs/GRMs. Examples include NIST SRMs 1646a Estuarine Sediment, 2709-2711 Soils, 113b Zinc Concentrate; Centre de Recherches Petrographiques et Geochemiques (CRPG) CRMs CHR-Pt+ and CHR-Bkgr; Canadian Certified Reference Materials Program (CCRMP) WGB-1 gabbro rock, TDB-1 diabase rock and three other CCRMP CRMs recently certified for the PGEs. NIST has used ICP-MS almost exclusively in conjunction with isotope dilution. This has not been the situation among other users, but is to be recommended in certification analysis for several reasons, which will be outlined.

Introduction

Inductively coupled plasma-mass spectrometry (ICP-MS) has been used in chemical analysis for about 10 years, and is applicable to most elements in the periodic table. The history of the development of this method[1,2]is outlined in Table 1. Date *et al.*[3–5] reported the earliest use specifically in geoanalysis; they analysed a varied set of geological sample matrices, including the United States Geological Survey (USGS) GXR samples[6] and Mn nodules,[7] and NIST Standard Reference Material (SRM)* limestones.

Applications for geochemistry developed rapidly, with ICP-MS becoming a routinely applied method for a variety of geochemical data collection programs.[8,9] These focused on the rare earth elements (REE),[10–14] the incompatible elements (U, Th, Rb, Nb, Ta and light REEs) in crustal rocks,[15–18] and the platinum group elements (PGEs).[13,19] These elements could not be determined routinely at crustal or depleted abundances[20] without the extremely low detection capability provided by ICP-MS. The lower detection limits for the method also permitted much more extensive use for water analysis in exploration geochemistry;[21] the extractive preconcentration steps needed for detection of ore metals and indicators needed for atomic absorption spectrometric (AAS) analyses could be eliminated using ICP-MS.

Simultaneously, ICP-MS began to be used to provide data from which certified and 'recommended' concentrations would be derived, not only for geological samples, but also for many other sample types.[22–33] At NIST and other metrology laboratories these certifications are accomplished largely through in-house measurements,[22–28] while in many other certification programs, for example those of the USGS, Centre de Recherches Petrographiques et Geochemiques (CRPG), Canadian Geological Survey (CGS) and Canadian Centre for Mineral Energy Technology (CANMET), they are accomplished through large interlaboratory analytical programmes.[29–33]

The rapid progress in the use of ICP-MS was due to the fact that both the ICP ion source and the quadrupole mass spectrometer were well-established when the two were combined. The progress in developing the method proceeded along two parallel paths, depending on whether that development was being carried out by practitioners of inductively coupled plasma-atomic emission spectrometry (ICP-AES)[10–19] or of traditional mass spectrometry [thermal ionization and spark-source mass spectrometry (TIMS and SSMS)].[34,35]

* NIST has registered the term Standard Reference Material as a Federal trademark to describe its certified reference materials. The term CRM is used generically to describe materials from producers world-wide which meet the International Organization for Standardization (ISO) guidelines for certification.

Practitioners of ICP-AES gravitated to ICP-MS because it offered greatly improved detection limits and much simpler spectra, while retaining the simultaneous multi-element nature of the analysis, and therefore maintaining a similar level of sample throughput, and the ability to use familiar calibration and interference correction techniques. These familiar calibration techniques include external standardization, with or without the concurrent use of an internal standard to ratio out nebulizer drift and plasma power fluctuations, and standard additions. While the mass spectrum has just under 300 lines in comparison to the thousands observed in ICP-AES, more than one species can possess the same mass, so that interference corrections may still be required; once identified, corrections for these have been applied as in ICP-AES.[5,36] Applying ICP-MS in the manner of ICP-AES, accuracies and precisions approaching 1% for certification analyses can be achieved under optimal circumstances, but not under routine operating conditions in most laboratories.

ICP-MS isotope dilution (ID) is better suited to certified reference material (CRM) certification, and is used extensively both by NIST and by the National Research Council of Canada (NRCC).[22–28] The elements that have most often been certified by NIST and NRCC using isotope dilution are the transition and heavy metals having significant environmental impact, rather than the REEs, PGEs and incompatibles that have dominated the geoanalytical use of ICP-MS. NIST certifications of geological matrices and similar materials since 1987 are listed in Table 2; NIST certifications have included many other matrices as well.[24]

Isotope dilution quantification is based solely on isotope ratio measurements. Isotopic ratios can be measured with higher precision and accuracy than the absolute elemental signal levels (external standardization), which are utilized in atomic spectroscopic methods of quantification, or ratios of elements (conventional internal standardization). Isotope dilution quantification is a specialized form of internal standardization in which the internal standard is an enriched minor isotope of the element itself. However, use of ID quantitation is restricted to the elements that are multi-isotopic. The 22 mononuclidic elements must be determined using external calibration and/or conventional internal standardization.

NIST validated the method of ID-ICP-MS for certifications through parallel analyses of a number of SRMs with the long-established mass spectrometric method, ID-TIMS, as well as with other recognized certification methods. Each ICP-MS isotope dilution analysis is designed so that the limiting factor for the precision of the total analytical procedure is the precision of the ratio measurement itself. In a properly adjusted ICP-MS instrument the precision of the isotope ratio measurement is approximately 0.1–0.2%, expressed as the relative standard deviation (s_r), for any given ratio set measured on the standard quadrupole instrument, and even less on one of the newer high-performance instrument designs.[37,38]

In this paper details are presented of the NIST approach to SRM certification based on ICP-MS with ID quantification. To follow, some of the major CRM work performed by the geoanalytical community, using the multi-element, conventional methods of quantification are summarized. Differences in results between the two approaches will be discussed, and recommendations will be made for future analytical programmes by International Working Group (IWG) and other laboratories using ICP-MS to characterize CRMs for use in geochemical investigations.

Table 1 ICP-MS chronology (Jarvis *et al.*[2])

Year	ICP-MS progress	Workers
1974, 1975	Gray demonstrated potential of plasma source mass spectrometry	
1980	Houk *et al.* extracted ions from ICP	
1983	First commercial instruments	
1983 and following	Extensive literature develops, data on CRMs validates method	
1983 and following	Lead isotopic analysis	Date and Gray, others
1985 and following	REE applications to existing CRMs	Doherty and Vandervoet, others
1985 and following	Transition and heavy metal applications Trace elements other than REE	Date and Gray, others
1986 and following	Os/Re applications	Richardson and others
1987 and following	PGE applications	Date *et al.*, others
1990 and following	Certifications of new CRMs use ICP-MS data	Beary and Paulsen
1990	USGS SDO-1	Kane and others
1992	IWG CHR-PT+ and CHR-Bkg	Potts and others
1994	CANMET WGB-1 and 5 others	Leaver
1994	IWG ZW-C	Govindaraju and others

NIST Certification Approach Using ID-ICPMS as a Certification Method

NIST has traditionally certified concentrations of analytes in its SRMs by agreement of results obtained by two or more independent methods (*e.g.*, ICP-AES, instrumental neutron activation analysis (INAA), X-ray fluorescence (XRF), ICP-MS, ID-ICP-MS, ID-TIMS, *etc.*).[39,40] Many other reference material producers adopt this same approach when possible. Occasionally, a single definitive method (*e.g.*, gravimetry, ID-MS) is used for certification. Definitive method certifications produce certified values that are considered free from systematic error; and, as such, they have very narrow uncertainties associated with the certified values. Typical 95% confidence interval bandwidths are <0.2–0.3% relative to the certified values.

Isotope dilution ICP-MS has become a definitive certification method at NIST, accessing a wider range of elements than ID-TIMS. The ID-ICP-MS procedures used at NIST are designed for each material and analyte to obtain the highest possible precision and accuracy. ID-ICP-MS as applied at NIST is unique and represents the apex of a measurement heirarchy. Therefore, the details of the ID-ICP-MS certification process at NIST are described in the following paragraphs, beginning with sample preparation, through to instrumental set-up and analysis.

Table 2 NIST geochemical certifications based on ICP-MS analyses

Matrix	SRM	Elements	Certificate date
Water	1643c	Mg	1991
Water	1643d	Ba, Cu, Li, Pb	In prep 1994 or 1995
Coal fly ash	1633b	Ba, Cu, Pb, Tl, Th, U	1993
Soil	2709-2711	Ag, Cd, Mo, Ni	1992
Sulfide concentrate	113b	Ag, Cd, Cu, Pb	In prep 1995
Sediment	1646a	Cu, Mg, Mo, Ni, Pb	In prep 1995
Al_2O_3	2556-2557	Pt, Pd, Pb, Rh*	1993

* Not ID; monoisotopic.

Sample Preparation

Samples mass basis

For SRMs, a drying protocol is established to provide the needed analytical basis mass. Failure to establish the most reproducible mass basis of the sample prior to analysis will result in poor analytical results, regardless of the instrumental technique. Different bottles of the same material can have different mass losses on drying, which do not remain constant over extended periods of time.[41,42] This variability is often greater than the 0.1–0.2% s_r of the ratio measurements, and could introduce analytical errors up to 3% or more if ignored. At NIST, analytical samples and samples for establishing the mass basis are taken and weighed at the same time. Loss in mass is determined according to the specified protocol, and a mass loss correction is applied to the initial sample mass.

Sample decomposition

A variety of vessels is used for sampling and digestion, depending on the dissolution technique employed. The method of decomposition depends on the analyte as well as the matrix. If indicated, results from more than one dissolution technique are compared to verify the dissolution methods. Conventional hotplate dissolution in PTFE containers is often used for convenience, and has the longest history at NIST for a wide variety of materials and analytes. The aggressive Carius tube decomposition was developed many years ago at NIST (then NBS) for the determination of PGEs[43–45] to ensure total solubilization of the PGEs. Specially designed PTFE vessels have been used in both microwave and conventional ovens, for high-pressure dissolutions of leaves and rocks. In the experience of NIST, the Carius tube provides the best sample decomposition for very difficult samples. It is used routinely for ID-TIMS determinations of sulfur in all NIST certifications for that element,[46,47] and was used in 1992, when the PGEs were certified in two used auto-catalyst SRMs by ICP-MS.[27,48]

The auto-catalyst materials presented challenges in achieving total decomposition, both in terms of the alumina-based ceramic, which constituted the matrix, and of the PGEs coated onto that matrix in producing the auto-catalysts. The Carius tube was the method of choice for these difficult samples; however, this technique is not in general laboratory use. Therefore, hot-plate dissolution was also used for several samples for comparison, as shown in Table 3. For the material tested, the hotplate results were not statistically different from Carius tube results for the Pt and Pd, but were slightly lower for the Rh.[27]

Round-robin results provided by a number of laboratories cooperating in the certification were based on fire assay and peroxide fusion decompositions. The comparison of results of these dissolution techniques demonstrated that between-laboratory variability rather than incomplete decomposition was the major source of scatter in the round-robin results. The interlaboratory mean agreed very well with the ICP-MS value.[27,48]

Table 3 Carius tube *versus* hot plate dissolution for Pt, Pd, and Rh in auto-catalyst SRM 2556

	Carius tube		Hot plate	
	Mean	Uncertainty s_r (%)	Mean	Uncertainty s_r (%)
Pt	697.4	0.78	696.3	0.53
Pd	326.0	0.40	324.6	0.28
Rh	51.18	0.78	50.67	1.27

Spiking details for ID quantification

The best precision and accuracy of an isotope ratio measurement is obtained for a ratio of near one, regardless of the mass spectrometer type. Accuracy of isotope dilution results requires that the altered elemental isotopic ratio of the spiked sample be significantly different from the ratios of either the pure spike or unspiked sample. The uncertainty in calculated result *versus* the measured ratio give a minimum error factor at the geometric mean of the spike and natural isotopic ratios.[49] However, with an isotopically pure spike the minimum is broad, and the error multiplication factor does not change much over a wide range of measured ratios. Therefore, it is better to spike closer to the optimum mass spectrometric ratio, than to the geometric mean. In practice, 1 μg of analyte spike per μg of natural analyte meets these criteria and yields an altered ratio of between 1 and 4.

Isotope dilution quantification is based on the measurement of the altered isotope ratio of the element. Quantitative elemental recovery is not required. For trace and ultratrace element determinations, spiking is performed immediately after sampling. Isotope equilibration is accomplished during sample dissolution/digestion and/or decomposition. Analytes above approximately 0.5 mg g^{-1} require sub-sampling procedures to conserve the very limited enriched isotope supply. In this instance, loss of the analyte during dissolution or sub-sampling would cause a negative bias in the analytical results as the enriched isotope is added only after aliquotting.

The zinc ore concentrate was initially certified in 1974 and is currently being recertified, as gradual degradation of such materials by the air oxidation of sulfide to sulfate is known to occur.[50,51] ID-ICPMS was used to determine the Cu, Ag, Cd and Pb in the zinc ore, while ID-TIMS was used for the Zn and S determinations. For most of the elements, sub-sampling procedures were used as their concentrations were in the mg g^{-1} to % range. For the Cd and Cu determinations, duplicate samples were taken from six bottles, dissolved, and diluted to a large volume. Duplicate aliquots of each of the 12 sample solutions were taken for Cu and Cd determinations. The spike for both elements was added from a single spike mixture. Quantitative recovery of the analyte through the sub-sampling procedure was confirmed when the 24 Cd determinations agreed to about 0.15%, equivalent to the ratio measurement uncertainty. In addition, the results showed that Cd was homogeneous within the measurement precision. In contrast, heterogenity for Cu in the zinc concentrate was established as the variability among samples was six times greater than that between the solution aliquots.

ICP-Mass Spectrometric Measurements

Instrument details

The ICP-MS used for NIST certification analyses is a PQ II Turbo Plus Mass Spectrometer from Fisons Instruments.* The operating parameters are radiofrequency (rf) power of 1.3 kW and coolant and auxiliary argon flow rate of 16 and 0.5 l min^{-1}, respectively. The nebulizer argon flow rate is controlled by a flow controller to 0.85 l min^{-1}. A peristaltic pump is used to introduce the sample at a rate of approximately 0.3 ml min^{-1}. Either a concentric or cross flow nebulizer is used, depending on the analyte and sample type. The spray chamber is water cooled to 2 °C. The nebulizer flow rate and the distance between the rf coil and the sample cone are adjusted to minimize oxide formation, yielding <0.4%

* This description is given for information only, and does not imply NIST endorsement of the product as the best for the purpose.

LaO^+/La^+ and CeO^+/Ce^+. The lens voltages are set to provide maximum signal for elements in the mass region of interest.

Data collection

All analytical data are taken in the peak jump mode. For each analyte (or group of analytes) the mass scale is adjusted to be centred on the peak tops, and is tested using multiple points per peak. When correctly centred, there will be <1% decrease in signal intensity per 0.02 u on either side of the peak top. Isotope ratio data is collected using one point per peak. Dwell times of 10 ms are used when measuring peaks of equal intensity. For isotopic ratios not equal to one, counting for longer on the smaller peak can moderately improve the uncertainty owing to counting statistics. For such samples, dwell times are adjusted so that the larger peak was measured for 10 ms and the smaller peak for longer times but <30 ms each cycle. Each analyte is measured separately for optimal precision, despite the multi-element capability of the ICP-MS instrumentation. However, several elements can be measured simultaneously with good precision, provided the elements all give count rates of approximately 2×10^5 cps.

Often trace element analyte concentrations are quite high relative to the instrument detection limits. In those instances, samples are diluted to give a maximum signal of 3×10^5 cps, to minimize ion multiplier errors at high count rates from loss of ion-multiplier gain and uncertainty in the deadtime correction. The counts on the peaks are accumulated for 50 s (approximately 1000 cycles).

A generic plot for a continuous dynode multiplier in the ion count mode indicates a constant gain *versus* input signal to 10^5 cps, but shows progressive loss in gain at input signals of 10^6 cps or greater. Even in the pulse counting mode, when the gain drops, counts will be lost due to changes in efficiency of the detector. In addition counts are lost to detector deadtime (ion count overlap). At NIST, the $^{144}Nd/^{145}Nd$ ratio (approximately 3:1) is measured over a range of count rates (concentrations) to select the dead-time correction and to assess the linearity of corrected data.

Mass bias correction

Under carefully controlled conditions, ICP-MS is capable of isotope ratio measurements with precisions that approach 0.1% s_r. However, this capability does not ensure equivalent accuracy or over-all analytical precision. All mass spectrometers exhibit mass bias, so that the measured ratio is not the true ratio. For most elements, solutions of high-purity natural materials can be used to determine the mass bias correction factor, by which the measured ratio must be multiplied to achieve the true value. IUPAC publications[52,53] provide periodic updates of the true isotopic composition of the elements as well as their atomic masses. For some elements such as Pb and Li, whose isotopic composition varies in nature, isotopic standards must be measured and the mass bias correction factor determined from the certified and measured ratios of those materials. NIST, for example, offers SRMs 981–983 as Pb isotopic standards.

The mass bias correction is normally greatest at low mass (6–8%), about 2–4% in the mid-mass region, and <1% at high mass. The bias changes with focusing, nebulizer gas flow rate and sample flow rate, among other parameter's and cannot be considered an instrument constant. The mass bias also drifts with time in ICP-MS, and during 1 h, that drift can be large relative to the uncertainty of the measurements. It is greatest in the first few hours of instrument operation and at low mass. To obtain the highest precision, not only the mass bias, but also its drift must be measured and appropriate corrections made.

The importance of correcting for mass bias drift can be illustrated with Ni data obtained recently for the renewal of SRM 1643d. The over-all precision of this determination is 0.3% relative. However, when the mass bias drift correction was ignored, the measurement precision was 0.48% relative (s_r), a significant increase over that obtained with drift correction.

As a practical approach, a synthetic mix of natural and spike (a spike calibration sample) is used as the working isotopic control for the analysis, with approximately the same ratio as the samples being analysed. This practice minimizes memory problems encountered when a natural isotopic standard that has a vastly different ratio from the spiked sample is used. The isotopic ratio in the control is determined by comparison with a natural isotopic standard at the start of the analysis.

Mass interferences

While the mass interferences are considerably fewer than spectral line overlaps encountered in ICP-AES, they represent a potential source of error in the ICP-MS results. Mass interferences can be caused by isotopes of neighbouring elements, doubly charged ions from higher mass elements, or polyatomic ions from combinations of lower mass elements, and were reported in earliest ICP-MS literature.[5,36] Polyatomic mass interferences occur for mid-mass elements in complex matrices, and are by far the most difficult to predict and identify. Low probability polyatomic ions from a combination of matrix elements, carrier gas (Ar), oxygen, nitrogen, acids *etc.*, are the source of these interferences. The oxides and double oxides of matrix elements are the most prevalent interferences.

Interferences are proven to be present when the isotope ratio of the unspiked analyte in the sample does not match the isotope ratio of the analyte in a pure spike solution within experimental error. In addition, poor precision relative to the signal level can be an indication of polyatomic ion interferences. When interferences are detected, chemical separations are required for accurate analysis.

Chemical separations are designed to eliminate the interfering matrix elements. At NIST, the chemical separations used for this purpose include ion-exchange chromatography, chelation chromatography, electrochemistry and precipitation techniques.[28] Because the chemical separations are normally not quantitative nor reproducible to the <0.2% s_r analytical goal, the analytical samples are always spiked before chemical separations to take full advantage of ID quantitation. Without ID quantitation, the removal of the interferents could lead to biased and/or imprecise results, due to variable recoveries in the separation step. After all chemical preparation procedures, samples are evaporated to dryness and redissolved in a suitable solvent, normally dilute HNO_3 due to its relatively low background.

Three new soil SRMs (2709–2711) of varying origin and type and a sediment (1646a) currently undergoing renewal certification, required separations in the certification analyses. Ni, Ag, Cd and Mo were certified using ID-ICP-MS determination after removal of the bulk matrix with Chelex-100.[28] As is common for mid-mass elements in complex matrices, molecular ion interferences existed. Table 4 lists the suspected interferences for these elements in the soil SRMs. In contrast, Mg and Pb were determined directly in SRM 1646a. In natural materials, molecular ion interferences are not likely to occur in the low mass (<26 u, *e.g.*, Mg) or high mass (>200 u, *e.g.*, Pb) region of the mass spectrum, as elements immediately downmass (for example, 16 mass units for oxides) are usually at lower concentrations than the analyte(s).

ICP-MS has also been applied to the certification of mononuclidic elements at NIST, for example Rh in auto-

catalysts, SRMs 2556 and 2557.[27,48] The Rh certification differs from those mentioned thus far, because an isotope ratio cannot be used to determine the presence or absence of interferences, or for quantification. Rh is a rare element found nearly exclusively in nickel sulfide and chromatite ores. Thus synthetic matrices can be prepared free of Rh content, which can be used to detect an interference at the Rh mass 103. The auto-catalyst support was predominantly Al oxide to which the PGEs were affixed using a multi-element washcoat. Synthetic mixtures were prepared to match the concentrations of all elements present in the two auto-catalysts downmass from Rh. As no peak was detected at mass 103 in either synthetic mixture, the absence of polyatomic interferences for Rh in both SRMs could be inferred. A correction of <0.5% was required for $^{206}Pb^{2+}$ at mass 103.[27]

Rhodium was quantified *versus* indium using conventional internal standardization. The precision of that quantitation can be compared to the precision of isotope dilution which was used for the quantification of Pt, Pd and Pb in the same SRMs. Precisions of 0.2% s_r were achieved for the Pt, Pd and Pb ID calibrations, while the In/Rh calibration exhibited a poorer precision of 0.5% s_r for 12 samples.

Other Recent Reference Material Characterizations based on ICP-MS Analysis

Prior to the development of ICP-MS, available CRM data for many elements of key importance in geochemistry, among them the REEs, incompatibles, and PGEs were dominated by data from one analytical method. In the instance of REEs, U, Th, and Ta that method was INAA; for Nd it was XRF, for the PGEs it was electrothermal atomic absorption spectrometry (ETAAS). Because of this reality, USGS, CRPG, and other producers of geochemical CRMs were previously not able to establish values for these elements following the NIST practice of demonstrating agreement between two or more independent methods of analysis.[39,40] Development of ICP-MS has allowed these organizations to make more extensive use of the NIST approach for key geochemical elements not typically certified by NIST or other metrology laboratories.

It has just been shown that NIST certifications based on definitive ID application of ICP-MS can produce uncertainties for certified values of 1% relative (s_r) or less. NIST certifications based on agreement between results from independent methods have uncertainty bandwidths wider by a factor of 2–5. Other producer certifications, which are usually accomplished through large interlaboratory data collection programs, have similar uncertainties to NIST certifications for major concentrations, but have somewhat larger uncertainties for trace concentrations.[54] In many instances, the increased uncertainty is rather small, but in others it is sizeable, and an improvement would be desirable. A summary of recent CRM certifications follows.

Table 4 Some potential interferences for mid-mass elements that could affect soil SRM certifications*

Interferent	Analyte
$^{44}Ca^{16}O^+$	^{60}Ni
$^{46}Ti^{16}O^+$	^{62}Ni
$^{a}X_2O^+$, $^{a}X_2OH^+$	^{97}Mo, ^{98}Mo
$X_2O_2^+$, $X_2O_2H^+$	^{110}Cd, ^{111}Cd, ^{112}Cd, ^{113}Cd
$^{91}Zr^{16}O^+$	^{107}Ag
$^{95}Mo^{16}O^+$	^{111}Cd
$^{98}Mo^{16}O^+$	^{114}Cd

* ^{a}X represents various combinations of ^{39}K, ^{41}K, ^{40}Ca and ^{40}Ar.

USGS Shale SDO-1

In 1990, USGS completed the characterization of an eastern gas shale as an RM.[32,42] Recommended concentrations were provided for a number of REEs, based on agreement of INAA and ICP-MS analyses. For previous USGS materials, the available REE data had been dominated by that obtained by just one method, INAA, though some very limited ID-MS data had also been available. In view of the importance of REE data to many geochemical investigations, the significance of the development of ICP-MS as a readily available additional method for certification cannot be under-estimated. The chondrite-normalized REE pattern based on these recommended concentrations shows the internal consistency of those values, unlike the recommended values for some earlier geological materials.[42,55]

PGEs in IWG and CANMET CRMs

The development of the CANMET[31] and IWG[30] PGE CRMs has been made possible largely because the ICP-MS technique allows analyses of the requisite accuracy for certification, at levels that were too close to detection levels of previous techniques to provide that accuracy. For those PGEs at higher concentrations, ICP-MS provides an independent technique the results of which can confirm or challenge those obtained by ETAAS or NAA. The number of certified CRMs and ranges of certified values, for the PGEs in these materials are: Pt, 7 CRMs, 0.0061–58 mg kg^{-1}; Pd, 7 CRMs, 0.014–80.8 mg kg^{-1}; Rh, 5 CRMs, 0.0095–4.7 mg kg^{-1}; Ru, 5 CRMs, 0.0109–9.2 mg kg^{-1}; Ir, 5 CRMs, 0.0088–6.2 mg kg^{-1}; and Os, 1 CRM, 1.9 mg kg^{-1}. Gold was also certified in seven CRMs, and information values were provided for other uncertified PGE elements, major matrix elements, and Cu, Co, Ni. Certified values for all the above are given in Table 5.

The CANMET series[31] includes TDB-1, a diabase rock from Tremblay Lake, Saskatchewan; UMT-1, ultramafic mill tailings from nickel–copper Giant Mascot Mines, Hope, British Columbia; WGB-1, a gabbroic rock from Wellgreen Complex, Yukon Territory; WMG-1, mineralized gabbro from the same location; WMS-1 massive sulfide and WPR-1 altered peridotite, both also from the Wellgreen Complex. TDB-1, WGB-1, and WMG-1 are all siliceous matrices with associated sulfides; UMT-1 and WPR-1 are also siliceous matrices, but much more iron- and magnesium-rich than the others. WMS-1 is a sulfide matrix material. Tellurides have been observed in the WPR-1 sample, and have been tentatively identified as PGE complexes.

The IWG materials,[30] CHR-Pt+ and CHR-Bkg, are chromatite samples from the Isle of Shetland (North Scotland), recently developed by the Open University and CRPG as RMs to meet the both the geoscience community's need for well-characterized chromatite matrices and the need for samples certified for the PGEs. The matrix represented in these CRMs differs greatly from that of the CANMET CRMs, but is the same matrix as SARM-7.[56] However, CHR-Pt+ and CHR-Bkg have the key certification elements at rather different concentrations than in SARM-7. CHR-Pt+ is enriched relative to SARM-7, while CHR-Bkg is considerably depleted. The three samples together then can provide method validation and instrument calibration over an extended range of concentrations for all PGEs in a sample matrix that is particularly difficult in terms of decomposition chemistry.

Numerous Constituents in Li Mica

Most recently, the IWG and the Czech Geological Survey issued a lithium mica RM, ZW-C,[33] the characterization of which involved extensive use of ICP-MS. This sample presents

considerable analytical challenge because of its high F and REE contents, and because of the occurrence of the refractory minerals cassiterite, wolframite, and topaz. Data were provided by 92 laboratories from around the world, from which the recommended concentrations were derived. The ranges of the ICP-MS data between laboratories for the Li Mica material were not generally larger than for other methods (Table 6); however they were considerably wider than the between-method range for a NIST certification.[33,54]

Compilation data

Similarly, the ranges for values published in the literature, and recently compiled by Gladney and others,[57] for ICP-MS analyses of NIST SRMs 1646 and 2704 are sizeable. The certified values were based on agreement of NIST analytical results between two independent methods, and not on isotope dilution as a definitive method of certification. The comparisons between certified values with their uncertainties and published ICP-MS data are shown in Table 7.

It is clear that the ranges exhibited for published data greatly exceed the 95% confidence intervals of certified values, as well as those that would have resulted from ID-ICPMS certification. For routine analytical purposes, it is not often necessary to achieve the accuracy typical of certification analyses. However, for RM characterization by IWG, USGS, and other organizations which use a consensus approach, the goal should be to achieve the narrowest possible range for other organizations which use a consensus approach, the goal should be to achieve the narrowest possible range, both between-method, and between-laboratory for each individual method. The literature indicates the need for some improvement in the generally-achieved accuracy of ICP-MS data if the technique is to make its potential impact on certification programmes, in addition to the very considerable impact already being made in programmes based on large geochemical survey analysis data sets.

Conclusions

It has been seen that ICP-MS data ranges of 10% relative (s_r) or more are frequently observed in compilation data sets of CRM analyses reported in the literature.[29,30,23–33,57] It has also been seen that very high accuracies and within-laboratory s_r values of less than 1.0% can be routinely achieved in national metrology or similar laboratories that specialize in certification analyses using ID quantification for ICP-MS analyses.[22–28,36] Using the Sutarno–Steger model for certification data evaluation, the between-laboratory s_r for analyses contributed by several metrology laboratories should be three times the within-laboratory s_r or less. Using as an upper limit the within-laboratory s_r of <1.0%, which NIST typically

Table 5 CRMs for Au and PGEs certified concentration in mg kg^{-1}*

	Au	Pt	Pd	Rh	Ru	Ir
NIST SRM 886	8.25 ± 0.13					
CANMET TBD-1	0.0063 ± 0.001	0.0063 ± 0.001	0.0224 ± 0.0014	(0.0007)	[0.0003]	(0.00015)
CANMET UMT-1	0.048 ± 0.002	0.129 ± 0.005	0.106 ± 0.003	0.0095 ± 0.0011	0.0109 ± 0.0015	0.0088 ± 0.006
CANMET WGB-1	0.0029 ± 0.0011	0.0061 ± 0.0016	0.0139 ± 0.0021	(0.00032)	[0.0003]	(0.00033)
CANMET WMG-1	0.110 ± 0.011	0.731 ± 0.035	0.382 ± 0.013	0.026 ± 0.002	0.035 ± 0.0005	0.046 ± 0.004
CANMET WMS-1	0.279 ± 0.033	1.741 ± 0.142	1.185 ± 0.044	0.225 ± 0.016	0.099 ± 0.016	0.235 ± 0.025
CANMET WPR-1	0.042 ± 0.003	0.285 ± 0.012	0.235 ± 0.009	0.0134 ± 0.0009	0.022 ± 0.004	0.0135 ± 0.0018
CRPG CHR-Pt-1	4.3	58.0	80.8	4.7	9.2	6.2
CRPG CHR-BKg	(0.028)	(0.05)	(0.770)	(0.0090)	(0.067)	(0.028)

* Values in parentheses are provisional; values in brackets are information.

Table 6 Characterization of Zinnwalditc reference material ZW-C

Element	Number of ICP-MS laboratories	ICP-MS mean value	Total no of laboratories	Mean value (all methods)	Recommended value
Be	(10)	37.50 ± 5.3	(30)	36.68 ± 4.33	35
Bi	(5)	14.58 ± 1.04	(13)	15.25 ± 4.68	15
Cd	(4)	2.04 ± 1.87	(16)	2.61 ± 2.27	1.5
Ce	(14)	100.33 ± 6.48	(50)	96.08 ± 11.15	97
Co	(13)	1.49 ± 0.63	(44)	2.96 ± 3.09	2
Cr	(11)	46.78 ± 17.78	(84)	54.87 ± 15.26	56
Cs	(10)	260 ± 21	(51)	270 ± 49	260
Cu	(9)	30.92 ± 8.7	(60)	39.57 ± 10.75	39

Table 7 ICP-MS data in the literature in comparison with certified values

			Literature data[57]			
SRM	Element	Certified value and uncertainty	(1)	(2)	(3)	(4)
1646a	Cd	0.36 ± 0.07	0.28			
	Cu	18 ± 3	14	23 ± 3		
	Zn	136 ± 6	98.3	126 ± 6		
2704	As	23.4 ± 0.8	20	21.9	22	23.6 ± 2.7
	Ba	414 ± 12	441			
	Cd	3.45 ± 0.22	3.2	3.6	4.0	
	Co	14.0 ±0.6	13	13.5	14	
	Cr	135 ± 5	104	106	107	

achieves for certification analyses even of monoisotopic elements by ICP-MS, over-all relative uncertainties of 3% for CRM certifications represent an achievable goal for all certifications using the method. It would also enable better estimations of the variance due to heterogeneous distribution of some constituents, which is inherent in the nature of highly mineralized samples, as illustrated above for Cu in SRM 113b.

Prior to the development of ICP-MS instrumentation, the definitive method of isotope dilution was beyond the reach of most laboratories. However, with the ready access to this instrumentation in many laboratories today, the ID approach can be used much more frequently in future geoanalytical programmes than it has been in the past. In addition to making it possible to certify geochemical CRMs to higher levels of accuracy, largely as a result of narrower uncertainties in all measurements, it would be possible to expand the isotopic composition data base for key isotopic ratio measurements, and to certify CRMs for these. Examples include the lead isotopes and the Pb–U–Th system[58,59] and Re–Os[60] ratio.

As instrumentation develops further,[37,38] routinely achievable precision for ICP-MS will improve.[37] Additionally, the best precision currently achievable by ID-TIMS should become achievable for ID-ICP-MS as well, using the double focusing magnetic sector ICP-mass spectrometer with multiple Faraday detectors which is being developed.[38] This would enable the use of the technique in certifying CRMs for geochronology and other studies that depend on very high precision (<0.02% relative uncertainties) isotope ratio measurements.

The future of ICP-MS offers another opportunity for the development of new knowledge in the geosciences. In conjunction with laser ablation sample introduction, ICP-MS provides the opportunity to perform microanalysis. It is not possible in this application to take full advantage of ID quantification, because spike equilibration with the analyte cannot be readily achieved. However, the very low detection limits for ICP-MS and the minute sample consumption with laser ablation lead to interesting possibilities in regard to studies of zoning within single crystals, of contrasts between fluid inclusion concentrations and those of surrounding host rocks, and other applications. For this application CRMs are needed as well. Work being carried out to characterize NIST glass SRM 610[61] is of importance in this respect.

The authors acknowledge the invitation from the organizing committee to present their opinions in this paper at Geoanalysis 94. J. D. Fassett and T. E. Gills are thanked for helpful comments which contributed to improving the presentation of ideas in this manuscript. U. B. Gray's assistance in the preparation of the tables is acknowledged.

References

1 Potts, P. J., Hawkesworth, C. J., van Calsteren, P., and Wright, I. P., in *Magmatic Processes and Plate Tectonics*, ed. Prichard, H. M., Alabaster, T., Harris, N. B. W., and Neary, C. D., Geological Society Special Publication No. 76, 1993, pp. 591–520.
2 Jarvis, K. E., Gray, A. L., and Houk, R. S., *Handbook of Inductively Coupled Plasma Mass Spectrometry*, Blackie, Glasgow, 1992.
3 Date, A. R., and Gray, A. L., *Spectrochim. Acta, Part B*, 1985, **40**, 115.
4 Date, A. R., and Hutchison, D., *Spectrochim. Acta, Part B*, 1986, **41**, 175.
5 Date, A. R., Cheung, Y. Y., and Stuart, M. E., *Spectrochim. Acta, Part B*, 1987, **42**, 3.
6 Allcott, G. H., and Lakin, H. W., in *Fifth International Geoexploration Symposium*, ed. Elliott, I. L., and Fletcher, W. K., Elsevier, Amsterdam, 1975, pp. 659–681.
7 Flanagan, F. J., and Gottfreid, D., United States Geological Survey, Professional Paper 1155, 1980.
8 Potts, P. J., in *Analysis of Geological Materials*, ed. Riddle, C., Marcel Dekker, New York, 1993, ch. 5.
9 Riddle, C., VanderVoet, A., and Doherty, W., *Geostand. Newsl.*, 1988, **12**, 203.
10 Doherty, W., and VanderVoet, A., *Can. J. Spectrosc.*, 1985, **30**, 135.
11 Lichte, F. E., Meier, A. L., and Crock, J. G., *Anal. Chem.*, 1987, **59**, 1150.
12 Longerich, H. P., Fryer, B. J., Strong, D. F., and Kantipuly, C. J., *Spectrochim. Acta, Part B*, 1987, **42**, 75.
13 Longerich, H. P., Jenner, G. A., Fryer, B. J., and Jackson, S. E., *Chem. Geol.*, 1990, **83**, 105.
14 Jarvis, K. E., *Chem. Geol.*, 1990, **83**, 89.
15 Jenner, G. A., Longerich, H. P., Jackson, S. E., and Fryer, B. J., *Chem. Geol.*, 1990, **83**, 133.
16 Hall, G. E. M., and Pelchat, J. C., *Geostand. Newsl.*, 1990, **14**, 197.
17 Ionov, D. A., Savoyant, L., and Dupuy, C., *Geostand. Newsl.*, 1992, **16**, 311.
18 Xie, Q., Jain, J., Sun, M., Kerrich, R., and Fan, J., *Geostand. Newsl.*, 1994, **18**, 53.
19 Jackson, S. E., Fryer, B. J., Gosse, W., Healey, D. C., Longerich, H. P., and Strong, D. F., *Chem. Geol.*, 1990, **83**, 119.
20 Mason, B., *Principles of Geochemistry*, Wiley, New York, 1966, pp. 45–46.
21 Hall, G. E. M., unpublished work.
22 McLaren, J. W., Beauchemin, D., and Berman, S. S., *Spectrochim Acta, Part B*, 1988, **43**, 413.
23 Beary, E. S., and Paulsen, P. J., unpbublished work.
24 Beary, E. S., Paulsen, P. J., and Fassett, J. D., *J. Anal. At. Spectrom.*, 1994, **9**, 1363.
25 Beary, E. S., Breitic, K. A., Paulsen, P. J., and Moody, J. R., *Analyst*, 1987, **112**, 441.
26 Beary, E. S., and Paulsen, P. J., unpublished work.
27 Beary, E. S., and Paulsen, P. J., *Anal. Chem.*, submitted for publication.
28 Beary, E. S., and Paulsen, P. J., *Anal. Chem.*, 1993, **65**, 1602.
29 Govindaraju, K., *Geostand. Newsl.*, 1987, **11**, 203.
30 Potts, P. J., Gowing, C. J. B., and Govindaraju, K., *Geostand. Newsl.*, 1992, **16**, 81.
31 Leaver, M., *Certificates for nine PGE Reference Materials, Certificates of Analysis*, CANMET, Ottawa, Canada, 1994.
32 Kane, J. S., Arbogast, B., and Leventhal, J., *Geostand. Newsl.*, 1990, **14**, 169.
33 Govindaraju, K., Rubeska, I., and Paukert, T., *Geostand. Newsl.*, 1994, **18**, 1.
34 Alvarez, R., Paulsen, P. J., and Kelleher, D. E., *Anal. Chem.*, 1969, **41**, 955.
35 Paulsen, P. J., Alvarez, R., and Kelleher, D. E., *Spectrochim. Acta, Part B*, 1969, **24**, 535.
36 McLaren, J. W., Beauchemin, D., and Berman, S. S., *Anal. Chem.*, 1987, **59**, 610.
37 Liezers, M., unpublished work.
38 Halladay, A. N., Christensen, J. C., Hall, C. M., Jones, C. E., Lee, D.-C., Teagle, D., Walder, A. J., and Entwistle, A., unpublished work.
39 Uriano, G. A., and Gravatt, C. A., *CRC Crit. Rev. Anal. Chem.*, 1977, **6**, 361.
40 Cali, J. P., Mears, T. W., Michaelis, H. E., Reed, W. P., Seward, R. W., Stanley, C. L., and Yolken, H. T., *NBS Monograph 148*, GPO, Washington, DC, 1975, p. 54.
41 Moody, J. R., *Anal. Chem.*, 1987, **59**, 1481.
42 *U.S. Geol. Surv. Bull. 2046*, ed. Kane, J. S., US Government Printing Office, 1993.
43 Gordon, C. L., *J. Res. Natl. Bur. Stand. (U.S.)*, 1943, **30**, 107.
44 Gordon, C. L., Schlecht, W. G., and Wichers, E., *J. Res. Natl. Bur. Stand. (U.S.)*, 1944, **33**, 457.
45 Wichers, E., Schlecht, W. G., and Gordon, C. L., *J. Res. Natl. Bur. Stand. (U.S.)*, 1944, **33**, 363.
46 Kelly, W. R., and Paulsen, P. J., *Talanta*, 1984, **31**, 1063.
47 Kelly, W. R., Paulsen, P. J., Murphy, K. E., Vocke, R. D., and Chen, L.-T., *Anal. Chem.*, 1994, **66**, 2505.

48 Gills, T. E., *NIST Certificates of Analysis*, SRMs 2556 and 2557, 1993.

49 Heumann, K. G., in *Inorganic Mass Spectrometry*, ed. Adams, F., Gijbels, R., and VanGreiken, R., John Wiley and Sons, New York, 1988, pp. 310–311.

50 Steger, H. G., and Sutarno, R., *Geostand. Newsl.*, 1986, **10**, 93.

51 Faye, G. H., and Steger, H. F., *Talanta*, 1979, **26**, 309.

52 IUPAC Inorganic Chemistry Division, *Pure Appl. Chem.*, 1991, **63**, 991.

53 IUPAC, Inorganic Chemistry Division, *Pure Appl. Chem.*, 1991, **63**, 975.

54 Kane, J. S., *Spectrochim. Acta, Part B*, 1991, **46**, 1623.

55 Jarvis, K. E., and Jarvis, I., *Geostand. Newsl.*, 1988, **12**, 1.

56 Steele, T. W., Levin, J., and Copelowitz, T., National Institute of Metallurgy of Johannesburg, Report No. 1696, 1975, p. 50.

57 Gladney, E. S., O'Malley, B. T., Roelandts, I., and Gills, T. E., *NIST Special Publication 260-111* (update), 1993.

58 Sutarno, R., and Steger, H. F., *Talanta*, 1985, **32**, 439.

59 Longerich, H. P., Fryer, B. F., and Strong, D. F., *Spectrochimica Acta, Part B*, 1987, **42**, 39.

60 Richardson, J. M., Dickin, A. P., and McNutt, R. H., in *Plasma Source Mass Spectrometry*, ed. Jarvis, K. E., Gray, A. L., Williams, J. G., and Jarvis, I., 1990, pp. 120–143.

61 Hinton, R. W., Witt-Eickschen, G., and Harte, B., *Analyst*, 1995, **120**, 1315.

The opinions expressed in the following article are entirely those of the author and do not necessarily represent the views of either The Royal Society of Chemistry or the Editor of *The Analyst*.

Perspective

Certified Ontario Reference Materials Programme at the Geoscience Laboratories, Sudbury, Ontario, Canada

Jean M. Richardson

Quality Control Supervisor, Geoscience Laboratories, Ontario GEOServices Centre, Sudbury, Ontario, Canada P3E 6B5

The Ontario Geoscience Laboratories (hereafter referred to as the Geoscience Laboratories) have produced 30 in-house materials since 1970. This experience, the limited availability of international rock standards in volume, and the recent acquisition of specialized equipment (capable of homogenizing up to 1 t of sample), has led to the development of the Certified Ontario Reference Materials programme for the production of certified reference materials (CRMs). Given the geological diversity of Ontario, the decision was made to create two streams of reference materials. One is a suite of unaltered and altered volcanic rock reference materials that reflected the wide compositional range of Archean rocks of Ontario. Sample sites are clustered in the Abitibi Greenstone Belt which includes the Timmins and Kirkland Lake mining camps. This region also hosts some of the world's largest and most prolific mines of Au and Cu–Zn, smaller Ni deposits and one of the two international type-localities of komatiite. Advantages of such a choice are extensive. The rocks in this area have been studied by the Ontario Geological Survey (OGS) for 50 years and this expertise is readily available both in terms of appropriate chemistry and in sampling sites. Geologically, Archean volcanic rocks were typically extruded into a subaqueous environment and cooled quickly. This facilitates a high degree of homogeneity. There are a wide variety of compositions available, clear association with mineral deposits and thus the reference materials may also provide excellent baseline material for environmental studies. In the 1970s, the OGS devised internationally used major element classification criteria which divided Archean volcanic rocks into three major clans that have several subtypes (komatiitic clan has ultramafic and basaltic members; tholeiitic clan has Fe-, Mg-, basaltic, dacitic, andesitic, and rhyolitic members; and calc-alkalic clan has basaltic, andesitic, dacitic and rhyolitic members). These rock types typically show different styles of alteration near ore deposits (*i.e.*, chloritization, sericitization, carbonatization). The Archean volcanic rock suite will be comprised of these unaltered and altered rock types. The other group will focus on materials that fill a specific geoanalytical need. Based on the information above and the capacity of the Geoscience Laboratories geostandards programme (5 CRMs per year), it is anticipated that several rock types will be prepared yearly. A calc-alkaline rhyolite and an ultramafic komatiite have now been collected and other sites have been identified. Collection has commenced. After the sample is bottled, the homogeneity will be tested in our laboratories using validated methods. This will provide a tentative composition and will be followed by round-robin determinations. The reference materials will be released in 100 and 500 g plastic bottles to both the geoanalytical community and the exploration industry to monitor precision and accuracy in commercial surveys.

Introduction

A geoanalytical 'reference material' or 'reference sample' is a finely ground material that is rendered as homogenous as possible and has an accurately known composition.[1] The 'best' reference materials are those that are proven to be homogenous and are certified for a large number (often exceeding 60) of elements (for example AC-E).[2]

Reference materials serve two primary functions. Traditionally, geoanalytical certified reference materials (CRMs) are used by analysts to verify new analytical methods, to resolve differences among analysts or methods, to monitor quality control programs and to enable matrix-matched calibrations. During method development and validation, CRMs have the advantage that they closely match the chemical, physical and mechanical properties of the samples to be analysed.[1] Thus, they are an inherent part of quality control within a laboratory and use ensures that procedures are precise and accurate. This type of market is small, but well established. This application makes stringent use of a valuable commodity. For instance, the use of 0.25 g might typically provide 6000 determinations, consisting of 20 elements each.

More recently, reference materials have been used as contract monitoring materials (CMM). These are used to ensure the client that the analytical laboratory is performing according to the terms of the agreement and is thus providing precise and accurate determinations. This use is less thrifty. Typically 10 g would generate only 60 single-element determinations on one sample. The fact that the reference materials with large numbers of well determined elements are available in highly restricted amounts (30–100 g per bottle at $100 a bottle) suggests that the supply of these materials is not meeting demand.

Traditionally, the geoanalytical community needs a variety of materials that span a compositional range for each element. Also, as there is only a finite amount (200–1000 kg) of most materials made, older materials must be replaced as they

become depleted. Furthermore, as the analytical instrumentation industry pushes determination limits for multi-element analysers lower, the need for reference materials that are well characterized for many elements at ppb levels will increase. Overall, the most important parameters for a good reference material include homogeneity, wide and appropriate elemental coverage in the range of interest (*i.e.*, ppb *versus* ppm range) and the credibility of the issuing organization.

The Geoscience Laboratories have been producing in-house reference materials (MRB series, Mineral Resources Branch) since 1970. At present over 30 are available to staff (the most recent compilation is given in ref. 3). Outside firms and agencies now request the MRB series materials to monitor contracts. The samples are invaluable in method development and validation, contract monitoring and quality control. This experience has provided an excellent springboard for producing international reference materials.

With the move of the Laboratories to Sudbury in 1992, a portion of the new facilities was commissioned as a geostandards preparation area containing equipment capable of pulverizing, screening, blending and bottling bulk samples exceeding 300 kg in size. Samples generated here are for international use and will be grouped under the program title 'Certified Ontario Reference Materials' (CORM).

The first subset of reference materials produced in this program will be the Archean volcanic rock suite. This suite consists of unaltered and altered volcanic rocks that reflect the wide compositional range of Archean rocks in Ontario. Sample sites will be clustered in the Abitibi Greenstone belt which includes the famous Timmins (Au, Cu, Zn, Ni) and Kirkland Lake (Au) mining camps (Fig. 1). Two samples have already been collected as part of this suite (a calc-alkaline rhyolite, ORCA and an ultramafic komatiite OKUM) (Tables 1 and 2).

The second subset consists of reference materials derived either from well known rock units within the province or rock-types that are a specific demand in the geoanalytical community (Fig. 1). NPD-1, currently undergoing laboratory testing, is an example of the former. It is a geostandard of hypersthene diabase, part of the 'Nipissing diabase', or a series of 2.2 Ga intrusions that have a total volume in excess of 10 000 km^3.[4] OPEG, now collected and being shipped to Sudbury, is a highly evolved rare-metal pegmatite enriched in Rb, Li, Cs, Ta, Sn and Be from Northwestern Ontario (Tables 1 and 2).

CRMs Currently Available Internationally

Historically, the CRMs normally used and easily available for geoanalysis were created from igneous rocks and ores.[5,6] Metamorphic, carbonate and clastic sedimentary rocks are now reasonably well represented and there are limited numbers of CRMs of unconsolidated materials (tills, soil, lake or stream sediments) available.[7] However, although it was realized almost 15 years ago[8] that sequential or partial extractions (*e.g.*, Tessier *et al.*[9]) are important for environmental studies, there appear to be only a few CRMs characterized using such procedures (*e.g.*, LKSD 1–4,[10] and MAG-1[11]). Finally, there is a need for isotopic, electron microprobe and laser ablation standards that is not being well serviced.[12]

Materials from Canada, S. Africa, Czechoslovakia, National Institute of Science and Technology (NIST, National Bureau of Standards, US) and China can be readily purchased for approximately $100–400 for every 50 to 200 g with no restrictions with respect to the amount acquired. Others are available gratis from the US Geological Survey or the International Working Group on Reference Materials on a limited amount, time-restricted basis (*e.g.*, 10–30 g every 12–36 months). Japan has a large suite of reference materials that are available on a project-participation basis.

Granites and basalts are among the most desired reference materials. The USGS has depleted two of their own suite of

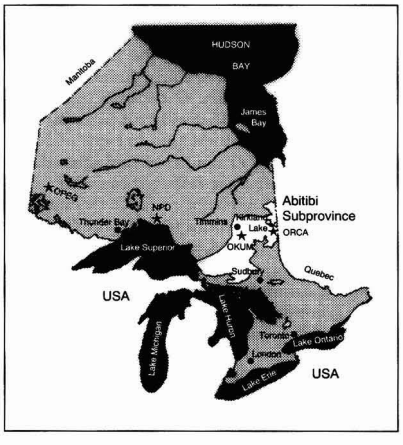

Fig. 1 Map of Ontario. Stars indicate the sample sites OPEG, NPD, OKUM and ORCA.

Table 1 Current status of geostandards of the CORM

Materials available								
Archean volcanic rock suite								
	Clan	Subclan	Site selected	Collected	Ground	Homogeneity testing	Round-robin	Released
OKUM	Komatiitic	Ultramafic	Yes	Yes	Yes	—	—	—
OKB		Basaltic	Yes	—	—	—	—	—
OTMG	Tholeiitic	Mg-rich	—	—	—	—	—	—
OTFE-		Fe-rich	Yes	—	—	—	—	—
OTB		Basaltic	—	—	—	—	—	—
OTA		Andesitic	—	—	—	—	—	—
OTD		Dacitic	—	—	—	—	—	—
OTR		Rhyolitic	—	—	—	—	—	—
OBCA	Calc-alkali	Basaltic	—	—	—	—	—	—
OACA		Andesitic	—	—	—	—	—	—
ODCA		Dacitic	—	—	—	—	—	—
ORCA		Rhyolitic	Yes	Yes	Yes	Yes	Yes	—
Other								
NPD		Diabase	Yes	Yes	Yes	Yes		
OPEG		Pegmatite	Yes	Yes	—	—		

Table 2 Preliminary composition of CORM geoanalytical reference materials

	OPEG Evolved pegmatite	NPD Nipissing diabase	ORCA Calc-alkalic rhyolite	OKUM Ultramafic komatite
Availability (mass-%)				
SiO_2	78.7	53.6	75.4	43.6
Al_2O_3	13.2	13.5	12.4	8.3
MnO	0.1	0.2	0.1	0.2
MgO	0.2	4.7	0.5	20.9
CaO	0.4	8.1	1.1	8.5
Na_2O	4.3	2.5	4.3	1.2
K_2O	1.7	1.4	2.2	0.0
TiO_2	0.0	1.2	0.3	0.4
P_2O_5	0.05	0.14	0.08	0.05
FeTot	0.3	12.7	2.9	12.3
LOI	1.3	1.3	0.8	4.1
Total	100.2	99.2	100.0	99.6
CO_2	0.2	0.2	0.02	<0.30
S	0.01	0.12	0.01	<0.03
FeO		9.4		
Availability (ppm)				
Ag		3.0	<20	<20
As	33	<6	<6	<6
Au		<3	<3	
Ba	370	306	370	29
Be	114	1	1	<0.2
Cd		<2		
Ce	2.3	36.4	63.3	1.0
Co	<5	44	<5	100
Cr	23	120	23	2350
Cs	133	1.1	0.6	0.1
Cu	<5	142	15	29
Dy	0.9	4.7	12.2	1.4
Er	0.1	2.7	7.8	0.9
Eu	0.0	0.9	1.4	0.2
Ga	32			
Gd	1.6	4.6	10.0	0.9
Hf	1.8	3.1	7.3	0.4
Ho	0.1	1.0	2.6	0.3
La	0.6	16.9	27.3	0.3
Li	High	20		
Lu	0.0	0.4	1.2	0.1
Mo	<6	<6	<6	<6
Nb	100	8.0	12.3	0.3
Nd	1.6	18.0	35.0	1.2
Ni	<5	60	8	1220
Pb	19	97	<7	<7
Pd		<10	<10	
Pr	0.4	4.6	8.7	0.2
Pt		6	<10	
Rb	2300	52	53	0.9
Sc	2	33	8	23
Sm	1.8	4.3	9.4	0.6
Sn	611			
Sr	29	175	72	13
Ta	139	0.5	1.0	0.1
Tb	0.2	0.7	1.8	0.2
Th	<10	<10	<10	<10
Th		4.6		
Tm	0.0	0.4	1.2	0.1
U		1.5		
V	<5	255	11	150
W	<35	<35	<35	<35
Y	3	24	73	8
Y	8.0	24.6	71.2	7.7
Yb	0.1	2.6	8.0	0.7
Zn	23	216	58	72
Zr	20	111	245	21

four of each of these rock types. One basalt, BCR-1 (Columbia River Basalt, created in 1967) is one of the most prized reference materials in existence. BCR-1 is used extensively for isotopic studies to ensure precision and accuracy to ensure compatibility beween studies and laboratories and is now depleted.[13] In total, there have been 15 basaltic reference materials generated. Of those, four can be acquired (from USGS, IWG-France and Japan) and four are now effectively depleted (BR, BCR-1, BHVO-1, JB-1, JB1-a). Thus, the materials of the Certified Ontario Reference Material programme will complement those currently available.

Rational for the Archean Volcanic Rock Suite

Geological and Geochemical Setting

Ontario is composed of greenstone belts comprised dominantly of mafic and, in some instances, ultramafic rocks. These rocks and their accompanying Au, Cu and Zn deposits have been extensively studied from the petrologic, tectonic and economic points of view for over 50 years by staff of the Ontario Geological Survey and others.[14,15] Archean volcanic rocks were typically extruded into a subaqueous environment that cooled quickly; some quenched. This facilitates a high degree of homogeneity. Later alteration has occurred but, since assistance is given by geologists of the OGS during site selection, such materials are avoided, unless specifically required.

Given the detailed information base available for Ontario, it was possible to focus the reference material programme in a limited geological region, clustering sampling sites in or near specific mining camps. This was an obvious starting point in the selection of reference materials as there is a well documented over-all geological and geochemical setting, a wide variety of compositions, a clear association with mineral deposits and an excellent background for environmental baseline samples. Thus these materials will complement those available internationally at present.

Because some of the world's largest and most prolific deposits are hosted in the mafic or ultramafic rocks of the Timmins-Kirkland Lake camp in the Abitibi Subprovince in Northeast Ontario (for instance the Dome, Hollinger, Kerr Addison, and MacIntyre Porcupine gold mines, the Kidd Creek Cu–Zn mine, the smaller Alexo Ni mine, Munroe-Croesus asbestos mine and the Pyke's Hill basaltic komatiitite locality), this area was chosen as the focus for the Abitibi volcanic rock suite (Fig. 1, Table 1). A suite of reference materials from this area would appeal to both the contract monitoring and the geoanalytical communities and also be a valuable research resource.

Chemical composition of the least altered rocks of the Abitibi Subprovince

The geochemical composition of the unaltered Archean volcanic rocks from the Timmins-Kirkland Lake area is very well known from the detailed work of the OGS. Geological attention has been focused on the area since 1909 when the first deposits were found. Two geological compilations have reviewed this information.[14,15] In 1976, based on the extensive compiled information and detailed field mapping, Jensen devised the internationally used major element volcanic rock classification scheme known as the Jensen Cation Plot (Fig. 2).[16] This scheme classified volcanic rocks generally, and those from the Archean specifically, into three major clans (komatiitic, tholeiitic and calc-alkalic) using Al, Mg, and Ti + Fe. This method has become the standard for characterizing Archean volcanic rocks.

Following from this, Grunski *et al.*[17] statistically profiled the Irvine and Baragar[18] profiles and the Jensen classification scheme to resolve the unaltered chemical signature of each of these magmatic clans and their subgroups (komtiitic clan, ultramafic and basaltic subsets, tholeiitic clan, Fe-, Mg-, basaltic, dacitic, andesitic, and rhyolitic subsets and calc-alkalic clan, basaltic, andesitic, dacitic and rhyolitic subsets, Table 1). A wide selection of these rock-types are present in the Timmins-Kirkland Lake area and are thus the focus of the Archean volcanic rock suite (Fig. 1).

Altered and ore-associated rocks

Within the Timmins-Kirkland Lake area, there are various styles of well documented ore deposits. Associated with each are usually several different styles of alteration with distinct chemical signatures (*i.e.*, chloritization, sericitization, carbonatization). When such alteration modifies the elemental signature to such an extent that the silicate matrix of the rock is totally replaced or the trace element signature is outside the normal calibration range for a particular element, then these materials could be useful standards. They will be included as the suite expands.

Site selection

Locations thought to represent target rock types and thus chemistries of the major groups of the Jensen Classification Scheme (Fig. 2) were sampled. Geologically, specific sites were selected on the basis of Dr. L. S. Jensen's (OGS) and P. Sangster's (Resident Geologists Office, Timmins, OGS) knowledge and experience in the area. The practical criteria used in determining potential sites are outlined in the Appendix.

The 1–2 kg grab samples were crushed to −170 mesh and analysed for major elements. The major element chemistry was then compared with the target chemical composition as defined by Jensen.[16] A traditional normalization plot was adapted to screen samples collected from potential sites. Such plots are typically used for rare earth element or spider diagrams use a reference composition on the *x*-axis and variation from this composition is represented on the *y*-axis. The reference composition was varied depending on the target rock type and all reference compositions are from Grunski *et al.*[17] Property ownership was then determined for targeted sites and the material collected.

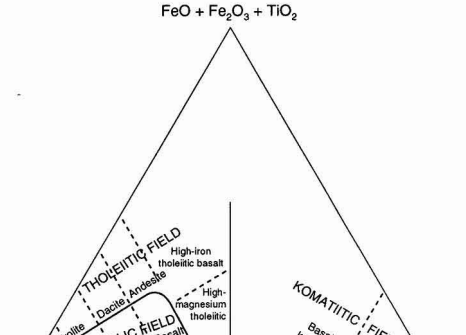

Fig. 2 Jensen cation plot showing classification of volcanic rocks into three major clans (Komatiitic, tholeiitic and calc-alkalic).[16]

Materials defined as being part of this suite

Using this approach, five collection sites have been delineated at present. Two bulk samples have been collected, a calc-alkalic rhyolite and an ultramafic komatiite and three others, a basaltic komatiite, a Mg-rich tholeiite and Fe-tholeiite will be collected in the near future. The field visits, site selection and standard collection will continue until the suite is completed (Table 1).

Description of Standards Collected to Date

ORCA-1

The first reference materials collected in this programme was a calc-alkalic rhyolite (ORCA) from Pontiac Township, 35 km northeast of Kirkland Lake (Fig. 1). This massive fine-grained slightly porphyritic grey rock contains minor amounts of feldspar phenocrysts and locally quartz eyes. Locally, the rock was weathered either chalky white (on weathered surfaces) or greenish in bands tens of metres away from the collection site. Both types of weathered material were removed mechanically or by blasting. Over 1000 kg were collected from a 2 × 4 m site that was part of a cliff 150 m high by 500 m long. The approximate chemical composition of this reference material is listed in Table 2.

OKUM

The second reference material, an ultramafic komatiite (OKUM), was collected at Serpentine Mountain in McArthur Township, 25 km south of Timmins (Fig. 1). OKUM represents a 1.5 m wide spinifex zone at the top of a 14 m wide flow that showed good differentiation into various units. The sample consists of black massive rocks composed of randomly oriented spinifex blades 5–10 cm long. A pronounced bluish-grey weathered surface extended 0.5–1 cm into the face that showed exceptional development of spinifex texture. This material was blasted or sawed off and was not incorporated into the sample. Over 700 kg were collected from a 2 × 3 m site that was part of flat glaciated outcrop over 100 m in diameter. The approximate chemical composition of this reference material is listed in Table 2.

Other Reference Materials Available Though CORM

Description of Other CORMs

NPD

NPD-1 was collected from the Basswood Lake intrusion 20 km north of Thessalon, northwest Ontario (Fig. 1). The diabase consists of hypersthene and plagioclase. All weathered surfaces were removed. The approximate chemical composition of this reference material is listed in Table 2.

OPEG

OPEG was collected 45 km north of Kenora, Ontario (Fig. 1). The bulk material was derived from the locality locally known as Lou's pegmatite. It consists of quartz, feldspar, tantalite, cassiterate, beryl and petalite. Chemically, the rock was chosen a geostandard as preliminary determinations indicated that it was high in SiO_2, Be, Rb, Cs, Ta and Nb and low in total iron, Y, Cd, Dy, La, Sc and Sr. The approximate chemical composition of this reference material is listed in Table 2.

General Preparation Techniques

The bulk samples are returned from the field in rock pails or canvas bags, sorted and broken down into small cobble-size

pieces. Weathered or altered material is removed mechanically or discarded and the cobbles stored in plastic bins.

The cobbles are crushed to approximately 2 mm in a Retsch BB3 jaw crusher and the pulp stored in numbered bins containing between 10–16 kg each. Then the bulk sample (*e.g.*, ORCA, approximately 1004 kg) is divided into subsamples of about 350 kg each. One subsample is designated the active sample (Portion A of ORCA consisted of 330 kg and is designated ORCA-1). The remainder is stored for future use (Portion B of ORCA consists of 370 kg and is designated ORCA-2).

In the instance of ORCA-1, 30 bins of the bulk sample were pulverized, screened and bottled. Grain size analyses were performed to ensure that the most effective screening procedures are used. No attempt was made to remove the steel introduced during crushing. Low Cr samples (*i.e.*, ORCA 23 ppm Cr *versus* OKUM 2000 ppm Cr) are pulverized in carbon steel mills to minimize contamination.

After bottling, the bulk sample is rigorously tested in-house to determine the composition of the material and to ensure the sample's homogeneity (Table 3). This comprehensive program will yield the chemical composition of the sample, the minimum sample size at which the sample is homogeneous (0.2–5 g), identify any problems that might be associated with a specific technique when analysing the sample and the grain size analysis of the final sample. Chemical testing is carried out to ensure the highest precision possible to avoid variation arising from use of several methods or different analysts. Factors that were especially assessed included the possibility of nugget effect for Sn, Cr, Au, PGEs, and the incomplete dissolution of specific mineral phases, especially zircon. Each element of interest in the sample must be proven to be homogeneous as the geostandards are being created for wide use as multi-element, multi-method reference materials.

After the homogeneity testing is satisfactorily completed, the materials will be released for a round-robin analytical programme to a selected group of laboratories to determine the elemental composition using a variety of methods.

Priorities for Collection

The Geoscience Laboratories geostandards programme is expected to produce 5 reference materials per year when fully operational. At present, production is 2–3 reference materials per year. Several of the members of the volcanic clan will be prepared each year, focusing on locations within the Timmins-Kirkland Lake area. These will be integrated with the other types of reference materials identified from the list of potential materials in Table 4. Interested parties are welcome to comment or join the round-robin programme by contacting the above. Reference materials and price lists will be available through the above address.

The authors gratefully acknowledge the geological support given by the staff of the Ontario Geological Survey in Sudbury, Timmins, Kirkland Lake and in particular that of Dr. L. S. Jensen, Dr. P. C. Lightfoot, Dr. F. Breaks, P. Sangster and D. Guindon. Dr. E. Grunski made available the computer files for the least altered chemistry. B.H.P. Minerals, Toronto, Ontario, allowed the collection of OKUM from their Serpentine Mountain property. P. Prince designed the crushing programme outlined and P. Larabie coordinated the collection and routine preparation.

Appendix

Practical Considerations Important to the Production of Reference Materials

Homogeneity

A reference material must be homogenous: otherwise it is useless. Unlike geological samples, it is not imperative that the sample represent the outcrop from which it came but the material must be similar from bottle to bottle. However, in many instances, the uniformity generated by geological processes can contribute to the homogeneity of a good reference material. Thus fine-grained rocks are preferred as targets for standard preparation, but medium- to coarse-grained rocks are also used. Porphyritic or porphyroblastic rocks and outcrops with veining are not optimal targets. Well thought through sample preparation procedures will overcome variation introduced by nature or, if not well controlled and planned, can create unacceptable variation.

Known geological context

It is strongly preferable that a given reference materials have a known geological context, but it is not vital. In many instances, the rock-units most suited by chemistry to be reference materials are insignificant from a geological point of view. However, if the aim of the programme is to provide a

Table 4 Other materials to be collected as part of the CORM geoanalytical reference material programme

(*i*)	Tills and related unconsolidated materials (typical composition ranges characteristic of areas of Cu–Ni, Cu–Zn and 'granitic' mineralization)
(*ii*)	Rocks of unusual composition that are needed by the analytical community rock (*e.g.*, granitic or carbonatite)
(*iii*)	Low grade gold in silicate rock (less than 100 ppb Au)
(*iv*)	Electron probe/laser ablation materials
(*v*)	Isotopic standards

Table 3 Summary of the homogeneity tests performed on geostandard materials, their purpose, the methodology used and the element determined for each test. Codes for elements determined: M1, majors, loss on ignition (LOI), C, S; T1, Li, Cd, Ag; T2, Be, Co, Cu, Mo, Ni, Sc, Sr, V, Y, W, Sr; T3, Rb, Sr, Nb, Th, Y, Zr; T3+, Ba, Cr, As, Sn, Ga, Pb; T4, lanthanoids, Y, Zr; T8, Rb, Sr, Cs, Hf, Nb, Ta; and T9, U, Th

Test	Purpose	Description	Elements determined
1	Variation amongst bottles	Test 1 in 30 bottles, analyse each bottle in duplicate	M1, T1, T2, T3, T3+, T4, T8, T9
2	Variation within bottles	7 Replicate analyses from 7 bottles	M1, T1, T2, T3, T3+, T4, T8
3	Analytical variation	7 Replicate measurements of 1 prepared sample (*i.e.*, 7 sips from one solution of 7 runs of one bead or pellet)	M1, T1, T, T3, T3+, T4, T8
4	Grain size analysis	7 Samples from 7 bottles	
5, 6, 8	Specific elemental composition tests (Hg, Au + PGEs, Sn)	1 Analysis of each of 7 bottles	Hg, Sn, Au, Pt, Pd
7	Variation owing to use of rotary splitter	1 × 50 g aliquot from 7 bottles, 3 × 50 g aliquots from 1 bottle	M1, T2, T3, T4, T8

representative composition for a specific purpose, obviously the geological content of the sample is critical and must be well determined before the sample or reference material is collected. For contract monitoring purposes, a suite of samples collected from a classic mining area could be a strong marketing factor.

Physical attributes of the collecting site

Suitable collecting sites have several common physical attributes. Frist, the outcrop must be large enough to allow a minimum of a 1 t sample be collected. Realistically, this means that outcrops less than about 10 m^2 are not suitable. Geological features that detract from compositional homogeneity should be avoided. This includes veining, fracturing, compositional layering, pillows or flow-top breccias. Strongly weathered outcrops should be avoided to decrease costs related to rind removal.

Access and permitting of collection site

Given the large amount of material to be removed, it is optimal if the selected site is on or very close to either a road or lakeshore. To minimize problems with obtaining permits, it is best if the selected site is on Crown Land. If the site is staked under a Mining Act or related legislation, permission should be obtained from the claim holder. The protected status of 'classic sites' (*e.g.*, Pyke's Hill, one of two international type-localities for komattites) must be respected.

Requirements within the laboratory

The samples should not pose hazards or any difficulties during either preparation or analysis. During sample preparation, the sample should not damage equipment or threaten safety. Thus, the preparation of SRMs of ultramafic, copper-, sulfur- or arsenic-rich compositions should be undertaken with care as such samples are not easily fusible for analysis by X-ray fluorescence (XRF). Damage to the platinum dishes that the fusions are performed in is expensive and should be avoided.

The standard reference materials selected should be able to be analysed using validated methods within the laboratories. The need for new method development and recalibration and revalidation should be avoided if possible. Limiting the reference programme to samples that the staff are familiar with is critical in the beginning of the programme. In the future it may be possible to branch out beyond these limitations.

Steps in certification of results

After the sample is bottled, the within-bottle and between-bottle heterogeneity must be assessed. If it is not homogenous, it must be reblended or abandoned. This process also provides both a tentative composition for the reference material and ensures that, when samples are sent out for round-robin certification, the time and money spent on gathering these results is worthwhile.

There will be variation in analytical results generated by the different laboratories and it is important that these differences be attributable to the methods used, not the homogeneity of the sample. As results are returned from the participating laboratories, the process of determining the certified values begins. A minimum of 20–40 laboratories should be used and several analytical methods would be employed. The statistical handling of the data must also be outlined.

References

1 Abbey, S., *Chem. Geol.*, 1992, **95**, 123.
2 Govindaraju, K., *Geostand. Newsl.*, 1987, **11**, 208.
3 Lightfoot, P. C., Chai, G., Hodges, A. E., and Rowell, D., Updated in-house report on the Certification of the OGS, 1991, pp. 231–236.
4 Lightfoot, P. C., de Souza, H., and Doherty, W., *Can. J. Earth Sci.*, 1993, **30**, 1123.
5 Fairburn, H. W., Schlecht, W. G., Stevens, R. E., Dennen, W. H., Ahrens, L. H., and Chayes, F., *U.S. Geol. Surv. Bull.*, 1951, **980**, 71P.
6 Flanagan, F. J., *Geochim. Cosmochim. Acta*, 1967, **31**, 289.
7 Govindaraju, K., *Geostand. Newsl.*, 1989, **13**, 1.
8 Flegal, A. R., *Geostand. Newsl.*, 1980, **4**, 17.
9 Tessier, A., Campbell, P. G. C., and Bisson, M., *Anal. Chem.*, 1979, **51**, 844.
10 Lynch, J., *Geostand. Newsl.*, 1990, **14**, 153.
11 Tessier, A., Campbell, P. G. C., and Bisson, M., *Geostand. Newsl.*, 1980, **4**, 145.
12 Kane, J., *Geostand. Newsl.*, 1993, **17**, 99.
13 Gladney, E. S., Jones, E. A., Nickel, E. J., and Roelandts, I., *Geostand. Newsl.*, 1990, **14**, 200.
14 Pyke, D. R., Ontario Geological Survey Report 219, 1982.
15 Jackson, S. L., and Fyon, J. A., *Geology of Ontario*, OGC Special vol. 4, ch. 11, pp. 405–485.
16 Jensen, L. S., Ontario Geological Survey, unpublished work.
17 Grunski, E., Easton, R. M., Thurston, P. C., and Jensen, L. J., in *Geology of Ontario*, OGC Special vol. 4, ch. 26, pp. 1397–1438.
18 Irvine, T. N., and Baragar, W. R. A., *Can. J. Earth Sci.*, 1971, **8**, 523.

The opinions expressed in the following article are entirely those of the authors and do not necessarily represent the views of either The Royal Society of Chemistry or the Editor of *The Analyst.*

Perspective

Method Validation in the Ontario Geoscience Laboratories

Jean M. Richardson and John L. Morrison

Geoscience Laboratories, Ontario GEOServices Centre, Ministry of Northern Development and Mines 933 Ramsey Lake Road, Sudbury, Ontario, Canada P3E 6B5

In 1992, the Ontario Geoscience Laboratories (hereafter referred to as the Geoscience Laboratories) moved from Toronto to Sudbury into a new 25 000 ft² facility. The acquisition of an extensive bank of new equipment and many staffing changes meant all methods were revised and then validated. Thus 7 single element tests, 2 precious metal packages, 2 major element packages by XRF, 7 elements determined by AA, 11 elements by ICP-OES, 8 elements by XRF and 24 elements by ICP-MS were validated. These methods represent the program needs of much of the Ontario Geological Survey. The task had to be completed 'as soon as possible' to minimize the impact on the mapping programs of the Survey which were not interrupted by the move. The tasks of building implementation, method development and validation were undertaken by approximately 12 staff members and were completed in 12 to 18 months. Method validation ensures that a particular analytical methodology using a specific combination of techniques will yield an analytical result that is proven to be correct. It is critical to perform such exercises when procedures are instituted or changed, new equipment procured or staff hired to ensure continuity of data quality. A generic validation program was documented, streamlined and used by all. A detailed outline was drawn up that explained the exercise and listed the steps required. For each method and element, precision, trueness, detection limit, quantification limit, working range, blank level and lack of inherent bias were quantified. These parameters were based on data from a minimum of seven replicates of five to seven SRMs that spanned a wide geological range. SRMs used in calibration or method development could not be included. The data quality objectives were approximately ± 5% precision (2σ) and trueness to meet the stringent data quality objectives of the Geoscience Laboratories. Here, over a 5-year period, precision and trueness are not expected to exceed ± 10% (2σ) when the concentration of an element is more than three times the limit of quantification or 10 times the limit of detection (LOD = 3s_b). Overall, the exercise was a resounding success. Data from the validation of Ba is used throughout the text to illustrate the principles discussed. The problems that were encountered typically included the availability of certain rock compositions, the level of characterization of some reference materials, the uncertainty on 'known' values and thus method trueness, the definition of detection limit and the difficulty in getting realistic 'blank' determinations for some methods. For the Geoscience Laboratories, the method validation exercise provides a standardized, non-subjective means to ensure the data quality objectives of the facility are met. It also convinces management, staff and clients that an appropriate level of expertise is achieved.

Keywords: *Method validation; trueness; precision; standard reference materials; certification; geoanalysis*

Introduction

Method validation is the process used to ensure that a particular analytical methodology using a specific combination of procedures (sample decomposition and instrumental procedures and data reduction) will yield a particular analytical result that has been proven to be correct.[1] As such, method validation is a form of certification. Such an exercise ensures that the specified combination of procedures will yield a precise and true analytical value for certain sample types during routine, specified analytical conditions. Preferred procedures are 'robust' or 'rugged', as they are more independent of human and support (*i.e.*, reagent blanks and mechanical service) conditions.

Reputable laboratories have documented, validated methodologies in place to assure that specific tests are performed correctly, meet data quality objectives and thus ensure client satisfaction. It is critical to perform method validation exercises when procedures are instituted or changed, new equipment procured or new staff hired to ensure continuity of quality control (QC) for clients and thus the preservation of the laboratory's standards.

The Geoscience Laboratories is an Ontario government laboratory that provides high-quality inorganic mineralogical and elemental analysis of rocks and minerals to geologists of the Ministry of Northern Development and Mines and the public at large. To meet client demand, the Geoscience Laboratories continually strives to meet very restrictive data quality objectives, achieve lower determination limits and faster turn-around times. In 1992, the Geoscience Laboratories were relocated 300 km north from Toronto to Sudbury, Ontario, Canada into a new purpose-built facility completely equipped with state-of-the-art instrumentation (wavelength and energy dispersive XRF, ICP-OES, ICP-MS, AA, INAA, SEM, XRD, TIMS, electron microprobe). This meant that for all procedures and methods, staff had to be retrained on the new equipment, methods revised or redeveloped and each method proven to work in the new setting in a consistent manner throughout the Geoscience Laboratories.

Thus the steps that comprise the method validation exercise traditionally used within this group were documented.[2] They parallel very closely the recently derived protocols outlined by the VAM–AMC (Valid Analytical Methods–Analytical Methods Committee) subcommittee for the quality assurance of trace analysis (Section 3.3 Validation).[3] The Geoscience Laboratories' procedures are outlined here and provide the background required to validate a method and determine the expected precision and trueness of a given method (sample preparation and instrumentation technique), the limit of quantification and the limit of detection, optimal working range, inherent bias, blank levels and sensitivity.

This method validation procedure proves the applicability of a given method. After this exercise, data quality, speed and cost of analysis, ease of operation, ruggedness, and a comparison with other methods can be assessed and optimized. The outlined exercise ensures that instruments, procedures and reagents are applicable and appropriate and that QC is maintained. Data from a Ba validation by XRF is used as an example.

How was This Exercise Used in the Geoscience Laboratories?

The general work pattern used to validate each method was very similar (Table 1). Computer templates were available to optimize the time spent handling data and to minimize errors. Data was not released until a written report was provided that outlined the salient points of method development (*i.e.*, interferences and analytical problems encountered), the operational parameters used (especially with respect to calibration), the validation data (seven replicates of a minimum of 5–10 SRMs and the figures of merit (Table 2) calculated. Thus, the method was demonstrated to have met the data quality objectives of the Laboratories for the sample types commonly expected. Typically training and method development took 3–6 months. Validation (data gathering and documentation) took about a week.

Table 1 Procedures used to implement methods at Geoscience Laboratories

1 Determine performance standards expected.
2 Collate and review historical documentation of method for both procedures and data quality.
3 Ensure safe installation of equipment and training.
4 Develop or revise method. Test spectroscopic and non-spectroscopic interferences, optimize operating conditions, test ruggedness for different sample types, check blanks, ensure check samples appropriate *etc.*
5 Validate method with a minimum of seven replicates of 5–10 carefully chosen SRMs. Focus first on precision to conserve SRMs. Calculate
- (*i*) Precision, method trueness, blank.
- (*ii*) Absolute (s_a) and relative standard deviations (s_r) of samples expressed at 2σ interval.
- (*iii*) Average s_r expected at 10 times LOD (or 3 times LOQ).
- (*iv*) Limit of detection, limit of quantification, analytical range, validated range, calibration range.
- (*v*) Plot of measured *versus* certified values for each element (trueness): slope, correlation coefficient and intercept of the line so created (bias).
- (*vi*) Plot of s_r (2σ) *versus* concentration.
- (*vii*) Regression of s_a *versus* measured concentration with correlation coefficient and intercept, plot if desired.

6 Determine if standards are met. If yes, use can begin at this stage.
7 Ensure written documentation of method for laboratory manual or use by others.
8 Determine composition of in-house reference materials or precision monitors by fiat.
9 Monitor generated data. Follow results from method closely when unusual samples come in, environmental conditions change, reagents change or when new staff or visitors use the methods or any other changes are made.
10 Review method in 12 months based on operational follow-up. Revise if necessary.

Procedural Information

Method validation exercises can be undertaken in four ways. Acceptable results can be obtained by (1) the analysis of synthetic formulations, (2) analysis of spiked samples (standard additions), (3) comparison of obtained results with those obtained by official or standard methods (*i.e.*, ASTM testing) or (4) by the analysis of certified reference materials of known concentrations.[4] The usefulness of any of these approaches is dependant upon the sample types expected and the availability of methods or standards.

Unlike in other fields of analysis, there is a wide range of rock, ore and related materials of certified composition that are known as SRMs and are available to geoanalysts (see Govindaraju[5,6]). These SRMs are produced and certified by several international organizations. This availability, coupled with the difficulty in matrix matching the complex composition of rocks means that option (4), analysis of certified material, is perhaps the most appropriate for geoanalysis and it is used almost exclusively for elemental analysis in the Geoscience Laboratories.

Setting Analytical Standards

Every laboratory has a set of general benchmark figures of merit or data quality objectives that each method and analyst must meet. At the Geoscience Laboratories, the expectation is that over a 5-year period, precision and trueness will not exceed ± 10% (2σ) for a given element when that element's concentration is more than 10 times the detection limit (LOD = $3s_o$) of the method in question (*i.e.*, $30s_o$ or 3 times LOQ). The long time-frame is required because data from any given year are typically integrated into larger projects that last up to five years. Precision is thus typically quoted in either parts per million or mass per cent. at the 95% confidence interval.[7] If the data are 100 to 300 times the detection limit, the relative standard deviation is typically less than 3%.[2]

To achieve the 5-year benchmark figure, precision and method trueness of about 3–5% is expected on a per batch or 'job' basis. Typically a batch or job would consist of 20 to 70 samples submitted by one geologist. Such stringent data quality objectives means that there is a 5% cushion over the long term. Thus variables such as reagent changes, personnel changes, technique changes, instrumentation changes or laboratory-setting changes can be absorbed and the data still be acceptable to the Ministry's long-term program objectives. Thus any method validation exercise must certify that the method in question can indeed generate data of sufficiently high quality to meet the short-term Laboratories' data quality objectives.

Table 2 Figures of merit determined in method validation exercise

Precision (2σ; s_r, s_a)
Method trueness (bias)
Limit of detection (LOD; $3s_o$)
Limit of quantification (LOQ; $10s_o$; 3.3 times LOD)
Limit of linearity (LOL)
Analytical range
Reagent blank
Ruggedness

Steps in Method Validation: Guidelines

Method validation consists of several that should be undertaken in a well constrained order (Table 1). Much of the exercise can be completed in a relatively short time-frame (*i.e.*, several days to one week). The second part of the process (operational compilation) requires a longer time-frame (*e.g.*, 6 months to one year) and results in a larger database. At the end of that time period, a statistically coherent body of data will have been gathered under a normal range of operating conditions. This data will be for a variety of reference sample types and the elemental contents will be well determined. At this point, factors contributing to ruggedness can also be evaluated.

To avoid the possible wastage of SRM, it is often appropriate to first determine precision using internal reference materials and samples of varied composition which span the advertised analytical range of the instrument. A minimum number of 12–15 samples is required to ensure that the range is properly tested. At least seven blanks should be determined at this stage as well. When the precision is established, the method trueness should be determined using an SRM. Depending on sample size and SRM availability, seven determinations should be undertaken of a minimum of 5–10 SRMs with diverse compositions. More SRMs should be used, if available. If possible, in-house reference materials should be analysed during this part of the exercise. From this data, the figures of merit for the method can be determined (Table 3). Any deviations from the procedures set forth here should be thoroughly discussed by all involved before the exercise begins to minimize the impact of compromises.

Training/Determining Operator Reproducibility

Any method validation exercise has as a fundamental tenet that the operator be fully trained, competent using the procedures and comfortable performing them routinely. Secondly, the instrument and/or equipment used must be fully functional to vendor specifications. To ensure this, the analyst in question should repeatedly analyse a small suite of samples of unknown compositions that are both within the middle of the advertised instrument analytical range and available in great quantity. Typical 'fodder' could be the remnants of previously submitted samples. This will ensure that he/she is comfortable with instrument operation and the performance of the samples while they are analysed. If is difficult to say exactly how many samples should be analysed before the validation exercise begins: it depends greatly on the experience and capabilities of the analyst. Given the importance of the method validation exercise, it is best if the analyst determines, in consultation with other staff, how soon after method development and/or training the validation can begin.

Selection and Use of Reference Materials

Reference materials to be used during a method validation exercise should be selected on the basis of similarity in

Table 3 Ba validation by pressed-pellet wavelength-dispersive XRF

Limit of detection, LOD (ppm Ba)	8.3
Limit of quantification, LOQ (ppm Ba)	27.6
10 × LOD (3 × LOQ) (ppm Ba)	83
Working range (ppm)	30–5000
Method trueness (within working range) (%)	±4.57
Method trueness (at 3 × LOQ) (%)	±2.87
Absolute precision (2σ, 95% confidence interval, within working range) ppm)	±19.14
Relative precision (2σ, 95% confidence interval, within working range (%)	4.62
Absolute precision (2σ, 95% at 3 × LOQ) (ppm)	±23.61
Relative precision (2σ, 95% at 3 × LOQ) (%)	2.29
No. of determinations/SRM	12
y-Intercept (s_a *versus* measured concentration)	2.760 ± 1.342
Correlation coefficient, *r*	0.727
y-Intercept (measured concentration *versus* certified concentration)	1.006 ± 9.968
Correlation coefficient, *r*	0.998
Slope	0.992

SRM	Rock type	Certified* (ppm)	Average (ppm)	s_{av} (2σ)	s_r (%) (2σ)	True (%)
FER3	Iron Formation	11	10	8.24	79.73	−6.06
GSD-10	Sediment	42	33	6.62	19.87	−20.63
NIM-N	Norite	100	111	9.80	8.83	11.00
GSR-6	Limestone	120	124	8.39	6.78	3.19
BHVO-1	Basalt	139	148	13.00	8.78	6.53
NBS-688	Basalt	200	200	8.79	4.40	−0.13
NIM-L	Lujavrite	450	422	14.71	3.49	−6.24
SY-2	Syenite	460	451	12.43	2.76	−1.94
SDC-1	Mica Schist	630	676	15.67	2.32	7.24
GA	Granite	840	799	19.92	2.49	−4.89
NBS-2709	Soil	968	962	22.87	2.38	−0.66
GSR-2	Andesite	1020	1020	12.89	1.26	−0.05
BR	Basalt	1050	1064	20.57	1.93	1.35
GSP-1	Granodiorite	1310	1247	39.12	3.14	−4.79
QLO-1	Quartz	1370	1400	18.60	1.33	2.20
GXR-4	Cu Head	1640	1604	23.25	1.45	−2.17
GXR-2	Soil	2240	2242	59.69	2.66	0.08
Mean, within working range ($n = 16$)				19.14	4.62	−0.62
(*i.e.*, excludes FER-3) (ppm)						4.57†

* Certified values from Govindaraju[5] and original certificates.
† Absolute value of the mean.

composition to typical sample material. This equivalence should encompass the expected concentration range, analytes of interest, various possible matrix, spectral interferences and sources of determinate and indeterminate error. If these criteria are not fulfilled, then the method will not be rugged and is thus limited. Where possible, the elemental range in the suite of reference materials should span both the analytical range of the instrument and the range of geological compositions found in nature or commonly submitted sample types. The method of Govindaraju[5] can be used to provide a first approximation of the compositional range of the analyte in most geological materials. This is supplemented with chemical summaries in sources such as petrology text books and discussions with clients.

Obviously other parameters to be considered include the degree and confidence with which the certified values of the reference materials are known and the availability of SRM based on the amount(s) required to complete the validation exercise. It is important that reference materials known to be well determined are selected for validation exercises. Unfortunately, such materials are scarce and treasured. However, given the analytical difficulties (poor calibrations and resulting biased data) that can arise if the compiled analytical values of the SRM are in error, it is imperative to understand the compromises. For instance, inhomogeneities in the GXR series of SRMs[8] have resulted in poor trueness and bad calibrations. Overall, it is better to use a limited number of SRMs that have well determined compositions than a wide variety of SRMs that are less well determined.

The Geoscience Laboratories has both SRM and in-house reference materials (known as 'MRB samples'). These serve several QC purposes. SRMs provide the authoritative measure of method trueness and are used sparingly. The composition of these samples is known and well documented (*e.g.*, Abbey,[9] Govindaraju[5,6]). Care must be taken not to waste them (either accidentally or as a result of poorly considered activities) to ensure a long-term supply. Typically 5–10 SRMs covering a wide compositional range should be used in a method validation exercise. They should not be analysed until the analyst is highly confident in his ability to perform the procedure correctly.

A suite of approximately 30 in-house reference materials comprise the Geoscience Laboratories 'MRB' samples. These were generated to support four important functions: firstly, they provide a good quantity of well characterized materials for in-house method development; secondly, they are used to routinely monitor analytical performance; thirdly, the analysis of these materials provides data for the Geoscience Laboratories' long-term QC program; and fourthly, they provide a means for the Geoscience Laboratories to monitor external analytical work done by contract agencies.[10] The MRB samples are collected from Ontario rock units and represent the various types of incoming samples. In contrast to SRMs, MRB samples are used more generously to monitor routine analytical work on a daily basis. These materials are known as the MRB samples because the first group (MRB 1–7) were developed in 1974 when the Geoscience Laboratories were part of the Mineral Resource Branch of the Ontario Ministry of Natural Resources.

Determination of Reagent Blank

The term 'reagent blank' is used to refer to any contamination that is added from all sources external to a sample. Such contaminants may be environmental (*i.e.*, the result of poor housekeeping, old equipment, downdraughts from fume hoods, equipment reacting with reagents) or due to contamination in reagents (purchased chemicals or water). Thus 'high blanks' can seriously effect the trueness of low or trace level determinations.[1] The main ways to minimize the reagent blank contribution to an analysis are to use minimal amounts of pure chemicals, to vigilantly keep records of chemical composition of reagents, sample passage through labware and vessels, isolating the usage of some to clean, conditioned areas; and by closely monitoring the level of blank determinations and taking early action if necessary.

Reagent blanks should be analysed with each batch of samples, when new reagents are opened for use and when operation conditions change (*i.e.*, fumehood supply air turned off and on). The results can be plotted on control charts or treated statistically[1] to allow the determination of systematic trends or outliers. Abnormalities can then be correlated with operational causes and corrective measures taken.

The level of the reagent blank value is determined by preparing a 'sample' that has been subjected to all the normal analytical conditions and procedures except for the addition of the actual sample powder or liquid to the vial. The measured elemental abundance derived from this 'sample' is said to be the reagent blank. If high blanks are determined, probable causes should be evaluated and minimized. A final, but not optimal, way to combat a high reagent blank is to determine the reagent blank and subtract it from the measured result for a sample, thus getting a 'true' value. High reagent blanks are most critical when the measurements are close to the limit of detection of the method used.

Determination of Measurement Precision

Precision is a measure of how closely one measurement agrees with a replicate generated by repeated application of the same process under specified conditions.[1] Precision is quantified by the standard deviation of the mean and is expressed in an absolute sense [eqn. (1) where σ is the population standard deviation (used with μ); s the sample standard deviation (used with X); X_i the individual analytical measurement; X the mean average measurement (used with s); μ the mean or average measurement (used with σ); and n is the number of measurements] or a relative or proportional sense [eqn. (2)].

$$s_a = \sigma = \sqrt{\frac{\Sigma (X_i - \mu)^2}{(n)}} \approx s = \sqrt{\frac{\Sigma (X_i - X)^2}{(n-1)}} \text{ (in ppm)} \quad (1)$$

$$s_r = \frac{s}{X} \times 100 \approx s_r = \frac{\sigma}{X} \times 100 \text{ (in \%)} \quad (2)$$

The relative precision is also known as the relative standard deviation (s_r). Doubling the value obtained from eqn. (1) (which generates a precision value at the 1σ interval) will yield the absolute uncertainty at 2σ or the 95% confidence interval. Either the 1σ or 2σ values can then be divided by the mean to get the s_r value at either 1σ or 2σ intervals, respectively. In the Geoscience Laboratories, the final figures of merit are always expressed at the 2σ interval.

In method validation, the generated data represent a small subset of all the true values (the sample), not the entire set of values available (the population). If the mean is derived from some components of a population (*i.e.*, a sampling), it is denoted as X. If it reflects all components of a population, the mean is denoted as μ. Thus X represents the average of some individual measurements, but not the average composition of the universe of those values which would be denoted by μ. Following through, the absolute standard deviation (s_a) derived from a sample or subgroup is denoted s, and that of a population as σ.

When standard deviation is being calculated for a population, the denominator of the equation is n (the number of measurements). In contrast, when calculating sample standard deviation, the denominator is $(n - 1)$. The value $(n - 1)$

represents the degrees of freedom or the number of independent deviation calculations that are possible within the sample after X has been calculated. This difference can result in distinctly different values for s and σ if n is very small or X is very low (*i.e.* close to the limit of detection). By either increasing the number of replicates or with larger elemental abundances, the difference between s and σ decreases.

In a typical method validation exercise, approximately seven replicates of each MRB sample, SRM and blank are generated, thus statistics that reflect 'sample testing' should be used (*i.e.*, s, X and $n - 1$). It is difficult to determine σ (as opposed to s) for an SRM: this would involve analysing a significant portion of the entire supply of the material, which is scattered throughout international laboratories. A possible exception to this might be statistical values determined from the compilation of analytical values for BCR-1,[11] a famous and now nearly depleted SRM.

Population statistics should be used for large groups of data drawn from a relatively small source. For instance, 10 l control solutions are created in the Geoscience Laboratories to monitor ICP instrument performance over 3–5 year periods. When determining figures of merit for a 3 year period, Beneteau[12] (ICP-MS) and Henri[13] (ICP-OES) reported data compilations based on 100 or 340 determinations and used population measures (σ).

The absolute standard deviation s_a and the s_r values both express the degree of uncertainty associated with a particular measurement either absolutely or relatively. The s_a value is most useful to the end user of a data set (*i.e.*, a geologist) as it indicates the total amount of uncertainty associated with one measurement expressed in the same units as the measurement. For instance, if a validation exercise was evaluating the determination of Rb and CaO by XRF, the s_a value would be expressed in ppm Rb and mass-% CaO. Per cent., in a proportional sense, is not part of the expression. In the case of BHVO-1, the measured Ba content of 148 ppm has a s_a value of 13 ppm (Table 3). This means that the 'error bars' associated with the measurement are ± 13 ppm 'wide' and that the true value lies between 135 and 161 ppm. There are not actually any errors in the measurement: the s_a value simply provides a quantification of the absolute uncertainty inherent in the method.

However, for geoanalysts assessing the validity of a method or for method comparison, the s_a value is not as useful as the s_r value as it increases linearly with concentration. The s_r value allows a better comparison of the degree of uncertainty because it is a proportional measure determined in per cent. and not as a unit related to the analyte composition (*i.e.*, per cent. as opposed to ppm Rb or mass-% CaO). Thus the s_r value provides a more meaningful measure of differences in precision across a wide compositional range by bring the apparent magnitude of the discrepancy to a common baseline (*i.e.*, normalizing it to 100). For example, for Ba by XRF (LOD = 8 ppm), NBS 688 (200 ppm Ba) and GSD 10 (42 ppm Ba) have similar s_a values of 8.8 and 6.6 ppm, respectively. However, the s_r values for these samples are different, 4.40 and 19.9%, respectively. Such a difference in s_r value is the result of the small amount of Ba present in GSD-10.

Limit of Detection, Limit of Quantification

The limit of detection (LOD) of a method is the point at which a measured value is larger than the uncertainty associated with it. Colloquially, it is equated with the point at which a peak can be distinguished from a background. It is defined as the 'lowest concentration that an analytical process can reliably detect' (IUPAC;[14] ACS,[15]) and thus is specific for a given sample preparation technique, instrument operating parameters and data reduction approach or 'method' in the terms of Abbey.[16] LOD is also defined as 3 times the value of the standard deviation of the noise that forms the background as the concentration approaches 0 (s_0).[1] Quantitative analytical measurements are not possible at the limit of detection: s_r = 100% (95% confidence internal). The lower limit at which measurements become quantitative is the limit of quantification (LOQ) or at 10 s_0. At the LOQ, the relative confidence in the measured value is about ± 30% (2σ) at the 95% confidence interval.[1]

However, the parameter s_0 or the standard deviation at 0 concentration (a form of 'blank') is difficult to measure. For instance, in ICP analysis, is the 'blank' a distilled water solution, a 10% nitric solution, a calibration solution of several elements in 10% nitric acid, a reagent blank or a rock which contains many other elements but not the element of interest? This final option is complicated by the nature of the rock. For instance, does it contain 3 or 30% iron and does this matter? In all analytical methods, the nature of the background is clearly dependant on the matrix of the samples being analysed and thus the value LOD and LOQ will vary as well. This is especially a problem in ultratrace analysis when analyte levels are typically near the LOD or LOQ. For rock analysis, the optimal background is that which is similar to the rocks samples expected to be routinely analysed.

Several approaches to LOD calculation are used at the Geoscience Laboratories, depending on the method in question, the ease with which a 'blank' can be defined for a given method and the reference materials available. First is a graphic approach where s_0 is the intercept of the line regressed through the absolute standard deviation data and the measured values that were generated by the replicates of validation samples analysed to determine precision. Thus it is expressed graphically on a plot of s_a *versus* concentration (Fig. 1) and is quantified *via* the slope, intercept and correlation coefficient. Typically the correlation coefficient (r) of such a plot is poor: 0.7–0.85 (*i.e.*, Ba by XRF, r = 0.727). This approach works best when the samples have a concentration range that begins at approximately 20 s_0. If the intercept is negative, the concentrations of the analyte in the SRM are too high or a single, high value is biasing the results (*i.e.*, Zr in NIM-L). This is discussed further in Potts.[17]

The second approach involves selection of 5–10 SRMs that encompass the working range of the method and thus have a range of sample matrices that might be expected during routine use. The following formulae:

$$\text{LOD} = \frac{s_1}{m} \text{ and } \text{LOQ} = \frac{10s_1}{m}$$

where s_1 is the (standard deviation of background signal)$^{1/2}$ and m is the sensitivity [*i.e.*, kcounts s^{-1}/oxide (%)], are used to calculate the LOQ and LOD respectively. The results are then averaged to yield an approximate LOQ or LOD for the entire method.

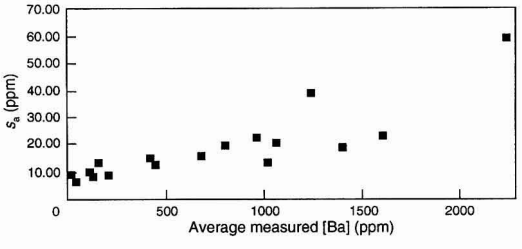

Fig. 1 Absolute standard deviation (s_a) *versus* measured abundance of Ba by XRF. r, 0.7275; intercept, 2.760 ± 1.342 ppm.

A third approach, unused in the Geoscience Laboratories, is to regress the median absolute differences against concentration for 10 to 200 duplicate pairs, when the concentration range is divided into equal frequency intervals (Thompson and Howarth[18]). The *y* intercept is the LOD. The strength of this method is its use of numerous duplicate pairs. It would be ideal for a laboratory validating methods already in production as it is most effective in the instances where there are data available for a large number of duplicate pairs.

Working Range *Versus* Geological Range

As the analyte concentration increases, signal intensity increases and the measurements taken become statistically more sound. The upper limit of reliable measurement is the point at which the relationship of concentration to intensity is no longer linear and thus calibrations cannot be carried out (*i.e.*, limit of linearity, LOL). Thus the LOD, LOQ and LOL delineate the dynamic range of an analytical method. The definition of the analytical working range varies depending upon the required precision and method trueness benchmarks. If very high precision results are required, then the analytical method will have a smaller analytical range. Typically the effective working range of the instrument in the Geoscience Laboratories setting is narrower than documented by the vendor.

Determination of Method Precision

Typically, precision degrades as the analytical signal decreases. The s_r value highlights these differences in a way that the s_a value cannot. Thompson and Howarth[18] portrayed this relationship by plotting s_r (%) (2σ) *versus* the measured concentration of the analyte (*e.g.*, Figs. 2 and 3) to illustrate how the uncertainty is magnified at the limits of detection and quantification of a method. The curve generated from such data is typically very steep at lower concentrations. LOD and LOQ typically occur near the inflection point of the graph. The over-all working range of the method is represented by a flattening of the curve. As the analytical limits of the method are approached, the curve gently inclines upwards as higher s_r values are generated (Fig. 2). These trends can be determined from replicate measurements of unknown-sample duplicates or reference materials. As SRMs must be analysed for accuracy, these data can also be used to determine method precision if the samples chosen reflect a range of compositions.

Using such a graph and the general laboratory precision benchmark points, the upper and lower limits of the effective working range can be determined and concentrations assigned to these end-points. If required, the uncertainty associated with measurements outside the normal working range can also be predicted with some confidence. Occasionally, the Geoscience Laboratories is asked to analyse unusual samples for which the elemental constituents are expected to be outside the normal working range of a particular method (*e.g.*, furnace matte). In such special circumstances, this graph allows some estimation of the minimum potential analytical uncertainties.

It can be desirable to calculate an 'average method precision'. Inspection of plots like Figs. 2 and 3 indicate that such an 'average' can be highly skewed. It is not appropriate to simply average all the results. It is better to determine the precision at a fixed point (*i.e.*, at three times LOQ) or to average the data within the working range of the method. The former has the advantage of being a single number but is independent of variation that might occur in slightly different matrices or with various interferences. The latter, while somewhat more subjective (it will depend on the SRMs used) are perhaps more representative of the results that a client might expect.

Determination of Trueness

Trueness is an absolute measurement of how closely a determined value approaches the known or certified value [eqn. (3)]. Method trueness is the average trueness of a suite of reference materials which approximate the materials that are to be analysed by that method. At the Geoscience Laboratories, SRM with well determined 'recommended' certified values (see classification of Abbey,[9] Govindaraju,[5,6]) are used to determine accuracy. A related quantity is the 'per cent. difference' which documents how closely a determined value approaches another value thought to be correct (*e.g.*, an analytical value determined 'by fiat', *i.e.*, best known value, during a method validation exercise), where the measured value is the analytical result determined experimentally or the mean of several of such results [eqn. (4)].

$$\text{Trueness} = \left(\frac{\text{Measured value} - \text{Certified value}}{\text{Certified value}}\right) \times 100 \text{ (result in per cent.)} \quad (3)$$

$$\text{Per cent. difference} = \left(\frac{\text{Measured value} - \text{Best known value}}{\text{Best known value}}\right) \times 100 \text{ (result in per cent.)} \quad (4)$$

The degree of trueness can be expressed in two ways. In one case, using eqn. (3), trueness can be expressed as a positive or negative quantity for each SRM. The data can be averaged for a suite of SRM that are represent the expected sample types and concentration ranges and expressed as ± the mean thus giving the method's trueness (*e.g.*, Table 3, 4.57 for Ba by XRF). This has the advantage of giving one value for the entire method averaged over a wide range of samples types

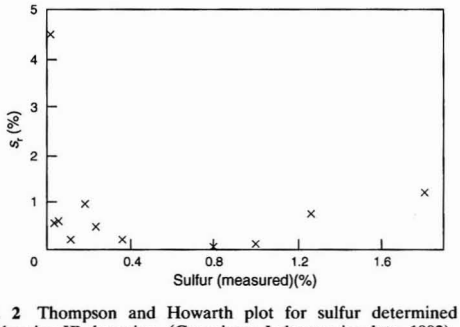

Fig. 2 Thompson and Howarth plot for sulfur determined by combustion IR detection. (Geoscience Laboratories data, 1992).

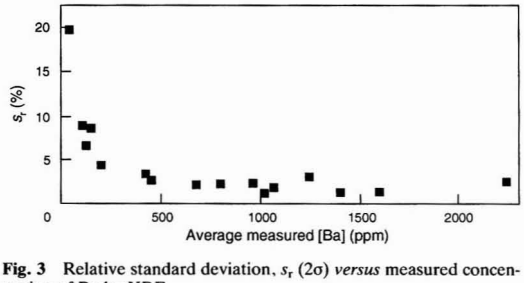

Fig. 3 Relative standard deviation, s_r (2σ) *versus* measured concentration of Ba by XRF.

and can be very useful in discussions with clients, but it is dependant on the availability of and how well individual elements are constrained.

Alternatively, bias in the method can be quantified graphically. This will identify the presence of conditions that either lead to incorrect results arising from a systematic error inherent in a method or cause an artifact of, or idiosyncrasy in, the measurement system. Measured values are plotted against the certified values for all SRM and a linear regression fitted to the data (Fig. 4). The slope of the line on a graph such as Fig. 4 should approach 1, the intercept approach 0 and the correlation coefficient approach 1. Otherwise there is bias in the data.[1] Bias to the data can be either positive or negative. A method with limited bias is accurate. A positive intercept could be generated by consistent contamination of the samples. This would also be observed in the blank determinations. If the correlation coefficient is low (<0.9), this indicates unacceptable scatter in the data, perhaps resulting from either the measured determinations or poorly determined SRMs were used. When investigating this, the first place to start is with the primary documentation for SRMs. Ripley and Thompson[19] recommend that this method only be used when SRM values are well determined as such treatment is not 'symmetrical, we talk of regressing y on x'.

Determination of the Composition of In-house Reference Materials by Fiat

The MRB samples are of prime importance to the Geoscience Laboratories as they are used to monitor most of the routine digestion/sample preparation procedures and as instrument control samples. However, the chemical composition of these samples is characterized in-house and they are not subjected to round robins. Instead, their composition is determined by association with the SRM usually as part of the method validation exercise. This provides the foundation for a 'best value' for the MRB sample that is well constrained by international SRMs. If the determinations of the SRM are accurate within the Geoscience Laboratories' standards, then it must follow that, if the MRB samples were analysed at the same time, by the sample procedures, by the same analyst, that the determined value represents the best value for the MRB sample. Thus the MRB composition is determined by association or by fiat. In no way do these values represent truly certified values: such determination are only 'best values'.

Ruggedness and Operational Follow-up

During method development, 'ruggedness' or tolerance of critical operational parameters must to be determined. Such factors could include variations in environmental considerations (humidity, temperature, pressure), chemical factors (reagent concentration, pH control, voltage). Such parameters should be determined functionally (*i.e.*, during application of the procedures), so that their relative effects on the measured analytical values be determined. If possible, these parameters should be optimized[1] before a method is validated (see Youden[20]).

Unfortunately, it is not practically possible to test all possible parameters before a method is validated and used. Problems with a method may only arise with the analysis of an unusual sample type or acquisition of new supporting apparatus. Thus, a 'compilation period' of 10–12 months is required after every method validation exercise, during which blanks, standards and duplicates are monitored assiduously, the data carefully charted and the results closely assessed. Experiences in this period will illustrate how rugged the method is or if redefinition of the method is required.

For example, after obtaining the method validation data outlined in Tait and Richardson[21] the method was put into routine use for 10 months. When evaluated after this interval, it appeared that the trueness of the method was improving and compiled values for MRB29 also were rising. This variation was finally correlated with the use of new crucibles with tightly fitting lids, thus limiting the rate at which Fe^{2+} oxidized to Fe^{3+}, even within the 20 min window that was set for analysis.

The T2 and T4 are two extremely well documented and rugged trace element packages in that have been used for several years in the Geoscience Laboratories and now have large integrated statistical databases of quality control data (Henri,[13] Beneteau[12]). Inconsistencies, if present, can easily be observed owing to the statistical tracking of each procedure. Long-term data collection such as this further supports the method validation exercise and ensures that QC benchmarks are met. For instance, we were able to compare the impact of two fully trained analysts in different years for the T2 package. The high correlation coefficient (0.9996) (Fig. 5) indicates that the method is exceedingly robust.

Benefits of the Method Validation Exercise

Overall, the method validation exercise outlined here has many advantages. Firstly, it provides a standardized means to determine the figures of merit for a method and thus can be used to compare methods. It becomes a vital over-all component of the delivery of a quality product to a client. Consistent product quality increases client confidence in and satisfaction with a laboratory. Secondly, it convinces laboratory staff that an appropriate level of expertise is achieved for any given method and that the method is functioning in an appropriate manner. Thirdly, it allows an analyst to demonstrate the quality of his/her work. Fourthly, it provides a

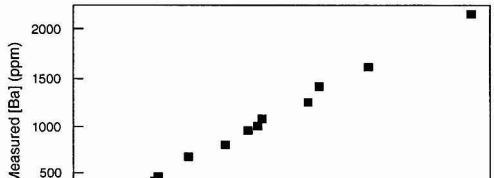

Fig. 4 Measured Ba abundance *versus* certified concentrations. Slope, 0.992; r, 0.998; intercept, 1.006 ± 9.968 ppm.

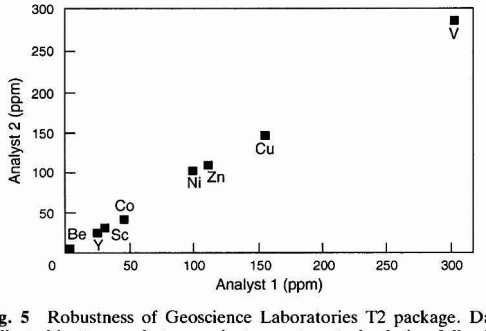

Fig. 5 Robustness of Geoscience Laboratories T2 package. Data collected by two analysts on a instrument control solution following same written procedure two years apart (data from Henri,[13]). Slope, 0.956; r, 0.9996; intercept, 1.425 ± 1.522 ppm.

consistent framework that can be used to compare various methods in terms of analytical figures of merit or time-effectiveness. Finally it provides consistent documentation important for quality assurance purposes. Such an exercise is an important building block in the QC program of a reputable laboratory.

Conclusions

A method validation exercise is documented that is regularly used to determine the figures of merit (precision, trueness, sensitivity, working range, limit of detection, blanks, limit of quantification) for data generated using a specific analytical method for a variety of expected sample types. It provides a consistent framework that can be used to compare analytical figures of merit determined by several methods. It provides a baseline against which cost, time effectiveness and other parameters can be assessed. Finally, it will convince all concerned (operator, supervisory staff and clients) that the data quality objectives of an organization are maintained. This procedure has been used to implement 29 methods consisting of 111 elements in the Geoscience Laboratories in Sudbury, Ontario, Canada in 12 to 18 months.

Overall, the new or relocated equipment was proven to produce similar or better quality determinations (*i.e.*, similar or higher figures of merit) in the Sudbury facility while generating a wide variety of elements in exceedingly varied and often complex sample matrices. In every instance, new instrumentation had to be proven to be compatible with old procedures (*i.e.*, OGS Staff[7]) to ensure that differences required by patent law, technological innovation or new analytical requirements did not negate existing protocols.

The staff of the Geoscience Laboratories are thanked for their help in clarifying and documenting the concepts presented here. In particular G. Henri, J. Tait and D. Romani are thanked for their help with the clarification of detection limit and trueness considerations.

References

1 Taylor, J. K., *Quality Assurance of Chemical Measurements*, Lewis Publishing, Chelsea, USA, 1989, p. 328.
2 Richardson, J. M., *Ont. Geol. Surv. Misc. Pap.*, 1992, **160**, 168.
3 Sargent, M., *Protocol for Quality Assurance of Trace Analysis*, National Measurement System Program on Valid Analytical Measurement, Laboratory of the Government Chemist, 1994, p. 7.
4 Garfield, F. M., *Quality Assurance Principles for Analytical Laboratories*, Associations of Official Analytical Chemists, Arlington, USA, 1991, p. 192.
5 Govindaraju, K., *Geostand. Newsl.*, 1994, **18**, 1.
6 Govindaraju, K., 1994.
7 OGS Staff *Analytical Capabilities and Services*, 1990.
8 Kane, J. S., Seims, D. F., and Arbogast, B. F., *Geostand. Newsl.*, 1992, **16**, 45.
9 Abbey, S., *Geol. Surv. Can.* Paper 83-15, 1983.
10 Lightfoot, P. C., Chai, G., Hodges, A. E., and Rowell, D., *An Update Report on the Certification of the OGS In-house MRB Standard Reference Materials. Summary of Field Work and Other Activities*, 1991, pp. 231–236.
11 Gladney, E. S., Jones, E. A., Nickell, E. J., and Roelandts, I., *Geostand. News.*, 1990, **14**, 200.
12 Beneteau, S. B., *Ont. Geol. Surv. Misc. Pap.*, 1992, **160**, 153.
13 Henri, G., *Ont. Geol. Surv. Misc. Pap.*, 1992, **160**, 159.
14 IUPAC, *Spectrochim. Acta, Part B*, 1978, **33**, 242.
15 American Chemical Society, *Anal. Chem.*, 1980, **52**, 2242.
16 Abbey, S., *Geostand. News.*, 1991, **15**, 191.
17 Potts. P. J., *Handbook of Silicate Rock Analysis*, Blackie, Glasgow, 1987, p. 622.
18 Thompson, M., and Howarth, R. J., *Analyst*, 1976, **101**, 690.
19 Ripley, B. D., and Thompson, M., *Analyst*, 1987, **112**, 377.
20 Youden, W. J., *Statistical Techniques for Collaborative Test*, Association of Official Analytical Chemists, Arlington, USA, 1975.
21 Tait, J., and Richardson, J. M., *Ont. Geol. Surv. Misc. Pap.*, 1992, **160**, 175.

The opinions expressed in the following article are entirely those of the author and do not necessarily represent the views of either The Royal Society of Chemistry or the Editor of *The Analyst.*

Perspective

Quality Management and Laboratory Accreditation at a University: What can be Learned From Experience?

Peter Bode

Interfaculty Reactor Institute, Delft University of Technology, Mekelweg 15, 2629 JB Delft, The Netherlands

Quality management has been introduced at the Laboratory for Instrumental Neutron Activation Analysis of the Interfaculty Reactor Institute at the Delft University of Technology. The laboratory has received accreditation for its quality system for compliance with the accreditation criteria of EN45001 closely following the ISO-25 guide. The laboratory's motivation for introducing quality management is given with emphasis on the aspects of a university environment. These motives include the need for a system of documentation, prevention of repetition of work, thorough traceability of experimental conditions, increased respect for and therefore, trustworthiness of the laboratory and improved chances for acquiring third party contracts. The route to accreditation is described briefly. The experience with the quality system is illustrated with examples of the consequences for research and routine operations, *e.g.*, related to technical competence of personnel, non-conformance management, audits and analytical quality. Unexpected spin-offs are presented and an outlook on the future is also given.

Introduction

Certification, accreditation and quality management have recently been discussed in a topical article by Nadkarni.[1] In the article, Nadkarni focuses initially on the chemical and process industries. In Europe, quality management is being emphasized at testing (service) laboratories to facilitate the mutual acceptance of services in the member states of the new unified internal market. A notifiable aspect of the 'new style of working, new style of thinking' (quoted by George Bush)[1] is that it has been introduced, supported and propagated by industry and commercial companies themselves, and that education in this area is almost absent at universities, which is even more remarkable as academics have a greater than average expectation to hold future positions where decisions are made.

Apparently universities are not yet sufficiently aware of the need for educating the students in the 'quality' lifestyle: not only teaching, but also educating students until it becomes second nature rather than a class to be taken. A few of the reasons for introducing quality practice at universities are given below.

(*i*) To reduce failure of experiments owing to improper planning and preparation, and to consequently reduce, repetition of experiments.

(*ii*) To enhance traceability of experiments.

(*iii*) To prevent professionals from becoming a 'single point to failure', Independent peer review of laboratories and methods.

(*iv*) To prepare young academics for the needs of society.

In answer to the first point (*i*) most university professionals have sufficient experience such that they do not require a written procedure to carry out their own work; however owing to this style of working the method in which results have been obtained is often poorly documented (if documented at all) with sometimes dramatic consequences if experiments have to be repeated when the results obtained are suspected to be wrong. Occasionally, tracing the reasons for inaccuracies is impossible owing to the absence of records.

Owing to poor documentation in many university laboratories the senior research scientist has become the 'single point of failure': he knows all the 'ins and outs' of the experiment but has documented the details in his head. When such a professional leaves the organization (for instance on sabbatical, or through illness or retirement) a tremendous amount of experience is lost from the organization. In addition to this, the mobility of students and PhD researchers tends to be rather high, and with it, the mobility of new expertise. More precise documentation of the universities' traditions is needed in order to expand on experiences and not to start anew, over and over again.

Documenting and archiving the many details of the analytical process are ever returning key-aspects of quality practice that make the training of new, unexperienced personnel much easier.

In answer to point (*ii*) sometimes it can be observed that university researchers have acquired a certain arrogance with respect to the quality of their analyses. Results of intercomparison laboratory tests have demonstrated that quite a number of laboratories that consider themselves to be 'highly experienced' do not present the outstanding results that one would expect from this classification. The professionals in these laboratories may be very knowledgeable on the fundamentals of their technique, but the absence of high quality results indicates that they have not mastered the entire analytical process in all its details.

Quality practice not only contributes to a better assessment of the quality of the analytical results, but it also challenges the university researcher to have his laboratory, his systems and his organization of work audited by external experts. Once accredited, the classification 'highly experienced' can be used in a more confident and justifiable way.

Peer review of one of the products of research, *viz.* a scientific article, is commonly accepted; therefore, why should

there be so much reluctance against a similar peer audit of the laboratory and its standard operating procedures?

The third point (*iii*) a characteristic aspect of experimental research and related analyses is that experiments sometimes fail: this may be justifiable when the obtained result appears to differ from the hypothesis, but it is unacceptable when an experiment fails because of bad planning, careless preparation (*i.e.*, not all conditions are fulfilled) and/or improper conduct.

It is common practice at universities that researchers always have ample time available to repeat experiments that have gone wrong; but that the same researchers apparently do not have the time to think things over properly in advance and during their experiments. This arrogant abuse of 'academic freedom' is not acceptable when the experiments are performed on a more or less routine basis *e.g.*, in some types of chemical analysis. As a result, at universities countless man-hours are lost and the economical consequences must be large.

(*iv*) It is reasonable for society to expect academics to be not only knowledgeable on the principles of quality practice but who have also been educated, trained and practised in such an environment. Universities should have, therefore, a mission to educate quality practice to present and future generations of scientists.

Perhaps universities fear that educating and introducing quality management into the curriculum might hamper the atmosphere of innovation and creativity? Perhaps there is too much ignorance on the implications of the quality lifestyle?

ISO/IEC 25 *versus* ISO 9000

International reference documents, the (International Standards Organisation/International Electrochemical Commission) ISO/IEC guides, have been developed to harmonize ways of implementing and evaluating quality assurance practices in laboratories, in connection with quality system certification (where 'certification' is defined as the 'procedure by which a third party gives written assurance that a product, process or service conforms to specific requirements') and laboratory accreditation (where 'accreditation' is defined as the 'procedure by which an independent authoritative body gives formal recognition that a body or person is competent to carry out specific tasks') and, more generally, to facilitate the acceptance of services, products and test results. Certification and accreditation are, as the definitions demonstrate, basically different concepts. The respective reference guides are the ISO 9000 series for certification and the ISO/IEC-25 for accreditation. The guide series differ from one another in principle as they have been developed with different intentions.

The ISO 9000 series are the most well-known. The purpose of this series is to insist on criteria to which a quality system has to comply in a contractual situation between supplier and buyer. As the ISO 9000 describes the quality system in a general way, certification bodies have to apply broad interpretations for the variety of industries and tertiary companies. These interpretations have not yet been firmed by reference documents. Quality system certification does not give any opinion on the quality of the product or service in view of the specific technical demands.

The ISO/IEC-25 guide (and the derived European Norm EN45001) differs from ISO 9000 by its emphasis on the demonstration of technical competence of personnel for the given jobs, ethical aspects, participation in laboratory intercomparisons and detailed descriptions of test and calibration methods. More detailed demands are made for the management of equipment and materials, the use of reference materials and reporting. Additionally the audit of the quality system is carried out by a team including one or more experts with technical knowledge of the methods to be accredited: a peer review.

A laboratory with an ISO 9000 certification therefore does not comply with the demands and interpretations of ISO/IEC-25; but, as stated in the ISO/IEC-25: 'Laboratories meeting the requirements of this guide comply, for calibration and testing activities, with the relevant requirements of the ISO 9000 series of standards, including those of the model described in ISO 9002, when they are acting as suppliers producing calibration and test results'.

When internal quality assurance in a laboratory is needed as a tool of management and when there is no formal reporting to a third party (*i.e.*, outside the laboratory), the ISO 9000 series may suit to implement a quality system to be certified. Still, such a laboratory may prefer the benefits of an independent audit of the technical competence of personnel and a peer review; however, when the laboratory issues certificates or reports, for instance on product specifications, material compositions or environmental analysis, the laboratory has to demonstrate that it is competent in performing its task. This can be accomplished by laboratory accreditation of the quality system complying with ISO/IEC-25. Such an accreditation also has distinct advantages in view of product liability, third party risks and related insurance premiums; and, in Europe because of European Union (formerly European Community) regulations.

Laboratory Accreditation: a Case History

Laboratory accreditation, rather than quality system certification, has been pursued by Interfaculty Reactor Institute's Laboratory for instrumental neutron activation analysis (INAA) for two reasons (in addition to the earlier mentioned considerations on the need for total quality management). Firstly, it is widely acknowledged that INAA may have a long-lasting position as one of the techniques of preference in the realization and particularly in the certification of reference materials. Traceability of INAA results may contribute to a further enhancement of the quality of certification processes. Peer review in the annual audit by the accreditation body, the demonstration of technical competence, the regular participation and evaluation of laboratory intercomparisons altogether ensure the certification organizing institution on the capability and quality of the participating laboratory. Secondly, in many research reactor institutions there is a tendency to use the INAA facilities for commercial services, either for economic reasons or to demonstrate the position of the institute in the technical and social community. As such, the INAA laboratory has to compete with other service laboratories on a commercial or industrial basis employing alternative techniques. To maintain and to improve the position of the INAA laboratory in this competition, accreditation may play an important and possibly vital role in the acquisition of contracts.

The quality system of the laboratory for INAA has been developed over a three year period. The path towards accreditation by the introduction of quality management at the laboratory has been published elsewhere.[2] On February 26, 1993 the laboratory was accredited by STERLAB, The Dutch Accreditation Board for Calibration Laboratories, Test Laboratories and Inspection Bodies (Fig. 1). This organization has declared that our laboratory procedures for INAA comply with the accreditation criteria for laboratories as described in STERLAB Criteria. These criteria contain all of the criteria from EN45001 (closely following the ISO/IEC guide 25) and the relevant criteria from ISO 9001 and ISO 9002. The accreditation covers the quality systems of the laboratory as well as the specified INAA activities.

The accreditation has made the laboratory for INAA the first accredited university laboratory in The Netherlands and probably the only accredited laboratory for INAA in the world. This accreditation demonstrates the viability of quality management in a university environment. In this paper an outline is given of the laboratories' experiences with the quality lifestyle, and also describes the unexpected spin-offs to the scientific research programme.

Practical Experience With Total Quality Management

A quality system cannot be purchased nor can it be tailor-made by a single person in the organization. It has to grow, and be created by the persons directly involved in the work-process as they need to have consensus on their future lifestyle of work and on the interpretation of the demands to be fulfilled. But realization of a quality system can only succeed when the directors of the organization proclaim it as one of their aims: it must have top-down support for any chance of successful bottom-up management. The most difficult stage (irrespective of the type of organization) is the period of developing awareness on quality management. It is difficult to speed-up the psychology of the workers in order to change their attitude; too much pressure on them may lead to a negative attitude against quality practice because only the top-down movement is then being recognized. It took about 1.5 years for employees in our laboratory to understand and accept the need for, and the philosophy of quality managment and laboratory accreditation both emotionally and rationally.

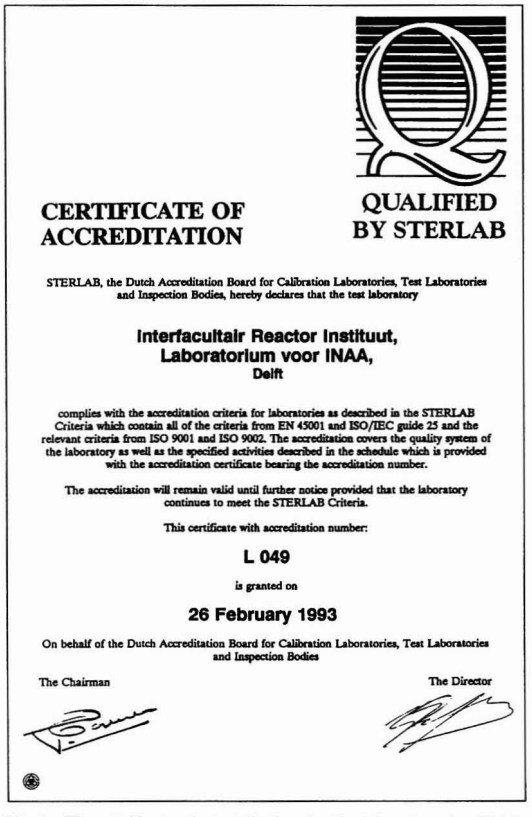

CERTIFICATE OF ACCREDITATION

QUALIFIED BY STERLAB

STERLAB, the Dutch Accreditation Board for Calibration Laboratories, Test Laboratories and Inspection Bodies, hereby declares that the test laboratory

Interfacultair Reactor Instituut, Laboratorium voor INAA, Delft

complies with the accreditation criteria for laboratories as described in the STERLAB Criteria which contain all of the criteria from EN 45001 and ISO/IEC guide 25 and the relevant criteria from ISO 9001 and ISO 9002. The accreditation covers the quality system of the laboratory as well as the specified activities described in the schedule which is provided with the accreditation certificate bearing the accreditation number.

The accreditation will remain valid until further notice provided that the laboratory continues to meet the STERLAB Criteria.

This certificate with accreditation number:

L 049

is granted on

26 February 1993

On behalf of the Dutch Accreditation Board for Calibration Laboratories, Test Laboratories and Inspection Bodies

The Chairman The Director

Fig. 1 The certificate of accreditation for the laboratory for INAA. The accreditation covers the quality system of the Laboratory as well as the specified Instrumental Neutron Activation Analysis (INAA) activities. The accreditation has made the laboratory for INAA the first accredited university laboratory in The Netherlands and probably the only accredited laboratory for INAA in the world.

Administration and Forms

In this process of developing awareness on quality management the difficulty was not so much agreement for the need to improve the organization but the consequences. Quality management requires, as an example, administrative management of equipment, laboratory tools including recordings of all settings, and also recording the reasons to change a setting. Manuals, electronic schemes, mechanical drawings are all systematically stored. Schemes and drawings of new tools are drawn 'as-built' implying that upon their completion, testing and first use the design schemes, *etc.* eventually have to be adapted.

Care for documentation also implies care for an adequate and demonstrable system of providing information to all employees. Minutes are preserved of group meetings and other institutes, and relevant information is distributed and the visa are also preserved.

The first form introduced is the most difficult to accept; once its usefulness has been recognized, many more easily follow. The most obvious ones to introduce at first were weighing forms, sample registration, calibrations and user lists. Later on came, *e.g.*, an extensive form to file training and qualification of personnel, user lists for reference materials and calibration chemicals and a form by which customers give their authorization before faxing them the analysis' report.

The introduction of forms has also been a good starting point for the introduction of stock control of consumables. A simple system was necessary to ensure that new forms, eventually with updated lay-outs, would be made in time before the existing ones ran out. Later on stock controls were introduced for tissues, pipette tips, weighing vials, *etc.*

Filling in forms is no longer considered to be some sort of enhanced bureaucracy. On several occasions, with thanks to the extensive documentation, *e.g.*, conditions under which a given analysis had been performed could be traced back, equipment settings could be reproduced to repeat a certain measurement, or correlations between several documented parameters could be used to locate a, until then unknown, contribution to inaccuracy or imprecision. Employees have regularly suggested further improvement of the forms and lists, not only for lay-out but also for amount and type of information to be recorded.

It is preferred at the laboratory to use hard-copy forms rather than forms on personal computers (PC) in a Laboratory Information Management System (LIMS). This is, partly, for 'psychological' reasons: by having the employees filling in the form by hand a little more awareness is introduced, it has to be done carefully in good handwriting and the employee has to put his name on the form. It also helps to enhance a 'feeling' for data. The use of hard-copy forms is also considerably easier in practice: a form just has to be taken from a shelf rather than having to find an available PC, start it, enter a program, file the data and ensure regular back-up and close it again.

Technical Competence of Personnel

Accreditation according to EN45001 (and thus in accordance with ISO/IEC 25) requires demonstration of technical competence of personnel. For each operation in INAA requiring some form of tutoring, supervisors have been named who have the authority to train newcomers to this specific operation, to

test their understanding of the training and to give them formal permission to perform the operation on their own. This process of training, testing of knowledge and giving permission is recorded on a person-related form; and the new permission is added to the list of qualified users present where the operation takes place, *e.g.*, with the balance, in the counting room, *etc.* This formal regulation met with less opposition because it was used to prevent unqualified persons from carrying out measurements without precise knowledge on how to handle the balance, or knowing how to calibrate a pipette, *etc.* Thus the new system means that for each distinguishable part of it, the analysis has been performed by technically competent employees.

Job descriptions are being written centrally by the university. Training programmes with details on the type of courses to be followed have been set up for every employee. A system has been set up for regular re-qualification of personnel even for given routine operations. This helps to assess that given and initial skills do not fade away when these operations haven't been performed for some time.

Appraisals on job fulfilment are held once a year and in between these evaluations employees have a less formal discussion in which agreements are made with the head of the laboratory on work priorities, where to improve on job fulfilment, social aspects of work, *etc.* Deputies have been assigned on the basis of tested technical capabilities for every employee who holds the power for a vital part of the work process such as management of laboratory tools or equipment, computer systems, authorization of the release of results, purchasing goods, liquid nitrogen filling, *etc.*

Chemical Compounds for Calibration and Reference Materials

Chemical compounds of high quality with respect to purity, stoichiometry and stability are used in the never-ending process of (re)determination of calibration parameters. Before introduction of the quality system, the laboratory had a stock of chemicals, collected over a 25 year period and some of the chemicals had even longer histories. Bearing in mind their impact on the final quality of the analytical result, it was questionable to what extent any certainty existed on the date of purchase, manufacturer, any certification on chemical purity or stoichiometry, hydrate water, their storage, their use or any tampering in the past. Sometimes labels were absent or incomplete to answer some of these questions. As a result, nearly all chemicals were disposed of, and a new collection for calibration purposes is being built-up. All calibration chemicals are now administrated and coded, recording not only their origin but also their use, date and name of the user. They are stored according to the guidelines given either by the supplier or by, *e.g.*, The Merck Index.[3] The chemicals are kept in a locked cabinet with admission for a few authorized users to prevent any accidental misusage, contamination or access to moisture. The same considerations were also applicable to the (certified) reference materials. These valuable materials are being brought into an extensive administration, they are also stored in a locked cabinet and only authorized users receive a personal key to that cabinet after a thorough instruction and test thereof on the use of these materials.

Non-conformance, Complaint Management and Corrective Actions

A characteristic feature of quality management is that it is considered an accepted fact that mistakes take place and never can be avoided. As a result, even the most bizarre mistake will be made sooner or later. However, by being aware of quality practice the probability of such a mistake being made will be reduced. Mistakes, and even blunders, once they have happened are welcomed as a tool for further improvement for the organization. Perhaps the documents were not understandable enough for everyone, perhaps oral instructions would have been better, perhaps...?! As a result, employees feel free to inform staff and colleagues of their mistakes which contributes to understanding and as such makes repetition less likely.

The ISO norm demands corrective actions in such non-conformance situations. These have been classified as deviations from expected situations, complaints from employees and customers, and ideas for improvement of the organization. For each type of non-conformance a form has to be completed, and corrective action being undertaken within a 2 week period, preferably as soon as possible.

However, a successful system for responding to non-conformance and complaint management requires more than administrative action and forms. Staff and employees have to learn that they must alter their own emotional reactions in such situations. Everyone must learn, with dogged perseverance, that a quality system will not improve by assignation of blame but by taking away the cause of the non-conformance. Attention must also be given to appropriate management of telephone suggestions and, eventually, complaints by customers.

This formal treatment of non-conformance and especially the rapid response *via* corrective action is considered to be a great success by all employees. It is one of the directly perceptible manifestations of the quality management with a more-or-less measurable benefit.

Laboratory Intercomparison

Regular participation in laboratory intercomparisons is mandatory for a quality system to be accredited. The results of such intercomparisons are used to trace systematic errors in the analysis routine (such as analyst dependent bias) to test organizational routines (often results have to be reported in formats deviating from the routine) and to compare the technical performance. These regular intercomparisons have economic consequences because the costs have to be paid by the laboratory itself. To ensure an effective tool for controlling the quality system for a fair price, some selection criteria have been set on the basis of which type of participation is considered: (*i*) the material to be analysed, the elements to be reported and their presumed concentration levels, all in view of the technical possibilities of state-of-the-art INAA; (*ii*) the quality of the material to be analysed in terms of homogeneity and stability. Previous experiences with, and the reputation of the issuing organization may play a role in this; (*iii*) the deadline set for reporting in view of the available capacity of personnel and facilities; (*iv*) the availability of the overall result of the intercomparison; and (*v*) insight into the handling of reported data and applied statistics. For instance, whether reported levels of imprecision are weighted in the data intercomparison and whether the method of analysis is described.

The laboratory for INAA participates bimonthly in the samples issued in the framework of the International Plant Analytical Exchange Programme and the International Soil Analytical Exchange Programme.[4] The laboratory offers its capacity for participation in intercomparisons organized by NIST, BCR, IAEA and others.

It should be stressed that samples are analysed under routine conditions with no extreme precautions whatsoever. Samples are handled as any other sample taking into account the directions for use. Results of intercomparisons, therefore, give insight into the state-of-the-practice of the technique when compared to other techniques rather than the state-of-the-art. State-of-the-art results under all extreme precautions

are required when analyses are being performed in the framework of certification of reference materials.

The results from these intercomparisons have always been satisfactory with respect to analytical quality. This does not come as a surprise because the extensive internal quality control implies the use of reference materials and well defined criteria for the release of analysis results (see below). However, in one particular case for a few elements the results were alarmingly deviant from the consensus value. Tracing back the particular analysis revealed that mistakes had been made in copying (by hand) the correct data in the official laboratory's report into the table provided by the issuing agency. Although, in retrospect, it is obvious that such transcripts had to be checked individually, it had not been done. Of course the procedure has now been altered; the administrative management of the laboratory now knows that authorizations should be present on each page of the tables before submitting them.

Quality System Management and Audits

The quality system and the underlying documents in the manual are both in a continuous state of improvement and growth. Suggestions for small changes in procedures and instructions for a better performance have to be processed, or new equipment and/or facilities have to be described. From the interpretation of the EN45001 guide and from the experience with regular audits of accredited quality systems, STERLAB (the accreditation board) may add new demands to which a quality system has to comply, or may change 'suggestions' for a quality system into 'demands' for a quality system. Management of the quality system belongs to the tasks of one of the laboratory's technical assistants. This quality coordinator has followed a dedicated practical training, organized by STERLAB on the interpretation and practical translation of EN45001. In practice, all associated work with the management of the quality system takes about 0.3 man-years.

Criteria for total quality management prescribe a system for an independent assessment of the performance of the laboratory in view of its quality system. The laboratory for INAA deals with three types of internal assessment: (*i*) the laboratory's quality coordinator checks bimonthly the extent to which the employees themselves conform to procedures and instructions. These checks may reveal the need for changes or more clarity in the written text; or that the forms need an update, *etc*. The report on these checks is submitted to the head of the laboratory and to the institute's quality manager; (*ii*) the institute's quality manager organizes, at least twice a year, an internal audit of all aspects of the laboratory. Being an outsider with respect to the conduct of analysis, but acquainted with the situation in the institute as such, he reports to the scientific director of IRI his findings on how the laboratory complies with its quality system as described in the quality manual; (*iii*) STERLAB, the Dutch Accreditation Board for Calibration Laboratories, Test Laboratories and Inspection Bodies, annually audits the laboratory for INAA. In this two day audit, STERLAB investigates to what extent the performance of the laboratory complies with the criteria given by EN45001 on the basis of which the accreditation has been given. This audit includes peer review by a scientist who is aware of the scientific aspects, and the technical state-of-the-art of INAA.

The findings of this annual audit are decisive for the continuation of the accreditation.

The experience with these audits is one of constructive criticism, aimed at the further improvement of the organization and the quality system rather than ventilating negative critique. As the members of STERLAB's audit team interview several employees of the laboratory themselves (staff, technicians, analysts, administrative support) the more enthusiastic and constructive the employees are themselves, the better the general impression of how the quality system is being implemented.

Unexpected Improvements as a Result of Total Quality Management

The introduction of total quality management was not primarily activated by a need for better analytical results but by, amongst others, a need for better organization of work. Comparing the performance of the laboratory in all its aspects as it is now with that in 1989 when the decision was taken, several improvements can be mentioned as side effects of the development of the quality system.

Analytical Quality

Over the several years of becoming aware of quality practice one develops an inevident but remarkably strong criticism of the criteria to be fulfilled during the analysis of the raw data; and on the criteria to be fulfilled upon release of the analysis report.

The development of the quality system accidentally but fortunately, coincided with the introduction of a new approach for computerizing the INAA facilities[5] and the development of new software for gamma-ray spectrum analysis and interpretation.[6] Particularly at the users-interface, many demands set with respect to quality assurance could be designed-in, and the interactively operating programs were thus designed such that mistakes at vital places, made by the users, could be accounted for. The history of the sample with respect to irradiation and measurement is automatically updated. Raw data can not be tampered with or deleted.

In each batch of samples to be analysed, a sample of a (certified) reference material or a control sample is included together with a blank and an adequate number of neutron flux monitors. The spectrum analysis software facilitates statistical treatment of the data of these controls and flux monitors in Shewhart control charts.

After the report has been printed, the analyst himself performs a 'first-line' control by the primary monitoring procedure in which all printed data is checked according to given criteria. Only when all checks are 'OK', is the report handed over for 'release control' by the staff of the Laboratory. Only when the staff have authorized the report, are the administrators allowed to mail the report. Actually, all contracts state that the Laboratory only takes responsibility for the quality of the results when the results have been authorized.

Results of analyses of reference materials (see Fig. 2) indicate that for routine analyses the differences between measured and certified concentrations (taking into account all uncertainties; measured peak areas, neutron flux, constants in the nuclear catalogue, uncertainty in the certified concentration) are not significant at the 95% confidence level. This is adequate for almost all requests for analysis, from samples related to applied scientific research to commercial services.

Additional Spin-offs

There have been some developments in the research programme of the laboratory for INAA in the past few years which have been initiated partly by the process of implementing total quality management.

(*i*) Insight in sources of error and sources of variation

Improvement of reliability of methods and procedures
Improvement of assurance of the various steps

(*ii*) Less repetition of analysis
Traceability of equipment settings
Certainty on calibrations
Certainty on quality of chemical compounds
No data 'forgotten' to be recorded

(*iii*) Improvement of atmosphere under which work is planned and carried out

(*iv*) Improvement of business position for commercial activities

It was mentioned above that the criteria to be fulfilled for the analysis of raw data were considered with more criticism; and equally so for the criteria to be fulfilled upon release of the analysis report. The changing attitude and style of working of the users led to less easier satisfaction with results which in their opinion 'wriggled'. It all coincided with the development of a new method for element assignment on the basis of observed gamma-ray lines, implementation of corrections for hitherto 'neglectable' effects[7,8] and better insight into, and a means for quickly assessing sources of variation in INAA.[9] Also shortcomings in tabulations of nuclear reaction parameters and decay schemes have been observed.

During the development of the quality system, the analytical process had to be unravelled up to the very last detail. After its evaluation, the process of INAA was 'built-up' again, with a systematic approach of assuring the various details which might affect the overall quality of the results and/or the work. It has led to a better understanding of the analytical aspects of INAA, improved methods and procedures and an increase in the reliability, quality and quantity of the analysis results and the work on it as such. It appears to be true that accreditation, and its maintenance, works as a generator of knowledge.

Therefore, perhaps most of the spin-offs from the application of total quality management to our scientific research (see earlier) are no longer recognized by the employees of the laboratory because their new style of working leading to these benefits is now taken for granted. As such they no longer observe directly that the organized way of training and qualification, the more careful working, the care for correct preconditions altogether has led to a far more reliable way of carrying out analyses; and thus, that far less analyses go wrong and have to repeated.

Additionally, there is less loss of time in tracing back equipment settings, manuals or schemes; certainty about the purity of chemicals, about calibration of all sort of tools, less annoyance because parameters have been forgotten because they were not recorded and so on. All of these factors contribute to a better and more constructive atmosphere; indispensable for project management of research plans.

The laboratory for INAA also has commercial activities which are not limited to customers in The Netherlands; marketing is also extended to other countries.

The fact that the laboratory is accredited is being used in the marketing activities, not only to profile the laboratory in relation to others, but also such that the customer sees the accreditation as a confirmation of reliability and value for money. Customers from other EU member states benefit from the accreditation because of the implicit international acceptance of the results.

Accreditation enables other accredited laboratories to contract-out part of their analyses for which it is obvious that INAA should be the method of choice.

Finally, the impression of the laboratory and its attitude to quality is enhanced by well cared for offices and laboratories. Working places and desks are cleaned after finishing a job, unfinished work on reports is stored in drawers out of sight rather than on desks or shelves. The only directions for use allowed to be present with equipment or facilities are the official ones and as such recognizable documents of the quality manual. All small, *e.g.*, hand-written guides, notes, remarks, *etc.* have been removed. Additionally, regularly small investments are made to improve on the comfort of the employees at their workstation: plants, better chairs, anti-reflecting screens on monitors, *etc.*

Outlook for the Future

The main change in attitude with respect to organization of work has been the acceptance of the necessity of (*i*) firstly, clearly defining the plan for work: *e.g.*, the purpose of the analysis, which elements have to be determined and under what conditions (accuracy, sensitivity, selected irradiation and counting facilities); (*ii*) then, working precisely according to what has been decided and agreed upon; (*iii*) the two stages above being accompanied by thorough documentation.

After getting used to this procedure, it is not such a big step to also see the benefits of quality practice for research plans. The simple fact that scientists often cannot reproduce their own experiments because of bad planning, careless preparation and/or absence of proper documentation, should be enough to convince everyone to start working even today on the introduction of quality practice...

The commonly heard argument against this invitation is always of the type: '...formal working according to quality practice and rigid documentation conflicts with the innovative and creative nature of the scientist...'. This appears to be quite understandable but nevertheless not justifiable: academic freedom does not imply the right to non-commitment. Perhaps only after having directly experienced total quality management in practice, may one understand and accept that quality management does not interfere with innovation and

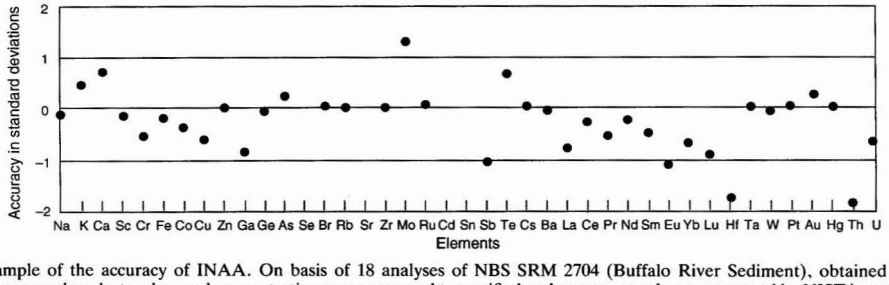

Fig. 2 Example of the accuracy of INAA. On basis of 18 analyses of NBS SRM 2704 (Buffalo River Sediment), obtained under routine conditions by several analysts, observed concentrations are compared to certified and consensus values as reported by NIST in terms of standard deviations ($n = 18$).

creativity. Of course, scientific research is always subject to unexpected situations, and it may be important to follow deviations from the projected pathway. Quality practice only demands a record of the reason for such a change, and to record that the deviation is authorized by the person formally responsible for the research plan. A new (of course, well-documented) plan is needed on what the change of pathway implies, what should be examined next, what should be measured or recorded. Not much more is required for good quality practice. Upon completion of the experiment it makes the entire research program traceable, all decisions are clear and all key elements should have been recorded.

Concluding Remarks

Universities and research institutes have to face the fact that the teaching and education of total quality management is no longer a matter of choice. Society has already made this choice and in many industries, laboratories and utilities, quality systems according to ISO 9000 or ISO/IEC-25 exist or are being prepared. It is even questionable whether these quality systems will withstand the consequences of one of the Japanese conceptions of quality management, KAIZEN; in short characterized by '... each employee should not let a day pass without having realized an improvement in quality anywhere in the company...'.

References

1 Nadkarni, R. A., *Anal. Chem.*, 1993, **65**, 387A.
2 Bode, P., and Van Dalen, J. P. J., *J. Radioanal. Nucl. Chem.*, 1994 **179**, 141.
3 *The Merck Index*, ed. Budavari, S., 11th edn. Merck, 1989, Rahway NJ, USA.
4 Organizer: Wageningen Agricultural University, Dept. of Soil Science and Plant Nutrition, P.O. Box 8005, 6700 EC Wageningen, The Netherlands.
5 Blaauw, M., and Lindstrom R. M., *J. Radioanal. Nucl. Chem.*, 1993, **169**, 443.
6 Blaauw, M., PhD Thesis, Delft University of Technology, 1993.
7 Blaauw, M., *Nucl. Instr. Methods*, 1993, **A332**, 493.
8 Blaauw, M., and Bode, P., *J. Radioanal. Nucl. Chem.*, 1993, **169**, 201.
9 Blaauw, M., Ammerlaan, M. J. J., and Bode, P., *Int. J. Appl. Rad. Isot.*, 1993, **44**, 547.

Paper 4/06132B
Received October 10, 1994
Accepted October 19, 1944

Instrumentation and Analytical Technique for the Analysis of Regional Geochemical Samples Used at the South African Council for Geoscience*

An Overview

J. H. Elsenbroek

Council for Geoscience, Private Bag X112, Pretoria 0001, South Africa

Regional geochemical stream sediment samples are analysed on a 26 fixed and 2 scanner channel simultaneous X-ray fluorescence spectrometer at the South African Council for Geoscience. Twenty-four elements are analysed simultaneously per sample: Sc, Ti, V, Cr, Mn, Fe, Co, Ni, Cu, Zn, As, Rb, Sr, Y, Zr, Nb, Mo, Sn, Sb, Ba, W, Pb, Th and U. Rapid quantitative analyses and a high daily sample throughput of 400 samples in a 20 h shift are obtained. The calibration of the instrument involves background determinations, inter-element interference and matrix corrections in order to obtain a good correlation between the X-ray net peak intensity (in kcounts s^{-1}) and the international reference material concentration value (in % or ppm). A wide range of international geological rock and soil reference materials are used for the calibration. Excellent geochemical data are obtained with respect to precision accuracy and determination limits. Precision of the data is of concern because decisions made in exploration geochemistry involve the interpretation of the relative difference in element concentrations and these may be masked by excessive noise. Systematic changes in the analytical system are of concern as they present a source of false geochemical patterns. Of the 24 chemical elements calibrated on the X-ray fluorescence spectrometer, 20 have determination limits significantly below that of the crustal abundance. This facilitates the demarcation of background geochemical trends. An example illustrating how the stream sediment geochemical data of the element Rb reflects the underlying host rocks on a regional scale is presented.

Keywords: *Simultaneous X-ray fluorescence spectrometry; regional geochemistry; trace element analysis; international reference material*

Introduction

The Council for Geoscience of South Africa has coordinated a regional geochemical stream sampling programme since 1973, which will eventually cover the entire 1.2×10^6 km^2 of the country. The prime objective of this programme is to locate mineralized bodies or provinces that may be of economic importance,[1] and to create a geochemical infrastructure. At present, the only analytical technique used for a variety of elements is X-ray fluorescence spectrometry.

Sampling and Sample Preparation

Samples are collected at a density of 1 km^2, which is amongst the highest sampling density in the world (Plant *et al.*[2,3]). Where possible, samples of approximately 5 kg are collected from first-order streams and ideally in such a way that the stream at the sampling point has drained an area of 1 km^2 (Labuschagne *et al.*[1]). When no first-order streams are available, a soil sample is taken. Prior to 1979, all sampling was carried out using foot traversing but this method proved to be tedious, time-consuming and unreliable. Helicopter supported transport was introduced in 1979, which speeded up the operation considerably.[1] Approximately 12 000 to 15 000 samples are taken annually. Samples are dried at ±75 °C and then sieved to the <75 μm fraction. A few drops of poly(vinyl alcohol) (PVA) is mixed with 20–25 g of the sieved powder sample and placed in an aluminium cup, from which a pellet is pressed at 30 tons in^{-2}. These pellets are then analysed for 24 elements using a simultaneous wavelength-dispersive X-ray fluorescence spectrometer (SWDXRF). The original sample and the remaining <75 μm fraction is stored for possible future use.

Experimental

Instrumentation

Analysis is performed on a Philips PW1606 SWDXRF with 28 channels. Of these 28 channels, 24 are used for element concentration determinations, while three channels are used for background determinations and one for measuring the RhKβ Compton peak for mass absorption coefficient determinations. A 3 kW Rh-target end-window tube is used which is operated at 60 kV and 40 mA. An Ag mask (shielding plate) is installed to eliminate spurious radiation. The elements, spectral lines, crystals, detectors, 2θ angles and counting times used are summarized in Table 1.

Procedures

The SWDXRF was calibrated by using the following steps: (*i*) pure chemcial standards were used for background determinations; (*ii*) interference standards were used for determining interference correction factors; and (*iii*) international reference materials, listed in Table 2 were used for the calibration of the net peak intensity (kcounts s^{-1}) to concentration (% or ppm).

Correction procedures

Although the SWDXRF is a very stable instrument, it is subject to a definite, though minimal, degree of drift. Compensation for this drift is made on the basis of corrections

* Presented at Geoanalysis 94: An International Symposium on the Analysis of Geological and Environmental Materials, Ambleside, England, September 18–22, 1994.

Table 1 Instrumental settings on the SWDXRF

Element	Line	Crystal	Detector	Count time/s	Angle 2θ
Sc	Kα	LiF200	Krypton, sealed	100	97.70
Ti	Kα	LiF200	Krypton, sealed	100	86.14
V	Kα	LiF200	Krypton, sealed	100	76.94
Cr	Kα	LiF200	Krypton, sealed	100	69.36
Mn	Kα	LiF200	Krypton, sealed	100	62.98
Fe	Kα	LiF200	Krypton, sealed	100	57.52
Co	Kα	LiF200	Krypton, sealed	100	52.80
Ni	Kα	LiF200	Krypton, sealed	100	48.66
Cu	Kα	LiF200	Krypton, sealed	100	45.03
Zn	Kα	LiF200	Xenon, sealed	100	41.80
As	Kβ1	LiF200	Xenon, sealed	100	30.44
Rb	Kα	LiF200	Xenon, sealed	100	26.62
Sr	Kα	LiF200	Xenon, sealed	100	25.16
Y	Kα	LiF200	Xenon, sealed	100	23.80
Zr	Kα	LiF200	Scintillation	100	22.56
Nb	Kα	LiF200	Scintillation	100	21.40
Mo	Kα	LiF200	Scintillation	100	20.33
Sn	Kα	LiF200	Scintillation	100	14.04
Sb	Kα	LiF220	Scintillation	100	19.07
Ba	Lα	LiF200	Krypton, sealed	100	87.18
W	Lα	LiF200	Xenon, sealed	100	43.02
Pb	Lβ	LiF200	Xenon, sealed	100	28.24
Th	Lα1	LiF200	Xenon, sealed	100	27.48
U	Lα1	LiF200	Xenon, sealed	100	26.14
Bg1	—	LiF200	Xenon, sealed	100	39.50
Bg2	—	LiF200	Xenon, sealed	100	33.20
Bg3	—	LiF200	Scintillation	100	15.00
Rh Comp	—	LiF200	Scintillation	100	16.365

to quantitative measurements using an internal monitor. The in-house internal monitor was prepared as a lithium tetraborate glass disc containing detectable concentrations of the analysed elements. Measurements of this internal monitor were carried out prior to the measurements of calibration reference materials and corrections for drift were applied to the calibration reference materials. Internal monitor sample measurements made during the analysis of geochemical stream sediment samples are compared with the original results. Any drift can thus be quantified and the calibration of the instrument can be maintained relative to its initial conditions. The internal monitor standard is measured regularly (approximately every 10th sample), and the appropriate corrections are made.

Background calibration graphs were set up by using blank samples where backgrounds below the spectral peaks related to a nearby interference-free background.[4] Using this relationship, the backgrounds below the spectral peaks in both reference material and unknowns were determined and the net spectral peak intensities were calculated. With the exception of the elements Ti, V and Fe, background determinations were made by using the three interference-free background channels. Fig. 1 shows the example of the background determination of the element Rb, where the Rb intensity (in kcounts s^{-1}) is plotted against the background intensity Bg2 (kcounts s^{-1}).

Interference standards of Hoechst Wax with 0.2% of the pure element were used to determine the degree of spectral line overlap and for the calculation of spectral line overlap correction factors, as described by Nisbet *et al.*[5]

Table 2 International reference materials used for instrument calibration

No.	Reference material	Origin*	Description	No.	Reference material	Origin	Description†
1	AGV-1	USGS	Andesite	31	GSD-1	IGGE	Str Sed
2	BCR-1	USGS	Basalt	32	GSD-2	IGGE	Str Sed
3	G-2	USGS	Granite	33	GSD-3	IGGE	Str Sed
4	GSP-1	USGS	Granodiorite	34	GSD-4	IGGE	Str Sed
5	PCC-1	USGS	Peridotite	35	GSD-5	IGGE	Str Sed
6	BHVO-1	USGS	Basalt	36	GSD-6	IGGE	Str Sed
7	MAG-1	USGS	Marine mud	37	GSD-7	IGGE	Str Sed
8	QLO-1	USGS	Quartz latite	38	GSD-8	IGGE	Str Sed
9	SCo-1	USGS	Cody shale	39	GSD-9	IGGE	Sed
10	SDC-1	USGS	Mica schist	40	GSD-10	IGGE	Sed
11	STM-1	USGS	Syenite	41	GSD-11	IGGE	Sed
12	BIR-1	USGS	Basalt	42	GSD-12	IGGE	Sed
13	DNC-1	USGS	Diabase	43	GSR-1	IGGE	Granite
14	W-2	USGS	Diabase	44	GSR-2	IGGE	Andesit
15	SY-2	Canmet	Syenite	45	GSR-3	IGGE	Basalt
16	SY-3	Canmet	Syenite	46	GSR-4	IGGE	Sandstone
17	MRG-1	Canmet	Gabbro	47	GSR-5	IGGE	Shale
18	GR	CRPG	Granite	48	GSR-6	IGGE	Limestone
19	GA	CRPG	Granite	49	GSS-1	IGGE	Soil
20	GS-N	ANRT	Glass	50	GSS-2	IGGE	Soil
21	FK-N	ANRT	Granite	51	GSS-3	IGGE	Soil
22	MW-1	IGEM	Miaskite	52	GSS-4	IGGE	Soil
23	JB-1	GSJ	Basalt	53	GSS-5	IGGE	Soil
24	NIM-D	MINTEK	Dunite	54	GSS-6	IGGE	Soil
25	NIM-G	MINTEK	Granite	55	GSS-7	IGGE	Soil
26	NIM-L	MINTEK	Lujavrite	56	GSS-8	IGGE	Soil
27	NIM-N	MINTEK	Norite	57	Fer-2	Canmet	Fe formation
28	NIM-P	MINTEK	Pyroxenite	58	Fer-3	Canmet	Fe formation
29	NIM-S	MINTEK	Syenite	59	Fer-3	Canmet	Fe formation
30	Fer-1	Canmet	Fe formation	60			

* USGS, United States Geological Survey; CCRMP, Canadian Certified Reference Materials Project; Canmet, Canada Centre for Mineral and Energy Technology; CRPG, Centre de Recherches Petrographiques et Geochimiques; ANRT, Association Nationale de la Recherche Technique, Paris; IGEM, Institute of Geology of Ore deposits, Petrology, Mineralogy and Geochemistry, Moscow; MINTEK, Council for Mineral Technology, South Africa; IGGE, Institute of Geophysical and Geochemical Prospecting, People's Republic of China; and GSJ, Geological Survey of Japan.

† Str Sed, stream sediment; Sed, sediment.

Matrix correction was carried out by using mass absorption coefficients to correct for absorption effects. The mass absorption coefficients were calculated from known international reference material major element compositions[6] using the following formula:

$$\mu_\lambda = \Sigma_i c_i \mu_i$$

where μ_λ is the mass absorption coefficient at wavelength λ; i the individual elements; c_i the mass fraction of element i; and μ_i the mass absorption coefficient of element i.

The values for μ_i were obtained from the tables of Heinrich.[7] The linear dependence of 1/RhKβ Compton intensity on the mass absorption coefficient of the CuKα wavelength (μ_{Cu}) for the international reference material was found by regressing the calculated μ_{Cu} on the measured 1/RhKβ Compton[8] as shown in Fig. 2. The regression equation was used to estimate μ_{Cu} for the unknowns. The μ_{Cu} value was multiplied by the geometric factor and the net peak intensities of all the elements on the short wavelength side of the FeKα absorption edge. For the elements Co, Fe, Mn, Cr, V, Ti and Sc the mass absorption coefficients of the CrKα wavelength (μ_{Cr}) were determined by using the FeKα net peak intensity in the following linear equation of the form $y = mx + c$

$$\frac{\mu_{Cu}}{\mu_{Cr}} = mI_{Fe} + c$$

where $y = \mu_{Cu}/\mu_{Cr}$; x is I_{Fe} (kcounts s^{-1}); m is the slope; and c is the intercept.

For all the 24 chemical elements the calibrations are simple linear fits between the net peak intensity (in kcounts s^{-1}) and the concentration (in % or ppm). The net peak intensity is the result of the following corrections: internal monitor drift, background, interference and mass absorption. Fig. 3 shows an example of the calibration of the element Rb where the Rb concentration (in ppm) is plotted against the Rb net intensity (in kcounts s^{-1}). A wide variety of geochemical reference samples that cover most typical rock, soil and stream sediment compositions was used for the calibration (Table 2).

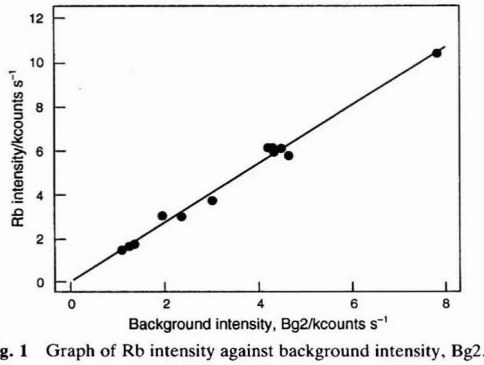

Fig. 1 Graph of Rb intensity against background intensity, Bg2.

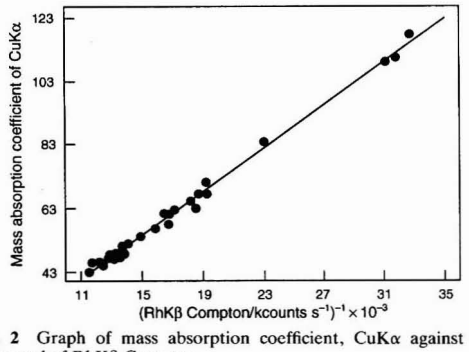

Fig. 2 Graph of mass absorption coefficient, CuKα against the reciprocal of RhKβ Compton.

Lower Limit of Detection and Determination Limit

The lower limit of detection is generally defined as that concentration equivalent to a certain number of standard deviations of the background count rate.[9] According to Jenkins[9] three major factors will affect the detection limit for a given element; (*i*) the sensitivity of the spectrometer for that element in terms of the counting rate per unit concentration of the analyte element; (*ii*) background (blank) counting rate; and (*iii*) the available time for counting peak and background photons.

The actual detection limit measurable also depends upon the characteristics of the specimen itself. Detection limits vary

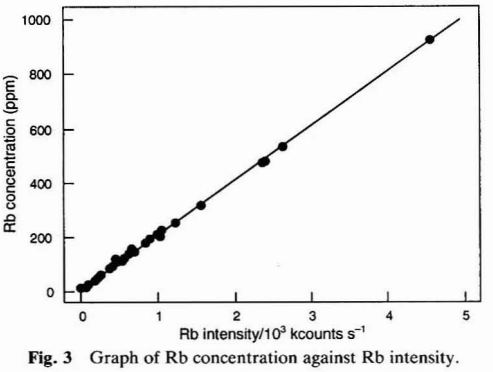

Fig. 3 Graph of Rb concentration against Rb intensity.

Table 3 Calibration concentration range of various elements and determination limits (DLs)

Element	Range (ppm)	DL (ppm)
Sc	1–55	1
TiO_2	0.20–3.77%	100
V	9–526	5
Cr	10–2900	4
MnO	0.01–0.32%	100
Fe_2O_3 (Total)	1.40–18.76%	100
Co	11–210	10
Ni	10–2380	10
Cu	19–1230	9
Zn	10–680	3
As	18–412	10
Rb	9–860	1
Sr	25–1100	1
Y	5–718	1
Zr	22–1210	1
Nb	10–960	5
Mo	1–92	0.2
Sn	3–370	2
Sb	10–2000	5
Ba	114–2400	10
W	24–490	4
Pb	11–636	4
Th	17–1000	4
U	9–650	2

not only with the atomic number of the measured element but also with the sample matrix. This is because both slope and background intensity are affected by changes in the matrix. In general, the background intensity increases with a decrease in average atomic number of the matrix. The slope decreases with an increase in the total absorption of the matrix for the measured wavelength.

According to Potts[10] lower limit of detection and determination limit are defined by the following equations. The lower limit of detection (LLD) is the smallest signal that can be qualitatively measured.

$$3s_p = 3\sqrt{2N_b} = \frac{3}{m}\sqrt{\frac{R_b}{T}}$$

The determination limit is the smallest signal that can be quantitatively measured.

$$6s_p = 6\sqrt{2N_b} = \frac{6}{m}\sqrt{\frac{R_b}{T}}$$

Where s_p is the standard deviation of the net analyte peak; N_b is the background counts; m, is the slope of the calibration graph; R_b is the background count rate under the peak; and T is total counting time on peak and background.

In this work the formula for calculating the determination limit (DL) was used (at 99% confidence). The 1σ counting error (CE) was calculated from the following equation:

$$1\sigma(\mathrm{CE}) = \frac{\sqrt{\frac{R_p + R_b}{T_p} + \frac{R_b}{T_b}}}{R_p} \times \text{concentration}$$

where R_p is the net peak in counts s^{-1}; R_b is the net background in counts s^{-1}; T_p is the peak counting time; and T_b is the background counting time.

The average determination limit (DL) of all 24 elements are summarized in Table 3, together with their calibration concentration ranges. The determination limit (DL) was calculated for calibration reference material together with the 1σ counting error for the calibration of the element Rb and is depicted in Table 4.

Table 4 Rubidium data for international reference materials

No.	Reference material	'True' value (ppm)	Observed value (ppm)	Absolute error (ppm)	Relative error (%)	DL (ppm)	Counting error
1	AGV-1	67	69	2	3	0.7	0.26
2	BCR-1	47	49	2	4	0.8	0.29
3	G-2	170	172	2	1	0.6	0.26
4	GSP-1	254	256	2	1	0.6	0.31
5	BHVO-1	11	12	1	9	1.6	0.53
6	MAG-1	149	135	−14	−9	0.6	0.27
7	QLO-1	74	74	0	0	0.6	0.24
8	SCO-1	112	111	−1	−1	0.6	0.25
9	SDC-1	127	124	−3	−2	0.6	0.27
10	STM-1	118	122	4	3	0.6	0.26
11	W-2	20	22	2	10	1.0	0.33
12	SY-2	217	213	−4	−2	0.7	0.32
13	SY-3	206	204	−2	−1	0.7	0.34
14	MRG-1	9	9	0	0	3.7	1.23
15	GA	175	173	−2	−1	0.6	0.26
16	GS-N	185	185	0	0	0.6	0.28
17	FK-N	860	859	−1	0	0.6	0.45
18	JB-1	41	43	2	5	0.8	0.28
19	NIM-G	320	324	4	1	0.5	0.30
20	NIM-S	530	534	4	1	0.6	0.39
1	GSD-1	116	121	5	4	0.6	0.27
2	GSD-2	470	489	19	4	0.5	0.34
3	GSD-3	79	76	−3	−4	0.6	0.25
4	GSD-4	130	127	−3	−2	0.6	0.26
5	GSD-5	118	101	−17	−14	0.7	0.27
6	GSD-6	107	108	1	1	0.6	0.25
7	GSD-7	147	104	−43	−29	0.8	0.30
8	GSD-8	132	135	3	2	0.5	0.23
9	GSD-9	80	82	2	3	0.6	0.24
10	GSD-11	408	327	−81	−20	0.8	0.37
11	GSD-12	270	234	−36	−13	0.7	0.32
12	GSS-1	140	131	−9	−6	0.6	0.26
13	GSS-2	88	89	1	1	0.6	0.23
14	GSS-3	85	89	4	5	0.6	0.22
15	GSS-4	75	63	−12	−16	0.7	0.26
16	GSS-6	237	177	−60	−25	0.8	0.32
17	GSS-7	16	16	0	0	1.2	0.40
18	GSS-8	96	98	2	2	0.6	0.25
19	GSR-1	466	483	17	4	0.5	0.35
20	GSR-2	38	42	4	11	0.7	0.24
21	GSR-3	37	42	5	14	0.8	0.30
22	GSR-4	29	30	1	3	0.6	0.23
23	GSR-5	205	212	7	3	0.6	0.29
24	GSR-6	32	35	3	9	0.8	0.28

Sources of Analytical Error in Quantitative X-ray Spectrometry

The major types of error in quantitative X-ray spectrometry are random and systematic errors. Random errors determine the precision of the result, whereas both systematic as well as random errors determine the accuracy of the result.

Random errors

According to Müller[11] precision or reproducibility of an analytical technique describes the magnitude of deviation that occurs after repeatedly measuring the same sample using the same technique. The major sources of random errors in an X-ray measurement are those due to the equipment and to the random nature of X-ray production.

The precision of the SWDXRF spectrometer was evaluated by a number of replicate analyses of the international reference material GSP-1, which were measured regularly over a period of three months. The elements, average concentration, standard deviation, minimum value, maximum value, range and precision are listed in Table 5. The statistical sample size is 75.

According to Fletcher *et al.*[12] exploration geochemists define analytical precision (PC), for concentration c, as the per cent. relative variation at the 95% (two standard deviations) confidence level:

$$PC(\%) = 200 \times s_c/c$$

where s_c is an estimate of the standard deviation at concentration c (the average concentration shown in Table 5). Fletcher *et al.*[12] considers the detection limit of an analytical technique to be reached when the 2σ standard deviation of repeated measurements approaches the concentration levels when precision becomes 100%. It thus follows that an acceptable precision can only be achieved at concentrations several times higher than the detection limit. This is the reason for the poor precision for the detection of Sc, Cr, Co and Mo in Table 5, as their concentrations are at or very close to the estimated lower limits of determination.

Systematic errors

According to Müller[11] accuracy includes reproducibility, and quantifies the deviation between the 'true' and the analytical value. Thus accuracy depends on both errors that arise from transformation of intensity measurements into concentrations, and from statistical scattering of the measurements.[11]

The most important source of systematic error is the sample. As X-ray fluorescence spectrometry is essentially a comparative technique, it is absolutely vital that calibration reference materials and specimens to be analysed are presented to the spectrometer in a reproducible and similar manner. The greatest difficulties are encountered in the analysis of powder specimens where local heterogeneity within particles tends to complicate specific absorption effects, the so-called particle size effects.[13]

The accuracy determined on the SWDXRF was evaluated by comparing the literature values (the so-called 'true' values) from Govindaraju[6] for the international reference material with the values calculated (the so-called 'observed' values) from the calibration graphs based on the assumption that the literature value is correct.

The element Rb will be used as an example. In Table 4 the reference material name, the 'true' value (literature value from Govindaraju[6]), the observed value (values from the SWDXRF), absolute error (observed value minus the 'true' value), relative error (absolute error/'true' value $\times$ 100), determination limit (DL) and counting error are tabulated.

Twenty international reference materials were used to calibrate the element Rb (Table 4). The relative error is high (10%) at a low concentration of 20 ppm with an absolute error of 2 ppm (reference material No. 11 W-2), whereas the relative error is zero (0%) at a higher concentration of 860 ppm with an absolute error of <1 ppm (reference material No. 17 FK-N). From the 20 international reference materials used for the calibration for the element Rb, four of these reference materials have a relative error between 4 and 11%, while 16 are below 5%. Also shown in Table 4 are 24 of the international reference materials of the Institute of Geophysical and Geochemical Prospecting (IGGE) that were analysed as 'unknown samples' and the observed values are compared with the recommended values. (Note that the IGGE reference materials were initially not included in the calibration and were compared as 'unknown' samples. At present all the reference materials mentioned in Table 2 are included in the calibrations). The relative error (in %) ranges from 1 to 29. Of the 24 reference materials, 8 have a relative error larger than 10%. These reference materials are GSD-5, GSD-7, GSD-11, GSD-12, GSS-4, GSS-6, GSR-2 and GSR-3. All of these materials have reasonably high Rb concentrations, from 37 ppm (GSR-3) to 408 ppm (GSD-11). Thus 67%

Table 5 Precision of the international reference material GSP-1

Element (ppm)	Average concentration	Standard deviation	Minimum	Maximum	Range	Precision (%)
TiO_2 %	0.62	0.005	0.61	0.62	0.01	1.61
MnO %	0.04	0	0.04	0.04	0	0.00
Fe_2O_3 (total)	4.07	0.004	4.06	4.08	0.02	0.20
Sc	9	0.70	8	11	3	15.6
V	57	1.29	54	60	6	4.5
Cr	14	2.33	8	19	11	33.3
Co	10	0.57	8	11	3	11.4
Ni	14	0.60	12	15	3	8.6
Cu	37	0.55	36	39	3	3.0
Zn	114	1.35	109	116	7	2.4
Rb	258	0.59	256	259	3	0.5
Sr	237	0.49	236	238	2	0.4
Y	27	0.37	26	28	2	2.7
Zr	475	0.64	473	476	3	0.3
Nb	20	0.23	19	20	1	2.3
Mo	6	0.50	5	6	1	16.7
Ba	1273	8.01	1253	1291	38	1.3
Pb	56	1.52	50	59	9	5.4
Th	91	0.86	87	93	6	1.9

of the IGGE reference material have a relative error below 10%. It is therefore difficult to quantify the over-all accuracy of the analysis as an 'average relative error'. The determination limit varies from 0.5 to 3.7 ppm on the different matrices of the international reference materials.

Crustal Abundances of the Chemical Elements

The crustal abundances of the chemical elements and their determination limits obtained on the SWDXRF are listed in Table 6. Of the 24 elements analysed on the SWDXRF 20 are significantly below the crustal abundances quoted by Reeves and Brookes[14] (column 1), Thalmann *et al.*[15] (column 2 for the average of rocks and column 3 for the average of soils) and Taylor[16] (column 4). The determination limits for the elements As, Sb, W and U are equal to or higher than the crustal abundances in the average rock or soil in Table 6. The method of analysis for these elements will not result in maps of background trends, but will highlight areas containing anomalous values.

One of the proposals made by the Analytical Committee of the International Geological Correlation Program (IGCP) Project 259 is that the determination limit must be below the average crustal abundance. Only four of the 24 elements (As, Sb, W and U) do not at present conform with this proposal. The remaining 20 determination limits are equal to or below the crustal abundances. Although the main purpose of this programme is to locate unknown mineralized ore bodies, the

Table 6 Crustal abundances of the elements compared to the determination limits (DL) of the 24 elements analysed on the SWDXRF (all values in ppm)*

Element	1	2	3	4	DL
Sc	20	22	16	22	1
Ti	5700	5700	5000	5700	100
V	180	135	60	135	5
Cr	71	100	40	100	4
Mn	1000	950	850	950	100
Fe	56000	56000	21000	56300	100
Co	26	25	8	25	10
Ni	75	75	17	75	10
Cu	60	55	15	55	9
Zn	70	70	50	70	3
As†	1.6	1.5	6	1.8	10
Rb	125	90	100	90	1
Sr	215	375	300	375	1
Y	19	33	50	33	1
Zr	155	165	300	165	1
Nb	15	20	15	20	5
Mo	2	1.5	2	1.5	0.2
Sn	4	2	10	2	2
Sb†	0.70	0.2	2	0.2	5
Ba	600	425	500	425	10
W†	0.40	1.5	1	1.5	4
Pb	14	12.5	10	12.5	4
Th	10	9.2	13	9.6	4
U†	2	2.7	1	2.7	2

* For columns 1 to 4, see text for description.
‡ Crustal abundance ≤ determination limit.

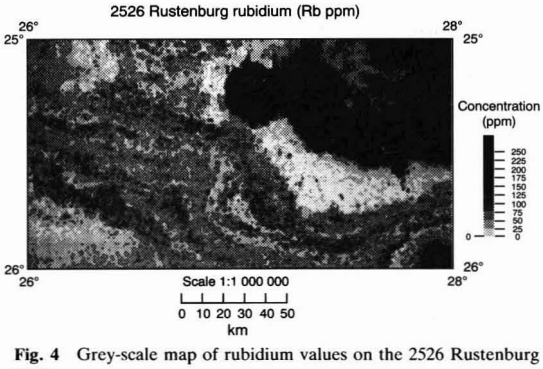

Fig. 4 Grey-scale map of rubidium values on the 2526 Rustenburg area.

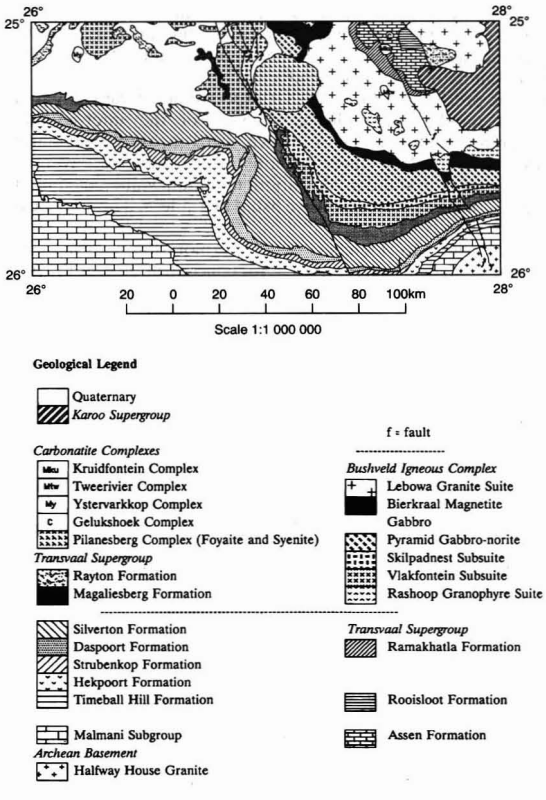

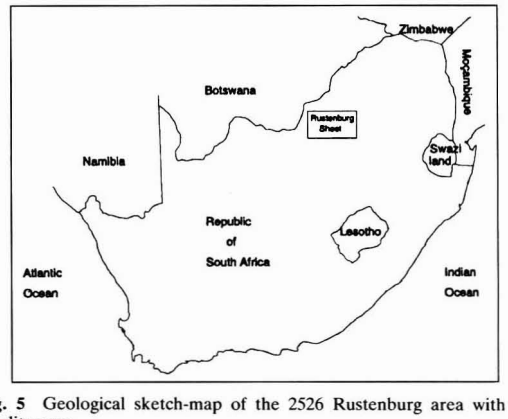

Fig. 5 Geological sketch-map of the 2526 Rustenburg area with locality map

majority of the elements analysed for on the SWDXRF can also be used for regional geochemical mapping.

Applications

To evaluate the results, a grey-scale map of Rb values (Fig. 4) is compared with the geology of the 2526 Rustenburg area in Fig. 5 (coordinates 25°00′S to 26°00′S and 26°00′E to 28°00′E). From the grey-scale map of the Rb values (Fig. 4) it is clear that high concentrations of the element Rb (>100 ppm) reflect the Halfway House Granites, the lithological units of the Lebowa Granite and the Rashoop Granophyre Suites, Pilanesberg Complex and mainly the Shale formations (Silverton and Timeball Hill of the Transvaal Sequence). Low concentrations of Rb (<50 ppm) reflect mainly the Bierkraal Magnetite Gabbro, Pyramid Gabbro-norite, the Skilpadnest and Vlakfontein Subsuites of the Bushveld Igneous Complex and the Dolomite and Chert of the Malmani Subgroup and the Assen Formation of the Transvaal Sequence. The determination limit of 1 ppm for the element Rb compared with the average crustal abundance of 90–125 ppm (Table 6) illustrates that the background trends are mapped below the element's crustal abundance. The eastern outcrops of the Lebowa Granite Suite is highly differentiated which is reflected by the anomolous values of Rb (>200 ppm). It is in this part of the granite where Sn mineralization occurs.

The repeatability or precision of the analytical technique is illustrated by the fact that 32 of the 1:50 000 scale maps were analysed at random over a period of several months to compile the final 1:1 000 000 scale map. The 1:50 000 scale maps consist of approximately 700 samples and no 'batch effects' or 'checker board effects' were observed. The accuracy of the analytical technique is illustrated by the demarcation of the geochemical trends that reflect the underlying geology.

Conclusions

The great advantage of simultaneous X-ray fluorescence spectroscopy for the multi-element determinations in regional geochemical mapping is the reproducibility, high speed and accuracy of the analyses. By using the automatic 300 position sample changer with the simultaneous X-ray fluorescence spectrometer, 24 element analyses can be made in 100 s per sample. Three hundred samples, plus the monitor sample at every tenth position, can be analysed in a 14 h shift, totalling to 1500 samples in a 5 d week. The 36 000 element analyses per week demonstrate the speed of the operation. The method is especially suitable for the large number of samples required for regional geochemical mapping.

The calibration of the Philips PW1606 SWDXRF spectrometer involved background determinations, inter-element interference and matrix corrections in order to obtain a good correlation between the X-ray net peak intensity (in kcount s^{-1}) and the international reference material concentration value (in % or ppm). All the calibrations were simple linear fits between net intensity (the product of above mentioned corrections) and concentration. For the calibration, a wide variety of geochemical reference samples which cover most typical rock compositions were used, including the stream sediment and soil sample reference material from IGGE. Of the 24 chemical elements calibrated on the Philips PW1606 SWDXRF spectrometer, 20 have a determination limit significantly below the crustal abundances. Although all of the 24 elements will show anomalous concentrations above background levels for the location of unknown mineralized ore bodies, the elements with determination limits significantly below the average crustal abundances will also map background trends which reflects the underlying geology. The stream sediment geochemical data can be used to aid geological mapping on a regional scale.

The Director of the Council for Geoscience of South Africa is thanked for granting permission to publish this work and Dr. D. De Bruin is thanked for critically reading this manuscript. M. Lombaard, and T. Laubscher are thanked for compiling the grey-scale map of Rb and W. van der Merwe for drawing the geological map of the Rustenburg area.

References

1 Labuschagne, L. S., Holdsworth, R., and Stone, T. P., *J. Geochem. Explor.*, 1993, **47**, 283.
2 Plant, J. A., Hale, M., and Ridgway, J., *Trans. Inst. Min. Metall. Sect. B*, 1988, **97**, 116.
3 Plant, J. A., Hale, M., and Ridgway, J., *Ontario Geol. Surv. Spec.*, 1989, **3**, 384.
4 Feather, C. E., and Willis, J. P., *X-ray Spectrom.*, 1976, **5**, 41.
5 Nisbet, E. G., Dietrich, C. J., and Esenwein, A., *Fortschr. Mineral.*, 1979, **7**, 264.
6 Govindaraju, K., *Geostand. Newsl.*, 1989, **13**, 113.
7 Heinrich, K. F. J., *Proceedings of the 11th International Congress on X-ray Optics and Microanalysis, London, (Canada)*, ed. Brown, J. B., and Packwood, R. H., 1986, pp. 67–119.
8 Willis, J. P., in *X-ray Fluorescence Analysis in the Geological Sciences. Advances in Methodology*, ed. Ahmedali, S. T., Geological Association of Canada, Short course GAC MAC, Annual Meeting Montreal, Quebec, Canada, 1989, vol. 7, p. 297.
9 Jenkins, R., *X-ray Fluorescence Spectrometry*, John Wiley and Sons, New York, 1988, vol. 99, p. 163.
10 Potts, P. J., *A Handbook of Silicate Rock Analysis*, Blackie and Son, London, 1987, p. 622.
11 Müller, R. O., *Spectrochemical Analysis by X-ray Fluorescence*, Adam Hilger, London, 1972, p. 326.
12 Fletcher, W. K., Hoffman, S. J., Mehrtens, M. B., Sinclair, A. J., and Thomson, I., *Exploration Geochemistry: Design and Interpretation of Soil Surveys*, ed. Robertson, J. M., *Reviews in Economic Geology*, Society of Economic Geologists, Chelsea, USA, 1987, vol. 3, 180.
13 Jekins, R., *An Introduction to X-ray Spectrometry*, Heyden, New York, 1976, p. 163.
14 Reeves, R. D., and Brooks, R. R., *Trace Element Analysis of Geological Materials. Chemical Analysis*, John Wiley & Sons, New York, 1978, vol. 51, 421.
15 Thalmann, F., Schermann, O., Schroll, E., and Hausberger, G., *Geochemical Atlas of the Republic of Austria 1:1 000 000. Bohemian Massif and Central Zone of the Eastern Alps (Stream Sediments <80 mesh)*, 1989, p. 141.
16 Taylor, S. R., *Geochim. Cosmochim. Acta*, 1964, **28**, 1273.

Paper 4/05898D
Received September 27, 1994
Accepted January 4, 1995

Investigation of Decomposition Products of Microwave Digestion of Food Samples

Helen J. Reid, Stanley Greenfield and Tony E. Edmonds*

Department of Chemistry, Loughborough University of Technology, Loughborough, Leicestershire, UK LE11 3TU

The involatile residues remaining after closed-vessel microwave digestion of various food samples, using nitric acid, with and without post-digestion treatment with hydrogen peroxide, have been studied. Decomposition products were found to include aliphatic and aromatic acids, nitro-compounds, oxalates and inorganic nitrates and phosphates. Measures of digestion completeness were provided by appearance, carbon content, infrared spectra and thin layer chromatograms of the residues, enabling a comparison of different digestion methods and sample types. Residual carbon levels varied linearly with the relative amounts of carboxylic acid and inorganic nitrate, as measured by infrared spectrometry of the residues. The formation of calcium oxalate was also a function of the degree of decomposition: the carboxylic acid : oxalate ratio increased in a logarithmic fashion with increasing residual carbon content.

Particularly high levels of residual carbon from nitric acid digestion of milk powder, due largely to carboxylic acid residues, were substantially decreased by post-digestion treatment with hydrogen peroxide. However, nitrobenzoic acids, which proved major interferents in electrochemical analysis, were only removed by treatment with perchloric acid.

Keywords: microwave digestion; sample preparation; food analysis; residual carbon

Introduction

Acid digestion in closed vessels using microwave heating is now a well established sample preparation technique, and many applications have been reported.[1,2] Whilst complete dissolution can usually be achieved with a suitable choice of conditions, complete decomposition of the organic matrix in food samples, especially those with a high protein and/or fat content, is much more difficult, and it has been noted by several workers[3–5] that microwave digestion with nitric acid alone is insufficient for complete oxidation of such materials.

Specific decomposition temperatures (as witnessed by a sharp rise in pressure at almost constant temperature) of the three basic components of biological and botanical matrices in nitric acid have been measured at 140 °C for carbohydrates, 150 °C for proteins and 160 °C for lipids.[6] This indicates that samples with a high fat content would be relatively difficult to decompose. Proteins also contain aromatic species such as phenylalanine, which give rise to aromatic acids particularly resistant to oxidation with nitric acid.

Studies of the decomposition products of nitric acid pressure digestion have been reported for microwave[7] and conventional[8] heating. Of particular interest are involatile compounds which cannot easily be removed by evaporation without loss of analyte. These include aromatic acids from protein decomposition, as mentioned above. Nitrobenzoic acid, especially the *para*-isomer, has been reported as a major interferent in electrochemical analysis of these digests.[7,9]

Studies of residual carbon content (RCC) as a measure of digestion efficiency, when comparing methods, have been reported.[5,10–13] Hee and Boyle[11] found it necessary to correct for carbon interference in ICP-AES analysis, while Friel *et al.*[4] found that a post-digestion, open beaker treatment with H_2O_2, on a hot-plate at 90 °C, effectively removed the problem. Krushevska *et al.*[5] compared RCCs of milk samples digested by hot-plate, high pressure ashing, closed microwave and open-focused microwave, and found the high pressure asher, with nitric acid only, and the open focused microwave system, using a mixture of HNO_3, H_2SO_4 and H_2O_2, gave very low residual carbon values (<1%, compared with up to 25% for other methods).

In the above studies, decomposition products of microwave digestion have not been identified in detail and have not been related to the RCC or digestion methods. The main aims of the current work were to study the effect of different digestion regimes on the quality and quantity of residual material, to identify the broad groups of compounds produced, to investigate their relative resistance to oxidation and to gauge their significance for analytical techniques particularly sensitive to organic interference.

Experimental

Apparatus

Digestions were carried out using a Model MDS-81D microwave unit [CEM Corporation, Matthews, NC, USA, supplied by CEM (Microwave Technology), Buckingham, UK], with a maximum power output measured at 675 ± 15 W and pressure monitoring *via* an external pressure transducer with operating range 100–1380 kPa (Data Instruments, Acton, MA, USA). The features and calibration of this equipment have been described previously.[14]

Samples were digested in CEM lined digestion vessels (Teflon PFA liner in polyetherimide outer casing) with a safety venting system incorporating a disposable membrane designed to rupture if the internal pressure exceeds 1380 kPa.

Elemental analyses were performed on a Perkin-Elmer 2400 CHN Analyzer (Beaconsfield, Bucks, UK). Fourier transform infrared analyses were carried out using a Perkin-Elmer 1600 Series FTIR instrument.

Voltammetric analysis was carried out using a Metrohm 626 Polarecord with 663 VA stand, with a hanging mercury drop electrode, saturated Ag/AgCl (3 mol l^{-1} KCl) reference electrode and glassy carbon auxiliary electrode.

Reagents

Digestions were carried out using ARISTAR-grade concentrated nitric acid, SpectrosoL grade hydrogen peroxide (30% m/v) (both from Merck, Poole, Dorset, UK) and AnalaR

* To whom correspondence should be addressed.

grade perchloric acid (71%) (Fisons, Loughborough, UK). Water purified by a Liquipure Modulab system (Liquipure Europe, Bicester, UK) was used for all dilutions. HiPerSolv (HPLC grade) methanol (Merck) was used for extraction of residues. Samples of milk powder, dried pet food, dried sweet bay leaves, tomato puree and sodium alginate (AMC samples) were provided by the Metallic Impurities in Organic matter Subcommittee of the Analytical Methods Committee of the Royal Society of Chemistry (Analytical Division). Aqueous standards for voltammetric analysis were prepared by dilution of standard solutions containing 1000 mg l^{-1} of copper and zinc, respectively (Merck), and by dissolution of solid samples of 2-, 3- and 4-nitrobenzoic acids (Merck, Fisons). Solutions were adjusted to pH 9 with analytical-reagent grade 88% ammonia solution (18 mol l^{-1}) (Fisons).

Digestion Methods

The AMC samples were all digested using each of the following three methods:

A, Microwave pressure digestion with nitric acid

Up to 12 vessels were each loaded with 0.5 g of sample (1 g in the case of tomato puree) and 10 ml of concentrated (16 mol l^{-1}) nitric acid, or nitric acid only for blanks. The turntable holding the sealed vessels was placed in the microwave cavity and one of the vessels was attached to the pressure-monitoring line. Microwave power was applied to give a steady pressure rise up to 1030 kPa over about 10 mins; the applied power level varied according to the number of vessels and the matrix being digested and was adjusted during the heating cycle according to the observed pressure rise. The applied power was then adjusted to maintain this pressure for a further 15 min. After cooling to room temperature in an ice-water bath, the vessels were vented and opened. Except where a second-stage microwave digestion using hydrogen peroxide was carried out, the digests were quantitatively transferred into volumetric flasks, or to beakers for further treatment, as required.

B, Post-digestion treatment with hydrogen peroxide, I

After carrying out the procedure described above for eight 0.5 g samples together with four blanks (except tomato puree: four 1 g samples and two blanks), the digests were combined in pairs to give four digests and two blanks. Two of the digests and one blank were diluted to 50 ml with water and transferred to polypropylene bottled for storage ('nitric acid only' digests). The other two digests and blank were transferred into beakers (with washing of the digestion vessels) and heated to bp on a hot-plate. Hydrogen peroxide was then gradually added dropwise until the digests became virtually colourless (*i.e.*, until addition of further peroxide produced no further decoloration). The treated digests were then cooled and made up to 50 ml with water and the addition of 2 ml of concentrated nitric acid (to maintain acid strength and prevent precipitation of insoluble salts).

C, Post-digestion treatment with hydrogen peroxide, II

A modified version of the procedure described by Friel *et al.*[4] was carried out, as follows: A 5 ml aliquot of 'nitric acid only' digest, prepared as described above, was evaporated to near dryness in a beaker or evaporating dish on a steam bath. After the addition of 2 ml of nitric acid, 1 ml of hydrogen peroxide was slowly added dropwise, and the solution evaporated to near dryness. This procedure was repeated until the solution appeared colourless, and foaming was reduced to that of the blank digest treated in parallel. Three to four repetitions were normally required.

In addition, samples of the milk powder were digested using the following two methods:

D, Second-stage microwave pressure digestion with hydrogen peroxide

Following the nitric acid digestion described above, 2 ml of hydrogen peroxide was added to each vessel, the vessels were sealed and the turntable returned to the microwave cavity. Microwave power (370–500 W) was applied, gradually increasing the pressure to a maximum of 700 kPa over a 15 min period. The applied power was then reduced to maintain pressure for up to 15 min. After cooling, the digests were transferred into calibrated flasks and diluted to 25 ml with water.

E, Post-digestion treatment with perchloric acid

Following the nitric acid digestion described above, the contents of each vessel were transferred (with washing of caps and vessels) into acid-washed glass beakers on a hot-plate. 2 ml of 71% perchloric acid was added to each digest. The beakers were covered with watch glasses and heated until dense white fumes of perchloric acid were evolved. After simmering for a further 15 min, the digests were cooled, transferred into calibrated flasks and diluted to 25 ml with water.

Preparation of Residues for Analysis

Aliquots of 5 ml of the diluted digests were transferred into pre-weighed evaporating dishes on a steam bath and evaporated to dryness. The residues were then dried to constant weight in an oven at 90 °C. In the case of the peroxide treatment (C), the residues were dried directly in the same vessels as used for the peroxide treatment. Aliquots of 5 ml of the corresponding blank digests were similarly treated and showed no significant residue originating from the reagents.

Some of the residual material was extracted with methanol and the soluble and insoluble fractions were retained separately for analysis.

Analysis of Residues

Carbon content analysis

The percentage carbon content of the original undigested samples (c_1) and of the dried digest residues (c_2), were determined by elemental analysis. The RCC as a percentage of the carbon content of the original sample (c_r) was then calculated from the formula

$$c_r = \frac{c_2 m_2}{c_1 m_1 \times F} \times 100\%$$

where m_1 and m_2 are the masses of the undigested sample and the digest residues, respectively, and F is the fraction of digest evaporated to dryness.

Infrared spectrometry

The infrared spectra of the residues and extracts were recorded, in the form of potassium bromide discs.

Thin layer chromatography

Thin layer chromatography was carried out on the methanol soluble fractions using silica plates with propan-2-ol–formic

acid–water, 20 + 1 + 5 as eluting solvent. Spots were viewed under UV light (254 nm) and acidic spots were visualized by spraying with Bromocresol Green (0.3% solution in 1 + 4 water–methanol containing four drops of 30% sodium hydroxide in 50 ml[15]).

Voltammetry

Several of the milk powder digests were analysed for zinc and copper by differential-pulse anodic stripping voltammetry (DPASV), using one of the following methods:

(*i*) A 5 ml aliquot of digest prepared as above was adjusted to pH 9 with ammonia and diluted to 25 ml with water prior to transfer into the polarographic cell.

(*ii*) In order to eliminate dissolved oxides of nitrogen, a 5 ml aliquot of digest was transferred into a small beaker and evaporated to dryness on a hot-plate. The residue was then taken up in dilute nitric acid, adjusted to pH 9 with ammonia and diluted to 25 ml with water.

DPASV was carried out at room temperature under oxygen-free nitrogen after purging with nitrogen for 5 min. Measuring conditions for the analysis were as follows: deposition potential, −1.30 V; deposition time 2 min with stirring (plus 20 s settling time); potential scan rate, 5 mV s^{-1} differential pulse, 50 mV.

Zinc and copper were determined by the addition of aqueous standard solutions; plots of peak height *versus* added zinc/copper were linear in each case. Solutions of the three nitrobenzoic acid (NBA) isomers were analysed, both separately (in 1% HNO_3 and after adjustment to pH 9 with ammonia) and by addition to the digest solutions, to compare with signals in the voltammograms which were not due to trace metals.

Results and Discussion

Appearance of Digests and Residues

The single stage, nitric acid digestion (A) produced clear, pale yellow solutions in all cases. The only exception was that the sweet bay digests contained a small amount of a fine, grey precipitate which infrared analysis indicated was due to siliceous material.

The colour, texture and mass of the dried residues varied considerably with digestion method and sample matrix, although replicates of the same sample/method combination were generally reproducible. Method A produced yellow, waxy residues in the cases of milk powder, sweet bay and pet food, pale yellow powder for tomato puree and white powder for sodium alginate. The peroxide treated digests gave paler, drier (less waxy) residues of lower mass than the nitric acid only digests.

Residual Carbon Content

The RCC results for digestion methods A–C are summarized in Fig. 1. As can be seen, the milk powder proved the least well digested sample for each method. This is almost certainly owing to its high protein and fat content, as it has been shown[6] that these compounds require higher temperatures for decomposition than do carbohydrates, which make up a greater proportion of the other samples.

The trace of carbon recorded in the case of sodium alginate was insignificantly low (below the standard error of the method), indicating essentially complete decomposition with nitric acid alone. The carbon remaining in the tomato puree, although detectable, was also very low indicating almost complete decomposition. Significant carbon remained in the other digests, except for the milk powder subjected to perchloric acid treatment, where the residues consisted essentially of inorganic perchlorates. (Solutions of the residues were tested with Brilliant Green dye, where the formation of a blue–green complex extractable into toluene confirmed the presence of perchlorate.[16]) Milk powder digested by method D (nitric acid–hydrogen peroxide with microwaves under pressure) resulted in an c_r value of 11%, which is slightly higher than the mean level from method C (nitric acid–hydrogen peroxide dropwise on a steam-bath).

Agreement between duplicates was generally very good (spread <1.5%). However, in the case of the second peroxide treatment (method C), the appearance and masses of the digest residues were more variable than with the other methods and replicate carbon content determinations confirmed this variability giving a range of 5.1–11.8% for milk powder ($n = 6$) and 2.7–5.8% for pet food ($n = 5$). However, the carbon content of the residues from this method were consistently lower than those from the first peroxide treatment method, B, which in turn were lower than those from the nitric acid only digests. The results indicate that for milk powders, sweet bay and pet food, the degree of decomposition was improved substantially using post-digestion peroxide treatment, particularly the more intensive (albeit slower) second method, C.

Infrared Spectrometry

Infrared analysis of the residues from the sodium alginate digests showed that oxidation to sodium nitrate was essentially complete, as witnessed by the elemental analysis results (15% nitrogen, negligible carbon and hydrogen). This was confirmed by mp determination. In addition, the mass of residue (334 mg per gram of sample) agreed well with the theoretical yield (373 mg per gram of sample) for complete conversion of sodium alginate to sodium nitrate (assuming the sodium content is unaffected by any cross-linkage of the alginate chains).

Infrared spectra of the tomato puree digests indicated a predominantly inorganic nitrate content (band at 1384 cm^{-1}), with a small carbonyl band at 1700 cm^{-1}, with virtually no difference between the nitric acid only and peroxide treated digests, as expected from their similar, low carbon contents.

The IR spectra of the other sample residues after digestions by methods A–C showed a mixture of organic material. The predominant bands in the spectra of residues from method A are attributable to carboxylic acids: characteristic bands in the

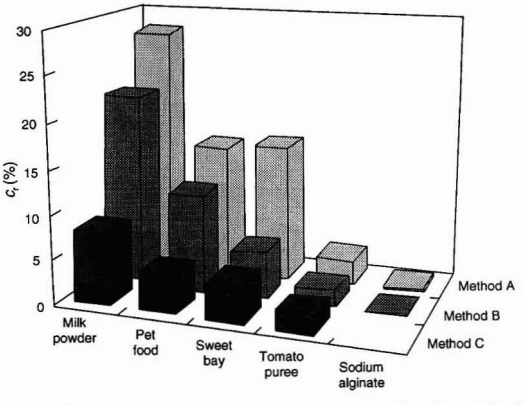

Fig. 1 Comparison of RCC following microwave digestion of food samples by method A, HNO_3 only; method B, HNO_3–H_2O_2 (I); and method C, HNO_3–H_2O_2 (II). Each column represents the mean result from analysis of at least two digests.

3000–2500 cm^{-1} region (O–H and C–H stretching), C=O stretch at 1700 cm^{-1}, together with multiple bands in the 1400–1100 cm^{-1} region and a band at 940 cm^{-1}. For the peroxide treated digests (method C), these bands were much weaker, and the spectra were dominated by bands due to inorganic nitrate (1384 cm^{-1}) and calcium oxalate (1620, 1320, 780, and 520 cm^{-1}), with an indication of inorganic phosphate (1000–1100 cm^{-1}).

These identifications were substantiated by extraction of the residues with methanol to give a white precipitate, identified as mainly calcium oxalate with a small amount of phosphate, and a yellow solution containing carboxylic acids and nitrate. Superimposition of the IR spectra of the methanol-soluble and -insoluble fractions gave patterns matching those of the total residue, indicating that no significant chemical change had resulted from the extraction procedure. In particular there was no apparent shift in the carbonyl absorption to higher wavenumber to indicate esterification of the acids in the presence of methanol.

A typical variation in the FTIR spectra between digestion methods is shown in Fig. 2, which shows the differences between sweet bay digests with and without peroxide treatment. Similar results were obtained for the milk powder and pet food digests. It can be seen that the peroxide treated digest shows a higher proportion of calcium oxalate and inorganic nitrate relative to the organic acid residues than the nitric acid only digest.

For milk powder digested by method D, the methanol soluble extract showed a similar IR spectrum to those from methods A–C. However, the precipitate from methanol extraction was found to be largely owing to phosphate residues, the FTIR spectrum closely resembling that of dibasic calcium phosphate ($CaHPO_4$), which is insoluble in methanol. The presence of orthophosphate was confirmed by treatment with acidified ammonium molybdate to form bright yellow ammonium molybdophosphate with addition of Crystal Violet to form a deep blue complex.[16] The IR spectrum also showed a small amount of calcium oxalate. The carbon content of the methanol-insoluble residue was measured to be 6%, compared to 19% if the residue had been entirely calcium oxalate, indicating 68% phosphate and 32% oxalate in the residue. This corresponds to a calcium phosphate yield of 41 mg per gram of sample digested, which compares with a theoretical yield of 37 mg g^{-1}, calculated from literature data for a typical phosphorus concentration in milk powder.[17] Hence it was shown that although method D produced a similar RCC to method C, the use of microwaves under pressure for the second stage produced a different decomposition profile, yielding far more phosphate and much less oxalate than peroxide treatment in open vessels using conventional heating.

It was observed that, for residues from digestion methods A–C, the higher the RCC was the stronger the carbonyl peak in the IR spectrum appeared, and it was felt that it might be useful to quantify this correlation, thus providing another measure of degree of decomposition to complement the RCC measurements. Clearly, owing to differences in sample loading, thickness and clarity of the KBr discs, the absolute peak heights would vary between similar samples, but if the relative absorbances of the carbonyl (1700 cm^{-1}) and inorganic nitrate (1384 cm^{-1}) bands were considered, the nitrate band would act as an internal reference and a meaningful parameter could be obtained. The relative absorbances (A) were calculated from the infrared spectra using the formula

$$A\,(x/y) = \frac{\log T_b - \log T_x}{\log T_b - \log T_y}$$

where T_b is the percentage transmittance at baseline in the spectra region of interest and T_x and T_y are the percentage transmittances at x and y cm^{-1}, respectively.

For each of the residues digested by methods A–C, plots of the relative absorbance at 1700 cm^{-1} to 1384 cm^{-1} (organic acid and inorganic nitrate, respectively) *versus* c_r were linear, indicating that residual carbon levels varied linearly with organic acid concentration (relative to inorganic nitrate as reference). When the RCC as a percentage of the mass of residue (c_2) was plotted against absorbance, straight lines were obtained for each sample type, but these did not coincide with each other. However, when the RCC expressed as a percentage of the original carbon content of the undigested sample c_r was plotted against absorbance, the lines coincided (see Fig. 3). This is apparently owing to the elimination of differences due to differing carbon contents of the original samples and differing masses of residual material remaining after digestion. For milk powder digested by method D, the results did not fall on this straight line, as the absorbance at 1700 cm^{-1} relative to that at 1384 cm^{-1} was higher for a given c_r value than for the other digests. This is presumably due to the much lower proportion of calcium oxalate, which was a major contributor to the carbon content (but not to the 1700 cm^{-1} absorption) for the residues from methods A–C.

The relative absorbance at 1700 to 1620 cm^{-1} (organic acid/oxalate) was also examined for its variation with RCC, for all matrices where oxalate was produced, *i.e.*, milk powder, sweet bay and pet food, digested by methods A–C. the absorbance ratio increased with increasing carbon content,

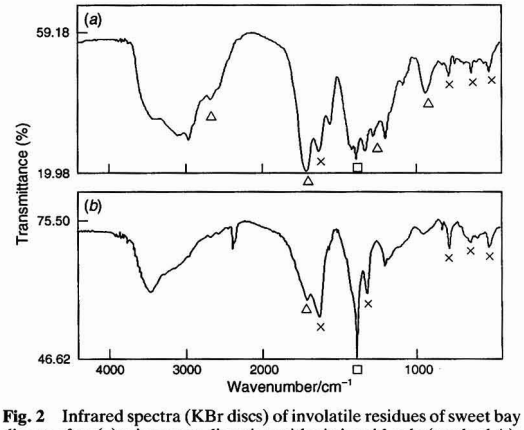

Fig. 2 Infrared spectra (KBr discs) of involatile residues of sweet bay digests after (*a*) microwave digestion with nitric acid only (method A); and (*b*) further treatment with hydrogen peroxide (method C). △, Carboxylic acid; □, inorganic nitrate; and ×, calcium oxalate.

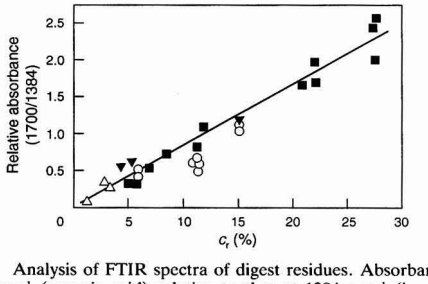

Fig. 3 Analysis of FTIR spectra of digest residues. Absorbance at 1700 cm^{-1} (organic acid) relative to that at 1384 cm^{-1} (inorganic nitrate) *versus* c_r (%). ■, Milk powder; ○, pet food; ▼, sweet bay; and △ tomato puree.

although the relationship was non-linear, as the relative absorbance increased very slowly at low values of c_r and much more rapidly at c_r levels of > 15% (such levels only being found in the milk powder digests), as shown in Fig. 4. When the values were plotted logarithmically, a straight line resulted.

An explanation of these findings is that early in the digestion process, the oxalate concentration is small; as the digestion progresses, the residual carbon content and the carboxylic acid concentration both decrease, whereas the oxalate concentration initially increases, reaching a maximum before falling gradually towards the end of the digestion. Evidence for this was provided by plotting the relative absorbance at 1620 to 1384 cm^{-1} (oxalate and nitrate, respectively) *versus* the residual carbon content, as shown in Fig. 5, where, in spite of the considerable scatter of results, the initial increase, followed by a decrease at c_r > 15%, can be seen. This is offered as a tentative explanation, as our experiments were not designed specifically to address this issue. Further work would need to be performed to be certain of the validity of this explanation.

Thin Layer Chromatography

Methanol extracts of milk powder, pet food and sweet bay digests all gave strong acidic spots having the same R_F value as 4-NBA, plus weaker spots corresponding to the other NBA isomers.

Voltammetric Analysis

The determination of zinc and copper in the milk powder digests by DPASV served to illustrate the effect of interfering species on this type of analysis. Zinc and copper were present at concentrations of approximately 0.1 μg ml^{-1} and 4 ng ml^{-1}, respectively, in the diluted digests (25 μg g^{-1} and 1 μg g^{-1} in the milk powder). By carrying out the analysis at pH 9 the adverse effect of the hydrogen wave was eliminated, enabling zinc to be determined much more easily than in acid solution, although there was a strong peak probably due to dissolved oxides of nitrogen (NO_x) very close to and partially overlapping the zinc wave. There were also several interfering peaks which rendered the determination of copper in the nitric acid and peroxide treated digests impossible. Fig. 6(*a*) shows a typical voltammogram. The determination of zinc could be performed successfully in the digests, but the NO_x peak sometimes interfered with accurate baseline estimation.

Comparison of the interfering peaks [Fig. 6(*a*), A, B and C] with signals produced by control samples of 2-, 3- and 4-nitrobenzoic acids (NBAs) at pH 9 indicated a mixture of 2- and 4-NBAs in the digests, with a trace of 3-NBA. 2-NBA and 4-NBA gave signals corresponding to A + C and B + C, respectively (3-NBA gave a signal between A and B and one at C). At acidic pH (1% HNO_3), the digests and control NBAs each gave one major signal at −0.1 V and a much broader, flatter signal at more negative potential (again masking any copper signal). These are reportedly due to the reduction of NBAs to amines *via* hydroxylamines in acidic soltions.[9] By comparing with mixtures of standard solutions of the NBAs at pH 9, the concentrations of 4- and 2-NBAs in the diluted digests, prepared by method D, were estimated at 40 and 10 μg ml^{-1}, respectively, which translates to a concentration of 12.5 mg of NBA per gram of sample digested. Assuming that the NBA results solely from the decomposition of phenylalanine in the original sample, as previously suggested,[7] the corresponding concentration of phenylalanine in the milk powder is 1.24%. This compares with a typical value for phenylalanine in milk powder of 1.40% calculated from the literature.[17]

Attempts to remove the NO_x peak by prolonged degassing prior to analysis, addition of sulfamic acid, or heating the digest to boiling before the final dilution were not very successful. However, the size of the peak diminished substantially on leaving the diluted digests in sealed poly(propylene)

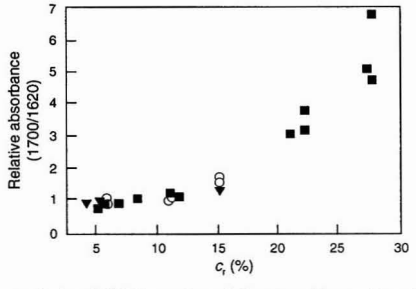

Fig. 4 analysis of FTIR spectra of digest residues. Absorbance at 1700 cm^{-1} (organic acid) relative to that at 1620 cm^{-1} (oxalate) *versus* c_r (%). ■, Milk powder; ○, pet food; ▼, sweet bay.

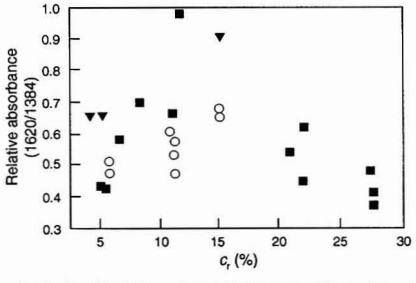

Fig. 5 Analysis of FTIR spectra of digest residues. Absorbance at 1620 cm^{-1} (oxalate) relative to that at 1384 cm^{-1} (organic acid) *versus* c_r (%). ■, Milk powder; ○, pet food; ▽, sweet bay.

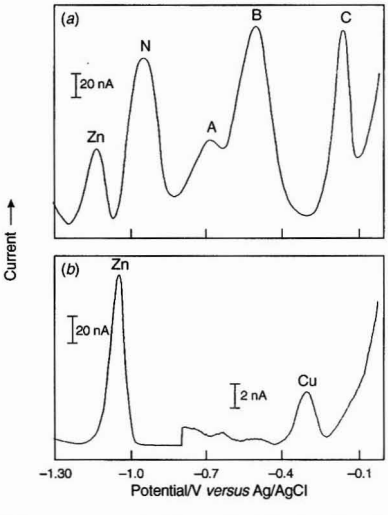

Fig. 6 Voltammograms of milk powder following digestion with (*a*) HNO_3–H_2O_2 (two stage microwave, method D), and (*b*) HNO_3–$HClO_4$ (microwave + hot-plate, method E), and adjustment to pH 9 with ammonia, showing signals due to Zn, Cu, nitrobenzoic acids (A, B and C) and probably nitrogen oxides (N).

bottles for a few days. Evaporation of the digests to dryness prior to dilution and pH adjustment, as has been previously recommended,[9] virtually eliminated the NO_x peak, but was slow and not very satisfactory in terms of possible loss of sample and introduction of contamination.

Complete decomposition of the milk powder using perchloric acid (method E) enabled copper to be successfully determined in the digests, as all the interfering peaks were removed [Fig. 6(*b*)]. By adjusting instrument sensitivity between the zinc and copper signals, to allow for the 25-fold difference in their concentration, both elements were determined simultaneously. The perchloric acid stage could not be carried out using microwave heating with the vessels used in this work, as the polyetherimide shell is attacked by perchloric acid. However, the use of all-Teflon PFA pressure vessels in a two-stage nitric–perchloric acid microwave digestion has been reported for the determination of copper in blood plasma by DPASV.[18]

The above results show the necessity of employing different sample decomposition methods according to the sample matrix and the analytical technique being used. For spectrometric methods that are tolerant of undigested organic material (such as ICP-AES) or for analysis of relatively easily decomposed materials, a single-stage digestion with nitric acid produces suitable solutions. Further digestion using hydrogen peroxide significantly reduces the RCC for samples of high protein and/or fat content, without further complicating the matrix (unlike, for example, the introduction of sulfuric acid), which may be important for some techniques (such as AAS or ICP-MS). However, complete decomposition is often needed for electrochemical analysis, and this can be readily accomplished using a straightforward post-digestion treatment with perchloric acid.

The authors thank A. Daley for performing the carbon content analyses. H. J. R. thanks the Trustees of the Analytical Chemistry Trust Fund of the Royal Society of Chemistry for the award of an SAC Research Studentship.

References

1 Kuss, H.-M., *Fresenius' J. Anal. Chem.*, 1992, **343**, 788.
2 Matusiewicz, H., and Sturgeon, R. E., *Prog. Anal. Spectrosc.*, 1989, **12**, 21.
3 Kingston, H. M., and Jassie, L. B., *Anal. Chem.*, 1986, **58**, 2534.
4 Friel, J. K., Skinner, C. S., Jackson, S. E., and Longerich, H. P., *Analyst*, 1990, **115**, 269.
5 Krushevska, A., Barnes, R. M., Amarasiriwaradena, C. J., Foner, H., and Martines, L., *J. Anal. At. Spectrom.*, 1992, **7**, 851.
6 Kingston, H. M., and Jassie, L. B., *J. Res. Natl. Bur. Stand (U.S.)*, 1988, **93**, 269.
7 Pratt, K. W., Kingston, H. M., MacCrehan, W. A., and Koch, W. F., *Anal. Chem.*, 1988, **60**, 2024.
8 Würfels, M., Jackwerth, E., and Stoeppler, M., *Anal. Chim. Acta*, 1989, **226**, 17.
9 Würfels, M., Jackwerth, E., and Stoeppler, M., *Anal. Chim. Acta*, 1989, **226**, 31.
10 Nakashima, S., Sturgeon, R. E., Willie, S. N., and Berman, S. S., *Analyst*, 1988, **113**, 159.
11 Hee, S. S. Q., and Boyle, J. R., *Anal. Chem.*, 1988, **60**, 1033.
12 Matusiewicz, H., Sturgeon, R. E., and Berman, S. S., *J. Anal. At. Spectrom.*, 1989, **4**, 323.
13 Krushevska, A., Barnes, R. M., and Amarasiriwaradena, C. J., *Analyst*, 1993, **118**, 1175.
14 Reid, H. J., Greenfield, S., and Edmonds, T. E., *Analyst*, 1993, **118**, 443.
15 Touchstone, J. C., and Dobbins, M. F., *Practice of Thin Layer Chromatography*, Wiley, New York, 1983, 2nd edn., p. 173.
16 Feigl, F., and Anger, V., *Spot Tests in Inorganic Analysis*, Elsevier, Amsterdam, 1972, 6th edn., p. 184, 392.
17 Paul, A. A., and Southgate, D. A. T., in *McCance and Widdowson's The Composition of Foods*, HM Stationery Office, London 1988, 4th edn.
18 Tahán, J. E., and Romero, R. A., *Anal. Chim. Acta*, 1993, **273**, 53.

Paper 4/06721E
Received November 3, 1994
Accepted January 6, 1995

Effect of the Coupling Reagent on the Metal Inhibition of Immobilized Urease in an Optical Biosensor

Roberto T. Andres and Ramaier Narayanaswamy*
Department of Instrumentation and Analytical Science, UMIST, P.O. Box 88, Sackville Street, Manchester, UK M60 10D

Urease was immobilized on aminopropyl glass through different bifunctional coupling reagents (cyanuric chloride, glutaraldehyde, hexamethylene diisocyanate, and phenylene diisothiocyanate) and their metal inhibition characteristics were compared. The inhibition studies were performed using a fibre-optic biosensor configuration, wherein the pH change resulting from the biocatalytic hydrolysis of urea was compared before and after the exposure to the metal samples. The different immobilized urease preparations exhibited varying metal inhibition behaviour: urease bound on cyanuric chloride- (1) and glutaraldehyde-activated (2) support were generally the most sensitive to the inhibition of seven test metal solutions (Hg^{2+}, Ag^{+}, Cu^{2+}, Zn^{2+}, Pb^{2+}, Cr^{3+}, and Co^{2+}), urease bonded through hexamethylene diisocyanate (3) coupling reagent suffered slightly lesser inhibition, while the enzyme bonded through phenylene diisothiocyanate (4) displayed excellent metal inhibition resistance. A similar trend was observed when the different urease reagents were subjected to long term exposure to a test metal ion (Cu^{2+}). Reagent 4 exhibited only a very slight decrease in its enzyme activity even after a 17 h continuous inhibition with the metal solution while the response of the other three enzyme reagents deteriorated significantly within 3–4 h. The unique inhibition property of urease bound on the diisothiocyanate glass was attributed to the metal binding property of the thiourea linkage formed during the immobilization process and to a more stabilized conformation of the immobilized urease in the said support. The usefulness of 4 was demonstrated in the biosensing of urea in the presence of an inhibiting metal ion, while 1 was applied to the biosensing of metal ion (Hg^{2+}) based on enzyme inhibition measurements.

Keywords: *Coupling agent; immobilized enzyme; metal inhibition; optical biosensor; urease*

Introduction

Numerous biosensors have been produced by integrating immobilized enzymes with different kinds of transducers.[1–4] These devices have found applications in various analytical fields including bioprocess control, biomedical analysis, environmental monitoring and control, food pharmaceutical or petrochemical analysis, and even defence. However, the performance and usefulness of these types of sensors are often dictated by the immobilization method employed for the deposition of the enzyme layer on the surface of the transducer.[5–12] For example, the sensor lifetime, its dynamic range, sensitivity, selectivity, response time, stability, and susceptibility to interferents are some of the operational parameters affected by the enzyme immobilization procedure and the type of support material used for the sensor fabrication.

There are five general methods of enzyme immobilization commonly employed for biosensor construction. These include physical adsorption of enzyme to water insoluble carriers, enzyme entrapment within the lattices of polymeric gels, simple containment of enzyme solution within a semipermeable membrane, intermolecular cross-linking of enzyme molecules around a carrier or the transducer surface using a bifunctional reagent, and the covalent coupling of the biocatalyst directly onto the transducer surface or to water-insoluble carrier maintained over the transducer. Presently, chemical coupling of the enzymes to reactive supports is a popular method of enzyme immobilization. This is owing to the high stability of the enzyme linkage and high enzyme loading achieved, and the wide diversity of solid supports and coupling chemistries available. There is also the added advantage that the immobilization is not easily reversed by pH, ionic strength, solvents or temperature.

The covalent coupling process is usually performed through the initial activation of the support matrix followed by the addition of the enzyme to the reactive support intermediate. In some cases, the coupling process is carried out in the presence of the enzyme, matrix, and a third reactive component, *e.g.*, carbodiimide. In these coupling procedures, the use of bi- or multifunctional reagents have proven to be a simple, yet effective and versatile approach for enzyme immobilization. These reagents are low molecular mass compounds, which contain two or more reactive functional groups, one of which forms a covalent linkage with the support and the other group(s) bind with the enzyme molecule. Several bifunctional reagents are available with varying reactivities towards different functional groups like –OH, –SH, –COOH, $-NH_2$, and these are described in the literature.[13–15]

In this work, four different kinds of bifunctional coupling reagents have been employed, namely glutaraldehyde, cyanuric chloride, hexamethylene diisocyanate and phenylene diisothiocyanate, in the immobilization of urease on an amino-derivatized controlled-pore glass in the construction of a fibre-optic biosensor. The different sensors were then tested for their resistance to heavy metal ion inhibition. Our interest in determining the metal inhibition characteristics of the optical urea biosensors is two-fold. Firstly, we would like to produce enzyme biosensors with enhanced resistance to metal inhibition. Interference from metal inhibitors is still one of the major problems facing enzyme biosensors even though immobilized enzymes are relatively less susceptible to metal inhibition than free enzymes in solution. Very few solutions have been proposed so far to circumvent the effects of metal ions on enzyme sensors.[5]. Secondly, we also want to fabricate fibre-optic enzyme biosensors for heavy metal determination based on enzyme inhibition. This technique of metal analysis has several attractive features, including high sensitivity, low

* To whom correspondence should be addressed.

cost, possibility for continuous and automated operations and the ability to reveal information on the toxicity of metal samples. This has been demonstrated in previous publications involving different types of enzyme biosensors[16–18] and enzyme reactor systems coupled with other transducers.[19–22] Obviously, for the latter purpose, biosensors with high sensitivity to metal ions are desirable.

Experimental

Materials

All reagents were obtained from commercial sources and were utilized without further purification. Urease (E.C. 3.5.1.5 from jack beans, Type III, U1500, 27200 U g^{-1}), aminopropyl glass (G4643, av. pore size, 50 nm; 200–400 mesh; 81 μmol of amine per gram of glass) were supplied by Sigma (St. Louis, MO, USA). Urea, Thymol Blue, Na salt and morpholine ethanesulfonic acid monohydrate (MES) were purchased from Aldrich (Gillingham, Dorset, UK). The four coupling reagents used for enzyme immobilization (cyanuric chloride, 25% aqueous glutaraldehyde, phenylene diisothiocyanate and hexamethylene diisocyanate) were also obtained from Aldrich. Formaldehyde solution (37–40%) and maleic acid were provided by BDH–Merck (Lutterwork, Leicestershire, UK).

The heavy metal compounds were obtained from different suppliers: mercury(II) chloride, silver nitrate, lead(II) nitrate, cobalt(II) nitrate hexahydrate, chromium(III) chloride, and zinc(II) nitrate hexahydrate were from BDH–Merck and copper(II) nitrate trihydrate was from Fluka Chemicals (Gillingham, Dorset, UK). The nylon mesh (pore diameter, 40 μm; thread diameter, 37 μm; 330 mesh/in; 27% open area) was kindly provided by Plastok Associations (Wirral, Middleside, UK).

All other chemicals utilized were of analytical-reagent grade. Unless otherwise stated, all reagents were prepared in distilled, de-ionized water.

Procedure

Immobilization of urease on aminopropyl glass resins

The immobilization of urease was carried out on aminopropyl glass resin using four different coupling reagents, namely cyanuric chloride, glutaraldehyde, hexamethylene diisocyanate and phenylene diisothiocyanate. Solutions of these bifunctional reagents were prepared freshly prior to the activation process: 0.025 g of phenylene diisothiocyanate was dissolved in 750 μl of dry acetone; 200 μl of hexamethylene diisocyanate was added to 1.3 ml of dry acetone; saturated solution of cyanuric chloride was made by mixing 0.75 g of the reagent with 2.5 ml of dry acetone, and 5.0% (v/v) glutaraldehyde was prepared by dilution of 25% aqueous stock solution with pH 7.0, 0.1 mol l^{-1} phosphate buffer.

In a typical batch preparation of the immobilized enzyme, 500 μl of the activating reagents were separately added to 10 mg portions of the aminopropyl glass. The reactions were allowed to proceed for at least 2 h at room temperature. Excess of the coupling reagents were carefully decanted and the resins were thoroughly washed with either dry acetone (for cyanuric chloride (**1**), phenylene diisothiocyanate (**2**), and hexamethylene diisocyanate (**3**)-activated resins) or cold pH 7.0, 0.1 mol l^{-1} phosphate buffer [for glutaraldehyde-activated resin (**4**)]. The glass materials were then dried in a desiccator under *vacuo* for around 15–20 min. The dried functionalized glass resins were immediately reacted with urease molecules. Firstly, around 150 μl of buffer solution (pH 8.5, 0.05 mol l^{-1} $Na_2B_4O_7$ buffer for **1**, **2**, and **3**; and pH 7.0, 0.1 mol l^{-1} phosphate buffer for **4**) was added to the glass resins, then 50 μl of urease solution (which was made by dissolving 1.7 mg of urease in 1.5 ml of cold water) was pipetted into the glass suspensions. The mixtures were gently swirled and then left in the refrigerator at 4 °C overnight to allow the covalent bonding of the enzyme. Excess of enzyme reagent and weakly bound biomolecules were removed by thorough washing first with cold water, followed by pH 7.0, 0.1 mol l^{-1} phosphate buffer.

Immobilization of Thymol Blue on aminopropyl glass resins

The covalent immobilization of the acid–base indicator, Thymol Blue, was also performed on aminopropyl glass materials. Around 200 μl of 0.01 mol l^{-1} formaldehyde in 0.1 mol l^{-1} MES solution were first added to 10 mg portions of the glass beads followed by 200 μl of 5 μmol l^{-1} aqueous Thymol Blue in a stoppered, small glass vial. The mixtures were carefully swirled then stored in a preheated oven (50–60 °C) for at least 48 h to effect the covalent binding of the indicator. Thereafter, the glass resins were washed with 2 mol l^{-1} NaCl, then alternately with pH 9.2 and pH 4.0 buffer solutions, followed by distilled water to remove weakly bound or unbound indicators. The washing procedure was also performed with intermittent (3–5 times) and short ultrasonic agitation (10 s) to facilitate a more thorough removal of excess of indicators. The dye-modified glass resins were then stored in pH 7.0, 0.1 mol l^{-1} phosphate buffer for future usage.

Sensor construction and flow cell configuration

The sensitive reagent phase of the biosensor consists of the immobilized urease intimately associated with the bound acid–base indicator. This was made by homogeneously mixing 10 mg portions of the urease-modified glass resins with an equivalent 10 mg aliquot of the Thymol Blue-modified controlled-pore glass. The glass resin mixtures, stored as suspensions in pH 7.0, 0.1 mol l^{-1} phosphate buffer, were kept in a refrigerator when not in use.

For the construction of the optical sensor, an aliquot of the reagent mixture was pipetted and carefully packed into the microwell (150–200 μm deep and 1.5 mm diameter) of a specially fabricated fibre-optic probe head (Fig. 1). The glass resins were tightly held in place using a nylon mesh, which in turn was supported by plastic tubing. The fibre-optic probe was then inserted into a flow cell assembly machined from a Perspex cylinder (1 cm diameter × 1 cm height). The flow cell device incorporated two 19G (1 mm od, 20 mm length) stainless-steel needles, positioned diametrically opposite each other, to serve as solution inlet/outlet. The bottom end of the flow cell was also fitted with a white PTFE plug (at 1.5 mm distance from the probe tip) to provide a reflective surface backing. The internal flow cell volume was approximately 25 μl.

Flow manifold configuration and measurement procedure

The flow cell set-up described above was integrated with the flow manifold shown in Fig. 2, where measurements of the enzymic activity of urease and inhibition by metal compounds were performed. A pH 6.0, 7.5 mmol l^{-1} maleate buffer was used as the carrier solution. To measure the immobilized urease activity, 100 mmol l^{-1} of urea (prepared in the maleate buffer solution) was introduced into the buffer stream, through the second valve, V2 (250 μl loop). Urease catalyses the hydrolysis of urea to ammonia and carbon dioxide, with the corresponding net increase in pH. The change in pH is manifested as a colour change of the immobilized Thymol Blue (brownish yellow → blue) leading to a decrease in the reflectance reading of the sensor (as measured at 600 nm). The

peak obtained is proportional to the urea concentration and corresponds to the reference signal for the inhibition reaction, *i.e.*, absence of inhibition (E_0). At the onset of peak recovery or return to the baseline signal, V2 is switched back to the load position and the metal solution (similarly prepared in the maleate buffer) is introduced through the first valve, V1 (sample loop, 5 ml). After the metal solution plug has completely passed through the flow cell (typically 10–12 min at the given flow rate of 0.5 ml min^{-1}), and when the baseline level has been regained, urea is re-injected to determine the inhibited enzyme activity, E. The percentage inhibition for each metal sample is calculated using the expression,

$$\text{Inhibition (\%)} = [(E_0 - E)/E_0] \times 100 \quad (1)$$

All fibre-optic reflectance measurements were obtained using an optical instrumentation system similar to that described previously.[23]

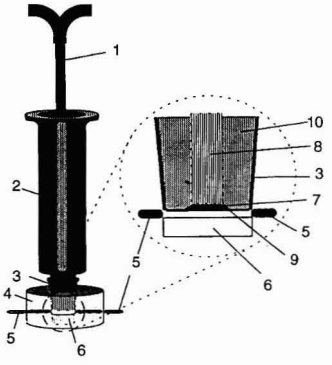

Fig. 1 Configuration of fibre-optic biosensor and flow cell set-up: 1, bifurcated optical fibre bundle; 2, plastic syringe cylinder; 3, body of plastic syringe needle; 4, Perspex cylinder; 5, 19G gauge syringe needles; 6, white PTFE cylinder as reflector; 7, glass resin mixture (containing immobilized urease and thymol blue) packed in a microwell; 8, bare 32-fibre plastic optical fibre bundle affixed to tip of plastic syringe using epoxy adhesive; 9, nylon mesh support; and 10, plastic syringe tip.

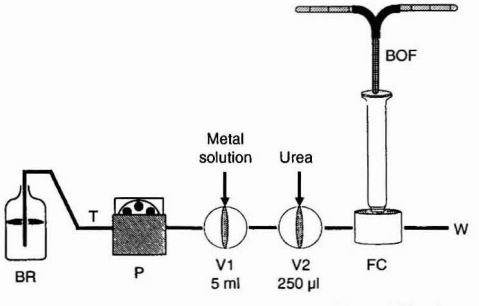

Fig. 2 Flow manifold used for measurement of immobilized urease activity and metal inhibition: BR, buffer reservoir (pH 6.0, 7.5 mmol l^{-1} maleate buffer); T, Teflon tubing (0.8 mm id, except for the sample loop of V1 (1.6 mm id); P, peristaltic pump (Watson Marlow, Model 202U) set at flow rate of 0.5 ml min^{-1}; V1 and V2, injection valves (Rheodyne 5020); FC, flow cell; W, waste; and BOF, bifurcated optical fibre. To maintain constant system temperature, all solution reservoirs, injection valve loops, and the flow cell were immersed in a water-bath kept at 25 °C.

Results and Discussion

Different Coupling Procedures for Urease Immobilization

An aminopropyl-functionalized controlled-pore glass was chosen as the base material for the immobilization of urease. This solid support is amenable to further activation through different chemistries,[24,25] and has proven thus far to be the most widely used for enzyme immobilization. Four coupling reagents were chosen for this study and the reaction schemes for the immobilization are illustrated in Fig. 3. The first method involves the arylation of the support with a trichloro-derivative of *s*-triazine (cyanuric chloride) forming an intermediate, which is reactive towards nucleophiles (especially amino groups and to lesser extent, phenolic-OH) at alkaline pH conditions (pH 8.5–9).[15] This procedure is similar to that commonly employed in the dyeing of cellulosic fibres using reactive dyes, such as Procion dyes.[26] The second procedure involves coupling through glutaraldehyde, which is the most commonly utilized approach for the covalent bonding of enzymes on supports. The method is based on the formation of a Schiff's base (aldimine) linkage between the free amino groups of the enzyme or support, and the carbonyl groups of the dialdehyde. Although, it has also been suggested that the reaction might actually involve the conjugate addition of enzyme amino groups to ethylene double bonds of α,β-unsaturated oligomers of glutaraldehyde, contained in the commercial aqueous preparations of the reagent.[27] The third and fourth immobilization schemes are based on the addition of unprotonated, nucleophilic amino groups on isocyanate and isothiocyanate groups to form stable substituted urea and thiourea products, respectively. The reaction with other nucleophiles of the enzymes, such as thiol, imidazole, aromatic hydroxy and carboxyl groups are not expected to produce stable derivatives here owing to the alkaline conditions employed in the two immobilization processes.[15] These four coupling procedures proved to be effective for the immobilization of urease molecules and for the preparation of the optical biosensors. Not only were the procedures simple, but the immobilized enzyme preparations achieved were also stable and highly active.

Inhibition of Immobilized Urease by Different Metal Ions

The inhibition of the four types of immobilized urease reagents by heavy metal ion salts was tested using two different concentration levels of metal ion solutions (10 and 100 µmol l^{-1}). For each measurement of inhibition, a fresh aliquot of the enzyme reagent (obtained from the stock immobilized enzyme preparation) was used to ensure that the reference signal was always taken from an uninhibited enzyme sensor. The results of this study is summarized in Fig. 4. All of the metal ions tested were inhibitory toward the different immobilized urease preparations, but exhibited varying degrees of inhibiting effects. The most potent inhibitor was Hg^{2+}, while Ag^{+} and Cu^{2+} also exerted strong inhibition on the immobilized urease. Moderate inhibitions were observed from Co^{2+}, Zn^{2+}, Cr^{3+} and Pb^{2+} ions. This variation in the metal inhibition efficiency is normally attributed to the different affinity of the metal ions with the thiol group of the enzyme, which in turn can be correlated with the stability of the respective sulfide salts of the metal ions.[28,29] However, other chemical effects like metal complexation or precipitation may also modify the relative inhibiting power of the metal ions.

It is also evident from Fig. 4, that the four types of immobilized urease preparations have different behaviours towards inhibition by the metal ions. Reagent **1** was generally the most sensitive to inhibition the seven test metal solutions. Slightly lesser inhibition effects were observed for reagents **2**

and **3**. However, in complete contrast with the other three immobilized urease reagents, reagent **4** was virtually immune to inhibition by metal ions. The unique metal inhibition behaviour of urease bound on the isothiocyanate glass can be attributed to the possible metal complexing property of the functionalized resin *via* the thiourea linkages (see Fig. 3). Indeed, the metal binding property of thiourea and some of its derivatives is well recognized and these reagents have found applications as masking reagents,[30–32] extractants,[33] eluents,[34] or preconcentrating agents[35] in metal analysis. Presumably in this study, the metal ions are also bound to the thiourea groups of the glass resins thus preventing or minimizing the inhibition of the immobilized urease.

Sensor Response to Continuous Metal Exposure

The behaviour of the different immobilized urease reagent phases on continuous exposure to a metal ion solution was also investigated. For this study, a 1 μmol l^{-1} Cu^{2+} solution prepared in the maleate buffer was used as the test metal ion solution. The initial response for each enzyme reagent phase was first obtained by injecting a plug of the substrate solution to the carrier buffer solution (pH 6.0, 7.5 mmol l^{-1} maleate buffer). The carrier buffer was then replaced with the copper solution and the sensor response was determined at 1 h intervals thereafter.

Fig. 5 shows the plots of the variation in enzyme activities of the different solid urease reagents as a function of their exposure time to the Cu^{2+} solution. It illustrates that the different immobilized enzymes also varied in their susceptibility towards prolonged contact with a metal ion. Within 2 h of continuous exposure to the copper solution, the urease bound to cyanuric chloride and glutaraldehyde-activated aminopropyl glass exhibited a considerable decrease in their biocatalytic activities. A less drastic decline in the sensor response was observed for urease coupled through hexamethylene diisocyanate linkage. In contrast with the three other immobilized urease preparations, the activity of urease bound onto phenylene diisothiocyanate-activated controlled-pore glass remained high even on prolonged contact with the metal ion. There was only a minimal decrease in the response even after a 6 h exposure to the copper solution. More significantly, the sensor response diminished only slightly even

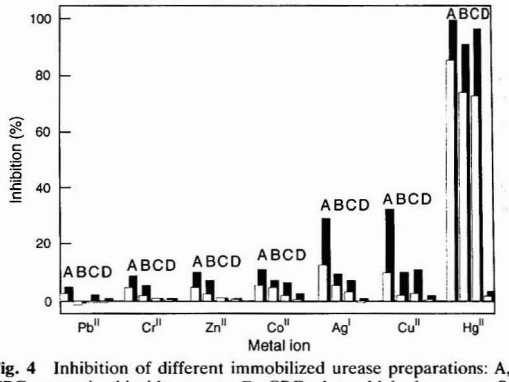

Fig. 4 Inhibition of different immobilized urease preparations: A, CPG–cyanuric chloride–urease; B, CPG–glutaraldehyde–urease; C, CPG–hexamethylene diisocyanate–urease; and D, CPG–phenylene diisothiocyanate–urease by various metal ions (clear bars, 1 μmol l^{-1} and solid black bars, 10 μmol l^{-1}.

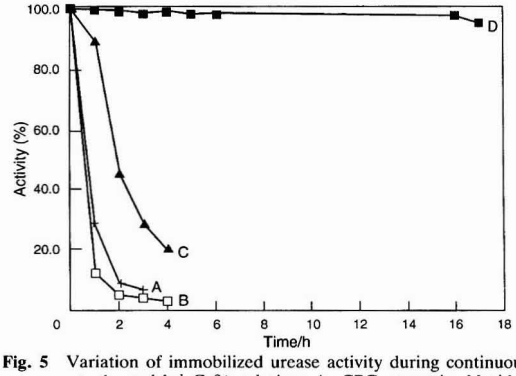

Fig. 5 Variation of immobilized urease activity during continuous exposure to 1 μmol l^{-1} Cu^{2+} solution: A, CPG–cyanuric chloride–urease; B, CPG–glutaraldehyde–urease; C, CPG–hexamethylene diisocyanate–urease; and D, CPG–phenylene diisothiocyanate–urease.

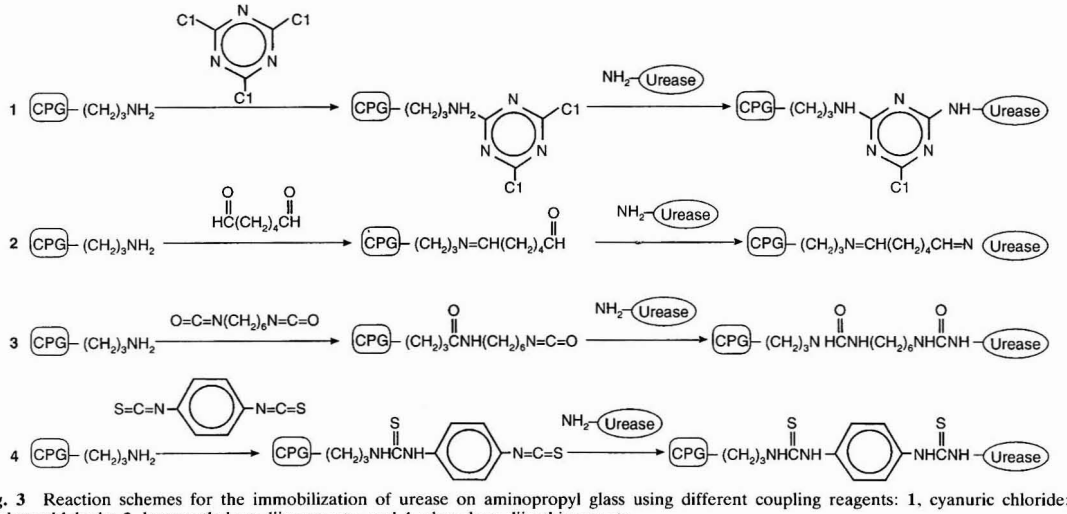

Fig. 3 Reaction schemes for the immobilization of urease on aminopropyl glass using different coupling reagents: **1**, cyanuric chloride; **2**, glutaraldehyde; **3**, hexamethylene diisocyanate; and **4**, phenylene diisothiocyanate.

though the inhibition experiment was continued for another 11 h. It appeared that the immobilized enzyme remained virtually uninhibited even at such exposure times when the metal-binding capacity of the isothiocyanate glass was expected to be exhausted. There are at least two possibilities, which can account for this behaviour. First, the immobilization of urease on isothiocyanate-glass may have induced some favourable conformational changes on the biomolecules that had lowered the accessibility of the essential sulfhydryl groups of urease to the inhibiting metal ions. Second, the flow nature of the measurement process may lead to the desorption of some of the bound metal ions exposing fresh surfaces for metal binding. Consequently, the support is not readily saturated as would be expected from irreversible metal ion attachment.

Urea Biosensing in the Absence/Presence of Metal Ion

In order to demonstrate the biosensing application of the different immobilized urease reagents, their responses to various urea concentrations were determined in the absence and presence of an inhibiting metal ion. Fig. 6(*a*)–(*d*) shows the different calibration graphs obtained for this experiment using 10 μmol l^{-1} Cu^{2+} as the test metal solution. The uninhibited enzyme sensors all exhibited sensitive and rectilinear responses toward urea up to 18 mmol l^{-1} urea concentration. However, in the presence of copper ion, the signals obtained from the immobilized urease reagent **1**, **2** and **3** were very low due to the severity of metal inhibition problems. As a result, the quantification of the urea substrate becomes impossible under these enzyme reagent systems. On the other hand, urease preparation **4** only suffered a relatively small decrease in its sensitivity that urea determination can still be conveniently performed even in the presence of the inhibitor.

However, we expect that a prolonged metal exposure or contact with higher metal concentrations will result in further decrease in the response of reagent **4**. This is owing to the possible eventual depletion of the metal binding sites of the solid support. It is probable that, the prevention or minimization of inhibition is only achieved in so far as there are uncoordinated ligand groups left in the enzyme immobilizing support. In this respect, it is advantageous to have a high initial loading of the coordinating groups in the functionalized solid support to minimize its saturation. Furthermore, the metal binding sites should have strong ligand properties to ensure that the metal ions are preferably attached to the solid support rather than the thiol moiety of the enzyme.

Nonetheless, it is clear from the above results that phenylene diisothiocyanate-activated glass support is a favourable matrix for urease immobilization as it enhances the resistance of the immobilized biocatalyst to metal inhibition. Immobilization on this support promises to improve the operational stability and lifetime of the biosensor, considering that one factor that limits the analytical usefulness of enzymes is their susceptibility to metal inhibition. This immobilization scheme would potentially extend the application of the biosensor in complex sample matrices, which contain relatively high levels of metal ions. It is also a convenient and simpler alternative to the present strategies (*e.g.*, passage through a chelating column or addition of masking reagents) of minimizing the inhibitory effects of metal ions to biosensors. It requires no addition of extraneous reagents to the immobilizing support (*e.g.*, co-entrapped EDTA[5]) as the matrix itself exhibits some metal binding properties. Although the concept presented here is done within the framework of an optical urease biosensor, it could be extended to other types of

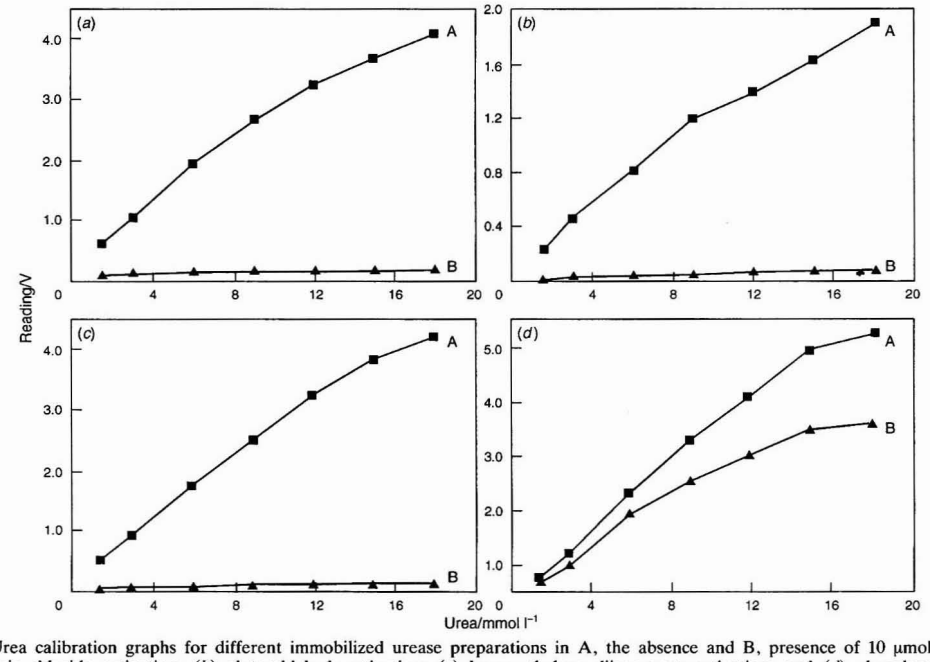

Fig. 6 Urea calibration graphs for different immobilized urease preparations in A, the absence and B, presence of 10 μmol l^{-1} Cu^{2+}: (*a*) cyanuric chloride activation; (*b*) glutaraldehyde-activation; (*c*) hexamethylene diisocyanate-activation; and (*d*) phenylene diisothiocyanate. Curves B were taken after a 30 min pre-incubation of the sensor in the copper solution, but measurements were usually completed only after another hour, throughout which the biosensor remained in continuous contact with the metal solution.

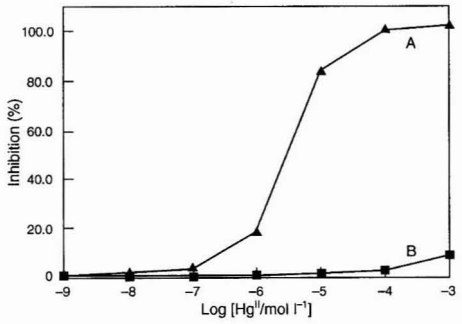

Fig. 7 Calibration graphs for Hg^{2+} based on the inhibition of immobilized urease: A, cyanuric chloride-activation; and B, phenylene diisothiocyanate-activation. Measurement was performed with alternate reactivation with pH 6.0, 0.75 mol l^{-1} diethylenetriaminepentaacetic acid (DTPA).

transducing devices and to other classes of immobilized enzymes.

Metal Ion Biosensing Based on Urease Inhibition

The results obtained also provide an important guideline in the fabrication of a toxic metal ion biosensor based on enzyme inhibition. Figs. 4–6 suggest that in order to produce a biosensor that is sensitive to metal ions, the immobilization scheme should not result in a matrix that contains functional groups, which can potentially interfere in the detection process by binding with the metal ions. One such immobilization strategy involves the use of cyanuric chloride-activated glass as the solid support material. Fig. 7 shows the calibration graphs obtained for the Hg^{2+} ion based on the inhibition of urease bound on cyanuric chloride-activated matrix and phenylene diisothiocyanate-activated glass. Again, the disparate metal inhibition patterns for the two immobilized urease reagents are very obvious. For the first type of glass resin, even a 10 nmol l^{-1} concentration of Hg^{2+} is enough to cause a discernable inhibition (1.7%) on urease, while a 0.1 mmol l^{-1} Hg^{2+} leads to an almost complete inactivation of the enzyme. On the other hand, the Hg^{2+} sensitivity of the latter type of urease reagent (**4**) is significantly lower; a 1 mmol l^{-1} concentration of Hg^{2+} causes only a moderate inhibition (<10%). The first type of biosensor would therefore find more practical application in the determination of toxic metal ions or in screening procedures for the detection for the presence of inhibiting metal ions, *e.g.*, in soil or water samples.

References

1 *Biosensor Principles and Applications*, ed. Blum, L. J., and Coulet, P. R., Marcel Dekker, New York, 1991.
2 Scheller, F., and Schubert, F., *Techniques and Instrumentation in Analytical Chemistry. Vol. 11. Biosensors*, Elsevier Science Publishers, Amsterdam, 1992.
3 *Biosensors: Fundamentals and Applications*, ed. Turner, A. P. F., Karube, I., and Wilson, G. S., Oxford University Press, Oxford, 1987.
4 Vadgama, P., and Crump, P. W., *Analyst*, 1992, **117**, 1657.
5 Wang, J., and Chen, Q., *Anal. Chem.*, 1993, **65**, 2698.
6 Sasso, S. V., Pierce, J. R., Walla, R., and Yacynych, A. M., *Anal. Chem.*, 1990, **62**, 1111.
7 Kallury, K. M. R., Lee, W. E., and Thompson, M., *Anal. Chem.*, 1993, **65**, 2459.
8 Beh, S. K., Moody, G. J., and Thomas, J. D. R., *Analyst*, 1989, **114**, 1421.
9 Gibson, T. D., Hulbert, J. N., Woodward, J. R., *Anal. Chim. Acta*, 1993, **279**, 185.
10 Campanella, L., Mazzei, F., Sammartino, M. P., and Tomassetti, M., *Bioelectrochem. Bioenerg.*, 1990, **23**, 195.
11 Stein, K., and Schwedt, G., *Anal. Chim. Acta*, 1993, **272**, 73.
12 Kumaran, S., and Tran-Minh, C., *Electroanalysis (N.Y.)*, 1992, **4**, 949.
13 *Pierce Catalog and Handbook*, Pierce Chemical Company, Illinois, 1994.
14 Wold, F., in *Methods in Enzymology. Vol. XXV. Enzyme Structure, Part B*, ed. Hirs, C. H. W., and Timasheff, S. N., Academic Press, New York, 1972, pp. 623–651.
15 Goldstein, L., and Manecke, G., in *Applied Biochemistry and Bioengineering, Vol. 1. Immobilised Enzyme Principles*, ed. Wingard, L. B., Katchalski-Katzir, E., and Goldstein, E., Academic Press, New York, 1976, pp. 23–126.
16 Sakai, H., Kaneki, N., Tanaka, H., and Hara, H., *Sens. Mater.*, 1991, **2**, 217.
17 Gayet, J. C., Haouz, A., Geloso-Meyer, A., and Burstein, C., *Biosens. Bioelectron.*, 1993, **8**, 177.
18 Shekhovstova, T. N., Chernetskaya, S. V., Belkova, N. V., and Dolmanova, I. F., *J. Anal. Chem.*, 1994, **49**, 709.
19 Donlan, A. M., Moody, G. J., and Thomas, J. D. R., *Anal. Lett.*, 1989, **22**, 1873.
20 Ogren, L., and Johannson, G., *Anal. Chim. Acta*, 1978, **96**, 1.
21 Bryce, D. W., Fernandez-Romero, J. M., and Luque de Castro, M. D., *Anal. Lett.*, 1994, **27**, 867.
22 Mattiasson, B., Danielsson, B., Hermansson, C., and Mosbach, K., *FEBS Lett.*, 1988, **85**, 203.
23 Ahmad, M., and Narayanaswamy, R., *Anal. Chim. Acta*, 1994, **291**, 255.
24 Lynn, M., in *Immobilised Enzymes, Antigens, Antibodies and Peptides. Preparation and Characterisation*, ed. Weetall, H. H., Marcel Dekker, New York, 1975, pp. 1–48.
25 Weetall, H. H., *Methods in Enzymology, Vol. XLIV. Immobilised Enzymes*, ed. Mosbach, K., Academic Press, New York, 1976, pp. 134–148.
26 Siegel, E., in *The Chemistry of Synthetic Dyes, Vol. VI. Reactive Dyes*, ed. Venkataraman, K., Academic Press, New York, 1972, pp. 1–209.
27 Means, G. E., and Feeney, R. E., *Chemical Modifications of Proteins*, Holden-Day, San Francisco, 1971.
28 Shaw, W. H. R., *J. Am. Chem. Soc.*, 1954, **76**, 2160.
29 Krajewska, B., *J. Chem. Technol. Biotechnol.*, 1991, **52**, 157.
30 Terashima, S., *Anal. Chim. Acta*, 1984, **156**, 301.
31 Desikan, N. R., and Vijayakumar, M., *Analyst*, 1985, **110**, 1399.
32 Suzuki, M., and Ohta, K., *Fresenius' Z. Anal. Chem.*, 1985, **322**, 480.
33 Zuo, G., and Muhammed, M., *Sep. Sci. Technol.*, 1990, **25**, 1785.
34 Hase, A., Kawabata, T., and Terada, K., *Anal. Sci.*, 1990, **6**, 747.
35 Shkinev, V. W., Gomolitskii, V. N., Spivakov, B. Y., Geckeler, K. E., and Bayer, E., *Talanta*, 1989, **36**, 861.

Paper 4/07076C
Received November 21, 1994
Accepted January 27, 1995

Determination of Cyanide Using a Tyrosinase Amperometric Biosensor with Catechol as Substrate

Xiaoya Hu and Zongzhou Leng

Department of Chemistry, Teachers College, Yangzhou University, Jiangsu 225002, China

Low cyanide concentrations are determined with a tyrosinase amperometric biosensor using enzyme immobilized on a preactivated polyamide membrane that is closely attached to the end of a wax-impregnated graphite electrode. The test is performed in the presence of the catechol substrate at −0.200 V *versus* SCE in 0.1 mol l^{-1} phosphate buffer (pH 7.5) (the reduction current results from *o*-benzoquinone, derived from the tyrosinase driving the oxidation of catechol, which is being measured). The decrease in substrate response within the linear range 2.0×10^{-7}–4.0×10^{-5} mol l^{-1} is proportional to the square-root of cyanide concentration. This method is characterized by high selectivity and reproducibility.

Keywords: Cyanide determination; amperometry; biosensor; enzyme electrodes; enzyme inhibition

Introduction

Cyanide is often present in waste water resulting from industrial processes such as electroplating, metal mining and organic synthesis. Because of its extreme toxicity, much research has been devoted to the determination of cyanide. The methods developed range from volumetric[1] to sensitive instrumental techniques such as electrochemical analysis,[2,3] spectrophotometry,[4] chromatography[5] and atomic absorption spectrometry.[6] These methods are typically based on the chemical properties of cyanide rather than its toxic properties. In the detection and determination of cyanide there are certain inherent difficulties. Many procedures require the purification or volatilization of cyanide and most suffer from a lack of specificity and from interferences.

Recently, a biosensor for cyanide detection that mimics the final steps of mitochondrial respiration has attracted increasing attention.[7,8] However, much is still to be desired with respect to the reproducibility and sensitivity of enzyme electrodes, and the process of determination is tedious and complex. In this work, we immobilized tyrosinase on a preactivated polyamide membrane. The immobilization and storage of the enzyme membrane and its replacement are simple and easy to handle. The detection of 1×10^{-7} mol l^{-1} cyanide can be achieved with amperometry in the presence of catechol. Good reproducibility and a useful linear range are obtained.

Experimental

Apparatus

All electrochemical experiments were carried out with a Model DH-1 potentiostat (Changchun Institute of Applied Chemistry, Changchun, China) and a Model 3036 *X–Y* recorder (Fourth Instrument and Meter Plant, Sichuan, China). pH Values were measured on a PDX-12 pH meter (Electroanalytical Instrument Factory, Jiangsu, China).

Reagents

Tyrosinase (EC 1.14.18.1, 2400 U mg^{-1}) was prepared from mushroom (Sigma). Pre-activated polyamide membranes (Immunodyne membrane, 120 μm thickness) were obtained from Pall Industrie (St. Germaine-en-Laye, France) and bovine serum albumin (BSA) from Boehringer (Mannheim, Germany). Other reagents were of analytical-reagent grade.

Immobilization Procedure

The preactivated polyamide membranes have a high density of covalent binding sites able to react with OH, COOH or NH_2 groups present in biomolecules. Enzyme immobilization is achieved by simple wetting of the preactivated polyamide membrane: 10 μl of enzyme solution of 10 mg ml^{-1} concentration in 0.1 mol l^{-1} phosphate buffer (pH 7.0) are applied to both sides of the membrane. The reaction is completed is less than 2 min. The enzymatic membranes on which the enzyme is immobilized with covalent binding are then washed twice with 1 mol l^{-1} KCl–1% m/m BSA and stored at −10 °C in 0.1 mol l^{-1} phosphate buffer (pH 7.0)–10% glycerol.

Enzyme Electrode

A wax-impregnated graphite electrode (WIGE) is polished with filter-paper and the enzymatic membrane is maintained in close contact with the end of this electrode with a screw-cap (Fig. 1). The cyclic voltammogram for catechol and *o*-benzoquinone is obtained with the WIGE in 0.1 mol l^{-1} phosphate buffer (pH 7.5) (Fig. 2). The peak potentials for *o*-benzoquinone reduction and catechol oxidation are −0.064 and 0.391 V (*versus* SCE), respectively.

Measuring Procedure

Experiments are carried out with the three-electrode system. The enzyme electrode is used as the working electrode, a

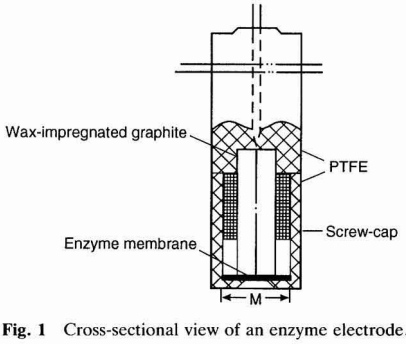

Fig. 1 Cross-sectional view of an enzyme electrode.

saturated calomel electrode (SCE) as the reference electrode and platinum as the counter electrode. The temperature is maintained at 25 °C with a thermostated circulating water-bath. The amperometric response to *o*-benzoquinone derived from the tyrosinase driving the oxidation of catechol is measured at −0.200 V *versus* SCE in 0.1 mol l^{-1} phosphate buffer (pH 7.5). The steady-state response toward the catechol declines on addition of cyanide inhibitor solution. The solutions are stirred with a magnetic stirrer.

Results and Discussion

Tyrosinase from the mushroom *Agaricus bisporus* contains four copper ions per molecule (compared with two copper ions from *Neurospora crassa*).[9,10] There are two active sites per molecule, each containing a pair of copper ions. The enzyme containing two coupled binuclear copper sites, in its resting state, exists mainly as met-tyrosinase. The mechanism of the diphenol reactivity at the coupled binuclear copper active site of tyrosinase has been described.[11] Inhibitor CN^- is known to bind with high affinity to Cu^I and stabilize it[12,13] in a manner that is competitive with oxygen.[11] *o*-Benzoquinone is reduced with the wax-impregnated graphite electrode at −0.200 V *versus* SCE.

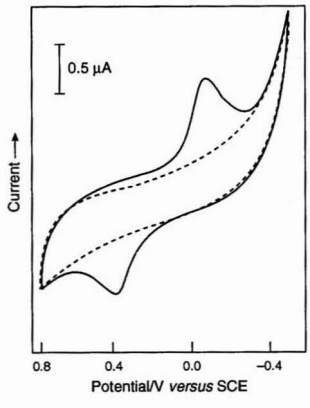

Fig. 2 Cyclic voltammograms for catechol in 0.1 mol l^{-1} phosphate buffer (pH 7.5): working electrode WIGE; scan rate, 36 mV s^{-1}; [catechol], 2.5×10^{-5} mol l^{-1}; and dashed line, catechol absent.

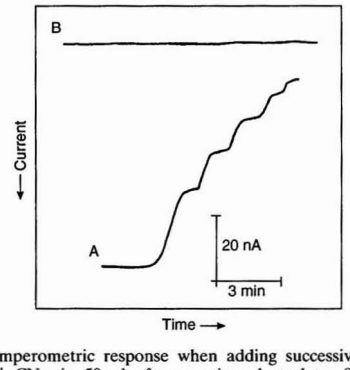

Fig. 3 Amperometric response when adding successively 5 μl of 0.1 mol l^{-1} CN^- in 50 ml of supporting electrolyte, 0.1 mol l^{-1} phosphate buffer (pH 7.5); 5×10^{-6} mol l^{-1} catechol; and potential, −0.200 V *versus* SCE. A, Enzyme electrode; and B, as A but with no enzyme present.

Dependence of Current on CN^- Concentration

The linear response range of the enzyme electrode to catechol is 2.0×10^{-7}–1.25×10^{-5} mol l^{-1} in 0.1 mol l^{-1} phosphate buffer (pH 6.5) at −0.200 V *versus* SCE. Fig. 3 shows the cathodic current with successive additions of CN^- solution at a catechol concentration of 5×10^{-6} mol l^{-1}. No response to CN^- is observed when tyrosinase is absent. Steady-state signals are achieved within 3 min. The decrease in substrate response is proportional to the square root of CN^- concentration with a linear range from 2×10^{-7} to 4.0×10^{-5} mol l^{-1} and a detection limit of 1×10^{-7} mol l^{-1}. The cathodic current is inversely proportional to $[CN^-]^{\frac{1}{2}}$ but not inversely proportional to $[CN^-]$ or $[CN^-]$.[2]

Influence of Substrate Concentration

The sensitivity of the enzyme electrode to CN^- varies with the catechol concentration. The calibration graphs of current *versus* $[CN^-]^{\frac{1}{2}}$ for CN^- in different concentrations of catechol show slopes that increase with increase in catechol concentration. A lower detection limit for CN^- is observed at higher catechol concentrations. Nevertheless, it takes a longer time to reach the steady-state current and the reductive current is unstable if the substrate concentration is too high (5×10^{-5} mol l^{-1}). At low concentrations of the substrate ($<1 \times 10^{-6}$ mol l^{-1}) the enzyme electrode is insensitive to CN^-, and there may even be no response to CN^-. The response of the enzyme electrode to catechol disappears when the CN^- concentration is greater than 7×10^{-5} mol l^{-1}.

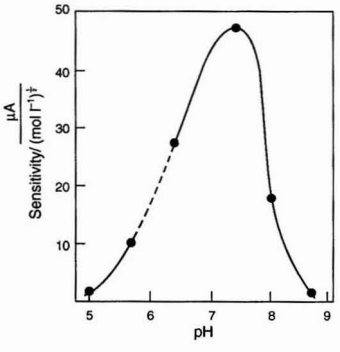

Fig. 4 Influence of pH on cyanide detection.

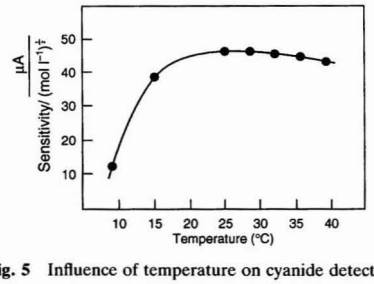

Fig. 5 Influence of temperature on cyanide detection.

Influence of pH

The influence of the pH of the reaction medium on the measurement of catechol and CN^- was studied with the enzyme electrode. The optimum sensitivity for catechol is observed in 0.1 mol l^{-1} phosphate buffer (pH 6.5). Fig. 4 indicates that the optimum sensitivity for CN^- occurs in 0.1 mol l^{-1} phosphate buffer (pH 7.5). The inhibitor exists as HCN in the acid solution, which makes it less likely for CN^- to bind with the copper active sites in tyrosinase. The sensitivity decreases sharply when the pH of medium is greater than 7.7.

Influence of Temperature

The relationship between the sensor sensitivity for cyanide and temperature was studied within the range 10–40 °C. Fig. 5 shows the influence of temperature on the determination of CN^-. The optimum temperature of CN^- detection is 20–30 °C. The sensor shows a slow response and has poor sensitivity below 10 °C. The stability and lifetime of enzyme electrode decrease when the temperature is greater than 35 °C.

Interferences

No interferences were observed in the presence of 500-fold concentrations of K^+, NH_4^+, Cl^-, NO_3^-, OAc^-, glucose, tartrate, citrate and EDTA and 250-fold concentrations of Ca^{2+} and Mg^{2+} when low concentrations of CN^-, *e.g.*, 2×10^{-6} mol l^{-1}, were measured. Large interferences from ascorbic acid and phenol are observed as phenol is the substrate of tyrosinase and ascorbic acid can react instantaneously with *o*-benzoquinone. The latter results in a decrease in the reductive current. The tyrosinase is not directly attacked by ascorbic acid.

Stability and Lifetime

The inhibition of cyanide to tyrosinase is reversible. Therefore, the enzyme membrane can be used repeatedly provided that the enzyme electrode is washed for 5 min with 0.1 mol l^{-1} phosphate buffer (pH 7.5) after each determiantion of CN^-. The enzyme membranes are stored in 0.1 mol l^{-1} phosphate buffer (pH 7.0)–10% glycerol at −10 °C. No decrease in the initial sensitivity was observed during 4 months. The same characteristics of the enzyme electrode are obtained when enzyme membranes are replaced. This is important for research on the characteristics of the enzyme or biosensor.

Table 1 Results of recovery of cyanide added to standard synthetic water samples

Cyanide added/μg	Cyanide found*/μg	Recovery* (%)
0.65	0.64	98.5
1.3	1.4	108
6.5	6.7	103
26	25	96.2

* Each value is the mean of three determinations.

Sample Analysis

The recovery from standard synthetic water samples was measured using the standard additions method with the tyrosinase amperometric biosensor and the results are given in Table 1. The average of recovery is 101.4%, with a standard deviation is of 5.2%.

We gratefully acknowledge financial support from the Natural Sciences Fund of Jiangsu Education Commission. The authors are also grateful to P. R. Coulet (Université Lyon, France) for kindly providing pre-activated polyamide membranes.

References

1 Singh, H. B., Wasi, N., and Wehra, W. C., *Int. J. Environ. Anal. Chem.*, 1986, **26**, 115.
2 Budimir, M. V., Sak-Bosnar, M., and Jovanovic, M. S., *Ion-Sel. Electrode, Proc. 5th Symp.*, 1988, **5**, 345.
3 Nikolic, S. D., Milosavljevic, E. B., Hendrix, J. L., and Nelson, J. H., 1992, **117**, 47.
4 Zhu, Z. H., and Fang, Z. L., *Anal. Chim. Acta*, 1987, **198**, 25.
5 Valentour, J. C., Aggarwal, V., and Sunshine, J., *Anal. Chem.*, 1974, **46**, 924.
6 Haj-Hussein, A. Y., Christian, G. D., and Růžička, J., *Anal. Chem.*, 1986, **58**, 38.
7 Smit, M. H., and Rechnitz, G. A., *Anal. Chem.*, 1993, **65**, 380.
8 Smit, M. H., and Cass, A. E. G., *Anal. Chem.*, 1990, **62**, 2429.
9 Yong, G., Leone, C., and Strothkamp, K. G., *Biochemistry*, 1990, **29**, 9684.
10 Himmelwright, R. S., Eickman, N. C., Lubien, C. D., Lerch, K., and Solomon, E. I., *J. Am. Chem. Soc.*, 1980, **102**, 7339.
11 Wilcox, D. E., Porras, A. G., Wang, Y. T., Lerch, K., Winkler, M. E., and Solomon, E. I., *J. Am. Chem. Soc.*, 1985, **107**, 4015.
12 Beltramini, M., Salvato, B., Santamaria, M., and Lerch, K., *Biochim. Biophys. Acta*, 1990, **1040**, 365.
13 Cotton, F. A., and Wilkinson, G., *Advanced Inorganic Chemistry*, Wiley, New York, 4th edn., 1980.

Paper 4/05957C
Received September 29, 1994
Accepted December 16, 1994

Flow Injection Detection of Tetracyclines by Electrocatalytic Oxidation at a Nickel-modified Glassy Carbon Electrode

W. Oungpipat

Department of Analytical Chemistry, School of Chemistry, The University of New South Wales, Sydney, NSW 2052, Australia

P. Southwell-Keely*

Department of Organic Chemistry, School of Chemistry, The University of New South Wales, Sydney, NSW 2052, Australia

P. W. Alexander*

Department of Physical Science, University of Tasmania, P.O. Box 1214, Launceston, TAS 7250, Australia

The electrocatalytic oxidation of tetracyclines in an alkaline solution at a nickel-modified glassy carbon electrode was investigated. The response of the modified electrode was characterized by voltammetry and flow injection. Subsequently, it was used for amperometric detection of tetracyclines in a flow injection system. The preparation of the modified electrode is carried out by simple deposition of Ni^{II} solution onto the glassy carbon-based electrode. The detection is based on the measurement of anodic current generated by the catalytic oxidation of the antibiotics at the surface of the electrode through the formation of a high-valent, oxyhydroxide species (NiOOH) at +550 V (*versus* Ag/AgCl). The modified electrode offers a stable and reproducible catalytic oxidation current for these antibiotics without recourse to pulsed waveform potential. Rapid quantification at the mg l^{-1} (ppm) level is achieved. Standard calibration graphs for tetracycline, doxycycline, oxytetracycline and chlortetracycline yielded linear ranges of 2.5–80, 2.5–100, 2.5–100 and 2.5–100 mg l^{-1}, respectively. Detection limits (S/N = 3) of (0.03, 0.92, 0.34 and 1.81 mg l^{-1} were obtained for tetracycline, doxycycline, oxytetracycline and chlortetracycline, respectively. The electrode was applied for the determination of the four antibiotics in single-component drug formulations.

Keywords: Nickel-modified glassy carbon electrode; tetracycline; doxycycline; oxytetracycline; chlortetracycline; flow injection

Introduction

Tetracyclines are a group of clinical, broad spectrum antibiotics having a wide range of activity against numerous human and animal pathogens. They are also found to be useful in agriculture and animal husbandry. Because of their practical importance, the assay of tetracyclines has received considerable attention.

Numerous methods have been reported for the determination of tetracyclines. These include titrimetric,[1] spectrophotometric,[2–5] spectrofluorimetric,[6–9] chemiluminescence,[10] high-pressure liquid chromatography[11–13] and electrochemical methods.[14–17] Among these methods, electrochemical detection is very attractive owing to the high sensitivity and wide dynamic range achievable.

Polarographic techniques[14–15] and stripping voltammetry[16] have been suggested for the analysis of tetracyclines. These methods offer a high sensitivity. The major disadvantage, however, is the need for complicated equipment that is not commonly available in all laboratories. In addition, these techniques involve the use of mercury, which is a toxic substance and may be undesirable for many practical applications, including flow injection. Ion-selective electrodes for tetracycline detection have also been reported;[17] however, long response times and a long preparation time for these electrodes are drawbacks. Unlike the methods mentioned above, amperometric detection has been shown to have a rapid response and high sensitivity while involving the use of simple equipment. The analytical performance of amperometry is, however, dependent on the electrode material.

Noble metals (*e.g.*, Pt and Au) have been used as electrode materials for electrochemical detection of many organic compounds including tetracyclines.[18] It has often been found that the accumulation of reactant and/or products onto the surface of these electrodes leads to electrode fouling. Glassy carbon is widely used in electroanalytical applications owing to its good electrical conductivity, large anodic window in several solvents, very low surface porosity and low residual current. The major drawback is owing to a high over-potential for the oxidation of many organic compounds.

Recently, the construction of chemically modified electrodes (CMEs) has attracted much interest for lowering the operational potential required to oxidize scarcely electroactive organic compounds. Reduced electrode fouling has also been reported. CMEs based on the modification of glassy carbon or graphite rods with metal (*e.g.*, copper,[19–21] cobalt[22] and nickel[23–27]) have shown a catalytic activity towards polyhydroxy compounds. These electrodes have been successfully applied to detect carbohydrates,[19,22–25] amino acids[25,27] sugars[20] and aliphatic alcohol[26] compounds using constant-potential amperometric detection. They have proved to offer a low detection limit and a stable response over a long operation time without using specialized pulse sequences to enhance electrode stability. However, the Ni–CME has not been used previously to detect tetracyclines.

The advantages of such CMEs and their application to the analysis of tetracyclines have prompted attempts to investigate the potential use of such electrodes for antibiotic assays. In addition, to the best of our knowledge, tetracyclines have not previously been determined in drug formulations by electrochemical catalysis in flow injection (FI) systems. in this

* To whom correspondence should be addressed.

work, a nickel-modified glassy carbon electrode (Ni–GCCME) in alkaline solution was therefore characterized and the application of this CME for the detection of tetracyclines in an FI system is described. Tetracyclines have a number of hydroxy groups available. These allow catalytic oxidation of the antibiotic at a Ni–GCCME to occur on electrooxidation of the Ni^{II} oxide to Ni^{III} oxide hydroxide (NiOOH) at +550 mV *versus* Ag/AgCl.

Experimental

Reagents

Tetracycline (TC), oxytetracycline (OTC), chlortetracycline (CTC) and doxycycline (DC) were purchased from Sigma–Aldrich (Castle Hill, New South Wales, Australia). All tetracyclines were in the form of their hydrochlorides. $Nickel^{II}$ sulfate and potassium hydroxide were obtained from Ajax Chemicals (Auburn, New South Wales, Australia). Samples of tetracycline capsules were purchased from a local pharmacy in Thailand and were kept in a desiccator placed in a refrigerator. All solutions were prepared from analytical-reagent grade materials as received in distilled, de-ionized water. Stock solutions of tetracyclines were prepared freshly prior to use.

Apparatus

Cyclic voltammetric experiments and static amperometric measurements were performed in a three-electrode cell using a nickel-modified working electrode, an Ag/AgCl reference electrode and a platinum wire counter electrode. The electrodes were connected to a cyclic voltammograph [Bioanalytical Systems (BAS), West Lafayette, IN, USA] Model CV-1b and a digital multimeter (Mironta). The output was displayed on a Graphtec *X–Y* recorder (Model WX 4425, Japan) and Omniscribe strip-chart recorder for cyclic voltammetric and amperometric measurements, respectively. A magnetic stirrer and a stirring bar provided the convective transport for the static amperometric experiments.

Amperometric measurements in the flow injection system were conducted using a BAS Model CV-1b cyclic voltammograph. A flow-through thin-layer electrochemical cell consisting of dual glassy carbon electrodes (GCEs) in serial configuration (BAS) was used. The working electrode was modified with nickel. The Ag/AgCl and stainless steel were used as reference and auxiliary electrodes, respectively. The output signal was recorded on an Omniscribe strip-chart recorder. Flow injection experiments were carried out using a peristaltic pump (Waters, Milford, MA, USA) Model 510 equipped with an injector valve using a 90 μl sample loop.

Electrode Preparation

Prior to modification with nickel, a GCE with an area of 0.47 cm^2 was polished with alumina slurries (BAS) for use in cyclic voltammetric and static amperometric measurements. The residual polishing material was subsequently removed from the surface by ultrasonication in doubly distilled water and the electrode allowed to dry in air.

The deposition of nickel onto the surface of the polished GCE was performed as follows. A measured volume (10 μl) of 0.1 mol l^{-1} nickel sulfate solution was deposited onto the electrode *via* a micropipette. The electrode was then allowed to dry in an air oven at 40 °C for 30 min and washed with distilled water.

The same procedure was followed for the deposition of Ni^{II} onto the surface of a dual GCE (surface area of 0.47 cm^2) for use in the amperometric measurements in the flow system. Except if stated otherwise, 5 μl of 1×10^{-4} mol l^{-1} nickel sulfate was applied to the electrode surface.

Procedures

Cyclic voltammetry was performed in an unstirred 0.1 mol l^{-1} potassium hydroxide solution. The test solutions were not deaerated. Voltammograms were recorded using a cyclic potential sweep between 0 and +900 mV with an initial value of 0.00 mV. The scan rate was 20 mV s^{-1}.

Static amperometric measurements were performed after successive injections of aliquots of stock tetracycline solutions. The electrodes were immersed into an electrochemical glass cell containing 10 ml of 0.10 mol l^{-1} potassium hydroxide. After a constant potential of +550 mV *versus* Ag/AgCl had been applied to the working electrode, the background current was allowed to decay to a steady-state. Following this initial stabilization step, aliquots of stock tetracycline solutions were added to the cell while the current–time data were recorded. The net signal (ΔI) obtained by subtracting the background current from the sample current was used for subsequent interpretation of the data. All experiments were performed at room temperature.

Flow amperometric measurements were conducted using the procedures described above. The electrode was conditioned in a solution of potassium hydroxide pumped through the flow system with a constant flow rate of 0.2 ml min^{-1} (except if stated otherwise) at +550 mV until a stable baseline was established. The sample was then injected into the flow injection system *via* an injection valve equipped with a fixed sample loop of 90 μl. The resulting peaks were recorded. Again, the net signal (ΔI) was used for subsequent interpretation of the data. All experiments were performed at room temperature.

Preparation of Samples

Samples of tetracycline capsules were treated as follows. The contents of 20 capsules were disintegrated and weighed. An accurately weighed portion of not less than 200 mg was transferred into a 100 ml calibrated flask and diluted to volume with water. The appropriate volume from this sample solution was taken and the same procedure followed as for the standard solution so that the final analyte concentration was within the working range.

Results and Discussion

Cyclic Voltammetry

The electrochemical response of the Ni–GCCME was first investigated by cyclic voltammetry in 0.10 mol l^{-1} KOH. The current–potential curves were recorded after attaining a steady-state response.

Fig. 1 demonstrates cyclic voltammograms of a GCE (A) and a Ni–GCCME (B) in 0.1 mol l^{-1} KOH. It can be seen that neither anodic nor cathodic waves were observed on the GCE. In contrast, well-defined waves were established on the Ni–GCCME. The fact that there were no redox-active substances present in the solution implies a deposition of the Ni^{II} onto the polished GCE. Therefore the oxidation and reduction responses for the Ni–GCCME obtained at an anodic peak current (E_{pa}) of + 550 mV and cathodic peak current (E_{pc}) of +450 mV can be assigned to the Ni^{II}/Ni^{III} couple. The proposed redox process may be represented by the following equation:[28]

$$Ni(OH)_2 + OH^- \leftrightharpoons NiO(OH) + H_2O + e^- \quad (1)$$

It was observed that the anodic peak current was dependent on scan rate. This behaviour is depicted in Fig. 2. A linear

relationship of the plot between the anodic peak current (I_{pa}) and square root of the scan rate was established. This indicates diffusion control[29,30] for the Ni^{II}/Ni^{III} redox response. In addition, it appeared that the anodic peak potential shifted towards the positive direction with an increase in scan rate, while the cathodic peak shifted towards a more negative potential.

When the Ni–GCCME was immersed in a KOH solution containing tetracyclines, an increase in the anodic current and a decrease in the cathodic current were observed. The results indicated that a Ni–GCCME can catalyse the electro-oxidation of tetracyclines due to the existence of Ni^{II} on the surface of the Ni–GCCME. By contrast, an electrocatalytic reaction was not observed at the GCE in the presence of tetracyclines. This is shown by the lack of change in the cyclic voltammograms on the GCE in the presence of tetracyclines compared with that in KOH alone. Typical cyclic voltammograms obtained on the GCE (Fig. 3, A) and Ni–GCCME (B) immersed in an alkaline solution in the presence of DC, TC, OTC and CTC are illustrated in Fig. 3, (*a*)–(*d*), respectively. Similar behaviour for each of the tetracyclines was observed. However, the difference in anodic currents generated by these tetracyclines at the Ni–GCCME indicates the different ability of such tetracyclines to be oxidized at the surface of the electrode.

The electrocatalytic mechanism observed is similar to that reported for electrocatalytic oxidation of other polyhydroxy compounds at a nickel wire electrode.[28] In strong alkaline solution, an active Ni^{III} oxide (NiOOH) is formed on the surface of the electrode. This species acts as a strong oxidant and reacts with tetracyclines resulting in the increase in anodic current. The catalytic oxidation was found to be proportional to the concentration of tetracyclines as shown in Fig. 4.

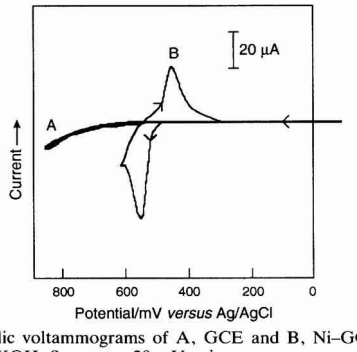

Fig. 1 Cyclic voltammograms of A, GCE and B, Ni–GCCME in 0.1 mol l^{-1} KOH. Scan rate, 20 mV s^{-1}.

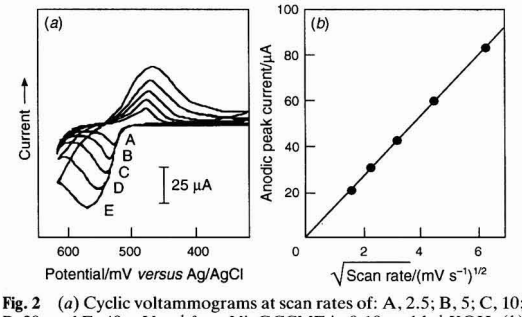

Fig. 2 (*a*) Cyclic voltammograms at scan rates of: A, 2.5; B, 5; C, 10; D, 20; and E, 40 mV s^{-1} for a Ni–GCCME in 0.10 mol l^{-1} KOH. (*b*) Graph of anodic peak current *versus* square root of scan rate.

Moreover, it was found that the catalytic current after the addition of the tetracyclines remained under diffusion control. This is shown by the linear relationship between peak current obtained in the presence of tetracyclines and the square root of the scan rate (not shown).

Constant-potential Amperometry in Stirred Solutions

Batch measurements at a fixed-potential were utilized to investigate amperometric applications of the Ni–GCCME.

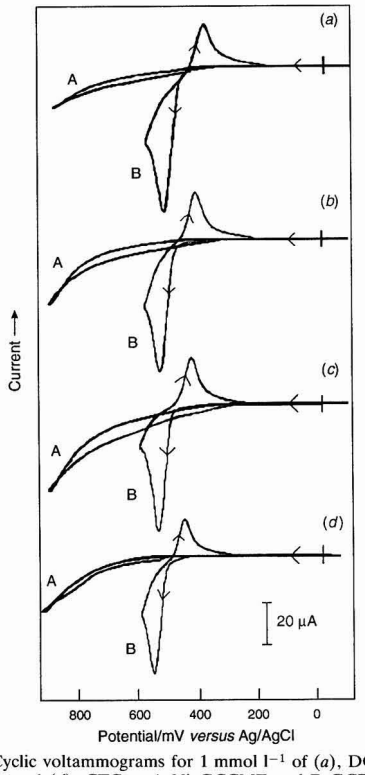

Fig. 3 Cyclic voltammograms for 1 mmol l^{-1} of (*a*), DC; (*b*), TC; (*c*), OTC; and (*d*), CTC at A Ni–GCCME and B GCE. Solution, 0.10 mol l^{-1} KOH; scan rate, 20 mV s^{-1}.

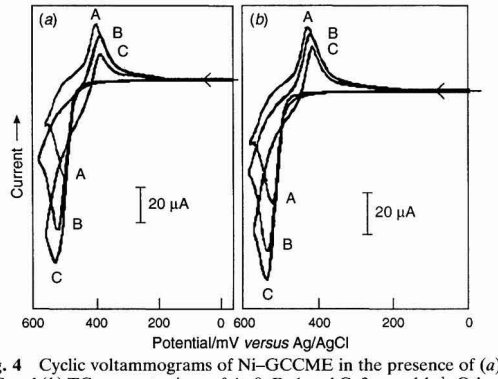

Fig. 4 Cyclic voltammograms of Ni–GCCME in the presence of (*a*) DC and (*b*) TC concentrations of A, 0; B, 1 and C, 3 mmol l^{-1}. Other experimental conditions as in Fig. 3.

Fig. 5 displays typical response of the Ni–GCCME and GCE to successive increments of 2 mg l^{-1} of tetracycline concentration. The modified electrode gives a rapid change in response to the added tetracyclines, yielding a steady-state response within 30 s. High sensitivity is indicated by well defined response at low concentrations (mg l^{-1}) of the substrate. The initial slopes of the linear range for CTC (E), OTC (F), TC (G) and DC (H) were found to be 0.05, 0.09, 0.12 and 0.13 μA l mg^{-1}, respectively. Deviation from linearity was observed at tetracycline concentrations of 9.76 (CTC), 29.63 (OTC), 19.05 (TC) and 13.53 (DC) mg l^{-1}. Detection limits (S/N = 3) of 0.19, 0.20, 0.27 and 0.17 mg l^{-1} were achieved for CTC, OTC, TC and DC, respectively. In contrast, no response was observed for analogous measurements at the GCE.

Flow Injection

Optimization of experimental variables

The effect of various parameters on the amperometric response of tetracyclines in flow injection was investigated to optimize the FI performance. These include the effect of applied potential, the hydroxide concentration, the flow rate and the Ni^{II} loading concentration.

Fig. 6 illustrates hydrodynamic voltammetric curves for CTC (A), OTC (B), TC (C) and DC (D) measured within the potential range +350 to +600 mV (*versus* Ag/AgCl). It can be seen that the optimum potential resulting in the highest electrode response for all the tetracyclines occurs at +550 mV. No significant current was observed within the same potential range for a plain GCE. This confirms the results for cyclic voltammetry described earlier, where the peak owing to tetracycline oxidation appeared when Ni^{III} species were produced. Based on these results, a potential of +550 mV was selected for amperometric studies in FI.

The electrode dependence on hydroxide concentration is shown in Fig. 7 for CTC (A), OTC (B), TC (C) and DC (D). The response was similar for all the tetracyclines studied. The response of the electrode increased as the hydroxide concentration was increased from 0.01 to 0.15 mol l^{-1}. Further increase in the hydroxide concentration beyond 0.15 mol l^{-1} caused a decrease in the electrode response. These results indicate that hydroxide ion is involved in the reaction mechanism. Moreover, it was observed that the higher the concentration of hydroxide concentration utilized, the higher the background current obtained. In fact, the current background increased from 0.10 to about 0.55 μA as the hydroxide concentration increased from 0.1 to 0.3 mol l^{-1}. Hence, the

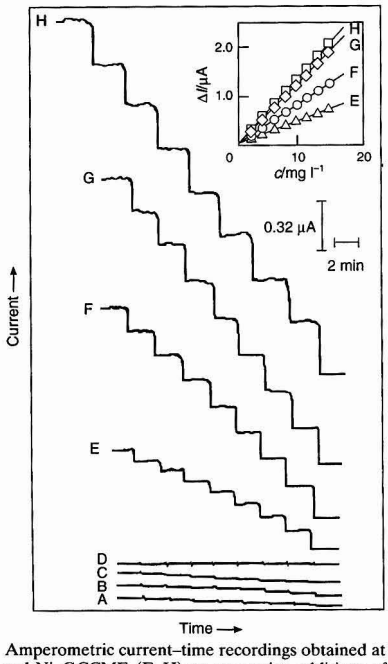

Fig. 5 Amperometric current–time recordings obtained at the GCE (A–D) and Ni–GCCME (E–H) on successive additions of 2 mg l^{-1} CTC (A and E), OTC (B and F), TC (C and G) and DC (D and H). Solution, 0.1 mol l^{-1} KOH; operating potential, +550 mV. Inset shows straight line calibrations for E–H.

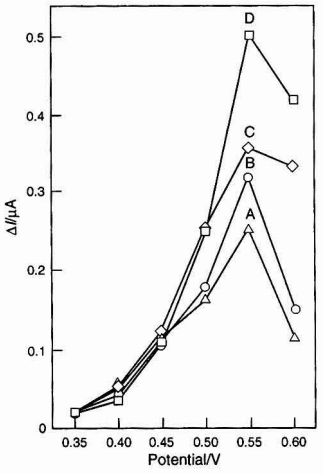

Fig. 6 Hydrodynamic voltammograms in FI at a Ni–GCCME for A, CTC; B, OTC; C, TC; and D, DC injection volume, 90 μl; carrier, 0.10 mol l^{-1} KOH; flow rate, 2 ml min^{-1}; analyte concentration, 20 mg l^{-1}.

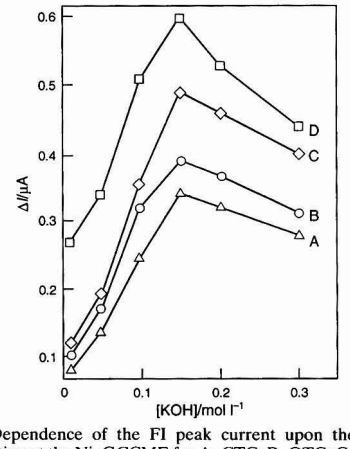

Fig. 7 Dependence of the FI peak current upon the hydroxide concentration at the Ni–GCCME for A, CTC; B, OTC; C, TC; and D, DC. Concentration of each compound, 20 mg l^{-1}; applied potential, +550 mV *versus* Ag/AgCl; carrier, 0.10 mol l^{-1} KOH; flow rate, 2 ml min^{-1}.

hydroxide concentration of 0.10 mol l^{-1} was chosen for further studies as the best compromise between the electrode sensitivity and the background current.

Fig. 8 shows the effect of the flow rate on the electrode response to CTC (A), OTC (B), TC (C) and DC (D) followed by varying the flow rate from 0.5 to 3.0 ml min^{-1}. Again, a similar trend for all the tetracyclines studied was observed. The electrode response increased rapidly when the flow rate of the hydroxide solution was increased from 0.5 to 1.0 ml min^{-1}. Increasing the flow rate to higher than 2.0 ml min^{-1} did not cause a significant change from that obtained for the lower flow rates. The dependence of electrode response on flow rate up to 2.0 ml min^{-1} may be attributed to the increase in convective mass transport at the electrode surface. The limited electrode response at flow rates higher than 2.0 ml min^{-1} may be due to the rate-limiting step for electron transfer at the electrode. The flow rate of the hydroxide carrier stream was therefore set at 2 ml min^{-1}.

The loading concentration of Ni^{II} on the surface of the GCE showed a profound effect on the Ni–GCCME response. Fig. 9 compares the electrode sensitivity obtained after varying the concentration of applied Ni^{II} solution from 2×10^{-5} to 2×10^{-4} mol l^{-1}. It was observed that the higher the concentration of Ni^{II} applied, the higher the electrode sensitivity and the background current obtained. This behaviour could be attributed to the higher concentration of the active nickel^{III} oxide (NiOOH) formed on the Ni–GCCME surface at higher Ni^{II} loading. This allows improved oxidation of tetracyclines to be achieved. The phenomenon again implies that the oxidation of tetracyclines at Ni–GCCME may occur on electro-oxidation of Ni^{II} oxide to Ni^{III} oxide hydroxide (NiOOH). The concentration of 1×10^{-4} mol l^{-1} of Ni^{II} solution was chosen for application to the GCE surface as a compromise of the highest electrode sensitivity and the signal-to-noise characteristic throughout the work.

Electrode calibration

Fig. 10 shows typical chart recordings for FI response. Calibration graphs were constructed for DC (*a*), TC (*b*), OTC (*c*) and CTC (*d*) using the optimized conditions described above. The graphs were found to be linear over the concentration range 0–125 μg ml^{-1} giving positive sloped lines of equation $y = mx + c$ and correlation coefficients of 0.997 (DC), 0.996 (TC), 0.996 (OTC) and 0.999 (CTC). Table 1 lists the analytical parameters obtained for the four antibiotics. The results show that the electrode sensitivity to the four antibiotics is of the following order: DC > TC > OTC > CTC. From the structures and molecular masses of the tetracyclines listed in Table 2, it appears that the rate of oxidation increases as the molecular mass of the antibiotic decreases. In addition, the steric effect of the group adjacent to the hydroxy groups could explain the reduced response obtained for TC in comparison with the response obtained for DC with the same molecular mass.

A linear calibration range up to 100 mg l^{-1} was found for DC, OTC and CTC and up to 80 mg l^{-1} for TC. These ranges are wider than those previously reported for tetracycline assay by chemiluminescence in a flow injection system.[10] Reasonable detection limits (S/N = 3) were obtained for the four antibiotics, the lowest value being 0.03 mg l^{-1} in the case of TC.

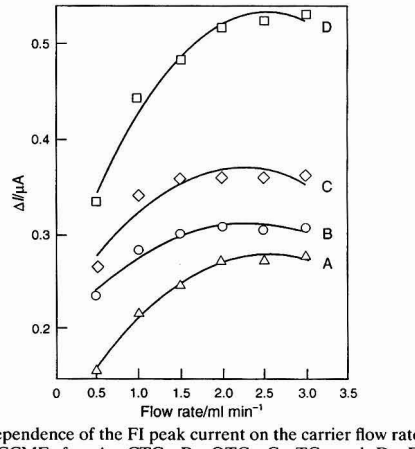

Fig. 8 Dependence of the FI peak current on the carrier flow rate at the Ni–GCCME for A, CTC; B, OTC; C, TC; and D, DC. Concentration of carrier, 0.10 mol l^{-1} KOH. Other experimental conditions as in Fig. 6.

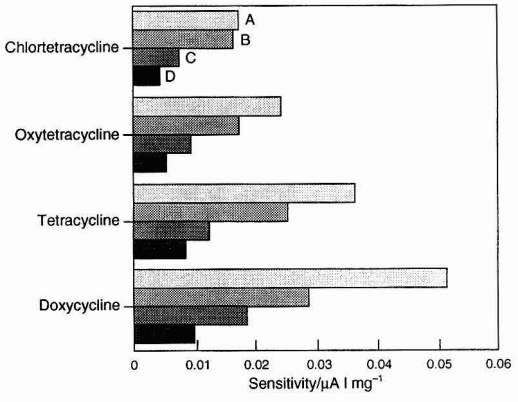

Fig. 9 Dependence of electrode sensitivity on the loading composition of Ni^{II} onto GCE at Ni–GCCME in FI of the antibiotics. A, 2.0×10^{-4}; B, 1.0×10^{-4}; C, 5.0×10^{-5}; and D, 2.5×10^{-5} mol l^{-1} Ni^{II}. Flow rate of carrier, 2 ml min^{-1}. Other experiment conditions as in Fig. 7.

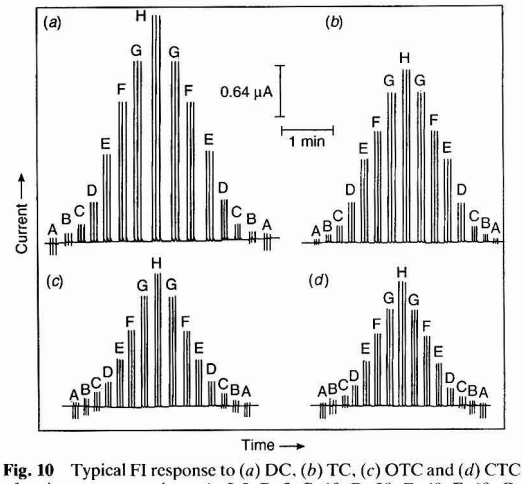

Fig. 10 Typical FI response to (*a*) DC, (*b*) TC, (*c*) OTC and (*d*) CTC of various concentrations: A, 2.5; B, 5; C, 10; D, 20; E, 40; F, 60; G, 80; and H, 100 mg l^{-1} at Ni–GCCME. Sample volume, 90 μl; carrier solution, 0.1 mol l^{-1} KOH; flow rate, 2 ml min^{-1}; potential, +550 mV *versus* Ag/AgCl.

The Ni–GCCME showed good reproducibility as evidenced by the results obtained for 30 repetitive injections of standard solutions. Low relative standard deviations of 1.58, 1.86, 2.57 and 3.20% were established for DC, TC, OTC and CTC, respectively. The half peak-widths were found to be 0.4 min for the oxidation of DC and TC and 0.2 min for OTC and CTC. These allow injection rates of 75 samples h^{-1} for DC and TC and 150 samples h^{-1} for OTC and CTC to be achieved. The high sample throughput reflects the inherent advantage of the FI technique over the batch measurements. The response time (time from injection to reading <6 s) was considered to be sufficiently fast to ensure that the degradation of tetracyclines in alkaline carrier solution was insignificant. No carry-over was noticed between repetitive sample injections, as shown in Fig. 10.

Electrode stability

One important parameter when considering the merit of the electrode in the flow system is the electrode stability. To investigate the present electrode stability, aliquots of a standard solution of DC (10 mg l^{-1}) were injected into the FI system under the optimized conditions. Fig. 11 illustrates the mean peak currents (B) for every 10 injections of DC, the corresponding relative standard deviation (A) and standard deviation (C). The results indicate a favourable stability with a relative standard deviation of 2.68% after 450 injections. The variation of background current within 450 injections was found to be less than 2%. A slight decline in the reproducibility after 400 repetitive injections of DC was noticed. This decline may be ascribed to the leaching of Ni^{II} from the surface of the Ni–GCCME during continuous rinsing with the alkaline carrier solution. The stable response over a long period of operation shows the great promise of such a CME for flow injection and indicates that there is little electrode fouling in the amperometric system achieved without the use of a pulsed waveform potential.

Electrode accuracy

The accuracy of determining tetracyclines using the Ni–GCCME was examined by performing recovery tests. These were carried out by adding a known amount of each of the tetracyclines to their corresponding drug formulations. The amount of tetracycline in commercial samples was also determined by the proposed method. The average results of six analyses of each sample are presented in Table 3. A mean recovery of 100.3% was found with a range of 98.60–101.78%. The proposed electrode, therefore, offers good accuracy, suitable for use in analysing the tetracyclines in commercial drug formulations.

Determination of Tetracyclines in Drug Formulations

The Ni–GCCME was evaluated for the analysis of commercial drug formulations of capsules in which tetracyclines were the only active component. The composition of each capsule formulation is listed in Table 4. Preparations of the drug

Table 2 Structures and molecular masses of the tetracyclines studied

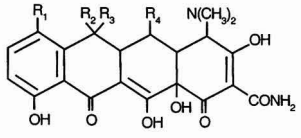

R^1	R^2	R^3	R^4	Name (abbreviation)	Molecular mass
H	OH	CH_3	H	Tetracycline (TC)	444.4
H	OH	CH_3	OH	Oxytetracycline (OTC)	460.0
Cl	OH	CH_3	H	Chlortetracycline (CTC)	478.8
H	H	CH_3	OH	Doxycycline (DC)	444.4

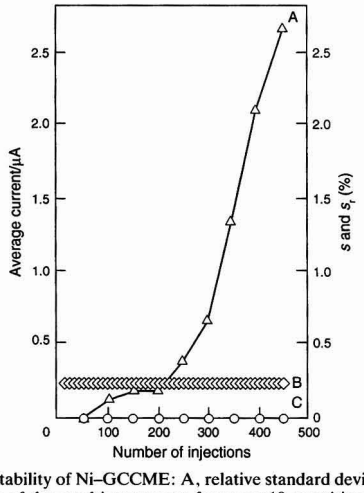

Fig. 11 Stability of Ni–GCCME: A, relative standard deviation (s_r); B, average of the resulting currents for every 10 repetitive injections of 10 mg l^{-1} DC; C, standard deviation, (s).

Table 3 Percentage recovery of tetracyclines added to sample solution of commercial formulations determined by the present method

	Standard tetracyclines/mg l^{-1}			
Formulation	Initially present	Added	Found	Recovery (%) ($n = 6$)
Medomycin (DC)	9.47	5.00	14.56	101.78
Tetracycline (TC)	8.90	5.00	13.88	99.60
Terramycin (OTC)	10.09	5.00	15.15	101.20
Aureomycin (CTC)	14.59	5.00	19.52	98.60
			Mean =	100.30

Table 1 Analytical characteristics for the determination of tetracycline by the present method

Antibiotic	Linear range/mg l^{-1}	Detection limit/mg l^{-1}	Regression equation*
Doxycycline	2.5–100.0	0.92	$y = -0.151 + s\,0.028x$ ($r^2 = 0.997$)
Tetracycline	2.5–80.0	0.03	$y = 0.148 + 0.025x$ ($r^2 = 0.996$)
Oxytetracycline	2.5–100.0	0.34	$y = 0.006 + 0.017x$ ($r^2 = 0.996$)
Chlortetracycline	2.5–100.0	1.81	$y = -0.019 + 0.016x$ ($r^2 = 0.999$)

* y = Current (μA), x = concentration (mg l^{-1}).

Table 4 Determination of some tetracyclines in commercial formulations by the present method and HPLC[31]

Formulation	Component	Source	Amount of antibiotic/mg: Labelled	Found: Present method (*A*)	Found: HPLC method (*B*)	Relative difference* (%)
Medomycin	DC	Medline	100	101.82	101.59	0.2
Tetracycline	TC	GPO†	250	256.06	258.08	−0.7
Tetracycline	TC	Liwinn Pharmaceutical	250	259.63	257.83	0.7
Terramycin	OTC	Pfizer	250	256.06	253.00	1.2
Aureomycin	CTC	F. E. Zuellig	250	255.36	254.66	0.3

* $[(A - B)/A \times 100$.
† GPO, Government Pharmaceutical Organisation (Bangkok).

samples (as described under Experimental) were analysed by the present method and the results compared with those obtained with an established HPLC method.[31] The results obtained are summarized in Table 4. A satisfactory agreement between the results was found with mean relative differences in the range 0.2–1.2%.

Conclusions

This work demonstrates the use of a Ni–GCCME as an amperometric detector in FI for tetracycline determination. The electrocatalytic oxidation of the antibiotic in an alkaline solution may proceed through the formation of a NiOOH surface layer as in the mechanism proposed for other polyhydroxy compounds (*e.g.*, carbohydrate).[28,32] The results reveal the distinct advantages of using the Ni–GCCME: it exhibits a rapid response, high sensitivity, low detection limits, a wide linear range and a reproducible response over a long period of time. The ease of preparation and simple equipment required are the additional advantages of the proposed assay method. The lower potential applied to the electrodes compared with that of Pt and Au[18] or a plain GCE[33] for oxidation of tetracycline provided increased selectivity. However, the general catalytic activity of Ni–GCCME towards hydroxylated compounds such as alcohols,[26] carbohydrates[23–25] and amino acids[27] limits the selectivity of the present electrode without the use of prior chromatographic separation of interfering compounds. The use of the proposed electrode as a detector following separation by liquid chromatography would extend its applications for analysing tetracyclines in complex biological matrices.

W. O. is grateful to the Australian International Development Assistance Bureau (AIDAB) and Thai Authorities especially DTEC and Rajamangala Institute of Technology for a fellowship.

References

1 Haroun, I., and Khattab, F., *Indian J. Pharmacol.*, 1978, **40**, 12.
2 Abdel-Khalek, M. S., and Mahrous, M. S., *Talanta*, 1983, **30**, 792.
3 Mahrous, M. S., and Abdel-Khalek, M. M., *Talanta*, 1984, **31**, 289.
4 Sultan, S. M., Al Zamil, I. Z., and Alarfaj, N. A., *Talanta*, 1988, **35**, 375.
5 Jelikić-Stankov, M., and Veselinović, D., *Analyst*, 1989, **114**, 719.
6 Poiger, H., and Schlatter, Ch., *Analyst*, 1976, **101**, 808.
7 Ragazzi, E., and Veronese, G., *J. Chromatogr.*, 1977, **132**, 105.
8 Regosz, A., *Pharmazie*, 1977, **32**, 681.
9 Salinas, F., Munoz de la Pena, A., and Duran Meras, I., *Anal. Lett.*, 1990, **23**, 863.
10 Syropoulos, A. B., and Calokerinos, A. C., *Anal. Chim. Acta*, 1991, **255**, 403.
11 Martinez, E. E., and Shimoda, W., *J. Assoc. Off. Anal. Chem.*, 1988, **71**, 477.
12 Björklund, H., *J. Chromatogr.*, 1988, **432**, 381.
13 LeDuc, B. W., Greenblatt, D. J., and Friedman, H., *J. Chromatogr.*, 1989, **490**, 474.
14 Olliff, C. J., and Chatten, L. G., *J. Pharm. Sci.*, 1977, **66**, 1564.
15 Sabharwal, S., Kishore, K., and Moorthy, P. N., *J. Pharm. Sci.*, 1988, **77**, 78.
16 Pinilla Gil, E., Calvo Blázquez, L., Garcia-Moncó Carra, R. M., and Sánchez Misiego, A., *Fresenius' Z. Anal. Chem.*, 1988, **332**, 821.
17 Yao, S. Z., Shiao, J., and Nie, L. H., *Talanta*, 1989, **36**, 849.
18 Chatten, L. G., Fleischmann, M., and Pletcher, D., *J. Electroanal. Chem.*, 1979, **102**, 407.
19 Prabhu, S. V., and Baldwin, R. P., *Anal. Chem.*, 1989, **61**, 852.
20 Prabhu, S. V., and Baldwin, R. P., *Anal. Chem.*, 1989, **61**, 2258.
21 Luo, P., Prabhu, S. V., and Baldwin, R. P., *Anal. Chem.*, 1990, **62**, 752.
22 Cataldi, T. R. I., Casella, I. G., Desimoni, E., and Rotunno, T., *Anal. Chim. Acta*, 1992, **270**, 161.
23 Casella, I. G., Desimoni, E., and Salvi, A. M., *Anal. Chim. Acta*, 1991, **243**, 61.
24 Casella, I. G., Desimoni, E., and Cataldi, T. R. I., *Anal. Chim. Acta*, 1991, **248**, 117.
25 Wang, E., and Liu, A., *J. Electroanal. Chem.*, 1991, **319**, 217.
26 Casella, I. G., Cataldi, T. R. I., Salvi, A. M., and Desimoni, E., *Anal. Chem.*, 1993, **65**, 3143.
27 Liu, A., and Wang, E., *Anal. Chim. Acta*, 1993, **280**, 223.
28 Fleischmann, M., Korinex, K., and Pletcher, D., *J. Electroanal. Chem.*, 1971, **31**, 39.
29 Zak, J., and Kuwana, T., *J. Electroanal. Chem.*, 1983, **150**, 645.
30 Beer, P. D., Kocian, O., Mortimer, R. J., and Ridgway, C., *Analyst*, 1992, **117**, 1247.
31 Oka, H., Matsumoto, H., Uno, K., Harada, K. I., Kadowaki, S., and Suzuki, M., *J. Chromatogr.*, 1985, **325**, 265.
32 Robertson, P. M., *J. Electroanal. Chem.*, 1980, **111**, 97.
33 Hou, W., and Wang, E., *Analyst*, 1989, **114**, 699.

Paper 4/06370H
Received October 18, 1994
Accepted December 5, 1994

Absorption Spectra and Multicapillary Imaging Detection for Capillary Isoelectric Focusing Using a Charge Coupled Device Camera

Jiaqi Wu and Janusz Pawliszyn*

Department of Chemistry, University of Waterloo, Waterloo, Ontario, Canada N2L 3G1

Two absorption imaging detectors using charge coupled device (CCD) cameras are designed for capillary isoelectric focusing (CIEF). In the first detector, a light beam passes through a 4 cm capillary and is dispersed by a grating onto a CCD camera. The two-dimensional CCD in the camera records the light absorption at different positions along the capillary in one dimension, and at different wavelengths in the second dimension, simultaneously. The resolution in wavelength is about 1 nm. Since the separation time in the 4 cm long capillary column is only 4 min, the complete analysis takes 4 min, which is much faster than conventional CIEF methods. In the second detector, a light beam passes through a capillary array and then onto a CCD camera. Isoelectric focusing separation and detection of several samples can be completed in about 4 min, and the focusing processes in all capillaries can be observed simultaneously by the real-time, on-line imaging detector. In both detectors, images are normalized by light intensity, recorded simultaneously with the images, to compensate for intensity fluctuation of the light source. The detection limit of the detector is 1.5×10^{-3} absorbance units. The pH resolution of the instrument with the 4 cm long capillaries is 0.01 which is the same or better than that of conventional CIEF instruments with much longer capillaries. The deviation in pH of replicate zone positions in different capillaries of the capillary array is less than 0.01 which is much better than capillary array IEF methods using the mobilization process.

Keywords: *Absorption imaging detection; capillary isoelectric focusing; capillary array; absorption spectra; charge coupled device camera*

Introduction

On-line, real-time imaging systems have proved to be ideal for capillary isoelectric focusing (CIEF)[1–4] because, unlike other capillary electrophoretic techniques, CIEF focuses all sample components inside the capillary column to stationary positions. The imaging detectors do not require the mobilization procedures[5–7] used in conventional CIEF instruments which employ on-column detectors for detection of all focused sample zones. Thus, they eliminate problems associated with the mobilization procedure such as distortion of the linear pH gradient,[7] long analysis times,[6] and difficulties in the determination of isoelectric points (pI) of protein samples.[8] Real-time imaging detectors also allow on-line optimization of separation conditions,[2] study of electrophoretic processes inside the capillary,[2] observation of interactions between proteins inside the capillary,[9] and detection of proteins labelled in-capillary.[4]

* To whom correspondence should be addressed.

In the previous research on the refractive index gradient[1,2,4] and absorption imaging detectors[3,4] for CIEF, a 1024-pixel, linear charge coupled device (CCD) was used as the light sensor. Each pixel of the linear CCD corresponds to a position along the capillary column, so that the zone positions inside the capillary can be determined in a real-time fashion directly from images recorded by the CCD sensor. For some applications, measuring the absorption spectra of zones is also required.[10] The only method reported until now to accomplish this detection used the mobilization process with a linear CCD or a scanning grating to measure the absorption spectra of eluting zones.[10]

One limitation of CIEF is that it is a single-channel separation method. Only one sample can be separated and detected at a time. The throughput of CIEF is much lower than that of isoelectric focusing (IEF) performed in gel slab, which can separate many samples and standards in different lanes simultaneously.[11] The imaging detector with the linear CCD sensor was applied to IEF performed in four capillaries simultaneously,[12] but, the mobilization process had to be again used in the experiment.

The above problems can be solved by using an absorption imaging detector with a CCD camera. In this paper, we report the construction of two kinds of three-dimensional absorption imaging detectors with CCD cameras. The first one uses a CCD camera with a grating to measure absorption spectra and positions of sample zones along the whole capillary simultaneously. The second one uses a CCD camera to detect sample zones along the full length of multiple capillaries simultaneously.

Experimental

Instrumental Procedures

In the CIEF instrument with the imaging detector capable of measuring absorption spectra, as shown in Fig. 1, the capillary cartridge was similar to that of our previous experiment.[4] A

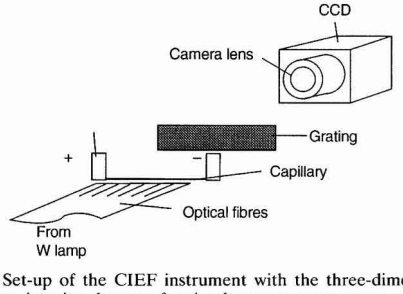

Fig. 1 Set-up of the CIEF instrument with the three-dimensional absorption imaging detector for simultaneous measurements of zone position and absorption spectrum.

100 μm id, 200 μm od, 4 cm long square silica capillary (Vitro Dynamics, Rockaway, NJ) was used as the separation column. The capillary inner wall was coated with non-cross-linked acrylamide to eliminate electro-osmotic flow.[5] The two ends of the capillary were connected to two 2 mm id, 15 mm long polyethylene buffer reservoirs. A 130 μm wide slit, made with two razor blades, was glued behind the capillary, so that only light rays passing through the capillary reached the grating.

In the instrument with a capillary array, two coated capillaries were used for separation. The structure of the cartridge is shown in Fig. 2. These two capillaries were fixed by three glass slides, and the capillary ends were connected to the buffer reservoirs. As shown in Fig. 2, two 130 μm wide slits made of razor blades were glued to the cartridge, just above the capillaries. The distance between the two capillaries was 8 mm.

The light source for the absorption imaging detectors was an 150 W tungsten lamp. In the first detector, the light beam was directed to the capillary by a bundle of 200, 200 μm od, optical fibres. The distance between the optical fibres and the capillary was 5 mm. As shown in Fig. 1, after the beam passed through the slit, the beam was dispersed by a 5 × 5 cm, 600 lines mm^{-1}, transparent grating. Then, the image was recorded by a 1752 × 532 pixel CCD camera (TEA/CCD-1752PF, Princeton Instruments, Trenton, NJ). The camera was cooled to −40 °C by a built-in electronic cooler.

For the multichannel CIEF, as shown in Fig. 2, the light beam from the optical fibre bundle was collimated by a 5 cm focal length cylindrical lens, and projected onto the capillary cartridge by a mirror. The images of the two capillaries were recorded simultaneously by one CCD camera. As shown in Fig. 3, only the light rays passing through the two capillaries could reach the CCD camera. A separate, single optical fibre carried part of the light beam directly to the CCD camera to monitor the light intensity of the lamp (point 1 in Fig. 3). Both alignments image almost the full length of the capillaries.

The recorded images were collected and processed by an ADC and CSMA software provided with the CCD camera by Princeton Instruments, in a personal computer. The time for the camera to record an image and store the image onto the computer hard disk is about 13 s. The images could be recorded by the detection system with the frequency of one image every 15 s.

In the two detectors, all images were normalized by the light beam intensity. Images recorded before the separation voltage was turned on were used as the background. The images recorded after the separation was complete, were divided by the background image, and the light intensity unit was changed into an absorption unit by the computer.

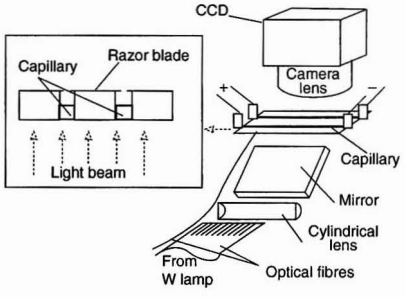

Fig. 2 Capillary array cartridge and the three-dimensional absorption imaging detector for detection of IEF performed in the capillary array.

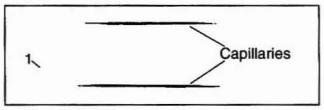

Fig. 3 Image of the two capillaries before the separation voltage is turned on, recorded by the CCD camera in the detector shown in Fig. 2. 1, The light spot directed by the independent optical fibre from lamp, which is used for measurement of light intensity of the lamp.

Reagents

Solutions of 10 mmol l^{-1} H_3PO_4 and 20 mmol l^{-1} NaOH were used as the anolyte and catholyte, respectively. All chemicals were of analytical-reagent grade, and solutions were prepared using de-ionized water, and filtered using 0.2 μm pore size cellulose acetate filters prior to use. Protein samples were human hemoglobin standard which contained variants A, F, S, and C (Hemo control AFSC, Helena Laboratories, Beaumont, TX), and myoglobin (horse skeletal muscle, Sigma, St. Louis, MO, USA). Samples were mixed with the carrier ampholytes (Pharmalyte pH 3–10 or pH 5–8, Sigma) to a final concentration of 2% ampholytes. The concentration of myoglobin was 0.3 mg ml^{-1}. The hemoglobin standard was diluted by 300–400-fold by the carrier ampholyte solution.

Isoelectric Focusing Process

The procedure was the same as that used in our previous experiment.[2] The mixture of protein sample and carrier ampholytes was injected into the capillary by pressure. Then, a plug of 1% agarose gel (prepared in the anolyte, 10 mmol l^{-1} H_3PO_4) was placed in the reservoirs at the anodic ends of the capillaries to avoid hydrodynamic flow inside the capillary. Finally, reservoirs at both ends of the capillaries were filled with their respective electrolytes, and the separation voltage was turned on. The separation voltage was 2 kV. The current passing through the capillary during the focusing process dropped from 15 to about 2 μA in 4 min and stabilized.

Results and Discussion

In the image recorded by the CCD with the detector shown in Fig. 1, one dimension corresponds to the position along the capillary, and another represents the wavelength. The optical light in the range 300–700 nm was found to be dispersed linearly with respect to wavelength by the grating used in the experiment. Thus, the wavelength of the light can be read directly from the positions of pixels perpendicular to the capillary in the two-dimensional CCD sensor. The zone positions can be determined by the positions of pixels in the other dimension of the CCD. By this alignment, the position of sample zones and their absorption spectra can be measured simultaneously from a single image recorded after the focusing process finishes.

Fig. 4 shows the three-dimensional electropherogram of the myoglobin sample. Two peaks are observed, which may correspond to oxygen-complexed and oxygen-free forms of the myoglobin. The zone positions of the two forms and their absorption spectra in the 300–430 nm wavelength range are obtained simultaneously in a real-time fashion. Since the focusing process takes less than 4 min for this sample, both measurements are completed in 4 min. This speed is much faster than the typical 20–30 min analysis time of the commercial CIEF instrument with a three-dimensional detector using a linear CCD sensor or a scanning grating. The resolution in wavelength in Fig. 4 is about 1 nm. The resolution can be enhanced if the absorption spectrum in a narrower range is measured with a higher resolution grating.

The detection limit of the detector in the 300–430 nm wavelength range, three times that of the baseline noise level, was calculated to be 0.003 absorbance units when the light intensity normalization method is used. This detection limit is higher than that of commercial single-wavelength, single-point, on-column absorption detectors, 5×10^{-4}–1×10^{-3} absorbance units. This lower sensitivity is attributed to the weak light intensity caused by the dispersion of the light beam, and the stray light rays caused by the grating. It was not possible to compare the detection limit with that of commercial CIEF three-dimensional absorption detectors with linear CCD sensors because no reports of such sensitivities are available.

Using a capillary array for IEF separation can greatly increase the sample throughput of CIEF, making it comparable with IEF performed in a gel slab. The analysis speed of CIEF is much faster than that of IEF in a gel slab. In order to perform detections for CIEF carried out in a capillary array, two problems have to be solved. The first is the illumination system for the capillary array, and the second is the simultaneous measurement of light intensity passing through the capillary array. The first problem was solved in our experiment by using a light collimating system with slits fixed above the capillaries, as shown in Fig. 2. In this way, all stray light rays were cut-off. Each capillary in the cartridge is independent, which eliminates any signal cross-talking problem between capillaries. The second problem was solved by using a two-dimensional CCD camera to measure the intensity of a light beam passing through all the capillaries simultaneously.

One advantage of using the CCD camera as the light sensor is that 'double beam' configuration can be employed in the absorption imaging detectors for compensation of low-frequency intensity fluctuation in light source. The high-frequency noise of the light source can be reduced by using a long exposure time for the CCD camera. In the present research, the exposure time was 2 s.

In an optical absorption detector, compensation of low-frequency light intensity fluctuation in light source is important for achieving good sensitivity. Usually, a double-beam configuration is utilized in conventional absorption detector, in which the reference beam is used for monitoring the light intensity of the source. The compensation is particularly essential for detectors used for separation methods, such as chromatography and capillary electrophoresis because the separation and the detection last from a few minutes to some hours, and the low-frequency fluctuation in intensity of the light source is avoidable during the long process. In the design of the absorption imaging detectors, a 'double beam' configuration is also used for the compensation of the low-frequency intensity fluctuation. In the first detector, the light intensity obtained from any pixel at which sample has no absorption is used as the reference which corresponds to the light intensity. In the second detector, a separate optical fibre is used to transport part of light beam directly to a certain area of the CCD sensor (point 1 in Fig. 3). In the designs of the two detectors, both the sample light beam which passes through the capillaries, and the reference light beam are recorded simultaneously in a single image by the CCD camera, and the sample images are normalized by the reference light intensity.

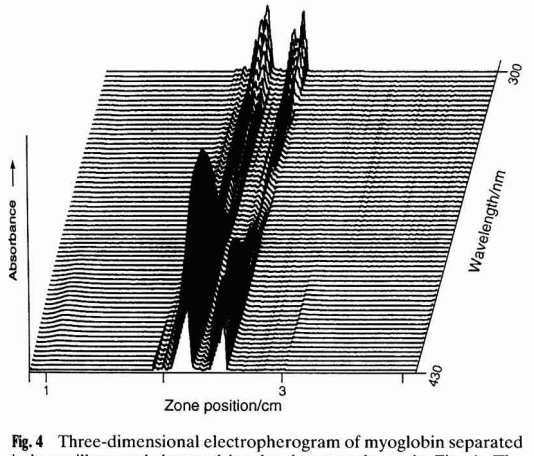

Fig. 4 Three-dimensional electropherogram of myoglobin separated in the capillary and detected by the detector shown in Fig. 1. The image was recorded 4 min after the separation voltage was turned on. Concentration of the sample is 300 μg ml^{-1}.

The use of the 'double beam' configuration improves the sensitivity of the detector. The low-frequency noise of the light source was measured in the following way. Ten images were recorded at 3 min intervals. From each image, the first image was subtracted, and then, the images were divided by the first image. The resulting images are the fluctuations of the light source, which is at 0.5% of the light intensity. In the 'double beam' configuration, all images are normalized by the light intensities recorded with the images simultaneously. After the normalization, the fluctuation is less than 0.13% of the light intensity, which correspond to about 5×10^{-4} absorbance units [log (1001.3/1000)]. Thus, the detection limit of the detector is about 1.5×10^{-3} absorbance units, which is close to that of single point, on-column detectors.

The CCD camera can monitor the separation processes in multiple capillaries simultaneously, and in real time. Fig. 5 shows the isoelectric focusing processes of hemoglobin variants inside the two capillaries, from 1–6 min after the separation voltage is turned on, as recorded by the absorption imaging detector. The results show that the focusing process stabilizes after 4 min. Isoelectric focusing separation can be finished in about 4 min in all the 4 cm long capillaries.

The reproducibility of the zone positions in the two capillaries is good as shown in Fig. 5. The differences of zone positions for the same variants in the two capillaries are less than 100 μm for the 4 cm long capillaries, which corresponds to an error in pH of 0.02 in pI determinations. This is much better than that of IEF performed in capillary array with a mobilization process,[12] because the mobilization speed in one capillary is different from that in another, causing error in the determination of pI values of protein samples from retention times.[8,12] Using the cartridge with two capillaries, a standard sample and an unknown sample could be run simultaneously. Because of the good reproducibility of the zone positions, the peaks in the sample could be identified directly against the standard peak positions without the use of inner pI standards.

One application of the instrument could be high-speed, high-sample-throughput hemoglobin variants screening. A hemoglobin sample can be diluted by 400-fold directly with the carrier ampholytes solution, and injected into the capillary array. As shown in Fig. 5, the separation and detection time for two samples is only 4 min, and then the capillaries are washed and a second group of samples can be run. The resolution of the instrument is good, as shown in Fig. 5(*h*).

Higher resolution is required for many applications of CIEF, including analysis of monoclonal antibodies,[13] and also hemoglobin variants screening.[6] The resolution of the instrument can be enhanced by using a narrow range of carrier ampholytes. The best resolution for hemoglobin variants can be achieved by using a mixture of wide range ampholytes and narrow range ampholytes.[6] Fig. 6 shows two electropherograms of the same hemoglobin sample separated and detected simultaneously in the two capillaries by the instrument using two different solutions of carrier ampholytes. Fig. 6(*a*) shows

the results using pH 3–10 carrier ampholytes, and in Fig. 6(*b*) a mixture of pH 5–8 and pH 3–10 carrier ampholytes was used (proportion is 2:1). The result in Fig. 6(*b*) shows better resolution. The pH resolution can be calculated from the pI value difference between variants A and F, a 0.05 pH difference, and the distance between the two peaks, to be 0.01. This resolution obtained with the 4 cm long capillaries is the same as or better than that of conventional CIEF instruments which use much longer capillaries (20–60 cm).[6,7]

A large linear range is also important in many applications. For example, quantitative determination of human hemoglobin variants requires higher linear range for the absorption detector because in normal human blood, the proportion between A and A_2 variants is in the range of 1:50. Diagnosis of some diseases requires that both variants be determined simultaneously with relative deviations of less than 10%. For such applications, a high quality CCD camera with a linear range greater than 10^3 is necessary. The camera used in the experiment has a linear range of more than 5000 when it is cooled to −40 °C. For applications which do not require a high linear range camera, however, an inexpensive industrial CCD camera with a linear range of 200 would be sufficient. Quantitative aspects of the instrument for protein analysis are currently under research.

Conclusion

This paper is the first report of the use of an absorption imaging detector for CIEF performed in a capillary array. The present design can be applied to more than two capillaries without changes in the detector configuration. Also, this cartridge design can be applied to capillary electrophoretic separation modes other than CIEF, such as capillary zone electrophoresis (CZE) performed in capillary array with short capillaries. The use of the CCD camera can enhance the separation speed of CZE. In conventional CZE instruments with an on-column detector, separation can only be completed when all sample zones have passed through the detection points of capillaries. The actual separation time for all components may be much shorter than this, and with a real-time imaging detector, as in electrophoresis performed in a gel slab, analysis can be complete when all the zones are separated.

In the future, this design can be developed into an inexpensive, conventional capillary electrophoresis instrument for fast analysis of proteins, which includes a high throughput capillary array cartridge equipped with an automated sampler for sample loading, and a three-dimensional absorption imaging detector using an inexpensive industrial CCD camera. This instrument would be capable of analysing a large number of samples in a short time.

This work was supported by the Natural Sciences and Engineering Research Council of Canada, and Sciex, a Division of MDS Health Group Limited, Canada. The

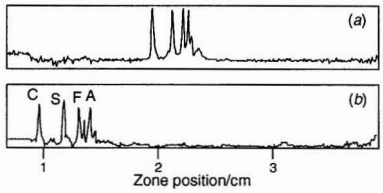

Fig. 6 Electropherograms of human hemoglobin variants A, F, S and C separated in the two-capillary cartridge using different carrier ampholytes, and detected by the detector shown in Fig. 2. (*a*) pH 3–10 carrier ampholytes, and (*b*) 2:1 mixture of pH 5–8 and pH 3–10 carrier ampholytes.

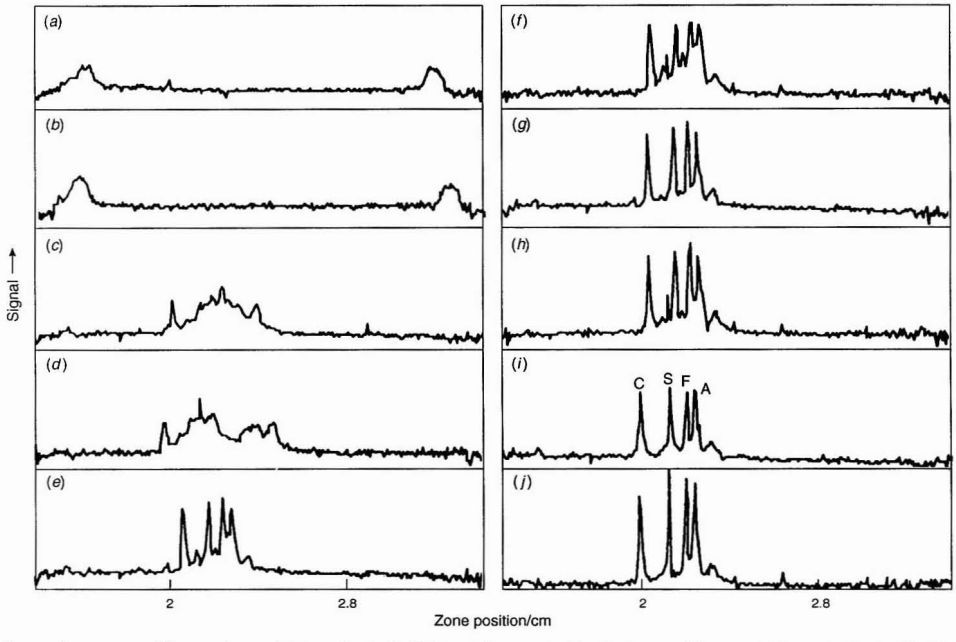

Fig. 5 Electropherograms of human hemoglobin variants A, F, S and C separated in the two-capillary cartridge and detected by the detector shown in Fig. 2 (*a*) and (*b*) are the images in the capillaries 1 and 2, respectively, at 1 min after the separation voltage is turned on, (*c*) and (*d*) at 2 min, (*e*) and (*f*) at 3 min, (*g*) and (*h*) at 4 min, and (*i*) and (*j*) at 6 min.

authors thank M. Adams for his editorial assistance in preparing this manuscript.

References

1 Wu, J., and Pawliszyn, J., *Anal. Chem.*, 1992, **64**, 224.
2 Wu, J., and Pawliszyn, J., *Anal. Chem.*, 1992, **64**, 2934.
3 Wu, J., and Pawliszyn, J., *J. Liq. Chromatogr.*, 1993, **16**, 1891.
4 Wu, J., and Pawliszyn, J., *Anal. Chem.*, 1994, **66**, 867.
5 Hjerten, S., and Zhu, M., *J. Chromatog.*, 1985, **346**, 265.
6 Molteni, S., Frischnecht, H., and Thormann, W., *Electrophoresis*, 1994, **15**, 22.
7 Zhu, M., Rodriguez, R., and Wehr, T., *J.Chromatogr.*, 1991, **559**, 479.
8 Kilar, F., *J. Chromatogr.*, 1991, **545**, 403.
9 Wu, J., and Pawliszyn, J., *J. Chromatogr.*, 1993, **652**, 295.
10 Zhu, M., Rodriguez, R., Wehr, T., and Siebert, C., *J. Chromatogr.*, 1992, **608**, 225.
11 Righetti, P. G., *Isoelectric Focusing: Theory, Methodology and Applications*; Elsevier, Amsterdam, 1983.
12 Wu, J., and Pawliszyn, J., *Electrophoresis*, 1993, **14**, 469.
13 Costello, M. A., Woititz, C., De Feo, J., Stremlo, D., Wen, L.-F., Pailling, D. J., Iqbal, K., and Guzman, N. A., *J. Liq. Chromatogr.*, 1992, **15**, 1081.

Paper 4/04818K
Received August 5, 1994
Accepted January 10, 1995

Determination of Oligomer Distribution of Alkylphenol Polyethoxylates and Fatty Alcohol Polyethoxylates by Positive-ion Atmospheric Pressure Chemical Ionization Mass Spectrometry

S. Pattanaargsorn, P. Sangvanich, A. Petsom and S. Roengsumran

Department of Chemistry, Faculty of Science, Chulalongkorn University, Bangkok 10330, Thailand

Positive-ion atmospheric pressure chemical ionization mass spectrometry was used to analyse commercial alkylphenol polyethoxylates and fatty alcohol polyethoxylates. The mass spectra show oligomer distributions with respect to (1) the degree of ethoxylation of each alkyl base and (2) different alkyl bases. Polyglycol ether and its molecular mass distribution could be identified from the mass spectra for all the surfactant samples tested. Relative amounts of each oligomer present in the sample could be calculated by scanning the sample at appropriate masses (selected ion monitoring mode). Mass-average molecular masses of each polymer series could therefore be calculated

Keywords: *Alkylphenol polyethoxylates; fatty alcohol polyethoxylates; atmospheric pressure chemical ionization mass spectrometry; molecular mass distribution*

Introduction

Alkylphenol polyethoxylates (alkylphenol polyethylene oxides, APEO) are widely used synthetic non-ionic surfactants.[1,2] The most commonly utilized APEO is nonylphenol polyethoxylate (nonylphenol polyethylene oxide, NPEO) of various polyethoxyl chain lengths.[3] The industrial preparation of NPEO is carried out in a batch process by reaction of highly branched 4-nonylphenol with ethylene oxides in the presence of alkaline catalysts. The NPEO obtained is usually a mixture of oligomers of various lengths of the polyethoxyl chain.[4–6]

For ecological reasons, APEO is increasingly being replaced by fatty alcohol polyethoxylates [fatty alcohol poly(ethylene oxide), FAEO], which is a biodegradable non-ionic surfactant.[7,8] In order to obtain satisfactory physical properties such as wetting, dispersing and foaming properties, detergency performance, viscosity and rinsability, commercial FAEO is normally formulated as a mixture of different fatty alcohols reacted with ethylene oxide. Because of the preparation method, each FAEO is also a series of homologues of the polyethoxylate chain differing from each other by one ethylene oxide unit.[5,6]

The standard method to determine the ethylene oxide content of polyethoxylated non-ionic surfactants is the use of hydroiodic acid to cleave ethylene oxide adducts and measuring the amounts of cleaved products.[9] This method gives the total content of ethylene oxide (EO number) resulting from the cleavage of all ethoxylated species present in the sample. Therefore, information on ethylene oxide contents of each particular species cannot be obtained. With the use of an appropriate stationary phase in HPLC, oligomer distribution patterns with respect to the degree of ethoxylation of some APEO could be resolved.[10–18] It was shown that lauryl alcohol polyethoxylates of various EO numbers could be resolved from each other by reversed-phase HPLC after fluorescent derivatization using 1-anthroylnitrile.[10] However, the range of degree of ethoxylation in the sample resolved by HPLC is usually only around 20 EO units.

As mentioned earlier, commercially available FAEO is normally a mixture of homologous FAEO series, *e.g.*, of various alkyl chain lengths. By selection of specific homologue mixtures, application advantages can be attained. Therefore, an analytical method that can determine the alkyl chain distribution of FAEO will provide information for further study on physico-chemical interrelationships. The determination of the alkyl chain distribution had been achieved with anionic surfactants, *e.g.*, linear alkylbenzene sulfonate (LAS), using GC[19,20] and HPLC.[21] The distribution of the degree of ethoxylation and alkyl bases of FAEO can also be obtained by derivatizing FAEO with a silylating agent and analysing the derivatives by GC–MS (unpublished data).

This paper describes the use of atmospheric pressure chemical ionization mass spectrometry (APCI-MS) for the simultaneous determination of the oligomer distribution of APEO and FAEO with respect to both the degree of ethoxylation and alkyl chain length. In addition, the method can detect contaminating polyglycol ether (PGE) and its molecular mass distribution simultaneously. For APCI-MS, ionization of the sample molecules occurs at atmospheric pressure with the aid of a discharge needle as the source of ionizing electrons. Ion–molecule collisions also occur in the source, hence the name atmospheric pressure chemical ionization. The method is considered to be a relatively mild ionization technique. The amount of sample fragmentation varies with the nature of the sample and also with the voltage applied to the discharge needle (corona discharge voltage) and the voltage applied to the two skimmers for accelerating and focusing ions into the mass analyser. Variations in the cone voltage can cause collision-induced dissociation through the increase in the transitional energy of the ions. In this experiment, APCI-MS was used to analyse non-ionic surfactants under conditions that minimized fragmentation of the sample molecules.

Experimental

Materials

Commercial surfactants, Tergitol NP-4, NP-6, NP-10, NP-13, NP-40 and 15-S-9, were a gift from Union Carbide Thailand (Bangkok, Thailand). Tergitol NP is NPEO with various polyethoxyl chain lengths; the number following NP indicates an average degree of ethoxylation (EO number) as indicated in the product description, *e.g.*, Tergitol NP-4 should contain

on average 4 mol of ethylene oxide per mole of surfactant molecules. Tergitol 15-S-9 is a mixture of linear secondary alcohols reacted with ethylene oxide. HPLC-grade acetonitrile and methanol were purchased from Biochemical Diagnostics Fine Chemicals (Poole, Dorset, UK).

Mass Spectrometry

Samples were dissolved in acetonitrile at a concentration of about 5.0 mg ml^{-1} and diluted to 1.0 mg ml^{-1} with acetonitrile–water mixture (60:40), and the solution was introduced directly into VG Trio 2000 mass spectrometer (Fisons Instruments, Manchester, UK), equipped with an atmospheric pressure chemical ionization (APCI) source and probe, *via* a 10 μl injection loop. The mobile phase was acetonitrile–water (1 + 1 v/v). The source and probe temperatures were both set at 120 °C. APCI was operated at a corona discharge voltage of 2.5 kV and at a cone voltage of 30 V. The flow rate was maintained at 0.4 ml min^{-1} with a Waters Model 510 isocratic pump (Millipore, Milford, MA, USA). Protonated molecular ions (MH^+) were monitored in the positive-ion APCI mode under the control of a MASSLYNX data system. Calibration was carried out with polyethylene glycol of appropriate molecular mass range. The mass spectra of each surfactant was obtained under continuum scanning at appropriate mass ranges. Scanning of various particular masses of interest was performed in the selected ion monitoring (SIM) mode by selecting appropriate masses previously obtained from the mass spectrum acquired under continuum scanning.

Result and Discussion

Nonylphenol Polyethoxylate (Tergitol NP)

Figs. 1(*a*), (*b*), (*c*), (*e*) and (*g*) show positive-ion APCI mass spectra of Tergitol NP-4, NP-6, NP-10, NP-13 and NP-40, respectively. Figs. 1(*d*) and (*f*) show expanded regions for Terigitol NP-10 and NP-13. The structure of NPEO is shown in Fig. 2(*a*).

A series of protonated molecular ion peaks of NPEO of various degrees of ethoxylation, which correspond to m/z 221 + 44n, are clearly shown in each spectrum. The spectra directly represent the oligomer distribution patterns of corresponding samples. The NPEO oligomer distribution pattern obtained by this method was reproducible and was independent of the corona discharge voltage and cone voltage, *i.e.*, no fragmentation was detected when the corona discharge voltage was varied from 1.0 to 3.5 kV and when the cone voltage was varied from 15 to 40 V. This indicates that the protonated NPEO species were not fragmented at the indicated potential of the corona pin. Variation of the cone voltage usually affects the collision among species and, therefore, may induces collision-induced dissociation of sample molecules into smaller fragments. However, in this instance, protonated NPEO ions could withstand the fragmentation energy when the cone voltage was varied from 15 V to as high as 40 V. Therefore, the mass spectra shown in Fig. 1 (the corona discharge voltage was set at 2.5 kV and the cone voltage at 30 V for optimum sensitivity) truly represent the approximate original abundances of various oligomers present in the samples, assuming equal sensitivity of the instrument for all oligomers (variations in the ion energy and ion energy ramp did not change the molecular mass distribution patterns of the samples).

In addition to the information on NPEO oligomer distribution patterns, each mass spectrum also indicates the contamination by PGE. Moreover, the oligomer distribution pattern of the contaminating PGE can also be obtained from the mass spectrum. A series of peaks at m/z 19 + 44n represent protonated molecular ions of PGE with various degrees of polymerization. The ratio of contaminating PGE to NPEO present in the sample was further determined by SIM scanning experiments at the m/z values of various NPEO and PGE peaks shown in the spectrum obtained previously (continuum mode, Fig. 1). Integration of the area under each peak was carried out and the mole ratios between NPEO and PGE were then calculated. The NPEO:PGE mole ratios for Tergitol NP-4, NP-6, NP-10 and NP-13 are 1:0.19, 1:0.19, 1:0.23 and 1:0.27, respectively. It is worth mentioning that the PGE is only a minor component.

The amount of PGE increases when the degree of polymerization increases greatly, as in the case of Tergitol NP-40, for which the NPEO:PGE mole ratio is 1:0.38. This might be a result of an increased concentration of ethylene oxide used during the preparation of Tergitol NP of high EO number. A small extent of contamination from other series of compounds, as shown by low-intensity series of peaks at m/z values other than those of NPEO and PGE, can also be seen in all spectra. Further studies should be carried out to identify the structures of these compounds, possible by MS–MS.

Fatty Alcohol Polyethoxylate (Tergitol 15-S-9)

Figs. 3(*a*) and (*b*) shows the positive-ion APCI mass spectrum of Tergitol 15-S-9. The spectrum indicates at least four series of compounds present in the sample. The first series is undecanol polyethoxylate $[C_{11}H_{23}O(CH_2CH_2O)_nH]$, which corresponds to a series of positive molecular ion peaks at m/z 173 + 44n. The second series is dodecanol polyethoxylate $[C_{12}H_{25}O(CH_2CH_2O)_nH]$, which corresponds to a series of peaks at m/z 187 + 44n. The third series is tridecanol polyethoxylate $[C_{13}H_{27}O(CH_2CH_2O)_nH]$, which corresponds to a series of peaks at m/z 201 + 44n. The last series of peaks is PGE $[HO(CH_2CH_2O)_nH]$. The contaminating PGE gives peaks at m/z 19 + 44n, similar to those found in all the previously discussed Tergitol NP spectra.

In addition to the information on oligomer distribution patterns with respect to different degrees of ethoxylation of the four compound series, the relative amounts of these four series (alkyl chain distribution) could also be determined by (1) calculating the relative amount of each oligomer within the series by the same procedure as used for NPEO, (2) picking eight representative m/z values that correspond to the eight most abundant oligomers of each series, (3) scanning the sample at m/z values corresponding to the m/z values representing all four series ($4 \times 8 = 32$ m/z values, which is the maximum number that could be scanned in one run) and (4) integrating the area under each peak and then calculating the relative abundances of each series. This SIM experiment gave an undecanol polyethoxylate : dodecanol polyethoxylate : tridecanol polyethoxylate : PGE ratio of about 38 : 24 : 22 : 16. In other words, the ratio between all three FAEO and PGE is 84 : 16. The mass average molecular masses of undecanol polyethoxylate, dodecanol polyethoxylate, tridecanol polyethoxylate and PGE in Tergitol 15-S-9 were then calculated from the relative amounts of each oligomer present in a particular series. The results are 698, 760, 684 and 597, which correspond to degrees of ethoxylation or EO numbers (n) of 12, 13, 11 and 13, respectively.

By using this technique, there is no need for chemical derivatization in order to obtain the oligomer distribution of FAEO with respect to degree of ethoxylation, as is required in a previous HPLC method.[10] This method can be used with samples that have a wide range of EO numbers without wasting a lot of analytical time (the limitation of the mass range that can be analysed will depend on the mass range capacity of the mass spectrometer used).

The standard method to determine the ethylene oxide content of polyethoxylated non-ionic surfactants is to use hydroiodic acid to cleave EO adducts and then measure the amount of free iodine formed.[9] The average EO number obtained by this method, therefore, represents ethylene oxide from all the ethoxylated compounds of different alkyl bases

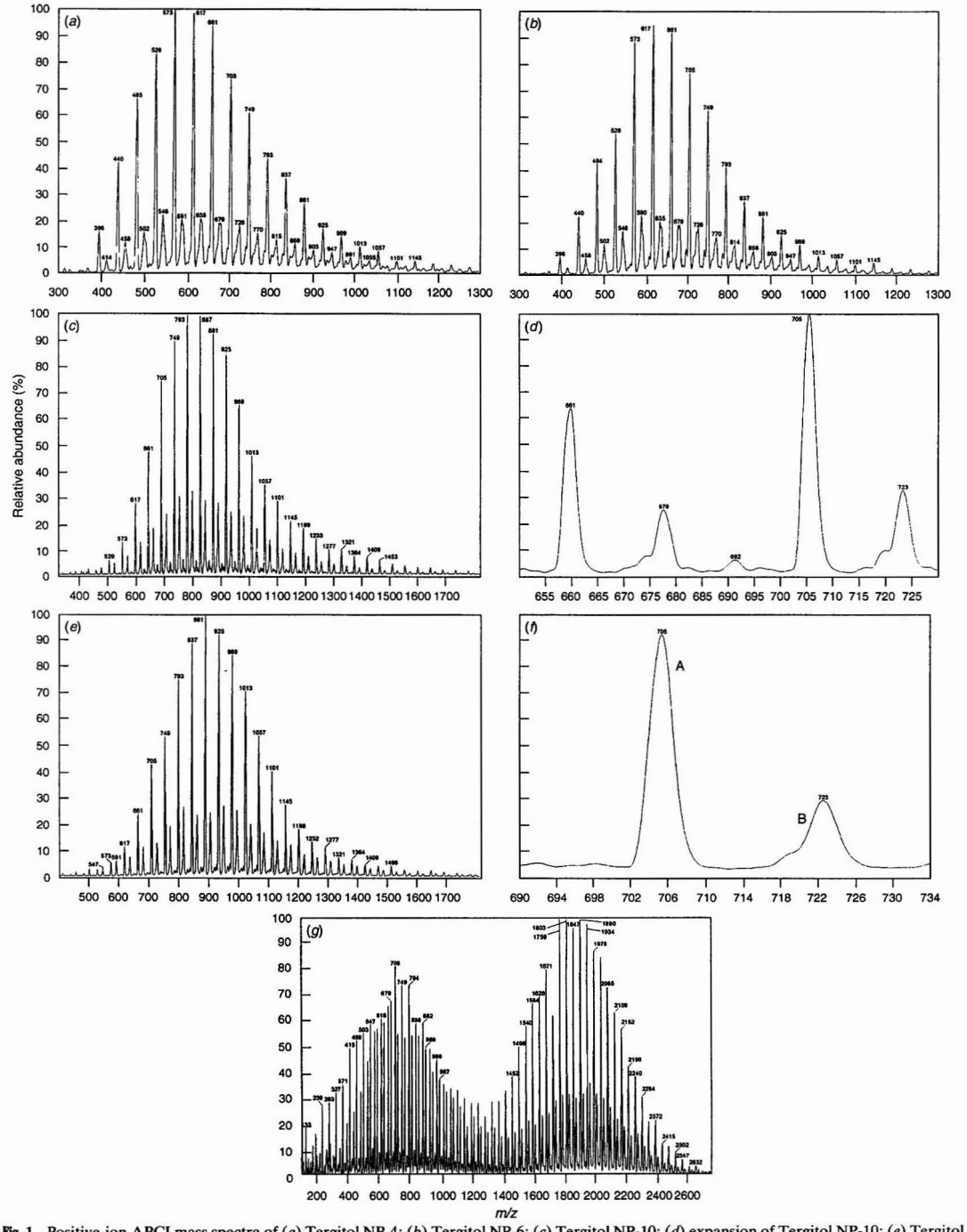

Fig. 1 Positive-ion APCI mass spectra of (*a*) Tergitol NP-4; (*b*) Tergitol NP-6; (*c*) Tergitol NP-10; (*d*) expansion of Tergitol NP-10; (*e*) Tergitol NP-13; (*f*) expansion of Tergitol NP-13 where A = Tergitol and B = PGE; (*g*) Tergitol NP-40.

present in the sample. Consequently, the physical and chemical properties of commercial APEO or FAEO represent the combination of all APEO species or all FAEO species together with PGE present in the product. The relative amount of each species present in the sample may vary from sample to sample. Unfortunately, available analytical techniques cannot conveniently reveal the ratio of APEO and PGE or the amount of each particular FAEO present in the product. Moreover, none of the methods mentioned earlier can reveal the molecular mass distribution pattern of each particular compound series in the sample. Therefore, the actual composition of sample batches with the same EO number will differ and this may cause slightly different physico-chemical properties between batches.

With the proposed method, information on the degree of ethoxylation of each particular species can be simultaneously obtained, *i.e.*, the distribution of the EO numbers of PGE, of undecanol polyethoxylate, of dodecanol polyethoxylate and of tridecanol polyethoxylate in Tergitol 15-S-9. Therefore, the average EO number for each alkyl base can be calculated. The method can be applied to aid studies on physico-chemical inter-relationships. To obtain a more precise average EO number of each alkyl base, SIM scanning of selected masses corresponding to the compounds of interest could also be performed and the mass-average molecular masses could then be calculated. With this method provided that the molecular masses of the alkyl bases are different from each other, the protonated molecular ion peaks of each polyethoxylated alkyl base will be resolved from each other. The limitation of the method is, perhaps, an inability to resolve (1) alkyl bases that are structural isomers of each other (this limitation can be solved by using MS–MS) and (2) non-ethoxylated species, *e.g.*, nonylphenol.

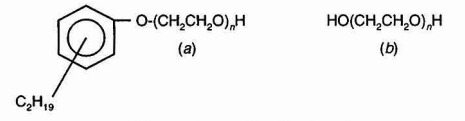

Fig. 2 Structures of (*a*) nonylphenol polyethoxylate and (*b*) polyglycol ether.

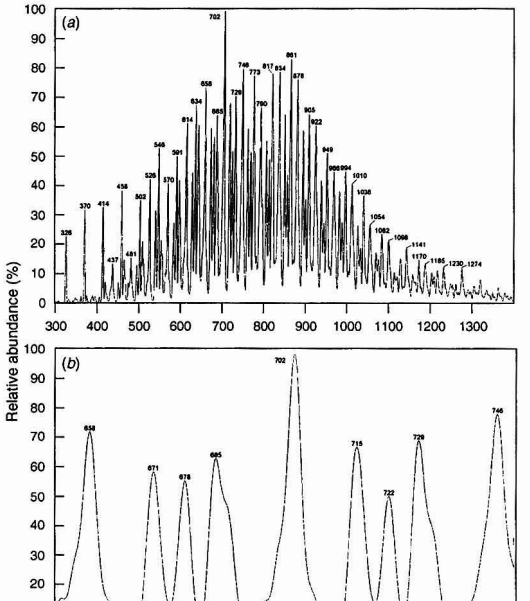

Fig. 3 (*a*) Positive-ion APCI mass spectrum of Tergitol 15-S-9 and (*b*) expanded spectrum.

Conclusion

The proposed method employing positive-ion APCI-MS permits the simultaneous determination of the oligomer distribution patterns of NPEO, PGE and FAEO present in surfactant samples without any need for chemical derivatization or a long analytical time as usually required in the previously used HPLC method. Moreover, this method can simultaneously give complete oligomer distribution information with regard to the EO distribution of each particular alkyl base and the alkyl chain distribution of the samples that contain more than one type of alkyl base.

By scanning the sample at appropriate masses in the SIM mode and integrating the peak areas, the relative amount of each particular oligomer in the sample could be calculated. The mass-average molecular mass of each polymer series could therefore be calculated. In addition, the method can also be used even with samples with a very broad oligomer distribution range.

References

1 Layman, P. L., *Chem. Eng. News*, 1984, January 23, 17.
2 Layman, P. L., *Chem. Eng. News*, 1986, January 20, 21.
3 Kunkel, E., *Tenside Deterg.*, 1980, **14**, 247.
4 Bolva, R. S., and Markov, K. M., *Tenside Deterg.*, 1981, **18**, 37.
5 Hettche, A., and Klahr, E., *Tenside Deterg.*, 1982, **19**, 127.
6 Maag, H. H., *Tenside Deterg.*, 1982, **19**, 144.
7 Kravetz, L., Chung, H., Guin, K. E., Shebs, W. T., and Smith, L. S., *Tenside Deterg.*, 1984, **21**, 1.
8 *Standard Test Method for Ethylene Oxide Content of Polyethoxylated Nonionic Surfactants*, ASTM D2959, American Society for Testing and Materials, Philadelphia, 1989.
9 Kudoh, M., Ozawa, H., Fudano, S. O., and Tsuij, K., *J. Chromatogr.*, 1984, **287**, 337.
10 Ahel, M., and Giger, W., *Anal. Chem.*, 1985, **57**, 1577.
11 Ahel, M., and Giger, W., *Anal. Chem.*, 1985, **57**, 2584.
12 Holt, M. S., McKerrell, E. H., Perry, J., and Watkinson, R. S., *J. Chromatogr.*, 1986, **362**, 419.
13 Clark, L. B., Rosen, R. T., Hartman, T. G., Louis, J. B., Suffet, I. H., Lippincott, R. L., and Rosen, J. D., *Int. J. Environ. Anal. Chem.*, 1992, **47**, 167.
14 Marcomini, A., Paroni, B., and Stelluto, S., *Int. J. Environ. Anal. Chem.*, 1989, **35**, 207.
15 Favretto, L., Stancher, B., and Tunis, B. F., *Analyst*, 1980, **105**, 833.
16 Marcomini, A., Capri, S., and Giger, W., *J. Chromatogr.*, 1987, **403**, 243.
17 Marcomini, A., and Giger, W., *Anal. Chem.*, 1987, **59**, 1709.
18 Jandera, P., Uzbanek, J., Prokers, B., and Churacek, J., *J. Chromatogr.*, 1990, **504**, 297.
19 Lew, H. Y., *J. Am. Oil Chem. Soc.*, 1972, **49**, 665.
20 Denig, R., *Tenside Deterg.*, 1973, **10**, 59.
21 Nakae, A., Tsuji, K., and Yamanaka, M., *Anal. Chem.*, 1981, **53**, 1818.

Paper 4/05078I
Received August 18, 1994
Accepted December 12, 1994

Determination of Trace Amounts of Sulfur in Hydrotreated Naphthas: Comparative Study Using Raney Nickel, Houston Atlas and Gas Chromatographic Methods

Mohamed M. Abdillahi, Khurshid Alam, Abdul Bari, M. Siddiqui and Mohammed A. Ali

Research Institute, King Fahd University of Petroleum and Minerals, Dhahran 31261, Saudi Arabia

Raney nickel, Houston Atlas and gas chromatographic–flame photometric detection (GC–FPD) methods were applied to the determination of trace amounts of sulfur in naphthas. The parameters investigated included the linearity, detection limits and the repeatability of the data. The analysis times were 2.0 h, 10 min and 30 min while the detection limits were 0.1 ppm, < 20 ppb and 20 ppb, respectively. These methods offer the determination of trace amounts of sulfur in the ranges 0.1–200 ppm (Raney nickel), 20 ppb–500 ppm (Houston Atlas) and 20 ppb–low per cent. (GC–FPD). The repeatability of the methods was determined at sulfur concentrations below 1.0 ppm.

Keywords: Trace sulfur determination; hydrotreated naphthas; Raney Nickel; Houston Atlas; gas chromatographic-flame photometric detection (GC–FPD)

Introduction

Hydrodesulfurization in petroleum refining demands very sensitive methods for the determination of sulfur at trace levels, because sulfur at these concentrations could be responsible for the poisoning of reforming catalysts in the reformer process. Therefore, low-level sulfur determinations have received considerable attention. Hydrodesulfurization of naphtha is performed by removing ppm levels of sulfur by mixing with a hydrogen-rich gas before it enters a catalytic bed utilizing a typical HDS catalyst of Co–Mo–Al oxides. The hydrotreating reactions in desulfurization can be summarized as follows

(i)	$RSH + H_2$	$\rightarrow RH + H_2S$	Thiols
(ii)	$R_2S + 2H_2$	$\rightarrow 2\,RH + H_2S$	Sulfides
(iii)	$(RS)_2 + 3H_2$	$\rightarrow 2\,RH + 2H_2S$	Disulfides
(iv)	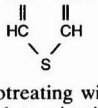 $+ 4\,H_2$	$\rightarrow C_4H_{10} + H_2S$	Thiophenes

Hydrotreating will therefore rely on sensitive procedures for the determination of trace amounts of sulfur before the product is further processed in catalytic reforming. The Wickbold[1] and Raney nickel[2] wet chemical methods were commonly employed for sulfur determinations at levels down to 0.2 and 0.1 ppm, respectively. However, each method requires a total analysis time of about 2–3 h and much larger sample volumes than other available techniques. Microcoulometric detection has been used for sulfur measurements from trace to per cent. levels.[3–5] However, this technique demands close attention to the operating parameters and is not precise below 1 ppm. Drushel[6] reported that the Houston Atlas analyser is a reliable and sensitive system, but is limited to lower concentrations owing to overloading of the lead acetate-impregnated paper used as the detector. ASTM Method D-4045[7] covers the determination of sulfur in petroleum products in the range 0.02–10.00 ppm. This method is applicable to liquids with boiling points in the range 30–371 °C and it includes naphtha. Gas chromatographic analysis of naphtha was discussed by Whittemore[8] with emphasis on columns, packings and identification techniques. Bradley and Schiller[9] have developed a calibration method for sulfur compounds in petroleum distillates. They have eliminated the non-linearity and variance of the flame photometric detector (FPD) response to different sulfur compounds.

This paper describes three alternative methods for the determination of trace amounts of sulfur in hydrotreated naphthas. The wet-chemical Raney nickel method, Houston Atlas analyser and gas chromatography with flame photometric detection (GC–FPD) were set up in our laboratory to conduct comparative studies of sulfur determinations in both feed and hydrotreated product naphthas. Calibration graphs for five model compounds were constructed and the detection limits of the techniques were determined. Both peak areas and peak heights were used for quantification of the GC–FPD results. This technique showed the presence of about 52 sulfur compounds in the feed naphtha that were virtually eliminated by the HDS treatment. The parameters of the Houston Atlas system were varied to achieve the best sensitivity for sulfur determinations in the range 0.1–500 ppm. The repeatability of the results relative to the levels of sulfur present in the naphtha (100 ppb) was established. As 0.1 ppm of sulfur was the detection limit with the Raney nickel method, 0.3 ppm was used instead for the repeatability measurements.

Experimental

Raney Nickel Method

In this method, the naphtha sample in the range 1–60 ml, depending on the sulfur concentration, was reacted with activated Raney nickel to produce nickel sulfide. Acidification of the NiS generated H_2S, which was trapped in NaOH solution. The absorber solution was then titrated with standard mercury(II) acetate solution with dithizone as the indicator.

The active Raney nickel was rinsed with isopropyl alcohol and then transferred into a reaction vessel containing 10 ml of the alcohol. A known amount of the naphtha was added to the flask. The experimental set-up shown in Fig. 1 was then installed according to Granatelli.[2] The leaks in the system were tested by using a stream of nitrogen. The stirrer, the heater and the water for condensation were turned on. Desulfurization proceeded and 10 ml each of 1 mol l^{-1} sodium hydroxide and acetone were charged in the absorber. The over-all reactions could proceed as follows:

$$Al + 2NaOH + 2H_2O \rightarrow 2NaAlO_2 + 3H_2$$
$$6Ni + 3H_2 \rightarrow 6NiH$$
$$NiH + SR \rightarrow NiS + HR$$
$$NiS + HCl \rightarrow NiCl_2 + H_2S$$

After desulfurization, 10 ml of HCl (2 + 1) was added to the acid reservoir. The heat was then turned off and the set-up was adjusted to connect the reaction flask to the absorber side-arm. Five drops of the indicator, dithizone solution, were placed in the absorber. The acid was then added to the reaction flask while maintaining the stirring, the heat and nitrogen flow.

The H_2S evolved was absorbed in NaOH solution. The mercury(II) acetate titrant was standardized and then titrated against the resulting solution until the colour changed to pink, marking the end-point. The concentration of sulfur was calculated as follows:

$$\text{sulfur (ppm)} = \frac{\text{net vol. of } Hg(OAc)_2 \text{ soln. consumed (ml)} \times \text{concn. of } Hg(OAc)_2 (\mu g\ S\ ml^{-1})}{\text{mass of the sample (g)}}$$

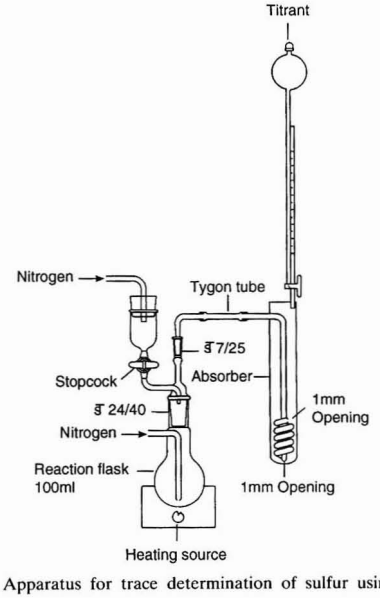

Fig. 1 Apparatus for trace determination of sulfur using Raney nickel.

Houston Atlas Sulfur Analyser

The naphtha is thermally cracked and is reduced to gaseous short chain hydrocarbons. In the presence of high-purity H_2 and at high temperatures, the total sulfur was reduced to H_2S. The rate of colour formation by H_2S on lead acetate-impregnated tape determines the concentration of sulfur in the naphtha. The Houston Atlas analyser consists of two parts, the hydrogenolysis unit and the H_2S analyser. The main components of hydrogenolysis unit are H_2 and inert gas flow meters, pyrolyser, temperature regulator and control panel. The inlet of the unit was connected to a source of ultra-high-purity hydrogen. Samples were injected into the hydrogenolysis tube with precision syringes attached to a slow-motion pump. The main parts of the H_2S analyser are the flow system, tape transport, optical system, rate-reading electronics and control panel. The thermally cracked products were transferred to this unit, which determines the total sulfur from the rate of the reaction between H_2S and lead acetate photometrically. This rate is translated into digital from the electronics. The over-all arrangement of the equipment is illustrated in Fig. 2.

The hydrogen gas flow was set at a pressure of 15 psig. The pyrolyser was heated up to the 1200 °C required to convert the sulfur compounds in the naphtha into H_2S. The instrument was set to the baseline and a blank of the isooctane solvent was measured (approximately 20 ppb). Samples were injected into the hydrogenolysis tube *via* precision syringes having capacities ranging from 10 to 100 μl. The thermally cracked products were directed to the detection system. The output was connected to the chart recorder and also read digitally on the rate-reading meter. A sharp decrease in response at higher concentrations of sulfur indicates colour saturation of the tape. Table 1 summarizes the operating conditions at various sulfur concentrations.

Gas Chromatography with Flame Photometric Detection

The growth of gas chromatography in recent decades is indicative of the wide acceptance of this technique as a means of separating components from complex mixtures such as naphtha. The column which is the heart of the GC was properly selected for the sulfur analysis and FPD was used for the sensitive detection of the sulfur-containing compounds.

A Perkin-Elmer PE-8700 gas chromatograph fitted with an FPD was used for the determination of individual compounds. The capillary column (DB-1, 30 m × 0.35 mm id) was used with helium as the carrier gas at a flow rate of 4.5 ml min^{-1}. The oven temperature was programmed at a rate of 4 °C min^{-1} from 45 °C (after an initial hold of 0.5 min) to 170 °C and held at this temperature for 30 min before completing the cycle. Both the detector and injector temperatures were 250 °C and

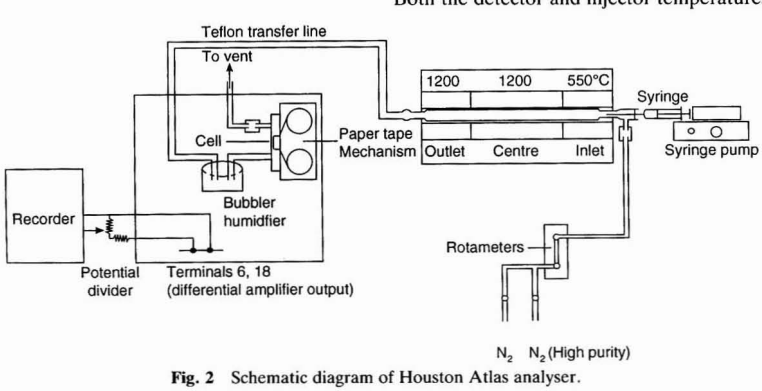

Fig. 2 Schematic diagram of Houston Atlas analyser.

the sulfur filter was set at 394 nm. The air and hydrogen flow rates were 90 and 65 ml min^{-1}, respectively. The detector output was recorded and quantified as either peak heights. Peak heights were found to be more precise than peak areas at lower concentrations. This is in accordance with some published data.[10] Because of the narrow linearity range inherent in FPD, different calibration graphs were constructed for various concentration ranges. The following model compounds were used: carbon disulfide, isobutanethiol, dipropyl sulfide, 3-methylthiophene and benzothiophene.

Results and Discussion

Comparative data for the three techniques are presented in Table 2. It is clear that each technique has its own merits, and the choice will depend on the precision, accuracy, range of sulfur concentration to be determined and the time available for the analysis. The repeatability, measured as the standard deviation of the data, varied with the level of sulfur concentrations. The relative standard deviations (s_r) of the measurements were calculated to be between 3.2% for the Houston Atlas method to 5.9% for the Raney nickel method. Table 3 shows the accuracy and the precision of the techniques studied.

Raney Nickel Method

The blank titration for the Raney nickel catalyst and isooctane solvent used as a standard were determined before each experiment. The feed naphtha was then analysed for sulfur, the concentration of which was 250 ppm. The hydrotreated naphtha products showed total sulfur in the range 0.15–0.70 ppm, depending on the catalysts and the operating conditions used. The Raney nickel method is suitable for the determination of sulfur in the range 0.1–300 ppm and can be used to determine sulfur in both feed and hydrotreated naphthas. Higher sulfur concentrations may be determined by dilution.

Houston Atlas Technique

Typical peaks of the instrument are shown in Fig. 3. The response on the right-hand side represents the isooctane blank. The signals that come after the blank are 20, 50 and 100 ppb. The repeatability of the data was tested, relative to 100 ppb, and was calculated to be s_r = 3.2% (Table 3). The detection limit was less than 10 ppb of sulfur, as is clear from the blank signal (see Fig. 3). Fig. 3 shows that the pure isooctane used as a blank contained about 10 ppb of sulfur. Therefore, the Houston Atlas method is suitable for sulfur determination and covers the range of concentrations expected in the feed and product naphthas. Calibration graphs were then constructed for different concentration ranges. Fig. 4(*a*) illustrates the calibration graph for sulfur determinations in the lower range from 0.1 to 2.0 μg ml^{-1} and Fig. 4(*b*) shows the calibrations in the range from 200 to 500 μg ml^{-1}.

Gas Chromatography with Flame Photometric Detection

The chemiluminescent sulfur band emission at 394 nm was used for the FPD measurements. The chemistry of the flame depends on the H_2-to-air ratio. It was observed that at the optimum flow rates of 65 and 90 ml min^{-1} of H_2 and air, respectively, the sulfur signals were recorded as peaks whereas the hydrocarbons were registered as dips in the chromatogram. Fig. 5 shows the quenching effect of isooctane used as a solvent in various concentrations. 3-Methylthiophene and dibutyl sulfide were tested and the results illustrate that 20 ppb of sulfur is the detection limit for GC–FPD (Fig. 5).

Calibrations for five compounds representing different groups were constructed and are given in Fig. 6. Fig. 6(*a*) presents the calibration graphs for CS_2, C_4H_9S and C_5H_6S and Fig. 6(*b*) those for $(C_3H_7)_2S$ and C_8H_6S. The sequence of the standards was (i) CS_2, (ii) C_4H_9S, (iii) C_5H_6S, (iv) $(C_3H_7)_2S$ and (v) C_8H_6S. Concave and convex calibration graphs were observed. The non-linear response of the FPD is normal for S_2^* detection at 394 nm. Fig. 7 illustrates the calibration graphs at the lower end below 2.5 μl ml^{-1} of sulfur. The repeatabilities of the results at 100 ppb of 3-methylthiophene and dibutyl sulfide was calculated to be s_r = 4.6% (see Table 3). The flame photometric detector was found to respond to

Table 1 Houston Atlas calibration parameters

	Concentration range/μg S ml^{-1}			
Parameter	0.1–2.0	2–20	25–100	200–500
Injector setting	20	20	20	10
Syringe size/μl	100	100	10	10
Sensitivity	High	Low	Low	Low
Attenuator setting	200	400	600	150
H_2 flow rate/ml min^{-1}	400	400	400	400
Pyrolyser temperature/°C	1300	1300	1300	1300

Table 2 Comparative data for determination of trace amounts of sulfur

	Technique		
Parameter	Raney nickel	Houston Atlas	GC–FPD
Principle	Wet chemistry	Hydrogenolysis/ H_2S detection	Separation/ detection of individual compounds
Range	0.1–200 ppm	20 ppb–500 ppm	ppb–% level
Detection limit	0.1 ppm	<20 ppb	20 ppb
Analysis time	2–3 h	10 min	30 min
Sample volume	Up to 60 ml	Up to 100 μl	<1 μl

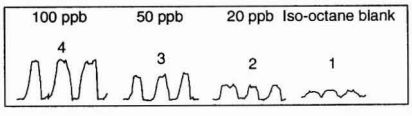

Fig. 3 Typical response peaks for the Houston Atlas method.

Table 3 Repeatability data for trace determination of sulfur

		Statistical values				
Method	No. of replicates	x	s_n1	t-Value	s_r(%)	Confidence limits (95%)
Raney nickel	8	0.51	0.031	2.31	5.9	±0.025
Houston Atlas	10	4.49	0.143	2.23	3.2	±0.10
GC–FPD	10	29.22	1.339	2.23	4.6	±0.94
GC–FPD	10	30.92	1.420	2.23	4.6	±1.0

different sulfur compounds with various selectivities depending on the rate of formation of S_2 molecules from the sulfur–hydrogen-rich flames. This can be seen from the unequal response factors for the individual sulfur compounds in Fig. 8. A typical FPD chromatogram of feed naphtha and hydrotreated products is shown in Fig. 9. The feed naphtha contains 52 sulfur compounds at appreciable concentrations (250 ppm), which was lowered to a total of 0.3 ppm as shown in the lower chromatogram.

Conclusions

The presence of ppm and sub-ppm levels of sulfur in naphtha can be accurately determined using Raney nickel, Houston Atlas and GC–FPD techniques. The temperature plays a dominant role in the Raney nickel method in the digestion of the sample for desulfurization and for the evolution of H_2S. The applicable concentration range of this wet-chemical method is from 0.1 to 300 ppm. However, it takes about 2 h and demands the attention of an experienced analyst. The Houston Atlas method is a reliable and sensitive technique suitable for the determination of trace amounts of sulfur, but, it is limited by the saturation of the lead acetate-impregnated tape detector. However, this could be extended by dilution. The effective concentration range is from 20 ppb to 500 ppm. Total trace sulfur determinations can be accomplished with the Raney nickel and Houston Atlas methods. The individual

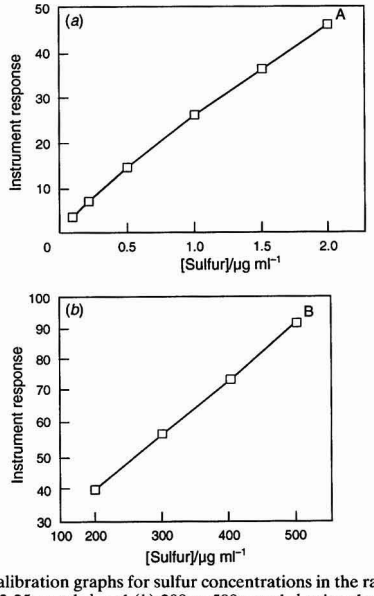

Fig. 4 Calibration graphs for sulfur concentrations in the range from (*a*) 0.1 to 2.25 μg ml^{-1} and (*b*) 200 to 500 μg ml^{-1} using the Houston Atlas method.

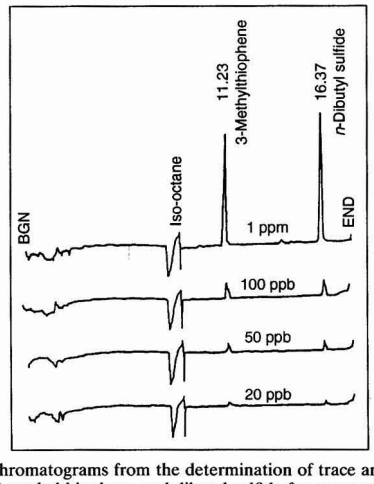

Fig. 5 Chromatograms from the determination of trace amounts of sulfur in 3-methylthiophene and dibutyl sulfide for concentrations of 20 ppb, 50 ppb, 100 ppb and 1 ppm.

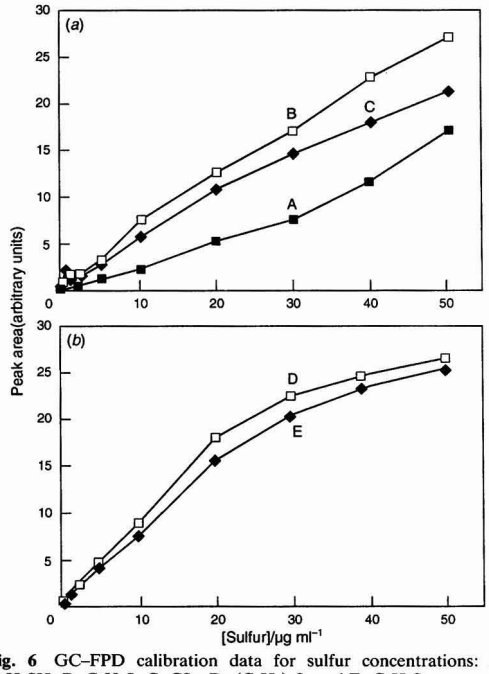

Fig. 6 GC–FPD calibration data for sulfur concentrations: A, C_4H_9SH; B, C_5H_6S; C, CS_2; D, $(C_3H_7)_2S$; and E, C_8H_6S.

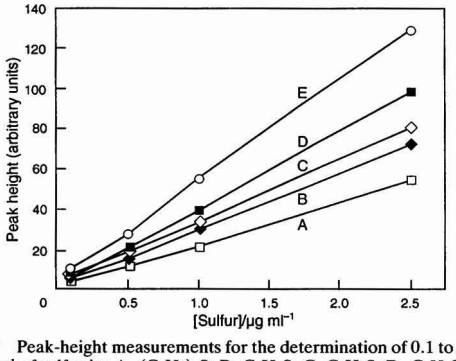

Fig. 7 Peak-height measurements for the determination of 0.1 to 2.5 μg ml^{-1} of sulfur in: A, $(C_3H_7)_2S$; B, C_8H_6S; C, C_5H_6S; D, C_4H_9SH; and E, CS_2.

sulfur compounds can be determined by the GC–FPD method at concentrations from as low as 20 ppb up to the lower per cent. levels. Peak heights gave precise measurements when compared with the peak areas at lower concentrations. FPD showed non-linearity of response depending on the S_2^* band emission at 394 nm. It also showed different selectivities towards sulfur compounds depending on the rate of S_2 formation for each compound, as illustrated in Fig. 8.

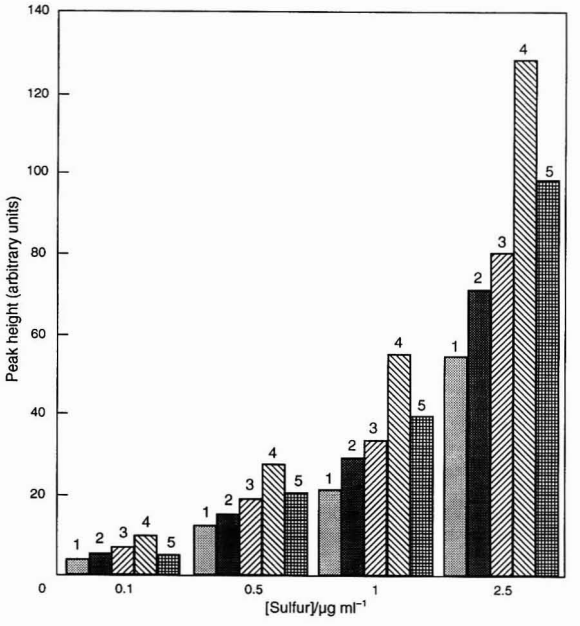

Fig. 8 Flame photometric detector responses for different sulfur compounds. 1. CS_2; 2, C_4H_9SH; 3, C_5H_6S; 4, $(C_3H_7)_2S$; and 5, C_8H_6S.

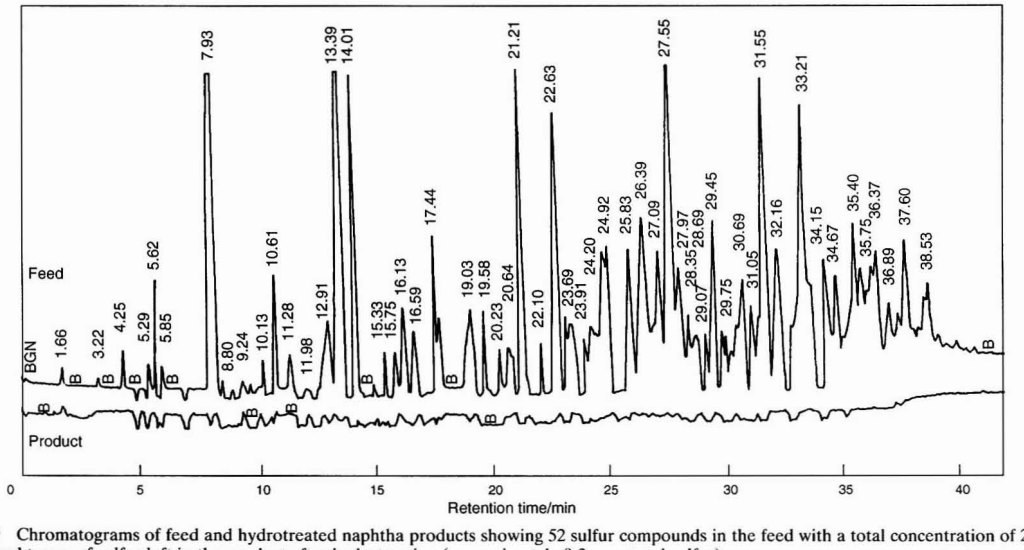

Fig. 9 Chromatograms of feed and hydrotreated naphtha products showing 52 sulfur compounds in the feed with a total concentration of 250 ppm and traces of sulfur left in the product after hydrotreating (approximately 0.3 ppm total sulfur).

The authors acknowledge the support of the Research Institute of the King Fahd University of Petroleum and Minerals, Dhahran, Saudi Arabia.

References

1 Wickbold, R., *Angew. Chem.*, 1957, **69**, 530.
2 Granatelli, R., *Anal. Chem.*, 1959, **31**, 434.
3 Drushel, H. V., *Anal. Lett.*, 1970, **3**, 353.
4 Carter, J. M. *Analyst*, 1972, **97**, 929.
5 Oita, I. J., *Anal. Chem.*, 1983, **55**, 2434.
6 Drushel, H. V., *Anal. Chem.*, 1978, **50**, 76.
7 *1992 Annual Book of ASTM Standards, Volume 05.03, ASTM D-4045. Test Method for Sulfur in Petroleum Products by Hydrogenolysis and Rateometric Colorimetry*, American Society for Testing and Materials, Philadelphia, PA, 1992.
8 Whittemore, I. M., in *Chromatography in Petroleum Analysis*, ed. Altgett, K. H., and Goun, T. N., Marcel Dekker, New York, 1979, ch. 3.
9 Bradley, C., and Schiller, D. J., *Anal. Chem.*, 1986, **58**, 3017.
10 Deans, D. R., *Chromatographia*, 1968, **1**, 187.

Paper 4/02187H
Received April 13, 1994
Accepted December 20, 1994

On-line Spectrophotometric Determination of Phosphate in Bioprocesses by Sequential Injection

Jorge C. Masini,* Pamela J. Baxter, Kandace R. Detwiler and Gary D. Christian

Department of Chemistry BG-10, University of Washington, Seattle, WA 98195, USA

Automation of a reduced molybdophosphoric acid method by sequential injection (SI) for the on-line monitoring of phosphate concentrations is presented. Simplicity, robustness and computer compatibility of the SI system has made possible the monitoring of a wide range of phosphate concentrations (0.1 to 30 mmol l^{-1}) without the necessity of mechanical reconfiguration of the manifold. Dilution, when required, was performed in a mixing chamber connected to the selector valve. Decisions about the necessity of dilution were made through software. Real-time data may be provided to process controllers. Results obtained on-line agreed with those obtained off-line. A sampling frequency of 25 per hour is possible. The method was demonstrated in a study of the influence of phosphate concentration on the production of biomass in aerobic fermentations of *Saccharomyces cerevisae*. The addition of phosphate to the fermentation before its depletion from the medium enhanced the production of biomass by 25 to 35%.

Keywords: *Phosphate; fermentation; sequential injection; automation; spectrophotometry*

Introduction

During fermentation, cell growth ceases when the carbon source is depleted from the medium. However, if the fermentor is fed with a carbon source, such as glucose, there is an increased period of linear growth that ceases before carbon depletion. This indicates that another component has become the limiting factor to the growth. The switch from the limitation by the carbon source to the limitation by another component has been used for the production of secondary metabolites in yeast, bacteria, plant, and mammalian cell cultures.[1–5]

Phosphorus is involved in all phases of cellular metabolism. A source of phosphorus is inorganic phosphate. Growth, limited by phosphate, has been used for the production of alkaloids in plant cell cultures.[1] Proteins, such as interferons, have also been produced in yeast and bacteria fermentations.[2–4]

In *Saccharomyces cerevisae* fermentations, phosphate has been used to control the expression of heterologous proteins (whose genes are linked to promoters of acid phosphatases).[3] Media with a high phosphate concentration repress the expression of heterologous proteins, whereas in media with low levels of phosphate, the production of acid phosphatases and related heterologous proteins is enhanced.

Thus, the production of heterologous proteins is performed through fermentations composed of two distinct phases; a growth phase and an induction phase.[5] During the growth phase there is enough phosphate present in the medium such that the growth is controlled by the carbon source, permitting a high cell density to be reached. By the end of the growth phase, the phosphate concentration depletes to levels below 1 mmol l^{-1} and the induction phase begins.[2] However, high levels of intracellular phosphate may suppress the production of secondary metabolites.[6–8] Better yields have been reached by keeping a low level of intracellular phosphate during the growth phase *via* fed-batch techniques.[8] Thus, in order to achieve maximum productivity of the whole process, a better understanding of the influence of key nutrients and their role in promoting growth and inhibiting secondary product formation is essential.[1,5] Studies on this subject require techniques for on-line monitoring of phosphate in media with a wide range of concentrations, and providing data with real-time characteristics.[5]

Flow injection (FI) is a rapid and reproducible technique, suitable for automating wet chemical methods.[9] Coupling FI with process controllers would allow the development of closed-loop control strategies using real-time data in order to improve and automate the whole process.[5]

Automation of the standard molybdophosphate[2] and molybdovanadate[10] methods by FI has been presented. The resulting manifolds are composed of several flow-channels, a multi-channel peristaltic pump and in some instances, as many as two injection valves. Such systems would require frequent maintenance. Additionally, if different dilution ratios are required, mechanical reconfiguration and, consequently, different calibrations would be necessary.

Sequential injection has been proposed to satisfy the demands for mechanical simplicity in FI techniques.[11–16] The main advantage of SI is that different conditions of analyses may be attained without reconfiguring the system but rather *via* the computer keyboard to change essential parameters, such as flow rate and direction, sample and reagent volumes, reactant ratio and reaction times. The inherent flexibility of SI makes it an ideal tool for monitoring bioprocesses where sample matrix changes with time and different conditions of analyses may be required.[11,12]

This paper describes the automation of the molybdophosphoric method by SI for on-line monitoring of phosphate concentrations in fermentation media. Short analysis times are required so that information with real-time characteristics is available, permitting the control of phosphate concentration, and leading to increased productivity of the process. The method was applied to study of the influence of phosphate concentration on the production of biomass in typical aerobic fermentations of *Saccharomyces cerevisae*.

Experimental

Fermentations

The medium composition and parameters of *Saccharomyces cerevisae* fermentation have been described in earlier work.[17]

*Permanent Address: Instituto de Química, Universidade de São Paulo, Caixa Postal 20780, 01498-970, São Paulo, SP, Brazil.

A 5 l fermentor Bioflo III (New Brunswick Scientific, Edison, USA) was used. A tangential filter was used in order to separate cells and solid particles from the broth before introducing the sample in the SI system (which also served as a sterile interface between fermentor and analyser). The microfiltration module consisted of two stainless-steel disc-shaped shells sandwiching two 0.1 μm pore size membranes (Millipore-waters, Milford, MA, USA) of diameter 47 mm. The sampling and filtration system has been described in earlier work.[18]

Apparatus

A modified Brinkmann PC 701 fibre optic spectrophotometer (Brinkmann Analytical, Westbury, NY, USA) was used in all experiments. The spectrophotometer was adapted into a sandwich flow cell with a 10 μl internal volume and 2 mm light path.[19] Relative absorbance was measured at 660 nm. An IBM compatible PC with FIALab (Alitea, Medina, WA, USA) or AT Matlab (The Mathworks, Natick, MA, USA) was used to control the pump, valve and data acquisition *via* a general purpose input–output board (Model ADA1100, Real Time Devices, State College, PA, USA).

Solutions were driven using a C4V Alitea peristaltic pump. A six port multi-position valve (Valco Instruments, Houston TX, USA) was used with fittings and tubings (Upchurch Scientific, Oak Harbor, WA, USA) to complete the system. Norprene tubing, size 13 (0.76 mm id) (Masterflex, Cole Parmer, Niles, IL, USA) was used with the peristaltic pump.

Chemicals

All reagents used were of analytical-reagent grade obtained from Aldrich (Milwaukee, WI, USA). Two reagent solutions were used for phosphate determination; reagent 1 consisted of 0.005 mol l^{-1} ammonium molybdate in 0.4 mol l^{-1} nitric acid, and reagent 2 consisted of 5% ascorbic acid (m/v) in the presence of 10% (v/v) glycerin (to prevent precipitation of reaction products). Monobasic potassium phosphate was used to prepare a 32.3 mmol l^{-1} stock solution (0.4390 g l^{-1}). Standard solutions with concentrations in a range of blank to 32.3 mmol l^{-1} were prepared by appropriate dilution of the stock solution. De-ionized water (Nanopure II Sybron Barnstead, Dubuque, IA, USA) was used to prepare all solutions.

Manifold

The system components were arranged as shown in Fig. 1. The holding coil was made of 160 cm × 0.8 mm id PTFE tubing and the connecting line to the detector was made of tightly knotted 25 cm × 0.8 mm id PTFE tubing. The sampling line was connected to position 2 of the multi-position valve and consisted of 5 cm × 0.5 mm id PTFE tubing. Between the filtration membrane and sampling line was 30 cm × 0.8 mm id stainless-steel tubing, giving a total dead volume of 160 μl between the membrane and the valve.

Ammonium molybdate (reagent 1) and ascorbic acid (reagent 2) lines were made of 10 cm × 0.5 mm id PTFE tubing connected, respectively, to position 4 and 6 of the multi-position valve. A mixing chamber, with an internal volume of 815 μl, was connected to position 5 using a 5 cm × 0.5 mm id PTFE tubing. The solution inside the mixing chamber was gently stirred by a magnetic stirrer.

Procedure

First, through anti-clockwise movements of the peristaltic pump, all lines were filled with the appropriate solutions. Excess reagent was flushed from the holding coil through an auxiliary waste position using a clockwise movement of the pump. The mixing chamber was filled with water.

Calibration Curves

Concentration range 2–30 mmol l^{-1}

A 120 μl volume of standard solution was aspirated into the holding coil *via* the sampling line (position 2). The valve was turned to position 5 and a clockwise pump movement expelled the sample into the mixing chamber, performing a desired dilution (ratio of 1:7) at 10 s stop time. A volume of 100 μl was aspirated from the mixing chamber towards the holding coil, in order to fill the connecting line with representative solution from inside the chamber. The excess, which reached the holding coil, was flushed through position 3. Then, 200 μl of reagent 1 (position 4), 50 μl of sample from the mixing chamber (position 5), and 200 μl of reagent 2 (position 6) were sequentially aspirated into the holding coil by anti-clockwise movements of the peristaltic pump. With the multi-position valve at position 1 and a clockwise pump movement, the interdispersed zone was propelled through the detector to waste. Simultaneously, the data acquisition began. When the dispersed-sample zone reached the detector (after a delay time of 20 s and a flow rate of 1.2 ml min^{-1}) the flow was stopped for 30 s, permitting the reaction to occur to a greater extent than in a continuous-flow mode. The detector line was washed with water for 40 s and data acquisition was finished. When delay times greater than 20 s are used, the measurement of absorbance is made in a highly dispersed slice of the sample zone, decreasing the sensitivity. Stopped-flow periods greater than 30 s do not lead to significant improvement, suggesting that at this time the reaction is almost complete.

Finally, the multi-position valve was turned to position 5 and water was pumped into the mixing chamber at a rate of 2.5 ml min^{-1} for 2 min, so that the whole system was cleaned for further analyses.

Concentration range 0.03–2.5 mmol l^{-1}

With these solutions, the dilution stage is not required, so 200 μl of reagent 1, 50 μl of standard, and 200 μl of reagent 2 were sequentially aspirated into the holding coil and then

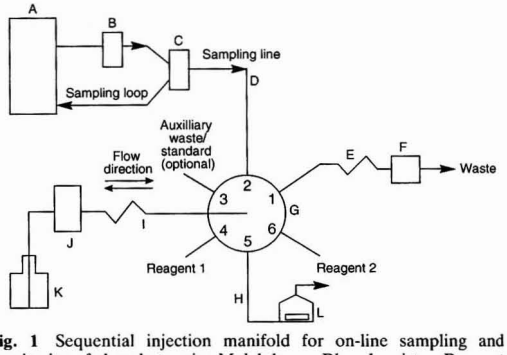

Fig. 1 Sequential injection manifold for on-line sampling and monitoring of phosphate using Molybdenum Blue chemistry. Reagent 1, 0.005 mol l^{-1} ammonium molybdate in 0.4 mol l^{-1} nitric acid; reagent 2, 5% ascorbic acid (m/v) in 10% glycerin (v/v); A = fermentor (5 l capacity); B = peristaltic pump (flow rate of 320 ml min^{-1}); C = tangential filter; D = stainless-steel tubing (30 cm × 0.8 mm id); E = PTFE reactor (25 cm × 0.8 mm id); F = detector (set at 660 nm); G = multi-position value; H = PTFE tube (5 cm × 0.5 mm id); I = PTFE holding coil (160 cm × 0.8 mm id); J = peristaltic pump (flow rate of 1.2 ml min^{-1}); K = carrier (water); and L = mixing chamber (815 μl internal volume).

propelled through the detector, using a procedure similar to that described above.

In all operations, the peristaltic pump was programmed to be stopped while the multi-position valve was rotating, in order to avoid cross-contamination problems as well as bubble formation and pressure surges.

Fermentation Monitoring

A program was written in MatLab (The Mathworks) for phosphate monitoring during fermentation. Before each analysis, 400 μl of sample was aspirated into the holding coil (position 2) and then flushed through the auxiliary waste position (in order to eliminate old solution contained in the sampling line dead volume of 160 μl, so that samples representative of the fermentor solution were used in each analysis). The program consists of two sub-routines. The first one executes the procedure described for construction of calibration curves of phosphate solutions with concentrations from 2 to 30 mmol l^{-1}. The value of the maximum absorbance previously determined for the 2 mmol l^{-1} solution is used as the criterion for calling a second sub-routine, which executes a procedure similar to that described for construction of calibration curves of phosphate solutions with concentrations between 0.03 and 2.5 mmol l^{-1}. In this case, fresh samples were aspirated directly from the sampling line (position 2) and sandwiched between reagent 1 and reagent 2 zones. The order of execution of both sub-routines may be reversed, permitting a higher sampling frequency during induction phases (no dilution necessary).

Off-line Phosphate Analyses and Dry Biomass Determination

Samples containing broth and cells were automatically withdrawn from the fermentor (*via* the same external loop used for on-line sampling) at intervals of 4 h and stored in a refrigerator in polyethylene bottles. Suspensions were manually mixed and either 10.0 or 5.0 ml were transferred to previously weighed centrifuge tubes using an EDP plus motorized pipette (Rainin Instrument, Woburn, MA, USA). The whole system was weighed and the mass of the sample was determined.

Suspensions were centrifuged for 2 min at approximately 100 *g*. Phosphate analyses were performed on the supernatant liquid after appropriate dilution in a calibrated flask. These analyses were performed using traditional FI system,[9] or by the SI system using an injected sample volume of 50 μl and a flow rate of 1.2 ml min^{-1}.

The determination of dry biomass was made with the pellet after supernatant was removed. Details are described elsewhere.[17]

Results and Discussion

Fig. 2 shows calibration curves obtained by aspirating 200 μl of ammonium molybdate and ascorbic acid spaced by different volumes (V) of phosphate standard solutions. It is possible to enlarge the dynamic range by using small volumes (20 or 40 μl) of standard. For more precise results, a syringe pump should be used at these volumes. However, larger volumes (80 μl) improve the sensitivity, so that one could work with solutions in a concentration range of 0.05 to 1.3 mmol l^{-1} with good accuracy and precision.

All experiments gave s_r values of 0.5 to 2.5%. However, according to Ivaska and Růžička,[14] as the angle of the total pump head rotation increases the reproducibility of SI measurements improves. The best s_r values are achieved at one full revolution of the pump head. Riley *et al.*[20] have recommended always starting sampling with the same roller at the same angle for optimum precision in FI. For the conditions of flow rate (1.2 ml min^{-1}) and pump tubing (Norprene 0.8 mm id) used in this work, a full revolution of the pump head is completed in 2.5 s, which means a volume of 50 μl. This value of V was aspirated from the mixing chamber, or from the sampling line when the samples did not require dilution before analysis.

A calibration curve for 2 to 30 mmol l^{-1} phosphate solutions is shown in Fig. 3. It is interesting to note that when measuring the absorbance after a 30 s stopped-flow period, an enlarged linear dynamic range is observed. The closeness of the two curves at lower concentrations suggests the reaction is nearly complete under continuous-flow conditions, but is less than complete at higher concentrations.

These experiments demonstrate that, once the SI system is configured, a wide range of phosphate concentrations might be monitored with the same manifold controlled by appropriate software. Thus, if the solution in the chamber (diluted at a ratio of 1 + 7) gives a signal lower than a previously determined threshold value of absorbance (observed for a 2.5 mmol l^{-1} solution), a second sub-routine is called. In such a situation, a 50 μl sample (without dilution) is directly aspirated from the sampling line and sandwiched between the ammonium molybdate and ascorbic acid zones. Typically, induction phases are carried out with phosphate concentrations of 0.2 to 1 mmol l^{-1},[1–4,25] so that software with the two sub-routines described here would be sufficient to monitor the whole fermentation.

It should be noted that the higher phosphate concentrations could, in principal, be determined without the need of the

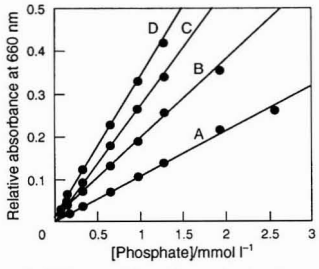

Fig. 2 Effect of different injected standard volumes, V, on the linearity of the calibration curves. Relative absorbance values were measured after a 30 s stopped-flow period. Delay time = 20 s. Flow rate = 1.2 ml min^{-1}. A, V = 20 μl, $y = 0.106x + 0.00049$ ($r^2 = 0.9998$); B, V = 40 μl, $y = 0.191x + 0.0059$ ($r^2 = 0.9997$); C, V = 60 μl, $y = 0.263x + 0.0047$ ($r^2 = 0.9996$); and D, V = 80 μl, $y = 0.321x + 0.012$ ($r^2 = 0.9990$). Linear regression calculated for the concentration range of 0 to 1.3 mmol l^{-1}.

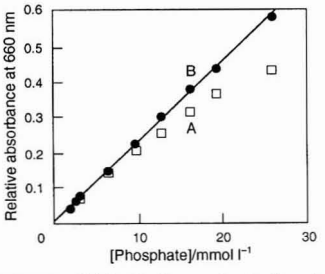

Fig. 3 Responses obtained from standard solutions (2 to 30 mmol l^{-1}) after injection of 120 μl into the mixing chamber (promoting a dilution of 1 + 7). Flow rate = 1.2 ml min^{-1}. Delay time = 20 s. Stopped flow period = 30 s. V = 50 μl (aspirated from the mixing chamber). A, continuous flow and B, stopped flow mode.

dilution chamber if unreduced molybdophosphoric acid had been measured, as the absorptivity of the unreduced form (at 400 nm) is about 3400 l per mol cm, one seventh that of the reduced form at 660 nm,[21] *i.e.*, by aspirating only ammonium molybdate reagent in instances where the mixing chamber was used. However, the fermentation medium exhibits significant absorbance at the 350–400 nm range, and substantially less at 660 nm, making use of the unreduced molybdophosphoric acid impractical. The mixing chamber method is, in addition, applicable to a wide range of analytes that require extensive dilutions. Unreduced molybdophosphoric acid methods have also been reported.[22–24]

Sampling

Problems related to cross-contamination through the multi-position valve are avoided by switching the pump off when the valve is rotating.[13] However, in bioprocess control, the sampling line (position 2) is constantly under a small pressure caused by the pumping (320 ml min^{-1}) of broth and cells through the fermentor external loop (filtrate flows spontaneously from the tangential filter at a rate of approximately 1 ml min^{-1} when unconnected to the SI system). This means that with the Valco valve specifically (and perhaps others), one must avoid rotation of the multi-position valve that would contact the sampling line and holding coil after ammonium molybdate solution and sample (from the mixing chamber) have been aspirated into the holding coil. This movement would cause the introduction of a small amount of undiluted sample into the holding coil and a systematic positive error.

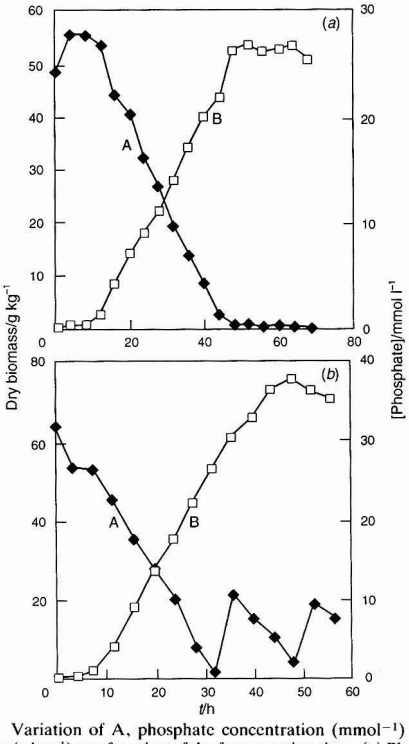

Fig. 4 Variation of A, phosphate concentration ($mmol^{-1}$) and B, biomass (g kg^{-1}) as a function of the fermentation time. (*a*) Phosphate added only at the start of the fermentation and (*b*) phosphate added at the start and before its depletion from the medium.

Monitoring

Fig. 4(*a*) shows the variation of phosphate and dry biomass as a function of the fermentation time for an experiment in which the phosphate was completely depleted from the medium after 48 h. A production of around 56 ± 8 g kg^{-1} (n = 5) was observed. Fig. 4(*b*) shows the same variation for a fermentation fed with phosphate after 32 and 48 h. A production of 77 ± 6 g kg^{-1} (n = 4) of biomass was attained at the end of the growth phase, which means an increased biomass production of 25 to 35%.

A comparison between results obtained on-line and off-line for phosphate concentrations is given in Table 1. The student t-test results at $P = 0.01$ are 0.075 compared with the tabulated value of 2.85, indicating no significant differences in the methods. Off-line analyses were performed by SI or classical FI. In these cases, sample dilution was performed manually and results are not available with real-time characteristics necessary for immediate medium control.

Fig. 5 shows the data obtained for seven measurement cycles, performed at intervals of 2 h, during a fermentation

Table 1 Comparison of phosphate concentrations obtained by on-line and off-line monitoring of fermentation samples. Average difference = −0.01 mmol l^{-1}

Phosphate concentration/mmol l^{-1}		
On-line	Off-line	Difference
4.34	4.20	0.14
5.34	5.63	−0.29
5.59	4.96	0.63
6.95	7.75	−0.80
7.61	7.97	−0.36
7.94	7.50	0.44
8.93	9.46	−0.53
10.06	10.08	−0.02
10.08	10.39	−0.31
10.17	11.70	−1.53
10.55	10.80	−0.25
14.86	14.21	0.65
17.91	17.17	0.74
18.19	17.84	0.35
23.15	22.76	0.39
24.66	25.26	−0.60
24.84	24.32	0.52
25.50	25.77	−0.27
25.94	26.73	−0.79
26.25	25.48	0.77
26.45	26.60	−0.15
26.61	26.65	−0.04
27.44	26.38	1.06

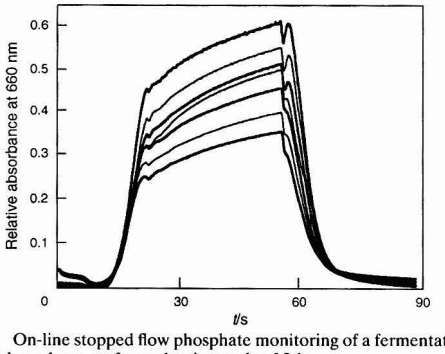

Fig. 5 On-line stopped flow phosphate monitoring of a fermentation run with analyses performed at intervals of 2 h.

experiment. The stability of the baseline is observed, as well as the effect of the stopped-flow period on the absorbance values.

Each analysis by on-line SI required 5 min, including sampling time and cleanup. However, when sample dilution is not necessary a sampling frequency of 25 h^{-1} is possible. It should be noted that the criterion used for calling the second sub-routine might be inverted so that the experiment could be run first without dilution. In this case, if the absorbance signal is higher than that obtained for a 2.5 mmol l^{-1} solution, a second sub-routine would be called in order to perform the dilution, so that the sampling frequency of 25 h^{-1} might be attained during induction phases.

The phosphate uptake by cells during the linear growth phase is around 2 to 3 mmol g^{-1} h^{-1}. Thus, the sampling frequency obtained is high enough to provide real-time data to process controllers.

Conclusion

Proven feasible for automating the 'Molybdenum Blue' method for phosphate monitoring in bioprocesses, SI presents some advantages in comparison to classical FI (such as the simplicity of the manifold). A small reduction in reagent consumption is observed. The flow detector fouling with the product of the reaction between ascorbic acid and ammonium molybdate does not occur in SI manifold as the detector is in contact with water between analyses. In FI manifolds, both reagents are mixed in the detector field causing fouling after a few hours of use. As a consequence, very stable base lines are obtained by SI and system cleaning during the operation time is unnecessary.

In addition, peristaltic pump tubing is never in contact with corrosive chemicals which extends its lifetime. Consequently, maintenance is unnecessary during an extended fermentation run. Re-calibration was performed daily and variations of 2 to 3% in phosphate concentration were observed. However, for process monitoring in laboratory environments this reproducibility is acceptable.

Another advantage of SI is the possibility of clustering standards around the multi-position valve, so that the system might be automatically recalibrated as required. There is also the possibility of two assays being performed with a unique SI system,[16] so that further studies could lead to the on-line monitoring of phosphate and biomass,[17] or phosphate and acid phosphatases.

Results showed the importance of controlling the phosphate concentration in fermentation medium of *Saccharomyces cerevisae* in order to realize an increased production of biomass, which is a first step in the production of secondary metabolites. In this case, on-line monitoring of phosphate would allow an appropriate balance between cell growth and secondary metabolite induction.

The authors express their gratitude to J. Růžička and L. Scampavia for suggestions and comments. J. C. M. acknowledges a fellowship from Fundação de Amparo a Pesquisa do Estado de São Paulo. K. R. D. acknowledges USDOE for financial support.

References

1 van Gulik, W. M., ten Hoopen, H. G. J., and Heijnen, J. J., *Biotechnol. Bioeng.*, 1993, **41**, 771.
2 Forman, L. M., Thomas, B. D., and Jacobson, F. S., *Anal. Chim. Acta*, 1991, **249**, 101.
3 Kramer, R. A., De Chiara, T. M., Schaber, M. D., and Hilliker, S., *Proc. Natl. Acad. Sci. U.S.A.*, 1984, **81**, 367.
4 Schendel, F. J., Baude, E. J., and Flickinger, M. C., *Biotechnol. Bioeng.*, 1989, **34**, 1023.
5 Bishop, B. F., and Lorber, S. J., in *Sensors in Bioprocess Control*, ed. Twork, J. V., and Yacynych, A. M., Marcel Dekker, New York, 1990, p. 1.
6 Bramble, J. L., Graves, D. J., and Brodelius, P., *Biotechnol. Bioeng.*, 1991, **37**, 859.
7 Mantell, S. H., Pearson, D. W., Hazell, L. P., and Smith, H., *Plant Cell Rep.*, 1983, **2**, 73.
8 Schiel, O., Jarchow-Redecker, K., Piehl, G. W., Lehmann, J., and Be, J., *Plant Cell Rep.*, 1984, **3**, 18.
9 Růžička, J., and Hansen, E. H., in *Flow Injection Analysis*, Wiley, New york, 2nd edn. 1988.
10 Parker, C. P., Gardell, M. G., and DiBiasio, P., *Am. Biotechnol. Lab.*, 1985, **3**(5), 37.
11 Růžička, J., and Marshall, G. D., *Anal. Chim. Acta*. 1990, **237**, 329.
12 Gübelli, T., Christian, G. D., and Růžička, J., *Anal. Chem.*, 1991, **63**, 2407.
13 Guzman, M., Pollema, C., Růžička, J., and Christian, G. D., *Talanta*, 1993, **1**, 81.
14 Ivaska, A., and Růžička, J., *Analyst*, 1993, **118**, 885.
15 Baron, A., Guzman, M., Růžička, J., and Christian, G. D., *Analyst*, 1992, **117**, 1839.
16 Růžička, J., *Anal. Chim. Acta*, 1992, **261**, 3.
17 Baxter, P. J., Christian, G., Růžička, J., *Analyst*, 1994, **119**, 1807.
18 Chung, S., Wen, X., Vilholm, K., De Bang, M., Christian, G. D., and Růžička, J., *Anal. Chim. Acta*, 1991, **249**, 77.
19 Pavón, J. L. P., Gonzalo, E. R., Christian, G. D., and Růžička, J., *Anal. Chem.*, 1992, **64**, 923.
20 Riley, C., Rocks, B. F., and Sherwood, R. A., *Anal. Chim. Acta*, 1986, **179**, 69.
21 Crouch, S. R., and Malmstadt, H. V., *Anal. Chem.*, 1967, **39**, 1084.
22 Amador, E., and Urban, J., *Clin. Chem. (Winston-Salem, N.C.)*, 1972, **18**, 601.
23 Munoz, M. A., Balon, M., and Fernandez, C., *Clin. Chem. (Winston-Salem, N.C.)*, 1983, **29**, 372.
24 Rubino, L., Catapano, V., and Guerra, G., *J. Autom. Chem.*, 1989, **11**, 164.
25 Toh-e, A., Ueda, Y., Kakimoto, S. I., Oshima, Y., *J. Bacteriol.*, 1973, **113**, 727.

Paper 4/05174B
Received August 24, 1994
Accepted January 6, 1995

Column Preconcentration of Cobalt with the Ion Pair of 2-Nitroso-1-naphthol-4-sulfonic Acid–Tetradecyldimethylbenzylammonium Chloride Supported on Naphthalene Using Second-derivative Spectrophotometry

Mohammad Ali Taher and Bal Krishan Puri

Chemistry Department, Indian Institute of Technology, Hauz Khas, New Delhi-110 016, India

Cobalt is quantitatively retained on 2-nitroso-1-naphthol-4-sulfonic acid–tetradecyldimethylbenzylammonium (TDBA$^+$)–naphthalene adsorbent in a chromatographic column in the pH range 6.1–9.0 at a flow rate of 1 ml min^{-1} from a large volume of aqueous solutions of various alloys. The solid mass consisting of the cobalt complex and naphthalene was dissolved out of the column with 5 ml of dimethylformamide (DMF) and the metal was determined by second-derivative spectrophotometry in the concentration range 1.0–60.0 μg per 5 ml of the final DMF solution. Seven replicate determinations of 20 μg of cobalt gave a mean peak height of 0.128 with a relative standard deviation of 1.4%. The sensitivity of the method is 0.019 μg ml^{-1}, found from the slope of the calibration graph. The interference of a large number of anions and cations was studied and the optimized conditions have been utilized for the trace determination of cobalt in standard reference materials. The method may also be applied to the trace determination of cobalt in various biological and environmental samples.

Keywords: Cobalt determination; derivative spectrophotometry; 2-nitroso-1-naphthol-4-sulfonic acid–tetradecyldimethylbenzylammonium–naphthalene adsorbent; standard alloys and steels

Introduction

The reagent 2-nitroso-1-naphthol-4-sulfonic acid (nitroso-S salt) was introduced by Hoffman[1] for the qualitative and later by Wise and Brandt[2] for the quantitative determination of cobalt. Although the reagent is highly sensitive for cobalt, it gives a large reagent blank, making the method troublesome. Attempts have also been made to determine some metals after extraction of the metal–nitroso-S–tetradecyldimethylbenzylammonium (TDBA) ion associated complexes into chloroform in the presence of a large amount of sodium chloride as a salting-out agent.[3] A survey of the literature revealed that various adsorbents, such as thiol cotton,[4] silanized glass beads,[5] C_{18}-bonded silica gel,[6] Amberlite XAD-4 resin.[7] cellulose,[8] silica gel,[9] green tea leaves[10] and polythioether foam[11] have been tried for the preconcentration of metal ions. Although some of these adsorbents are fairly effective, their methods of preparation are lengthy and involve rigid control of the conditions. The desorption of the metal is carried out by a slow process of elution (probably the metal complex may be held by interior surfaces of the adsorbent and hence is not eluted easily), so the procedure is time consuming.

In this paper, an efficient method for the preconcentration of cobalt from a large volume of the aqueous solutions of various standard reference materials with 2-nitroso-1-naphthol–TDBA–naphthalene adsorbent is described. The method is economical (all reagents are cheap and only 0.3 g of the adsorbent and not much glassware are needed), rapid (the adsorbent is dissolved out of the column instead of being eluted), simple (the metal solution at a definite pH is passed over the adsorbent), sensitive (the adsorbent can be dissolved in 2–5 ml of an organic solvent, and the whole of the solution may be used for the absorbance measurement) and highly selective (the reagent nitroso-S salt is specific for cobalt. It is relatively cheap and selective compared with many other reagents used recently[12–18]). The solid mass, consisting of the metal ion associated complex and naphthalene, can easily be dissolved out of the column with a suitable organic solvent such as dimethylformamide (DMF) and the cobalt is determined by second-derivative spectrophotometry. The metal can also be determined by directly aspirating the DMF solution into the flame of an AAS instrument, but the instrument is relatively expensive, maintainence is high and it is not free from matrix effects. Various parameters were evaluated and the optimized conditions were utilized for the trace determination of cobalt in certified alloys and steel samples. The method may also be employed for the determination of cobalt in various environmental and biological samples.

Experimental

Apparatus

A Hitachi Model 330 UV/VIS spectrophotometer with a 1 cm pathlength (quartz cell) and an Elico pH meter with a glass electrode and calomel combination were used. A funnel-tipped glass tube (60 × 6 mm id) was used as a preconcentration column (Fig. 1). It was plugged with poly(propylene) fibres and filled with the slurry (adsorbent) to a height of 1.0–1.2 cm after slightly pressing the adsorbent in the column with a flat glass rod.

Reagents

All reagents were of analytical-reagent grade. Cobalt(II) chloride was dissolved in distilled water and standardized complexometrically. A 2 ppm solution was prepared by appropriate dilution of the standard solution. Buffer solutions of pH 8–11 and 4–7 were prepared by mixing 0.5 mol l^{-1} solutions of each of ammonium acetate and ammonia and of acetic acid and ammonium acetate, respectively, appropriate ratios.

Preparation of Nitrosos-S–TDBA–Naphthalene Adsorbent

A solution of naphthalene was prepared by dissolving 20 g in 40 ml of acetone on a hot-plate stirrer at approximately 35 °C. It was transferred into a beaker containing 1500 ml of distilled water and 0.9 g (0.0028 mol) of nitroso-S salt in a fast stream with continuous stirring at room temperature. $TDBA^+Cl^-$ (1.2 g, 0.0031 mol) was dissolved in 500 ml of distilled water by warming on a hot-plate. It was mixed with the above solution of naphthalene–acetone–nitroso-S salt in water. The yellow naphthalene material coprecipitated with TDBA and nitroso-S was stirred for about 2 h and then allowed to stand for another 2 h at room temperature. The supernatant solution was decanted off and the residue was washed twice with distilled water. The adsorbent in the form of a slurry was stored in a brown bottle for subsequent use.

General Procedure

An aliquot of cobalt solution containing 1–60 μg of cobalt was taken in a 25 ml beaker. The pH of this solution was adjusted to 8 with the addition of 1 ml of buffer solution (pH 8.0–8.5) and diluted to about 15 ml with distilled water. The column loaded with the nitroso-S–TDBA–naphthalene adsorbent was conditioned to pH 8.0 with 2–3 ml of buffer and then the metal solution was passed through the column at a flow rate of 1 ml min^{-1}. The packing was washed with a small volume of water and then aspirated strongly for a few minutes, pushing down the naphthalene material with a flat glass rod to eliminate the excess of water attached to the naphthalene. The solid mass, consisting of the metal complex along with naphthalene, was dissolved out of the column with 5 ml of DMF. The second-derivative spectrum of this solution was recorded from 520 to 660 nm against a reagent blank at a scan rate of 60 nm min^{-1} with $\Delta\lambda$ = 10 nm.

Results and Discussion

Spectral Characteristics (Zero Order)

The absorption spectrum of the ion-associated Co–nitroso-S–TDBA in DMF against the reagent blank prepared under similar conditions was recorded (Fig. 2) and the second-derivative spectrum is shown in Fig. 3. Derivatization of the spectrum leads to sharper zero-order bands and gives higher signals. The main instrumental parameters affecting the shape of the derivative spectra are the wavelength, scanning speed, the wavelength increment over which the derivative is obtained ($\Delta\lambda$) and the response time. These parameters need to be optimized to give a well resolved peak (better resolution), *i.e.*, to give good selectivity and higher sensitivity in a determination. Preliminary observations revealed that the best results were obtained from the second-derivative spectrum with scale range of 0.3, a wavelength interval ($\Delta\lambda$) of 10 nm and a scan speed of 60 nm min^{-1}. The response time is automatically selected by the spectrophotometer in accordance with the optical energy and the scanning speed. Fig. 3 indicates that a calibration graph may be obtained by measuring the peak heights in the second-derivative spectrum at 620, 592 or 564 nm from the baseline. This method is easier than the peak-to-peak method, especially when interfering ions are present. In this study, the peak height at 620 nm was measured in all instances against the reagent blank.

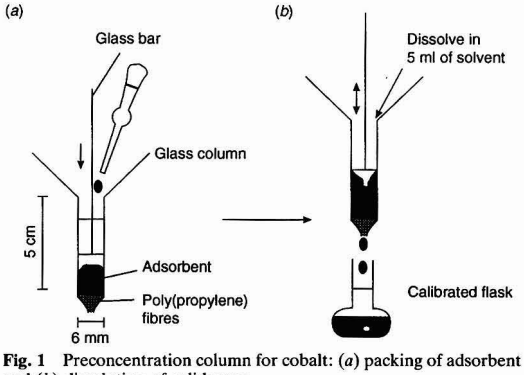

Fig. 1 Preconcentration column for cobalt: (*a*) packing of adsorbent and (*b*) dissolution of solid mass.

Retention Characteristics of Nitroso-S–TDBA–Naphthalene

TDBA chloride is a well known water-soluble quaternary ammonium salt widely used as the counter ion in anionic metal complexes in the solvent extraction of metals.[19] The reagent 2-nitroso-1-naphthol-4-sulfonic acid has one sulfonic acid group capable of dissociation and thus it can form ion pairs (nitroso-S:TDBA = 1:1) with quaternary ammonium cations as follows:

$$C_{10}H_5(OH)(NO)SO_3^- + (R)_4N^+ \rightleftharpoons [C_{10}H_5(OH)(NO)SO_3]^-[R_4N]^+ \quad (1)$$

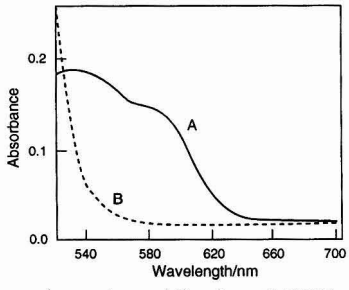

Fig. 2 Zero-order spectrum of Co–nitroso-S–TDBA–naphthalene complex in DMF solution (A) and against reagent blank (B): Co, 20 μg; pH 8.0; buffer, 1.0 ml; and flow rate, 1 ml min^{-1}.

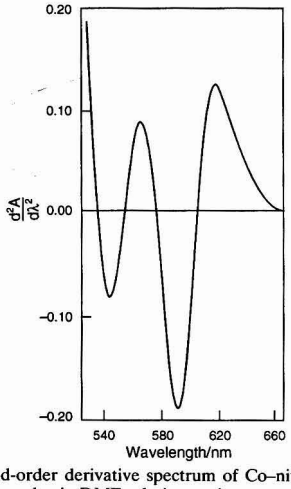

Fig. 3 Second-order derivative spectrum of Co–nitroso-S–TDBA–naphthalene complex in DMF solution against reagent blank: Co, 20 μg; pH, 8.0; scan speed, 60 nm min^{-1}; and $\Delta\lambda$, 10.

The ion pair formed between the nitroso-S anion and $TDBA^+$ cation is easily coprecipitated with microcrystalline naphthalene. The ion-pair reactions between nitroso-S and several well known quaternary ammonium salts were therefore tried in order to develop new adsorbents. Preliminary results indicated that only $TDBA^+$ and cetyltrimethylammonium ($CTMA^+$) can form ion pairs with nitroso-S. In this study, $TDBA^+$ was selected as the counter ion as it is cheaper than $CTMA^+$ and has excellent retention characteristics for metal ions.

Reaction Conditions

The conditions were established by use of 20 μg of cobalt. The adsorption of cobalt on this absorbent was found to be maximum in the pH range 6.1–9.0 (Fig. 4). In subsequent studies, the pH was maintained at about 8.0. Addition of 0.5–15.0 ml of the buffer (pH 8.0–8.5) did not affect the retention of cobalt and the use of 1.0 ml was recommended. The flow rate was varied from 0.2 to 8 ml min^{-1} and was found not to affect adsorption within this range. A flow rate of 1–2 ml min^{-1} was adopted in all subsequent experiments. With larger volumes of the aqueous phase, a flow rate of 8 ml min^{-1} can be used in order to decrease the time of analysis. The effect of the volume of the aqueous phase on the retention of cobalt was investigated using the general procedure. The adsorption was constant and maximum when the volume of the aqueous phase did not exceed 200 ml, resulting in a preconcentration factor of about 40. The solid mass can be completely dissolved out of the column with less than 3 ml of the solvent (DMF), hence a preconcentration factor of about 67 can be achieved. In subsequent studies, 20 ml of the aqueous phase were used for convenience.

Retention Capacity of the Adsorbent

The retention capacity of the adsorbent was determined by a batch method. The experiment was performed by taking 500 μg of cobalt, 1 ml of buffer solution (pH 8.0–8.5) and 40 ml of water in a beaker. This solution was transferred into a separating funnel and then a suitable amount of the nitroso-S–TDBA–naphthalene adsorbent was added. The separating funnel was shaken vigorously on a mechanical shaker for 5 min. The solid mass was separated by filtration and cobalt was determined from the filtrate by AAS. The solid mass on the filter-paper was dried in an oven, kept in a desiccator and then weighed to determine the mass of the adsorbent. The maximum amount of cobalt retained with 15.5 mg g^{-1} of nitroso-S-salt in the adsorbent. It was also noted that the retention capacity depends on the amount of TDBA and nitroso-S supported on naphthalene. From the stoichiometry in reaction (1), the molar ratio of nitroso-S and $TDBA^+$ is 1:1. From the observations on the preparation of the adsorbent, it was found that with the use of nitroso-S (0.9 g, 0.0028 mol) and $TDBA^+$ (1.2 g, 0.0031 mol), a slight excess of nitroso-S and 20 g of naphthalene were sufficient for the complete retention of the metal ions.

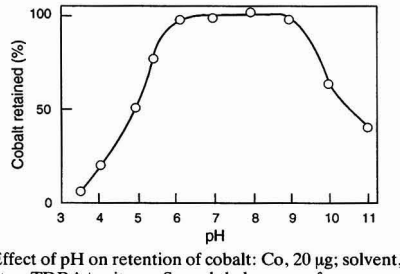

Fig. 4 Effect of pH on retention of cobalt: Co, 20 μg; solvent, DMF; adsorbent, $TDBA^+$–nitroso-S–naphthalene; reference, reagent blank.

Choice of Solvent

A number of solvents were tried for dissolving the Co–nitroso-S–TDBA–naphthalene from the column. As the solid mass was dissolved in a small volume (3–5 ml) of the solvent from the column, it was essential to select a solvent in which the chelate is highly soluble in order to achieve a high sensitivity for the spectrophotometric measurements. The solid material was found to be insoluble in ordinary organic solvents such as toluene, 1,2-dichloroethane, hexane, nitrobenzene, isoamyl alcohol, amyl alcohol, ethyl acetate, methylisobutyl ketone,

Table 1 Effect of diverse salts and ions

Salt or ion	Tolerance limit	Salt or ion	Tolerance limit
$CH_3COONa·3H_2O$, KNO_3, NH_4Cl, Na_2SO_4	1 g	Trisodium citrate	10 mg
NaCl, KI, $Na_3PO_4·12H_2O$, K_2CO_3, K_2SO_4, NaF	200 mg	Mn^{II}, Ag^{I}	6.5 mg
		Pb^{II}, Sb^{III}	12 mg
		Zn^{II}	4.5
$(CH_3COO)_2$ Mg·$4H_2O$	500 mg	Ni^{II}	2 mg
		Mo^{VI}	2.7 mg
$CaCl_2$, $Na_2S_2O_3$	100 mg	Cd^{II}	7.3 mg
Thiourea	500 mg	Cr^{VI}	3.3
Na_3EDTA	10 μg	Al^{III}	30 μg, 3 mg*
KSCN, KNa tartrate	20 mg	Fe^{III}	30 μg*, 1 mg*
		Cu^{II}	25 μg, 0.25 mg†

* Masked with 200 mg of NaF + 10 mg of tri sodium citrate.
† Masked with 500 mg of thiourea + 0.1 g of $Na_2S_2O_3$.

Table 2 Analysis of standard reference materials for cobalt

		Concentration or cobalt (%)	
Sample	Composition (%)	Certified value	Found*
JSS 651-7 Stainless steel	C, 0.047; Si, 0.72; Mn, 1.72; P, 0.028; Cr, 18.60; S, 0.0063 Mo, 0.84; Cu, 0.082 Al, 0.002; N, 0.0312; Ni, 9.20	0.22	0.23 ± 0.02
JSS 653-7 Stainless Steel	C, 0.068; Si, 0.63; Cu, 0.030; Ni, 13.91; Mn, 1.72; Cr, 22.53; N, 0.0276	0.35	0.37 ± 0.03
NKK 916 Aluminium Alloy	Si, 0.41; Fe, 0.54; Cu, 0.27; Mn, 0.11; Mg, 0.10; Cr, 0.05; Ni, 0.06; Zn, 0.30; Ti, 0.10; Sn, 0.05; Pb, 0.04; V, 0.02; Zr, 0.05; Bi, 0.03; Sb, 0.01; B, 0.0006	0.03	0.03 ± 0.01

* Mean of four determinations ± standard deviation; 0.5 g of thiourea, 10 mg of trisodium citrate, 0.1 g of $Na_2S_2O_3$ and 0.2 g of NaF were added as masking reagents at pH ≈ 8.

chloroform and dioxane, but soluble in dimethyl sulfoxide, DMF and propylene carbonate. DMF was preferred owing to the high solubility and stability. It was found that 2–3 ml of this solvent were sufficient to dissolve the mixture, thus enhancing the sensitivity of the method. As only a small volume (3–5 ml) of the solvent was used to dissolve the complex and naphthalene, it was essential to study the effect of the surplus water attached to naphthalene. It was noted that the surplus water decreased the absorbance by 12–15% and led to an error in the determination. Hence it was necessary to eliminate the water attached to the naphthalene in the column completely by aspirating it.

Linearity, Sensitivity, Precision and Stability

On the basis of the optimum conditions developed above, a calibration graph was constructed between the peak height and the concentration of cobalt. The graph was found to be linear over the concentration range 1–60 μg of cobalt in 5 ml of the final DMF solution. Seven replicate determinations of 20 μg of cobalt gave a mean peak height of 0.128 with a relative standard deviation of 1.4%. The sensitivity of the method was found to be 0.019 μg ml^{-1} from the slope of the calibration graph.

Effect of Diverse Ions

Various salts and metal ions were added individually to a solution containing 20 μg of cobalt and the general procedure was applied. The tolerance limit was set as the ion concentration required to cause a ±3% error in the determination of cobalt. The results obtained are given in Table 1. Among the salts examined, most could not be tolerated up to gram or milligram levels, except BDTA (10 μg). Of the metal ions examined, most metal ions could be tolerated up to the 1 mg level, except Cu^{II} (25 μg), Al^{III} (30 μg) and Fe^{III} (30 μg). However, these could be easily masked with the addition of sodium fluoride (200 mg)–trisodium citrate (10 mg) for Al^{III} and Fe^{III} and thiourea (500 mg)–$Na_2S_2O_3$ (0.1 g) for Cu^{II}. Hence the method is highly selective and may safely be applied to the determination of cobalt in reference materials.

Determination of Cobalt in Standard Aluminium Alloys and Steel Samples

The proposed method was applied to the determination of cobalt in Nippon Keikinzoku Kogyo (NKK) CRM 916 aluminium alloy and Japanese standards of iron and steel (JSS) CRM 651-7 and 653-7 stainless steel. A 0.1 g sample of the standard aluminium alloy or steel was completely dissolved in 6–14 ml of hydrochloric acid (1 + 1) by heating on a water-bath and then 1 ml of 30% v/v hydrogen peroxide was added. The excess of peroxide was decomposed by heating the sample on the water-bath. The solution was cooled, filtered if necessary and diluted to 100 ml with distilled water in a calibrated flask. An aliquot (1–2 ml) of this sample was taken in a 20 ml beaker, 0.5 g of thiourea, 10 mg of trisodium citrate, 0.1 g of $Na_2S_2O_3$ and 0.2 g of NaF were added as masking reagents at pH ≈ 8 and the general procedure was applied. The results obtained are given in Table 2. These results are in agreement with the certified values.

Conclusion

A simple, economical and highly selective adsorbent was obtained simply by mixing aqueous solutions of nitroso-S salt and $TDBA^+ Cl^-$ with an acetone solution of naphthalene and applied to the preconcentration of cobalt from a large volume of the aqueous solutions of alloy and steel samples. As nitroso-S salt reacts with several metal ions, similar procedure may also be developed for them. The reagent is cheap and highly selective for cobalt and the use of second-derivative spectrophotometry further increased the sensitivity and selectivity of the method. Cobalt may also be determined by directly aspirating the DMF solution of the metal complex after preconcentration into the flame of an AAS instrument or by pulse polarography. Preliminary experiments also indicated that the cobalt–nitroso-S–TDBA ion associated complex, which cannot be extracted into many organic solvents owing to its low solubility, may be coprecipitated with 2 ml of 20% naphthalene solution. Although this method is less time consuming than the reported column method, the preconcentration factor is low (approximately 20).

References

1 Hoffman, O., *Chem. Ber.*, 1985, **18**, 46.
2 Wise, W. M., and Brandt, W. W., *Anal. Chem.*, 1954, **26**, 693.
3 Motomizu, S., and Toei, K., *Bunseki Kagaku*, 1981, **30**, 245.
4 Yu, M.-Q., and Liu, G.-Q., *Talanta*, 1983, **30**, 265.
5 Taguchi, S., Yal, T., Shimada, Y., and Goto, K., *Talanta*, 1983, **30**, 169.
6 Watanabe, H., Goto, K., Taguchi, S., McLaren, J. W., Berman, S. S., and Russell, D. S., *Anal. Chem.*, 1981, **53**, 738.
7 Sakai, Y., and Mori, N., *Talanta*, 1986, **33**, 161.
8 Burba, P., and Willmer, P. G., *Talanta*, 1983, **30**, 381.
9 Kubota, M., Matsumoto, K., and Terada, K., *Anal. Sci.*, 1987, **3**, 45.
10 Kimura, M., Yamashita, H., and Komada, J., *Bunseki Kagaku*, 1986, **35**, 400.
11 Khan, A. S., and Chow, A., *Talanta*, 1986, **33**, 182.
12 Barrera, A. B., Barrera, P. B., and Martinez, F. B., *Analyst*, 1985, **110**, 1313.
13 Odashima, T., Kibuchi, T., Ohtani, W., and Ishii, H., *Analyst*, 1986, **111**, 1383.
14 Sanchez, F. G., Lopez, M. H., and Gomez, T. C., *Talanta*, 1987, **197**, 275.
15 Murillo, J. A., and Lemus, M., *Analyst*, 1988, **113**, 1439.
16 Jimenez, A. I., Jimenez, F., and Arias, J. J., *Analyst*, 1989, **114**, 93.
17 Satake, M., Nagahiro, T., and Puri, B. K., *Analyst*, 1993, **118**, 85.
18 Toral, M. I., Richter, P., and Silva, L., *Talanta*, 1993, **40**, 1405.
19 Bandyopadhyay, S., and Das, A. K., *J. Indian Chem. Soc.*, 1989, **66**, 427.

Paper 4/07190E
Received November 25, 1994
Accepted December 14, 1994

Selective Spectrophotometric Determination of Cobalt(II) Using 2,2′-Dipyridyl-2-Pyridylhydrazone and a Flow Injection Manifold

Demetrius G. Themelis, George A. Zachariadis and John A. Stratis

Department of Chemistry, Laboratory of Analytical Chemistry, Aristotle University of Thessaloniki, 54006 5Thessaloniki, Macedonia, Greece

Micro-amounts of cobalt(II) were determined spectrophotometrically at 500 nm using a flow injection manifold and 2,2′-dipyridyl-2-pyridylhydrazone (DPPH) as a colour-forming reagent. The various chemical and physical variables were optimized and a study of interfering ions was also carried out. A linear calibration graph was obtained for 0–12.0 mg l^{-1} cobalt(II), at a sampling rate of 90 injections per hour. The accuracy and reproducibility were very good (s_r = 0.4%), the limit of detection was 0.017 mg l^{-1} and the limit of quantitation was 0.031 mg l^{-1}. The method was found to be adequately selective owing to the fact that the strongly acidic medium used prevented the formation of complexes of the reagent with other ions. The method has been successfully applied to the determination of cobalt in cyanocobalamin (vitamin B_{12}).

Keywords: Cobalt; spectrophotometry; 2,2′-dipyridyl-2-pyridylhydrazone; flow injection; cyanocobalamin

Introduction

Continuous-flow methods have been developed extensively for the determination of many metals and non-metals. There are two types of continuous-flow analysis; the air-segmented flow type[1] and the unsegmented flow type[2] (flow injection, FI). Since its inception, FI has undergone continued development as demonstrated by the number of analytical methods that have been proposed to determine numerous species in several matrices with good precision, accuracy, and sensitivity. Flow injection is a kinetic-based technique[3] which does not require the reaction being monitored to undergo completion prior to analysis. This is due to the reproducible timing and controlled dispersion of FI.[4] One of the advantages of FI is its higher throughput rate, because of the shorter residence time of the sample in the flow system. Also, several on-line separation and concentration techniques have been coupled to FI systems in order to permit determinations, particularly at trace level concentrations. Several books on this technique have been published.[4–6]

As regards the automated determination of cobalt, several FI procedures have been reported in the last few years, the majority of them based on the complex-formation reaction between cobalt and a ligand. Among the detectors used are chemiluminescence,[7–9] flame atomic absorbance spectrometry[10–12] (AAS), electrothermal atomic absorbance spectrometry[13] and spectrophotometry.[14–17]

A number of the above methods were applied to water samples,[10,11,14] reference materials,[13] and steels.[15,16] However, although they are generally sensitive, the procedures involved are complex and they are subject to a number of interferences which require the use of masking agents or prior separations and on-line preconcentration procedures that often make them time-consuming. Moreover, the application of on-line column preconcentration is not without problems and in some cases the improvement in efficiency is only marginal and, occasionally, interference effects even seem to be enhanced.

Nitrogen-containing heterocyclic hydrazone compounds are selective and sensitive reagents for the spectrophotometric determination of trace amounts of many transition metal ions. 2,2′-Dipyridyl-2-pyridylhydrazone (DPPH) was first synthesized in our laboratory by Alexaki-Tzivanidou[18,19] and has been used for the spectrophotometric determination of iron(II),[20] cadmium(II),[21] cobalt(II),[19,22] copper(II),[23] zinc(II)[24] and palladium(II).[25] Using DPPH, the spectrophotometic determination of cobalt(II)[19] was recognized[26] to be sensitive and very selective and seems to be unique, in the sense that it is suitable for the microdetermination of cobalt(II) in the presence of large quantities of other ions.

For routine analysis, a developed method must be selective, sensitive at the sub-milligram per litre level, simple to operate and must exhibit good sample throughput. This is accomplished through the use of FI. Thus, the goal of this research was to develop a simple, sensitive and very selective method for the FI spectrophotometric determination of cobalt(II) based on the formation of a very stable complex between cobalt(II) and DPPH[19] in an acidic medium, that prevents the formation of complexes of other cations. The method has been successfully applied to the determination of cobalt(II) in cyanocobalamin (vitamin B_{12}) after wet digestion.

Experimental

Instrumentation

The FI system used was a Tecator 5010 analyser (Tecator, Höganäs, Sweden) with a Tecator chemifold SR II manifold which is shown schematically in Fig. 1. The detector used was a Tecator 5023 FI star double-beam spectrophotometer, consisting of a 5032 detector controller and a 5023-011 spectrophotometer optical unit. A printer was included with the detection system and allowed modification of the readout from the 5032 detector controller by means of direct digital communication with the 5010 analyser. The absorbance of the coloured Co^{II}–DPPH complex produced was monitored at 500 nm with a 1 cm path length flow cell with an internal volume of 18 μl. The flow sytem used was 0.5 mm id Teflon tubing throughout. Tygon pump tubes were used for aqueous solutions while solvent flexible and acid-flex pump tubes were used for alcoholic and highly concentrated (above 2 mol l^{-1}) hydrochloric acid solutions, respectively. The FI system had a programmable cycle time which was divided into the cycle injection time and the cycle delay time. The cycle time was the period of time between consecutive sample injections and was set by determining the time required from the point of sample

injection to the return to baseline. The cycle injection time was the period of time that the injector remained in the inject position. The cycle delay time was the period of time that the injector remained in the filling position. Using the appropriate commands, the injection time and the duration of the sample filling period were set in the cycle injection time and in the cycle delay time display.

An Orion EA940 pH-meter was employed for the pH measurements with absolute accuracy limits at the pH measurements being defined by NIST buffers.

Reagents

All chemicals were of analytical-reagent grade and were provided by Merck (Darmstadt, Germany), unless stated otherwise, and all the solutions were made up in de-ionized water.

The stock cobalt(II) solution (50 mg l^{-1}) was prepared from cobalt nitrate, $Co(NO_3)_2 \cdot 6H_2O$, and was standardized by EDTA titration. Hydrolysis was prevented by adjusting the pH to about 3.3 with 2 mol l^{-1} HCl.[27]

2,2-Dipyridyl-2-pyridylhydrazone (DPPH) was synthesized and identified as previously reported.[18,20] The stock of 0.1 mol l^{-1} DPPH solution was prepared by dissolving the required amount in ethanol. The ethanolic solution was stable and could be kept for several weeks in an amber glass bottle.

The buffer solution (pH 7.24) was prepared from H_3PO_4, CH_3COOH, H_3BO_3 (0.4 mol l^{-1} each) and 0.2 mol l^{-1} NaOH.[28]

All solutions were de-gassed with purified nitrogen, except for hydrochloric acid which was de-gassed by ultrasonication. All the stock solutions were stored in polyethylene containers. All the polyethylene containers and glassware used for aqueous solutions were cleaned in nitric acid (1 + 1) while the ethanolic solutions were cleaned in 3% Decon 90 and then all were rinsed with de-ionized water before use.[29] Working solutions of cobalt(II) and DPPH were prepared by dilution immediately before use.

Procedure

Using the FI set up shown in Fig. 1, 100 μl of a solution containing between 0 and 12.0 mg l^{-1} cobalt(II) were injected into the carrier stream (Fig. 1, C), the pH adjusting stream which merged with the reagent stream (Fig. 1, R_1), and the DPPH stream. A water-soluble orange-yellow complex (λ_{max} = 480 nm) was formed on the passage of the reagent and metal solution through the 60 cm reaction coil. The coloured zone then merged with the reagent stream (Fig. 1, R_2), the hydrochloric acid stream. Passage of the coloured zone through the 12 cm reaction coil resulted in the change in colour of the complex to pink (λ_{max} = 500 nm). After the pink colour had developed, the absorbance was measured in the flow-through cell at 500 nm. The transient signal was recorded as a peak, the height of which was proportional to the cobalt(II) concentration in the sample, and was used for all measurements. Five replicate injections per sample were made in all instances.

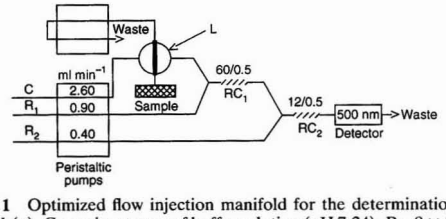

Fig. 1 Optimized flow injection manifold for the determination of cobalt(II). C, carrier stream of buffer solution (pH 7.24); $R:_1$ 8×10^{-4} mol l^{-1} (40% v/v ethanol) DPPH reagent stream; R_2, 1.5 mol l^{-1} hydrochloric acid reagent stream; L, sample loop (100 μl); RC_1, reagent coil 1; RC_2, reagent coil 2. Numbers above coils denote coil length/cm : id/mm ratio.

For the determination of cobalt(II), the cycle time was set to 40 s with a 15 s cycle injection time. Using the cycle time of 40 s, 90 injections per hour were made. The recorded peaks were sharp and the baseline was stable.

To determine Co^{II} in cyanocobalamin, an accurately weighed amount of the vitamin was dissolved in doubly de-ionized water. The resulting solution had a dark red colour. The absorption spectrum showed a large absorption band in the range 470 to 580 nm. Thus, for the determination of Co^{II} with the proposed FI method, it was necessary to digest the aqueous solution of B_{12} until decolourization. Aliquots of 2–5 ml of this solution were transferred into a series of 50 ml glass beakers. To the contents of each beaker, 10 ml of about 16 mol l^{-1} HNO_3 were added and the resulting mixture was heated on a hot plate. Then, 1 ml of about 12 mol l^{-1} HCl was added and the colour immediately turned yellow. The mixture was heated almost to dryness and the residue was dissolved in doubly de-ionized water and the solution was adjusted to pH 2.5–3.0 with 2 mol l^{-1} NaOH. The resulting solutions were transferred into a series of 25 ml calibrated flasks and diluted to the mark with doubly de-ionized water. These solutions were used for the determination of cobalt using the above described FI procedure.

Results and Discussion

Study of the Co^{II}–DPPH Complex

In aqueous solution, pH 2–11, DPPH reacted instantly with cobalt(II) to form a water-soluble orange-yellow complex (λ_{max} = 480 nm). On adding a strong acid only, a bathochromic shift took place and the colour changed to pink (λ_{max} = 500 nm, $\varepsilon_{max} = 4.2 \times 10^4$ l mol^{-1} cm^{-1}). This shift, from 480 nm to 500 nm was probably due to a characteristic protonation of the complex with a simultaneous redistribution of the electrons. The system was reversible.[19] The complex formation was independent of pH over the range 2–11 and the maximal absorbance showed no shift between pH 4 and 10. The complex was kinetically stable to protons, even in the presence of a very high concentration of acid, so it could be used for a specific determination of cobalt(II), as the reaction of DPPH with other transition metal cations was pH-dependent. The molar ratio method applied for both complex forms showed that the ratio of metal ions to ligand molecules was 1 : 2.

Developing a FI method based on the above reaction,[19] it was necessary to check if the mentioned complex could be formed under flow conditions. Preliminary experiments showed that 40% v/v ethanolic DPPH solutions of different concentrations caused no 'matrix effects' (negative and positive deflections before and after the peak) when a spectrophotometric detector was employed.[6] Using the FI set up shown in Fig. 1, but without the hydrochloric acid solution stream, the absorbance of the Co^{II}–DPPH complex showed a maximum at 480 nm which was in agreement with the batch value. Then, the formation of the pink Co^{II}–DPPH complex (λ_{max} = 500 nm) was examined using 1.5 mol l^{-1} hydrochloric acid. The absorbance of the complex showed a maximum of 500 nm which was again in agreement with the batch value. The FI set up shown in Fig. 1 was also used and in both cases the main experimental variables were: [Co^{II}] = 3 mg l^{-1} (pH 4 with 0.1 mol l^{-1} HCl); [DPPH] = 1.6×10^{-3} mol l^{-1} (40% v/v ethanol in water); carrier stream pH 7.02; injection loop = 300 μl; reaction coil 1 = 120 cm; reaction coil 2 = 60 cm; cycle time

= 65 s; cycle injection time = 30 s and the flow rate of each stream was 0.9 ml min^{-1}.

Optimization of Chemical Variables

The chemical variables were optimized for the FI system shown in Fig. 1 using a fixed Co^{II} concentration of 3 mg l^{-1} (pH 4 with 0.1 mol l^{-1} HCl) and the same FI operating variables mentioned above. The absorbance was read in the flow-through cell at 500 nm.

In the batch method,[19] 20% perchloric acid was used for converting the orange-yellow complex into the pink complex. It was also mentioned that the same results were obtained with hydrochloric acid and sulfuric acid. However, perchloric acid is difficult to handle properly, so 1.5 mol l^{-1} hydrochloric acid was used in the present work for three reasons: (*i*) to avoid precipitation of perchloric salts; (*ii*) to protect the analyst from the corrosive properties of concentrated perchloric acid; and (*iii*) to avoid the use of acid-flex pump tubes, thus, lowering the cost of the system.

When the buffer containing stream and DPPH stream were fixed at pH 7.02 and [DPPH] = 1.6×10^{-3} mol l^{-1} (40% v/v ethanol in water), respectively, the peak heights were independent of hydrochloric acid concentration from 1–12 mol l^{-1}, indicating that the conversion of the orange-yellow complex to the pink complex was complete and effective in this range. Stopped-flow experiments showed that the conversion and the formation of the pink complex was instantaneous, as the reaction had reached at least 97% of the 'steady state value' within 20 s.

Finally a concentration of 1.5 mol l^{-1} hydrochloric acid was used thereafter. This variable was examined first because the proposed FI method for determining cobalt(II) was strongly dependant on the efficiency of the above mentioned conversion.

The influence of the pH of the carrier stream on reaction development was studied in the range 2.8–12.0. The DPPH and hydrochloric acid streams were fixed at [DPPH] = 1.6×10^{-3} mol l^{-1} (40% v/v ethanol in water) and [HCl] = 1.5 mol l^{-1}, respectively. Several well known buffer systems were used. The most suitable and the one selected was a modified universal buffer prepared from H_3PO_4, CH_3COOH, H_3BO_3 (0.4 mol l^{-1} each) and 0.2 mol l^{-1} NaOH. The results are shown in Fig. 2. The maximum extent of complex formation was observed to be at pH 7–9. Also, as can be seen from Fig. 2, exactly the same pH 'window' was found when the pH-dependence on the FI orange-yellow Co^{II}–DPPH complex formation was tested in a separate experiment using the same universal buffer system. In this case, the FI set up shown in Fig. 1 was used, but without the 1.5 mol l^{-1} hydrochloric acid solution stream keeping the rest of the experimental variables the same (as mentioned above). The absorbance was read at 480 nm. The pH was measured in the waste line. A carrier buffer stream of optimal pH 7.24 was chosen. At the detector the pH of the stream was approximately 7.85, due to dilution. In both cases, stopped-flow experiments showed that the reaction had reached at least 96% of the 'steady state value' within 30 s, indicating that the fast chemical reaction was almost complete.

When the buffer containing stream and hydrochloric acid stream were fixed at pH 7.24 and [HCl] = 1.5 mol l^{-1}, respectively, the analytical signal was independent of DPPH concentration from 0.8×10^{-3} to 2×10^{-3} mol l^{-1}. A DPPH concentration of 0.8×10^{-3} mol l^{-1} (40% v/v ethanol in water) was selected for further study. Under these conditions, the reaction was near to completion, as demonstrated by stopped-flow experiments and measurement of the temporal variation of absorbance.

Optimization of the Flow Injection Manifold

In order to proceed with the final system design, the FI variables were studied by using the univariate method. The effects of sample injection volume, reaction coil lengths and the flow rate of each stream were studied under the above optimum concentrations of pH, DPPH and hydrochloric acid in the sample solutions. The cycle time was set within the range of 40–75 s with a 15–30 s cycle injection time depending on the variable examined. Cobalt(II) standards were prepared at 0.5 mg l^{-1}, 3.0 mg l^{-1} and 7.0 mg l^{-1}. The three standards were investigated as a function of the FI operating variables.

In FI, the sensitivity of a method may be varied as a function of sample injection volume. To increase the sensitivity, a larger volume of sample is injected and, thus, a higher product concentration is observed. This is especially important when using a fixed path length spectrophotometric detector. The injection loop volume was varied from 30 to 300 μl by changing the length of sample loop in the injection valve. The results are shown in Fig. 3. The peak heights increased non-linearly with increasing sample size. This property of FI is a result of sample zone dispersion.[6] The concentration maximum of the sample zone is a function of sample zone size, with the concentration maximum of the large sample zone not being significantly affected by dispersion after a limiting injection volume. A sample injection volume of 100 μl was selected as a compromise between sensitivity and sample injection rate.

The influence of the first reaction coil length was investigated in the range 12–150 cm. In this reaction coil, Co^{II} was reacting with the DPPH to form the orange-yellow Co^{II}–DPPH complex (λ_{max} = 480 nm). The length of the reaction coil determined the time the reaction was allowed to proceed prior to the hydrochloric acid stream. The sample was reacting to form the above mentioned complex, but at the same time

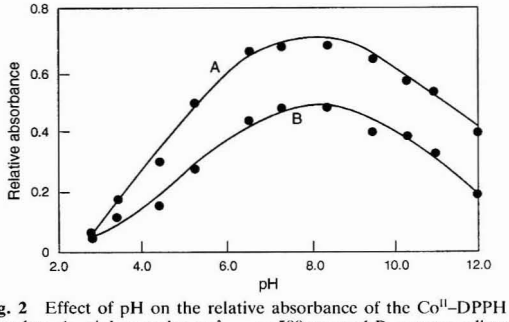

Fig. 2 Effect of pH on the relative absorbance of the Co^{II}–DPPH complex. A, pink complex at λ_{max} = 500 nm and B, orange-yellow complex at λ_{max} = 480 nm.

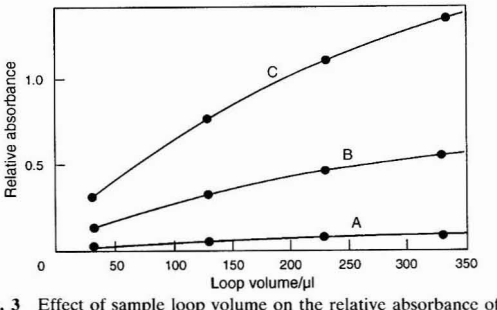

Fig. 3 Effect of sample loop volume on the relative absorbance of the Co^{II}–DPPH complex. [Co^{II} = 0.5 (A); 3.0 (B); and 7.0 (C) mg l^{-1}.

the sample was subject to dispersion as it travelled through the tubing. There was an optimal coil length which maximized the reaction before the dispersion effects began to predominate. The signals from the Co^{II} standards as a function of the first reaction coil length is shown in Fig. 4. The signal intensity goes through a maximum at a reaction coil length of 60 cm, thus, a 60 cm first reaction coil was chosen as optimal. Fig. 4 indicates that the reaction is near to completion as increasing the length of reaction coil to more than 60 cm and, thus, allowing the reaction to continue for a longer time period, failed to show an increase in the signal intensity from the Co^{II} standards. At a length greater than 60 cm any further production of Co^{II}–DPPH complex was negated by the dispersion effects.

The second reaction coil length was also investigated in the range 12–150 cm. The results of the experiment are shown in Fig. 5. In this second reaction coil the conversion of the orange-yellow Co^{II}–DPPH complex to the pink complex (λ_{max} = 500 nm) takes place by the use of 1.5 mol l^{-1} hydrochloric acid. This bathochromic shift was very fast and, therefore, only a short length of coil was necessary. The results showed that with increasing coil length the sensitivity decreased slightly. The slow decrease in signal as a function of coil length was due to dispersion effects. These dispersion effects, however, were slight and a large increase in coil length was necessary to change the signal significantly. Therefore, a coil length of 12 cm was chosen as optimal.

The carrier-buffer solution flow rate was studied at between 0.38 and 2.60 ml min^{-1}. The results are shown in Fig. 6. The peak heights increased non-linearly with increasing carrier flow rate, but levelled off at a flow rate of above 2.22 ml min^{-1}. A flow rate of about 2.60 ml min^{-1} was selected as optimal. It has been established[6] that differential flow rate variations between the carrier and reagent produce significant changes in sample dispersion. The explanation is straightforward. At the merging point of the carrier and reagent, different degrees of dilution occur. Thus, for maximum sensitivity the carrier flow rate should be high while the reagent flow rate should be kept low.

The DPPH stream flow rate was studied in the range of 0.38–2.19 ml min^{-1}. The results of the experiment are shown in Fig. 7. The signal intensity goes through a maximum at a DPPH solution flow rate of 0.94 ml min^{-1}, thus, a flow rate of about 0.90 ml min^{-1} was chosen as optimal. As can be seen from Fig. 7 the reaction between cobalt(II) and DPPH is near to completion. Stopped-flow experiments showed that the reaction had reached at least 98% of the 'steady state value' within 15 s. At a flow rate greater than 0.94 ml min^{-1}, any further production of Co^{II}–DPPH complex was negated by dispersion effects.

Finally, the hydrochloric acid solution flow rate was studied in the range 0.42–2.19 ml min^{-1}. The results are shown in Fig. 8. The results show that with increasing flow rate the

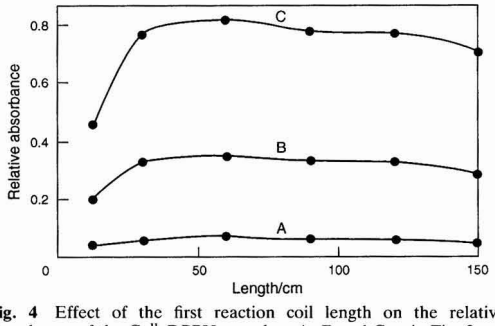

Fig. 4 Effect of the first reaction coil length on the relative absorbance of the Co^{II}–DPPH complex. A, B and C as in Fig. 3.

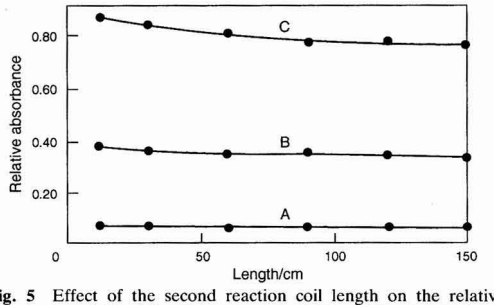

Fig. 5 Effect of the second reaction coil length on the relative absorbance of the Co^{II}–DPPH complex. A, B and C as in Fig. 3.

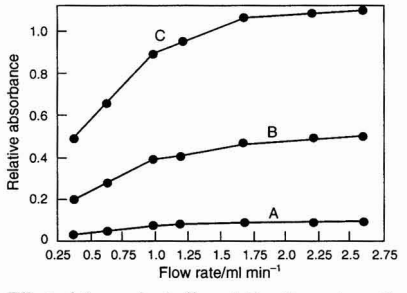

Fig. 6 Effect of the carrier-buffer solution flow rate on the relative absorbance of the Co^{II}–DPPH complex. A, B and C as in Fig. 3.

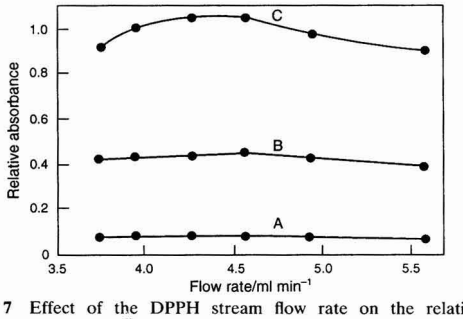

Fig. 7 Effect of the DPPH stream flow rate on the relative absorbance of the Co^{II}–DPPH complex. A, B and C as in Fig. 3.

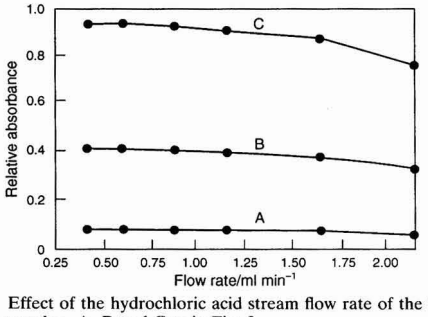

Fig. 8 Effect of the hydrochloric acid stream flow rate of the Co^{II}–DPPH complex. A, B and C as in Fig. 3.

sensitivity decreases slightly due to dispersion effects. A high increase in flow rate is necessary to change the signal significantly. Therefore, a flow rate of about 0.40 ml min^{-1} was chosen as optimal. Stopped-flow experiments showed that the conversion of the orange-yellow Co^{II}–DPPH complex to the pink complex was instantaneous, and the maximum absorbance was always observed to be at λ_{max} = 500 nm.

Calibration Curve, Accuracy and Precision

A calibration graph for 0 to 12.0 mg l^{-1} cobalt(II) solutions was recorded under the optimum conditions described above. The standards were run in five replicate injections (n = 5). The calibration graph was linear and was described by the least-squares equation of the peak height absorbance, A, *versus* cobalt concentration mg l^{-1}:

$$A = (7.62 \pm 2.75) \times 10^{-3} + (136.81 \pm 0.53) \times 10^{-3} [Co^{II}]$$

A correlation coefficient of r = 0.99992 was yielded with good accuracy and reproducibility (s_r = 0.4%). The calculated detection limit[30] was 0.017 mg l^{-1} (n = 10) with a limit of determination[31,32] of 0.031 mg l^{-1}.

Interference Studies

The interference effects of many cations and anions on the determination of cobalt(II) ([Co^{II} = 1 mg l^{-1}) were examined using the flow system shown in Fig. 1 and optimum conditions described above. The results are summarized in Table 1. The following ions were studied in addition to those included in Table 1: K^+, Na^+, NH_4^+, F^-, Cl^-, Br^-, I^-, NO_2^-, NO_3^-, SCN^-, SO_4^{2-}, CO_3^{2-}, HCO_3^-, PO_4^{3-}, HPO_4^{2-}, $H_2PO_4^-$, $H_2BO_3^-$ and CH_3COO^-. These ions do not interfere, even at a maximum ion [Co^{II}] molar ratio of 1000 : 1. The criterion for interference was fixed at a s_r of less than ±2% variation of the average FI signal, calculated for the established level of Co^{II}.

Determination of Cobalt in Cyanocobalamin Samples

A series of five cyanocobalamin solutions with different Co^{II} concentrations were analysed. The concentrations of cobalt were: 0.9, 1.8, 2.7, 3.6, and 4.5 mg l^{-1}, and checked by flame AAS. Experiments applying the proposed FI procedure to the above samples showed recoveries between 98.5–102.7% with an s_r value of less than 0.9% for n = 5 replicate determinations for each cyanocobalamin solution.

Conclusion

The proposed FI method offers many significant improvements, not only over the manual batch method[19] but other direct FI spectrophotometric methods for Co^{II} as well, *e.g.*, low cost instrumentation, manifold simplicity, higher throughput rate (90 injections per hour), good dynamic range (0 to 12.0 mg l^{-1}), better reproducibility (s_r = 0.4%), lower detection limit (0.017 mg l^{-1}), no complicated procedures before the determination of the analyte, no dangerous reagents used and few interferences, as most of the complexes of DPPH with other ions are destroyed on adding hydrochloric acid. Finally, the method is convenient for the determination of sub-milligram per litre level of Co^{II} in cyanocobalamin. The reliability and suitability of the proposed method is illustrated by the recovery of cobalt(II) from cyanocobalamin samples of between 98.5 and 102.7%, with an s_r value of less than 0.9% (n = 5).

Table 1 Effect of various ions on the determination of 1.7×10^{-5} mol l^{-1} (1 mg l^{-1}) Co^{II} using the optimum conditions given under the procedure for aqueous solutions

Ion added*	Molar ratio of ion to Co^{II}
Ca^{2+}, Mg^{2+}	500
Sr^{2+}	200
Cu^{2+}, Ni^{2+}	50
Fe^{3+}	30
Zn^{2+}, Mn^{2+}, Pb^{2+}	15
Cd^{2+}, Sb^{3+}, Pd^{2+}	5
Hg^{2+}, Cr^{3+}	4
Fe^{2+}, Al^{3+}, CrO_4^{2-}	1

* These ions in the stated ratio caused a relative error of less than ±2%.

References

1 Skeggs, L. T., *Am. J. Clin. Pathol.*, 1957, **28**, 311.
2 Růžička, J., and Hansen, E. H., *Anal. Chim. Acta*, 1975, **78**, 145.
3 Gordon, G., Yoshino, K., Themelis, D. G., Wood, D., and Pacey, G. E., *Anal. Chim. Acta*, 1989, **224**, 383.
4 Růžička, J., and Hansen, E. H., in *Flow Injection Analysis*, ed. Winefordner, J. D., and Kolthoff, I. M., Wiley-Interscience, New York, 2nd edn., 1988.
5 Valcarcel, M., and Luque de Castro, M. D., in *Flow Injection Analysis; Principles and Applications*, ed. Chalmers, R. A., Masson, M., and Miller, J. N., Ellis Horwood, Chichester, 1987.
6 Karlberg, B., and Pacey, G. E., in *Flow Injection Analysis; A Practical Guide*, Elsevier, Amsterdam, 1989.
7 Burguera, J. L., and Townshend, A., *Proc. Anal. Div. Chem. Soc.*, 1979, **16**, 263.
8 Burguera, J. L., Townshend, A., and Greenfield, S., *Anal. Chim. Acta*, 1980, **114**, 209.
9 Lin, Q., Guiraum, A., Escobar, R., and De la Rosa, F., *Anal. Chim. Acta*, 1993, **283**, 379.
10 Fang, Z., Xu, S., and Zhang, S., *Anal. Chim. Acta*, 1987, **200**, 35.
11 Fang, Z., Zhu, Z., Zhang, S., Xu, S., Guo, L., and Sun, L., *Anal. Chim. Acta*, 1988, **214**, 41.
12 Trojanowicz, M., and Pyrzynkska, K., *Anal. Chim. Acta*, 1994, **287**, 247.
13 Sperling, M., Yin, X., and Welz, B., *J. Anal. At. Spectrom.*, 1991, **6**, 615.
14 Isshiki, K., and Nakayama, E., *Talanta*, 1987, **34**, 277.
15 Thorburn Burns, D., Chimpalee, N., and Harriott, M., *Anal. Chim. Acta*, 1989, **225**, 123.
16 Cristofol de Alcaraz, E., Rojas, F. S., and Cano Pavon, J. M., *Fresenius' J. Anal. Chem.*, 1991, **340**, 175.
17 Arruda, M., Zagatto, E., and Maniasso, N., *Anal. Chim. Acta*, 1993, **283**, 476.
18 Alexaki-Tzivanidou, H., PhD Thesis, University of Thessaloniki, Greece, 1972.
19 Vasilikiotis, G. S., Kouimtzis, T., Apostolopoulou, C., and Voulgaropoulos, A., *Anal. Chim. Acta*, 1974, **70**, 319.
20 Alexaki-Tzivanidou, H., *Anal. Chim. Acta*, 1975, **75**, 231.
21 Alexaki-Tzivanidou, H., Kounenis, G., and Elezoglou, B., *Microchem. J.*, 1978, **23**, 329.
22 Kouimtzis, T., Apostolopoulou, C., and Stafylakis, I., *Anal. Chim. Acta*, 1980, **113**, 205.
23 Alexaki-Tzivanidou, H., and Vasilikiotis, G. S., *Microchem. J.*, 1981, **26**, 1.
24 Vasilikiotis, G. S., and Alexaki-Tzivanidou, H., *Microchem. J.*, 1981, **26**, 519.
25 Stratis, J. A., Anthemidis, A. M., and Vasilikiotis, G. S., *Analyst*, 1984, **109**, 373.
26 Sandell, E. B., and Onishi, H., in *Photometric Determination of Trace Metals. General Aspects. Colorimetric Determination of Traces of Metals, Part I. Chem. Anal. Ser. Vol. 3*, ed. Elving, P. J., Winefordner, J. D., and Kolthoff, I. M., Wiley-Interscience, New York, 4th edn., 1978, p. 360.
27 Smith, A. E., *Analyst*, 1973, **98**, 65.

28 Britton, H., and Robinson, R., *J. Chem. Soc.*, 1931, 1456.
29 Holz, F., *Fresenius' Z. Anal. Chem.*, 1984, **319**, 29.
30 Long, G. L., and Winefordner, J. D., *Anal. Chem.*, 1983, **55**, 713A.
31 ACS Committee on Environmental Improvement, *Anal. Chem.*, 1980, **52**, 2242.
32 ACS Committee on Environmental Improvement, *Anal. Chem.*, 1983, **55**, 2210.

Paper 4/07507B
Received December 8, 1994
Accepted January 3, 1995

Synthesis and Studies on the Analytical Functions of a Highly Selective Spectrophotometric Reagent 2-(8-Quinolylazo)-5-*N,N'*-dimethylaminobenzoic Acid

Hanxi Shen and Yuanping Tang
Department of Chemistry, Nankai University, Tianjin, 300071, China
Xinliang Xiao, Shufen Zhang and Ruixian Liu
Department of Chemistry, Tianjin University, Tianjin, 300072, China

A new highly-selective chromogenic reagent, 2-(8-quinolylazo)-5-*N,N'*-dimethylaminobenzoic acid (QAMB) has been synthesized. In pH 4.0–8.0 medium, the reagent reacts only with cobalt or copper ions to form blue–green complexes. In alkaline medium, the reagent also reacts with nickel, mercury and palladium ions to form blue complexes. Therefore, QAMB may be the most selective among heterocyclic azo-chromogenic reagents. The physical and chemical properties of QAMB and its colour-formation reaction with cobalt ions have been studied in detail. A new spectrophotometric method for the determination of cobalt in iron and steel samples has been developed.

Keywords: Spectrophotometric reagent; 2-(8-quinolylazo)-5-N,N'-dimethylaminobenzoic acid; cobalt

Introduction

Research into the selectivity and sensitivity of analytical methods is an area of current interest. Although there has been considerable success in enhancing sensitivity, there has been little improvement in the selectivity of reactions.

This paper describes a new, highly selective heterocyclic azo-chromogenic reagent, 2-(8-quinolylazo)-5-*N,N'*-dimethylaminobenzoic acid (QAMB). Designed and synthesized to emphasize the effects of cyclization and steric hindrance in complexes, QAMB follows the rule of reaction for metal ions with chromogenic reagents. In pH 4.0–8.0 medium, the reagent reacts only with cobalt or copper ions to form blue–green complexes (λ_{max} = 645 nm). In alkaline medium, the reagent may react with cobalt, copper, nickel, mercury and palladium ions to form coloured compounds. QAMB is the most selective reagent of its kind.[2–7] The synthesis, separation and purification of the reagent and its physical and chemical properties (and colour-formation reaction with cobalt ions) have been studied in detail. A novel method for the determination of cobalt in iron and steel samples has been developed.

Experimental

Synthesis of Reagent

Procedure for the synthesis of QAMB

The route of the synthesis is shown below.

A 1.44 g amount of 8-aminoquinoline was dissolved in 20 ml of 2 mol l^{-1} HCl solution and cooled to 0 °C in an ice-bath. A 10 ml volume of $NaNO_2$ (1.42 g) solution was added dropwise and stirred. A red–brown diazo-salt solution was prepared after further stirring for 30 min at 0–5 °C. Separately, an equal quantity of *m*-dimethylaminobenzoic acid was dissolved in 20 ml of ethanol and cooled to 0–5 °C. The above diazo-salt solution was added dropwise to this solution, with vigorous stirring. After mechanically stirring for a further 4 h the mixture was allowed to stand overnight. A red–purple solution was obtained, from which, by means of a rotary evaporator, any ethanol was expelled. An excess of solid sodium acetate was added to separate the precipitate. The crude product was obtained by filtering and dissolving in dilute HCl solution. A purified dark-red solid was obtained by filtering and dissolving in ethanol. This was further purified by column chromatography with a stationary phase of silica-gel G and a mixture of ethanol–chloroform as the eluent. A re-purified powder was obtained by evaporation and concentration of the eluent.

Analysis of the product

The IR spectrum of QAMB gave an absorption band at: 3410.5 cm^{-1}, for a hydroxy group (–OH); 3057.8 cm^{-1}, for an unsaturated hydrocarbon group; 2901.8 and 2803.5 cm^{-1}, for two methyl groups ($-CH_3$); 1696.1 cm^{-1}, for a carbonyl group (–C=O–); and 1597.7 and 1507.4 cm^{-1}, for phenyl and –N=N– groups, respectively. Elemental analysis gave the molecular

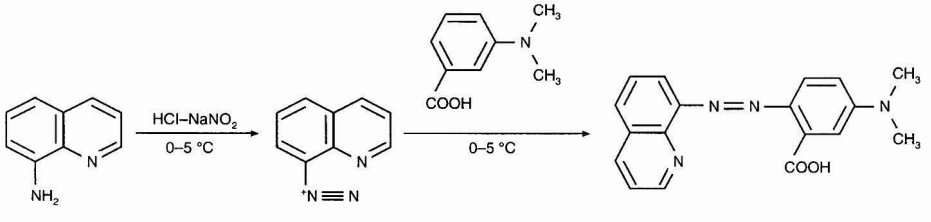

mass of QAMB to be 320.354 ($C_{18}H_{16}N_4O_2$). Analysis of QAMB gave the following calculated values (%): C, 67.49; H, 5.03; N, 17.49; and found values (%) C, 67.45; H, 5.06; N, 17.46.

Reagents

Standard cobalt solution. 5.3240 g of $CoSO_4 \cdot 6H_2O$ was dissolved in distilled water, 10 ml of H_2SO_4 (1 + 1) was added and diluted to 1000 ml with distilled water. The solution contained cobalt 1.20 mg ml^{-1}. This was further diluted to 6.0 μg ml^{-1} with distilled water, as used.

QAMB solution, 1.0×10^{-4} mol l^{-1}. QAMB (0.0321 g) was dissolved with <1 ml of ethanol. This was transferred into a 1000 ml calibrated flask and diluted up to the mark with distilled water.

Acetic acid–sodium acetate buffer solution pH 5.2. The solutions of acetic acid (0.1 mol l^{-1}) and sodium acetate (0.1 ml l^{-1}) were mixed in a ratio of (1 + 3) to give a pH value of 5.2.

Experimental Procedure

A volume of 2 ml of 1.0×10^{-4} mol l^{-1} QAMB solution and <1.6 ml of 6.0 μg l^{-1} standard cobalt solution were mixed in a 10 ml calibrated flask. A volume of 1.0 ml of the buffer solution (pH 5.2) was added and diluted to volume with distilled water. After 30 min the absorbance was measured at 645 nm against a reagent blank in a 1 ml cell, using a Shimadzu UV240 spectrophotometer (Shimadzu, Kyoto, Japan).

Results and Discussion

Properties of QAMB

Physical properties

QAMB is a dark-red powder which is slightly soluble in water. It is soluble in organic solvents, such as, ethanol, diethyl ether, acetone and *N,N'*-dimethylformamide, and in acidic and basic aqueous solutions.

Absorption spectra and dissociation constant of QAMB

In acidic medium, QAMB solution appears as purple–red in colour and yellow in basic medium. Absorption spectra for QAMB are shown in Fig. 1. The species and number for the reagent in solutions with various pH values need further determination according to the spectra.

The spectra at 380–700 nm was recorded for reagent solutions at a set of pH values. If the absorbances of all species of the reagent obey Beer's law,the absorbances are additive:

$$A^{\lambda} = \sum_{i-1}^{m} \varepsilon_i^{\lambda} c_i,$$

where A^{λ} is the absorbance at the wavelength of the reagent, containing m species, ε_i^{λ} and c_i are the molar absorption coefficient and the concentration of species i, respectively.

Using the measured absorption spectra, a matrix was constructed, $A_{p \times n} = \varepsilon_{p \times m} c_{m \times n}$, where p is the number of wavelengths, n is the number of determinations and m is the number of species.

By calculating with TRIANG program[7] (redesigned to FORTRAN 77 compile system) the rank of matrix was found for the species form of the reagent. The result gave two species; HL, and L^-, in pH 1.0–8.0 media.

The dissociation constant was calculated to be $pK = 5.72$ using a BASIC program written according to the A–pH curve and the equation $pK_a = pH + \log(A - A_L)/(A_{HL} - A)$.

Chromogenic Properties of QAMB With Metal Ions

Chromogenic testing of the reagent with metal ions was carried out in acidic, neutral and basic media, respectively. Only cobalt and copper ions formed the blue–green complexes with QAMB at pH 4.0–8.0. In alkaline conditions when the amount of nickel, mercury or palladium ions was over 3 μg, they also formed blue complexes. There was no apparent colour changes when using other metal ions with QAMB.

Absorption Spectra of the Complex

The absorption spectra of the complex formed between cobalt and QAMB are shown in Fig. 2. The absorption peaks of QAMB and its cobalt complex were located at 510 and 645 nm, respectively, at pH 5.2. The contrast of wavelengths is 135 nm.

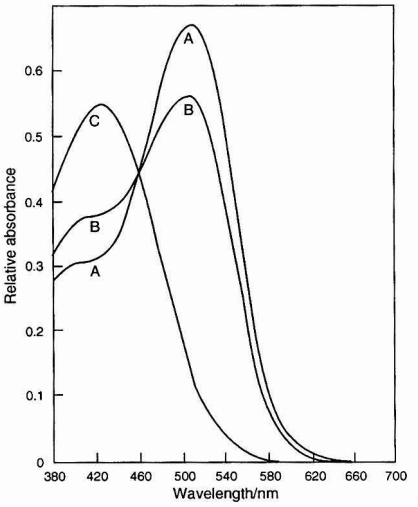

Fig. 1 Absorption spectra of QAMB at pH: A, 1.0; B, 5.0; and C, 8.0.

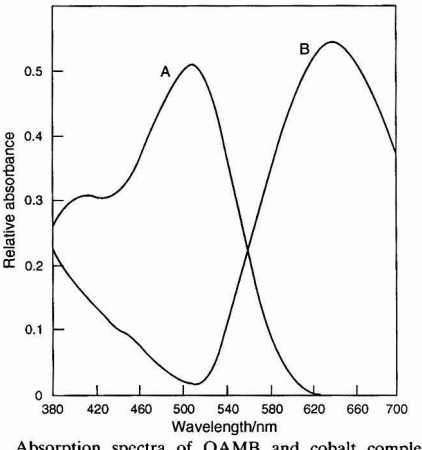

Fig. 2 Absorption spectra of QAMB and cobalt complex. A, [QAMB] = 2.0×10^{-5} mol l^{-1} and B, [QAMB] = 2.0×10^{-5} mol l^{-1} plus [Co] = 1.0×10^{-5} mol l^{-1} (against reagent blank).

Conditions for Testing the Colour of Cobalt Complexes

Amount of QAMB

When the amount of cobalt was 10 μg and the amount of 1.0×10^{-4} mol l^{-1} QAMB was >2.0 ml, the absorbance of the cobalt complex was at a maximum and remained constant. Hence, 2.0 ml of QAMB was chosen for this procedure.

Effect of reaction acidity

Results showed that the optimal reaction acidity for cobalt ions with QAMB is at pH 4.0–8.0. A 1 ml volume of acetic acid–sodium acetate (pH 5.2) buffer solution was used for pH adjustment. Once the cobalt complex has formed, it is unaffected by the addition of a strong acid (2 mol l^{-1}). Hence, a strong acid may be added in order to eliminate copper ion interference.

Rate of colour reaction

The colour developed after 5 min of adding QAMB with cobalt ions. The absorbance reached a maximum after 30 min and remained stable for at least 24 h.

Measurement of complex composition

The isomolar continuous variation method and the equilibrium shift method (Figs. 3 and 4, respectively) gave a concentration ratio of cobalt to QAMB of 1 : 2 in the complex.

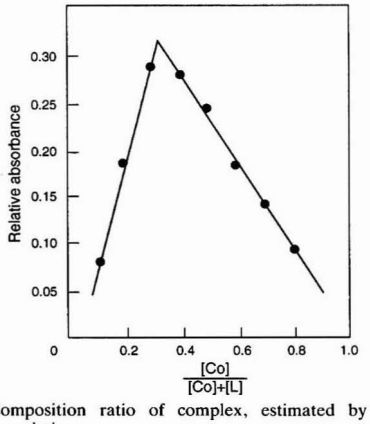

Fig. 3 Composition ratio of complex, estimated by isomolar continuous variation.

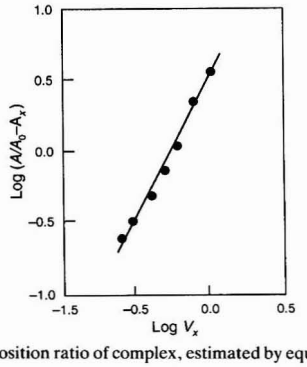

Fig. 4 Composition ratio of complex, estimated by equilibrium shift.

Effect of Co-existing Ions

When determining 6 μg of cobalt, the relative error was <5% and 1.0 mg of K^+, Na^+, Ca^{2+} or Mg^{2+}; 0.5 mg of Al^{3+}, Pb^{2+}, Zn^{2+}, Bi^{3+} or Cr^{6+}; 0.1 mg of Mn^{2+}, Fe^{3+}, Cr^{3+} or V^{4+}; and 0.02 mg of Ni^{2+}, Hg^{2+}, Pd^{2+} or rare earth ions did not interfere in the determination. An amount of 6 μg of Cu^{2+} does interfere, but the copper complex formed discolours after the addition of HCl. For Ni and Hg complexes in alkaline medium, both complexes are decomposed by HCl. Common anions, such as EDTA, F^-, SO_4^{2-}, phosphate, oxalate, glycerine, tartrate, thiourea, citrate and triethanolamine, do not interfere with the determination of cobalt.

Calibration Graph

The calibration graph for the determination of cobalt in the range of 0–10 μg showed linearity. The regression equation of the curve is given by

$$A = -0.007 + 0.0737\, c_{Co}$$

where $r = 0.999$, the molar absorption coefficient determined for the cobalt complex is 4.34×10^4 l mol^{-1} cm^{-1}. As the amount of QAMB increases, the linear range of determination also increases.

Analysis of Sample

Determination of trace amounts of cobalt in low-alloyed steel

An amount of 0.1 g of the steel sample, along with 3–4 pellets of H_2O_2 were added to 20 ml of HCl (1 + 1) in a 100 ml Erlenmeyer's flask. When the vigorous reaction stopped, the sample was dissolved by heating. Perchloric acid (5 ml) was added and allowed to fume. This was cooled and water was added to dissolve the salt. The solution was transferred to a 250 ml calibrated flask and diluted to volume with water. An aliquot of the solution was used for the chromogenic reaction to be carried out (following the experimental procedure) and for the absorbance to be measured. The results are presented in Table 1.

Discussion

Furukawa *et al.* discussed one heterocyclic azo-reagent.[2] It was suggested that a change of coordinate group in the reagent or the size of the chelate rings would improve the selectivity. The reagent groups were arranged in order of selectivity, $-NH_2$ > –COOH > –OH. A series of new heterocyclic-azo benzoic acid compounds, including 2-(2-thiazolylazo)-5-*N*,*N*′-dimethylaminobenzoic acid (TAMB), 2-(2-benzothiazolylazo)-5-*N*,*N*′-dimethylaminobenzoic acid (BTAMB) and 2-[2-(3,5-dibromopyridine)azo]-5-*N*,*N*′-dimethylaminobenzoic acid (3,5-diBr-PAMB) were successfully synthesized.[2,8,10]

Only the size of the chelate rings were changed, based on the unchanged coordinate atoms. The reagent QAMB (which can form two six-membered rings) is shown for comparison of the selectivities of all three heterocyclic-azo reagents.

The size of the chelate ring plays an important role in the selectivity of reagents. There are two six-membered rings in the complex between reagent QAMB with metal ions, a 5-membered and a six-membered ring for 3,5-diBr-PAMB, and

Table 1 The determination of cobalt in low-alloyed steel

Sample No.	Standard (%)	Determination (%)	Average (%)
7137	0.016	0.016; 0.015; 0.018; 0.017; 0.014; 0.017	0.016
7138	0.17	0.165; 0.171; 0.170; 0.179; 0.162; 0.161	0.168

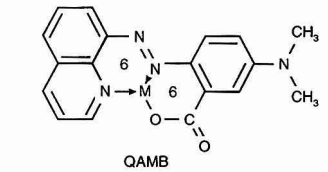

QAMB

M = Co; Cu; Ni; Hg; Pd

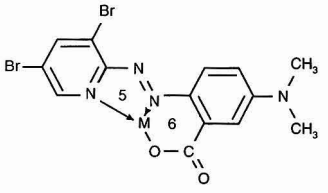

3,5–diBr–PAMB[8]

M = Fe; Co; Cu; Ni; Pd; V; Mn; Zn; Ga; (Nb; Cr; Ru; Cd; In; Os; Pt)

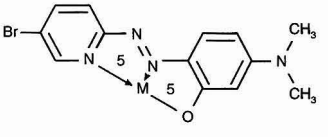

5–Br–DMPAP[9]

M = Co; Cu; Ni; Pd; V; Mn; Zn; Ga; Nb; Cr; Ru; Rh; Cd; In; Os; Pt; Mg; Ca; Sr; Sr; Ba; Se; Y; Ti; Zr; Ag; Sn; Sb; Ta; Ir; Hg; Tl; Bi; Th; La; Lu; U; Np

only two five-membered rings for 5-Br-DMPAP. As the five-membered ring is more stable than the six-membered ring, 5-Br-DMPAP forms complexes with more metal ions but loses selectivity. However, for 3,5-diBr-PAMB, the selectivity was improved because of the formation of a six-membered ring. The selectivity for reagent QAMB was further improved as it was noticed that QAMB did not react with Fe^{III} ions. The steric hindrance of the quinoline ring also improved the selectivity of QAMB.

The authors thank the National Natural Science Foundation Commission and State Education Commission for their financial support.

References

1 National Natural Science Foundation Commission of China, The Research Report on Natural Science Branch Developmental Strategy, *Fenxi Huaxue*, Science Press, Beijing, 1983, 46.
2 Furukawa, M., and Shibata, S., *Bunseki*, 1980, **6**, 330.
3 Ishizuki, T., Wada, H., and Nakagawa, G., *Bunseki Kagaku*, 1979, **28**, 535.
4 Katami, T., Hakayawa, T., Furukawa, M., and Shibata, S., *Analyst*, 1984, **109**, 159.
5 Shen, H., and Li, J., *Fenxi Huaxue*, 1988, **16**, 301.
6 Shen, H., Wang, Z., Li, W., Ye, J., Pan, X., and Jiao, F., *Huaxue Xuebao*, 1988, **46**, 285.
7 Shen, H., and Li, J., *Fenxi Huaxue*, 1989, **17**, 279.
8 Furukawa, M., and Shibata, S., *Anal. Chim. Acta*, 1982, **140**, 301.
9 Shibata, S., Furukawa, M., and Toei, K., *Anal. Chim. Acta*, 1973, **66**, 397.
10 Furukawa, M., *Anal. Chim. Acta*, 1982, **140**, 281.

Paper 4/06518B
Received October 25, 1994
Accepted January 1, 1995

Application of Pattern Recognition in a Factor Analysis–Spectrophotometric Method for the Simultaneous Determination of Rare Earth Elements in Geological Samples

Hong-yan Wang, Duo-xi Wang, Ying-hua Wang, Shu-gui Chen and Feng-jun Zhang

Department of Applied Chemistry, Changchun Geological College, Changchun 130026, China

A factor analysis–spectrophotometric method was used to determine simultaneously 15 rare earth elements (REEs) in the REE–tribromochlorophosphonazo system. It adopts the singular value decomposition method to decompose the original data matrix of absorbance and the iterative target transformation factor analysis method to carry out the quantitative analysis. Because a pattern recognition method was used to optimize the calibration model, the accuracy of the analytical results was apparently increased. The standard deviations were 3.8×10^{-4}–5.5×10^{-2} and the relative standard deviations were 0.22–3.5%. A detailed discussion is given of the selection of the calibration model and the features of classification.

Keywords: *Simultaneous rare earth element determination; geological samples; pattern recognition; spectrophotometry; factor analysis*

Introduction

Factor analysis is a multivariate statistical method. Although it was developed originally to solve psychological and social science problems, it has rapidly been applied to a wide variety of chemical problems such as in inductively coupled plasma atomic emission spectrometry,[1] spectrophotometry[2,3] and mass spectrometry.[4] In recent studies factor analysis was used to resolve the overlapped absorption spectra of complex mixtures[5,6] and improved factor analysis has been reported.[7,8] However, almost all of the methods reported for factor analysis–spectrophotometry have been concerned mostly with organic compounds or synthetic sample analyses for some inorganic compounds and the analysis of complex systems, especially complex geological samples, has rarely been reported. In multivariate statistical spectrophotometric analysis, the closer the concentration ratio among components in a calibration model is to the unknown samples, the more accurate the results for concentration are. However, information on unknown samples is still difficult to acquire. Pattern recognition as a chemometric method[9] has been used in chemical area, and by adopting pattern recognition[10] we can recognize some concealed properties from a large number of obtained data.

Kowalski *et al.*[11] were able to classify the geographical sources of obsidian samples using the concentrations of ten elements obtained by X-ray fluorescence spectrometry. Saxberg *et al.*[12] showed that different brands of whisky can be discriminated on the basis of gas chromatography. Wirsz and Blades[1] applied pattern recognition to inductively coupled plasma atomic emission spectra.

Classification analysis can be effected using pattern recognition. The classes of unknown samples can be discriminated using the Euclidean distance, *t*-test value and *F*-test value, which are regarded as features of recognition spectral properties. The correction model can be optimized by the improved continuous Hamming method (ICHM).[13] Many methods of classification can be used such as the least-distance Bayes method, the Hamming method and the basic event generation method.[13] The ICHM method is suitable for any distributive samples, concentrated and dispersed.

This paper shows that it is possible to apply the factor analysis–spectrophotometric method to the analyses of unknown samples. Because the chemical properties of rare earth elements (REEs) are fairly similar, the absorption spectra of their complex compounds are nearly linearly related. This may cause the problem of matrix loss, rank by decomposing the original data. The problem can be solved easily by the singular value decomposition (SVD) method. By using the SVD and iterative target transformation factor analysis (ITTFA) methods, we can make a conversion from a normal projection matrix to a concentration target vector, so that the converse operation of the matrix in general factor analysis is avoided. By use of this method, the 15 REEs in more than 200 geological samples selected from different areas in China were determined simultaneously. After a sampled test with ICP-AES (for the results see Table 8), we conclude that the errors of the concentration results conform to the requirements of the Ministry of Geological Minerals for relative errors in geological sample analysis.

Theory

ITTFA Method

The original data matrix consists of $L - 1$, the theoretical absorbance of a standard mixture ($L - 1$ column), and the determined absorbance of one unknown sample (L column) at r wavelengths (rows):

$$D_{r\times L} = \begin{bmatrix} d_{11}, d_{12}, \ldots, d_{1L-1}, d_{1L} \\ d_{21}, d_{22}, \ldots, d_{2L-1}, d_{2L} \\ \ldots\ldots\ldots\ldots \\ d_{r1}, d_{r2}, \ldots, d_{rL-1}, d_{rL} \end{bmatrix}$$

where r is the number of analytical wavelengths and L is the number of samples. It can be decomposed into three matrices, $U_{r\times 1}$, $V_{L\times L}$ and $S_{L\times L}$ by the SVD method:

$$D = USV^t$$

The reproduced data matrix ($\bar{D}$) is obtained after defining the number of factors (n):

$$\bar{D} = \bar{U}\bar{S}\bar{V}^T$$

The concentration target vector, $C_i = (C_{i1}, C_{i2}, \ldots, C_{iL-1}, C_{iL})$, is formed by $L - 1$ known samples and one unknown sample (C_{iL}) which can be given an arbitrary initial value (common for zero) as the initial forecast value of the concentration. Now the target vector is $C_i = (C_{i1}, C_{i2}, \ldots, C_{iL-1}, 0)$. Brayden *et al.*[14] proved that the initial value of an unknown sample had no effect on the ultimate forecast of concentration.

According to the theory of projection matrix, we can obtain a projection matrix, P:

$$P = DD^+ = VV^t$$

By using this matrix, the target vector of concentration is projected to the rows vector of $\bar{D}$ for realizing target transformation. The projection R_i is

$$R^T{}_i = PC^T{}_i$$

In the matrix R_i, R_{iL} ($R_{iL} = P_{L1}C_{iL} + p_{L2}C_{i2} + \ldots + P_{1L-1}C_{iL-1} + P_{LL}C_{iL}$) is the concentration forecast value of an unknown sample. Keeping other elements unchanged, the iteration is repeated by using R_{iL} instead of C_{iL} until,

$$|{}^{(m)}R_{iL} - {}^{(m-1)}R_{iL}| < e(10^{-4})$$

where ${}^{(m)}R_{iL}$ is the approximate optimum concentration of component i.

Method of Classification

Characteristic parameter

Consider a point set of samples $W = (x_1, x_2, \ldots, x_i, \ldots, x_N)$, in which x_i is a point of N-dimensional characteristic space. Assume that there are N_1 points belonging in class w_1, there are N_2 points belonging in class $w_2, \ldots$, and there are N_m points belonging in class w_m in the space. The samples of the same class should have the same place in characteristic space. In this paper, the following three parameters are regarded as the recognition features for recognizing whether the correction sample is in the same class as the unknown sample.

(1) Euclidean distance (E_d). This indicates the diverse degree of the place between two samples in characteristic space:

$$E_{d_{ij}} = \sum_{k=1}^{r} \sqrt{(x_{ki} - x_{kj})^2} \quad (1)$$

where $E_{d_{ij}}$ is the distance between sample i and sample j and k is the number of analytical wavelengths. Obviously, the smaller E_d is, the smaller is the difference degree.

(2) F-Test. This can test whether the variance of two samples has a marked difference:

$$F = \frac{S_A{}^2}{S_B{}^2} \quad (2)$$

If F is less than $F_{0.05,27,27}$, we shall consider that the variance of two samples does not have marked difference and $S_A{}^2$ and $S_B{}^2$ come from the same estimate of variance.

(3) t-Test. If there is no marked difference between $S_A{}^2$ and $S_B{}^2$, the difference between the average values of two samples will be verified by the t-test:

$$t = \frac{\overline{x_A} - \overline{x_B}}{\sqrt{[(S_A{}^2 + S_B{}^2)/r]}} \quad (3)$$

where r is the number of analytical wavelengths. If t is less than $t_{0.05,2(r-1)}$, we can say that the two samples come from the same parent.

Method of classification

Here E_d, t-test and F-test values are taken as the recognition features, and unknown samples are classified and recognized with the improved continuous Hamming method (ICHM). The process of recognition is as follows.

(1) Setting up the table of classification. The table of classification is constructed with the recognition features (E_d, t and F) of the known class samples (class D; this corresponds to a correction model) and unknown class samples (class N) (see Table 5).

(2) Calculating the mean values $\bar{x}_j^D$ and $\bar{x}_j^N$ and the sum of variances, $S(D)$ and $S(N)$:

$$\bar{x}_j^D = \left(\sum_{x_i \in D} x_i^D \right) / N_1 \quad (4)$$

$$\bar{x}_j^N = \left(\sum_{x_i \in D} x_{ij}^N \right) / N_2 \quad (5)$$

where N_1 is the number of known class samples, N_2 is the number of unknown class samples, $j = 1, 2, \ldots, n$ is the number of features and $i = 1, 2, \ldots, m$ is the number of samples:

$$S(D) = \sum_{j=1}^{n} \left[\sum_{x_i \in D} (x_{ij} - \bar{x}_j^D)^2 \right] / (N_1 - 1) \quad (6)$$

$$S(N) = \sum_{j=1}^{n} \left[\sum_{x_i \in D} (x_{ij} - \bar{x}_j^N)^2 \right] / (N_2 - 1) \quad (7)$$

(3) Calculating the Hamming nucleus $Z = (Z_1, Z_2, \ldots, Z_j, \ldots, Z_n)^T$:

$$Z_j = \begin{cases} \bar{x}_j^D & \text{when } S(D) \leqslant S(N) \\ \bar{x}_j^N & S(D) > S(N) \end{cases}$$

(4) Calculating the distance between the characteristic of samples and the Hamming nucleus, d_i:

$$d_i(x_i, z) = \sum_{j=1}^{n} (x_{ij} - z_j)^2$$

(5) Choosing the proper threshold value (Δ) and defining the class. If $d_i(x_i, z) \leqslant \Delta$, then $x_i \in D$, or else the correction model will be exchanged until the successful model is selected.

(6) The unknown sample is calculated with the successful calibration model by the ITTFA method.

Experimental

Apparatus

A UV-3000 spectrophotometer (Japan) and a Universe-68 computer (USA) were used.

Reagents

All reagents were of analytical-reagent grade. All solutions were prepared with ion-exchanged water. REE stock solution (1 mg ml^{-1}) were prepared by dissolving suitable amounts of the oxides of the 15 REEs in 10 ml of 6 mol l^{-1} hydrochloric acid, except for cerium, which was dissolved using hydrochloric acid and hydrogen peroxide. A 0.05% solution of tribromochlorophosphonazo (TBCPA) was prepared.

Preparation of Sample Solution

A 0.5000 g amount of geological sample was mixed with 3 g of sodium hydroxide and melted at 650 °C for 10 min. A 1 g amount of EDTA and 1 ml of 2% $MgCl_2$ solution were added after extracting the melt materials with 100 ml of water. The precipitates were filtered and dissolved in concentrated

hydrochloric acid. The solution was transferred into 50 ml calibrated flask and diluted to volume with water.

Procedure

A 5.00 ml volume of sample solution was placed in a 25 ml calibrated flask and 1 ml of 20% ascorbic acid solution and 0.5 ml of 5% ammonium oxalate solution as masking agents, 2.5 ml of 0.05% TBCPA solution and 0.2 ml of 2.5% KF solution were added. The absorbances of 27 analytical wavelengths between 634 and 660 nm were measured with the UV-3000 spectrophotometer and the concentrations of the elements were calculated with the computer using the ITTFA program. The details of the calculation procedure are shown in Fig. 1.

Results and Discussion

Properties of Absorption Spectra

The properties of the absorption spectra and the ranges in which Beer's law is obeyed for the 15 REE complexes are shown in Table 1. The additivity ranges of the absorbances of the 15 REE mixture is 0–20 μg per 25 ml.

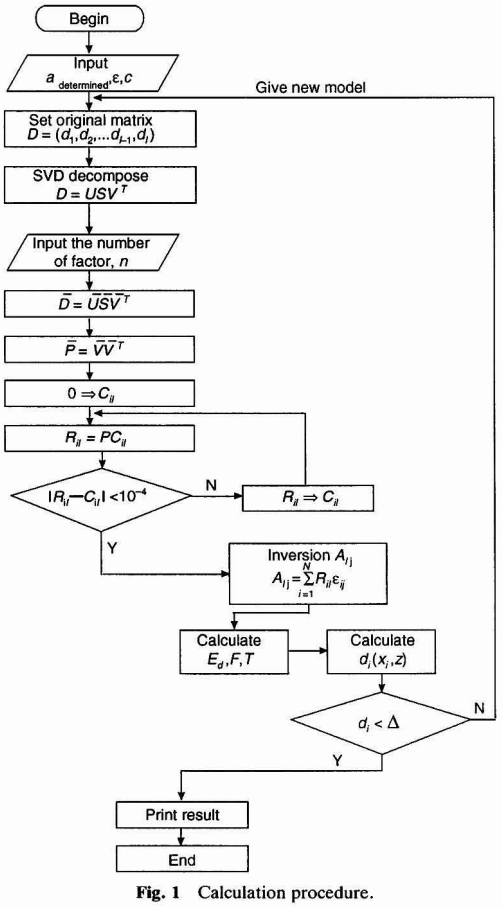

Fig. 1 Calculation procedure.

Definition of the Number of Factors

In general factor analysis, the number of factors (n) is defined by a set of criteria of errors.[15] The number of factors is often considered as the number of components contributing to the absorbance. However, if there are many components in a system, the definition of the number of factors will be difficult, and an incorrect judgement could be made. In this work, the first n factors were selected as the number of factors that had made a considerable contribution to the variance of the original data matrix. Now the number of factors (n) was not equal to the number of components. Decomposing many absorbance data matrices of the 15 REE mixtures made it clear that the maximum eigenvalue accounts for 99.999% of the summation value of the eigenvalue by only a single factor (see Table 2). The contribution to the variance of the original data matrix was decided mainly by the feature vector corresponding to the maximum eigenvalue. Hence the number of factors was one in this system and the analytical results for the 15 REEs also showed that the error of the calculated concentration was the least by only a single factor. When the number of factors was one, the reproduced data matrix was given by

$$\bar{D} = \bar{U}_{r\times 1}\bar{S}_{1\times l}\bar{V}_{1\times l}^{t}$$

where r is the number of wavelengths and l is the number of samples (correction samples and unknown sample). The projection vector was obtained as

$$p(i, j) = v(i, l)v(j, l), \quad i, j = 1, 2, \ldots, l$$

The target transformation was completed as follows:

$$R(i, l) = \sum_{j=1}^{l} p(l, j)c(i, j)$$

If $|R(i, l) - C(i, l)| > 10^{-4}$ [$C(i, l)$ is the initial value of the unknown sample, common for zero, $R(i, l)$ is the predicted

Table 1 Properties of absorption spectra of REEs complexes

Element	Wavelength of maximum absorption/nm	Molar absorptivity/ 10^5 l mol^{-1} cm^{-1}	Ranges in which Beer's law is obeyed/ μg ml^{-1}
La	642	1.14	0–0.8
Ce	643	1.11	0–0.8
Pr	643	1.18	0–0.8
Nd	645	1.16	0–0.8
Sm	644	1.23	0–0.8
Eu	646	1.19	0–0.8
Gd	645	1.23	0–0.8
Tb	646	1.22	0–0.8
Ho	647	1.15	0–0.4
Dy	646	1.21	0–0.4
Er	649	1.11	0–0.4
Tm	648	1.14	0–0.4
Yb	647	1.05	0–0.4
Lu	645	0.99	0–0.24
Y	647	1.23	0–0.48

Table 2 Variation of eigenvalue with the number of factors

Number of factors (n)	Eigenvalue (λ)	$\lambda_i/\Sigma\lambda_i$ (%)
1	0.48×10^2	99.999
2	0.13×10^{-3}	2.71×10^{-4}
3	0.46×10^{-5}	9.58×10^{-6}
4	0.57×10^{-7}	1.19×10^{-7}
$\Sigma\lambda_i$	48.000 13	

concentration of component i in the unknown sample], then $C(il) \Rightarrow R(il)$ and iteration was repeated until the difference between ${}^{(m)}R(il)$ and ${}^{(m-1)}R(il)$ was less than 10^{-4}, where ${}^{(m)}R(il)$ is the concentration of components i in the unknown sample.

Selection of Classification Characteristic

The selection of a proper characteristic that can designate the properties of a certain kind of sample is an important problem in pattern recognition. If there are many characteristics, we can make full use of useful information. However, too many characteristics will result in the information being used repeatedly and less useful information is introduced. Generally, the characteristics may be more than the required number at the beginning. Subsequently, the characteristics that have more influence on the classification can be selected by test. The Euclidean distance (E_d), t-test value (t), F-test value (F), variance (s^2) and similarity coefficient (sc) are taken as the characteristics at the beginning. Using the information about the samples of a known class, a weight function of classification was constructed:

$$g_j = \frac{U_{\text{different class},j}}{U_{\text{same class},j}}$$

$$U_{\text{same class},j} = \sum_i (x_{ij} - \overline{x_j})^2; x_{ij} \text{ and } \overline{x_j} \text{ are in the same class}$$

$$U_{\text{different class},j} = \sum_k (x_{kj} - \overline{x_j})^2; x_{kj} \text{ and } \overline{x_j} \text{ are in different classes}$$

where i, k (i, $k = 1, 2, \ldots, m$) are the numer of samples and j ($j = 1, 2, \ldots, n$) is the number of characteristics. All the weight functions (g_j) are shown in Table 3. As can be seen, the values of the weight function for E_d, t, F and s^2 are larger and therefore their contributions to classification are larger. Therefore, E_d, F, t and s^2 were selected as the features of classification. If the features describing the sample properties come from the same calculation, they will play the same role in the classification, which causes the information to be used repeatedly. The similarity coefficient may test the similarity between features. Table 4 gives the similarity coefficients among E_d, s^2, F and t. The data indicate that E_d and s^2 are similar and we can give up either of them. Finally, E_d, F and t were selected as the features of classification.

Selection of Correction Model

According to the relationship of concentration ratios among REEs of samples of national origin and from the Jilin province area (China), a series of concentration matrix clusters of different ratios were made. When unknown samples are analysed, one of them is chosen as the calibration model and the concentrations (c_i) of the 15 REEs are calculated by the ITTFA method. Then, a theoretical spectrum (A_j) can be obtained from the calculated concentrations by Beer's law. Comparing the absorbances of the theoretical spectrum with the determined absorbance, we can obtain the classification

Table 3 Selection of class characteristics

Power function	Characteristic				
	E_d	s^2	s_r	F	t
g_j	22.13	19.36	23	13.2	24.6

Table 4 Similarity coefficient

	s^2	E_d	F	t
s^2	1	0.992	0.328	0.247
E_d		1	0.272	0.302
F			1	0.248
t				1

Table 7 Limit of quantitative detection, accuracy and precision

Element	LOQ/μg ml^{-1}	t-Test value ($t_{0.05,6} = 2.45$)	s_r (%) ($n = 9$)
La	0.02	1.69	1.98
Ce	0.02	0.42	1.92
Pr	0.019	2.20	1.87
Nd	0.02	0.06	2.24
Sm	0.019	0.18	2.44
Eu	0.02	0.94	2.10
Gd	0.02	0.00	3.3
Tb	0.02	1.45	2.70
Dy	0.022	0.53	3.49
Ho	0.023	1.33	3.58
Er	0.024	1.65	1.83
Tm	0.022	0.21	2.29
Yb	0.024	1.09	1.94
Lu	0.026	0.88	3.09
Y	0.011	0.06	0.22

Table 5 Characteristics of samples

	Sample*											
	Class D						Class N					
Characteristic	1	2	3	4	5	6	J1	J2	J3	J4	J5	J6
E_d	4.19	4.14	4.92	4.82	2.97	2.95	0.36	5.28	1.43	3.42	0.89	0.73
F	1.29	1.45	1.17	1.18	1.23	1.08	1.02	1.31	1.70	1.33	1.30	1.47
t	1.97	1.93	1.82	2.12	1.62	1.89	1.27	1.25	1.02	1.68	1.35	1.00

* Samples 1–6 are geochemical standard samples (China) and samples J1–J6 are unknown samples from Jilin.

Table 6 Classification result of ICHM

	Sample											
	1	2	3	4	5	6	J1	J2	J3	J4	J5	J6
$d_i(x_i, z)$	0.07	0.89	0.77	1.0	1.1	1.2	13	1.7	7.4	0.35	9.6	10
$\Delta = 0.23$	D	D	D	D	D	D	N	D	N	D	N	N

Table 8 Results of the analysis of geological samples for the 15 REEs

Element	Sample* J2 Present method (ppm)			Average (ppm)	ICP-AES (ppm)	RE† (%)	J4 Present method (ppm)			Average (ppm)	ICP-AES (ppm)	RE† (%)
La	14.7	14.5	14.8	14.7	14.2	0.35	23.7	23.9	23.5	23.7	23.6	−0.4
Ce	27.0	27.6	27.8	27.5	26.2	5.0	38.9	39.2	38.5	38.9	40.2	3.2
Pr	3.4	3.5	3.6	3.5	3.2	5.5	5.4	5.6	5.4	5.5	5.6	1.8
Nd	12.8	12.6	12.9	12.8	14.1	−9.2	22.4	22.5	22.2	22.4	22.4	0.0
Sm	2.3	2.4	2.2	2.2	2.4	−8.3	4.4	4.6	4.5	4.5	4.8	−6.2
Eu	0.57	0.57	0.59	0.58	0.54	7.4	1.1	1.1	1.2	1.1	1.2	−8.3
Gd	2.1	2.0	2.1	2.1	2.0	−5.0	3.8	3.9	3.5	3.7	3.7	0.0
Tb	0.34	0.31	0.33	0.33	0.31	−6.4	0.57	0.5	0.57	0.57	0.59	−3.4
Dy	1.5	1.6	1.3	1.5	1.4	7.1	3.0	3.5	3.2	3.2	3.4	−5.9
Ho	0.24	0.27	0.28	0.26	0.28	−7.1	0.68	0.65	0.69	0.67	0.64	4.7
Er	0.85	0.87	0.86	0.86	0.80	7.5	1.7	1.8	1.8	1.8	1.8	0.0
Tm	0.15	0.14	0.17	0.15	0.15	0.0	0.30	0.29	0.31	0.30	0.30	0.0
Yb	0.80	0.78	0.79	0.79	0.76	3.9	2.0	1.98	1.92	1.97	1.93	2.1
Lu	0.13	0.12	0.15	0.13	0.14	−7.1	0.29	0.28	0.31	0.29	0.28	3.6
Y	8.3	8.0	8.1	8.1	8.4	−3.6	17.8	18.0	17.9	17.9	17.7	1.1

Element	GSS-6 Present method (ppm)			Average (ppm)	Certified value (ppm)	RE† (%)	GSS-8 Present method (ppm)			Average (ppm)	Certified value (ppm)	RE† (%)
La	42.1	42.6	42.8	42.5	40.0	6.2	12.2	12.5	12.0	12.3	13.0	−5.7
Ce	79.2	78.9	79.0	79.0	78.0	1.3	37.5	37.7	37.4	37.5	38.0	−1.3
Pr	9.3	9.2	9.2	9.2	9.2	0.0	3.1	3.0	3.0	3.0	3.2	−6.25
Nd	35.5	35.7	35.0	35.4	34.1	3.8	10.9	11.0	11.2	11.0	11.8	−7.2
Sm	6.0	6.5	6.4	6.3	6.3	0.0	2.3	2.2	2.3	2.3	2.4	−4.2
Eu	1.5	1.3	1.4	1.4	1.3	7.6	0.48	0.46	0.47	0.47	0.47	0.0
Gd	5.6	5.7	5.8	5.7	5.5	3.6	2.1	2.0	2.2	2.1	2.3	−8.9
Tb	0.76	0.78	0.77	0.77	0.77	0.0	0.38	0.40	0.39	0.39	0.42	−7.1
Dy	4.7	4.9	4.6	4.7	5.1	−7.8	2.2	2.4	2.3	2.3	2.2	4.5
Ho	0.96	0.95	0.95	0.95	0.96	−1.04	0.74	0.77	0.76	0.76	0.75	1.3
Er	2.6	2.5	2.4	2.5	2.8	−10.7	1.2	1.3	1.3	1.3	1.3	0.0
Tm	0.42	0.46	0.45	0.44	0.44	0.0	0.18	0.20	0.18	0.19	0.20	−5.0
Yb	2.5	2.6	2.7	2.6	2.8	−7.1	1.1	1.0	1.1	1.1	1.2	−8.3
Lu	0.41	0.43	0.41	0.42	0.45	−6.7	0.18	0.16	0.17	0.17	0.19	−10.5
Y	24.5	24.9	25.0	24.8	26.8	−7.5	13.0	12.9	13.4	13.1	13.8	−5.1

* J2 and J4 are geochemical samples from Jilin; GSS-6 and GSS-8 are geochemical standard samples (China).
† Relative error.

features value of an unknown sample, E_d, F and t. Employing the E_d, F and t values for samples of a known class, which includes the training points of the known class, and an unknown class, the calibration model that has the same class as the unknown samples was chosen by the ICHM. For example, using calibration model four, the concentrations of the 15 REEs of unknown samples J1, J2, J3, J4, J5 and J6 from the Jilin area were obtained. The classification characteristics of the known class samples and unknown class samples are given in Table 5. The distances d_i between the features of the sample and the Hamming nucleus and the results of classification according to the threshold ($\Delta = 2.3$) defined by experiment are given in Table 6. It is clear that J2 and J4 belong in class D and that model four is suitable for J2 and J4. By using correction model four and the ITTFA method, the calculated concentrations of J2 and J4 are as shown in Table 8. J1, J3, J5 and J6 did not belong in class D and the calibration model was changed until the successful model was selected.

Analysis of Geological Samples

The limit of quantitative detection (LOQ), accuracy (t-test) and relative standard deviation (s_r) of the method are given in Table 7. By using this method, national standard samples and more than 200 geological samples selected from different areas in China were analysed. A selection of the results is given in Table 8. The results show that the method is suitable for the determination of the 15 ERRs at high, medium and low concentrations in geological samples. Satisfactory results can still be obtained when the concentration ratios among the 15 REEs are 1:200.

References

1 Wirsz, D. F., and Blades, M. W., *Anal. Chem.*, 1986, **58**, 51.
2 Zhou, W. L., Pan, J. M., Sun, J., and Chen, Y., *Fenxi Ceshi Tongbao*, 1993, **5**, 27.
3 Wang, B. N., Tang, G. N., and Huang, K. L., *Analyst*, 1993, **2**, 205.
4 Ritter, G. L., Lowry, S. R., and Isenhour, T. L., *Anal. Chem.*, 1976, **3**, 591.
5 He, X. W., Tang, Z. X., Yang, W. L., Zhang, G. Z., Yu, G. Y., and Shi, H. M., *Fenxi Huaxue*, 1994, **3**, 218.
6 Wang, H. Y., and Wang, D. X., *Fenxi Shiyan Shi*, 1993, **12**, 82.
7 He, X. W., Ren, H. J., and Shi, H. M., *Fenxi Huaxue*, 1988, **12**, 1109.

8 Dong, K. L., Wang, H. Y., Zhou, H., and Wang, D. X., *Fenxi Huaxue*, 1992, **20**, 1252.
9 Yu, R. Q., *Introduction to Chemometrics*, Hunan Education Publishing House, Hunan, 1990, ch. 8.
10 Varnuza, K., *Pattern Recognition in Chemistry*, Springer, Berlin, 1980.
11 Kowalski, B. R., Schatzki, T. F., and Stross, F. H., *Anal. Chem.*, 1972, **44**, 2176.
12 Saxberg, B. E. H., Duewer, D. L., Booker, J. L., and Kowalski, B. R., *Anal. Chim. Acta*, 1978, **103**, 201.
13 Wang, B. Q., and Chen, Z. Y., *Moshi Shibie*, Dizhen Publishing House, Beijing, 1989, ch. 4.
14 Brayden, T. H., Poropatic, P. A., and Watanabe, J. L., *Anal. Chem.*, 1988, **60**, 1154.
15 Malinowski, E. R., *Anal. Chem.*, 1977, **49**, 606.

Paper 4/05241B
Received August 26, 1994
Accepted December 12, 1994

Determination of Benomyl Residues in Waters by Solid-phase Spectrofluorimetry

José Luis Vilchez, Luis Fermín Capitán-Vallvey, Jamal Rohand, Alberto Navalón and Ramiro Avidad*

Department of Analytical Chemistry, University of Granada, E-18071 Granada, Spain

A sensitive spectrofluorimetric method for the determination of trace amounts of benomyl was developed, based on solid-phase spectrofluorimetry. The relative fluorescence intensity of the benomyl fixed on C_{18} silica gel was measured directly after packing the gel beads in a 1 mm silica cell, using a solid-phase attachment. The wavelengths of excitation and emission were 293 and 375 nm, respectively. The applicable concentration range was from 0.2 to 20.0 ng ml^{-1}, with a relative standard deviation of 1.1% and a detection limit of 0.04 ng ml^{-1}. The method was applied to the determination of benomyl residues in natural waters. Recoveries were 96–103%. The method is more sensitive and selective than other methods described in the literature.

Keywords: Benomyl determination; solid-phase spectrofluorimetry; pesticide residues; water analysis

Introduction

Methyl[1-(butylcarbamoyl)benzimidazol-2-yl]carbamate (benomyl) is a fungicide with systemic activity, effective against a wide range of fungi affecting field crops, fruits and ornamentals. The US National Research Council has estimated the use of benomyl at 2×10^6 per annum as active ingredient in several commercial pesticides. Because of its suspected carcinogenic activity and wide use, the determination of benomyl in crops and waters is very important.

Owing to the instability of benomyl in water and organic solvents,[1] for its determination by the use of HPLC it is first quantitatively converted into carbendazim (MBC).[2–4] The major problem is that the carbendazim produced from benomyl during the analysis and the carbendazim that was already present in the sample at the beginning of the analysis cannot be distinguished. The biological activities of MBC and benomyl differ and for this reason the determination of benomyl as MBC has only limited applications. Other methods[5] rely on the simultaneous determination of benomyl and carbendazim in water using HPLC after previous quantitative conversion of benomyl into 3-butyl-2,4-dioxo-*s*-triazino[1,2-*a*]benzimidazole (STB) at pH 13.0.

More recently, Marvin *et al.*[6] published a method for the simultaneous determination of trace concentrations of benomyl and MBC in water using automated on-line preconcentration by HPLC. However, the difficulty was the instability of the solution of benomyl, which is rapidly converted into carbendazim.

Solid-phase spectrofluorimetry (SPF) has been found to be useful for the determination of trace amounts of pesticides in water, showing several advantages such as low interference levels, low detection limit, high sensitivity and the use of conventional instrumentation.[7–10] In this paper, a method for determination of trace amounts of benomyl, in the presence of carbendazim, by SPF is described. The method was applied satisfactorily to the determination of benomyl residues in natural waters.

* To whom correspondence should be addressed.

Experimental

Apparatus and Software

A Perkin-Elmer (Norwalk, CT, USA) LS-5 luminescence spectrometer fitted with accessories described previously[11] was used to perform all spectrofluorimetric measurements, and variable-angle surface accessory designed and constructed by the authors[11] was also used to carry out the measurements of relative fluorescence intensity (RFI). A standard rectangular silica cell with a 1 mm pathlength was used as a container for the fluorescence measurements.

A Crison Model 501 digital pH meter (Crison Instruments, Barcelona, Spain) with a combined glass–saturated calomel electrode and an Agitaser 2000 rotating agitator (Tecnotrans, Barcelona, Spain) were also used.

The Statgraphics (Statistical Graphics, Version 6.0) software package was used for regression analysis (linear model).

Reagents

All reagents were of analytical-reagent grade unless stated otherwise. Reverse osmosis quality water was used throughout.

Benomyl stock standard solution (100 mg l^{-1}) was prepared by dissolution of 10.00 mg of the reagent (Riedel-de Haën, Seelze, Germany) in 100 ml of 5 mol l^{-1} hydrochloric acid. This solution was stable for at least 2 weeks. Working standard solutions (5, 2 and 1 μg ml^{-1}) were prepared by appropriate dilutions with 5 mol l^{-1} hydrochloric acid.

C_{18} silica gel (40–63 μm particle size) (Sigma, St. Louis, MO, USA) was used as the solid support without any pre-treatment.

Fluorescence Measurements

The measured RFI of the gel beads containing the fluorescent analyte and packed in a 1 mm silica cell was the diffuse transmitted fluorescence emitted from the gel at the unirradiated face of the cell. The optimum angle between the cell plane and the excitation beam was 45° in all instances.[11]

Procedures

Basic procedure

A 500 ml water sample containing between 0.2 and 20.0 ng ml^{-1} of benomyl was acidified with concentrated hydrochloric acid to pH 1.0, transferred into a 1 l glass bottle and 250 mg of C_{18} silica gel were added. The mixture was shaken mechanically for 30 min, after which the gel beads were collected by filtration under suction, dried and packed into a 1

mm silica cell. A blank sample containing all reagents except benomyl was prepared and treated in the same way as described for the sample. The fluorescence intensities (20.0 ± 0.5 °C) of the sample and blank were always measured at λ_{em} = 375 nm with λ_{ex} = 293 nm. A calibration graph was constructed in the same way using benomyl solutions of known concentration.

Procedure for natural waters

The above-mentioned reagents were added to 500 ml of natural water sample (for tap water, addition of 5 ml of 100 μg ml^{-1} sodium sulfite solution was also necessary to eliminate the interference from chlorine) and placed in a 1 l glass bottle. The subsequent steps were as described under *Basic procedure*. The standard additions method was used for calibration.

Sample treatment

Water samples, appropriately acidified with concentrated hydrochloric acid to pH 1.0, were filtered through a cellulose acetate filter (0.45 μm pore size, Millipore HA WP 04700) and the filtrates were collected in glass containers that had been cleaned carefully with hydrochloric acid. The samples were stored at 4 °C until analysis. Analyses were performed with the least possible delay (1–2 d). The usual precautions were taken to avoid contamination.[12]

Results and Discussion

Spectral Characteristics

In aqueous solutions, benomyl shows native fluorescence that remains stable only in an acidic medium.[13] The peak wavelength in the emission spectrum of benomyl solution is 400 nm and the excitation maximum is located at 280 nm. When the benomyl is fixed on C_{18} silica gel, the maxima of emission and excitation were 375 and 293 nm, respectively.

From a study of the half-life of the excited state of the system in the solid phase at different temperatures, it was concluded that the luminescence process was fluorescence ($\tau < 5 \times 10^{-6}$ s).

Optimization of Variables

pH dependence

As aqueous solutions of benomyl are stable only in an acidic medium, the effect of pH was studied using hydrochloric acid for adjustment.[13] The optimum pH for the fixation of the benomyl was found to be 1.0.

The fluorescence was independent of ionic strength, adjusted with NaCl or $NaClO_4$, up to 0.1 mol l^{-1}.

Influence of temperature

The dependence of the RFI (of benomyl fixed on the gel) on temperature is critical (−1.2% °C^{-1}). The RFI decrease with temperature was totally reversible. All RFI measurements reported here were performed at 20.0 ± 0.5 °C. As the fixation process was independent of temperature in the range 0–40 °C, the fixation of benomyl on the gel was carried out at room temperature.

Other experimental conditions

The stirring time necessary for maximum RFI development was 30 min for 100, 200 and 500 ml sample volumes. Longer times did not result in any improvement. As the use of a large amount of silica gel lowered the RFI, only the amount required to fill the cell and facilitate handling, *i.e.*, 250 mg, was used in all measurements. With regard to the stability of the C_{18} silica gel–benomyl system, the RFI remained constant for at least 1 h. The order of addition of the reagents did not affect the results obtained.

Effect of sample volume on sensitivity

In previous papers,[7–11] it was mentioned that one of the main advantages of the SPF method is the potential increase in sensitivity with increase in the sample volume taken for analysis. This effect can be assessed by measuring the RFI of C_{18} silica gel equilibrated with different volumes of solutions containing the same concentration of benomyl and proportional amounts of the other reagents.

Plots of RFI *versus* sample volume show an increase in fluorescence signal with sample volume, tending asymptotically to a constant RFI value above a certain volume (500 ml in this study) The shape of the graphs suggests a Langmuir-type isotherm, as was observed in some solid-phase spectrofluorimetic studies.[11]

Calibration and Precision

The calibration graphs for the samples treated according to the procedure described above are linear for the concentration range 1.0–40.0 ng ml^{-1} for a 100 ml, 0.8–30.0 ng ml^{-1} for a 200 ml and 0.2–20.0 ng ml^{-1} for a 500 ml sample volume. The analytical parameters are summarized in Table 1.

The repeatability of the proposed method and of the packing of the gel in the 1 mm silica cell was determined. The precision was measured for a benomyl concentration of 10.0 ng ml^{-1} by performing ten independent determinations. The relative standard deviations (s_r) ($P = 0.05$, $n = 10$) were 1.0%, 1.1% and 1.1% for 100, 200 and 500 ml samples, respectively. The precision (s_r) of the packing operation, calculated from ten measurements, was 1.0% for the benomyl fixed on the silica gel and 0.9% for the silica gel blank. The precision (s_r) of the fluorescence measurements (noise) was about 0.5% in all instances.

Sensitivity and Detection Limit

The sensitivity of SPF methods can be enhanced by increasing the volume of the sample. In practice, this increase can be calculated from the slope of the calibration graphs. The calculated values of the sensitivity ratio (S) for the samples analysed in this study were $S_{500/100} = 1.81$ and $S_{500/200} = 1.35$, where the subscripts represent the sample volumes (ml). The non-linear dependence of sensitivity *versus* sample volume can be attributed to the decrease in the distribution coefficient

Table 1 Analytical parameters. Ten standards were used for statistical calculation of calibration graphs

	Sample volume/ml		
Parameter	100	200	500
Intercept	−0.3	−0.6	0.1
Slope	7.98	10.76	14.48
Linear dynamic range/ng ml^{-1}	1.0–40.0	0.8–30.0	0.2–20.0
Correlation coefficient	0.999	0.999	0.999
Detection limit/ng ml^{-1}	0.2	0.1	0.04
Quantification limit/ng ml^{-1}	0.5	0.4	0.1
s_r (%)*	1.0	1.1	1.1

* Relative standard deviation for 10 ng ml^{-1} of benomyl and ten replicates.

with analyte concentration, as is usual for a non-linear isotherm.

The IUPAC detection limits ($k = 3$)[14] and the quantification limits ($k = 10$)[15] were calculated for 100, 200 and 500 ml sample volumes. The results are reported in Table 1.

Effect of Foreign Species

In order to determine the potential effect of foreign species and/or different fluorescent and non-fluorescent pesticides on the determination of benomyl at the 1.0 ng ml^{-1} level, a systematic study was carried out. A 20.0 μg ml^{-1} level of potentially interfering ionic species was tested first and if interference occurred the ratio was reduced progressively until interference ceased. Organic species were tested at different concentration levels depending on their respective solubilities in water. Tolerance was defined as the amount of foreign species that produced an error not exceeding ±5% in the determination of the analyte. Table 2 gives the results obtained.

Applications of the Method

The proposed method was applied to the determination of benomyl in water samples by using the standard additions method. Tap water from Granada, raw water from the supply to Granada (Genil River), mineral water from Lanjarón (Granada) and underground water from a well located in the aquifer of the fertile plain of Granada were selected as representative samples. The volume of water used was 500 ml in all instances. The effect produced by the usual level of chlorine in tap water (0.6 μg ml^{-1}) was eliminated by the addition of an appropriate amount of sodium sulfite.

The benomyl content of all of the water samples was found to be lower than the detection limit of the method. Therefore, in order to determine the accuracy of the proposed method, a recovery study was carried out on the waters mentioned above. For this, various volumes (between 0.15 and 0.5 ml) of 5 ng ml^{-1} benomyl solution were added to 500 ml of water samples and after adjusting the pH to 1 (maintaining a final volume of 525 ml in all instances) the percentage recovery was determined. Table 3 gives the results obtained.

In conclusion, solid-phase spectrofluorimetry can be used with advantage over other methods for the determination of benomyl residues in waters, although benomyl is known to be unstable in water and organic solvents. Further, benomyl is distinguished from carbendazim, which permits the elucidation of the extent to which both compounds are initially present, an important problem owing to their different interactions with biological systems.

Table 2 Effect of foreign species on the determination of 1.0 ng ml^{-1} of benomyl

Foreign species	Tolerance level/ng ml^{-1}
F^-, Cl^-, Br^-, I^-, ClO_3^-, CO_3^{2-}, PO_4^{3-}, SO_4^{2-}, NO_3^-, acetate, Ca^{2+}, Mg^{2+}	>20 000
Carbendazim	6 000
Humic acid	1 000
Lindane	500
Thiabendazole	260
Carbaryl	200
Folpet	200
Dichlone	50
o-Phenylphenol	15
Morestan	2

Table 3 Recovery study of benomyl in natural waters

	Benomyl/ng ml^{-1}		
Sample	Taken	Found*	Recovery (%)
Tap water	1.50	1.45 ± 0.02	96.7
(Granada)	3.50	3.50 ± 0.04	100.0
	5.00	5.10 ± 0.05	102.0
Surface water	1.50	1.50 ± 0.02	100.0
(Genil River)	3.50	3.50 ± 0.03	100.0
	5.00	4.95 ± 0.05	99.0
Mineral water	1.50	1.50 ± 0.03	100.0
(Lanjarón)	3.50	3.45 ± 0.04	98.6
	5.00	5.10 ± 0.06	102.0
Underground water	1.50	1.55 ± 0.03	103.3
	3.50	3.45 ± 0.05	98.6
	5.00	5.05 ± 0.06	101.0

* Average value ± standard deviation of six determinations.

This study was funded by the Dirección General de Investigación Científica y Técnica (DGICYT) del Ministerio de Educación y Ciencia (Spain) (Project No. NAT91-0407).

References

1 Chiba, M., and Doornbos, F., *Bull. Environ. Contam. Toxicol.*, 1974, **11**, 273.
2 Austin, D. J., Lord, K. A., and Williams, I. H., *Pestic. Sci.*, 1976, **7**, 211.
3 Bardalaye, P. C., and Wheeler, W. B., *J. Chromatogr.*, 1985, **330**, 403.
4 Spittler, T. D., Marafioti, R. A., and Lahr, L. M., *J. Chromatogr.*, 1984, **317**, 527.
5 Chiba, M., and Singh, R. P., *J. Agric. Food Chem.*, 1986, **34**, 108.
6 Marvin, C. H., Brindle, I. D., Singh, R. P., Hall, C. D., and Chiba, M., *J. Chromatogr.*, 1990, **518**, 242.
7 Vilchez, J. L., Avidad, R., Navalón, A., Rohand, J., and Capitán-Vallvey, L. F., *Int. J. Environ. Anal. Chem.*, 1993, **53**, 139.
8 Vilchez, J. L., Navalón, A., Avidad, R., Rohand, J., and Capitán-Vallvey, L. F., *Fresenius' J. Anal. Chem.*, 1993, **345**, 716.
9 Capitán, F., Alonso, E. J., Avidad, R., Capitán-Vallvey, L. F., and Vilchez, J. L., *Anal. Chem.*, 1993, **65**, 1336.
10 Vilchez, J. L., Avidad, R., Rohand, J., Navalón, A., and Capitán-Vallvey, L. F., *Anal. Chim. Acta*, 1993, **282**, 445.
11 Vilchez, J. L., Navalón, A., Avidad, R., García-López, T., and Capitán-Vallvey, L. F., *Analyst*, 1993, **118**, 303.
12 American Public Health Authority, American Water Works Association and Water Pollution Control Federation, *Standard Methods for the Examination of Water and Waste Water*, APHA, Washington, DC, 15th edn., 1980.
13 Singh, R. P., Marvin, C. H., Brindle, I. D., Hall, C. D., and Chiba, M., *J. Agric. Food Chem.*, 1992, **40**, 1303.
14 IUPAC, *Pure Appl. Chem.*, 1976, **45**, 105.
15 Guidelines for Data Acquisition and Data Quality Evaluation in Environmental Chemistry, *Anal. Chem.*, 1980, **52**, 2242.

Paper 4/06718E
Received November 3, 1994
Accepted January 3, 1995

CUMULATIVE AUTHOR INDEX

JANUARY–MAY 1995

Aaseth, Jan, 779, 853, 931
Abdillahi, Mohamed M., 1577
Abou-Shakra, Fadi R., 341
Abramova, Natalia E., 859
Abrigo, C., 47
Adkins, Rob L., 1433
Afanas'ev, Igor B., 859
Aggarwal, Jugdeep K., 1301
Åkesson, B., 833
Ala-Kleme, Timo, 367
Alam, Khurshid, 1577
Alava, Izaskun, 1069
Albero, Mª Isabel, 129
Alexander, Jan, 931, 935
Alexander, P. W., 1559
Alfthan, Georg, 841
Ali, Azza M..M., 1065
Ali, Mohammed A., 1577
Allard, Bert, 603
Allen, Lawrence H., 1163
Amin, Alaa S., 1189
Analytical Methods Committee, 29
Andersen, Ole, 853
Anderson, Richard A., 867
Andersson, Örjan, 423
Andrade, J. M., 249
Andrés, J. Verdú, 299
Andres, Roberto T., 1549
Angeletti, Roberto, 577
Anjaiah, K. V., 1401
Antolovich, Michael, 1
Aoki, Nobumi, 135
Arakawa, Hiromi, 1083
Araujo, Pedro W., 295
Argyraki, Ariadni, 1353
Arias, J. J., 313
Aro, Antti, 841
Arruebarrena-Baez, Morella, 985
Arthur, John R., 827
Astruc, A., 79
Astruc, M., 79
Augugliaro, Vincenzo, 237
Avidad, Ramiro, 1609
Axner, Ove, 635
Azani, R., 395
Bacigalupo, Maria A., 1153
Bacsó, Jozsef, 871
Badini, G. E., 1025
Baeyens, W. R. G., 463
Baggiani, Claudio, 1153
Balaram, V., 1401
Balazs, G. Bryan, 523
Baldin, C., 47
Balint, Judit, 871
Barrero, J. M., 431
Barrow, Ian S., 1357
Bastiani, E., 577
Baumann, Wolfram, 243
Baxter, Douglas C., 69, 755
Baxter, Pamela J., 1583
Beary, Ellyn S., 1505
Beck, Rolf, 1327
Beckett, Geoffrey J., 827
Beech, Stuart G., 827
Behne, Dietrich, 823
Bekessy, Lambert K., 211
Beltran, R., 1171
Bentley, Philip A., 985
Benzo, Zully, 1215
Beran, Miloš, 979
Beran, Miloš, Jr., 979
Bergdahl, Ingvar A., 1205
Berglöf, Tomas, 755
Berzas Nevado, J. J., 171
Bhilare, N. G., 391
Bishop, Nicholas J., 705
Bissonnette, M. C., 395
Bjennes, Heidi, 367
Blais, Jean-Simon, 395, 629
Blanchflower, W. John, 331, 1129
Blanuša, Maja, 951
Bode, Peter, 1527
Bolyos, Maria, 733
Borch-Iohnsen, Berit, 891
Bos, Martinus, 1009
Bottazzi, Piero, 1309
Bouropoulos, Nicolaos Ch., 347
Brandvold, Donald K., 1485
Brandvold, Lynn A., 1485
Branth, Stefan, 837
Brekke, Trond, 1379
Brereton, Richard G., 295, 1107
Brindle, Ian D., 183
Brunmark, Per, 41
Bryden, Noella A., 867
Bulnayev, A. I., 1445
Cámara, C., 431
Cai, Qiantao, 1047
Calokerinos, A. C., 463
Calos, Nicholas, 211
Cammack, Richard, 699
Cannavan, A., 331
Capellmann, Michaela, 935
Capitán-Vallvey, Luis Fermín, 1609
Carbonell, Vicente, 231
Cargnello, Jill A., 783, 789, 793
Caruso, Joseph A., 583
Cave, Mark, 1341
Cawley, Jess, 1267
Ceramelli, Giuseppe, 319, 1005
Cerdà, V., 1181
Chakraborti, Dipankar, 643, 917
Chambon, P., 1133
Chambon, R., 1133
Chan, Albert C., 651
Chan, Wing Hong, 1055
Chanda, Bhabatosh, 917
Chatterjee, Amit, 643, 917
Chau, Y. K., 667, 721
Chee, Kok Kay, 273, 281
Chen, Ni, 1115
Chen, Shu-gui, 1603
Cheremisina, Zinaida P., 859
Chi, Nai-Yuen, 511
Chłopicka, Joanna, 943
Chow, P. Y. T., 1221
Chowdhury, Tarit Roy, 643
Christian, Gary D., 1583
Chromiak, Edward, 149
Chua, T. H., 1221
Chung, Mu-Jye, 511
Cirello-Egamino, Joanne, 183
Cladera, A., 1181
Cohen, David, 1327
Coles, Barry J., 1415, 1421
Colombi, Stefano, 1153
Cook, Robert L., 591
Cordos, Emil A., 725
Corocher, Nadia, 1153
Corti, Piero, 319, 1005
Crews, Helen M., 705
Crichton, Robert R., 693
Crocker, Peter R., 783
Cser, Agnes, 905
Cui, Xiao-Yuan, 699
Curtius, Adilson J., 947
Dalene, Marianne, 41
Damiani, Patricia, 443
Danielson, Neil D., 1091
Danielsson, Bengt, 155
Danielsson, Lars-Göran, 713
Das, Dipankar, 643, 917
Date, Yuuko, 1141
Dauphin, Jean François, 967
De Bock, Lieve, 681
de Campos, Reinaldo Calixto, 947
de la Fuente, Miguel Angel, 107
de la Guardia, Miguel, 231, 313
De Medina, Hilda Ledo, 761
De Vargas, Marinela Colina, 761
Dean, J. R., 355
Deby, Carol, 967
Deby-Dupont, Ginette, 967
del Barrio Martín, S., 85
Delgado Zamarreño, M. M., 139
Delves, H. Trevor, 793
Detwiler, Kandace R., 1583
Deuster, Patricia A., 867
Devi, Surekha, 555
Diaz-Garcia, Marta Elena, 457
Djane, Nii-Koley, 1471
Doklea, Erika, 771
Dowle, C. J., 355
Dreassi, Elena, 319, 1005
Dressler, Valderi L., 1185
Dubest, Roger, 447
Ducaroir, Jacques, 741
Düker, Anders, 603
Dutka, B. J., 721
Dyer, Christopher D., 985
Echols, Roger T., 1175
Ede, Roland J., 789
Edmonds, Tony E., 1543
Edmunds, Mike, 1433
Edwards, Robert, 117
Eisenhut, S., 1291
El-Sayed, Gamal O., 1189
El-Shahat, Mohamed F., 549, 1201
El-Zawawy, F. M., 549
Elizalde, María P., 1069
Elsenbroek, J. H., 1535
Emteborg, Håkan, 69
Enger, Jonas, 635
Enzweiler, Jacinta, 1391
Ersoy, Lale, 373
Estela, J. M., 1181
Evans, Paul A., 985
Eybl, Vladislav, 855
Fabelinsky, Yury I., 1427
Falcó, P. Campíns, 299
Fernández, L., 431
Fernandez-Romero, J. M., 179
Fichtl, Burckhard, 771
Figueiredo, Ana M. G., 1441
Filby, Roy H., 1379
Fischer, Anna B., 975
Fogg, Arnold G., 505
Folta, Maria, 943
Foote, John W., 887
Forth, Wolfgang, 771
Fouillet, B., 1133
Frech, Wolfgang, 69, 755
Frentiu, Tiberiu, 725
Frontasyeva, M. V., 1437
Fu, Cheng-Guang, 1147
Fuchs, Anette, 905
Fujita, Tomio, 1137
Fukasawa, Tsutomu, 543, 1201
Fukushima, Takeshi, 381
Fung, Paul K., 1159
Furusawa, Motohisa, 437
Gallus, S., 1291
Gao, De, 499
García, J. M., 313
García, Mª Soledad, 129
García Pinto, Carmelo, 53
Gennaro, M. C., 47
Gessner, Hildegard, 823
Ghandour, M. A., 1065
Gilkes, R. J., 1335
Gilles, C., 1247
Gilmartin, Markas A. T., 1029
Giraldez, I., 1171
Giraudi, Gianfranco, 1153
Głąb, Stanisław, 489
Glass, Robert S., 523
Gleeson, Sarah A., 1421
Glynn, Anders Wicklund, 713
Gnaneshwara Rao, T., 1279
Godlewska, Beata, 143
Gómez, E., 1181
Gómez-Hens, Agustina, 125
Gómez Laguna, M. A., 171
Golimowski, Jerzy, 143
Gomez-Ariza, J. L., 1171
González, Elisa Blanco, 809
Govil, Pradip K., 1279
Grattan, K. T. V., 1025
Greenfield, Simon M., 793
Greenfield, Stanley, 1543
Greenway, Gillian M., 477, 1077
Groves, John A., 1107
Gu, Jun, 499
Güçer, Şeref, 101
Gupta, Vinod K., 495
Gurden, Stephen P., 1107
Gutierrez, Elizabeth, 761
Haapakka, Keijo, 367
Haas, Ulrich, 351
Haigh, James A., 985
Hallén, Ira Palminger, 765
Hamano, Takashi, 135
Hamilton, David L., 1373
Hansson, Gert-Åke, 1205
Hart, John P., 1029, 1059
Harte, B., 1315
Hasan, Berween A., 231
Hayakawa, Kazuichi, 377, 1137
Hebeda, E. H., 1291
Heinen Brown, Judy, 1215
Heinonen, Olli, 837
Hempel, M., 721
Hendra, Patrick J., 985
Herbert, Hugh K., 1357
Hernández Artiga, Maria Purificación, 485
Hernández-Cassou, S., 305
Hernandez Mendez, J., 139
Heumann, K. G., 1291
High, Kim A., 629
Hill, Steve J., 413
Hinton, R. W., 1315
Hitchen, S. M., 355
Hjelstuen, Ole K., 863
Hopkins, Timothy C., 1373
Hori, Yoshikazu, 187
House, Ivan, 793
Howard, Alan N., 887
Hsu, Fu-Shien, 511
Hu, Jingbo, 1073
Hu, Xiaoya, 1555
Huang, P. M., 659
Huang, W., 833
Huebra, Marta M., 1069
Hughes, Martin N., 699
Hulanicki, Adam, 143
Hunter, Thomas C., 161
Ibáñez, Gabriela, 443
Ibrahim, Hosny, 1211
Igarashi, Shukuro, 539

Imai, Kazuhiro, 381
Inoue, Hirofumi, 1141
Irons, Gordon P., 477
Isaksen, Gary H., 1379
Ishida, Junichi, 1083
Ishiyama, Munetaka, 113
Issa, Yousry M., 1189, 1211
Ito, Yoshio, 135
Iwatsuki, Masaaki, 543, 1201
Jacobsen, Dag, 853
Jain, Suresh, 495
Jambers, Wendy, 681
Jane, Yih-Song, 517
Jantzen, Eckard, 667
Jarvis, Kym E., 1391, 1397
Jeffries, Teresa E., 1365
Jervis, Robert E., 651
Jiménez, A. I., 313
Jinyu, Zhao, 1199
Joannou, Chris. L., 699
Jochum, Frank, 905
Johannsen, Bernd, 775
Johansson, Karin, 423
Johansson, Magnus, 755
Jones, Mark M., 855, 951
Jönsson, Jon Åke, 1471
Josowicz, Mira, 1019
Juárez, Manuela, 107
Kakehi, Kazuaki, 63
Kalcklösch, Margrit, 823
Kale, Uma, 325
Kan, Jin-qing, 573
Kane, Jean S., 1505
Kane, M., 355
Kankare, Jouko, 367
Karlsson, Stefan, 603
Kato, Masaru, 381
Kavianpour, Keyhandokht, 295
Kawakami, Takanori, 539
Kendall, Marion D., 793
Kennard, Colin H. L., 211
Kennedy, D. Glenn, 331, 1129
Khalaf, Karim D., 231, 313
Khan, Shazia, 699
Khodari, Mahmoud, 1065
Khoo, Soo Beng, 1047
Kilworth, Richard, 1273
Kitaoka, Mitsuo, 1137
Knight, Andrew W., 1077
Ko, Matthew M., 651
Kohashi, Kazuya, 1141
Koizumi, Yoshiyuki, 89
Kojima, Nobuaki, 135
Kolesov, Gennady M., 1457, 1461
Kolotyrkina, Irina Ya., 201
Koncki, Robert, 489
Kontoghiorghes, George J., 845
Kontoyannis, Christos G., 347
Korkina, Ludmila G., 859
Kostial, Krista, 951
Kotyzová, Dana, 855
Koutenský, Jaroslav, 855
Koutsoukos, Petros G., 347
Kozak, L. M., 659
Krishnamurti, G. S. R., 659
Krishnana, S. S., 651
Krośniak, Mirosław, 943
Kuballa, Jürgen, 667
Kuralay, Ayses, 1087
Kvíčala, Jan, 959
Kwan, K. K., 667, 721
Kyriakopoulos, Antonios, 823
Lamble, Kathryn, 413
Lamy, Isabelle, 741
Lan, Wei Guang, 273, 281, 1115
Landsberg, Judith P., 789, 793
Langford, Cooper H., 591
Latva, Martti, 367
Lau, Oi-Wah, 1125
Ledin, Anna, 603
Lee, David, 827
Lee, Hian Kee, 281
Leguille, F., 79
Lehnert, Ralph, 985
Leng, Zongzhou, 1555
Leung, Ka-Sing, 1125
Levoir, Patrick, 447
Li, Ke, 361
Li, Lin, 583
Li, Qilong, 1073
Li, Sam F. Y., 361
Li, Xiangdong, 1415
Liang, Bing, 543
Liebl, Bernhard, 771
Lindeberg, S., 833
Linke, Krzysztof, 939
Liu, D., 721
Liu, Daojie, 565, 569, 1195
Liu, Guihua, 565, 569
Liu, Renmin, 565, 569, 1195
Liu, Ruixian, 1599
Liu, Yi-Ming, 385
Ljungberg, Peter, 635
Łobiński, Ryszard, 615
López, P., 249
Lombeck, Ingrid, 905
Lonardi, Silvano, 319, 1005
Loukas, Yannis L., 533
Lowthian, Philip J., 271
Lu, Jianzhong, 453
Lu, Xing, 651
Luppino, Maria A., 883
Luque De Castro, M. D., 179
Luterotti, Svjetlana, 925
Lyon, Ian C., 1321
McCulloch, M. T., 35
Machado, Enio L., 1185
Machill, S., 1465
McInnis, R., 721
Mackay-Sim, Alan, 1013
McKee, Chris, 1261
McLaren, James W., 629
McLean, Allan J., 883
McLemore, Virginia T., 1485
MacPherson, Allan, 871
Mäkelä, Anna-Liisa, 837, 955
Mäkelä, Pekka, 837, 955
Malahoff, Alexander, 201
Malmsten, Yvonne, 635
Mandal, Badal K., 643, 917
Maraj, Shaun R., 699
Marengo, E., 47
Marina, M. L., 255
Marsh, James R., 1091
Marshall, William D., 623
Martelletti, M. T., 47
Martínez-Lozano, Carmen, 471, 1103
Martins, Ayrton F., 1185
Martins, Jorge L. S., 193
Masini, Jorge C., 1583
Massey, Robert C., 705
Masuda, Akimasa, 335
Mathew, Biju, 1097
Mathiasson, Lennart, 1471
Matni, G., 395
Matsunaga, Akinobu, 377, 1137
Mattos, I. L., 179
Matveeva, Svetlana S., 1427
Mazurek, Roman, 761
Mecklenburg, Michael, 155
Menzel, Helmut, 905
Methven, Bradley A. J., 629
Meyer, Jean-Jacques, 447
Mikalsen, Arne, 935
Mikasa, Hiroshi, 187
Miki, Yasuyoshi, 63
Millward, Geoffrey E., 609
Mishra, Rajendra Kumar, 197
Mitsuhashi, Yukimasa, 135
Miyake, Yasuko, 63
Miyazaki, Motoichi, 377, 1137
Mizukami, Eiichi, 377, 1137
Mohamed, A. A., 549
Mohamed, Ashraf A., 1201
Mohamed, Sabry K., 1211
Moiny, Georges, 967
Morales, E., 1171
Morales-Rubio, Angel, 231, 313
Moreira, Josino C., 505
Moreira, Maria de Fátima R., 947
Moreno Cordero, Bernardo, 53
Moritani, Kazuhiro, 1141
Morrison, John L., 1519
Moser-Veillon, Phylis B., 895
Motomizu, Shoji, 187
Mückter, Harald, 771
Muniategui, S., 249
Muñoz, Amalia, 529
Muñoz Leyva, Juan Antonio, 485
Munro, C. H., 993
Muralidhara Rao, B., 1097
Murillo Pulgarín, J. A., 171
Murphy, Karen E., 1505
Nachtmann, Carlo, 577
Nakamura, Toshihiro, 89
Näntö, Veikko, 837, 955
Narasimha Murty, B., 1099
Narayana, B., 1097
Narayanaswamy, Ramaier, 1549
Nashine, Neena, 197
Navalón, Alberto, 1609
Navarro, Mª Pilar, 899
Ndung'u, Kuria, 1471
Nerín, Cristina, 751
Nicol, Fergus, 827
Nieboer, Evert, 733
Nigdikar, Shailja V., 887
Nishimura, Masayuki, 1137
Nishiyama, Katsuhiko, 113
Niwa, Tomoko, 167
Njåstad, Oddvar, 1479
Nogueira, Claudio A., 1441
Noike, Yuji, 89
Nomura, Satoshi, 503
Norlin, Peter, 155
Norman, Michael D., 1059
Nouri, B., 1133
Nowak, Barbara, 737, 747
Nusko, R., 1291
Nyarku, Samuel, 1163
O'Connor, Catherine, 1485
Oguri, Shigeyuki, 63
Ohkura, Yosuke, 113
Öhman, Ove, 155
Ohto, Mikiya, 377
Oji, Yoshikiyo, 135
Olin, Åke, 423
Olivieri, Alejandro C., 443
Olsen, Samuel D., 1379
Oriundi, Maurizio Paleologo, 577
Ortapamuk, Oya, 1087
Oshima, Mitsuko, 187
Oskarsson, Agneta, 765, 911
Ottolini, Luisa, 1309
Oungpipat, W., 1559
Ow, B. Y., 1221
Owen, Linda M. W., 705
Özer, Inci, 1087
Packwood, R. H., 1247
Palmer, Martin R., 1301
Palmisano, Leonardo, 237
Panadero, Sagrario, 125
Papantoni, Margareta, 1471
Parini, Cornelia, 1153
Pattanaargsorn, S., 1573
Paulls, David A., 467
Paulsen, Paul J., 1505
Pawliszyn, Janusz, 1567
Pearce, Nicholas J. G., 1365
Pérez-Bendito, Dolores, 125
Pérez-Conde, M. C., 431
Pérez-Granados, Ana Mª, 899
Pérez Pavón, José Luis, 53
Pérez-Ruiz, Tomás, 471, 1103
Pellow-Jarman, Martin V., 985
Pereiro-García, Rosario, 457
Perkins, William T., 1365
Perruccio, Piero Luigi, 319, 1005
Persson-Moschos, M., 833
Pets, Liidia I., 1453
Petsom, A., 1573
Piasek, Martina, 951
Pinel, R., 79
Pires Valente, Antonio L., 419
Polansky, Marilyn M., 867
Pons, Begoña, 751
Poole, Colin F., 289
Poole, Salwa K., 289
Porteous, Nikki C., 1397
Potts, Philip J., 1273, 1391
Powell, Jonathan J., 783, 789, 793
Prada, D., 249
Pramauro, Edmondo, 237
Prevot, Alessandra Bianco, 237
Price, Gareth J., 161
Pringle, T. Glenn, 651
Puacz, Wojciech, 939
Puri, Bal Krishan, 1589
Purohit, Rajesh, 555
Quevauviller, Ph., 597
Rajput-Williams, Jayshri, 887
Ramsey, Michael H., 261, 1353, 1407, 1415, 1421
Rathore, Devendra P. S., 403
Reddy, M. R. P., 1401
Reeder, Shaun, 1341
Regoeczi, Erwin, 733
Reid, Helen J., 1543
Reig, F. Bosch, 299
Remond, G., 1247
Renault, Jacques, 1261
Ribone, María Elida, 443
Richardson, Jean M., 1513, 1519
Robards, Kevin, 1
Rodríguez, Adela Rosa, 529
Roengsumran, S., 1573
Rózańska, Barbara, 407
Rohand, Jamal, 1609
Rongsheng, Zhou, 1453
Rostad, H. P. W., 659
Rucklidge, John, 1283
Ruiz-Benitez, M., 1171
Russ, K., 1465
Rusu, Ana-Maria, 725
Ryabukhin, Valentin A., 1427
Saad, Bahruddin B., 561
Sánchez-Pedreño, Concepción, 129
Safronova, Natalia S., 1427
Sahoo, Sarata K., 335
Samanta, Gautam, 643, 917
Sams, Mark S., 1407
San Andres, M. P., 255
San José, C., 431
Sanchez Perez, A., 139
Sandström, Brittmarie, 911, 913
Sangvanich, P., 1573
Santa, Tomofumi, 381
Sanz-Medel, Alfredo, 799, 809
Sapozhnikov, Dmitry Yu., 1461
Saraswati, Rajananda, 95
Sarradin, P. M., 79
Sasamoto, Kazumi, 113
Sato, Jun, 89
Saunders, Bruce W., 1013
Saurina, J., 305
Savini, Luisa, 319
Saxena, Reena, 403
Saxton, John M., 1321
Schiffrin, David J., 175
Schulman, S. G., 463
Schütz, Andrejs, 1205
Semma, Masanori, 135
Sharp, Michael, 69
Shen, Hanxi, 1599
Shi, Yujun, 573
Shiga, Masanobu, 113
Shih, Jeng-Shong, 517
Shinde, V. M., 391
Shoukry, Adel F., 1211
Shpigun, Lilija K., 201
Siddiqui, Abdul Bari M., 1577
Sidrach, Ciriaco, 1103
Sievert, Ramón Cózar, 485
Simons, Jo, 1009
Sin, Yoke Min, 273, 281, 1115
Singh, Ajai K., 403
Singh, Balwant, 1335
Singh, Pramod K., 855, 951

Sitholé, B. Bruce, 1163
Skarping, Gunnar, 41
Smeller, Johanna M., 207
Smith, Joseph V., 1231
Smith, W. E., 993
Southwell-Keely, P., 1559
Soutorová, Milena, 959
Sparén, Anders, 713
Spies, Hartmut, 775
Srikumar, T. S., 833
Srivastava, Suresh K., 495
Stahl, Ralph, 979
Steger, W. E., 1465
Steien, Sissel, 779
Steinnes, Eiliv, 1437, 1479
Stoddart, Barry, 117
Stratis, John A., 1593
Suliman, Fakhr Eldin O., 561
Sultan, Salah M., 561
Sümer, Nilgün, 1087
Summers, Leslie J., 523
Sun, Ailing, 565, 569
Sundberg, Johanna, 765
Susanto, Joko P., 187
Suslova, Tatjana B., 859
Syamsundar, S., 1099
Szahun, Wieslaw, 939
Tachibana, Masaki, 437
Taher, Mohammad Ali, 1589
Takada, Maki, 1083
Tang, K. F., 1221
Tang, Yuanping, 1599
Taniguchi, Isao, 113
Tarp, Ulrik, 877
Themelis, Demetrius G., 1593
Thiel, David V., 1013
Thomas, Allen G., 1357
Thompson, Michael, 261, 271, 1353
Thompson, Richard P. H., 783, 789, 793
Thornton, Iain, 1415
Thunus, Léopold, 967
Tobal, Lorenzo, 129
Tomás, C., 1181
Tomás, Virginia, 471, 1103
Tomíška, František, 959
Tomlinson, Medha J., 583
Tosunoğlu, Sedat, 373
Toussaint, G., 1133
Townshend, Alan, 117, 467
Toyo'oka, Toshimasa, 385
Trafford, Janice M., 1433
Tranter, R. L., 355
Tsai, Perng-Jy, 675
Tsang, Stephen, 1059
Tseung, A. C. C., 1025
Tsuruta, Yasuto, 1141
Tsyb, Anatoli F., 817
Turner, Grenville, 1321
Turrion Nieves, M. B., 139
Tyson, Julian F., 1175
Uchida, Chikako, 63
Uden, Peter C., 419
Ueno, Keiyu, 113
Umamaheshwari, A., 1099
Vaganov, Peter A., 1453
Val, Otilia, 471
Valcárcel, M., 179
Valiraki, Aspasia P., 533
Valle Fuentes, F. J., 85
Van Calsteren, M. R., 395
van den Berg, Constant M. G., 143
Van den Borre, A., 463
van der Linden, Willem E., 1009
Van der Weken, G., 463
Van Grieken, René, 681
Van Peteghem, Carlos, 577
Van Rees, K. C. J., 659
Vannucci, Riccardo, 1309
Vanoosthuyze, Kristina E., 577
Vaquero, Mª Pilar, 899
Varo, Pertti, 841
Vatca, George, 725
Vaz, Jesus E., 1215
Vela, Lukias D., 651
Velasco-García, Nieves, 457
Velosa, Manuela, 1215
Vengosh, A., 1291
Vera, S., 255
Vetter, Thomas W., 95
Vianna-Soares, Cristina D., 193
Vilchez, José Luis, 1609
Villalobos, Enrique, 761
Vincent, James H., 675
Vinha, Carlos A., 351
Voigtman, Edward, 325
Volker, F., 35
Vtyurin, Boris M., 817
Vyza, Ekaterini A., 533
Wada, Hiroko, 167
Walczyk, T., 1291
Walker, Simon W., 827
Wallen, Peter J., 985
Walsh, J. Nick, 1397, 1433
Wang, Duo-xi, 1603
Wang, Hong-yan, 1603
Wang, Jin, 623
Wang, Qiong-e, 121
Wang, Shuhao, 1195
Wang, Wan-Chun, 837, 955
Wang, Ying-hua, 1603
Ward, Neil I., 341
Ward, Roberta J., 693
Warner, J. Stuart, 675
Watkins, Peter J., 1407
Watling, R. John, 1357
Watt, Frank, 783, 789, 793
Watters, Jr., Robert L., 95
Webb, Peter C., 1273
Weiss-Nowak, Christian, 823
Wesley, Ian J., 985
West, H. Margaret, 1267
West, Judy A., 887
Westphal, Christian, 823
White, P. C., 993
Wickstrøm, Elsa, 853
Wilken, Rolf-Dieter, 667
Wilkinson, Jamie J., 1421
Williams, Carl A., 341
Williams, Norman R., 887
Williams-Thorpe, Olwen, 1273
Wills, Robert, 1267
Wilson, Heather M. M., 985
Wilson, Robert, 175
Winquist, Fredrik, 155
Witt-Eickschen, G., 1315
Wong, Ming Keong, 273, 281, 1115
Wong, Siu-Kay, 1125
Woodhead, Jon D., 35
Wróbel, Katarzyna, 809
Wróbel, Kazimierz, 809
Wu, Jiaqi, 1567
Wu, Weh S., 1159
Xiao, Xinliang, 1599
Xie, Bin, 155
Xin, Zhang, 1199
Xu, Hong-Da, 1147
Xuejing, Xie, 1497
Yadav, R. B., 1099
Yamaguchi, Masatoshi, 1083
Yamamoto, Atsushi, 377, 1137
Yaman, Mehmet, 101
Yang, Yu, 243
Yılmaz, Selma, 1087
Yu, Ru-Qin, 499
Yuan, Ruo, 1055
Yuchi, Akio, 167
Zachariadis, George A., 1593
Zachwieja, Zofia, 943
Zagrodzki, Paweł, 943
Zaichick, Vladimir Ye., 817
Zaki, M. T. M., 549
Zamrazil, Václav, 959
Zanetti, Alberto, 1309
Zanoni, Maria Valnice B., 505
Zen, Jyh-Myng, 511
Zhang, Aimei, 1195
Zhang, Fan, 121
Zhang, Feng-jun, 1603
Zhang, Shufen, 1599
Zhang, X. R., 463
Zhang, Zhujun, 453
Zheng, Guo-Dong, 499
Zhuang, Hui-sheng, 121
Zolotov, Yury A., 201
Zufiaurre, Raquel, 751

5th SYMPOSIUM ON KINETICS IN ANALYTICAL CHEMISTRY

(KAC '95)
September 25-28, 1995
Moscow, Russia

You are cordially invited to participate in the 5th Symposium on Kinetics in Analytical Chemistry (KAC). This symposium is intended to continue the series of KAC meetings which were initiated in Cordoba, Spain in 1983 and continued in Preveza, Greece (1986), Cavtat, Yugoslavia (1989) and Erlangen, Germany (1992).

The meeting will be particularly important to all scientists involved with kinetic techniques in analytical chemistry and/or interested in different kinetic aspects in analytical chemistry.

The scientific programme will feature the latest developments in various areas including:

Kinetic determination of materials with catalytic or inhibitory effects

Differential rate methods

Enzymic methods

Electrochemical methods (electrocatalysis and chemically-modified electrodes)

Flow methods

Chemical and biochemical sensors

Luminescence

Kinetics in pharmaceutical analysis

Instrumental and environmental applications

Error-compensated kinetic methods

Chromatographic methods

The programme will include keynote lectures, oral sessions, poster sessions and workshop seminars to present the latest developments in commercial instrumentation.

Scientific Committee

Professor M.I. Karayannis (Greece)

Professor U. Nickel (Germany)

Professor M.D. Perez-Bendito (Spain)

Professor K.B. Yatzimirsky (Ukraine)

Professor H.A. Mottola (USA)

Professor H.L. Pardue (USA)

Professor G. Werner (Germany)

Professor Yu. A. Zolotov (Russia)

Local Organizers:

Dr I.F. Dolmanova (Moscow)
Dr T.N. Shekhovtsova (Moscow)
Tel : (7-095) 939 33 46
Fax : (7-095) 939 25 79

Analytical Chemistry Division, Chemical Department, Lomonosov Moscow State University, 119899 Moscow, Russia

To participate in the scientific sessions, please submit an abstract of 300 words or less ready for direct reproduction (DIN A4, including title, authors and address) to the address given above for Dr Shekhovtsova.

The Analyst ***will be the official journal for papers resulting from this meeting.***

Book Reviews

ICUMSA. International Commission for Uniform Methods of Sugar Analysis. Methods Book
Pp. 250. ICUMSA. 1994. Price £100.00 (surface mail); £112.00 (airmail). ISBN 0-905003-13-6.

This book includes all the Commissions' recognized methods of analysis and is presented in a loose leaf format for ease of updating.

The analytical methods are divided into sections based on the following product lines; raw sugar, refined products, molasses, sugar cane, sugar beet, cane sugar processing, beet sugar processing and starch derived sweeteners. Whilst all the methods are numbered, finding a particular method is somewhat tedious and could have been improved by the inclusion of dividers to mark the beginning of each section.

The book includes approximately 70 methods of analysis of which 5 are microbiological assays. The methods are defined as 'official', 'accepted' or 'tentative' and encompass a wide range of analytical techniques including gas chromatography and atomic absorption spectrometry as well as the more traditional techniques such as polarimetry and volumetric analysis.

'the book provides a wealth of information on the analysis of sugar products'

The methods are well laid out in a standard format which will satisfy most quality system requirements. For this reason alone, the book is invaluable to those laboratories which are accredited or seeking accreditation in this field.

Some very old techniques are included, such as lead by dithizone and arsenic using silver diethyldithiocarbamate. Whilst complementary modern techniques, such as atomic absorption are included, the modern techniques are not all accompanied by repeatability and reproducibility data. The absence of analytical quality assurance data for a significant number of the methods is one of the disappointing aspects of this book.

Over-all the book provides a wealth of information on the analysis of sugar products and is recommended to anyone involved in this field of work.

Alan Kay
Public Protection Department
County Offices, Derbyshire, UK

Lipid Chromatographic Analysis
Edited by Takayuki Shibamoto. *Chromatographic Science Series. Volume 65.* Pp. viii + 412. Marcel Dekker. 1994. Price £135.00. ISBN 0-8247-8941-5.

Of all the techniques that contribute to analytical science, chromatography in its various forms is amongst the forefront. It would be no exaggeration to state that the advances made in lipid chemistry and in the understanding of the role lipids play in animal and, particularly, human nutrition have been wholly dependent on the ability to separate and quantify lipid components by chromatographic techniques. These techniques and their applications have been well documented but such is their plethora that lipid researchers, who may not be particularly interested in analytical chemistry *per se*, may have some difficulty in selecting the technique which may be of greatest benefit to them. This publication seeks to address that issue.

'highly recommended and it should be an addition to all libraries of laboratories in which there is an interest in the chemical and biochemical aspects of lipids'.

This book covers most of the traditional methods of lipid analyses but also incorporates relatively new approaches such as solid phase extraction and supercritical fluid chromatography. Not surprisingly, gas liquid chromatography and high-performance liquid chromatography, two of the major techniques used in lipid analyses, are features in nine of the twelve chapters of the book and their use in a range of applications is described. Many of the chapters start with an introduction to the technique and there is duplication that can be a source of annoyance, but to those who are interested in the application of the technique these introductions may be wholly acceptable. It is gratifying to note that a technique such as thin-layer chromatography, which tends to be viewed as routine and non-glamorous is accorded prominence in a chapter describing the use of flame ionization for the detection of components separated by thin-layer chromatography.

Contributions to the book are made by authors, many of whom are well known in the field of lipid analyses, and their presentations are made in a clear, precise manner which enable the reader to follow methods with ease. Each chapter is well documented with comprehensive references and the experimental details are easily followed. In addition, the book is remarkably devoid of typographical errors.

This excellent, practical book with its detailed methodology will be a constant source of reference to those actively engaged in lipid research in relation to the effect and influence of lipids on biological processes. It is highly recommended and it should be an addition to all libraries of laboratories in which there is an interest in the chemical and biochemical aspects of lipids.

A. Smith
The Macaulay Land Use Research Institute
Aberdeen, UK

Flow-through (Bio)Chemical Sensors
M. Valcárcel and M. D. Luque de Castro. *Techniques and Instrumentation in Analytical Chemistry. Volume 16.* Pp. 332. Elsevier. 1994. US $202.75. ISBN 0-444-89866-2.

Chemical sensors and biosensors are now being championed by scientists from increasingly diverse backgrounds. The positive aspect of this is that fresh ideas and new concepts are introduced into this fast moving field; the occasional negative aspect is that additional conceptual stances sometimes confuse basic priorities. There is something of both in this two author appraisal of so-called flow-through sensors. Without doubt, use of a sensor without careful consideration of sampling and flow system requirements can lead to failure. These authors have rightly focused on a key issue of integrated sensor/measurement cell performance, and of its particular relevance to practical analysis. They set out, in 5 chapters, a logical build from sensors types through to the added contribution of separation and reaction schemes used in continuous flow. Their effort is laudable, their success is variable.

The first chapter on basic sensors is a rather detailed attempt at formal definitions of sensors, various measurement hierarchies, transduction interfaces with many attempted (re-) classifications, even down to terms such as 'probe' *versus*

'sensor'. One wonders about the need for all this at this stage; such conceptual reworking of established ground will fail to gain agreement of those established in the field and confuses priorities in a book that purports to be dealing with the specific science of flow-through sensors.

'As such, this is a useful repository of information on FI that could serve as a general literature source, though somewhat marred by the limited offering on background aspects and a liberal definition of sensors'.

The second chapter on 'fundamentals' of continuous flow, fares rather better in that it describes in well-illustrated detail, flow geometries, flow cells and the fabrication needs for particular measurement problems, *e.g.*, reagent loss, lack of sensor reversibility. It would have been helpful if the basic principles of segmental flow, FI, continuous flow dynamics and flow/surface interfaces, *etc.*, could also have been introduced.

The next chapter, dealing with integrated reaction and detection, includes a spectrum of entities from flow-through cells integrated with spectrophotometers, to descriptions of chemical sensors and biosensors not yet used under flow conditions. However, a sufficient number of true sensor/flow combinations is also provided and gives an idea of general progress, covering a comprehensive range of chemical sensors up to whole cell-based analyte binding and recognition. A subsequent chapter on integrated separation and detection also takes a very liberal interpretation of the term 'sensing', with FI–spectrophotometric combinations being a major part of the descriptions on offer. Rather more relevant is a 'mini-review' of separation membranes in electrochemical sensors, and the description of ISEs employed under continuous flow conditions. The final chapter covers flow analysis, where both analyte separation and reaction are involved. Examples are given of a variety of detector systems, including enzymic, made more selective by means of membranes or some partitioning process.

This book gives practical reminders of flow systems, but for fundamentals the reader will need to look elsewhere. The individual descriptions of literature reports, it has to be said, are thorough and replete with data, and there are ample illustrations of both flow constructs and reaction chemistries. As such, this is a useful repository of information on FI that could serve as a general literature source, though somewhat marred by the limited offering on background aspects and a liberal definition of sensors.

Pankaj Vadgama
Department of Medicine
University of Manchester, UK

Analytical Electrochemistry
By Joseph Wang. Pp xi + 198. VCH. 1994. Price DM98.00; £39.50. ISBN 0-1-56081-575-2.

As the title suggests, the main emphasis of this book is on electroanalysis, rather than on physical aspects of electrochemistry. It is designed to be a suitable text for graduate-level courses in electroanalytical chemistry, or as a supplement to Masters courses in Instrumental Analysis. It pays particular importance in presenting recent advances in the areas of new methodologies, sensors and detectors, in a clear and concise manner.

The book is divided into six chapters. The first deals with some fundamental concepts such as mass transport and the electrical double layer. This is by no means extensive, but adequate reference is made to more specialized texts which would need to be consulted for a more in-depth treatment of the fundamentals of the subject. The second chapter then deals with controlled potential techniques, such as chronoamperometry, polarography, pulse voltammetry, AC voltammetry, stripping analysis and electrochemical detection in flowing-solution analysis. The main equations and waveforms for these techniques are given in the chapter, along with some representative applications of how these techniques are applied. In chapter three, the emphasis is on practical applications such as design of electrochemical cells, choice of electrode materials, and instrumentation. In particular, emphasis is placed on discussing the newer forms of electrode materials which are of importance in modern day applications, namely microelectrodes and modified electrodes.

The next two chapters deal with potentiometric- and amperometric-sensors. Because of the nature of the book, neither of these important subjects is dealt with exhaustively, and the reader can really only get a basic understanding of the principles involved. Again, these subjects would need to be reinforced by consultation with more specialized texts. The final chapter then shows how a combination of voltammetric, spectroscopic and microscopic techniques can be used to study electrode reactions.

'for students who know very little about the subject, the text would be a very useful introduction to this exciting field of study'.

Most chapters contain some relatively basic worked examples, which nevertheless illustrate some of the quantitative aspects of the subject. All in all, I found the text to be very readable, and for students who know very little about the subject, the text would be a very useful introduction to this exciting field of study. The text is relatively inexpensive for student purchase, and provides good value for money. My only concern is that it has, by its very nature, a limited depth of coverage, which for some courses would necessitate additional reading material from other standard texts. It certainly should be on all library shelves of institutions where electroanalytical chemistry or instrumental analysis is preached and practised.

Malcolm R. Smyth
Dublin City University
Dublin 9, Ireland

Electroanalytical Chemistry. Volume 18. A Series of Advances
Edited by Allen J. Bard. Pp. xii + 400. Marcel Dekker. New York. 1993. Price US$165.00. ISBN 0-8247-9092-8.

While this volume, like the others in the series, will be of great interest to those working in the area of electroanalytical chemistry, I must take issue with the cover note which claims the text to be suitable for the non-specialist. This, in my opinion, is most definitely not the case. However, this comment aside, there can be no doubt that this is an extremely thorough and well-researched text, providing as is intended a snapshot of the current state-of-the-art in certain areas of electroanalytical chemistry.

The three topics covered in this volume are Electrochemistry in Micelles, Microemulsions and Related Microheterogeneous Fluids (James F. Rusling, with 182 references), Mechanisms of Charge Transport in Polymer-modified Electrodes (Gyorgy Inzelt, with 294 references) and Scanning Electrochemical Microscopy (Allen J. Bard, Fu-Ren F. Fan and Michael V. Mirkin, with 95 references). This last topic is relatively young in comparison with the others, arising as it does from the advent of scanning probe microscopies such as

the scanning tunneling microscope and the atomic force microscope. The 'newness' of this field is illustrated by the dramatically lower number of references provided for this section in relation to the other two sections. I confess that this topic, in which the probe tip may be used either as a probe of localized electrochemistry or indeed to induce local electrochemistry at an appropriate substrate, is the one that I personally find the most innovative. This section includes discussion of a number of applications of the SECM, including the localized deposition of fine metal lines using a moving tip and the etching of GaAs surfaces *via* a hole-stimulating reaction in the region of the substrate closest to the tip. Apart from these examples, there is also some extremely useful practical details on such matters as how to produce a suitable probe tip. I feel sure that this area of electroanalytical chemistry will receive a great deal more attention in the near future.

'this is an extremely thorough and well-researched text, providing as is intended a snapshot of the current state-of-the-art in certain areas of electroanalytical chemistry'.

The section on micelles and related systems begins with a very thorough introduction to these systems, which is extremely easy to follow. There has, of course, been a resurgence of interest in these systems resulting from their ability to act as templates for the production of micro- and mesoporous-systems. However, in this text, emphasis is placed upon the electrochemistry that may occur when such systems are assembled at an appropriate conducting interface. The examples detailed are far too many to describe, but I note that of particular interest to me was the section on *in-situ* spectroscopy of such systems. This section describes the many ways in which the molecular structure of these systems has been probed using non-invasive techniques. This section attracted my attention because it revealed how the technique of surface enhanced Raman scattering may be used to determine potential-dependent changes in orientation of these surfactant systems at a silver electrode surface.

Polymer-modified electrodes are of course a 'very hot topic' at the moment from the point of view of their myriad potential applications and more importantly, the ability to tailor the properties of the system using chemistry. Despite this, it was of great interest to me to discover just how far back the theory of these systems extends, although Gyorgy Inzelt makes the comment that no real comprehensive theory describing the conduction mechanisms in the polymer systems exists at the present time. I was familiar with some of the more popular polymer systems that have been studied, including the substituted polyanilines which, when deposited on a conducting surface, exhibit complex chromophore behaviour often involving several visible colour changes. However, these are only a fraction of the systems described in this very comprehensive section.

Overall, at $165.00, this volume in my opinion represents good value for money and is a must for those enthusiasts of the topics described.

Martyn E. Pemble
The Solid State Chemistry Group,
University of Manchester, UK

Time of Flight Mass Spectrometry and its Applications
Edited by E. W. Schlag. Pp. x + 413. Elsevier. 1994. Price US $122.75. ISBN 0-444-8188 75-8.

The recent dynamic resurgence in time-of-flight mass spectrometry has thrust this previously overlooked technique at the cutting edge of mass spectrometry development. This has come about because of the inherent ability of the time-of-flight instrument to provide a complete mass spectral analysis per event, *e.g.*, pulsed laser ionization coupled with an unlimited mass range and high ion transmission characteristics. The time-of-flight system is by far the fastest scanning of the mass spectrometric techniques, being able to provide complete spectra in tens of microseconds. It is, therefore, able to provide real-time analysis of very rapid transient events such as laser ablation or rapid compositional changes occurring, *e.g.*, during the scanning of gas or liquid chromatography effluents and capillary zone electrophoresis systems. The major problem with these latter applications is the requirement for data handling systems able to cope with the mass of information produced.

This rapid expansion of the time-of-flight technique has resulted in an avalanche of publications and it is appropriate that suitable review articles/papers appear to provide a starting point for researchers entering the field. This book contains such a compilation which has also been published as Volume 131 of the International Journal of Mass Spectrometry and Ion Processes. There are some 21 articles, appropriately commencing with an account by Mamyrin describing his development of the reflection technique and how it has subsequently been used to investigate a range of problems. The reflectron can enhance the resolving power of the time-of-flight mass spectrometer some 10-fold, overcoming its early handicap of being a low resolution instrument.

'The breadth and quality of the work described makes this compendium an excellent entry point or reference for time-of-flight mass spectrometry'.

Further contributions provide detailed consideration of ion optics and ion-source design whilst elsewhere ion, particularly heavy ion, detection is of importance. A major advantage of the time-of-flight mass spectrometer is its relatively simple concept and construction which makes it adaptable to solve particular applications. Many of these are amenable to inexpensive 'in house' instruments in contrast to large expensive conventional mass spectrometers. This aspect is well illustrated within this book. Several of the articles present novel applications which open up new directions for the future development of mass spectrometry. Examples are extreme state selection *via* ZEKE techniques and the now well publicized extremely high-mass ion work pioneered for biomolecules by Hillenkamp and also used herein for DNA analysis.

The breadth and quality of the work described makes this compendium an excellent entry point or reference for time-of-flight mass spectrometry. It should be available, either in Journal or Book form, to any laboratory concerned with time-of-flight mass spectrometry or considering entering this field. Together with Cotter's book in the ACS Symposium series, it provides an excellent account of the current state of time-of-flight mass spectrometry.

Dennis Price
Department of Chemistry and Applied Chemistry
University of Salford, UK

Sample Preparation for Biomedical and Environmental Analysis
Edited by D. Stevenson and I. D. Wilson. *Chromatographic Society Symposium*. Pp. x + 246. Plenum. 1994. Price US$75.00. ISBN 0-306-44663.

Sampling and sample preparation are the hidden problems of analytical chemistry; the 'skeletons' we keep hidden in our

cupboards! In this respect, this volume might appear to be well overdue. It is not however, immediately obvious from the title, (though it is from that of the Series) that this work consists of the proceedings of a Symposium of the same name held in July 1991. As with many volumes of symposium papers it is, like the 'parson's egg', good in parts.

The book contains some 24 contributions, of which 16 seem to be full papers (although rather uneven both in length and quality) and 8 are described on the page, if not in the contents list, as 'notes'. A wide range of topics more or less related to the symposium title is covered. No attempt seems to have been made to organize the papers in any logical way.

'the lions share of the work is concerned with solid-phase extraction techniques'.

The book contains some excellent papers. In particular, the papers by Watson on 'Clinical Analysis' and by Snowdon on 'Pesticide Residues' are wider in scope than most and attempt to cover their topics reasonably comprehensively. Watson's paper, in particular, ought to be compulsory reading for all chromatographers. However, the lions share of the work (8 contributions) is concerned with solid-phase extraction techniques. Further papers deal with superfluid extraction, column switching, capillary electrophoresis, automation, a proprietary membrane technique, pre-column derivatization and post-column derivatization, the latter suggesting that sample preparation is not necessary, which leaves one wondering why it was included.

To be of real use, a book such as this needs to be fully indexed. A few random checks suggest that this has not been carried out. Thus, 'derivatization, post-column' and 'derivatization, pre-column are each only mentioned once, in both cases to the same paper by Cooper *et al.* Yet the first mention of pre-column derivatization is to be found on page 1 and a complete paper (Lingeman and Brinkman) is devoted to 'post-column reaction-detection', an expression which does not occur in the index at all.

There is not doubt that there is much in this volume to interest the practising chromatographer. It is a pity that in an age which talks so glibly of 'information highways', it has taken so long to reach publication. I suspect that much of the work described in this volume may already have been published elsewhere.

M. A. Russell
Dorset, UK

Circular Dichroism: Principles and Applications
By K. Nakanishi, N. Berova and R. W. Woody. Pp xvii + 570. VCH. 1994. Price £83.00. ISBN 1-56081-618-X.

About thirty years ago, *The Analyst* published a review concerned with the analytical applications of circular dichroism. Little analytical work involving the use of circular dichroism had appeared at that time, and the last sentence of that review said, 'However, circular dichroism has many potential applications, particularly in the field of natural products, for which the technique may prove useful for handling mixtures now amenable only to complicated treatments.'

With the increasing emphasis on all aspects of chirality, and of the use of natural products in synthesis of pharmaceuticals and the like, the analytical applications of any method involving optical activity should be increasing sharply. A survey of those applications would be very useful. In that respect, and only in that respect, this well-edited book is something of a disappointment. It indeed contains a very full treatment of the principles and many applications of circular dichroism, but the applications described are chiefly stereochemical and spectroscopic, emphasizing the theoretical, rather than the practical, applications of the method.

Having said that, within its objectives, this is a very good book indeed. It contains chapters by experts on all aspects of circular dichroism, ranging from the emission of chiral excited states to the circular dichroism of nucleic acids. All the chapters seem to be of a high standard, with some that are outstandingly good. I noticed particularly the treatment by H. E. Smith of the benzene chromophore in its optically active derivatives, and that by Dekkers on circularly polarized luminescence, which contains a useful discussion of experimental methods. In all chapters, the quality of the figures is excellent.

'circular dichroism is full of potential for the solution of analytical problems'.

The title of only one of the 20 chapters contains the word 'analytical'. That is the last chapter of the book, on circular dichroism coupled with HPLC, where Salvadori, Bertucci, and Rosini give a good description of this extremely useful method. There is a substantial section on the measurement of circular dichroism on-line, which shows the utility of the technique. However, even this single analytical chapter reveals that the authors are perhaps not primarily interested in analyses. No reference is made to the early use of a circular dichroism spectrometer as a detection system in HPLC by Westwood, Games and Sheen. That included the use of a device for on-line measurement, and was published in an analytical journal.

This particular book is unlikely to be of direct interest to analysts, although it is clear from almost every page in it that circular dichroism is full of potential for the solution of analytical problems, particularly those related to natural products. The methodology of those solutions is not really tackled in this book. There have been a number of applications, fully worked out, particularly in pharmacology and similar areas, which have not even been touched on, *e.g.*, relating to measurement of nicotine in extracts.

The book is dedicated to the memory of the late Professor Snatzke, a pioneer in modern applications of circular dichroism, who contributed the first chapter, a characteristic wide-ranging and clear statement. The volume reflects his interests very well, which were in stereochemistry and chiroptical properties of natural and synthetic materials. It is a fine book, but it is not a handbook of analytical methods and applications of circular dichroism.

R. D. Gillard
Department of Chemistry
University of Wales, Cardiff, UK

Trace Element Analysis in Biological Specimens
Edited by R. F. M. Herber and M. Stoeppler. *Techniques and Instrumentation in Analytical Chemistry. Volume 15.* Pp. xiii + 576. Elsevier. 1994. Price US$ 271.50. ISBN 0-444-89867-0.

If you are engaged in the trace element analysis of human biological specimens, such as blood, urine, teeth, bone, hair, nails and soft tissues, then this is the reference text for you! It has been well-conceived and structured by the editors; written with authority by the contributors; and neatly produced by the

publishers. As its pages contain much of value for all, from the experienced professional to the comparative novice, there should be a copy on the shelves of every laboratory engaged in such work, especially in the fields of clinical chemistry and forensic toxicology.

'If you are engaged in the trace element analysis of human biological specimens, such as blood, urine, teeth, bone, hair, nails and soft tissues, then this is the reference text for you!'

The book has been divided into two parts of almost equal length; Basic Principles and Methods (Part 1, containing 12 chapters on various protocols and individual analytical techniques), and Elements (Part 2, containing 13 chapters, each on a specific element). By so doing, the editors have greatly improved on the approach adopted in an earlier book in this series, 'Evaluation of Analytical Methods in Biological Systems, Part B, Hazardous Metals in Human Toxicology. Volume 4, edited by A. Vercruysse'.

The chapters in Part 1 are entitled: Sampling and sample storage (Aitio); Sample treatment of human biological materials (Sansoni and Panday); Graphite furnace AAS and Atomic absorption spectrometry; Flame AAS (both by Slavin); Atomic emission spectrometry (Schramel); Voltammetry (Wang); Neutron activation analysis (Versieck); Isotope dilution mass spectrometry (de Bievre); The chemical speciation of trace elements in biomedical specimens: Analytical techniques (Gardiner and Delves); Interlaboratory and intralaboratory surveys. Reference methods and reference materials (Braithwaite); Reference materials for trace element analysis (Parr and Stoeppler); and Statistics and data evaluation (Herber and Salle). The message of the importance of appropriate sample collection, treatment and storage procedures, the correct choice and application of sophisticated analytical instrumentation, and the need to ensure the delivery of high quality data if results are to be at all meaningful, is driven home powerfully. The chapter on flame AAS is very short, perhaps understandably, but less forgivable is the omission of one on inductively coupled plasma mass spectrometry, although applications of this technique are occasionally mentioned elsewhere in the book. Chapter 8 on isotope dilution mass spectrometry is given the wrongly-numbered header 'Chapter 7' throughout the text.

The 13 chapters of Part 2 focus on the obvious elements of importance: aluminium (Savory); arsenic (Stoeppler and Vahter); cadmium (Herber); chromium (Cornelis); copper (Delves and Stoeppler); lead (Ewers); manganese (Halls); mercury (Schutz); nickel (Templeton); selenium (Thomassen); thallium (Sager); vanadium (Schaller); and zinc (Fell and Lyon). If the editors could have foreseen the controversy over antimony, at least in Britain, where it has recently been suggested, in a very public fashion, that the element is implicated in cot deaths, they might have increased the number under consideration by one. Overall, however, the balance of coverage both between and within chapters is very good, save perhaps for the chapter on mercury, which, at 65 pages, is more than twice the length of any other. Each chapter is a gold mine of selected information and considered recommendations concerning the determination of the element in question in a variety of human biological matrices. In general, authors draw on references up until the early 1990s. Rather irritatingly, neither Cornelis nor Halls give the titles of papers listed in the reference sections for their chapters, a fault of which Slavin and Schramel are also guilty in Part 1.

The appeal of this excellent book will be largely to clinical chemists, toxicologists and biochemists, and, despite the editors' stated claims, somewhat less to the environmental analytical chemist, especially at the quoted price. North Americans may be a little disappointed that only nine of the 38 authors involved are presently employed on their sub-continent, the other 29 emanating from Europe, but, like the rest of the world, can be assured that the purchase of this book will be an excellent investment, which will pay for itself many times over.

J. G. Farmer
Department of Chemistry
University of Edinburgh, UK

Biofluid and Tissue Analysis for Drugs Including Hypolipidaemics

Edited by Eric Reid, Howard M. Hill and Ian D. Watson. *Methodological Surveys in Bioanalysis of Drugs, Volume 23.* Series editor Eric Reid. Pp. xviii + 420. Price £98.00. Royal Society of Chemistry. 1994. ISBN 0-85186-644-1.

This is the type of book you will either love or hate because of the way in which it has been produced. It is a collection of papers presented at the Tenth International Forum on Biofluid and Tissue Analysis for Drugs held at Guildford, England in 1993, and is the 23rd volume in this series.

As a result, it covers a large number of topics ranging from the education and training of analysts to the analysis of phospholipid hydroperoxides and microdialysis. There is certainly something of interest in this volume for all analysts, especially in the papers showing the advances made in the applications of capillary electrophoresis and hyphenated- and automated-systems. However, the book will probably be more comprehensible and useful to those who attended the Forum than it is to the general reader, who will probably use it with specific interest topics in mind.

'something of interest in this volume for all analysts'.

For an expensive scientific volume, it is poorly laid out and, at times, difficult to follow. Apart from unnecessary and excessive use of the # symbol, there are errors and variations in typefaces, a proliferation of confusing footnotes and repeated explanations of abbreviations, such as ASPEC, cropping up in several places. It would have benefited from heavy editing of the comments following each group of papers, and fewer citations and annotations contributed by the editors.

The compendium on drug assay would have been better placed at the end of the book rather than coming in the middle and splitting the main text. The cross-referencing of authors as primary and co-, in separate columns, appears unnecessary and divisive.

There are several very useful papers on the application of derivatization as a prelude to gas chromatography and HPLC of several drugs suitable for use with other compounds. Fluorimetric detectors come in for regular discussion, with some useful suggestions for signal enhancement being given. Also, of wider value, are the papers dealing with various pre-treatments of drugs and standards. For the general reader seeking new analytical approaches and procedures there is a great deal of value, but at times, searching it out is not always easy.

The wide coverage in the book guarantees it a place on many company shelves, but the user will need to become familiar with the approach, layout and abbreviations employed.

Ronald C. Denney
Sevenoaks, Kent, UK

Conference Diary

Date	Conference	Location	Contact
1995			
June			
5–7	**Image Techniques and Analysis in Fluid Mechanics**	Rome, Italy	**A. Cehedese,** Department of Mechanics and Aeronautics, University La Sapienza, Via Eudossiana 18, 00184 Rome, Italy
5–8	**5th Symposium on our Environment and 1st Asia–Pacific Workshop on Pesticides**	Convention City, Singapore	**The Secretariat,** 5th Symposium on our Environment, c/o Department of Chemistry, National University of Singapore, Kent Ridge, Republic of Singapore 0511 **Fax:** +65 779 1691
6–9	**8th International Symposium on Loss Prevention and Safety Promotion in the Process Industries**	Antwerp, Belgium	**The Organising Committee,** 8th International Symposium on Loss Prevention, c/o Ingenieurshuis V2W, Desguinlei 214, B-2018 Antwerpen, Belgium
7	**Joint Meeting of the Molecular Spectroscopy Group and the Infrared and Raman Discussion Group—Vibrational Spectroscopy and Imaging**	Oxford, UK	**Dr. J. M. Chalmers,** ICI plc, Wilton Research Centre, P.O. Box 90, Wilton, Middlesbrough, UK TS90 8JE
7–9	**LIMS 95—International Conference and Exhibition**	Bonn, Germany	**JAY Conference Services,** 45 Hilltop Avenue, Hullbridge, Hockley, Essex, UK SS5 6BL
11–14	**PREP '95: 1995 International Symposium, Exhibit and Workshops on Preparative Chromatography, Ion Exchange, and Adsorption/Desorption Processes and Related Techniques**	Washington DC, USA	**Mrs. Janet Cunningham,** PREP '95 Symposium/ Exhibits Manager, Barr Enterprises, 10120 Kelly Road, P.O. Box 279, Walkersville, MD 21793, USA **Tel:** +1 301 898 3772. **Fax:** +1 301 898 5596
12–16	**50th Annual Molecular Spectroscopy Symposium**	Columbus, USA	**T. A. Miller,** International Symposium on Molecular Spectroscopy, Department of Chemistry, Ohio State University, 120 West 18th Avenue, Columbus, Ohio 43210, USA
13–16	**ESIS 95—New Infrared Spectroscopy and Microspectroscopy: FTIR and Raman**	Lyon, France	**G. Lachenal,** Laboratoire des Materiaux Plastiques et Biomateriaux, Université Claude Bernard Lyon 1, 43 Boulevard du 11 Novembre, 69622 Villeurbanne Cedex, France
July			
2–6	**VII International Congress of Toxicology**	Seattle, USA	**Jada Hill,** The Sterling Group, 9393 W, 110th Street, Suite, Overland Park, KS 66210, USA **Tel:** +1 913 345 2228. **Fax:** +1 913 345 0893
2–7	**12th International NMR Meeting**	Manchester, UK	**Dr. J. E. Gibson,** Royal Society of Chemistry, Burlington House, Piccadilly, London, UK W1V 0BN **Tel:** +44 (6)171 437 8656. **Fax:** +44 (0)171 734 1227
9–13	**3rd International Symposium on Applied Mass Spectrometry in Health Sciences and 3rd European Tandem Mass Spectrometry Conference**	Barcelona, Spain	**Professor Emilio Gelpi,** Palau de Congressos, Departamento de Convencions, Avda, Reina Ma Christina, 08004 Barcelona, Spain
9–14	**13th Australian Symposium on Analytical Chemistry/4th Environmental Chemistry Conference**	Darwin, Australia	**13AC/4EC, Symposium Secretariat,** Convention Catalyst Int., GPO Box 2541, Darwin NT 0801, Australia **Tel:** +61 89 811 875. **Fax:** +61 89 411 639
9–15	**SAC 95**	Hull, UK	**Analytical Division,** The Royal Society of Chemistry, Burlington House, Piccadilly, London, UK W1V 0BN **Tel:** +44 (0)171 437 8656. **Fax:** +44 (0)171 734 1227
10–13	**Vth COMTOX Symposium on Toxicology and Clinical Chemistry of Metals**	Vancouver, Canada	**F. William Sunderman, Jr., M.D.,** Departments of Laboratory Medicine and Pharmacology, University of Connecticut Medical School, P.O. Box 1292, Farmington, CT 06034-1292, USA **Tel:** +1 203 679 2328. **Fax:** +1 203 679 2154

Date	Conference	Location	Contact
30–5/8	**XXIInd International Conference on Phenomena in Ionized Gases**	Hoboken, USA	**E. E. Kunhardt,** Physics Department, Stevens Institute of Technology, Hoboken, NJ 07030 USA **Tel:** +1 201 216 5099. **Fax:** +1 201 216 5638

August

5–10	**1995 International Symposium on Soil and Plant Analysis**	Wageningen, The Netherlands	**Soil and Plant Analysis Council,** Georgia University Station, P.O. Box 2007, Athens, GA 30612-2007, USA **Tel:** +1 706 546 0425. **Fax:** +1 706 548 4891
6–11	**NIR '95—The Future Waves**	Montreal, Canada	**NIR '95, The Canadian Grain Commission,** Grain Research Laboratory, 1403-303 Main Street, Winnipeg, Manitoba, Canada R3C 3G8
13–17	**ICFIA '95, 7th International Conference on Flow Injection Analysis and JAFIA, Japanese Association for Flow Injection Analysis**	Seattle, USA	**Gary D. Christian,** Department of Chemistry, BG-10, University of Washington, Seattle, WA 98195, USA **Tel:** +1 206 685 3478. **Fax:** +1 206 543 5340. **E-Mail**: christia@chem.washington.edu
14–16	**41st International Conference on Analytical Science and Spectroscopy**	Windsor, Canada	**William E. Jones,** Department of Chemistry and Biochemistry, University of Windsor, Windsor, Ontario, Canada N9B 3P4
20–25	**12th International Symposium on Plasma Chemistry**	Minneapolis, USA	**L. Graven,** 315 Pillsbury Drive, SE, University of Minnesota, Minneapolis, MN 55455-0139, USA **Tel:** +1 612 625 9023. **Fax:** +1 612 626 1623
27–2/9	**CSI XXIX: Colloquium Spectroscopicum Internationale**	Leipzig, Germany	**GDCh-Geschäftsstelle, Abt. Tagungen,** Varrentrappestr. 40–42, Postfach 90 04 40, D-6000 Frankfurt am Main 90, Germany **Tel:** +49 69 791 7358. **Fax:** +49 69 791 7475
27–1/9	**46th Annual Meeting of the International Society of Electrochemistry (ISE46)**	Xiamen, China	**Secretariat,** XLVIth ISE Annual Meeting, P.O. Box 1995, Xiamen University, Xiamen 361005, China **Tel:** +86 592 208 5349. **Fax:** +86 592 208 8054
27–1/9	**Third International Conference on Magnetic Resonance Microscopy**	Würzburg, Germany	**Dr. A. Haas,** Physikalisches Institute, Universität Würzburg, Am Hubland, D-97074 Würzburg, Germany
27–30	**EUROTOX**	Prague, Czech Republic	**Czech Medical Association J. E. Purkyně,** EUROTOX '95, P.O. Box 88, Sokolská 31, 120 26 Prague 2, Czech Republic **Tel:** +42 2 24 915195. **Fax:** +42 2 24 216836

September

1–4	**CSI XXIX, Post-symposium ICP-MS and 11th German ICP-MS Users Meeting**	Wernigerode, Germany	**Professor Lieselotte Moenke,** Department of Chemistry, Martin-Luther University, Halle-Wittenberg, Institute of Analytical and Environmental Chemistry, Weinbergweg 16, D-06120 Halle, Germany
3–6	**Third International Meeting on Recent Advances in Magnetic Resonance Application to Porous Media**	Louvain la Neuve, Belgium	**Professor J. M. Dereppe,** Université de Louvain, Place Louis Pasteur 1, B-1348, Louvain la Neuve, Belgium
3–8	**6th European Conference on the Spectroscopy of Biological Molecules**	Villeneuve d'Ascq, France	**Professor J. C. Merlin,** ECSBM '95, LASIR, UST Lille Bât. C5, 59655 Villeneuve d'Ascq Cedex, France
5–8	**RSC Autumn Meeting. Analytical and Faraday Symposium: Ions in Solution**	Sheffield, UK	**Dr. J. F. Gibson,** The Royal Society of Chemistry, Burlington House, Piccadilly, London, UK W1V 0BN **Tel:** +44 (0)171 437 8656. **Fax:** +44 (0)171 734 1227
6–8	**5th Symposium on Chemistry and Fate of Modern Pesticides**	Paris, France	**Mrs. Frei-Häusler,** IAEAC Office, Postfach 46, CH-4123 Allschuril 2, Switzerland **Fax:** +41 61 482 08 05

Date	Conference	Location	Contact
6–9	**Joint Meeting of the Royal Society of Chemistry Fast Reactions in Solution Discussion Group and the Molecular Spectroscopy Group on Ultrafast Processes in Laser Spectroscopy**	Norwich, UK	**Professor B. H. Robinson,** School of Chemical Sciences, University of East Anglia, Norwich, UK NR4 7TJ
10–14	**Ion-Ex '95, The Fourth International Conference and Industrial Exhibition on Ion Exchange Processes**	Wrexham, UK	**Ion-Ex '95 Conference Secretariat,** Faculty of Science, The North East Wales Institute, Connah's Quay, Deeside, Clwyd, UK CH5 4BR **Fax:** +44 (0)1244 814305
12–15	**5th International Symposium on Drug Analysis**	Leuven, Belgium	**Professor J. Hoogmartens,** Institute of Pharmaceutical Sciences, Van Evenstraat 4, B-3000 Leuven, Belgium **Tel:** +32 16 32 34 40. **Fax:** +32 16 32 34 48
12–16	**European Symposium on BiOS Europe '95: The European Biomedical Optics Symposium Week**	Barcelona, Spain	**Ms. Karin Burger,** BiOS Europe '95, EUROPTO Series, c/o Direct Communications GmbH, Xantener Strasse 22, D-10707 Berlin, Germany **Tel:** +49 30 881 50 47. **Fax:** +49 30 881 50 40 **E-Mail:** Burger,100140.3211@compuserve.com
17–20	**6th Surrey Conference on Plasma Source Spectrometry**	Jersey, UK	**Dr. Kym Jarvis,** NERC ICP-MS Facility, CARE, Imperial College, Silwood Park, Ascot, Berkshire, UK SL5 7TE **Tel:** +44 (0)1344 294517/6. **Fax:** +44 (0)1344 873997
17–21	**109th AOAC International Annual Meeting and Exposition**	Tennessee, USA	**Meetings and Education Department,** AOAC International, 2200 Wilson Boulevard, Suite 400, Arlington, Virginia, 22201-3301, USA **Tel:** +1 703 522 3032.
24–28	**11th Asilomar Conference on Mass Spectrometry—Molecular Structure Determination: Activation, Mass Analysis and Detection**	Pacific Grove, USA	**Professor R. Graham Cooks,** Department of Chemistry, 1393 Brown Building, Purdue University, West Lafayette, IN 47907, USA
25–28	**5th Symposium on 'Kinetics in Analytical Chemistry' (KAC '95)**	Moscow, Russia	**Dr. I. F. Dolmanova,** Analytical Chemistry Division, Chemical Department, Lomonosov Moscow State University, 119899 Moscow, Russia **Tel:** +7 095 939 3346. **Fax:** +7 095 939 2579
October			
1–5	**21st World Congress of the International Society for Fat Research (ISF)**	The Hague, The Netherlands	**Mrs. J. Wills,** ISF Secretariat, P.O. Box 3489, Champaign, IL 61826–3489, USA **Tel:** +1 217 359 2344. **Fax:** +1 217 351 8091
9–13	**ECASIA '95**	Montreux, Switzerland	**EPEL-ECASIA 95,** Department des Materiaux/ LMCH, CH-1015 Lausanne, Switzerland **Fax:** +41 21 693 3946
15–20	**22nd Annual Conference of the Federation of Analytical Chemistry and Spectroscopy Societies**	Cincinnati, USA	**Joseph A. Caruso,** FACSS National Office, 198 Thomas Johnson Dr., Suite S-2, Frederick, MD 21702, USA **Tel:** +1 301 694 8122. **Fax:** +1 301 694 6860
16–18	**Image Enhancement and Analysis**	Washington DC, USA	**Mr. Ben Keddy,** Cambridge Healthtech Institute, 1037, Chestnut Street, Newton Upper Falls, MA 02164, USA **Tel:** +1 617 487 7989.
19–20	**Biotechnology Now and Tomorrow**	Bucharest, Romania	**Mrs. Gestiana Munteanu,** Biotechnos S.A., Str. Dumbrava Rosie, nr. 18, Bucuresti 70254, Romania **Tel:** +40 1 210 20 15. **Fax:** +40 1 210 97 05
23–25	**2nd Annual Blood Safety and Screening**	Washington DC, USA	**Mr. Ben Keddy,** Cambridge Healthtech Institute, 1037, Chestnut Street, Newton Upper Falls, MA 02164, USA **Tel:** +1 617 487 7989.
24–27	**BCEIA '95—The International Sixth Beijing Conference and Exhibition on Instrumental Analysis**	Beijing, China	**General Service Office,** The International Sixth BCEIA, Room 585, Chinese Academy of Science Room, San Li He, Xi Jiao, P.O. Box 2143, Beijing 100045, China

Date	Conference	Location	Contact
26–27	**Sensors and Signals**	County Dublin, Ireland	**Dr. D. Diamond,** School of Chemical Sciences, Dublin City University, Glasnevin, Dublin, Ireland **Tel:** +353 1 704 5308. **Fax:** +353 1 704 5503
November			
5–10	**1st Mediterranean Basin Conference on Analytical Chemistry**	Cordoba, Spain	**Professor Alfredo Sanz-Medel,** Department of Physical and Analytical Chemistry, Faculty of Chemistry, University of Oviedo, C/Julían Clavería, no. 8 33006 Oviedo, Spain **Tel:** +34 85 10 34 74. **Fax:** +34 85 10 31 25
5–10	**OPTCON '95**	San Jose, USA	**Meetings Department,** Optical Society of America, 2010 Massachusetts Avenue, NW, Washington, DC 20036-1023, USA **Tel:** +1 202 223 9034. **Fax:** +1 202 416 6100
8–9	**Biological Applications of Inorganic Mass Spectrometry**	Norwich, UK	**Ms. Helen Phipps,** Institute of Food Research, Norwich Laboratory, Norwich Research Park, Colney, Norwich, UK NR4 7UA **Tel:** +44 (0)1603 255219. **Fax:** +44 (0)1603 255168
14–15	**International Conference for Chemical Information Users**	Manchester, UK	**Dr. M. P. Coward,** Chemistry Department, UMIST, P.O. Box 88, Manchester, UK M60 1QD **Tel:** +44 (0)161 200 4491. **Fax:** +44 (0)161 228 1250
December			
13–14	**2nd LC/MS Symposium**	Cambridge, UK	**Dr. J. Oxford,** Glaxo Research and Development Ltd., Park Road, Ware, Hertfordshire, UK SG12 0DJ
17–22	**International Symposium on Environmental Biomonitoring and Specimen Banking**	Hawaii, USA	**K. S. Subramanian,** Environmental Health Directorate, Health Canada, Tunney's Pasture, Ottawa, Ontario, Canada K1A OL2 **Tel:** +1 613 957 1874. **Fax:** +1 613 941 4545
1996			
January			
8–13	**1996 Winter Conference on Plasma Spectrometry**	Florida, USA	**R. Barnes,** Department of Chemistry, Lederle GRC Tower, University of Massachusettes, P.O. Box 34510, Amherst, MA 01003-4510, USA **Tel:** +1 413 545 2294. **Fax:** +1 413 545 4490
21–25	**VIth Latin American Congress on Chromatography**	Caracas, Venezuela	**Irene Romero,** Interep SA, P.O. Box 76343, Caracas 1070-A, Venezuela
February			
6–9	**Fourth International Symposium on Hyphenated Techniques in Chromatography (HTC 4); Hyphenated Chromatographic Analysers**	Bruges, Belgium	**Dr. R. Smits, Royal Flemish Chemical Society (KVCV), Working Party on Chromatography,** BASF Antwerpen N.V., Central Laboratory, Haven 725, Scheldelaan 600, B-2040 Antwerp, Belgium **Tel:** +32 3 561 2831. **Fax:** +32 3 561 3250
March			
17–21	**47th Pittsburgh Conference on Analytical Chemistry and Applied Spectroscopy**	Chicago, USA	**The Pittsburgh Conference,** 300 Penn Center Boulevard, Suite 332, Pittsburgh, PA 15235-5503 USA **Tel:** +1 412 825 3220. **Fax:** +1 412 825 3224

Date	Conference	Location	Contact
25–29	**ESEAC '96, 6th European Conference on ElectroAnalysis**	Durham, UK	**Dr. A. G. Fogg,** Loughborough University of Technology, Loughborough, Leicestershire, UK LE11 3TU **Tel:** +44 (0)1509 263171. **Fax:** +44 (0)1509 233163
31–4/4	**7th International Symposium on Supercritical Fluid Chromatography and Extraction**	Indianapolis, USA	**Mrs. Janet Cunningham,** Barr Enterprises, 10120 Kelly Road, P.O. Box 279, Walkersville, MD 21793 USA **Tel:** +1 301 898 3772. **Fax:** +1 301 898 5596
April			
9–12	**26th International Symposium on Environmental Analytical Chemistry**	Vienna, Austria	**Professor Dr. M. Grasserbauer,** Institute for Analytical Chemistry, Vienna University of Technology, Getreidemarkt 9/151, A-1060 Wien, Austria **Fax:** +43 1 5867813
23–26	**Analytica Conference '96**	Münich, Germany	**Congress Center,** Messegelände, D-80325 München, Germany **Tel:** +49 89 5107 159. **Fax:** +49 89 5107 180
May			
7–9	**VIIth International Symposium on Luminescence Spectrometry in Biomedical Analysis—Detection Techniques and Applications in Chromatography and Capillary Electrophoresis**	Monte-Carlo, Monaco	**Professor Willy R. G. Baeyens,** University of Ghent, Pharmaceutical Institute, Department of Pharmaceutical Analysis, Harelbekestraat 72, B-9000 Ghent, Belgium **Tel:** +32 9 221 8951. **Fax:** +32 9 221 4175
20–24	**18th International Symposium on Capillary Chromatography**	Riva del Garda, Italy	**Professor D. P. Sandra,** I.O.P.M.S., Kennedypark 20, B-8500 Kortrijk, Belgium **Tel:** +32 56 204960. **Fax:** +32 56 204859
23–25	**XIIIth National Conference on Analytical Chemistry**	Craiova, Romania	**Romanian Society of Analytical Chemistry,** 13 Boulevard Republicii, Sector 3, 70346 Bucharest, Romania **Tel:** +40 1 631 00 60. **Fax:** +40 1 631 00 60
June			
16–21	**HPLC '96: 20th International Symposium on High Performance Liquid Phase Separations and Related Techniques**	California, USA	**Mrs. Janet Cunningham,** Barr Enterprises, 10120 Kelly Road, P.O. Box 279, Walkersville, MD 21793, USA **Tel:** +1 301 898 3772. **Fax:** +1 301 898 5596
July			
8–12	**XVI International Congress of Clinical Chemistry**	London, UK	**Mrs. Pat Nielsen,** XVIth International Congress of Clinical Chemistry, P.O. Box 227, Buckingham, UK MK18 5PN **Fax:** +44 (0)1280 6487
17–19	**8th Biennial National Atomic Spectroscopy Symposium (BNASS)**	Norwich, UK	**Dr. S. J. Haswell,** School of Chemistry, University of Hull, Hull, UK HU6 7RX **Tel:** +44 (0)1482 465469. **Fax:** +44 (0)1482 466410
August			
20–23	**7th International Symposium on Pharmaceutical and Biomedical Analysis (PBA '96)**	Osaka, Japan	**Professor Susumu Honda,** Faculty of Pharmaceutical Sciences, Kinki University, Kowakae 3-4-1, Higashi Osaka 577, Japan **Fax:** +81 6 721 2353
September			
1–7	**Euroanalysis IX**	Bologna, Italy	**Professor Luigia Sabbatini,** Euroanalysis IX, Dipartimento di Chimica, Università di Bari, Via Orabona, 4, 70126 Bari, Italy **Tel:** +39 80 242020. **Fax:** +39 80 242026
15–20	**21st International Symposium on Chromatography**	Stuttgart, Germany	**GDCh-Geschäftsstelle, Abt. Tagungen,** Varrentrappestr. 40–42, Postfach 90 04 40, D-6000 Frankfurt am Main 90, Germany **Tel:** +49 69 791 7358. **Fax:** +49 69 791 7475

Courses

Date	Conference	Location	Contact
1995			
June			
5–7	**Advanced HPLC Short Course**	Pensylvania, USA	**Jim Alexander,** Rohm and Haas Laboratories, 727 Norristown Road, Spring House, PA 19477, USA **Tel:** +1 610 619 5226.
7–12	**4th Annual Course on Practical Methods of Digestion for Trace Analysis**	Amherst, USA	**Nancy Teranto,** Questron Corporation, 4044 Quakerbridge Road, Mercerville, NJ 08619, USA **Tel:** +1 609 587 6898. **Fax:** +1 609 587 0513
6–7	**Industrial Waste Water Part I**	Sheffield, UK	**Maria Baldham,** The Division of Adult Continuing Education, The University of Sheffield, 196–198 West Street, Sheffield, UK S1 4ET **Tel:** +44 (0)114 282 5391. **Fax:** +44 (0)114 270 8653
6–8	**5th Annual Flow Injection Atomic Spectrometry Short Course**	Amherst, USA	**J. Tyson,** Department of Chemistry, LGRC Tower, University of Massachusetts, Box 34510, Amherst, MA 01003-4510 USA **Tel:** +1 413 545 0195. **Fax:** +1 413 545 4846
8	**DSC Calibration—Temperature, Enthalpy, Heat Capacity Short Course**	Leeds, UK	**Professor Edward Charsley,** Head of the Thermal Analysis Consultancy Service, Leeds Metropolitan University, Calverley Street, Leeds LS1 3HE **Tel:** +44 (0)113 283 3121/3122. **Fax:** +44 (0)113 283 3120
16–20	**Capillary Electrophoresis, Routine Method for the Quality Control of Drugs: Practical Approach**	Montpellier, France	**Professor H. Fabre,** Laboratory of Analytical Chemistry, Faculty of Pharmacy, 15 Avenue Charles Flahault 34060 Montpellier, France **Tel:** +33 67 54 45 20. **Fax:** +33 67 52 89 15
26–30	**Radioisotope Techniques Short Course**	Loughborough, UK	**Dr. P. Warwick,** Department of Chemistry, Loughborough University of Technology, Loughborough, Leicestershire, UK LE11 3TU **Tel:** +44 (0)1509 222585.
26–30	**Summer School in Spectroscopic Interpretation**	Manchester, UK	**Mr. M. P. Coward,** Chemistry Department, UMIST, P.O. Box 88, Manchester, UK M60 1QD
29–30	**Industrial Waste Water Part II**	Sheffield, UK	**Maria Baldham,** The Division of Adult Continuing Education, The University of Sheffield, 196–198 West Street, Sheffield, UK S1 4ET **Tel:** +44 (0)114 282 5391. **Fax:** +44 (0)114 276 8653
July			
3	**Fourier Transform Infrared Spectroscopy**	Manchester, UK	**Dr. M. P. Coward,** Chemistry Department, UMIST, P.O. Box 88, Manchester, UK M60 1QD
17–19	**Techniques Workshop (Chemometrics)**	Hull, UK	**Dr. M. J. Adams,** School of Applied Sciences, University of Wolverhampton, Wulfruna Street, Wolverhampton, UK WV1 1SB **Tel:** +44 (0)1902 322141. **Fax:** +44 (0)1902 322680
September			
4–5	**Short Course on Sample Handling of Pesticides in the Aquatic Environment**	Paris, France	**Mrs. Frei-Häusler,** IAEAC Office, Postfach 46, CH-4123 Allschuril 2, Switzerland **Fax:** +41 61 482 08 05

Entries in the above listing are included at the discretion of the Editor and are free of charge. If you wish to publicize a forthcoming meeting please send full details to: *The Analyst* Editorial Office, Thomas Graham House, Science Park, Milton Road, Cambridge, UK CB4 4WF. Tel: +44 (0)1223 420066. Fax: +44 (0)1223 420247. E-mail:Analyst@RSC.ORG.

Conference Reports

Promoting the Potential of Analytical Chemistry: Electrochemical Sensors—Symposium Dedicated to the Memory of Professor Wilhelm Simon, Mátrafüred, Hungary, September 15–18, 1994, and SCAR '94–XIIth National Conference on Analytical Chemistry, Constanta, Romania, September 22–24, 1994

Conferences and symposia, as meetings principally for discussion or instruction, normally through oral and other presentations by several persons, are essentially occasions for exchanging views to promote a given topic or to solve a problem. Their success can be governed by the extent to which they lean towards the alternative concepts of 'symposium' as a 'drinking together' or 'merry feast', with the most effective being appropriate blends of discussion and moderate relaxation. The events of September 1994 in Hungary and Romania turned out, in their respective ways, to be vintage blends.

In deference to the Electrochemical Sensors Symposium in Mátrafüred being in memory of the late Professor W. Simon, the event was opened with due reverence by a musical dedication in his honour followed by a worthily generous tribute by Dr. Werner E. Morf, on behalf of himself and Dr. Erno Pretsch, on the 'Reminiscences of Wilhelm Simon and of his Research Work at ETH Zürich'. Together, these laid the way for the kind of happy event in which Wili Simon revelled for twenty years by his participation in the regular discussion symposia on electrochemical sensors held at Mátrafüred.

In a different way, SCAR '94 in Constanta marked a rebirth, by being only the second occasion since 1971 (the first being at the XIth National Conference in Analytical Chemistry in Cluj-Napoca in 1992) that foreign lecturers were invited to these Romanian events. By its nature SCAR '94, that is, the XIIth National Symposium on Analytical Chemistry was geared to helping the re-integration of Romanian analytical chemistry into the international scene, and to indicate opportunities for young people to contribute to analytical chemistry.

Electrochemical Sensors

Events in Mátrafüred, the location of the Wilhelm Simon Memorial Symposium, by being held in this quiet village set in forest and hilly countryside an hour or more by bus or car in the Mátra to the East of Budapest, bring to mind lines from Liebig's friendly letter to Faraday[1] in 1844. These said 'how quietly we live . . . except for scientific pursuits we have no other excitements of mind. We take walks in our beautiful green woods and in the evening drink tea at the neighbouring old castles. This is our recreation'. One can only surmize that Liebig's 'tea' was of a special brew. Instead of castles there is at Mátrafüred the comfortable Hotel Avar for relaxation, where the day's science from presentations and discussions

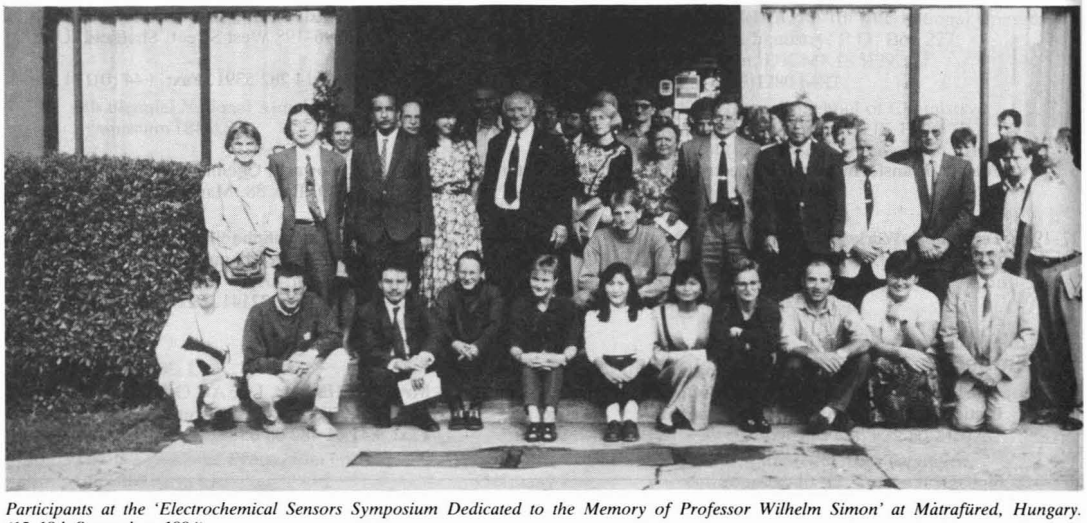

Participants at the 'Electrochemical Sensors Symposium Dedicated to the Memory of Professor Wilhelm Simon' at Mátrafüred, Hungary. (15–18th September, 1994).

which already have gone on well into the evening will usually continue informally deep into the night. This time though, there were more oral presentations than usual, so that the formal discussion periods were curtailed. Nevertheless, the scientific programme was a hefty one, and Wili Simon would have been exhilarated by it.

By having all participants resident in Hotel Avar, the mealtimes and breaks were arranged to accommodate the tight schedule of invited lectures and discussion papers. For this purpose an international audience in excess of 75 having left Budapest for Mátrafüred in the morning of Thursday, 15th September, assembled for an early afternoon start to the Symposium.

Following the opening musical and oral tribute items, mentioned above, Dr. Kazuo Yasuda of Hitachi gave an appreciation of the contributions of Professor Simon to the development of ion-selective electrode (ISE) instrument technology in Japan for blood electrolyte measurements. A significant stage in this development was the adoption by Simon[2] for his valinomycin-based potassium ISE of the PVC support matrix membrane concept for trapping the ion sensor as described in earlier studies at the University of Wales in Cardiff on a calcium ISE.[3] As a result, as Dr. Yasuda reminded the audience, by 1985 the numbers of instruments produced for sodium and potassium measurements with ISEs exceeded the number of flame photometers. Today, through the activities of the International Federation of Clinical Chemistry, blood electrolyte measurements in clinical work are usually made by ISEs rather than by flame photometry.

Rather fittingly, the first main invited contribution was by Dr. Erno Pretsch on behalf of the eight co-authors from the Department of Organic Chemistry at ETH, Zürich on 'New Insights into the Planning of Ionophores and the Compositions of Membranes'. Alongside ISEs, this took on board optodes, which had commanded Simon's attention in his later years. Pretsch considered the membranes' intimate and complex relationships in terms of ion-exchange equilibria which determine response function, selectivity, detection limits and measuring ranges. Professor Richard P. Buck then followed in his characteristic affluent manner with a discourse on 'Microfabrication Technology of Flexible Membrane-based Sensors for *In Vivo* Applications', when he described studies to fulfil the desire of cardiovascular physiologists to use flexible multielectrode probes to help describe the potential and ionic distribution in the heart as a function of time. This again served to emphasize the significance of the pioneering development of flexible PVC matrix membranes, which here had progressed to aminated PVC matrices.

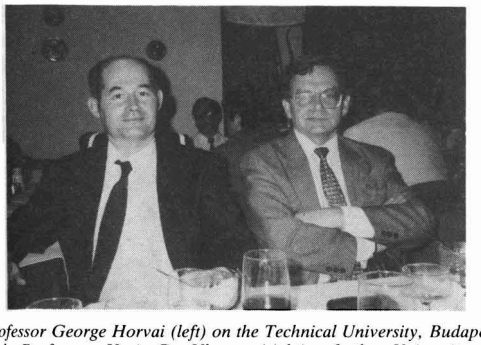

Professor George Horvai (left) on the Technical University, Budapest and Professor Yuri G. Vlasov (right) of the University of St. Petersburg, Russia, relaxing during the Electrochemical Sensors Symposium.

This first block of invited lectures, after a short coffee break, was followed by five short discussion papers, each of twenty minutes duration, to take the Symposium through to the end of the first day's proceedings in time for dinner. These reported studies in the USA, Switzerland, Hungary and Russia, and sometimes involving degrees of international collaboration. They were devoted to ISEs in various guises and covered a thermodynamic basis for selectivity, measurement accuracy, effect of ionic additives on electrically charged carriers, matters concerning the interface between two immiscible electrolyte solutions (ITIES) and diffusion features in lithium-selective membranes.

On the second day, there was an early start to hear the seven full invited lectures plus a further eight short discussion papers, thus bringing the day's proceedings right up to dinner at seven o'clock in the evening. Professor Andrzej Lewenstam, in the dual role of representing Finland and Poland, opened the day by addressing 'Integrated Potentiometric Electrodes' wherein he dealt with solid contact interfaces *vis-a-vis* liquid junctions, and conducting polymers. Dr. Geža Nagy covered 'New Applications of Potentiometric Microelectrodes' in terms of Scanning Electrochemical Microscopy (SECM) directed at providing information about the chemical nature and chemical environment of the substrate of interest and topographic imaging of surfaces. This represented co-operation between himself and Professor Klara Tóth from Hungary and their co-authors at the University of Texas at Austin.

Professor M. E. Meyerhoff described work at the University of Michigan on 'Polymer Membrane-based Polyion Sensors' which focused on poorly plasticized PVC membranes doped with lipophilic anion- and cation-exchangers for the unexpectedly large and reproducible potentiometric responses to μmol l^{-1} levels of polyionic species like heparin and protamine. The multi-centre programme linking Budapest, Hungary with centres at Chapel Hill, Raleigh and Cleveland, USA, and devoted to sensor design for minimizing deleterious interactions by the use of small size and mass, and biocompatible materials was described by Dr. Erno Lindner under the theme of 'Electroanalytical and Biocompatibility Studies on Microfabricated Array Sensors'.

The invited lecture of Dr. Elizabeth A. H. Hall of Cambridge, UK was true to the title of 'Investigating Polymers and Organic Metals as Transduction Mediators or Immobilization Matrices' with the focus of attention being on whether immittance spectroscopy can be employed for investigating the mechanism of operation of electrically deposited polymers and charge-transfer salts. In his lecture on 'Ionophores Containing Ethoxylate Units for Ion Sensing' Professor J. D. R. Thomas described the studies of his group at the University of Wales on the ISE qualities of a range of acyclic polyethers and of crown and bis-crown ethers. Here, the discussion confirmed a need for further attention to the mechanism and other features of the potentiometric sensing of alkoxylate non-ionic surfactants.

The last of the second day's invited lectures, by being from ETH, Zürich, served to remind participants of the connection with the late Professor Wilhelm Simon. Thus, by considering 'From Molecular Recognition to Analytical Information by Chemical Sensors' Dr. Ursula E. Spichiger explored the potential for analytical chemistry of carrier-based sensors in relation to the validity of data produced. She exemplified difficulties that can arise by the quality assessment of gastric juice pH data obtained by a pH probe based on ETH 2418 (4-dipropylamino-2′-azobenzene-carboxylic acid octadecyl ester). The subsequent discussion papers included such diverse topics as an amperometric sensor using immobilized bacteria, assays of vitamin B_6, electrochemical detection in capillary systems, dual microdisk electrodes, and a drug-

sensitive electrode based on trimethoprimium-phosphotungstate ion associate as sensing ion-exchanger. With an even more arduous day ahead for the morrow, participants were more than ready for dinner and informal exchanges recapping on the day's proceedings.

The third day, Saturday, September 17th was opened with the first invited lecture being by Dr. Werner E. Morf, formerly of Professor Simon's group, considering the 'Lifetime of Glass Membrane Electrodes: Theoretical Model for the Corrosion of Silicate Glasses'. He applied the concepts adopted by geologists for simulating the corrosion of minerals under hydrogeochemical conditions. The matter of modelling was continued by Professor G. Horvai speaking on 'Computer Modelling of the Membrane/Solution Interface of Liquid Membrane Electrodes', leading to an iterative solution of a set of equations giving the equilibrium distributions of the interface components, which was tested for the practical system of a liquid membrane doped with a carrier.

Professor Y. Umezawa of Tokyo University, in his lecture on 'Optical Second-harmonic Generation (SHG) at the Surface of Ionophore-incorporated Polymeric Liquid Membranes', used the premise that it is only the molecules of the interface between two centrosymmetric media, such as the surface between two liquids, that participate in the asymmetry of the interface that will contribute to the SHG. He discussed the application of SHG to measurements at the surface of PVC membranes with trapped ionophores. A more general theme was adopted by Professor Yuri G. Vlasov of St. Petersburg University, by first of all relating to the range and market size of sensors then within the title of 'Development of Solid-state Chemical Sensors for Industrial, Environmental and Medical Applications' turning to some new developments in solid-state sensors.

Flow injection was associated early on with electrochemical sensors. Here, Professor Richard A. Durst of Cornell University discussed a computer-controlled system under the title 'Flow-injection Liposome Immunoanalysis (FILIA) with Electrochemical Detection'. The system consists of an immunoreactor column of glass beads covalently coated with an antibody specific for the analyte of interest set in a flow system linked to a flow-through detector operated in the controlled-potential amperometric mode.

The last two billed invited lectures of the whole programme were set for the mid-afternoon of the third day. The first was 'Advanced Methods for the Characterization of Modified Electrodes', directed at electrochemical impedance spectroscopy, quartz crystal microbalance and radiotracer methods, by Dr. G. Inzelt of Eötvös Loránd University, Budapest. The second involved the specialist applications area of 'Some Recent Studies on the Use of Electrochemical Sensors in Non-aqueous Solution Chemistry' under the co-authorship of Kosuke Izutsu and T. Nakamura of Shinshu University, Japan and delivered by Professor Izutsu. This covered a pH ISFET, fluoride and cyanide ion-sensors, and liquid junction potentials between different solvents.

The discussion papers which occupied the rest of the third day's proceedings ahead of the excellent Symposium Banquet were broadly devoted to ISE systems in various guises, although they included two on optical sensors. The final set of discussion papers which came on the final morning, that is on Sunday, 18th September were similarly devoted to ion-sensors, after which there was a final discussion session which decided that the Mátrafüred meetings should continue with an event in October 1996. However, it is evident that they need to be broadened in scope to embrace the full area of electrochemical sensing and include aspects of the field that were clearly not in evidence on this occasion. Nevertheless, as well as remembering the contributions of the late Professor Wilhelm Simon, this was an event that had promoted the field by discourse across both scientific and international boundaries.

XIIth National Conference on Analytical Chemistry

The Romanian National Conferences on Analytical Chemistry are peripatetic. Constanta, the Black Sea resort, was a truly delightful place for holding this twelfth event in the series, with the host location being the newly founded (March 1990) 'Ovidius' University, supplemented by hotel accommodation in the nearby resort of Mamaia for accommodating both foreign guests and some of the Romanian participants.

As already mentioned, the aim of this Conference was for foreign lecturers to present accounts of their research, in order that Romanian analytical chemists be given an informed view of recent progress in aspects of the subject. This was undertaken against a background of years of difficulty for Romanians in terms of the non-availability of international scientific literature and even of laboratory materials. However, opportunities such as the 'TEMPUS', 'Go-West' and 'Go-East' programmes of the European Union, and other means of travel to, and co-operating with, foreign countries have alleviated the position for some Romanian colleagues.

The events of December 1989 in Romania caused a big hiccup and many changes. Adjustments to these have inevitably been patchy. Many problems clearly remain, especially of the environmental kind and these can be a fruitful field for receiving the attention of analytical chemists. There are also possibilities in the industrial, biomedical and clinical fields.

Foreign Lecturers

For the Conference, the Chairman, Professor George-Emil Bailuescu, with the help of a long list of sponsors, and a Committee under the Secretaryship of Dr. G. L. Radu drawn from the Romanian Society of Analytical Chemistry and 'Ovidius' University, Constanta, had brought in a dozen foreign lecturers as the mainstay of the oral programme. To complement this, there were posters on display throughout the Conference. The posters (157 were listed in the programme) were mainly from Romania and were classified under the headings of Separations, Electrometric Methods, Spectrometric Methods, Analytical Biochemistry, Environmental Analysis, and Miscellaneous.

The pre-opening event of the Conference was a truly hospitable Welcome Reception at the Cazinoul din Constanta on the evening of Wednesday, September 21st. Following the introductions and the renewal and making of friendships

Serious discussion during SCAR '94. Left to right: Professor Adam Hulanicki (University of Warsaw, Poland), Professor Richard P. Buck (University of North Carolina, USA) and Professor P. R. Coulet (University of Lyon, France).

among the 200 or so participants there was a solid foundation for effective communication, and especially since so many of the Romanians spoke English fluently.

After the formal Opening Ceremony on the morning of Thursday, September 22nd, the main Conference business got under way with strict instructions by Professor G. E. Bailuescu to the first Chairman, Professor J. D. R. Thomas, that the programme was to stick to the planned time schedules. In setting an example, Professor Bailuescu (Bucharest) kept his Opening Lecture on 'Sampling', to well within the time limits, and he also allowed room for the discussion of his lecture. In his presentation, Professor Bailuescu indicated, perhaps controversially, that sampling also included pre-treatment stages and separations; this can be a matter of continuing debate.

Professor Adam Hulanicki (Warsaw, Poland), having already been on stage at the Opening Ceremony in his capacity as President of the Analytical Division of IUPAC, gave an illuminating address on 'Improvement of Detection Limit in Absorption Atomic Spectometry'. During the ensuing coffee break the foreign lecturers were introduced to the Rector of the host 'Ovidius' University.

Next came the electrochemically based lectures, firstly by Professor Richard P. Buck (Chapel Hill, USA), billed to speak on '*In Vivo* Monitoring Using Microchemical Sensors', but who, by request, broadened his theme to embrace microfabrication technology and flexible membrane-based sensors. Second was the lecture on 'Design of Selective Electrodes for Analysis' by Professor J. D. R. Thomas (Wales, UK) who summarized the scope of the design and application of ion-selective electrodes and briefly described the design of amperometric oxidase enzyme electrodes set up for the flow injection.

The late afternoon lecture session followed lunch and poster viewing, and was devoted to chromatographic themes, with the opener, Professor H. Y. Aboul (Riyadh, Saudi Arabia) relating his experiences in the 'Applications of Chiral Chromatography in Biomedical Analysis'. Next came Professor H. A. Claessens (Eindhoven, The Netherlands) to address 'Properties, Stability, and Characterization of Reversed-phase Stationary Phases for HPLC'. The day's formal events were drawn to a close by Professor R. P. Baldwin (Louisville, USA) attending to what is among the most recent areas of focus for analytical chemists and biochemists, namely capillary electrophoresis, and specifically on 'Electrochemical Detection in Capillary Electrophoresis'. Dinner followed.

The programme of Friday, 23rd September, was devoted firstly to 'Amperometric Biosensors Based on Redox Enzymes Immobilized in Carbon Paste' by a true expert in the field, Professor L. Gorton (Lund, Sweden). Such a topic by its nature, and since it is pursued in Romania was bound to create good discussion, as was also the case for the lecture of Professor P. R. Coulet (Lyon, France) on 'Molecular Recognition and Transduction in Biosensors'.

For the first lecture after coffee, Professor Yohichi Goshi (Nagoya, Japan) took on the rather difficult and esoteric theme of the kind of events that inspire the generation of ideas. His mentor example type, Professor V. A. Fassell, was a good one, and the talk made interesting listening. Next came, 'Sampling and Pre-treatment of Gases for Gas Chromatographic Analysis' by Professor J. Namiesnik (Gdansk, Poland).

According to the pattern of lunch followed by poster viewing the participants sat down for the late afternoon and final session of lectures. The first lecture was directed at an application of analytical chemistry and the second at a technique. They provided a good base for appreciating progress made and for generating further research ideas. Thus, Professor M. Biziuk (Gdansk, Poland) addressed 'Occurrence and Determination of Organohalogen Compounds in Tap and Surface Water', while Professor N. H. Velthorst (Amsterdam, The Netherlands), elucidated the theme of 'High-resolution Spectroscopy in Analytical and Environmental Chemistry: Identification and Quantification'.

Although the formal scientific presentations ended at six o'clock on the evening of Friday, 23 September, conference participants were kept together by the Romanian folk dancing evening which followed. Furthermore, the post conference tour to the Danube Delta on Saturday, 24th September, starting at Tulcea ready for sailing along the Bratul Sfintu Gheorghe branch of the Danube gave the opportunity for sealing the valuable informal discussions, whilst at the same time savouring a sample of one of the touristic gems of Romania.

Posters: The Romanian Analytical Scene

Except for 16 contributions from foreign countries (half from Moldova and three from Belorussia), most of which were not on display, more than two thirds of the billed posters were from centres in Bucharest (66 listed) and Cluj-Napoca (41 listed). Even without allowing for the fact that there were few submissions from at least one significant group in Bucharest it is evident that Romanian analytical chemistry is dominated by centres situated in Bucharest. There is much activity in Cluj-Napoca, but over half the listed posters from this city were attributable to two research leaders (Professor E. Cordos with 16 and Dr. E. Hopirtean with eight). The main minor geographical centres of analytical chemical research, as deduced from the poster list are at Timisoara, Iasi, Craiova and Constanta.

The leading research group, as deduced from poster author lists is clearly that of Professor E. Cordos of the Research Centre for Analytical Instrumentation at Cluj-Napoca, whose researches on spectroscopic instrumentation and sensors are of high repute. At least some of the output of this group merits the entrepreneural attention of instrument makers and laboratory suppliers, and finance from venture capitalists. Indeed, Professor Cordos and his colleagues ought themselves to look at 'promoting the potential of analytical chemistry' by marketing their spectrophotometers, automatic analyser and tubidimeter, devices for atomic spectrometry, sensors and analysers for humidity, NO_x, carbon monoxide, sulfur dioxide and other toxic gases. Romania is now committed to a free market economy, and there is plenty of evidence of new business activity.

Of course, as in any conference, many of the posters were on fairly routine separation, spectral, electrometric, assessment, method for . . ., determination of . . . , content of . . ., and other type of work. Nevertheless, most of the work presented was of modern flavour, covering chromatography in its various forms, polarography and stripping voltammetry, ion-sensing, spectrometric methods including fluorescence and chemiluminescence, flow methods, enzyme methods and biosensors, surface analysis, and even neural networks.

Conclusion

By being respectively devoted to the specific and the general, these two events provided different views of analytical chemistry in Eastern Europe. The Hungarian scene is clearly in tow with the international line, while that in Romania is still reeling from the lost momentum of the last twenty years or so. However, both are geared to promoting the potential of analytical chemistry. As in Hungary, there are in Romania agencies of leading scientific instrument suppliers, and at SCAR '94 there were many participants from industrial

organizations and oil companies to inter-relate with what was said and seen.

Financial resources are still a problem, but there is an enthusiasm among both Romanians and Hungarians for the potential of having science play its role. Conferences and symposia have their part to play, but also there are the roles of more dedicated long-term initiatives like the new Master's course in environmental and analytical chemistry at the University Politehnica in Bucharest, the environmental problems are there and personnel must be trained for tackling them. Every success is wished on 'Promoting the Potential of Analytical Chemistry'.

References

1 Reed, J., *Humour and Humanism in Chemistry*, G. Bell & Sons, London, 1947, p. 246.
2 Simon, W., Lecture to Electroanalytical Group of The Society for Analytical Chemistry on *Some Developments in Antibiotic Liquid Membrane Ion-selective Electrodes* at Imperial College, London on 26th November 1971.
3 Moody, G. J., Oke, R. B., and Thomas, J. D. R., *Analyst*, 1970, **95**, 910.

Professor J. D. R. Thomas*
School of Chemistry
University of Wales
Cardiff, UK

* Present address: 4 Orchard Court, Gresford, Wrexham, UK LL12 8EB.

The Tenth Russian National Conference on Solvent Extraction, Ufa, Russia, November 14–18, 1994

This series of meetings started in 1959 in Moscow (Vernadskii Institute of Geochemistry and Analytical Chemistry). Since the fourth conference, these meetings have been organized by the Commission on Solvent Extraction of the Russian Academy of Sciences. Seven meetings (1959–1984) were called 'All-Union Conferences on Extraction Chemistry' but since the eighth conference held in Divnogorsk in 1987, the coverage of these scientific events has widened.

The tenth conference covered all of the most important areas of solvent extraction, namely thermodynamics and kinetics of solvent extraction, interphase phenomena, liquid membranes, chemistry of metals and acids, extraction with neutral, cationic and anionic extractants, separation of organic substances, mass transfer, modelling of equipment, and technological and analytical applications of solvent extraction. More than 100 participants presented 13 plenary, 41 oral papers in sections and 76 posters.

The next conference will be organized in 1996 in Moscow or Minsk.

Professor Yu. A. Zolotov
Kurnakov Institute of General and Inorganic Chemistry,
Moscow

Future Issues will Include—

Principal Component Analysis Applied to Admittance Spectra of Quartz Crystal Microbalance in Liquids—**Shouzhuo Yao, Kang Chen, Ze Tan and Lihua Nie**

Method for the Analysis of Selected Non-*ortho* Chlorinated Chlorobiphenyls in Shell Fish Tissue—**Thomas L. King, John F. Uthe and Charles J. Musial**

Trace Enrichment of Metals Using Supported Liquid Membrane Technique—**L. Mathiasson, M. Papantoni, N-K. Djane, K. Ndung'u and J. A. Jonsson**

Quantitative Analysis of Binary Aqueous Sodium Chlorate and Sodium Perchlorate Solution in the Presence of Sodium Bichromate, Using Fourier Transform Infrared Spectrometry—**Kazem Kargosha, Hosainy Said Davarani and Reza Moosavi**

Effect of Dimethylsulfoxide as a Masking Agent for Aqueous Chlorine in the Determination of Oxychlorines—**Noriko Imaizumi, Toshiki Kanayama and Kikug Oikawa**

Comparison of Time-resolved Fluorimmunoassay and Immunoenzymic Assay for Clenbuterol—**Maria A. Bacigalupo, A. Ius, G. Meroni, M. Dovis and E. Petruzzelli**

Open-focussed Microwave-assisted Digestion for the Preparation of Large Mass Samples—**Ralph E. Sturgeon, Jianhua Liu and S. N. Willie**

Study of the Polarographic and Voltammetric Behaviour of Enoxacin—**Jinghao Pan, Gerong Zhou and Hiuzhi Fan**

Sensitive Determination of Manganese using Flow Injection and Chemiluminescent Detection—**R. D. Snook, Andrew R. Bowie, Peter R. Fielden and Roger D. Lowe**

Flow Injection Determination of Uranium with In-Value Ion-exchange Column Preconcentration and Separation—**Kate Grudpan, Saisunee Laiwraungrath and Ponlayuth Sooksamiti**

Simultaneous Determination of Guanine, Uric Acid, Hypoxanthine and Xanthine in Human Plasma by Reversed-phase High-performance Liquid Chromatography With Amperometric Detection—**Erkang Wang, Tao Li and Zhiming Liu**

Investigation on the Factors Influencing the Aluminium Speciation in Natural Waters Equilibria with Mineral Phase of Gibbsite—**Shuping Bi**

Deconvolution of Mixtures by Chemometric Factor Analysis—**R. G. Brereton**

Reversible Potentiometric Ascorbic Acid Solid Membrane Sensor Based on 4,4′,4″,4‴-Tetra-*tert*-butylphthalocyanine Cobalt(II)—**Ruqin Yu, Jun-Zhong Li and Guoli Shen**

Rapid and Sensitive Assay for Some Protease Enzymes Using à fluorosubstrate-immobilized Bioreactor—**Frederick J. Rowell, L. X. Tang and R. A. Cumming**

Separation of Inorganic Selenium Species on Anion-exchange Resins—**Krystyna Pyrzynska**

Trace Detection of Benzene Vapour in a Simple Ion Chamber Employing Laser-induced Resonance-enhanced Multiphoton Ionization in the Wavelength Region 246–264 nm—**K. W. D. Ledingham, Archibald Marshall and Ravi P. Singhal**

Palladium-doped Screen-printed Electrodes for Monitoring Formaldehyde—**Joseph Wang, Maria Pedrero and Xiaohua Cai**

Acid–Base Indicators: Transition Colours and pH Ranges Determined in Select Aqueous–Organic Mixed Solvents—**William E. Acree, Sheryl A. Tucker and Heather C. Bates**

Simultaneous Determination of Arsenic, Cadmium and Lead in Swine and Bovine Kidneys by Electrothermal Atomic Absorption Spectrometry—**Margarida Ferreira, M. Elisa Soares and M. Lourdes Bastos**

Determination of Organotin Compounds in Marine Mussel Samples by High-performance Liquid Chromatography, Hydride Generation With Inductively Coupled Plasma Atomic Emission Spectrometric Detection—**P. Rivaro, Laura Zaratin, Roberto Frache and Ambrogio Mazzucotelli**

On-line Preconcentration of Silver on Sulfydryl Cotton Microcolumn and Determination by Flow Injection-Atomic Absorption Spectrometry—**M. M. Gomez Gomez, M. M. Hidalgo Garcia and M. A. Palacios Corvillo**

Fast Determination of Total Fluoride by Direct Potentiometry in Samples of Aluminium Fluoride and Cryolite—**M. S. Corbillon, M. P. Carril, J. M. Madariaga and Ignacio Uriarte**

Direct Determination of Dissolved Uranyl(VI) in Sea-water by Cathodic Stripping Voltammetry—**Renata Djogic and Marko Branica**

Comparison of Reverse Polarity Capillary Electrophoresis and Adsorptive Stripping Voltammetry for the Detection and Determination of Reactive Textile Dyes—**W. F. Smyth, D. A. Oxspring and R. Marchant**

Retention Behaviour of Some Commercial Pesticides on Porous Graphitized Carbon Column—**Esther Forgacs, Cserhati Tibor**

Use of a Model Gut System to Study the Effect of Dietary Fibre and Multivitamins on the Speciation of Copper, Zinc and Iron—**Stephen J. Haswell and Mustafa S. Dundar**

Traceability in Analytical Chemistry—**Miguel Valcarcel and Angel Rios**

Nitrogen Factors for Sheepmeat. Part 1. Mutton—**Analytical Methods Committee**

COPIES OF CITED ARTICLES

The Royal Society of Chemistry Library can usually supply copies of cited articles. For further details contact: The Library, Royal Society of Chemistry, Burlington House, Piccadilly, London W1V 0BN, UK. Tel: +44 (0)171-437 8656. Fax: +44 (0)171-287 9798. Telecom Gold 84: BUR210. Electronic Mailbox (Internet) LIBRARY@RSC.ORG.

If the material is not available from the Society's Library, the staff will be pleased to advise on its availability from other sources.

Please note that copies are not available from the RSC at Thomas Graham House, Cambridge.

Technical Abbreviations and Acronyms

The presence of an abbreviation or acronym in this list should NOT be read as a recommendation for its use. However those defined here, need not be defined in the text of your manuscript.

AAS	atomic absorption spectrometry
ac	alternating current
A/D	analogue-to-digital
ADC	analogue-to-digital converter
ANOVA	analysis of variance
AOAC	Association of Official Analytical Chemists
ASTM	American Society for Testing and Materials
bp	boiling point
BSA	bovine serum albumin
BSI	British Standards Institution
CEN	European Committee for Standardization
cpm	counts per minute
CMOS	complementary metal oxide silicon
c.m.c.	critical micellization concentration
CRM	certified reference material
CVAAS	cold vapour atomic absorption spectrometry
c.w.	continuous wave
CZE	capillary zone electrophoresis
dc	direct current
dpm	disintegrations per minute
DRIFT	diffuse reflectance infrared Fourier transform spectroscopy
DELFIA	dissociation enhanced lanthanide fluorescence immunoassay
DNA	deoxyribose nucleic acid
EDTA	ethylenediaminetetraacetic acid
ELISA	enzyme linked immunosorbent assay
emf	electromotive force
ETAAS	electrothermal atomic absorption spectrometry
EXAFS	extended X-ray absorption fine structure spectroscopy
EPA	Environmental Protection Agency
FAAS	flame atomic absorption spectrometry
FAB	fast atom bombardment
FAO-WHO	Food and Agriculture Organization, World Health Organization
FIR	far-infrared
FT	Fourier transform
FPLC	fast protein liquid chromatography
FPD	flame photometric detector
GC	gas chromatography
GLC	gas–liquid chromatography
HGAAS	hydride generation atomic absorption spectroscopy
HPLC	high-performance liquid chromatography
ICP	inductively coupled plasma
id	internal diameter
INAA	instrumental neutron activation analysis
IR	infrared
ISFET	ion-selective field effect transistor
iv	intravenous
im	intramuscular
IGFET	insulated gate field effect transistor
ISE	ion-selective electrode
LC	liquid chromatography
LED	light emitting diode
LOD	limit of determination
LOQ	limit of quantification
mp	melting point
MRL	maximum residue limit
mRNA	messenger ribonucleic acid
MS	mass spectrometry
NIR	near-infrared
NMR	nuclear magnetic resonance
NIST	National Institute of Standards and Technology
od	outer diameter
OES	optical emission spectrometry
PBS	phosphate buffered saline
PCB	polychlorinated biphenyl
PAH	polycyclic aromatic hydrocarbon
PGE	platinum group element
PIXE	particle/proton-induced X-ray emission
ppt	parts per trillion (10^{12}; pg g^{-1})
ppb	parts per billion (10^{9}; ng g^{-1})
ppm	parts per million (10^{6}; μg g^{-1})
PTFE	poly(tetrafluoroethylene)
PVC	poly(vinyl chloride)
PDVB	poly(divinyl benzene)
QC	quality control
QA	quality assurance
REE	rare earth element
rf	radiofrequency
RIMS	resonance-ionization mass spectrometry
rms	root mean square
rpm	revolutions per minute
RNA	ribonucleic acid
SCE	saturated calomel (reference) electrode
SE	standard error
SEM	scanning/surface (reflection) electron microscopy
SIMS	secondary-ion mass spectrometry
SIMCA	soft independent modelling of class analogy, statistical isolinear multicategory analysis
SRM	Standard Reference Material
STM	scanning tunnelling (electron) microscopy
STP	standard temperature and pressure
TIMS	thermal ionization mass spectrometry
TLC	thin-layer chromatography
TOF	time-of-flight
TGA	thermogravimetric analysis
TMS	trimethylsilane
tris	2-amino-2-(hydroxymethyl)-propane-1,3-diol
TRIS	tris(hydroxymethyl)methylamine
UV	ultraviolet
UV/VIS	ultraviolet–visible
VDU	visual display unit
XRD	X-ray diffraction
XRF	X-ray fluorescence
YAG	yttrium aluminium garnet

Commonly Used Symbols

M	molecular mass
M_r	relative molecular mass
r	correlation coefficient
s	standard deviation
u	atomic mass

BAS

NEW Catalogue of BAS Certified Reference Materials

NEW Catalogue of Outside-Source Reference Materials

now available

For copies, please apply to:

BUREAU OF ANALYSED SAMPLES LTD
Newham Hall, Newby, Middlesbrough
Cleveland, England, TS8 9EA

Telephone: (01642) 300500
Fax: (01642) 315209

Circle 001 for further information

NEW BOOK FROM THE ROYAL SOCIETY OF CHEMISTRY

LIMS: Implementation and Management

By A.S. Nakagawa, *Analytical Systems Inc., Pennsylvania, USA*

There is currently a high level of interest in Laboratory Information Management Systems (LIMS), which, when successfully implemented, can revitalize the operations of a laboratory and contribute significantly to the effectiveness and efficiency of the overall enterprise. **LIMS: Implementation and Management** describes the strategy, planning, resources, and activities needed to integrate LIMS and its supporting technologies into an organization. It covers all aspects of implementation and management and has the benefit of not being product specific. This book will not date as it is not restricted to a particular software product, hardware platform, or technical automation approach. Instead it deals with the issues, expertise, organization, and resources that contribute to the successful implementation of LIMS.

The author has wide experience of automated laboratory systems in the chemical, pharmaceutical, environmental, and biotechnology industries, and for the past 15 years has been intimately involved in every aspect of LIMS implementations including justification, system selection, installation, project management, development, training, validation, performance optimization, and maintenance.

LIMS: Implementation and Management contains numerous illustrations and tables to highlight concisely the major points and concepts discussed in each chapter. The book is essential reading for laboratory, information systems and project managers responsible for the implementation of LIMS and, as it does not require any previous knowledge of computers or laboratory information management systems, is easily accessible to all.

Hardcover **xiv + 180 pages** **ISBN 0 85186 824 X** **1994**
Price £37.50

To order please contact:
The Royal Society of Chemistry, Turpin Distribution Services Limited, Blackhorse Road, Letchworth, Herts SG6 1HN, United Kingdom.
Telephone: +44 (0) 1462 672555. Fax: +44 (0) 1462 480947. Telex: 825372.
Please quote your credit card details. We can now accept Access/Visa/Mastercard/EuroCard.

Turpin Distribution Services Limited is wholly owned by The Royal Society of Chemistry.

For information on other books and journals please contact:
Sales and Promotion Department, The Royal Society of Chemistry, Thomas Graham House, Science Park, Milton Road, Cambridge CB4 4WF, United Kingdom.
Telephone: +44 (0) 1223 420066. Fax: +44 (0) 1223 423429. E-mail: (Internet) RSC1@RSC.ORG.

RSC Members are entitled to a discount on most RSC publications. Details available from:
Membership Administration Department at the Cambridge address above.

K VOS/LUMSDAF/GR

SENSORS AND SIGNALS

The third in a series of meetings, dedicated to bringing together scientists working in the area of sensors, sensor arrays, signal processing and chemometrics, will be held at the Grand Hotel, Malahide, Co. Dublin on 26-27 October, 1995. The meeting is being organised jointly by the Chemometrics Group, the Electroanalytical Group and the Republic of Ireland Sub-region of the Analytical Division of The Royal Society of Chemistry.

Speakers will include **G.G. Guilbault** (*University College Cork*), **G.G. Wallace** (*University of Wollongong*), **J. Slater** (*Birkbeck College*), **P. Hailey** (*Pfizer Central Research*), **R. Forster** (*Dublin City University*), **J. McLaughlin** (*University of Ulster*). Topics will include Chemometrics in the Industrial Situation, Piezoelectric Sensors for Environmental Monitoring, Interpreting Signals from Gas Sensor Arrays and New Developments in Biomedical Implant Sensors.

All contributed papers will be presented as posters, and all papers presented at the meeting can be submitted for publication in a special issue of ***The Analyst***, subject to the normal refereeing procedures of the journal.

Those wishing to submit an abstract, or obtain further details of the meeting, should contact :

Dr Dermot Diamond, *School of Chemical Sciences, Dublin City University, Dublin 9, Ireland.*
FAX: 353 1 7045503
Abstracts should be submitted to Dr Diamond before August 31, 1995 at the very latest

The final circular, including details of the registration fee, accommodation, *etc.*, will be sent to interested parties in June/July 1995.

FIRST FOLD HERE

THE ANALYST READER ENQUIRY SERVICE
For further information about any of the products featured in the advertisements in this issue, write the appropriate number on the postcard, detach and post.

FOLD HERE

THE ANALYST READER ENQUIRY SERVICE

MAY'95

For further information about any of the products featured in the advertisements in this issue, please write the appropriate number in one of the boxes below.
Postage paid if posted in the British Isles but overseas readers must affix a stamp.

PLEASE USE BLOCK CAPITALS LEAVING A SPACE BETWEEN WORDS *Valid 12 months*

1 NAME

2 COMPANY

PLEASE GIVE YOUR BUSINESS ADDRESS IF POSSIBLE. IF NOT, PLEASE TICK HERE ☐

3 STREET

4 TOWN

5 COUNTY
POST CODE

6 COUNTRY

7 DEPARTMENT/
DIVISION

8 YOUR JOB TITLE/
POSITION

9 TELEPHONE NO

OFFICE USE ONLY REC'D PROC'D

FOLD HERE

Postage will be paid by Licensee

Do not affix Postage Stamps if posted in Gt. Britain, Channel Islands, N. Ireland or the Isle of Man

BUSINESS REPLY SERVICE
Licence No. WD 106

Reader Enquiry Service
The Analyst
The Royal Society of Chemistry
Burlington House, Piccadilly
LONDON
W1E 6WF
England

The unique source of information on analytical techniques

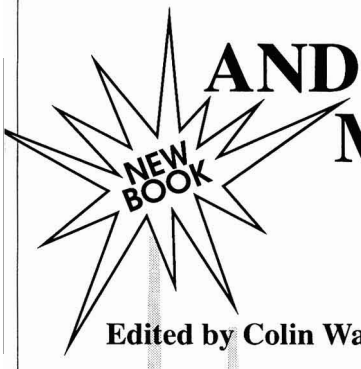

OFFICIAL AND STANDARDIZED METHODS OF ANALYSIS

Third Edition

Edited by Colin Watson, *Atomic Spectrometry Consultancy, Ilford, Essex*

This important new book contains summaries of the analytical methods used in many areas, notably: health and safety; environmental monitoring; food analysis; quality control; water quality.

It enables analysts to assess all the options before committing to the particular technique that best suits their circumstances, whether performing only occasional analyses, analysing a wide variety of substances, or specializing in particular areas.

It provides details on development and evaluation of methods; the very latest techniques; detailed methods recommended by the Analytical Methods Committee of The Royal Society of Chemistry; food analysis methods approved by the Ministry of Agriculture, Fisheries and Food; water analysis; chromatographic and spectrometric methods; traditional 'wet' chemical tests.

It guarantees the analytical scientist certain benefits: informed purchasing and experimental decisions - saving time and money; confidence in achieving the most accurate, reliable results possible; and a sense of where given work and techniques fit in to the wider analytical picture.

Hardcover **xxiv + 778 pages** **ISBN 0 85186 441 4** **1994** **Price £110.00**

PLACE YOUR ORDER FOR THIS UNIQUE BOOK TODAY!

THE ROYAL SOCIETY OF CHEMISTRY
Information Services

To order, please contact:
The Royal Society of Chemistry, Turpin Distribution Services Limited, Blackhorse Road, Letchworth, Herts SG6 1HN, United Kingdom.
Telephone: +44 (0) 1462 672555. Fax: +44 (0) 1462 480947. Telex: 825372

RSC members wishing to purchase for personal use should contact:
The Royal Society of Chemistry, Membership Administration Department, Thomas Graham House, Science Park, Milton Road, Cambridge CB4 4WF, United Kingdom.
Telephone: +44 (0) 1223 420066. Fax: +44 (0) 1223 423623

JAASbase

An essential time-saving PC literature search tool for the analytical chemist

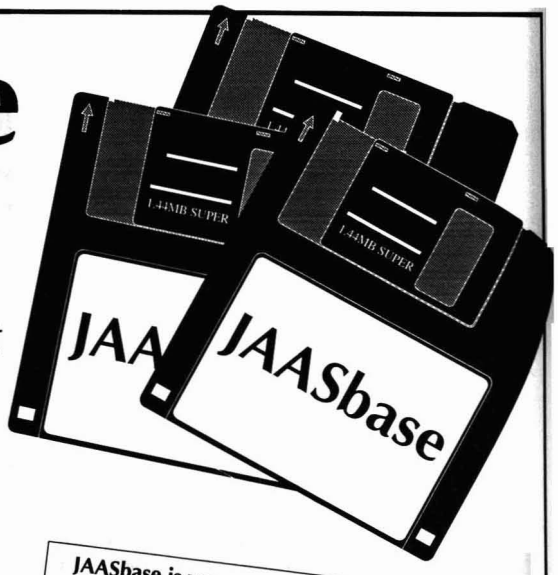

What JAASbase is ...

JAASbase is a unique database of atomic spectrometry reference information, containing full bibliographic references to journal articles and conference papers in the field of atomic spectrometry published since 1985. These references are selected by expert atomic spectroscopists, who add supplementary information that allows you to search for the references you require. The backfile (covering 1985 to 1994) contains over 28,000 references. Update disks add around another 4,000 references a year. JAASbase has been designed to work with the database manager Idealist, a fully indexed, free-text retrieval system.

How will JAASbase help you?

If you are an analytical scientist with a need for rapid access to information on techniques used in atomic spectrometry, JAASbase is the tool you need. Particularly if you work in an applications laboratory with a restricted budget for primary journals and little or no access to library facilities - JAASbase gives you instant access at your bench. Whether your area of analysis is food, the environment, quality control, geology, metallurgy, or whatever, JAASbase will quickly become an essential part of your working life.

JAASbase is your

- key to all atomic spectrometry literature
- user friendly guide to applications literature in many fields - geology, industrial analysis, the environment, food, clinical analysis ...
- easy way of keeping up with the growing volume of publications in your field
- convenient, time-saving, inexpensive searching facility on your PC
- own database - customize it to meet your specific requirements

1995 Subscription Price

JAASbase Backfile (1986-94)	£280.00/$490.00	Plus VAT in the UK
JAASbase Updates 1995	£ 99.00/$174.00	
Idealist Software	£210.00/$368.00	Available in disk size 3.5" or 5.25"

To order, please contact:

The Royal Society of Chemistry, Turpin Distribution Services Limited, Blackhorse Road, Letchworth, Herts SG6 1HN, United Kingdom. Telephone: +44 (0) 1462 672555. Fax: +44 (0) 1462 480947. Turpin Distribution Services Limited is wholly owned by The Royal Society of Chemistry.

RSC members' should order from:

The Royal Society of Chemistry, Membership Administration, Thomas Graham House, Science Park, Milton Road, Cambridge CB4 4WF, United Kingdom. Telephone: +44 (0) 1223 420066. Fax: +44 (0) 1223 423623. E-Mail: (Internet) RSC1@RSC.ORG.

THE ROYAL SOCIETY OF CHEMISTRY

Information Services

© LASER-CLAASBASE CD/98

One of the world's leading analytical chemistry journals

Journal of Analytical Atomic Spectrometry

Covering the development and application of atomic spectrometric techniques

The Journal of Analytical Atomic Spectrometry (JAAS) is an international journal publishing original research papers, communications and letters covering the development and analytical application of atomic spectrometric techniques. It also includes comprehensive reviews of specific topics of interest to practising atomic spectroscopists.

The journal is published 12 times a year, including two special issues, and contains papers on all aspects of the subject. It features information on forthcoming conferences and meetings, recent awards, items of historical interest, book reviews and conference reports.

A special feature of ***JAAS***, which makes it significantly different from all other journals in the field, is the inclusion of Atomic Spectrometry Updates. The six regular issues each contain a major review of the whole range of topics previously covered by ***ARAAS*** (Annual Reports on Analytical Atomic Spectroscopy) providing a unique appreciation of developments in analytical atomic spectrometry.

JAAS provides an excellent publications service supporting growing research into, and applications of, atomic spectrometric techniques.

Editor: Janice M. Gordon, The Royal Society of Chemistry, Thomas Graham House, Science Park, Milton Road, Cambridge CB4 4WF, UK
US Associate Editor: J.M. Harnly, Department of Agriculture, Beltsville Human Nutrition Research Center, BLDG 161, BARC-EAST, Beltsville, MD 20705, USA

1995 Price (12 issues plus annual author and subject index)

ISSN 0267-9477 EEA £512.00 USA $941.50 Canada £538.00 (+GST)
Rest of World £538.00

Order today from the address below . .

To order, please contact:

The Royal Society of Chemistry, Turpin Distribution Services Limited, Blackhorse Road, Letchworth, Herts SG6 1HN, United Kingdom. Tel: +44(0)1462 672555. Fax: +44 (0)1462 480947.

RSC members ordering for personal use are entitled to a discount on most RSC products, and should contact:

Membership Administration Department, The Royal Society of Chemistry, Thomas Graham House, Science Park, Milton Road, Cambridge CB4 4WF, United Kingdom.
Tel: +44 (0)1223 420066. Fax: +44 (0)1223 423623. E-mail (Internet): RSC1@RSC.ORG

For further information on RSC products, please contact the Sales and Promotion Department at our Cambridge address.

THE ROYAL SOCIETY OF CHEMISTRY

Information Services

Solvent Safety Sheets

A Compendium for the Working Chemist

Edited by H Henning, Consultant, ex-Factory Inspectorate

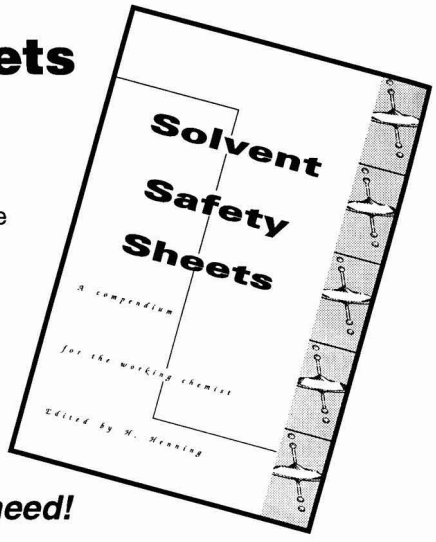

When knowing the hazard is not always enough . . .

There are many publications available providing hazard data on a wide variety of chemicals, but what is more often required is safety information which can be immediately followed should the need arise.

NOW - a new publication to meet that need!

Solvent Safety Sheets: A Compendium for the Working Chemist provides full safety information on approximately 120 solvents in common usage. It takes account of the UK's new Chemical Hazards Information and Packaging (CHIP) regulations, published in August 1993, by using the required new datasheet format (which incorporates an eco-toxicity section) and including the new risk and safety phrases for individual chemicals. The publication has been independently edited by an expert in the field and is indexed by chemical name and synonym.

Use Solvent Safety Sheets to:

- identify chemical hazards in the work environment
- follow essential first aid steps
- identify precautions to be taken during use or disposal
- find remedial action to be taken in case of accidental release
- gain knowledge of the ecological effects of specific chemicals

Softcover
Approx 250 pages
ISBN 0 85186 471 6
Price £39.95
1993

Solvent Safety Sheets: A Compendium for the Working Chemist is an essential handbook for those in small to medium-sized companies who work directly with the chemicals in question and who may not have direct access to a safety professional. With **Solvent Safety Sheets** you will be in a position to take immediate action yourself!

Don't take chances with hazardous substances - keep informed and safe! Make sure you have access to a copy of* Solvent Safety Sheets *by placing your order today.

To order, please contact:
The Royal Society of Chemistry, Turpin Distribution Services Limited
Blackhorse Road, Letchworth, Herts SG6 1HN, United Kingdom
Telephone: +44 (0) 1462 672555. Fax: +44 (0) 1462 480947

Turpin Distribution Services Limited is wholly owned by The Royal Society of Chemistry

RSC Members
There is no members' discount for this title. RSC members, ordering for their own use, should contact: Membership Administration, The Royal Society of Chemistry
Thomas Graham House, Science Park, Milton Road, Cambridge CB4 4WF, United Kingdom
Tel: +44 (0) 1223 420066. Fax: +44 (0) 1223 423623

THE ROYAL SOCIETY OF CHEMISTRY
Information Services

INTERACTIVE CHEMISTRY TRAINING SOFTWARE

FROM THE ROYAL SOCIETY OF CHEMISTRY

Interactive Chemistry Training Software offers a first-class range of computer packages for analytical chemists, spectroscopists, and health and safety officers, produced by **Cognitive Solutions Ltd.,** a software house specialising in the development of packages for computer-based interactive training. There are currently five software packages available:

GC SoftBook **SoftCOSHH™ v2.0**

HPLC SoftBook **AAS SoftBook** **ICP SoftBook**

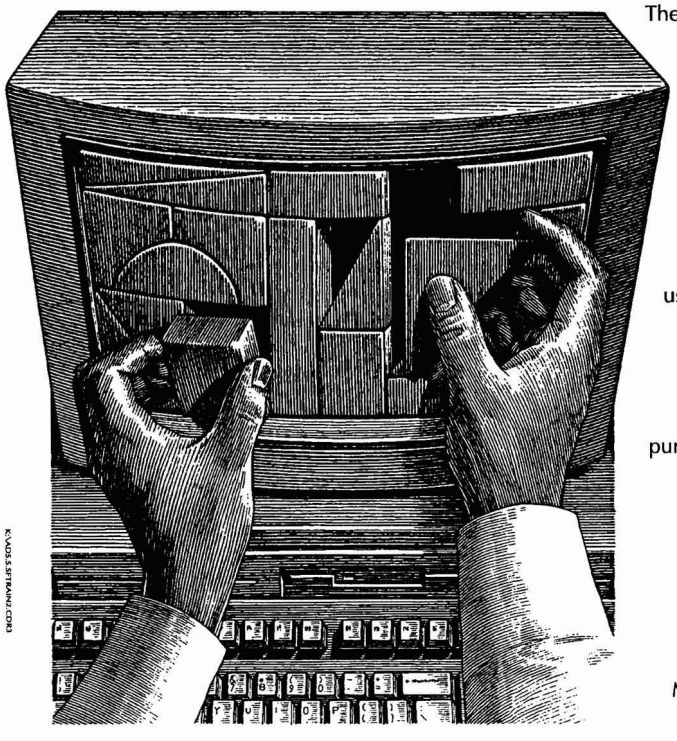

The visual, interactive nature of the product offers a much fuller and more effective method of training than conventional methods. The various principles and practical applications are presented in a colourful, animated form which is easy to use and requires minimal computer knowledge.

Each package is relatively inexpensive, representing a much more cost-effective training facility than more conventional techniques. Learning proceeds at the user's own pace, and any given section of the packages can be readily replayed, ensuring that principles can be grasped thoroughly before laboratory equipment is handled.

Full technical support is available to the purchaser, providing advice on content and usage of each package.

1995 Prices (VAT to be added)

All Packages are £295.00

SoftCOSHH™ v2.0 is £695.00

15% discount for educational users.
Multiple user discount prices available.

To order please contact:

The Royal Society of Chemistry, Turpin Distribution Services Limited, Blackhorse Road, Letchworth, Herts SG6 1HN, United Kingdom.
Telephone: +44 (0) 1462 672555. Fax: +44 (0) 1462 480947.
Please quote your credit card details. We can accept Access/Visa/Mastercard/EuroCard.

Turpin Distribution Services Limited is wholly owned by The Royal Society of Chemistry.

For information on RSC books and journals please contact:

Sales and Promotion Department, The Royal Society of Chemistry, Thomas Graham House, Science Park,
Milton Road, Cambridge CB4 4WF, United Kingdom.
Telephone: +44 (0) 1223 420066. Fax: +44 (0) 1223 423429. E-mail (Internet): RSC1@RSC.ORG.

RSC Members should order from the Membership Administration Department at the Cambridge address above.

THE ROYAL SOCIETY OF CHEMISTRY

Information Services

1527 Quality Management and Laboratory Accreditation at a University: What can be Learned From Experience?—Peter Bode

1535 Instrumentation and Analytical Technique for the Analysis of Regional Geochemical Samples Used at the South African Council for Geoscience. An Overview—J. H. Elsenbroek

SAMPLE HANDLING

1543 Investigation of Decomposition Products of Microwave Digestion of Food Samples—Helen J. Reid, Stanley Greenfield, Tony E. Edmonds

SENSORS/ELECTRODES

1549 Effect of the Coupling Reagent on the Metal Inhibition of Immobilized Urease in an Optical Biosensor—Roberto T. Andres, Ramaier Narayanaswamy

1555 Determination of Cyanide Using a Tyrosinase Amperometric Biosensor with Catechol as Substrate—Xiaoya Hu, Zongzhou Leng

1559 Flow Injection Detection of Tetracyclines by Electrocatalytic Oxidation at a Nickel-modified Glassy Carbon Electrode—W. Oungpipat, P. Southwell-Keely, P. W. Alexander

SEPARATION SCIENCE

1567 Absorption Spectra and Multicapillary Imaging Detection for Capillary Isoelectric Focusing Using a Charge Coupled Device Camera—Jiaqi Wu, Janusz Pawliszyn

1573 Determination of Oligomer Distribution of Alkylphenol Polyethoxylates and Fatty Alcohol Polyethoxylates by Positive-ion Atmospheric Pressure Chemical Ionization Mass Spectrometry—S. Pattanaargsorn, P. Sangvanich, A. Petsom, S. Roengsumran

1577 Determination of Trace Amounts of Sulfur in Hydrotreated Naphthas: Comparative Study Using Raney Nickel, Houston Atlas and Gas Chromatographic Methods—Mohamed M. Abdillahi, Khurshid Alam, Abdul Bari M. Siddiqui, Mohammed A. Ali

SPECTROPHOTOMETRY

1583 On-line Spectrophotometric Determination of Phosphate in Bioprocesses by Sequential Injection—Jorge C. Masini, Pamela J. Baxter, Kandace R. Detwiler, Gary D. Christian

1589 Column Preconcentration of Cobalt With the Ion Pair of 2-Nitroso-1-naphthol-4-sulfonic Acid–Tetradecyldimethylbenzylammonium Chloride Supported on Naphthalene Using Second-derivative Spectrophotometry—Mohammad Ali Taher, Bal Krishan Puri

1593 Selective Spectrophotometric Determination of Cobalt(II) Using 2,2′-Dipyridyl-2-pyridylhydrazone and a Flow Injection Manifold—Demetrius G. Themelis, George A. Zachariadis, John A. Stratis

1599 Synthesis and Studies on the Analytical Functions of a Highly Selective Spectrophotometric Reagent 2-(8-Quinolylazo)-5-*N,N′*-dimethylaminobenzoic Acid—Hanxi Shen, Yuanping Tang, Xinliang Xiao, Shufen Zhang, Ruixian Liu

1603 Application of Pattern Recognition in a Factor Analysis–Spectrophotometric Method for the Simultaneous Determination of Rare Earth Elements in Geological Samples—Hong-yan Wang, Duo-xi Wang, Ying-hua Wang, Shu-gui Chen, Feng-jun Zhang

1609 Determination of Benomyl Residues in Waters by Solid-phase Spectrofluorimetry—José Luis Vilchez, Luis Fermín Capitán-Vallvey, Jamal Rohand, Alberto Navalón, Ramiro Avidad

1613 CUMULATIVE AUTHOR INDEX

NEWS AND VIEWS

55N Book Reviews

60N Conference Diary

65N Courses

66N Conference Reports—J. D. R. Thomas, Yu. A. Zolotov

71N Papers in Future Issues

72N List of Abbreviations and Acronyms

Cover picture: Conference logo for the Geoanalysis 94 Symposium.

ICP-MS

1357 Analysis of Diamonds and Indicator Minerals for Diamond Exploration by Laser Ablation–Inductively Coupled Plasma Mass Spectrometry—R. John Watling, Hugh K. Herbert, Ian S. Barrow, Allen G. Thomas

1365 Comparisons of Infrared and Ultraviolet Laser Probe Microanalysis Inductively Coupled Plasma Mass Spectrometry in Mineral Analysis—Teresa E. Jeffries, William T. Perkins, Nicholas J. G. Pearce

1373 Preparation of Glasses for use as Chemical Standards Involving the Coprecipitated Gel Technique—David L. Hamilton, Timothy C. Hopkins

1379 Determination of Trace Elements in Petroleum Exploration Samples by Inductively Coupled Plasma Mass Spectrometry and Instrumental Neutron Activation Analysis—Samuel D. Olsen, Roy H. Filby, Trond Brekke, Gary H. Isaksen

1391 Determination of Platinum, Palladium, Ruthenium and Iridium in Geological Samples by Isotope Dilution Inductively Coupled Plasma Mass Spectrometry Using a Sodium Peroxide Fusion and Tellurium Coprecipitation—Jacinta Enzweiler, Philip J. Potts, Kym E. Jarvis

1397 Measurement of Boron Isotope Ratios in Groundwater Studies—Nikki C. Porteous, J. Nick Walsh, Kym E. Jarvis

1401 Comparative Study on the Trace and Rare Earth Element Analysis of an Indian Polymetallic Nodule Reference Sample by Inductively Coupled Plasma Atomic Emission Spectrometry and Inductively Coupled Plasma Mass Spectrometry—V. Balaram, K. V. Anjaiah, M. R. P. Reddy

ICP-AES

1407 Validation of a Geochemical Logging Tool for *In Situ* Major Element Analysis in Boreholes Using Inductively Coupled Plasma Atomic Emission Spectrometry—Mark S. Sams, Peter J. Watkins, Michael H. Ramsey

1415 Chemical Partitioning of the New National Institute of Standards and Technology Standard Reference Materials (SRM 2709–2711) by Sequential Extraction Using Inductively Coupled Plasma Atomic Emission Spectrometry—Xiangdong Li, Barry J. Coles, Michael H. Ramsey, Iain Thornton

1421 Improved Detection Limits for Transient Signal Analysis of Fluid Inclusions by Inductively Coupled Plasma Atomic Emission Spectrometry Using Correlated Background Correction—Barry J. Coles, Sarah A. Gleeson, Jamie J. Wilkinson, Michael H. Ramsey

1427 Inductively Coupled Plasma Atomic Emission Spectrometric Determination of Rare Earth Elements in Granites and Greisens Using Thin-layer Chromatographic Preconcentration—Natalia S. Safronova, Svetlana S. Matveeva, Yury I. Fabelinsky, Valentin A. Ryabukhin

1433 Inductively Coupled Plasma Atomic Emission Spectrometric Analysis of Low Levels of Selenium in Natural Waters—Rob L. Adkins, J. Nick Walsh, Mike Edmunds, Janice M. Trafford

NEUTRON ACTIVATION ANALYSIS

1437 Epithermal Neutron Activation Analysis of Mosses Used to Monitor Heavy Metal Deposition Around an Iron Smelter Complex—M. V. Frontasyeva, E. Steinnes

1441 Determination of Platinum, Palladium, Iridium and Gold in Selected Geological Reference Materials by Radiochemical Neutron Activation Analysis: Comparison of Procedures Based on *Aqua Regia* Leaching and Sodium Peroxide Sintering—Claudio A. Nogueira, Ana M. G. Figueiredo

1445 Neutron Activation Analysis Investigation of the Composition and Geochemical Peculiarities of Lake Baikal Bottom Sediments—A. I. Bulnayev

1453 Evolution, Using Instrumental Neutron Activation Analysis, of the Element Composition of Coal and Oil Shale Fuel at Consecutive Stages of Its Combustion—Peter A. Vaganov, Zhou Rongsheng, Liidia I. Pets

1457 Neutron Activation Analysis of Environmental Materials—Gennady M. Kolesov

1461 Neutron Activation Determination of Noble Metals in Samples of Terrestrial and Cosmic Origin Using Microfire Assay Concentration—Gennady M. Kolesov, Dmitry Yu. Sapozhnikov

OTHER TECHNIQUES

1465 Analysis of Weathering Products Formed on Saxonean Cretaceous Sandstones—K. Russ, S. Machill, W. E. Steger

1471 Trace Enrichment of Metals Using a Supported Liquid Membrane Technique—Margareta Papantoni, Nii-Koley Djane, Kuria Ndung'u, Jon Åke Jönsson, Lennart Mathiasson

1479 Enrichment of Metals in the Organic Surface Layer of Natural Soil: Identification of Contributions From Different Sources—Eiliv Steinnes, Oddvar Njåstad

1485 Distribution and Partitioning of Copper, Lead and Zinc in Stream Sediments Above and Below an Abandoned Mining and Milling Area Near Pecos, New Mexico, USA—Lynn A. Brandvold, Virginia T. McLemore, Catherine O'Connor, Donald K. Brandvold

PERSPECTIVES

1497 Analytical Requirements in International Geochemical Mapping—Xie Xuejing

1505 Impact of Inductively Coupled Plasma Mass Spectrometry on Certification Programmes for Geochemical Reference Materials—Jean S. Kane, Ellyn S. Beary, Karen E. Murphy, Paul J. Paulsen

1513 Certified Ontario Reference Materials Programme at the Geoscience Laboratories, Sudbury, Ontario, Canada—Jean M. Richardson

1519 Method Validation in the Ontario Geoscience Laboratories—Jean M. Richardson, John L. Morrison

Continued on facing page—

ICP-MS

1357 Analysis of Diamonds and Indicator Minerals for Diamond Exploration by Laser Ablation–Inductively Coupled Plasma Mass Spectrometry—R. John Watling, Hugh K. Herbert, Ian S. Barrow, Allen G. Thomas

1365 Comparisons of Infrared and Ultraviolet Laser Probe Microanalysis Inductively Coupled Plasma Mass Spectrometry in Mineral Analysis—Teresa E. Jeffries, William T. Perkins, Nicholas J. G. Pearce

1373 Preparation of Glasses for use as Chemical Standards Involving the Coprecipitated Gel Technique—David L. Hamilton, Timothy C. Hopkins

1379 Determination of Trace Elements in Petroleum Exploration Samples by Inductively Coupled Plasma Mass Spectrometry and Instrumental Neutron Activation Analysis—Samuel D. Olsen, Roy H. Filby, Trond Brekke, Gary H. Isaksen

1391 Determination of Platinum, Palladium, Ruthenium and Iridium in Geological Samples by Isotope Dilution Inductively Coupled Plasma Mass Spectrometry Using a Sodium Peroxide Fusion and Tellurium Coprecipitation—Jacinta Enzweiler, Philip J. Potts, Kym E. Jarvis

1397 Measurement of Boron Isotope Ratios in Groundwater Studies—Nikki C. Porteous, J. Nick Walsh, Kym E. Jarvis

1401 Comparative Study on the Trace and Rare Earth Element Analysis of an Indian Polymetallic Nodule Reference Sample by Inductively Coupled Plasma Atomic Emission Spectrometry and Inductively Coupled Plasma Mass Spectrometry—V. Balaram, K. V. Anjaiah, M. R. P. Reddy

ICP-AES

1407 Validation of a Geochemical Logging Tool for *In Situ* Major Element Analysis in Boreholes Using Inductively Coupled Plasma Atomic Emission Spectrometry—Mark S. Sams, Peter J. Watkins, Michael H. Ramsey

1415 Chemical Partitioning of the New National Institute of Standards and Technology Standard Reference Materials (SRM 2709–2711) by Sequential Extraction Using Inductively Coupled Plasma Atomic Emission Spectrometry—Xiangdong Li, Barry J. Coles, Michael H. Ramsey, Iain Thornton

1421 Improved Detection Limits for Transient Signal Analysis of Fluid Inclusions by Inductively Coupled Plasma Atomic Emission Spectrometry Using Correlated Background Correction—Barry J. Coles, Sarah A. Gleeson, Jamie J. Wilkinson, Michael H. Ramsey

1427 Inductively Coupled Plasma Atomic Emission Spectrometric Determination of Rare Earth Elements in Granites and Greisens Using Thin-layer Chromatographic Preconcentration—Natalia S. Safronova, Svetlana S. Matveeva, Yury I. Fabelinsky, Valentin A. Ryabukhin

1433 Inductively Coupled Plasma Atomic Emission Spectrometric Analysis of Low Levels of Selenium in Natural Waters—Rob L. Adkins, J. Nick Walsh, Mike Edmunds, Janice M. Trafford

NEUTRON ACTIVATION ANALYSIS

1437 Epithermal Neutron Activation Analysis of Mosses Used to Monitor Heavy Metal Deposition Around an Iron Smelter Complex—M. V. Frontasyeva, E. Steinnes

1441 Determination of Platinum, Palladium, Iridium and Gold in Selected Geological Reference Materials by Radiochemical Neutron Activation Analysis: Comparison of Procedures Based on *Aqua Regia* Leaching and Sodium Peroxide Sintering—Claudio A. Nogueira, Ana M. G. Figueiredo

1445 Neutron Activation Analysis Investigation of the Composition and Geochemical Peculiarities of Lake Baikal Bottom Sediments—A. I. Bulnayev

1453 Evolution, Using Instrumental Neutron Activation Analysis, of the Element Composition of Coal and Oil Shale Fuel at Consecutive Stages of Its Combustion—Peter A. Vaganov, Zhou Rongsheng, Liidia I. Pets

1457 Neutron Activation Analysis of Environmental Materials—Gennady M. Kolesov

1461 Neutron Activation Determination of Noble Metals in Samples of Terrestrial and Cosmic Origin Using Microfire Assay Concentration—Gennady M. Kolesov, Dmitry Yu. Sapozhnikov

OTHER TECHNIQUES

1465 Analysis of Weathering Products Formed on Saxonean Cretaceous Sandstones—K. Russ, S. Machill, W. E. Steger

1471 Trace Enrichment of Metals Using a Supported Liquid Membrane Technique—Margareta Papantoni, Nii-Koley Djane, Kuria Ndung'u, Jon Åke Jönsson, Lennart Mathiasson

1479 Enrichment of Metals in the Organic Surface Layer of Natural Soil: Identification of Contributions From Different Sources—Eiliv Steinnes, Oddvar Njåstad

1485 Distribution and Partitioning of Copper, Lead and Zinc in Stream Sediments Above and Below an Abandoned Mining and Milling Area Near Pecos, New Mexico, USA—Lynn A. Brandvold, Virginia T. McLemore, Catherine O'Connor, Donald K. Brandvold

PERSPECTIVES

1497 Analytical Requirements in International Geochemical Mapping—Xie Xuejing

1505 Impact of Inductively Coupled Plasma Mass Spectrometry on Certification Programmes for Geochemical Reference Materials—Jean S. Kane, Ellyn S. Beary, Karen E. Murphy, Paul J. Paulsen

1513 Certified Ontario Reference Materials Programme at the Geoscience Laboratories, Sudbury, Ontario, Canada—Jean M. Richardson

1519 Method Validation in the Ontario Geoscience Laboratories—Jean M. Richardson, John L. Morrison

Continued on facing page—

ANALAO 120(5) 1227–1616 55N–72N (1995) MAY 1995

The Analyst

The analytical journal of The Royal Society of Chemistry

CONTENTS

GUEST EDITOR 1227 Dr. Michael Ramsey

FOREWORD 1228 Geoanalysis 94: An International Symposium on the Analysis of Geological and Environmental Materials

X-RAY TECHNIQUES

TUTORIAL REVIEW 1231 Synchrotron X-ray Sources: Instrumental Characteristics, New Applications in Microanalysis, Tomography, Absorption Spectroscopy and Diffraction—Joseph V. Smith

1247 Trace Element Standards for the Electron Microanalyser Using Layered and Ion-implanted Materials—C. Remond, R. H. Packwood, C. Gilles

1261 Method of X-ray Fluorescence Analysis for Environmental Lead, Especially in Household Dust, Using Thin-film Principles—Jacques Renault, Chris McKee

1267 Analysis and Characterization of Water Treatment Plant Sludges by X-ray Fluorescence Spectrometry—H. Margaret West, Jess Cawley, Robert Wills

1273 Analysis of Silicate Rocks Using Field-portable X-ray Fluorescence Instrumentation Incorporating a Mercury(II) Iodide Detector: A Preliminary Assessment of Analytical Performance—Philip J. Potts, Peter C. Webb, Olwen Williams-Thorpe, Richard Kilworth

1279 Merits of Using Barium as a Heavy Absorber in Major Element Analysis of Rock Samples by X-ray Fluorescence: New Data on ASK-1 and ASK-2 Reference Samples—T. Gnaneshwara Rao, Pradip K. Govil

MASS SPECTROMETRY

REVIEW 1283 Accelerator Mass Spectrometry in Environmental Geoscience—John Rucklidge

REVIEW 1291 Recent Developments in Thermal Ionization Mass Spectrometric Techniques for Isotope Analysis—K. G. Heumann, S. Eisenhut, S. Gallus, E. H. Hebeda, R. Nusko, A. Vengosh, T. Walczyk

REVIEW 1301 Boron Isotope Analysis—Jugdeep K. Aggarwal, Martin R. Palmer

1309 Determination of Hydrogen in Silicates by Secondary Ion Mass Spectrometry—Luisa Ottolini, Piero Bottazzi, Alberto Zanetti, Riccardo Vannucci

ION PROBE TECHNIQUES

1315 Ion Probe Measurements of National Institute of Standards and Technology Standard Reference Material SRM 610 Glass, Trace Elements—R. W. Hinton, B. Harte, G. Witt-Eickschen

1321 High-precision, *In Situ* Oxygen Isotope Ratio Measurements Obtained From Geological and Extra-terrestrial Materials Using an Isolab 54 Ion Microprobe—John M. Saxton, Ian C. Lyon, Grenville Turner

MICROSCOPY

1327 A New Type of Synthetic Geochemical Reference Material—SynTERM—David Cohen, Rolf Beck

1335 Application of Analytical Transmission Electron Microscopy to Identifying Intercrystal Variations in the Composition of Clay Minerals—Balwant Singh, R. J. Gilkes

1341 Reconstruction of *In Situ* Pore-water Compositions Obtained by Aqueous Leaching of Drill Core: An Evaluation Using Multivariate Statistical Deconvolution—Mark Cave, Shaun Reeder

1353 Estimation of Sampling Bias Between Different Sampling Protocols on Contaminated Land—Michael H. Ramsey, Ariadni Argyraki, Michael Thompson

Continued on inside back cover—

Typeset and printed by Black Bear Press Limited, Cambridge, England

0003-2654(1995)5:1-Y